E15PC00012/100068825

# Research on Safety Technology Verification for Materials and Corrosions in the U.S. Outer Continental Shelf (OCS), High Pressure High Temperature (HPHT) Material Evaluation

## Final Report

Prepared by: Joel D. Elhard, Andrew Duguid, and Michael Heinrichs

Battelle
505 King Avenue
Columbus, Ohio 43201

Submitted to: Bureau of Safety and Environmental Enforcement (BSEE)

July 2017

BATTELLE

BATTELLE

# EXECUTIVE SUMMARY

## Objectives

Offshore oil and gas (O&G) exploration, drilling, and production are moving to high pressure, high temperature (HPHT) environments by the integration of the use of new materials technologies for operations. An integral part of these new technologies is advanced materials including new elastomers and composite media which may be used in downhole equipment such as packers and measurement tools. As these material components are developed, there is a need to demonstrate material properties and compatibility for use in downhole applications under HPHT conditions (greater than 15,000 pounds per square inch [psi] and 176°C [350°F]). This is especially important because elastomers are used in critical components for maintaining safe operations and well control.

While industry standards have been outlined to guide the use of materials for oilfield operations, they remain insufficient to demonstrate the materials properties and compatibility for use in downhole applications, particularly under HPHT conditions. Industry standards provide some guidance on the use of materials for oilfield operations in HPHT environments, such as acceptable hardness ranges, tensile strength ranges, and volume swell parameters, however, the existing standards associated with overall component testing (e.g., wellhead, packer, blow-out preventer [BOP], or sub-surface safety valve [SSSV]) do not provide recommendations for individual elastomeric materials qualification (e.g., individual components of an overall system, such as seals) in HPHT environments. Current industry standards do not include testing protocols to verify component/material compatibility with HPHT environments. Extreme environments have the potential to cause wear more quickly and more severely than standard applications for these material components, which increases the risk of component failure. It is critical to use proper material selection based on qualification testing approaches to validate that an elastomer is suited for HPHT use prior to component selection.

The objectives of this project were to perform a feasibility study to test and validate standard test protocols, laboratory testing procedures, and analyses for a subset of materials properties suitable for HPHT operations. This overarching objective was accomplished by performing five major tasks:

1. Evaluation of potential failure modes of seal elastomers and composites for HPHT O&G applications through understanding the materials that are used, the manufacturing processes, and their failure modes.
2. Evaluation of existing industry standards for materials used for O&G operations under HPHT conditions by reviewing the existing industry literature and industry standards for elastomeric and composite materials in subsea, downhole, and HPHT applications.
3. Assessment of test protocols and experimental analysis for materials used for O&G operations under HPHT conditions and collection of material property data for five elastomers commonly used by the O&G industry for use in the development of a finite element analysis (FEA) model.

4. Creation of an FEA model using material property data for each elastomer studied.
5. Testing of elastomer O-rings in a test fixture capable of HPHT conditions to determine the onset of extrusion for a series of clearance gaps, and compilation of test data for validation of an FEA model.

The results of this study are applicable to offshore HPHT operators as use of validated FEA models may quickly and cost effectively predict the performance of elastomer behavior in wellheads, packers, BOPs and SSSVs. This project represents the first step of creating such a validated model, the results of which may be incorporated into Application for Permit to Drill (APD), Application for Permit to Modify (APM) and Deepwater Operation Plan (DWOP) submittals to provide predictive material performance information during design consideration for HPHT operations.

**Project Execution**

The foundation of this project was a thorough literature review of existing industry standards and elastomer failure mechanisms to compile the set of current knowledge of material behavior and testing protocols. The applicable industry standards reviewed in this study included those from the following organizations:

- American National Standards Institute (ANSI)
- American Petroleum Institute (API)
- American Society for Testing Materials (ASTM)
- International Organization for Standardization (ISO)
- National Association for Corrosion Engineers (NACE)
- Aerospace Material Specifications (AMS)
- Military Specifications (MIL-SPEC)
- Norsk Sokkels Konkuranseposisjon (NORSOK)

Six direct failure mechanisms of elastomeric seals used in O&G applications were studied and reported on. The failure mechanisms were:

- Extrusion and nibbling
- Compression set
- Explosive decompression
- Wear
- Chemical degradation
- Spiral failure

Five elastomer types were used for the development of data to validate the FEA model. The elastomers were:

- Acrylonitrile butadiene nitrile rubber (NBR)
- Hydrogenated acrylonitrile butadiene nitrile rubber (HNBR)
- Fluoroelastomers based on vinylidene fluoride (FKM; Viton®)
- Fluoroelastomers based on propylene tetrafluoroethylene copolymers (FEPM; Aflas®)
- Perfluoroelastomers (FFKM; Kalrez®).

The FEA model developed in this program is specific to the conditions of the experiments conducted under HPHT conditions on O-rings and the independent measurements of basic elastomer properties. Assumptions of the model include:

- Constant temperature
- Constant pressure
- Chemically inert environment
- Chemically static elastomer materials
- Static O-ring seal

**Key Findings**

The following key findings are based on the results of this project:

- New or revised guidance, followed by formal industry standards, are needed to ensure safe operation in HPHT environments (over 15,000 psi and 175ºC) since current industry standards only provide guidance for elastomer use at pressures up to 5,000 psi.
- The dominant HPHT failure mechanism in observed during elastomer testing and FEA model development was crack tear propagation via extrusion-initiated spiral failure. Understanding of this failure mechanism could guide development of new crack resistant materials.
- A FEA-based computer model was developed using ABAQUS software to predict the onset of tearing and failure of elastomer O-rings operating under HPHT conditions. The FEA (M-CTP) model was parameterized with a comprehensive set of elastomer mechanical property data at multiple temperatures, including multi-axial, compression, hyper-elastic, crack-initiation and creep-crack-growth tests. The model was successfully validated by comparing the experimental (E-CTP) test results from a HPHT test cell.
- The outcome of this work supports the use of FEA in the design and evaluation of elastomer seals in downhole tools and well control applications such as BOPs, as illustrated for the case of an annular BOP in Figure 108. Battelle emphasizes that any large-scale extension of the FEA model that was developed and validated on AS568-210 size O-ring seal fixtures should be revalidated on larger scale devices before implementation.

- The correlation between the model (M-CTP) and experimental data (E-CTP) was very high with average deviation[1] of 9% for all O-ring materials at all tested clearance gaps and all test temperatures. This provides users with high confidence in the M-CTP accuracy (Figure 103a,b). The FEA (M-CTP) model was also parameterized with elastomer property data at multiple temperatures and confirmed through experimental data.
- O&G elastomers have much lower mechanical properties (tensile modulus, tensile strength and elongation at break) at temperatures above 75°C (Section 6.7, 6.8) Therefore, although elastomers may be in compression mode, the O&G operator should require higher temperature test data for HPHT applications.
    - The performance of the O&G elastomer seal materials was determined to depend on critical tear pressures as a function of temperature. For 90 Shore A Hardness Elastomers: HNBR-90 and FKM-90 are superior to FFKM-90 and FEPM-90 at 150°C to 175°C across all clearance gaps (Figure 110). Lower hardness elastomers (Figure 111) have similar E-CTP at 150°C to 175°C across all clearance gaps (Figure ES-7), which is much lower than HNBR-90 and FKM-90, but similar to FFKM-90 and FEPM-90.
    - The experimental critical tear pressure (E-CTP) results for elastomer O-rings were consistent with a Power Law expression that allows for accurate prediction at a range of clearance gaps at temperatures up to 175ºC and pressures of 15,000 psi. These results provide guidelines for O-ring seal design and selection for HPHT conditions.

**Recommendations**

- O-ring seal failures can be caused by other stresses encountered under HPHT conditions, including corrosive environments ($H_2S$, $CO_2$, and chlorides). Additional testing and model development are recommended for these conditions so that the FEA can more accurately represent actual working conditions.
- Testing in this program was conducted using an O-ring of the same size. Future testing should be expanded to component and device level (i.e., BOPs, SSSVs, packers, etc.).
- Future studies can include extending the FEA model and HPHT testing to include aging effects in corrosive and non-corrosive environments as well as extended lifecycle testing (cyclic pressurization and associated crack growth) under these conditions.

[1] Defined as the average of the individual M-CTP and E-CTP deviations, calculated as: $\frac{|(M-CTP)-(E-CTP)|}{E-CTP} \cdot 100$

- Future development efforts should expand the FEA model to include longer term creep crack growth of elastomers in combination with experimental validation (Figure ES-1).

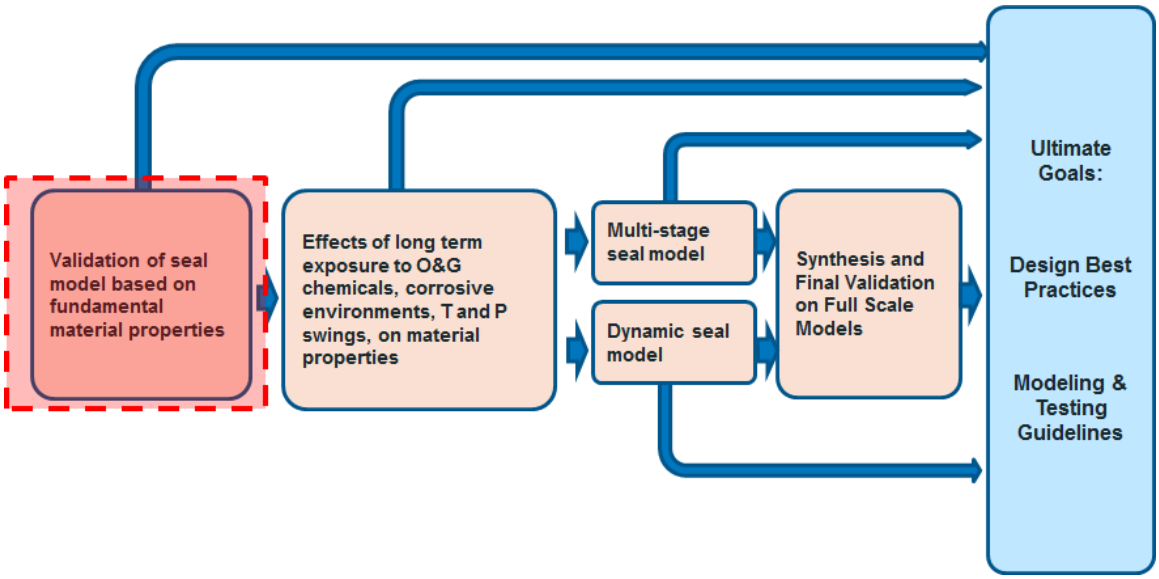


**Figure ES-1. Recommendation Roadmap**

The elastomers evaluated in this study with the resulting FEA model constitute the development and validation of a baseline FEA model. This model serves as a building block toward the eventual goal of developing a complete computer-based model that can be used to develop best practices and guidelines for elastomer use under HPHT conditions. A complete model would include predictive failure capabilities for various downhole HPHT environments (including sweet and sour gas conditions) encountered by operators.

**TABLE OF CONTENTS**

## LIST OF TABLES

Page

## LIST OF FIGURES

Page

## LIST OF APPENDICES

## LIST OF ACRONYMS AND ABBREVIATIONS

| Acronym | Definition |
|---|---|
| AMS | Aerospace Material Specifications |
| ANSI | American National Standards Institute |
| APD | Appliation for Permit to Drill |
| API | American Petroleum Institute |
| APM | Application for Permit to Modify |
| ASTM | American Society for Testing Materials |
| BOP | blow-out preventer |
| BSEE | Bureau of Safety and Environmental Enforcement |
| CSM | cure site monomer |
| CAD | computer aided design |
| $CO_2$ | carbon dioxide |
| CTE | coefficient of thermal expansion |
| CTP | critical tearing pressure (Endurica model) |
| CTS | critical Tresca stress |
| DMA | dynamic mechanical analysis |
| DoD | Department of Defense |
| DWOP | Deepwater Operation Plan |
| E-CTP | experimental critical tearing pressure |
| ETP | perfluoromethyl vinyl ether |
| FEA | finite element analysis |
| FEPM | Propylene tetrafluroethylene copolymers class of fluoroelastomers (such as Aflas®) |
| FFKM | perfluorinated elastomers class of perfluoroelastomers (such as Kalrez®) |
| FKM | fluoroelastomers class of fluoroelastomers (such as Viton®) |
| FLE | first large extrusion |
| $H_2S$ | hydrogen sulfide |
| HCl | hydrochloric acid |
| HF | hydrofluoric acid |
| HFP | hexafluoropropylene |
| HNBR | hydrogenated acrylonitrile butadiene nitrile rubber |
| HPHT | high pressure, high temperature |
| HSE | health, safety, and environment |
| Hz | Hertz unit |

| | |
|---|---|
| IRM | Industry Reference Materials |
| ISO | International Organization for Standardization |
| ksi | kilopound per square inch |
| M-CTP | measured critical tearing pressure |
| MIL-SPEC | Military Standard |
| MPa | Mega Pascals unit |
| NACE | National Association for Corrosion Engineers |
| NBR | acrylonitrile butadiene nitrile rubber |
| NORSOK | Norsk Sokkels Konkuranseposisjon |
| O&G | oil and gas |
| OCS | Outer Continental Shelf |
| PMVE | perfluoromethyl vinyl ether |
| PSIG | pounds per square inch gauge |
| RGD | rapid gas decompression |
| RSD | relative standard deviation |
| SAE | Society of Automotive Engineers |
| SINTEF | Stiftelsen for INdustriell og TEknisk Forskning |
| SPM | sub-plate mounted valve |
| SSSV | sub-surface safety valve |
| VDF | vinylidene fluoride |
| TFE | tetrafluoroethylene |
| TM | Test Method |
| UK | United Kingdom |

# 1.0 INTRODUCTION

Offshore exploration and drilling are moving to higher pressure and higher temperature environments, enabled by the integration of new elastomers and composites into downhole operations. Elastomers can be used in components including packers, subsurface safety valves (SSSVs), well heads, and blow-out preventers (BOPs) operating under high pressure, high temperature (HPHT) conditions. Industry standards provide guidance on the use of materials for oilfield operations; however, there is a need to demonstrate material properties and compatibility for use in downhole applications, particularly under HPHT conditions (greater than 15,000 pounds per square inch [psi] and 350°F). Uncertainty of elastomer performance in HPHT systems poses a potential safety risk on oil and gas (O&G) subsea operations in the Outer Continental Shelf (OCS).

The overall project effort was divided into five main tasks.

Task 1: Battelle documented the associated material properties of elastomers and composites, and reviewed the critical failure modes of elastomers in HPHT environments. Battelle gathered and presented information on the manufacture of HPHT service elastomers and the types of O&G equipment that may rely on elastomer seals.

Tasks 2 and 3: Battelle identified available standards, test protocols, and conducted analyses for the material properties of common O&G elastomers identified in Task 1.

Task 4: Battelle characterized failures of common O&G industry elastomer O-ring seals. Specifically, in Task 4, the Battelle team conducted tests to better understand elastomer failure modes of common industry elastomers. Tests were conducted in a custom-designed HPHT test cell capable of operating at elevated temperatures (up to 175°C or ~350°F) and pressures (up to 15,000 psig).

Task 5: Battelle developed and parameterized a FEA model of the thermomechanical behavior of an elastomer in an O-ring seal/gland configuration under HPHT operating conditions. The model accurately characterized the extrusion crack tear process. The HPHT test data were used to validate the FEA model.

Figure 1 illustrates the five-task approach for this project.

This final project report summarizes the approach used and findings of this study. Sections 2.0 and 3.0 provide the objectives and approach for this project, respectively. Section 4.0 provides a review of critical elastomer properties. The review identifies parameters that framed the balance of the study, such as batch, cure, and mold variabilities between O-rings. Section 5.0 provides a review of current standards that guide O&G use of elastomers, including those used in HPHT applications. This review was used, in part, to guide the design of experiments for the remainder of the study, including material testing temperatures. Section 6.0 provides material property data used to construct the FEA model. The material property data include thermal expansion data, volumetric compression data, critical tension, and critical tearing energy. The approach to the FEA model setup is presented in Section 7.0, followed by the HPHT experimental setup and testing approach data collected in Section 8.0. Finally,

Section 9.0 presents a comparison of the FEA model against the resulting HPHT data, as well as additional developmental steps to further expand the applications of the model in the future.

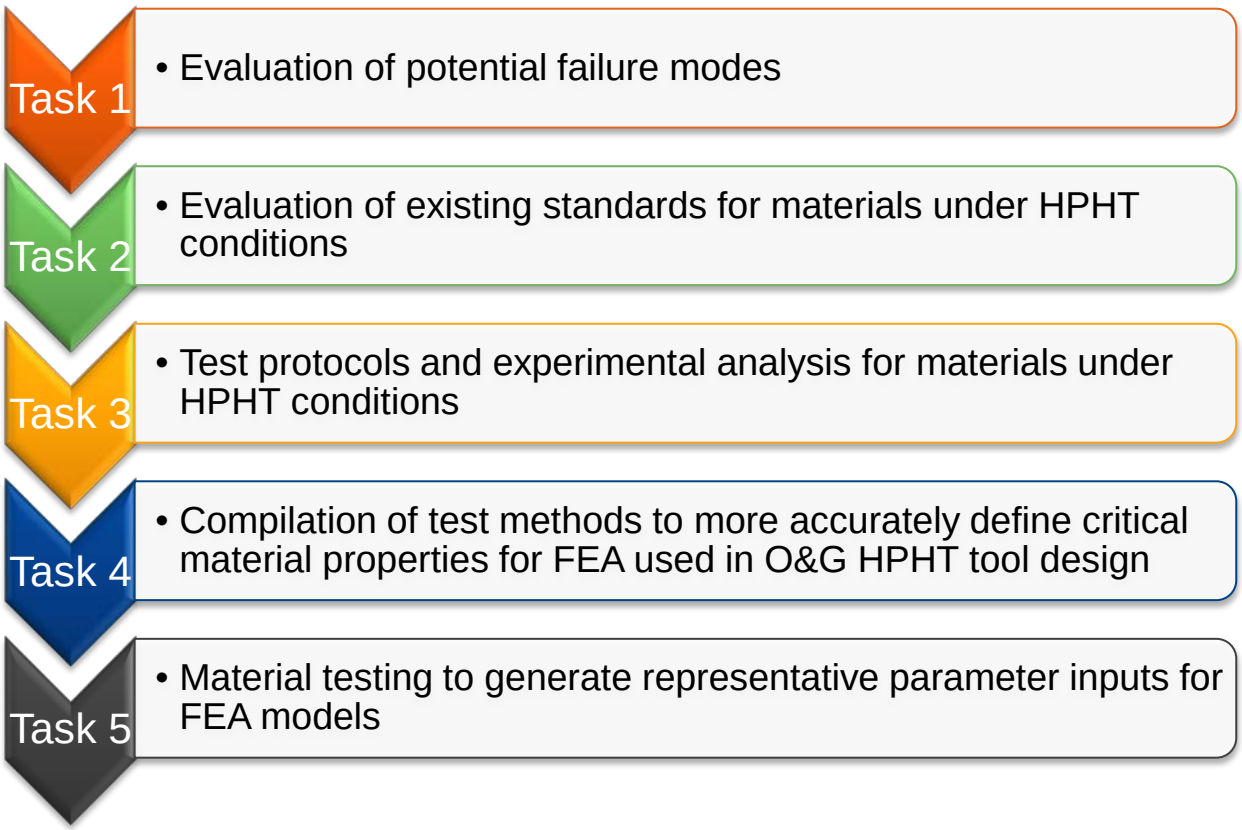


**Figure 1. Project tasks.**

## 2.0 OBJECTIVES

The objective of this program was to evaluate current test protocols, procedures, and material property analyses that are conducted by O&G operators to demonstrate equipment is fit for service in HPHT conditions. This objective was accomplished through reviewing material properties and existing test methods for elastomers that are being currently used, and evaluating how well those test methods replicate HPHT environments. In addition, since O&G operators rely on FEA modeling to design down-hole seals and tools, a second objective was to develop a FEA model of an O-ring seal that would be validated through elastomer testing under elevated temperature and pressure conditions and demonstrate the feasibility to predict the onset of failure.

## 3.0 APPROACH

Five different types of elastomer materials were evaluated as part of this study: acrylonitrile butadiene nitrile rubber (NBR), hydrogenated acrylonitrile butadiene nitrile rubber (HNBR), fluoroelastomers (FKM), propylene tetrafluoroethylene copolymers (FEPM), and perfluorinated elastomers (FFKM). These materials were selected due to their prevalent use by the O&G industry in HPHT applications. Table 1 lists the elastomers that were evaluated, with their respective common industry trade names.

**Table 1. Elastomers evaluated as part of this study and examples of associated trade names.**

| Elastomer | Abbreviation | Common Industry Trade Names |
|---|---|---|
| Acrylonitrile butadiene rubber | NBR | KRYNAC®, Nipol® |
| Hydrogenated acrylonitrile butadiene rubber | HNBR | Elasto-Lion® |
| Fluoroelastomers | FKM | Viton®, Fluorel®, Daiel®, Tecnoflon® |
| Perfluorinated elastomers | FFKM | Kalrez®, Tecnoflon®, Chemraz® |
| Propylene tetrafluoroethylene copolymers | FEPM | Alfas®, Viton® Extreme™ |

As part of the first task, a literature search and review were conducted for common elastomers in HPHT O&G applications. The objective was to gather data on the current elastomer types and composites used for O&G applications, the manufacturing processes used to fabricate these materials into parts, the types of devices these materials are incorporated into, and their corresponding operating conditions.

As an example, James Walker and Co. produces a wide range of O&G production elastomer seal products such as their Springsele® and Teesele® from Elasto-Lion® (HNBR), FR58/90 (FKM), and FEPM. ERIKS® Seals and Plastics produces seal products for downhole completion, production and subsea applications from each of the elastomers included in this study: NBR, HNBR, FKM, FFKM, and FEPM. Pioneer Weston also produces single-acting cap seals with elastomer “energizer” materials from each of the elastomers in this study as well as spring S-seals and T-seals used in reciprocating and high pressure static applications from HNBR and FKM.

Additionally, failure modes of elastomer devices in O&G applications including frequency and criticality of failures were explored. Identifying the level of understanding for failure modes of

materials used in current applications will lend insight into the design and testing for this project and improve overall selection of materials for HPHT O&G tooling and component design.

Following the review of elastomers and their properties, an evaluation of existing standards for materials used in HPHT O&G environments was conducted. The standards reviewed are applicable to the use of elastomeric materials in the O&G downhole equipment identified as part of this study: packers, SSSVs, wellheads, and BOPs.

Standards evaluated include:

- American National Standards Institute (ANSI)
- American Petroleum Institute (API)
- American Society for Testing Materials (ASTM) International
- International Organization for Standardization (ISO)
- National Association of Corrosion Engineers (NACE)
- Aerospace Material Specifications (AMS)
- United States Military Standard (MIL-SPEC)
- Norsk Sokkels Konkuranseposisjon (NORSOK)

API, Aerospace, MILSPEC, NACE and other standards evaluated for this study are listed in Table 2 through Table 5.

**Table 2. Selection of ISO standards evaluated in this study.**

| Standard Number | Standard Description |
|---|---|
| ISO 10417/API 14B (International Standard, 2004) | Petroleum and natural gas industries — Subsurface safety valve systems — Design, installation, operation and redress |
| ISO 13533/API 16A (International Organization for Standardization, 2001) | Petroleum and natural gas industries — Drilling and production equipment — Drill through equipment |
| ISO 23936-2 (International Organization for Standardization, 2011) | Petroleum, petrochemical and natural gas industries — Non-metallic materials in contact with media related to oil and gas production — Part 2: Elastomers |
| ISO 10423/API 6A (International Organization for Standardization, 2005) | Specification for Wellhead and Christmas Tree Equipment |

**Table 2. Selection of ISO standards evaluated in this study (continued).**

| Standard Number | Standard Description |
|---|---|
| ISO 14310/API 11D (International Organization for Standardization, 2008) | Petroleum and natural gas industries — Downhole Equipment — Packers and bridge plugs |
| ISO 13628-4/API 17B (ISO 13628-4, 2011) | Design and Operation of Subsea Production Systems — Subsea Wellhead and Tree Equipment |
| ISO 10423/API 6A (International Organization for Standardization, 2005) | Specification for Wellhead and Christmas Tree Equipment |
| ISO 14310/API 11D (International Organization for Standardization, 2008) | Petroleum and natural gas industries — Downhole Equipment — Packers and bridge plugs |
| ISO 13628-4/API 17B (ISO 13628-4, 2011) | Design and Operation of Subsea Production Systems — Subsea Wellhead and Tree Equipment |

**Table 3. Selection of ISO, API, and NORSOK standards evaluated in this study.**

| Standard Number | Standard Description |
|---|---|
| ISO 27996 (International Organization for Standardization, 2009) | Aerospace fluid systems — Elastomer seals — Storage and shelf life |
| ISO 10432 (International Organization for Standardization, 2006) | Petroleum and natural gas industries—Downhole equipment—Subsurface safety valve equipment |
| API STD 53 (American Petroleum Institute, 2012) | Blowout Prevention Equipment Systems for Drilling Wells |
| NORSOK 710 (CDI Energy Products, 2014) | Qualification of non-metallic materials and manufacturers – Polymers |

**Table 4. Selection of NACE standards evaluated in this study.**

| Standard Number | Standard Description |
|---|---|
| NACE TM0187 (NACE TM0187, 2001) | Evaluating Elastomeric Materials in Sour Gas Environments |
| NACE TM0296 (NACE TM0296, 2014) | Evaluating Elastomeric Materials in Sour Liquid Environments |
| NACE TM0297 (NACE, 2008) | Effects of High-Temperature, High-Pressure Carbon Dioxide Decompression of Elastomeric Materials |

**Table 5. Selection of MILSPEC and Society of Automotive Engineers standards evaluated in this study.**

| Standard Number | Standard Description |
|---|---|
| MIL-G-21569 (United States Department of Defense [DoD], 1965) | Gaskets, Cylinder Liner Seal, Synthetic Rubber |
| MIL-P-25732 (United States DoD, 1980) | Packing, Preformed, Petroleum Hydraulic Fluid Resistant, Limited Service at 275°F |
| MIL-PRF-1149D (United States DoD, 1998) | Gasket Materials, Synthetic Rubber, 50 and 65 Durometer Hardness |
| SAE/ARP 5316C (SAE Aerospace, 2010) | Storage of Elastomer Seals and Seal Assemblies Which Include an Elastomer Element Prior to Hardware Assembly |

These industry standards provide guidelines for elastomer selection (including critical material properties: acceptable hardness ranges, tensile strength ranges, and volume swell parameters), elastomer qualification testing for specific equipment, requirements for shipment and storage/shelf life of elastomers, and laboratory testing procedures to evaluate elastomer properties and failure characteristics. To ensure an accurate depiction of the current status of HPHT elastomer standards, Battelle reached out to industry stakeholders (see Section 5.2.2) to solicit feedback on ways in which current industry standards could be improved to better reflect the requirements of the current HPHT elastomer applications.

After reviewing applicable material industry standards, material characterization testing under elevated temperature conditions was conducted to gather critical material property information for inputs into the FEA model. Testing was conducted by both Battelle and Battelle's subcontractor, Endurica, on NBR, HNBR, FKM, FEPM, and FFKM. Testing included traditional material tests to evaluate hyperelastic[2] material behaviors for use in FEA model development (see Section 7.0 of this report). The following hyperelastic material tests were conducted for each of the five elastomers evaluated as part of this study:

- Quasi-static Cyclic Simple Tension
- Quasi-static Cyclic Planar Tension
- Quasi-static Cyclic Equibiaxial Tension

[2] An ideal, elastic material model for which the stress-strain relation is provided from a strain energy density function.

- Volumetric Compression
- Thermal Expansion
- Tearing Energy
- Creep Crack Growth Rate

The material property data collected were used to construct the FEA model of a 1-inch O-ring subjected to HPHT conditions in a test cell designed to produce replicable failures of O-rings. The computer aided design (CAD) drawing file of the test cell for HPHT testing was used to generate the initial model geometry, and actual measurements were used to update design measurements of the test cell. A mesh optimization study was conducted to determine the optimal mesh number which balanced model fidelity with computational resources. The primary model output of interest was the Tresca stress, defined as one half the differences between the maximum and minimum principle stresses. This model was used to predict the onset of failure (or tearing) of the O-ring, which would then be compared to HPHT test data. The onset of failure predicted from the FEA model, defined as the pressure at which the Tresca stress calculated in the model, exceeded that of the critical tearing pressure (CTP) of the material.

The resulting FEA model was validated using data collected as part of HPHT testing conducted under controlled conditions in a custom test fixture (Section 8.0). Stepped-scan testing and dwell testing were used to measure the CTP. Each elastomer was tested at two temperatures based on their maximum recommended service temperature. The test results quantified the experimental critical tearing pressure (E-CTP) as well as the first large extrusion pressure for each elastomer. The E-CTP is defined as the pressure at which the first signs of extrusion (or failure) were observed on the O-ring. The E-CTPs for each elastomer were plotted (see Section 8.7) to allow relative comparison of the elastomers. The plots provide perspective on where different elastomers may be used depending on temperature, pressure, and clearance gap. The FEA model predicted material failure points (M-CTPs) and was compared against E-CTP data collected in the laboratory experiments.

# 4.0 ELASTOMER PROPERTIES

## 4.1 Use Conditions of High Pressure, High Temperature Oil and Gas Devices

### *4.1.1 Temperatures and Pressures*

Prior to analyzing the different elastomers used in offshore HPHT environments, typical use conditions for these devices must be specified. API 17TR8 (High-pressure High-temperature Design Guidelines, as published February 2015) defines HPHT as any pressure greater than 15,000 psi and any temperature greater than 350°F. However, descriptions of HPHT conditions and the associated interrelationship between temperature and pressure vary from operator to operator. For example, Schlumberger identifies HPHT as any pressure greater than 10,000 psi and any temperature greater than 300°F (Figure 2) (High-Pressure, High-Temperature Technologies, 2008). The Bureau of Safety and Environmental Enforcement (BSEE) has sponsored standards workshops and projects (SPE-174995-MS, ANL) to refine API 17TR8 (API Standards 17 Workshop, January 11, 2017). Other organizations have differing definitions; therefore, for the purposes of this project, Battelle used the API 17TR8 definition of an HPHT environment.

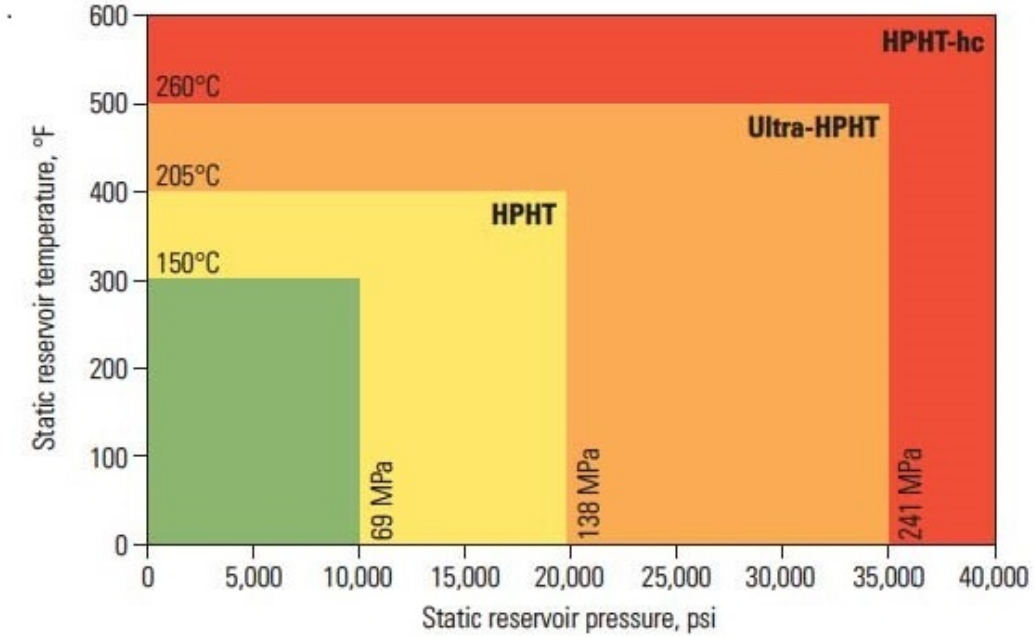


**Figure 2. Schlumberger's HPHT classification system showing common well service tool components, elastomeric seals and electronic device boundaries (High-Pressure, High-Temperature Technologies, 2008).**

### *4.1.2 Gaseous and Liquid Hydrocarbons*

Under standard temperature and pressure conditions, hydrocarbons exist as either gases (low molecular weight, volatile species), or as liquids or solids (higher molecular weight, less volatile species). Under HPHT conditions, the fraction of liquid compared to gas may increase, depending on the specific temperature and pressure of the reservoir. Natural gas reservoirs can be considered "sweet" or "sour" depending on the content of hydrogen sulfide ($H_2S$) in the gas. The Schlumberger Oilfield glossary defines "sweet" gas as: "Natural gas that does not contain hydrogen sulfide [$H_2S$] or significant quantities of carbon dioxide [$CO_2$]", and "sour" gas as: A gas containing hydrogen sulfide, carbon dioxide or mercaptans, all of which are extremely harmful". Gas containing greater than 5.7 milligrams of $H_2S$ per standard cubic meter of natural gas, which is equivalent to approximately 4 parts per million by volume under standard temperature and pressure, is considered sour (Environmental Protection Agency, n.d.). Sour gas can also contain carbon dioxide ($CO_2$), water or organic acids that can naturally exist in these reservoirs. These components can combine to create a corrosive environment for both metals and elastomers (Hertz, 1996). Elastomers affected by sour gas may experience increased hardness and cracking. Additionally, elastomers placed in HPHT environments of liquid/gas mixtures are susceptible to explosive decompression failures if they are rapidly exposed to atmospheric pressure.

### *4.1.3 Corrosion Inhibitors, Solvents, and Other Additives*

To enhance drilling or production operations, additives are frequently introduced in the downhole environment at various times throughout a well's lifetime. Due to the corrosive nature of downhole environments, corrosion inhibitors are often added to the drilling mud to protect critical equipment by slowing the corrosion process. Corrosion inhibitors can either be water or hydrocarbon soluble, based on the carrier fluid used to deliver them downhole (NACE International, 2002). Because of the delivery methods used to place corrosion inhibitors downhole, elastomeric compounds are frequently in contact with the corrosion inhibitor. Elastomer seals in the wellhead and SSSV are of primary concern for exposure, as packers are typically not yet installed when corrosion inhibitors are introduced. The Schlumberger Oilfield Glossary define packer fluid as: "The fluid that remains in the tubing-casing annulus above the packer after the completion has been run and all circulation devices have been isolated". Packers need to withstand any corrosion inhibitors that may be blended with the packer fluid to balance downhole pressures after the packer is installed (NACE International, 2002). Each elastomer type will interact with corrosion inhibitors in different ways; an overview about elastomer-corrosion inhibitor interaction is provided in Section 4.2.6.

In addition to corrosion inhibitors, solvents, surfactants, and additives may be introduced to the formation to enhance production. These well stimulation fluids include fracturing fluids, acidification chemicals, and solvents. Fracturing fluids typically contain a blend of several different chemicals to achieve the proper physical and chemical properties for each fracturing job. In general, fracturing fluids are neutral to slightly caustic in pH, and contain high levels of total dissolved solids. Elastomer applications in contact with fracturing fluids include downhole equipment such as SSSVs and packers.

Additional well stimulation fluids can contain solvents or acids that increase production from the well. Various solvents can be used in dewaxing procedures to clean the wellbore, and each elastomer

interacts differently with different types of solvents (Tukenov). Examples of this are presented in Table 6. Additionally, strong acids can be used to increase porosity, including mixtures of hydrochloric acid (HCl) and hydrofluoric acid (HF). Strong acids can affect elastomeric properties, and may cause swelling or changes in hardness (Hertz, 1996).

## 4.2 Types of Elastomers and Composites Used in HPHT O&G Applications

Five different types of elastomer (rubber) materials (ASTM D1418-2017; Standard Practice for Rubber and Rubber Latices—Nomenclature) were evaluated as part of this project: NBR, HNBR, FKM, FEPM, and FFKM. While each of the elastomers studied have known applications in downhole tools such as packers, the ultimate selection of material for HPHT service is dependent on specific exposure conditions for the equipment, with each elastomer tolerant of different temperature ranges and chemical exposures. Moldability of the elastomer is also a factor for parts that require more complex shapes. As a general rule, fluoroelastomers and perfluoroelastomers (FKM, FEPM, and FFKM) are more expensive and demonstrate greater chemical resistance and higher operating temperatures, but struggle at lower temperatures and with certain chemicals. Certain formulations of fluoroelastomers address these shortcomings and are described further below. NBR has good mechanical properties and is less expensive than fluoroelastomers, but has lower temperature and chemical tolerance. Hydrogenating NBR rubber used to prepare HNBR improves its temperature and some chemical resistance, but also adds cost. Temperature and pressure resistance of the elastomers depends on the design of the final part as well as the degree to which its physical properties are affected by temperature and chemical environments.

All elastomers consist of a crosslinked network of polymers, with mechanical and chemical properties that are a function of the type of monomer, molecular weight, number, and type of crosslinks. Many elastomers are co-polymers, a combination of two different monomers, or terpolymers composed of three monomers, where the addition of different monomers improves the final elastomer properties, such as hardness, thermal, or chemical durability, among others. Even within families of elastomers there will be different formulations from different manufacturers where the molecular weight, degree of crosslinking, and ratio of monomers change the chemical and mechanical properties of the elastomer. These formulations are frequently tailored to lend resistance to a particular chemical, improve high or low temperature properties, or change the mechanical properties. Besides the elastomer formulation, fillers such as carbon black or precipitated calcium carbonate can be added to improve mechanical or chemical properties. Other additives can be added to improve curing or mold release behavior, including silicone or polytetrafluoroethylene telomer emulsions. Because of the variability from manufacturers and compounders, this review will address each family in general terms. Although specific properties will be reported from various vendors, any reported properties should be taken as representative and not specific to the family. The design and selection of the particular elastomer (rubber compound, formulation) for an application should be confirmed with the individual vendor.

Table 6 provides characteristic properties for the five elastomer families considered for this project, as reported by the manufacturers.

**Table 6. General properties of NBR, HNBR, FKM, FEPM and FFKM elastomers.**

| | FKM | FEPM | FFKM | NBR | HNBR |
|---|---|---|---|---|---|
| **High Temperature Limit** | 204°C [1] (400°F) (continuous) 250°C [7] (482°F) (intermittent) | 230°C [2] (446°F) 260°C [7] (500°F) (in steam) | 327°C [3] (621°F) 220°C to 316°C [4] (428°F to 601°F) | 100°C [7] (248°F) (continuous) 130°C [7] (266°F) (intermittent) | 150°C [7] (302°F) (continuous) 180°C [7] (356°F) (intermittent) |
| **Low Temperature Limit** | -30 to -8°C[1] (-22 to 18°F) | -12[1] to -3°C[6] (10 to 27°F) | -5°C [5] (23°F) | -50 to -5°C[7] (-58 to 23°F) | -30°C[7] (-22°F) |
| **Chemicals Suitable for Sealing with the Material** | Hydrocarbon fuels, oil, aliphatic and aromatic chemicals.[1] | Strong acids and bases, steam, light oxygenates (MeOH) and amines.[2] | Fuels, oils, solvents, alcohols, ketones, mineral acids and bases.[3] | Aliphatic oils and fuels, lower alcohols.[7] | Aliphatic oils and fuels, lower alcohols.[7] |
| **Chemicals Incompatible with the Sealing Material Applications** | High pH caustic and amines, low molecular weight carbonyls. Some concerns with light oxygenates (MeOH), steam and mineral acids.[1] | Esters and ketones, light oils, gasoline, chlorinated and hydrocarbon solvents.[2] | Some concern with hot water and amines.[4] | Aromatic hydrocarbons, ketones, acids and bases, ketones.[3] UV and weathering, ethers, aldehydes, chlorinated solvents, phosphate esters.[7] | Aromatic hydrocarbons, ethers, ketones, phosphate esters.[7] |
| **Compression Set** | 12 to 40%[1] | 35[6] to 40%[7] | 14 to 29%[4] | 2 to 20%[8] | 20%[9] |

Note that due to the different temperature range of applications for the elastomers, the compression set values are at different times and temperatures; see the references for specific test conditions.

[1] DuPont FKM Selection Guide. Compression Set is a 70 hr. /200°C (392°F) test. Low temperature limit is the temperature of retraction 10% result. High temperature limit is for continued exposure.

[2]FEPM Fluoroelastomers Guide.

[3]Dupont FFKM Parts Chemical Resistance

[4]3M Dyneon Fluoroelastomers Product Comparison Guide. Compression Set is a 70 hr/200°C (392°F) test.

[5]Dupont FFKM Spectrum 7090 Technical Information

[6]FEPM 100-150 Series Standard Grade, Commercial Polymer Types and Physical Properties. Compression Set is a 70 hr/200°C (392°F) test. Low temperature service is the glass transition point.

[7]James Walker Elastomer Engineering Guide.

[8]Parco Nitrile Selection Guide. Compression set is at 22 hrs. and 100°C (212°F).

[9]Lanxess Therban Technical Information. Compression set is at 70hr and 150°C (302°F).

An additional concern for elastomers in HPHT O&G applications is being exposed to $CO_2$ and $H_2S$ gases. The critical temperatures and pressures for $CO_2$ and $H_2S$ are 31°C, 73.8 bar (88°F, 1,070 psi), and 100°C, 89.7 bar (212°F, 1,300 psi), which can both be exceeded in downhole conditions (National Institute of Standards and Technology, 2011). Supercritical fluids are exceptionally good solvents and can be exacerbated when $H_2S$ and $CO_2$ are both present in sour wells since it creates a mixed solvent system. This can cause leaching of seal materials, swelling of seals or explosive decompression, where gases such as $CO_2$, $H_2S$, or hydrocarbons migrate into the elastomer at high pressures, then expand and destroy the part when pressure is released too quickly (Hertz, 1996). In addition, as the downhole temperature increases, the degree of swelling and the permeation rate into and out of the seal are higher.

### *4.2.1 FKM Class Elastomers (ASTM D1418-17, Class M)*

FKM is a classification of fluoroelastomers in ASTM D1418-17 (Standard Practice for Rubber and Rubber Latices—Nomenclature). FKM elastomers are typically copolymers containing vinylidene fluoride (VDF, $CF_2=CH_2$) and hexafluoropropylene (HFP, $CF_3$-$CF=CF_2$), where VDF provides methylene group (-$CH_2$-) cure sites and the HFP adds bulky side chains to allow flexibility within the backbone by preventing crystallinity. Terpolymers also exist where a tetrafluoroethylene (TFE, $CF_2=CF_2$) monomer is added to increase the fluorine content; this improves chemical stability but tends to decrease performance at low temperatures. Substitution of fluorinated vinyl ethers, such as perfluoromethyl vinyl ether, for the HFP in the terpolymer improves the low temperature performance.

Typically, fluoroelastomers contain a cure site monomer (CSM), which is added in small amounts to the polymer to enable crosslinking during curing. The cure systems used in crosslinking fluoroelastomers are generally diamine, bisphenol or peroxide systems, with each adding certain properties to the final product. The diamine system was the first system used. However, in comparison to bisphenol and peroxide systems it cures more slowly, has more mold release problems, poorer compression set resistance, poorer steam, water and acid resistance, and poorer high temperature resistance. The diamine system does enable better adhesion to metal inserts in the part, but its drawbacks limit its importance in current FKM systems. The bisphenol cure system has largely replaced the diamine system and provides better performance in nearly all categories previously listed for the diamine process. However, the phenols include unsaturated bonds in the final rubber, which are susceptible to chemical attack. Additionally, bisphenol cures are generally not compatible with the inclusion of vinyl ether monomers due to degradation of the ether. Peroxide cure systems use an organic peroxide to form crosslinks from free-radical susceptible CSMs, which commonly contain bromine or iodine atoms. Peroxide systems generally have better resistance to aqueous environments including steam, high temperature water, and mineral acids than bisphenol or diamine cured systems.

FKM fluoroelastomers generally demonstrate good chemical resistance, but with notable exceptions for mineral acids and bases and low molecular weight carbonyls such as ketones. Mineral acids attack primarily amine and phenol crosslinked systems; however, its acid resistance is greatly improved with peroxide cure systems. Fluoroelastomers containing VDF and

HFP are susceptible to dehydrofluorination reactions at the VDF/HFP sequence from bases such as hydroxides and amines, leaving a carbon-carbon unsaturated double bond. This is necessary for crosslinking reactions but can also cause the seal to lose elasticity and fail. Additionally, acetone and other low molecular weight carbonyls cause excessive swelling in FKM fluoroelastomers.

Table 7 summarizes relative properties of the common fluoroelastomer compositions and curing systems.

**Table 7. Relative properties of fluoroelastomer polymer compositions and cure systems.**

| Type | General Characteristic Properties |
|---|---|
| ***Polymers*** | |
| VDF (vinylidene fluoride) + HFP (hexafluoropropylene) copolymer | Good compression set resistance, high temperature performance, and chemical resistance to fuels and oils. But susceptible to attack by oxygenated automotive fuels, acids and bases and light carbonyls. |
| VDF + HFP + TFE (tetrafluoroethylene) terpolymer | As above, with generally higher chemical resistance to oxygenated fuel and acids. But less compression set resistance and low temperature performance. |
| VDF + TFE + PMVE (perfluoromethyl vinyl ether) terpolymer | Similar to VDF + HFP + TFE, but with better low temperature performance and susceptible to oxygenated fuels. |
| ***Crosslinking (Curing) Systems*** | |
| Diamine | Very good adhesion to metal parts, but comparatively poor mold release, compression set resistance and steam, water and acid resistance. |
| Bisphenol | Very good compression set resistance and improved mold release, cure rate and steam, water and acid resistance. |
| Peroxide | As bisphenol, but with better steam, water and acid resistance. |

### *4.2.2 FEPM Class Elastomers (ASTM D1418-17, Class M)*

FEPM is a classification of fluoroelastomers in ASTM D1418-17 (Standard Practice for Rubber and Rubber Latices—Nomenclature) developed to provide better base resistance than FKM types. This base resistance generally comes at the expense of low temperature performance, and

less fuel and oil resistance than FKM fluoroelastomers. The base resistance is improved by eliminating the VDF/HFP sites, which are base active, and replacing them with TFE monomers.

Two common FEPM formulations are an alternating copolymer of TFE and propylene ($CH_2$=CH-$CH_3$), and a terpolymer of ethylene (E, $CH_2$=$CH_2$), TFE (T), and perfluoromethyl (P) vinyl ether ($CF_2$=CF-O-$CF_3$) (or ETP). Common trade names are Alfas® and Viton® Extreme™ ETP-S, respectively. Aflas® was developed to provide improved resistance to strong bases, amines, and steam treatment compared to conventional FKM, but has lower chemical resistance to aliphatic and aromatic hydrocarbons (AFLAS Fluoroelastomers, 2015). Viton® Extreme™ ETP-S was developed to regain the lower temperature flexibility and resistance to light oils, gasoline, and light carbonyls such as acetone (DuPont, 2010). FEPM fluoroelastomers still contain hydrogen atoms in the backbone, making them more susceptible to degradation than perfluorinated compounds.

### *4.2.3 Perfluorinated Elastomers: FKM, FFKM (ASTM D1418-17 Class M)*

Perfluorinated elastomer is a classification of fluoroelastomers in ASTM D1418-17 (Standard Practice for Rubber and Rubber Latices—Nomenclature). FFKM currently provide the highest chemical and temperature resistance of elastomer materials, but are also more expensive than FEPM and FKM elastomers. The backbone of FFKM materials is completely fluorinated, eliminating hydrogen atoms such as in FKM and FEPM. This is commonly accomplished using TFE and perfluoromethyl vinyl ether (PMVE) copolymers, with incorporation of a small amount of CSM to enable crosslinking. Common tradenames for FFKM are Kalrez®, Tecnoflon® and Chemraz®. Specific products vary in the ratio of monomers, specific vinyl ether monomer used, and crosslinking system.

The crosslinking or curing system for FFKM materials impacts the final temperature and chemical resistance properties. Four common linkages are employed: peroxide cures, bisphenol cures, triazine cures, and less commonly irradiation cures. Peroxide and bisphenol cures are done similarly as described in Section 4.1. Triazine cures utilize a pendant nitrile group in one of the monomers to form a triazine ring crosslink when three nitrile groups come together. Irradiation cures use high energy radiation such as electron beams or gamma rays to affect crosslinking, which appears to be by generation of carbon-carbon bonds. Peroxide cure systems generally present the best chemical resistance properties and good high temperature performance. Bisphenol systems, as in FKMs, are less suited to acid and hot water/steam applications, but are applicable to temperatures higher than peroxide cure systems. Triazine systems are exceptional in thermal performance, able to maintain integrity under continuous use in applications up to 300°C (572°F) (Moore, 2006). However, they exhibit poor chemical resistance to hot water/steam and bases/amines due to vulnerability of the triazine linkages. Irradiation cured FFKM is primarily used in the semiconductor industry, as the final product contains very few added chemicals and no fillers that could leach into process fluids. Table 8 contains general properties for FFKM crosslinked by bisphenol, peroxides and triazine methods. Note that these properties are not for any particular product; some product formulations may perform better or worse than listed in Table 8.

**Table 8. General properties for FFKM crosslink systems.**

| | Bisphenol Cure | Peroxide Cure | Triazine Cure |
|---|---|---|---|
| **Approximate high temperature limit** | 275°C[1] (527°F) | 230°C[1] (446°F) | 315°C[1](599°F) |
| **Chemicals compatible with these materials** | Organic solvents, ketones, aldehydes, ethylenediamine.[2] | Organic solvents, ketones, aldehydes.[2] Steam, acid, bases and hot water.[1] | Organic solvents, ketones, aldehydes.[2] Acids.[3] |
| **Chemical Incompatibilities** | Acids, less effective than peroxide cure for steam, hot water, alkali and amines.[3] | Less effective in acids than triazine cure.[3] | Alkali, amines and hot water/steam.[3] |

[1]Ed Cole, "An Introduction to Perfluoroelastomers", *Rubber World*, 2013.
[2] Anestis Logothetis, "Perfluoroelastomers and Their Functionalization", 1997.
[3]Precix P03 FFKM data sheet.

### *4.2.4 Acrylonitrile Butadiene Nitrile Rubber (ASTM D1418-17 Class R)*

Nitrile rubber is a classification of elastomers in ASTM D1418-17 (Standard Practice for Rubber and Rubber Latices—Nomenclature). Nitrile rubber, also known as NBR or Buna-N, is a copolymer of acrylonitrile and butadiene. Butadiene provides the elastomer with a necessary crosslinking site, as well as elasticity and flexibility. Acrylonitrile adds oil and fuel resistance as well as strength. Increasing the acrylonitrile content generally will improve oil and fuel resistance, tensile strength, and abrasion resistance, but also decrease compression set resistance and low temperature performance. Inclusion of a carboxylated terpolymer improves the rubber's tensile strength, modulus and abrasion resistance, but also negatively impacts compression set, water resistance, and low temperature performance.

NBR is generally resistant to aliphatic oils and fuels, aqueous salts, and alcohols, but should not be used with steam, acids, oxidizers, aromatics, chlorinated solvents, ethers, light carbonyls, hydrogen sulfide (which attacks carbon-to-carbon double bonds), and amines. Sulfur crosslinking and peroxide crosslinking are the two common cure systems, with peroxide systems improving physical and thermal properties as well as chemical resistance. NBR is susceptible to weathering by ultraviolet light or other oxidizers due to the double bonds present in the butadiene portions of the polymer backbone. The maximum continuous operating temperature range of NBR is limited to approximately 125°C (257°F).

### *4.2.5 Hydrogenated Acrylonitrile Butadiene Nitrile Rubber (ASTM D1418-17 Class R)*

HNBR is a classification of elastomers in ASTM D1418-17 (Standard Practice for Rubber and Rubber Latices—Nomenclature). HNBR was developed to improve the cost and performance gap between NBR and FKM elastomers for resistance to oil. HNBR is made by dissolving the acrylonitrile-butadiene polymer, then treating with hydrogen gas and a catalyst to saturate, the addition of hydrogen to the carbon-to-carbon double bonds. HBNR's properties are dependent on

the acrylonitrile to butadiene ratio and cure system as in NBR and described in Section 4.2.4. However, the properties of crosslinked HNBR depend on the balance between the amount of remaining butadiene unsaturation, which is needed for sulfur cure (vulcanization), and the low temperature performance which is better with more saturated polymer (fewer double bonds). HBNR trade names are Zetpol® and Therban® from Zeon Corporation and Lanxess, respectively.

Tensile strength, abrasion resistance, and thermal properties of HNBR generally exceed those of NBR and FKM. Also, chemical resistance is improved with good performance in acids, bases, and amines, and improved performance against weathering, oxidizers, and steam. HNBR is not suitable for exposure to light carbonyls or ethers, and the acrylonitrile group can be attacked by hydrogen sulfide at high temperatures. The elimination of residual unsaturation in the polymer backbone by hydrogenation increases the use temperature of HNBR by 50°C compared to NBR.

### *4.2.6 Elastomer Property Performance under Oil and Gas Well Conditions*

Elastomer materials can be affected by many conditions experienced in exploration and production. High temperatures can cause additional excess crosslinking of the elastomer if the cure system is not fully consumed or deactivated in treatment of the part. Other thermal degradation effects include decomposition of chemical moieties (functional groups) within the polymer or reaction of fillers and other additives. Elevated temperature will also increase the rate at which any possible reactions occur. Typically, thermal degradation will cause hardening of the elastomer, which reduces seal strength. One example of thermal degradation is the reaction of FKM elastomers cured with calcium or magnesium salts, where water at 150°C (302°F) will cause delayed decomposition (MERL Ltd, 2005). High temperature will affect the physical properties of elastomers, potentially causing excessive swelling or reduced strength within the seal.

Oilfield elastomers may also experience very low temperatures due to the adiabatic effect from gas expansion and low temperature subsea conditions. When elastomers drop below their glass transition temperature, they can become brittle and potentially fail, especially in dynamic sealing applications.

As described previously, certain chemicals can degrade elastomers by reacting with their constituents. For example, strong bases and amines will dehydrofluorinate FKMs that incorporate vinylidene fluoride and hexafluoropropylene. Acids can attack bisphenol crosslinks (Ameduri, Boutevin, & Kostov, 2001). Bases and hot water will attack triazine crosslinks in FFKMs (Cole, 2015). In addition, oxidizers will attack double bonds in NBR and HNBR seals (Cheremisinoff & Cheremisinoff, 1993). Typically, this degradation results in embrittlement of the seal and potential seal failure.

Explosive decompression, also called rapid gas decompression (RGD), occurs when liquified (supercritical fluid) gases migrate into a seal at high pressures. If pressure is released too quickly, a strong pressure gradient is created between the gas formed inside the seal and outside the seal. If the gas cannot permeate out of the seal quickly enough, bubbles may form inside the seal material, causing irreversible seal damage and potential failure. One procedure to mitigate this

issue is to apply low decompression rates. RGD is heavily dependent upon a balance between the concentration of liquified gas inside the elastomer and how readily it can permeate out of the seal. Good barrier polymer properties will reduce the level of swelling, but inhibit the corresponding release rate when the pressure is reduced. Therefore, conducting seal material testing with a realistic service gas under HPHT conditions (e.g., NORSOK M-710 [Qualification of non-metallic sealing materials and manufactures] or NACE TM-0187 [Standard Test Method - Evaluating Elastomeric Materials in Sour Gas Environments]) is the best way to select a seal material.

When rubber seals come in contact with fluids of similar chemical properties, the fluid can enter into the polymer network, expanding it and causing swelling. This swelling can generally be reduced via removal of the fluid solvent. Physical properties of the part are generally diminished in a swelled state, and if swelling is too extreme, the seal can be extruded and/or cause undue stresses in the seal housing.

For example, a polar liquid could be expected to swell a polymer composed of polar components in its polymer chain. The Hildebrand solubility parameter, commonly represented as 'δ', is related to the strength of secondary bonds (such as dipole-dipole interactions between molecules), and provides a simple, qualitative assessment of whether a liquid will swell a polymer. When the Hildebrand solubility parameter of the polymer is close to the Hildebrand solubility parameter of the fluid, the two are chemically similar and swelling is more likely to occur. Hildebrand solubility parameters for some relevant polymers and solvents have been calculated by group-contribution methods by MERL Ltd. (now Element Materials Technology, Ltd.) and are available in a report for the U.K. Health and Safety Executive; guidance to this report can be found in the references section (MERL Ltd, 2005). Additionally, Sambasiva Allada preformed research and correlated a generalized solubility parameter for non-polar gases in the supercritical regime that can be used to understand how some supercritical gases interact with elastomers (Allada, 1984).

A drawback to Hildebrand solubility parameters is that they are for ideal mixtures, but do not account well for polar liquids and polar polymers, as the fundamental Hildebrand equation does not include terms for these interactive forces.

Hansen three-dimensional solubility parameters account for this by incorporation of factors for non-polar dispersive interactions (represented as $\delta_d$), polar interactions ($\delta_p$), and hydrogen bonding interactions ($\delta_h$), with a total parameter determined according to Equation 1 (Rodriguez, Cohen, Ober, & Archer, 2003). Polymers exposed to liquids with similar values for their $\delta_d$, $\delta_p$, and $\delta_h$ terms are more likely to experience polymer swelling.

$$\delta_{total}{}^2 = \delta_d{}^2 + \delta_p{}^2 + \delta_h{}^2 \qquad \text{Equation 1}$$

For example, both NBR and HNBR are not useful as seals against carbonyl containing solvents e.g. acetone, methylethylketone (MEK) or ether-like solvents because of the very high solubility of the polar acrylonitrile component of NBR and HNBR in the polar ketone and ether component solvents. The degree of swelling of HNBR and NBR in these polar solvents can be estimated by the similarity between the polymer and solvent Hansen Solubility Parameters as shown in Table 9.

The results show that butyl rubber absorbs much lower levels of these polar solvents compared to NBR and that solvents that have matching Hansen solubility parameters swell NBR to a much higher degree than those that only have similar γT (which is equivalent to the Hildebrand solubility parameter).

Table 10 provides the relative elastomer compatibility for a range of common conditions experienced in O&G applications. The specific vendor formulation, cure and compounding will affect the performance of the rubber in these conditions. Therefore, testing should be performed to ensure the integrity of the elastomer part in the expected conditions.

**Table 9. Hansen Solubility Parameters and Solvent Swelling of Elastomers (Hansen, 2007)**

| Material | $\gamma_D$ ($Mpa^{0.5}$) | $\gamma_P$ ($Mpa^{0.5}$) | $\gamma_H$ ($Mpa^{0.5}$) | $\gamma_T$ ($Mpa^{0.5}$) | Butyl Rubber (wt.% gain) | Nitrile Rubber (wt. % gain) |
|---|---|---|---|---|---|---|
| Elastomer | | | | | | |
| Butyl Rubber (BR) | 16.0 | 2.3 | 3.3 | 16.5 | | |
| Nitrile Rubber (NBR) | 19.0 | 9.2 | 4.1 | 21.5 | | |
| Solvent | | | | | | |
| 2-Butoxyethanol | 16.0 | 5.1 | 12.3 | 20.8 | 6.2 ± 14.3 | 47 ± 0.4 |
| 2-Ethoxyethanol | 16.2 | 9.2 | 14.3 | 23.5 | 2.3 ± 5.4 | 64 ± 0.1 |
| 2-Methoxyethanol | 16.2 | 9.2 | 16.4 | 24.8 | 1.5 ± 10.4 | 90 ± 4.7 |
| Diethyl carbonate | 16.6 | 3.1 | 6.1 | 18.0 | 15.0 ± 0.1 | 106 ± 1.2 |
| 2-(2-Methoxyethoxy) ethanol | 16.2 | 7.8 | 12.6 | 22.0 | 1.8 ± 2.0 | 119 ± 3.7 |
| Ethyl acetate | 15.8 | 5.3 | 7.2 | 18.2 | 15 ± 1.5 | 133 ± 7.7 |
| Methyl acetate | 15.5 | 7.2 | 7.6 | 18.7 | 9.2 ± 0.2 | 141 ± 4.1 |
| Acetone | 15.5 | 10.4 | 7.0 | 19.9 | 5.1 ± 2.9 | 163 ± 0.3 |
| Methyl ethyl ketone | 16.0 | 9.0 | 5.1 | 19.1 | 11 ± 0.4 | 247 ± 5.9 |
| 3-Pentanone | 15.8 | 7.6 | 4.7 | 18.2 | 22 ± 1.4 | 251 ± 3.4 |
| Dioxane | 19.0 | 1.8 | 7.4 | 20.5 | 19 ± 0.2 | 263 ± 1.8 |
| Ethyl formate | 15.5 | 8.4 | 8.4 | 19.5 | 9.7 ± 7.7 | 288 ± 5.0 |
| 2-Pyrrolidone | 19.4 | 17.4 | 11.3 | 28.4 | 5.2 ± 9.8 | 304 ± 4.3 |
| Tetrahydrofuran | 16.8 | 5.7 | 8.0 | 19.5 | 179 ± 6.7 | 352 ± 0.4 |
| Dimethylformamide | 17.4 | 13.7 | 11.3 | 24.9 | 2.8 ±13.6 | 428 ± 2.8 |
| Furfural | 18.6 | 14.9 | 5.1 | 24.4 | 4.5 ± 4.3 | 458 ± 8.2 |
| Cyclohexanone | 17.8 | 6.3 | 5.1 | 19.6 | 28 ± 1.7 | 508 ± 0.7 |
| N,N-Dimethylacetamide | 16.8 | 11.5 | 10.2 | 22.8 | 4.9 ± 6.0 | 548 ± 1.6 |
| *N*- Methy1-2-pyrrolidone | 18.0 | 12.3 | 7.2 | 23.0 | 6.7 ± 22.5 | 798 ± 1.0 |

**Table 10. Relative elastomer compatibility for a range of common oilfield conditions.**

| Condition | More Suitable Elastomers | Less Suitable Elastomers |
|---|---|---|
| **Temperature above 280°C (536°F)** | FFKM<br>triazine cure | FKM, FEPM<br>FFKM bisphenol and peroxide cures |
| **Temperature above 200°C (392°F)** | FFKM | FKM, FEPM |
| **Temperature above 150°C (302°F)** | FKM, FEPM, FFKM | HNBR |
| **Temperature above 100°C (212°F)** | HNBR, FKM, FEPM, FFKM | NBR |
| **High pH Corrosion Inhibitors** | FEPM<br>FFKM<br>peroxide cure | FKM, NBR |
| **Acid Treatments** | FEPM<br>FKM<br>peroxide cure<br>FFKM<br>triazine and peroxide cures<br>HNBR | NBR<br>FKM<br>bisphenol cure |
| **Sour Gas Conditions** | FEPM, FFKM | NBR, HNBR<br>FKM<br>bisphenol cure |
| **Aromatic Solvents** | FKM, FEPM, FFKM | NBR, HNBR |
| **Light Carbonyl Solvents (Acetone, MEK, etc.)** | FKM<br>terpolymers with higher fluorine content<br>FEPM<br>TFE/E/PMVE terpolymers<br>FFKM | NBR<br>HNBR<br>FKM<br>VDF/HFP copolymers, lower fluorine contents<br>FEPM<br>TFE/P copolymers |
| **Sub-Freezing Temperatures** | NBR, HNBR<br>FKM<br>(PMVE co- and ter-polymers) | FFKM, FEPM |

## 4.3 Processing Techniques Used for Compounding and Parts Fabrication

Battelle reviewed several common processing techniques used to manufacture O-rings and seals. Strict control of polymer processing is required to achieve the desired qualities in the final product. The processing techniques evaluated included mixing, molding, and finishing processes. Mixing, or compounding processes, are used to manufacture discrete elastomers from a blend of polymers. Once an elastomer has been mixed, it is then formed into the specific end use part where crosslinking reactions fuse it into the final shape. Battelle will describe three common methods: compression molding, injection molding, and transfer molding, as well as a polishing step (cryogenic deflashing) to remove defects from the manufacturing process.

### *4.3.1 Elastomer Compounding*

Fluoroelastomers as well as NBR and HNBR can be compounded easily by conventional means, such as internal (or Banbury) mixing and open two roll water cooled rubber mill mixing. The role of mixing is to incorporate all of the ingredients into a homogeneous mixture that can be molded into parts. Insufficient mixing leads to heterogeneities of physical and chemical properties within the part (for example, crosslinking may be heavier in one portion of the part, or there may be more filler in one section). A variety of ingredients can be added to an elastomer to affect its processing and final physical and chemical characteristics. Some general classes of elastomer ingredients include (James Walker, 2012):

- **Fillers**, such as carbon black and clays, can be reinforcing if small enough, or simply diluting such as talc. As a rule, smaller particle sizes increase physical properties since their higher surface energy allows adhesion to the polymer. Fillers can chemically affect how the part cures.

- **Accelerators**, which speed up the curing process. When peroxide curing, a coagent is often used to improve effectiveness by selecting for favorable reactions, and in many formulations more than one accelerator is used.

- **Activators**, which initiate the curing process.

- **Curatives**, which are the active crosslinking components, and depend on the specific cure chemistry.

- **Desiccants**, such as lime, remove trace amounts of water which could impact the cure and final physical properties.

- **Flame Retardants**, are additives such as halogen-containing compounds or inorganic oxides that can be added to suppress flame generation for elastomers that will support a flame, and therefore improve fire resistance.

- **Plasticizers**, which generally reduce rubber hardness and improve molding behavior. Plasticizers can increase the low temperature performance of a rubber, but are also subject to leaching out of the part through means described in Section 4.2.6.

- **Process Aids**, which help to integrate fillers or improve molding performance (such as mold release).

- **Retarders**, which keep the compound from curing too early.

- **Coupling Agents**, which are added to allow the elastomer to bond better to filler materials or pieces within the part.

The specific ingredients and concentrations vary between compounders and products to achieve target physical and chemical properties. Because of their high fluorine content, fluoroelastomers have fewer potential additives that are compatible compared with other hydrocarbon elastomer types. For example, very few plasticizers exist for fluoroelastomers. A typical fluoroelastomer compound contains metal oxides (3-15 parts per hundred of fluoroelastomer) to capture hydrogen fluoride generated during the vulcanization process or improve metal adhesion. Calcium hydroxide and magnesium oxide are commonly used, with lower concentrations typically used in peroxide cure systems. Zinc oxide can be used to improve acid and steam resistance. Fillers (around 10-30 parts per hundred of fluoroelastomer) such as carbon black, barium sulfate, calcium carbonate or other minerals, can be added to improve hardness, compression set resistance, swelling, and tensile strength. Processing aids (0.5 to 2.0 parts per hundred of fluoroelastomer) can be added to improve mold release or extrusion, but can lower the compression set resistance. The curing agents (0.5-4.0 parts per hundred of fluoroelastomer) that are used are composed of crosslinkers and coagents (Ogunniyi, 2003).

Several types of mixers are available for compounding elastomers, but generally they can be classified as mills or internal mixers. Mills are typically open to the atmosphere and have two counter-rotating rollers that squeeze the rubber that is fed between them. An operator cuts the sheet of rubber and re-feeds them along with the ingredients to homogenize the elastomer. The rollers are often water cooled to regulate temperature. Internal mixers are isolated from the atmosphere, and ingredients are fed by a ram into two counter-rotating lobes. Mixing occurs by shearing the elastomer between the walls of the mixer and the two lobes. After mixing, the elastomer is formed into a part typically by molding, which is covered in the following sections. Gaskets can also be formed by calendaring or tubing and hose liners can be formed by extrusion.

### *4.3.2 Compression Molding*

Compression molding is a simple process where a mass of material is put into the pre-shaped mold cavity, and pressed into the final part. An excess of material is required in the pre-form to ensure good filling of the mold and overflow grooves are employed to catch it. However, too much excess can cause the final part to be out of specification as it will push on the mold plates and prevent complete closure. The mold is typically heated to start the curing process, and the

final cycle time is dictated by the cure time requirements. Figure 3 illustrates the compression molding process.

Compression molding has a low tooling cost and is typically used for low volumes of high value parts or materials. The amount of waste material is less compared to transfer molding (Section 4.3.4), but extra work is required to make pre-forms. There is risk of material contamination by the addition of the pre-form step.

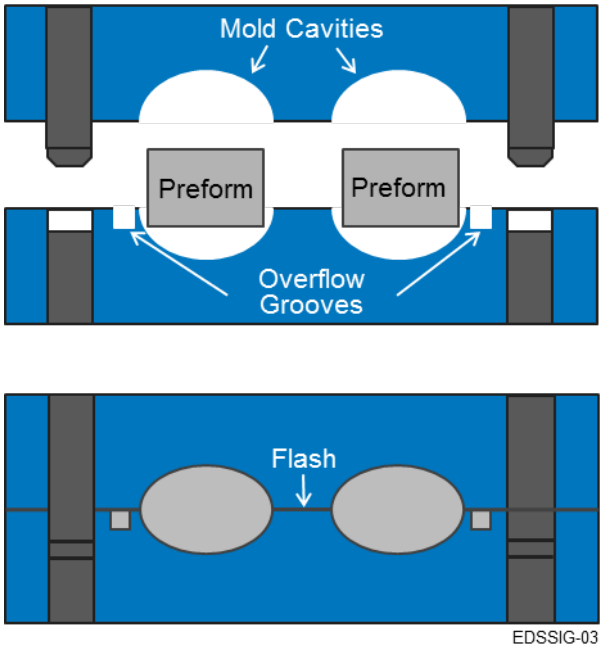


**Figure 3. Simple illustration of the compression molding process. Adapted from (Columbia Engineered Rubber, Inc., 2006 -2013).**

### *4.3.3 Injection Molding*

Injection molding of rubber begins with the feeding of strips of uncured feedstock, where it is heated and compressed into a nozzle for injection into the mold. The heating within the nozzle generally reduces viscosity and allows for the rubber to fill the entire mold. The material temperature is maintained high enough to initiate the curing process. Figure 4 provides a schematic of the injection molding process.

Injection molding is particularly suitable for making large lots with high quality reproducibility. Mold costs are much higher than compression molding, but the process also eliminates the pre-form process and preheating of material can reduce cycle times. Material losses associated with the runners, and residual material in the barrel and nozzle can be high. Since injection molding machines are typically expensive, the same machine is often used for multiple feedstocks, and

therefore contamination is a risk if the equipment is not cleaned properly between different feedstock batches.

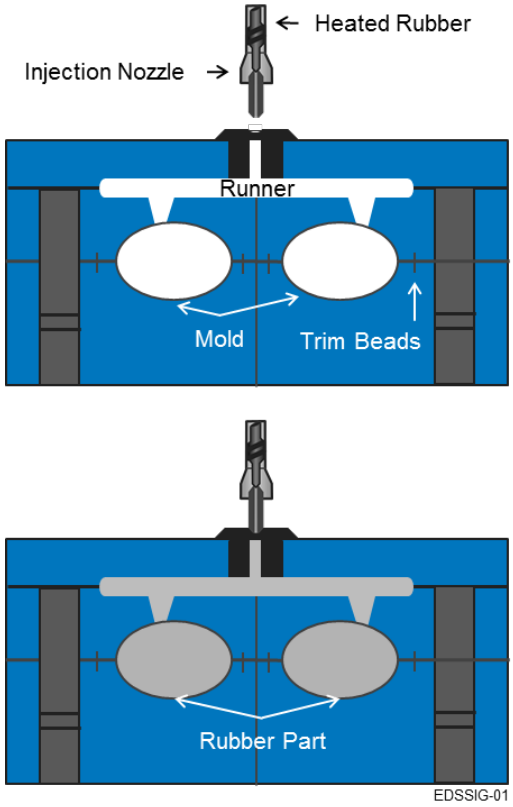


**Figure 4. Simple illustration of the injection molding process. Adapted from (Columbia Engineered Rubber, Inc., 2006 -2013).**

### *4.3.4 Transfer Molding*

Transfer molding is similar to compression molding, but has the advantage of a closed mold which allows for better replication between batches. Pre-forms are placed in a transfer pot above the mold, and a ram forces the material down into the mold. Excess material stays between the ram and transfer pot, rather than between two halves of the mold in compression molding, which generates a part with consistently higher dimensional accuracy. Figure 5 illustrates the transfer molding process.

Transfer molding costs more than compression molding because a more accurate pre-form must be created, but less than injection molding, where no pre-form is required. Transfer molding (as well as injection molding) generates higher dimensional accuracy parts than compression molding, but generally uses more material.

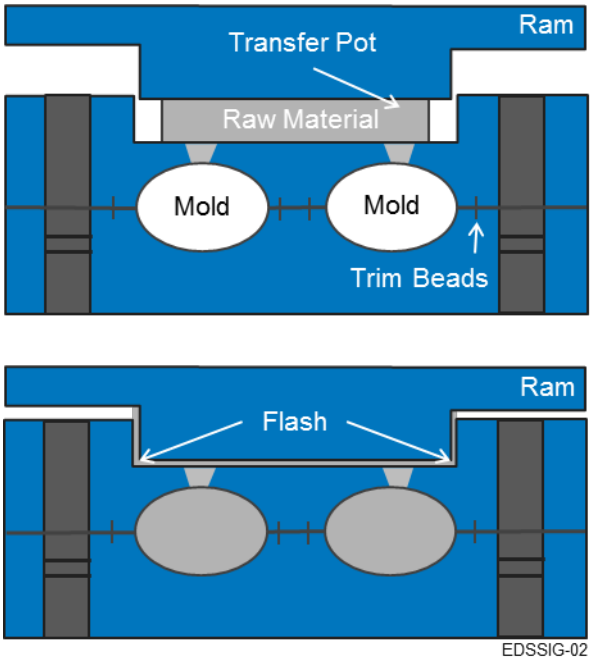


**Figure 5. Simple illustration of the transfer molding process. Adapted from (Columbia Engineered Rubber, Inc., 2006 -2013).**

### *4.3.5 Curing*

Curing is the process of crosslinking the rubber, and is essential for generating a part with the desired properties. Several curing systems are available for elastomers, including peroxide cures, ionic cures, and irradiation cures. For fluoroelastomers, a typical cure consists of two steps: application of heat (150-180°C, 302-356°F) and pressure (1,450 to 4,350 psi, 100 to 300 bar) within the mold until the part is strong enough to hold its shape (roughly 10-15 minutes), followed by a post cure in air and atmospheric pressure between 200-250°C (392-482°F) for 12-24 hours (Ameduri, Boutevin, & Kostov, 2001). The post cure heating process removes residual water, which drives condensation reactions, and improves physical properties particularly with bisphenol cure systems. Molds may need to be agitated by mechanical means such as vertical alignment and vibration to remove trapped gases during the primary cure and prevent void formation. Perfluoroelastomers are cured very similarly to fluoroelastomers, but can also be post cured in nitrogen rather than air to improve high temperature compression set resistance.

NBR and HNBR parts are commonly cured between 20 and 40 minutes around 125 to 200°C (257-392°F) within the mold, with a post cure of around 4 hours at 150°C (302°F) (Arkema Inc., 2009) and (Files, Jones, & Wood, 2001).

In general, when the higher range of molding temperatures (~ 200°C) are employed, shorter initial cure times can be used which reduces the cycle time. It should also be noted that when peroxide cure systems are used, oxygen can interfere with the cure, causing tackiness at the

surface of the part and degradation of properties. Finally, scorching can occur in curing when the reaction proceeds too quickly, causing a runaway exotherm within the material. Scorching can be caused by too high of a cure temperature or improper selection of curing additives.

### *4.3.6 Deflashing*

Flash (also called flashing), is the excess material attached to the part during the molding process, and must be removed from the final part to properly fit seal grooves. This removal process is called 'deflashing', and is frequently done by manual trimming, tumbling, media blasting, or cryogenic deflashing. Manual trimming can be done with any number of tools or grinders, and is typically less precise than other methods. Tumbling removes the flash by tumbling multiple parts in a bin, where contact of two parts or an added media causes the flash to be knocked from the part. Media blasting uses a media such as sand in a carrier fluid like water or air. The carrier fluid and media are flowed over the parts quickly to remove the flash. Cryogenic deflashing cools the parts, typically to below glass transition temperatures, so that the flash becomes brittle, and tumbling with or without another media or media blasting to clear the part off. For complex shapes, such as O-rings, media blasting or cryogenic processes tend to be more effective, but care should be taken to avoid damaging the part if media blasting is used.

## 4.4 Oil and Gas Equipment Incorporating Elastomer and Composite Seals

Battelle has evaluated elastomer use in four critical HPHT device applications (i.e., packers, BOPs, SSSVs, and wellheads), which were selected based on discussions with both internal and industry experts. The particular elastomeric components and end-use conditions, as well as pertinent regulations that these devices must conform to prior to use in the O&G industry are summarized below. Each of the five elastomers evaluated in this study may be used in the devices summarized below depending on anticipated operating conditions.

### *4.4.1 Packers*

One of the more common applications of elastomers in HPHT offshore operations is their use in packers. Packers are used in numerous configurations during both testing and completion activities, which can be retrievable or permanently installed in the well. HPHT offshore wells typically make use of permanent packers during the production phase due to the more extreme conditions these wells operate under. The packer's primary function is to seal off the annular space between the steel casing and a test string or production tubing, preventing fluid from reaching the surface by means of the annular space. Alternatively, packers can be used to isolate production zones within a single well. As a secondary function, packers can be used to support the tubing string. The elastomeric seal of the packer must stand up to in situ conditions including 15,000 psig and 350°F in HPHT wells, and must be compatible with the fluid used to inflate the element. Figure 6 shows a configuration of an example packer. Elastomeric-based compounds typically are used to make up the packing element.

The elastomer packing element is one of the most critical components of the packer. The packer achieves its objective of sealing the annular space by first being lowered into the well by either

the drill string or wireline, until it reaches the required depth. Once at the required depth, packers can be set either mechanically or hydraulically. Hydraulically set packers are more commonly used. When the hydraulically set packer is lowered into the well, it is automatically deployed when it experiences a certain pressure, corresponding to its target deployment depth (Bellarby, 2009). Deployment involves setting the slips against the casing, as well as inflation of the packing element. The packing element may be inflated with drilling fluid, or in permanent applications, cement. Alternatively, the elastomeric packing element may be designed to swell when it encounters certain fluid types. These packers are more permanent, and rely on chemical interactions with the elastomer packing element to swell the packing element and create a tight seal (Offshore, 2008). Swellable packers may function as the primary packer device, or an in-situ backup in the event of a primary packer failure.

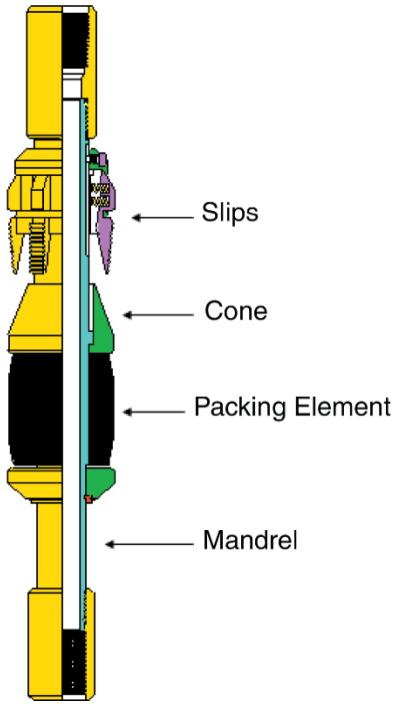


**Figure 6. Example packer. Note the elastomer based packing element which forms a seal between the drill string and the casing (Society of Petroleum Engineers, 2015).**

Industry standards, including ISO 14310 (Petroleum and natural gas industries -- Downhole equipment -- Packers and bridge plugs) and API 11D1 (Packers and Bridge Plugs), outline criteria that packers (and bridge plugs) must comply with during manufacturing, installation, and operation. In general, existing standards simply state which requirements for elastomeric compounds must be defined by the end user, and what documentation must be supplied with the elastomer materials by the manufacturer to the end user. The final packer product is validated in one of seven grades, each with increasing testing criteria that must be conducted prior to

completing validation. Testing can include basic supplier/manufacturer defined acceptance criteria, liquid or gas pressurization tests, loading tests, or a combination of each (International Standards, 2008). Standards for these tests are a combination of ISO defined parameters and supplier/manufacturer defined parameters.

### *4.4.2 Blow-Out Preventers*

BOPs are used during the drilling process to seal the wellbore in the event of a formation kick or external event that requires the drill platform to disconnect from the well. BOPs can be classified into two primary categories: annular and ram. Ram BOPs do not commonly make use of elastomers in their critical components, and one or more are typically installed at the base of the BOP stack. Annular BOPs are typically installed at the top of the BOP stack, and are typically a secondary barrier to prevent a blowout from occurring (the primary barrier is the drilling mud in the hole). Annular BOPs make use of a solid, elastomer-based donut which is compressed around the drill pipe using hydraulic pressure to seal off the well opening around the drill string (shown in Figure 7). When a potential blowout is detected, hydraulic pressure is applied to the donut, forcing it to conform tightly around the drill pipe. In this configuration, the elastomer donut is directly exposed to the formation temperature and pressure, which may exceed several thousand psig. As the elastomer is directly exposed to formation fluids, it must be made of materials compatible with the formation fluid components (Society of Petroleum Engineers, 2015).

30 CFR Part 250 Oil and Gas and Sulfur Operations in the Outer Continental Shelf—Blowout Preventer Systems and Well Control; Final Rule Effective July 28, 2016 was recently issued by BSEE. This regulation requires that subsea wells need to include a minimum of four remote controlled hydraulic BOPs, at least one of which needs to be an annular-style BOP (30 CFR 250.733, BSEE). Annular BOPs are required to be tested every seven days to ensure functionality. Failure of BOPs to function as designed have led to many blowout events, therefore proper functionality of these units is essential.

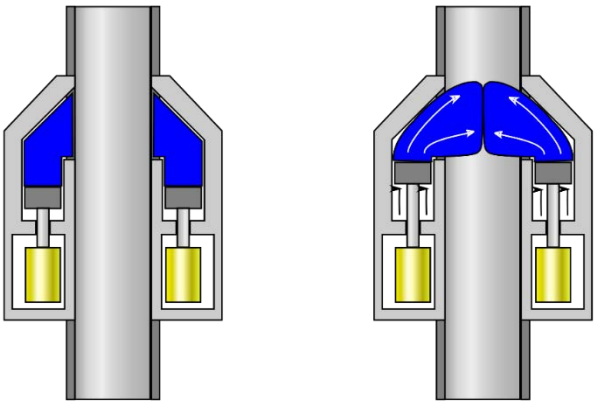

**Figure 7. Cross sectional view of an annular BOP in both the standby (left) and activated (right) positions) (Ocean & Aerospace Research Institute, 2016).**

### *4.4.3 Subsurface Safety Valve*

SSSVs are installed within the wellbore and function to stop flow in the event of an emergency. These valves are normally closed, and held open by hydraulic pressure provided from the surface. In the event of a power failure or other emergency on the surface, the hydraulic pressure is released and the safety valve closes and seals off the well. To provide an effective seal, these valves may incorporate either elastomer-based seals or metal-to-metal seals. The SSSV must withstand conditions similar to the packer (15,000 psig and 350°F in HPHT wells), but also maintain the ability to properly close and seal the well after spending much of the time in the "open" position. This requires that the elastomer seals be extremely resistant to degradation through continuous exposure to produced fluids. Figure 8 shows an example SSSV.

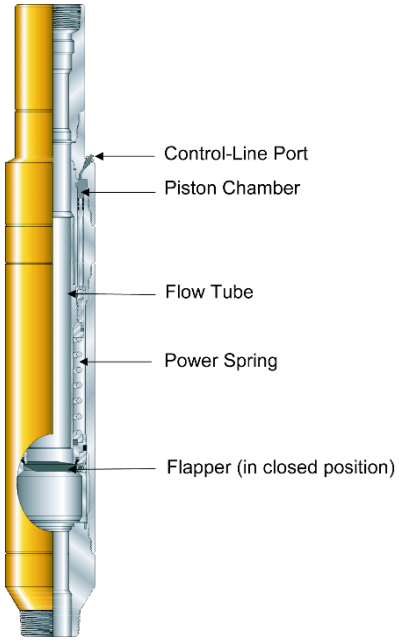


**Figure 8. Example subsurface safety valve (SSSV). Note the elastomer seal on the flapper. (Society of Petroleum Engineers, 2015).**

SSSVs must conform to regulations which have been recently issued by BSEE such as 30 CFR Part 250 Oil and Gas and Sulfur Operations on the Outer Continental Shelf—Oil and Gas Production Safety Systems; Final Rule, effective November 7, 2016 (30 CFR 250.801, 30 CFR 250.802). Other specifications are provided by the API (API 14A/B; Subsurface Safety Valve Equipment; Design, Installation, Operation, Test, and Redress of Subsurface Safety Valve Systems), which have been incorporated into ISO 10432:2004/10417:2004 (Petroleum and natural gas industries -- Subsurface safety valve systems -- Design, installation, operation and redress) standards (Bellarby, 2009). In order to ensure that SSSVs are working properly, they are typically tested every three to 12 months, depending on typical failure rates for a given application. SSSVs may leak at a rate no greater than 400 cc/min for liquid applications, or 15 scf/min for gas applications (Bellarby, 2009). SSSVs must be removed from the well every 12

months for inspection, testing, and recalibration to current well conditions for operators meeting ISO 10417 (International Standard, 2004).

### *4.4.4 Wellhead*

The wellhead functions to transition the subsurface well components (casing and tubing) with components external to the subsurface well (Christmas tree, risers, and flowlines). Wellheads can function as structures from which to hang the first casing structure, and during well completion, the Christmas tree is attached to the wellhead. Therefore, the wellhead functions as a critical seal, providing a barrier to prevent well fluids from escaping the well.

In offshore drilling environments, wellhead configurations have traditionally made use of metal-to-metal seal assemblies at critical interfaces, although elastomers are often used as a backup to these metal-to-metal seals (Bellarby, 2009). When used as a backup seal, the elastomer is not continuously exposed to the working fluids of the well, although it may be exposed to the same pressure as the rest of the wellhead. Figure 9 shows a typical offshore, subsurface wellhead component, with the locations of the metal-to-metal seals as well as the elastomeric backup seals.

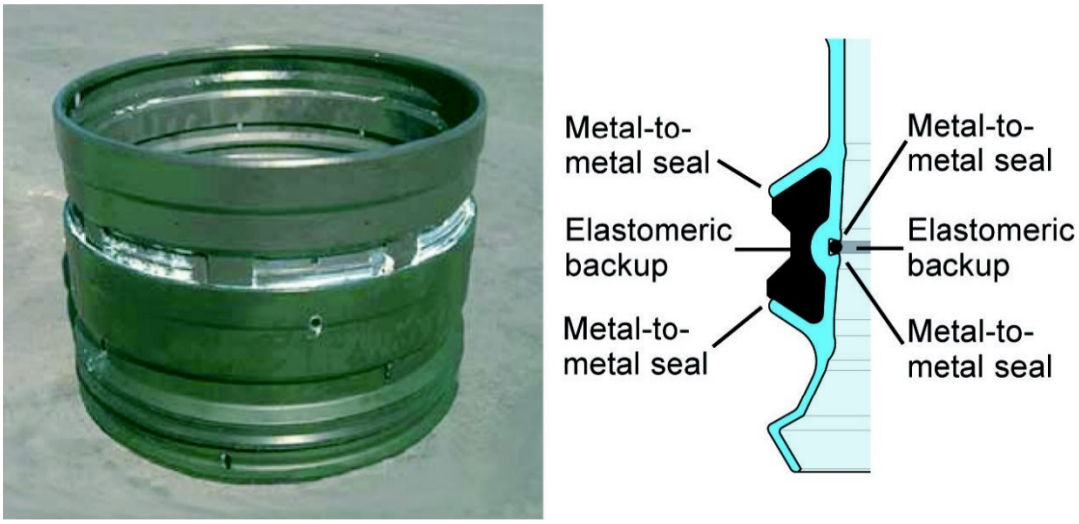


**Figure 9. Offshore, subsurface wellhead configuration (left) with seal cross-section (right) (Society of Petroleum Engineers, 2015).**

ISO 13628 (Petroleum and natural gas industries -- Design and operation of subsea production systems -- Part 15: Subsea structures and manifolds) and API 17E (Specification for Subsea Umbilicals) dictate some of the parameters that subsea wellheads must adhere to prior to being placed into service. The end user is required to specify the materials to be used in the construction of the unit. Standard pressure ratings for subsea wellheads may be as high as 15,000 psi. Similar to packers, validation testing must be conducted prior to acceptance of the wellhead unit. This testing includes pressure and temperature cycling, but again the final acceptance testing criteria are set by the manufacturer, and not typically specified by the standard.

## 4.5 Failure Modes of Elastomer and Composite Seals in HPHT Oil and Gas Applications

Elastomers fail in numerous ways depending on their function and the extremes of their operating environment. Identification of the failure mechanisms of elastomers will influence which elastomers are selected for specific applications, how long they are placed in service, and what backup protection methods may be used to prevent a failure. Since the HPHT testing and modeling will focus on O-rings, Battelle has identified the top six O-ring failure mechanisms for discussion in this report. These failure mechanisms include: extrusion and nibbling, compression set, explosive decompression, wear, chemical degradation, and spiral failure. Temperature, storage effects and poor installation are also discussed. In discussions with project stakeholders, the majority of failures can be attributed to human error during storage and installation. O-rings that are overstretched or rolled during installation are prone to failure.

### *4.5.1 Extrusion and Nibbling*

Extrusion and nibbling occur most often in O-rings that seal under dynamic conditions. These conditions exist if the O-ring seals between two moving interfaces, or between static interfaces which experience pulsating pressures and cause stress to the O-ring. As the O-ring gets caught between interfaces, the trapped O-ring portions are pulled or nibbled, effectively eating away at the O-ring material. As the O-ring loses material, its structure weakens and it is more prone to leaks or complete failures (Daemar Inc., 2015). Failures such as these can occur in any application in which the elastomer experiences friction against a stationary object, including packers (interface between elastomer and casing) and SSSVs (interface between flapper seal and annular region).

### *4.5.2 Compression Set*

Compression set failures are one of the more commonly observed failure mechanisms. In order for an O-ring to seal correctly, proper dimensions for both the O-ring and the gland are critical. Both the O-ring and the gland must be clean, such that a proper sealing surface can develop. The proper deformation of the O-ring (squeeze) must also be achieved to prevent leaks (Parker Hannifin Corporation, 1947). A compression set failure occurs when improper compression of the O-ring in the gland is applied or the material undergoes a permanent deformation (Daemar Inc., 2015). Improperly dimensioned O-rings or glands can lead to leaks or premature extrusion failures. O-rings that are too large for a given gland are prone to extrusion failures, while O-rings that are too small will not develop sufficient squeeze when compressed to achieve a proper seal. Additionally, any swelling that may occur due to exposure to various constituents present in the service environment must be considered when calculating proper O-ring squeeze.

### *4.5.3 Rapid Gas Decompression (RGD)*

RGD, also known as explosive decompression, occurs when an O-ring is operated in high temperature and high pressure gas environments, causing supercritical fluid gases to become trapped within the internal structure of the O-ring. When pressure on the O-ring is rapidly

relieved, the gases trapped inside the O-ring rapidly expand and rupture the O-ring material (Daemar Inc., 2015), resulting in blistering and pitting on the surface. In general, higher durometer elastomers (EPM, Inc., 2015) will have higher stiffness and resist rupturing compared to a lower durometer material at the same clearance gap. A higher potential for RGD occurs during situations where the pressure may cycle quickly (for example, when HPHT elastomers are rapidly pulled out of a high pressure environment during drilling or testing activities).

### *4.5.4 Wear*

Abrasive or wear failure can be caused by several factors, including human error during the handling or installation process, and in applications involving moving surfaces. If sealing surfaces are damaged, improperly lubricated, or improperly finished, an abrasive type wear failure can occur. Wear failures can cause an elastomeric seal to deform, causing a leak or catastrophic failure (Daemar Inc., 2015). This failure mechanism is of particular concern to any temporary tool used in HPHT environments that is moved on a consistent basis. The more frequently a tool is handled, the greater an opportunity for an accidental abrasive wear failure to occur.

### *4.5.5 Chemical Degradation*

Chemical degradation occurs when incompatible materials are exposed to one another. Each well application contains different combinations of hydrocarbon compounds, drilling fluids, strong acids or caustics, and corrosive gases including hydrogen sulfide. Elastomers in the presence of solvents or chemicals may be subject to leaching of soluble components from the elastomer into the bulk fluid, weakening and degrading the polymeric structure of the elastomer (Campion, Thomson, & Harris, 2005). Typically, leaching rates increase as temperature increases, making this condition an increased concern in HPHT environments. Additionally, as bulk fluid is absorbed into the elastomer, the elastomer will often swell, increasing the chances of other types of failure mechanisms (including extrusion and abrasive failure) occurring.

Additionally, oxidation agents can oxidize the elastomer material, which undergoes a chain scission reaction (Campion, Thomson, & Harris, 2005). This reaction serves to lower the average molecular weight of the elastomer, weakening it and making it more susceptible to failure. Oxidizing agents can be both liquid and gaseous. A common gaseous oxidizing agent is ozone, which often contributes to the failure of elastomers that are stored over a long period of time. Ozone and reactive singlet oxygen may be formed in the presence of ultraviolet radiation (sunlight) and oxygen; therefore, elastomers stored in the presence of these components (such as in storage yards, or on decks of ships or offshore drill rigs) are susceptible to degradation.

Elastomers are qualified for service based on their initial factory properties. Feedback from industry stakeholders who provide elastomer devices for use in the offshore O&G industry stressed that the manufacturer cannot control storage, installation, maintenance, and service conditions necessary for long-term in-service safety of the device.

### *4.5.6 Spiral Failure*

Spiral failures occur in O-rings that are used in applications involving motion. If the O-ring is installed improperly, or if an external force acts upon it, a portion of the O-ring may become caught between two moving parts and held in a stationary position. The remainder of the O-ring may then become rolled as parts move, causing the O-ring to twist (Daemar Inc., 2015). Repeated twisting of the O-ring can cause a series of spiral grooves to appear on the O-ring, diminishing its ability to seal properly. The metal surfaces that will be in contact with the O-ring should be well-designed and machined to a smooth surface so that the O-ring elastomer does not have the opportunity to catch and become twisted. This will help ensure proper installation of the O-rings.

## 4.6 The Critical Role of O&G Elastomer Components in Environmental Safety

If an O-ring fails in a seal, redundant back-up seals prevent the "leak" from having more impact on the operational readiness of a well or a rig. O-ring failure would be less critical due to component redundancy.

Battelle conducted a failure analysis with a risk assessment for the larger and more mission critical drilling and production equipment in which HPHT elastomers are used as sealing components. The service provider and operator companies interviewed for this project rated all safety equipment as equally critical for providing health, safety, and environment (HSE) protection. However, some inference to the criticality of the equipment described in this report can be drawn from the work that has been conducted on blowouts by (SINTEF, 2013) and (Holand, 1997). In this report blowout is defined as "An uncontrolled flow of gas, oil, or other fluids from a well to the atmosphere" B or the sea floor. BSEE has issued 30 CFR Part 250 Oil and Gas and Sulfur Operations in the Outer Continental Shelf—Blowout Preventer Systems and Well Control; Final Rule effective July 28, 2016 where BOP is involved in a subset of a loss of well control incidents which also includes uncontrolled flow between formations. Blowouts can be divided into several categories to aid in understanding what critical HSE equipment may have been in use at the time of the blowout. This report will consider blowouts during drilling, completion, and workover. A blowout is the uncontrolled release of formation fluids or crude oil and/or natural gas from an oil well or gas well after pressure control systems and all HSE barriers have failed. Stiftelsen for INdustriell og TEknisk Forskning (SINTEF) keeps a database of well blowouts and reports that most blowouts occur during drilling, followed by workover, completion, and production (with no external cause). These data (Table 11) can be narrowed down by removing the production with external cause (e.g., accidents and sabotage), abandoned wells, and unknown data (Table 12), which are used to determine the likelihoods that specific equipment types may be in the well at the time of a blowout (Table 13). These likelihoods are not for failure of specific equipment, but rather the likelihood of being present in a well during a blowout assuming that wells suffering blowouts are comparable to wells that have not suffered a blowout. Estimates indicate that the wellhead and BOP are far more likely to be present when a blowout occurs in comparison to the packer and SSSV.

Equipment failure data are sparse. Based on an earlier SINTEF database and data acquired from 124 blowout cases in the same categories between 1980 and 1994, wellhead seal failure occurred only twice out of all of the blowout failures attributed to the equipment included in this study (Table 14) (SINTEF, 2013).

The infrequency of blowout leads combined with the remoteness of failed components in wells experiencing blowouts causes difficulty in estimating the likelihood of occurrence of seal failure in critical applications (i.e., even if the overall component failed it is difficult to say if it was the seal or another subcomponent). However, the likelihood of equipment present in a well experiencing a blowout can be ranked from wellhead (most likely) to SSSV (least likely).

Cai et al. (2013) estimated BOP failure rates as part of a study evaluated the probability of failure on demand of closing subsea rams in BOPs. The inner and outer BOP seals are typically composed of carbon steel with an HNBR elastomer seal material. The study indicated mechanical and hydraulic factors are most important with software and hardware factors least important. Cai et. al. report BOP failure rates related to leakage (seals) in the range of $10^{-5}$ and $10^{-6}$ (Table 15) (Cai, et al., 2013).

**Table 11. SINTEF database data on blowouts between 1980 and 2012 (SINTEF, 2013).**

| | Number of Blowouts | | | | | | | | | | |
|---|---|---|---|---|---|---|---|---|---|---|---|
| **Area** | Developmental Drilling | Exploration Drilling | Unknown Drilling | Completion | Workover | Production with external cause | Production without external cause | Wireline | Abandoned Well | Unknown | Total |
| **US GoM OCS** | 54 | 55 | | 13 | 44 | 8 | 13 | 5 | 2 | 2 | 196 |
| **UK and Norway Waters** | 9 | 33 | 1 | 7 | 9 | 1 | 2 | 4 | 1 | | 67 |
| **Total** | 63 | 88 | 1 | 20 | 53 | 9 | 15 | 9 | 3 | 2 | 263 |

**Table 12. Simplified blowout data used to estimate equipment likelihood of being in a well during a blowout, excluding production with external cause (e.g., accidents and sabotage), abandoned wells, and unknown data.**

| Well Activity | | | | | | |
|---|---|---|---|---|---|---|
| | Drilling | Completion | Workover | Production without external cause | Wireline | Total |
| **Number of blowouts** | 152 | 20 | 53 | 15 | 9 | 249 |
| **Percent** | 61.0 | 8.0 | 21.3 | 6.0 | 3.6 | 100.0 |

**Table 13. Estimated likelihood of equipment being in the well during a blowout. "X" indicates that equipment is expected to be in the well during the process, "P" indicates that it is possible that the equipment is in the well during the process.**

| Well Activity | | | | | | |
|---|---|---|---|---|---|---|
| **Likely HSE Equipment** | **Drilling** | **Completion** | **Workover** | **Production without external cause** | **Wireline** | **Likelihood of being present during a blowout** |
| **BOP** | x | x | x | | x | 94.0 |
| **SSSV** | | | p | x | | 27.3 |
| **Packer** | | p | p | x | p | 35.3 |
| **Wellhead** | x | x | x | x | x | 100.0 |

**Table 14. Failures based on SINTEF data between 1980 and 1994 showing failure rates for well equipment included in this study (SINTEF, 2013).**

| Category/sub category | Failures | Blowout Subtotal per category | Percent Failure (Subtotal) | Total Blowouts | Percent Failure (Total Blowouts) |
|---|---|---|---|---|---|
| **Drilling** | | | | | |
| **BOP failed after closure** | 6 | 88 | 6.8 | 124 | 4.8 |
| **Wellhead seal failed** | 1 | 88 | 1.1 | 124 | 0.8 |
| **Workover** | | | | | |
| **Casing head (Wellhead) failed** | 1 | 20 | 5.0 | 124 | 0.8 |
| **Production without external cause** | | | | | |
| **SSSV failure** | 2 | 6 | 33.3 | 124 | 1.6 |
| **Wellhead seal failed** | 1 | 6 | 16.7 | 124 | 0.8 |
| **Wireline** | | | | | |
| **SSSV failure** | 1 | 3 | 33.3 | 124 | 0.8 |

**Table 15. BOP failure rates related to mechanical and hydraulic factors (Cai, et al., 2013).**

| Factor | Node | Description | Failure Rate x $10^{-6}$ |
|---|---|---|---|
| Mechanical | BOP Internal Leakage Failure | The BOP has failed due to internal leakage | 6.26 |
| Mechanical | Sub-plate Mounted Valve (SPM) Internal Leakage/Failure | The SPM in control pod has failed due to internal leakage | 9.20 |
| Mechanical | BOP External Leakage Failure | The BOP has failed due to external leakage | 13.50 |
| Hydraulic | External leakage/Failure | External leakage with low pressure in control pod occurs | 6.90 |
| Hydraulic | External leakage High Failure | External leakage with high pressure occurs | 11.50 |

# 5.0 INDUSTRY STANDARDS REVIEW AND GAP ANALYSIS

A literature review of existing O&G industry-specific standards was conducted, as well as other industries' standards with similar HPHT operating environments. Battelle reached out to industry stakeholders to solicit feedback on ways in which current industry standards could be improved to better reflect the needs of the current HPHT elastomer applications. These standards were reviewed to determine if any discrepancies between existing standards and any major gaps in the current standards. Standards that were evaluated are:

- Aerospace Material Specifications (AMS)
- American National Standards Institute (ANSI)
- American Petroleum Institute (API)
- American Society for Testing Materials (ASTM) International
- International Organization for Standardization (ISO)
- National Association of Corrosion Engineers (NACE)
- Norsk Sokkels Konkuranseposisjon (NORSOK)
- United States Military Standard (MIL-SPEC)

Industry standards were initially categorized according to their scope. The industry standards fell predominantly into one of four following categories:

a) standards aligned with end use of tools in drilling and production applications,

b) standards aligned with similar applications within other industries,

c) standards associated with laboratory testing, and

d) standards associated with storing and shipping of elastomer-based materials.

After categorization, each standard was summarized such that comparisons could be made between the standards. Standards that referenced other standards were identified, and contradictions between standards were noted. A gap analysis was conducted to identify aspects of the elastomer qualification process and material properties analysis that may require additional regulatory guidance to improve the safety practices of offshore HPHT O&G operations. Finally, project stakeholders were consulted about perceived gaps in existing standards associated with HPHT elastomer use (see Section 5.2.2). Key findings are presented in Section 5.4. A complete summary of standards, including standard titles, is presented in Appendix A.1.

## 5.1 Discussion of Standards Reviewed

Temperature and pressure requirements for elastomers covered in these standards vary, with some being closer to HPHT conditions than others. Many of these standards can likely be adapted to represent HPHT conditions with minor modifications. A large majority of standards, such as API, ISO, and NORSOK, provide guidance for elastomer qualification testing explicitly for drilling and production equipment. Often, the standard applies to the entire component or tool assembly, and not just the elastomer components. Other standards reviewed include laboratory-based test protocols to evaluate elastomer properties and failure characteristics after exposure to various fluids, temperatures, and pressures. Standards for these protocols include ASTM standards and NACE standards. ASTM standards in particular are frequently referenced by other standards (including ISO and API) as a method to conduct material property analysis. AMS and MIL-SPEC standards also adapt ASTM standards to use as qualification standards for elastomer materials for aerospace and military applications. A complete table of summarized standards relevant to this project can be found in Appendix A.1. Appendix A.2 contains a list of all standards evaluated, while Appendix A.3 includes specific tables or figures presented in the standards discussed in this report.

### *5.1.1 ISO, API, and NORSOK Standards*

Many of the API standards evaluated have similar corresponding ISO standards, as API historically had drafted and issued standards in coordination with ISO. For example, the versions of API 17D (Specification for Design and Operation of Subsea Production Systems—Subsea Wellhead and Tree Equipment) and ISO 13628 (Petroleum and natural gas industries -- Design and operation of subsea production systems -- Part 15: Subsea structures and manifolds) (both of 2011) are identical adaptations. However, newer API standards reviewed, those from 2015 onwards, are separate from ISO. Standards API 14B: Design, Installation, Operation, Test, and Redress of. Subsurface Safety Valve Systems (similar to ISO 10417: Petroleum and natural gas industries -- Subsurface safety valve systems -- Design, installation, operation and redress), API 16A: Specification for Drill-through Equipment (similar to ISO 13533: Petroleum and natural gas industries -- Drilling and production equipment -- Drill-through equipment), API 6A: Specification for Wellhead and Christmas Tree Equipment (similar to ISO 10423: Petroleum and natural gas industries -- Drilling and production equipment -- Wellhead and christmas tree equipment), and API 11D: Specification for Miscellaneous Production Equipment (similar to ISO 14310: Petroleum and natural gas industries -- Downhole equipment -- Packers and bridge plugs) which were reviewed provide standards for required equipment specifications for SSSVs, BOPs, wellheads, and packers, respectively (Table 16).

In particular API 11D, as well as API 14A (Addressing Critical Service and HPHT SSSV Applications), have portions of the standard dedicated to HPHT service. ISO 10417, Section 5.2.3.4, states that SSSVs as a unit must be tested to withstand a differential pressure of 200 psi, but does not state explicitly for which pressure elastomeric components must be qualified. ISO 13533 (Petroleum and natural gas industries -- Drilling and production equipment -- Drill-through equipment) calls for non-metallic BOP components to be qualified to a maximum temperature rating of 177°C, depending on the code of BOP selected (see Table A.3-1). API 6A,

Sections 4.2.1.1 and 4.2.2.3, present temperature and pressure requirements for wellheads, indicating that the maximum pressure for a wellhead to be qualified is 20,000 psi at 121°C. This is within the range of HPHT pressure conditions, but falls short of qualifying the unit for high temperature service. Note that these temperature and pressure qualification levels are for the overall unit and not the elastomeric components explicitly. ISO 14310, Section 5.3.3.3 lists material characterization tests that must be conducted for non-metallic materials used in packers. These tests include tensile strength, elongation, and tensile modulus tests, as well as compression set and durometer hardness tests. Note that no minimum elastomer modulus properties are provided to guide elastomer selection in this standard.

**Table 16. Comparison on API standards against HPHT conditions.**

| | HPHT Conditions | API 6A (12th Edition) | API 11D (3rd Edition) | API 14A (12th Edition) | API 14B 6th Edition | API 16A (3rd Edition) | API 17D** (2nd Edition) |
|---|---|---|---|---|---|---|---|
| Temperature (°F) | >350 | Varies* | >350 | >350 | N/A | <350 | <140*** |
| Pressure (psi) | >15k | 1k | >15k | >15k | N/A | <20k | <15k |
| Chemical Compatibility Issues | Yes | Yes | Yes | Yes | N/A | No | No |
| Rapid Gas Decompression Issues | Yes | No | Yes | Yes | N/A | No | No |

*listed as the maximum specified temperature for the given application
**Identical to ISO 13628: Petroleum and natural gas industries -- Design and operation of subsea production systems -- Part 15: Subsea structures and manifolds
***End use temperature and pressure to be specified by user.

In general, these standards do not specify an explicit selection criteria for elastomeric components but rather stating that the operator and supplier must mutually agree upon material type and material selection criteria. For packers, BOPs, and SSSVs, ISO defines overall functionality test requirements, which are considered to be outside the scope of this report, but it should be noted that these tests are not explicit tests for the elastomer components themselves.

Some initial storage criteria for elastomer components is outlined in API 14B (Design, Installation, Operation, Test, and Redress of Subsurface Safety Valve Systems) and ISO 27996 (Aerospace fluid systems – Elastomer Seals – Storage and Shelf Life). API 14B Section 5.2.3.4 requires that elastomer components of SSSVs cannot be exposed to ultraviolet light (sunlight) during storage. Additionally, other oxidizing agents, such as ozone, should be avoided when storing the elastomeric components for extended durations. No maximum storage timeframes are provided in the standard, and no requalification criteria are defined for elastomers taken from storage prior to being installed in service. In addition, the SSSV equipment shall be packaged for transport per the written specifications of the equipment manufacturer to prevent normal

handling loads and contamination from harming the equipment. API 14A Section 9 cover storage and preparation for transport and state that SSSV equipment shall be stored per the written specifications of the equipment manufacturer to prevent deterioration (for example, caused by atmospheric conditions, debris, radiation, etc.) prior to transport. However, for storage after transport, one is to consult the operating manual for the device. These specifications address the protection of: external sealing elements, sealing surfaces, exposed threaded connections, access port(s) sealing and contamination from fluids and debris. ISO 27996 (Aerospace fluid systems -- Elastomer seals -- Storage and shelf life), Section 6 is primarily used in the aerospace industry to evaluate storage parameters for elastomer components similar to those used in O&G applications. In addition to storage conditions that should be avoided (similar to those presented in ISO 10417 (Petroleum and natural gas industries -- Subsurface safety valve systems -- Design, installation, operation and redress), Section 5.2.3.4), humidity and temperature ranges recommended for storage are also stated (between 40% and 70% humidity, between 41°F and 86°F temperature range). Finally, for each of the elastomers considered as part of this study (NBR, HNBR, FKM, FFKM, and FEPM), recommended maximum storage timeframes (reported in quarters of a year per ISO 27996) are provided (28 quarters of a year, or 112 months, for NBR and HNBR, 40 quarters of a year, or 160 months, for FKM, FFKM, and FEPM), as well as packaging, shipping, and labeling methods (including use of packaging free of chemicals capable of degrading the elastomer, packaging that will block ultraviolet light). In general, standards for elastomer storage are not well documented in O&G-specific ISO standards which provide guidance for BOPs, wellheads, and packers.

NORSOK M-710 (Qualification of non-metallic sealing materials and manufactures) and ISO 23936-2 (Petroleum, petrochemical and natural gas industries -- Non-metallic materials in contact with media related to oil and gas production -- Part 2: Elastomers) provide qualification of elastomeric components for O&G service, including chemical compatibility, accelerated age evaluation, and RGD testing. Documentation requirements and physical material property tests to be conducted during the qualification process are provided in Table 1 of the ISO 23936-2 standard (see Table A.3-2 of this report). These standards indicate that elastomer selection will vary based on the end service environment, but care should be taken to ensure that the appropriate material is selected for each application. Criteria specified to aid in the selection process that are pertinent to HPHT applications include adequate physical and chemical properties, resistance to RGD, long life, resistance to extrusion or creep under high pressures, and resistance to changes in properties at high temperature. Accelerated age testing can assist in determining the appropriate elastomer type for specific use conditions. ISO 23936-2 Section 7 specifies accelerated age testing conditions, which include exposure to a similar chemical medium found downhole at three elevated temperatures, which shall be 15°C, 30°C, and 45°C higher than that of expected service temperatures (which range from 66°C to 180°C in ISO 23936, Table A.3-3 of this report). It should be noted that this standard qualifies elastomers for minimum HPHT service (defined as greater than 350°F, or 176°C), but does not require testing to be conducted at temperatures greater than 180°C. HPHT conditions can far exceed 180°C, with temperatures up to 260°C.API 14A references ISO 23936-2 frequently for elastomer test procedures to qualify the components for service.

Recommended fluids for exposure testing are listed in Tables A.1-A.5 of ISO 23936-2. These fluids include representative gas and liquid hydrocarbons commonly found downhole (including heptane and methane), but fail to include other chemicals commonly found downhole that are capable of degrading elastomers, including drilling fluids, hydrates, and scale and corrosion inhibitors. Testing performed at elevated temperature causes chemical aging to occur more rapidly. NORSOK M-710 Sections 7 and 8, reference and follow the same testing guidelines presented in ISO 23936, however stricter qualification standards in terms of volume change after chemical aging are applied. The chemical aging methods in NORSOK M-710 and ISO 23936-2 may not be sufficient for qualifying seal systems in deep-water completions due to the large range of acceptance criteria of ±50% change in tensile properties (Slay & Ferrell, 2008). Material characterization tests performed at pre- and post-aging are specified, and include hardness and tensile testing (modulus, tensile strength, and elongation at break), as well as volume measurements. Acceptable deviations of these parameters after exposure to the fluid medium are specified in Table 17.

**Table 17. Acceptable material characterization deviations after age testing, per ISO 23936-2, Section 7.2.2.**

| Measurement | ISO 23936-2 | NORSOK M-710 |
|---|---|---|
| Hardness | +10/-20 units | Not provided |
| Volume | +25%/-5% | +5%/-1% |
| Tensile | +/- 50% | +/- 50% |

RGD testing of elastomers is also specified in ISO 23936-2, Annex B, where methane ($CH_4$) and carbon dioxide ($CO_2$) are the test gases. Testing should be conducted in an environment similar to downhole conditions. Liquid, gas, or combined phases should be used depending on anticipated use conditions. Sample fluid compositions are outlined in the standard for use during RGD testing, although any fluid composition can be used if agreed upon by the end user. The typical test temperature for ISO 23936-2 Annex B test is 212°F, while the recommended test pressure in this standard is 2,175 psi. Although these RGD test temperatures and pressures involving $CO_2$ and $CH_4$ are far below the minimum expected temperatures and pressures associated with HPHT applications, both compounds are already in supercritical phase conditions. For $CO_2$, the critical temperature is 87.9 °F and critical pressure of $CO_2$ is 1070.0 psi. For $CH_4$ the critical temperature is -117.3°F and the critical pressure is 668.6 psi. Since the test gases are in the condensed supercritical phase, reducing the temperature, or pressure will cause them to return to gas phase and expand rapidly. A cyclical pressurization-depressurization test procedure is defined, during which the test cell containing the elastomer is pressurized and depressurized twice each day for an eight-day period. The maximum constant depressurization rate during the test is limited to below ~20 psi/minute to prevent inducing RGD-type failure during sample removal.

The sour gas testing of elastomers specified in ISO 23936-2, Annex B, uses $CO_2$ and $H_2S$ as the test gases. The sample test exposure media contains 10 vol% water and 60 vol% hydrocarbon

liquid along with 30 vol% $CH_4$, $CO_2$, and $H_2S$ pressurized to 1450 psi initially with inert gas. Three test temperatures are selected depending. on the elastomer composition, for example, FKM is typically tested at 195°C, 210°C, 220°C (Parker Handbook), which are above the service temperature of the elastomer. The test pressure is determined by the vapor pressure of all the components at the test temperature. The maximum constant depressurization rate during the test is limited to below ~20 psi/minute to prevent inducing RGD-type failure during sample removal.

Collectively, the ISO, API, and NORSOK standards evaluated provide guidance regarding the end use requirements of SSSVs, BOPs, wellheads, and packers under non-HPHT operating conditions. However, explicit required characteristics for HPHT environments are not presented in all of the API standards reviewed, with the exception of API 11D and 14A. To supplement this, API published API 17TR8 (HPHT Design Guidelines) to provide design information for service environments with temperatures exceeding 350°F and pressures exceeding 15,000 psi. Section 5.2 of this technical report contains step by step guidance (through API 17TR8) of design and validation requirements for a series of service conditions. Specific consideration is given in this report about corrosive service conditions, and recommendations associated with component design.

Some additional guidance is provided to assist with elastomer selection for a given application, and recommended procedures for accelerated age testing and testing for resistance to RGD are provided as part of ISO 23936, NACE TM0187-2011, NORSOK M-710, and API 6A. It should be noted that these test procedures do not align specifically with HPHT environments.

### *5.1.2 NACE and ASTM Standards*

NACE and ASTM standards contain laboratory-based test protocols intended to evaluate elastomer properties and failure characteristics after exposure to various fluids, temperatures, and pressures. The NACE and ASTM standards described here evaluate elastomeric characteristics in environments applicable to O&G HPHT such as petroleum-based oils, $CO_2$, and compressive regimes.

NACE standards provide test procedures along with protocols for test conditions, specimen preparation, equipment, and reporting of results. The tests described in NACE TM0187 (Standard Test Method - Evaluating Elastomeric Materials in Sour Gas Environments), TM0192 (Evaluating Elastomeric Materials in Carbon Dioxide Decompression Environments), TM0296 (Evaluating Elastomeric Materials in Sour Liquid Environments), and TM0297 (Effects of High-Temperature, High-Pressure Carbon Dioxide Decompression on Elastomeric Materials) all provide relative resistance measurements for O-rings or other elastomers to the specific test environments existing in oil fields and other energy-related applications. Similarly, ASTM's D471 (Standard Test Method for Rubber Property—Effect of Liquids), D575 (Standard Test Methods for Rubber Properties in Compression), D945 (Standard Test Methods for Rubber Properties in Compression or Shear (Mechanical Oscillograph), and D6147 (Standard Test Method for Vulcanized Rubber and Thermoplastic Elastomer—Determination of Force Decay (Stress Relaxation) in Compression) provide test procedures to determine chemical and physical properties of elastomers in laboratory environments. While ASTM provides test procedures for

determining relevant elastomer properties and some may be carried out at temperatures up to 482°F, they are not commonly intended for testing elastomers in HPHT environments of O&G production. Results of both NACE and ASTM tests can be used to help qualify elastomers for service in HPHT O&G service, but should not be used alone for qualification.

NACE TM0296 (Evaluating Elastomeric Materials in Sour Liquid Environments) provides a standard test method for evaluation of the resistance of elastomeric materials to sour liquid (hydrocarbon, water, or mixtures of each with $H_2S$) environments. It is stated in the standard that the test procedure of accelerated aging is similar to ASTM D471 (Standard Test Method for Rubber Property— Effects of Liquids). The results of the tests provide a relative measure of the resistance of elastomeric materials to a sour liquid environment. Section 5.1 of NACE TM0296 states that the standard temperatures for conducting this test are 212, 250, 302, and 347°F, though others can be used if agreed upon between all parties involved. The final test pressure shall be 1,000 ± 100 psig (Section 5.2.1 of TM0296), far below the standard minimum of 15,000 psi to qualify as a high pressure environment. The testing procedures determine compression set, change in mass/volume, tensile properties, and hardness to evaluate the resistance of the elastomeric materials to sour liquid environments.

NACE TM0187 (Standard Test Method - Evaluating Elastomeric Materials in Sour Gas Environments) describes test procedures to evaluate elastomeric materials for use in oil fields and other energy-related areas where vapor phase sour gaseous environments (gaseous hydrocarbons containing $H_2S$) exist. Similar to NACE TM0296, test procedures in NACE TM0187 also consist of determination of compression set, change in mass/volume, tensile properties, and hardness to evaluate the resistance of the elastomeric materials to the environment of interest (sour gas in this case). Test temperatures of NACE TM0187 (Section 5.1 of standard) are also similar to those of NACE TM0296: 212, 302, and 347°F. The initial pressure should be 1,000 ±100 psig and the pressure during the test should be dictated by the test vessel (Section 5.2 of TM0187). While the test temperatures almost achieve the threshold of 350°F for high temperature, the pressure after temperature elevation is expected to be much lower than high pressure conditions.

ASTM D471 (Standard Test Method for Rubber Property— Effects of Liquids) outlines methods for the evaluation of the relative ability of elastomers to withstand the effects of petroleum-based industry reference materials (IRM) and ASTM oils. Test procedures are specified in ISO 13628-4 (see Appendix A.3-6) and include high temperature conditions applicable to the downhole O&G environment with a range of -103 ± 4°F to 482 ± 4°F (Section 5.1 of D471); however, these tests are not performed at high pressure. The procedures in this standard used to evaluate an elastomer's resistance to petroleum-based oils include, but are not limited to: change in mass and/or volume after immersion, change in tensile strength, change in elongation, and hardness after immersion.

NACE TM0297 (Effects of High-Temperature, High-Pressure Carbon Dioxide Decompression on Elastomeric Materials) presents a standard test method to evaluate the resistance of elastomeric materials to high temperature, elevated pressure, and gaseous $CO_2$ environments. The tests are to be performed at an elevated pressure of 1,000 to 5,500 psig (Section 4.2 of

TM0297) and a temperature of 122 to 446°F (Section 4.1 of TM0297). Temperatures above 350°F are considered high; however, the elevated pressure at which the tests should be performed does not qualify as high pressure. Test results provide a relative measure of the resistance to rapid depressurization in dry $CO_2$ environments by determination of change in visual appearance, in tensile properties, in cross-sectional diameter, and in durometer hardness. NACE TM0192 is similar to NACE TM0297, where the objective of the test method is to measure the effect of rapid depressurization from elevated pressure in dry $CO_2$ environments on elastomeric materials. However, the test detailed in NACE TM0192 is to be conducted at 77 ± 9°F (Section 4.1 of TM0297) at 750 ± 50 psig (Section 4.2 of TM0297). According to Halliburton's test results (Slay & Ferrell, 2008), the test temperature used in NACE TM0192 can be considered a good representation of tests performed at higher temperatures and pressures for HNBR. Testing at 72°F causes more damage than testing at 302°F because a lower temperature does not allow gas to escape as quickly as testing at higher temperature (Slay & Ferrell, 2008).

ASTM D575 (Standard Test Methods for Rubber Properties in Compression) describes two methods for measuring compression stiffness through compression-deflection of rubber compounds (Section 2 of D575). Compression-deflection is the change in thickness of a specimen upon the application of a compressive force. ASTM D575 Method A (Section 3.1.1 of D575) is a compression test that measures the force needed to cause a specified deflection while ASTM D575 Method B (Section 3.1.2 of D575) measures the deflection of an elastomer resulting from a specified compression force at ambient temperature and pressure.

ASTM D945 (Standard Test Methods for Rubber Properties in Compression or Shear (Mechanical Oscillograph) presents test methods for measuring the mechanical and deformation properties such as Yerzley resilience and hysteresis, dynamic and static modulus, creep and set, and kinetic energy of elastomers through the use of Yerzley mechanical oscillography. These are addressed in Part A of the standard (*Measurements in Compression*), and Part B of the standard (*Measurements in Shear*). The Yerzley oscillograph predicts the properties of elastomers through analysis of the vibrational frequency and damping rate of free oscillations which are the result of the initial known energy applied to the specimen. The deformation properties of an elastomer are imperative for isolation and absorption of shock and/or vibration. Test conditions such as pressure and temperature are not specified in the standard.

ASTM D6147 (Standard Test Method for Vulcanized Rubber and Thermoplastic Elastomer—Determination of Force Decay (Stress Relaxation) in Compression) specifies test methods for determination of the force decay (or stress relaxation) of an elastomer in air or liquids. Force decay is the decrease in stress that occurs after a given time interval during the application of a constant deformation load and is expressed as a percentage of the initial stress that was measured at the start of the time interval. This standard states that testing temperatures in the range of -103 ± 3.6°F to 572 ± 5.4°F may be selected (see Appendix A.3-15) in order to measure the thermal effect on the stress relaxation properties of the elastomer. This is important for determining low temperature flexibility of the seal. Table 18 shows a comparison of test conditions for these relevant NACE and ASTM standards.

**Table 18. Comparison of relevant testing conditions.**

| Standard | Test Type | Test Temperature | Test Pressure |
|---|---|---|---|
| NACE TM0296 | Elastomer resistance to sour liquids | 212, 250, 302, 347°F | 1,000 ± 100 psig |
| NACE TM0187 | Elastomer resistance to sour gas | 212, 302, 347°F | 1,000 ±100 psig |
| ASTM D471 | Elastomer resistance to petroleum-based IRM and ASTM oils | -103 ± 4°F to 482 ± 4°F | Atmospheric (14.7 psi) |
| NACE TM0297 | Elastomer resistance to elevated temperature and pressure gaseous $CO_2$ environment | 122-446°F | 1,000-5,500 psig |
| NACE TM0192 | Effect of rapid depressurization from elevated pressure in dry $CO_2$ environments | 77 ± 9°F | 750 ± 50 psig |
| ASTM D575 | Compression-deflection of rubber compounds | 73.4 ± 3.6°F | Atmospheric (14.7 psi) |
| ASTM D945 | Mechanical and deformation properties | N/A | N/A |
| ASTM D6147 | Force decay in air or liquid | -103 ± 3.6°F to 572 ± 5.4°F | N/A |

### *5.1.3 Standards from Adjacent Industries*

Standards used by other industries to govern similar elastomer materials in applications similar to HPHT O&G environments were evaluated to determine any similarities to standards used by the O&G industry. AMS and MIL-SPEC standards were evaluated to determine areas of commonality with API, ISO, ASTM, and NACE standards. AMS standards reviewed were primarily associated with elastomeric formulations or installations typical of aerospace applications, and often referenced similar ASTM standards to those described in this report for the qualification of elastomers. As such, the relevant ASTM standards preferential to the AMS standards reviewed are summarized (see Section 5.1.2), as they are more applicable to qualification of elastomers for HPHT O&G service. Since limited storage guidelines have been developed specifically for O&G elastomers, one aerospace standard, SAE ARP 5316C (Storage of Aerospace Elastomeric Seals and Seal Assemblies Which Include an Elastomer Element Prior to Hardware Assembly), is included, as it details how to store elastomers used in aerospace applications (Sections 4 and 5 of ARP5316C). These storage guidelines align closely with ISO 27996 (Aerospace fluid systems -- Elastomer seals -- Storage and shelf life; Sections 5 and 6 of ISO 27996) and ISO 10417 (Petroleum and natural gas industries -- Subsurface safety valve

systems -- Design, installation, operation and redress; Section 5 of ISO 10417, similar to API 14B), and are believed to be readily transferrable to most O&G elastomer applications. Table 19 compares recommended storage conditions across these three standards.

**Table 19. Comparison of pertinent storage conditions.**

| Standard | Storage Conditions | Storage Temperature | Packaging |
|---|---|---|---|
| SAE ARP 5316C | Humidity <75% | <100°F | Individually packaged, protection against ultraviolet light |
| ISO 27996 | Humidity < 65% | 41°F-86°F | Individually packaged to prevent damage |
| ISO 10417 | N/A | N/A | Protection against ultraviolet light |

### *5.1.4 MIL-SPEC Standards*

Several MIL-SPECs were evaluated to determine what standards the U.S. Military follows for elastomer qualifications. The majority of the MIL-SPECs reviewed pertained to inspection of elastomer components after being received by the end user, and how to statistically test a fraction of the elastomer components for acceptance of the shipment. A few relevant MIL-SPECs included in this study pertain to qualification of elastomers for non-O&G service conditions. MIL-P-25732C (Packing, Preformed, Petroleum Hydraulic Fluid Resistant, Section 3), MIL-G-21569B (Nitrile 70 Durometer O-ring, Section 4), and MIL-PRF-1149D (Performance Specification: Gasket Materials, Synthetic Rubber, 50 and 65 Durometer Hardness, Table II) are representative of classes of MIL-SPECs that cover acceptance testing of elastomers for military applications which are exposed to hydrocarbons at elevated temperatures but ambient pressures. Part of the recommended acceptance testing includes both dry heat elevated temperature testing and exposure to anticipated working fluids. Characteristic tests, such as tensile, compression set, and hardness are performed before and after testing to determine how the elastomer properties have changed. Acceptable ranges for changes in properties are provided, and select examples are shown in Table 20. While the materials specifications in these MIL-SPECs are not explicitly aligned with HPHT O&G needs, they do provide more assurance that such materials have good quality control tests compared to non-MIL-SPEC materials. It is still necessary to demonstrate that they will perform as required in the proposed HPHT environment.

**Table 20. Material property change criteria for selected MIL-SPEC standards.**

| Property Change | MIL-P-25732C | MIL-PRF-1149D |
|---|---|---|
| Hardness Change | +/- 10 | +/- 10 |
| Tensile Strength Decrease | 40% | 20% |
| Elongation Decrease | 45% | 35% |
| Compression Set Change | 55% | 25% |

## 5.2 Relevancy of Standards to HPHT Applications

### *5.2.1 Relevancy of Laboratory Qualification Testing*

It is the design engineer's responsibility to work with equipment manufacturers to determine threshold physical properties for elastomers in HPHT conditions. ASTM standards summarized as part of Table 18 include laboratory testing procedures for many of these standards. Material properties that may be pertinent include (WEST Engineering Services, 2009) the following below:

- High and low temperature testing;
- Hardness;
- Modulus at predetermined elongations;
- Ultimate elongation and tensile strength;
- Compression set; and
- Fluid compatibility.

Although ultimate tensile strength and elongation are easily measured in the laboratory, in most sealing applications the elastomer is confined in a gland, slot or housing and not completely free to move. Therefore, the elastomer is compressed and cannot experience these extreme forces, except in the narrow gland region where extrusion and crack tear propagation can occur.

The relative changes in the elastomer stiffness or modulus at various elongations, in particular 50% and 100%, are followed as a function of time to monitor aging and other property changes.

Hardness is the most universally reported characterization test result since it provides a reasonable correlation to the stiffness or compressive modulus of the material. It is relatively easy to measure and is used to monitor any changes in elastomer properties. For example, NBR rubber can get "harder", become brittle, and more likely to crumble at elevated temperature due to additional excess crosslinking. Other crosslinked elastomers with less residual unsaturation

can undergo chain scission and a softening of the material. However, hardness alone does not provide a complete depiction of the viscoelastic properties of elastomer formulations, since many compounds (NBR, FKM) can be cured to the same hardness, but have dramatically different mechanical and thermal performance. The low temperature performance of an elastomer is still important, even when service temperatures are elevated, because rapid, localized cooling can occur during depressurization events and cool the material below the glass transition temperature, where it becomes "glass-like" and brittle.

Elastomers are viscoelastic materials which once compressed into a gland and pressurized, may not recover its original dimensions once the pressure is reduced. When the elastomer does not return to its original shape the problem is called "compression set". How well the seal returns to its original form is typically a function of the temperature of the seal when it is deformed and released. This effect is magnified if the elastomer seal is over-compressed, in which case the seal may adapt the deformed geometry permanently, and cause leaks in the seal after pressure cycles.

### *5.2.2 Industry Feedback*

Most companies surveyed indicate that they comply with guidelines set forth by the API and ISO. They often follow their own internal standards as well. These internal standards frequently are not publicly available and may likely differ from organization to organization.

Service companies identified two primary areas where revised standards would be beneficial. First, service companies note that there are few common standards associated with storage or shelf life of elastomer components. If drilling or completion schedules are delayed, the possibility exists for downhole tools to arrive at the drill site for long-term storage prior to installation. A major complaint was that there are few standards that are required for the storage, handling, expiration dates and requalification procedures of elastomer component suppliers. Because of the unknown sample storage history, transportation conditions, and chain of custody issues, service companies can only guarantee performance of downhole equipment in its factory-accepted condition. Once the component is transported, service companies cannot guarantee performance.

Second, service companies indicate that they adhere to developed internal standards, which may meet, or even exceed, standards put in place by regulatory agencies such as BSEE. These internal standards are often required by other standards that do not explicitly specify material acceptance criteria (e.g., ISO14310:2008 or API 11D), but rather they require that suppliers/manufacturers (often service companies) follow their own documented specifications and acceptance criteria for elastomer components. While this regulatory approach allows for autonomy of service companies to create internal standards that best fits their products' needs, no universal standards are followed industry wide for elastomer use in HPHT applications. Development of industry-wide standards for HPHT elastomer selection would allow the industry as a whole to make selection decisions of elastomers to be used in their downhole tools and equipment based on the same criteria and encourages collaborative advancement of HPHT technologies.

## 5.3 Gap Analysis

Based on the selected standards reviewed as part of this study, a gap analysis, spanning gaps in elastomer material characterization and qualification testing, was conducted to determine in which areas standards could be improved to better reflect the requirements of service in HPHT environments. For this gap analysis, an oilfield component, such as a packer, was reviewed through each of the design steps. Each family of standards was evaluated across several categories, discussed below, designed to span the development of critical well components. A sample outline of the anticipated component development process is outlined in Figure 10. As part of this gap analysis, the development process of a well component (e.g., wellhead, packer, BOP, or SSSV) was broken down into six steps:

1. First, the overall component design is established between the operator and the service company. Guidance from some of the standards, as well as previous field experience, will help to shape the design requirements.

2. Second, appropriate materials of construction, including elastomers, will be selected based upon the design requirements.

3. Third, laboratory testing and qualification of materials is typically conducted to ensure that they will meet design requirements. This should include compatibility testing with chemicals anticipated to be present in the service environment, as well as elevated temperature and pressure testing which is representative of HPHT operating environment conditions.

4. Fourth, the component in its entirety should be tested to ensure that it functions properly fully assembled, and meets all design requirements.

5. Fifth, after acceptance testing of the component, the component should be properly packaged for shipment and storage, to ensure critical components, including elastomers, are protected.

6. Sixth, it is anticipated that validation testing will be performed on the component after installation in the well.

For each identified primary component design steps, standards were reviewed to determine the degree of guidance provided to evaluate key elastomer properties for HPHT environments. Standards were grouped by issuing organization for this evaluation. Table 21 shows which standards were found to be associated with specific steps in the component design process. Note that HPHT testing and chemical compatibility testing categories were identified as steps in this process.

As shown in Table 21, ISO and API standards typically provide guidance on overall well and component design criteria, as well as some component qualification and testing parameters (see Section 5.1.1 of this report). For select components, storage guidance is provided as part of ISO

10417 (or API 14B). NORSOK standards reviewed as part of this effort were focused on the elastomer materials present in components. Selection criteria for elastomers were provided in the NORSOK standards reviewed, as well as recommended chemical exposure testing processes. NACE and ASTM standards (see Section 5.1.2 of this report) each provide laboratory testing protocols for critical elastomer material properties, including chemical exposure suitability testing, but may not always be reflective of the range of all well chemistries. Although many standards recommend different chemicals be used for exposure testing (such as ISO 23936, ASTM D471, and NACE TM0297, TM0187, TM0296), no standard reviewed details how to best develop a surrogate chemical exposure testing environment reflective of actual well conditions.

One group of standards reviewed, MIL-SPEC, represents an adjacent standard covering military operations outside of the O&G industry. This was conducted to gather relevant information that might be transitioned into O&G standards. MIL-SPEC standards reviewed include those related to the qualification and inspection of elastomers used as seals in oil-based service environments, similar to chemical conditions encountered in drilling and production applications. MIL-SPEC standards MIL-G-21569B and MIL-PRF-1149D were found to contain useful guidance on selection of elastomers for military applications, qualification of the elastomers under relevant test conditions, laboratory testing procedures to document critical material properties, packaging, shipping, and storage procedures, as well as procedures for how to validate the properties of the elastomer product received in the field (see discussion in Section 5.1.4).

Standards reviewed show lack of performance criteria covering material property testing conducted at high pressure and high temperature (15,000 psi, 350°F) downhole conditions. Laboratory testing to identify changes in material properties after exposure to high temperature and high pressure conditions is necessary to fully qualify a given elastomer formulation for service in such an environment. Existing ISO, NORSOK, NACE, or ASTM standards do not require or provide guidance for testing at pressures exceeding the 15,000-psi definition of high pressure service for individual elastomers. Some of the material property tests call for exposure testing to be conducted at or near 350°F, but few tests require elevated temperature testing to be conducted beyond the threshold of high temperature O&G service. Since 350°F is the threshold for HPHT conditions, if materials are not tested beyond 350°F, they cannot be fully qualified for HPHT service. Laboratory testing of elastomeric properties at HPHT conditions is essential to fully understand the behavior of critical elastomer components under expected service conditions.

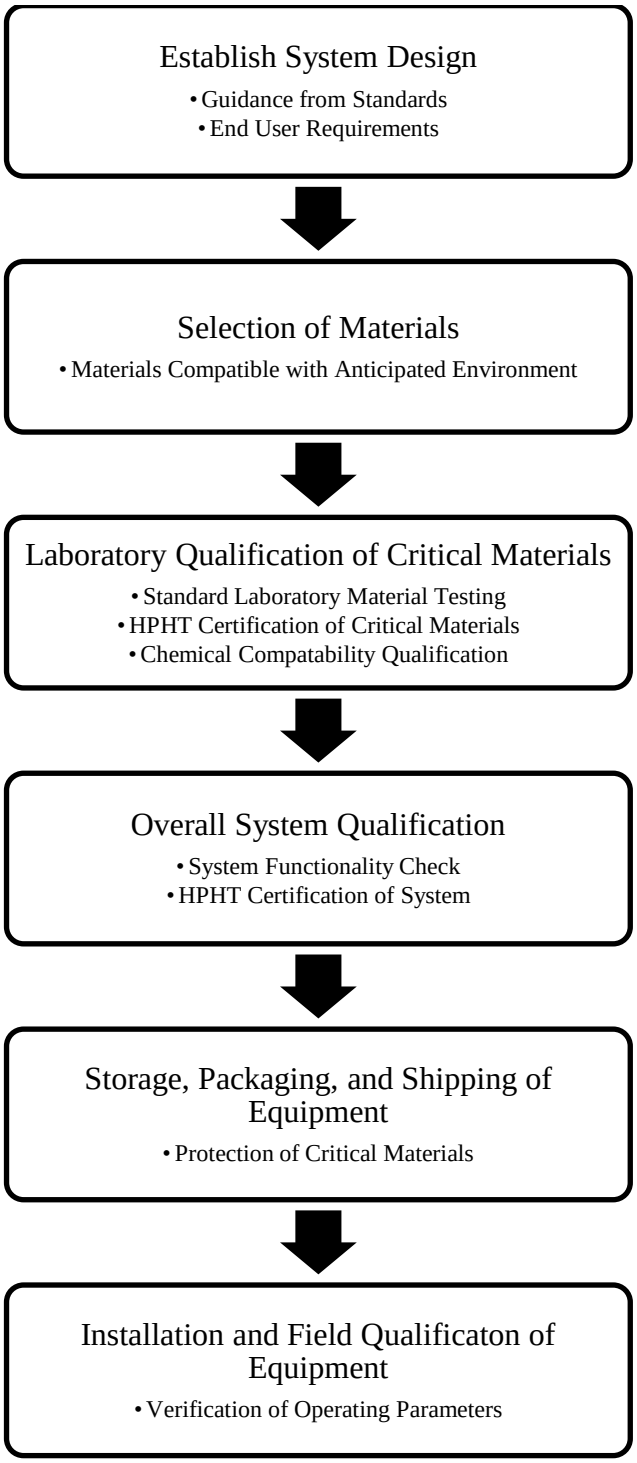


**Figure 10. Sample component development process derived for use in this gap analysis.**

In addition to laboratory testing of elastomer components under HPHT conditions, the entire component (e.g., entire wellhead, packer, BOP, or SSSV) should be evaluated for overall functionality at HPHT conditions prior to being placed in service. Few ISO and API (with exception of API 11D and 14A) standards reviewed do not indicate that HPHT conditions must be used to test the component before installation. However, care must be taken to ensure that QC tests that are developed do not permanently damage each component before sale. Evaluation of the component's performance after shipping and storage is essential, as elastomers can become damaged if improperly protected during shipment or storage. Damage in shipping may result in a change in the material properties of the elastomer, often compromising the functionality of the overall component.

MIL-SPEC standards reviewed present an example of how standards can be adapted to include all aspects of the product development lifecycle. MIL-SPECS provide the most guidance of any standard agency evaluated for all points in a component development process. New or revised standards specifically designed for O&G applications can be focused to better address the gaps in current ISO or API standards which MIL-SPEC standards address for military industries.

In some instances, notable differences exist in testing standards for the same material properties. For example, both ISO 23936-2 Annex B and NACE TM0192 Section 4 provide guidelines for RGD testing of elastomers, but require vastly different test conditions. The NACE standard (TM0192) requires tests to be conducted at room temperature and pressures not to exceed 750 psi. The recommended test gas is $CO_2$. ISO 23936-2 provides several available temperature test options up to 212°F and allows for pressures up to 2,175 psi. These tests are conducted in a more complex gas environment, comprising a mixture of $CO_2$ and $CH_4$.

Each test detailed in ISO 23936-2 Annex B and NACE TM0192 predicts different RGD properties for the same material (Edmond, et al., 2001) due to the different test conditions. This shows the importance of not only selecting the correct temperature and pressure for testing that are representative of downhole conditions, but selecting appropriate test media and parameters (e.g., decompression rate) that are representative of field service conditions. This illustrates a critical conclusion from this gap analysis is that standards need to provide testing guidance that reflects actual downhole conditions encountered before and after elastomer components are placed into service. This unmet need is illustrated by the lack of test protocols for high pressure testing, and tests that incorporate chemical compatibility tests using constituents found downhole.

**Table 21. Standard issuing agencies which provide guidance to different steps in the component design process.**

| | | Evaluated Standard | | | | | |
|---|---|---|---|---|---|---|---|
| **Process** | **Notes** | **API** | **ISO** | **NORSOK** | **NACE** | **ASTM** | **MIL-SPEC** |
| System Design Guidance | Overall system/tool performance criteria | X | X | | | | |
| Material Selection Guidance | Selection of most appropriate elastomer | | | X | | | X |
| Laboratory Material Qualification | Lab testing of material properties | | | | X | X | X |
| HPHT Laboratory Qualification | HPHT laboratory testing of properties | | | | | | |
| Chemical Compatibility Qualification | Lab chemical compatibility testing | | | X | X | X | X |
| Installed System Qualification | Performance testing of system/tool | X | X | | | | |
| HPHT System Qualification | HPHT testing of system/tool | | | | | | |
| Storage/Shipping Guidance | Packaging and storage considerations | X | X | | | | X |
| Field Requalification | Evaluation of system components in field | | | | | | X |

## 5.4 Primary Findings and Recommendations from Standards Analysis

*Finding 1: Temperatures and pressures for recommended testing are specified below HPHT thresholds.*

One of the largest gaps identified was that recommended testing standards, including ISO, NACE and NORSOK, were designed to be conducted at temperatures and pressures not reflective of extreme HPHT conditions. For example, ISO 23936 and NORSOK M-710 identify maximum pressures of 2,175 psi and maximum temperatures of 212°F to conduct materials compatibility testing. The temperature and pressure recommendations are well below the HPHT threshold pressure and temperature of 15,000 psi and 350°F. Conducting qualification tests for critical elastomer properties at temperatures and pressures less than anticipated HPHT conditions can result in improper conclusions being reached pertaining to material properties. For example, materials not susceptible to degradation at room temperature may experience softening and loss of critical properties at elevated temperatures. If critical material properties are not validated in the laboratory, field failures in the field are likely to occur, which are more detrimental to project safety, schedule, and budget.

*Finding 2: Complex downhole chemical environments are not accounted for in most existing standards.*

In addition, most chemical exposure suitability or compatibility tests were not required to be conducted with chemicals or chemical mixtures that accurately represent those constituents found downhole. ISO 23936 Section A.1.1 provides some guidance for exposure to chemical fluids, but does not define acceptable concentrations of downhole chemicals often present, including drilling fluids, hydrate, scale and corrosion inhibitors. Rather, simple hydrocarbon gases and liquid are used (such as methane and heptane).

The tests described in NACE TM0187, TM0296, and TM0297 all include laboratory testing of elastomers under elevated temperatures and pressures (up to 5,000 psi and 445°F) after exposure to working fluids similar to those found in O&G applications. Similarly, ASTM D471 provides test procedures to determine chemical and physical properties of elastomers in laboratory environments. The ASTM standard calls for testing to be conducted at elevated temperatures; however ambient pressures are used during testing. Table 18 compares these standards in additional detail.

*Finding 3: Shipping and storage conditions for elastomers are often not specified by existing standards.*

Many of the API, ISO, and NORSOK standards reviewed do not include guidance pertaining to how elastomer components should be protected during shipment and stored prior to installation. The storage duration and conditions can alter the elastomer's performance; therefore, it is critical that shipping and storage operations be conducted in a manner such that the elastomeric properties of components are not compromised. In general, storage temperatures should be less than 100°F with a humidity level of less than 75% (see Table 18). Elastomer products should be individually packaged and protected from ultraviolet exposure. ISO 27996 Section 6 states that the recommended maximum storage timeframes for NBR and HNBR shall be 112 months, and for FKM, FFKM, and FEPM, for 160 months. After this period of time, elastomers are not guaranteed to function as designed. MIL-SPEC standards MIL-P-25732 (Section 3) and MIL-PRF-1149D (Table II) were reviewed and appeared to provide sufficient guidance regarding acceptance criteria in these areas (see Appendix A.3). A similar approach may be applied to ISO/API standards governing elastomer use in HPHT environments. Additionally, MIL-G-21569 Section 4 provides examples of how to requalify elastomers for service after long periods of storage, including selection criteria for statistical qualification analysis, which may also be applicable to the O&G industry.

*Recommendation:*

The gap analysis conducted shows that no single family of standard provides complete guidance for elastomer selection, qualification, packaging, and storage for HPHT conditions (see Table 22). Consolidation of standards under a single standard organization (such as API) would allow for more uniform coverage of "cradle to grave" standardization of elastomer use in O&G operations.

# 6.0 MATERIAL PROPERTY TESTING

## 6.1 Technical Approach

Three different sets of material property tests were conducted to aid in the development of the FEA model.

In the first set of tests, Battelle conducted baseline testing using both slabs (~1 mm x ~ 160 mm x 160 mm) and O-rings (AS568-210) for each material. AS568 refers to the Aerospace Standard 568 published by the Society of Automotive Engineers where the size is shown after the hyphen (e.g., -210). Small samples (per ASTM D471) from the material slabs were used to conduct exposure testing in the silicone hydraulic fluid used in the HPHT experimental test cell. Exposure testing allowed Battelle to evaluate whether swelling of elastomers would need to be accounted for during HPHT testing or FEA model development. Additionally, O-rings themselves were tested in accordance with associated MIL-SPEC guidelines to ensure that the O-rings procured for use in this study conformed to design specifications.

During the second set of testing, traditional material tests were used to evaluate hyperelastic material behaviors for use in FEA model development. This testing was led by Battelle's subcontractor Endurica. The following hyperelastic material tests were conducted for each of the five elastomers evaluated as part of this study:

a) Quasi-static Cyclic Simple Tension

b) Quasi-static Cyclic Planar Tension

c) Quasi-static Cyclic Equibiaxial Tension

d) Volumetric Compression

e) Thermal Expansion

f) Tearing Energy

g) Creep Crack Growth Rate

When required, test procedures were modified to allow for testing at elevated temperatures, ensuring results were aligned with high temperature field service conditions. All materials were tested at temperatures of 100°C (212°F). Materials with recommended service temperatures above 200°C (FKM, FFKM, and FEPM) were also tested at an elevated temperature of 175°C (347°F). HNBR has a recommended maximum operating temperature of 160°C, so it was tested at a maximum of 150°C (302°F). NBR was the only material not tested above 100°C, as its maximum operating temperature is 120°C.

Finally, Battelle conducted a series of additional materials characterization testing to provide an additional level of precision to the data previously gathered for model development. This testing included dynamic mechanical analysis (DMA) and multiaxial expansion membrane inflation tests. Sections 6.8 and 6.9 of this report provide information about these tests.

## 6.2 Elastomer Tests for Hyperelastic Material Models in Finite Element Analysis

### *6.2.1 Quasi-static Cyclic Tension*

Quasi-static cyclic tension testing was conducted by Battelle's subcontractor Endurica. The test objective was to collect data inputs for use in development of the FEA model. Stress and strain data sets were collected by stretching the elastomer in a series of tests, and then fitting the data set to curves which in turn describe the material parameters. The curves fit to the test data were then used as inputs for the FEA model. The different stress-strain tests conducted include:

a) Quasi-static Cyclic Simple Tension: (no lateral constraint to prevent specimen thinning; a pure tensile strain)

b) Quasi-static Cyclic Planar Tension: (completely constrained in the lateral direction: a pure shear strain test)

c) Quasi-static Cyclic Equibiaxial Tension: (equally constrained in radial direction; a pure compression strain test)

Figure 11 shows representative fitted curves of simple tension, planar tension, and biaxial tension for the FKM-75 elastomer. The measured stress versus strain at 20% strain is proportional to the values of yield stress at break for each elastomer material, so stretching each coupon to failure is not required for accurate inputs to the FEA model.

For each of the materials tested, three simple tension specimens, three planar tension specimens, and three equibiaxial specimens were cut from slabs of each elastomer material (measuring 150 mm by 150 mm by 1.0 to 2.0 mm thick). The specimens were loaded slowly between zero force and the defined stretch level for five cycles of loading and unloading at four different strain levels. This provided the initial stress-strain behavior and the "stabilized"[3] stress-strain behavior at each of the strain conditions.

[3] Mullins effect

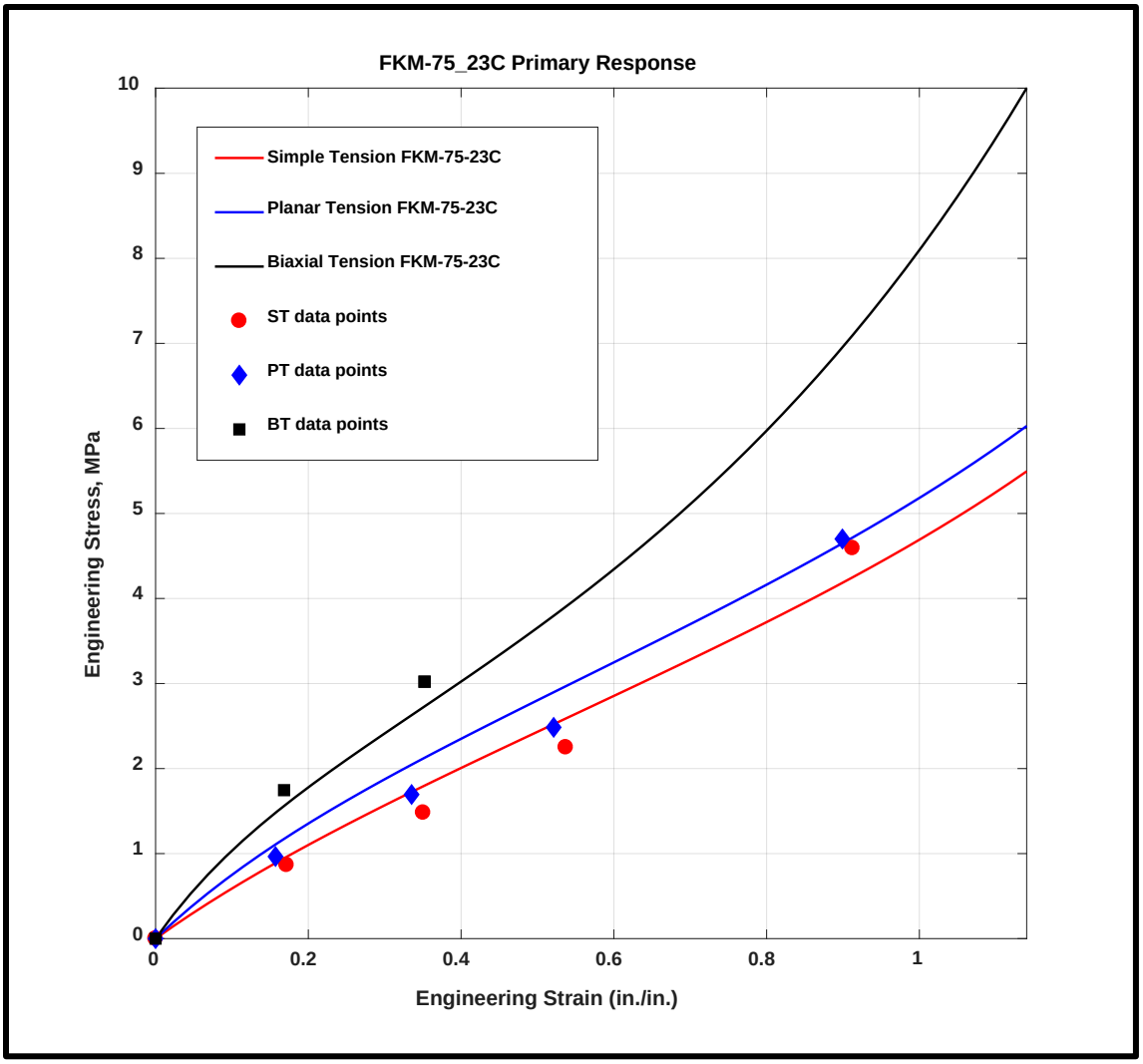


**Figure 11. Representative plot of stress versus strain data for FKM-75 elastomer.**

Figure 12 shows force diagrams for each of the three types of tests, and Figure 13 shows representative test coupons used for testing.

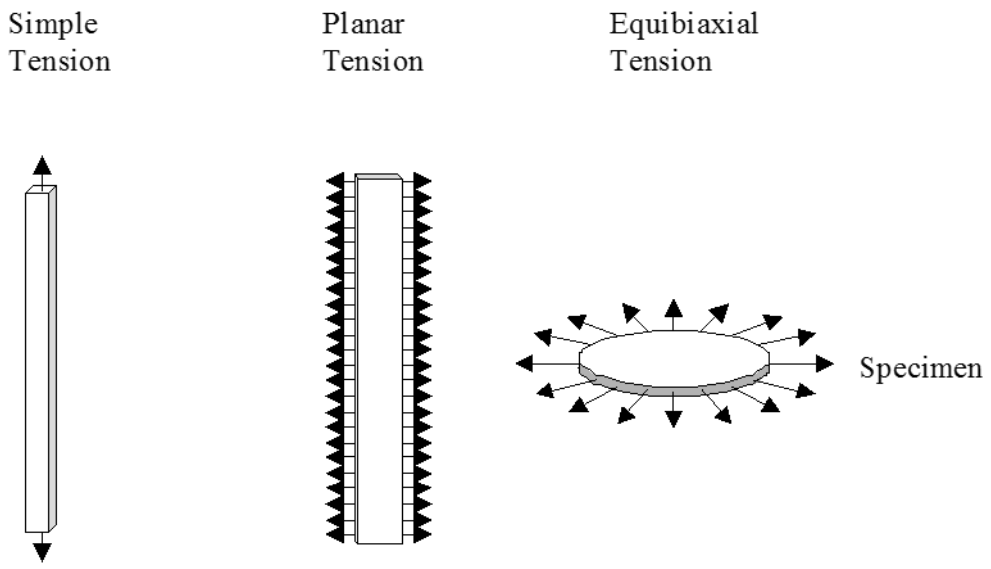


**Figure 12. Force diagrams for simple, planar, and equibiaxial tension tests (Endurica, LLC, 2015).**

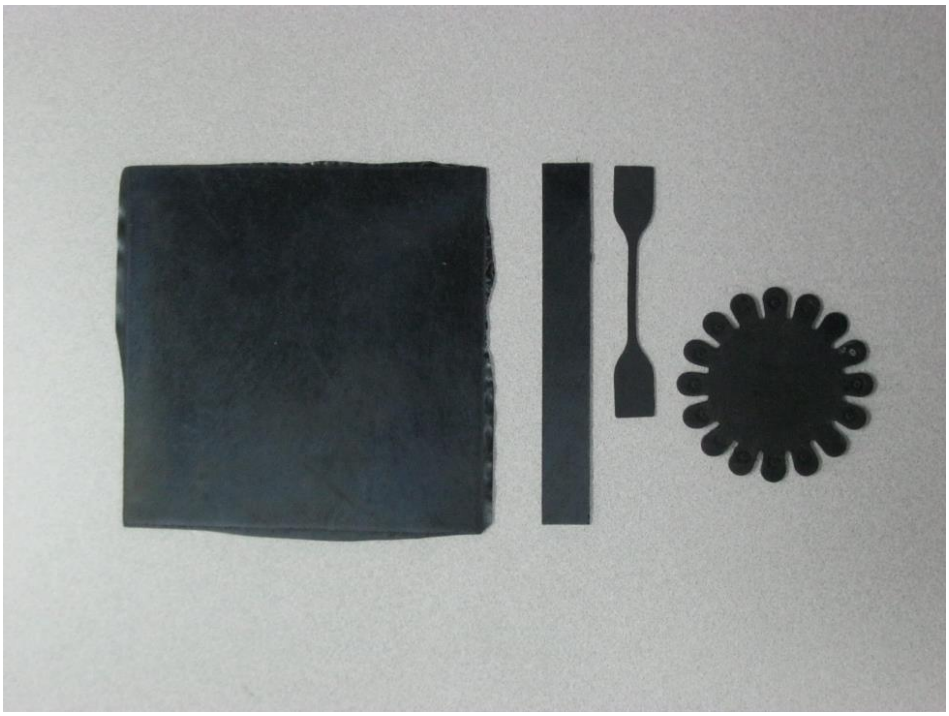

**Figure 13. Uncut slab (left), planar tension test coupon (second from left), simple tension test coupon (second from right), and equibiaxial test coupon (right) (stock photo, (Endurica, LLC, 2015).**

Figure 14 shows the test apparatus used for simple tension testing. For a test, a load is applied only in the longitudinal direction of the test coupon.

**Figure 14. Simple tension test apparatus stock photo, (Endurica, LLC, 2015).**

Figures 15 and 16 show raw data plots from the testing of FKM-75 and FKM-90 test coupons. Each plot shows the cycles applied to the test coupon during the test sequence. Note the first pull of each test coupon results in a higher stress for a given strain level than the following pulls. This behavior is referred to as the Mullins effect. A full data analysis for each of the elastomers is included in Appendix A.4.

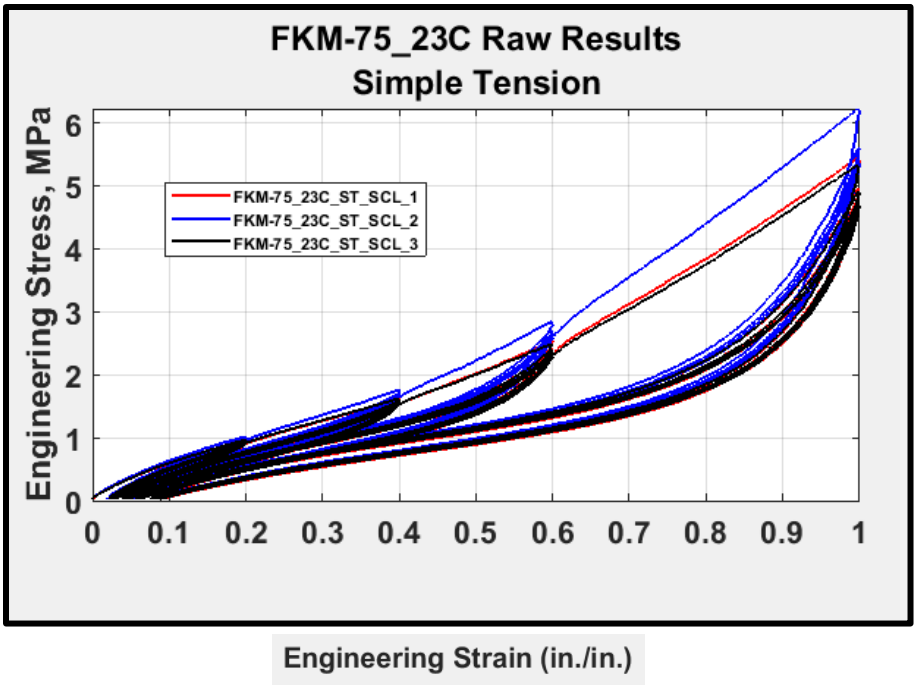


**Figure 15. Raw stress-strain results in simple tension for FKM-75 at 23°C.**

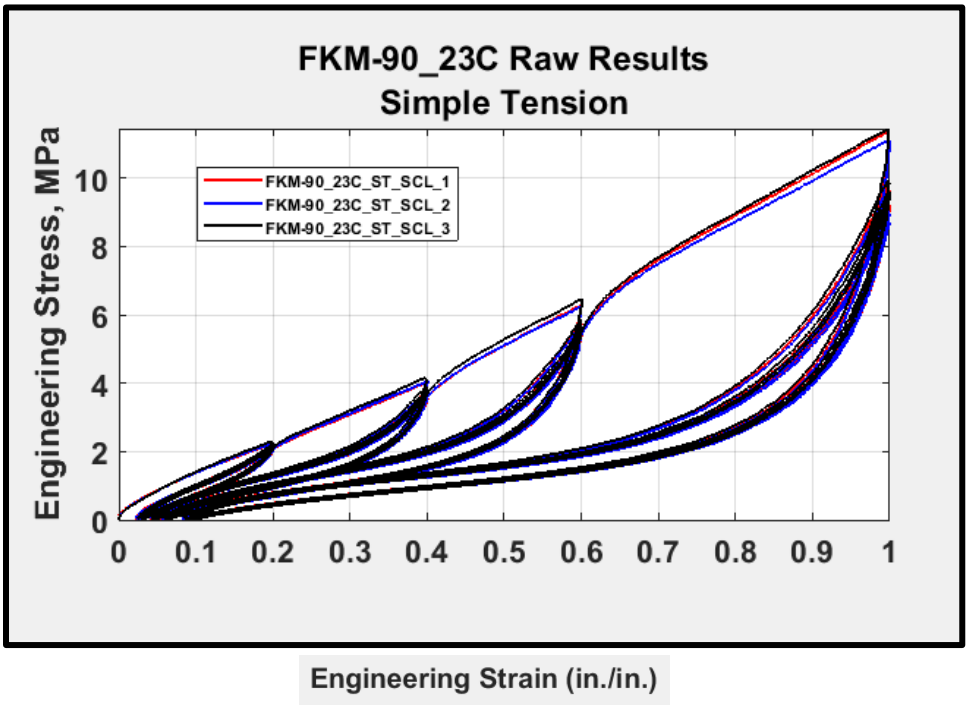


**Figure 16. Raw stress-strain results in simple tension for FKM-90 (left to right) at 23°C.**

Figure 17 shows the test apparatus used for planar tension evaluation. For these tests, the load was applied in the planar direction of the test coupon.

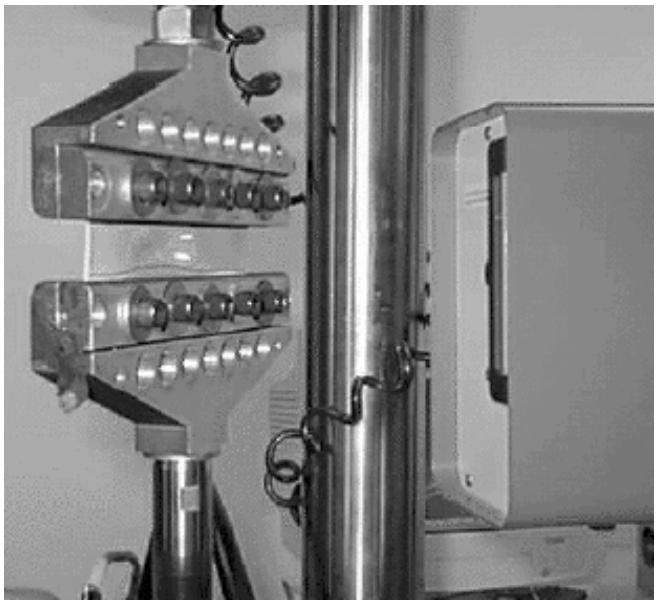

**Figure 17. Planar tension test apparatus (Endurica, LLC, 2015).**

Figures 18 and 19 show raw data plots from the testing of FKM-75 and FKM-90 test coupons. Each plot shows the cycles applied to the test coupon during the test sequence. Again, the Mullins effect can be seen on the first pull of each test coupon. A full data analysis for each of the elastomers is included in Appendix A.4.

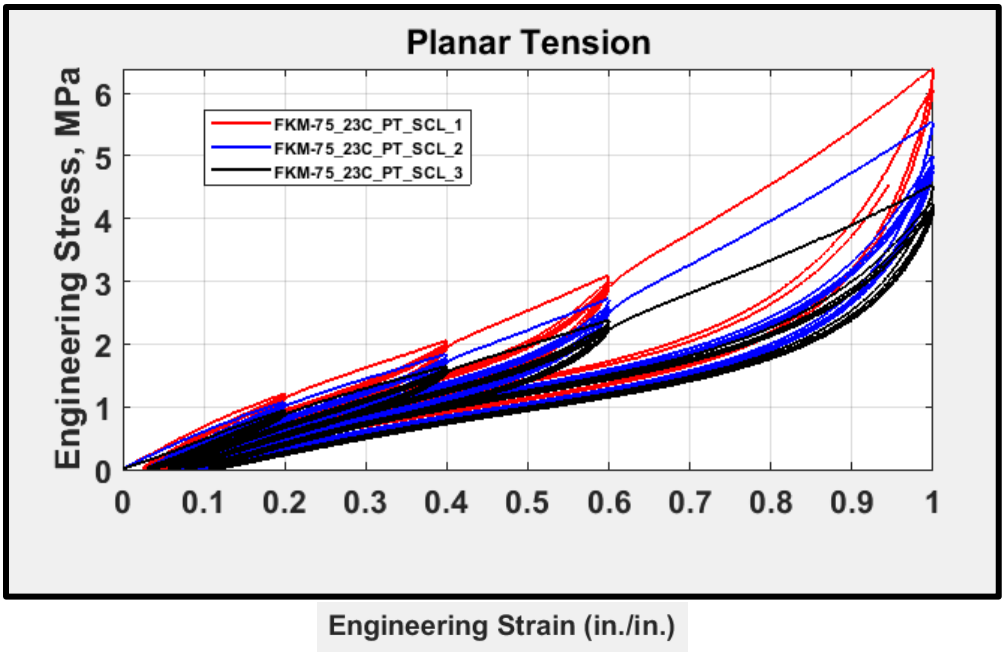


**Figure 18. Raw stress-strain results in planar tension for FKM-75 at 23°C.**

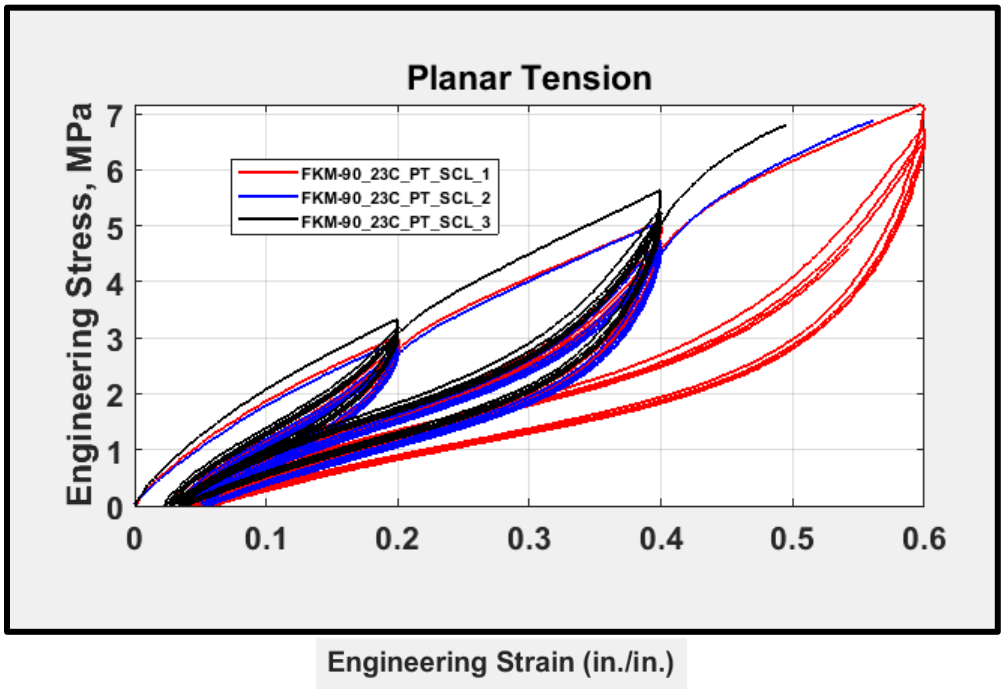


**Figure 19. Raw stress-strain results in planar tension for FKM-90 at 23°C.**

Figure 20 shows the test apparatus used for equal biaxial extension evaluation (referred to as equibiaxial tension). For incompressible or nearly incompressible materials, equibiaxial tension

creates a state of strain equivalent to pure compression. For these tests, load is applied equally in all directions in the plane of the test coupon.

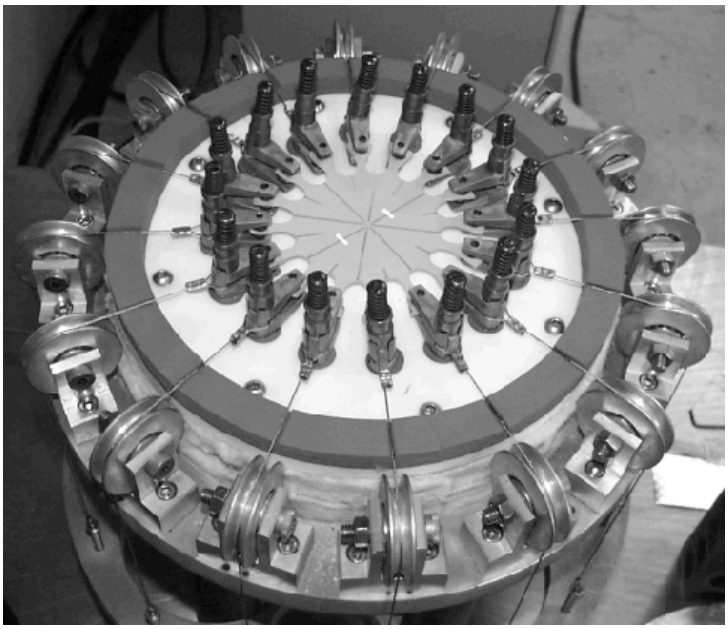

**Figure 20. Equibiaxial tension test apparatus (Endurica, LLC, 2015).**

Figures 21 and 22 show raw data plots from the testing of FKM-75 and FKM-90 test coupons. Each plot shows the cycles applied to the test coupon during the test sequence. The results of these tests also show the Mullins effect on the first pull of each test. A full data analysis for each of the elastomers is included in Appendix A.4.

The simple, planar, and equibiaxial data were fitted to curves to develop Mooney-Rivlin coefficients needed as inputs for the FEA model. The results of the fitting with associated coefficients are included in Appendix A.4.

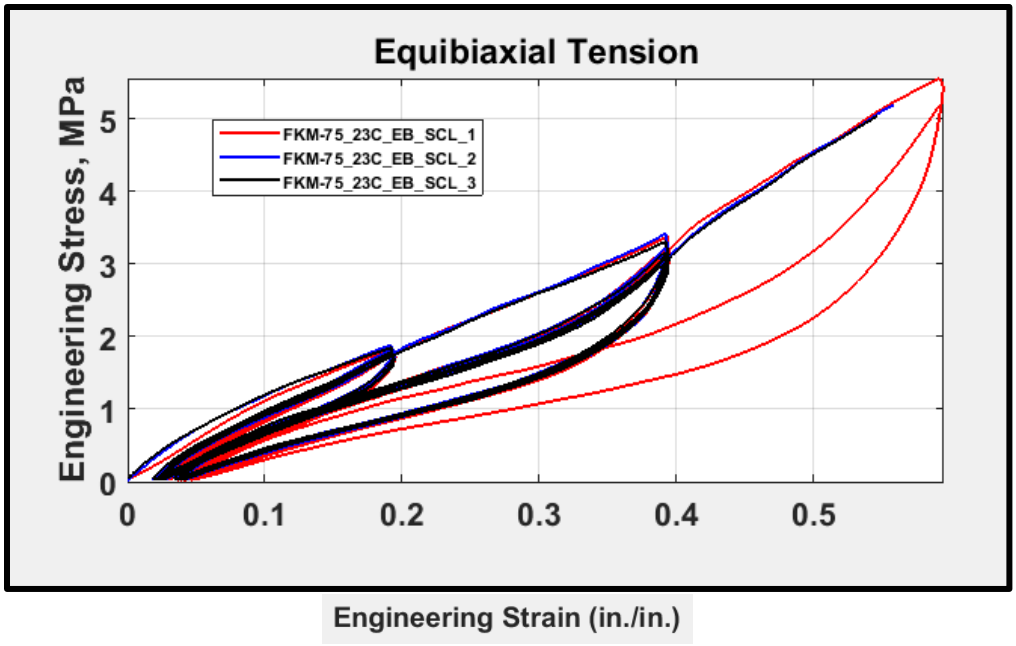


**Figure 21. Raw stress-strain results in equibiaxial tension for FKM-75 at 23°C.**

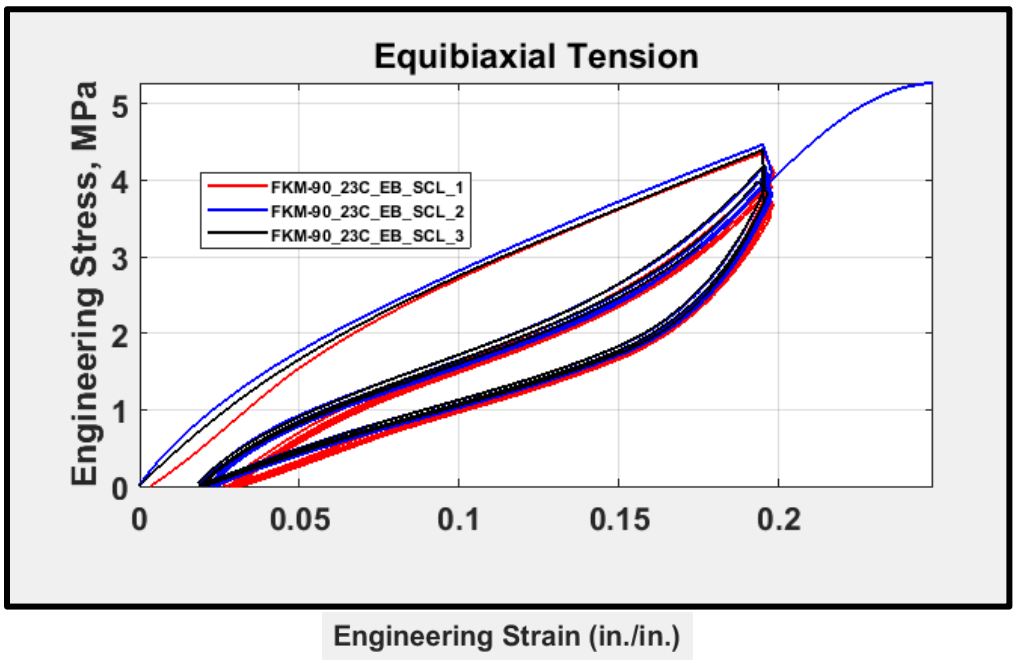


**Figure 22. Raw stress-strain results in equibiaxial tension for FKM-90 at 23°C.**

### *6.2.2 Volumetric Compression*

Testing to determine the elastomers' response to physical compression (volumetric compression), expansion, and temperature change was also conducted for each material.

Volumetric compression testing was conducted to determine the bulk modulus of each elastomer. Test coupons were 6.35 mm diameter disks cut from standard slabs and stacked within the test apparatus. A piston was then used to apply force to the elastomer, and its stress under the applied force was measured. Figure 23 shows the apparatus used in testing. Figure 24 and Figure 25 show representative data for FKM-75 and FKM-90 materials, respectively. The initial slope of the curves up to a strain of approximately 0.03 (3% compression) in Figure 24 and Figure 25 is defined as the bulk modulus or the compressive modulus.

**Figure 23. Volumetric compression test apparatus (Endurica, LLC, 2015).**

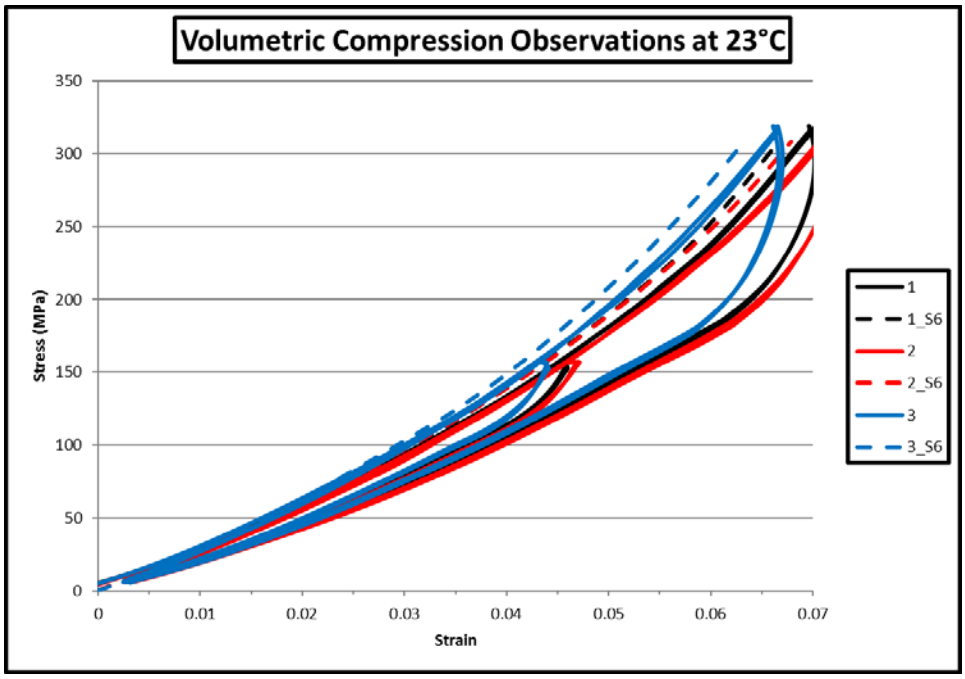


**Figure 24. Raw stress-strain results for volumetric compression testing of FKM-75 at 23°C.**

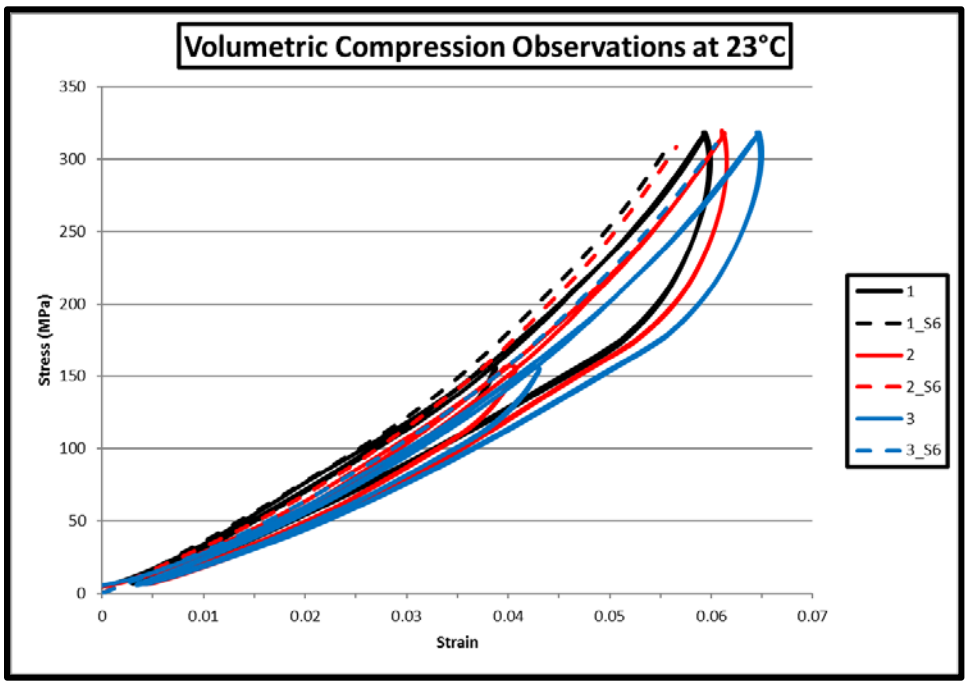


**Figure 25. Raw stress-strain results for volumetric compression testing of FKM-90 at 23°C.**

Thermal expansion testing was conducted to determine how the elastomers expand with increasing temperature. A thermomechanical analyzer (Figure 26) was used for thermal expansion testing. Test coupons were cut and held in the test apparatus, while temperature was varied between -75°C and 150°C at 0.5°C/min. The expansion ratio of the material, defined as the ratio of its size at the test temperature compared to the reference temperature (room temperature), was determined throughout the temperature range. The resulting data are shown in Figures 27 and 28. Two coefficients of thermal expansion were measured as the slopes of the linear regions of the plots, one for low temperature (below 0°C) and one for high temperature (above 50°C).

**Figure 26. Thermomechanical analyzer used for thermal expansion testing (Miller).**

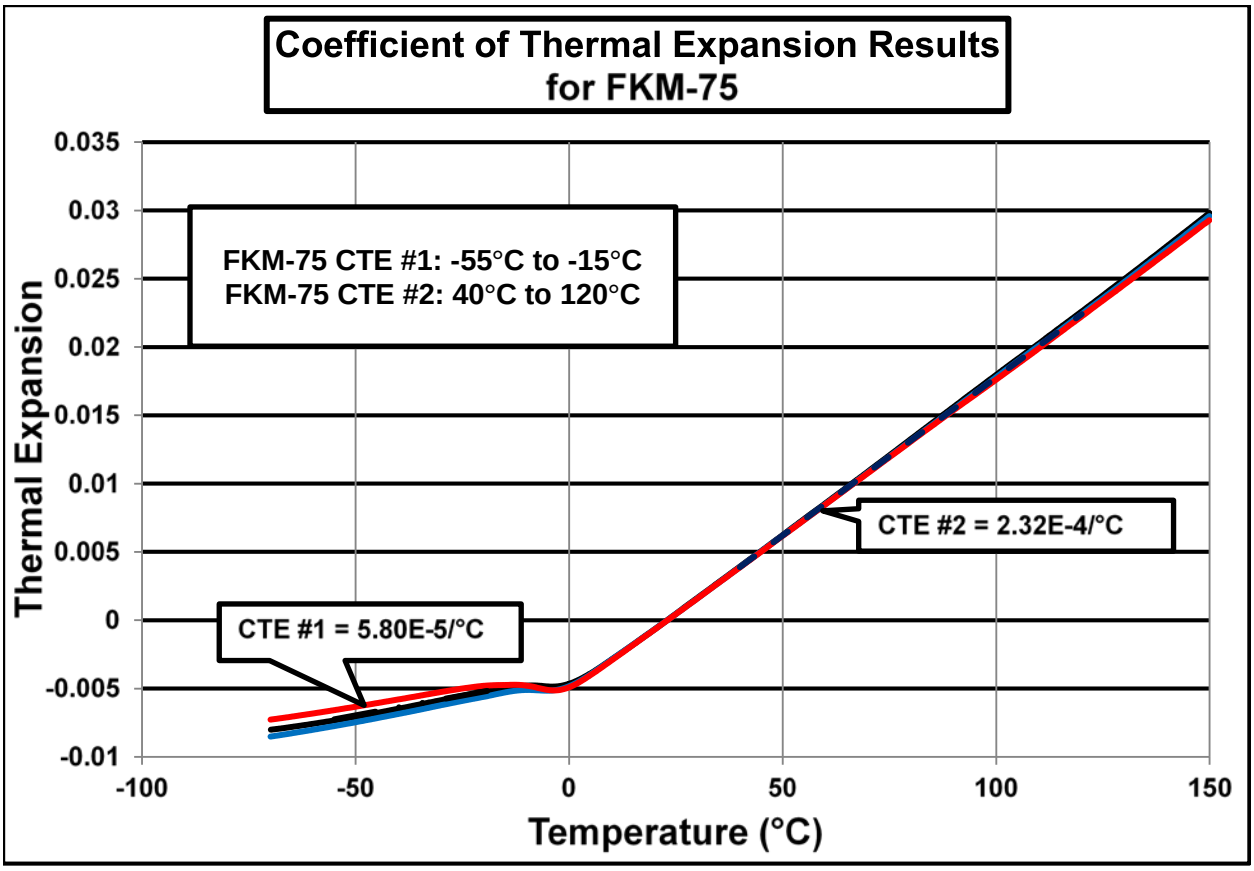


**Figure 27. Thermal expansion fit and observations of three replicates of FKM-75.**

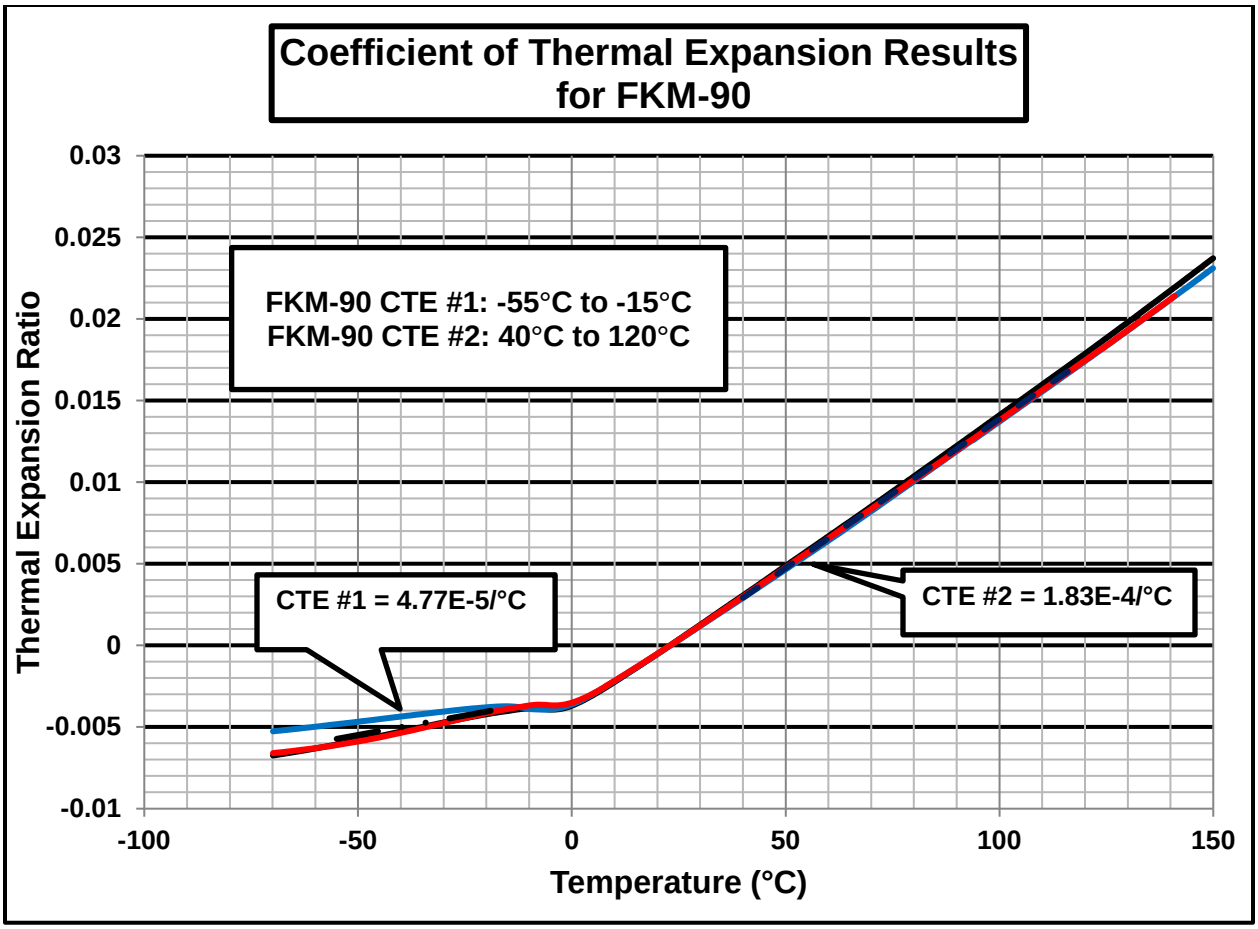


**Figure 28. Thermal expansion fit and observations of three replicates of FKM-90.**

### *6.2.3 Tearing Energy*

During initial O-ring HPHT testing (Task 4), the Battelle team observed tearing of the O-rings as they were extruded in the test fixture. This tearing is believed to occur as the O-ring material is extruded from the gap due to the high energy state of the elastomer during compression. In order to incorporate this phenomena into the FEA model, measurements of the tearing energy and crack growth rates were obtained through laboratory tests.

The tearing energy was identified as the energy that caused catastrophic crack growth in a single loading. The tearing energy test was conducted using the same test coupon dimension for the planar test; however, an initial cut was placed in the test coupon (approximately 25 mm in depth [Figure 29]). A load was applied to the specimen to create a strain of 1% per second. This test was conducted at temperatures of 23°C, 100°C, 150°C, and 175°C. Figure 30 shows a representative plot of FEPM-80 material. The resulting data were compiled into inputs for the FEA model.

**Figure 29. Image of initial tear in elastomer test coupon for tearing energy test (Endurica, LLC, 2015).**

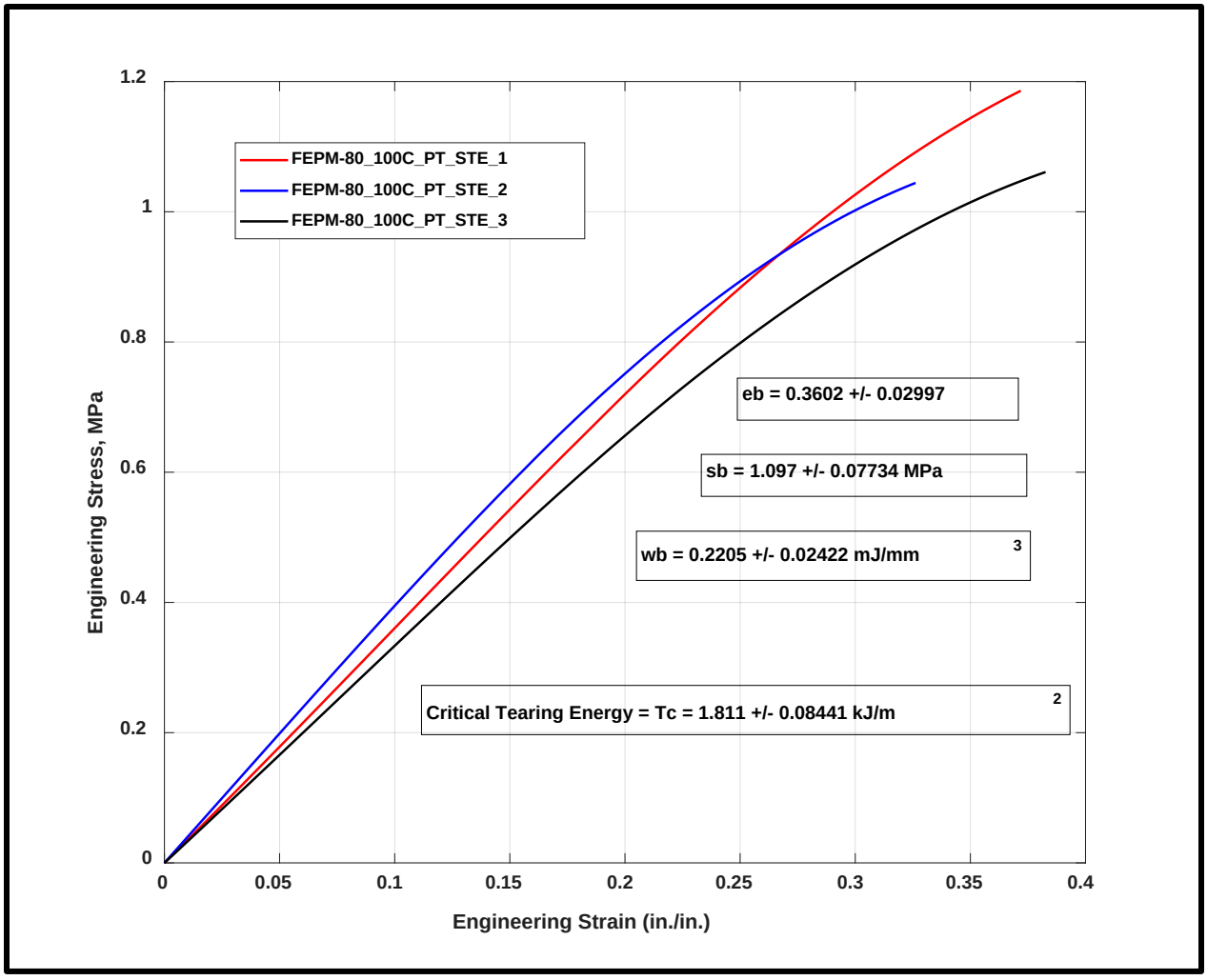


**Figure 30. Critical tearing energy plot of stress versus strain for FEPM-80.**

### *6.2.4 Creep Crack Growth Rate*

Creep crack growth rate is a measure of the crack propagation of an elastomer at a given strain rate. The crack growth rate test uses the same type of test coupon as the planar tension test. A camera was used to track the propagation of the crack over time. The apparatus is shown in Figure 31. Figure 32 shows a closeup view of the camera with the hot box installed. The hot box was used to maintain test coupon temperature during the elevated temperature test runs.

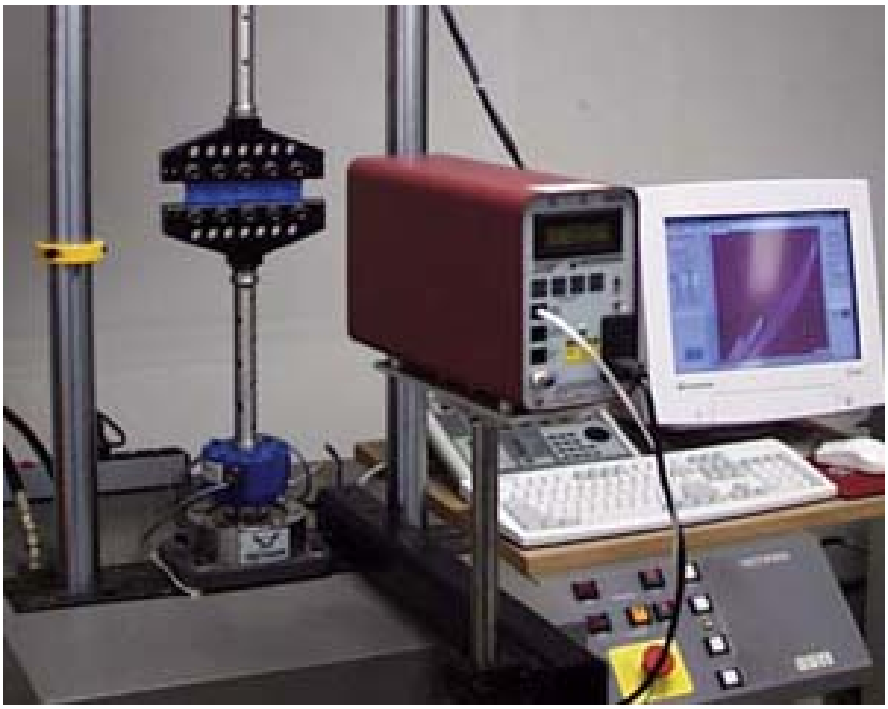

**Figure 31. Creep crack growth test apparatus (Endurica, LLC, 2015).**

**Figure 32. Camera and heat box for creep crack growth test (Endurica, LLC, 2015).**

During the test, the crack growth rate was observed by the camera; the data were plotted as the length of the crack versus time. This can be seen in Figure 33, which is a digitized image based on the observations recorded by the camera throughout the experiment. Crack propagation was tracked in both the vertical (y) and horizontal (x) axes of movement. Figure 34 shows a graph of the crack length in the x axis plotted against the experiment time. From this plot, crack propagation rates can be determined. Figure 35 shows stress plotted against strain for the test. Note that Figures 33 through 35 show individual plots for each of the three replicates of the test.

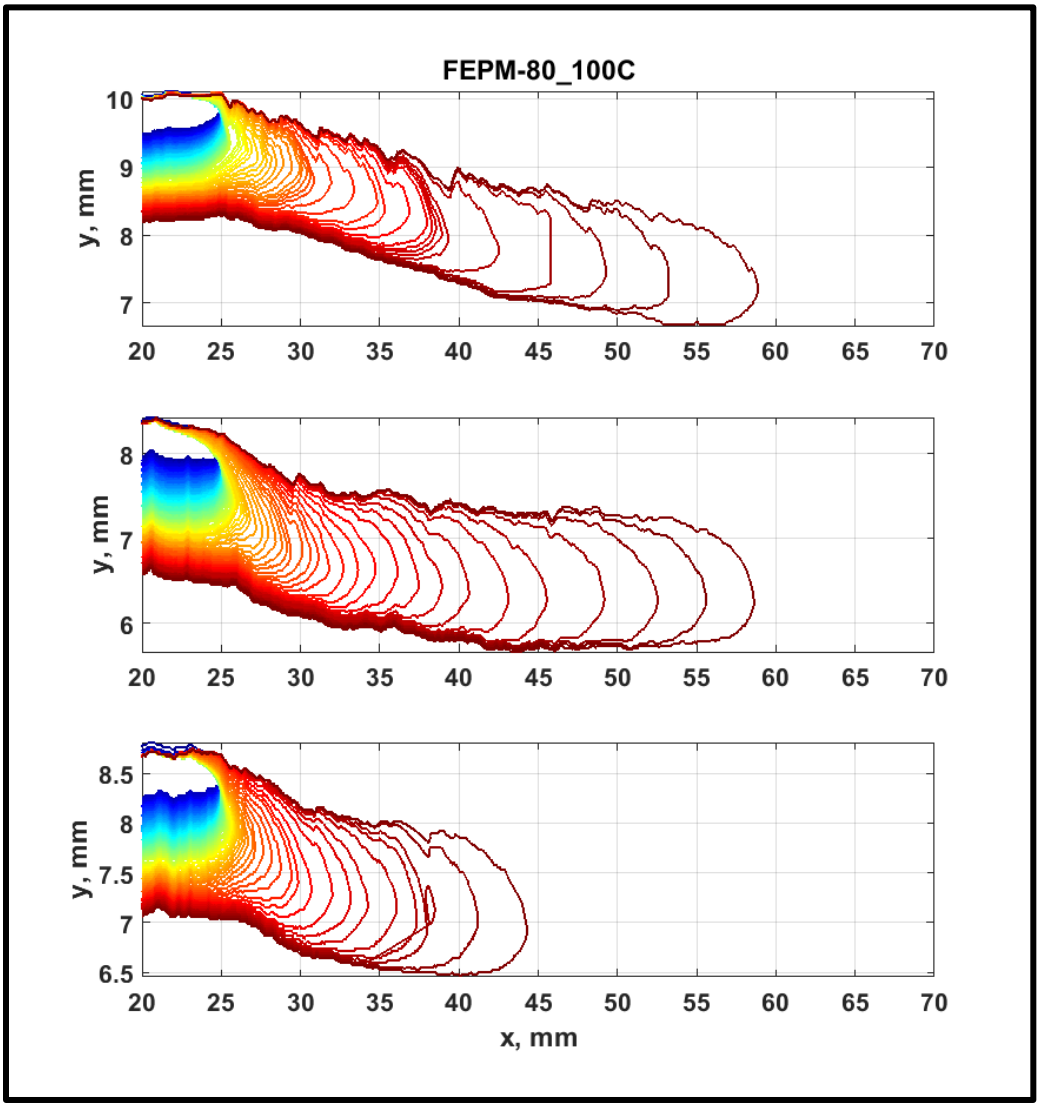


**Figure 33. Digitized camera view of the crack propagation of FEPM-80 material.**

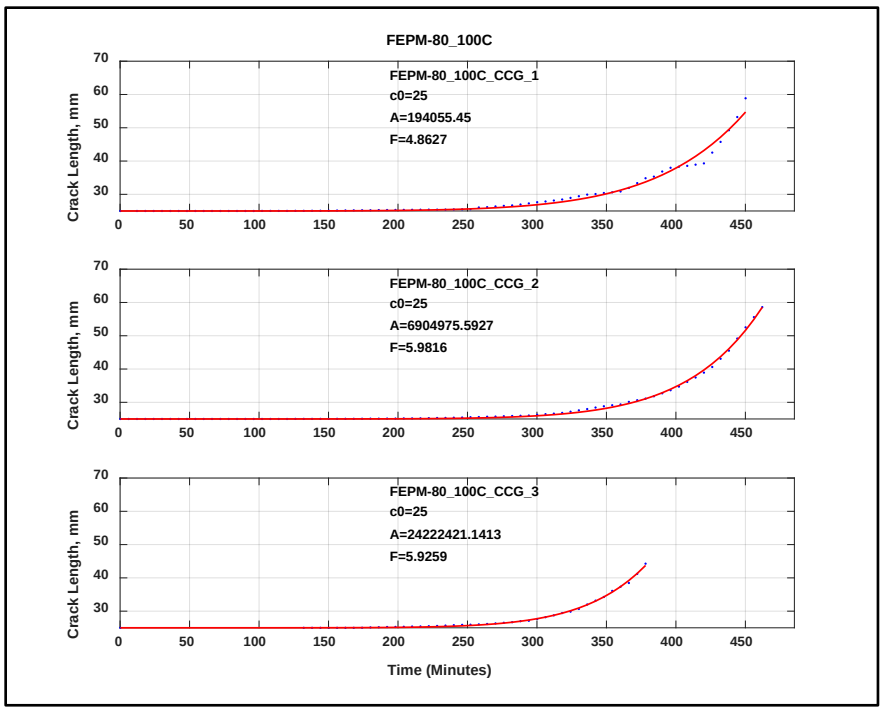


**Figure 34. Crack length versus time for FEPM-80 material.**

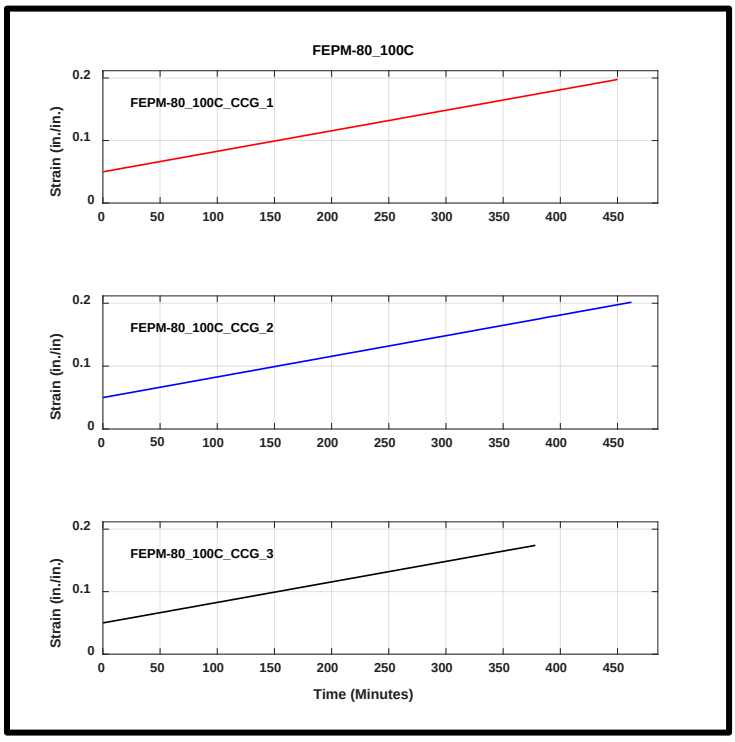


**Figure 35. Stress versus strain details for FEPM-80 material.**

## 6.3 HPHT Elastomer Property Testing at Battelle

### *6.3.1 Swelling Tests for Elastomers*

When seals come in contact with fluids having chemical properties similar to the elastomer, the fluid can enter into the polymer network resulting in swelling. Most of the time this swelling is reversible once the fluid is removed; however, the elastomer's physical properties are generally diminished in a swelled state. Further, if swelling is too extreme, the seal can be extruded and/or cause undue stresses in the seal housing. ISO 23936-2:2011 Annex E was presented as one of the standards providing guidance for elastomer exposure testing. This approach was used as a starting point for swell testing, which was based on ASTM D471.

Battelle conducted a literature review to determine the effect of fluid medium on the expected solvent resistance properties for the five types of elastomers in the same fluid to be used by PetroMar for the HPHT testing (silicone oil, polydimethylsiloxane fluid). Table 22 outlines the overall compatibility ratings for elastomers with silicone oil, showing that they would all be resistant to solvents (Precision Polymer Engineering, n.d.).

**Table 22. Compatibility ratings for elastomers with silicone oil (Precision Polymer Engineering, n.d.).**

| Elastomers | | | | | |
|---|---|---|---|---|---|
| | FFKM | FEPM | FKM | HNBR | NBR |
| Minimum Temperature °C | -15 | -25 | -40 | -30 | -50 |
| Maximum Temperature °C | 325 | 290 | 275 | 175 | 125 |
| **Overall Compatibility Rating for Silicone Oil** | **1** | **1** | **1** | **1** | **1** |

| Key | |
|---|---|
| 1 | Excellent |
| 2 | Good |
| 3 | Doubtful |
| 4 | Do not use |

To confirm the swelling effects level, Battelle conducted elevated temperature exposure of samples of FKM and NBR. The testing followed ASTM D471-15, which has a default ambient test temperature of 23 ± 2°C, and with Table 3A providing an alternative test temperature of 175 ± 2°C (347 ± 4°F). This was also in agreement with recommendations outlined in ISO 1817:2011 "Rubber, vulcanized or thermoplastic- Determination of the effect of liquids". From Section 7.1 *"Temperature, tests intended to simulate service conditions using the actual liquid with which the rubber will be used the test temperature should be equal to or greater than the*

*service temperature."* For that reason, room temperature immersion testing was not conducted. Another example of industry standard exposure testing specific for FKM in DC-200 silicone fluid at elevated temperature (175 ºC) is shown in Table 23.

The samples were exposed to the same DC-200 silicone fluid (also called E200; 100 centipoise) being used by PetroMar to conduct the HPHT testing for Task 4. The exposure was for 28 days at 175°C. Changes in mass or dimensions for the FKM samples were recorded and are shown in Table 24 and Table 25, respectively. The results are similar to published immersion properties for FKM in DC-200 silicone fluid (Table 23) which showed little change in volume. The mass changes were 0.71 +/- 0.44% mass/mass and 0.42 +/- 0.10 % mass/mass for FKM-75 and FKM-90, respectively. Dimensional changes were 0.09 +/- 0.21% (thickness/thickness) and 0.48 +/- 0.26% (thickness/thickness) for the FKM-75 and FKM-90, respectively. In addition, hardness values for the samples were measured before and after exposure and are presented in Table 26. Both the FKM-75 and FKM-90 samples showed an increase in hardness of about six units after the prolonged elevated temperature immersion exposure. This is larger than the literature value of two units, but still less than 10% relative change to the initial hardness value of the material.

**Table 23. Fluid resistance of FKM at elevated temperature (DuPont, 2010).**

| Fluid | Concentration | Temperature, °C (°F) | Time | Polymer Type | % of Original Property Retained | | Durometer A, Points Change in Hardness | % Volume Change |
|---|---|---|---|---|---|---|---|---|
| | | | | | Tensile Strength | Elongation at Break | | |
| DC-200 Silicone Oil | | 175 (347) | 28 days | A | | | 2 | –2 |

**Table 24. ASTM D471-15 (ISO 23936-2) swell testing results for FKM-75 and FKM-90 in DC200 (by mass change) percent change in mass post 28 days at 175ºC in ESCO silicone fluid E200=DC200, 100CS.**

| Sample (n=3; avg.) | M1 (g) | M2 (g) | ΔM (%) | Std Dev (%) |
|---|---|---|---|---|
| FKM M83248/1 75 hardness | 3.974 | 4.002 | 0.713 | 0.438 |
| FKM M83248/2 90 hardness | 4.042 | 4.059 | 0.420 | 0.106 |

$$\Delta M = \frac{(M2 - M1)}{M1} 100$$

M1 = initial mass of specimen
M2= mass of specimen after immersion

**Table 25. ASTM D471-15 (ISO 23936-2) swell testing results for FKM-75 and FKM-90 (percent change in thickness post 28 days at 175ºC in ESCO silicone fluid E200 = DC200, 100CS).**

| Sample (n=3; avg.) | T1 (in) | T2 (in) | ΔT (%) | Std Dev (%) |
|---|---|---|---|---|
| FKM M83248/1 75 hardness | 0.074 | 0.074 | 0.083 | 0.074 |
| FKM M83248/2 90 hardness | 0.075 | 0.076 | 0.480 | 0.075 |

$$\Delta T = \frac{(T2 - T1)}{T1} 100$$

T1 = initial thickness of specimen
T2 = thickness of specimen after immersion

**Table 26. Hardness change for FKM-75 and FKM-90 after exposure.**

| Sample (n=3; avg.) | H1 (Shore A, initial) | H2 (Shore A, final) | ΔH (H2-H1) | Std Dev |
|---|---|---|---|---|
| FKM M83248/1 75 hardness | 74.0 | 80.5 | 6.5 | 0.89 |
| FKM M83248/2 90 hardness | 85.0 | 91.1 | 6.1 | 0.30 |

Similarly, the results for the corresponding swelling tests at elevated temperature (175°C) for the NBR are included in Table 27. The results show a small decrease in thickness of 1 to 2% and a significant decrease in mass of 8 to 15% compared to the pre-exposed NBR material. A very large increase in hardness to a final value of 95 to 99 from initial values of 40 to 80 was observed.

**Table 27. Results of exposure testing for NBR.**

| NBR, immersed for 28 days at 175ºC in ESCO Silicone fluid, E200, 100 CS | | | Hardness | Thickness | Mass |
|---|---|---|---|---|---|
| **Sample ID** | **Pre-hardness** | **Post hardness** | **%Δ** | **%Δ** | **%Δ** |
| NBR-40A | 40 | 96.0 | 140.0 | -0.4 | -8.3 |
| NBR-50A | 50 | 95.3 | 90.7 | -1.2 | -10.0 |
| NBR-60A | 60 | 94.8 | 58.0 | -1.1 | -14.8 |
| NBR-80A | 80 | 98.5 | 23.1 | -1.7 | -9.1 |

The large increase in hardness confirms the property degradation of NBR elastomers when exposed above the maximum use temperature of 125ºC, which can be explained as due to excessive crosslinking of residual unstauration sites. The decrease in thickness and mass of the elastomer from swelling and leaching also suggest that changes in composition of the elastomer may have taken place.

The objective of the "wet" material property testing was to capture severe changes in material properties due to physical aging and provide corrective data for model development. Testing has shown that with the silicone-based oil, severe physical aging effects will not occur during the short time (less than 8 hours) that O-rings will be exposed to the fluid during HPHT testing.

## 6.4 Tensile Testing at Multiple Strain Rates

Battelle conducted tensile testing of elastomer samples to provide additional information for FEA model development. This testing supplemented the testing referenced in Section 6.2.3 which was conducted at moderate strain levels. The supplemental testing provided the complete stress-strain curve which includes the ultimate tensile strength, elongation at break, and the slope of the stress-strain curve at different levels of elongation (providing "stiffness" values). The various test apparatus used are illustrated in Figure 36 and Figure 37. Additional testing of both M83248-1 (FKM-75) and M83248-2 (FKM-90) are presented in Section 6.7. Slab testing of the remaining elastomers was replaced by corresponding testing of the actual O-rings under test (Section 6.5).

### *6.4.1 Slab Sample Testing*

Figure 38 provides results for the uniaxial tensile testing for commercial slabs (non-MIL-SPEC) of FKM-75. Testing was conducted using an Instron Tensile Testing Machine with a 200 foot-pound load cell and computer controlled data acquisition. Two regions of elongation are depicted on the plot. The applicability of each region depends on the extent of deformation in the elastomer part under consideration. The resistance to stretching in the initial 0 to 10% elongation region is typically called Young's Modulus and can be related to flexibility. The second region of ~50 to 150% elongation is typically used when conducting aging studies of elastomers. The FEA incorporates both of these regions.

**Figure 36. A tensile sample pulled at high strain (Endurica, LLC, 2015).**

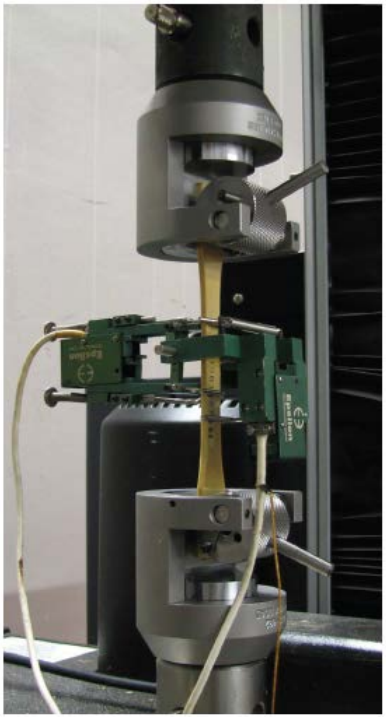

**Figure 37. A tensile specimen with an extensometer installed (Endurica, 2015).**

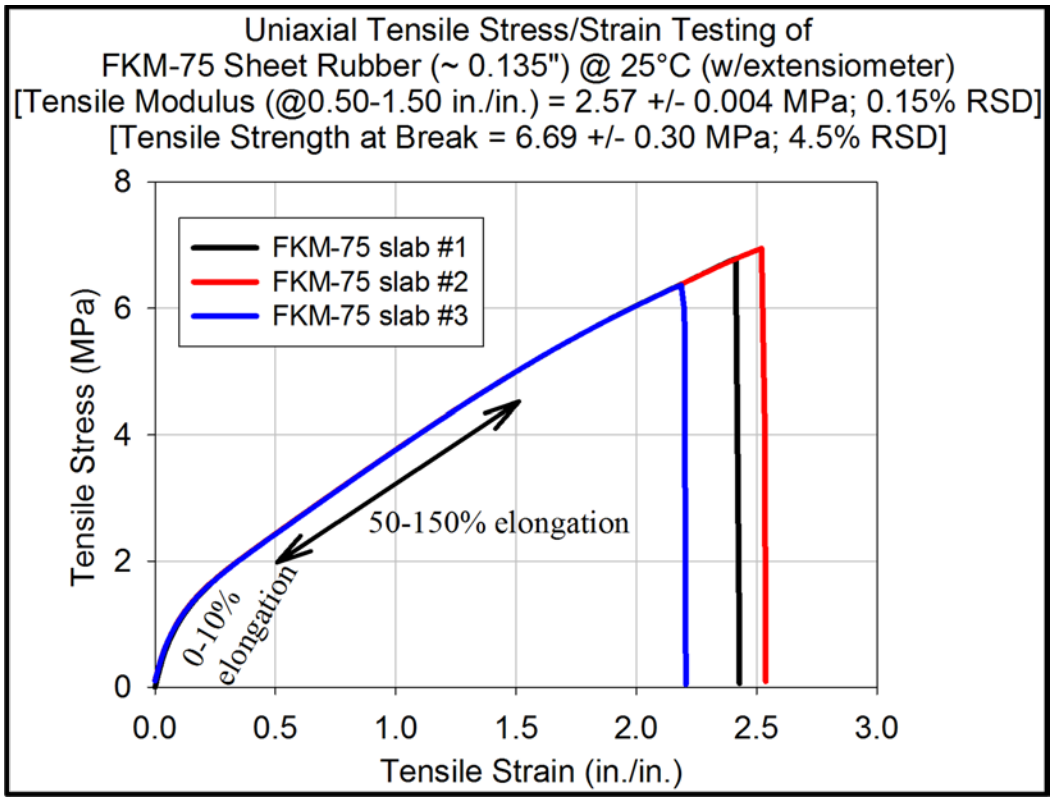


**Figure 38. Stress-strain curve for FKM-75 sheet showing tensile modulus measurement regions.**

The results shown in Figure 38 show a tensile modulus of 2.57 ± 0.004 MPa (at 50-100% elongation) with a tensile strength of 6.69 ± 0.30 MPa for FKM-75 elastomer at 25°C. The corresponding tensile modulus values for the slope of lower strain portion of the curve (0 to 10% elongation) were 9.44 ± 0.35 MPa. The shape of the stress-strain curve depends on the strain rate. A strain rate of 33%/second (~30 seconds/test) was used for these elastomer slab tests. The tensile testing of the O-ring samples was conducted at a strain rate of 15%/second (~30 seconds/test) (see Section 6.4). A much slower strain rate corresponding to the slab testing discussed in this section (Figure 38) of 1%/second (~6 minutes per test) was used to mimic the testing at Endurica. At a very slow strain rate, the shape of the curve is flatter. Figure 39 shows the linear regression results for the Young's Modulus region of the plot.

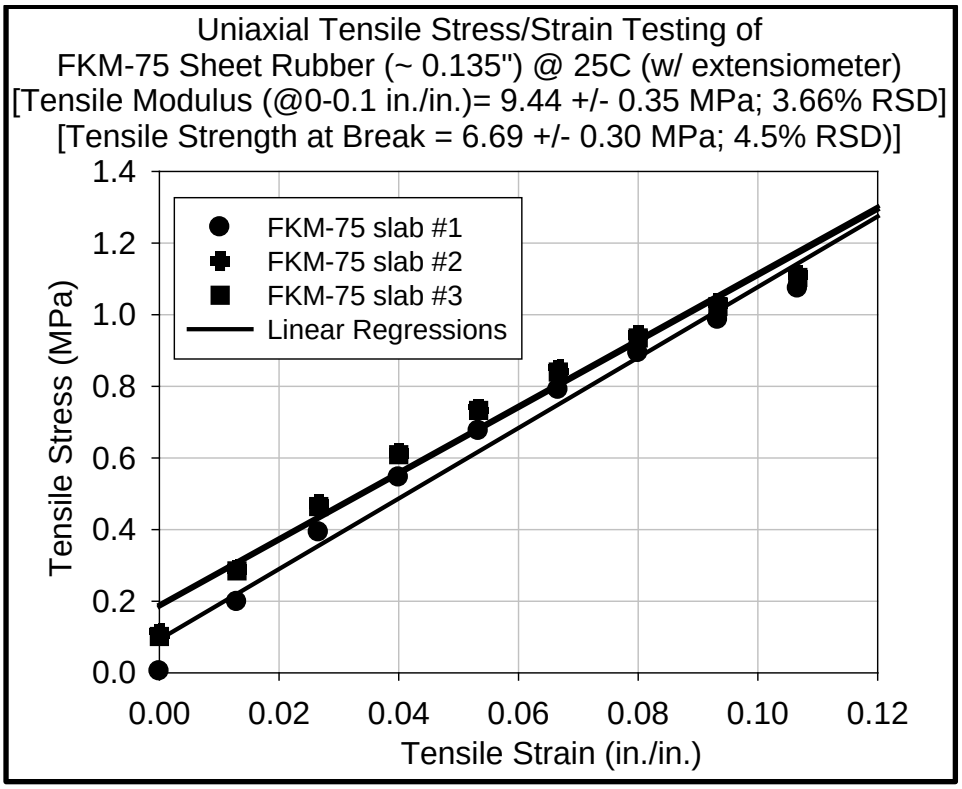


**Figure 39. Tensile modulus calculations at 0 to 10% elongation for FKM-75 sheet.**

## 6.5 Direct Mechanical Testing

Direct mechanical testing of FKM O-rings was accomplished by using the same test setup as shown in Figure 37, with a different fixture capable of holding an O-ring test coupon rather than a slab-form test coupon. The results for the uniaxial O-ring tests conducted at Battelle found that the tensile strengths for the 210-75 and 210-90 O-rings were 9.30 +/- 2.08 MPa, and 10.90 +/- 0.69 MPa, respectively, close to the FKM M83248-1 (FKM-75) and FKM M83248-2 (FKM-90) specification values of 9.65 psi (min.) for each, respectively. The elongation percent change for the 210-75 and 210-90 O-rings was found to be 262 +/- 36% and 214 +/- 10%, respectively, exceeding the M83248C specifications of 125% and 100% elongation respectively. The results are shown in Table 28 and the raw stress-strain data plots are provided in Figures 40 and 41.

**Table 28. FKM-75 and 90 hardness O-ring properties: Mil-R-83248-210.**

| | Young's Modulus (MPa) (0.5-1.5 in/in) | Ultimate Tensile Strength (MPa) | Elongation at Break (%) |
|---|---|---|---|
| Mil-R-83248-210-75 O-ring | 2.88± 0.08 | 9.30±2.08 | 261.5± 35.9 |
| Mil-R-83248-210-90 O-ring | 5.23± 0.04 | 10.90± 0.69 | 213.5± 10.2 |

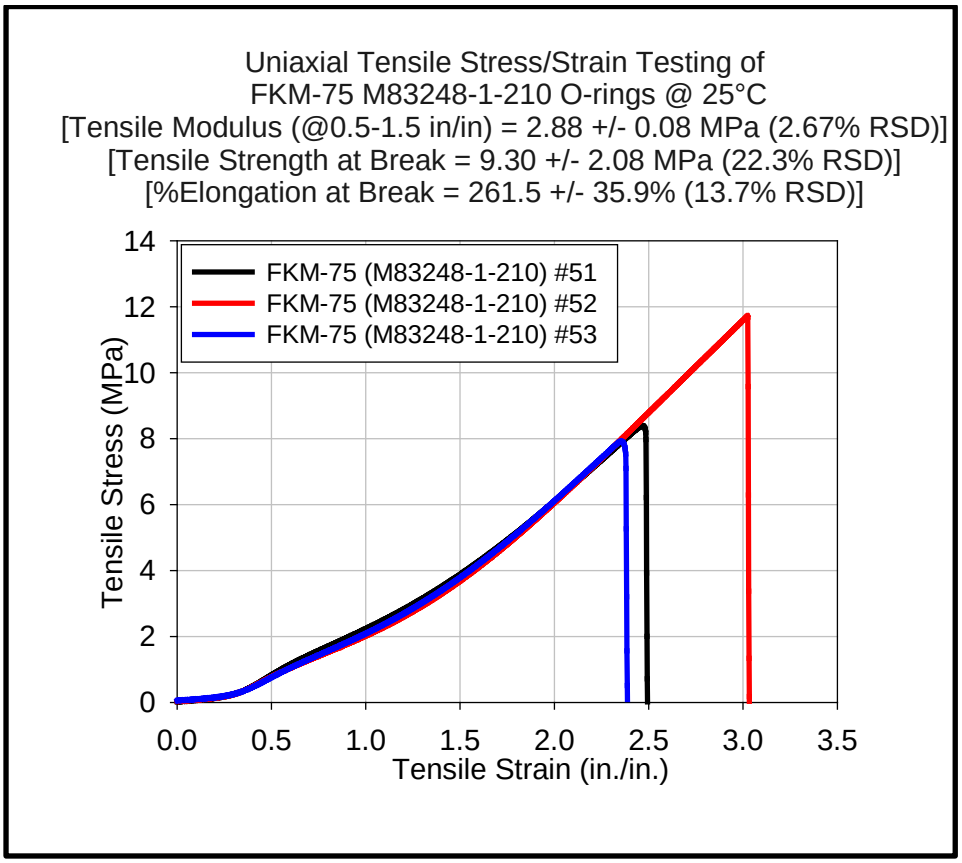


**Figure 40. Tensile stress-strain curves for FKM-75 M83248-1-210 O-rings at 25°C.**

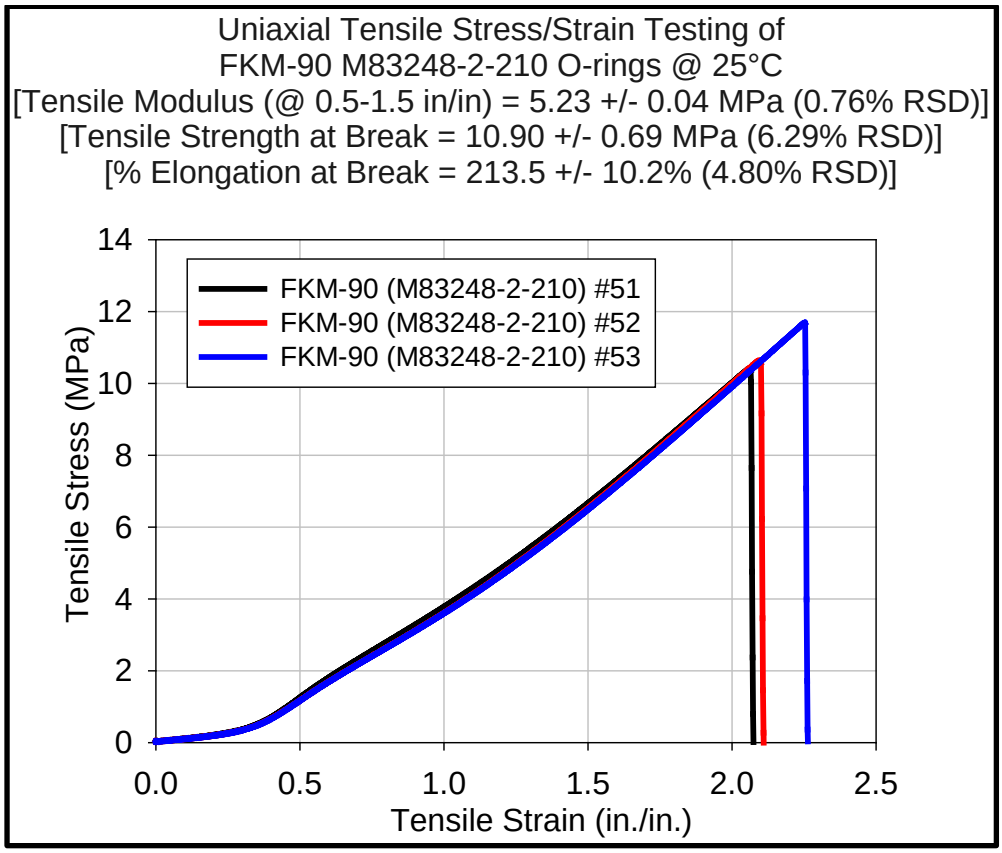


**Figure 41. Tensile stress-strain curves for FKM-90 M83248-2-210 O-rings at 25°C.**

## 6.6 Elevated Temperature Effects on Bulk Elastomer (Sheet) Properties

The change in physical properties of the same FKM-75 sheet rubber as a function of increasing temperature from 25°C to 75°C to 125°C to 175°C is shown in Table 29, with raw data plots shown in Figure 42. This testing was conducted in triplicate. The tensile modulus of the FKM-75 material is reported for two strain regions. The first one is the stress/strain region up to about 10% elongation and is typically called the Young's Modulus of a material (Figure 43). For the FKM-75 sheet rubber this value decreases considerably from 25ºC (8.82 MPa) to 75ºC (5.59 MPa), a 36.6% reduction. A modest general decrease in tensile modulus is observed from 75ºC to 125ºC and then slightly increased over the 175°C readings. The second stress-strain region is from about 50% to 150% elongation. This tensile modulus region is sometimes used as a general stiffness value. For FKM-75 rubber sheet this modulus region is much less affected by the increase in temperature with an average value of 2.40 ± 0.09 MPa with only a 3.7% relative standard deviation across the 25ºC to 175ºC temperature range. The ultimate tensile strength of FKM-75 sheet also decreases significantly from 25ºC (6.71 MPa) to 75ºC (4.49 MPa), a 33% decline and continues to decrease across the 75ºC to 175ºC region (Figure 44). The ultimate elongation at break properties of the FKM-75 sheet decreases significantly between 25ºC (262.0%) and 75ºC (164.2%) as well, a 37% relative reduction that continues from 75ºC to

175ºC. This is shown in Figure 44 and Figure 45. The reduction of mechanical properties (Young's Modulus, tensile strength, and elongation at break) suggests that the exudation of elastomers like FKM would increase at elevated temperatures as low as 75°C. Room temperature characterization data are inadequate to predict the extent of this exudation behavior at elevated temperature and high pressure conditions.

**Table 29. Effect of elevated temperature on mechanical properties of FKM-75 sheet.**

| Test Temperature (°C) | Tensile Modulus (MPa) (Young's) (0.0-0.1 in/in) | Tensile Modulus (MPa) (0.5-1.5 in/in) | Ultimate Tensile Strength (MPa) | Elongation at Break (%) |
|---|---|---|---|---|
| **25** | 8.82±0.46 (5.18% RSD) | 2.41±0.007 (0.30% RSD) | 6.71± 0.35 (5.24% RSD) | 262.0±21.9 (8.38% RSD) |
| **75** | 5.59±0.03 (0.51% RSD) | 2.42 ± 0.012 (0.51% RSD) | 4.49±0.28 (6.27% RSD) | 164.2 ±15.4 (9.37% RSD) |
| **125** | 4.93±0.08 (1.57% RSD) | 2.27±0.004 (0.20% RSD) | 3.19±0.08 (2.52% RSD) | 115.3±4.0 (3.47% RSD) |
| **175** | 5.13±0.09 (1.67% RSD) | 2.48±0.01 (0.29% RSD) | 2.56±0.07 (2.58% RSD) | 82.0±4.0 (4.88% RSD) |

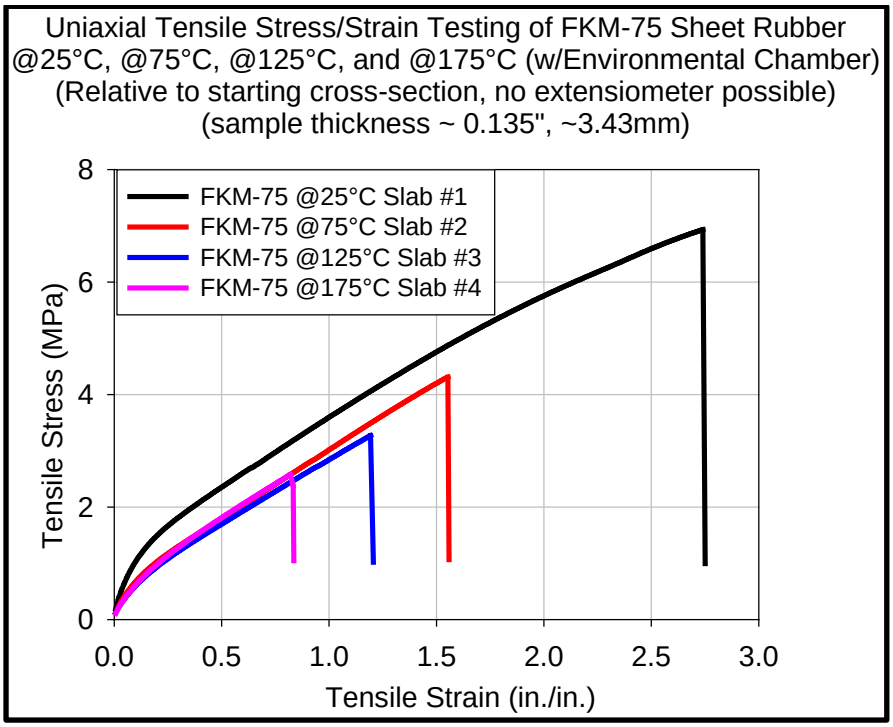


**Figure 42. Effect of elevated temperature on the tensile properties of FKM-75 sheet.**

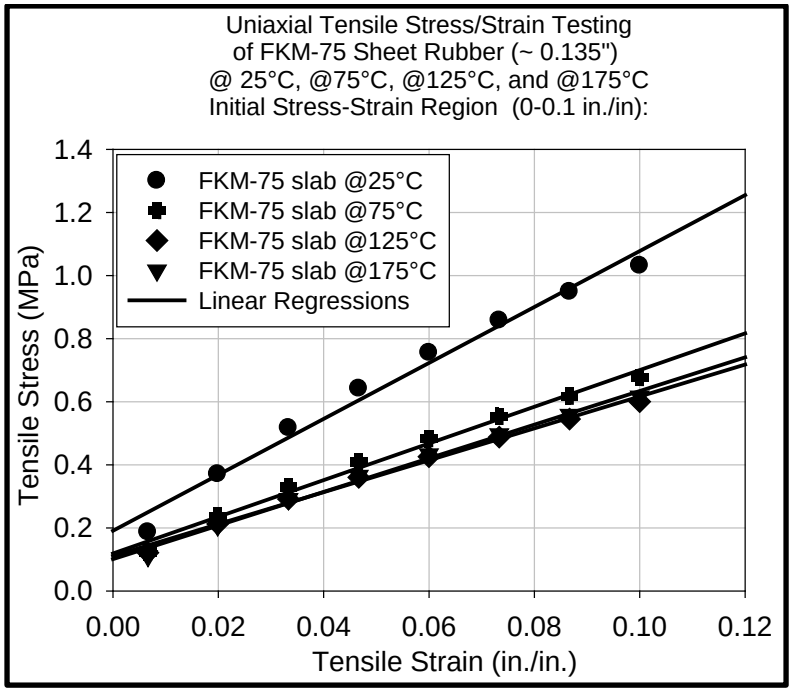


**Figure 43. Effect of temperature on the tensile modulus (0 to 10% elongation) of a FKM-75 sheet.**

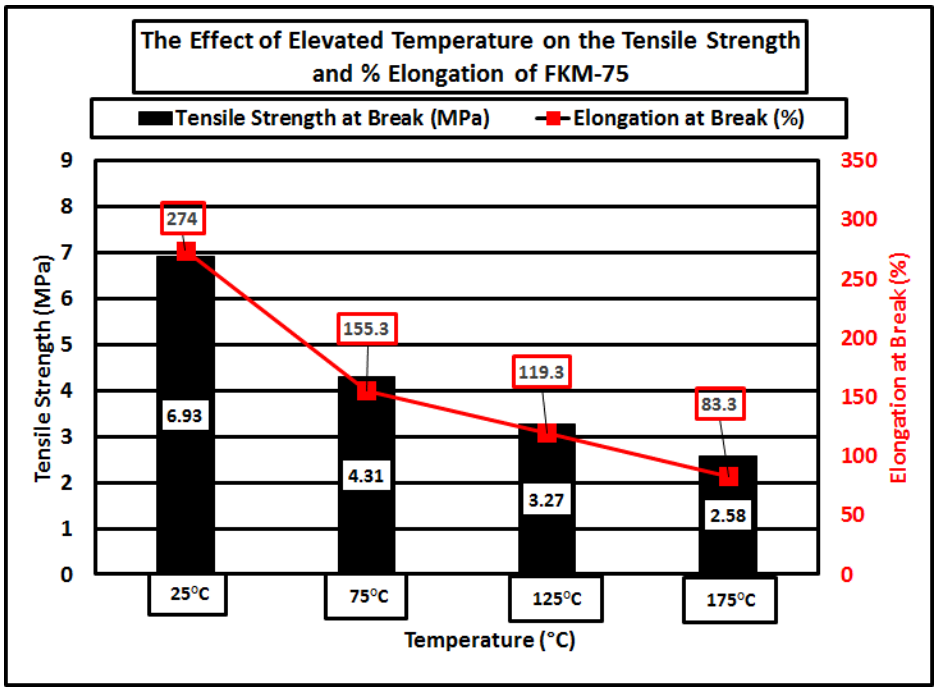


**Figure 44. Plot of reduction in tensile strength (MPa) and elongation at break (%) of FKM-75 at elevated temperature (25-175°C).**

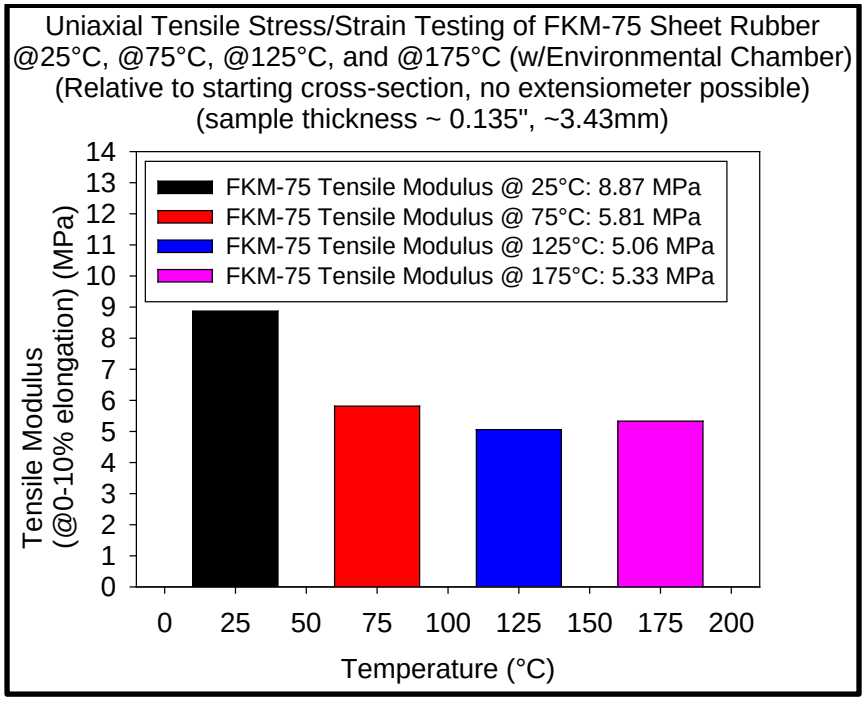


**Figure 45. Effect of elevated temperature on the tensile modulus (0 to 10% elongation) of FKM-75 sheet.**

## 6.7 Elevated Temperature Effects on Elastomer Properties

### *6.7.1 FKM Elastomer O-rings*

The effect of elevated temperature on the mechanical properties of actual O-rings (M83248-1) used in the HPHT testing conducted at PetroMar was conducted using an environmental chamber with the same test apparatus as shown in Figure 36. Figure 46 shows an overlay of the stress-strain curves for the FKM-75 elastomer (M83248-1; size -020) O-rings at 25ºC, 75ºC, 125ºC and 175ºC, while Table 30 shows the elongation data in tabular form.

The results are similar to the FKM slab results showing significant reduction in tensile strength (37% at 75ºC) and elongation at break (38% at 75ºC) with little change in stiffness (3.6 ± 0.1 MPa) in the strain region of 50 to 100% elongation. The initial 0 to 10% strain tensile stiffness (Young's Modulus) was more difficult to quantitate in the O-ring test configuration compared to the larger cross-section slab samples. Therefore, the different elastomers (FKM, FEPM, and FFKM) were compared over the 50 to 100% strain regime.

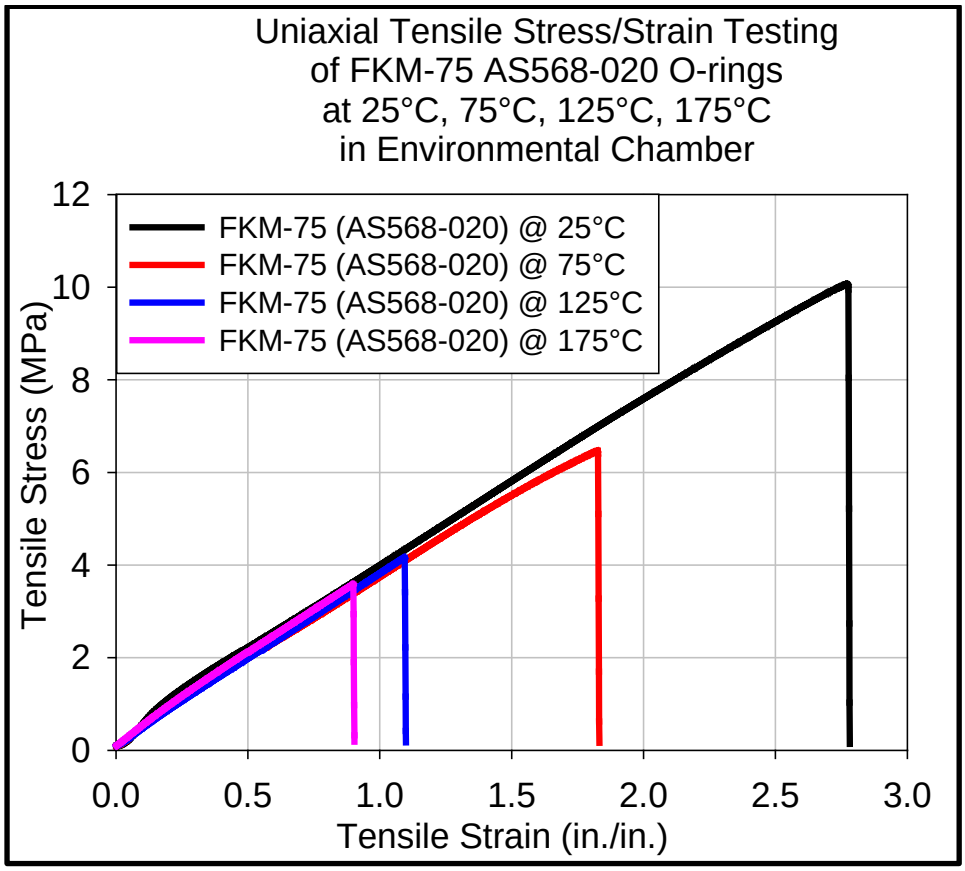


**Figure 46. Elevated temperature tensile test results for FKM-75 AS568-020 O-rings.**

**Table 30. Elevated temperature tensile test results for FKM M83248-1 75 O-rings -020.**

| Temperature (ºC) | Tensile Modulus (MPa) (0.5-1.00 in/in) | Tensile Strength (MPa) | Elongation % |
|---|---|---|---|
| **25** | 3.60± 0.02 (0.66% RSD) | 10.33±0.63 (6.11% RSD) | 291±27.50 (9.44% RSD) |
| **75** | 3.61±0.07 (2.03 % RSD) | 6.47± 0.21 (3.21% RSD) | 180±12.17 (6.74% RSD) |
| **125** | 3.56± 0.14 (3.99% RSD) | 4.28±0.28 (6.65% RSD) | 114±6.11 (5.35% RSD) |
| **175** | 3.75±0.01 (0.34% RSD) | 3.53± 0.19 (5.30 % RSD) | 89± 3.44 (3.87% RSD) |

### *6.7.2 FEPM O-ring Tests*

To determine any variability in material properties caused by the O-ring molding process, Battelle conducted elevated temperature testing of FEPM on two O-rings of the same cross-section (0.0625 inch), different outer diameter, 1.00 inch and 1.06 inch (sizes AS568-020 and AS568-021) and the same durometer (hardness of 80). Testing of two sizes of O-rings (-020 and -021) of the same elastomer material allowed for O-rings with different physical mold sizes to be compared. Table 31 presents the dimensions of the FEPM O-rings tested. The FEPM results for the two O-ring samples are summarized in Table 32 and Table 33, and compared directly in Table 34.

**Table 31. FEPM O-ring dimensions.**

| AS568 | Nominal Reference | | | Actual Dimensions | |
|---|---|---|---|---|---|
| **Sample Number** | **ID (in)** | **OD (in)** | **Cross Section Diameter (in)** | **ID (in)** | **ID (mm)** |
| **-20** | 0.875 | 1.00 | 0.0625 | 0.864±.009 | 21.95±0.23 |
| **-21** | 0.938 | 1.0625 | 0.0625 | 0.926±.009 | 23.52±0.23 |

**Table 32. Tensile testing results of FEPM-80 Size AS568-020 O-ring product at 25°C, 75°C, 125°C, and 175°C.**

| Temperature (ºC) | Tensile Modulus (MPa) (0.5-1.25 in/in) | Tensile Strength (MPa) | Elongation % |
|---|---|---|---|
| **25** | 5.97± 0.12 (1.97% RSD) | 11.60±0.27 (2.34% RSD) | 263±20.80 (7.92% RSD) |
| **75** | 3.26±0.04 (1.21 % RSD) | 7.06± 0.51 (7.22% RSD) | 195±17.95 (9.19% RSD) |
| **125** | 3.02± 0.15 (5.12% RSD) | 4.64±0.40 (8.55% RSD) | 147±12.73 (8.66% RSD) |
| **175** | 3.11±0.06 (1.82% RSD) | 3.82± 0.15 (3.99 % RSD) | 123± 2.39 (1.95% RSD) |

**Table 33. Tensile testing results of FEPM-80 O-ring size AS568-021 (Sample A80-021) at 25°C, 75°C, 125°C, and 175°C.**

| Temperature (C) | Tensile Modulus (MPa) (0.5-1.25 in/in) | Tensile Strength (MPa) | Elongation % |
|---|---|---|---|
| **25** | 6.61±0.07 1.02 % RSD) | 15.69± 0.37 (2.37 % RSD) | 298± 14.35 (4.82 %RSD) |
| **75** | 3.50± 0.25 (7.13 % RSD) | 7.93±0.75 (9.46 % RSD) | 214± 21.04 (9.85 % RSD) |
| **125** | 3.52± 0.19 (5.43 % RSD) | 5.42± 0.26 (4.80 % RSD) | 152± 12.41 (8.17 % RSD) |
| **175** | 2.91± 0.12 (4.09 % RSD) | 3.21± 0.67 (20.88 % RSD) | 98± 19.00 (19.46 % RSD) |

The results indicate that FEPM-80, although stiffer than both FKM-75 and FFKM-75 at ambient temperature, loses stiffness (by approximately 50%) at temperatures of 75°C (167°F) or higher to be at about the same stiffness as FKM-75 at these temperatures. This suggests that there may be a thermal transition for the FEPM copolymer that occurs at moderate temperatures and should be taken into consideration in FEA model development for FEPM. The tensile strength and percent elongation for the FEPM decreased substantially as the temperature increased.

**Table 34. Percentage change of tensile modulus, ultimate tensile strength, and elongation and break for FEPM-80 size AS568-020 and AS568-021 O-rings.**

| | Sample: FEPM-80 - size -020 O-rings | | | Sample: FEPM-80 - size -021 O-rings | | |
|---|---|---|---|---|---|---|
| **Test Temp. (°C)** | **Tensile Modulus (MPa) (0.5-1.5 in/in)** | **Tensile Strength (MPa)** | **Elongation at Break (%)** | **Tensile Modulus (MPa) (0.5-1.5 in/in)** | **Tensile Strength (MPa)** | **Elongation at Break (%)** |
| **25** | 0 | 0 | 0 | 0 | 0 | 0 |
| **75** | -45.4 | -39.1 | -25.9 | -47.0 | -49.5 | -28.2 |
| **125** | -49.4 | -60.0 | -44.1 | -46.7 | -65.5 | -49.0 |
| **175** | -47.9 | -67.1 | -53.2 | -56.0 | -79.5 | -67.1 |

The results of the tensile testing show that the tensile modulus, tensile strength, and elongation at break for the FEPM-80 hardness O-rings are significantly reduced, even at temperatures as low as 75ºC (167ºF) compared to the ambient temperature (25ºC) properties. This loss in modulus (stiffness) and strength are likely important contributors to the exudation resistance of O-rings at elevated temperature. Both sizes of O-rings evaluated exhibited similar levels of property degradation at elevated temperatures, indicating that the molding process did not appear to affect the properties of the elastomer O-rings.

### *6.7.3 FFKM O-ring Testing*

Similar thermal characterization testing was conducted for FFKM in an O-ring seal gasket. The results indicate that FFKM-75 retained a higher tensile modulus (stiffness) at 75ºC (8% loss) than FEPM-80, but not as well as FKM-75, which showed no change compared to room temperature. The change in stiffness of the elastomers versus temperature is a function of polymer viscoelastic properties and were more fully explored in DMA testing Section 6.8.

As summarized in Table 35 and Figure 47, the reduction in tensile strength at break (MPa) and elongation at break (%) were more pronounced, especially at 125°C and 175°C. The higher tensile modulus or stiffness (lower percent property loss) at 175°C versus 125°C is the result of increased crosslinking that occurs at the highest temperature, leading to a reduction in tensile strength and elongation at break.

**Table 35. The effect of elevated temperature on the mechanical properties of FFKM O-ring gasket material FFKM 3753-6230.**

| Test Temperature (°C) | Tensile Modulus (MPa) | Tensile Strength (MPa) | Elongation at Break (%) |
|---|---|---|---|
| **25** | 2.26 ±0.09 (3.82% RSD) [from 0.5-1.25 in/in] | 5.64 ± 0.10 (1.80% RSD) | 206 ± 8.80 (4.28% RSD) |
| **75** | 2.08 ± 0.12 (5.71% RSD) [from 0.5-1.25 in/in] | 2.49 ± 0.04 (1.61 %RSD) | 128 ± 4.2 (3.25% RSD) |
| **125** | 1.375 ± 0.004 (0.26% RSD) [from 0.4-0.9 in/in] | 1.24 ± 0.14 (11.31% RSD) | 106.1 ± 11.8 (11.15 %RSD) |
| **175** | 1.706 ± 0.03 (1.98% RSD) [from 0.3-0.6 in/in] | 1.068 ± 0.16 (14.79% RSD) | 75.2 ± 11.5 (15.31% RSD) |

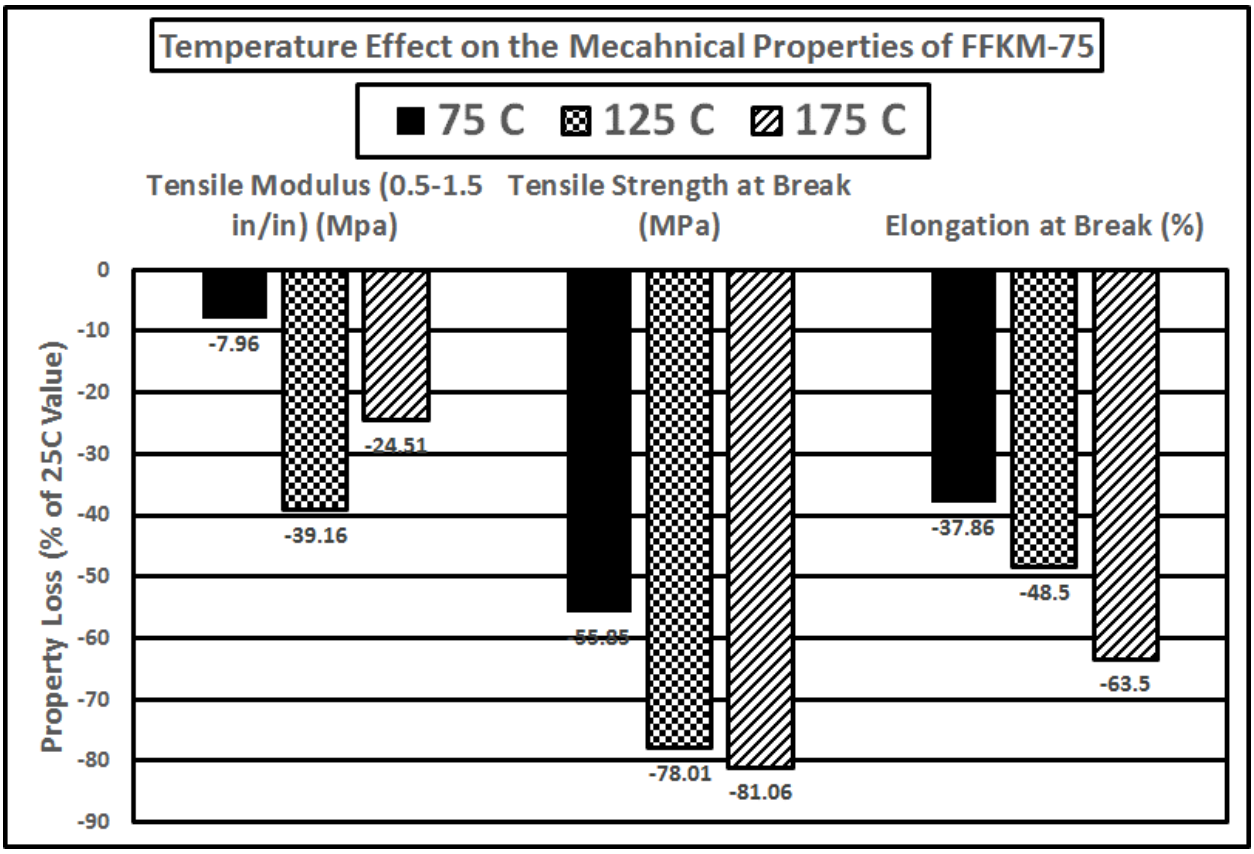


**Figure 47. Reduction of mechanical properties of FFKM O-ring gasket versus temperature (°C).**

## 6.8 Dynamic Mechanical Analysis Properties

DMA is a technique that measures the properties of materials as they are deformed under stress at elevated temperatures. Stress is applied in a variable, sinusoidal pattern, and the resulting strain on the material (also sinusoidal in nature) is measured. For elastic materials, the delta phase between the stress and measured strain sine waves is 0° (i.e., "they are in phase"), while for viscous materials the phase delta is closer to 90° (i.e., "the phases are shifted"). The polymers selected for this study exhibited behaviors in between these two extremes (TA Instruments, 1997). The dynamic modulus, storage modulus, and loss modulus can be calculated as follows:

- Dynamic Modulus (E*) = (Stress Amplitude)/(Strain Amplitude)
- Storage Modulus = E* cosδ
- Loss Modulus = E* sinδ

where δ is the phase angle. DMA was conducted on sections of FKM, NBR, FEPM and FFKM. The sections were placed in a sample holder and analyzed in tensile mode using a TA Instruments Q800 DMA (Figure 48).

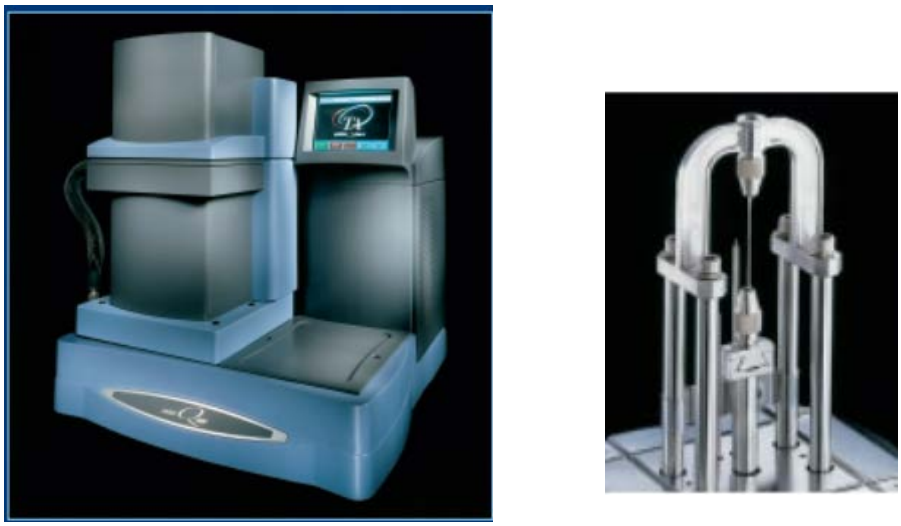

**Figure 48. DMA instrument (left) and sample holder illustrations (right) (TA Instruments, 2016).**

The instrument sample chamber temperature was controlled accurately with a combination of liquid nitrogen cooling and pulsed resistive heating. Table 36 shows the results for each of the elastomers tested. Storage moduli decreased for all materials as the temperature values increased. Fluorinated elastomers (such as FKM, FEPM, and FFKM) exhibited a more rapid decrease in material properties at elevated temperatures when compared to NBR elastomers. Additionally, harder elastomers tended to lose a greater percentage of their modulus as temperature increased,

although they maintained a greater modulus value than their softer analogues at elevated temperatures.

**Table 36. The effect of temperature on the storage modulus of O-ring elastomers.**

| Storage Modulus (MPa) Change as a function of temperature (ºC) | | | | | | | | | | | |
|---|---|---|---|---|---|---|---|---|---|---|---|
| Sample | **at 25 ºC** | **at 50 ºC** | **-% change** | **at 90 ºC** | **-% change** | **at 120 ºC** | **-% change** | **at 160 ºC** | **-% change** | **at 175 ºC** | **-% change** |
| HNBR-70 | 9.9 | 8.9 | 10.1 | 7.9 | 20.2 | 7.6 | 23.2 | 7.6 | 23.2 | 7.7 | 22.2 |
| FFKM-75 | 9.1 | 7 | 23.1 | 6 | 34.1 | 6.1 | 33 | 6.5 | 28.6 | 6.7 | 26.4 |
| FKM-75 | 9.6 | 8.5 | 11.5 | 6.9 | 28.1 | 6.5 | 32.3 | 6.5 | 32.3 | 6.6 | 31.3 |
| FKM-90 | 22.5 | 19 | 15.6 | 14.5 | 35.6 | 12.9 | 42.7 | 12.4 | 44.9 | 12.3 | 45.3 |
| NBR-70 | 17.2 | 13.6 | 20.9 | 9.7 | 43.6 | 8.1 | 52.9 | 7.4 | 57 | 7.4 | 57 |
| NBR-90 | 54 | 41.7 | 22.8 | 31.7 | 41.3 | 25.7 | 52.4 | 22.7 | 58 | 22.2 | 58.9 |
| FEPM-80 | 16 | 11.3 | 29.4 | 7.8 | 51.3 | 6.8 | 57.5 | 6 | 62.5 | 6 | 62.5 |

Figures 49 and 50 depict the storage modulus (MPa) changes as the temperature increases for FKM-75 (Figure 49) compared to FFKM-75 (Figure 50), respectively.

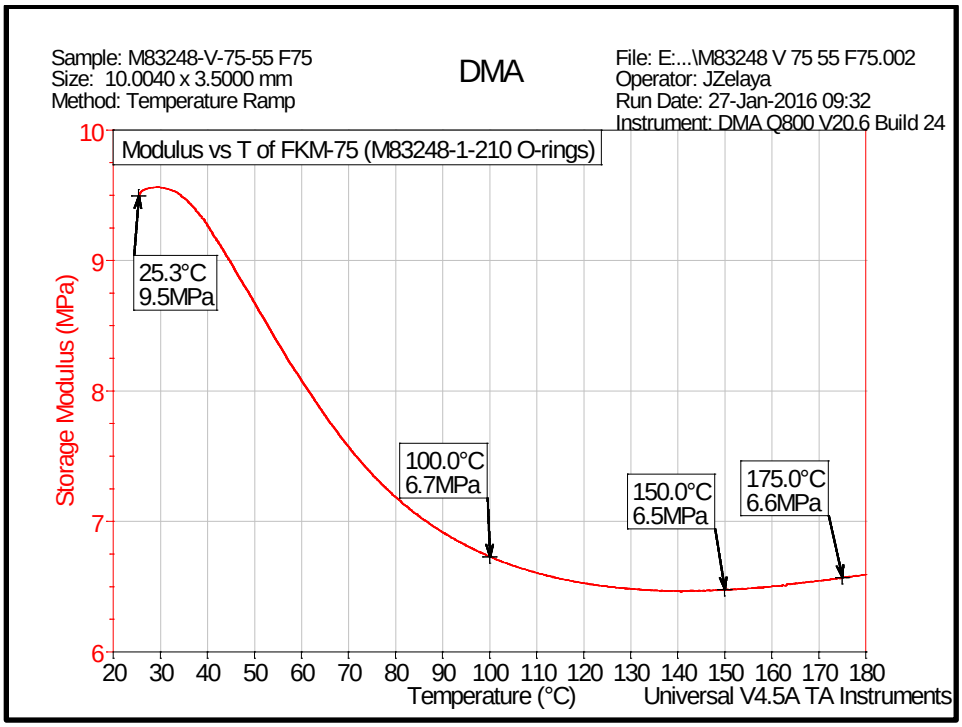


**Figure 49. DMA results for FKM-75 versus temperature.**

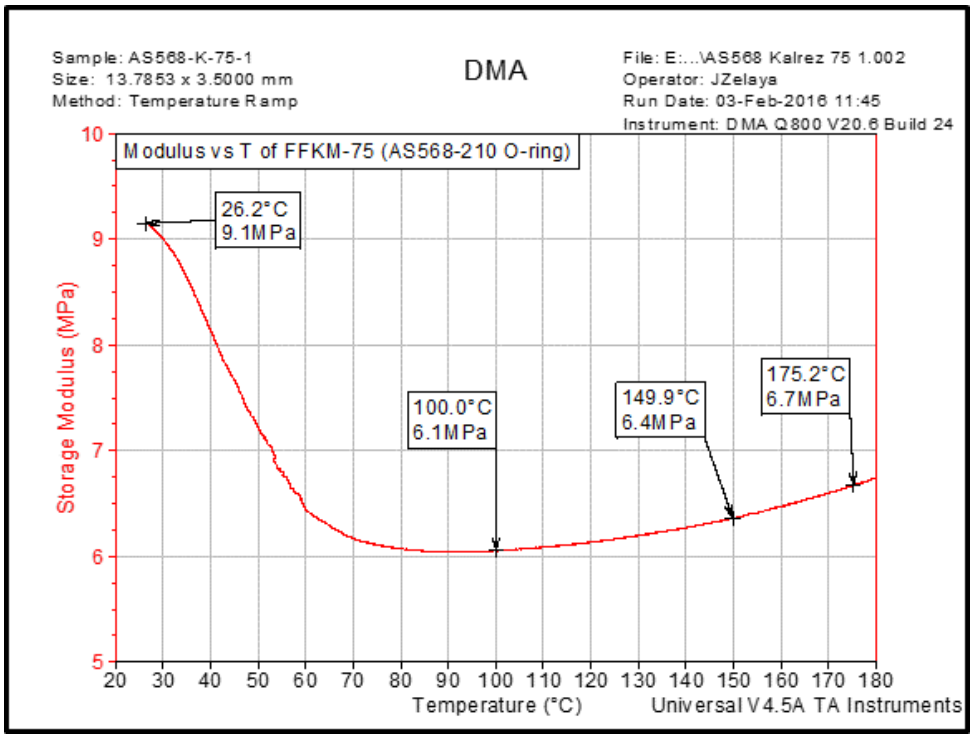


**Figure 50. DMA results for FFKM-75 versus temperature.**

DMA plots for other elastomers tested are included in Appendix A.5. In addition to the temperature scan DMA at a fixed frequency (1 Hz), Battelle also conducted frequency dependent temperature scans from 1 Hz to 200 Hz. This testing provided additional information on the flexibility of the elastomers at different strain rates. Figure 51 shows the frequency dependent modulus versus temperature for FFKM-75 from -20ºC to 80ºC.

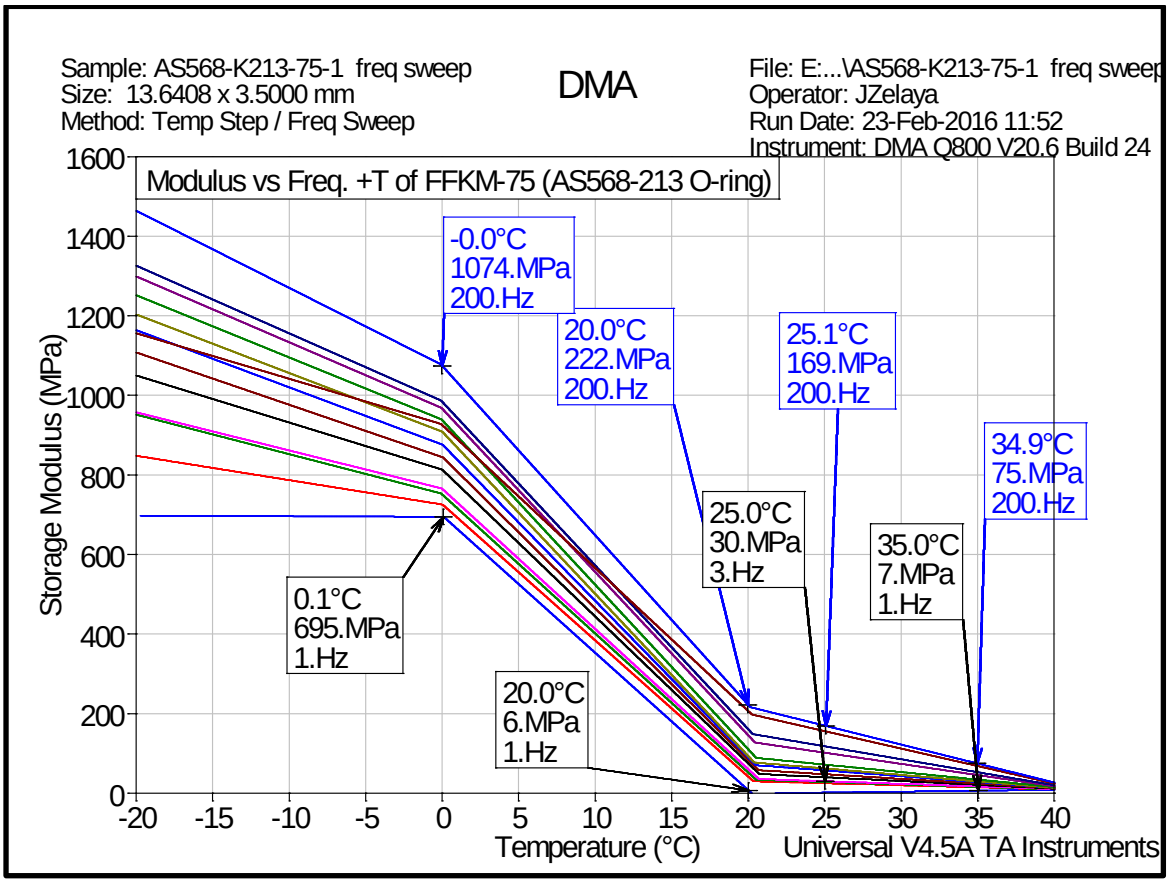


**Figure 51. Frequency dependent, temperature versus modulus measurements for FFKM-75 (AS568-213 O-ring).**

The results illustrate how the low temperature properties of O&G elastomers can also be important when dynamic seal applications are involved. Additionally, during rapid gas decompression events, the localized temperature can decrease in the elastomer.

## 6.9 Multiaxial Expansion: Membrane Inflation Tests

Battelle conducted membrane inflation testing of elastomers to collect critical material properties. Membrane inflation testing requires that a circular test coupon of the selected material

(NBR, HNBR, FKM, FFKM, or FEPM) be clamped in a test fixture radially. The coupon is marked with identifier markings; the movement is tracked by a camera throughout the test. Pressure is applied to the membrane coupon, using either a compressed gas or liquid medium. As the membrane inflates, the movement of the material under strain is tracked by the translation of the markings on the membrane. From the known amount of stress applied to the membrane, and the measured translation of the markings on the membrane, critical material properties including stretch ratio and Mooney Rivlin material coefficients can be determined. Figure 52 shows Battelle's membrane inflation test rig, while Figure 53 and Figure 54 illustrate how points on the membrane were tracked during the inflation process.

Cyclic testing conducted indicates that during the first stretch of the material, higher pressures are needed to displace the membrane. Subsequent inflations require lower pressure to achieve the same level of displacement. This may be representative of the Mullins effect for the material.

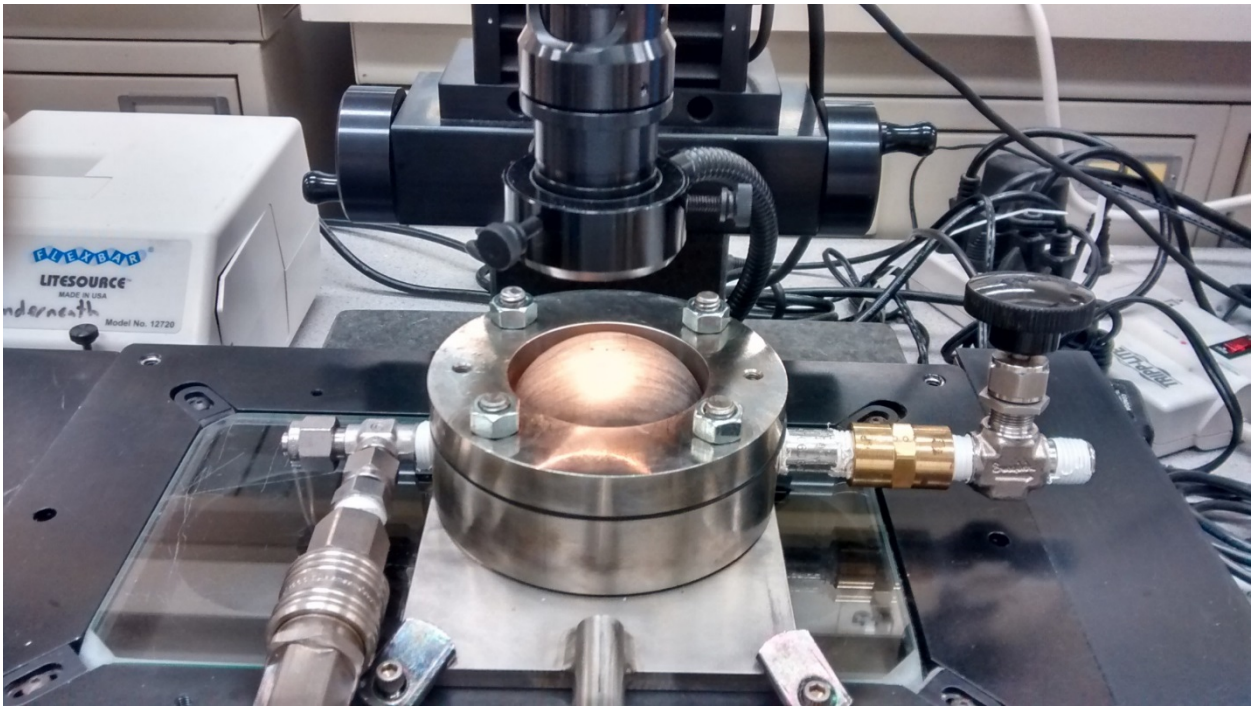


**Figure 52. Battelle's elastomer membrane inflation test apparatus.**

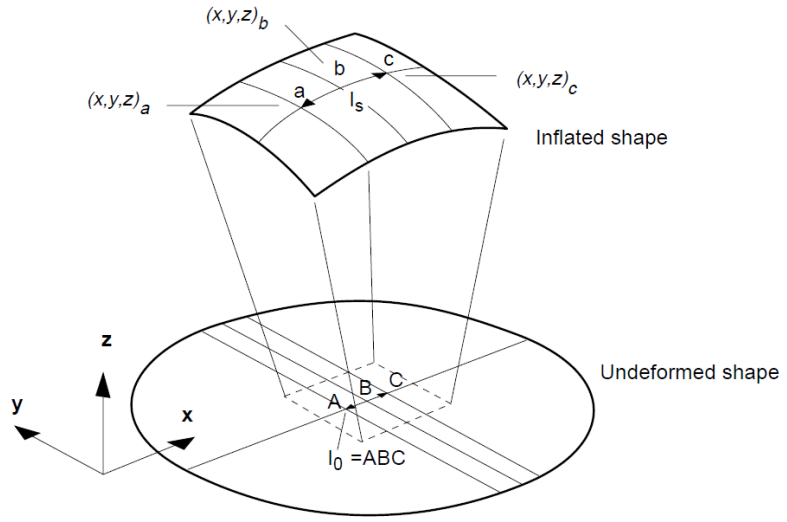


**Figure 53. Example coordinate system showing translation of marked points from the undeformed shape to the inflated shape (Makino, Hamburgen, & Fitch, 1993).**

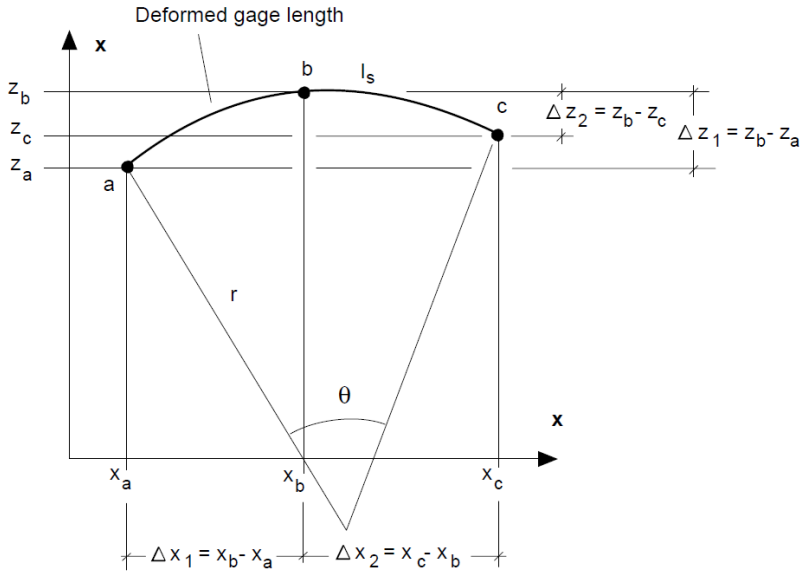


**Figure 54. Side view of Figure 2, showing radial coordinate calculations (Makino, Hamburgen, & Fitch, 1993).**

Figure 55 shows a representative example of the cyclic pressure versus stretch ratio graphs which are generated during this testing. In this particular graph, a total of five inflations were conducted, with inflations one, three, and five plotted. Note that the inflation "path" for inflations three and five follow the deflation "path" of inflation one.

Additional membrane inflation tests for other elastomers are included in Appendix A.5.

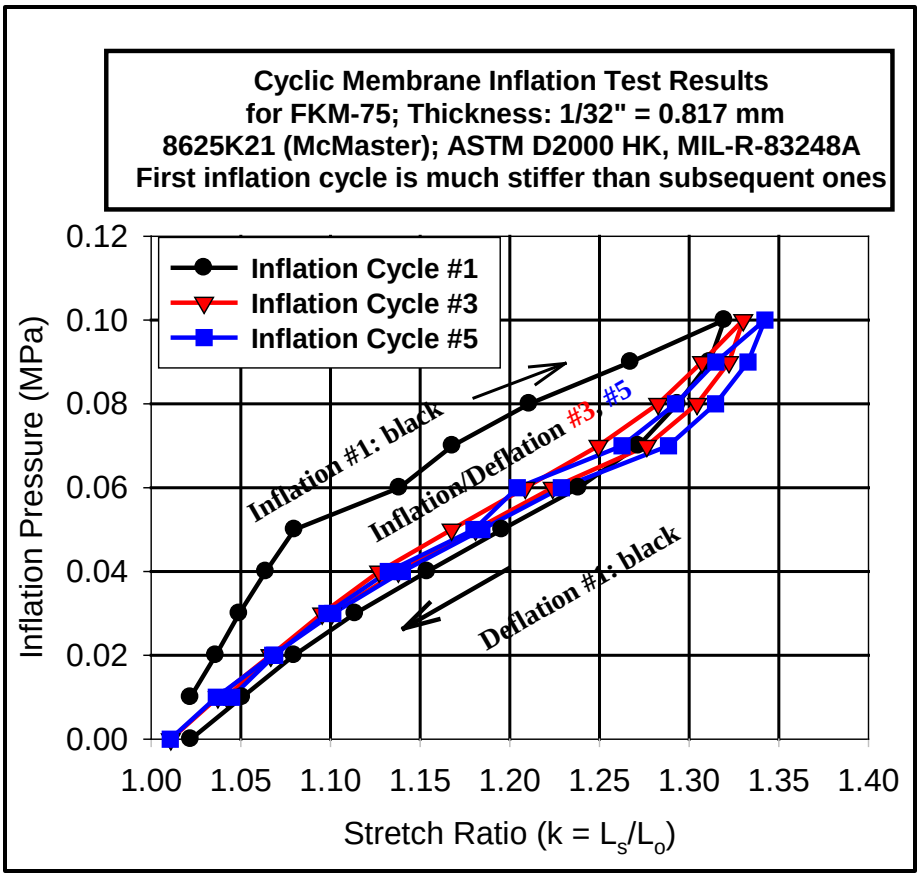


**Figure 55. Inflation pressure versus stretch ratio for FKM-75 hardness membrane.**

Figure 56 shows an example of how the inflation pressure can be used to determine the corresponding membrane stresses in MPa that are created.

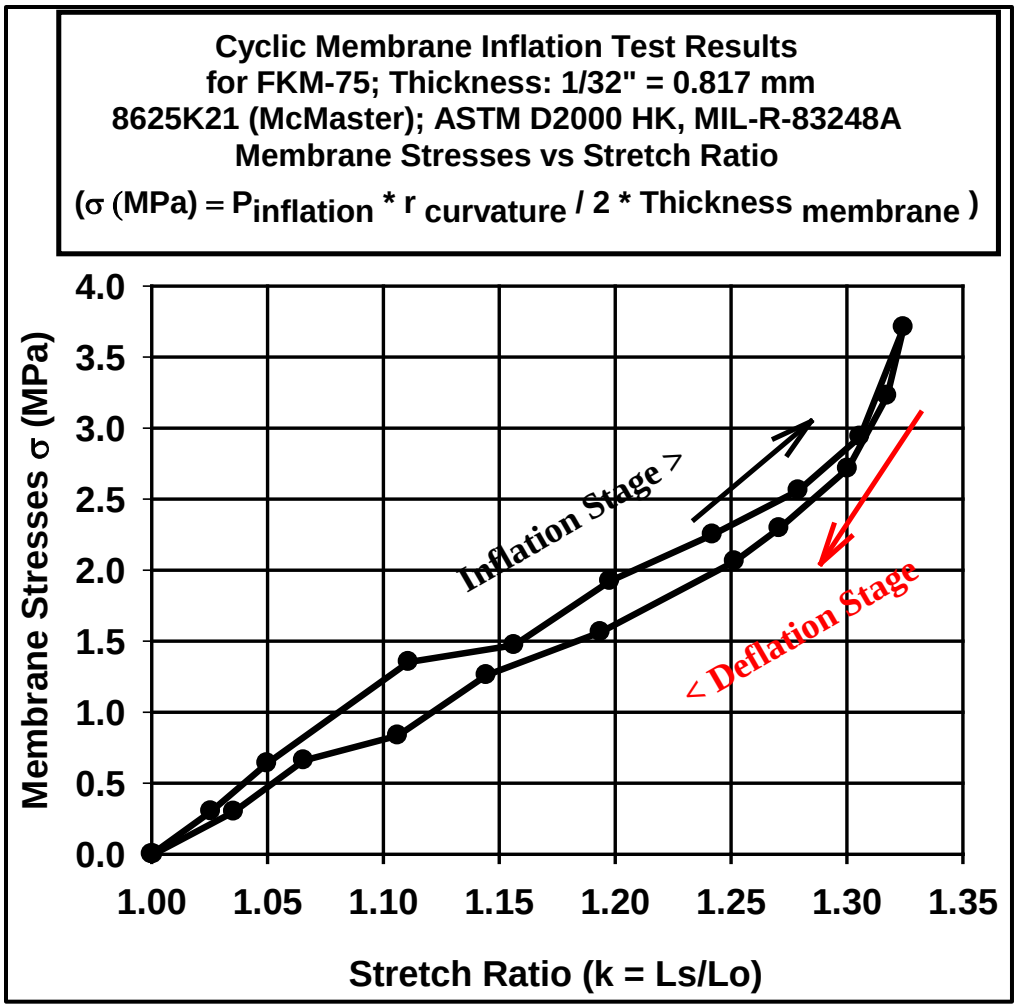


**Figure 56. Example of how the inflation pressure can be used to determine the corresponding membrane stresses.**

### 6.10 Cyclic Testing of Elastomers II: Mullins Effect at Sequentially Higher Strains

One objective of the elastomer testing conducted at Battelle was to provide supplemental information on the level of the Mullins effect on the mechanical properties of the O&G elastomers when subjected to cyclic loadings. This is especially important when the strain from one loading exceeded the previous ones. The results of the cyclic tests showed that the stiffness encountered when stretching the elastomer is highest the first-time a given strain is used and always lower up to that strain on subsequent cycles.

Conventional uniaxial stress-strain testing for each elastomer was conducted to the point of failure to determine the maximum stress limit for the test so that several intermediate stress levels could be assigned for cyclic testing (Figure 57). This test was conducted at the same slow 1% strain/second strain rate.

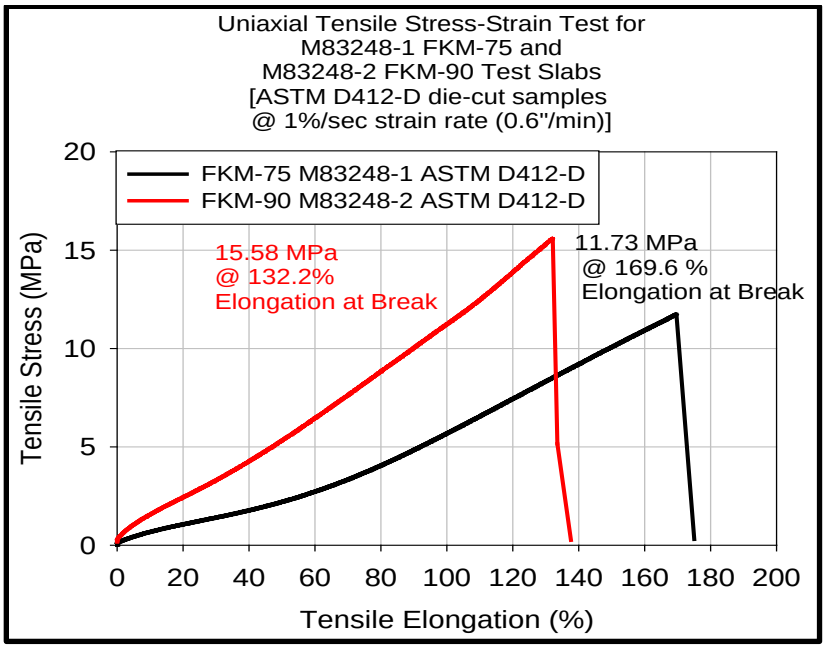


**Figure 57. Uniaxial tensile tests for M83248 FKM slab material.**

Subsequent cyclic loading tests were then conducted on new samples of elastomer (Figures 58 and 59).

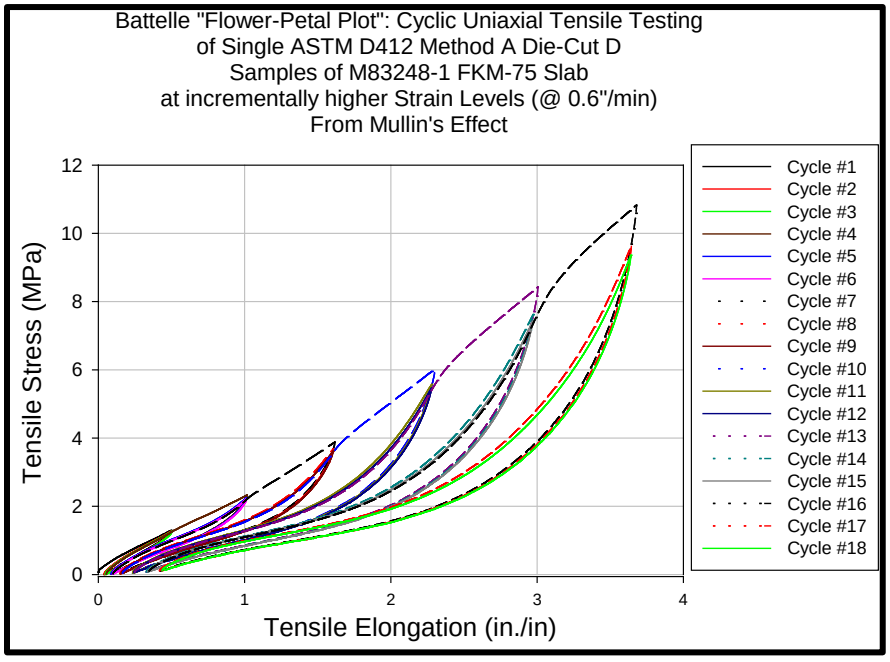


**Figure 58. Battelle cyclic tensile testing of FKM-75 M83248-1.**

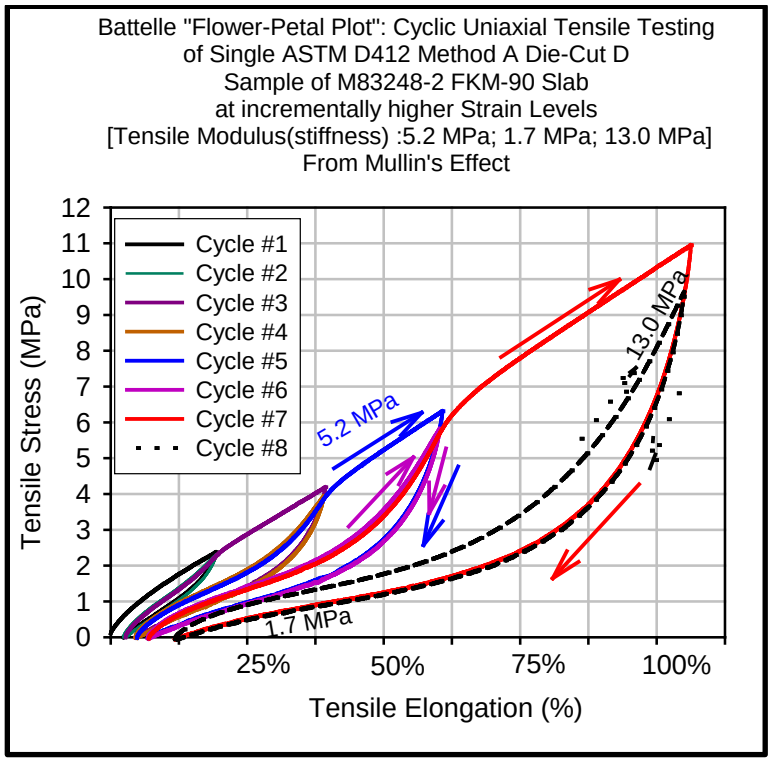


**Figure 59. Battelle cyclic tensile testing of FKM-90 M83248-2.**

# 7.0 FEA MODEL SETUP

## 7.1 Model Setup

The O-ring FEA model consists of three parts: O-ring, piston, and cylinder. The piston and cylinder are modeled as rigid. Measurements of the deformation of the vessel bore under high pressure loading in Task 4 confirm this assumption is valid. The test cell gland was designed and built to test size 210 O-rings under HPHT conditions in a static radial seal. The test cell used pistons of slightly different diameters to vary the extrusion gap between the vessel's bore and the piston, as shown in Figure 60. Figure 61 shows a schematic of the cross-section of an O-ring extruded into the clearance gap of the test setup.

**Figure 60. Pistons and pressure vessel used for the HPHT O-ring testing (PetroMar, Inc.).**

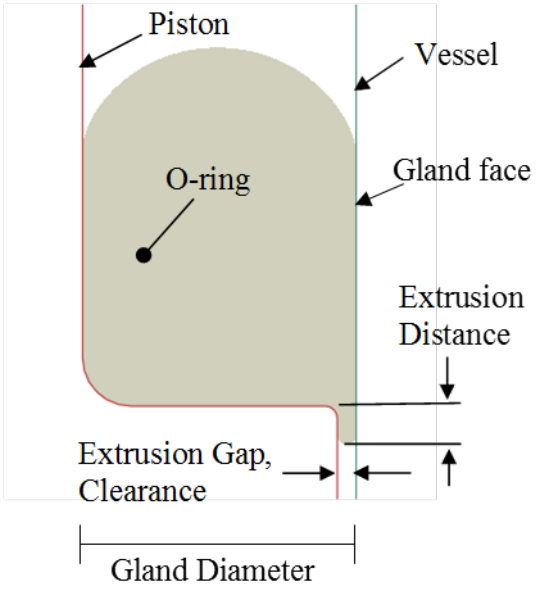


**Figure 61. Diagram of terms used to describe testing (Endurica, LLC).**

The FEA model uses the material properties measured in previous tasks for each material. The material properties are included in the FEA model as a three-term Ogden hyperelastic law including the volumetric compression response, a Mullins model, and the thermal expansion coefficient. Surface-to-surface contact interactions were created between the O-ring and piston and between the O-ring and cylinder. The contact interactions allow the friction to be modeled using the coefficient of friction that was found to be ≈0.05 based on friction force measurements conducted during Task 4 between the piston gland and the O-ring in the test fixture. The temperature field in the model allows the temperature to be controlled during the thermal expansion step. The coefficient of thermal expansion (CTE) for each material that had been previously measured was input into the model to calculate this volume expansion. A constant, steady-state temperature was then applied to the model through the entire O-ring cross section to mimic the experimental temperature stabilization. The fluid pressure was applied to the O-ring in the model using pressure penetration interactions. As pressure was applied to the O-ring, the area of the O-ring exposed to the fluid pressure changed as the O-ring deforms. These pressure penetration interactions apply fluid pressure only to the free surface area of the O-ring that is exposed to the fluid, not the portion against the wall.

The O-ring mesh used an approximate element size of 1.5 mils that was refined to smaller elements of approximate size 0.18 mils near the extrusion gap. The overall mesh is shown in Figure 62, and a detail view of the clearance gap is shown in Figure 63.

The entire mesh on the O-ring includes 30,458 elements of type CAX4RH modeled using ABAQUS software. The CAX4RH element type is a linear axisymmetric stress element that uses a hybrid formulation and reduced integration; they are recommended for materials such as rubber that have a high Poisson's ratio close to 0.5.

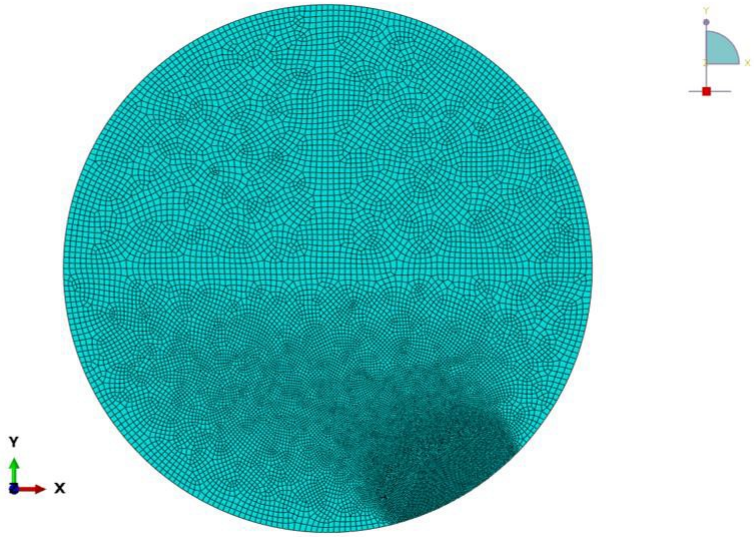


**Figure 62. Mesh on O-ring showing the refined mesh at area that was be extruded (Endurica, LLC).**

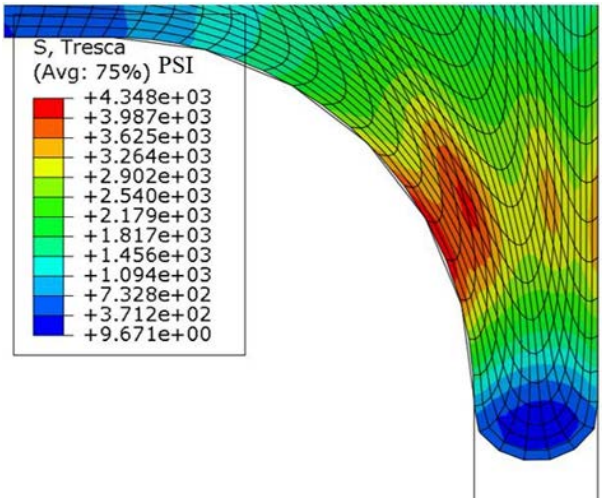


**Figure 63. Detail view of extrusion gap (Endurica, LLC).**

The mesh shown in Figure 62 was generated for an FEPM-80 O-ring at 100°C with a 0.002 in. nominal clearance gap at the CTP. The mesh has sufficient elements across the smallest clearance gap to accurately capture the stress gradients.

Assumptions of the model include:

- Constant temperature
- Constant pressure
- Chemically inert environment
- Chemically static elastomer materials
- Static O-ring seal

## 7.2 Model Run Sequence

The finite element simulation was set up to mimic as closely as possible the steps used in the HPHT O-ring test cell experiments executed during Task 4. The steps presented in Figure 64 were modeled as follows:

1. Initial unstressed, room temperature geometry, with unconstrained O-ring and piston.
2. Installation of the O-ring and interference fit on the inside gland diameter.
3. Closure of the test cell and contact with the outside cylinder wall.
4. Thermal equilibration at test temperature.
5. Establishment of initial, zero-pressure contact with the gland face.
6. Pressurization.

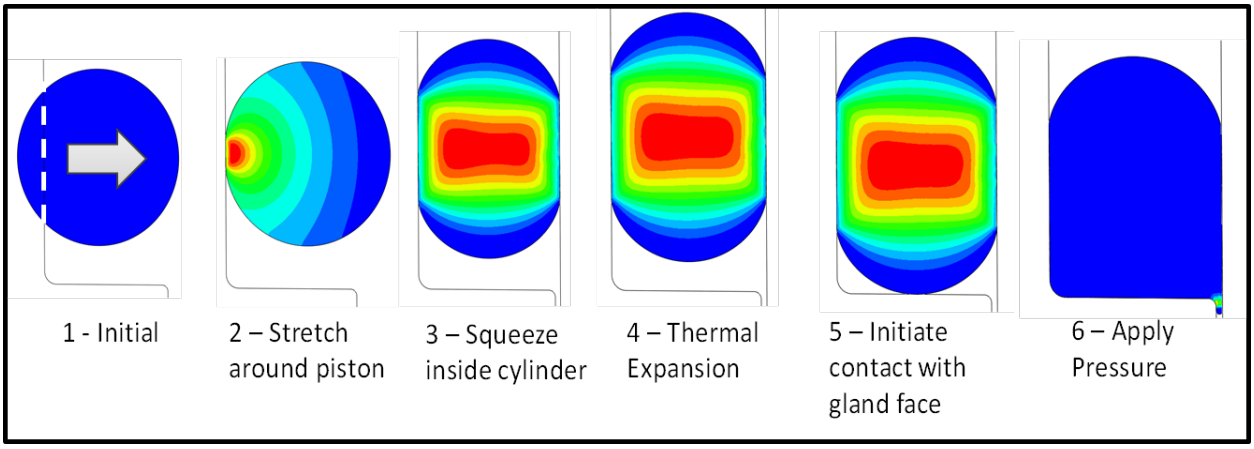


**Figure 64. Analysis steps for computing stress-distribution in O-ring as a function of pressure (Endurica, LLC).**

The FEA model was calibrated using the HPHT experimental E-CTP determined by PetroMar for each combination of material, hardness, temperature, and clearance gap. The PetroMar E-CTP pressure was used as the input pressure (blue p(θ) box in Figure 65) to the FEA simulation pushing the O-ring material. Each of these combinations generates a family of Tresca stress τ (pc,θ) curves (right side Figure 66) that are used along with the shear modulus (Gθ) and Tc(θ) from tear crack propagation tests run on slab samples to calculate the critical flaw size a0 for each material combination. The pressure/flaw-size calibrated FEA model simulations then are run and the initiation of tearing is analyzed, using the procedure shown in Figure 66. Further details can be found in the tearing criterion section of Appendix A.7.

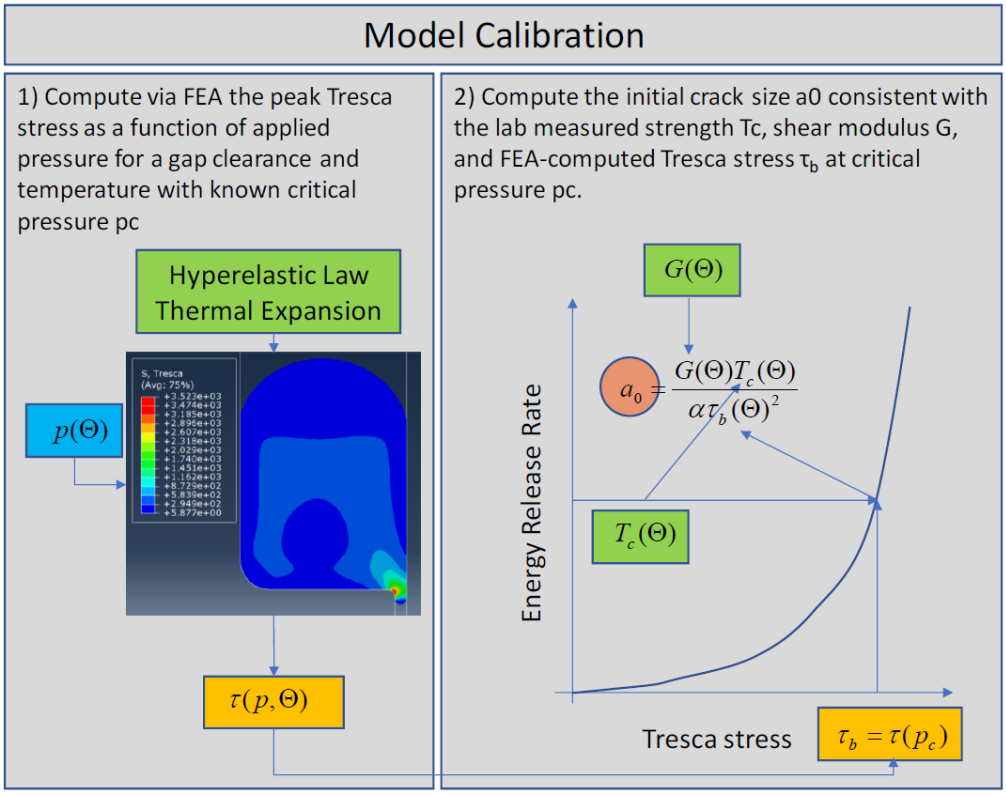


**Figure 65. Calibration of FEA model with HPHT E-CTP from PetroMar (Endurica, LLC).**

In both stepped pressure scan experiments following tear initiation, further extrusion of the O-ring was observed to occur via the propagation of a crack along an inward-spiraling path. Tear propagation resulted in a flap of roughly constant thickness being separated from the O-ring, and fed through the gap clearance. In the FEA model simulations, the continued extrusion of the O-ring into each gap clearance was monitored and the final extrusion distance was reported.

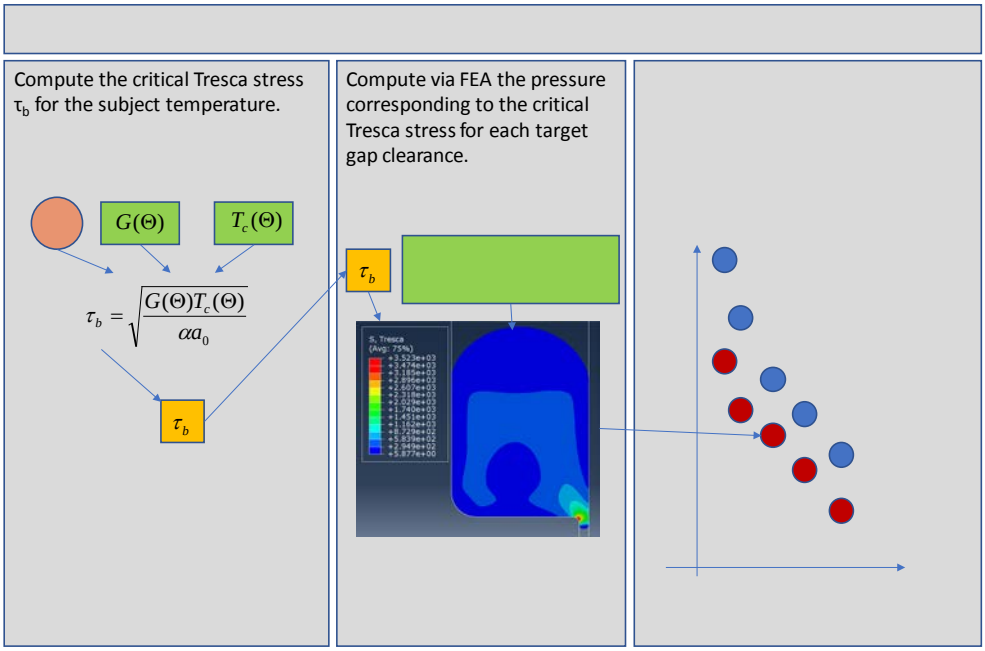


**Figure 66. Diagram showing the process for CTP determination (Endurica, LLC).**

## 7.3 Model Outputs

The mechanical state of the O-ring was recorded as a function of time during the simulation. The following outputs were estimated using the model:

1. Tresca stress distribution
2. Total recoverable strain energy
3. Total deformed O-ring volume
4. Strain energy density distribution
5. Extrusion distance: The extrusion distance was measured as the axial distance from the lower gland face to the furthest extruded point of the O-ring in the extrusion gap (see Figure 67).
6. Applied pressure to the O-ring.

Example Tresca stress maps generated from the model are shown in Figures 67 and 68, respectively. In each respective figure, the left image shows the O-ring that was extruded through the gap between the vessel and the piston. The colors on the map correlate to the Tresca stress levels experienced by the O-ring. The image on the right preserves the Tresca stress levels across the O-ring cross section, while "reversing" the model, and presenting the O-ring in its original form. This is useful to show how the O-ring material moved throughout the extrusion process, and which portions of the O-ring cross section exhibited the most stress. Images for each of the materials can be found in Appendix A.7.

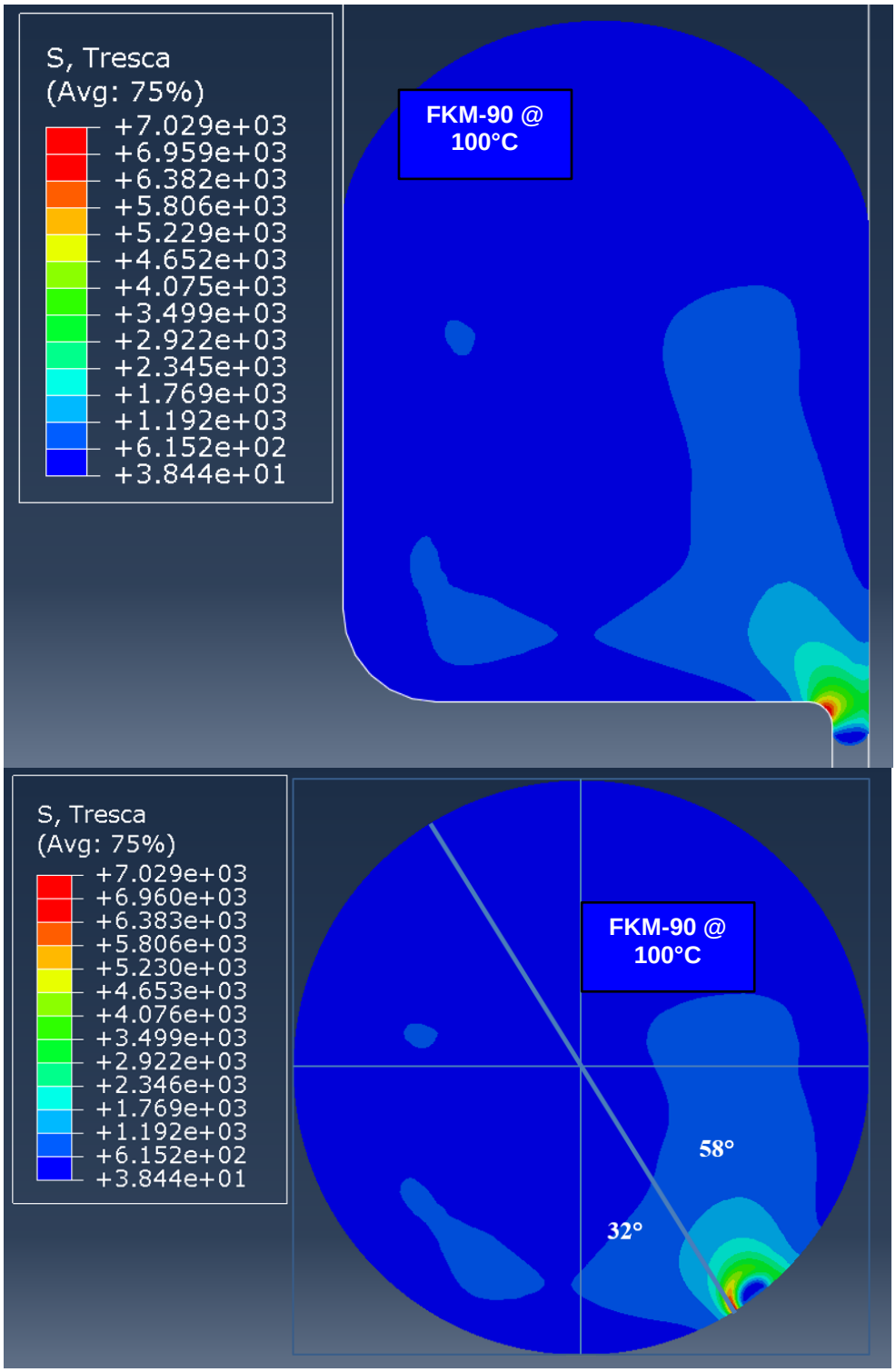


**Figure 67. Tresca stress maps (extruded top, recovered bottom) for FKM-90 O-ring at 100°C (Endurica, LLC).**

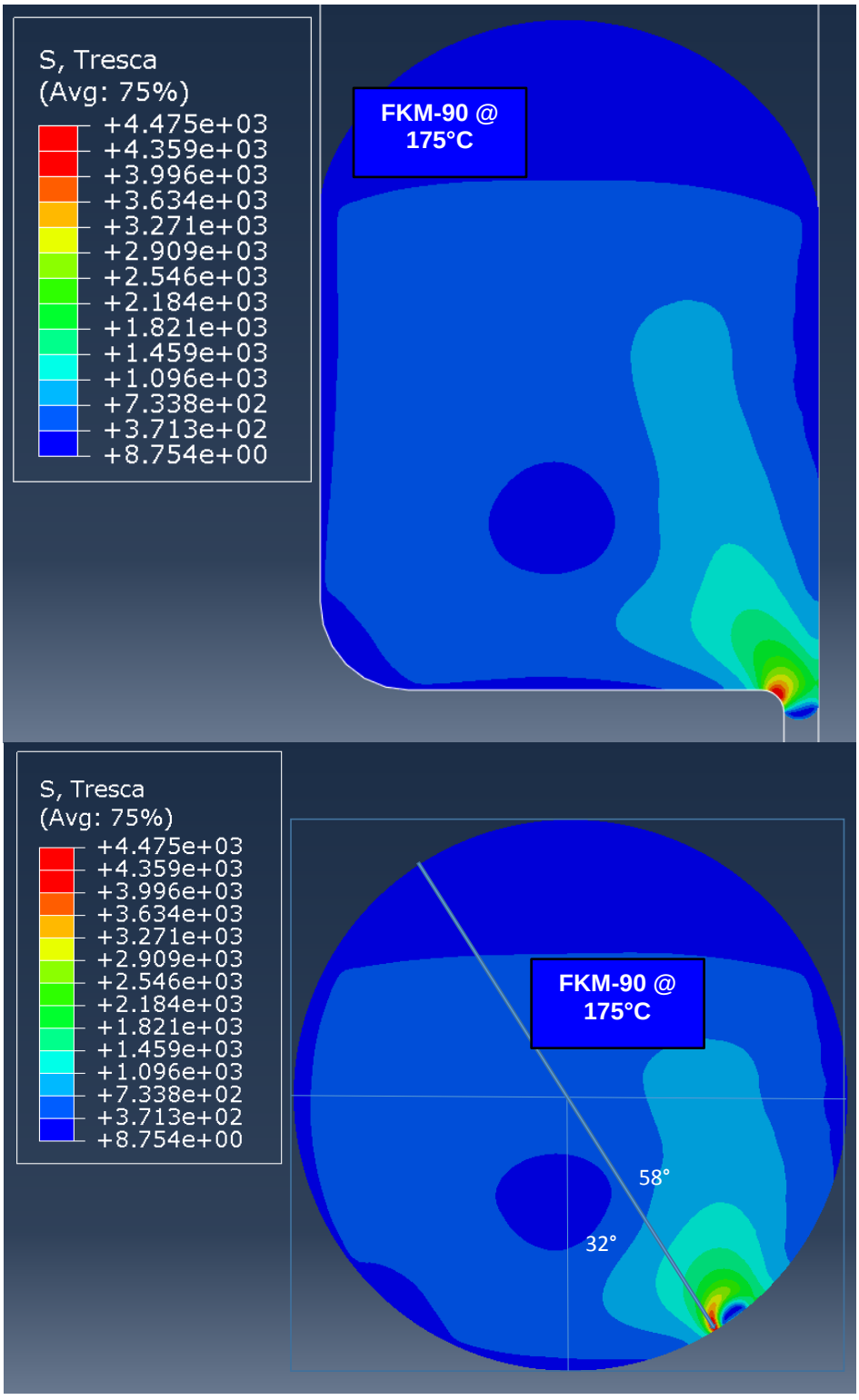


**Figure 68. Tresca stress maps (extruded top, recovered right) for FKM-90 O-ring at 175°C (Endurica, LLC).**

For each of the materials, the maximum Tresca stress identified in the Tresca stress maps (see Figures 67 and 68) was compared against critical Tresca stress (CTS) values obtained in the FEA model. In situations where the Tresca stress predicted by the FEA model exceeded the CTS for the material, it was assumed that a crack would develop, and the O-ring was considered to have failed. These data were then compared against the HPHT test data for validation. A representative plot comparing the FEA model results and the HPHT test results is shown in Figure 69 for the HNBR-90 material for all clearance gaps and temperatures evaluated.

Reasonable agreement was shown between the FEA model and HPHT test results. Complete plots comparing the FEA model and HPHT test results for all materials can be found in Appendix A.7.

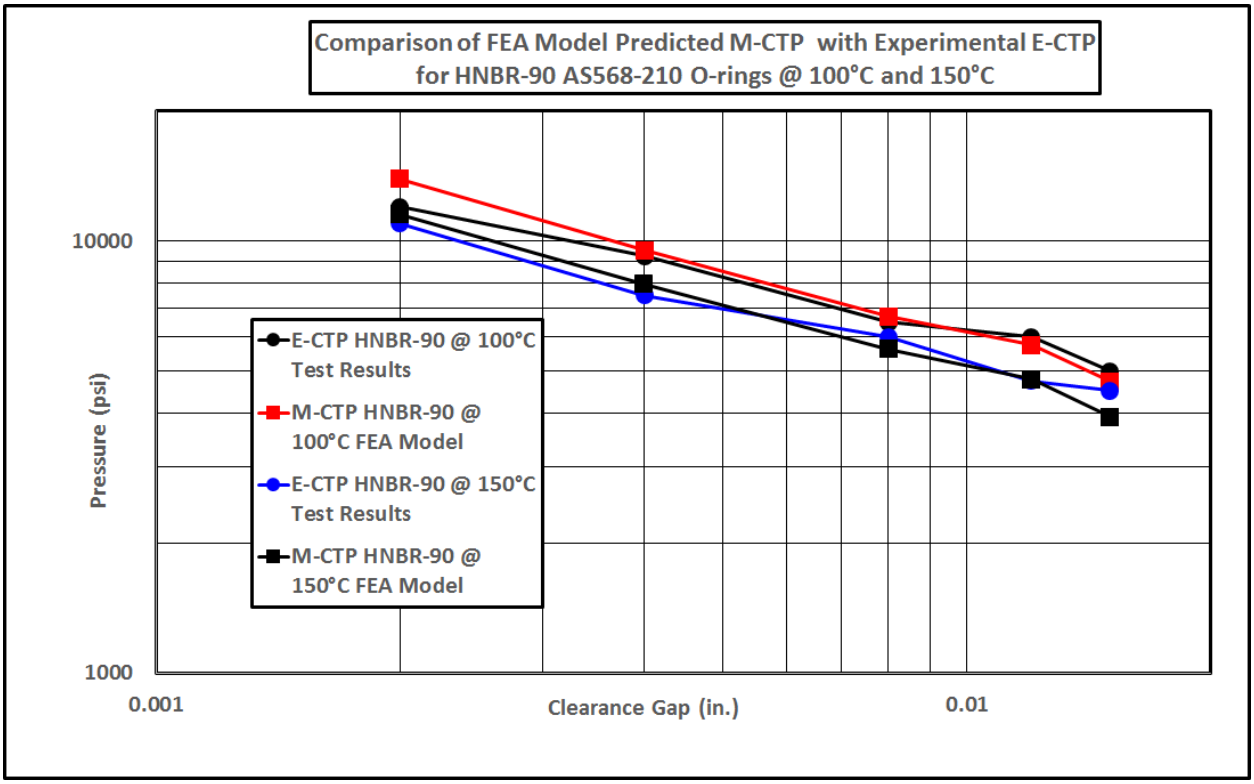


**Figure 69. Comparison of FEA (M-CTP) and HPHT Task 4 test results (E-CTP) for HNBR-90 material (Endurica, LLC).**

## 8.0 HPHT TESTING

### 8.1 HPHT Test Equipment and Fixture

PetroMar designed and constructed a special fixture and hydraulic system to test O-rings under HPHT conditions. Figures 70 and 71 illustrate the main components and features of the HPHT setup. The high-pressure hydraulic system test setup rated to 30,000 psi included:

- Manual fluid pump;
- Pressure vessel and a set of pistons accepting a AS568-210-size O-ring;
- Valves, tubes and fittings;
- Heater band;
- Oil-fill system capable of circulating oil under vacuum and filled with Rhodorsil 47V100 silicone fluid; and
- Pressure transducer and temperature sensors connected to the acquisition system.

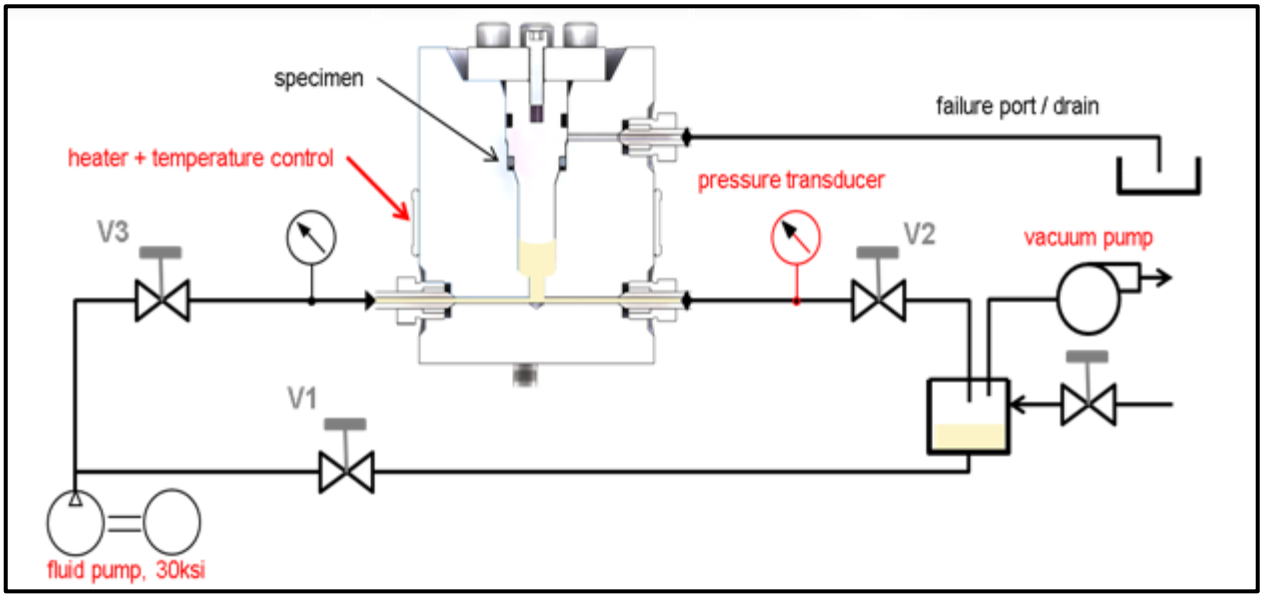


**Figure 70. HPHT O-ring schematic of the test system.**

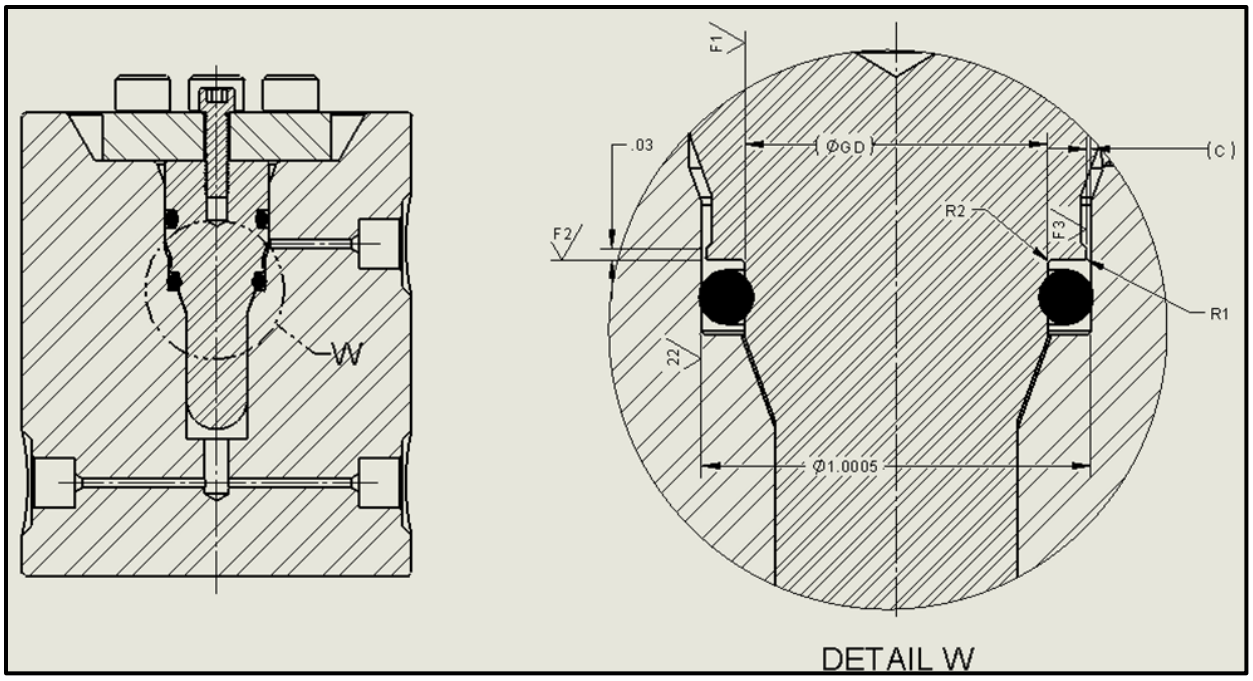


| PMT105302 | C | GD | R1 | R2 | F1 | F2 | F3 | PD |
|---|---|---|---|---|---|---|---|---|
| -10 | 0.0017 | 0.7779 | 0.0050 | 0.0150 | 9 | 9 | 9 | 0.9970 |
| -20 | 0.0037 | 0.7778 | 0.0050 | 0.0197 | 10 | 10 | 32 | 0.9930 |
| -30 | 0.0077 | 0.7778 | 0.0050 | 0.0197 | 12 | 12 | 32 | 0.9850 |
| -40 | 0.0120 | 0.7772 | 0.0060 | 0.0196 | 32 | 63 | 32 | 0.9765 |
| -50 | 0.0148 | 0.7780 | 0.0050 | 0.0197 | 16 | 16 | 16 | 0.9710 |

**Figure 71. Actual dimensions of the test fixture including set of pistons used (in.).**

Other important design and test considerations and parameters chosen for enhanced accuracy and precision of results were:

- Only new AS568-210 size O-rings were utilized;
- Other than the clearance gap, the gland dimensions were based on the Parker O-ring Handbook (Parker, 2007) recommendations for static seals;
- The initial squeeze was set to be 18% for each gap; and
- All tests were single-cycle tests.

## 8.2 Stepped-scan Tests

Under given temperature and clearance gap conditions, stepped-scan tests were conducted to indicate (1) pressure levels at which a specimen starts to extrude and (2) the highest pressure an O-ring can sustain before it either suffers the first large extrusion (FLE) event or a leak ($P_{ss\text{-}FLE}$).

During a stepped-scan test the temperature was kept constant, and the specimen was soaked at a given pressure level for five-minute durations, after which the pressure was stepped up every five minutes in increments of 500 psi. Evaluation of pressure stability on each level revealed whether a specimen sealed without extrusion (stable pressure levels) or partially extruded into the clearance gap. When a specimen extrudes, it leaves an additional volume for oil to occupy, which results in a small but detectable pressure decrease during that interval (creating a saw-tooth shaped step). The typical profile of a stepped-scan test is shown in Figure 72.

The presence of the "saw-tooth" shape provided initial estimates of the pressure where longer term dwell tests at constant pressure should be conducted. In some cases, this was about one-half of the corresponding FLE event pressure ($P_{ss}$-FLE).

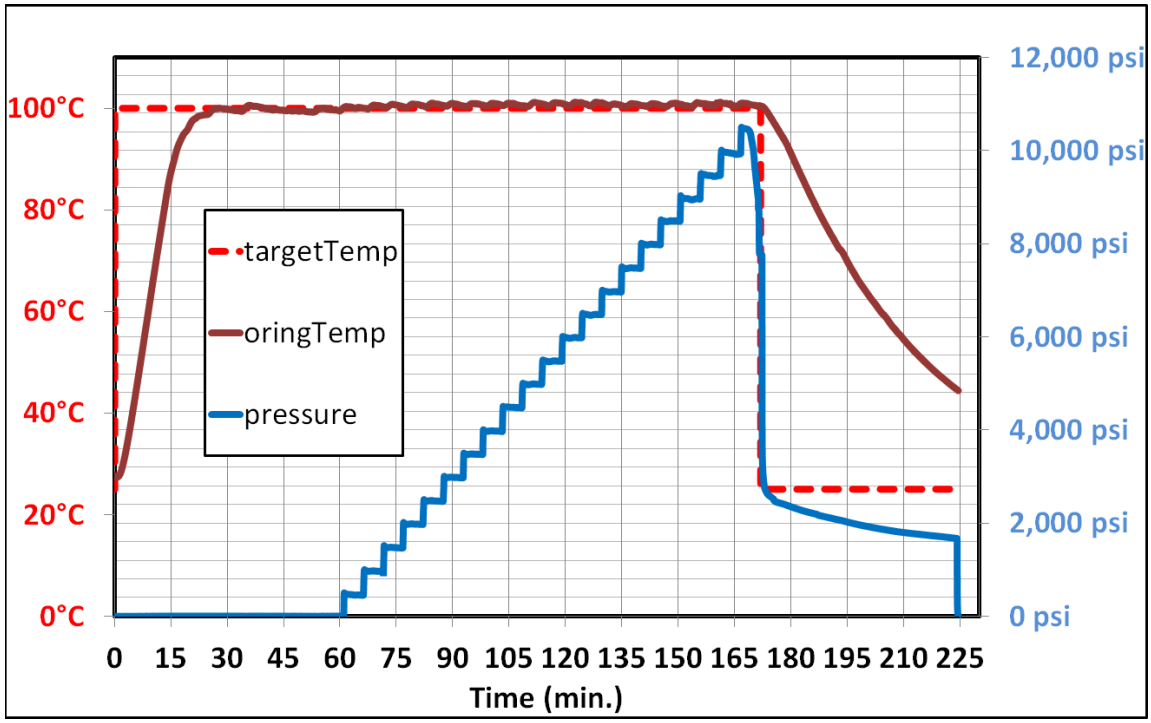


**Figure 72. Stepped-scan HPHT test profile per the D100511 procedure.**

## 8.3 Removal and Examination of O-Rings (Color Coding)

The determination of the critical pressure level that initiates tears or cuts on the O-ring surface was an iterative process. For every combination of test parameters, this search required a series of up to five specimens dwell tested (dwell tests described below) at different pressure levels. Although all tested specimens were documented and stored, only one specimen per series was used to define the experimentally derived E-CTP. The remaining specimens will have different levels of damage, but not damage corresponding to E-CTP. To simplify the classification of data, the tested specimens were sorted into three main groups: green, yellow, and red based on the extent of the damage (see Appendix 6, Figures 8, 9, and 10):

Green group:

- No visible damage
- Seating

Yellow group:

- Thin-band cut off
- Small-size extrusion with visible damage
- Visible localized cuts/tears
- Nibbled surface

Red group:

- FLE event (after stepped-scans)
- Large extrusion/deep circumferential cuts

Each O-ring from the green group was examined under a microscope to find small cuts and tears otherwise invisible to the naked eye. If these tiny damages were found, the pressure to which this O-ring was subjected was defined to be the E-CTP for that material at that durometer, temperature, and clearance. This pressure was on the borderline between the green and yellow groups, that is, at the transition of an undamaged O-ring to a damaged O-ring. These O-rings were marked as green-yellow and kept in the green group on plots.

## 8.4 Dwell Testing to Determine Experimental Critical Tearing Pressure (E-CTP)

PetroMar used the results of the stepped-scan tests to provide insight in the starting search for the minimal pressure at which an O-ring of a material and durometer is expected to tear at a given temperature (E-CTP). This was achieved by running a series of dwell tests utilizing up to five nominally identical O-rings exposed to different pressure levels. The strategy was to test the first

O-ring at a fixed pressure, examine the O-ring for damage, and then deciding which way to adjust the pressure for the next O-ring. Once an O-ring exhibited only visible localized cuts and tears under a microscope (yellow criterion), the pressure was reduced until no-damage (green criterion) and that pressure was defined to be the E-CTP for that combination of material, durometer, temperature, and clearance. Typically, the iterations continued until the pressure difference between the damaged and undamaged O-rings was less than 100 psi. The HPHT profile used in the dwell tests is shown in Figure 73.

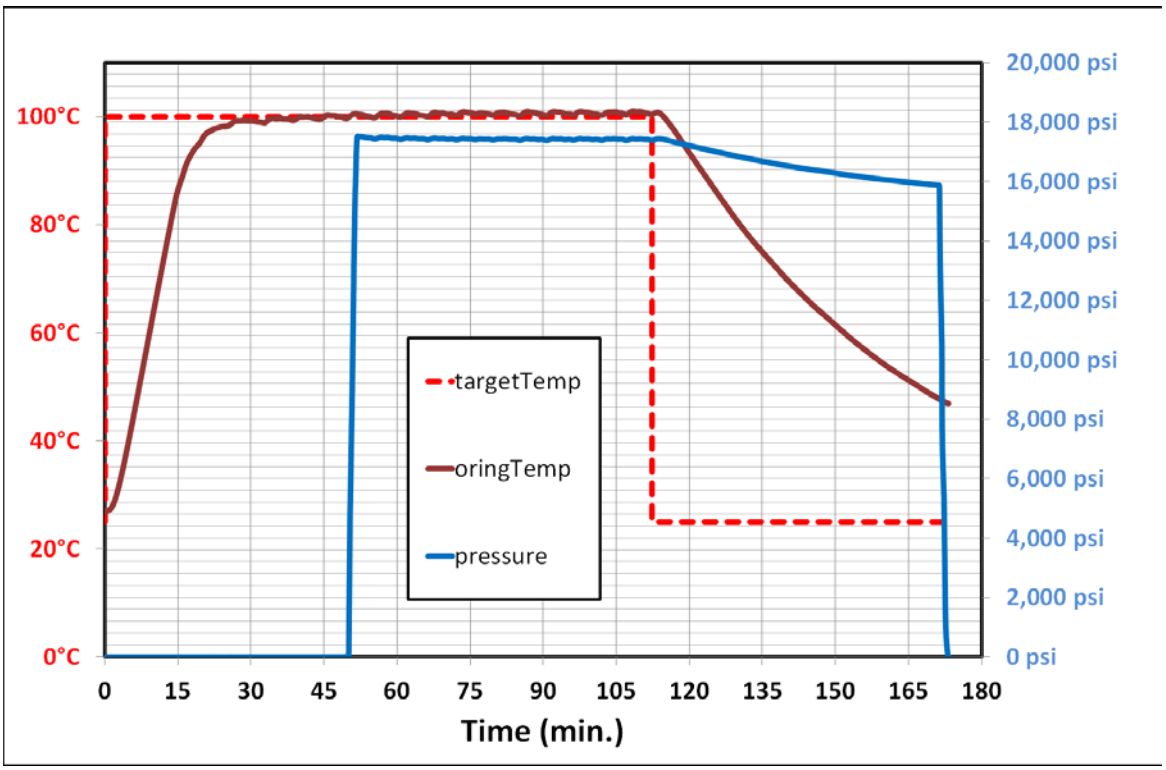


**Figure 73. HPHT O-ring dwell test profile per PetroMar D100511 procedure.**

Table 37 shows the matrix of dwell tests conducted based on the results of the stepped-scan testing.

**Table 37. Test matrix for dwell testing.**

| Material | Compound Reference | Nominal Hardness | Actual Hardness Mean | Service Temperature [°C] | Test Temp#1 [°C] | Test Temp#2 [°C] |
|---|---|---|---|---|---|---|
| FKM-75 | F-13664 (F75) / Mil-83248-1 | 75 | 77 | -20 to +200 | 100 | 175 |
| FKM-90 | F-13681 (F90) / Mil-83248-2 | 90 | 91 | -20 to +200 | 100 | 175 |
| NBR-75 | B1016 | 75 | 76 | -30 to +120 | 100 | n/a |
| NBR-90 | B1001 | 90 | 94 | -30 to +120 | 100 | n/a |
| HNBR-75 | R1006 | 75 | 76 | -35 to +160 | 100 | 150 |
| HNBR-90 | R1003 | 90 | 92 | -35 to +160 | 100 | 150 |
| FEPM-80 | L1000 | 80 | 89 | -20 to +230 | 100 | 175 |
| FEPM-83 | 210-A-83 | 83 | 83 | -20 to +230 | 100 | 175 |
| FFKM-75 | K4079 | 75 | 76 | -2 to +316 | 100 | 175 |
| FFKM-90 | K3018 | 90 | 94 | -40 to +270 | 100 | 175 |

## 8.5 Power Law Data Analysis Procedures

The upper pressure level of the green criterion or “no-damage” group defines the E-CTP for each set of test parameters. The critical pressures for the five clearances tested can be interpolated using power law regression

$$E\text{-}CTP = A * C^{B} \qquad \text{Equation 2}$$

where:

E-CTP is a critical tearing pressure [psi],
C is clearance gap [inch],
A and B are coefficients.

Figure 74 illustrates how E-CTP is defined for each of the five clearance gaps (green circles). It also illustrates the power regression coefficients and the corresponding fit curve.

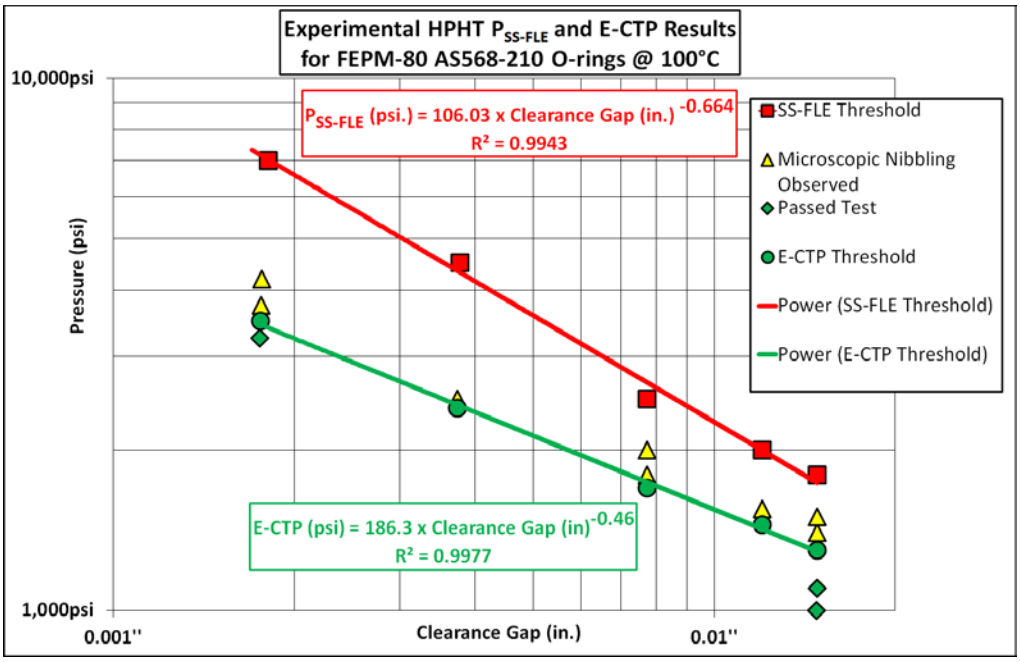


**Figure 74. Example of the E-CTP levels versus clearance gap and their interpolation using power regression with coefficients A=186.3 and B=-0.46 (black line). Red line represents interpolation of the pressure-stepped large extrusion results.**

## 8.6 Hardness Measurement

Shore A hardness was measured on elastomer material (slabs, test coupons and O-rings) as a check that the nominal value was close to the actual value. Hardness and tensile modulus are traditionally used to select elastomers and composites in O&G operations based on “rules of thumb” derived from decades of experience and empirical information.

The test method used for hardness measurement is ASTM D2240-15 “Standard Test Method for Rubber Property—Durometer Hardness”. The method uses an indenter (Figure 75) on the surface of the material; indentation hardness is inversely related to the penetration and is related to the elastic modulus and viscoelastic behavior of the material. The indenter is formed from steel rod, hardened to 500 HV10, and sharpened to the dimensions indicated. The penetration depth of the test is approximately 2.5 mm (0.100 inches).

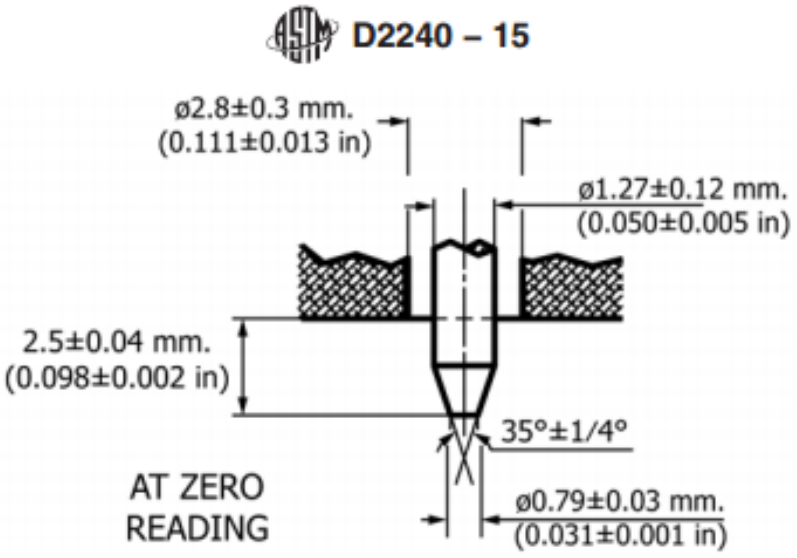


**Figure 75. Diagram of indenter used in hardness testing (ASTM, 2015).**

To ensure precision and accuracy of the hardness measuring apparatus, the durometer must be mounted in an operating stand with a cylindrical weight that is brought down on the indenter using a lever action. Special fixtures were employed to hold the O-ring in place (Figure 76). Immediately after testing an indentation hole was visible, confirming that penetration into the sample had occurred. Because of the potential for this to produce a defect site in test specimens, surplus test articles (slabs and O-rings) were reserved for these tests. Testing was performed on 10 slab material samples and 100 O-ring samples for each elastomer in this study.

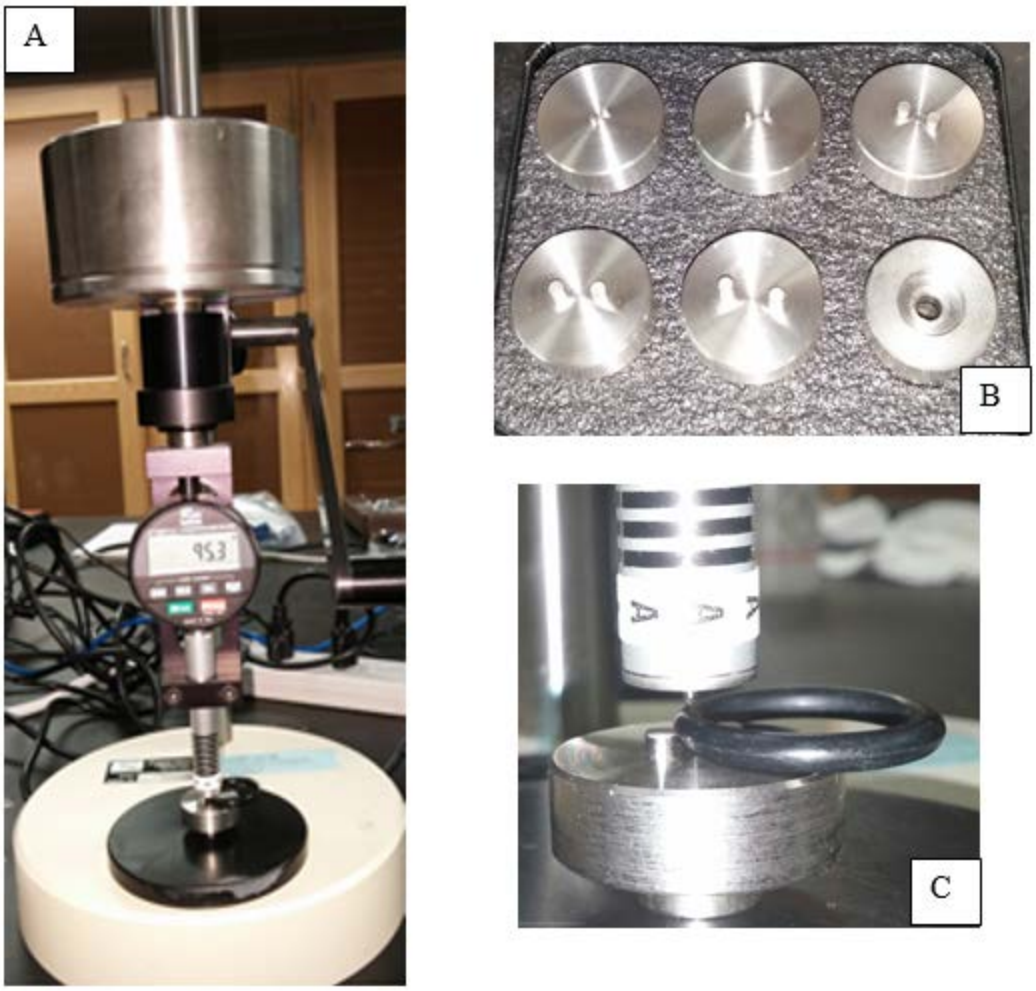


**Figure 76. A) Rex durometer Model OS-1 operating stand serial # 2259964; B) Rex durometer Model OS-1 operating stand serial # 2259964; C) hardness test being conducted on -210 O-ring.**

## 8.7 Results

### *8.7.1 Test Results for E-CTP and FLE*

The test results for the dwell testing to calculate the E-CTP and FLE for each elastomer and each set of conditions are presented in Table 38 through Table 42 and Figures 77 through 86.

#### *8.7.1.1 FKM*

**Table 38. E-CTP and SS-FLE pressure versus clearance gap for FKM-75 and FKM-90 at 100°C and 175°C.**

| E-CTP FKM-75, FKM-90 | | | | | | | | |
|---|---|---|---|---|---|---|---|---|
| Nominal Clearance Gap (@ 25°C) | Clearance Gap (in.) @ 100°C | E-CTP, FKM-75 @ 100°C (psi) | Clearance Gap (in.) @ 100°C | E-CTP, FKM-90 (psi) | Clearance Gap (in.) @175°C | E-CTP, FKM-75 @175°C (psi) | Clearance Gap (in.) @ 175°C | E-CTP, FKM-90 @ 175°C (psi) |
| 0.0148" | 0.0148336 | 2,100 | 0.0148672 | 4,200 | 0.014824 | 1,500 | 0.014848 | 3,000 |
| 0.012" | 0.0120392 | 2,450 | 0.0120672 | 4,200 | 0.012028 | 1,750 | 0.012048 | 3,000 |
| 0.0077" | 0.007752 | 3,250 | 0.007784 | 5,250 | 0.007736 | 2,250 | 0.0077612 | 3,825 |
| 0.0037" | 0.0037784 | 4,900 | 0.0038312 | 8,200 | 0.0037512 | 3,200 | 0.00378 | 5,000 |
| 0.0017" | 0.0018152 | 7,200 | 0.001868 | 10,500 | 0.0017704 | 4,400 | 0.001812 | 7,000 |
| SS-FLE FKM-75, FKM-90 | | | | | | | | |
| Nominal Clearance Gap (@ 25°C) | Clearance Gap (in.) @ 100°C | SS-FLE, FKM-75 @100°C (psi) | Clearance Gap @ 100°C (in.) | SS-FLE, FKM-90 @100°C (psi) | Clearance Gap (in.) @175°C | SS-FLE, FKM-75 @175°C (psi) | Clearance Gap @175°C (in.) | SS-FLE, FKM-90 @175°C (psi) |
| 0.0148" | 0.014856 | 3,500 | 0.014904 | 6,500 | 0.014832 | 2,000 | 0.014864 | 4,000 |
| 0.012" | 0.012064 | 4,000 | 0.012112 | 7,000 | 0.012048 | 3,000 | 0.01208 | 5,000 |
| 0.0077" | 0.007788 | 5,500 | 0.007868 | 10,500 | 0.007756 | 3500 | 0.007796 | 6,000 |
| 0.0037" | 0.00386 | 10,000 | 0.004028 | 20,500 | 0.003804 | 6,500 | 0.003868 | 10,500 |
| 0.0017" | 0.002044 | 21,500 | 0.0017 | Use power law | 0.001868 | 10,500 | 0.00202 | 20,000 |

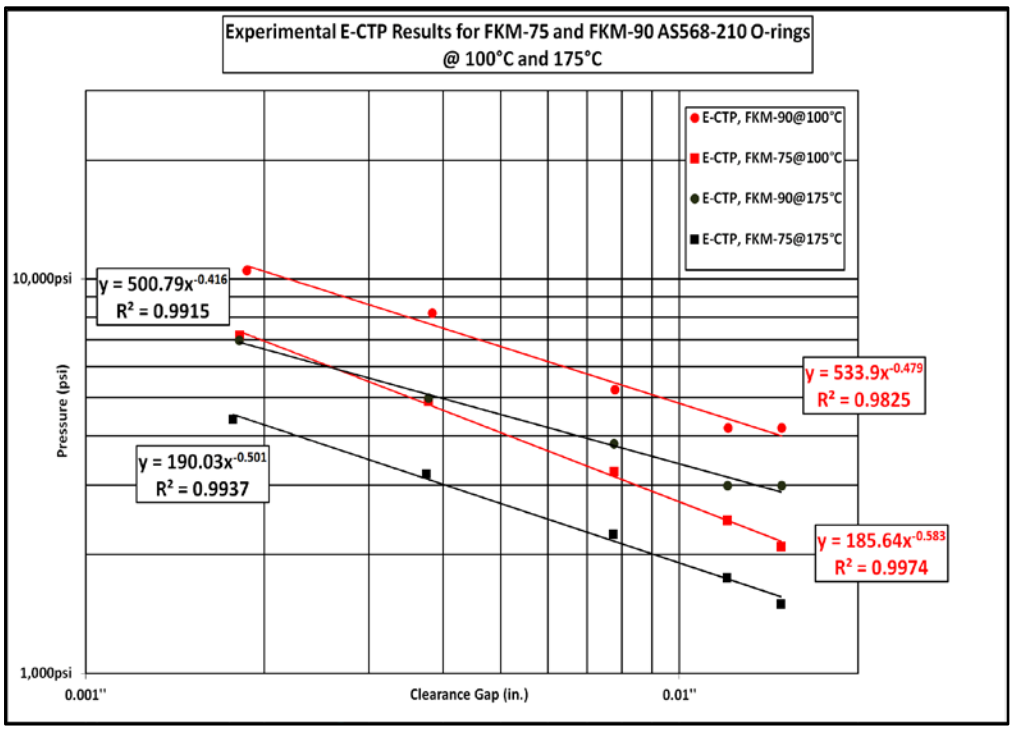


**Figure 77. Experimental E-CTP versus clearance gap for FKM-75 and FKM-90 at 100°C and 175°C.**

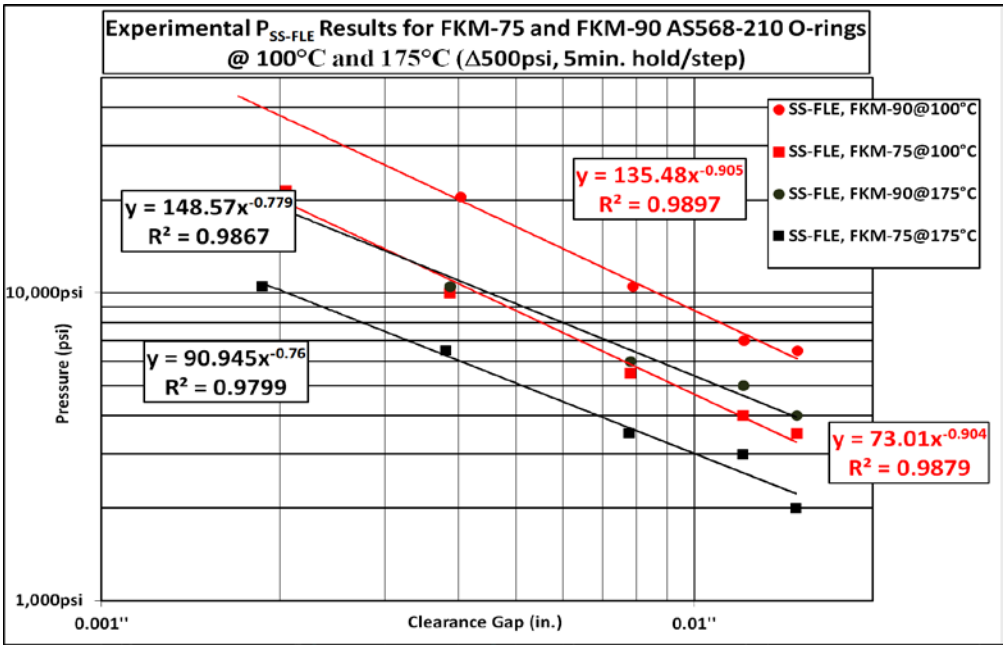


**Figure 78. Experimental Stepped-Scan (SS-FLE) threshold pressure versus clearance gap for FKM-75 and FKM-90 at 100°C and 175°C.**

#### *8.7.1.2 NBR*

**Table 39. E-CTP and SS-FLE pressure versus clearance gap for NBR-75 and NBR-90 at 100°C.**

| E-CTP NBR-75, NBR-90 | | | | |
|---|---|---|---|---|
| Nominal Clearance Gap (@ 25°C) | Clearance Gap (in.) @ 100°C | E-CTP, NBR-75 @ 100°C (psi) | Clearance Gap (in.) @ 100°C | E-CTP, NBR-90 @ 100°C (psi) |
| 0.0148" | 0.014856 | 3,500 | 0.0149 | 6,250 |
| 0.012" | 0.0120604 | 4,000 | 0.0121 | 6,250 |
| 0.0077" | 0.07776 | 4,750 | 0.07812 | 7,000 |
| 0.0037" | 0.03808 | 6,750 | 0.03868 | 10,500 |
| 0.0017" | 0.01824 | 7,750 | 0.01956 | 16,000 |
| **SS-FLE NBR-75, NBR-90** | | | | |
| Nominal Clearance Gap (@ 25°C) | Clearance Gap (in.) @ 100°C | SS-FLE, NBR-75 @100°C (psi) | Clearance Gap (in.) @ 100°C | SS-FLE, NBR-90 @100°C (psi) |
| 0.0148" | 0.014888 | 5,500 | 0.014.36 | 8,500 |
| 0.012" | 0.0120604 | 6,500 | 0.0121 | 10,500 |
| 0.0077" | 0.07844 | 9,000 | 0.07956 | 16,000 |
| 0.0037" | 0.04004 | 19,000 | 0.037 | Use Power Law |
| 0.0017" | 0.01876 | 25000 | 0.017 | Use Power Law |

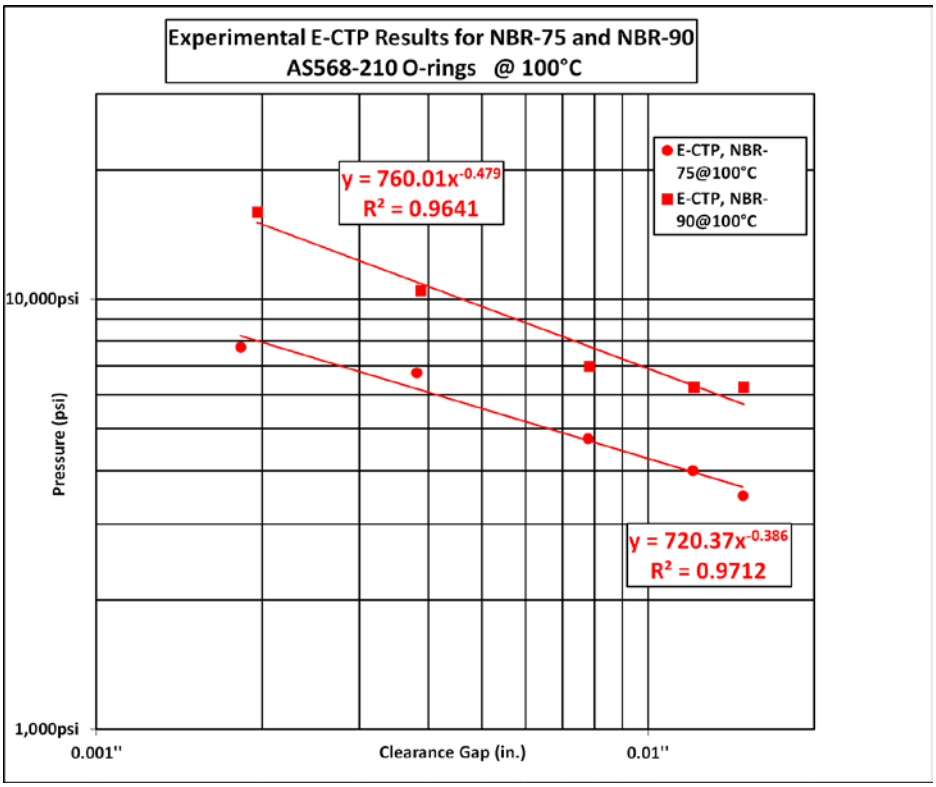


**Figure 79. E-CTP versus clearance gap for NBR-75 and NBR-90 at 100°C.**

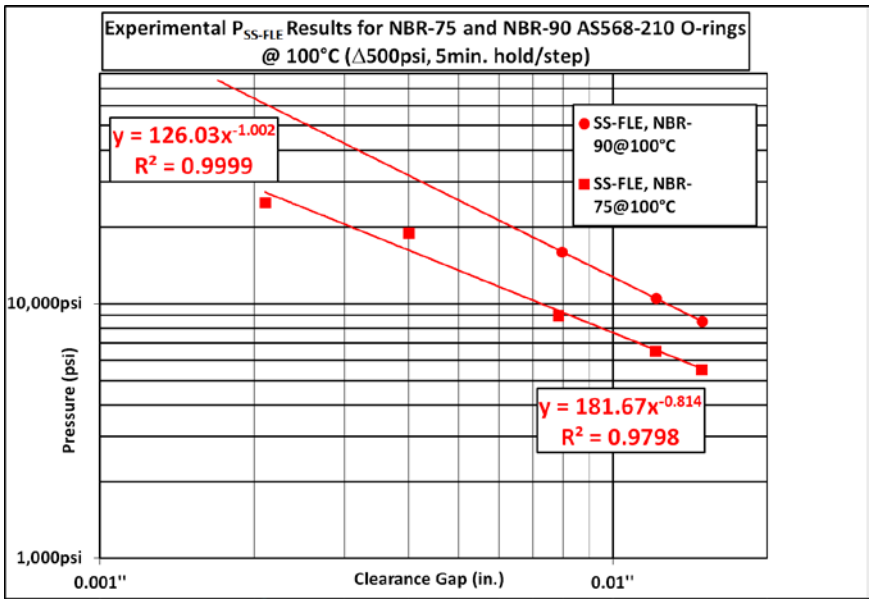


**Figure 80. FLE pressure versus clearance gap for NBR-75 and NBR-90 at 100°C.**

### *8.7.1.3 HNBR*

**Table 40. E-CTP and SS-FLE pressure versus clearance gap (in.) for HNBR-75 and HNBR-90 at 100°C and 150°C.**

| E-CTP HNBR-75, HNBR-90 | | | | | | | | |
|---|---|---|---|---|---|---|---|---|
| Nominal Clearance Gap (@ 25°C) | Clearance Gap (in.) @ 100°C | E-CTP, HNBR-75 @ 100°C (psi) | Clearance Gap (in.) @ 100°C | E-CTP, HNBR-90 @ 100°C (psi) | Clearance Gap (in.) @ 175°C | E-CTP, HNBR-75 @175°C (psi) | Clearance Gap @ 175°C (0.000”s) | E-CTP, HNBR-90 @ 175°C (psi) |
| 0.0148" | 0.0148288 | 1,800 | 0.01488 | 5,000 | 0.014828 | 1,750 | 0.014872 | 4,500 |
| 0.012" | 0.0120304 | 1,900 | 0.012096 | 6,000 | 0.012036 | 2,250 | 0.012076 | 4,750 |
| 0.0077" | 0.0774 | 2,500 | 0.07804 | 6,500 | 0.07736 | 2,250 | 0.07796 | 6,000 |
| 0.0037" | 0.03764 | 4,000 | 0.03848 | 9,250 | 0.03752 | 3,250 | 0.0382 | 7,500 |
| 0.0017" | 0.018 | 6,250 | 0.01892 | 12,000 | 0.0176 | 3,750 | 0.01876 | 11,000 |
| **SS-FLE HNBR-75, HNBR-90** | | | | | | | | |
| Nominal Clearance Gap (@ 25°C) | Clearance Gap (in.) @ 100°C | SS-FLE, HNBR-75 @ 100°C (psi) | Clearance Gap (in.) @ 100°C | SS-FLE, HNBR-90 @ 100°C (psi) | Clearance Gap (in.) @ 175°C | SS-FLE, HNBR-75 @ 175°C (psi) | Clearance Gap (in.) @ 175°C | SS-FLE, HNBR-90 @ 175°C (psi) |
| 0.0148" | 0.01484 | 2,500 | 0.014912 | 7,000 | 0.01484 | 3,000 | 0.014848 | 6,500 |
| 0.012" | 0.012048 | 3,000 | 0.012128 | 8,000 | 0.012048 | 4,000 | 0.012048 | 7,500 |
| 0.0077" | 0.07756 | 3,500 | 0.07884 | 11,500 | 0.0778 | 4000 | 0.07764 | 11,000 |
| 0.0037" | 0.03796 | 6,000 | 0.04036 | 21,000 | 0.0386 | 5,000 | 0.038248 | 17,500 |
| 0.0017" | 0.01876 | 11000 | 0.017 | Use Power law | 0.01996 | 10,000 | 0.01908 | Use Power law |

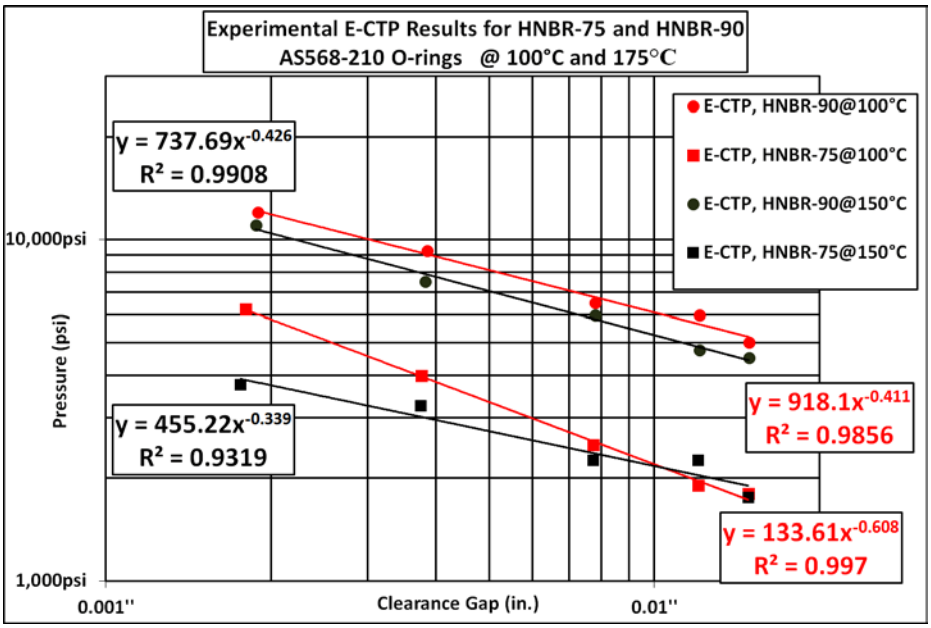


**Figure 81. Experimental E-CTP versus clearance gap for HNBR-75 and HNBR-90 at 100°C and 150°C**

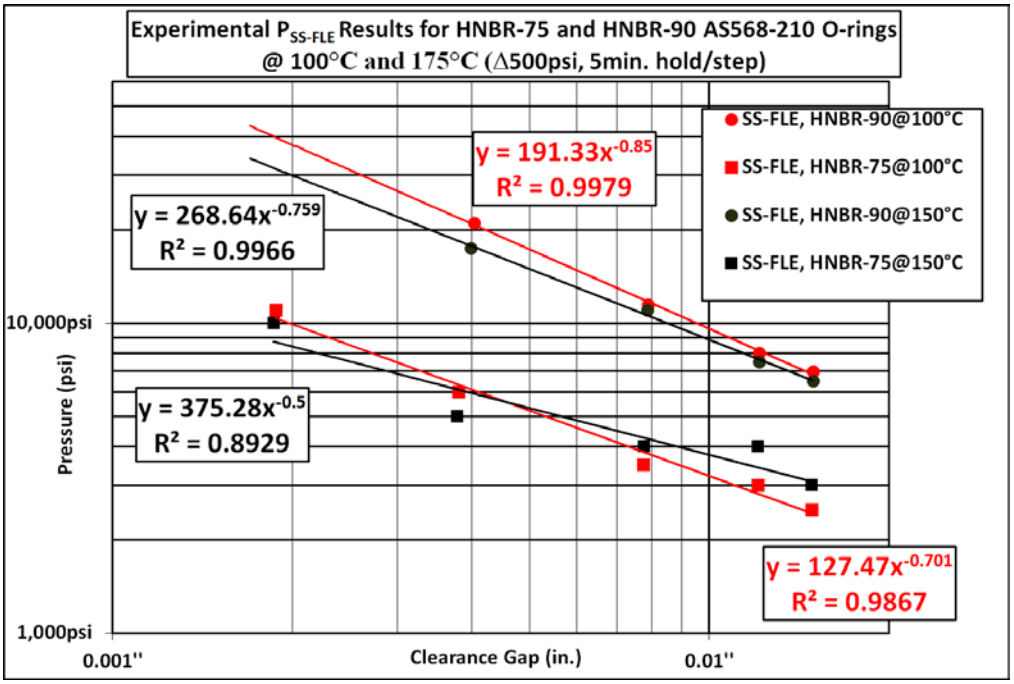


**Figure 82. Experimental SS-FLE pressure versus clearance gap for HNBR-75 and HNBR-90 at 100°C and 150°C**

### *8.7.1.4 FEPM*

**Table 41. E-CTP and SS-FLE pressure versus clearance gaps (in.) for FEPM-80 (89) and FEPM-83 (83) at 100°C and 175°C.**

| E-CTP FEPM-80 (89), FEPM-83 | | | | | | | | |
|---|---|---|---|---|---|---|---|---|
| Nominal Clearance Gap (@ 25°C) | Clearance Gap (in.) @ 100°C | E-CTP, FEPM-80 @ 100°C (psi) | Clearance Gap (in.) @ 100°C | E-CTP, FEPM-83 @ 100°C (psi) | Clearance Gap (in.) @ 175°C | E-CTP, FEPM-80 @ 175°C (psi) | Clearance Gap (in.) @ 175°C | E-CTP, FEPM-83 @ 175°C (psi) |
| 0.0148" | 0.0148336 | 1,750 | 0.014856 | 1,750 | 0.0148256 | 1,300 | 0.014824 | 1,600 |
| 0.012" | 0.01204 | 1,900 | 0.0120576 | 1,900 | 0.012028 | 1,450 | 0.0120256 | 1,675 |
| 0.0077" | 0.07756 | 2,250 | 0.07772 | 2,350 | 0.07736 | 1,700 | 0.07732 | 1,950 |
| 0.0037" | 0.0378 | 3,500 | 0.03796 | 3,300 | 0.03752 | 2,400 | 0.03748 | 2,600 |
| 0.0017" | 0.01792 | 4,800 | 0.0186 | 4,250 | 0.01772 | 3,500 | 0.01756 | 3,250 |
| **SS-FLE FEPM-80 (89), FEPM-83** | | | | | | | | |
| Nominal Clearance Gap (@ 25°C) | Clearance Gap (in.) @ 100°C | SS-FLE, FEPM-80 @ 100°C (psi) | Clearance Gap (in.) @ 100°C | SS-FLE, FEPM-83 @ 100°C (psi) | Clearance Gap (in.) @ 175°C | SS-FLE, FEPM-80 @ 175°C (psi) | Clearance Gap (in.) @ 175°C | SS-FLE, FEPM-83 @ 175°C (psi) |
| 0.0148" | 0.01484 | 2,500 | 0.014896 | 2,500 | 0.01484 | 1,800 | 0.014848 | 2,000 |
| 0.012" | 0.012056 | 3,000 | 0.01212 | 2,500 | 0.012048 | 2,000 | 0.012048 | 2,200 |
| 0.0077" | 0.07804 | 3,500 | 0.07868 | 3,000 | 0.0778 | 2,500 | 0.07764 | 3,000 |
| 0.0037" | 0.03972 | 6,500 | 0.041 | 6,000 | 0.0386 | 4,500 | 0.038248 | 5,000 |
| 0.0017" | 0.017 | 11,000 | 0.017 | 9,000 | 0.01996 | 7,000 | 0.01908 | 7,500 |

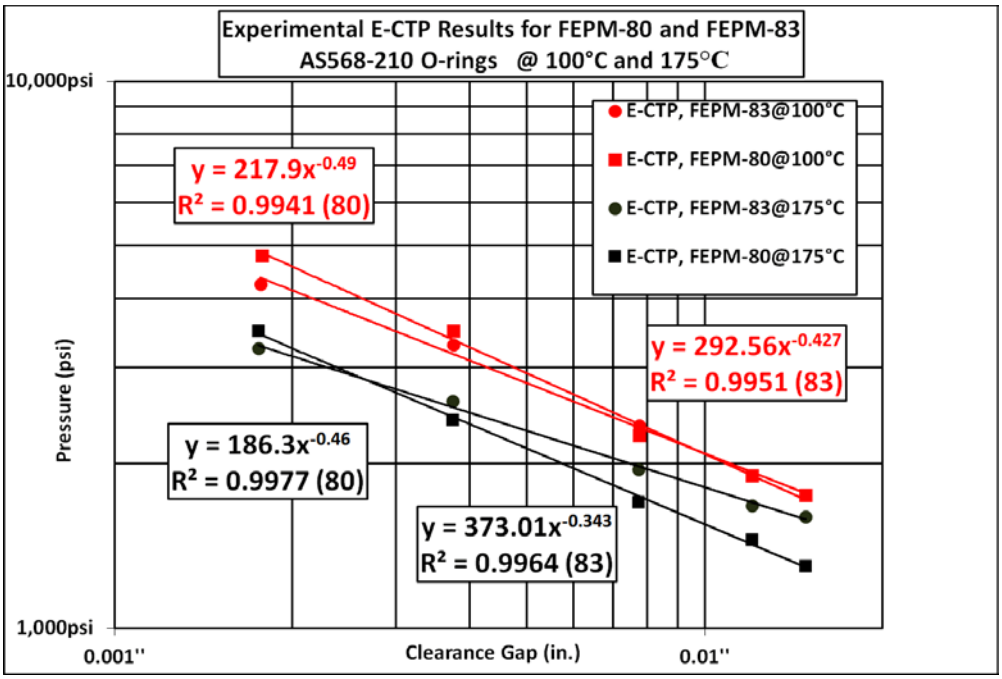


**Figure 83. E-CTP versus clearance gap for FEPM-80 (~89 durometer actual) and FEPM-83 (~ 83 durometer actual) at 100°C and 175°C.**

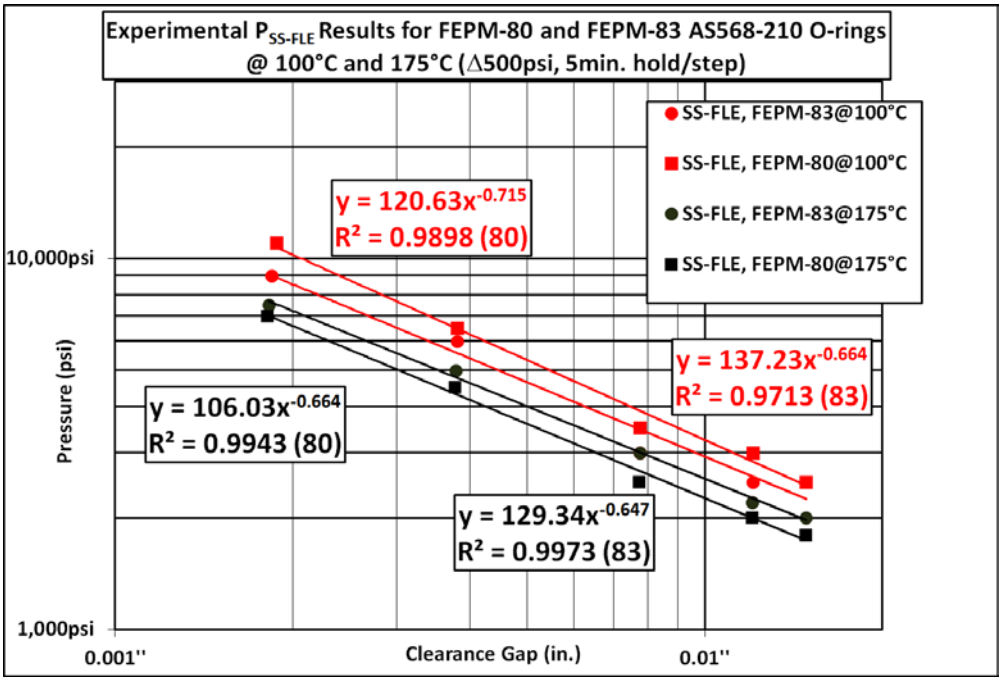


**Figure 84. Experimental SS-FLE pressure versus clearance gap for FEPM-80 (~89 durometer actual) and FEPM-83 (~ 83 durometer actual) at 100°C and 175°C.**

### *8.7.1.5 FFKM E-CTP and SS-FLE*

**Table 42. E-CTP and SS-FLE Threshold pressures versus clearance gap (in.) for FFKM-75 and FFKM-90 at 100°C and 175°C.**

| E-CTP FFKM-75, FFKM-90 | | | | | | | | |
|---|---|---|---|---|---|---|---|---|
| Nominal Clearance Gap (@ 25°C) | Clearance Gap (in.) @ 100°C | E-CTP, FFKM-75 @ 100°C (psi) | Clearance Gap (in.) @ 100°C | E-CTP, FFKM-90 (psi) | Clearance Gap (in.) @175°C | E-CTP, FFKM-75 @175°C (psi) | Clearance Gap (in.) @175°C | E-CTP, FFKM-90 @ 175°C (psi) |
| 0.0148" | 0.0148336 | 2,100 | 0.014856 | 3,500 | 0.0148256 | 1,600 | 0.014824 | 1,500 |
| 0.012" | 0.01204 | 2,500 | 0.0120576 | 3,600 | 0.012028 | 1,750 | 0.0120256 | 1,600 |
| 0.0077" | 0.07756 | 3,500 | 0.07772 | 4,500 | 0.07736 | 2,250 | 0.07732 | 2,000 |
| 0.0037" | 0.0378 | 5,000 | 0.03796 | 6,000 | 0.03752 | 3,250 | 0.03748 | 3,000 |
| 0.0017" | 0.01792 | 5,750 | 0.0186 | 10,000 | 0.01772 | 4,500 | 0.01756 | 3,500 |
| **SS-FLE FFKM-75, FFKM-90** | | | | | | | | |
| Nominal Clearance Gap (@ 25°C) | Clearance Gap (in.) @ 100°C | SS-FLE, FFKM-75 @ 100°C (psi) | Clearance Gap @ (in.) 100°C | SS-FLE, FFKM-90 @ 100°C (psi) | Clearance Gap (in.) @175°C | SS-FLE, FFKM-75 @175°C (psi) | Clearance Gap (in.) @ 175°C | SS-FLE, FFKM-90 @ 175°C (psi) |
| 0.0148" | 0.01484 | 2,500 | 0.014896 | 6,000 | 0.01484 | 2,500 | 0.014848 | 3,000 |
| 0.012" | 0.012056 | 3,500 | 0.01212 | 7,500 | 0.012048 | 3,000 | 0.012048 | 3,000 |
| 0.0077" | 0.07804 | 6,500 | 0.07868 | 10,500 | 0.0778 | 5,000 | 0.07764 | 4,000 |
| 0.0037" | 0.03972 | 17,000 | 0.041 | 25,000 | 0.0386 | 10,000 | 0.038248 | 7,800 |
| 0.0017" | 0.017 | Use Power law | 0.017 | Use Power law | 0.01996 | 18,500 | 0.01908 | 13,000 |

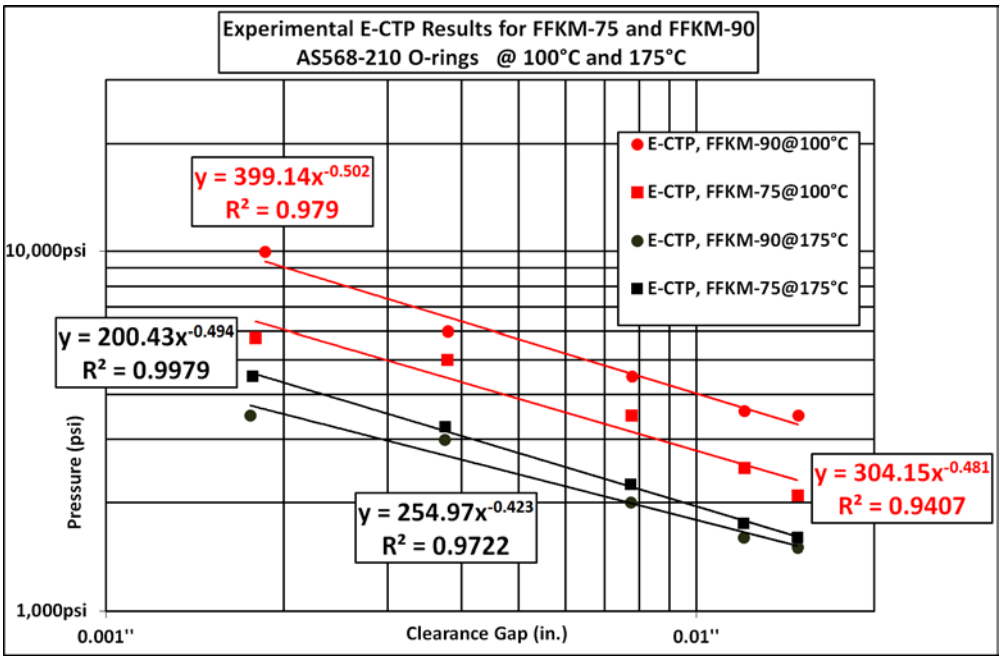


**Figure 85. Experimental E-CTP versus clearance gap for FFKM-75 and FFKM- 90 at 100°C and 175°C.**

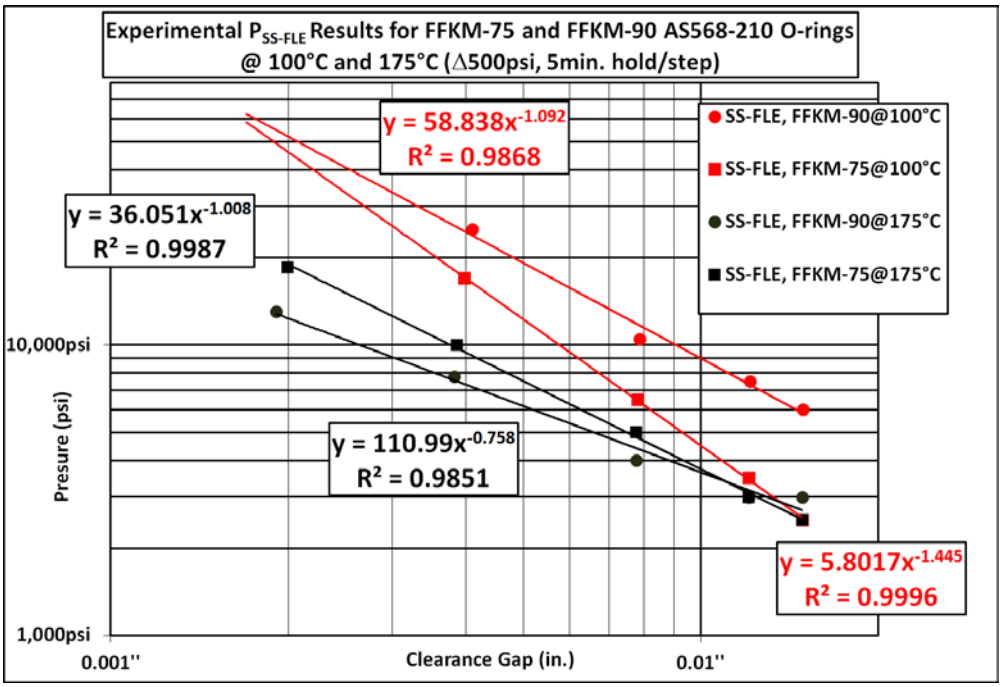


**Figure 86. Experimental SS-FLE pressure versus clearance gap for FFKM-75 and FFKM-90 at 100°C and 175°C.**

Unlike all other materials tested, in terms of CTP, the low-durometer FFKM durometer 75 slightly outperformed the high-durometer FFKM durometer 90 for all clearance gaps at 175°C.

The change in FLE pressure for a given change in clearance gap appears to be steeper for the FFKM than the other elastomers included in the study (i.e., Power Law coefficients).

### *8.7.2 Critical Tearing Pressure (E-CTP) Coefficient Estimation*

The data collected from the dwell test for each elastomer were fit using a power law regression to estimate coefficients A and B, as indicated in the below power law expression.

$$P=A*C\text{^}(B), \text{ where P [psi] \& C [inch]}$$

Tables 43 and 44 summarize coefficients of power regression for E-CTP based on the test results in Section 6.0.

**Table 43. Coefficients of E-CTP power regression for extrusion tests conducted at 100°C.**

| Material | Compound Reference | Durometer (measured) | Temperature (°C) | Coefficient A | Coefficient B |
|---|---|---|---|---|---|
| FKM-75 | F-13664 (F75) / Mil-83248-1 | 77 | 100 | 184.572 | -0.584 |
| FKM-90 | F-13681 (F90) / Mil-83248-2 | 91 | 100 | 533.899 | -0.479 |
| NBR-75 | B1016 | 76 | 100 | 720.374 | -0.386 |
| NBR-90 | B1001 | 94 | 100 | 760.005 | -0.479 |
| HNBR-75 | R1006 | 76 | 100 | 133.608 | -0.608 |
| HNBR-90 | R1003 | 92 | 100 | 918.098 | -0.411 |
| FEPM-80 | L1000 | 89 | 100 | 217.904 | -0.490 |
| FEPM-83 | 210-A-83 | 83 | 100 | 292.565 | -0.427 |
| FFKM-75 | K4079 | 76 | 100 | 304.152 | -0.481 |
| FFKM-90 | K3018 | 94 | 100 | 399.140 | -0.502 |

**Table 44. Coefficients of E-CTP power regression for extrusion tests conducted at 150°C and 175°C.**

| Material | Compound Reference | Durometer (measured) | Temperature (°C) | Coefficient A | Coefficient B |
|---|---|---|---|---|---|
| FKM-75 | F-13664 (F75) / Mil-83248-1 | 77 | 175 | 190.034 | -0.501 |
| FKM-90 | F-13681 (F90) / Mil-83248-2 | 91 | 175 | 500.792 | -0.416 |
| NBR-75 | B1016 | 76 | >> use T | >> use T | >> use T |
| NBR-90 | B1001 | 94 | >> use T | >> use T | >> use T |
| HNBR-75 | R1006 | 76 | 150 | 455.224 | -0.339 |
| HNBR-90 | R1003 | 92 | 150 | 737.688 | -0.426 |
| FEPM-80 | L1000 | 89 | 175 | 186.302 | -0.460 |
| FEPM-83 | 210-A-83 | 83 | 175 | 373.009 | -0.343 |
| FFKM-75 | K4079 | 76 | 175 | 200.431 | -0.494 |
| FFKM-90 | K3018 | 94 | 175 | 254.974 | -0.423 |

### *8.7.3 Traditional Elastomer Property Testing*

Hardness measurements were conducted as described in Section 8.6. The results of the testing are presented in Table 45.

The original batch of FEPM-80 durometer O-rings tested had an actual durometer closer to 89.3. Similarly, the FEPM-90 durometer O-rings had an actual durometer of 94.4, which was determined to be too hard for this testing. Therefore, a new supplier of FEPM O-rings was selected that offered a product with an 83 hardness value. The new FEPM-83 O-rings were confirmed to have an 83 hardness and were used as O-rings with a hardness of approximately 80. Data comparing the originally tested FEPM-80 durometer material with the new supplier's FEPM-83 durometer material are shown in Figure 87. The results were that both O-rings performed reproducibly, with the FEPM-80 (89 actual) providing a slightly higher E-CTP at smaller clearance gaps compared to the FEPM-83 (83 actual) as shown by the corresponding Power-Law coefficients for each material.

**Table 45. Material test hardness results. The non-specification FEPM materials are shown highlighted in yellow and were replaced with new samples.**

| Material | Compound Reference | Manufacturer /Vendor /Supplier | Specified Hardness | Measured Hardness (150 mm x 150 mm slab) | Measured Hardness AS568-210 size O-rings |
|---|---|---|---|---|---|
| FKM-75 | Slab-M83248/I | Vendor B | 75 | 76.2 ± 0.7 (0.9% RSD) | |
| FKM-75 | M83248/I -210 F-13664 | Vendor B | 75 | | 77.4 ± 2.1 (2.7% RSD) |
| FKM-90 | Slab-M83248/2 | Vendor B | 90 | 86.8 ± 0.3 (0.3% RSD) | |
| FKM-90 | M83248/2 -210 F13681 | Vendor B | 90 | | 91.4 ± 0.5 (0.5% RSD) |
| NBR-75 | Slab-B1016 | Vendor A | 75 | 76.0 ± 0.6 (0.7% RSD) | |
| NBR-75 | B1016-210 | Vendor A | 75 | | 75.9 ± 0.9 (1.2% RSD) |
| NBR-90 | Slab-B1001 | Vendor A | 90 | 89.0 ± 0.1 (0.1% RSD) | |
| NBR-90 | B1001-210 | Vendor A | 90 | | 93.8 ± 0.8 (0.9% RSD) |
| HNBR-75 | Slab-R1006 | Vendor A | 75 | 75.6 ± 1.7 (2.2% RSD) | |
| HNBR-75 | R1006-210 | Vendor A | 75 | | 75.8 ± 0.9 (1.1% RSD) |
| HNBR-90 | Slab-R1003 | Vendor A | 90 | 89.6 ± 1.6 (1.8% RSD) | |
| HNBR-90 | R1003-210 | Vendor A | 90 | | 92.2 ± 1.0 (1.1% RSD) |
| FEPM-80 | Slab-L1000 | Vendor A | 80 | 78.9 ± 0.6 (0.7% RSD) | |
| FEPM-80 | L1000-210 | Vendor A | 80 | | 89.3 ± 1.2 (1.3% RSD) (+9 units from Target) |
| FEPM-80 | B0020525/2q16 | Vendor C | 80 | | 86.6 ± 1.1 (1.3% RSD) (+7 units from Target) |
| FEPM-83 | 210-A-83 | Vendor D | 83 | | 83.5 ± 0.9 (1.1% RSD) |
| FEPM-90 | Slab-L1003 | Vendor A | 90 | 86.2 ± 1.0 (1.2% RSD) | |
| FEPM-90 | L1003-210 | Vendor A | 90 | | 94.4 ± 2.5 (2.7% RSD) |
| FFKM-75 | Slab-K4079 | Vendor A | 75 | 76.7 ± 0.6 (0.8% RSD) | |
| FFKM-75 | K4079-210 | Vendor A | 75 | | 75.7 ± 0.9 (1.2% RSD) |
| FFKM-90 | Slab-K3018 | Vendor A | 90 | 91.5 ± 0.7 (0.7% RSD) | |
| FFKM-90 | K3018-210 | Vendor A | 90 | | 93.8 ± 0.9 (1.0% RSD) |

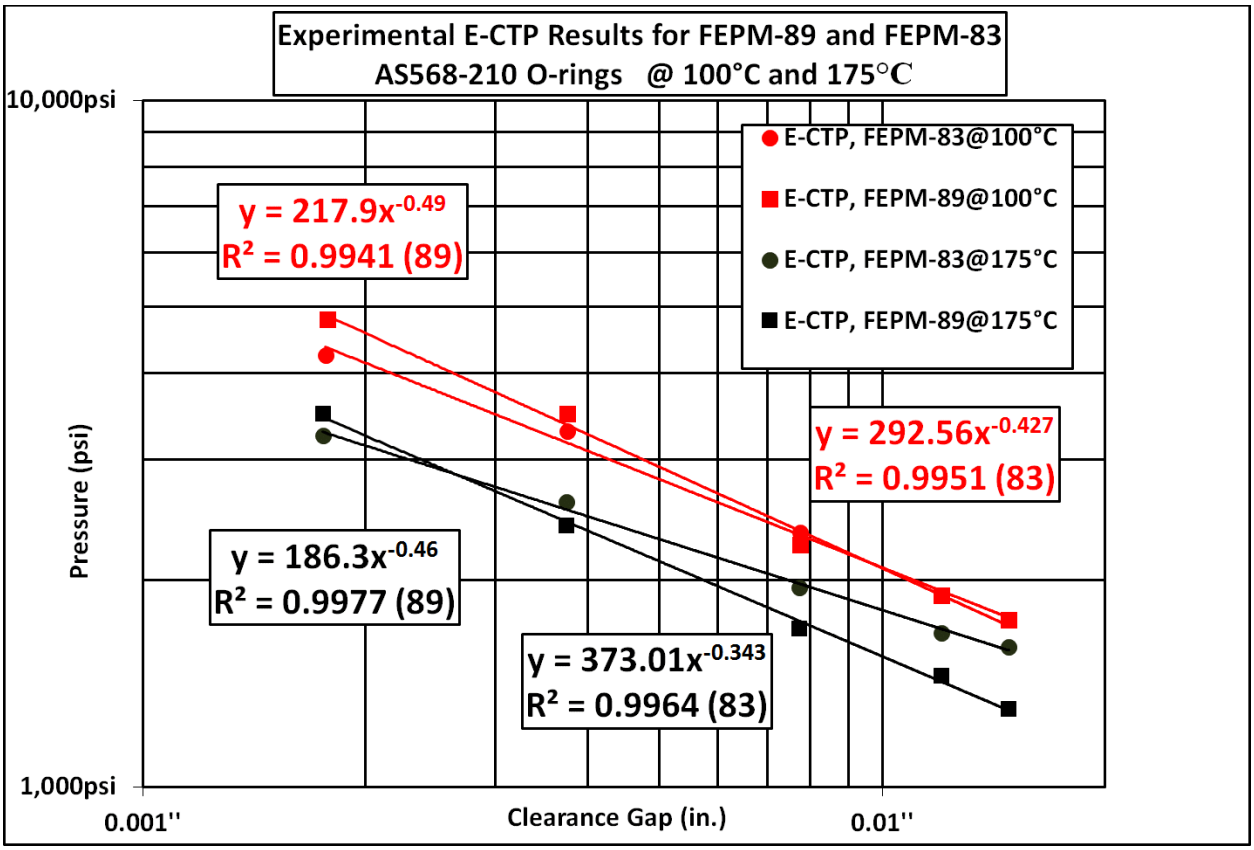


**Figure 87. Results of FEPM-89 (nominal 80) and FEPM-83 (nominal 83) materials. Note that an O-ring batch FEPM-80 durometer had an actual hardness of approximately 89 (and is shown as FEPM-89).**

## 8.8 Discussion

### *8.8.1 Cross-Material Plots and Ranking of Critical Tearing Pressures (E-CTP)*

The results of the dwell testing were used to compare the E-CTP of the five elastomers tested at similar conditions. Figure 88 through Figure 91 show plots of the E-CTP for each elastomer to allow comparison between materials at similar temperatures and durometers. It must be noted that the arrangement of the elastomers in the figures from highest to lowest corresponds only to the test conditions for a single-cycle dwell test using new O-rings. The ability of the O-rings' material to resist tear may be affected by different factors that could alter their relative ranking; this includes the duration of exposure to temperature, pressure, aging and load history. The rankings indicate that, under the conditions of the tests, NBR performs the best of the elastomers tested in the 75 and 83 durometer range as well as for 90 durometer at 100°C, which is also its maximum continuous use temperature. The results of the higher temperature range 150°C and 175°C tests for the lower durometer (75 to 83) elastomers were similar for FKM, FFKM and HNBR, which all outperformed FEPM. For the 90 (nominal) durometer elastomers, HNBR, tested at its

maximum use temperature of 150°C, significantly outperformed FKM at 175°C, which in turn significantly outperformed FFKM at 175°C.

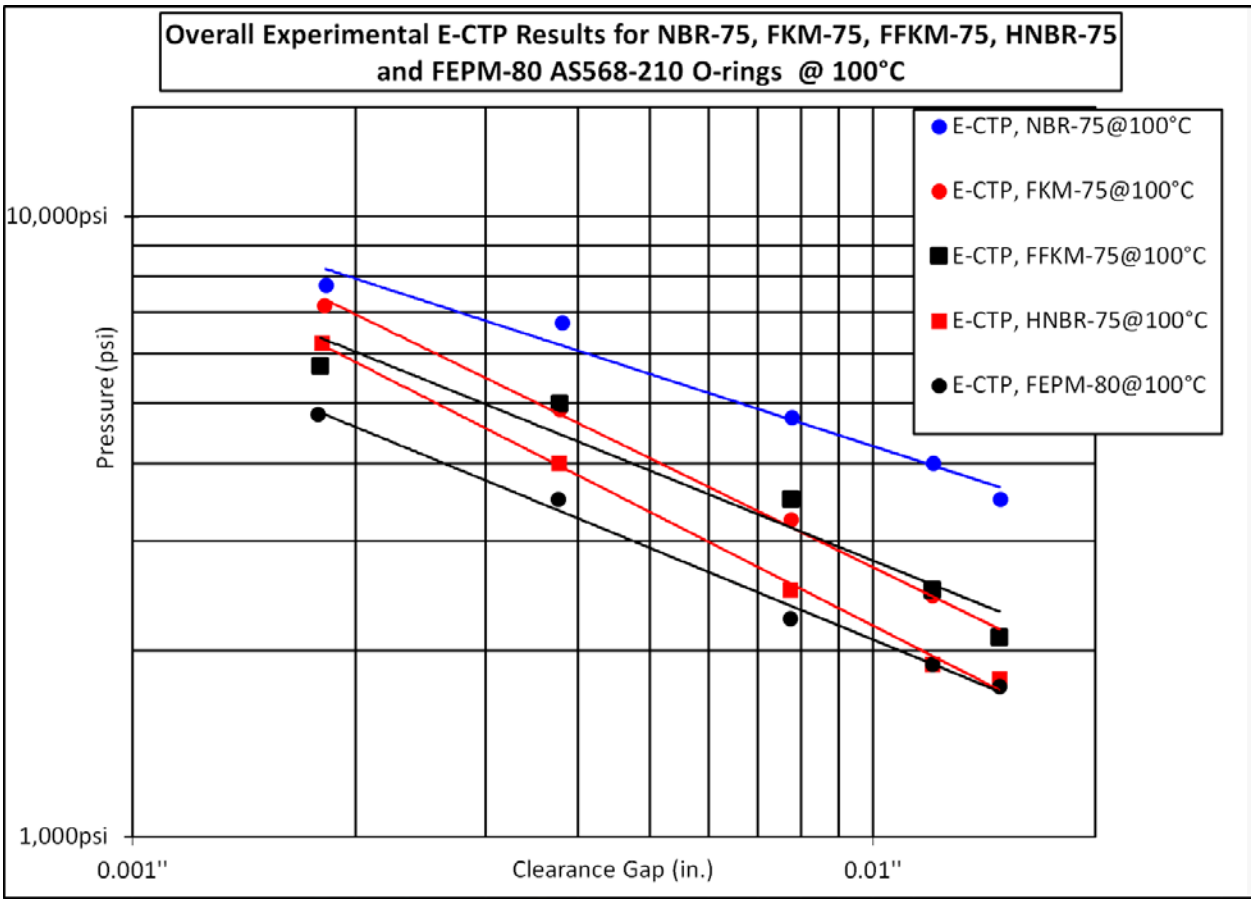


**Figure 88. Comparison of experimental E-CTP for NBR-75, FKM-75, FFKM-75, HNBR-75 and FEPM-80 O-rings at 100°C. The legend lists all materials in the descending E-CTP order.**

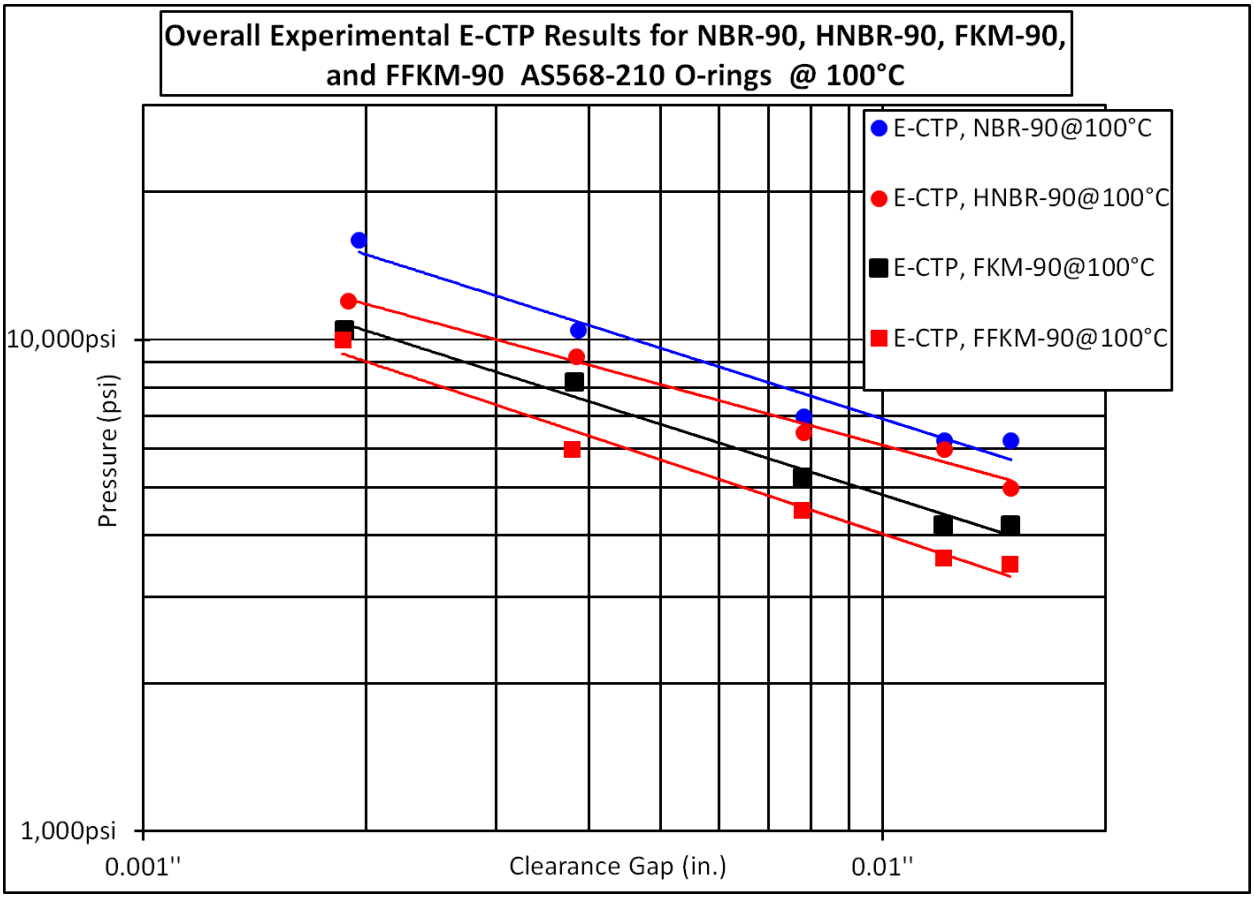


**Figure 89. Comparison of experimental E-CTP for NBR-90, HNBR-90, FKM-90, and FFKM-90 O-rings at 100°C. The legend lists all materials in the descending E-CTP order.**

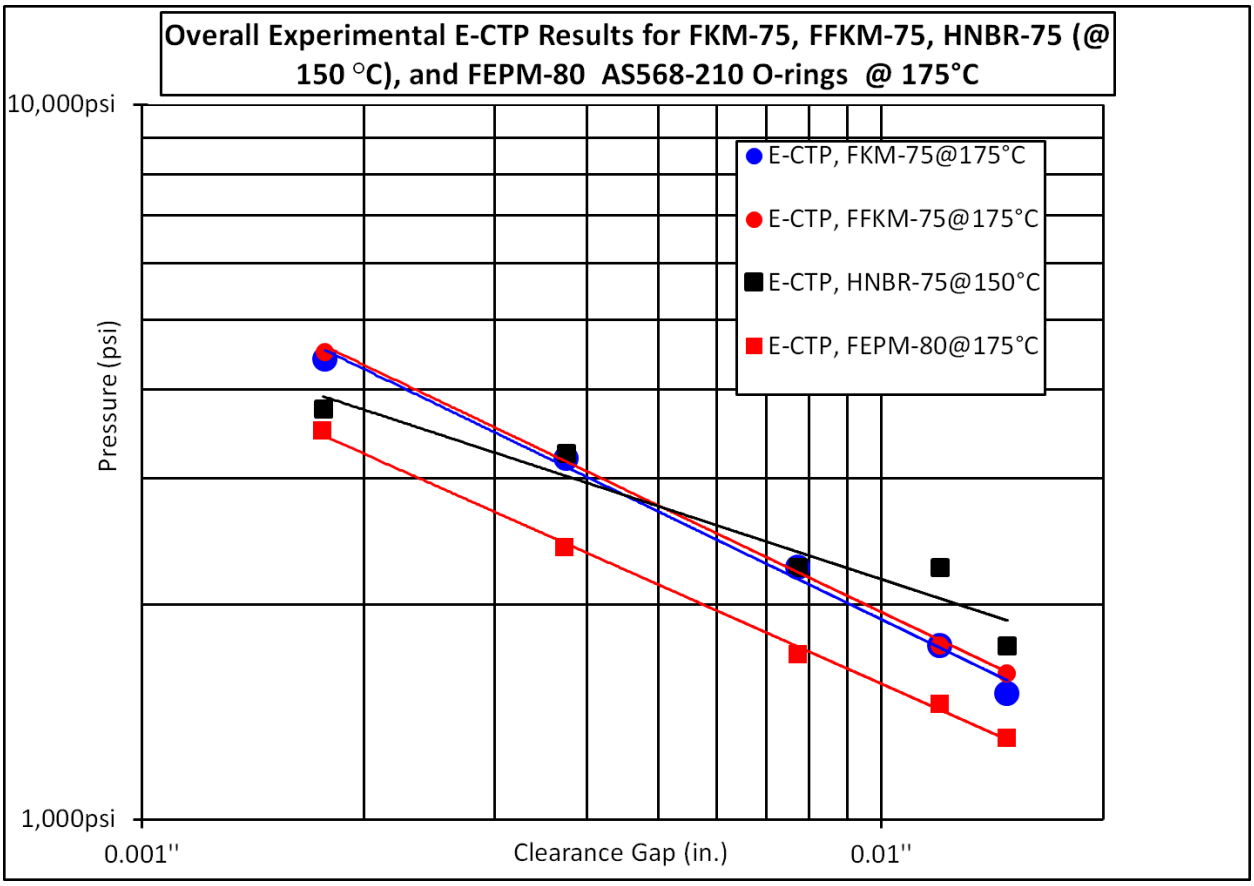


**Figure 90. Comparison of experimental E-CTP for FKM-75, FFKM-75, HNBR-75 (@ 150°C) and FEPM-80 O-rings at 175°C. The legend lists all materials in the descending E-CTP order.**

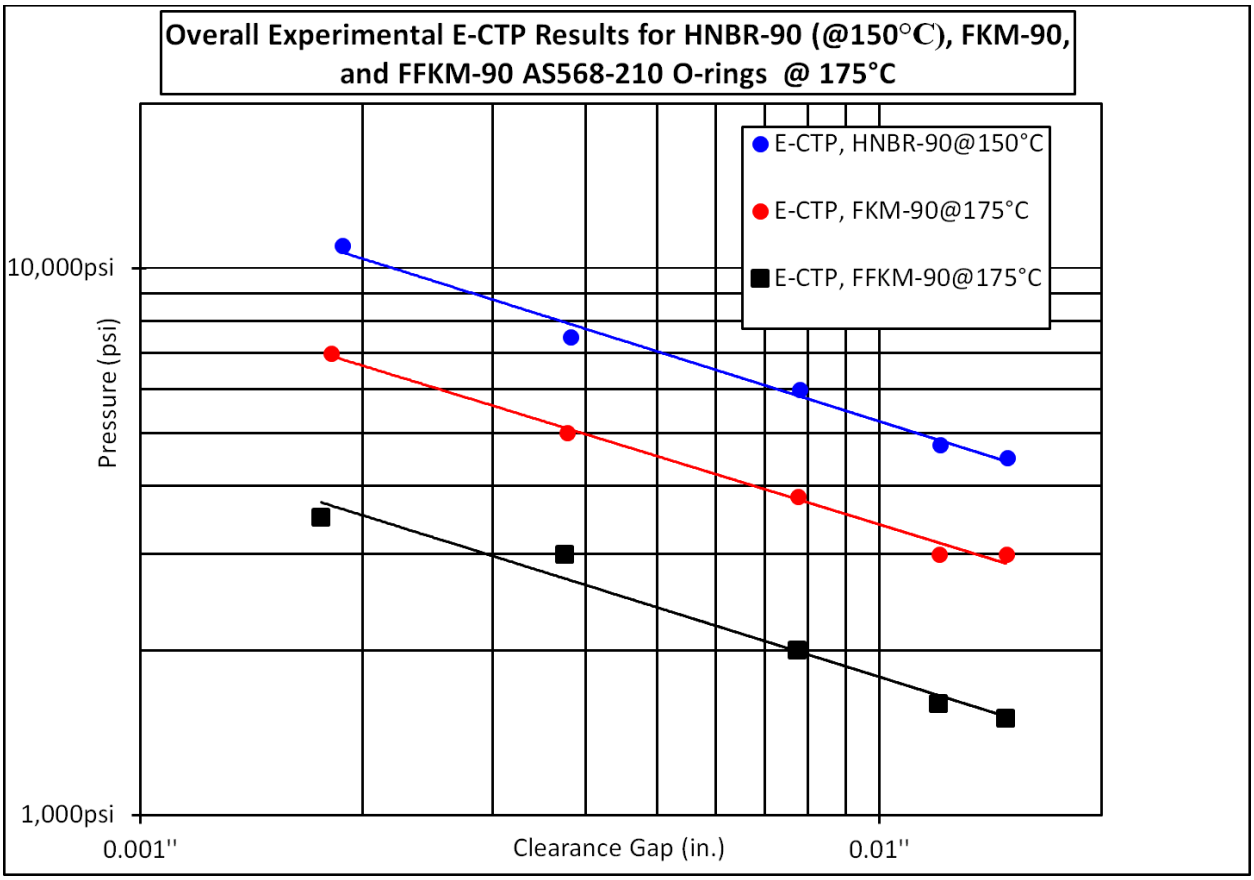


**Figure 91. Comparison of experimental E-CTP ranking for HNBR-90 (@ 150°C), FKM-90, and FFKM-90 O-rings @ 175°C. The legend lists all materials in the descending E-CTP order.**

Plotting the E-CTP for all materials tested against temperature for a single clearance of 0.002 in. shows 90 durometer NBR performed best with an E-CTP of approximately 15,000 psi and FEPM durometer 83 was the lowest performing material with an E-CTP of approximately 4 ksi at 100°C (Figure 92).

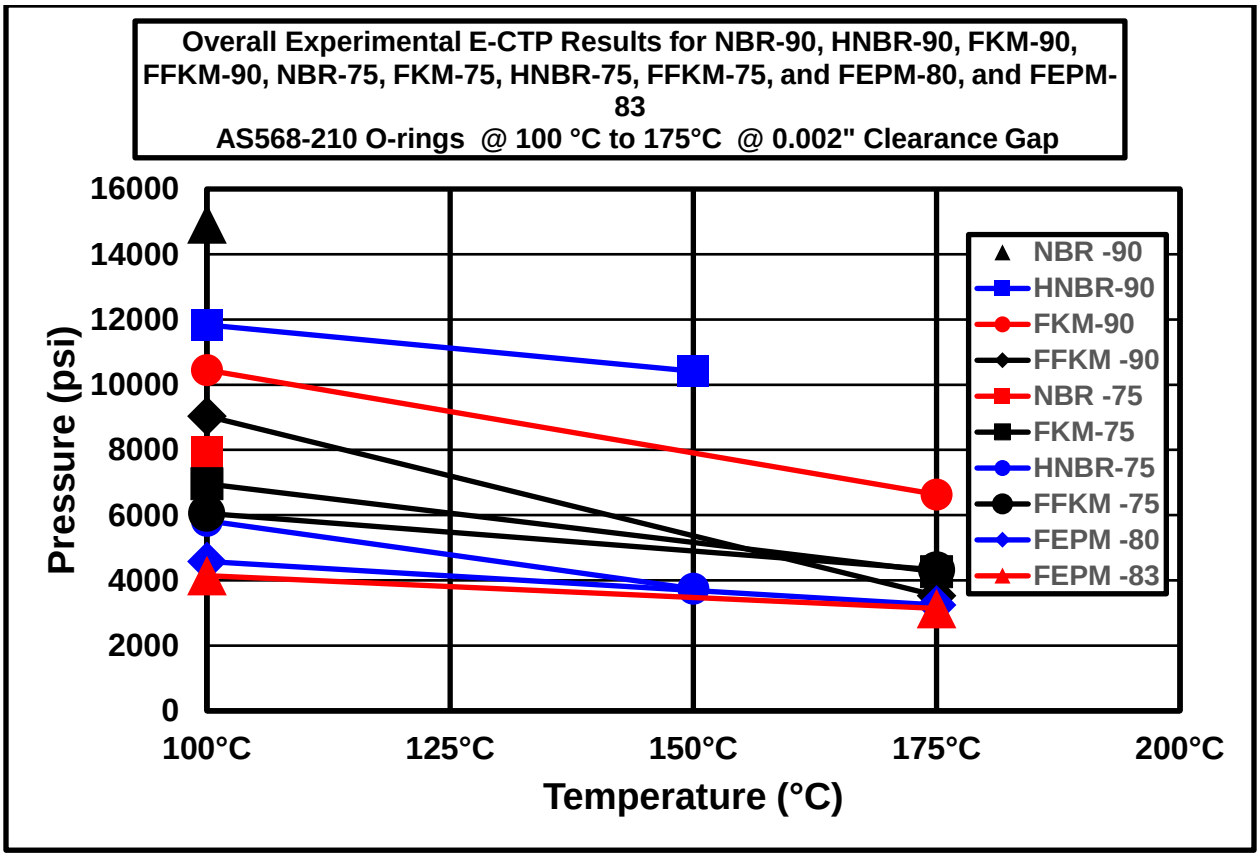


**Figure 92. Overall material ranking of experimental E-CTP versus temperature for NBR-90, HNBR-90, FKM-90, FFKM-90, NBR-75, FKM-75, HNBR-75, FFKM-75, FEPM-80, and FEPM-83 AS568-210 O-rings using a 0.002-inch clearance gap. The legend lists all materials in the descending E-CTP order.**

As expected, for all materials, E-CTP levels decreased as temperature increased from 100°C to 175°C. The most interesting temperature dependence is seen with FFKM (black lines); the 90 durometer FFKM has the highest rate of the CTP drop in the temperature range from 100°C to 175°C (~60%), while the 75 durometer FFKM is in line with other materials and its CTP decreased by only 29%. As a result, the 75 durometer FFKM outperformed the 90 durometer FFKM at the highest temperature tested of 175°C, but they were quite similar.

The comparisons of E-CTP provide information that may be useful in selecting elastomers for HPHT service. The results indicate that elastomer selection should be based not only on pressure and temperature conditions but also on the clearance associated with the machinery being sealed.

# 9.0 FEA MODEL VALIDATION

## 9.1 Results

The CTS determined by the FEA model for each elastomer/temperature combination are shown in Table 46 and Table 47.

**Table 46. Critical Tresca stress at 100°C.**

| Material at 100 °C | Critical Tresca Stress (psi) |
|---|---|
| HNBR-90 | 16,064 |
| NBR 90 | 14,044 |
| NBR-75 | 10,964 |
| FKM-90 | 7,948 |
| FFKM-75 | 7,181 |
| FFKM-90 | 6,773 |
| FKM-75 | 5,457 |
| FEPM-90 | 4,891 |
| FEPM-80 | 4,443 |
| HNBR-75 | 4,408 |

The CTS FEA model material rankings at 100°C were from highest to lowest: HNBR-90 (1) > NBR 90 (2) > NBR-75 (3) > FKM-90 (4) > FFKM-75 (5) ≈ FFKM-90 (5) > FKM-75 (6) > FEPM-90 (7) > FEPM-80 (8) ≈ HNBR-75 (8).

**Table 47. Critical Tresca stress at 150°C and 175°C.**

| Material at 175°C | Critical Tresca Stress (psi) |
|---|---|
| HNBR-90 (tested at 150°C) | 11,678 |
| FKM-90 | 4,680 |
| FKM-75 | 3,472 |
| FFKM-75 | 3,404 |
| HNBR-75 (tested at 150°C) | 3,184 |
| FFKM-90 | 3,175 |
| FEPM-90 | 2,384 |
| FEPM-80 | 2,351 |

The CTS FEA model material rankings at 150 to 175°C were, from highest to lowest: HNBR-90 (1) > FKM-90 (2) > FEPM-90 (2) > FKM-75 (3) ≈ FFKM-75 (3) > HNBR-75 (4) ≈ FFKM-90 (4) > FEPM-80 (5).

These CTS values were used in the FEA O-ring model extrusion simulation as a "breakpoint" for the material mesh as the input pressure was increased at a given temperature to the M-CTP as shown in Figure 69. Figure 93 through Figure 96 show plots of the M-CTP for each elastomer to allow comparison between materials at similar temperatures and durometers. It should be noted that the FEA model is for a single-cycle dwell test of a new O-ring.

The following charts arrange FEA results of M-CTP for O-rings of the elastomer materials for similar temperatures and durometers. It should be noted that the FEA model is for a single-cycle dwell test of a new O-ring. The ability of the O-ring material to resist tear may be affected by different factors that could alter the relative ranking, e.g., duration of exposure to temperature and pressure, aging and load prehistory, including Mullins effect and HPHT cycling.

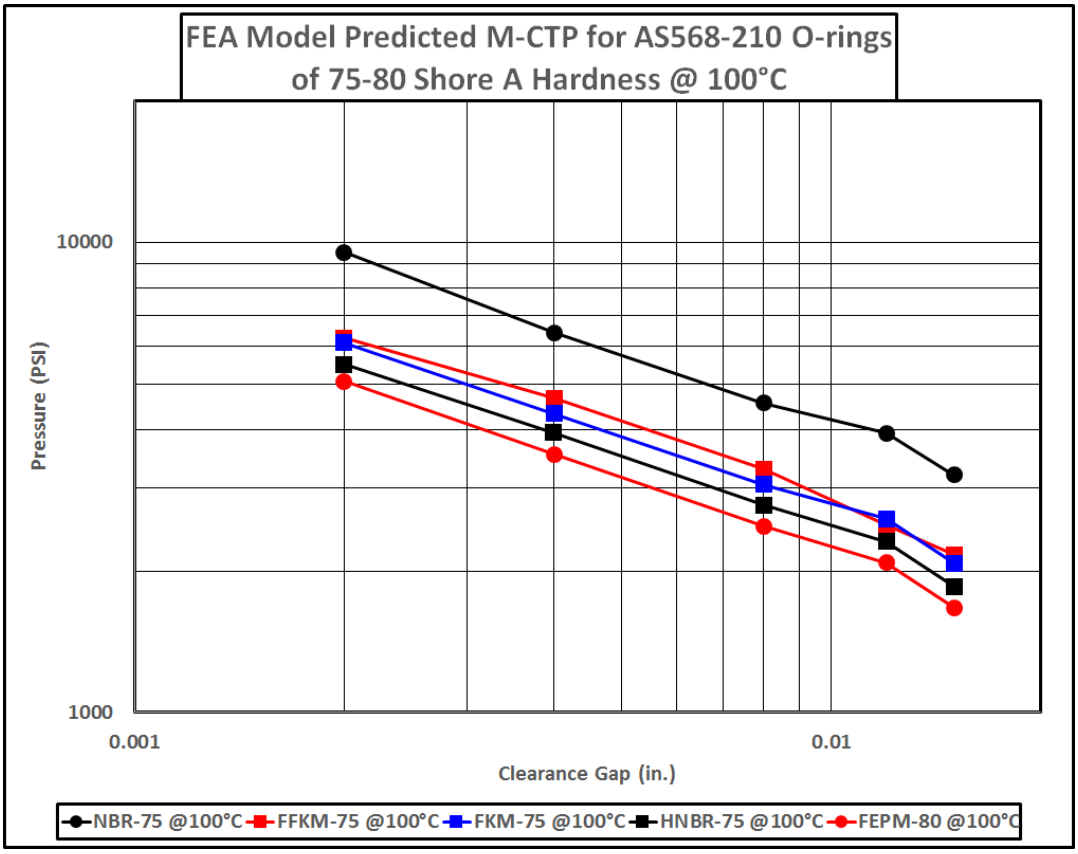


**Figure 93. M-CTP ranking for O-rings with hardness of 75 and 80 at 100°C.**

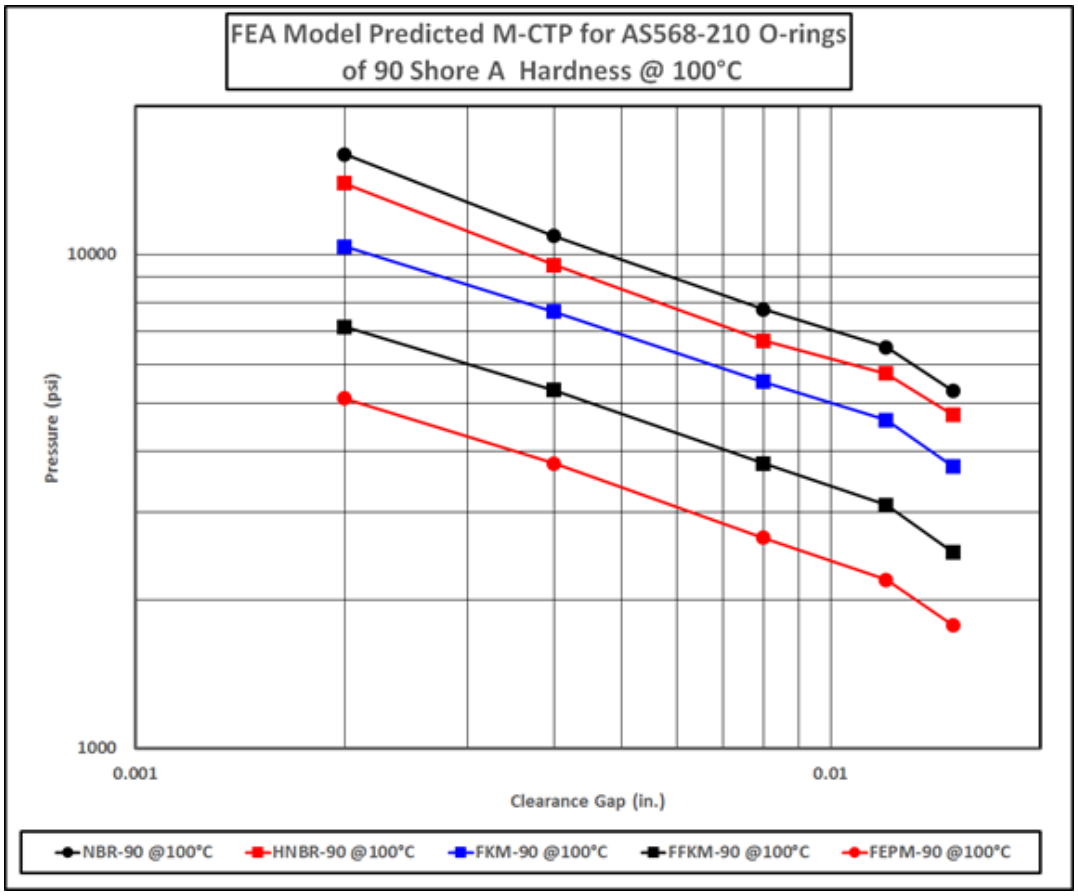


**Figure 94. M-CTP ranking for O-rings with a hardness of 90 at 100°C (Endurica, LLC).**

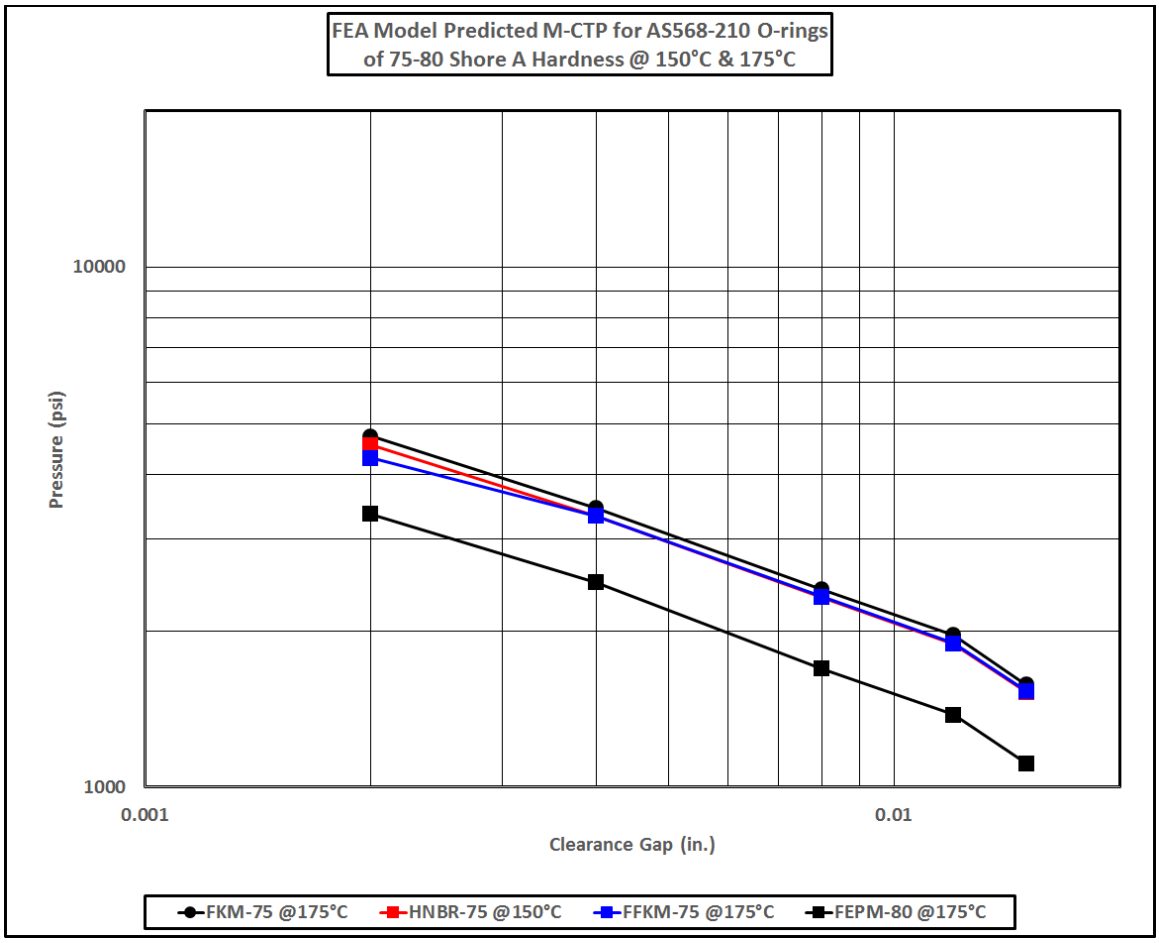


**Figure 95. M-CTP ranking for O-rings with a hardness of 75 and 80 at 150°C and 175°C (Endurica, LLC).**

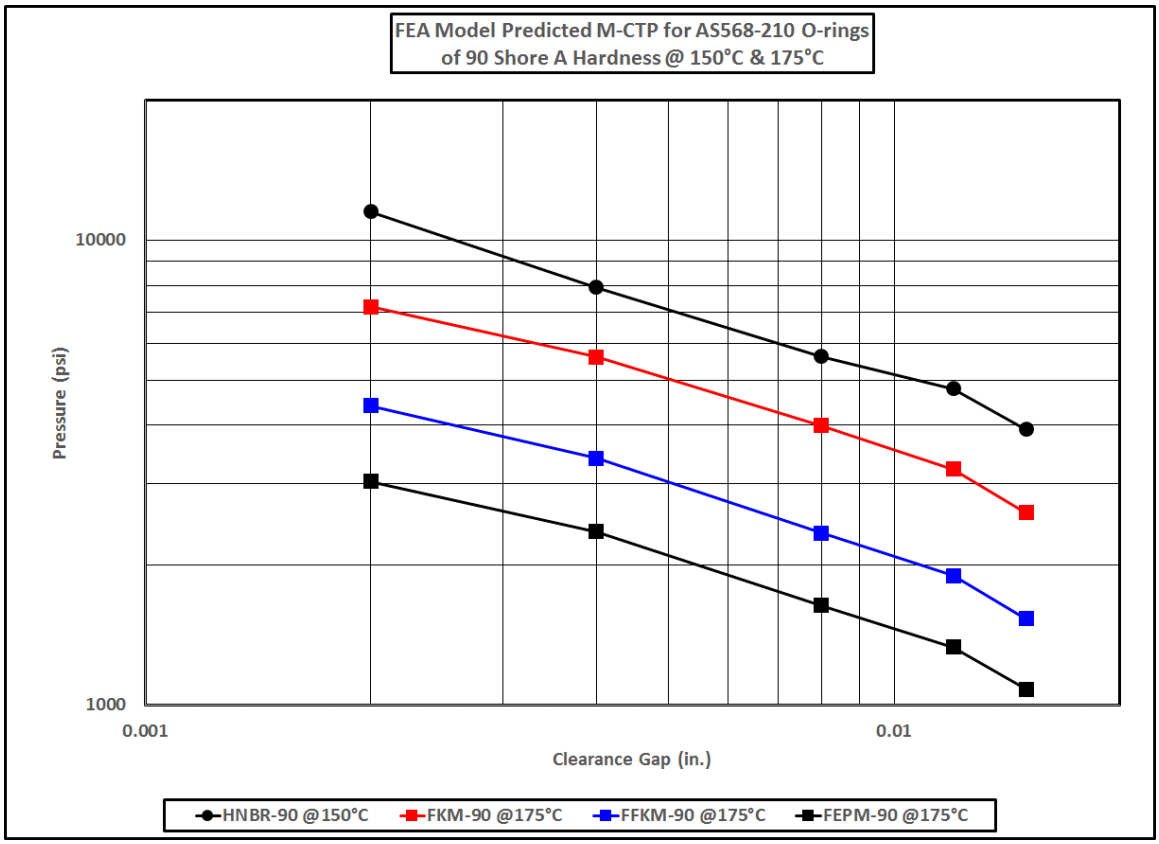


**Figure 96. M-CTP rankings for O-rings with a hardness of 90 at 150 and 175 V (Endurica, LLC).**

The relative M-CTP for the elastomer types at a temperature of 100°C is included in Table 48.

The FEA Model M-CTP material rankings at 100°C were NBR 90 (1) > HNBR-90 (2) > FKM-90 (3) > NBR-75 (4) > FKFM 90 (5) > FFKM-75 (6) ≈ FKM-75 (6) > HNBR-75 (7) > FEPM-90 (8) > FEPM-80 (9).

**Table 48. FEA M-CTP estimates at 100°C.**

| Material | M-CTP at 0.015-inch clearance gap | M-CTP at 0.012-inch clearance gap | M-CTP at 0.008-inch clearance gap | M-CTP at 0.004-inch clearance gap | M-CTP at 0.002-inch clearance gap |
|---|---|---|---|---|---|
| **NBR-90** | 5,294 | 6,495 | 7,746 | 10,912 | 16,123 |
| **HNBR-90** | 4,731 | 5,739 | 6,695 | 9,521 | 13,783 |
| **FKM-90** | 3,714 | 4,623 | 5,521 | 7,658 | 10,392 |
| **NBR-75** | 3,203 | 3,931 | 4,547 | 6,428 | 9,516 |
| **FFKM-90** | 2,488 | 3,109 | 3,773 | 5,315 | 7,183 |
| **FFKM-75** | 2,165 | 2,504 | 3,292 | 4,653 | 6,250 |
| **FKM-75** | 2,077 | 2,582 | 3,058 | 4,325 | 6,119 |
| **HNBR-75** | 1,853 | 2,309 | 2,764 | 3,927 | 5,504 |
| **FEPM-90** | 1,773 | 2,193 | 2,667 | 3,769 | 5,114 |
| **FEPM-80** | 1,673 | 2,080 | 2,490 | 3,540 | 5,055 |

Table 49 shows the corresponding Task 4 HPHT E-CTP material rankings at a temperature of 100°C (in the same order as the FEA model M-CTP results).

The Task 4 HPHT material E-CTP rankings at 100°C were NBR-90 (1) > HNBR-90 (2) > FKM-90 (3) > NBR-75 (4) > FFKM-90 (5) > FFKM-75 (6) ≈ FKM-75 (6) > HNBR-75(7) ≈ FEPM-90 (7) ≈ FEPM-80 (7).

The corresponding overall M-CTP material rankings from the FEA model at a temperature of 175°C are shown in Table 50.

The FEA model M-CTP material rankings at 150°C to 175°C were: HNBR-90 (@ 150 °C) (1) > FKM-90 (2) > FKM-75 (3) ≈ FFKM-90 (3) ≈ FFKM-75 (3) ≈ HNBR-75 (@150 °C) (3) > FEPM-80 (4), ≈ FEPM-90 (4). The HNBR-90 and FKM-90 performed the best and the FEPM-80 and FEPM-90 performed the worst. Recall that the NBR elastomer was not modeled at these temperatures because the 150°C to 175°C range is greater than its maximum temperature (120°C).

**Table 49. Critical tearing pressure (E-CTP) from HPHT laboratory testing at 100°C.**

| Material | E-CTP at 0.015-inch clearance gap | E-CTP at 0.012-inch clearance gap | E-CTP at 0.008-inch clearance gap | E-CTP at 0.004-inch clearance gap | E-CTP at 0.002-inch clearance gap |
|---|---|---|---|---|---|
| **NBR-90** | 6,250 | 6,250 | 7,000 | 10,500 | 16,000 |
| **HNBR-90** | 5,000 | 6,000 | 6,500 | 9,250 | 12,000 |
| **FKM-90** | 4,200 | 4,200 | 5,250 | 8,200 | 10,500 |
| **NBR-75** | 3,500 | 4,000 | 4,750 | 6,750 | 7,750 |
| **FFKM-90** | 3,500 | 3,600 | 4,500 | 6,000 | 10,000 |
| **FFKM-75** | 2,100 | 2,500 | 3,500 | 5,000 | 5,750 |
| **FKM-75** | 2,100 | 2,450 | 3,250 | 4,900 | 7,200 |
| **HNBR-75** | 1,800 | 1,900 | 2,500 | 4,000 | 6,250 |
| **FEPM-90** | 1,750 | 1,900 | 2,350 | 3,500 | 4,800 |
| **FEPM-80** | 1,750 | 1,900 | 2,250 | 3,300 | 4,250 |

**Table 50. FEA M-CTP estimates at 150°C and 175°C.**

| Material | M-CTP at 0.015-inch clearance gap | M-CTP at 0.012-inch clearance gap | M-CTP at 0.008-inch clearance gap | M-CTP at 0.004-inch clearance gap | M-CTP at 0.002-inch clearance gap |
|---|---|---|---|---|---|
| **HNBR-90 at 150 °C** | 3,920 | 4,792 | 5,610 | 7,926 | 11,668 |
| **FKM-90** | 2,597 | 3,221 | 3,995 | 5,610 | 7,194 |
| **FKM-75** | 1,577 | 1,963 | 2,401 | 3,447 | 4,732 |
| **FFKM-90** | 1,534 | 1,899 | 2,346 | 3,394 | 4,406 |
| **FFKM-75** | 1,531 | 1,892 | 2,323 | 3,325 | 4,292 |
| **HNBR-75 at 150 °C** | 1,525 | 1,888 | 2,321 | 3,323 | 4,552 |
| **FEPM-80** | 1,113 | 1,376 | 1,692 | 2,481 | 3,350 |
| **FEPM-90** | 1,083 | 1,333 | 1,640 | 2,356 | 3,028 |

Table 51 shows the corresponding HPHT test-based material E-CTP rankings at a temperature of 175°C. The results compare favorably with the FEA model M-CTP results with HNBR-90 and FKM-90 elastomers outperforming all others.

The HPHT test-based E-CTP material rankings at 175°C were: HNBR-90 (1)> FKM-90 (2) > HNBR-75 (3) ≈ FKM-75 (3) ≈ FFKM-75 (3) ≈ FFKM-90 (3) ≈ FEPM-90 (3) > FEPM-80 (4).

Recall that NBR elastomer was not evaluated at these temperatures because the 150°C to 175°C range is greater than its maximum use temperature (120°C).

**Table 51. Critical tearing pressure (E-CTP) from HPHT laboratory testing at 150°C and 175°C.**

| Material | E-CTP at 0.015-inch clearance gap | E-CTP at 0.012-inch clearance gap | E-CTP at 0.008-inch clearance gap | E-CTP at 0.004-inch clearance gap | E-CTP at 0.002-inch clearance gap |
|---|---|---|---|---|---|
| **HNBR-90 at 150 °C** | 4,500 | 4,750 | 6,000 | 7,500 | 11,000 |
| **FKM-90** | 3,000 | 3,000 | 3,825 | 5,000 | 7,000 |
| **HNBR-75 at 150 °C** | 1,750 | 2,250 | 2,250 | 3,250 | 3,750 |
| **FKM-75** | 1,500 | 1,750 | 2,250 | 3,200 | 4,000 |
| **FFKM-75** | 1,600 | 1,750 | 2,250 | 3,250 | 4,500 |
| **FFKM-90** | 1,500 | 1,600 | 2,000 | 3,000 | 3,500 |
| **FEPM-90** | 1,600 | 1,675 | 1,950 | 2,600 | 3,500 |
| **FEPM-80** | 1,300 | 1,450 | 1,700 | 2,400 | 3,250 |

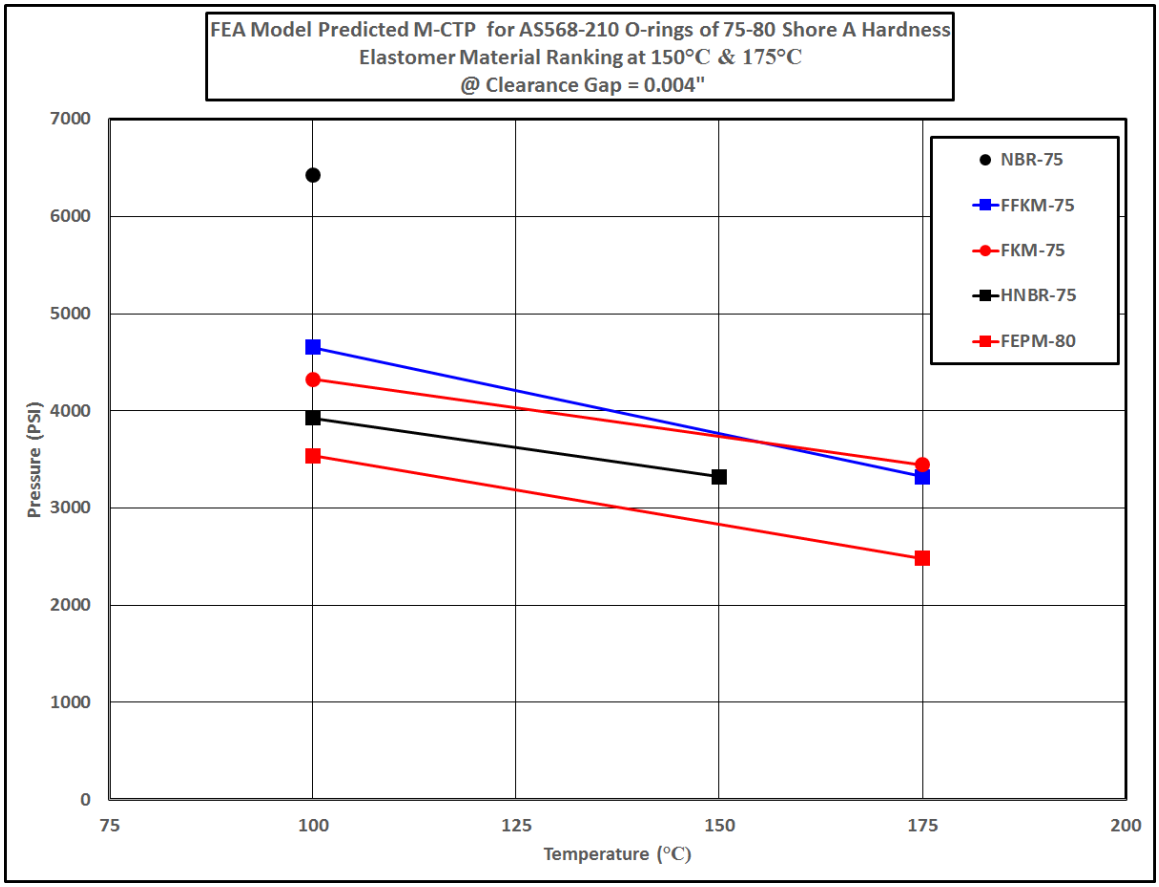


**Figure 97. Ranking of M-CTP for 75-80 durometer materials at 100°C to 175°C for 0.004-inch clearance gap and AS568-210 size O-rings.**

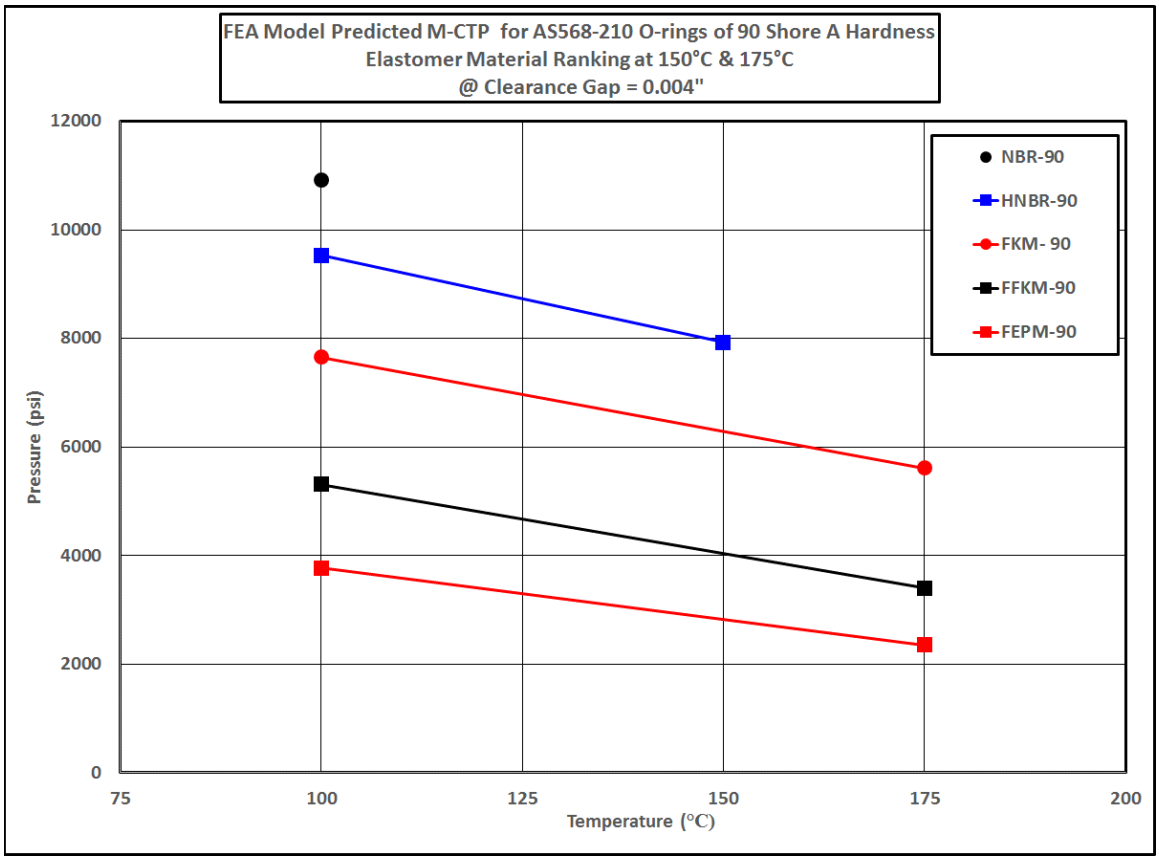


**Figure 98. Ranking of M-CTP for 90 durometer materials at 100°C to 175°C for 0.004-inch clearance gap and AS568-210 size O-rings. Note: NBR could only be tested at 100 °C**

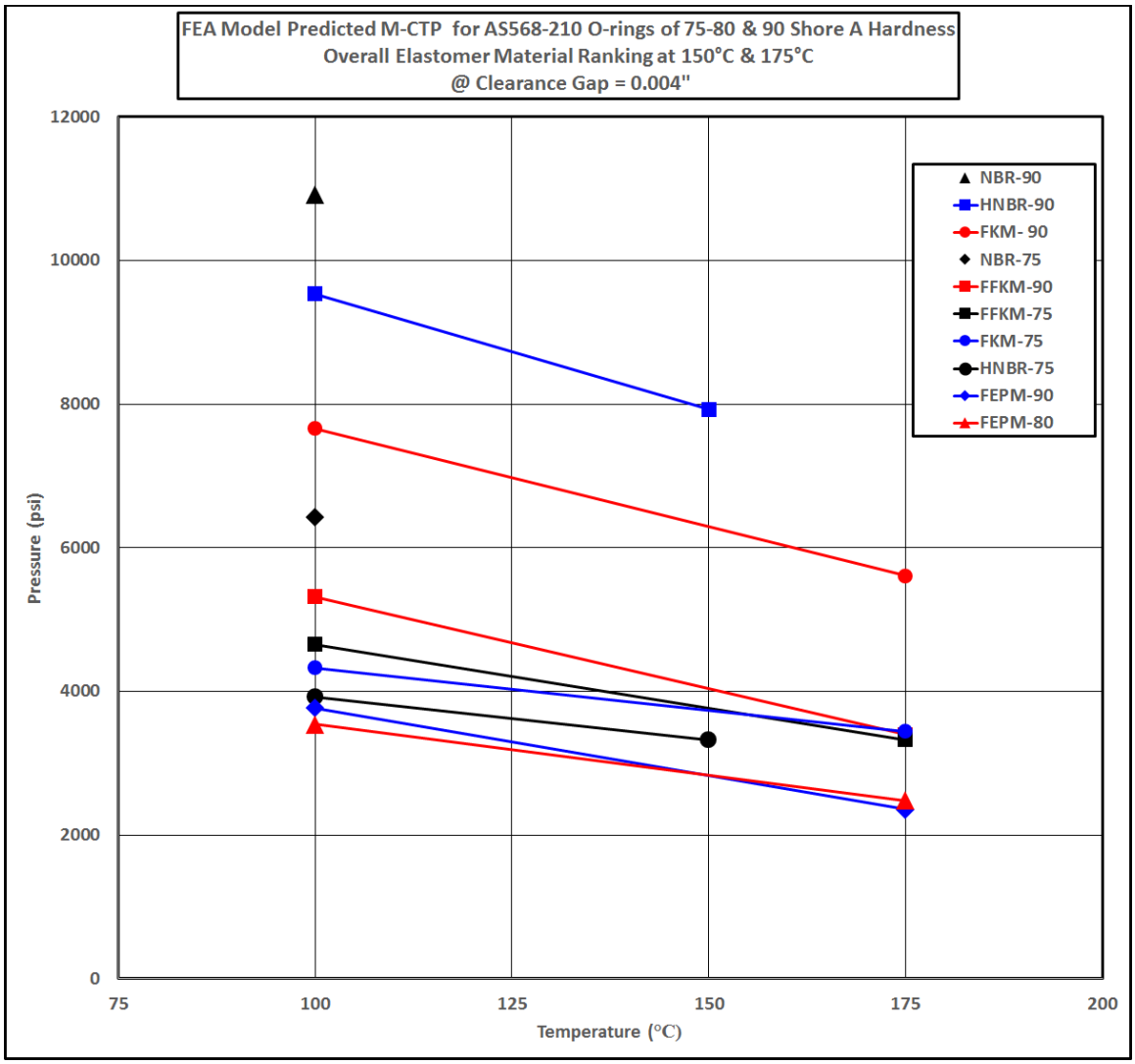


**Figure 99. Ranking of M-CTP for 75-90 durometer materials at 100°C to 175°C for 0.004-inch clearance gap and AS568-210 size O-rings. Note: NBR could only be tested at 100 °C.**

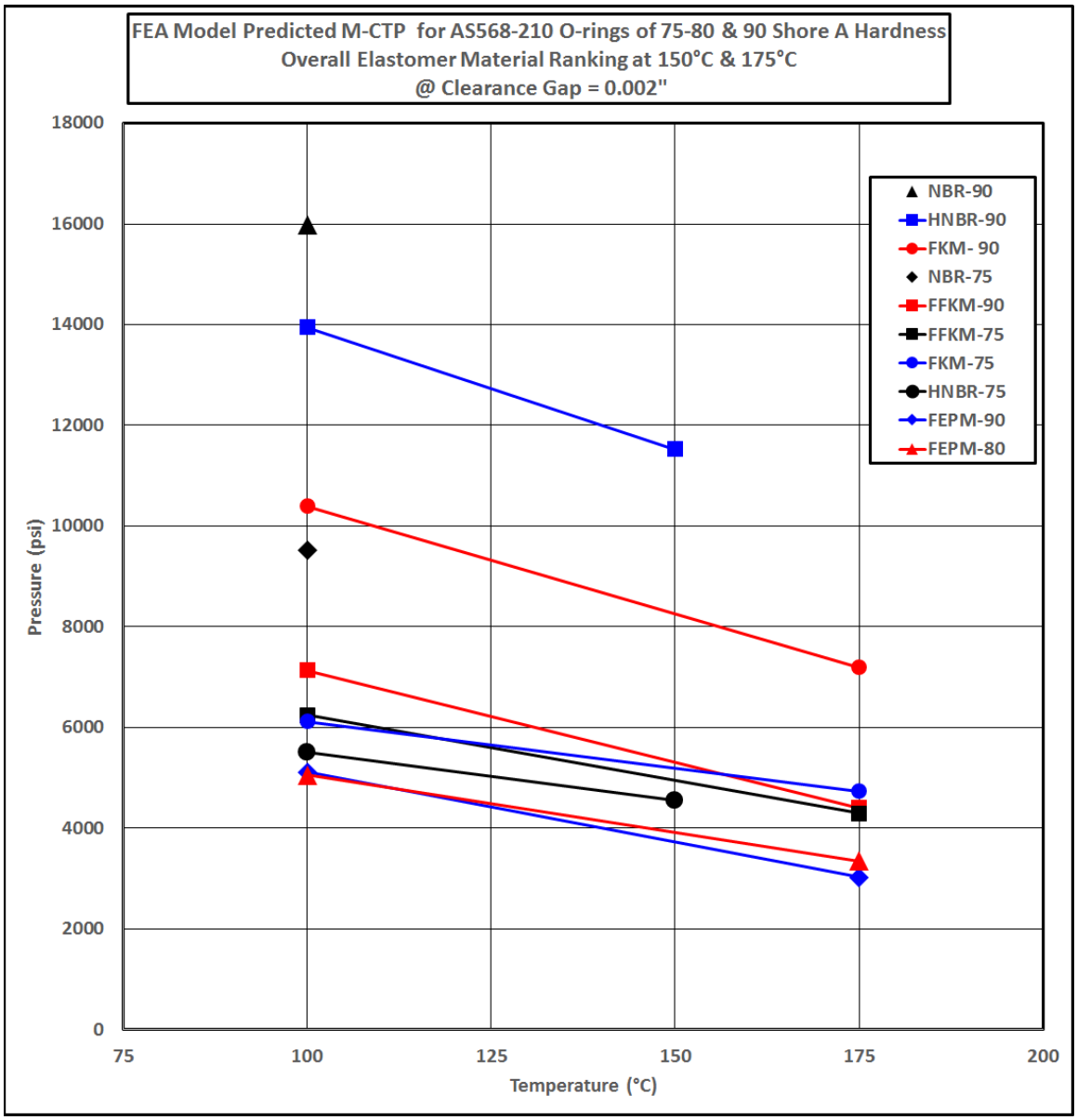


**Figure 100. Ranking of M-CTP for 75-90 durometer materials at 100°C to 175°C for 0.002-inch clearance gap and AS568-210 size O-rings. Note: NBR could only be tested at 100 °C.**

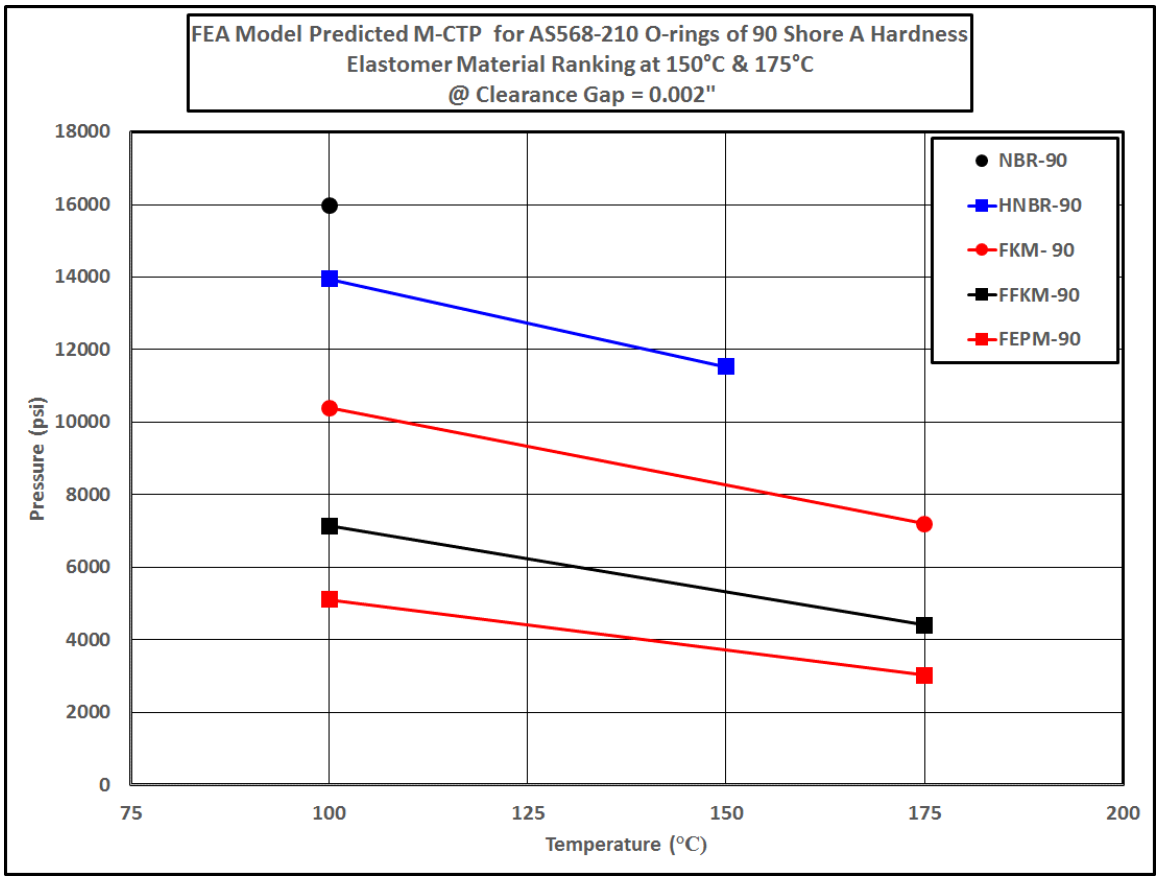


**Figure 101. Ranking of M-CTP for 90 durometer materials at 100°C to 175°C for 0.002-inch clearance gap and AS568-210 size O-rings. Note: NBR could only be tested at 100 °C.**

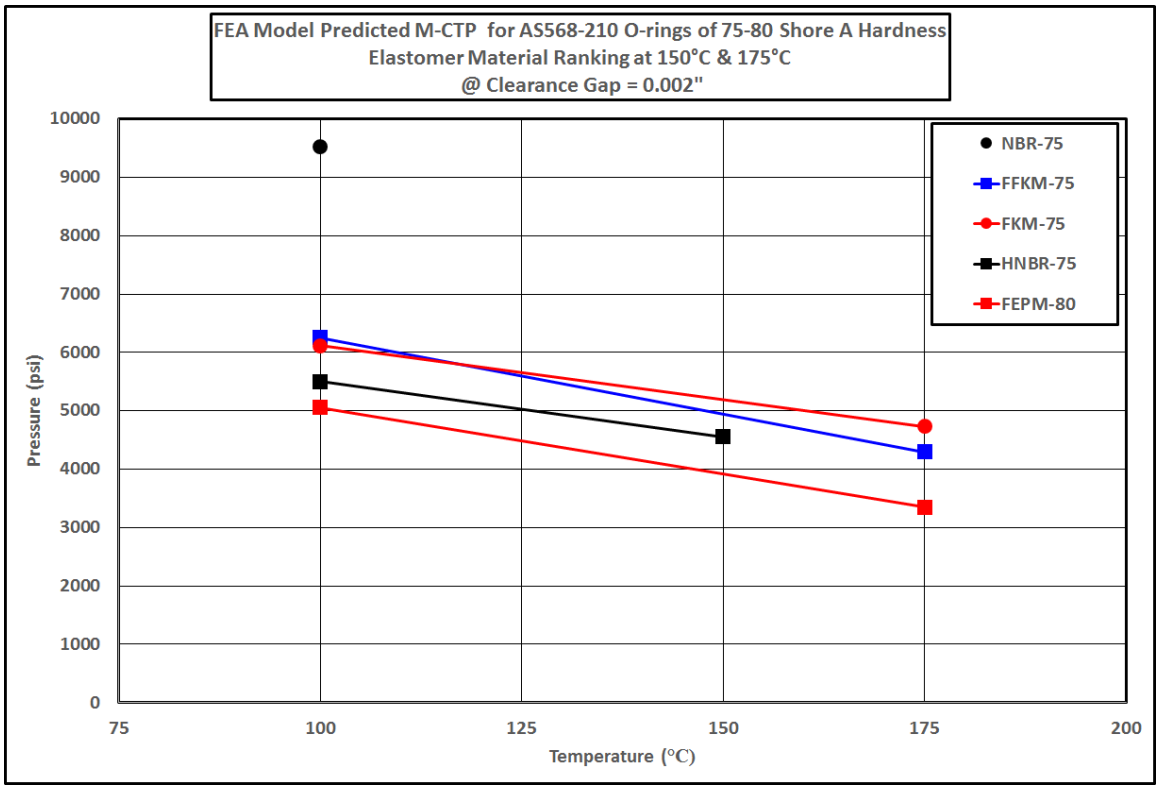


**Figure 102 Ranking of M-CTP for 75-80 durometer materials at 100°C to 175°C for 0.002-inch clearance gap and AS568-210 size O-rings. Note: NBR could only be tested at 100 °C.**

## 9.2 Discussion

CTS results and sensitivity analyses for each of the elastomers studied are summarized in the detailed FEA modeling report (Appendix A.7). These values identify the pressure at which extrusion and tearing begin to occur as predicted by the FEA model. At elevated temperatures under the test conditions explored, NBR and HNBR performed best under the majority of temperature and clearance gap conditions evaluated. Note that these tests do not explore material compatibility issues between elastomers and their environment. Severe environment conditions (see Section 4.1) led to the creation of some of the fluorinated elastomers that were also tested (i.e., FFKM, FEPM, and FKM). These data can be used with reasonable certainty to predict failure conditions for elastomer O-rings at elevated temperatures. The current model could reasonably be used for the elastomers and conditions used in this study to assess seal integrity for similar gland or lip geometries and scenarios.

### *9.2.1 FEA versus Experiment*

The FEA computed pressure at tear initiation (M-CTP) is plotted in Figure 103 against experimentally observed tear initiation pressure test results. The black 1:1 linear regression fit

line indicates ideal agreement. The distance of a point from the line shows the difference between the two results. The correlation coefficient $R^2$ for the regression line is 0.96 with an average deviation of 9% between model M-CTP and E-CTP. This is a good level of agreement covering all elastomers at multiple hardness values and at multiple exposure temperatures. In the plot, data points are coded by polymer family (symbol style), shore hardness (edge bordered or no border symbols), and temperature (blue or red symbols).

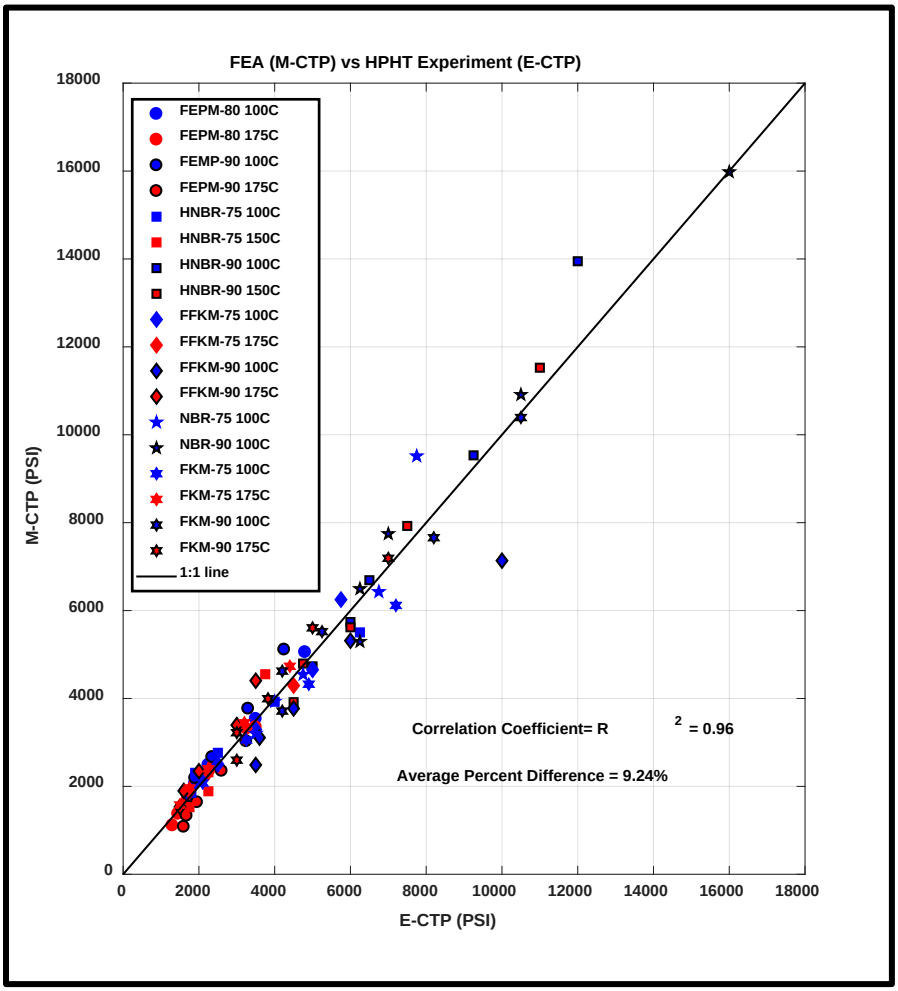


**Figure 103a. Black bordered symbols are for the harder 90 durometer materials. No border symbols are for the softer 75-80 durometer materials. Red symbols are for higher temperatures of 150°C to 175°C. Blue symbols are for lower temperature of 100°C (Endurica, LLC).**

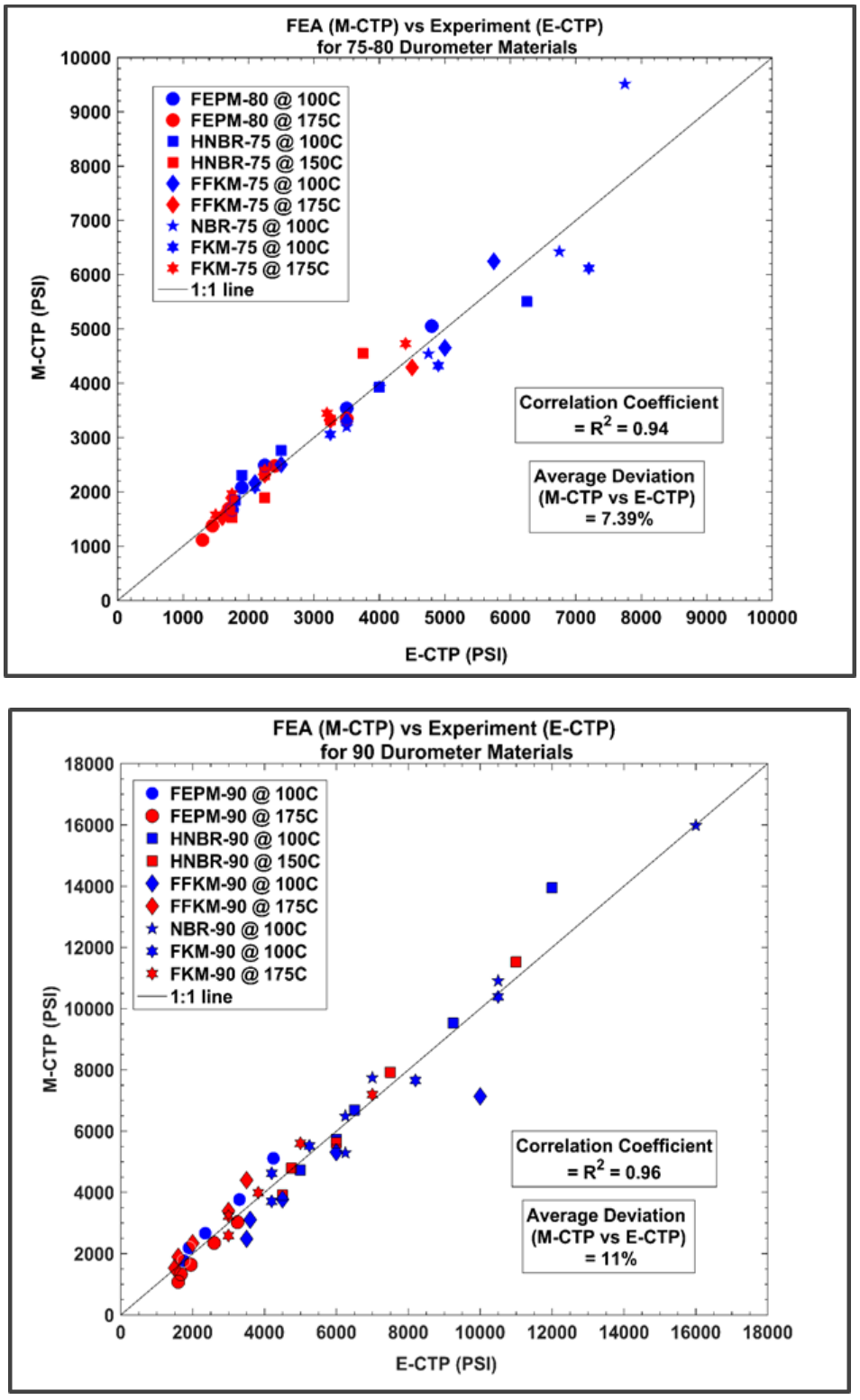


**Figure 103b. Comparison of tear initiation pressure predictions by FEA (M-CTP, psi) versus HPHT experiment (E-CTP, psi). Each polymer family uses a different marker symbol shape.**

Sensitivity analyses were conducted to provide insight into aspects of testing that could not be varied in the current study. A sensitivity study was conducted to examine the effect of the fillet radius on the gland of the piston next to the clearance gap (refer to Figure 104). The study used one test setup, FKM-75 at 100°C with a 0.004-inch clearance gap and four different fillet radii.. The pressure when the Tresca stress reaches the critical level when tearing initiates was determined for each fillet radius. The fillet radius versus pressure results show that a larger fillet radius enables the O-ring to withstand greater pressure before tearing initiates. This can be useful to keep in mind when designing new tools or sealing surfaces to ensure that they can withstand required pressures while maintaining seal integrity. The fillet radius versus pressure relationship can be approximated by a log-linear relationship. The results of the sensitivity study are shown in Figure 104.

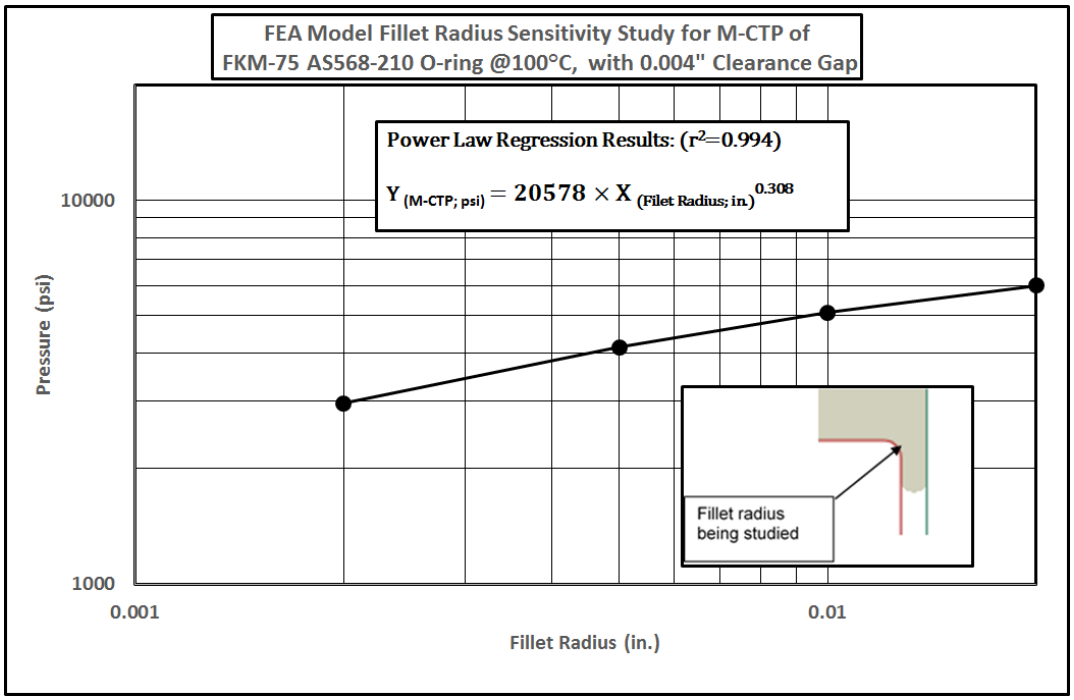


**Figure 104. Results of the fillet radius study (Endurica, LLC).**

The results indicate that an FEA model can be constructed such that failure conditions that correlate well with laboratory test results can be predicted. Several aspects of O-ring seals were not included in the scope of this task, and present opportunities for further study. These include scenarios related to chemical exposure, different sealing geometries, presence of backup rings, and extended lifecycle testing (cyclic pressurization and associated crack growth). Additionally, it may be useful to develop the model to include creep crack growth for estimating the effects of long-duration pressurization periods. The current model has not been validated against long-term sealing experiments, but this could be done using the existing HPHT experimental hardware.

Such evaluations would greatly benefit efforts to establish effective guidance on the conditions that ensure safe operation of O-rings in the long term.

### *9.2.2 Longer-term O-ring Performance: M-CTP Propagation after 1 Year at Temperature, Pressure*

Table 52 provides estimates of the effect of long-term thermal aging under the high pressure conditions determined for each elastomer O-ring on the M-CTP (psi) performance.

Most elastomers were predicted to lose about 50% of their M-CTP pressure resistance when held up to 175°C at their maximum pressure rating. The model-predicted best performing elastomer with regard to long-term temperature performance reduction was FKM-75 (Viton 75) which lost only 28% of its M-CTP, with the harder FKM-90 (Viton 90) also performing above average (42% reduction) after 1 year at 175°C. Of course, these elastomers also had a lower initial M-CTP compared to the others.

**Table 52. Relative change in M-CTP predicted by FEA model after 1 year at maximum pressure (for 0.004" Clearance Gap).**

| Elastomer | M-CTP Initial (psi) | M-CTP after 1 month (psi) | Relative Decrease in M-CTP after 1 month (%) | M-CTP after 1 year (psi) | Relative Decrease in M-CTP after 1 year (%) |
|---|---|---|---|---|---|
| NBR-90 @100°C | 10,912 | 5,210 | -52 | 3,935 | -64 |
| HNBR-90 @100°C | 9,521 | 4,931 | -48 | 3,841 | -60 |
| FKM-90 @100°C | 7,658 | 3,977 | -48 | 3,101 | -60 |
| NBR-75 @100°C | 6,428 | 3,841 | -40 | 3,159 | -51 |
| FKM-90 @175°C | 5,610 | 3,767 | -33 | 3,238 | -42 |
| FFKM-90 @ 100°C | 5,315 | 2,110 | -60 | 1,485 | -72 |
| FFKM-75 @ 100°C | 4,653 | 3,431 | -26 | 3,056 | -34 |
| FKM-75 @ 100°C | 4,325 | 2,411 | -44 | 1,931 | -55 |
| HNBR-75 @100°C | 3,927 | 2,316 | -41 | 1,895 | -52 |
| FEPM-90 @ 100°C | 3,769 | 2,158 | -43 | 1,746 | -54 |
| FEPM-80 @ 100°C | 3,540 | 1,965 | -44 | 1,572 | -56 |
| FKM-75 @ 175°C | 3,447 | 2,716 | -21 | 2,481 | -28 |
| FFKM-90 @ 175°C | 3,394 | 2,451 | -28 | 2,165 | -36 |
| FFKM-75 @ 175°C | 3,325 | 1,997 | -40 | 1,645 | -51 |
| FEPM-80 @ 175°C | 2,481 | 1,548 | -38 | 1,294 | -48 |
| FEPM-90 @ 175°C | 2,356 | 1,500 | -36 | 1,264 | -46 |

Appendix A.7 includes plots of the comparative retention of M-CTP performance for all elastomers included in the study as a function of pressure hold time with one-month and one-year values highlighted.

## 10.0 CONCLUSIONS

Current industry standards and literature on elastomer performance were used as guidance for the development of laboratory experiments and FEA model to simulate elastomer behavior in HPHT environments. The best fit agreement between the FEA model and the HPHT experiments (Figure 103a) of 0.96 illustrates that all of the O&G elastomers studied under steady-state HPHT conditions can be successfully modeled using FEA.

The agreement between the model and HPHT experiment served as validation for the model with respect to modeling the specific conditions tested. The results of the HPHT experiments were not inherently obvious. An initial hypothesis for a failure mechanism was reversible extrusion of the elastomer through the clearance gap and leading to a loss of sealing capability. Examination of some preliminary failed ("red") O-rings showed the development of a crack at the fillet radius adjacent to the clearance gap in the test apparatus. Based on visual analysis of the O-rings, the elastomer material on the non-fillet radius side of the apparatus was pushed into the clearance gap as the test progressed, resulting in a crack in the O-ring that spiraled from the outside of the O-ring toward the center (Figure 105).

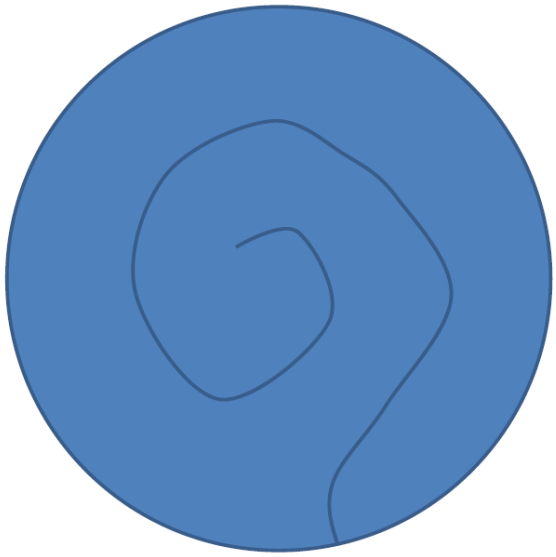

**Figure 105. Tear propagation path observed during HPHT testing.**

Discovery of the crack behavior supported a hypothesis that the critical failure mode from extrusion involved crack generation and tearing (Figure 106). This required additional laboratory property measurements to determine creep-crack growth rate and onset for the study elastomers. The FEA model was then developed including the effect of creep-crack growth.

Figure 107 illustrates how the FEA model developed in this program could be used in a design analysis of elastomer seal components for annular blow out preventers as depicted in Figure 108.

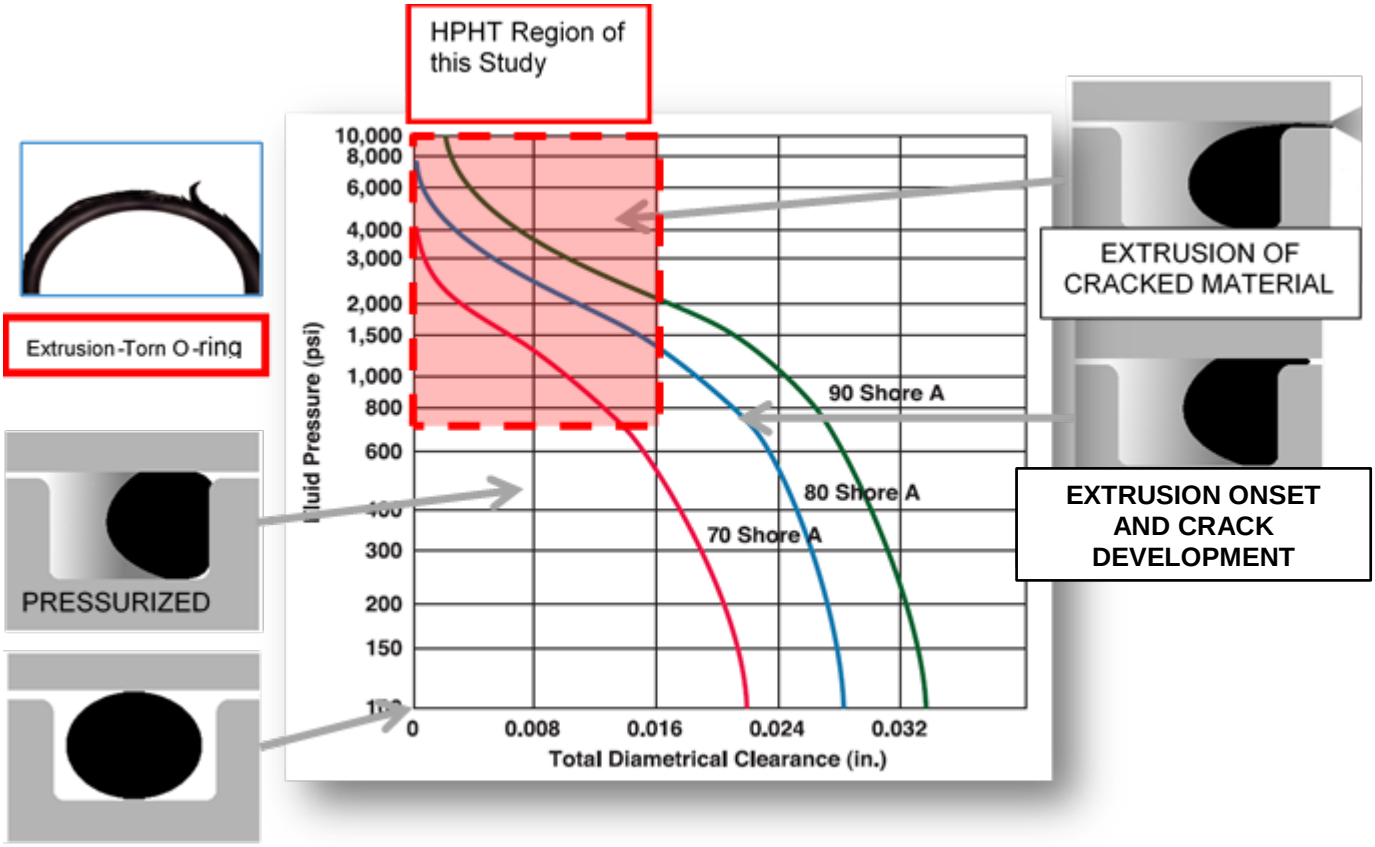


**Figure 106. Traditional published O-ring extrusion limit guidelines and cracked, failed O-ring (upper left).**

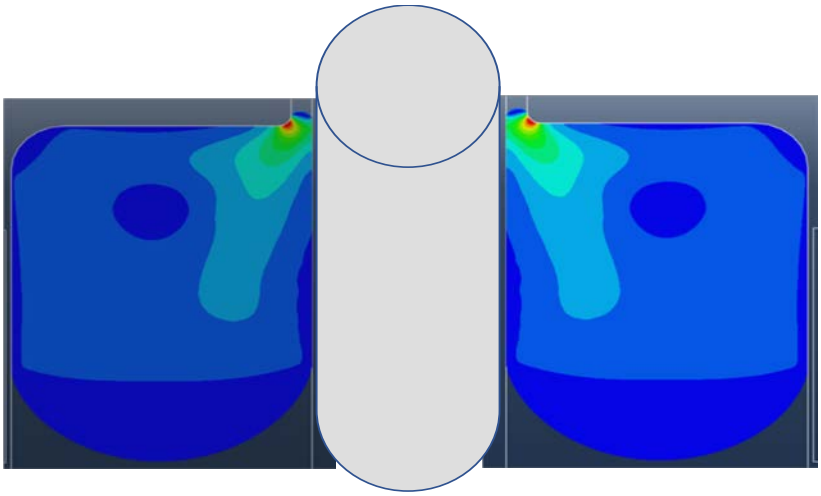

**Figure 107. Illustration of scaled-up FEA analysis of BOP elastomer seal using M-CTP model approach (FKM-90 at 175°C shown).**

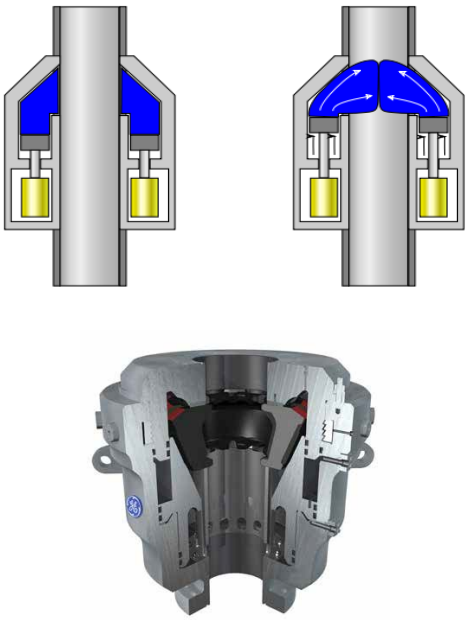

**Figure 108. Annular blow-out preventer uses flow extrusion of elastomer for well-control (7-inch GK* BOP for 15,000-20,000 psi shown) [4].**

[4] GE Oil & Gas, 3300 North Sam Houston Parkway East Houston, TX 77032

## Key Findings

The following key findings are based on the results of this project:

- New or revised guidance, followed by formal industry standards, are needed to ensure safe operation in HPHT environments (over 15,000 psi and 175ºC) since current industry standards only provide guidance for elastomer use at pressures up to 5,000 psi.
- The dominant failure mechanism in HPHT elastomer testing and FEA model development was crack tear propagation via extrusion-initiated spiral failure. Understanding of this failure mechanism could guide development of new crack resistant materials.
- A FEA-based computer model was developed using ABAQUS software to predict the onset of tearing and failure of elastomer O-rings under HPHT conditions. The FEA (M-CTP) model was parameterized with a comprehensive set of elastomer mechanical property data at multiple temperatures, including multi-axial, compression, hyper-elastic, crack-initiation and creep-crack-growth tests. The model was successfully validated by comparing the experimental (E-CTP) test results from a HPHT test cell.
- The outcome of this work supports the use of FEA in the design and evaluation of elastomer seals in downhole tools and well control applications such as BOPs, as illustrated for the case of an annular BOP in Figure 107 and Figure 108. Battelle emphasizes that any large-scale extension of the FEA model that was developed and validated on AS568-210 size O-ring seal fixtures should be revalidated on larger scale devices before implementation.
- The correlation between the model (M-CTP) and experimental data (E-CTP) was very high with average deviation[5] of 9% for all O-ring materials at all tested clearance gaps and all test temperatures. This provides users with high confidence in the M-CTP accuracy (Figure 103a,b). The FEA (M-CTP) model was also parameterized with elastomer property data at multiple temperatures and confirmed through experimental data.
- O&G elastomers have much lower mechanical properties (tensile modulus, tensile strength and elongation at break) at temperatures above 75°C (Section 6.7, 6.8). Therefore, even though elastomers may be in compression mode, the O&G operator should require higher temperature test data for HPHT applications.

[5] Defined as the average of the individual M-CTP and E-CTP deviations, calculated as: $\frac{|(M-CTP)-(E-CTP)|}{E-CTP} \cdot 100$

- The performance of the O&G elastomer seal materials was determined to depend on CTPs as a function of temperature. The relative ranking of the elastomer seal materials was found to be (Table 53 and 54):
  - For 90 Hardness Elastomers: HNBR-90 and FKM-90 are superior to FFKM-90 and FEPM-90 at 150°C to 175°C across all clearance gaps (see Figure 109).
  - Lower Hardness elastomers (hardness of ~75-83) have similar E-CTP at 150°C to 175°C across all clearance gaps, which is much lower than HNBR-90 and FKM-90, but similar to FFKM-90 and FEPM-89 (see Figure 110).
  - The outcome of this work supports the use of FEA in the design and evaluation of elastomer seals in downhole tools and well control applications such as BOPs.

  Battelle emphasizes that any large-scale extension of the FEA model that was developed and validated on AS568-210 size O-ring seal fixtures should be revalidated on larger scale devices before implementation.

  - The correlation between the model (M-CTP) and experimental data (E-CTP) was very high with average deviation of 9% (500 to 1,000 psi) for all O-ring materials at all clearance gaps and all test temperatures. This provides users with high confidence in the M-CTP accuracy.
  - The current version of the FEA model accurately predicts the elastomer seal crack initiation pressure, but does not explicitly monitor creep crack growth after tearing begins. Power-law predictions of the change in M-CTP over time indicate approximately 50% reduction after 1 year exposure at maximum pressurization specific for each elastomer at 0.004-inch clearance gap (see Table 53 and Table 54, Figure 110 and Figure 111, and Appendix A-8 [Figures 88-95]).

**Table 53. Comparison of M-CTP and E-CTP at 100°C and 0.004-inch clearance gap.**

| Material | M-CTP at 100°C 0.004-inch clearance gap | E-CTP at 100°C 0.004-inch clearance gap |
|---|---|---|
| **NBR 90** | 10,912 | 10,500 |
| **HNBR-90** | 9,521 | 9,250 |
| **FKM-90** | 7,658 | 8,200 |
| **NBR-75** | 6,428 | 6,750 |
| **FFKM-90** | 5,315 | 6,000 |
| **FFKM-75** | 4,653 | 5,000 |
| **FKM-75** | 4,325 | 4,900 |
| **HNBR-75** | 3,927 | 4,000 |
| **FEPM-90** | 3,769 | 3,500 |
| **FEPM-80** | 3,540 | 3,300 |

**Table 54. Comparison of M-CTP and E-CTP at 175°C and 0.004-inch clearance.**

| Material | M-CTP at 175°C 0.004-inch clearance gap | E-CTP at 175°C 0.004-inch clearance gap |
|---|---|---|
| **HNBR-90 at 150°C** | 7,926 | 7,500 |
| **FKM-90** | 5,610 | 5,000 |
| **FKM-75** | 3,447 | 3,200 |
| **FFKM-90** | 3,394 | 3,000 |
| **FFKM-75** | 3,325 | 3,250 |
| **HNBR-75 at 150°C** | 3,323 | 3,250 |
| **FEPM-80** | 2,481 | 2,400 |
| **FEPM-90** | 2,356 | 2,600 |

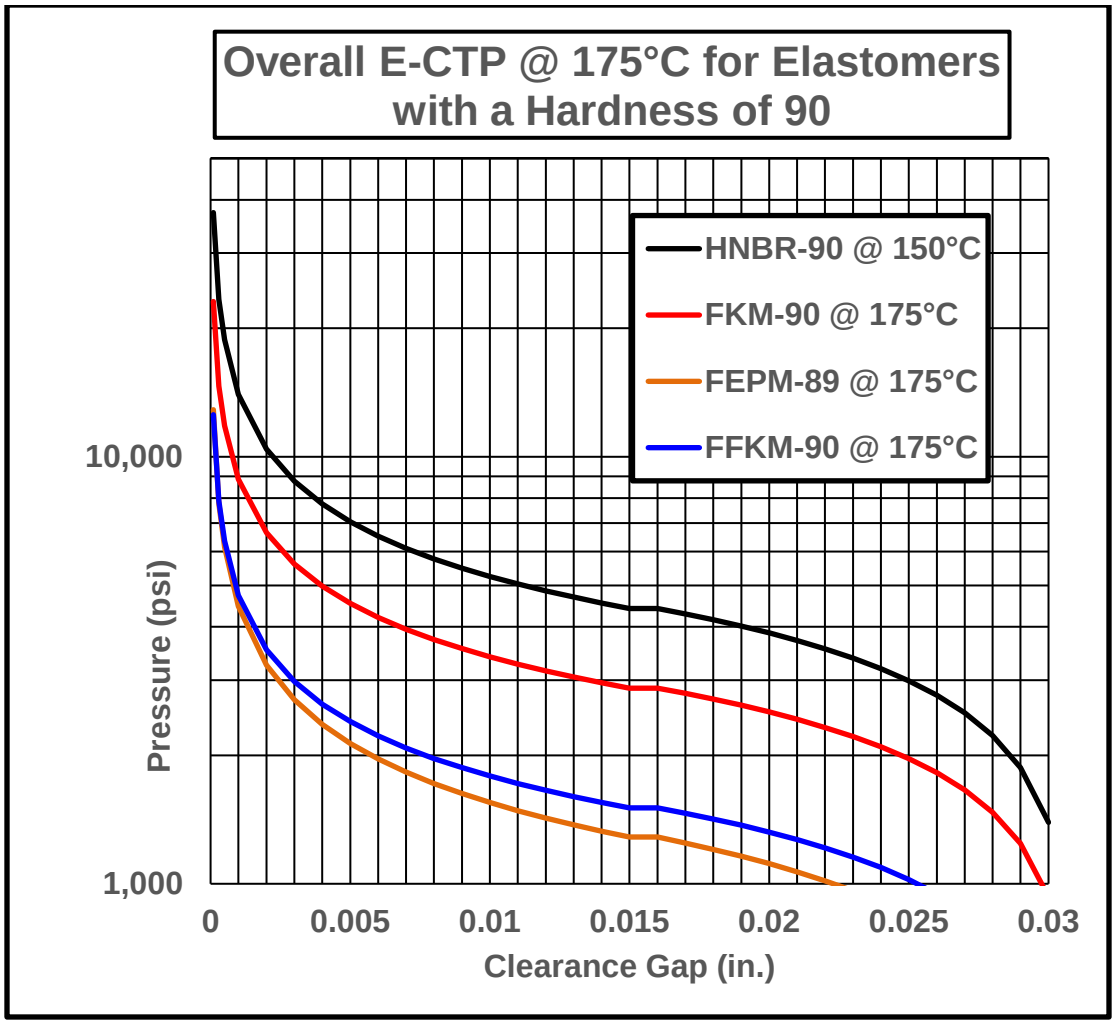


**Figure 109. Relative ranking of E-CTP for elastomers with a hardness of 90 at 175°C.**

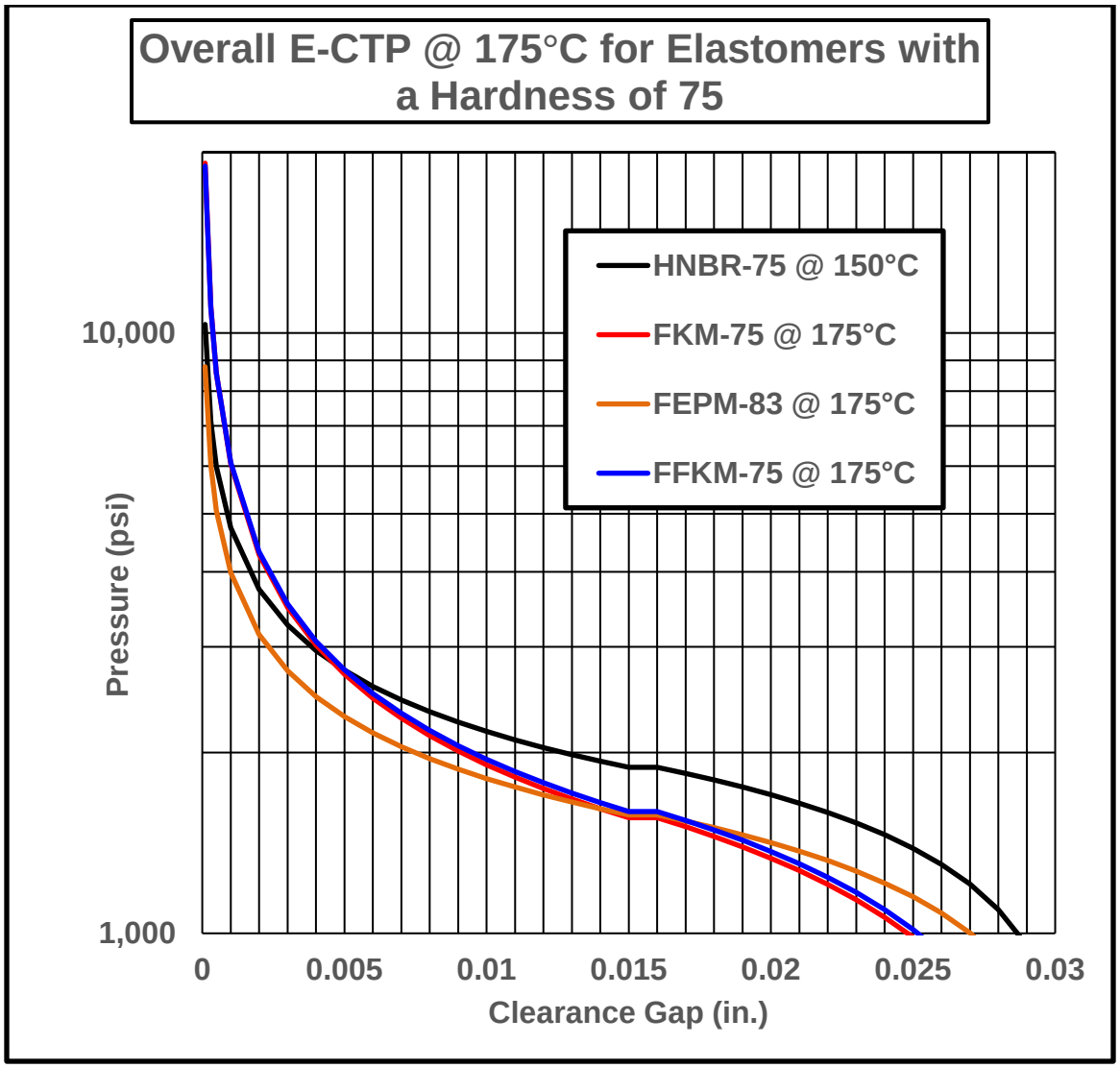


**Figure 110. Relative similarity of E-CTP for elastomers with a hardness of 75 at 175°C.**

- The FEA model accurately predicts the elastomer seal crack initiation pressure (M-CTP) and Power-law predictions of the change in M-CTP over time indicate approximately 50% reduction after 1 year exposure to maximum pressure (Figure 111 and Figure 112). The FEA model estimate of aging behavior can be improved by validation of creep crack growth at several time points after tearing begins.

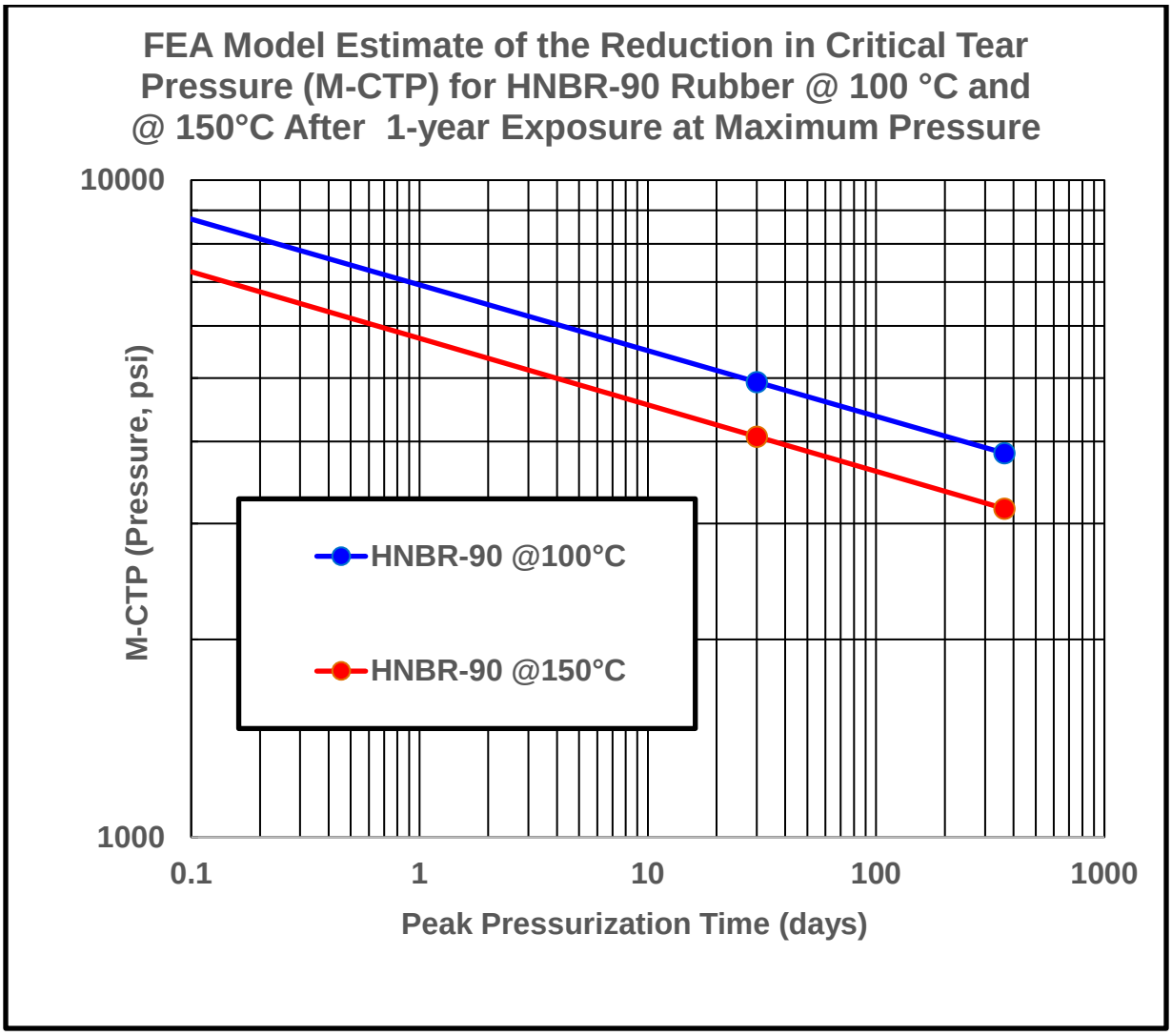


**Figure 111. FEA model Estimate of the reduction in M-CTP for HNBR-90 at 100°C and 150°C after 1-year exposure at maximum pressure at 0.004-inch clearance gap.**

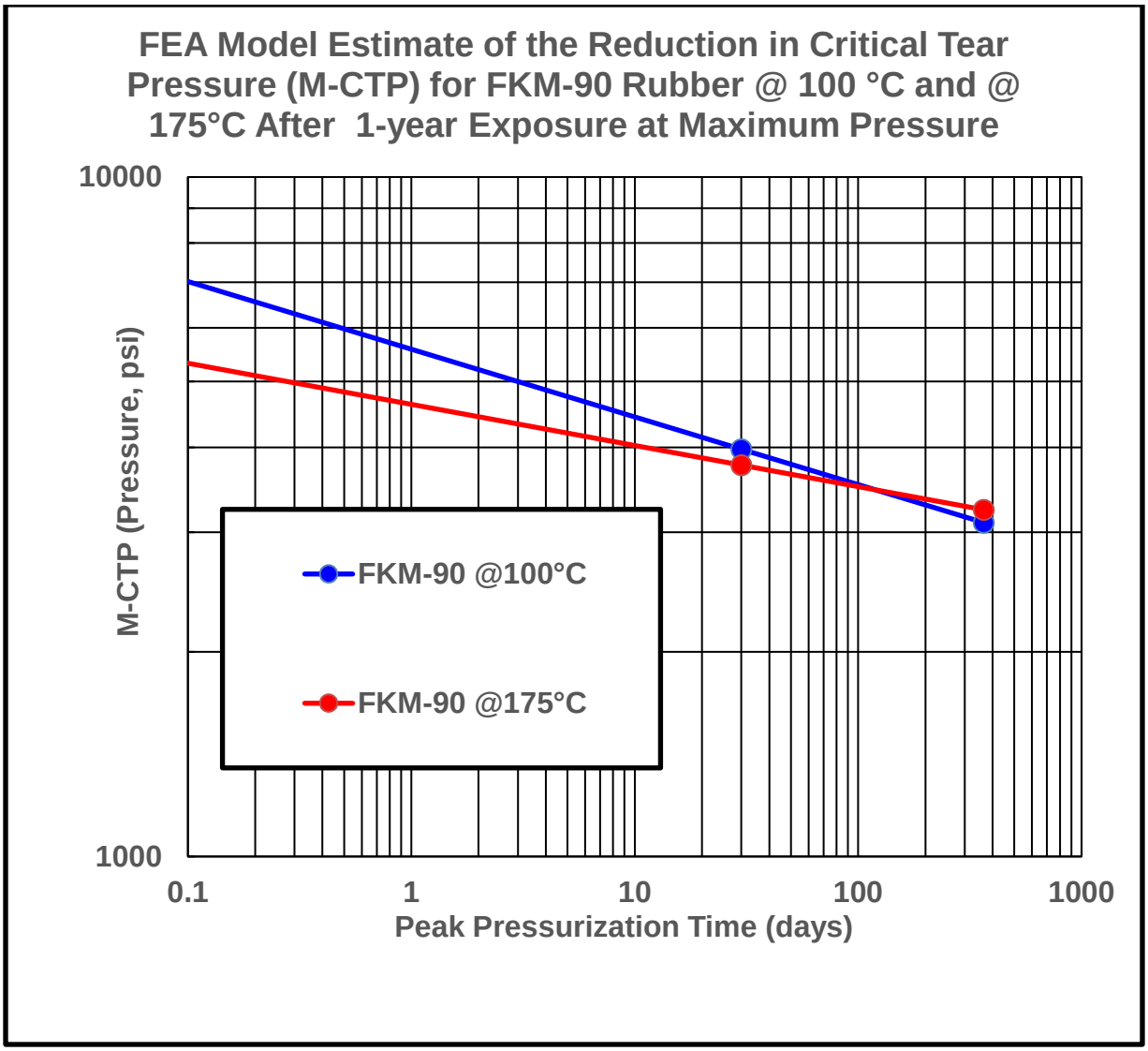


**Figure 112. FEA model estimate of the reduction in M-CTP for FKM-90 at 100°C and 175°C after 1-year exposure at maximum pressure at 0.004-inch clearance gap.**

**Recommendations**

- O-ring seal failures can be caused by other stresses encountered under HPHT conditions, including chemical environments ($H_2S$, $CO_2$, hydrocarbon liquid and vapor). Additional testing and model development are recommended for these conditions so that the FEA can more accurately represent real HPHT operating environment conditions.

- The testing in this program was done at the O-ring level and should be expanded to component and device level (i.e., BOPs, SSVs, packers, etc.).
- Future studies can include extending the FEA model and HPHT testing to include aging effects in corrosive and non-corrosive environments as well as extended lifecycle testing (cyclic pressurization and associated crack growth) under these conditions.
- Future development efforts should expand the FEA model to include longer term creep crack growth of elastomers in combination with experimental validation (Figure 113).

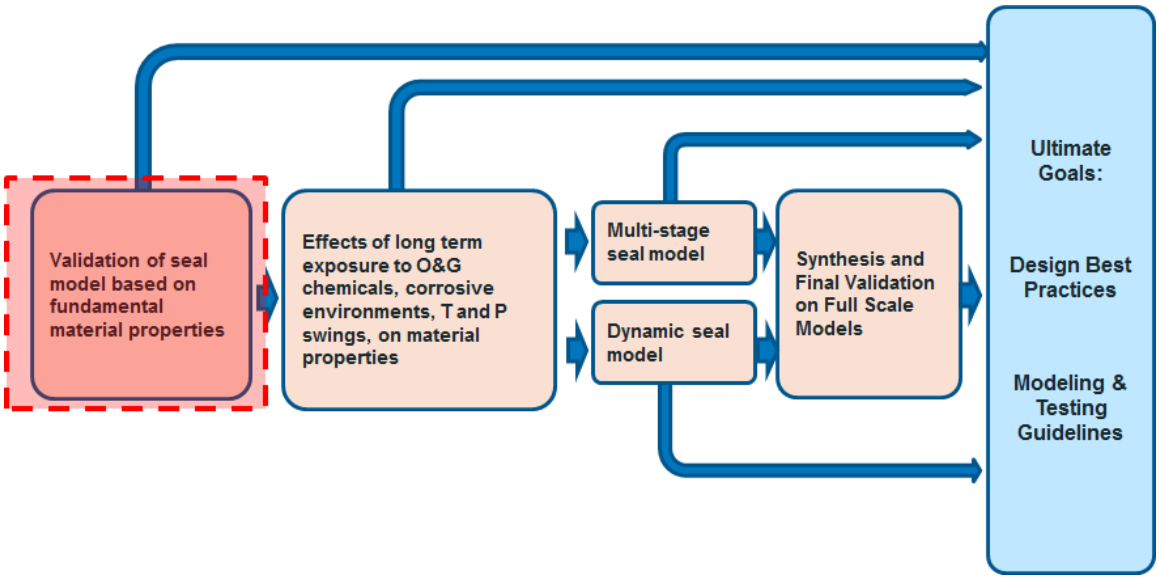


**Figure 113. Recommendation Roadmap**

The evaluations of elastomers performed in this study, and the FEA model produced, constitute the development and validation of a baseline FEA model. This model serves as a building block toward the eventual goal of developing a complete computer-based model that can be used to develop best practices and guidelines for elastomer use under HPHT conditions. A complete model would include predictive failure capabilities for various downhole environments (including sweet and sour gas conditions) encountered by HPHT operators.

## 11.0 REFERENCES


AFLAS Fluoroelastomers. (2015, November 30). *AFLAS 100-150 Series Standard Grade*. Retrieved from www.aflas.jp: http://www.aflas.jp/english/products/100-150.html

Allada, S. R. (1984). Solubility Parameters of Supercritical Fluids. *Industrial and Engineering Chemistry Process Design and Development*, 344-348.

Ameduri, B., Boutevin, B., & Kostov, G. (2001). Fluoroelastomers: Synthesis, Properties and Applications. *Progress in Polymer Science*, 105-187.

American Petroleum Institute. (2012, November). API STD 53. *Blowout Prevention Equipment Systems for Drilling Wells*. API.

API. (2010). *Specification for Wellhead and Christmas Tree Equipment.*

API. (2015). *Design, Installation, Operation, Test, and Redress of Subsurface Safety Valve Systems.*

API. (2015). *High-pressure High-temperature Design Guidelines.*

API. (2015). *Packers and Bridge PlugsPetroleum* .

API. (2015). *Specification for Subsurface Safety Valve Equipment.*

Arkema Inc. (2009, April). *Technical Information DI-CUP and VUL-CUP Peroxides.* Retrieved from luperox.com: http://www.luperox.com/export/sites/organicperoxide/.content/medias/downloads/literature/di-cup-and-vul-cup-vulcanizing-nitrile-rubber.pdf

ASTM . (n.d.). ASTM D1349-14. *Standard Practice for Rubber – Standard Conditions for Testing*. ASTM .

ASTM. (2010). ASTM D6546-00. *Standard Test Methods for Suffested Limits for Determining Compatibility of Elastomer Seals for Industrial Hydraulic Fluid Applications*. ASTM.

ASTM. (2012). ASTM D430-08. *Standard Test Methods for Rubber Deterioration – Dynamic Fatigue*. ASTM.

ASTM. (2012). ASTM D575-91. *Standard Test Methods for Rubber Properties in Compression*. ASTM.

ASTM. (2012). ASTM D7127-05. *Standard Test Method for Rubber Property—Resilience Using Schob Type Rebound Pendulum*. ASTM.

ASTM. (2012). ASTM D945-08. *Standard Test Methods for Rubber Properties in Compression or Shear (Mechanical Oscillograph)*. ASTM.

ASTM. (2013). ASTM D926-08. *Standard Test Method for Rubber Property – Plasticity and Recovery (Parallel Plate Method)*. ASTM.

ASTM. (2014). ASTM D6147-97. *Standard Test Method for Vulcanized Rubber and Thermoplastic Elastomer – Determination of Force Decay (Stress Relaxation) in Compression*. ASTM.

ASTM. (2014). ASTM D623-07. *Standard Test Method for Rubber Property – Heat Generation and Flexing Fatigue in Compression*. ASTM.

ASTM. (2015). *Standard Test Method for Rubber Property - Durometer Hardness.*

ASTM. (n.d.). ASTM D2000-12. *Standard Classification System for Rubber Products in Automotive Applications*. ASTM.

ASTM. (n.d.). ASTM D2632-15. *Standard Test Method for Rubber Property – Resilience by Vertical Rebound*. ASTM.

ASTM. (n.d.). ASTM D471-12a. *Standard Test Method for Rubber Property— Effects of Liquids*. ASTM.

ASTM. (n.d.). ASTM D5662-14. *Standard Test Method for Determining Automotive Gear Oil Compatibility with Typical Oil Seal Elastomers*. ASTM.

ASTM. (n.d.). ASTM D7216-15. *Standard Test Method for Determining Automotive Engine Oil Compatibility with Typical Seal Elastomers*. ASTM.

ASTM D573-04. (2010). *Standard Test Method for Rubber- Deterioration in an Air Oven*. ASTM.

Bellarby, J. (2009). Well Completion Design. *Developments in Petroleum Science*, pp. 557-593.

Cai, B., Liu, Y., Liu, Z., Tian, X., Zhang, Y., & Ji, R. (2013). Application of Bayesian Networks in Quantitative Risk Assessment of Subsea Blowout Preventer Operations. *Risk Analysis, 33*(7).

Campion, R. P., Thomson, B., & Harris, J. A. (2005). *Elastomers for fluid containment in offshore oil and gas production: Guidelines and review*. HSE.

CDI Energy Products. (2014, September). NORSOCK 710. *Qualification of non-metallic materials and manufactureres- Polymers*. NORSOCK.

Cheremisinoff, N. P., & Cheremisinoff, P. N. (1993). *Elastomer Technology Handbook.* CRC Press.

Cole, E. (2015, December 1). *An Introduction to Perfluoroelastomers.* Retrieved from Rubber World - December 2013: http://digitaleditions.walsworthprintgroup.com/article/An+introduction+to+perfluoroelastomers/1582871/0/article.html

Columbia Engineered Rubber, Inc. (2006 -2013). *Rubber Compression Molding, Compression Molding Process*. Retrieved from Rubber Compression Molding, Compression Molding Process: http://www.columbiaerd.com/compression-molding.html

Daemar Inc. (2015). *Causes of O-Ring Failure*. Retrieved from http://daemar.com/o-rings_causesoffailure_117.html/

DuPont. (2010). *DuPont Viton(TM) Selection Guide.* DuPont.

Edmond, K., Ho, E., Flitney, R., Embury, P., Groves, S., & Rivereau, J.-M. (2001). Comparison of Explosive Decompression Test Protocols for Elastomer Seals in High Pressure Gas Service. *Corrosion 2001*. Nace International.

Endurica, LLC. (2015). *BSEE Project Kickoff Meeting Presentation.*

Environmental Protection Agency. (n.d.). *Natural Gas Processing*. Retrieved from http://www3.epa.gov/ttnchie1/ap42/ch05/final/c05s03.pdf

EPM, Inc. (2015). *The Seal Man's O-Ring Handbook*. Retrieved from https://www.physics.harvard.edu/uploads/files/machineshop/epm_oring_handbook.pdf

Files, E., Jones, M., & Wood, M. E. (2001, December 1). Post Cure Thermo-oxidative Effects on HNBR. *Rubber World*.

Hansen, C. M. (2007). *Hansen Solubility Parameters; A User's Handbook.* CRC Press.

Hertz, D. L. (1996). Oil and Gas Industry Seals and Sealing - Success and Failure. *ERG Fall Technical Meeting.* Houston.

Holand, P. (1997). *Offshore Blowouts Causes and Control.* Houston, TX: Gulf Publishing Company.

International Organization for Standardization. (2001, 12 1). ISO 13533. *Drilling and production equipment — Drillthrough equipment*. ISO.

International Organization for Standardization. (2005, 2 1). ISO 10423. *Drilling and production equipment- Wellhead and Christmass tree equipment.* ISO.

International Organization for Standardization. (2006, May 1). ISO 10432. *Petroleum and natural gas industries- Downhole equipment- Subsurface safety valve equipment.* International Organization for Standardization.

International Organization for Standardization. (2008). ISO 14310. *Downhole equipment-Packers and bridge plugs*. ISO.

International Organization for Standardization. (2009, 2 1). ISO 27996. *Aerospace fluid systems — Elastomer seals—Storage and shelf life*. ISO.

International Organization for Standardization. (2011, 12 15). ISO 23936-2. *Non-metallic materials in contact with media related to oil and gas production — Part 2: Elastomers*. ISO.

International Standard. (2004, 07 01). Petroleum and Natural Gas Industries - Subsurface Safety Valve Systems - Design, Installation, Operation, and Redress. International Standards Organization.

International Standards. (2008, November). Petroleum and natural gas industries - downhole equipment - Packers and bridge plugs. *14310:2008*.

International Standards. (2011, November 1). Design and operation of subsea production systems - Part 4: Subsea wellhead and tree equipment. *13628-4*.

ISO 13628-4. (2011, 5). *Design and Operation of Subsea Productions Systems— Subsea Wellhead and Tree Equipment*. ISO.

James Walker. (2012). *Elastomer Engineering Guide.* Woking: James Walker Sealing Products and Services, Ltd.

Makino, A., Hamburgen, W. R., & Fitch, J. S. (1993). *Fluoroelastomer Pressure Pad Design for Microelectronic Applications.* California: WRL Research Report 93/7.

MERL Ltd. (2005). *Elastomers for Fluid Containment in Offshore Oil and Gas Production: Guidelines and Review. Research Report 320.* Retrieved from www.hse.gov.uk: http://www.hse.gov.uk/research/rrpdf/rr320.pdf

Miller, K. (n.d.). *Testing Elastomers for Hyperelastic Material Models in Finite Element Analysis.* Axel Products, Inc.

Moore, A. L. (2006). *Fluoroelastomers Handbook: The Definitive User's Guide and Databook.* Taylor and Francis.

NACE. (2008, March 15). NACE 0297. *Effects of High-Temperature, High-Pressure Carbon Dioxide Decompressions of Elastomeric Materials*. NACE.

NACE International. (2002). Oilfield Corrosion Inhibitors and Their Effects on Elastomeric Seals. *NACE International Publication 1G286*.

NACE TM0187. (2001, June 18). *Evaluating Elastomeric Materials in Sour Gas Environments*. NACE.

NACE TM0296. (2014, June 26). *Evaluating Elastomeric Materials in Sour Liquid Environments*. NACE.

National Institute of Standards and Technology. (2011). *Carbon Dioxide*. Retrieved from webbook.nist.gov: http://webbook.nist.gov/cgi/cbook.cgi?ID=C124389&Mask=4

Offshore. (2008, October 1). Swelling Elastomers set to Supersede Cement in Well Completions. *Offshore, 68*(10).

Ogunniyi, S. S. (2003). Compounding Studies of a Fluoroelastomer. *Iranian Polymer Journal*, 367-371.

Parker. (2007). *The Parker O-Ring Handbook.*

Precision Polymer Engineering. (n.d.). Retrieved from http://www.prepol.com/my-ppe/chemical-compatibility

Rodriguez, F., Cohen, C., Ober, C. K., & Archer, L. A. (2003). *Principles of Polymer Systems, Fifth Edition.* Taylor and Francis.

SAE Aerospace. (2010, December). Storage of Elastomer Seals and Seal Assemblies Which Include an Elastomer Element Prior to Hardware Assembly. *Aerospace Recommended Practice*. SAE.

SINTEF. (2013). *Offshore Blowout Database.* Retrieved from https://www.sintef.no/en/projects/sintef-offshore-blowout-database/

Slay, B., & Ferrell, K. (2008, May). Performance Qualification of Seal Systems for Deepwater Completions. *Offshore Technology Conference*. Houston, TX, United States: Offshore Technology Conference.

Society of Petroleum Engineers. (2015). *Completion Flow Control Accessories*. Retrieved from PetroWiki: http://petrowiki.org/images/0/05/Vol4prt_Page_071_Image_0001.png

TA Instruments. (1997). *Dynamic Mechanical Analysis of Polymers.*

TA Instruments. (2016, June). Retrieved from http://www.tainstruments.com/

Tukenov, D. (n.d.). Nanochemistry Drives New Method for Removal and Control of Wax. *Journal of Petroleum Technology*.

United States DOD. (1965, February 5). MIL-G-21569. *Gaskets, Cylinder Liner Seal, Synthetic RUbber*. United States DOD.

United States DOD. (1980, February 25). MIL-P-25732. *Packing, Preformed, Petroleum Hydraulic Fluid Resistant, Limited Service at 275°F*. United States DOD.

United States DOD. (1998, June 10). MIL-PRF-1149D. *Gasket Materials, Synthetic Rubber, 50 and 65 Durometer Hardness*. United States DOD.

WEST Engineering Services. (2009). *High Temperature Elastomer Study for MMS.*

## A.1 Appendix 1 – Summary Table of Relevant Industry Standards

Standards directly and indirectly related to elastomeric materials used in O&G HPHT environments are summarized in the table below. Standards are grouped by the organization – API, ISO, NORSOK, NACE, MIL-SPEC and ASTM. The ‘Summary of Standard’ column includes a bulleted synopsis of the relevant sections of each standard. The ‘Cross References’ column lists standards that are referenced within the relevant sections of the standard being summarized for test conditions, procedures, or other relevant topics. Complete citations of standards summarized can be found in the reference section.

## Table A.1-1: Summary of Reviewed Standards Relevant to Elastomer use in HPHT O&G Service

| STANDARD NUMBER | STANDARD DESCRIPTION | SUMMARY OF STANDARD | CROSS REFERENCES |
|---|---|---|---|
| **API 6A, 12th Edition** (API, 2010) | Specification for Wellhead and Christmas Tree Equipment | Modified from ISO 10423:2009. Sections pertinent for elastomer design are similar to ISO 10423 requirements. | ISO 10423 |
| **API 11D, 3rd Edition (API, 2015)** | Packers and Bridge Plugs | Modified from ISO 14310:2008. Contains Annex B (Requirements for HPHT Environment Equipment) and Annex C (Requirements for HPHT Operational Tools).<br>Annex B – covers packers and bridge plugs in service of >350°F and >15,000 psi. Functional requirements pertaining to elastomer service environments (including chemical exposures) required to be identified. Aging testing under well conditions identified as a recommended test. | ISO 14310 |
| **API 14A, 12th Edition (API, 2015)** | Specification for Subsurface Safety Valve Equipment | Similar to ISO 10432:2004, although new HPHT information is added in API14A 12th Edition.<br>Annex H – user to fully specify environmental conditions which elastomers will be exposed to. Ageing and RGD testing to be completed by ISO23936-2, Annex B (100°C, 145 psi). For elastomers, Tensile strength, Tensile modulus, Elongation, Compression set, Tear resistance, Low temperature limit of brittleness, and Low temperature stiffening/flexibility testing shall be conducted per specifications in H.2 | ISO 23936 |
| **API 14B, 6th Edition (API, 2015)** | Design, Installation, Operation, Test, and Redress of Subsurface Safety Valve Systems | Storage conditions presented similar to ISO 10417, Section 5. When packaging, SSSV equipment with exposed elastomeric seals shall be protected from UV light and shall not be in contact with contaminants.<br>SSSV equipment with elastomeric materials shall not be stored near ozone (produced from electrical devices) or radiation equipment and shelf life shall be accounted for in storage.<br>Annex A provides testing procedures for SSSVs, although not explicitly associated with HPHT conditions. | |

| | | | |
|---|---|---|---|
| **API 16A, 3rd Edition** | Petroleum and natural gas industries — Drilling and production equipment — Drillthrough equipment | See ISO 13533:2001 | ISO 13533:2001 |
| **API 17D, 2nd Edition** | Design and Operation of Subsea Production Systems – Subsea Wellhead and Tree Equipment | See ISO 13628-4:2011 | ISO 13628-4:2001 |
| **API 17TR10, 1st Edition** ***(Technical Report – Not a Standard)*** **(API, 2015)** | High-pressure High-temperature Design Guidelines | Service temperatures above 550 °F are excluded from this technical report. Report main topics include Design Verification, Materials for HPHT Equipment, Seals and Bolting/Fasteners, Design Validation, and Hydrostatic Tests for HPHT Equipment.<br>Figure 1 shows an HPHT Design Flow Chart used as guidance for conducting of HPHT designs.<br>Functional specifications (Section 5.3.1) shall include well fluid properties or compositions – a topic which is typically not included in other design standards from ISO or ASTM.<br>NACE TM0177 or MR0175/ISO15156-3 specified as acceptable produced/condensed fluid compositions for HPHT evaluation testing.<br>Section 7.1.1.2 specifies HT tests (including RGD and fluid compatibility), which shall mimic service conditions to the extent possible, which are typically not specified in traditional ASTM elastomer tests (such as D471). Tables 2 and 3 specify industry standards for determination of rubber (elastomer) properties. | NACE TM0177<br><br>NACE MR0175/ISO15156-3 |

## Table A.1-1: Summary of Reviewed Standards Relevant to Elastomer use in HPHT O&G Service (continued)

| STANDARD NUMBER | STANDARD DESCRIPTION | SUMMARY OF STANDARD | CROSS REFERENCES |
|---|---|---|---|
| ISO 10417 (International Standard, 2004) | Petroleum and natural gas industries — Subsurface safety valve systems — Design, installation, operation and redress | Section 5- System Configuration<br>This standard states that sealing devices and all related equipment shall be compatible with the dimensions and configurations of permanent well equipment and servicing tools.<br>Surface controlled SSSVs shall be tested for leaks by checking for flow after opening the surface valves.<br>When packaging, SSSV equipment with exposed elastomeric seals shall be protected from UV light and shall not be in contact with contaminants.<br>SSSV equipment with elastomeric materials shall not be stored near ozone (produced from electrical devices) or radiation equipment and shelf life shall be accounted for in storage.<br>The replacement of seals in tubing-retrievable SSSVs shall be limited to seals that do not require the breaking of a body-joint connection as defined by the manufacturer.<br>Replacement of wireline/through-flowline-retrievable SSSVs elastomeric seals is acceptable as defined by the manufacturer.<br>Pressure differential of pressure testing for closure mechanism shall be 200 psi ± 5%.<br>When hydraulic or pneumatic control systems are used, components must be capable of meeting all anticipated environmental conditions.<br>Wellhead passages/connectors materials must be compatible with any fluids that may come in contact.<br>**For seal material applications for working pressures ≥10,000 psi requires special consideration.** | |
| ISO 13533 (International Organization for Standardization, 2001) | **Petroleum and natural gas industries — Drilling and production equipment — Drillthrough equipment** | Section 5- Design requirements<br>Equipment design shall be such that wellbore elastomeric materials operate within the temperature classifications in Table 4 (see Appendix B, Code F: 40-350°F).<br>Section 5.8- Design temperature verification testing for non-metallic sealing materials and molded sealing assemblies | |

| STANDARD NUMBER | STANDARD DESCRIPTION | SUMMARY OF STANDARD | CROSS REFERENCES |
|---|---|---|---|
| | | Non-metallic seals used in the ram-type and annular-type blowout preventers as pressure-controlling members shall be tested to verify performance at extreme temperatures.<br>Section 10- Storage and Shipping<br>**Manufacturers shall specify appropriate storage and shipping conditions of elastomeric seals.** | |
| ISO 23936-2 (International Organization for Standardization, 2011) | Petroleum, petrochemical and natural gas industries — Non-metallic materials in contact with media related to oil and gas production — Part 2: Elastomers | This standard provides appropriate considerations for elastomer selection based on physical and mechanical properties, resistance to rapid gas decompression (RGD) events, temperature flexibility, high pressure gas permeation, resistance to high pressure extrusion or creep, resistance to thermal cycling and dynamic movement.<br>Section 5 outlines documentation requirements for properties and quality control of elastomer materials.<br>The manufacturer is responsible for testing elastomer materials to verify that quality control requirements are met (Section 5).<br>Section 7.2.2 provides acceptance criteria for results of age control and RGD testing of elastomers.<br>Section 9.2.1 states that vendor will facilitate fatigue test to assure acceptable life of the design of elastomeric materials in flexible joints.<br>Ageing test temperatures for elastomeric materials specified in Table A.6 in Section A.1.2.1 (see Appendix B).<br>Elastomeric materials in blowout preventers (Sections 9.3) and in packer assemblies (Section 9.4) shall be tested for appropriateness using procedures from ISO 13533 and ISO 14310 respectively. Inflatable packers shall be tested for high tear strength magnitudes and high extensibility at high temperatures selected from Table A.6 (see Appendix B).<br>**Annex C includes table of most commonly used elastomeric materials (see Appendix B).** | **ISO 13533**<br>**ISO 14310**<br>**NORSOK 710** |

## Table A.1-1: Summary of Reviewed Standards Relevant to Elastomer use in HPHT O&G Service (continued)

| STANDARD NUMBER | STANDARD DESCRIPTION | SUMMARY OF STANDARD | CROSS REFERENCES |
|---|---|---|---|
| **ISO 10423 (International Organization for Standardization, 2005)** | Specification for Wellhead and Christmas Tree Equipment | This standard states that qualification of physical properties and quality control requirements of elastomers shall include hardness testing, tensile testing elongation, compressions set, modulus, and fluid immersion according to ASTM procedures (see Cross References column).<br>Non-metallic seals intended for reuse shall be examined according to manufacturer's requirements (Section Q.7.9).<br>Manufacturers shall produce written requirements which define physical property requirements, generic base polymers, material qualification, and storage/age-control requirements for non-metallic seals (Section 5.2.3).<br>This standard lists standard test fluids for non-metallic seals used in immersion testing to determine fluid compatibility in Table F.2 in Section F.1.13.5.2 (see Appendix B)<br>Annex A of this standard describes Product Specification Levels (PSL) for PSL 1-5. | ASTM D 1414<br>ASTM 2240<br>ASTM D 412<br>ASTM 395<br>ASTM D 471 |
| **ISO 14310 (International Organization for Standardization, 2008)** | Petroleum and natural gas industries — Downhole Equipment — Packers and bridge plugs | This standard provides requirements specifically for packers and bridge plugs.<br>Both metallic and non-metallic material specifications shall be stated by the supplier/manufacturer Section 6.5.1).<br>The user/purchaser shall specify the required equipment compatibility, design, and quality grade (Section 5.6).<br>Suppliers/manufacturers shall document specifications for handling, storage, and labelling of non-metallic compounds and shall define compound type, mechanical properties (tensile strength, elongation, and tensile modulus), compression set, and durometer hardness (Section 6.3.3.3).<br>Suppliers/manufacturers shall state pressure, temperature, and axial performance ratings as applicable for materials (Section 6.3.4).<br>Test methods and results of validation of design requirements for products shall be documented by suppliers/manufacturers (Section 5.7).<br>Storage and shipment of packers and bridge plugs shall meet requirements stated by suppliers/manufacturers (Section 9). | |

## Table A.1-1: Summary of Reviewed Standards Relevant to Elastomer use in HPHT O&G Service (continued)

| STANDARD NUMBER | STANDARD DESCRIPTION | SUMMARY OF STANDARD | CROSS REFERENCES |
|---|---|---|---|
| **ISO 13628-4 (ISO 13628-4, 2011)** | Design and Operation of Subsea Production Systems—Subsea Wellhead and Tree Equipment | Section 5- Common System Requirements<br>The standard requires that manufacturer shall define product capabilities based on validation testing and performance requirements.<br>This standard references ISO 10423 for information for design and rating of equipment use at elevated temperatures.<br>The potential for external hydrostatic pressure exceeding internal bore pressure in deep water environments resulting in reverse pressure on the seal shall be considered in seal design.<br>The manufacturer should document if special surface storage or surface testing procedures are recommended for subsea equipment.<br>Minimum validation test requirements are provided in Table 3 in Section 5.1.7.7 of the standard (see Appendix B).<br>Seals shall be protected such that equipment does not rest on a seal during shipment or storage. Loose seals shall be boxed individually.<br>Elastomeric seal storage environment, age control procedures, and protection shall be documented by manufacturer.<br>Section 8- Specifications for Subsea Wellheads:<br>All pressure containing components of wellhead shall be designed to meet ISO 15156 requirements.<br>Subsea annulus seal assemblies;<br>Shall be treated as pressure controlling equipment defined in ISO 10423.<br>Factory acceptance testing is not required.<br>When there is potential for corrosion or loss of inhibited fluids, it is advised that the production annulus seal assembly be isolated from the production annulus.<br>Loads shall be considered during design.<br>Working pressure of annulus seals shall be greater than or equal to the working pressure of the casing hanger.<br>Annex J- Screening Tests for Material Compatibility | ISO 10423<br>ISO 15156 |

| STANDARD NUMBER | STANDARD DESCRIPTION | SUMMARY OF STANDARD | CROSS REFERENCES |
|---|---|---|---|
| | | Procedures are specified to verify compatibility of chemical additive with subsea completion materials including screening tests for degradation or erosion of non-metallic seals at 140°F for 32 days. | |
| **ISO 27996 (International Organization for Standardization, 2009)** | Aerospace fluid systems — Elastomer seals — Storage and shelf life | This standard states that the life of elastomeric seal elements may be extended by the manufacturer with prompt and proper packaging after vulcanization. Labels shall indicate limited storage life if elements were not properly packaged by manufacturer.<br>Packaging (Section 5) of elastomeric seals by the manufacturer shall occur below 65% relative humidity and free from contaminates. Seals or seal assemblies shall be sealed in individual envelops or in individually sealed packets in multiple envelopes so that seals or assemblies can be removed without impacting the integrity of other packets. The standard also states that all components of a seal assembly must be packaged in the same sealed envelope so that all elements are present when the package is opened. Packaging material and labelling is also addressed in the standard.<br>The storage environment (Section 6) is specified as follows: the temperature may range from 41-86°F, humidity shall be between 40-70% if the elastomer is not in a moisture-proof bag, elastomer must be protected from UV light, must not be near radiation or ozone, must be free from superimposed stress, shall not contact liquid, semi-solid materials, metals with deleterious effects, excess dusting powder, or other elastomers, and shall be rotated in the "first in, first out" principle.<br>Storage life requirements (Section 9) are as follows; NBR, HNBR- 28 quarters of a year, FKM, FFKM, FEPM- 40 quarters of a year. | ISO 27996 (International Organization for Standardization, 2009) |
| **ISO 10432 (International Organization for Standardization, 2006)** | Petroleum and natural gas industries—Downhole equipment—Subsurface safety valve equipment | This standard provides requirements for SSSV equipment not specific to the elastomeric components for environmental compatibility, design validation, supplier/manufacturer requirements, quality control, and storage requirements.<br>Mechanical properties (tensile, elongations, modulus, compression set, and durometer hardness) of non-metallic materials used in SSSVs shall be determined from the test methods listed in the Cross References column. | ASTM D 1414<br>ASTM D 412<br>ASTM D 395<br>ASTM D 2240 |

## Table A.1-1: Summary of Reviewed Standards Relevant to Elastomer use in HPHT O&G Service (continued)

| STANDARD NUMBER | STANDARD DESCRIPTION | SUMMARY OF STANDARD | CROSS REFERENCES |
|---|---|---|---|
| **API STD 53 (American Petroleum Institute, 2012)** | Blowout Prevention Equipment Systems for Drilling Wells | This standard specifies that elastomeric seal compatibility with HPHT conditions requires special consideration.<br>Both a low and high pressure test must be carried out on all BOP components exposed to well pressure according to Table 3 in Section 6.5.3.7 in standard (see Appendix B).<br>Compatibility of elastomeric seals with drilling and completion fluids shall be addressed by manufacturers.<br>Manufacturers shall provide guidelines for frequency of inspection/renewal and acceptance criteria for elastomeric materials.<br>After exposure under pressure to H2S and/or CO2 elastomeric seals shall be replaced per the manufacturer's requirements.<br>Section 5.2.10 of standard states that some nitrile elastomeric components may be suitable for H2S service when drilling fluids are properly treated. It should be noted that service life decreases as temperature increases from 150°F to 200°F. If flowline temperatures exceed 200°F, equipment manufacturer shall be consulted.<br>If BOP is activated and shut in for an emergency events during a sour well drilling operation, rubber elements must be inspected, tested, or replaced according to the equipment owner's PM program.<br>Proper storage of elastomeric materials shall be defined by manufacturer.<br>If well control equipment has been out of service for 6 months or longer, standard states consideration must be given to the replacement of critical BOP elastomer components. | |
| **NORSOK 710 (CDI Energy Products, 2014)** | Qualification of non-metallic materials and manufacturers – Polymers | NORSOK 710 refers to requirements in ISO 23936-2 for elastomers.<br>This standard describes methodology for establishing long term chemical compatibility for elastomers using accelerated aging testing.<br>Conditions for accelerated age testing of elastomers is specified; three different elevated temperatures above the anticipated service temperature are required to be tested.<br>Changes in elastomer volume (+5%, -1%) and tensile strength (+/- 50%) is specified, although a manufacturer can adjust these standards as required. A visual inspection also must occur (Section 8.2.2). | ISO 23936-2 |

## Table A.1-1: Summary of Reviewed Standards Relevant to Elastomer use in HPHT O&G Service (continued)

| STANDARD NUMBER | STANDARD DESCRIPTION | SUMMARY OF STANDARD | CROSS REFERENCES |
|---|---|---|---|
| | | Recommended liquid and gas phase compositions for accelerated aging testing are provided for both sweet and sour wells, although compositions may be altered as long as they are agreed upon between interested parties. | |
| **NACE TM0187 (NACE TM0187, 2001)** | Evaluating Elastomeric Materials in Sour Gas Environments | Guidelines are provided for accelerated aging of elastomers in sour gas environments.<br>Compositions of the fluids used in testing is provided as part of the standard.<br>Three temperatures are given for the testing (212°F, 302°F, and 347°F); one of which is to be selected for testing (Section 5.1).<br>Ambient temperature-based pressures of 1,000 ± 100 psig are specified for testing (Section 5.2)<br>The test duration shall be approximately 160 hours (Section 5.3).<br>The standard provides specifications for test coupon criteria.<br>Mass and volume changes of the elastomer are recorded after exposure testing. Tensile properties, compression set changes, and changes in hardness are evaluated pre and post exposure. | |
| **NACE TM0296 (NACE TM0296, 2014)** | Evaluating Elastomeric Materials in Sour Liquid Environments | This standard provides a test procedure to measure the resistance of elastomeric materials to sour liquid environments through the determination of compression set and changes in mass, volume, tensile properties, and hardness.<br>Gases used in testing (H2S, CO2, CH4) shall be reagent or chemically pure grade.<br>Test temperature shall be agreed upon prior to testing by all parties involved. The standard test temperatures are 212, 250, 302, and 347 ± 5°F (Section 5.1).<br>The final test pressure shall be 1,000 ±100 psig (Section 5.2).<br>Standard exposure period is stated as 160 ±2 hours (Section 5.3).<br>Requirements for test specimen and vessels are stated. | |
| **NACE TM0297 (NACE, 2008)** | Effects of High-Temperature, High-Pressure Carbon Dioxide | This standard provides test procedures to measure the effect of rapid depressurization in dry CO2 environments from temperatures greater than 122°F on elastomeric materials. The test determines changes in visual | |

## Table A.1-1: Summary of Reviewed Standards Relevant to Elastomer use in HPHT O&G Service (continued)

| STANDARD NUMBER | STANDARD DESCRIPTION | SUMMARY OF STANDARD | CROSS REFERENCES |
|---|---|---|---|
| | Decompression of Elastomeric Materials | appearance, tensile properties, tensile strength, ultimate elongations, cross-sectional diameter, and durometer hardness.<br>Testing requires the use of standard industrial-grade CO2.<br>Testing shall be performed at a temperature of 122, 212, 302, 347, or 446 ± 5°F (Section 4.1) and a pressure of 1,000, 2,500, 4,000, 5,500 ±100 psig (Section 4.2) and stated in the test report.<br>Testing duration other than 24 ±1 hour shall be agreed on by parties involved prior to testing (section 4.3).<br>Criteria for test coupons and test vessels are provided. | |

## Table A.1-1: Summary of Reviewed Standards Relevant to Elastomer use in HPHT O&G Service (continued)

| STANDARD NUMBER | STANDARD DESCRIPTION | SUMMARY OF STANDARD | CROSS REFERENCES |
|---|---|---|---|
| **MIL-G-21569 (United States DOD, 1965)** | Gaskets, Cylinder Liner Seal, Synthetic Rubber | This standard states requirements for oil resistance and high temperature resistant synthetic rubber O-rings and other forms of gaskets.<br>Physical and quality assurance requirements of rubber material used in gaskets are specified.<br>Test methods referenced for tensile strength and ultimate elongation, hardness, oven aging, hot compression set, immersion in liquids, volume changes, and compression stress relaxation.<br>Shipment and storage requirements for gaskets and O-rings are included. | FED-STD 601<br>ASTM D 1390 |
| **MIL-P-25732 (United States DOD, 1980)** | Packing, Preformed, Petroleum Hydraulic Fluid Resistant, Limited Service at 275°F | Specifications are presented for O-ring packings for use with petroleum based hydraulic fluids from temperatures of -65 - 275°F (Section 1.1).<br>The standard states requirements for qualification, materials, dimensions and tolerances, and physical properties of O-rings.<br>O-rings shall be individually packaged with required labels.<br>Quality assurance requirements for O-rings are addressed.<br>Test methods are provided for physical properties, fluid aging, corrosion and adhesion, and dynamic cycling. | |
| **MIL-PRF-1149D (United States DOD, 1998)** | Gasket Materials, Synthetic Rubber, 50 and 65 Durometer Hardness | This standard states physical and age requirements for vulcanized synthetic rubber gasket materials of nominal hardness 50 and 65 durometer hardness.<br>Inspection requirements for verification of materials are presented.<br>The standard references test methods for tensile strength and ultimate elongation, hardness, specific gravity, oven aging, hot compression set, brittleness point, extraction in distilled water, oil resistance, phosphate ester resistance, and fuel resistance. | ASTM D 412<br>ASTM D 2240<br>ASTM D 792<br>ASTM D 573<br>ASTM D 395<br>ASTM D 2137<br>ASTM D 471 |
| **SAE/ARP 5316C (SAE Aerospace, 2010)** | Storage of Elastomer Seals and Seal Assemblies Which Include an Elastomer Element Prior to Hardware Assembly | This standard confirms storage life and proper storage of elastomeric seals and seal assemblies.<br>Manufacturer will package and label elastomers according to Section 4 of this standard. | |

| | | | |
|---|---|---|---|
| | | Standard states the elastomer seals shall be stored below 100°F. If stored below 59°F, elastomer temperature must be raised to 68°F prior to installation (Section 5.1)<br>Relative humidity be such that condensation does not occur. Humidity of storage environment must be below 75% if elastomer is not stored in moisture proof bag (Section 5.2).<br>Elastomers must be protected from light when stored- individual opaque bags are recommended (Section 5.3).<br>Radiation and ozone shall be avoided in storage (Sections 5.4-5.5).<br>No tensions or stresses shall impact elastomers during storage (Section 5.6).<br>Contact of elastomers with liquid, semi-solid materials, metals, dusting powder, and other elastomers shall be avoided (Sections 5.7-5.11).<br>First in-first out rotation shall be applied to elastomeric seal stock (Section 5.12).<br>Records of elastomers' physical properties (including numerical resulted of physical property tests) shall be maintained and kept in storage with the elastomer (Section 6).<br>Tables 1 and 2 in standard (see Appendix B) provide storage life of elastomers. After storage life has been exceeded, elastomers shall be discarded via internal company procedures (Sections 7-8). | |

## Table A.1-1: Summary of Reviewed Standards Relevant to Elastomer use in HPHT O&G Service (continued)

| STANDARD NUMBER | STANDARD DESCRIPTION | SUMMARY OF STANDARD | CROSS REFERENCES |
|---|---|---|---|
| **ASTM D471-12a (ASTM)** | Standard Test Method for Rubber Property— Effects of Liquids | This standard provides test methods for evaluating the relative ability of vulcanized rubber to withstand the effect of liquids.<br>Includes procedures for measuring change in mass after immersion, measuring change in volume after immersion, use of dimensional-change method for water-insoluble liquids and mixed liquids, change in mass with liquid on surface only, determining mass of soluble matter extracted by the liquid, change in tensile strength, elongation and hardness after immersion, change in breaking resistance, burst strength, tear strength and adhesions for coated fabrics.<br>Table 3 in Section 5.1 in the standard (See Appendix B) presents test temperatures and immersions periods ranging from -103 - 482°F and 22 - 4990 h respectively.<br>This standard states requirements for testing apparatus and that test specimens shall be prepared according to ASTM D3182 and D3183. | ASTM D3182<br>ASTM D3183 |
| **ASTM D573-04 (ASTM D573-04, 2010)** | Standard Test Method for Rubber—Deterioration in an Air Oven | This standard provides a test procedure for determining the influence of elevated temperature on the physical properties of vulcanized rubber.<br>Standard states requirements for testing apparatus and for preparing test specimens.<br>Test method for accelerated aging can be carried out at any elevated standard temperature from Practice D1349 (range -103 - 482°F).<br>Determination of physical properties after accelerated aging shall conform to Test Methods D412.<br>The standard states how to express results of the tests. | ASTM D1349<br>ASTM D412 |
| **ASTM D430-06 (ASTM, 2012)** | Standard Test Methods for Rubber Deterioration – Dynamic Fatigue | This standard describes three methodologies for determining dynamic fatigue of soft rubber materials. Dynamic Fatigue is deterioration of a material as the result of repeated deformation due to extension, compression, or bending forces or any combination thereof. The deformation causes weakening of the material until either surface cracking or rupture occurs.<br>The two types of fatigue failures described in the standard are as follows: Type I seeks to produce separation of rubber and fabric in a composite specimen and is not applicable to this work. Type II seeks to produce cracking on the surface of specimens. | |

| STANDARD NUMBER | STANDARD DESCRIPTION | SUMMARY OF STANDARD | CROSS REFERENCES |
|---|---|---|---|
| | | For Type II testing, two test methodologies apply: Method B – DeMattia Flexing Machine (Type II testing only) and Method C – E. I. DuPont de Nemours and Co. Flexing Machine (either Type I or II testing)<br>Both test methods require a controlled environment during testing and conditioning of specimens prior to testing.<br>Testing shall be performed in a Standard Laboratory Atmosphere [73.4 ± 3.6°F], conditions other than this are acceptable and shall be reported (Section 7).<br>Specimens shall be brought to the specified conditions for no less than 12 hours prior to testing.<br>METHOD B: DeMattia Flexing Machine<br>This method may be used to test for resistance to cracking produced by either extension or bending.<br>METHOD C: E.I. DuPont De Nemours and Co. Flexing Machine<br>Grade from 0-10 assigned based on cracking results (Table 1 in standard, see Appendix B). | |

## Table A.1-1: Summary of Reviewed Standards Relevant to Elastomer use in HPHT O&G Service (continued)

| STANDARD NUMBER | STANDARD DESCRIPTION | SUMMARY OF STANDARD | CROSS REFERENCES |
|---|---|---|---|
| **ASTM D575-91 (ASTM, 2012)** | Standard Test Methods for Rubber Properties in Compression | This standard describes two methods of measuring compression stiffness through compression-deflection of rubber compounds. Compression-deflection is the change in thickness of a specimen upon the application of a compressive force.<br>The two methods described are:<br>Method A, Compression Test of Specified Deflection – Measuring the force required to cause a specific deflection.<br>Method B, Compression Test at Specified Force – Measuring the deflection that results from the application of a specified mass or compressive force.<br>Both test methods require a controlled environment during testing and conditioning of specimens prior to testing (Section 8).<br>Testing shall be performed at Standard Laboratory Atmosphere [73.4 ± 3.6°F].<br>Specimens shall be conditioned at the specified conditions for no less than 3 hours prior to testing.<br>Specimens that are affected by atmospheric moisture shall be conditioned at 50 ± 6% relative humidity for a minimum of 24 hours prior to testing.<br>METHOD A: Compression Test at Specified Deflection<br>Compressive forces are applied and removed in three successive cycles with the first two cycles intended as conditioning for the specimen and the third as the test cycle.<br>METHOD B: Compression Test at Specified Force<br>This test is intended for rapid testing with reasonable accuracy, therefore a single force application cycle is used. | |

## Table A.1-1: Summary of Reviewed Standards Relevant to Elastomer use in HPHT O&G Service (continued)

| STANDARD NUMBER | STANDARD DESCRIPTION | SUMMARY OF STANDARD | CROSS REFERENCES |
|---|---|---|---|
| **ASTM D945-06 (ASTM, 2012)** | Standard Test Methods for Rubber Properties in Compression or Shear (Mechanical Oscillograph) | This standard describes the test methods for use of Yerzley mechanical oscillography for measuring deformation properties of rubber vulcanizates. These properties include resilience, dynamic modulus, static modulus, kinetic energy, creep, and set under a given force. Measurements of compression and shear are described.<br>The described test is primarily, but not solely, applicable to materials with static moduli at the test temperature such that forces below 280 psi in compression or 140 psi in shear will produced 20% deformation, and having resilience such that at least three complete cycles are produced when obtaining the damped oscillatory curve.<br>An unbalanced lever applies a load to the test specimen and the resulting deflections are recorded by a chronograph, allowing for calculations of static modulus at any stage of a stepwise loading or unloading procedure. Creep and recovery rates, including set, can also be obtained. Dynamic modulus, which is a resilience index, an oscillation frequency, and a measurement of stored energy can also be determined due to the lever's positioning on a knife edge that can be impact-loaded that produces a damped free oscillation trace.<br>There are three categories of testing for either compression or shear specimens:<br>Initial creep and set under a given load<br>Yerzley resilience and hysteresis, point modulus, frequency in hertz, effective dynamic modulus, and maximum impact energy absorbed at a given test load value.<br>Stepwise loading and unloading and hysteresis loop, stresses in pascals or pounds-force per square inch at any deformation. | |

| STANDARD NUMBER | STANDARD DESCRIPTION | SUMMARY OF STANDARD | CROSS REFERENCES |
|---|---|---|---|
| **ASTM D6147-97 (ASTM, 2014)** | Standard Test Method for Vulcanized Rubber and Thermoplastic Elastomer – Determination of Force Decay (Stress Relaxation) in Compression | This standard describes two methods to determine the force decay of a material that is compressed at a constant deformation for a given time and temperature. Testing may be performed in either air or liquids.<br>Force decay (or stress relaxation) is the decrease in stress that occurs after a given time interval during the application of a constant deformation load. It is expressed as a percentage of the stress measured at the start of the time interval.<br>METHOD A (Section 8.3) is the most applicable to this work. In it a specimen is tested at a single (potentially elevated) temperature for 168 hours, however longer time periods may be used. Elevated temperatures may be selected from ASTM D1349-14.<br>Preheat the compression device and test specimen to the test temperature. Recommended specimen preheating time is 31 ± 1 minutes.<br>Apply the compression to the specimen within 30 seconds and compress by 25 ± 1%. When the final compression is reached it is fixed and maintained for the entire test period.<br>After 31 ± 1 minutes under compression, measure the counterforce exerted by the specimen with an accuracy of ±1%. Repeat the measurements at additional times over the duration of the test.<br>Counterforce measurements should be performed three times for each test specimen and the median value reported in order to account for operator variability. | ASTM D1349-14 |
| **ASTM D6546-00 (ASTM, 2010)** | Standard Test Methods for and Suggested Limits for Determining Compatibility of Elastomer Seals for Industrial Hydraulic Fluid Applications | This specification describes how to simulate the service conditions experienced by elastomer seals in industrial hydraulic fluid through a process of controlled thermal aging. The aging procedure is then followed by evaluation of property changes of the material in order to determine compatibility and anticipated service quality. Suggested properties and acceptable change limits are supplied.<br>Tests should be performed at the maximum sustained temperature anticipated during use and in the fluid with which the elastomer will come into contact during service (Section 6.1). | ASTM D 412<br>ASTM D 1414<br>ASTM D 471<br>ASTM D 2240<br>ASTM D 3677<br>ASTM E 1131<br>ASTM D 5028 |

| STANDARD NUMBER | STANDARD DESCRIPTION | SUMMARY OF STANDARD | CROSS REFERENCES |
|---|---|---|---|
| | | Recommended immersion periods (Section 6.2) are 24, 72, 100, 250, 500, and 1000 hours with the final immersion period dependent upon the performance of the material in the previous period. If the physical properties have degraded beyond acceptable limits, no further testing is required.<br>The recommended physical properties tests and corresponding ASTM methods are:<br>Tension – methods D412 and D1414<br>Compression set – methods D395 and D1414<br>Fluid aging – methods D471 and D1414<br>Hardness – method D2240<br>Compositional analysis – methods D3677 and E1131<br>Degree of cure – method D5028<br>Change in volume – procedure 10 of this method<br>Acceptable property change limits are provided in Table 1 in standard (see Appendix B). | |

| STANDARD NUMBER | STANDARD DESCRIPTION | SUMMARY OF STANDARD | CROSS REFERENCES |
|---|---|---|---|
| **ASTM D7121-05 (ASTM, 2012)** | Standard Test Method for Rubber Property – Resilience Using Schob Type Rebound Pendulum | This specification describes the determination of percentage resilience or rebound resilience of thermoset rubbers and thermoplastic elastomers at either standard laboratory atmosphere or other temperatures as agreed upon by customer and supplier.<br>The Schob Type rebound pendulum is designed to measure the percentage resilience as an indication of hysteretic energy loss as the measured rebound is inversely proportional to the hysteretic loss.<br>The test procedure requires the mechanical conditioning of the specimen by subjecting it to a minimum of three and a maximum of seven successive impacts in order to reach what is essentially a constant rebound amplitude. Once this point has been reached, the specimen is subjected to three more impacts at the same velocity and the readings are recorded. The three readings can then be converted to resilience values, expressed as a percentage, and the median values reported as the rebound resilience. | |
| **ASTM D7216-15 (ASTM)** | Standard Test Method for Determining Automotive Engine Oil Compatibility with Typical Seal Elastomers | This test method describes procedures for evaluating the compatibility of automotive engine oils with several elastomers by determining the changes in volume, Durometer A hardness, and tensile properties.<br>The procedure can be applied to elastomer formulations and test durations/temperatures other than those specified in the procedure.<br>Specific elastomer formulations of interest, test temperatures, and immersion times referenced in this standard are listed in Table 1 of the standard (see Appendix B).<br>Table A1.1 of the standard provides the formulations and initial physical properties of the elastomers for testing (see Appendix B). | |
| **ASTM D5662-14 (ASTM)** | Standard Test Method for Determining Automotive Gear Oil Compatibility with Typical Oil Seal Elastomers | This test method describes procedures for evaluating the compatibility of automotive gear oils with several elastomers by determining the changes in volume, Durometer A hardness, and percent elongation.<br>Specific elastomer formulations of interest, and test oil temperatures are referenced in this document in Table 1;Nitrile (NBR) test oil temperature: 212°F, and Fluoroelastomer (FKM) test oil temperature: 302°F (see Appendix B). | |

## Table A.1-1: Summary of Reviewed Standards Relevant to Elastomer use in HPHT O&G Service (continued)

| STANDARD NUMBER | STANDARD DESCRIPTION | SUMMARY OF STANDARD | CROSS REFERENCES |
|---|---|---|---|
| **ASTM D1349-14 (ASTM )** | Standard Practice for Rubber – Standard Conditions for Testing | This document sets forth the standard laboratory environment for testing and conditioning rubber samples in order to provide reliable comparison data between different materials and different test facilities. These conditions apply to all test methods unless specific conditions are detailed in that method or are agreed upon by customer and supplier.<br>Standard Laboratory Atmosphere: 73.4 ± 3.6°F and 50 ± 10 % relative humidity (Section 2.1.2).<br>Table 1 in Section 3og the standard provides additional test temperatures and associated tolerances with recommended temperatures ranging from -103 ± 3.6°F to 572 ± 5.4°F (see Appendix B).<br>Relative humidity requirements are given in relation to the temperature tolerance and vary from 50 ± 5% to 50 ± 15% for temperature tolerance of ± 3.6°F to ± 5.4°F respectively (section 4).<br>Test specimens should be conditioned at the standard conditions for a minimum of 12 hours prior to testing, although the conditioning time may be modified if agreed upon by customer and supplier or if a specific test method requires it (Section 5.6). | |

| STANDARD NUMBER | STANDARD DESCRIPTION | SUMMARY OF STANDARD | CROSS REFERENCES |
|---|---|---|---|
| **ASTM D2632-15 (ASTM)** | Standard Test Method for Rubber Property – Resilience by Vertical Rebound | This standard covers the determination of impact resilience by measuring the vertical rebound of a dropped object of given mass. Resilience is very sensitive to temperature changes as well as the rate and depth of penetration of the dropped object.<br>Resiliency is defined as the difference between the recovered thickness and thickness under total load, divided by the difference between the unloaded thickness and the thickness under total load; it is expressed as a percentage.<br>Testing is typically performed at the standard laboratory atmosphere (73.4 ± 3.6°F and 50 ± 10% Relative Humidity), however other conditions may be used. Test temperatures (as prescribed in ASTM D1349-14) may reach 572 ± 5.4°F (Section 8). | ASTM D1349-14 |
| **ASTM D623-07 (ASTM, 2014)** | Standard Test Method for Rubber Property – Heat Generation and Flexing Fatigue in Compression | This standard describes the methods for determining the flexing fatigue characteristics of rubber materials under dynamic compressive strains.<br>The test consists of subjecting a specimen of definite size and shape to rapidly oscillating compressive stresses under controlled conditions and measuring the temperature increase as well as the degree of permanent set or other dimensional changes at certain test conditions. The test also measures the time required for a fatigue failure.<br>The standard covers two methods, Method A – Goodrich Flexometer, and Method B – Firestone Flexometer.<br>METHOD A: Goodrich Flexometer (Sections 6-13)<br>This test requires that a definite compressive load be applied to a specimen while it is undergoing an additional high-frequency cyclic compression of given amplitude. Specimens may be tested under constant applied load or initial compression with the change in height continuously monitored during flexure. Comparing the change in height with the permanent set after testing will allow for determination of either the stiffening or softening of the material.<br>Tests may be performed under varying loads, strokes, and test temperatures. Tests conducted at 122°F and 212°F are recommended.<br>METHOD B: Firestone Flexometer (Sections 14-19) | |

| STANDARD NUMBER | STANDARD DESCRIPTION | SUMMARY OF STANDARD | CROSS REFERENCES |
|---|---|---|---|
| | | This test applies a rotary motion to one end of a test specimen which is held under a constant compressive load before determining the time required for a change in height of the test specimen.<br>The speed of oscillation of the plate is held constant at 13.3 Hz but the compressive load and magnitude of oscillation may be varied over a wide range. | |
| **ASTM D926-08 (ASTM, 2013)** | Standard Test Method for Rubber Property – Plasticity and Recovery (Parallel Plate Method) | This standard provides test methods for determining plasticity and recovery of vulcanized rubber.<br>Plasticity is the tendency of a material that has been deformed due to stress to remain deformed after that stress has been removed.<br>Recovery is the tendency of a material that has been deformed due to stress to return to its normal state after that stress has been removed. The test can be run at various temperatures. Recommended temperatures are 73.4, 104, 158, 185, and 212°F although other temperatures may be used (Section 8.2). | |
| **ASTM D2000-12 (ASTM)** | Standard Classification System for Rubber Products in Automotive Applications | This standard provides a classification systems of rubber materials from designations of types and classes in Table 4 (see Appendix B).<br>Types are based on resistance to heat aging. Test temperatures range from 158°F for Type A to 572°F for Type K.<br>Classes are based on resistance to swelling in oil.<br>The classification system contains basic requirements for physical properties determined through standard laboratory tests carried out according to the applicable ASTM test methods (See Table 5 in this report for relevant ASTM test methods).<br>Provides basic requirements for classification of elastomeric materials include durometer hardness, tensile strength, ultimate elongation, heat aged, oil immersion, and compression set. | |

## A.2 Appendix 2 – Complete Listing of Standards Evaluated for Relevancy

**Table A.2-1: General Specifications/All Materials**

| STANDARD NUMBER | MATERIAL | HARDNESS | TEMPERATURE | STANDARD DESCRIPTION |
|---|---|---|---|---|
| **ASTM D395-14** | ALL | Unspecified | Unspecified; Conditioned at 23.0 ± 2.0°C (73.4 ± 3.6°F). | Standard Test Methods for Rubber Property - Compression Set |
| **ASTM D412-06a (2013)** | ALL | Unspecified | 73.4 ± 3.6°F, unless otherwise specified | Standard Test Methods for Vulcanized Rubber and Thermoplastic Elastomers – Tension |
| **ASTM D2137-11** | ALL | Unspecified | Conditioned at 23.0 ± 2.0°C (73.4 ± 3.6°F).<br>Method A: Dipping in methanol:<br>-90°C/ -130°F<br>Method C: at a specified temperature | Standard Test Methods for Rubber Property - Brittleness Point of Flexible Polymers and Coated Fabrics |
| **ASTM D2240-05 (2010)** | ALL | Unspecified | 23.0 ± 2.0°C (73.4 ± 3.6°F) | Standard Test Method for Rubber Property - Durometer Hardness |
| **MIL-G-21569** | ALL | Unspecified | 194°F ± 2°F. | Gaskets, Cylinder Liner Seal, Synthetic Rubber |
| **MIL-P-82745** | ALL | 65-75 | Testing of physical properties after aging at 212°F ± 5°F | Packing, Preformed, Hydraulic Oil Compatible, Specification For |
| **SAE AS871B** | ALL | Unspecified | Conditioned at 21 to 25°C (69.8 to 77°F) | Manufacturing and Inspection Standards for Preformed Packings (O-Rings) |
| **SAE AMS-P-83461** | ALL | Unspecified | Cured at 370°F.<br>Physical properties after aging for 70hrs. at 275°F ± 5°F and 60 days at 75°F ± 5°F.<br>Dynamic cycling: 275°F at 1500 psig | Packing, Preformed, Petroleum Hydraulic Fluid Resistant, Improved Performance At 275°F - SUPERSEDES MIL-P-83461B |
| **AMS-P-5510A** | ALL | >88 | Unspecified | O-Ring, Preformed, Straight Thread Tube Fitting Boss, Type I Hydraulic |

## Table A.2-1: General Specifications/All Materials (continued)

| STANDARD NUMBER | MATERIAL | HARDNESS | TEMPERATURE | STANDARD DESCRIPTION |
|---|---|---|---|---|
| | | | | (-65 to 160°F) - SUPERSEDES MIL-P-5510C |
| **SAE AMS2817F** | ALL | Unspecified | Unspecified | Packaging and Identification - Preformed Packings |
| **SAE ARP5316C** | ALL | Unspecified | Storage shall be below 100°F (38°C) | Storage of Elastomer Seals and Seal Assemblies Which Include an Elastomer Element Prior to Hardware Assembly |
| **AS568D** | ALL | Unspecified | Unspecified | Aerospace Size Standard for O-Rings |
| **MIL-R-3065** | ALL | Unspecified | Unspecified | SUPERSEDED BY ASTM D2000; Rubber, Fabricated Products |
| **MIL-P-83461** | ALL | Unspecified | Cured at 370°F.<br>Physical properties after aging for 70hrs. at 275°F ± 5°F and 60 days at 75°F ± 5°F.<br>Dynamic cycling: 275°F at 1500 psig | SUPERSEDED BY AMS-P-83461; Packing, Preformed, Petroleum Hydraulic Fluid Resistant, Improved Performance At 275°F |
| **MIL-P-4861** | ALL | Unspecified | Storage shall not exceed 125°F | SUPERSEDED BY SAE AMS2817; Packing, Preformed, Rubber: Packaging Of |
| **SAE J120** | ALL | Unspecified | Unspecified | CANCELLED, ASTMS LISTED AS REPLACEMENTS; Rubber Rings for Automotive Applications. Class 1 & 2 |

**Table A.2-2: NBR and HNBR*/Buna-N®**

| STANDARD NUMBER | MATERIAL | HARDNESS | TEMPERATURE | STANDARD DESCRIPTION |
|---|---|---|---|---|
| **MIL-DTL-5516D** | NBR | >88 | High-temperature: 70°C (158°F) at 1500psi (10.34Mpa).<br>Low-temperature: -54° to -57°C. (-65° to -70°F) | Packing, Preformed, Petroleum Hydraulic Fluid Resistant, 160°F |
| **MIL-PRF-6855F** | NBR | 25-85 | Standard conditions: 75±5 °F (24±3 °C). Accelerated aging, water/oil immersion: 212±2 °F (100±1 °C) for ~70hrs.<br>Cold bend: pre-soak in fuels at 158±2 °F (70±1 °C); dry, then mounted to device at -67±2 °F (-55±1 °C) in a cold Chamber. | Rubber, Synthetic, Sheets, Strips, Molded or Extruded Shapes, General Specification For – SUPERSEDES MIL-R-6855 AND AMS-R-6855 |
| **MIL-PRF-1149** | NBR | Type I= 50, Type II= 65 | Pre-test conditioning: 80 ± 9°F (27 ± 5 °C). Oven aging: 158 ± 2°F (70 ± 1.1 °C).<br>Brittleness Point: -20 ± 2°F (-29 ± 1.1 °C).<br>Extraction in water, oil and phosphate ester resistance: 212°F/ 100°C.<br>Fuel Resistance: 73.4 ± 3.6°F (23 ± 2°C). | Gasket Materials, Synthetic Rubber, 50 and 65 Durometer Hardness |
| **MIL-P-25732** | NBR | 68 minimum | Standard conditions: 75±5 °F (24±3 °C). Aging: 275°F ± 5°F.<br>Fluid Aging: 77°F ± 5°F.<br>Dynamic Cycling: 275°F at 1500 psig | Packing, Preformed, Petroleum Hydraulic Fluid Resistant, Limited Service At 275°F |
| **SAE AMS3201L** | NBR | 35-45 | Compression Set and Oil resistance: 212 ± 2°F (100 ± 1°C) for ~70hrs.<br>Dry Heat Resistance: 302 ± 5°F (150 ± 3°C) for ~70hrs.<br>Brittleness: -40 ± 1°F (-40 ± 2°C). | Butadiene Acrylonitrile (NBR) Rubber, Dry Heat Resistant, 35-45 |

## Table A.2-2: NBR and HNBR*/Buna-N® (continued)

| STANDARD NUMBER | MATERIAL | HARDNESS | TEMPERATURE | STANDARD DESCRIPTION |
|---|---|---|---|---|
| **SAE AMS3205M** | NBR | 45-55 | Oil Resistance: 158 ±2°F (70 ± 1°C) for 70 hrs. ±0.5.<br>Dry Heat Resistance, Compression Set: 212 ± 2°F (100 ± 1°C) for 70 hrs. ±0.5.<br>Brittleness: -40 ± 1°F (-40 ± 2°C).<br>Weathering: 104°F ± 2°F (40°C ± 1°C). | Synthetic Rubber, Low-Temperature Resistant, 45-55 |
| **SAE AMS3212N** | NBR | 55-65 | Aliphatic Fuel Resistance: (after drying at 158 ± 2°F / 70 ± 1°C) Fuel at 20 to 30°C (68 to 86°F).<br>Aromatic Fuel Resistance: 20 to 30°C (68 to 86°F).<br>Dry heat resistance and compression set: 212 ± 2°F (100 ± 1°C) for 70 hrs. ±0.5.<br>Brittleness: 0 ± 2°F (-18 ± 1°C) for 10 minutes ± 1. | Acrylonitrile Butadiene (NBR) Rubber, Aromatic Fuel Resistant, 55-65 |
| **SAE AMS3215M** | NBR | 65-75 | Aliphatic Fuel Resistance: (after drying at 158 ± 2°F / 70 ± 1°C) Fuel at 20 to 30°C (68 to 86°F) for 168hrs ± 0.5.<br>Dry heat resistance and compression set: 212 ± 2°F (100 ± 1°C) for 70 hrs. ±0.5.<br>Brittleness: 0 ± 2°F (-18 ± 1°C) for 10 minutes ± 1.<br>Weathering: 104 ± 2°F (40 ± 1°C) for 7days. | Acrylonitrile Butadiene (NBR) Rubber, Aromatic Fuel Resistant, 65-75 |

## Table A.2-2: NBR and HNBR*/Buna-N® (continued)

| STANDARD NUMBER | MATERIAL | HARDNESS | TEMPERATURE | STANDARD DESCRIPTION |
|---|---|---|---|---|
| **SAE AMS3227H** | NBR | 55-65 | Lubricating, processing oil, coolant resistance: 302 ± 5°F (150 ± 3°C) for 70 hrs. ±0.5.<br>Dry heat resistance: 212 ± 2°F (100 ± 1°C) for 70 hrs. ±0.5.<br>Compression set: 257 ± 4°F (125 ± 2°C) for 70 hrs. ±0.5.<br>Brittleness: -40 ± 2°F (-40 ± 0.2°C) for 5 minutes ± 0.2. | Acrylonitrile Butadiene (NBR) Rubber, Hot Oil and Coolant Resistant, Low Swell, 55-65 |
| **SAE AMS7260E** | NBR | 70-80 | Aromatic/non-aromatic fuel resistance: immersed aromatic fuel then non-aromatic at 20 to 30°C (68 to 86 °F); then dried at 70°C ± 1 (158 °F ± 2) for 48 hours ± 0.5.<br>Low-temperature flexibility: (as received) -50°C ± 1 (-58°F ± 2) at 5hrs ± 0.25; (after heat aging at 100 °C ± 1 (212°F ± 2) for 70 hrs., plus the aromatic/ non-aromatic fuel testing) -40 °C ± 1 (-40°F ± 2) at 5hrs ± 0.25.<br>Compression set: 257 ± 4°F (125 ± 2°C) for 70 hrs. ±0.5. | Rings, Butadiene-Acrylonitrile (NBR) Rubber, Molded, Fuel and Low Temperature Resistant, 70-80 |
| **SAE AMS 7270L** | NBR | 65-75 | Aromatic/non-aromatic fuel resistance: immersed aromatic fuel then non-aromatic at 20 to 30°C (68 to 86 °F); then dried at 70°C ± 1 (158 °F ± 2) for 24 hours ± 0.5.<br>Oil Resistance: 302°F ± 5 (150°C ± 3) for 70 hrs. ± 0.5<br>Dry Heat Resistance: 212 ± 2°F (100 ± 1°C) for 70 hrs. ±0.5. | Rings, Sealings, Butadiene-Acrylonitrile (NBR) Rubber, Fuel Resistant, 65-75 |

## Table A.2-2: NBR and HNBR*/Buna-N® (continued)

| STANDARD NUMBER | MATERIAL | HARDNESS | TEMPERATURE | STANDARD DESCRIPTION |
|---|---|---|---|---|
| | | | Compression set: 257 ± 4°F (125 ± 2°C) for 70 hrs. ±0.5.<br><br>Low-temperature brittleness: (after aromatic/ non-aromatic fuel testing) -40°C ± 1 (-40°F ± 2) at 5hrs ± 0.25. | |
| **SAE AMS7271J** | NBR | 60-70 | Aromatic/non-aromatic fuel resistance: immersed aromatic fuel then non-aromatic at 20 to 30 °C (68 to 86 °F); then dried at 70°C ± 1 (158°F ± 2) for 48 hours ± 0.5.<br><br>Low-temperature flexibility: (as received) -50°C ± 1 (-58 °F ± 2) at 5hrs ± 0.25; (after fuel immersion and then heat drying) -47°C ± 1 (-53°F ± 2) at 5hrs ± 0.25.<br><br>Dry Heat Resistance: 257 ± 5°F (125 ± 3°C) for 70 hrs. ±0.5<br><br>Compression set: 257 ± 4°F (125 ± 2°C) for 70 hrs. ±0.5.<br><br>Simulated Component Test: involves various oils, subjected to pressures 50, 500, and 1500psi at -67 °F ± 2 (-55°C± 1), 158 °F ± 2 (70°C ± 1), -53°F ± 2 (-47°C ± 1), 158°F ± 2 (70°C ± 1), and lastly -53 °F ± 2 (-47°C ± 1).<br><br>Wet Neckdown Test: soaked in fuel 20 to 30°C (68 to 86°F) to see swelling | Rings, Sealing, Butadiene-Acrylonitrile (NBR) Rubber, Fuel and Low Temperature Resistant, 60-70 |
| **SAE AMS7274J** | NBR | 65-75 | Lubricating Oil Resistance: 302 °F ± 5 (150°C ± 3) for 96 hrs. ± 0.5 | Rubber, Butadiene-Acrylonitrile (NBR), 65 to 75 Hardness, For |

## Table A.2-2: NBR and HNBR*/Buna-N® (continued)

| STANDARD NUMBER | MATERIAL | HARDNESS | TEMPERATURE | STANDARD DESCRIPTION |
|---|---|---|---|---|
| | | | Processing Oil Resistance: 302 °F ± 5 (150°C ± 3) for 70 hrs. ± 0.5<br>Dry Heat Resistance: 212 ± 2°F (100 ± 1°C) for 70 hrs. ±0.5.<br>Compression set: 257 ± 4°F (125 ± 2°C) for 70 hrs. ±0.5.<br>Low-temperature flexibility (after aging in lubricating oil) -40 °C ± 1 (-40 °F ± 2) at 5hrs ± 0.1. | Elastomeric Seals in Aircraft Engine Oil Systems |
| **SAE AS3578** | NBR | Unspecified | Unspecified | Packing, Preformed - O-Ring Seal, Type AMS7271 |
| **AMS-P-5315 (MIL-P-5315)** | NBR | 60-70 | Low-temperature flexibility (after aging in lubricating oil) -54°C ± 1 (-65 °F ± 2) for 70 hrs.<br>Fuel resistance: 158 °F ± 2 (70°C ± 1) | Acrylonitrile-Butadiene (NBR) Rubber For Fuel-Resistant Seals 60-70 – SUPERSEDES MIL-P-5315 |
| **AMS 7362A (MIL-R-7362)** | NBR | 65-75 | Compression set: 257 ± 2°F (125 ± 1°C) for 70hrs.<br>Oil resistance: 257 ± 2°F (125 ± 1°C) for 70hrs. | Nitrile Rubber, Synthetic, Solid, Sheet, Strip and Fabricated Parts, Synthetic Oil Resistant – SUPERSEDES MIL-R-7362 |
| **SAE AMS3217/2C** | NBR | Unspecified | Press cured: 311 ± 5°F (155 ± 3°C) for 20 minutes ±0.5.<br>Synthetic lubricant immersion: 158 °F ± 5 (70°C ± 3) for 70 hrs. ±0.5. | Standard Elastomer Stocks; Test Slabs, Acrylonitrile Butadiene (NBR), Low Acrylonitrile |

## Table A.2-2: NBR and HNBR*/Buna-N® (continued)

| STANDARD NUMBER | MATERIAL | HARDNESS | TEMPERATURE | STANDARD DESCRIPTION |
|---|---|---|---|---|
| **MIL-R-6855** | NBR | 60 | Accelerating aging: 212 ± 2°F (100 ± 1°C) for 70 hrs. ±1.<br>Water immersion and oil conditioning: 212 ± 2°F (100 ± 1°C) for 70 hrs. ±1.<br>Fuel immersion: subjected to two fuels for 7 days each, then dried at 158°F ± 2 (70 °C ± 1) for 4hrs.<br>Low temperature: (after immersed fuel)-67°F ± 2 (-55°C ± 1) for 300 minutes ± 15. | SUPERSEDED BY MIL-PRF-6855 |
| **AMS-R-6855** | NBR | 60 | Unspecified | SUPERSEDED BY MIL-PRF-6855; Class 2A |

**Table A.2-3: Fluorocarbon Elastomer (FKM)/FKM®**

| STANDARD NUMBER | MATERIAL | HARDNESS | TEMPERATURE | STANDARD DESCRIPTION |
|---|---|---|---|---|
| **SAE AMS 3138D** | FKM | Unspecified | FKM coating shall be stored below 100 °F | Coating Materials, Fluorocarbon (FKM) Elastomeric |
| **DTD-5613** | FKM | Unspecified | For static purposes: -58 to 437 °F; for dynamic purposes only down to -4 °F | British Defense Standards: Elastomeric Toroidal Sealing Rings, (O-Rings) Low Compression Set Fluorocarbon Type (05.82) |
| **SAE AMS3216G** | FKM | 70-80 | Operational temperature range:<br>-20 to +400 °F | Fluorocarbon (FKM) Rubber, High-Temperature - Fluid Resistant, Low Compression Set, 70-80 |
| **SAE AMS3217/4B** | FKM | 65-75 | Unspecified | Standard Elastomer Stocks; Test Slabs, Fluoroelastomer (FKM), 65-75 |
| **SAE AMS3384** | FKM | 70-80 | Operational temperature range:<br>-40 to +400 °F | Rubber, Fluorocarbon Elastomer (FKM), 70 to 80 Hardness, Low Temperature Sealing Tg -22°F, For Elastomeric Shapes or Parts in Gas Turbine Engine Oil, Fuel and Hydraulic Systems - SUPERSEDES AMS-R-83485 TYPE II |
| **SAE AMS7259E** | FKM | 85-95 | Operational temperature range:<br>-20 to +400 °F | Rubber: Fluorocarbon (FKM), High Temperature/Fluid Resistant, Low Compression Set/85-95 Hardness, For Seals In Fuel Systems and Specific Engine Oil Systems |
| **SAE AMS7276H** | **FKM** | 70-80 | Operational temperature range: | Rubber: Fluorocarbon (FKM), High-Temperature-Fluid Resistant, Low Compression Set, For Seals in Fuel Systems and Specific Engine Oil Systems |

## Table A.2-3: Fluorocarbon Elastomer (FKM)/FKM® (continued)

| STANDARD NUMBER | MATERIAL | HARDNESS | TEMPERATURE | STANDARD DESCRIPTION |
|---|---|---|---|---|
| | | | -20 to +400 °F | |
| **SAE AMS7287** | **FKM** | 70-80 | Operational temperature range:<br>-40 to +400 °F | Fluorocarbon Elastomer (FKM), High Temperature/HTS Oil Resistant/Fuel Resistant, Low Compression Set/70 to 80 Hardness, Low Temperature Tg -22°F, For Seals in Oil/Fuel/Specific Hydraulic Systems - SUPERSEDES AMS-R-83485 Type I for Compression Seals |
| **AMS-R-83485 (MIL-P-83485)** | FKM | Unspecified | Operational temperature range:<br>-40 to +400 °F | SUPERSEDED by AMS 7287 for Type I parts, compression seals; Class 1 & 2, Type 1 |
| **AMS7277C** | FKM | 70-85 | Unspecified | CANCELLED: Rings, Sealing, Synthetic Rubber Phosphate Ester Hydraulic Fluid resistant, Butyl Type 70-85 - NO REPLACEMENT LISTED |
| **AMS7278F** | FKM | 70-80 | Operational temperature range:<br>-20 to +400 °F (AMS7276) | CANCELLED, USE AMS7276 OR 7280: Rings, Sealing, Fluorocarbon Rubber High Temperature-Fluid-Resistant, 70-80 |
| **AMS7279** | FKM | 85-95 | Operational temperature range:<br>-20 to +400 °F (AMS7259E) | SUPERSEDED by AMS 7259; Rings, Sealing, Fluorocarbon Rubber High-Temperature-Fluid-Resistant 85-95 |
| **AMS7279G** | FKM | 85-95 | Unspecified | CANCELLED: Sealing, Fluorocarbon Rubber High Temperature Fluid Resistant 85-95 - NO REPLACEMENT LISTED |

**Table A.2-4: Tetrafluoroethylene-Propylene Elastomer (FEPM)/FEPM®**

| STANDARD NUMBER | MATERIAL | HARDNESS | TEMPERATURE | STANDARD DESCRIPTION |
|---|---|---|---|---|
| **SAE AMS3382C** | FEPM | Class 1: 70-80, Class 2: 85-95 | Operational temperature range: +23 to +450 °F | Tetrafluoroethylene/Propylene Rubber (FEPM), Hydraulic Fluid and Synthetic Oil Resistant, 70-80 and 85-95 |
| **SAE AMS7255D** | FEPM | 70-80 | Operational temperature range: +23 to +450 °F | Rings, Sealing, Tetrafluoroethylene/Propylene Rubber (FEPM), Hydraulic Fluid and Synthetic Oil Resistant, 70-80 |
| **SAE AMS7256B** | FEPM | 85-95 | Operational temperature range: +23 to +450 °F | Rings, Sealing, Tetrafluoroethylene/Propylene Rubber (FEPM), Hydraulic Fluid and Synthetic Oil Resistant, 85-95 |

**Table A.2-5: Perfluorocarbon Elastomer (FFKM)/FFKM®**

| STANDARD NUMBER | MATERIAL | HARDNESS | TEMPERATURE | STANDARD DESCRIPTION |
|---|---|---|---|---|
| **SAE AMS7257E** | FFKM | 70-80 | Operational temperature range:<br>+5 to 554 °F<br>Testing: 392 °F | Perfluorocarbon (FFKM), Engine Oil, Fuel and Hydraulic Fluid Resistant, 70-80 Hardness, For High Temperature Seals in Engine Oil Systems, Fuel Systems and Hydraulic Systems |

## A.3 Appendix 3 – Select tables and Figures from Referenced Standards

**Table A.3-1: Table 4 from ISO 13533 (International Organization for Standardization, 2001): Temperature Rating for Non-Metallic Sealing Materials.**

| Lower limit (first digit) | | | Upper limit (second digit) | | |
|---|---|---|---|---|---|
| Code | Temperature | | Code | Temperature | |
| | °C | (°F) | | °C | (°F) |
| A | – 26 | – 15 | A | 82 | 180 |
| B | – 18 | 0 | B | 93 | 200 |
| C | – 12 | 10 | C | 104 | 220 |
| D | – 7 | 20 | D | 121 | 250 |
| E | – 1 | 30 | E | 149 | 300 |
| F | 4 | 40 | F | 177 | 350 |
| G | Other | Other | G | Other | Other |
| X | See note | See note | X | See note | See note |

NOTE These components may carry a temperature class of 4 °C to 82 °C (40 °F to 180 °F) without performing temperature verification testing provided they are marked as temperature class "XX".

EXAMPLE Material "EB" has a temperature rating of – 1 °C to 93 °C (30 °F to 200 °F).

**Table A.3-2: Table 1 from ISO 23936-2 (International Organization for Standardization, 2011): Required documentation for elastomer material properties**

| Properties | Documentation | Quality control tests |
|---|---|---|
| Density (ISO 2781 or ASTM D297) | D[a] | B[c] |
| Hardness (IRHD/Shore A) (ISO 48/ISO 7619-1, ASTM D2240/ ASTM D1415) | D | B |
| Tensile and elongation properties (ISO 37, ASTM D1414, ASTM D412) | D | B |
| Compression set (ISO 815-1, ASTM D395/ASTM D1414) | D | |
| Low temperature characteristics by DSC, DMA or TMA | D | |
| Tear strength (ISO 34-1:2010, Method A, ASTM D624) | D | |
| Temperature of retraction (ISO 2921) | D | |
| Ageing/RGD characteristics (Annexes A/B) | D | |
| High pressure gas permeation | DH[b] | |

[a] D: Properties to be documented for each supplier for each type of material. Nominal values with tolerances shall be given (Data Sheet).

[b] DH: As for D, but specifically when using all large components exposed to high pressure gas.

[c] B: Properties to be documented on a batch-wise basis, minimum 5 samples per test per batch with all results presented. The acceptance criteria shall be established prior to the test and based on qualification test results.

**Table A.3-3: Table A.6 from ISO 23936-2 (International Organization for Standardization, 2011): Test temperature.**

| Temperature classification | Operating minimum °C | Operating maximum °C | Elevated test temperatures °C |
|---|---|---|---|
| K | –60 | 82 | 97, 112, 127 |
| L | –46 | 82 | 97, 112, 127 |
| P | –29 | 82 | 97, 112, 127 |
| R | Room temperature | Room temperature | 36, 51, 66 |
| S | –18 | 66 | 81, 96, 111 |
| T | –18 | 82 | 97, 112, 127 |
| U | –18 | 121 | 136, 151, 166 |
| V | 2 | 121 | 136, 151, 166 |
| X | –18 | 180 | 195, 210, 225 |
| Y | –18 | 345 | Not possible |
| Non-ISO/API | 0 | 150 | 165,180,195 |
| Bespoke | As shall be agreed between interested parties | | |

**Table A.3-4: Table C.1 from ISO 23936-2 (International Organization for Standardization, 2011): Characteristics of most commonly used elastomeric materials including Four of the Elastomers (NBR, HNBR, FEPM, FKM, FFKM).**

| Elastomer type | Upper temp [a] °C | Characteristics | Selected general fluid resistance | | | | |
|---|---|---|---|---|---|---|---|
| | | | Crude oil | Alkaline | MeOH | Water | $H_2S$ |
| EPDM | 150 | Good in water and steam; poor in hydrocarbons | NO [b] | OK [c] | OK | OK | OK |
| CR | 100 | Good in water; can be used as a hose cover, good weathering properties | C [d] | NO | OK | OK | C |
| NBR | 120 | Nitrile; highly unsaturated; a good general purpose sealing material, susceptible to ageing; vary acrylonitrile content to affect low temperature performance and oil swell | OK | OK | OK | OK | NO |
| HNBR | 160 | Hydrogenated nitrile; largely saturated, improved heat ageing, chemical and weather resistance; vary acrylonitrile content to affect low temperature performance and oil swell | OK | OK | OK | OK | C |
| FKM 1 | 200 | Copolymer; most widely specified type; poor in methanol and alkaline fluids | OK | NO | NO | OK | C |
| FKM 2 | 200 | Terpolymer; high fluorine grades good in methanol | OK | NO | OK | OK | C |
| FKM 3 | 200 | Terpolmer; low $T_g$; low fluorine grades not good in methanol | OK | NO | NO | OK | C |
| FKM 5 | 200 | Pentapolymer; developed for alkaline fluid resistance; very little performance info available | OK | OK | OK | OK | C |
| FEPM | 230 | TFE/P copolymer; poor in aromatic solvents; good $H_2S$, steam and alkaline resistance; high $T_g$ | C | OK | OK | OK | OK |
| | 200 | ETP – Ethylene containing terpolymer; developed for alkaline resistance | OK | OK | OK | OK | C |
| FFKM | 220 to 315 | Thermal performance depends on crosslink chemistry; very good fluid/chemical resistance; | OK | OK | OK | OK | OK |

[a] Maximum rated temperature in air.

[b] NO: considered unsuitable for service; excessive volume swell at equilibrium: also, chemical ageing may occur.

[c] OK: considered suitable for service, in terms of volume swelling (< 20 %) and ageing.

[d] C: could be suitable for service, in terms of volume swelling and ageing, but refer to qualifying notes: also, fluid contact may not be relevant.

NOTE 1 OK covers a range of performance, e.g. FKM crude oil resistance is better than that of NBR/HNBR, although nitrile are usually considered as acceptable.

NOTE 2 Service situations involving CR contact with $H_2S$ are unlikely to exist.

NOTE 3 Nitriles will chemically age, NBR more readily than HNBR, in contact with $H_2S$; temperature and concentration factors apply.

NOTE 4 Methanol is 100 % (neat); dilution with water will make methanol less aggressive.

NOTE 5 FKM 5 has better resistance than FKM 1-3. As some fluids may degrade this elastomer type testing is recommended.

NOTE 6 FKM cure important; generally, peroxide cure gives better chemical resistance than bisphenol cure chemistry.

**Table A.3-5: Table F.2 from ISO 10423 (International Organization for Standardization, 2005): Standard test fluids for non-metallic seals.**

| Material class | Hydrocarbon liquid phase | Gas phase |
|---|---|---|
| AA/BB | [a] | 5 % vol. fraction $CO_2$/95 % vol. fraction $CH_4$ |
| CC | [a] | 80 % vol. fraction $CO_2$/20 % vol. fraction $CH_4$ |
| DD/EE | [a] | 10 % vol. fraction $H_2S$/5 % vol. fraction $CO_2$/85 % vol. fraction $CH_4$ |
| FF/HH | [a] | 10 % vol. fraction $H_2S$/80 % vol. fraction $CO_2$/10 % vol. fraction $CH_4$ |
| Water shall be added to the liquid phase. | | |
| [a] Hydrocarbon liquid phase is selected at the manufacturer's discretion, which may include, but is not limited to, jet fuel, diesel, kerosene, etc. | | |

**Table A.3-6: Table 3 from ISO 13628-4 (ISO 13628-4, 2011): Minimum Validation Test Requirements.**

| Component | Pressure/load cycling test | Temperature cycling test[a] | Endurance cycling test (total cumulative cycles) |
|---|---|---|---|
| Metal seal exposed to well bore in production | 200 | 3 | PMR[c] |
| Metal seal not exposed to well bore in production | 3 | 3 | PMR[c] |
| Non-metallic seal exposed to well bore in production | 200 | 3 | PMR[c] |
| Non-metallic seal not exposed to well bore in production | 3 | 3 | PMR[c] |
| OEC | 200 | NA | PMR[c] |
| Wellhead/tree/tubing head connectors | 3 | NA | PMR[c] |
| Workover/intervention connectors | 3 | NA | 100 |
| Tubing heads | 3 | NA | NA |
| Valves[b] | 200 | 3 | 600 |
| Valve actuators | 200 | 3 | 600 |
| Tree cap connectors | 3 | NA | PMR[c] |
| Flowline connectors | 200 | NA | PMR[c] |
| Subsea chokes | 200 | 3 | 500 |
| Subsea choke actuators | 200 | 3 | 1 000[e] |
| Subsea wellhead casing hangers | 3 | NA | NA |
| Subsea wellhead annulus seal assemblies (including emergency seal assemblies) | 3 | 3 | NA |
| Subsea tubing hangers, HXT internal tree caps and crown plugs | 3 | NA | NA |
| Poppets, sliding sleeves, and check valves | 200 | 3 | PMR[c] |
| Mudline tubing heads | 3 | NA | NA |
| Mudline wellhead, casing hangers, tubing hangers | 3 | NA | NA |
| Running tools[d] | 3 | NA | PMR[c] |

NOTE Pressure cycles, temperature cycles and endurance cycles are run as specified above in a cumulative test with one product without changing seals or components.

[a] Temperature cycles shall be in accordance with ISO 10423.

[b] Before and after the pressure cycle test a low-pressure, 2 MPa (300 psi) ± 10 %, leak-tightness test shall be performed.

[c] PMR signifies "per manufacturer rating".

[d] Subsea wellhead running tools are not included.

[e] A choke-actuator cycle is defined as total choke stroke from full-open to full-close or full-close to full-open.

**Table A.3-7: Table 3 from API STD 53 (American Petroleum Institute, 2012): Pressure Test, Surface BOP Systems, Subsequent Tests.**

| Component to Be Tested | Pressure Test—Low Pressure [a] psi (MPa) | Pressure Test—High Pressure [b c] psi (MPa) |
|---|---|---|
| Annular preventer | 250 to 350 (1.72 to 2.41) | Minimum of MASP for the hole section or 70 % of annular RWP, whichever is lower. |
| Ram preventers | | |
| Fixed pipe | 250 to 350 (1.72 to 2.41) | MASP of the hole section. |
| Variable bore | | |
| Blind/blind shear | | |
| Casing rams (prior to running casing) | | |
| Choke and kill lines and valves | | |
| Choke manifold | | |
| Upstream of choke(s) | 250 to 350 (1.72 to 2.41) | Same as the ram preventer. |
| Downstream of choke(s) | 250 to 350 (1.72 to 2.41) | RWP of choke(s) outlet, valve(s), or line(s), whichever is lower. |
| Adjustable chokes | Function test only. | Verification of backup control system. |
| BOP control system | | |
| Manifold and BOP lines | Function test in accordance with equipment owner's PM program. | In accordance with equipment owner's PM program. |
| Accumulator pressure | Function test in accordance with equipment owner's PM program. | |
| Close time | Verify functionality of backup systems. | |
| Pump capability | | |
| Control stations | | |
| Safety valves | | |
| Kelly, kelly valves, and safety valves | 250 to 350 (1.72 to 2.41) | MASP of the hole section. |
| Auxiliary equipment | | |
| Poor boy degasser/MGS [d] | Optional flow test. | N/A |
| Trip tank, flo-show, etc. | Visual and manual verification. | Daily. |

[a] The low-pressure test shall be stabilized for at least 5 minutes with no visible leaks. Flow-type test shall be of sufficient duration to observe for significant leaks.

[b] The high-pressure test shall be stabilized for at least 5 minutes with no visible leaks.

[c] Well control equipment may have a higher rated working pressure than required for the well site. The site-specific test requirements shall be used for these situations.

[d] The MGS requires a one-time hydrostatic test during manufacturing or upon installation. Subsequent welding on the MGS vessel shall require an additional hydrostatic test to be performed.

**Table A.3-8: Table 1 from ARP 5316C (SAE Aerospace, 2010): Aerospace material specifications for Two of the Elastomers (NBR, FKM).**

| Specification | Title | Polymer | Maximum Storage Life (Years) |
|---|---|---|---|
| AMS3200 | Butadiene-Acrylonitrile (NBR) Rubber Petroleum-Base Hydraulic Fluid Resistant (55-65) | NBR | 15 |
| AMS3201 | Butadiene Acrylonitrile (NBR) Rubber, Dry Heat Resistant, 35-45 | NBR | 15 |
| AMS3202 | Butadiene-Acrylonitrile (NBR) Rubber Dry Heat Resistant (55-65) | NBR | 15 |
| AMS3205 | Synthetic Rubber Low-Temperature Resistant, 45-55 | CR | 15 |
| AMS3208 | Chloroprene (CR) Rubber, Weather Resistant, 45-55 | CR | 15 |
| AMS3209 | Chloroprene Rubber, Weather Resistant (65-75) | CR | 15 |
| AMS3210 | Chloroprene Rubber, Electrical Resistant (65-75) | CR | 15 |
| AMS3212 | Acrylonitrile Butadiene (NBR) Rubber Aromatic Fuel Resistant (55-65) | NBR | 15 |
| AMS3213 | Acrylonitrile Butadiene (NBR) Rubber Aromatic Fuel Resistant (75-85) | NBR | 15 |
| AMS3214 | Acrylonitrile Butadiene (NBR) Rubber, Aromatic Fuel Resistant, 35-45 | NBR | 15 |
| AMS3215 | Acrylonitrile Butadiene (NBR) Rubber Aromatic Fuel Resistant (65-75) | NBR | 15 |
| AMS3216 | Fluorocarbon (FKM) Rubber, High Temperature - Fluid Resistant Low Compression Set (70-80) | FKM | Unlimited |
| AMS3218 | Fluorocarbon (FKM) Rubber, High Temperature - Fluid Resistant Low Compression Set (85-95) | FKM | Unlimited |
| AMS3220 | Rubber, Synthetic General Purpose, Fluid Resistant, 55-65 | NBR | 15 |
| AMS3227 | Acrylonitrile Butadiene (NBR) Rubber, Hot Oil and Coolant Resistant, Low Swell (55-65) | NBR | 15 |
| AMS3228 (CANCELLED) | Acrylonitrile Butadiene (NBR) Rubber, Hot Oil and Coolant Resistant, Low Swell (65-75) | NBR | 15 |
| AMS3229 (NONCURRENT) | Acrylonitrile Butadiene (NBR) Rubber, Hot Oil and Coolant Resistant, Low Swell (75-85) | NBR | 15 |
| AMS3237 | Butyl (IIR) Rubber, Phosphate Ester Resistant, 35-45 | IIR | Unlimited |
| AMS3238 | Butyl (IIR) Rubber, Phosphate Ester Resistant (65-75) | IIR | Unlimited |
| AMS3239 | Butyl (IIR) Rubber, Phosphate Ester Resistant (85-95) | IIR | Unlimited |
| AMS3240 | Chloroprene (CR) Rubber, Weather Resistant, 35-45 | CR | 15 |

**Table A.3-8 (cont'd): Table 1 continued from ARP 5316C (SAE Aerospace, 2010): Aerospace material specifications for Four of the Elastomers (NBR, FEPM, FKM, FFKM).**

| Specification | Title | Polymer | Maximum Storage Life (Years) |
|---|---|---|---|
| AMS3346 | Silicone Rubber - 1000 psi (55-65) | Q | Unlimited |
| AMS3347 | Silicone Rubber - 1200 psi, High Modulus (45-55) | Q | Unlimited |
| AMS3348 | Silicone (VMQ) Rubber 1150 psi (7.93 MPa) Tensile Strength, High Resiliency 25-35 | VMQ | Unlimited |
| AMS3349 | Silicone (VMQ) Rubber, 1100 psi (7.58 MPa) Tensile Strength, High Resiliency, 65-75 | VMQ | Unlimited |
| AMS3356 | Silicone (VMQ) Rubber, Lubricating Oil and Compression Set Resistant, Electrical Grade (55-65) | VMQ | Unlimited |
| AMS3357 | Rubber, Silicone (VMQ), Lubricating Oil and Compression Set Resistant, 65-75 | VMQ | Unlimited |
| AMS3382 | Tetrafluoroethylene/Propylene Rubber (FEPM) Hydraulic Fluid and Synthetic Oil Resistant 70 to 80 and 85 to 95 | FEPM | Unlimited |
| AMS7255 | Rings, Sealing, Tetrafluoroethylene/Propylene Rubber (FEPM) Hydraulic Fluid and Synthetic Oil Resistance 70 to 80 | FEPM | Unlimited |
| AMS7256 | Rings, Sealing, Tetrafluoroethylene/Propylene Rubber (FEPM) Hydraulic Fluid and Synthetic Oil Resistance 85 to 95 | FEPM | Unlimited |
| AMS7257 | Rings, Sealing, Perfluorocarbon (FFKM), Rubber, High-Temperature-Fluid Resistant (70-80) | FFKM | Unlimited |
| AMS7258 | Rings, Sealing, Acrylonitrile Butadiene (NBR) Rubber Fuel Resistant, Low Shrinkage (65-75) | NBR | 15 |
| AMS7259 | Rings, Sealing, Fluorocarbon (FKM) Rubber High-Temperature-Fluid Resistant, Very Low Compression Set (85-95) | FKM | Unlimited |
| AMS7260 | Rings, Butadiene-Acrylonitrile (NBR) Rubber, Molded Fuel and Low Temperature Resistant 70-80 | NBR | 15 |
| AMS7264 | Rings, Sealing, Silicone Rubber, High Temperature Resistant, Low Compression Set, 65-75 | Q | Unlimited |
| AMS7266 | Rings, Sealing, Fluorosilicone Rubber, General Purpose, High Temperature, Fuel and Oil Resistant 65-75 | FVMQ | Unlimited |
| AMS7267 | Rings, Sealing, Silicone (VSI) Rubber Heat Resistant, Low Compression Set (70-80) | VSI | Unlimited |
| AMS7268 | Rings, Sealing, Silicone Rubber, Low Compression Set, Non-Oil Resistant (65-75) | Q | Unlimited |
| AMS7269 | Rings, Sealing, Silicone (PVMQ) Rubber, Low Outgassing, Space and Vacuum Service (45-55) | PVMQ | Unlimited |
| AMS7270 | Rings, Sealing, Butadiene-Acrylonitrile (NBR) Rubber, Fuel Resistant (65-65) | NBR | 15 |
| AMS7271 | Rings, Sealing, Butadiene-Acrylonitrile (NBR) Rubber Fuel and Low Temperature Resistant (60-70) | NBR | 15 |
| AMS7272 | Rings, Sealing, Butadiene-Acrylonitrile (NBR) | NBR | 15 |

**Table A.3-8 (cont'd): Table 1 continued from ARP 5316C (SAE Aerospace, 2010): Aerospace material specifications for Two of the Elastomers (NBR, FKM).**

| Specification | Title | Polymer | Maximum Storage Life (Years) |
|---|---|---|---|
| | Rubber Synthetic Lubricant Resistant 67-75 | | |
| AMS7273 | Rings, Sealing, Fluorosilicone (FVMQ) Rubber, High Temperature Fuel and Oil Resistant 70-80 | FVMQ | Unlimited |
| AMS7274 | Rings, Sealing, Butadiene-Acrylonitrile (NBR) Rubber Oil Resistant (65-75) | NBR | 15 |
| AMS7276 | Rings, Sealing Fluorocarbon (FKM) Rubber High-Temperature - Fluid Resistant Very-Low Compression Set (70-80) | FKM | Unlimited |
| AMS-P-5315 | Packing, Preformed, Hydrocarbon Fuel Resistant | NBR | 15 |
| AMS-P-5510 | Packing, Preformed, Straight Thread Tube Fitting Boss, Type Hydraulic (-65° to 160°F) | NBR | 15 |
| AMS-P-5516 | Packing, Preformed, Petroleum Hydraulic Fluid Resistant, 160°F | NBR | 15 |
| AMS-P-25732 (CANCELLED S/S by MIL-P-25732) | Packaging, Preformed, Petroleum Hydraulic Fluid Resistant, Limited Service at 275°F (135°C) | NBR | 15 |
| AMS-P-83461 | Packing, Preformed, Petroleum Hydraulic Fluid Resistant, Improved Performance at 275°F (135°C) | NBR | 15 |
| AMS-R-6855 | Rubber, Synthetic, Sheets, Strips, Molded or Extruded Shapes | | |
| | Class 1 - All Grades | NBR | 15 |
| | Class 2 - All Grades | CR | 15 |
| | Class 3 - All Grades | SBR | 3 |
| | Class 4 - All Grades | CR | 15 |
| | Class 5 - All Grades | SBR | 3 |
| AMS-R-7362 | Rubber, Synthetic, Solid, Sheet, Strip and Fabricated Parts, Synthetic Oil Resistant | NBR | 15 |
| AMS-R-25988 | Rubber, Fluorosilicone Elastomer, Oil and Fuel Resistant, Sheets, Strips, Molded Parts and Extruded Shapes | FVMQ | Unlimited |
| AMS-R-83248 (CANCELLED – S/S by AMS3216,3218,7259,7276) | Rubber, Fluorocarbon Elastomer, High Temperature, Fluid, and Compression Set Resistant | FKM | Unlimited |
| AMS-R-83285 | Rubber, Ethylene-Propylene, General Purpose | EPDM | Unlimited |
| AMS-R-83412 | Rubber, Ethylene-Propylene, Hydrazine Resistant | EPDM | Unlimited |
| AMS-R-83485 | Rubber, Fluorocarbon Elastomer, Improved Performance at Low Temperature | FKM | Unlimited |
| NAS1613 | Seal Element, Packing, Preformed, Ethylene Propylene Rubber | EPDM | Unlimited |

**NOTE: Some organizations condsider "UNLIMITED" as the equivalent of 25 years.**

**Table A.3-9: Table 2 from ARP 5316C (SAE Aerospace, 2010): Military and federal specifications for Two of the Elastomers (NBR, FKM).**

| Specification | Title | Polymer | Maximum Storage Life (Years) |
|---|---|---|---|
| MIL-DTL-432 (INACTIVE) | Gaskets, Nonmetallic, Synthetic Rubber | NBR | 15 |
| MIL- DTL-81716 (INACTIVE) | Packing, Preformed, Straight Thread Tube Fitting Boss, Type II Hydraulic (Minus 65°F to Plus 275°) | NBR | 15 |
| MIL- DTL-83397 (INACTIVE) | Rubber, Polyurethane, Castable, Humidity Resistant | AU or EU | 5 |
| MIL-P-5315 (CANCELLED S/S by AMS-P-5315)) | Packing, preformed, hydrocarbon fuel resistant | NBR | 15 |
| MIL-P-5510 (CANCELLED S/S by AMS-P-5510)) | Packing, preformed, straight tube fitting boss, type 1 hydraulic (-65 deg to 160 deg F) | NBR | 15 |
| MIL-P-5516 (INACTIVE) | Packing, preformed, petroleum hydraulic fluid resistant, 160 deg F | NBR | 15 |
| MIL-P-25732 (INACTIVE) | Packing, preformed, petroleum hydraulic fluid | NBR | 15 |
| MIL- PRF-2765 | Rubber Sheet, Strip, Extruded, & Molded Shapes, Synthetic, Oil Resistant | NBR | 15 |
| MIL- PRF-6855 (~~CANCELED~~) | Rubber, Synthetic, Sheets, Strips, Molded or Extruded Shapes | | |
| | Class 1 - All Grades | NBR | 15 |
| | Class 2 - All Grades | CR | 15 |
| | Class 3 - All Grades | SBR | 3 |
| | Class 4 - All Grades | CR | 15 |
| | Class 5 - All Grades | SBR | 3 |
| MIL-R-7362 (CANCELLED S/S by AMS-R-7362) | Rubber, synthetic, solid, sheet, strip and fabricated parts, synthetic oil resistant | NBR | 15 |
| MIL- DTL-25988 () | Rubber, fluorosilicone elastomer, oil-and-fuel-resistant, sheets, strips, molded & extruded | FVMQ | Unlimited |
| MIL-R-81828 (CANCELLED) | Rubber, Chlorosulfonated Polyethylene Elastomer, Sheet & Molded Shapes, Ozone Resistant | CSM | 15 |
| MIL-R-83248 (~~INACTIVE~~)CANCELLED S/S by ams3216,3218,7259,7272) | Rubber, Fluorocarbon Elastomer, High Temperature, Fluid and Compression Set Resistant | FKM | Unlimited |
| MIL-R-83285 (CANCELLED S/S by AMS-R-83285) | Rubber, Ethylene-Propylene, General Purpose | EPDM | Unlimited |
| MIL-R-83412 (CANCELLED S/S by AMS-R-83412) | Rubber, Ethylene-propylene, Hydrazine Resistant | EPDM | Unlimited |

**Table A.3-9 (cont'd): Table 2 continued from ARP 5316C (SAE Aerospace, 2010): Military and federal specifications for Two of the Elastomers (NBR, FKM).**

| Specification | Title | Polymer | Maximum Storage Life (Years) |
|---|---|---|---|
| MIL-P-83461 (CANCELLED S/S by AMS-P-83461) | Packing, Preformed, Petroleum Hydraulic Fluid Resistant, Improved Performance at 275°F (135°C) | NBR | 15 |
| MIL-R-83485 (CANCELLED S/S by AMS-R-83485) | Rubber, fluorocarbon elastomer, improved performance at low temperatures | FKM | Unlimited |
| FED-ZZ-R-765 (CANCELLED S/S by A-A-59588) | Silicone Rubber, General Purpose | Q | Unlimited |
| A-A-59588 | RUBBER, SILICONE | Q | Unlimited |

NOTE: Some organizations condsider "UNLIMITED" as the equivalent of 25 years.

**Table A.3-10: Table 3 from ASTM D471-12a ( (ASTM): Test Temperatures and Immersion Periods.**

| Temperature in °C (°F) | | Immersion Period, h |
|---|---|---|
| −75 ± 2 (−103 ± 4) | 85 ± 2 (185 ± 4) | 22 |
| −55 ± 2 (−67 ± 4) | 100 ± 2 (212 ± 4) | 46 |
| −40 ± 2 (−40 ± 4) | 125 ± 2 (257 ± 4) | 70 |
| −25 ± 2 (−13 ± 4) | 150 ± 2 (302 ± 4) | 166 |
| −10 ± 2 (14 ± 4) | 175 ± 2 (347 ± 4) | 670 |
| 0 ± 2 (32 ± 4) | 200 ± 2 (392 ± 4) | 1006 |
| 23 ± 2 (73 ± 4) | 225 ± 2 (437 ± 4) | 2998 |
| 50 ± 2 (122 ± 4) | 250 ± 2 (482 ± 4) | 4990 |
| 70 ± 2 (158 ± 4) | | |

**Table A.3-11: Table 1 from ASTM D6546 (ASTM, 2010): Property Change Limits**

| Time, h | Maximum Volume Swell, % | Maximum Volume Shrinkage, % | Hardness Change, Shore A Points |
|---|---|---|---|
| 24 | 15 | –3 | ±7 |
| 70 | 15 | –3 | ±7 |
| 100 | 15 | –3 | ±8 |
| 250 | 15 | –4 | ±8 |
| 500 | 20 | –4 | ±10 |
| 1000 | 20 | –5 | ±10 |

| Maximum Tensile Strength Change, % | Maximum Elongation Change, % | Maximum Work Function Change, % | Maximum Compression Set, % |
|---|---|---|---|
| –20 | –20 | ±12 | . . . |
| –20 | –20 | ±12 | 20 |
| –20 | –20 | ±12 | 20 |
| –20 | –20 | ±12 | 25 |
| –25 | –25 | ±17 | 30 |
| –30 | –30 | ±20 | 35 |

**Table A.3-12: Table 1 from ASTM D 7216-15 (ASTM): Immersion Temperatures and Times for Two of the Reference Elastomers (NBR, FKM).**

| Elastomer | Immersion Test Temperature, °C | Immersion Test Time, h |
|---|---|---|
| Nitrile (NBR) | 100 ± 1 | 336.0 ± 0.5 |
| Polyacrylate (ACM) | 150 ± 1 | 336.0 ± 0.5 |
| Fluoroelastomer (FKM) | 150 ± 1 | 336.0 ± 0.5 |
| Silicone (VMQ) | 150 ± 1 | 336.0 ± 0.5 |
| VAMAC (MAC) | 150 ± 1 | 336.0 ± 0.5 |

[A] Some lubricant specifications might require immersion times other than 336 h. For times < 70 h the tolerance is ± 0.25 h and for times ≥ 70 h the tolerance is ± 0.5 h (see also 1.4).

**Table A.3-13: Table A1.1 from ASTM D 7216-15 (ASTM): Formulation Data and Typical Physical Properties for Two of the Reference Elastomer Materials (FKM, NBR) in 7.4.**

| Elastomer | Ingredients | Parts, by Mass | Durometer A Hardness,[B] Points | Tensile Strength,[C] MPa | Ultimate Elongation,[B] % | Specific Gravity[D] mg/m³ |
|---|---|---|---|---|---|---|
| Fluoroelastomer (FKM) | Rubber[E] | 100.00 | 71 | ≥13 | 270 | 1.84 |
| | Maglite D | 3.00 | | | | |
| | N-990 Carbon Black | 30.00 | | | | |
| | Calcium Hydroxide – Reagent Grade | 6.00 | | | | |
| | --- | | | | | |
| | Press Cure: 10 min @ 177 °C | | | | | |
| | Post Cure: 16 h @ 232 °C | | | | | |
| Polyacrylate (ACM) | Rubber[F] | 100.00 | 66 | 11.9 | 175 | 1.31 |
| | N-550 Carbon Black | 65.00 | | | | |
| | Stearic Acid | 1.00 | | | | |
| | Substituted diphenylamine[G] | 2.00 | | | | |
| | Processing aid[H] | 2.00 | | | | |
| | Sodium Stearate | 4.00 | | | | |
| | Quaternary ammonium compound[I] | 2.00 | | | | |
| | --- | | | | | |
| | Press cure: 12 min @ 170 °C | | | | | |
| | Post cure: None | | | | | |
| Silicone (VMQ) | Rubber[J] | | 30 to 80 | 50 to 400 | 400 to 1200 | 1.10 to 2.20 |
| | --- | | | | | |
| | Press cure: 5 min @ 188 °C | | | | | |
| | Post cure: 4 h @ 200 °C | | | | | |
| Nitrile (NBR) | Rubber[K] | 100.00 | 68 | 19.6 | 290 | 1.25 |
| | Zinc Oxide | 5.00 | | | | |
| | Stearic Acid | 2.00 | | | | |
| | Antidegradent[L] | 2.00 | | | | |
| | N-774 Carbon Black | 70.00 | | | | |
| | Polysulfide[M] | 5.00 | | | | |
| | Dicumyl peroxide[N] | 3.00 | | | | |
| | --- | | | | | |
| | Press cure: 12 min @ 170 °C | | | | | |
| | Post cure: None | | | | | |

[A] Manufacturer shall mark each elastomer sheet to designate the direction of the grain of the material.
[B] Test Method D2240.
[C] Test Method D412.
[D] Test Method D297.
[E] Viton A-275C or Fluorel FC-2123 have been found satisfactory for this purpose. (Viton is a trademark of Dupont Dow Elastomers; Fluorel is the trademark of 3M.)
[F] HyTemp 4051 EP has been found satisfactory for this purpose. (HyTemp is a trademark of Zeon Chemicals.)
[G] Naugard 445 has been found satisfactory for this purpose. (Naugard is a trademark of Uniroyal Chemical.)
[H] TE 80 has been found satisfactory for this purpose. (TE is a trademark of Technical Processing.)
[I] HyTemp NPC-50 has been found satisfactory for this purpose.
[J] Dow Corning Product ID.24122V-BLK has been found satisfactory for this purpose.
[K] Nipol DN3350 has been found to be satisfactory for this purpose. (Nipol is a trademark of Zeon Chemicals.)
[L] Stangard has been found satisfactory for this purpose. (Stangard is a trademark of Harwick Chemical.)
[M] Thiokol TP-95 has been found satisfactory for this purpose. (Thiokol is a trademark of Morton International.)
[N] Varox DCP40KE has been found satisfactory for this purpose. (Varox is a trademark of R.T. Vanderbilt.)

**Table A.3-14: Table 1 from ASTM D5662-14 (ASTM): Test oil temperatures.**

| Material | Test Oil Temperature, °C | Percent Deviation Limits |
|---|---|---|
| Nitrile | 100 ± 1 | 1% |
| Polyacrylate | 150 ± 1 | 1% |
| Fluoroelastomer | 150 ± 1 | 1% |

**Table A.3-15: Table 1 from ASTM D1349-14 (ASTM ): Test Temperatures and Tolerances.**

| Test Temperatures, °C (°F)[A] | Tolerance, plus or minus, °C (°F) |
|---|---|
| –75 (–103) | 2.0 (3.6) |
| –70 (–94) | 2.0 (3.6) |
| –55 (–67) | 2.0 (3.6) |
| –40 (–40) | 2.0 (3.6) |
| –25 (–13) | 2.0 (3.6) |
| –10 (14) | 2.0 (3.6) |
| 0 (32) | 2.0 (3.6) |
| 23 (73)[B] | 2.0 (3.6) |
| 35 (95) | 2.0 (3.6) |
| 40 (104) | 2.0 (3.6) |
| 50 (122) | 2.0 (3.6) |
| 55 (131) | 2.0 (3.6) |
| 70 (158) | 2.0 (3.6) |
| 85 (185) | 2.0 (3.6) |
| 90 (194) | 2.0 (3.6) |
| 100 (212) | 2.0 (3.6) |
| 105 (221) | 2.0 (3.6) |
| 120 (248) | 2.0 (3.6) |
| 125 (257) | 2.0 (3.6) |
| 130 (266) | 2.0 (3.6) |
| 135 (275) | 2.0 (3.6) |
| 155 (311) | 2.0 (3.6) |
| 160 (320) | 2.0 (3.6) |
| 175 (347) | 2.0 (3.6) |
| 180 (356) | 2.0 (3.6) |
| 200 (392) | 3.0 (5.4) |
| 225 (437) | 3.0 (5.4) |
| 250 (482) | 3.0 (5.4) |
| 275 (527) | 3.0 (5.4) |
| 300 (572) | 3.0 (5.4) |

[A] The test temperature is the (set point) temperature to which the testing environment is controlled (tolerance). The tolerance is the maximum allowable variation of the instrument's (chamber or room) indicated temperature during test conditions. If the indicated temperature is beyond the tolerance, immediately implement procedures to correct the problem.
[B] Standard laboratory temperature.

**Table A.3-16: Table 4 from ASTM D2000-12 (ASTM): Suffix number to indicate temperature of test.**

| Applicable Suffix Requirements | Second Suffix Number | Test Temperature, °C[A] |
|---|---|---|
| A, B, C, EA, EF, EO, G, K | 11 | 275 |
| | 10 | 250 |
| | 9 | 225 |
| | 8 | 200 |
| | 7 | 175 |
| | 6 | 150 |
| | 5 | 125 |
| | 4 | 100 |
| | 3 | 70 |
| | 2 | 38 |
| | 1 | 23 |
| | 0 | [B] |
| F | 1 | 23 |
| | 2 | 0 |
| | 3 | –10 |
| | 4 | –18 |
| | 5 | –25 |
| | 6 | –35 |
| | 7 | –40 |
| | 8 | –50 |
| | 9 | –55 |
| | 10 | –65 |
| | 11 | –75 |
| | 12 | –80 |

[A] These test temperatures are based on Practice D1349.
[B] Ambient temperature in the case of outdoor testing.

## A.4 Appendix 4 – Material Characterization Testing Report for FEA Model Input Parameters (courtesy of Endurica, LLC)

# Characterization of High Pressure / High Temperature (HPHT) Sealing Materials for Finite Element Analysis

**Endurica Project Number:** P077

**Materials**:

FEPM-80
FEPM-90
HNBR-75
HNBR-90
FFKM-75
FFKM-90
NBR-75
NBR-90
FKM-75
FKM-90

July 2017

| Experiments Conducted by: | Analysis and Reporting Prepared by: |
|---|---|
| Axel Products, Inc.<br>Industrial Highway<br>Ann Arbor, Michigan<br><br>www.axelproducts.com | Endurica LLC<br>1219 W. Main Cross St., Ste 201<br>Findlay, Ohio 45840<br><br>www.endurica.com |

# Endurica Subcontractor Report: Executive Summary

A series of High Pressure / High Temperature (HPHT) rated elastomers was characterized to provide material parameters for finite element analysis of a seal under quasi-static loading. The characterization provides information on the nonlinear stress-strain behavior, tearing behavior, and thermal behavior across a broad range of operating conditions.

The Hyperelastic module provides information needed to define the stress-strain law for Finite Element Analysis. A 3rd order Ogden hyperelastic law has been selected, and its parameters determined. The volumetric compression has been measured and a 2nd order Ogden volumetric law has been selected as well as an initial bulk modulus. Parameters for describing the Mullins effect are also provided.

The creep crack growth module provides information that indicates how quickly damage will accumulate when an elastomer is held under load. A power law was selected to fit crack growth measurements. The power law allows estimates crack growth rate vs energy release rate.

Temperature effects on the elastomers were measured. A thermal expansion test measured the expansion of materials under temperature changes. A linear coefficient of thermal expansion was fit to the data. Each experiment and module was run at multiple temperatures to measure the material properties at a range of temperatures.

# Contents

# Legal Notices



# Materials

10 materials were characterized, as follows:

| Name | Detailed Material Description |
|---|---|
| FEPM-80 | Aflas®-80 Durometer |
| FEPM-90 | Aflas®-90 Durometer |
| HNBR-75 | HNBR-75 Durometer |
| HNBR-90 | HNBR-90 Durometer |
| FFKM-75 | Kalrez®-75 Durometer |
| FFKM-90 | Kalrez®-90 Durometer |
| NBR-75 | Nitrile-75 Durometer |
| NBR-90 | Nitrile-90 Durometer |
| FKM-75 | Viton®-75 Durometer |
| FKM-90 | Viton®-90 Durometer |

# Raw Measurements

The data files containing all raw measurements are indexed in a separately provided excel spreadsheet *Data File Summary final.xlsx*, and have been separately provided in the archives named *Axel Raw Results END_16037.zip* and *Axel Raw Results END_15120.zip*. The archive files together contain 1994 individual data files.

## Tests Performed

Table A.4-1. Table of tests performed on each material and test temperature.

| Material | Temp, °C | Critical Tearing Energy | Hyper-elastic Parameters | Mullins effect | Volumetric Compression | Creep Crack Growth | Thermal Expansion |
|---|---|---|---|---|---|---|---|
| **FEPM-80** | 100 | X | X | X | X | X | X |
| **FEPM-80** | 175 | X | X | X | X | X | |
| **FEPM-90** | 100 | X | X | X | X | X | X |
| **FEPM-90** | 175 | X | X | X | X | X | |
| **HNBR-75** | 100 | X | X | X | X | X | X |
| **HNBR-90** | 100 | X | X | X | X | X | X |
| **HNBR-90** | 150 | X | X | X | X | X | |
| **FFKM-75** | 100 | X | X | X | X | X | X |
| **FFKM-75** | 175 | X | X | X | X | X | |
| **FFKM-90** | 100 | X | X | X | X | X | X |
| **FFKM-90** | 175 | X | X | X | X | X | |
| **NBR-75** | 100 | X | X | X | X | X | X |
| **NBR-90** | 100 | X | X | X | X | X | X |
| **FKM-75** | 23 | | X | X | X | | X |
| **FKM-75** | 100 | X | | | | X | |
| **FKM-75** | 175 | X | X | X | X | X | |
| **FKM-90** | 23 | | X | X | X | | X |
| **FKM-90** | 100 | X | | | | X | |
| **FKM-90** | 175 | X | X | X | X | X | |

## Summary of Material Parameters

The set of material parameters shown may be used for FEA modeling.

Table A.4-2. SI Units Material Properties – Hyperelastic Parameters.

| Material | Temp, °C | $\mu_1$, MPa | $\mu_2$, MPa | $\mu_3$, MPa | $\alpha_1$ | $\alpha_2$ | $\alpha_3$ | Young's Modulus, MPa |
|---|---|---|---|---|---|---|---|---|
| **FEPM-80** | 100 | 1.354 | 0.109 | 0.005495 | 3.151 | -3.151 | 8.559 | 1.468 |
| **FEPM-80** | 175 | 1.31 | 0.1055 | 0.005317 | 3.151 | -3.151 | 8.559 | 1.421 |
| **FEPM-90** | 100 | 1.773 | 0.1972 | 0.01231 | 1.184 | -1.184 | 11.2 | 1.983 |
| **FEPM-90** | 175 | 1.49 | 0.1657 | 0.01034 | 1.184 | -1.184 | 11.2 | 1.666 |
| **HNBR-75** | 100 | 2.007 | 0.1698 | 0.007936 | 2.339 | -2.339 | 8.023 | 2.185 |
| **HNBR-90** | 100 | 2.514 | 0.328 | 0.0132 | 2.756 | -2.756 | 9.097 | 2.855 |
| **HNBR-90** | 150 | 2.531 | 0.3302 | 0.01329 | 2.756 | -2.756 | 9.097 | 2.874 |
| **FFKM-75** | 100 | 1.79 | 0.06131 | 0.008854 | 1.431 | -1.431 | 13.66 | 1.860 |
| **FFKM-75** | 175 | 2.167 | 0.07421 | 0.01072 | 1.431 | -1.431 | 13.66 | 2.252 |
| **FFKM-90** | 100 | 1.329 | 0.6496 | 0.003826 | 3.469 | -3.469 | 13.32 | 1.982 |
| **FFKM-90** | 175 | 1.305 | 0.6375 | 0.003755 | 3.469 | -3.469 | 13.32 | 1.946 |
| **NBR-75** | 100 | 1.743 | 0.1984 | 0.000745 | 2.648 | -2.648 | 8.738 | 1.942 |
| **NBR-90** | 100 | 4.724 | 5.72E-9 | 0.008121 | 2.736 | -2.736 | 4.154 | 4.732 |
| **FKM-75** | 23 | 1.917 | 0.2228 | 0.001367 | 2.661 | -2.661 | 10.79 | 2.141 |
| **FKM-75** | 175 | 1.724 | 0.2003 | 0.001229 | 2.661 | -2.661 | 10.79 | 1.926 |
| **FKM-90** | 23 | 3.865 | 1.055 | 0.009981 | 2.38 | -2.38 | 10.31 | 4.930 |
| **FKM-90** | 175 | 3.41 | 0.9303 | 0.008805 | 2.38 | -2.38 | 10.31 | 4.349 |

Table A.4-3. SI Units Material Properties – Mullins, Volumetric Compression

| Material | Temp, °C | r | m, MPa | β | Bulk Modulus, MPa | D1, 1/MPa | D2, 1/MPa |
|---|---|---|---|---|---|---|---|
| **FEPM-80** | 100 | 2.865 | 0.24 | 0.1 | 2363 | 0.002682 | 0.001122 |
| **FEPM-80** | 175 | 3.564 | 0.1457 | 0.1 | 3141 | 0.002922 | 0.001697 |
| **FEPM-90** | 100 | 2.722 | 0.1049 | 0.1 | 2503 | 0.002386 | 0.0007123 |
| **FEPM-90** | 175 | 3.508 | 0.05697 | 3.11E-8 | 3087 | 0.002836 | 0.001628 |
| **HNBR-75** | 100 | 3.327 | 0.419 | 1.29E-7 | 2605 | 0.002215 | 0.001082 |
| **HNBR-90** | 100 | 2.851 | 0.3597 | 0.1 | 2525 | 0.002032 | 0.0008483 |
| **HNBR-90** | 150 | 3.775 | 0.3629 | 0.1 | 2224 | 0.002388 | 0.00101 |
| **FFKM-75** | 100 | 8.694 | 0.1112 | 0.1 | 1180 | 0.004156 | 0.002139 |
| **FFKM-75** | 175 | 120 | 0.00867E | 0.1 | 1251 | 0.005677 | 0.003555 |
| **FFKM-90** | 100 | 4.281 | 0.1873 | 0.1 | 1206 | 0.004404 | 0.002078 |
| **FFKM-90** | 175 | 7.949 | 0.08966 | 0.1 | 1302 | 0.005466 | 0.003177 |
| **NBR-75** | 100 | 4.596 | 0.474 | 1.37E-8 | 2325 | 0.002391 | 0.001183 |
| **NBR-90** | 100 | 7.018 | 0.1606 | 0.1 | 2764 | 0.001978 | 0.0006899 |
| **FKM-75** | 23 | 3.663 | 0.2337 | 0.1 | 2800 | 0.002033 | 0.000392 |
| **FKM-75** | 175 | 12.73 | 0.05536 | 0.1 | 1582 | 0.003336 | 0.001915 |
| **FKM-90** | 23 | 2.091 | 0.4503 | 0.01788 | 3145 | 0.001825 | 0.0002386 |
| **FKM-90** | 175 | 4.303 | 0.09003 | 0.1 | 1702 | 0.003016 | 0.001349 |

Table A.4-4. SI Units Material Properties – Creep Crack Growth Law Parameters, Critical Tearing Energy, Coefficient of Thermal Expansion.

| Material | Temp, °C | Fq | Tq, J/m2 | rq, mm/min | Tc, kJ/ m^2 | Coef Therm, 10^-6/ °C |
|---|---|---|---|---|---|---|
| **FEPM-80** | 100 | 5.59 | 409 | 0.04 | 1.811 | 244 |
| **FEPM-80** | 175 | 6.97 | 239 | 0.021 | 0.5244 | 244 |
| **FEPM-90** | 100 | 5.9 | 554 | 0.0354 | 2.625 | 203 |
| **FEPM-90** | 175 | 7.29 | 273 | 0.05 | 0.7422 | 203 |
| **HNBR-75** | 100 | 6.23 | 755 | 0.0315 | 2.314 | 201 |
| **HNBR-90** | 100 | 5.00 | 624 | 0.0316 | 2.665 | 147 |
| **HNBR-90** | 150 | 4.94 | 497 | 0.0332 | 1.399 | 147 |
| **FFKM-75** | 100 | 10.8 | 226 | 0.00968 | 0.4483 | 298 |
| **FFKM-75** | 175 | 6.45 | 102 | 0.00142 | 0.09397 | 298 |
| **FFKM-90** | 100 | 3.56 | 204 | 0.0545 | 1.021 | 430 |
| **FFKM-90** | 175 | 10.1 | 103 | 0.0374 | 0.2286 | 430 |
| **NBR-75** | 100 | 6.39 | 564 | 0.0541 | 2.056 | 176 |
| **NBR-90** | 100 | 4.45 | 276 | 0.0506 | 1.853 | 89 |
| **FKM-75** | 100 | 5.63 | 222 | 0.0362 | 0.7701 | 232 |
| **FKM-75** | 175 | 13.8 | 144 | 0.026 | 0.35 | 232 |
| **FKM-90** | 100 | 5.02 | 257 | 0.00514 | 1.091 | 185 |
| **FKM-90** | 175 | 8.26 | 155 | 0.00608 | 0.4034 | 185 |

Table A.4-5. English Units Material Properties – Hyperelastic Parameters.

| Material | Temp, °C | $\mu_1$, PSI | $\mu_2$, PSI | $\mu_3$, PSI | $\alpha_1$ | $\alpha_2$ | $\alpha_3$ | Young's Modulus, PSI |
|---|---|---|---|---|---|---|---|---|
| **FEPM-80** | 100 | 196.3 | 15.81 | 0.797 | 3.151 | -3.151 | 8.559 | 212.9 |
| **FEPM-80** | 175 | 190.0 | 15.30 | 0.771 | 3.151 | -3.151 | 8.559 | 206.0 |
| **FEPM-90** | 100 | 257.1 | 28.59 | 1.785 | 1.184 | -1.184 | 11.2 | 287.5 |
| **FEPM-90** | 175 | 216.1 | 24.03 | 1.499 | 1.184 | -1.184 | 11.2 | 241.6 |
| **HNBR-75** | 100 | 291.0 | 24.62 | 1.151 | 2.339 | -2.339 | 8.023 | 316.8 |
| **HNBR-90** | 100 | 364.5 | 47.56 | 1.914 | 2.756 | -2.756 | 9.097 | 414.0 |
| **HNBR-90** | 150 | 367.0 | 47.88 | 1.927 | 2.756 | -2.756 | 9.097 | 416.8 |
| **FFKM-75** | 100 | 259.6 | 8.89 | 1.284 | 1.431 | -1.431 | 13.66 | 269.7 |
| **FFKM-75** | 175 | 314.2 | 10.76 | 1.554 | 1.431 | -1.431 | 13.66 | 326.5 |
| **FFKM-90** | 100 | 192.7 | 94.19 | 0.555 | 3.469 | -3.469 | 13.32 | 287.5 |
| **FFKM-90** | 175 | 189.2 | 92.44 | 0.544 | 3.469 | -3.469 | 13.32 | 282.2 |
| **NBR-75** | 100 | 252.7 | 28.77 | 0.108 | 2.648 | -2.648 | 8.738 | 281.6 |
| **NBR-90** | 100 | 685.0 | 8.30E-7 | 1.178 | 2.736 | -2.736 | 4.154 | 686.2 |
| **FKM-75** | 23 | 278.0 | 32.31 | 0.198 | 2.661 | -2.661 | 10.79 | 310.5 |
| **FKM-75** | 175 | 250.0 | 29.04 | 0.178 | 2.661 | -2.661 | 10.79 | 279.2 |
| **FKM-90** | 23 | 560.4 | 152.98 | 1.447 | 2.38 | -2.38 | 10.31 | 714.8 |
| **FKM-90** | 175 | 494.5 | 134.89 | 1.277 | 2.38 | -2.38 | 10.31 | 630.6 |

Table A.4-6. English Units Material Properties – Mullins, Volumetric Compression

| Material | Temp, °C | r | m, PSI | β | Bulk Modulus, PSI | D1, 1/PSI | D2, 1/PSI |
|---|---|---|---|---|---|---|---|
| **FEPM-80** | 100 | 2.865 | 34.80 | 0.1 | 342635 | 1.850E-5 | 7.738E-6 |
| **FEPM-80** | 175 | 3.564 | 21.13 | 0.1 | 455445 | 2.015E-5 | 1.170E-5 |
| **FEPM-90** | 100 | 2.722 | 15.21 | 0.1 | 362935 | 1.646E-5 | 4.912E-6 |
| **FEPM-90** | 175 | 3.508 | 8.26 | 3.107E-8 | 447615 | 1.956E-5 | 1.123E-5 |
| **HNBR-75** | 100 | 3.327 | 60.76 | 1.291E-7 | 377725 | 1.528E-5 | 7.462E-6 |
| **HNBR-90** | 100 | 2.851 | 52.16 | 0.1 | 366125 | 1.401E-5 | 5.850E-6 |
| **HNBR-90** | 150 | 3.775 | 52.62 | 0.1 | 322480 | 1.647E-5 | 6.966E-6 |
| **FFKM-75** | 100 | 8.694 | 16.12 | 0.1 | 171100 | 2.866E-5 | 1.475E-5 |
| **FFKM-75** | 175 | 120 | 1.26 | 0.1 | 181395 | 3.915E-5 | 2.452E-5 |
| **FFKM-90** | 100 | 4.281 | 27.16 | 0.1 | 174870 | 3.037E-5 | 1.433E-5 |
| **FFKM-90** | 175 | 7.949 | 13.00 | 0.1 | 188790 | 3.770E-5 | 2.191E-5 |
| **NBR-75** | 100 | 4.596 | 68.73 | 1.366E-8 | 337125 | 1.649E-5 | 8.159E-6 |
| **NBR-90** | 100 | 7.018 | 23.29 | 0.1 | 400780 | 1.364E-5 | 4.758E-6 |
| **FKM-75** | 23 | 3.663 | 33.89 | 0.1 | 406000 | 1.402E-5 | 2.703E-6 |
| **FKM-75** | 175 | 12.73 | 8.03 | 0.1 | 229390 | 2.301E-5 | 1.321E-5 |
| **FKM-90** | 23 | 2.091 | 65.29 | 0.01788 | 456025 | 1.259E-5 | 1.646E-6 |
| **FKM-90** | 175 | 4.303 | 13.05 | 0.1 | 246790 | 2.080E-5 | 9.303E-6 |

Table A.4-7. English Units Material Properties – Creep Crack Growth Law Parameters, Critical Tearing Energy, Coefficient of Thermal Expansion.

| Material | Temp, °C | Fq | Tq, in*lbf/in$^2$ | rq, in/min | Tc, in*lbf/in$^2$ | Coef Therm, 10^-6/ °F |
|---|---|---|---|---|---|---|
| **FEPM-80** | 100 | 5.59 | 2.335 | 0.001575 | 10.341 | 136 |
| **FEPM-80** | 175 | 6.97 | 1.365 | 0.000827 | 2.994 | 136 |
| **FEPM-90** | 100 | 5.9 | 3.163 | 0.001394 | 14.989 | 113 |
| **FEPM-90** | 175 | 7.29 | 1.559 | 0.001969 | 4.238 | 113 |
| **HNBR-75** | 100 | 6.23 | 4.311 | 0.001240 | 13.213 | 112 |
| **HNBR-90** | 100 | 5 | 3.563 | 0.001244 | 15.217 | 82 |
| **HNBR-90** | 150 | 4.94 | 2.838 | 0.001307 | 7.988 | 82 |
| **FFKM-75** | 100 | 10.8 | 1.290 | 0.000381 | 2.560 | 166 |
| **FFKM-75** | 175 | 6.45 | 0.582 | 0.000056 | 0.537 | 166 |
| **FFKM-90** | 100 | 3.56 | 1.165 | 0.002146 | 5.830 | 239 |
| **FFKM-90** | 175 | 10.1 | 0.588 | 0.001472 | 1.305 | 239 |
| **NBR-75** | 100 | 6.39 | 3.220 | 0.002130 | 11.740 | 98 |
| **NBR-90** | 100 | 4.45 | 1.576 | 0.001992 | 10.581 | 49 |
| **FKM-75** | 100 | 5.63 | 1.268 | 0.001425 | 4.397 | 129 |
| **FKM-75** | 175 | 13.8 | 0.822 | 0.001024 | 1.999 | 129 |
| **FKM-90** | 100 | 5.02 | 1.467 | 0.000202 | 6.230 | 103 |
| **FKM-90** | 175 | 8.26 | 0.885 | 0.000239 | 2.303 | 103 |

# Base Characterization

## *Experiment 1: Critical Tearing Energy*

Purpose: Identify tearing energy that causes catastrophic crack growth in single loading.

Specimen: Planar Tension with initial cut. 150 mm x 10 mm x 1 mm.
Initial Cut: 25 mm, inserted via razor blade.
Strain Rate: 1% / sec.
Ambient temperatures: 100, 150, 175°C

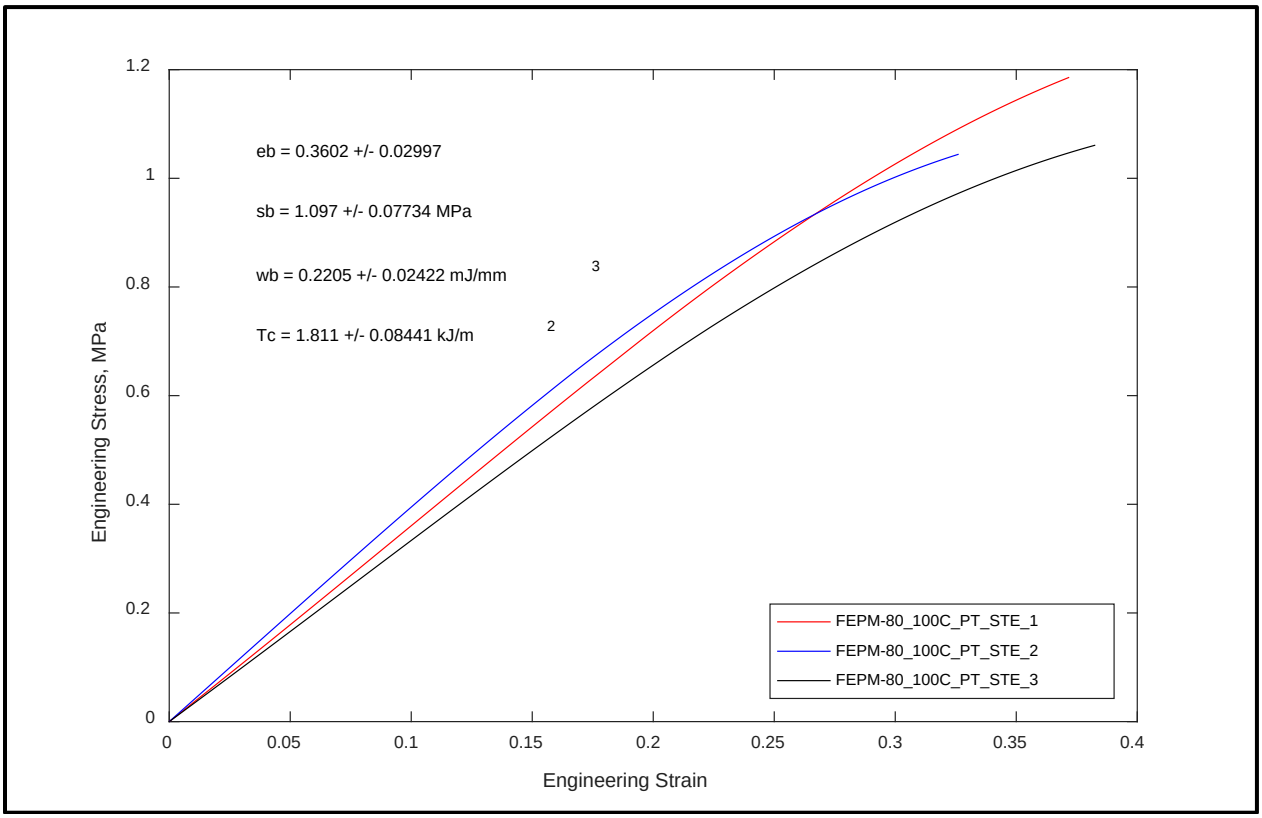

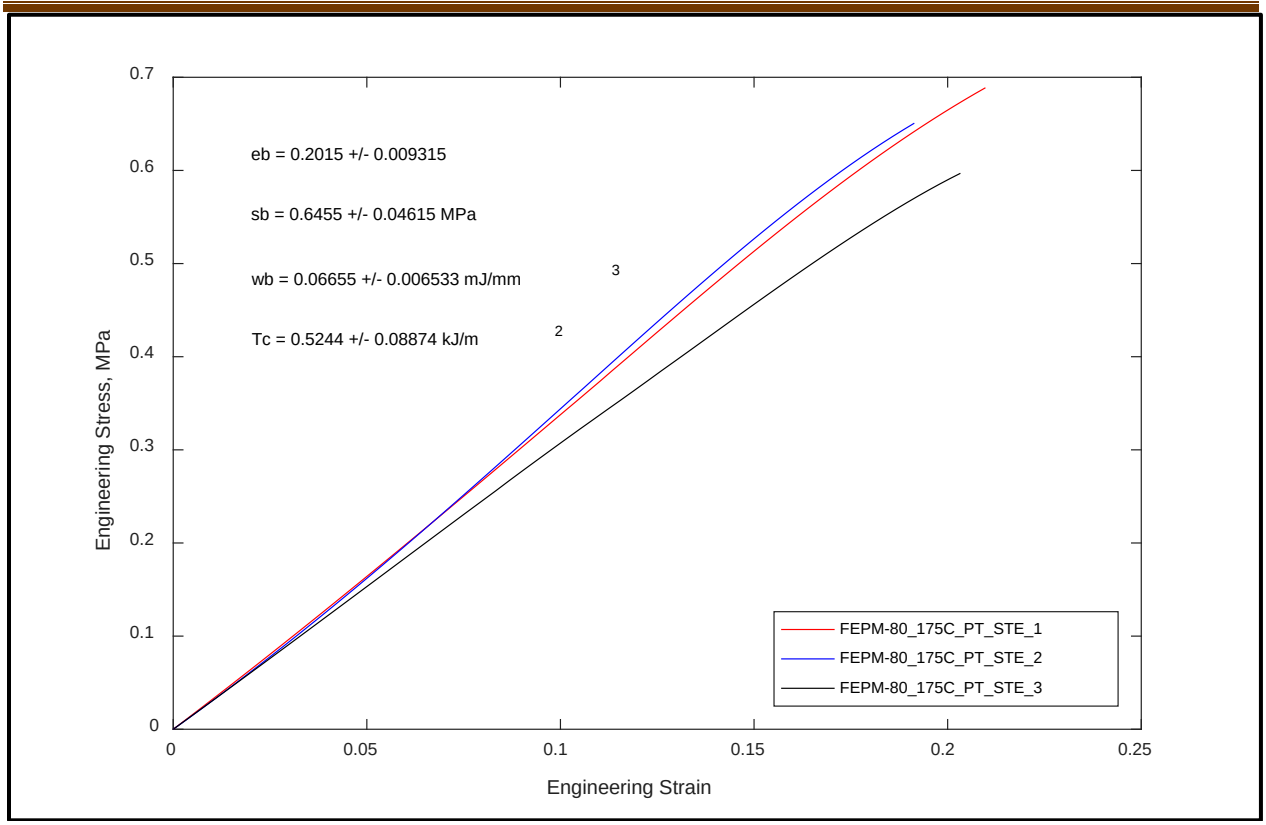
eb = 0.2015 +/- 0.009315
sb = 0.6455 +/- 0.04615 MPa
wb = 0.06655 +/- 0.006533 mJ/mm
Tc = 0.5244 +/- 0.08874 kJ/m
3
2
FEPM-80_175C_PT_STE_1
FEPM-80_175C_PT_STE_2
FEPM-80_175C_PT_STE_3
Engineering Stress, MPa
Engineering Strain
0
0.1
0.2
0.3
0.4
0.5
0.6
0.7
0.05
0.15
0.25

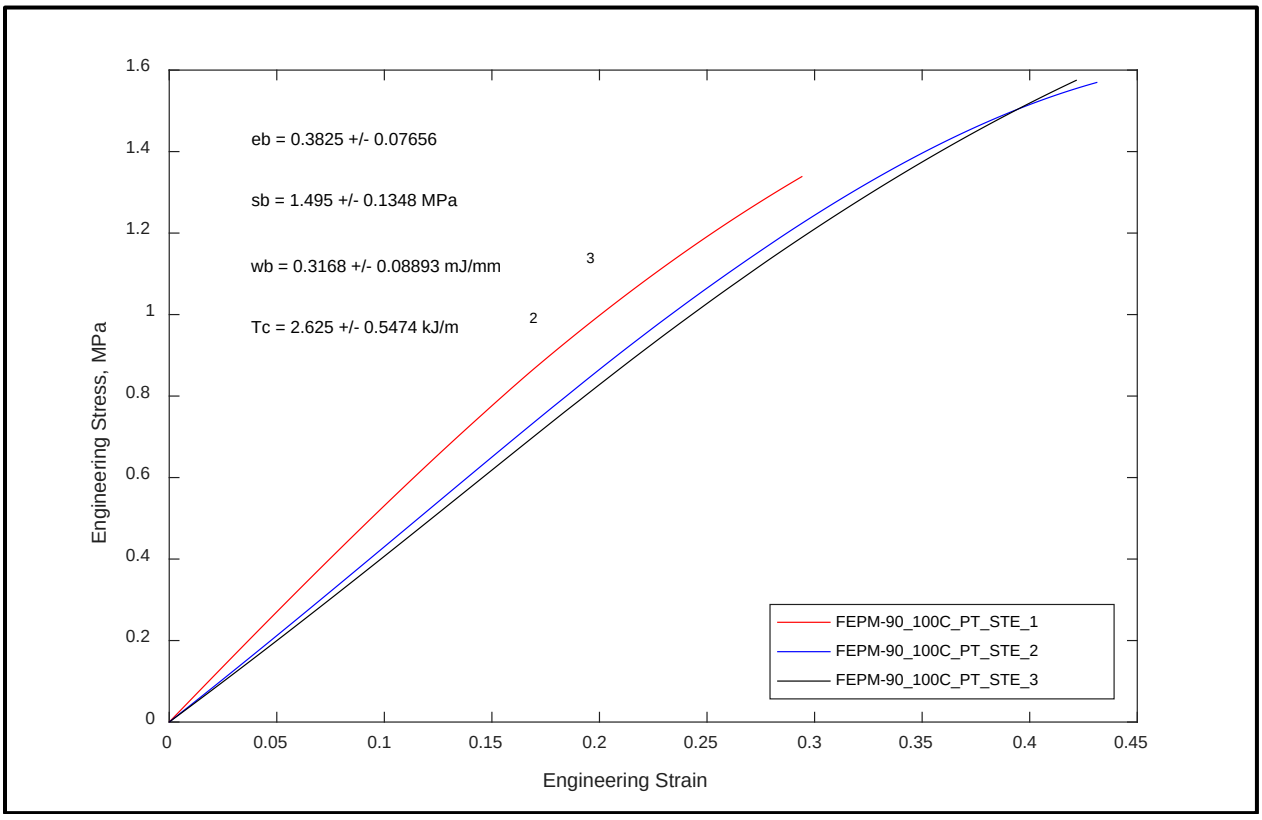
eb = 0.3825 +/- 0.07656
sb = 1.495 +/- 0.1348 MPa
wb = 0.3168 +/- 0.08893 mJ/mm
Tc = 2.625 +/- 0.5474 kJ/m
3
2
FEPM-90_100C_PT_STE_1
FEPM-90_100C_PT_STE_2
FEPM-90_100C_PT_STE_3
Engineering Stress, MPa
Engineering Strain
0
0.2
0.4
0.6
0.8
1
1.2
1.4
1.6
0.05
0.1
0.15
0.2
0.25
0.3
0.35
0.4
0.45

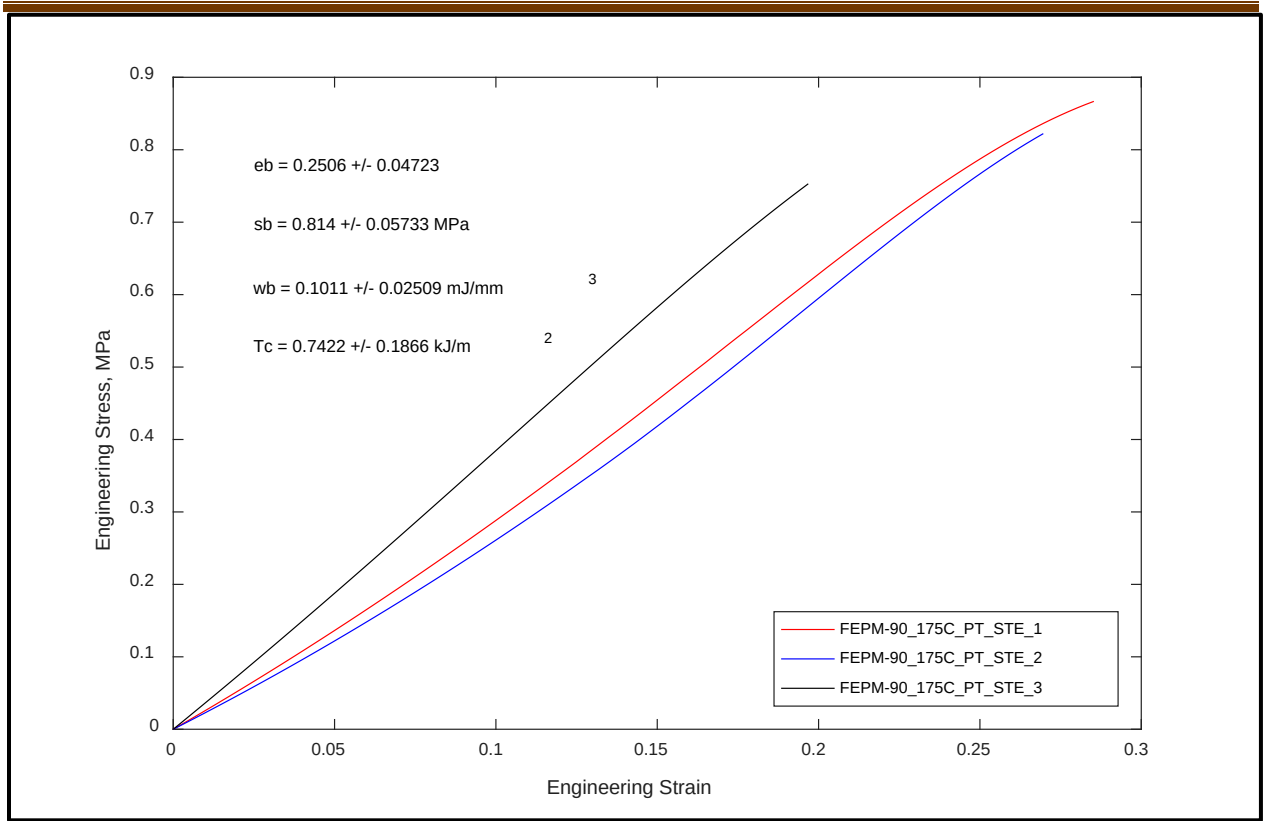
eb = 0.2506 +/- 0.04723
sb = 0.814 +/- 0.05733 MPa
wb = 0.1011 +/- 0.02509 mJ/mm
Tc = 0.7422 +/- 0.1866 kJ/m
3
2
FEPM-90_175C_PT_STE_1
FEPM-90_175C_PT_STE_2
FEPM-90_175C_PT_STE_3
Engineering Stress, MPa
Engineering Strain
0
0.1
0.2
0.3
0.4
0.5
0.6
0.7
0.8
0.9
0.05
0.15
0.25

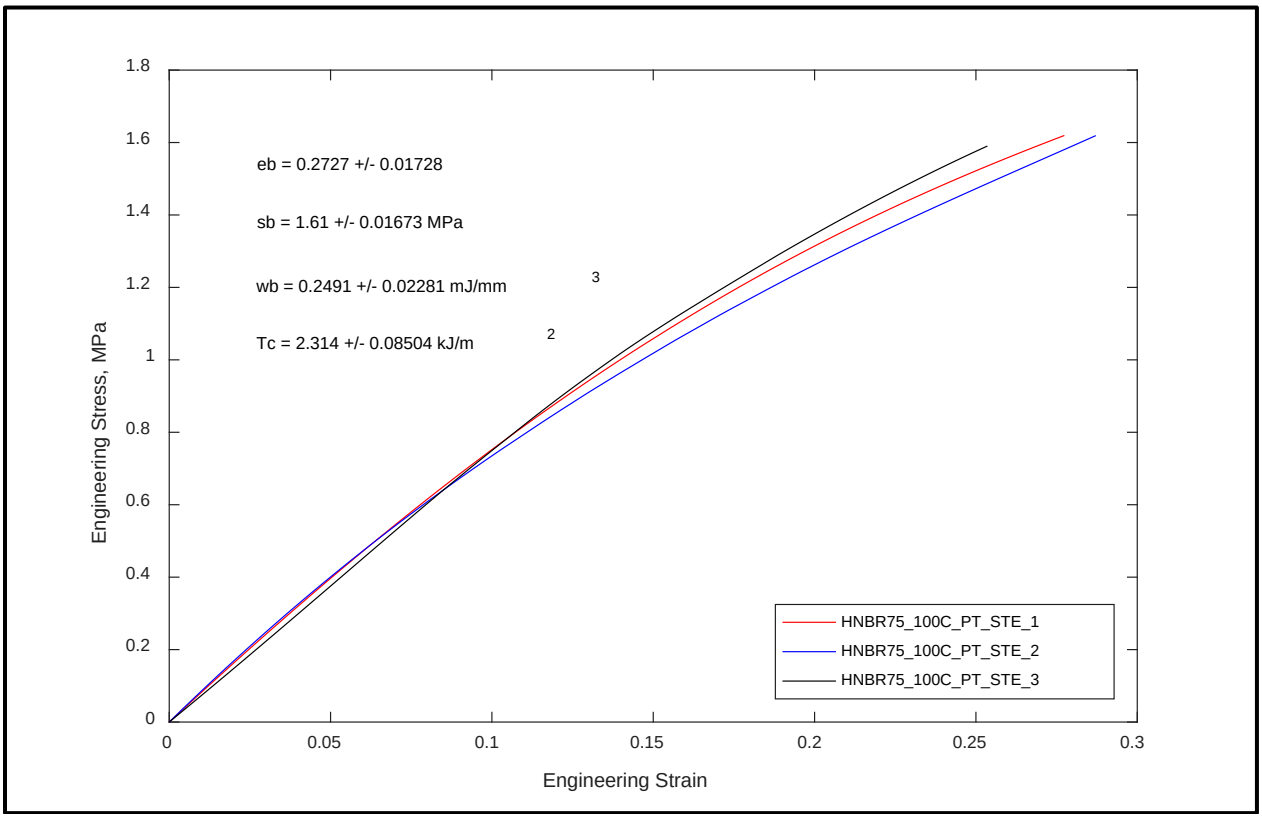
eb = 0.2727 +/- 0.01728
sb = 1.61 +/- 0.01673 MPa
wb = 0.2491 +/- 0.02281 mJ/mm
Tc = 2.314 +/- 0.08504 kJ/m
3
2
HNBR75_100C_PT_STE_1
HNBR75_100C_PT_STE_2
HNBR75_100C_PT_STE_3
Engineering Stress, MPa
Engineering Strain
0
0.2
0.4
0.6
0.8
1
1.2
1.4
1.6
1.8
0.05
0.1
0.15
0.2
0.25
0.3

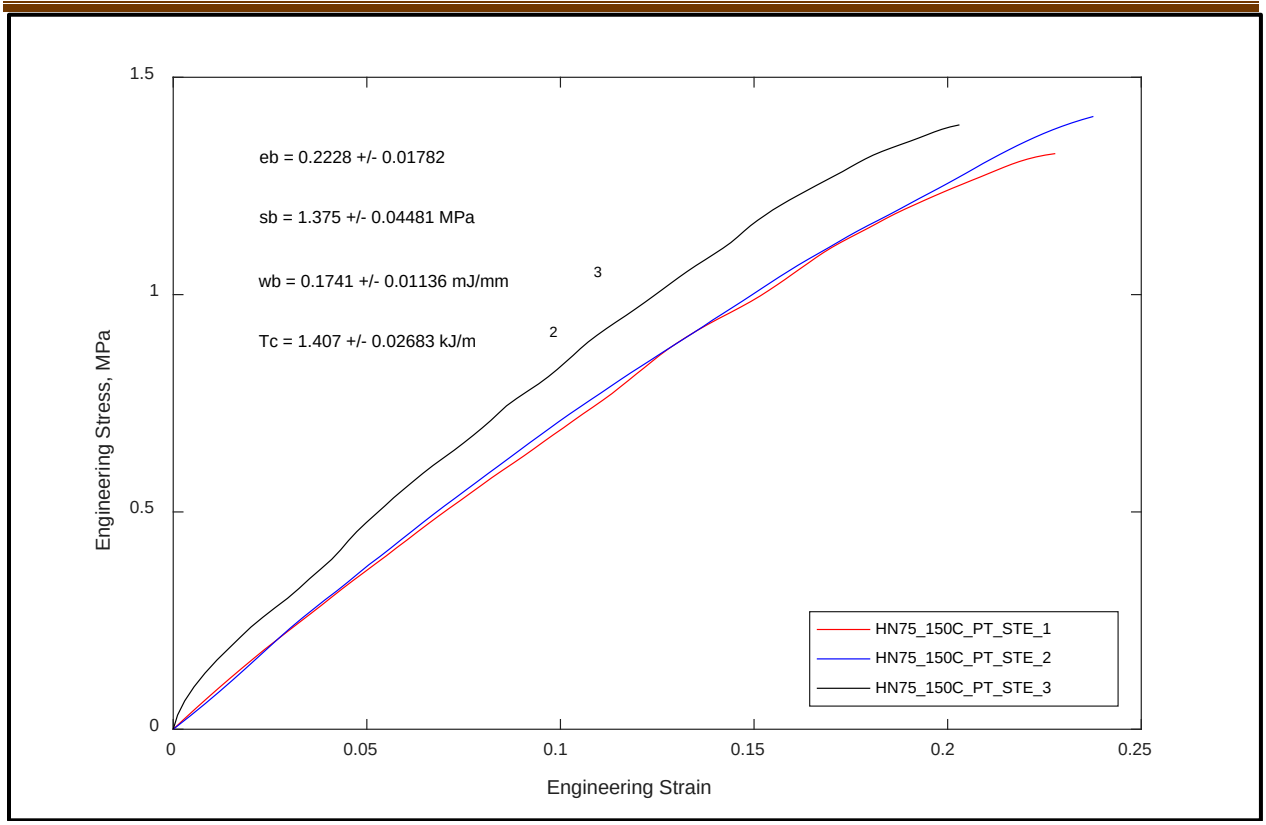
eb = 0.2228 +/- 0.01782
sb = 1.375 +/- 0.04481 MPa
wb = 0.1741 +/- 0.01136 mJ/mm
Tc = 1.407 +/- 0.02683 kJ/m
3
2
HN75_150C_PT_STE_1
HN75_150C_PT_STE_2
HN75_150C_PT_STE_3
Engineering Stress, MPa
Engineering Strain
0
0.5
1
1.5
0.05
0.1
0.15
0.2
0.25

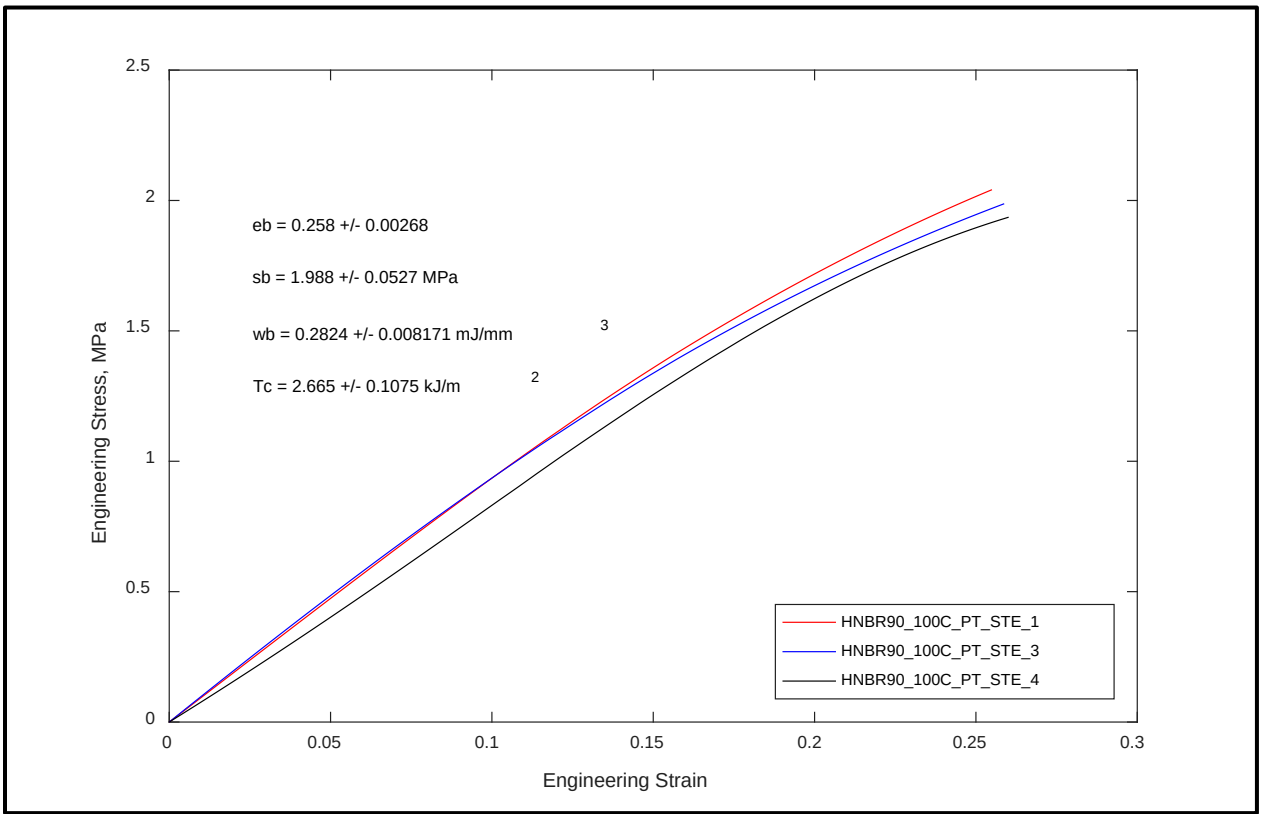
eb = 0.258 +/- 0.00268
sb = 1.988 +/- 0.0527 MPa
wb = 0.2824 +/- 0.008171 mJ/mm
Tc = 2.665 +/- 0.1075 kJ/m
3
2
HNBR90_100C_PT_STE_1
HNBR90_100C_PT_STE_3
HNBR90_100C_PT_STE_4
Engineering Stress, MPa
Engineering Strain
0
0.5
1
1.5
2
2.5
0.05
0.1
0.15
0.2
0.25
0.3

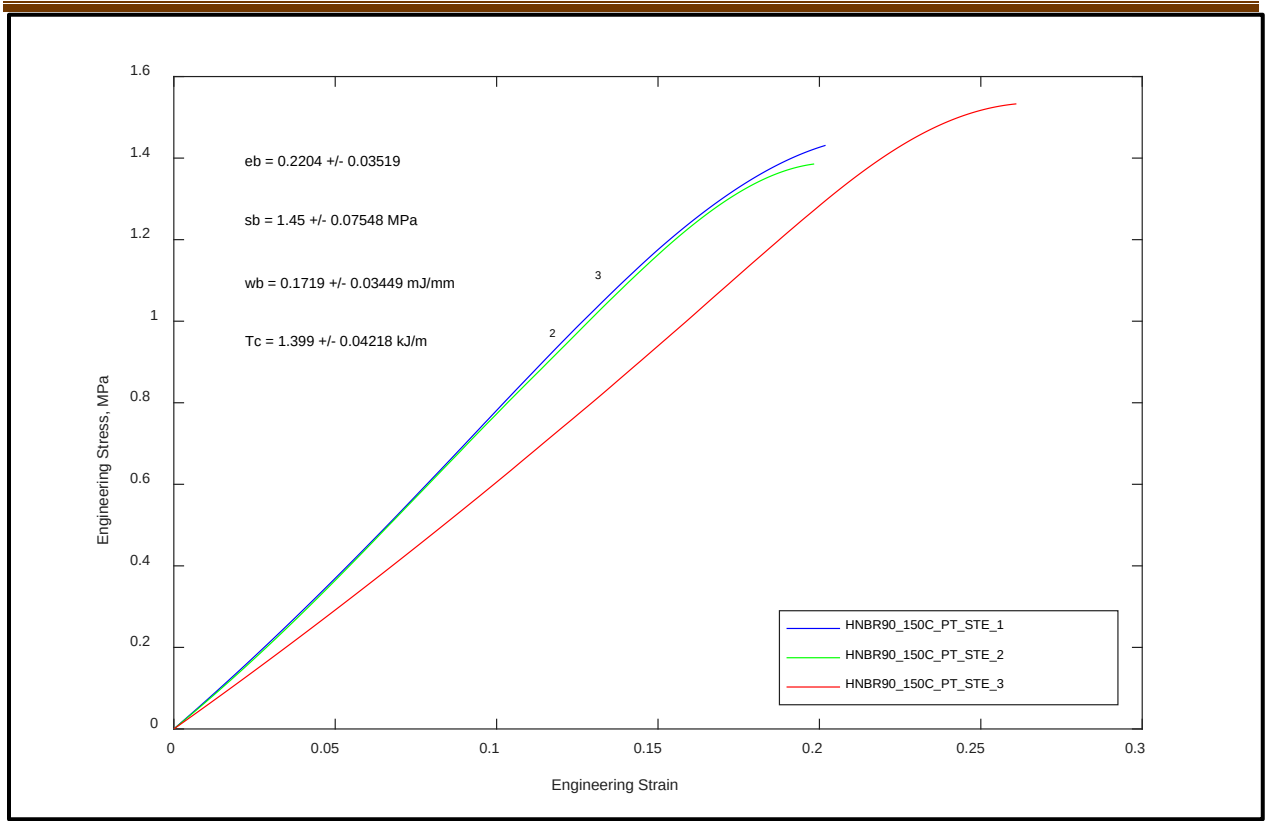
eb = 0.2204 +/- 0.03519
sb = 1.45 +/- 0.07548 MPa
wb = 0.1719 +/- 0.03449 mJ/mm
Tc = 1.399 +/- 0.04218 kJ/m
HNBR90_150C_PT_STE_1
HNBR90_150C_PT_STE_2
HNBR90_150C_PT_STE_3
Engineering Stress, MPa
Engineering Strain

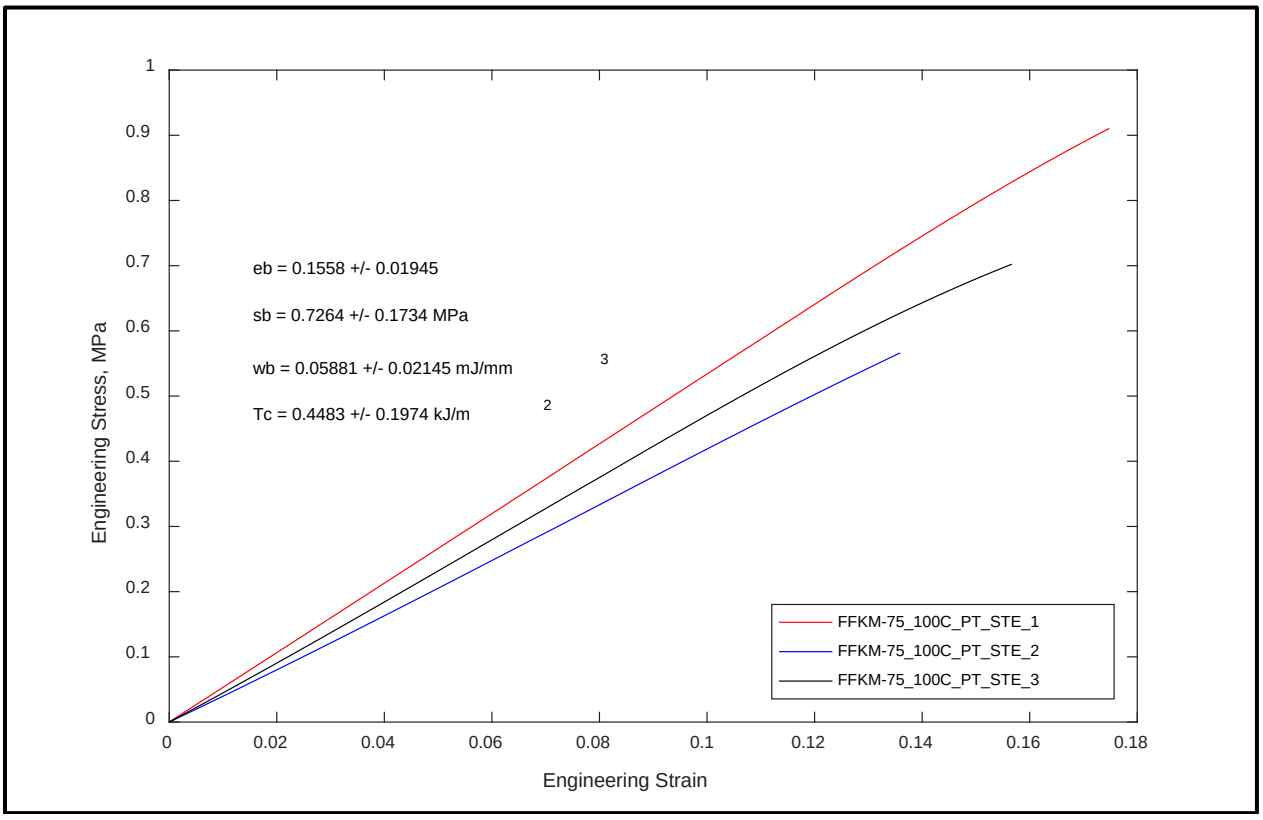
eb = 0.1558 +/- 0.01945
sb = 0.7264 +/- 0.1734 MPa
wb = 0.05881 +/- 0.02145 mJ/mm
Tc = 0.4483 +/- 0.1974 kJ/m
FFKM-75_100C_PT_STE_1
FFKM-75_100C_PT_STE_2
FFKM-75_100C_PT_STE_3
Engineering Stress, MPa
Engineering Strain

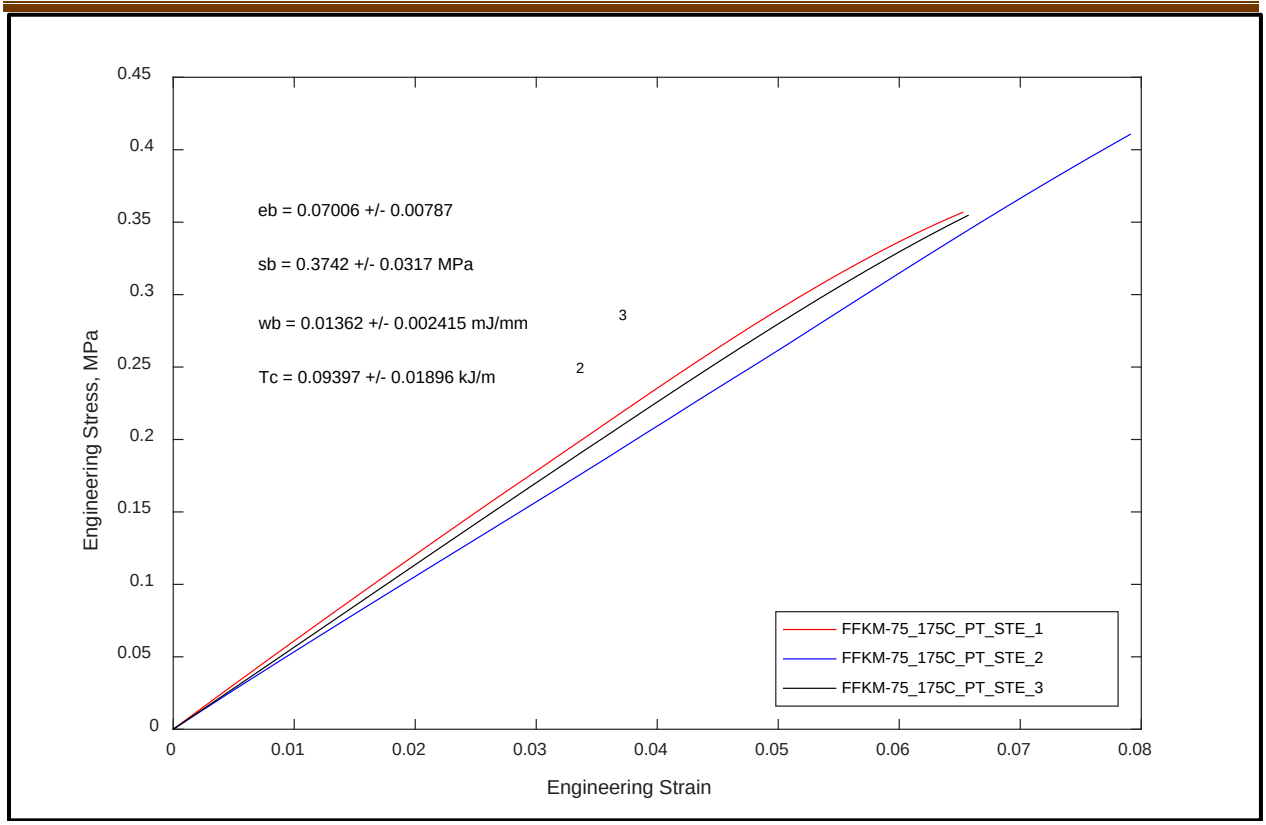
eb = 0.07006 +/- 0.00787
sb = 0.3742 +/- 0.0317 MPa
wb = 0.01362 +/- 0.002415 mJ/mm
Tc = 0.09397 +/- 0.01896 kJ/m
FFKM-75_175C_PT_STE_1
FFKM-75_175C_PT_STE_2
FFKM-75_175C_PT_STE_3
Engineering Stress, MPa
Engineering Strain
0
0.05
0.1
0.15
0.2
0.25
0.3
0.35
0.4
0.45
0.01
0.02
0.03
0.04
0.05
0.06
0.07
0.08

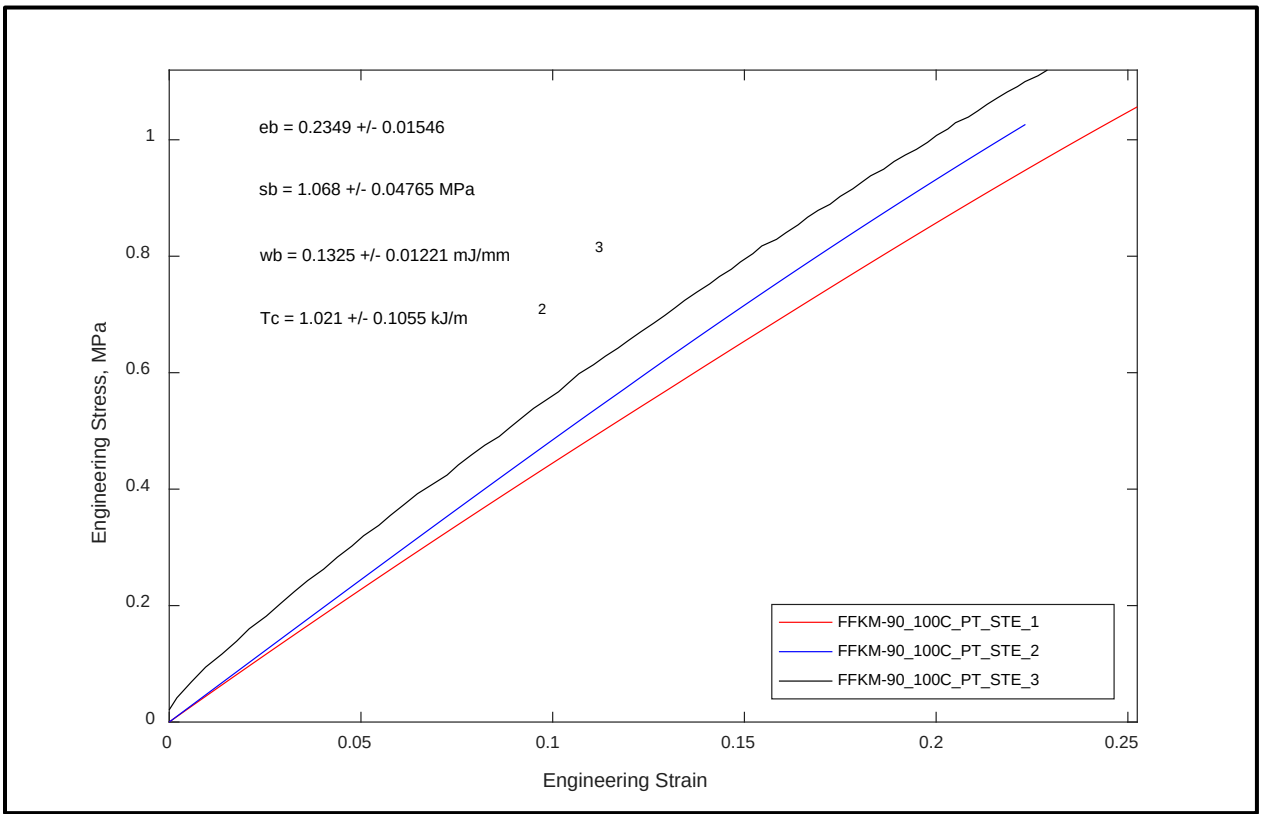
eb = 0.2349 +/- 0.01546
sb = 1.068 +/- 0.04765 MPa
wb = 0.1325 +/- 0.01221 mJ/mm
Tc = 1.021 +/- 0.1055 kJ/m
FFKM-90_100C_PT_STE_1
FFKM-90_100C_PT_STE_2
FFKM-90_100C_PT_STE_3
Engineering Stress, MPa
Engineering Strain
0
0.2
0.4
0.6
0.8
1
0.05
0.1
0.15
0.2
0.25

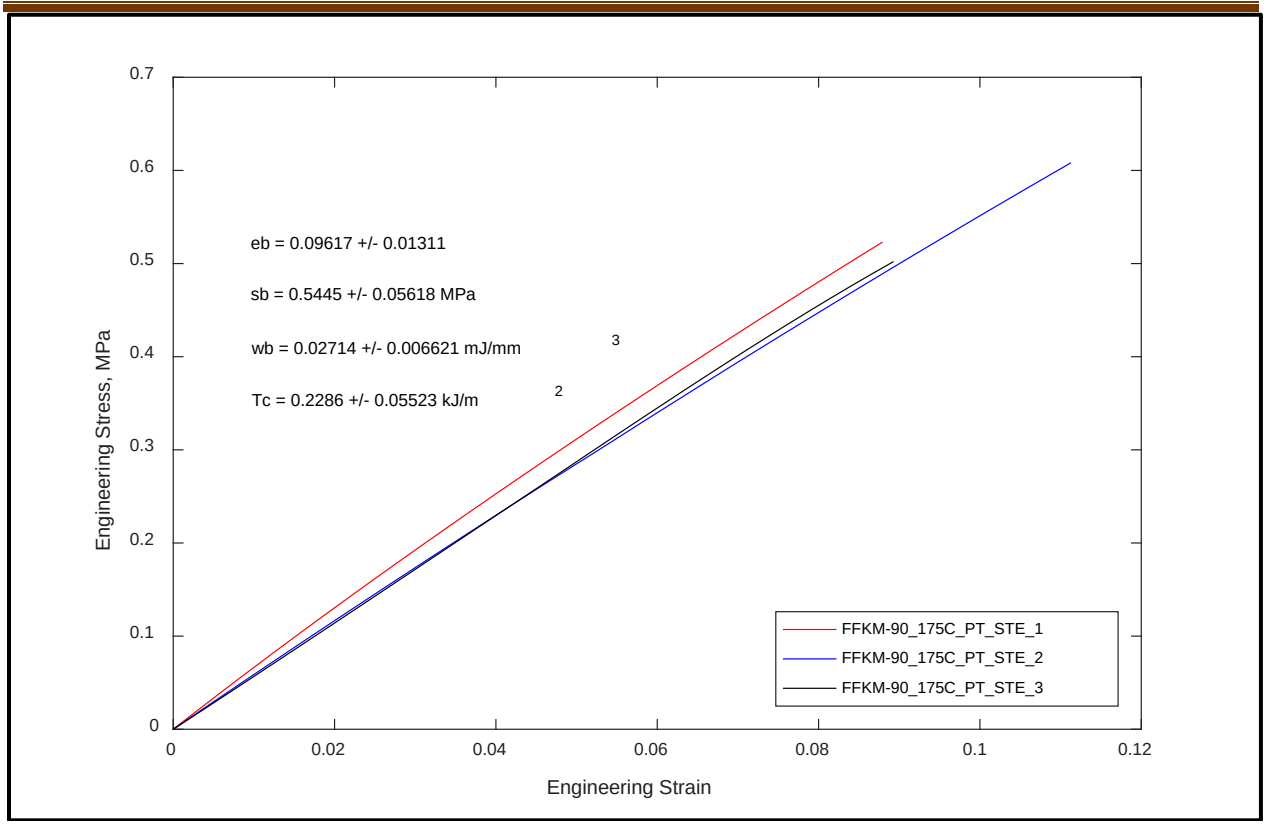
eb = 0.09617 +/- 0.01311
sb = 0.5445 +/- 0.05618 MPa
wb = 0.02714 +/- 0.006621 mJ/mm
Tc = 0.2286 +/- 0.05523 kJ/m
2
3
FFKM-90_175C_PT_STE_1
FFKM-90_175C_PT_STE_2
FFKM-90_175C_PT_STE_3
Engineering Stress, MPa
Engineering Strain
0
0.1
0.2
0.3
0.4
0.5
0.6
0.7
0.02
0.04
0.06
0.08
0.1
0.12

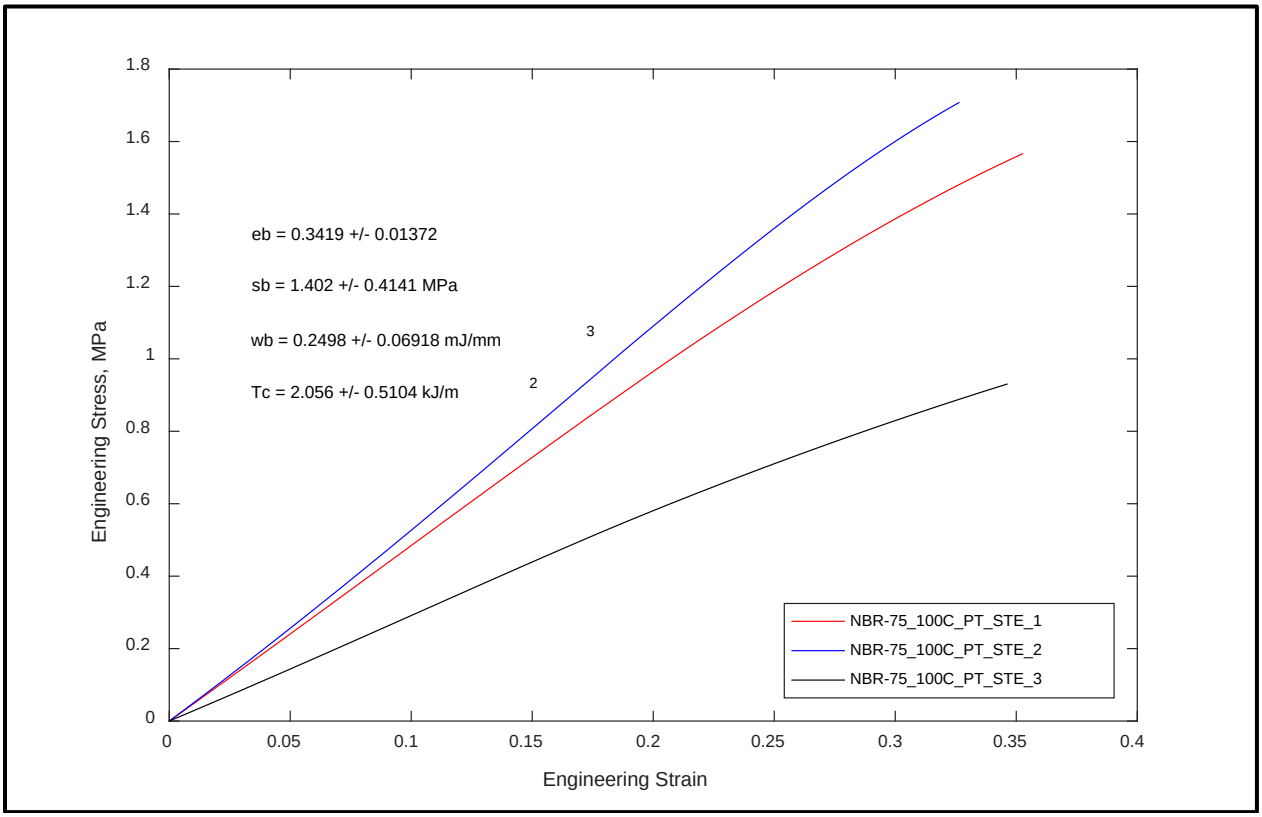
eb = 0.3419 +/- 0.01372
sb = 1.402 +/- 0.4141 MPa
wb = 0.2498 +/- 0.06918 mJ/mm
Tc = 2.056 +/- 0.5104 kJ/m
2
3
NBR-75_100C_PT_STE_1
NBR-75_100C_PT_STE_2
NBR-75_100C_PT_STE_3
Engineering Stress, MPa
Engineering Strain
0
0.2
0.4
0.6
0.8
1
1.2
1.4
1.6
1.8
0.05
0.1
0.15
0.2
0.25
0.3
0.35
0.4

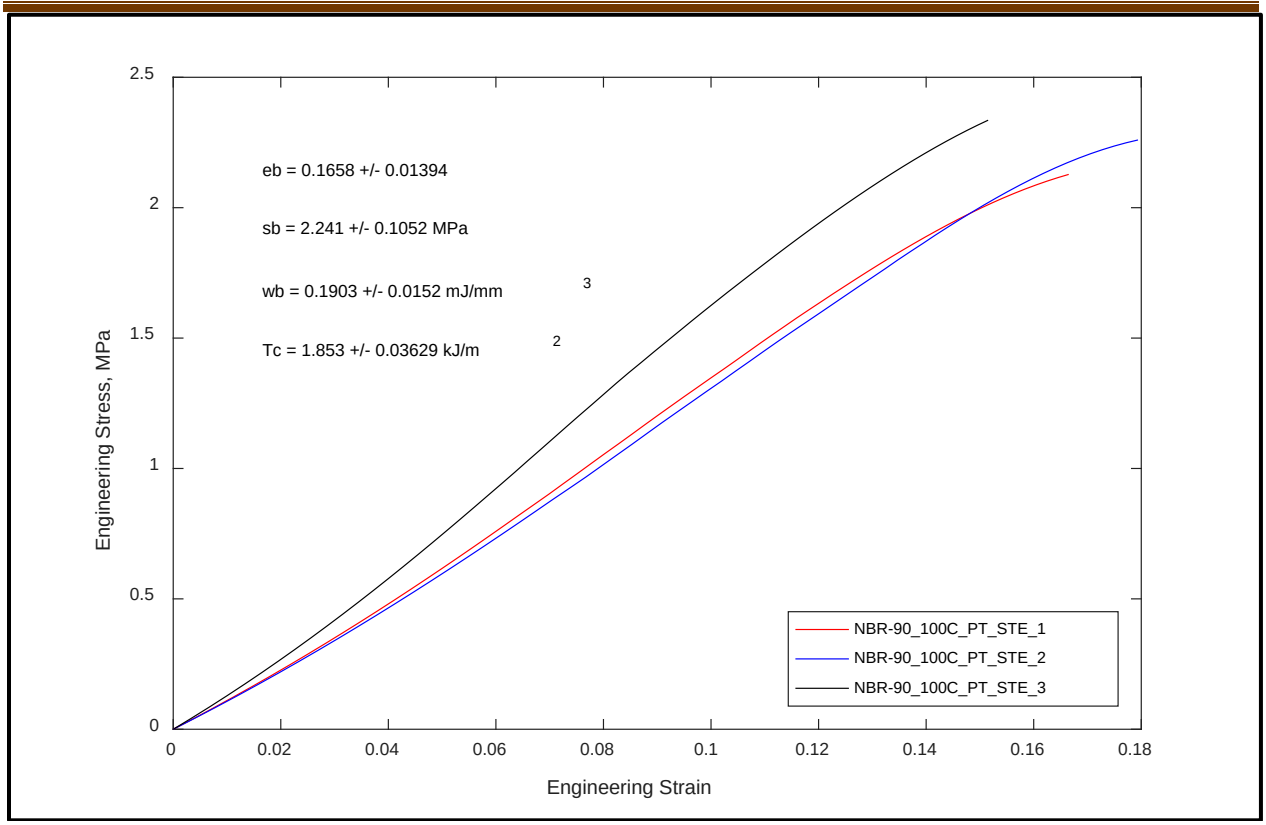
eb = 0.1658 +/- 0.01394
sb = 2.241 +/- 0.1052 MPa
wb = 0.1903 +/- 0.0152 mJ/mm
Tc = 1.853 +/- 0.03629 kJ/m
3
2
NBR-90_100C_PT_STE_1
NBR-90_100C_PT_STE_2
NBR-90_100C_PT_STE_3
Engineering Stress, MPa
Engineering Strain
0
0.5
1
1.5
2
2.5
0.02
0.04
0.06
0.08
0.1
0.12
0.14
0.16
0.18

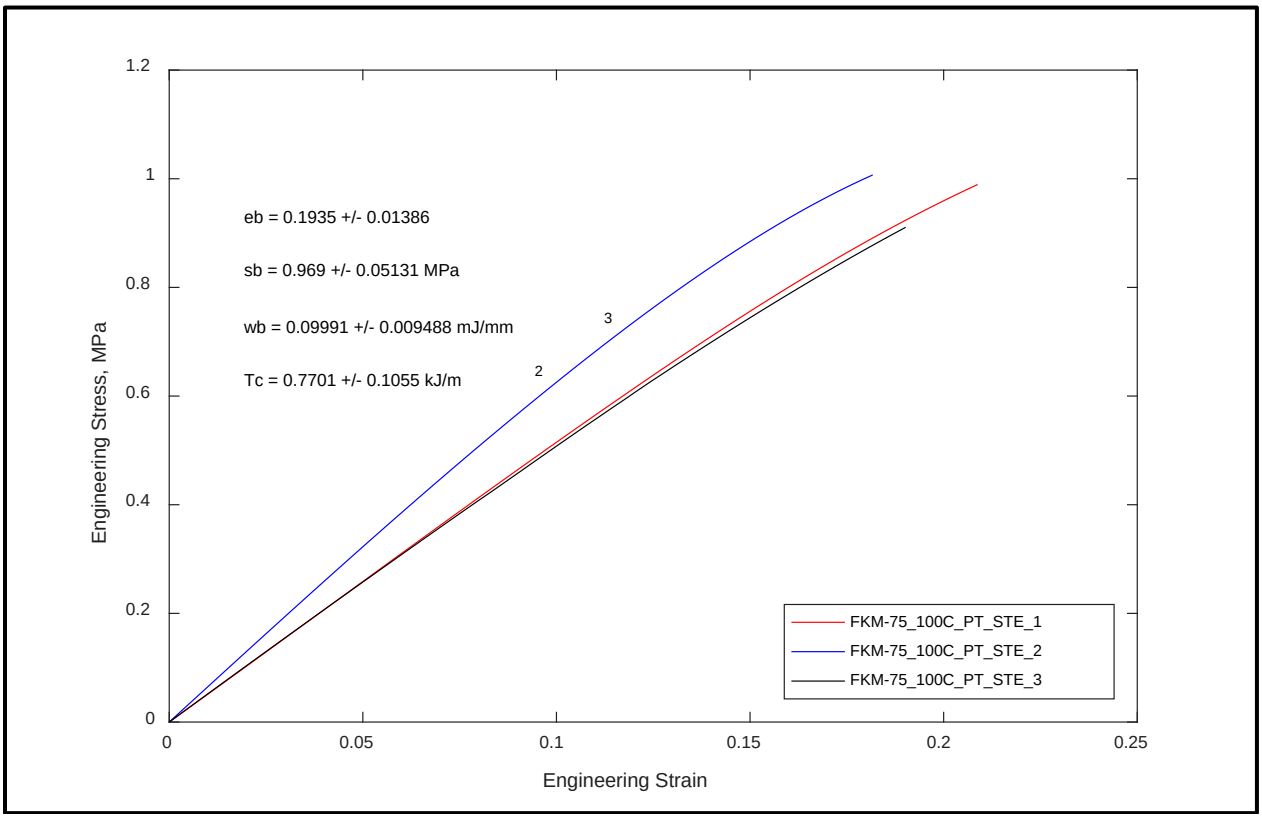
eb = 0.1935 +/- 0.01386
sb = 0.969 +/- 0.05131 MPa
wb = 0.09991 +/- 0.009488 mJ/mm
Tc = 0.7701 +/- 0.1055 kJ/m
3
2
FKM-75_100C_PT_STE_1
FKM-75_100C_PT_STE_2
FKM-75_100C_PT_STE_3
Engineering Stress, MPa
Engineering Strain
0
0.2
0.4
0.6
0.8
1
1.2
0.05
0.1
0.15
0.2
0.25

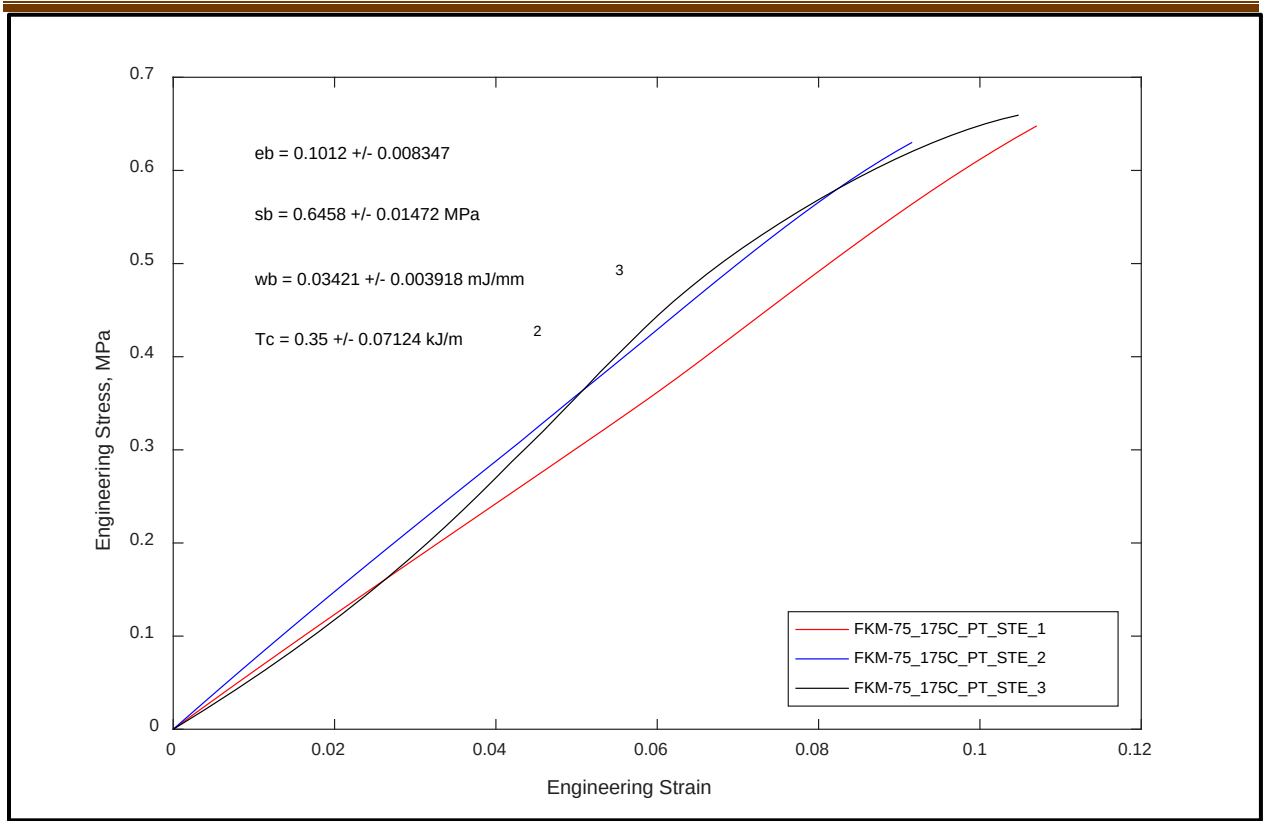
eb = 0.1012 +/- 0.008347
sb = 0.6458 +/- 0.01472 MPa
wb = 0.03421 +/- 0.003918 mJ/mm
Tc = 0.35 +/- 0.07124 kJ/m
FKM-75_175C_PT_STE_1
FKM-75_175C_PT_STE_2
FKM-75_175C_PT_STE_3
Engineering Stress, MPa
Engineering Strain
0
0.1
0.2
0.3
0.4
0.5
0.6
0.7
0.02
0.04
0.06
0.08
0.1
0.12

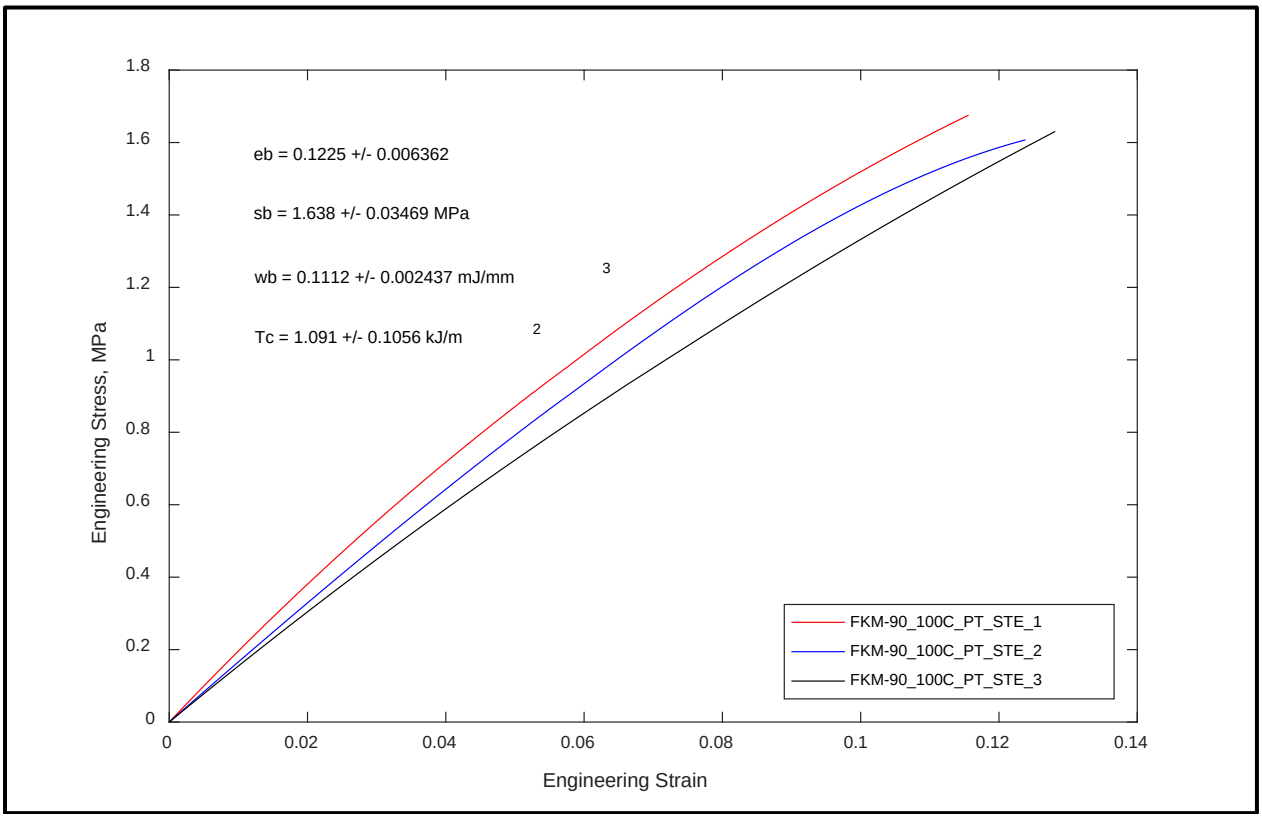
eb = 0.1225 +/- 0.006362
sb = 1.638 +/- 0.03469 MPa
wb = 0.1112 +/- 0.002437 mJ/mm
Tc = 1.091 +/- 0.1056 kJ/m
FKM-90_100C_PT_STE_1
FKM-90_100C_PT_STE_2
FKM-90_100C_PT_STE_3
Engineering Stress, MPa
Engineering Strain
0
0.2
0.4
0.6
0.8
1
1.2
1.4
1.6
1.8
0.02
0.04
0.06
0.08
0.1
0.12
0.14

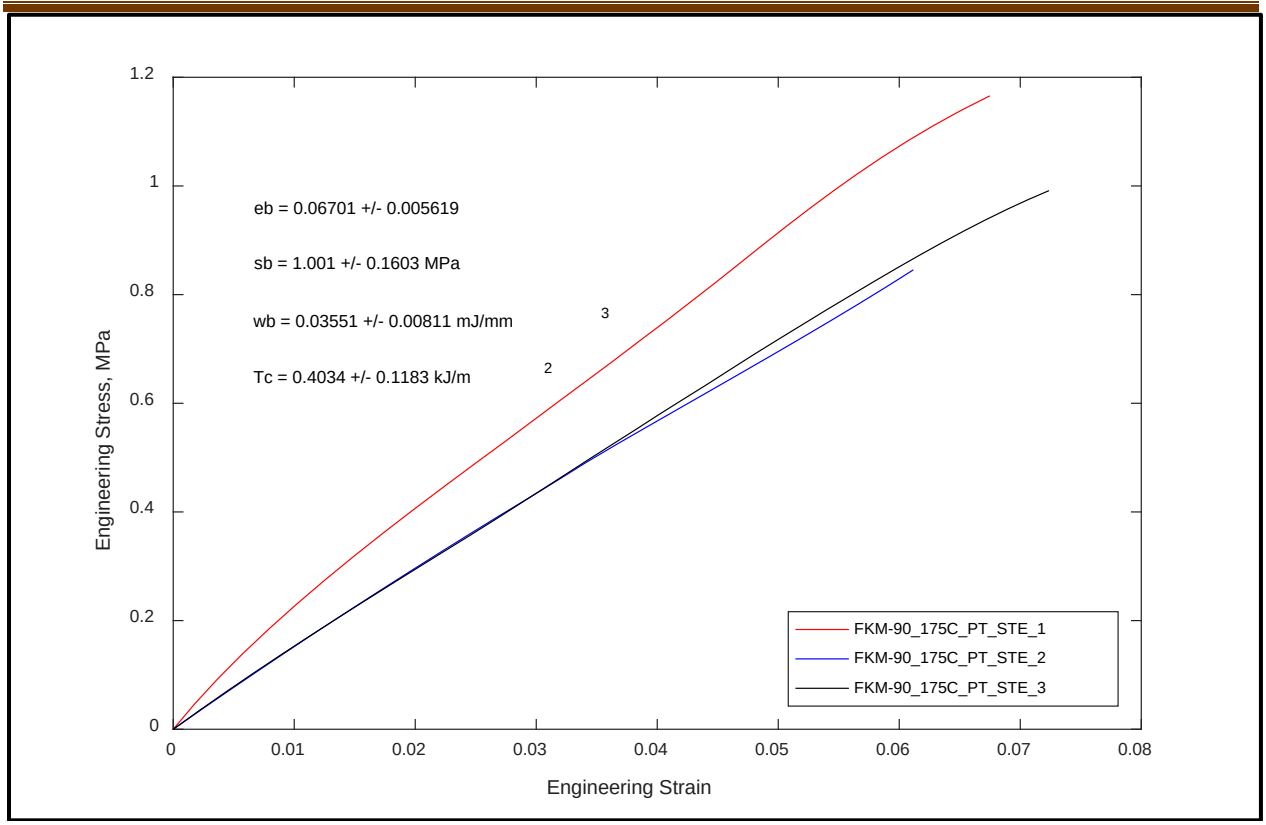


Figure A.4-1. Comparison of strain to break experiments on edge pre-cracked planar tension specimen. 3 replicates.

Table A.4-8. Strength parameters derived from edge cracked planar tension tests.

| Material | Test Temperature °C | Engineering Strain at break | Engineering Stress at break, MPa | Strain Energy Density at break, mJ / mm^3 | Critical Tearing Energy, kJ/m$^2$ |
|---|---|---|---|---|---|
| FEPM-80 | 100 | 0.3602 | 1.097 | 0.2205 | 1.811 |
| FEPM-80 | 175 | 0.2015 | 0.6455 | 0.06655 | 0.5244 |
| FEPM-90 | 100 | 0.3825 | 1.495 | 0.3168 | 2.625 |
| FEPM-90 | 175 | 0.2506 | 0.814 | 0.1011 | 0.7422 |
| HNBR-75 | 100 | 0.2727 | 1.61 | 0.2491 | 2.314 |
| HNBR-90 | 100 | 0.2580 | 1.988 | 0.2824 | 2.665 |
| HNBR-90 | 150 | 0.2204 | 1.45 | 0.1719 | 1.399 |
| FFKM-75 | 100 | 0.1558 | 0.7264 | 0.05881 | 0.4483 |
| FFKM-75 | 175 | 0.07006 | 0.3742 | 0.01362 | 0.09397 |
| FFKM-90 | 100 | 0.2349 | 1.068 | 0.1325 | 1.021 |
| FFKM-90 | 175 | 0.09617 | 0.5445 | 0.02714 | 0.2286 |
| NBR-75 | 100 | 0.3419 | 1.402 | 0.2498 | 2.056 |
| NBR-90 | 100 | 0.1658 | 2.241 | 0.1903 | 1.853 |
| FKM-75 | 100 | 0.1935 | 0.969 | 0.09991 | 0.7701 |
| FKM-75 | 175 | 0.1012 | 0.6458 | 0.03421 | 0.35 |
| FKM-90 | 100 | 0.1225 | 1.638 | 0.1112 | 1.091 |
| FKM-90 | 175 | 0.06701 | 1.001 | 0.03551 | 0.4034 |

# Hyperelastic Module

## *Experiment 2 – Quasistatic Cyclic Simple, Planar, and Equibiaxial Tension*

Purpose: Cyclic tension experiments in simple tension, planar tension, and equibiaxial tension are needed to define the hyperelastic and Mullins law parameters for finite element analysis.

Specimens: Simple tension – Dumbbell specimen
Planar tension – Rectangular specimen
Equibiaxial tension – Circular specimen

Strain Rate: 1% / sec.

Ambient temperature: 23°C, 100°C, 150°C, 175°C. Test temperature noted in figures.

Cycles: 5 per strain level

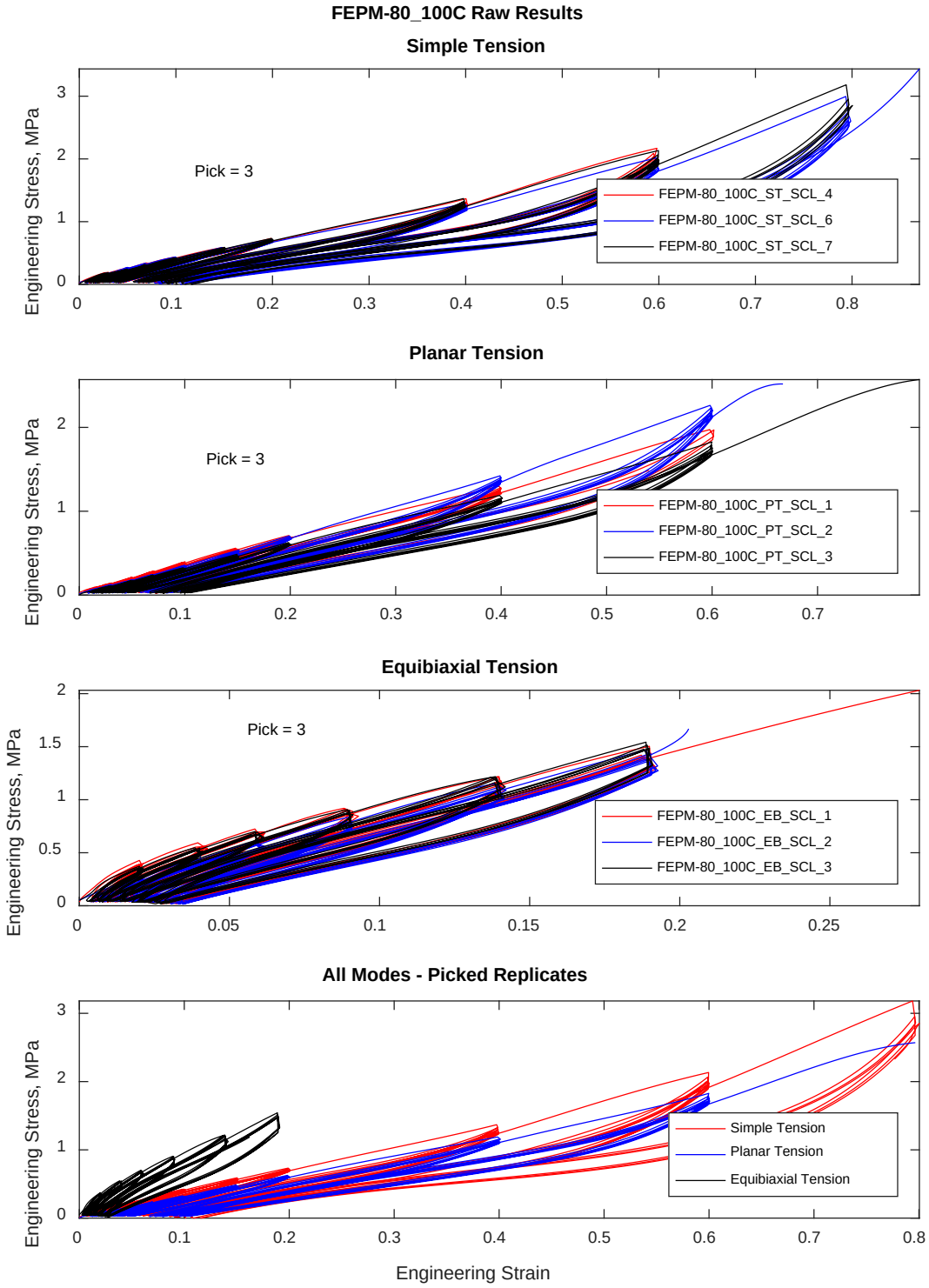
FEPM-80_100C Raw Results
Simple Tension
Engineering Stress, MPa
Pick = 3
FEPM-80_100C_ST_SCL_4
FEPM-80_100C_ST_SCL_6
FEPM-80_100C_ST_SCL_7
Planar Tension
Engineering Stress, MPa
Pick = 3
FEPM-80_100C_PT_SCL_1
FEPM-80_100C_PT_SCL_2
FEPM-80_100C_PT_SCL_3
Equibiaxial Tension
Engineering Stress, MPa
Pick = 3
FEPM-80_100C_EB_SCL_1
FEPM-80_100C_EB_SCL_2
FEPM-80_100C_EB_SCL_3
All Modes - Picked Replicates
Engineering Stress, MPa
Simple Tension
Planar Tension
Equibiaxial Tension
Engineering Strain

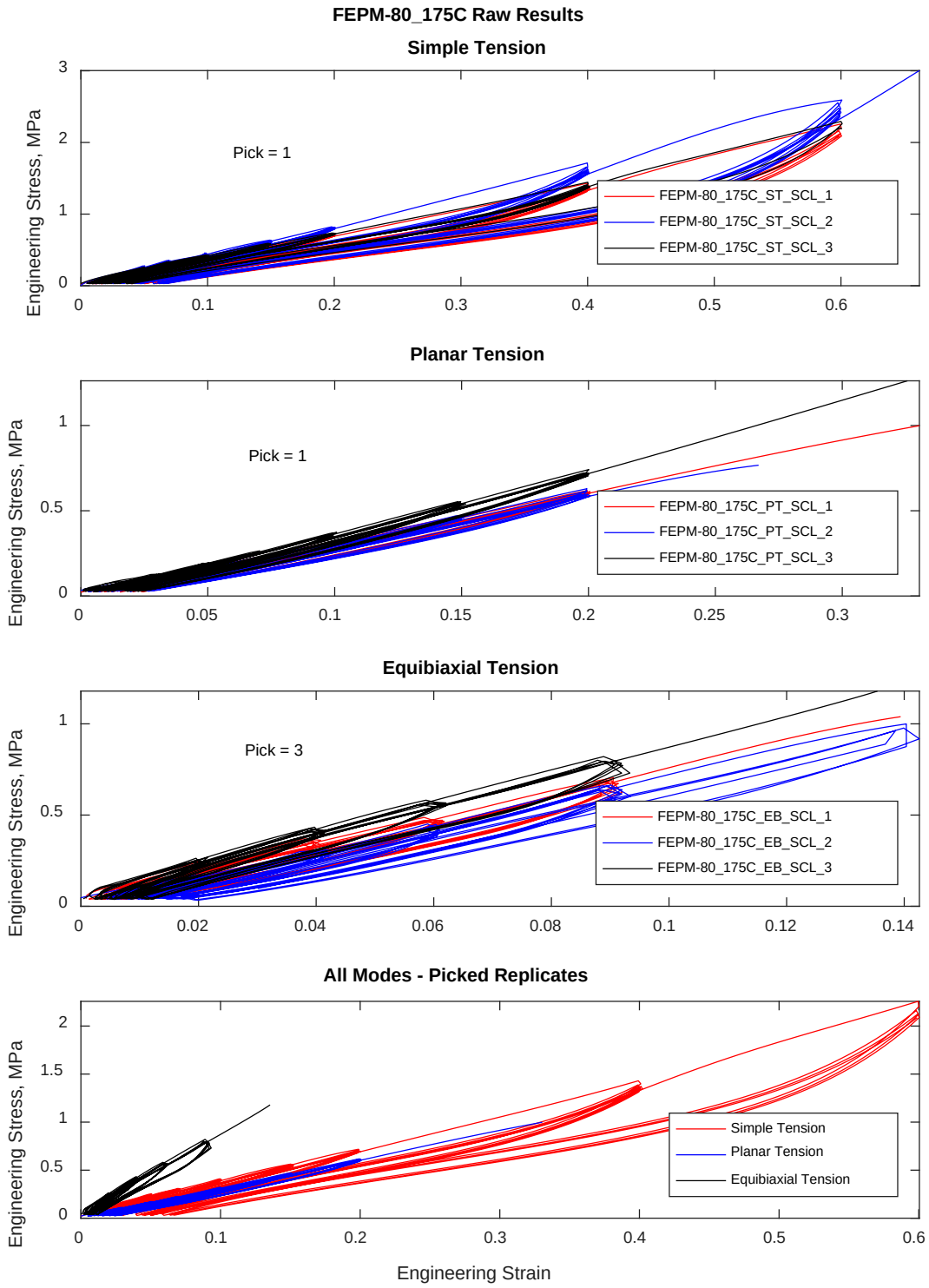
FEPM-80_175C Raw Results
Simple Tension
Engineering Stress, MPa
Pick = 1
FEPM-80_175C_ST_SCL_1
FEPM-80_175C_ST_SCL_2
FEPM-80_175C_ST_SCL_3
Planar Tension
Engineering Stress, MPa
Pick = 1
FEPM-80_175C_PT_SCL_1
FEPM-80_175C_PT_SCL_2
FEPM-80_175C_PT_SCL_3
Equibiaxial Tension
Engineering Stress, MPa
Pick = 3
FEPM-80_175C_EB_SCL_1
FEPM-80_175C_EB_SCL_2
FEPM-80_175C_EB_SCL_3
All Modes - Picked Replicates
Engineering Stress, MPa
Simple Tension
Planar Tension
Equibiaxial Tension
Engineering Strain

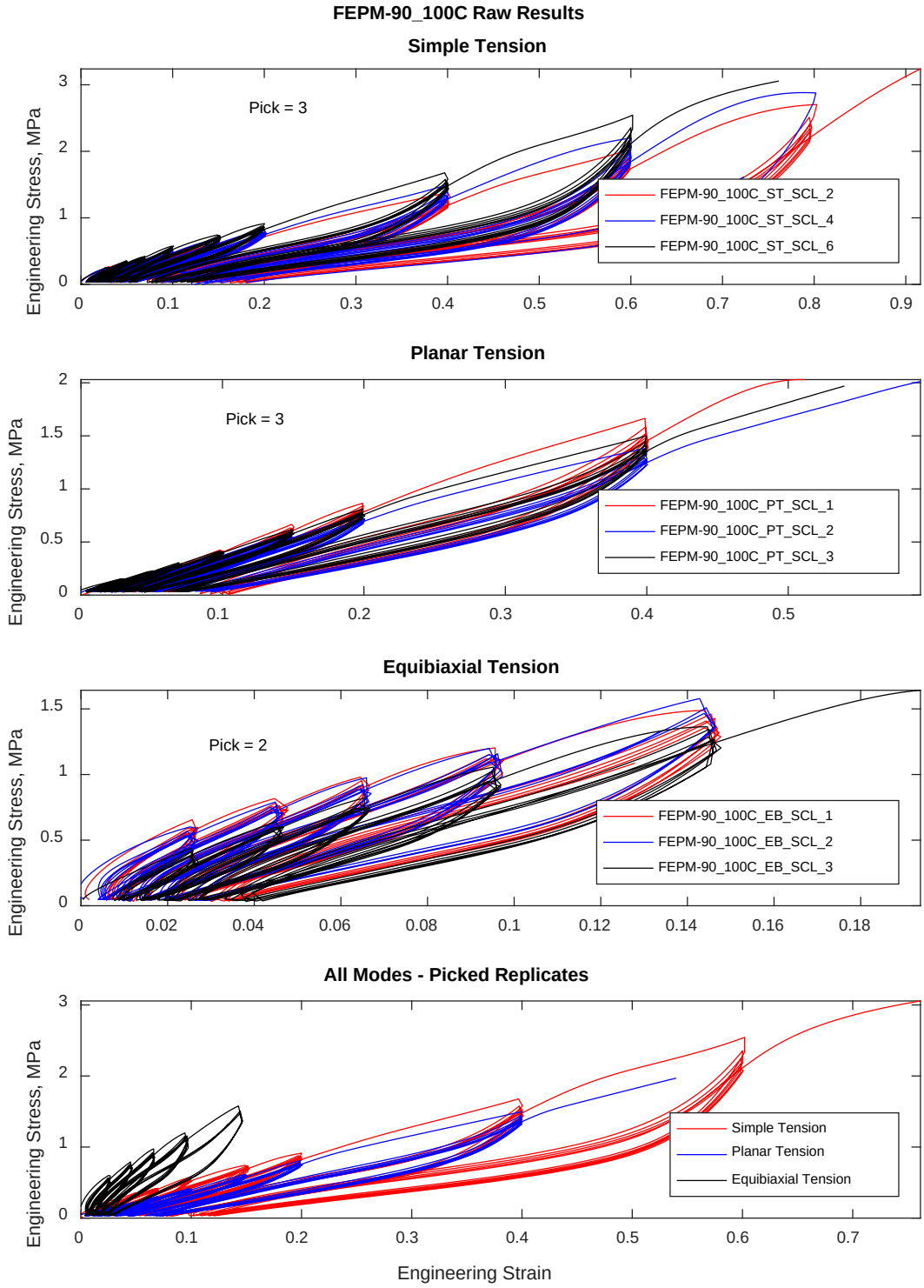
FEPM-90_100C Raw Results
Simple Tension
Pick = 3
Engineering Stress, MPa
FEPM-90_100C_ST_SCL_2
FEPM-90_100C_ST_SCL_4
FEPM-90_100C_ST_SCL_6
Planar Tension
Pick = 3
Engineering Stress, MPa
FEPM-90_100C_PT_SCL_1
FEPM-90_100C_PT_SCL_2
FEPM-90_100C_PT_SCL_3
Equibiaxial Tension
Pick = 2
Engineering Stress, MPa
FEPM-90_100C_EB_SCL_1
FEPM-90_100C_EB_SCL_2
FEPM-90_100C_EB_SCL_3
All Modes - Picked Replicates
Engineering Stress, MPa
Simple Tension
Planar Tension
Equibiaxial Tension
Engineering Strain

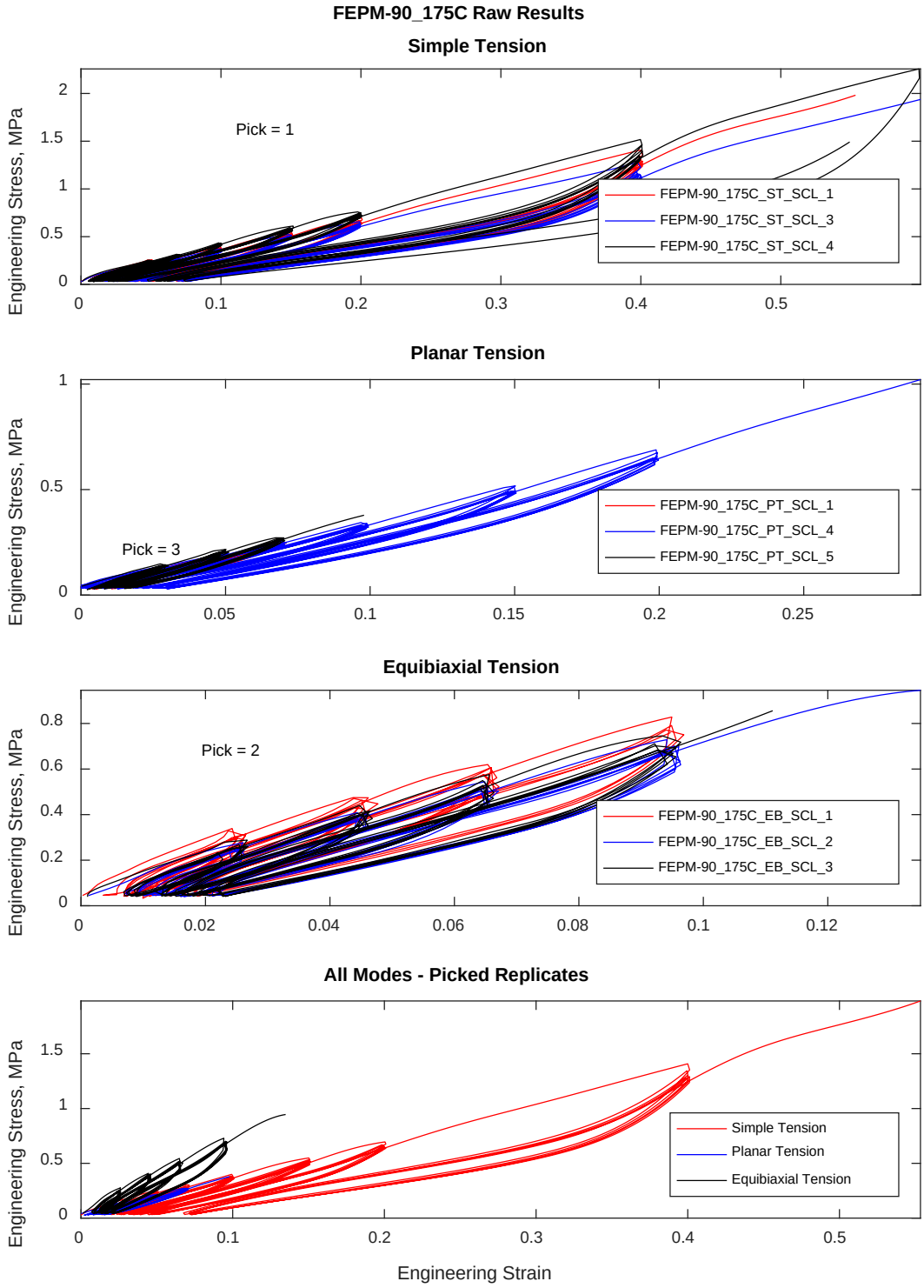
FEPM-90_175C Raw Results
Simple Tension
Engineering Stress, MPa
Pick = 1
FEPM-90_175C_ST_SCL_1
FEPM-90_175C_ST_SCL_3
FEPM-90_175C_ST_SCL_4
Planar Tension
Engineering Stress, MPa
Pick = 3
FEPM-90_175C_PT_SCL_1
FEPM-90_175C_PT_SCL_4
FEPM-90_175C_PT_SCL_5
Equibiaxial Tension
Engineering Stress, MPa
Pick = 2
FEPM-90_175C_EB_SCL_1
FEPM-90_175C_EB_SCL_2
FEPM-90_175C_EB_SCL_3
All Modes - Picked Replicates
Engineering Stress, MPa
Simple Tension
Planar Tension
Equibiaxial Tension
Engineering Strain

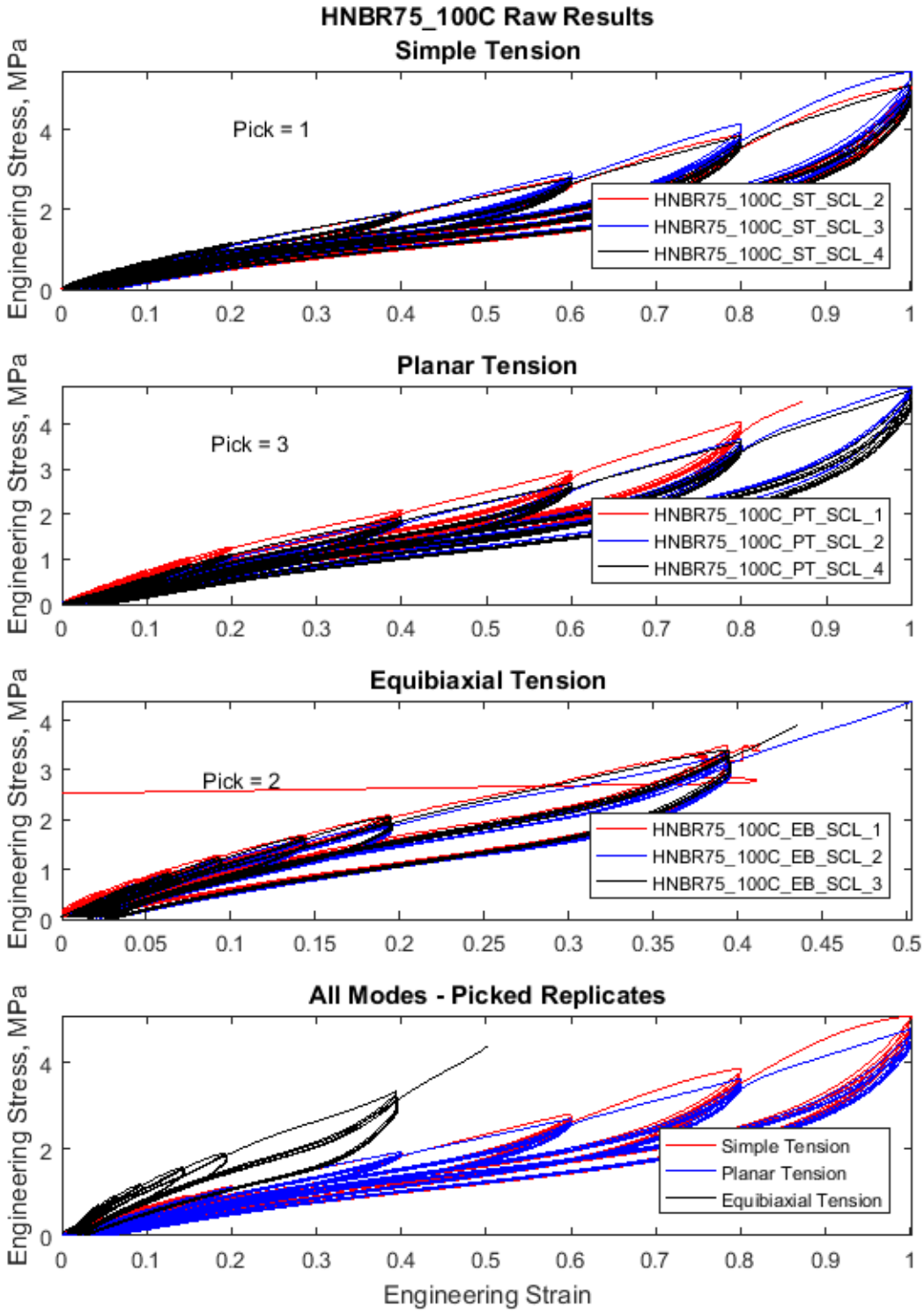
HNBR75_100C Raw Results
Simple Tension
Pick = 1
HNBR75_100C_ST_SCL_2
HNBR75_100C_ST_SCL_3
HNBR75_100C_ST_SCL_4
Planar Tension
Pick = 3
HNBR75_100C_PT_SCL_1
HNBR75_100C_PT_SCL_2
HNBR75_100C_PT_SCL_4
Equibiaxial Tension
Pick = 2
HNBR75_100C_EB_SCL_1
HNBR75_100C_EB_SCL_2
HNBR75_100C_EB_SCL_3
All Modes - Picked Replicates
Simple Tension
Planar Tension
Equibiaxial Tension
Engineering Stress, MPa
Engineering Strain

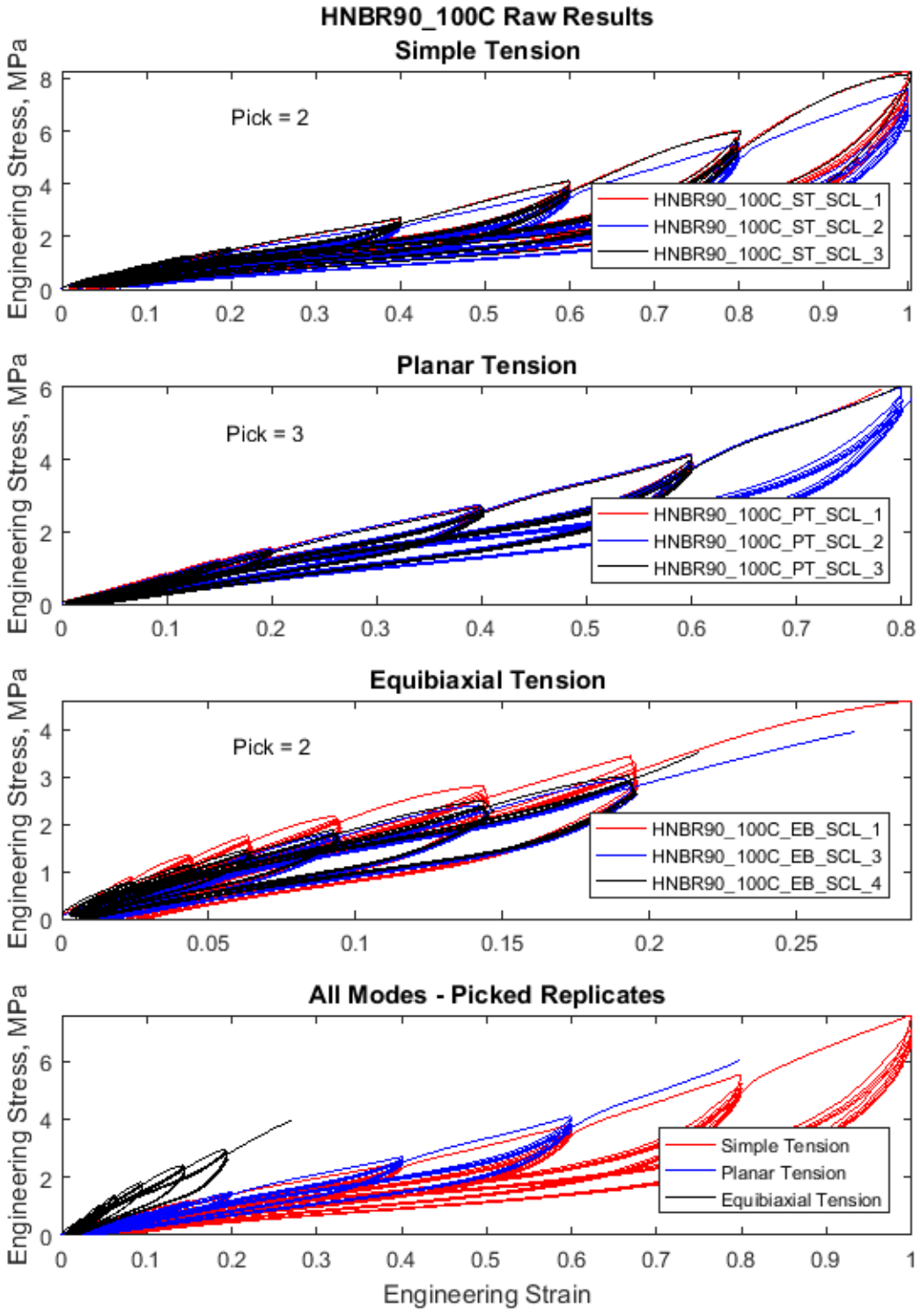
HNBR90_100C Raw Results
Simple Tension
Pick = 2
HNBR90_100C_ST_SCL_1
HNBR90_100C_ST_SCL_2
HNBR90_100C_ST_SCL_3
Planar Tension
Pick = 3
HNBR90_100C_PT_SCL_1
HNBR90_100C_PT_SCL_2
HNBR90_100C_PT_SCL_3
Equibiaxial Tension
Pick = 2
HNBR90_100C_EB_SCL_1
HNBR90_100C_EB_SCL_3
HNBR90_100C_EB_SCL_4
All Modes - Picked Replicates
Simple Tension
Planar Tension
Equibiaxial Tension
Engineering Stress, MPa
Engineering Strain

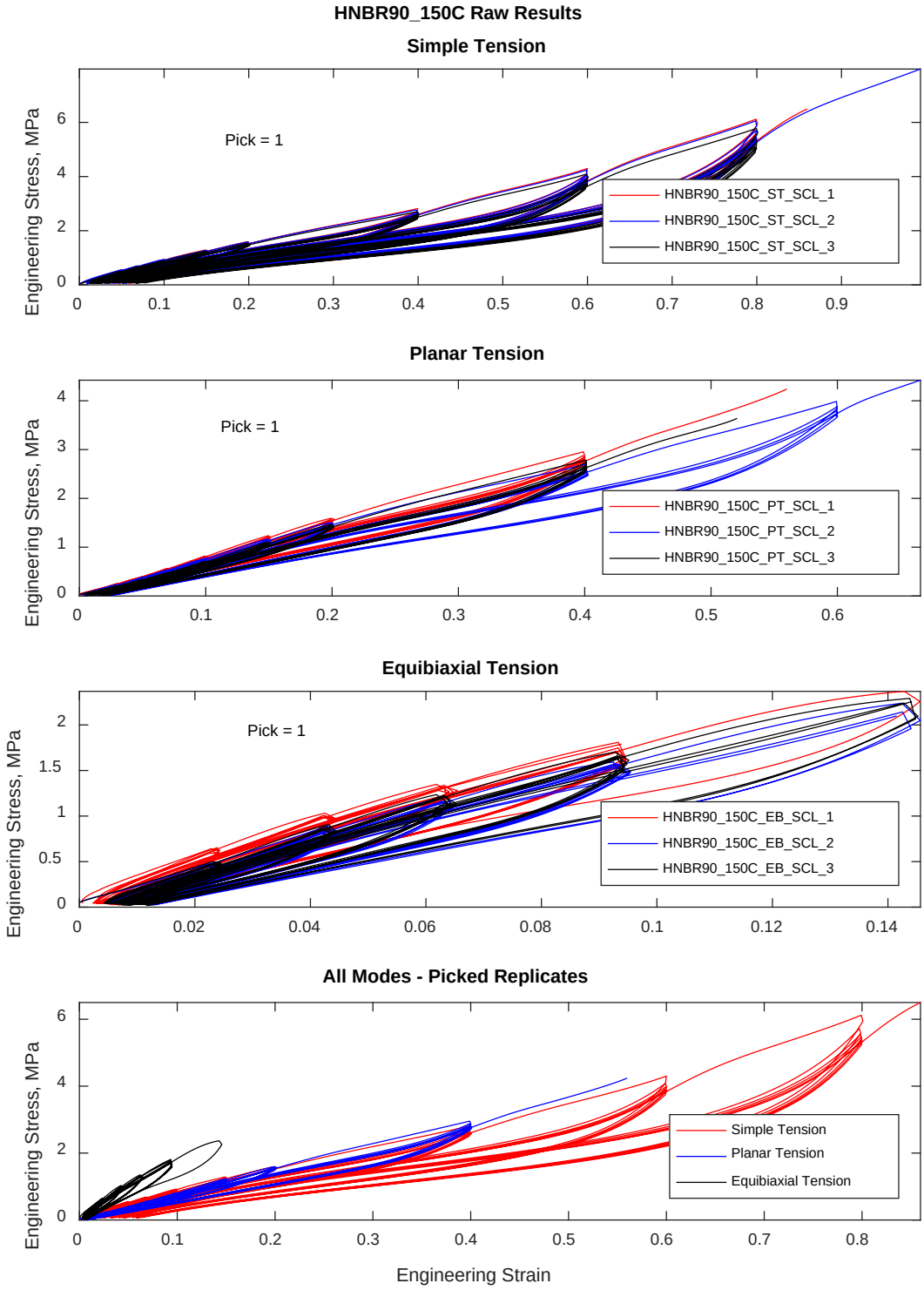
HNBR90_150C Raw Results
Simple Tension
Engineering Stress, MPa
Pick = 1
HNBR90_150C_ST_SCL_1
HNBR90_150C_ST_SCL_2
HNBR90_150C_ST_SCL_3
Planar Tension
Engineering Stress, MPa
Pick = 1
HNBR90_150C_PT_SCL_1
HNBR90_150C_PT_SCL_2
HNBR90_150C_PT_SCL_3
Equibiaxial Tension
Engineering Stress, MPa
Pick = 1
HNBR90_150C_EB_SCL_1
HNBR90_150C_EB_SCL_2
HNBR90_150C_EB_SCL_3
All Modes - Picked Replicates
Engineering Stress, MPa
Simple Tension
Planar Tension
Equibiaxial Tension
Engineering Strain

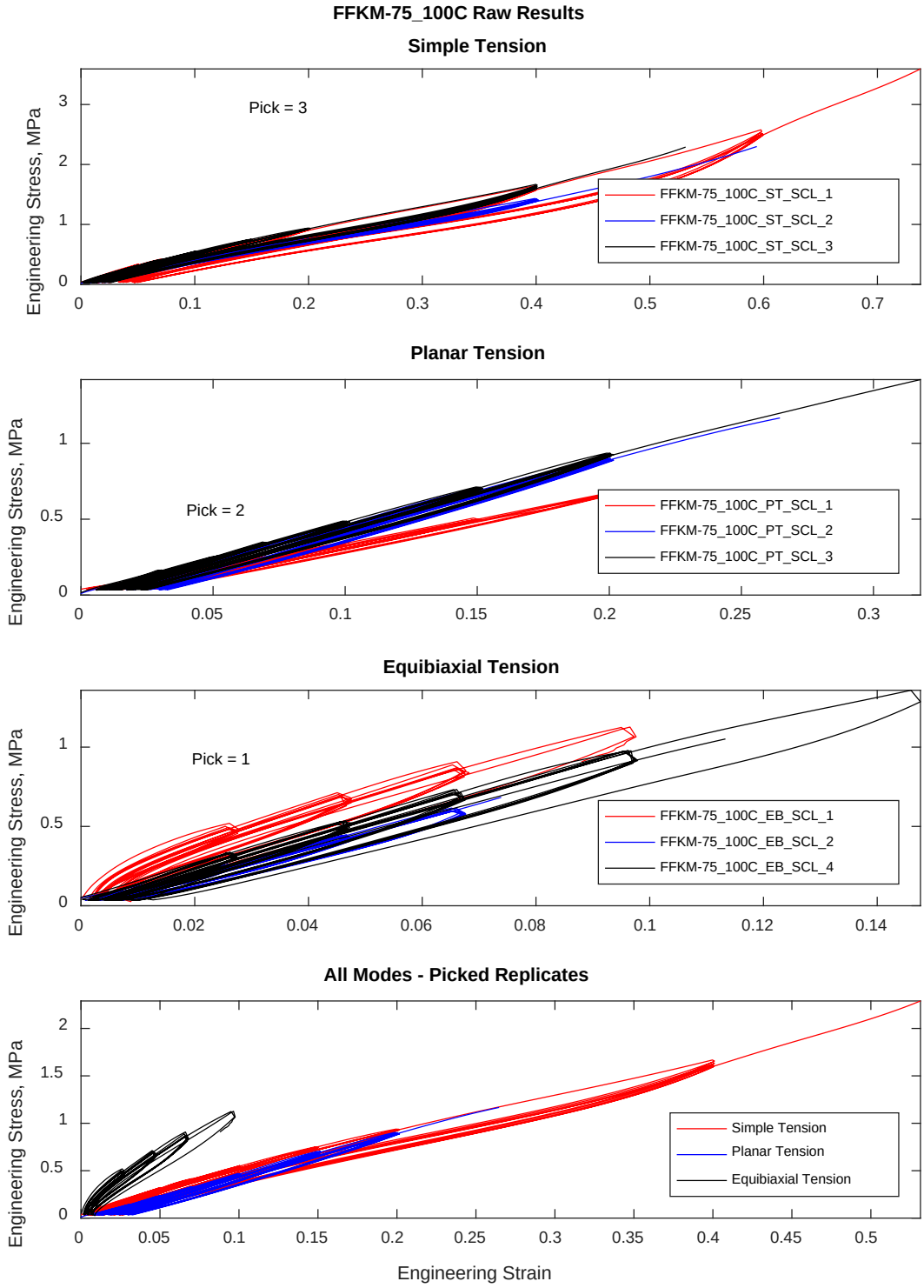
FFKM-75_100C Raw Results
Simple Tension
Pick = 3
Engineering Stress, MPa
FFKM-75_100C_ST_SCL_1
FFKM-75_100C_ST_SCL_2
FFKM-75_100C_ST_SCL_3
Planar Tension
Pick = 2
Engineering Stress, MPa
FFKM-75_100C_PT_SCL_1
FFKM-75_100C_PT_SCL_2
FFKM-75_100C_PT_SCL_3
Equibiaxial Tension
Pick = 1
Engineering Stress, MPa
FFKM-75_100C_EB_SCL_1
FFKM-75_100C_EB_SCL_2
FFKM-75_100C_EB_SCL_4
All Modes - Picked Replicates
Engineering Stress, MPa
Simple Tension
Planar Tension
Equibiaxial Tension
Engineering Strain

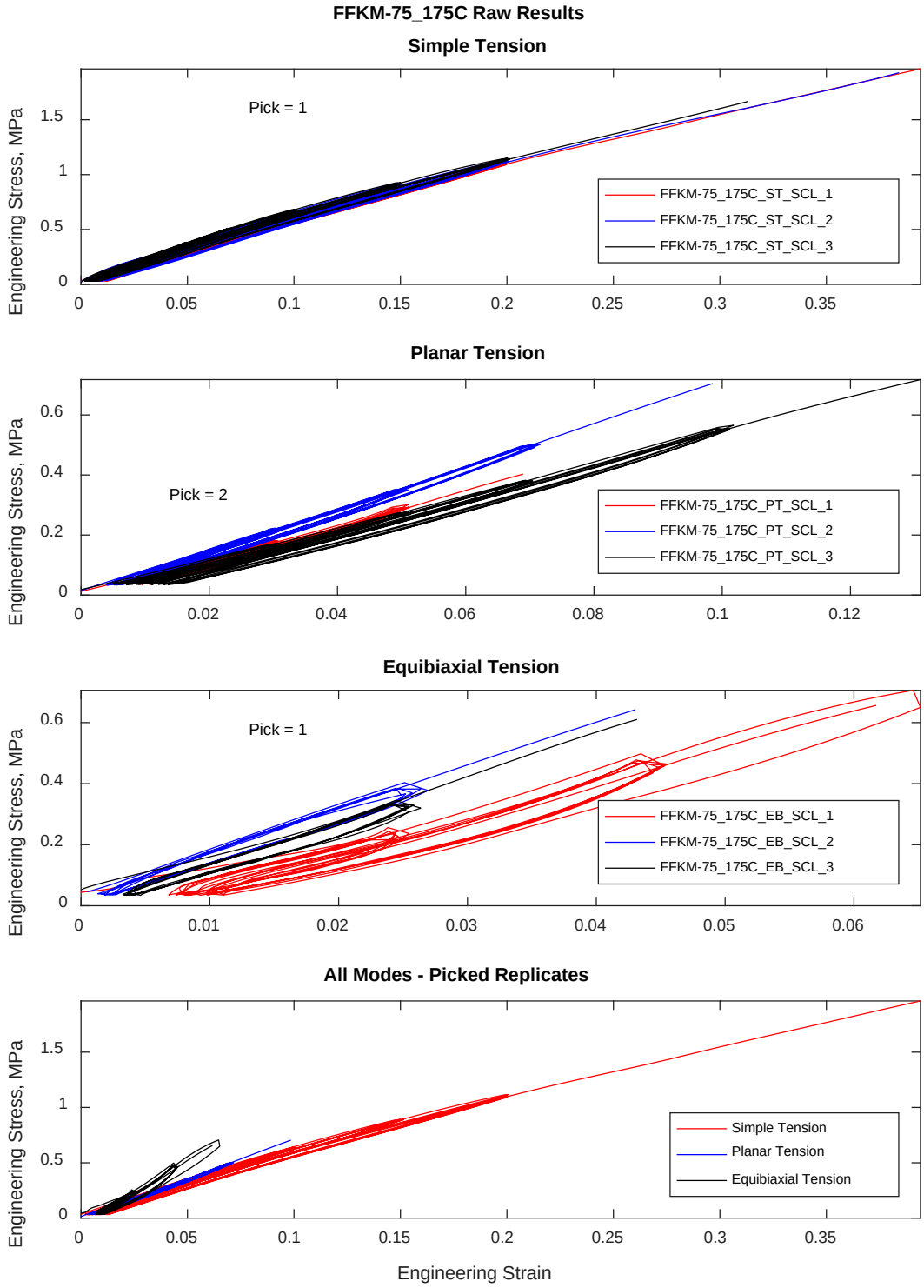
FFKM-75_175C Raw Results
Simple Tension
Pick = 1
Engineering Stress, MPa
FFKM-75_175C_ST_SCL_1
FFKM-75_175C_ST_SCL_2
FFKM-75_175C_ST_SCL_3
Planar Tension
Pick = 2
FFKM-75_175C_PT_SCL_1
FFKM-75_175C_PT_SCL_2
FFKM-75_175C_PT_SCL_3
Equibiaxial Tension
Pick = 1
FFKM-75_175C_EB_SCL_1
FFKM-75_175C_EB_SCL_2
FFKM-75_175C_EB_SCL_3
All Modes - Picked Replicates
Simple Tension
Planar Tension
Equibiaxial Tension
Engineering Strain

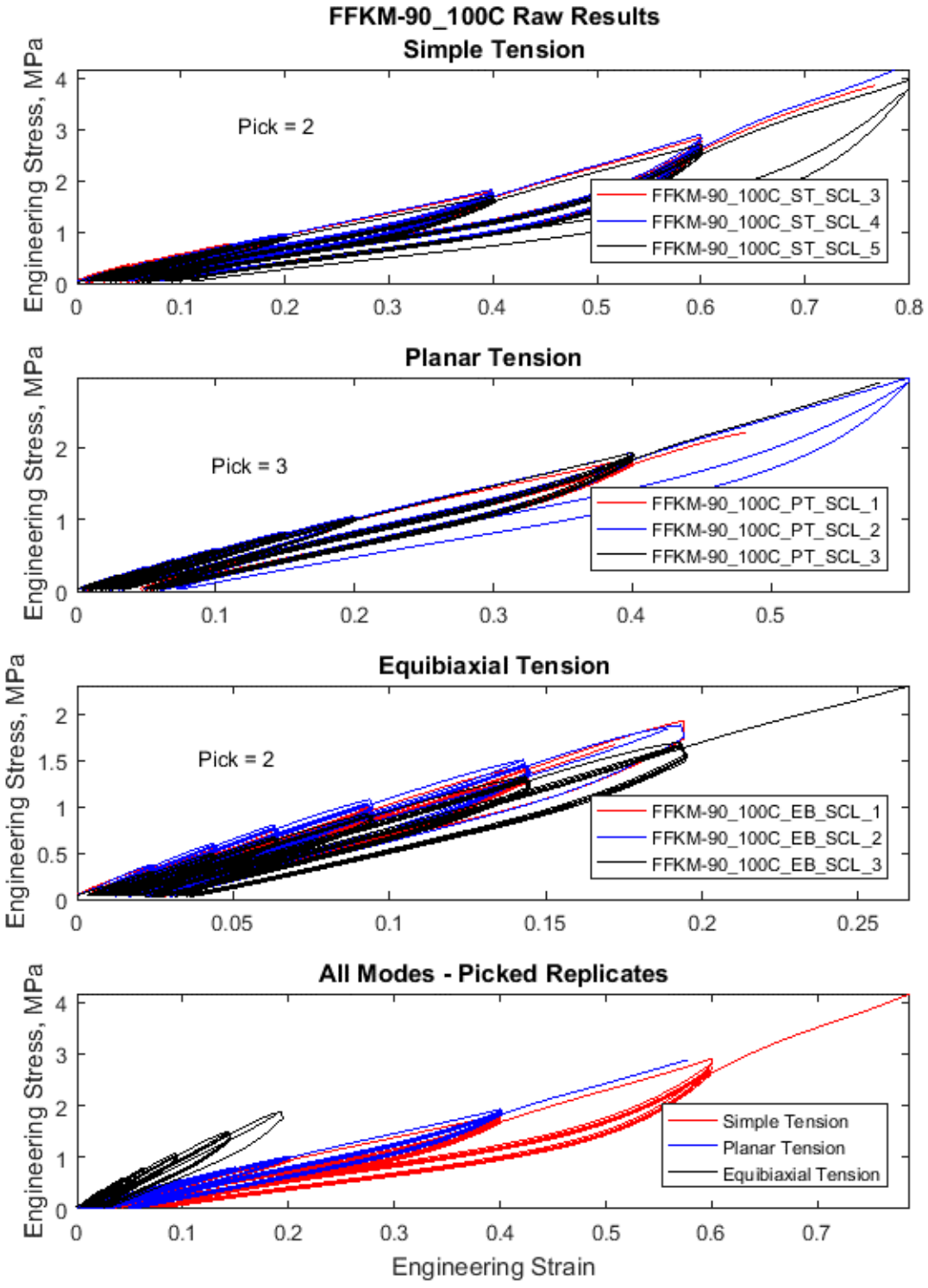
FFKM-90_100C Raw Results
Simple Tension
Engineering Stress, MPa
Pick = 2
FFKM-90_100C_ST_SCL_3
FFKM-90_100C_ST_SCL_4
FFKM-90_100C_ST_SCL_5
Planar Tension
Engineering Stress, MPa
Pick = 3
FFKM-90_100C_PT_SCL_1
FFKM-90_100C_PT_SCL_2
FFKM-90_100C_PT_SCL_3
Equibiaxial Tension
Engineering Stress, MPa
Pick = 2
FFKM-90_100C_EB_SCL_1
FFKM-90_100C_EB_SCL_2
FFKM-90_100C_EB_SCL_3
All Modes - Picked Replicates
Engineering Stress, MPa
Simple Tension
Planar Tension
Equibiaxial Tension
Engineering Strain

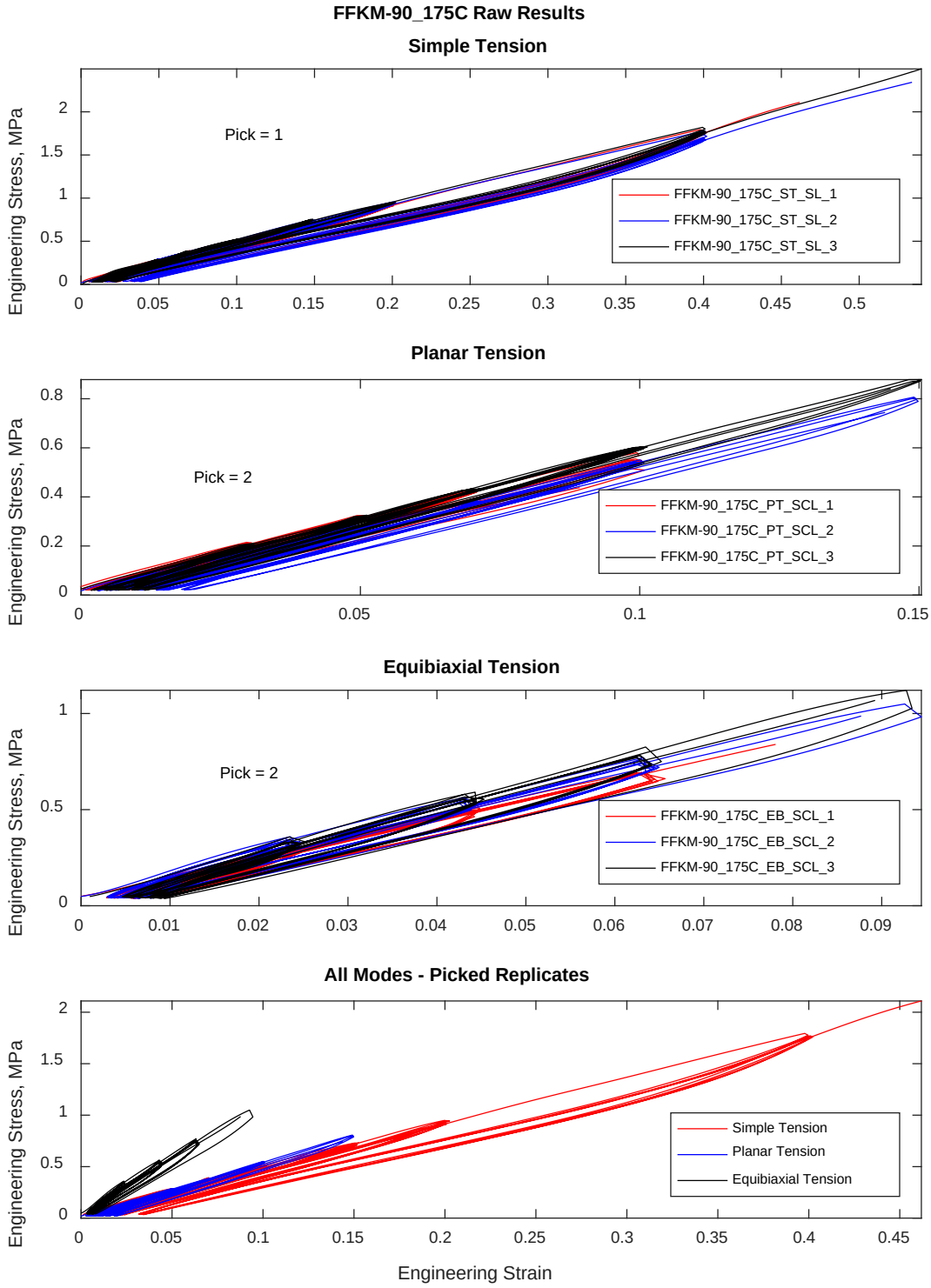
FFKM-90_175C Raw Results
Simple Tension
Pick = 1
Engineering Stress, MPa
FFKM-90_175C_ST_SL_1
FFKM-90_175C_ST_SL_2
FFKM-90_175C_ST_SL_3
Planar Tension
Pick = 2
FFKM-90_175C_PT_SCL_1
FFKM-90_175C_PT_SCL_2
FFKM-90_175C_PT_SCL_3
Equibiaxial Tension
Pick = 2
FFKM-90_175C_EB_SCL_1
FFKM-90_175C_EB_SCL_2
FFKM-90_175C_EB_SCL_3
All Modes - Picked Replicates
Simple Tension
Planar Tension
Equibiaxial Tension
Engineering Strain

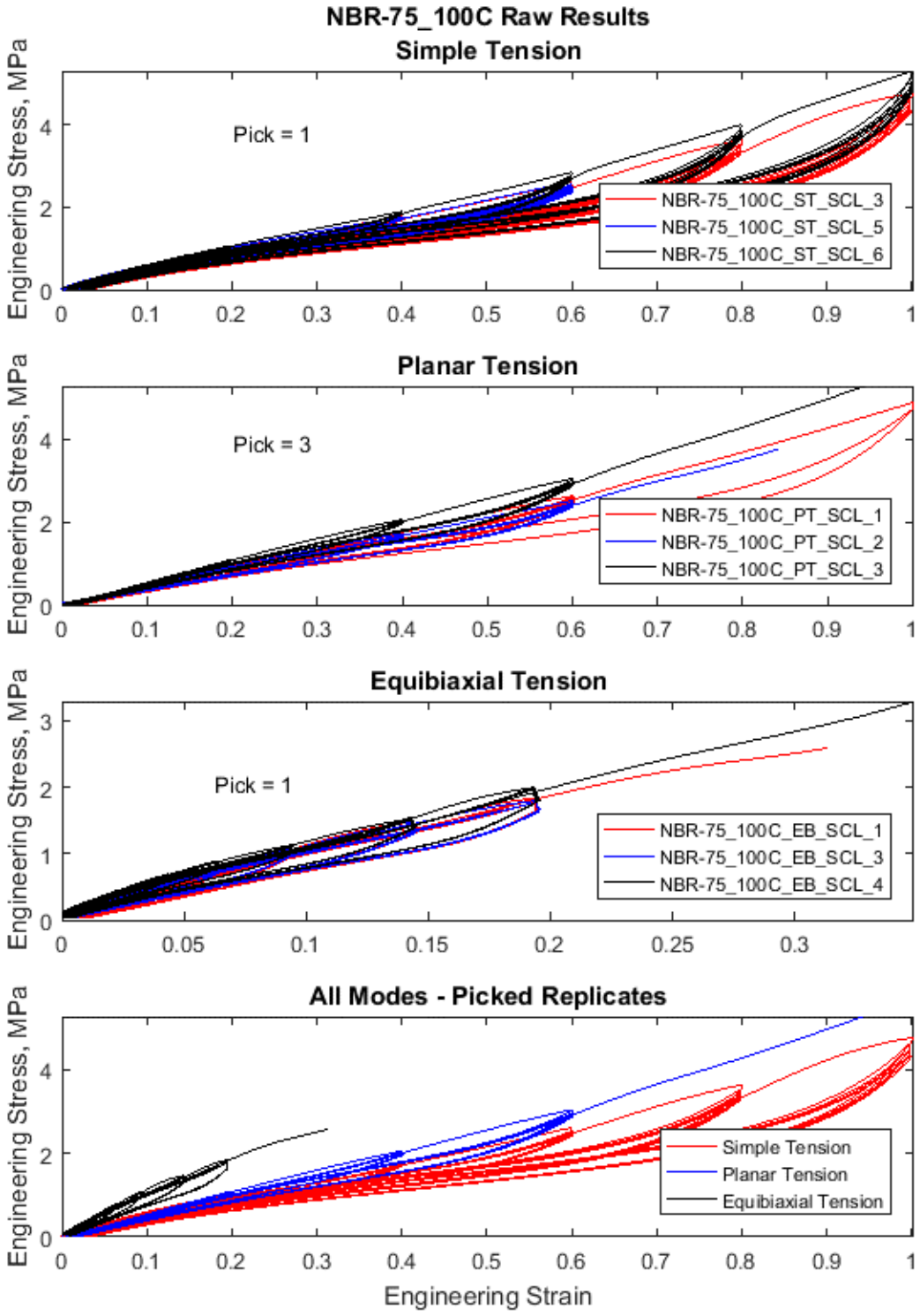
NBR-75_100C Raw Results
Simple Tension
Pick = 1
NBR-75_100C_ST_SCL_3
NBR-75_100C_ST_SCL_5
NBR-75_100C_ST_SCL_6
Planar Tension
Pick = 3
NBR-75_100C_PT_SCL_1
NBR-75_100C_PT_SCL_2
NBR-75_100C_PT_SCL_3
Equibiaxial Tension
Pick = 1
NBR-75_100C_EB_SCL_1
NBR-75_100C_EB_SCL_3
NBR-75_100C_EB_SCL_4
All Modes - Picked Replicates
Simple Tension
Planar Tension
Equibiaxial Tension
Engineering Stress, MPa
Engineering Strain

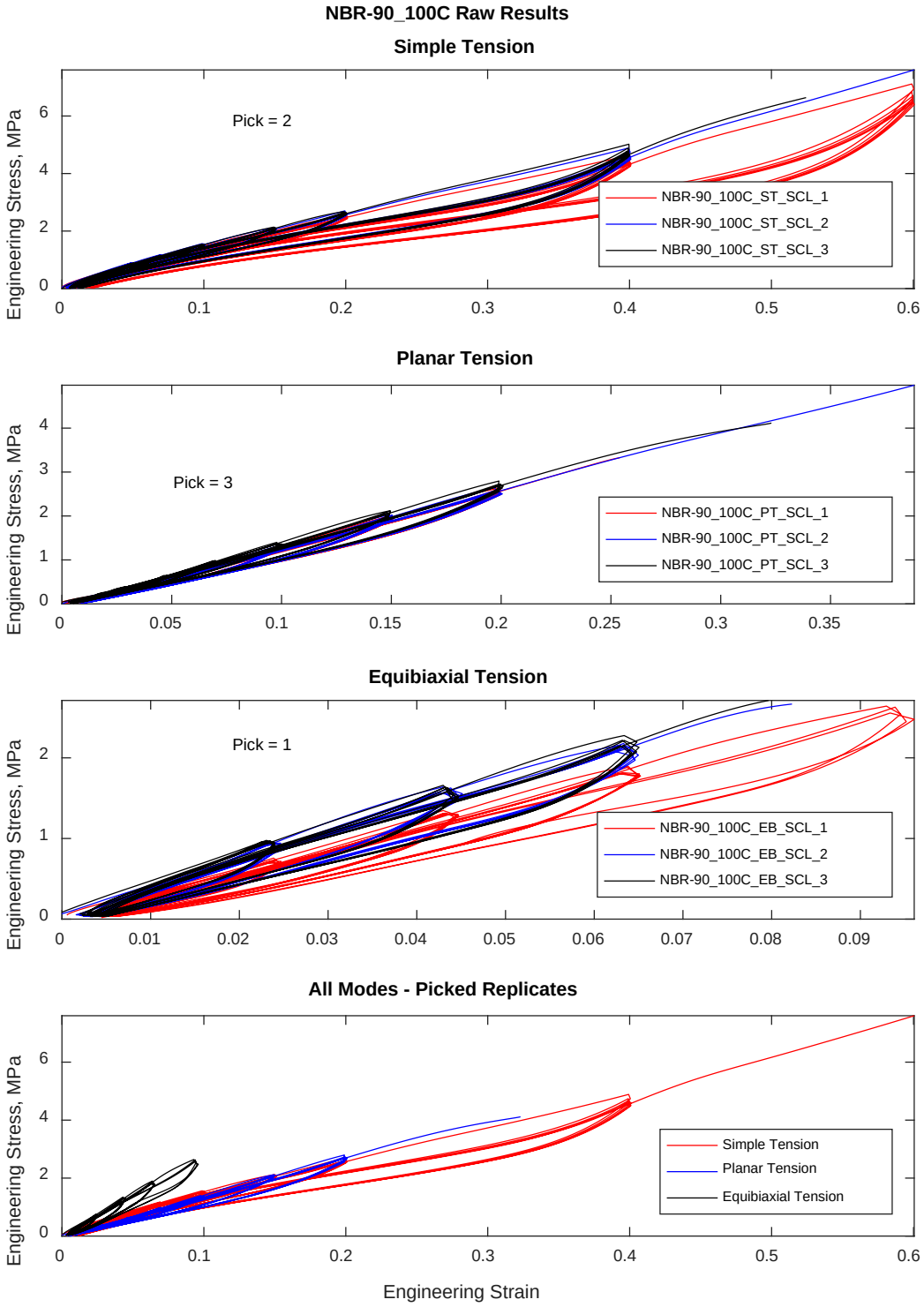
NBR-90_100C Raw Results
Simple Tension
Pick = 2
Engineering Stress, MPa
NBR-90_100C_ST_SCL_1
NBR-90_100C_ST_SCL_2
NBR-90_100C_ST_SCL_3
Planar Tension
Pick = 3
NBR-90_100C_PT_SCL_1
NBR-90_100C_PT_SCL_2
NBR-90_100C_PT_SCL_3
Equibiaxial Tension
Pick = 1
NBR-90_100C_EB_SCL_1
NBR-90_100C_EB_SCL_2
NBR-90_100C_EB_SCL_3
All Modes - Picked Replicates
Simple Tension
Planar Tension
Equibiaxial Tension
Engineering Strain

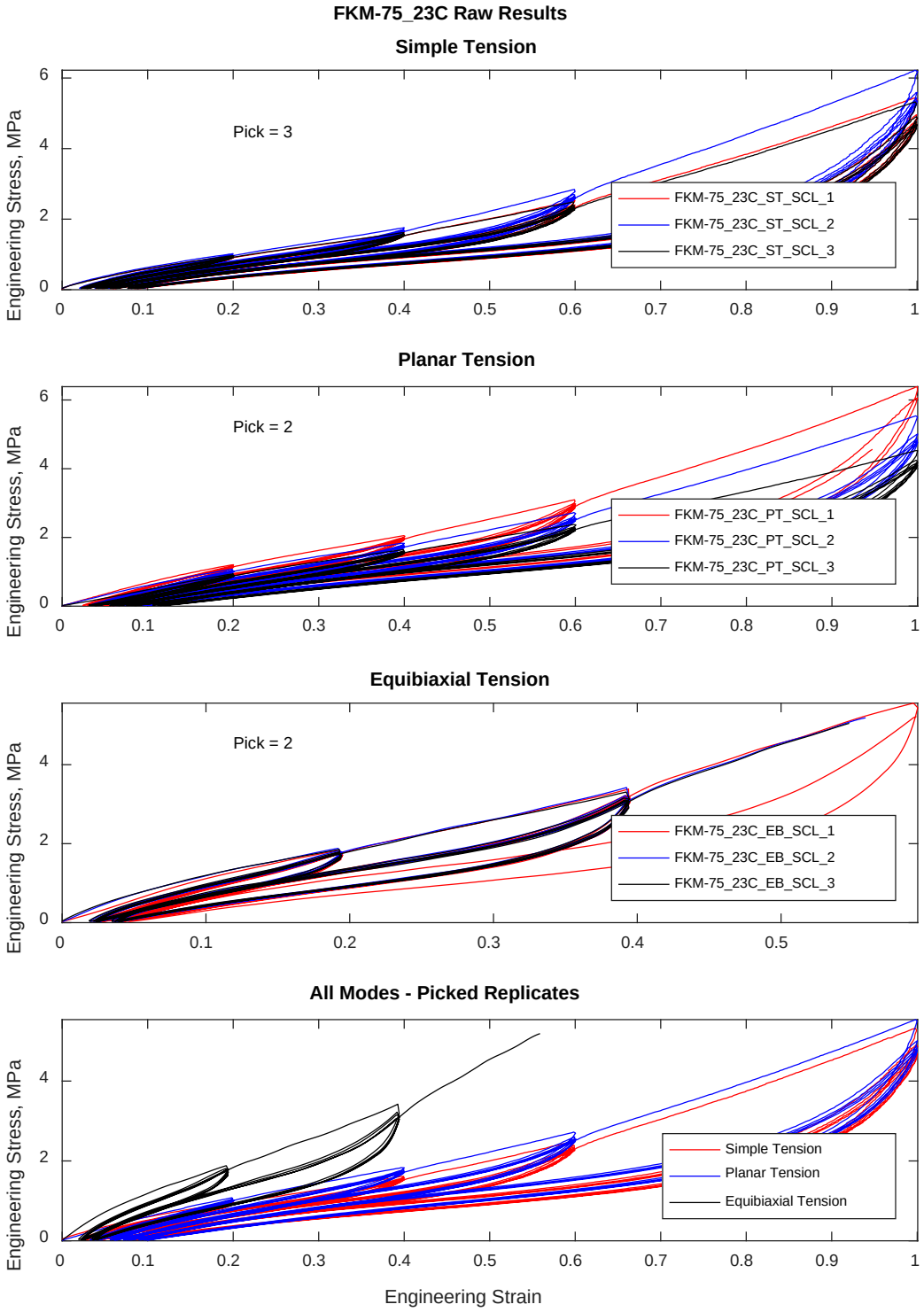
FKM-75_23C Raw Results
Simple Tension
Pick = 3
Engineering Stress, MPa
FKM-75_23C_ST_SCL_1
FKM-75_23C_ST_SCL_2
FKM-75_23C_ST_SCL_3
Planar Tension
Pick = 2
FKM-75_23C_PT_SCL_1
FKM-75_23C_PT_SCL_2
FKM-75_23C_PT_SCL_3
Equibiaxial Tension
Pick = 2
FKM-75_23C_EB_SCL_1
FKM-75_23C_EB_SCL_2
FKM-75_23C_EB_SCL_3
All Modes - Picked Replicates
Simple Tension
Planar Tension
Equibiaxial Tension
Engineering Strain

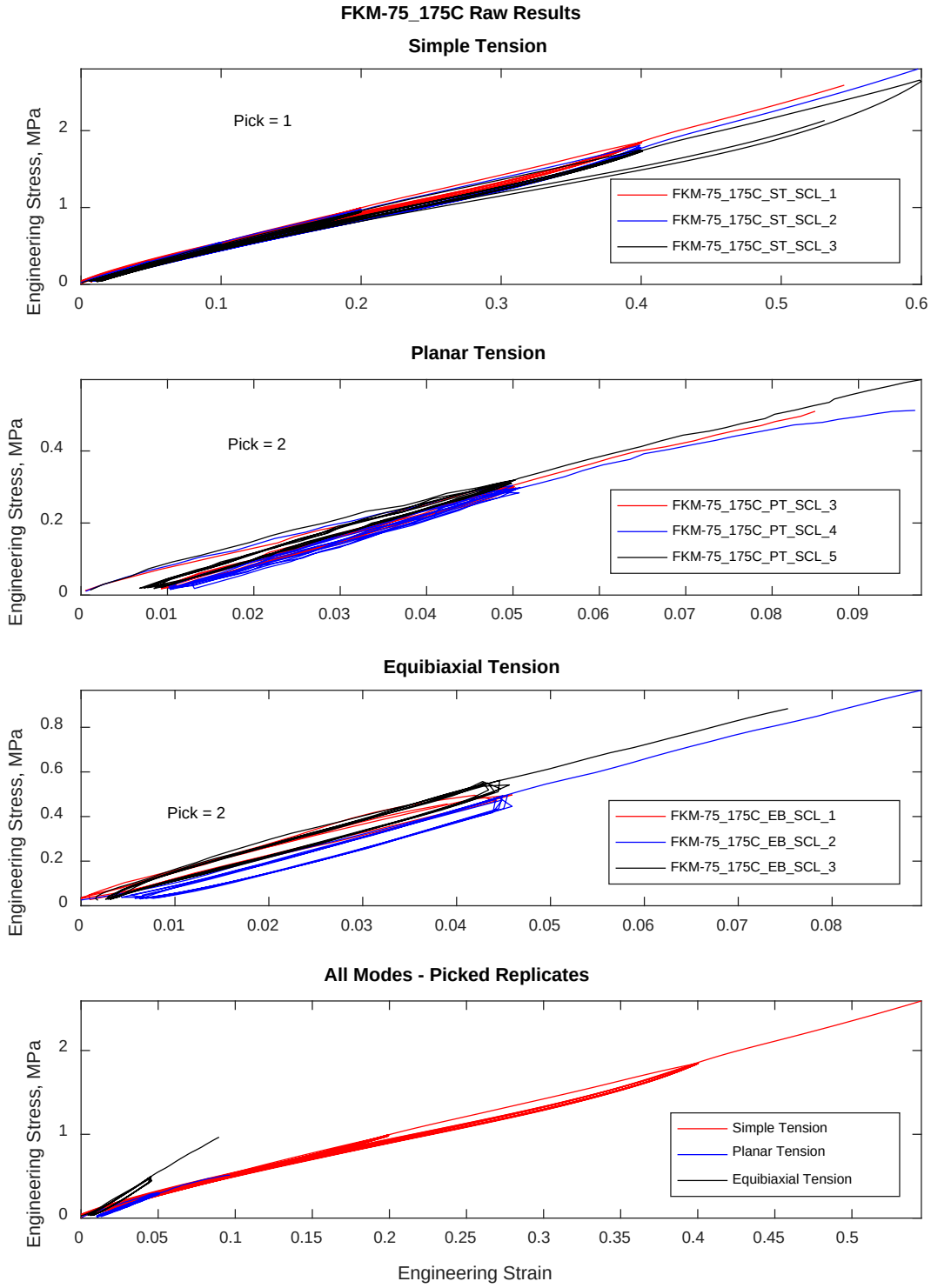
FKM-75_175C Raw Results
Simple Tension
Pick = 1
Engineering Stress, MPa
FKM-75_175C_ST_SCL_1
FKM-75_175C_ST_SCL_2
FKM-75_175C_ST_SCL_3
Planar Tension
Pick = 2
Engineering Stress, MPa
FKM-75_175C_PT_SCL_3
FKM-75_175C_PT_SCL_4
FKM-75_175C_PT_SCL_5
Equibiaxial Tension
Pick = 2
Engineering Stress, MPa
FKM-75_175C_EB_SCL_1
FKM-75_175C_EB_SCL_2
FKM-75_175C_EB_SCL_3
All Modes - Picked Replicates
Engineering Stress, MPa
Simple Tension
Planar Tension
Equibiaxial Tension
Engineering Strain

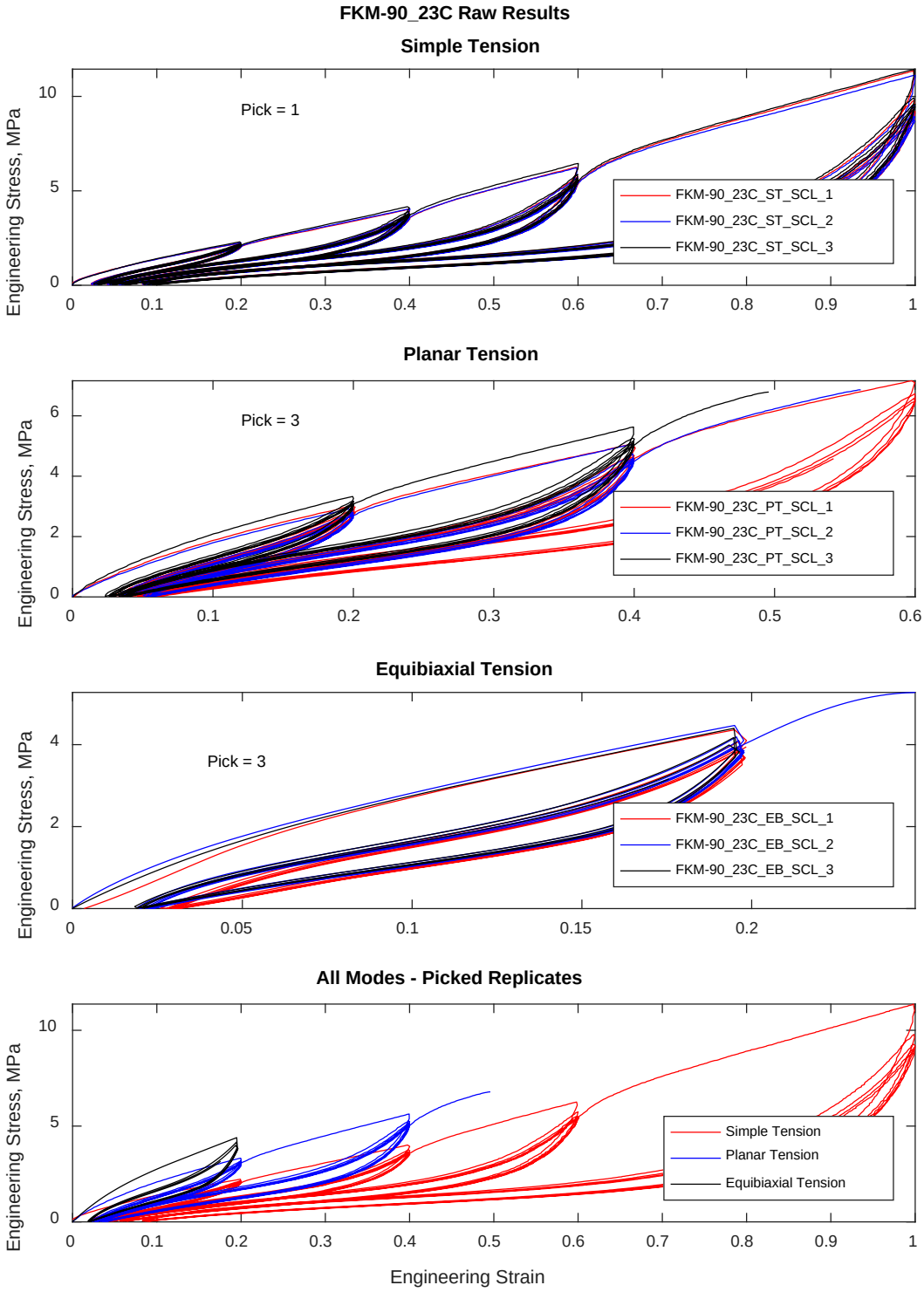
FKM-90_23C Raw Results
Simple Tension
Pick = 1
Engineering Stress, MPa
FKM-90_23C_ST_SCL_1
FKM-90_23C_ST_SCL_2
FKM-90_23C_ST_SCL_3
Planar Tension
Pick = 3
Engineering Stress, MPa
FKM-90_23C_PT_SCL_1
FKM-90_23C_PT_SCL_2
FKM-90_23C_PT_SCL_3
Equibiaxial Tension
Pick = 3
Engineering Stress, MPa
FKM-90_23C_EB_SCL_1
FKM-90_23C_EB_SCL_2
FKM-90_23C_EB_SCL_3
All Modes - Picked Replicates
Engineering Stress, MPa
Simple Tension
Planar Tension
Equibiaxial Tension
Engineering Strain

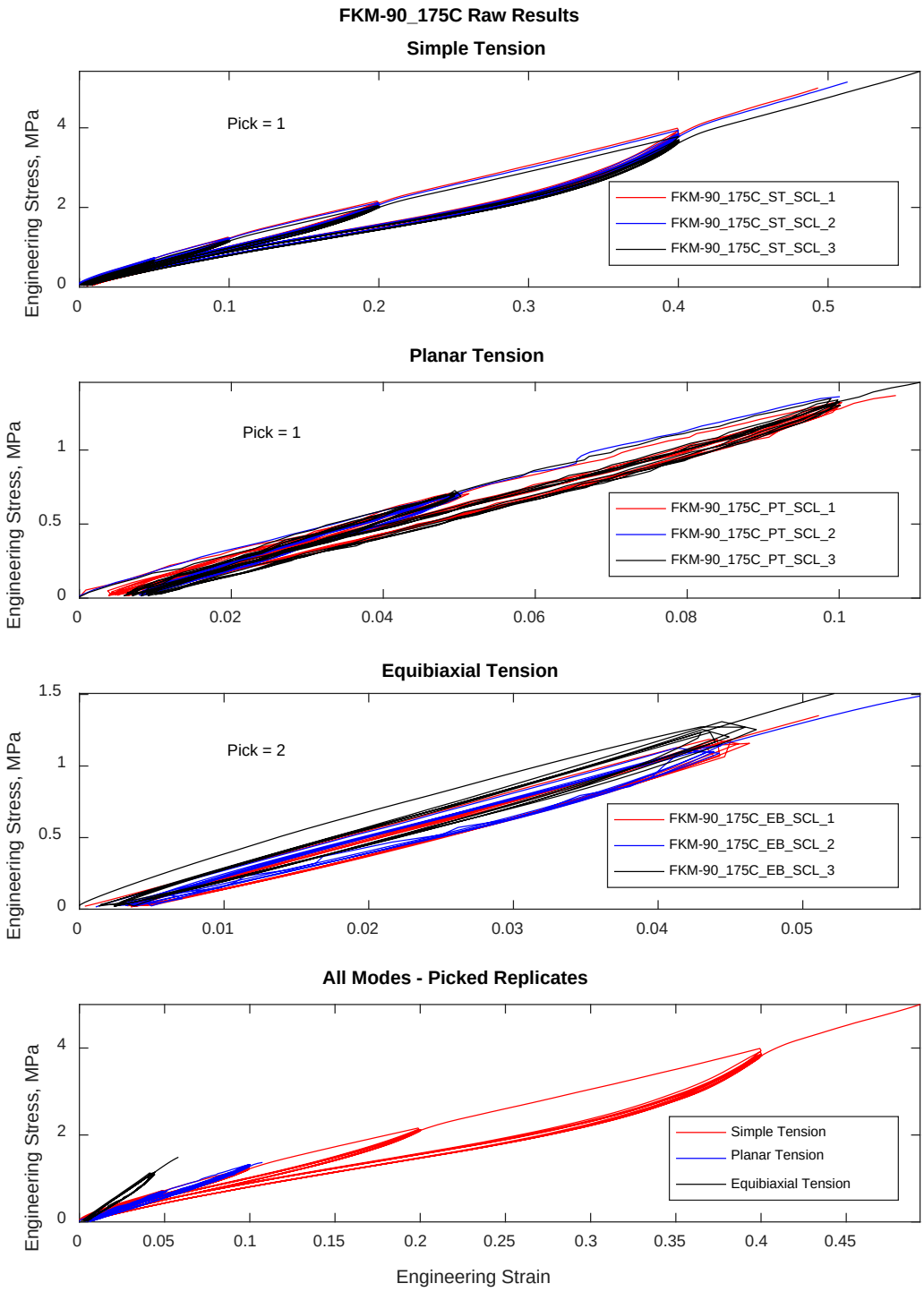


Figure A.4-2. Raw results for simple, planar, and equibiaxial tension.

## *Analysis 1 – Hyperelastic Law Parameters*

Purpose: The hyperelastic law is used to define reversible stress-strain behavior of an elastomer for finite element analysis. In cases involving cyclic loading, it may also be used to define the monotonic stress-strain curve.

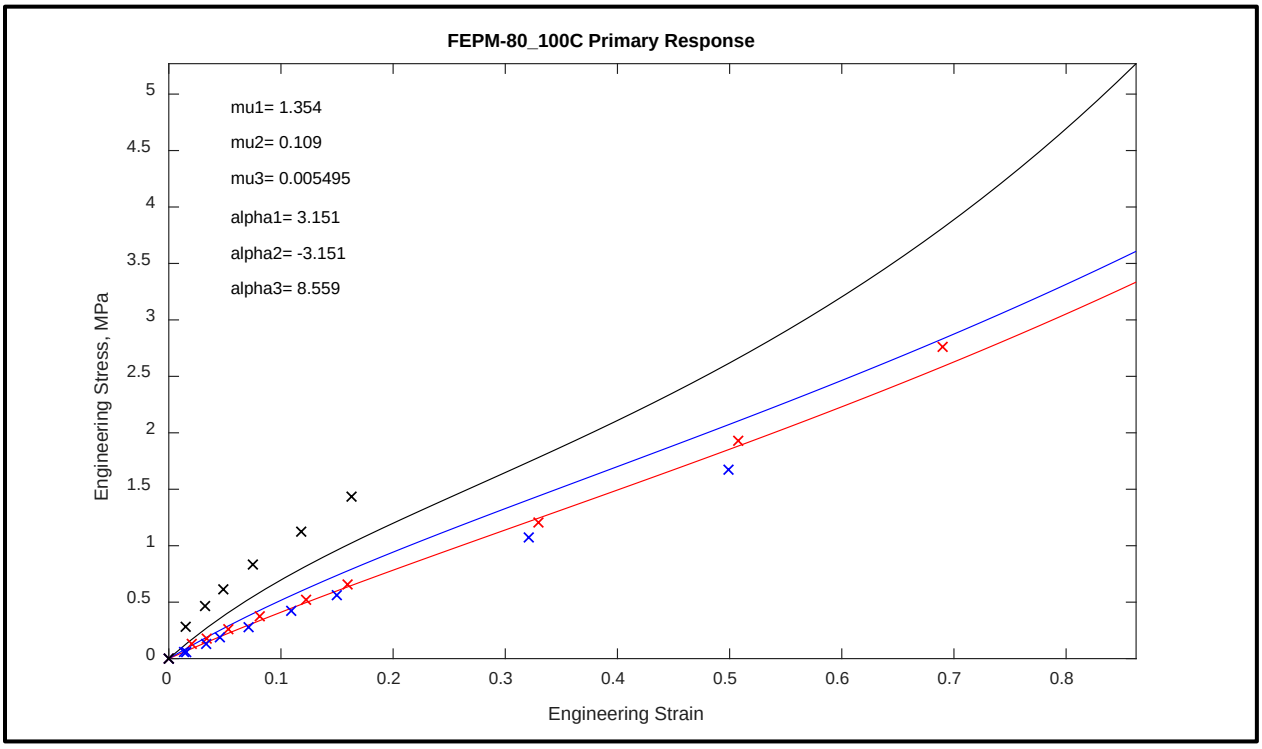

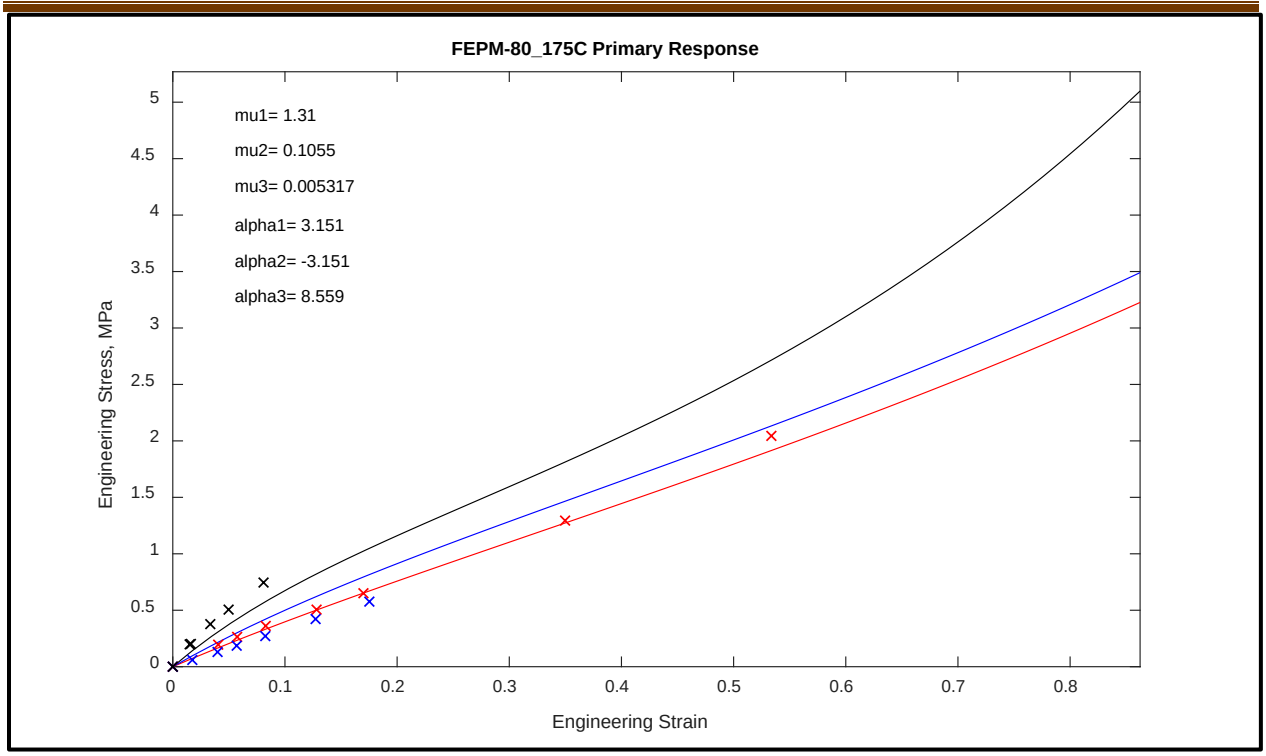
FEPM-80_175C Primary Response
mu1= 1.31
mu2= 0.1055
mu3= 0.005317
alpha1= 3.151
alpha2= -3.151
alpha3= 8.559
Engineering Stress, MPa
Engineering Strain
0
0.5
1
1.5
2
2.5
3
3.5
4
4.5
5
0.1
0.2
0.3
0.4
0.5
0.6
0.7
0.8

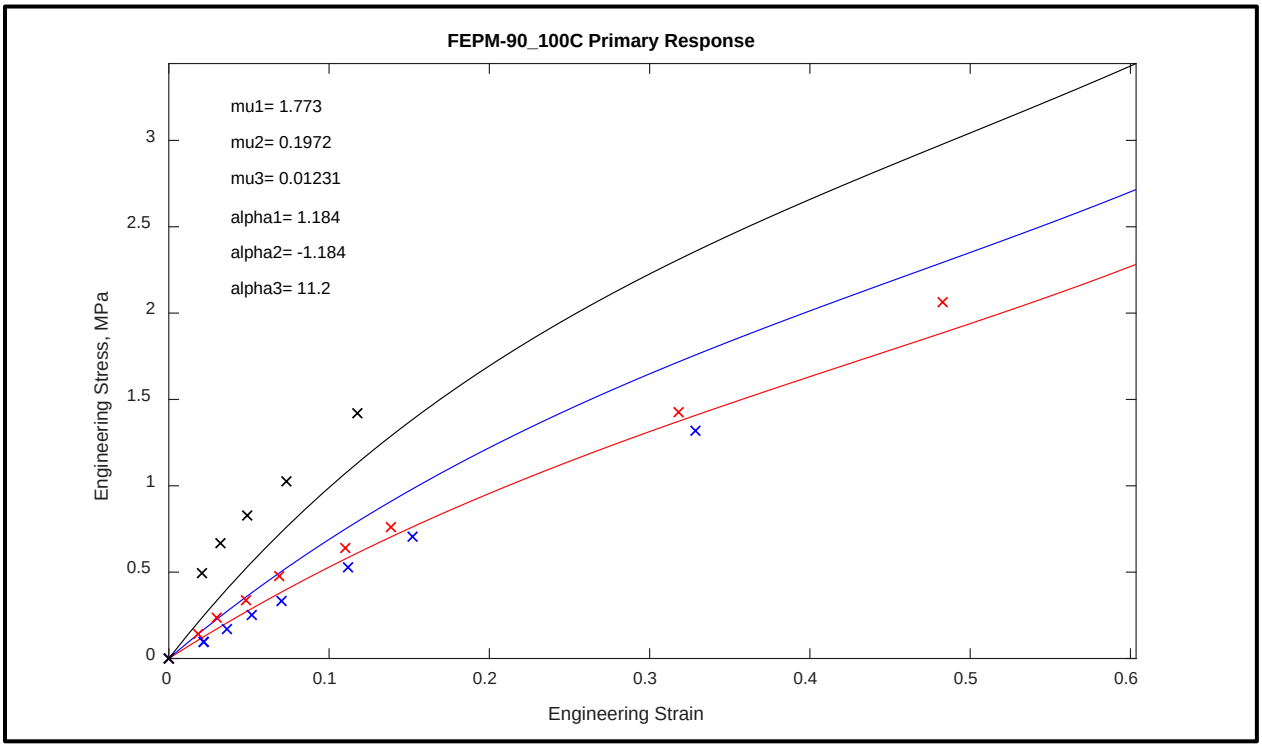
FEPM-90_100C Primary Response
mu1= 1.773
mu2= 0.1972
mu3= 0.01231
alpha1= 1.184
alpha2= -1.184
alpha3= 11.2
Engineering Stress, MPa
Engineering Strain
0
0.5
1
1.5
2
2.5
3
0.1
0.2
0.3
0.4
0.5
0.6

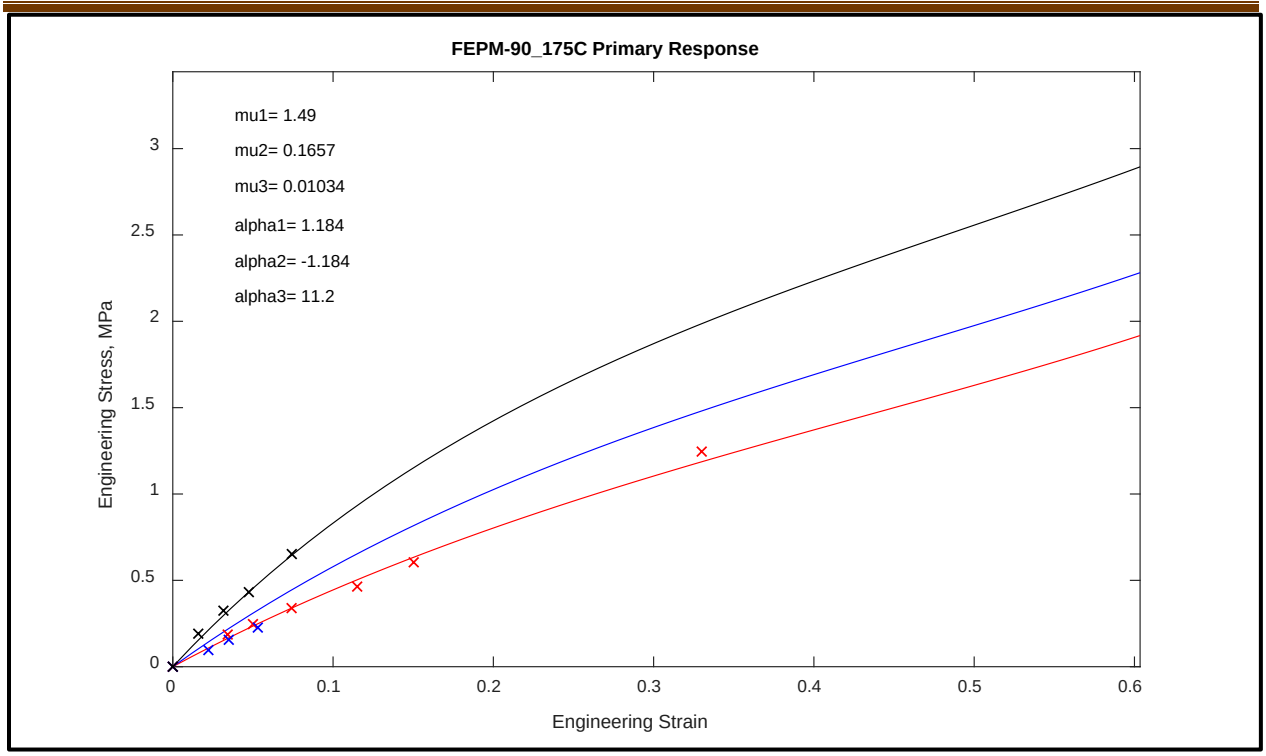
FEPM-90_175C Primary Response
mu1= 1.49
mu2= 0.1657
mu3= 0.01034
alpha1= 1.184
alpha2= -1.184
alpha3= 11.2
Engineering Stress, MPa
Engineering Strain
0
0.5
1
1.5
2
2.5
3
0.1
0.2
0.3
0.4
0.5
0.6

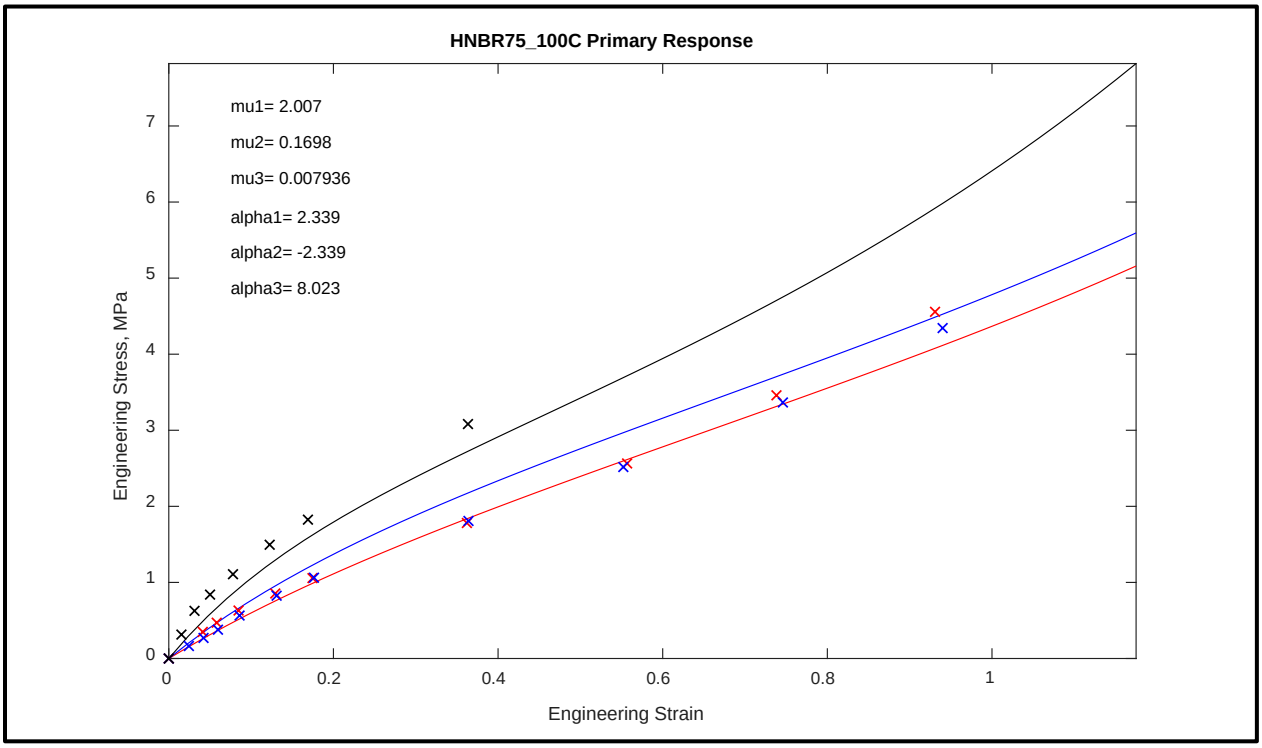
HNBR75_100C Primary Response
mu1= 2.007
mu2= 0.1698
mu3= 0.007936
alpha1= 2.339
alpha2= -2.339
alpha3= 8.023
Engineering Stress, MPa
Engineering Strain
0
1
2
3
4
5
6
7
0.2
0.4
0.6
0.8
1

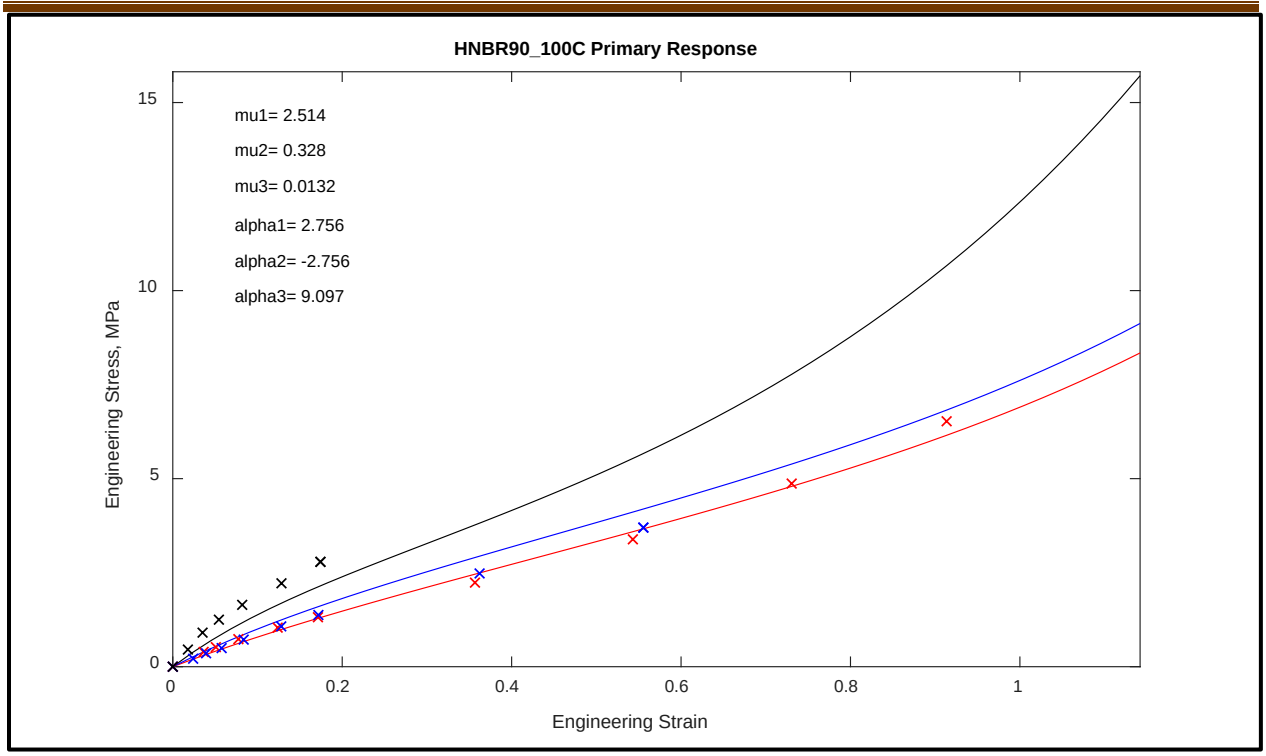
HNBR90_100C Primary Response
mu1= 2.514
mu2= 0.328
mu3= 0.0132
alpha1= 2.756
alpha2= -2.756
alpha3= 9.097
Engineering Stress, MPa
Engineering Strain
0
5
10
15
0
0.2
0.4
0.6
0.8
1

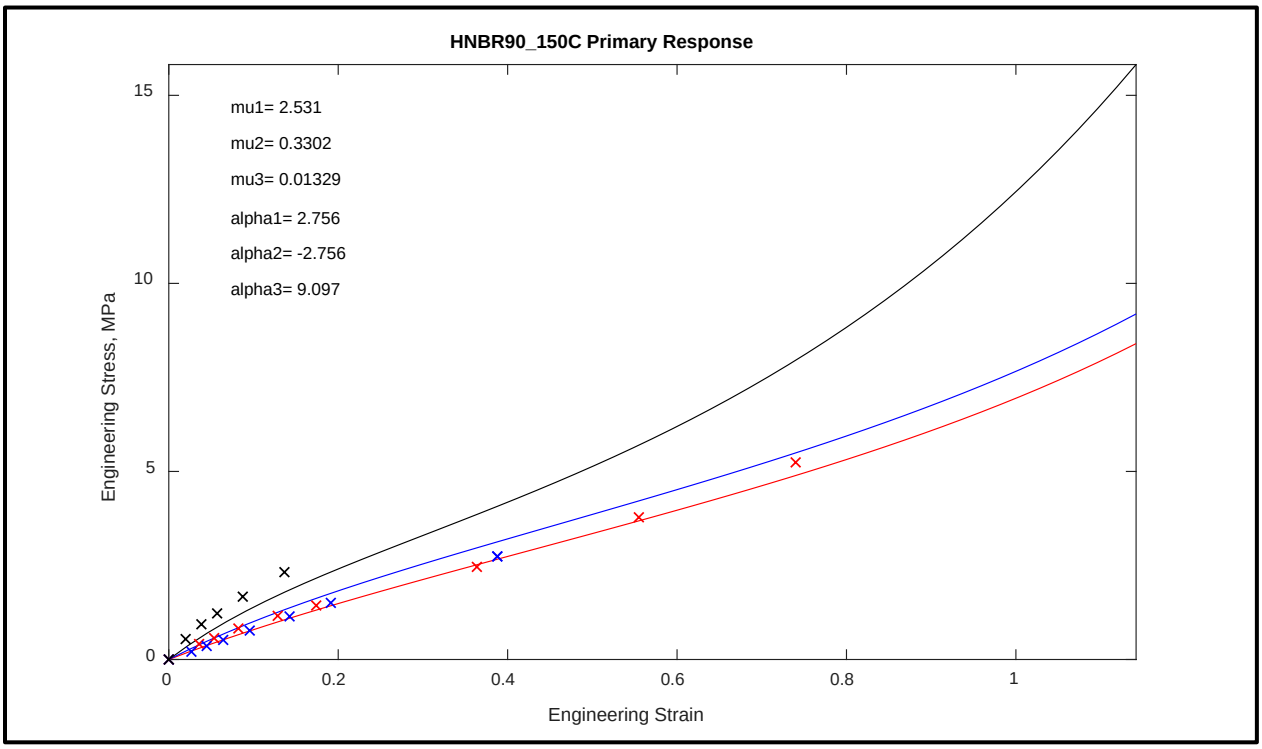
HNBR90_150C Primary Response
mu1= 2.531
mu2= 0.3302
mu3= 0.01329
alpha1= 2.756
alpha2= -2.756
alpha3= 9.097
Engineering Stress, MPa
Engineering Strain
0
5
10
15
0
0.2
0.4
0.6
0.8
1

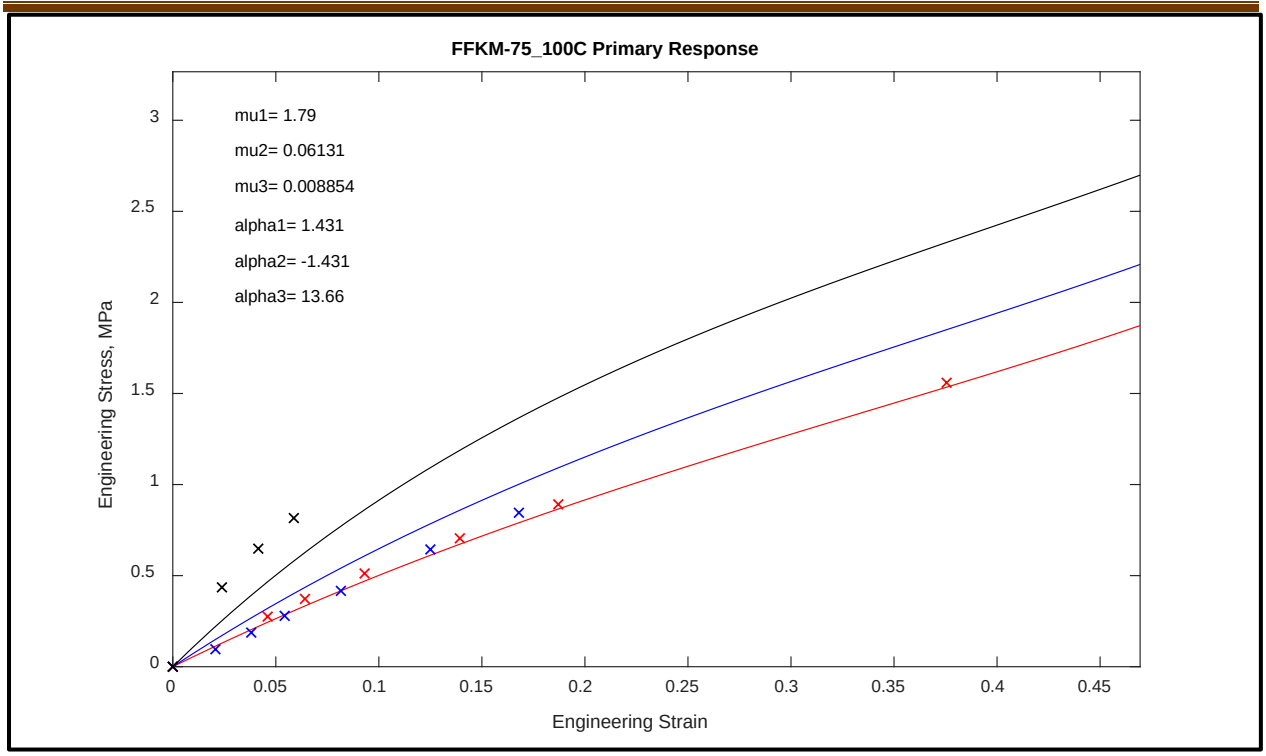
FFKM-75_100C Primary Response
mu1= 1.79
mu2= 0.06131
mu3= 0.008854
alpha1= 1.431
alpha2= -1.431
alpha3= 13.66
Engineering Stress, MPa
Engineering Strain
0
0.5
1
1.5
2
2.5
3
0.05
0.1
0.15
0.2
0.25
0.3
0.35
0.4
0.45

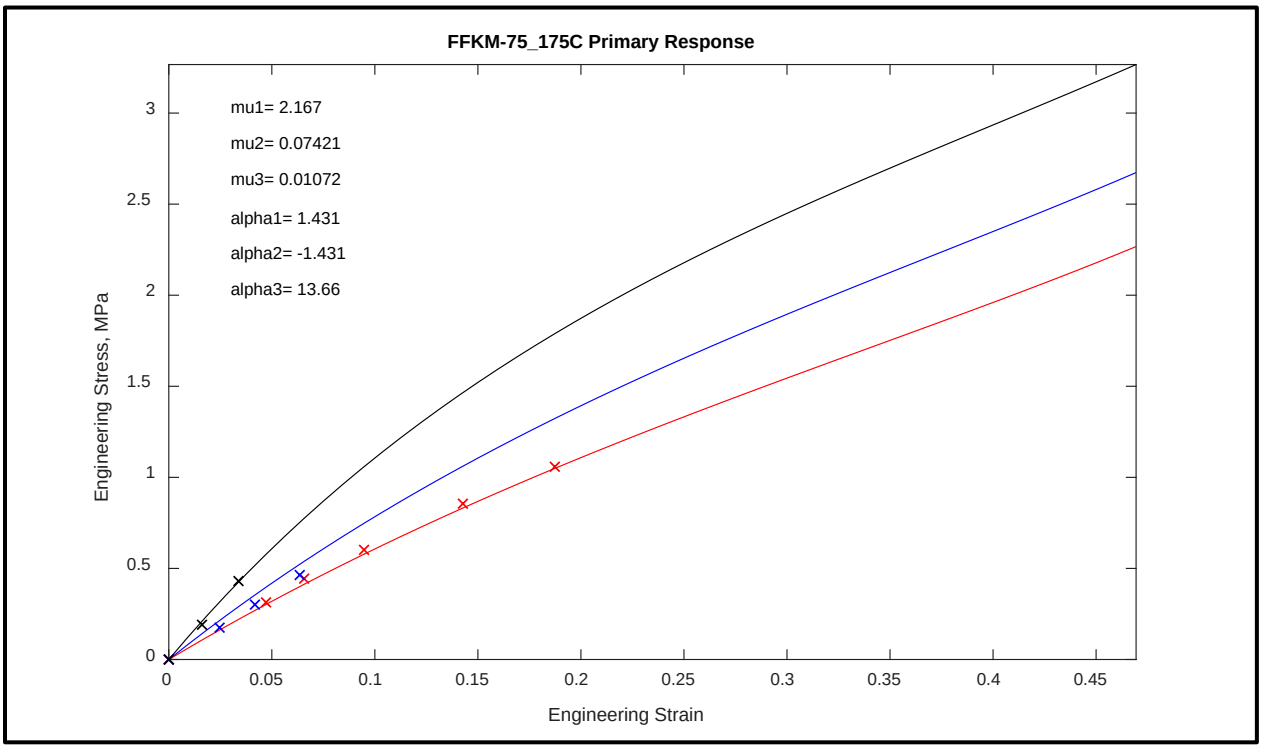
FFKM-75_175C Primary Response
mu1= 2.167
mu2= 0.07421
mu3= 0.01072
alpha1= 1.431
alpha2= -1.431
alpha3= 13.66
Engineering Stress, MPa
Engineering Strain
0
0.5
1
1.5
2
2.5
3
0.05
0.1
0.15
0.2
0.25
0.3
0.35
0.4
0.45

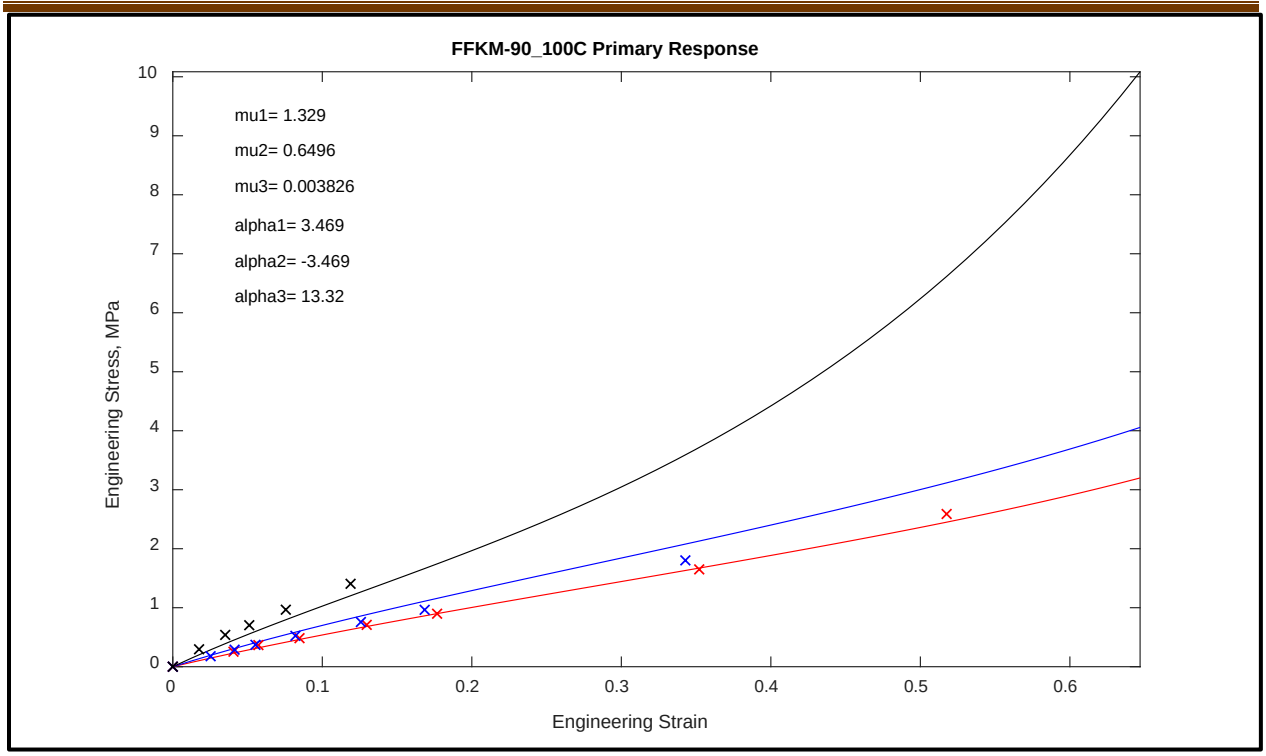
FFKM-90_100C Primary Response
mu1= 1.329
mu2= 0.6496
mu3= 0.003826
alpha1= 3.469
alpha2= -3.469
alpha3= 13.32
Engineering Stress, MPa
Engineering Strain
0
1
2
3
4
5
6
7
8
9
10
0
0.1
0.2
0.3
0.4
0.5
0.6

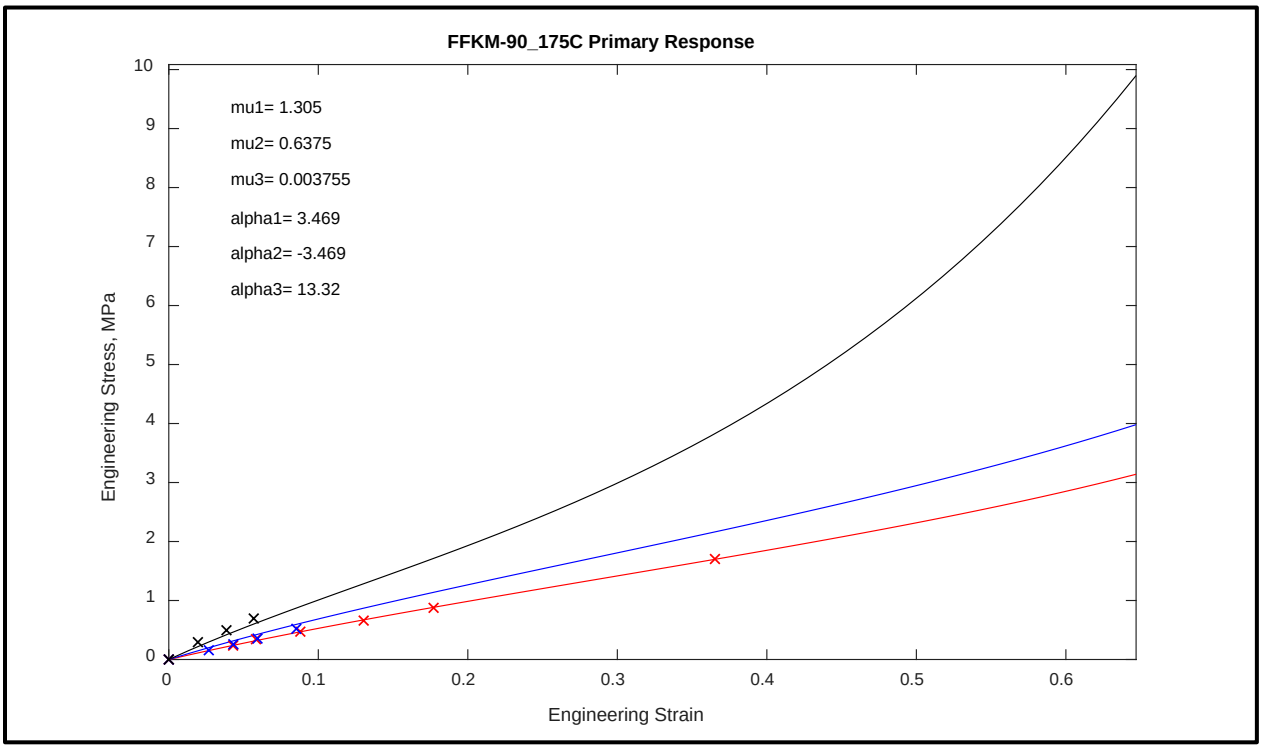
FFKM-90_175C Primary Response
mu1= 1.305
mu2= 0.6375
mu3= 0.003755
alpha1= 3.469
alpha2= -3.469
alpha3= 13.32
Engineering Stress, MPa
Engineering Strain
0
1
2
3
4
5
6
7
8
9
10
0
0.1
0.2
0.3
0.4
0.5
0.6

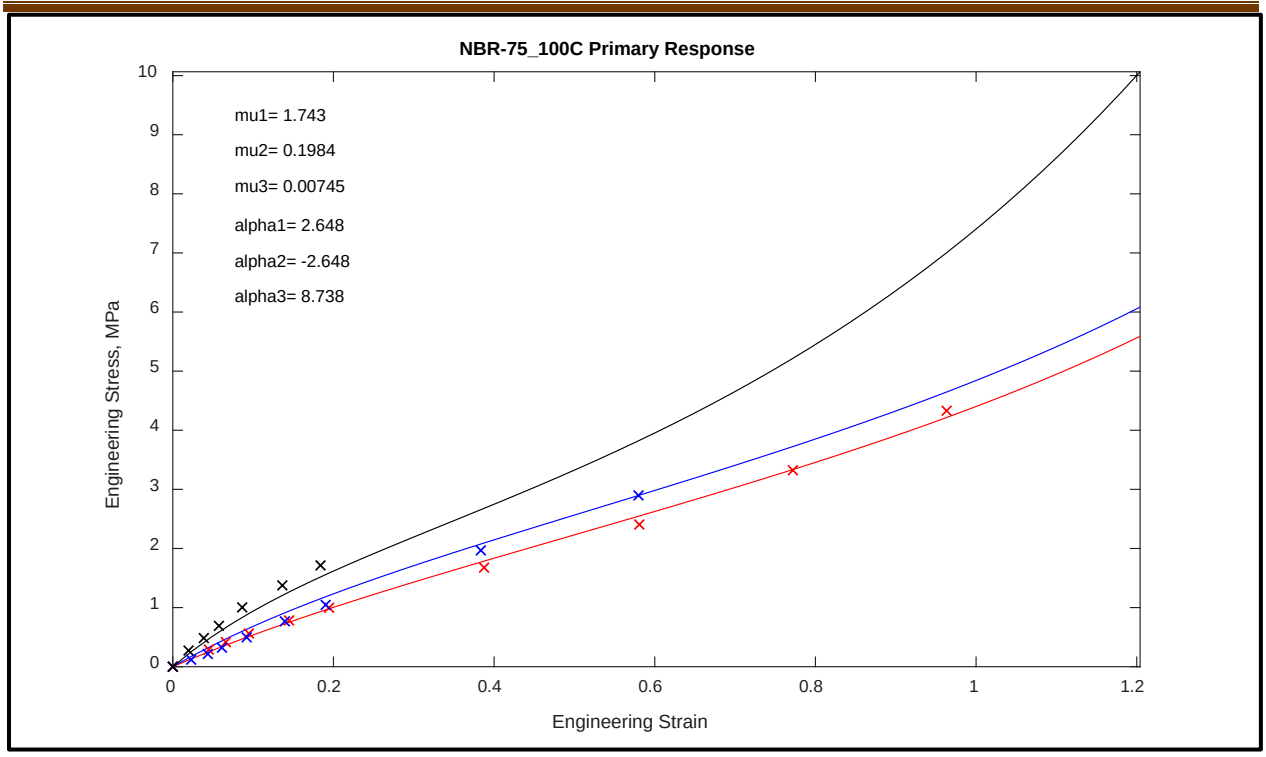
NBR-75_100C Primary Response
mu1= 1.743
mu2= 0.1984
mu3= 0.00745
alpha1= 2.648
alpha2= -2.648
alpha3= 8.738
Engineering Stress, MPa
Engineering Strain
0
1
2
3
4
5
6
7
8
9
10
0.2
0.4
0.6
0.8
1
1.2

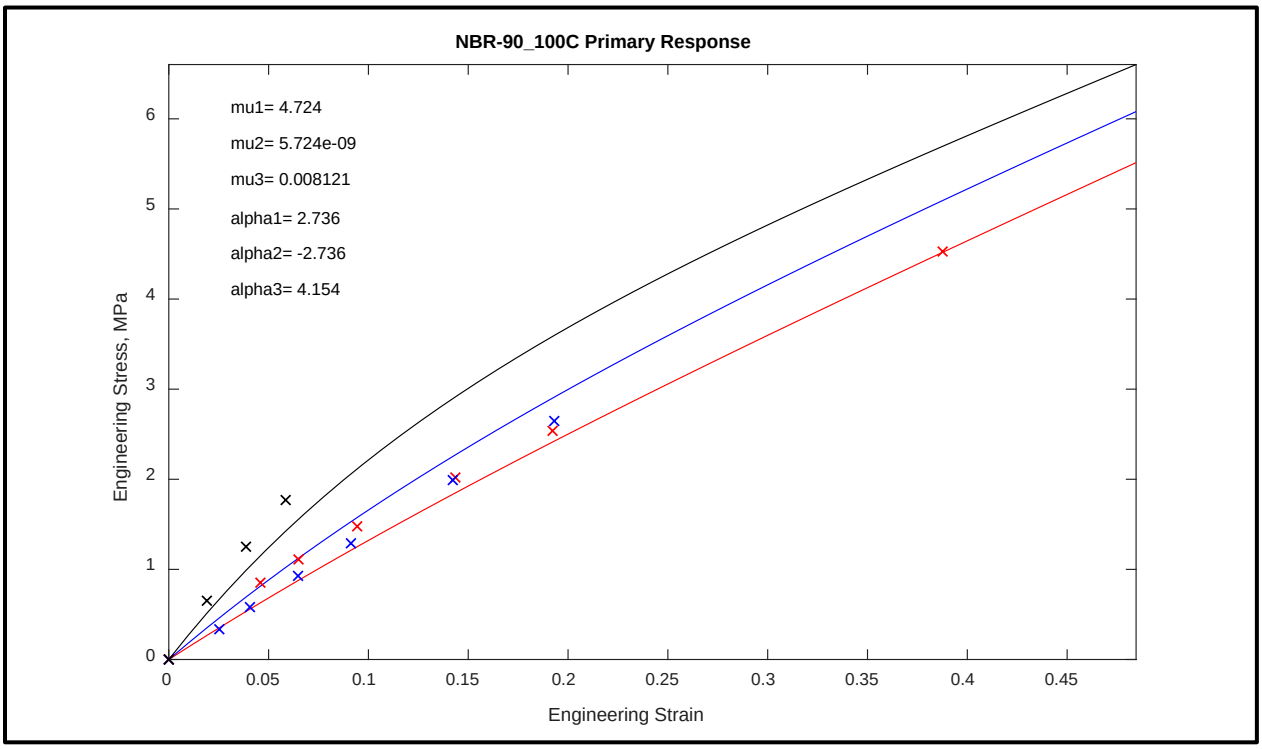
NBR-90_100C Primary Response
mu1= 4.724
mu2= 5.724e-09
mu3= 0.008121
alpha1= 2.736
alpha2= -2.736
alpha3= 4.154
Engineering Stress, MPa
Engineering Strain
0
1
2
3
4
5
6
0.05
0.1
0.15
0.2
0.25
0.3
0.35
0.4
0.45

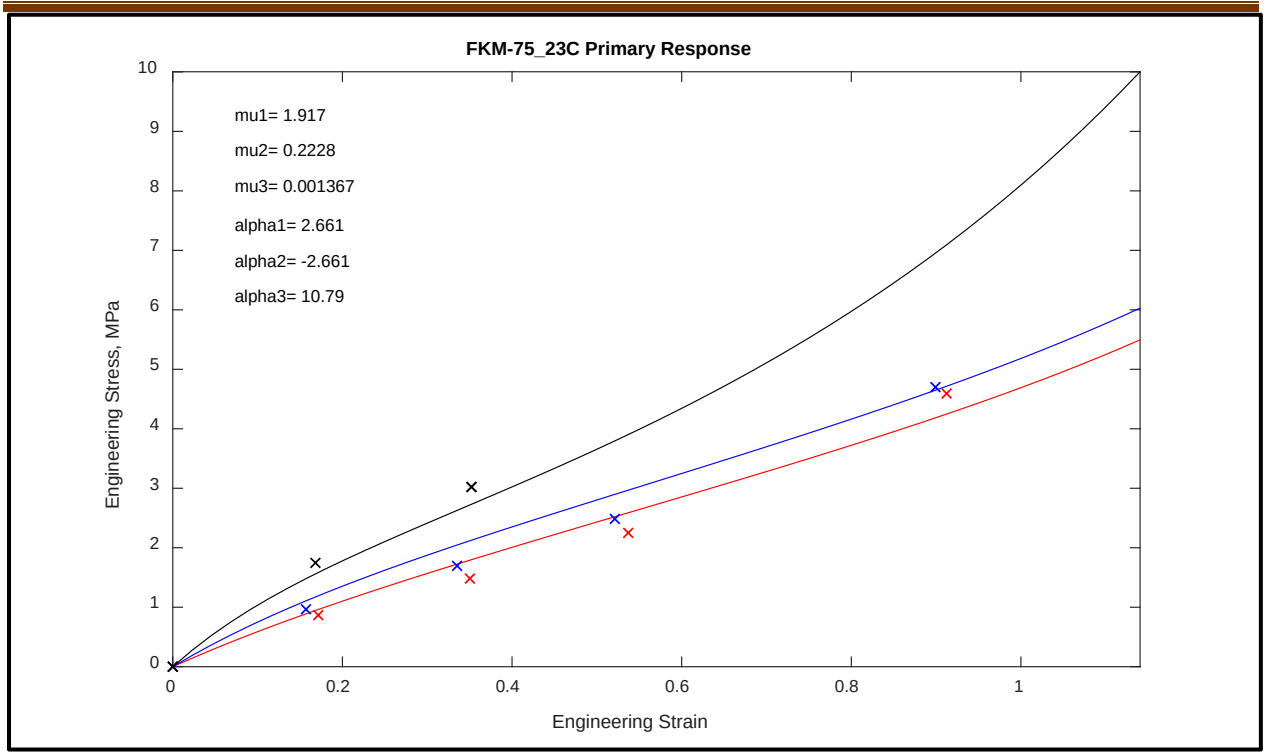
FKM-75_23C Primary Response
mu1= 1.917
mu2= 0.2228
mu3= 0.001367
alpha1= 2.661
alpha2= -2.661
alpha3= 10.79
Engineering Stress, MPa
Engineering Strain
0
1
2
3
4
5
6
7
8
9
10
0
0.2
0.4
0.6
0.8
1

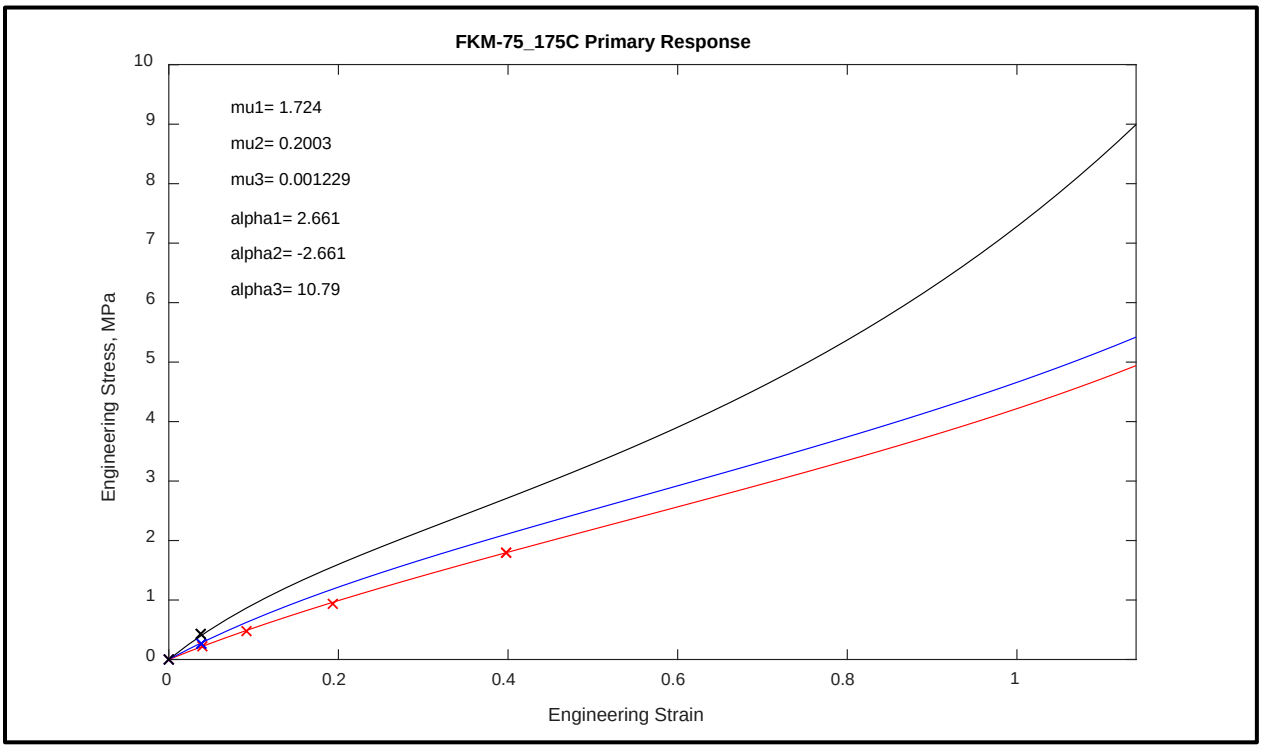
FKM-75_175C Primary Response
mu1= 1.724
mu2= 0.2003
mu3= 0.001229
alpha1= 2.661
alpha2= -2.661
alpha3= 10.79
Engineering Stress, MPa
Engineering Strain
0
1
2
3
4
5
6
7
8
9
10
0
0.2
0.4
0.6
0.8
1

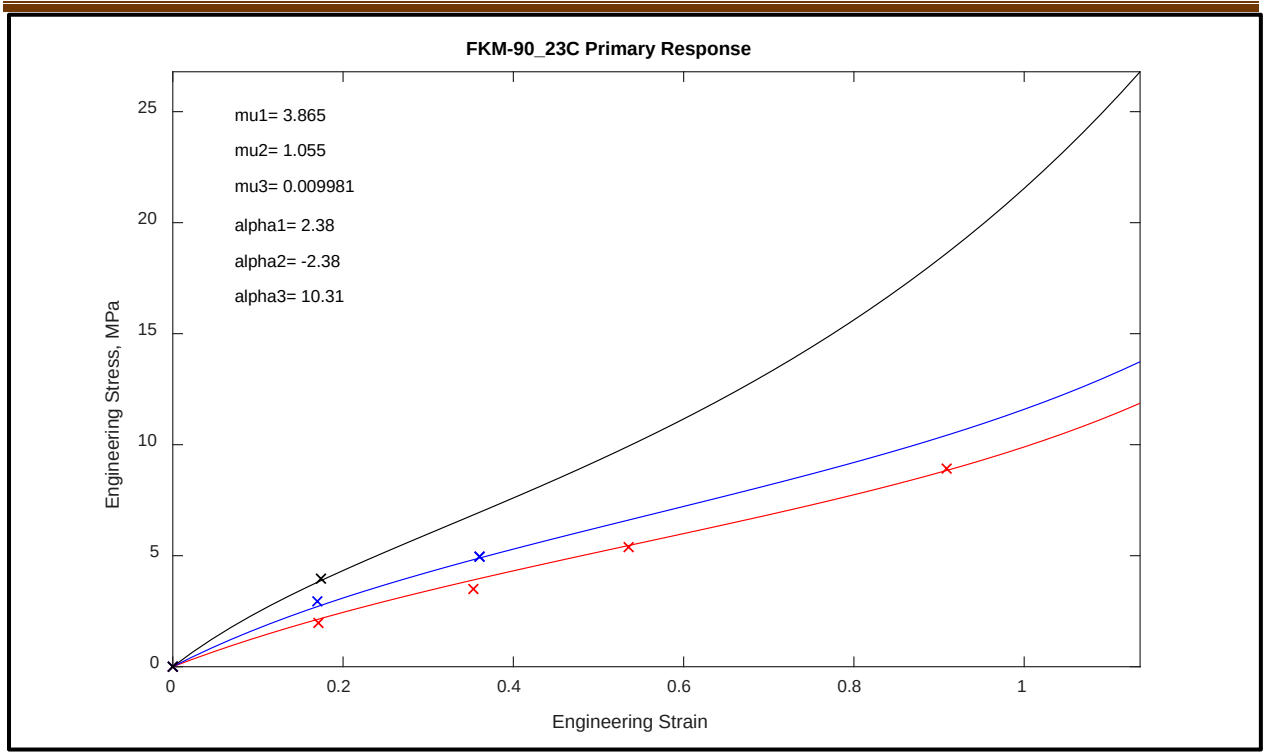


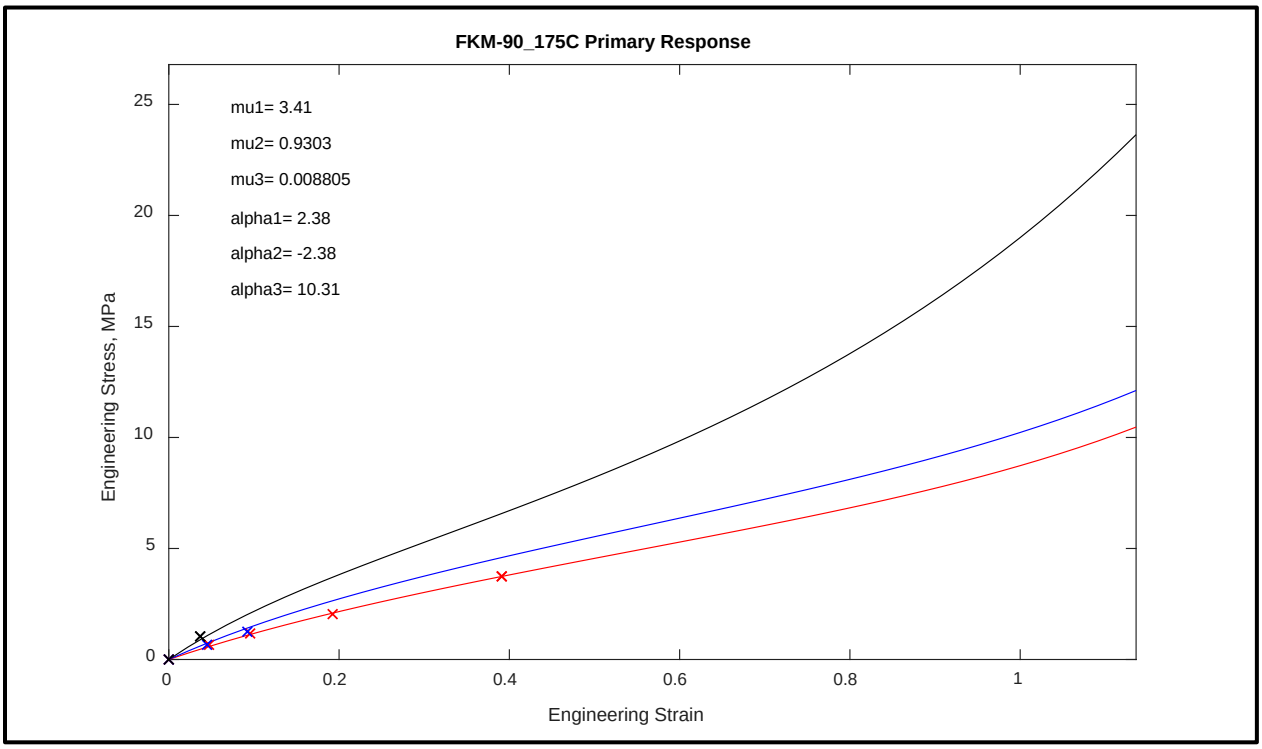


Figure A.4-3. Fit of 3 term Ogden hyperelastic law to cyclic stabilized peak stress-strain observations.

The distortional portion of the Ogden strain energy potential *W*, containing *N* terms, is defined with the material parameters $\mu_i$ and $\alpha_i$ according to:

$$W = \sum_{i=1}^{N} \frac{2\mu_i}{\alpha_i^2}\left(\bar{\lambda}_1^{\alpha_i} + \bar{\lambda}_2^{\alpha_i} + \bar{\lambda}_3^{\alpha_i} - 3\right) \quad (1)$$

Table A.4-9. Ogden model parameters for cyclic stabilized peak stress-strain observations.

| Material | Test Temp, °C | $\mu_1$, MPa | $\mu_2$, MPa | $\mu_3$, MPa | $\alpha_1$ | $\alpha_2$ | $\alpha_3$ |
|---|---|---|---|---|---|---|---|
| FEPM-80 | 100 | 1.354 | 0.109 | 0.005495 | 3.151 | -3.151 | 8.559 |
| FEPM-80 | 175 | 1.31 | 0.1055 | 0.005317 | 3.151 | -3.151 | 8.559 |
| FEPM-90 | 100 | 1.773 | 0.1972 | 0.01231 | 1.184 | -1.184 | 11.2 |
| FEPM-90 | 175 | 1.49 | 0.1657 | 0.01034 | 1.184 | -1.184 | 11.2 |
| HNBR-75 | 100 | 2.007 | 0.1698 | 0.007936 | 2.339 | -2.339 | 8.023 |
| HNBR-90 | 100 | 2.514 | 0.3280 | 0.01320 | 2.756 | -2.756 | 9.097 |
| HNBR-90 | 150 | 2.531 | 0.3302 | 0.01329 | 2.756 | -2.756 | 9.097 |
| FFKM-75 | 100 | 1.79 | 0.06131 | 0.008854 | 1.431 | -1.431 | 13.66 |
| FFKM- 5 | 175 | 2.167 | 0.07421 | 0.01072 | 1.431 | -1.431 | 13.66 |
| FFKM-90 | 100 | 1.329 | 0.6496 | 0.003826 | 3.469 | -3.469 | 13.32 |
| FFKM-90 | 175 | 1.305 | 0.6375 | 0.003755 | 3.469 | -3.469 | 13.32 |
| NBR-75 | 100 | 1.743 | 0.1984 | 0.000745 | 2.648 | -2.648 | 8.738 |
| NBR-90 | 100 | 4.724 | 5.724e-9 | 0.008121 | 2.736 | -2.736 | 4.154 |
| FKM-75 | 23 | 1.917 | 0.2228 | 0.001367 | 2.661 | -2.661 | 10.79 |
| FKM-75 | 175 | 1.724 | 0.2003 | 0.001229 | 2.661 | -2.661 | 10.79 |
| FKM-90 | 23 | 3.865 | 1.055 | 0.009981 | 2.38 | -2.38 | 10.31 |
| FKM-90 | 175 | 3.41 | 0.9303 | 0.008805 | 2.38 | -2.38 | 10.31 |

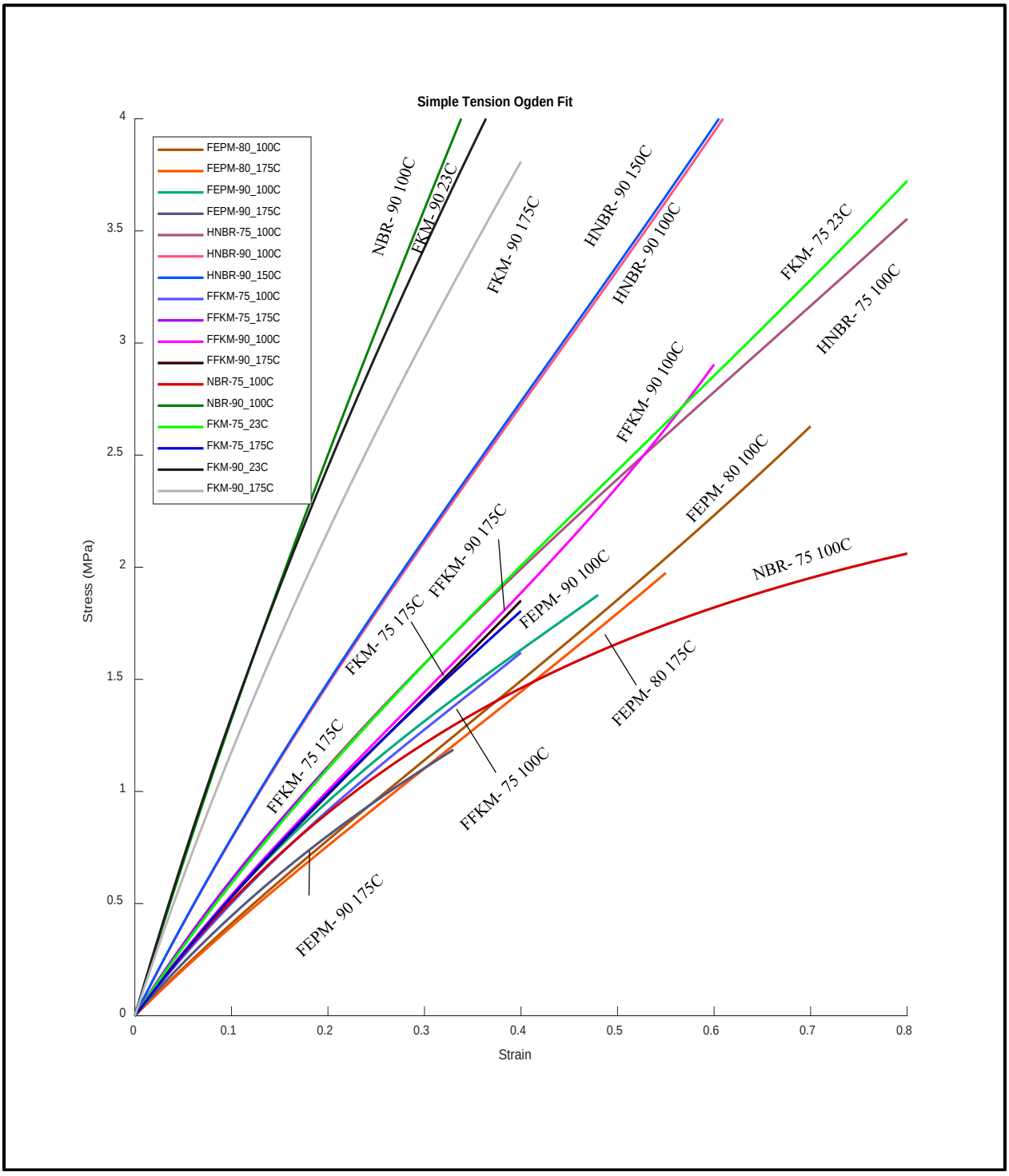


Figure A.4-4. Simple Tension Ogden fit.

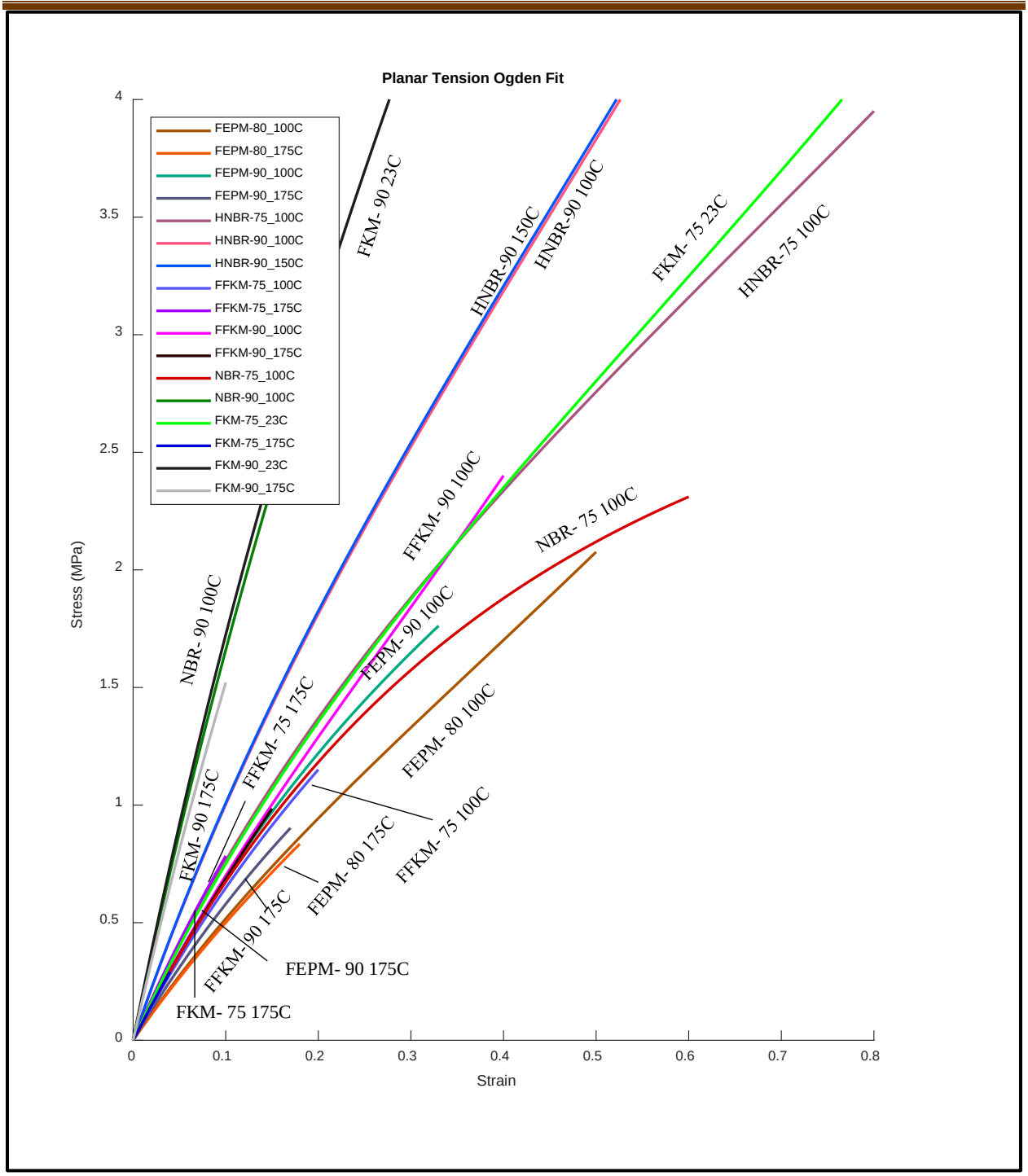


Figure A.4-5. Planar Tension Ogden Fit.

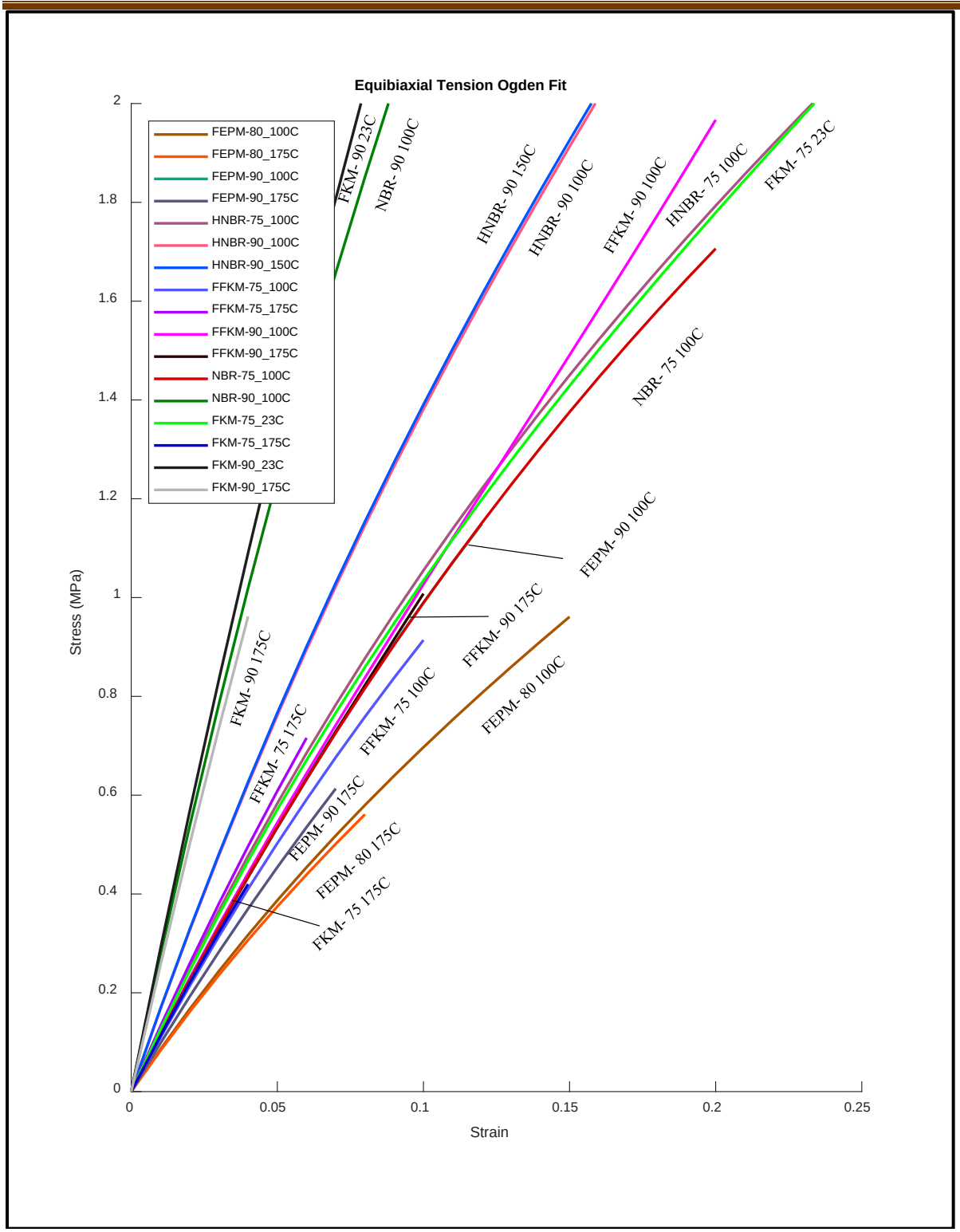


Figure A.4-6. Equibiaxial Tension Ogden Fit.

## *Analysis 2 – Mullins Effect Parameters*

Purpose: The Mullins law is used to define how an elastomer's stress-strain behavior depends on the most extreme prior loading event. Some finite element codes are able to capture this effect using these parameters.

The Mullins law is defined via the softening function $\eta$.

$$\eta = 1 - \frac{1}{r}\,\mathrm{erf}\left[\frac{\tilde{W}(I_{1,\max}) - \tilde{W}(I_1)}{m + \beta\tilde{W}(I_{1,\max})}\right] \qquad (2)$$

$\tilde{W}$ is the strain energy density on the primary (monotonic) stress-strain curve

$I_1$ is the instantaneous value of the 1st Invariant (measures state of deformation)

$I_{1,\max}$ is the maximum prior value of the 1st Invariant (measures state of deformation).

r, m and β are material constants

If the stress on the primary stress-strain curve is $\tilde{\sigma}$, then the stress on the unloading curve after softening due to prior deformation is given by $\sigma = \eta\tilde{\sigma}$.

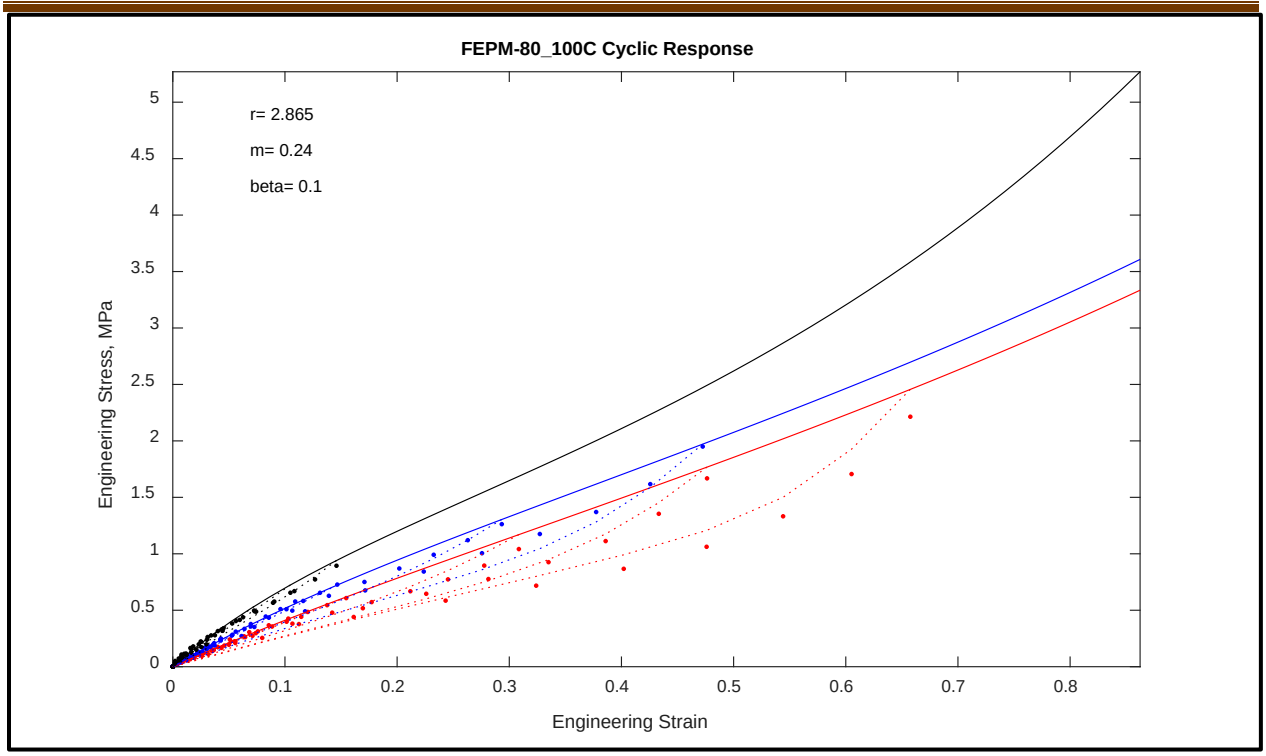
FEPM-80_100C Cyclic Response
r= 2.865
m= 0.24
beta= 0.1
Engineering Stress, MPa
Engineering Strain
0
0.5
1
1.5
2
2.5
3
3.5
4
4.5
5
0.1
0.2
0.3
0.4
0.5
0.6
0.7
0.8

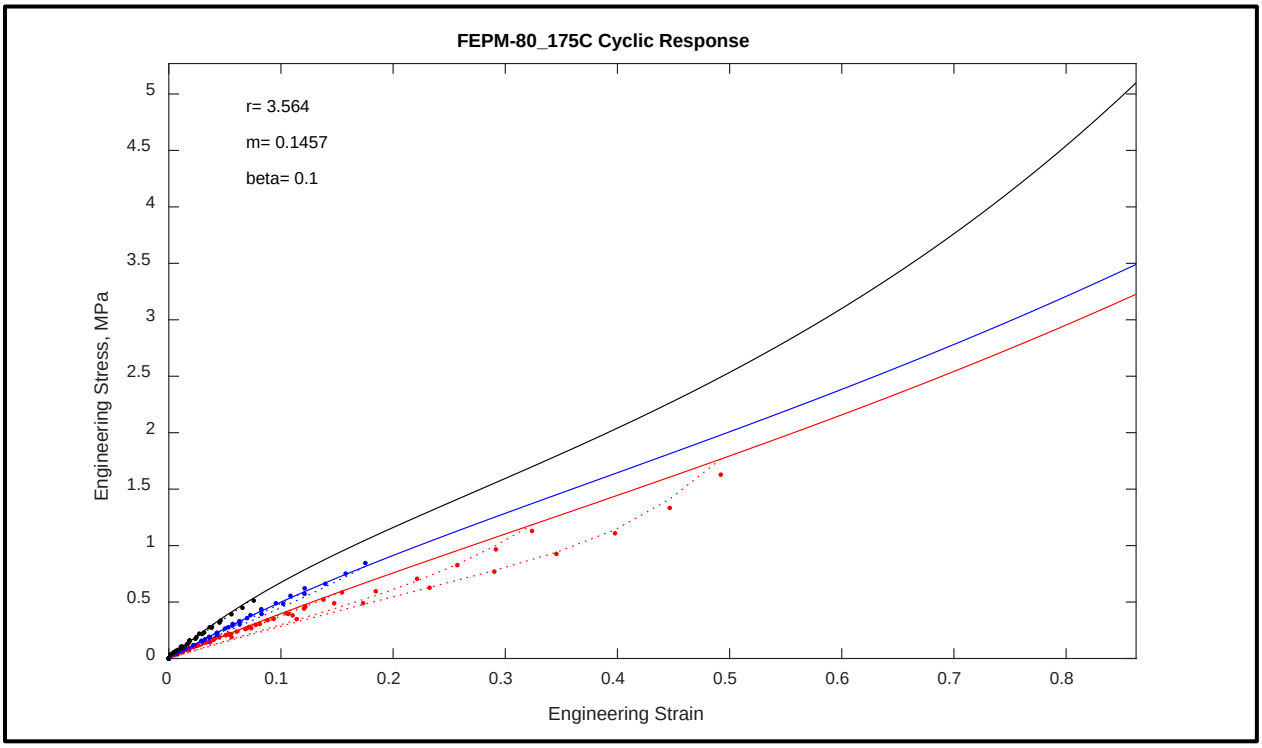
FEPM-80_175C Cyclic Response
r= 3.564
m= 0.1457
beta= 0.1
Engineering Stress, MPa
Engineering Strain
0
0.5
1
1.5
2
2.5
3
3.5
4
4.5
5
0.1
0.2
0.3
0.4
0.5
0.6
0.7
0.8

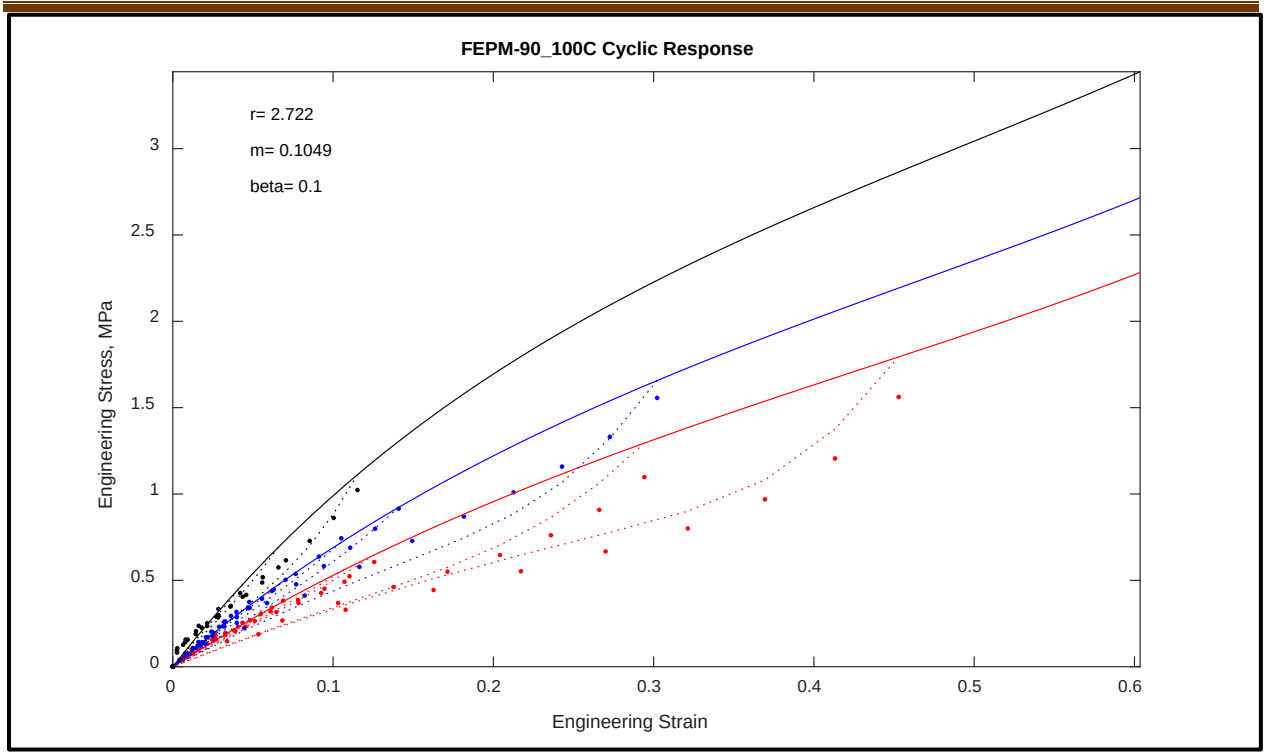
FEPM-90_100C Cyclic Response
r= 2.722
m= 0.1049
beta= 0.1
Engineering Stress, MPa
Engineering Strain
0
0.5
1
1.5
2
2.5
3
0.1
0.2
0.3
0.4
0.5
0.6

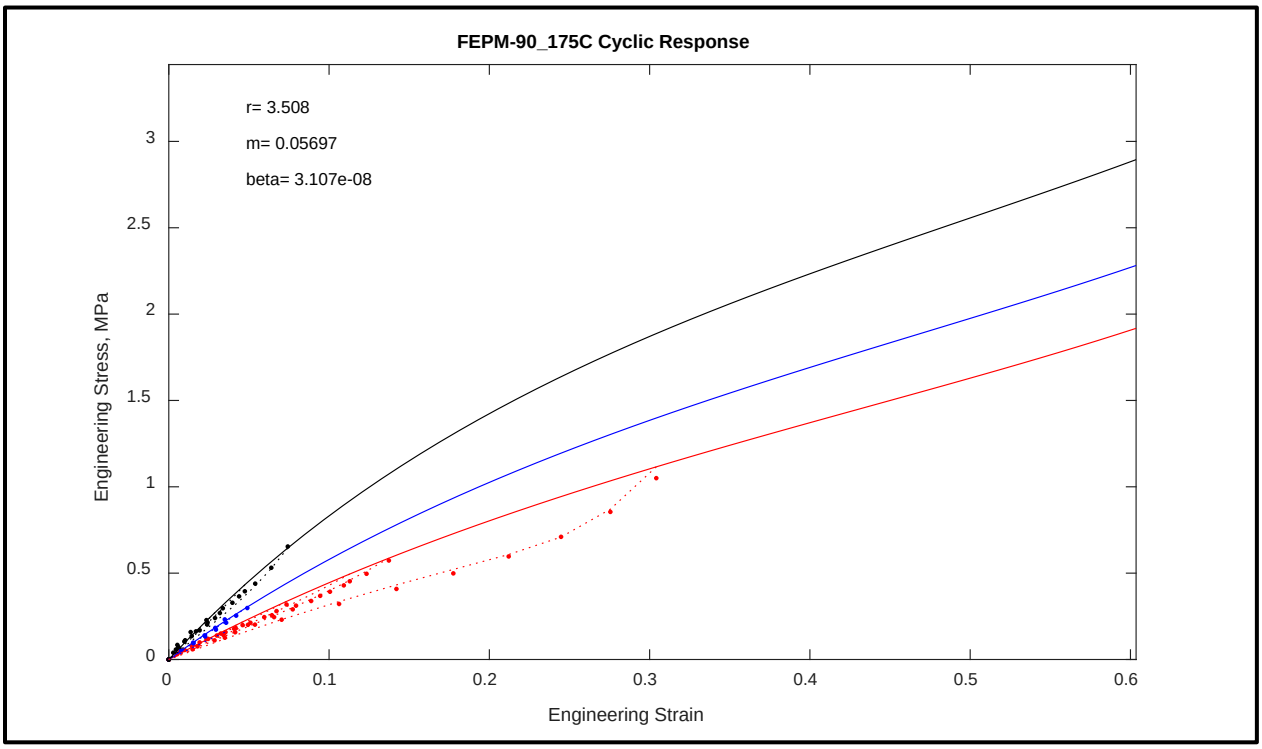
FEPM-90_175C Cyclic Response
r= 3.508
m= 0.05697
beta= 3.107e-08
Engineering Stress, MPa
Engineering Strain
0
0.5
1
1.5
2
2.5
3
0.1
0.2
0.3
0.4
0.5
0.6

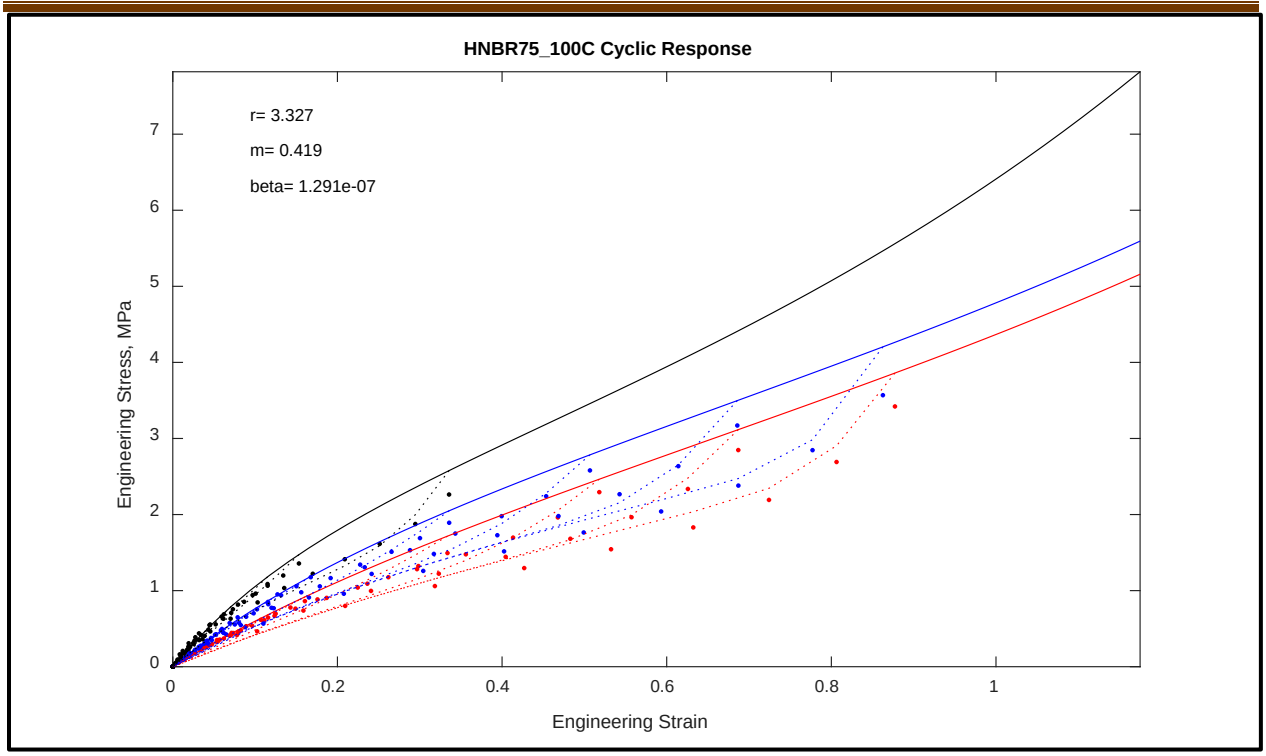
HNBR75_100C Cyclic Response
r= 3.327
m= 0.419
beta= 1.291e-07
Engineering Stress, MPa
Engineering Strain
0
1
2
3
4
5
6
7
0
0.2
0.4
0.6
0.8
1

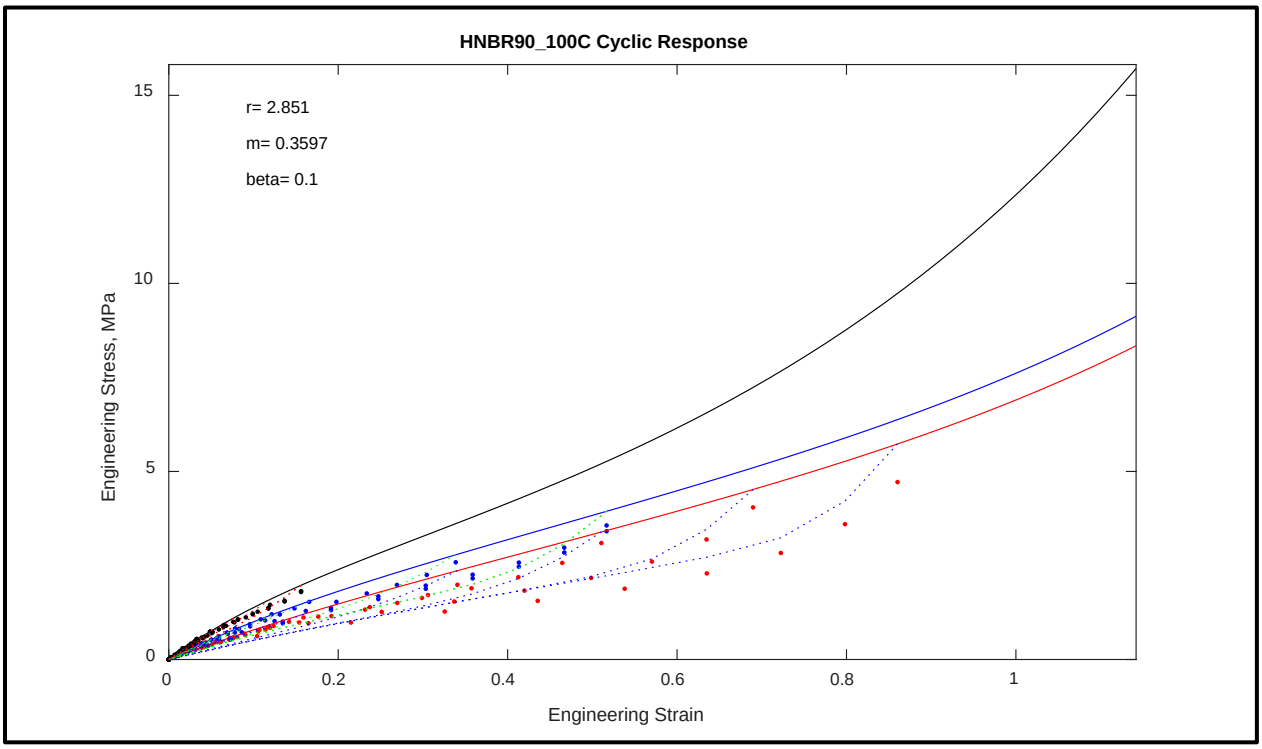
HNBR90_100C Cyclic Response
r= 2.851
m= 0.3597
beta= 0.1
Engineering Stress, MPa
Engineering Strain
0
5
10
15
0
0.2
0.4
0.6
0.8
1

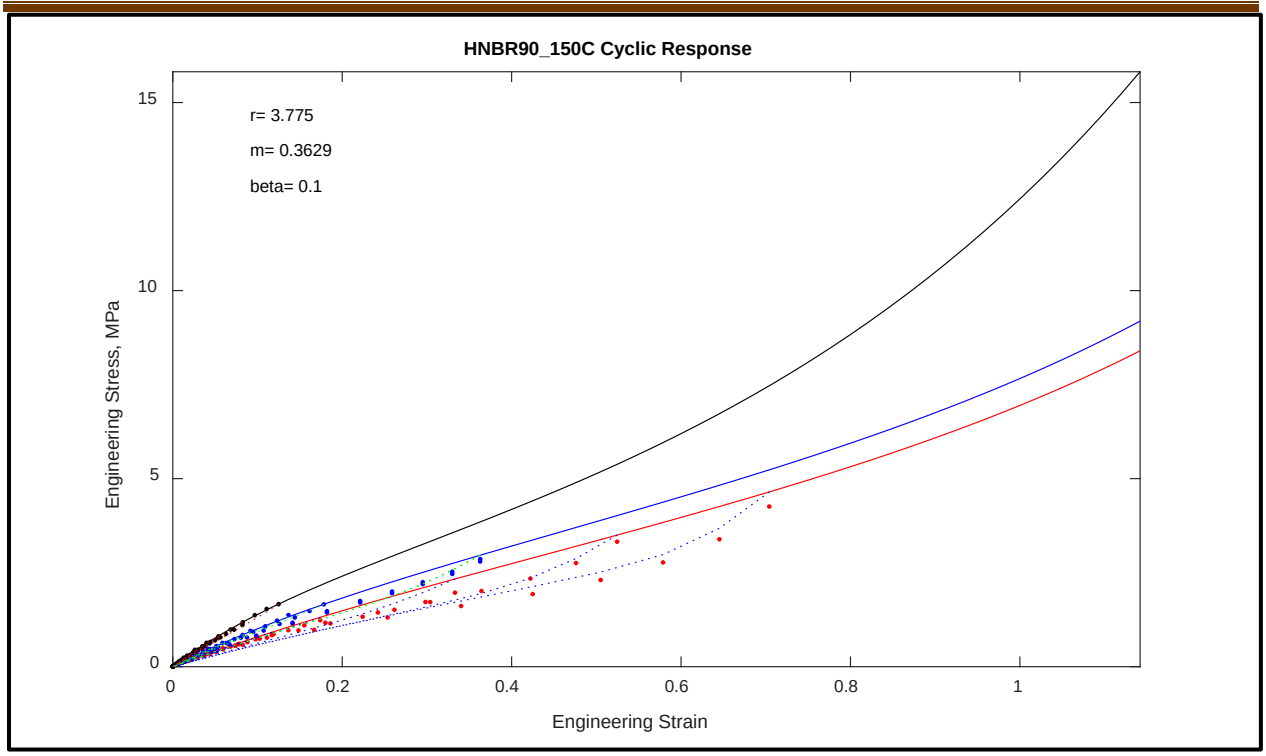
HNBR90_150C Cyclic Response
r= 3.775
m= 0.3629
beta= 0.1
Engineering Stress, MPa
Engineering Strain
0
5
10
15
0
0.2
0.4
0.6
0.8
1

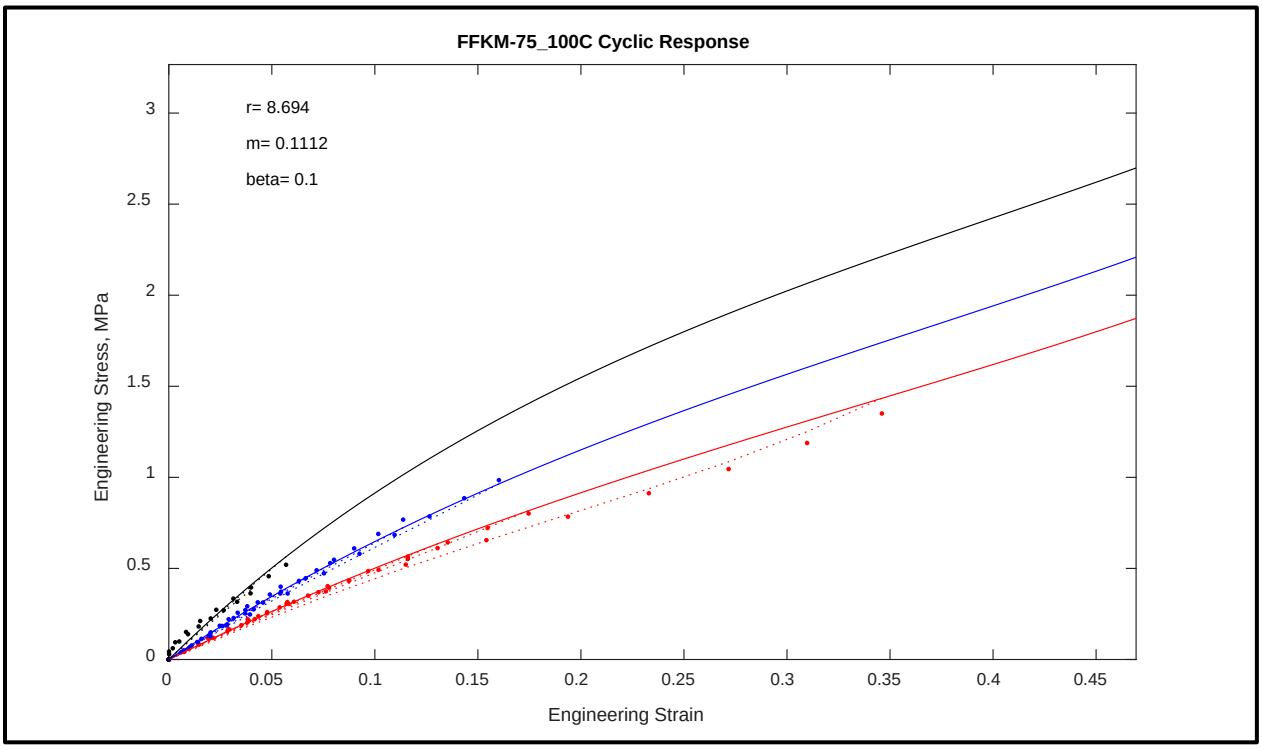
FFKM-75_100C Cyclic Response
r= 8.694
m= 0.1112
beta= 0.1
Engineering Stress, MPa
Engineering Strain
0
0.5
1
1.5
2
2.5
3
0
0.05
0.1
0.15
0.2
0.25
0.3
0.35
0.4
0.45

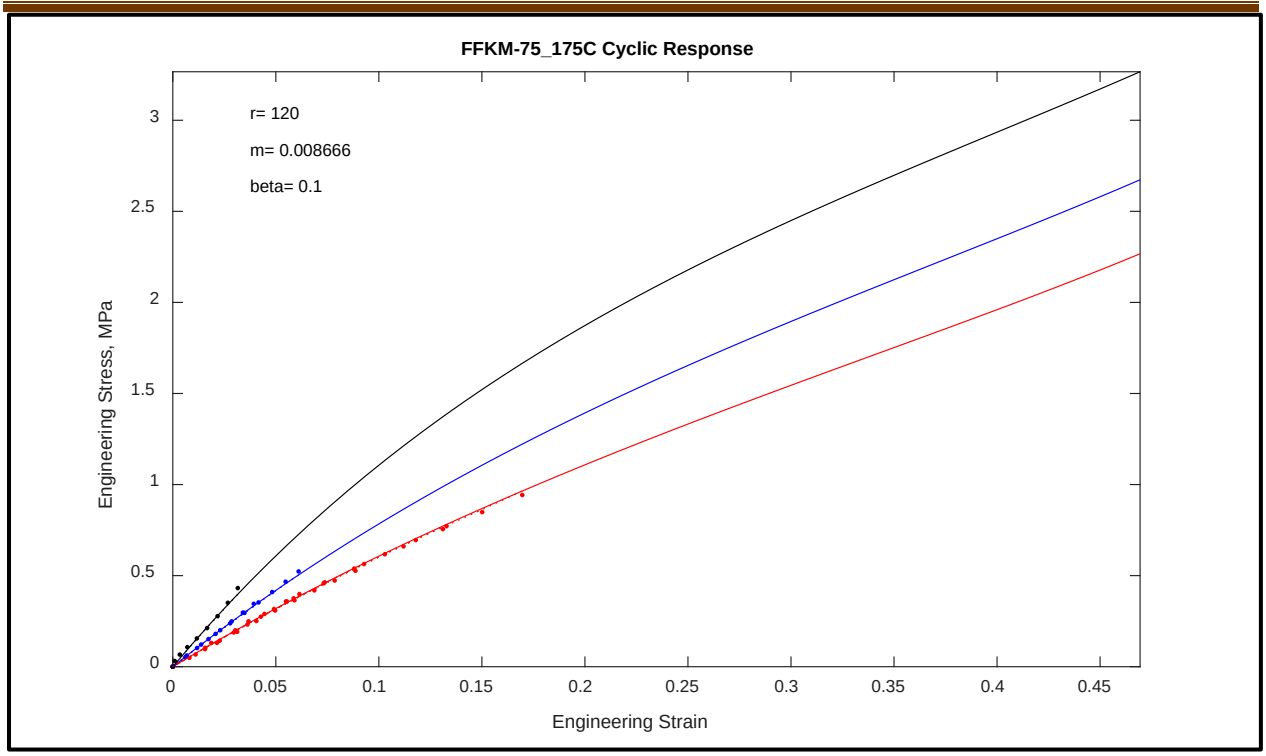
FFKM-75_175C Cyclic Response
r= 120
m= 0.008666
beta= 0.1
Engineering Stress, MPa
Engineering Strain
0
0.5
1
1.5
2
2.5
3
0.05
0.1
0.15
0.2
0.25
0.3
0.35
0.4
0.45

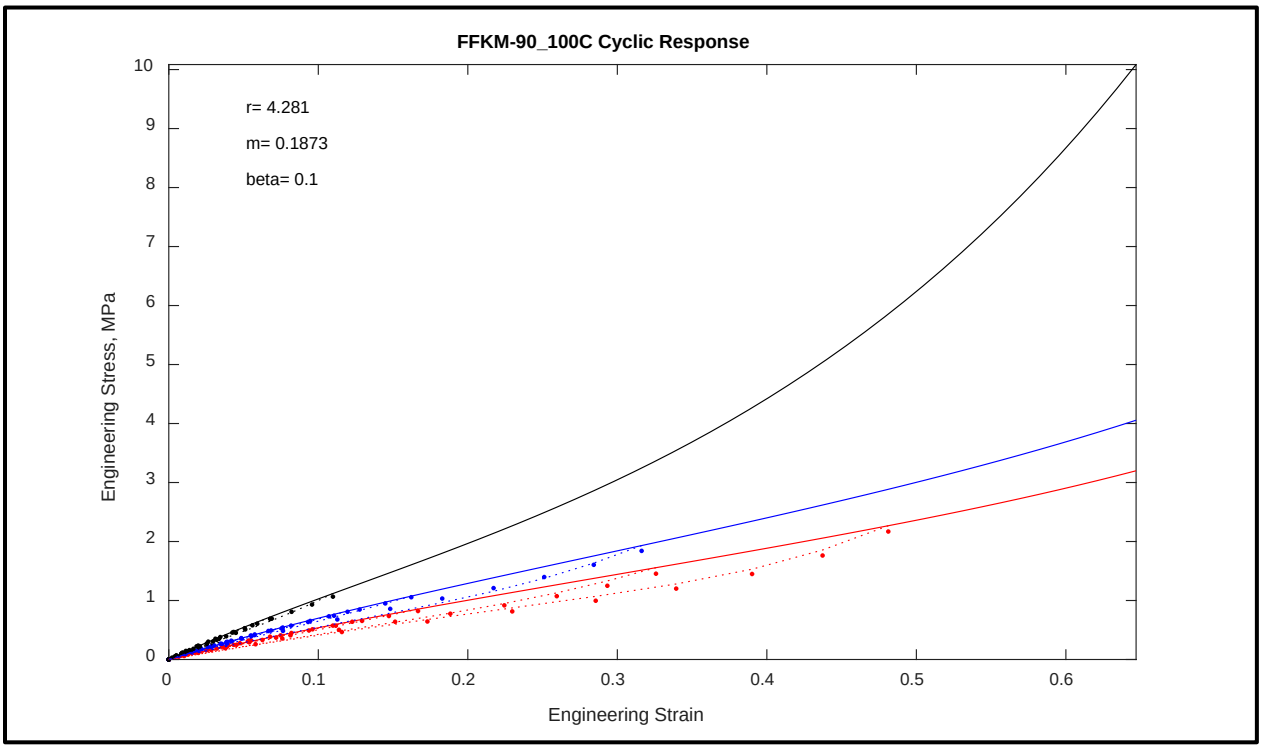
FFKM-90_100C Cyclic Response
r= 4.281
m= 0.1873
beta= 0.1
Engineering Stress, MPa
Engineering Strain
0
1
2
3
4
5
6
7
8
9
10
0.1
0.2
0.3
0.4
0.5
0.6

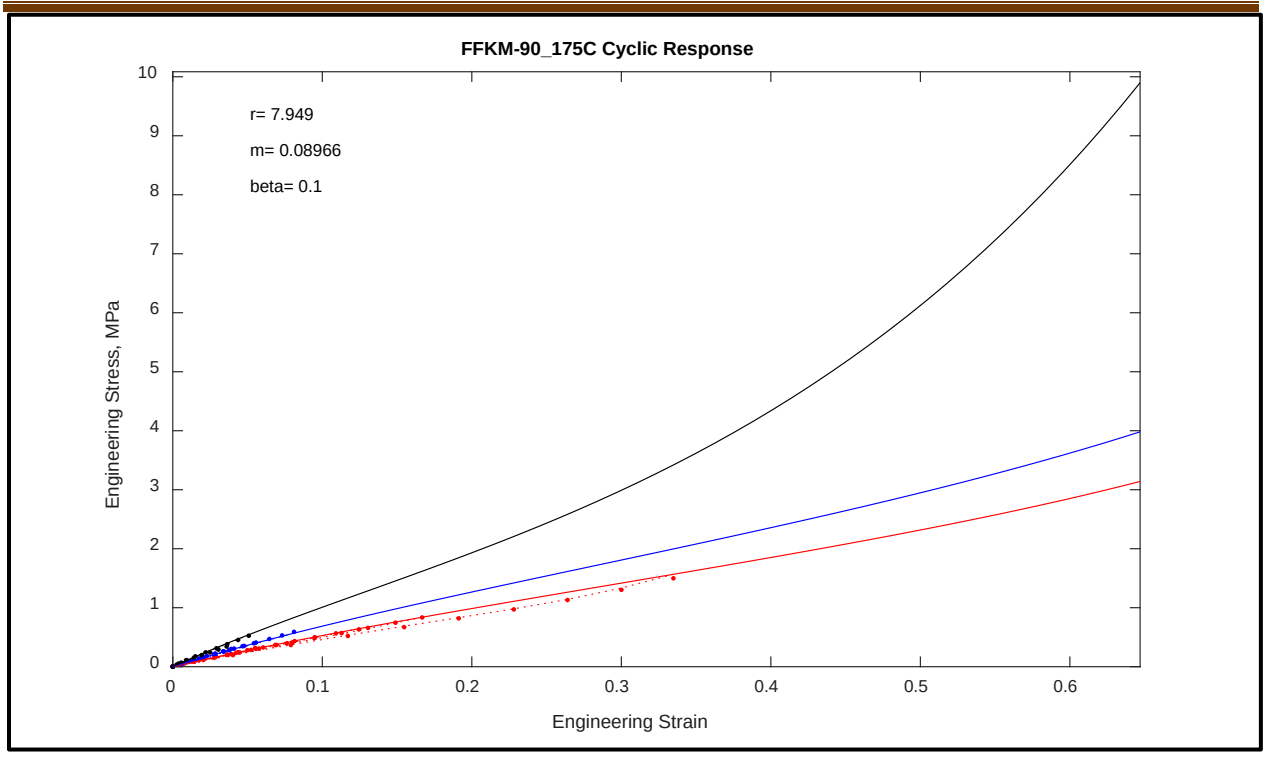
FFKM-90_175C Cyclic Response
r= 7.949
m= 0.08966
beta= 0.1
Engineering Stress, MPa
Engineering Strain
0
1
2
3
4
5
6
7
8
9
10
0
0.1
0.2
0.3
0.4
0.5
0.6

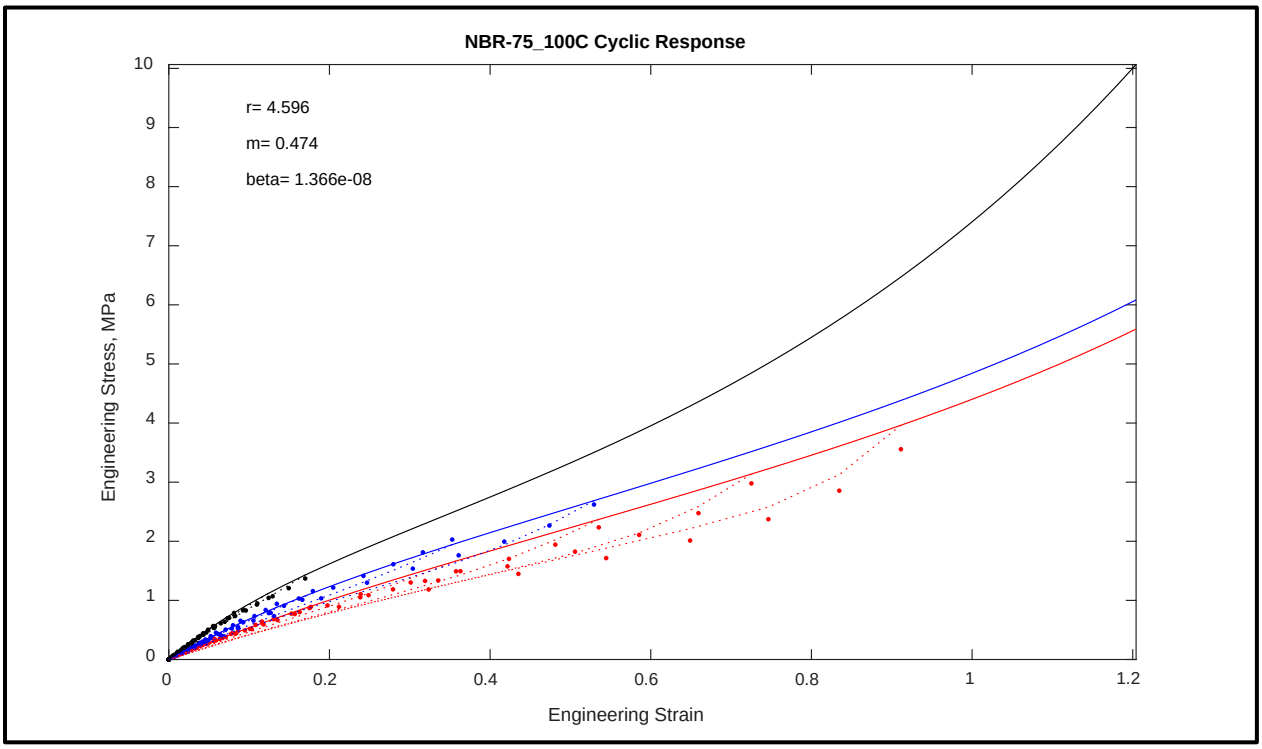
NBR-75_100C Cyclic Response
r= 4.596
m= 0.474
beta= 1.366e-08
Engineering Stress, MPa
Engineering Strain
0
1
2
3
4
5
6
7
8
9
10
0
0.2
0.4
0.6
0.8
1
1.2

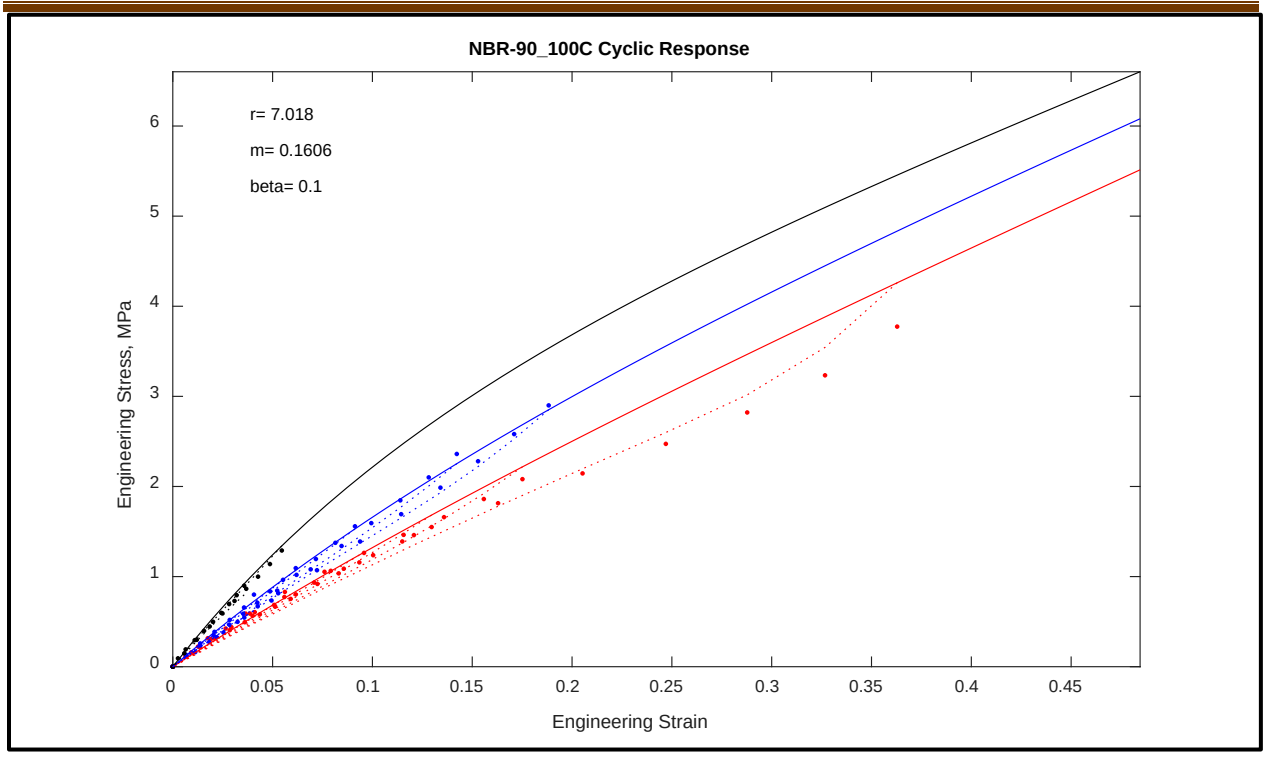
NBR-90_100C Cyclic Response
r= 7.018
m= 0.1606
beta= 0.1
Engineering Stress, MPa
Engineering Strain
0
1
2
3
4
5
6
0
0.05
0.1
0.15
0.2
0.25
0.3
0.35
0.4
0.45

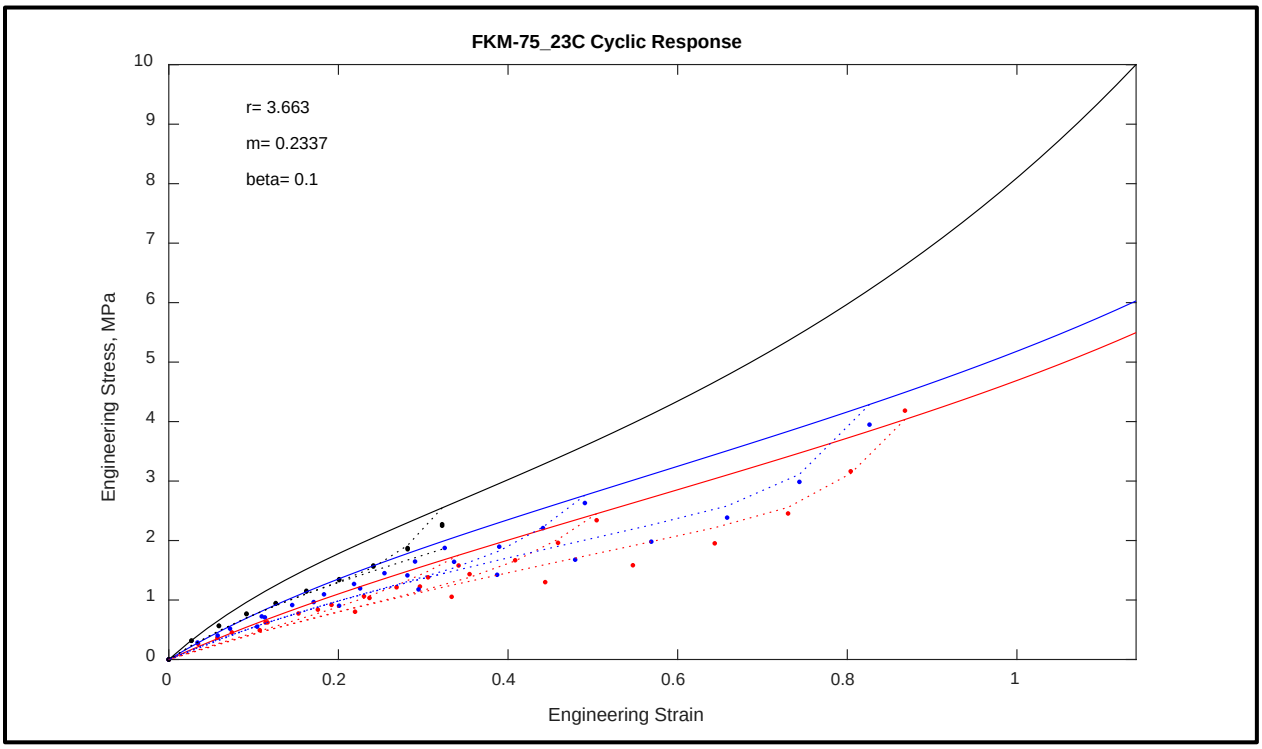
FKM-75_23C Cyclic Response
r= 3.663
m= 0.2337
beta= 0.1
Engineering Stress, MPa
Engineering Strain
0
1
2
3
4
5
6
7
8
9
10
0
0.2
0.4
0.6
0.8
1

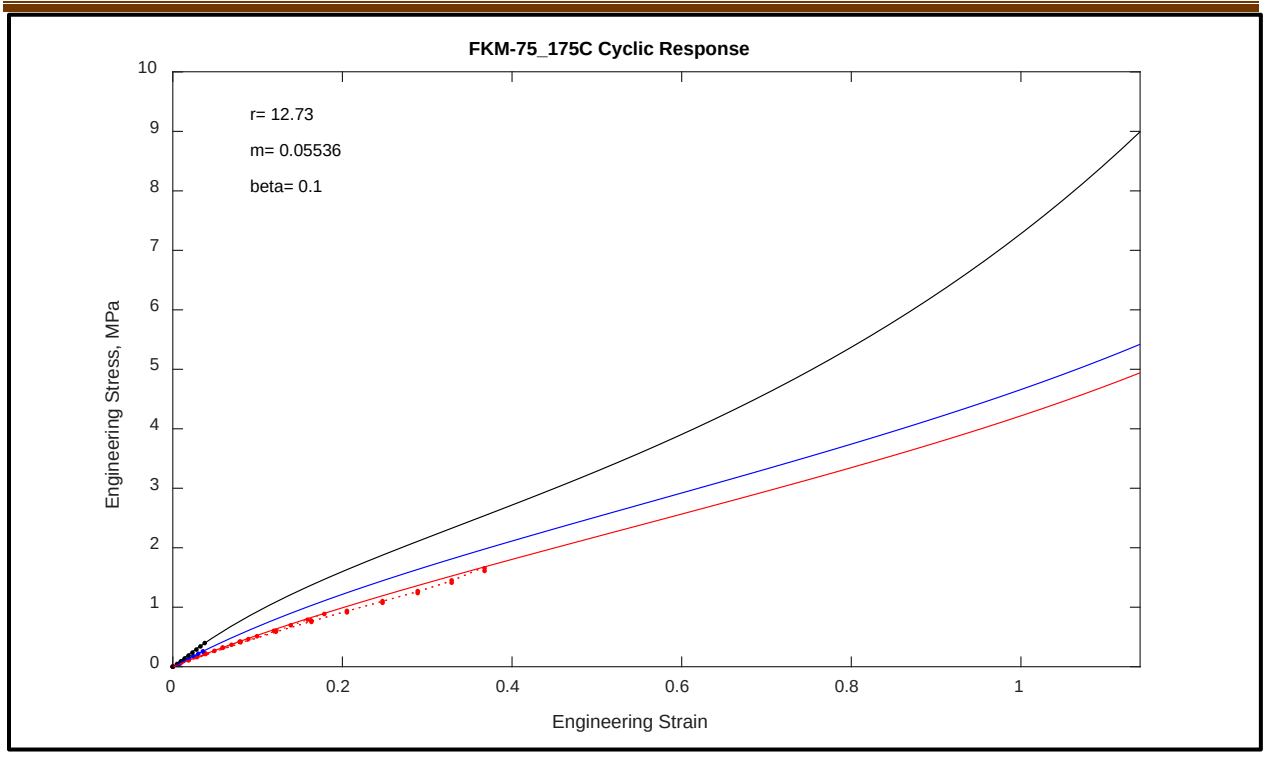
FKM-75_175C Cyclic Response
r= 12.73
m= 0.05536
beta= 0.1
Engineering Stress, MPa
Engineering Strain
0
1
2
3
4
5
6
7
8
9
10
0
0.2
0.4
0.6
0.8
1

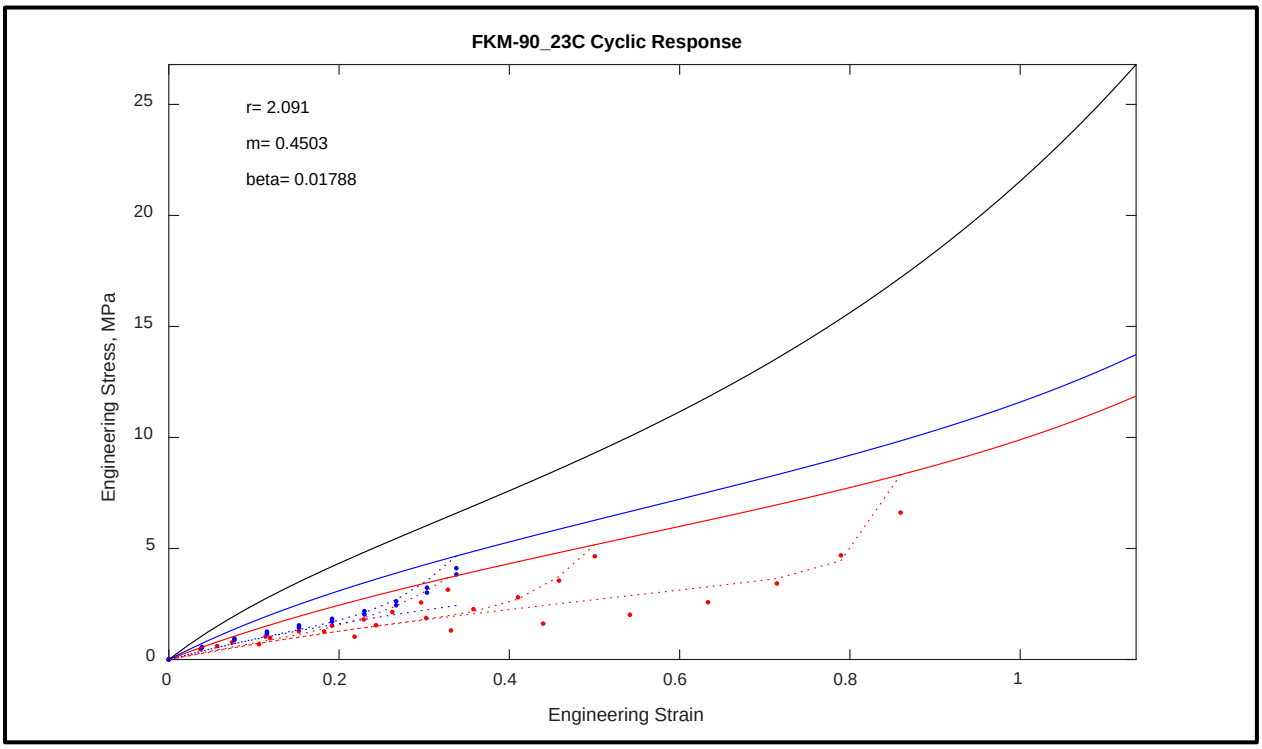
FKM-90_23C Cyclic Response
r= 2.091
m= 0.4503
beta= 0.01788
Engineering Stress, MPa
Engineering Strain
0
5
10
15
20
25
0
0.2
0.4
0.6
0.8
1

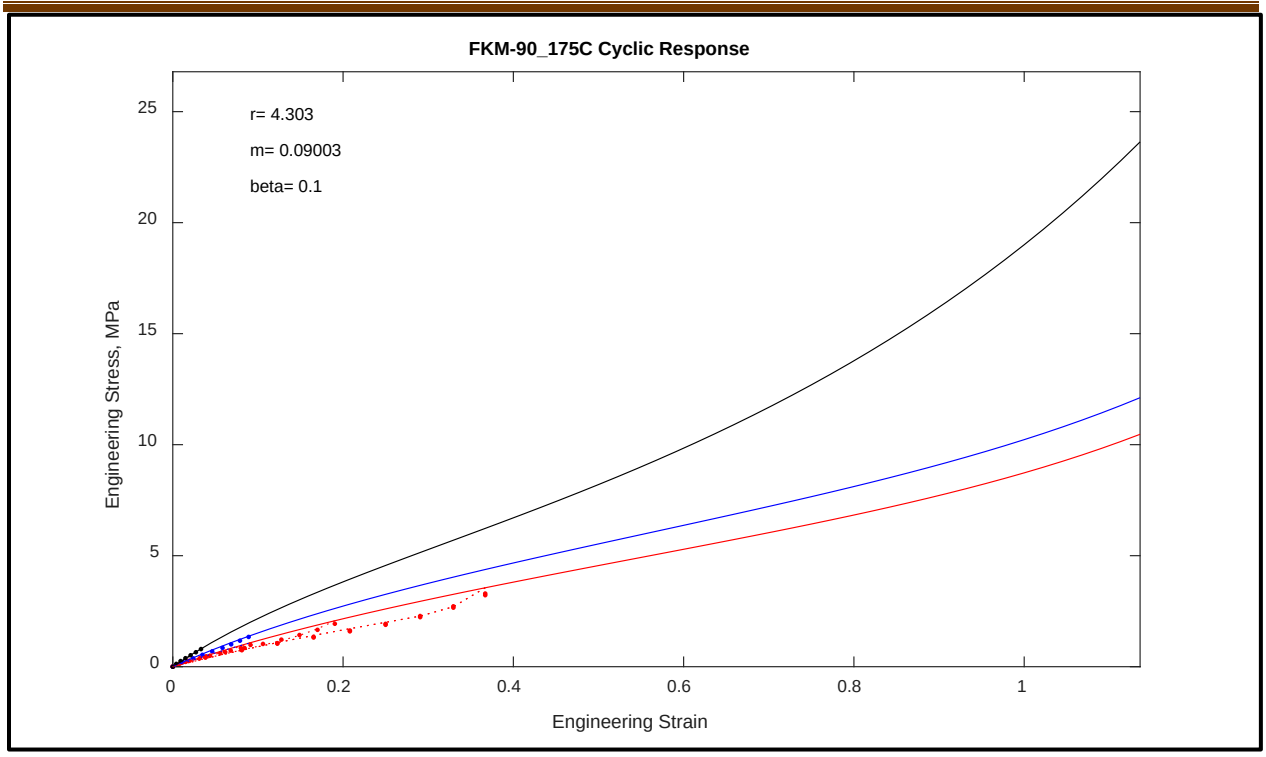


Figure A.4-7. Fit of Mullins law to a series of cyclic stabilized unloading curves in simple, planar, and equibiaxial tension.

Table A.4-10. Mullins law parameters.

| Material | Test Temperature, °C | r | m, MPa | β |
|---|---|---|---|---|
| FEPM-80 | 100 | 2.865 | 0.24 | 0.1 |
| FEPM-80 | 175 | 3.564 | 0.1457 | 0.1 |
| FEPM-90 | 100 | 2.722 | 0.1049 | 0.1 |
| FEPM-90 | 175 | 3.508 | 0.05697 | 3.107e-8 |
| HNBR-75 | 100 | 3.327 | 0.419 | 1.291e-7 |
| HNBR-90 | 100 | 2.851 | 0.3597 | 0.1 |
| HNBR-90 | 150 | 3.775 | 0.3629 | 0.1 |
| FFKM-75 | 100 | 8.694 | 0.1112 | 0.1 |
| FFKM-75 | 175 | 120 | 0.008666 | 0.1 |
| FFKM-90 | 100 | 4.281 | 0.1873 | 0.1 |
| FFKM-90 | 175 | 7.949 | 0.08966 | 0.1 |
| NBR-75 | 100 | 4.596 | 0.474 | 1.366e-8 |
| NBR-90 | 100 | 7.018 | 0.1606 | 0.1 |
| FKM-75 | 23 | 3.663 | 0.2337 | 0.1 |
| FKM-75 | 175 | 12.73 | 0.05536 | 0.1 |
| FKM-90 | 23 | 2.091 | 0.4503 | 0.01788 |
| FKM-90 | 175 | 4.303 | 0.09003 | 0.1 |

## *Experiment 3: Volumetric Compression*

Purpose: The volumetric compressibility of the material provides information needed to accurately model the material deformation under highly confined loading.

Specimen: Cylindrical specimen contained within a fixture and compressed.
Ambient temperature: 100°C, 150°C, 175°C. Test temperature noted in figures.

The dilatational portion of the Ogden strain energy potential *W*, containing *N* terms, is defined with material parameter *Di* according to:

$$W = \sum_{i=1}^{N} \frac{1}{D_i} \left( J_{el} - 1 \right)^{2i} \qquad (3)$$

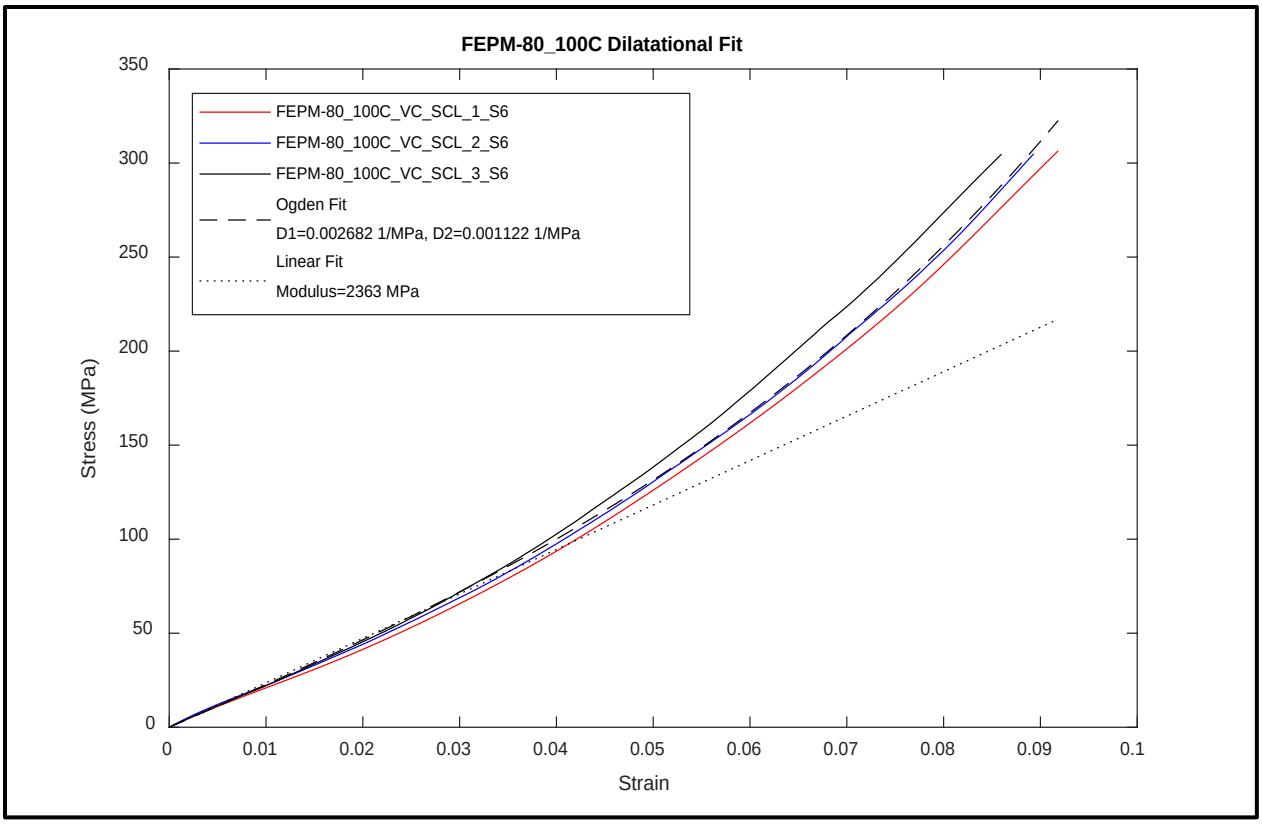

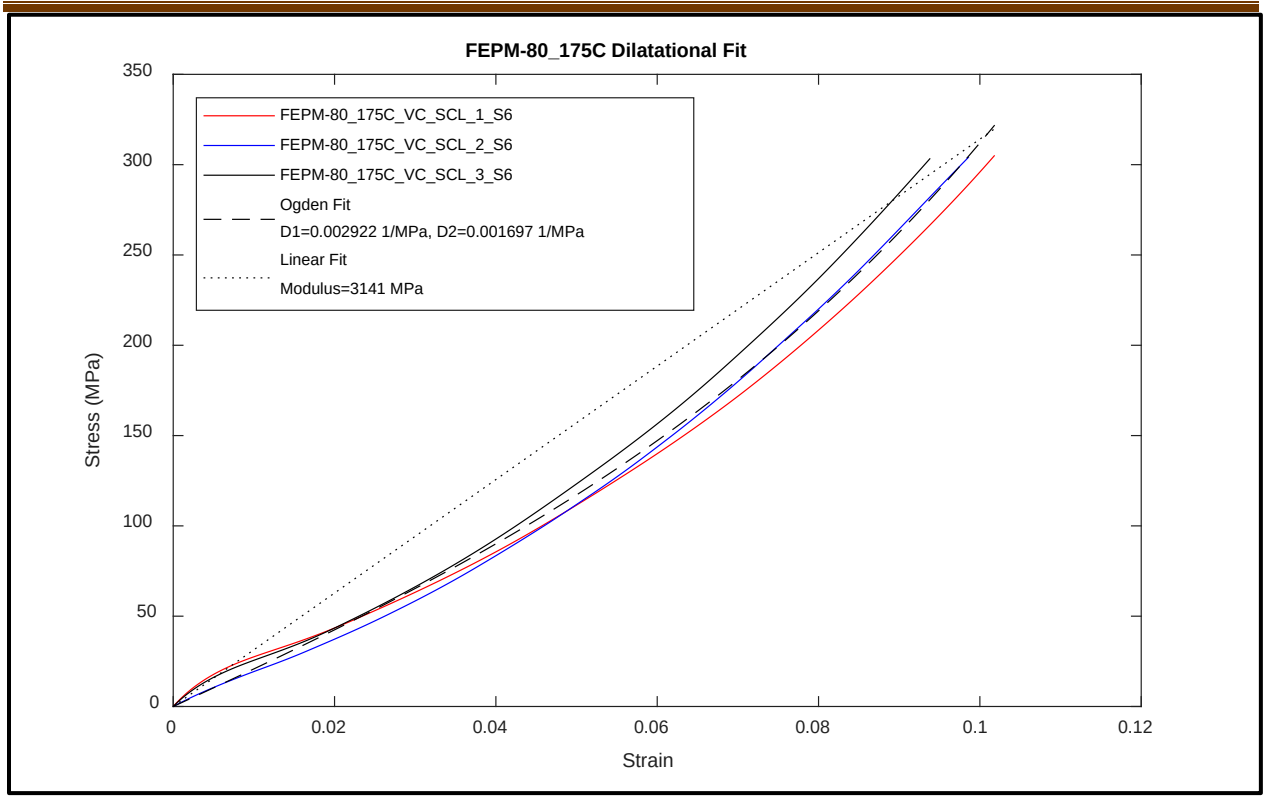
FEPM-80_175C Dilatational Fit
FEPM-80_175C_VC_SCL_1_S6
FEPM-80_175C_VC_SCL_2_S6
FEPM-80_175C_VC_SCL_3_S6
Ogden Fit
D1=0.002922 1/MPa, D2=0.001697 1/MPa
Linear Fit
Modulus=3141 MPa
Stress (MPa)
Strain
0
50
100
150
200
250
300
350
0
0.02
0.04
0.06
0.08
0.1
0.12

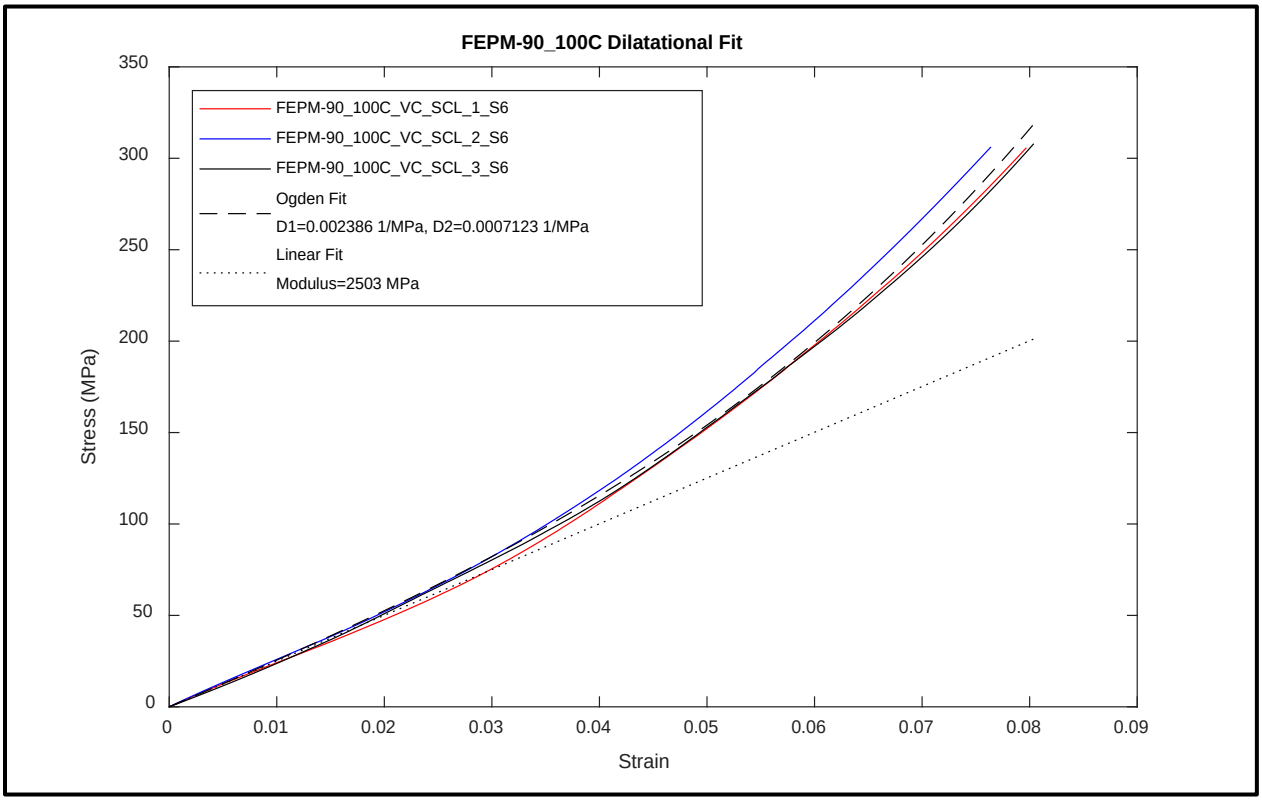
FEPM-90_100C Dilatational Fit
FEPM-90_100C_VC_SCL_1_S6
FEPM-90_100C_VC_SCL_2_S6
FEPM-90_100C_VC_SCL_3_S6
Ogden Fit
D1=0.002386 1/MPa, D2=0.0007123 1/MPa
Linear Fit
Modulus=2503 MPa
Stress (MPa)
Strain
0
50
100
150
200
250
300
350
0
0.01
0.02
0.03
0.04
0.05
0.06
0.07
0.08
0.09

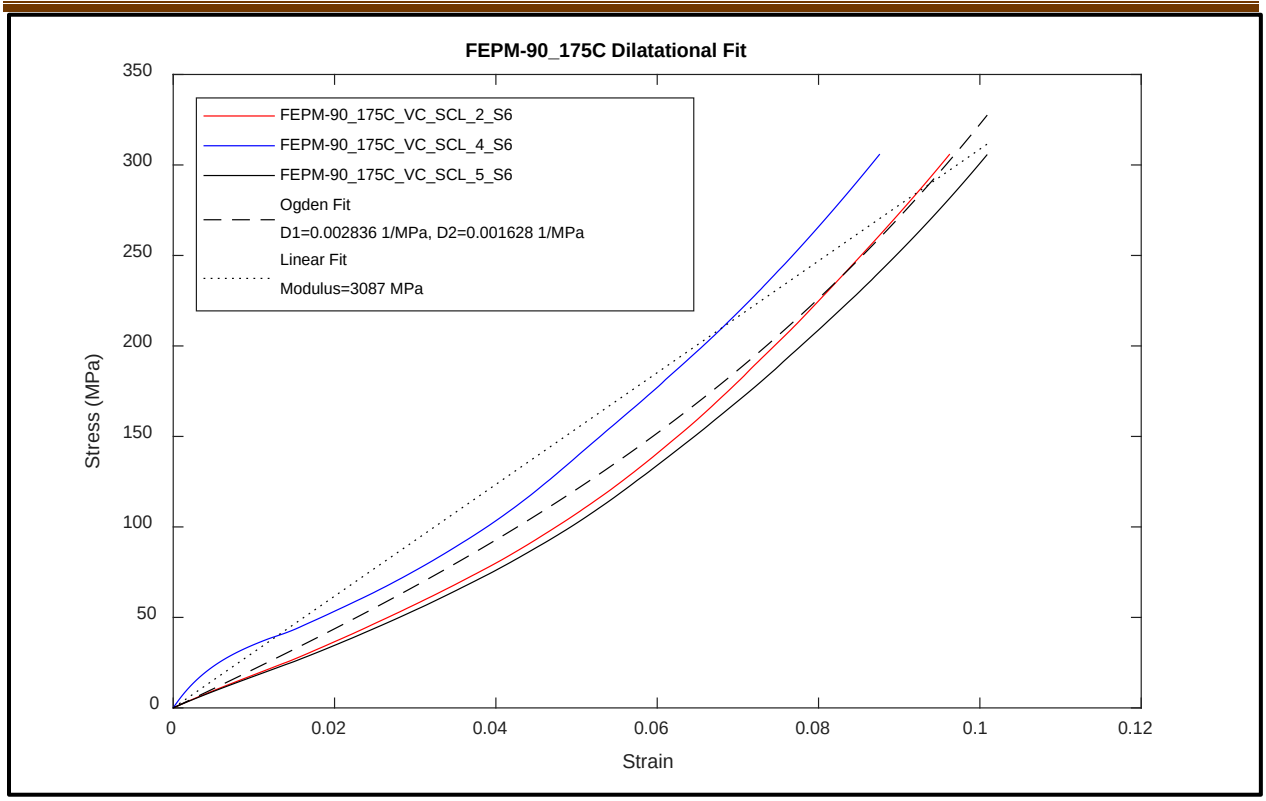
FEPM-90_175C Dilatational Fit
FEPM-90_175C_VC_SCL_2_S6
FEPM-90_175C_VC_SCL_4_S6
FEPM-90_175C_VC_SCL_5_S6
Ogden Fit
D1=0.002836 1/MPa, D2=0.001628 1/MPa
Linear Fit
Modulus=3087 MPa
Stress (MPa)
Strain
0
50
100
150
200
250
300
350
0
0.02
0.04
0.06
0.08
0.1
0.12

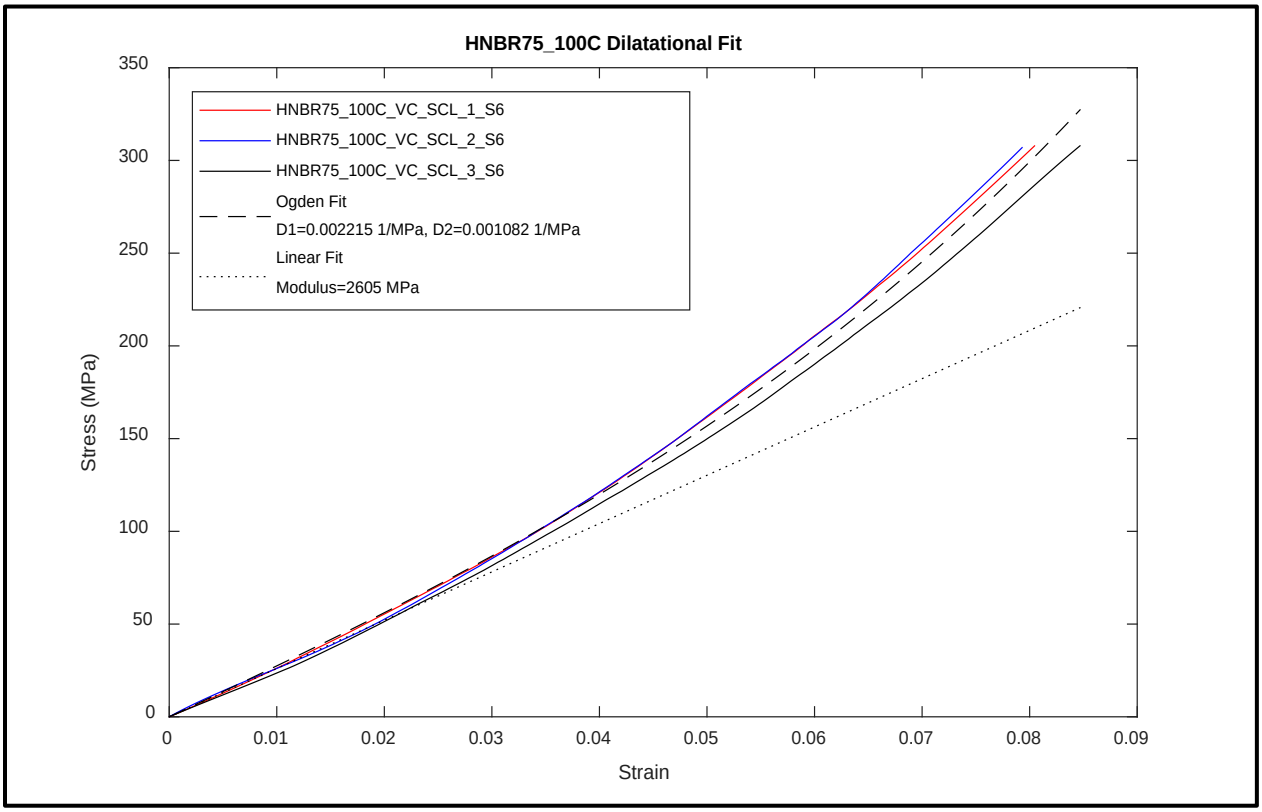
HNBR75_100C Dilatational Fit
HNBR75_100C_VC_SCL_1_S6
HNBR75_100C_VC_SCL_2_S6
HNBR75_100C_VC_SCL_3_S6
Ogden Fit
D1=0.002215 1/MPa, D2=0.001082 1/MPa
Linear Fit
Modulus=2605 MPa
Stress (MPa)
Strain
0
50
100
150
200
250
300
350
0
0.01
0.02
0.03
0.04
0.05
0.06
0.07
0.08
0.09

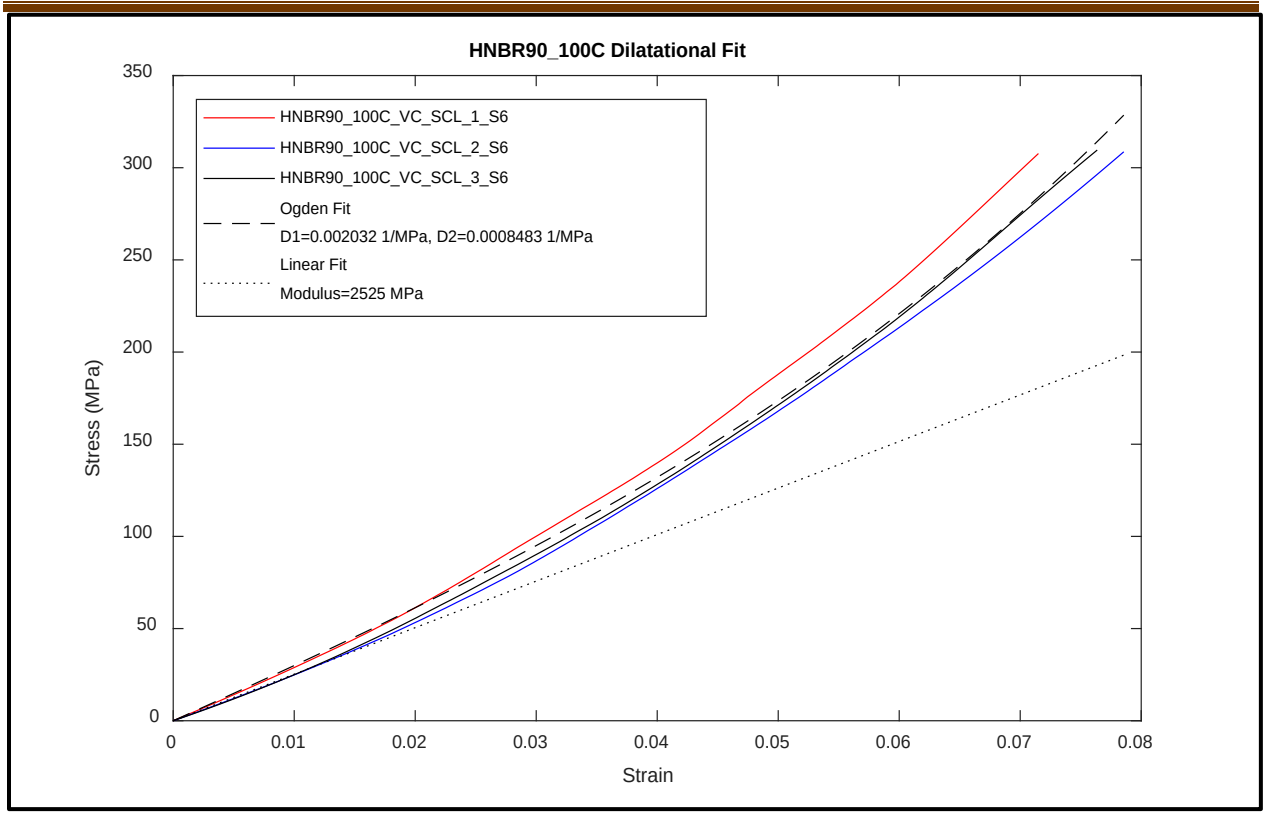
HNBR90_100C Dilatational Fit
HNBR90_100C_VC_SCL_1_S6
HNBR90_100C_VC_SCL_2_S6
HNBR90_100C_VC_SCL_3_S6
Ogden Fit
D1=0.002032 1/MPa, D2=0.0008483 1/MPa
Linear Fit
Modulus=2525 MPa
Stress (MPa)
Strain
0
50
100
150
200
250
300
350
0
0.01
0.02
0.03
0.04
0.05
0.06
0.07
0.08

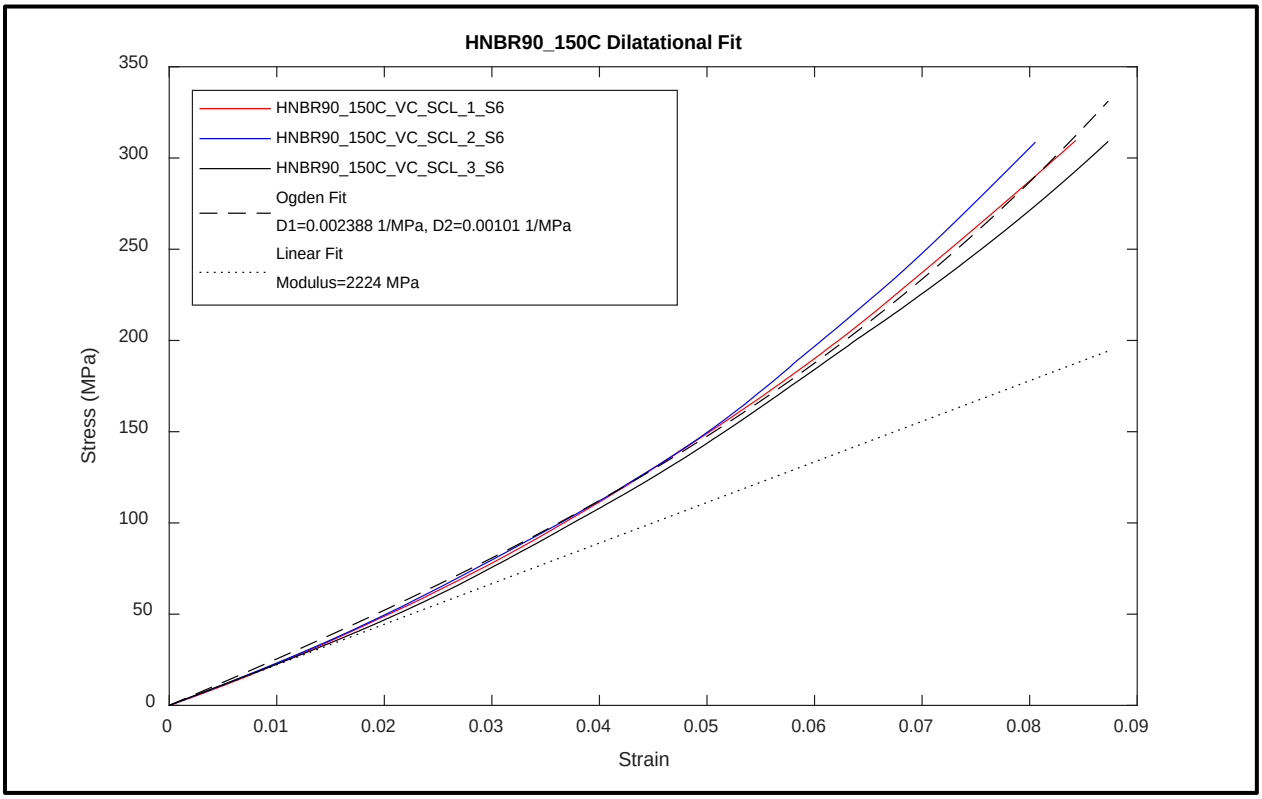
HNBR90_150C Dilatational Fit
HNBR90_150C_VC_SCL_1_S6
HNBR90_150C_VC_SCL_2_S6
HNBR90_150C_VC_SCL_3_S6
Ogden Fit
D1=0.002388 1/MPa, D2=0.00101 1/MPa
Linear Fit
Modulus=2224 MPa
Stress (MPa)
Strain
0
50
100
150
200
250
300
350
0
0.01
0.02
0.03
0.04
0.05
0.06
0.07
0.08
0.09

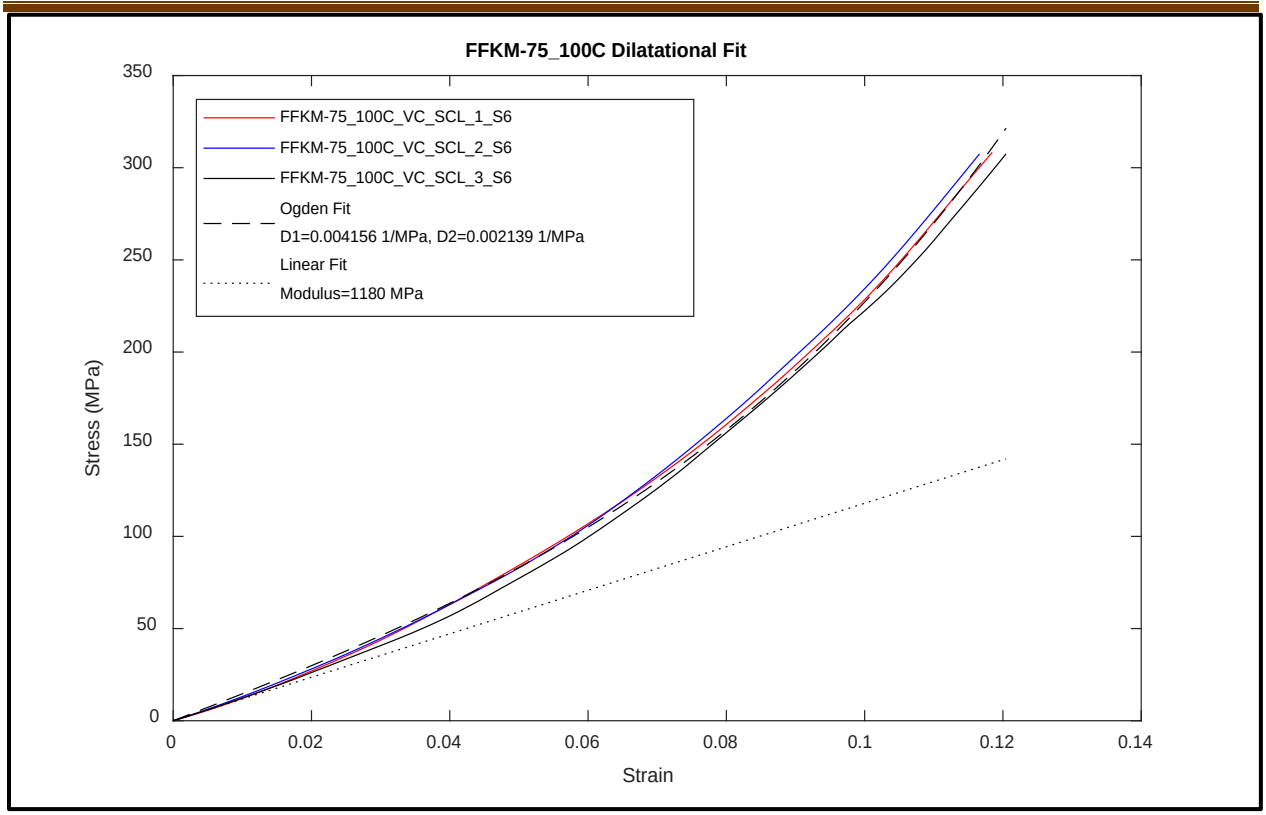
FFKM-75_100C Dilatational Fit
FFKM-75_100C_VC_SCL_1_S6
FFKM-75_100C_VC_SCL_2_S6
FFKM-75_100C_VC_SCL_3_S6
Ogden Fit
D1=0.004156 1/MPa, D2=0.002139 1/MPa
Linear Fit
Modulus=1180 MPa
Stress (MPa)
Strain
0
50
100
150
200
250
300
350
0
0.02
0.04
0.06
0.08
0.1
0.12
0.14

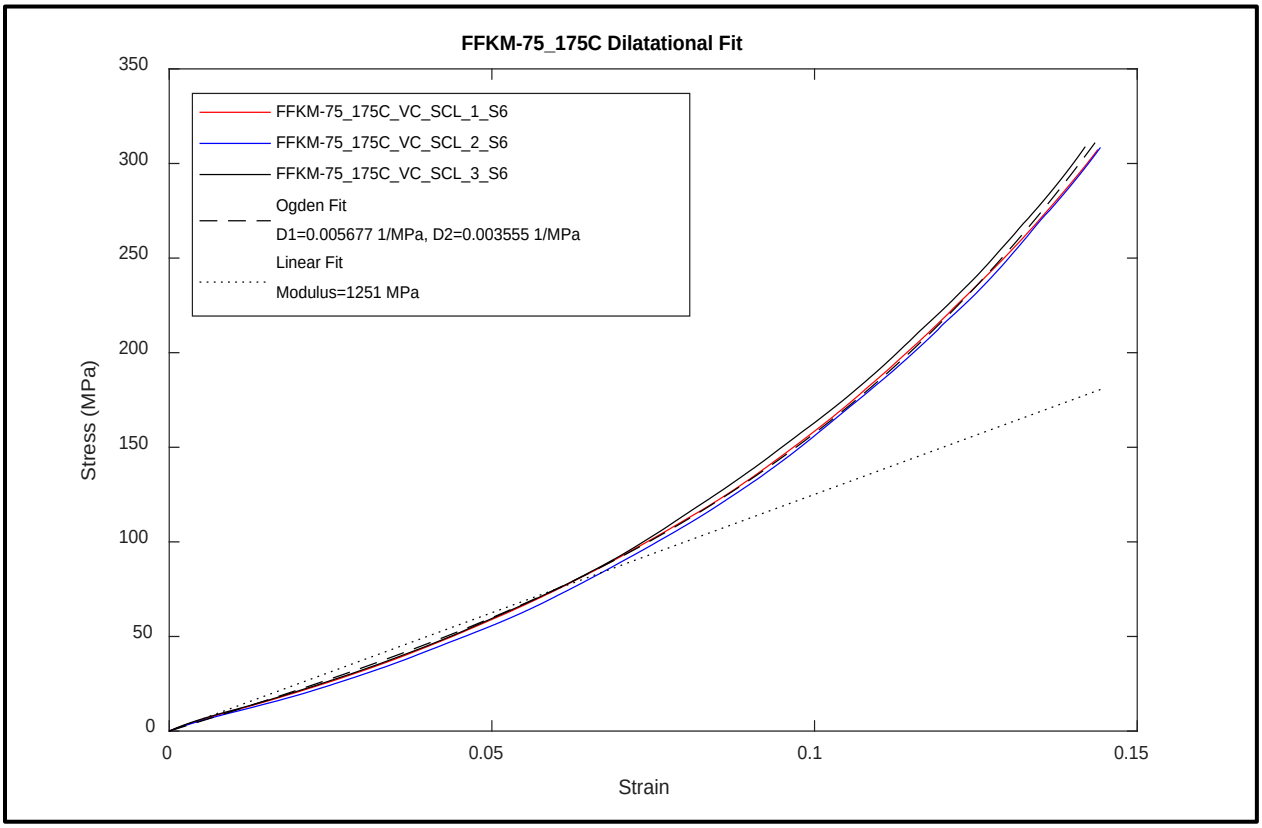
FFKM-75_175C Dilatational Fit
FFKM-75_175C_VC_SCL_1_S6
FFKM-75_175C_VC_SCL_2_S6
FFKM-75_175C_VC_SCL_3_S6
Ogden Fit
D1=0.005677 1/MPa, D2=0.003555 1/MPa
Linear Fit
Modulus=1251 MPa
Stress (MPa)
Strain
0
50
100
150
200
250
300
350
0
0.05
0.1
0.15

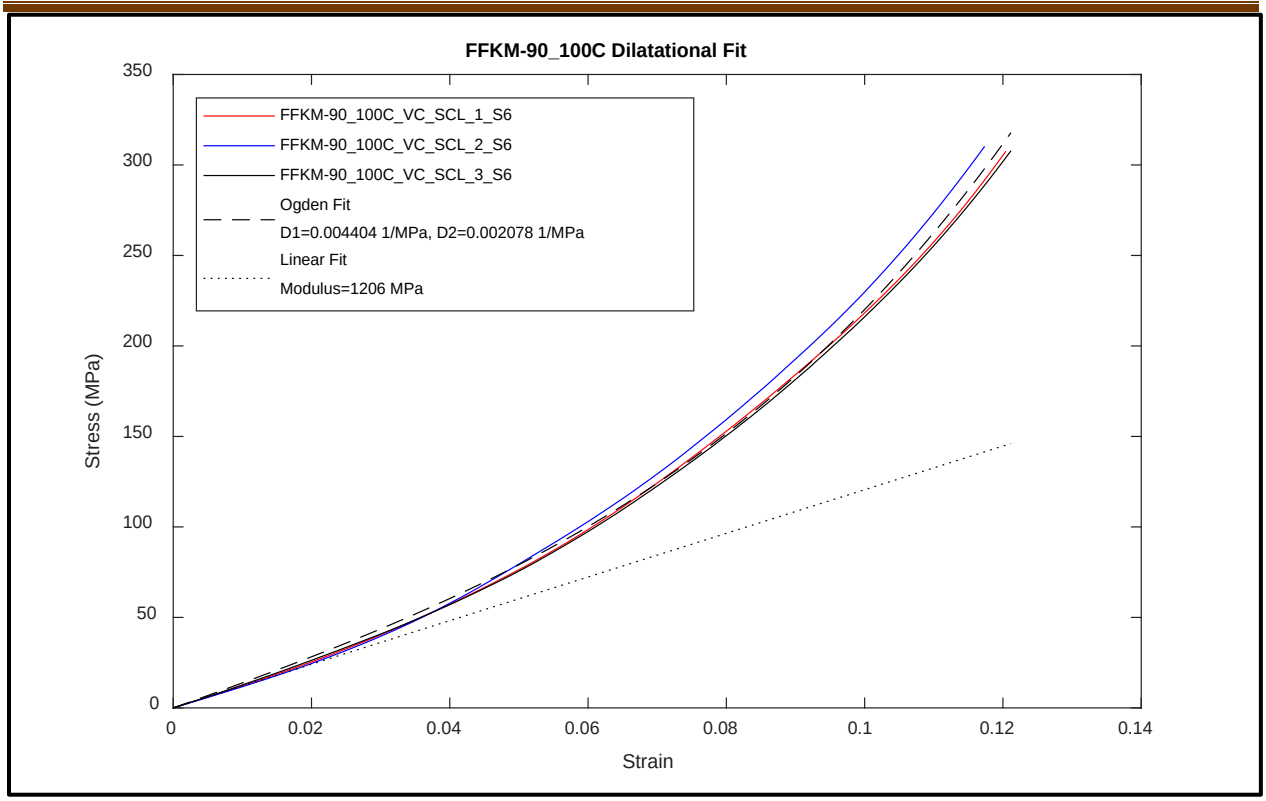
FFKM-90_100C Dilatational Fit
FFKM-90_100C_VC_SCL_1_S6
FFKM-90_100C_VC_SCL_2_S6
FFKM-90_100C_VC_SCL_3_S6
Ogden Fit
D1=0.004404 1/MPa, D2=0.002078 1/MPa
Linear Fit
Modulus=1206 MPa
Stress (MPa)
Strain
0
50
100
150
200
250
300
350
0
0.02
0.04
0.06
0.08
0.1
0.12
0.14

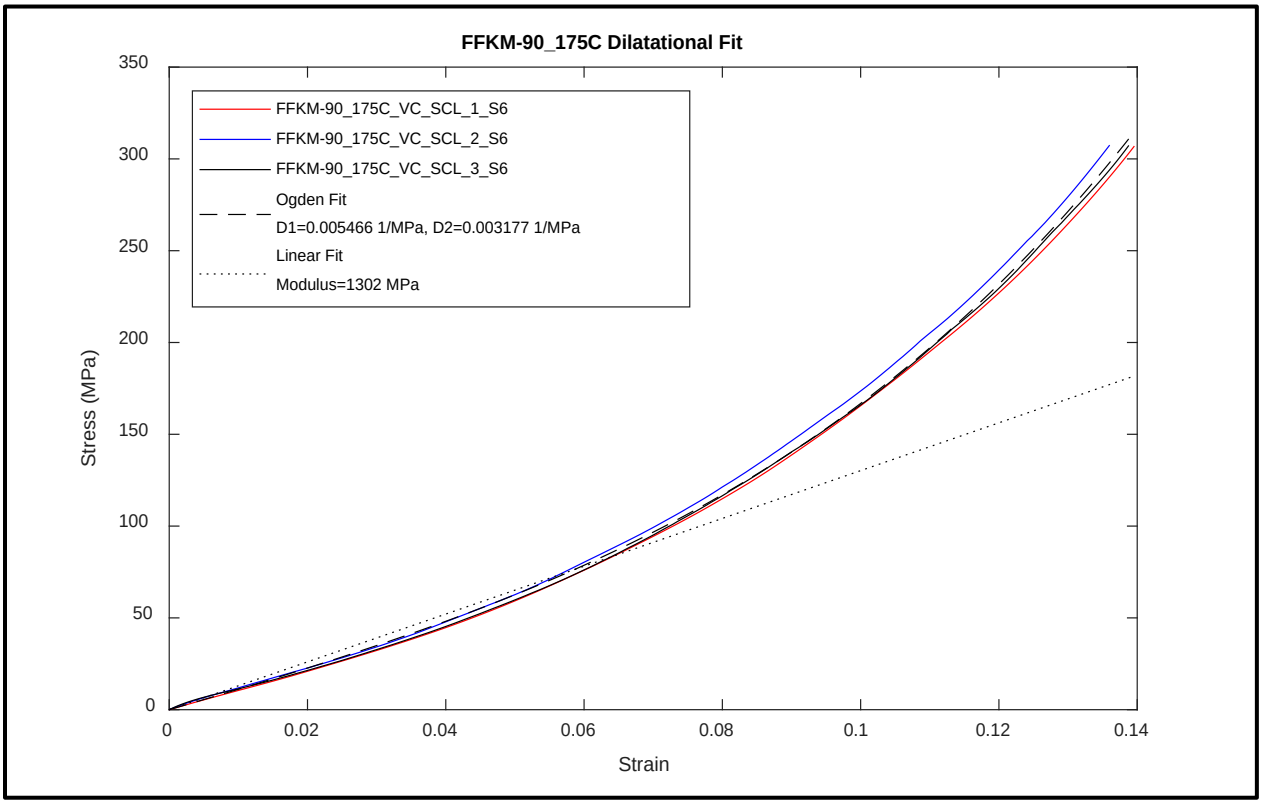
FFKM-90_175C Dilatational Fit
FFKM-90_175C_VC_SCL_1_S6
FFKM-90_175C_VC_SCL_2_S6
FFKM-90_175C_VC_SCL_3_S6
Ogden Fit
D1=0.005466 1/MPa, D2=0.003177 1/MPa
Linear Fit
Modulus=1302 MPa
Stress (MPa)
Strain
0
50
100
150
200
250
300
350
0
0.02
0.04
0.06
0.08
0.1
0.12
0.14

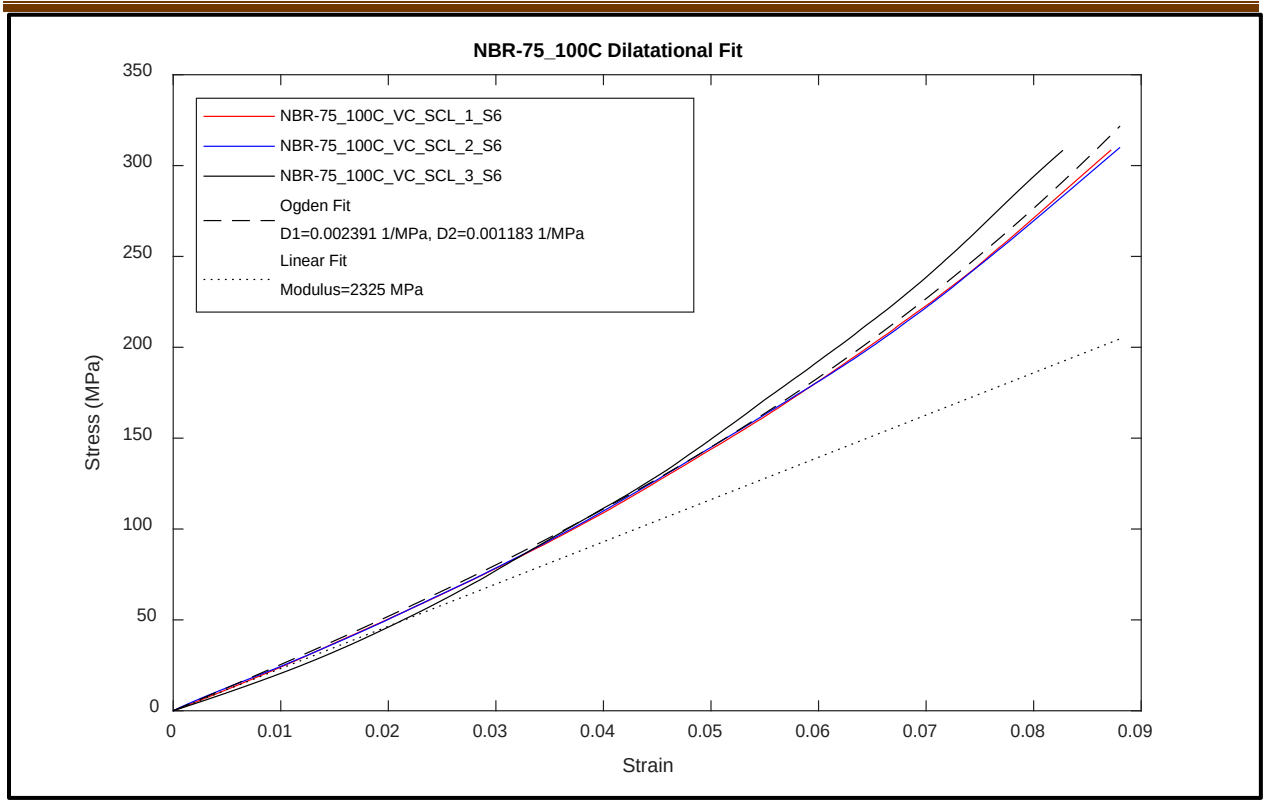
NBR-75_100C Dilatational Fit
NBR-75_100C_VC_SCL_1_S6
NBR-75_100C_VC_SCL_2_S6
NBR-75_100C_VC_SCL_3_S6
Ogden Fit
D1=0.002391 1/MPa, D2=0.001183 1/MPa
Linear Fit
Modulus=2325 MPa
Stress (MPa)
Strain
0
50
100
150
200
250
300
350
0
0.01
0.02
0.03
0.04
0.05
0.06
0.07
0.08
0.09

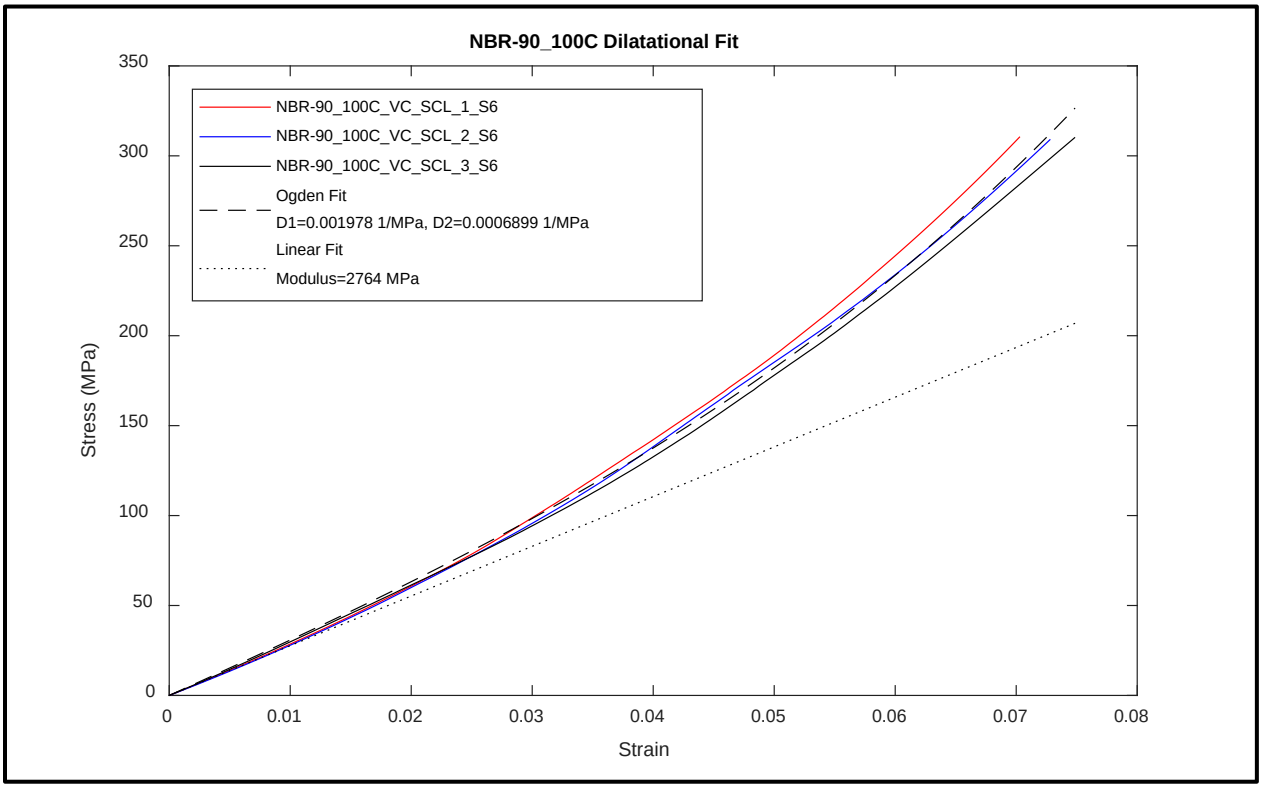
NBR-90_100C Dilatational Fit
NBR-90_100C_VC_SCL_1_S6
NBR-90_100C_VC_SCL_2_S6
NBR-90_100C_VC_SCL_3_S6
Ogden Fit
D1=0.001978 1/MPa, D2=0.0006899 1/MPa
Linear Fit
Modulus=2764 MPa
Stress (MPa)
Strain
0
50
100
150
200
250
300
350
0
0.01
0.02
0.03
0.04
0.05
0.06
0.07
0.08

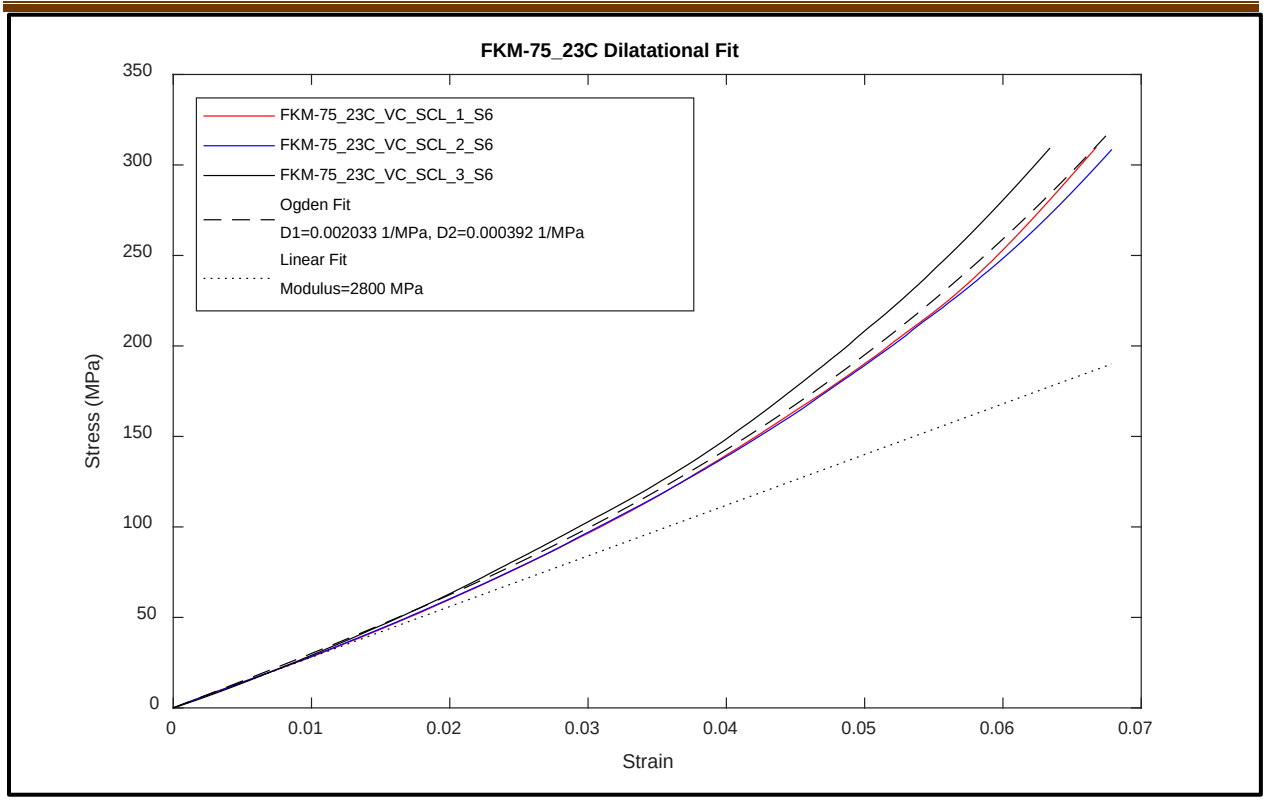
FKM-75_23C Dilatational Fit
FKM-75_23C_VC_SCL_1_S6
FKM-75_23C_VC_SCL_2_S6
FKM-75_23C_VC_SCL_3_S6
Ogden Fit
D1=0.002033 1/MPa, D2=0.000392 1/MPa
Linear Fit
Modulus=2800 MPa
Stress (MPa)
Strain
0
50
100
150
200
250
300
350
0
0.01
0.02
0.03
0.04
0.05
0.06
0.07

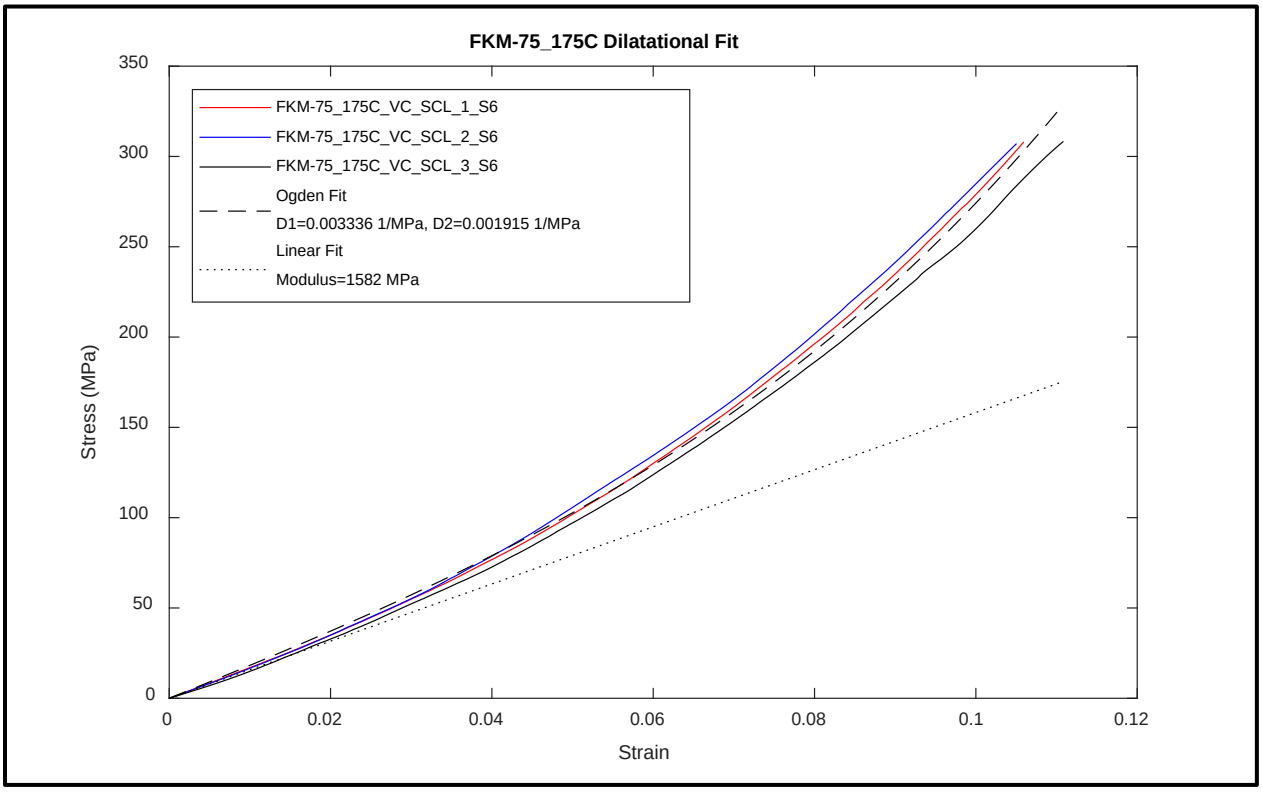
FKM-75_175C Dilatational Fit
FKM-75_175C_VC_SCL_1_S6
FKM-75_175C_VC_SCL_2_S6
FKM-75_175C_VC_SCL_3_S6
Ogden Fit
D1=0.003336 1/MPa, D2=0.001915 1/MPa
Linear Fit
Modulus=1582 MPa
Stress (MPa)
Strain
0
50
100
150
200
250
300
350
0
0.02
0.04
0.06
0.08
0.1
0.12

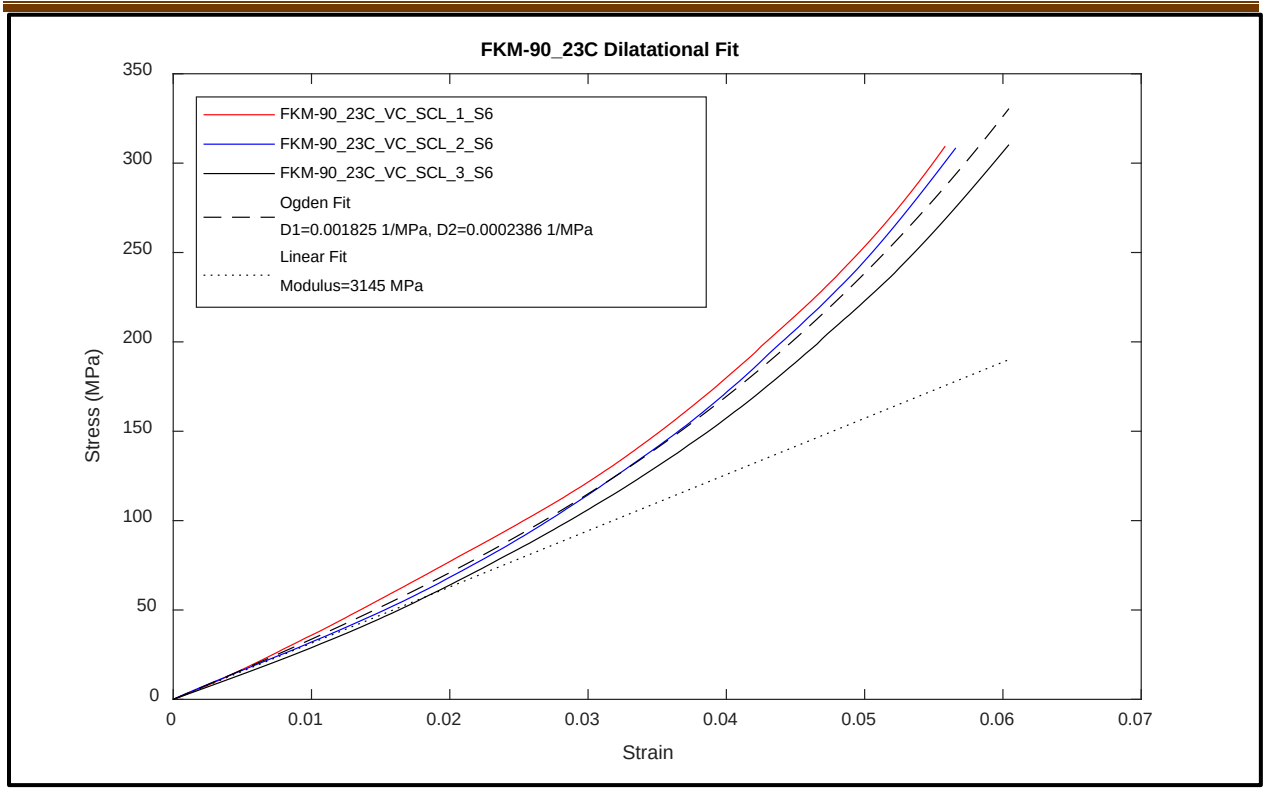


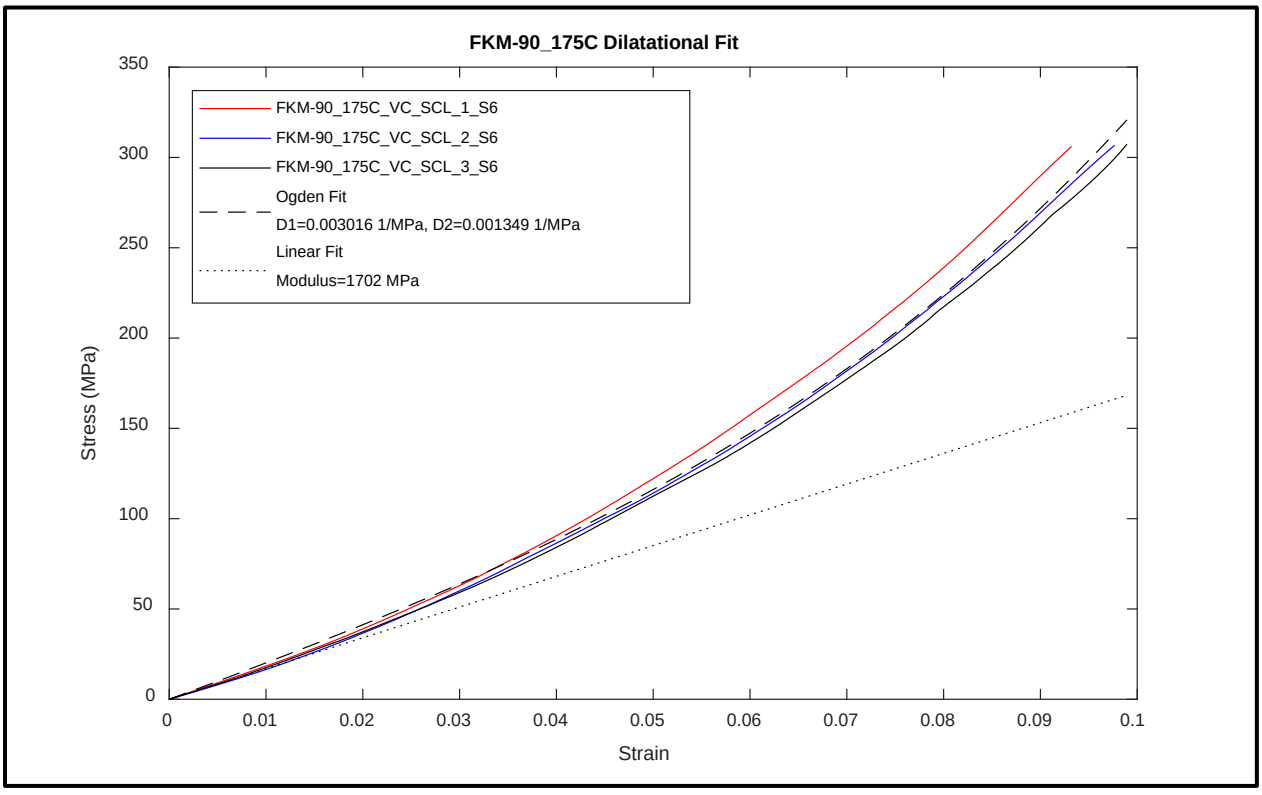


Figure A.4-8. Dilatational Fit.

Table A.4-11. Mullins Law Parameters.

| Material | Test Temperature, °C | Bulk Modulus, MPa | D1, 1/MPa | D2, 1/MPa |
|---|---|---|---|---|
| FEPM-80 | 100 | 2363 | 0.002682 | 0.001122 |
| FEPM-80 | 175 | 3141 | 0.002922 | 0.001697 |
| FEPM-90 | 100 | 2503 | 0.002386 | 0.0007123 |
| FEPM-90 | 175 | 3087 | 0.002836 | 0.001628 |
| HNBR-75 | 100 | 2605 | 0.002215 | 0.001082 |
| HNBR-90 | 100 | 2525 | 0.002032 | 0.0008483 |
| HNBR-90 | 150 | 2224 | 0.002388 | 0.00101 |
| FFKM-75 | 100 | 1180 | 0.004156 | 0.002139 |
| FFKM-75 | 175 | 1251 | 0.005677 | 0.003555 |
| FFKM-90 | 100 | 1206 | 0.004404 | 0.002078 |
| FFKM-90 | 175 | 1302 | 0.005466 | 0.003177 |
| NBR-75 | 100 | 2325 | 0.002391 | 0.001183 |
| NBR-90 | 100 | 2764 | 0.001978 | 0.0006899 |
| FKM-75 | 23 | 2800 | 0.002033 | 0.000392 |
| FKM-75 | 175 | 1582 | 0.003336 | 0.001915 |
| FKM-90 | 23 | 3145 | 0.001825 | 0.0002386 |
| FKM-90 | 175 | 1702 | 0.003016 | 0.001349 |

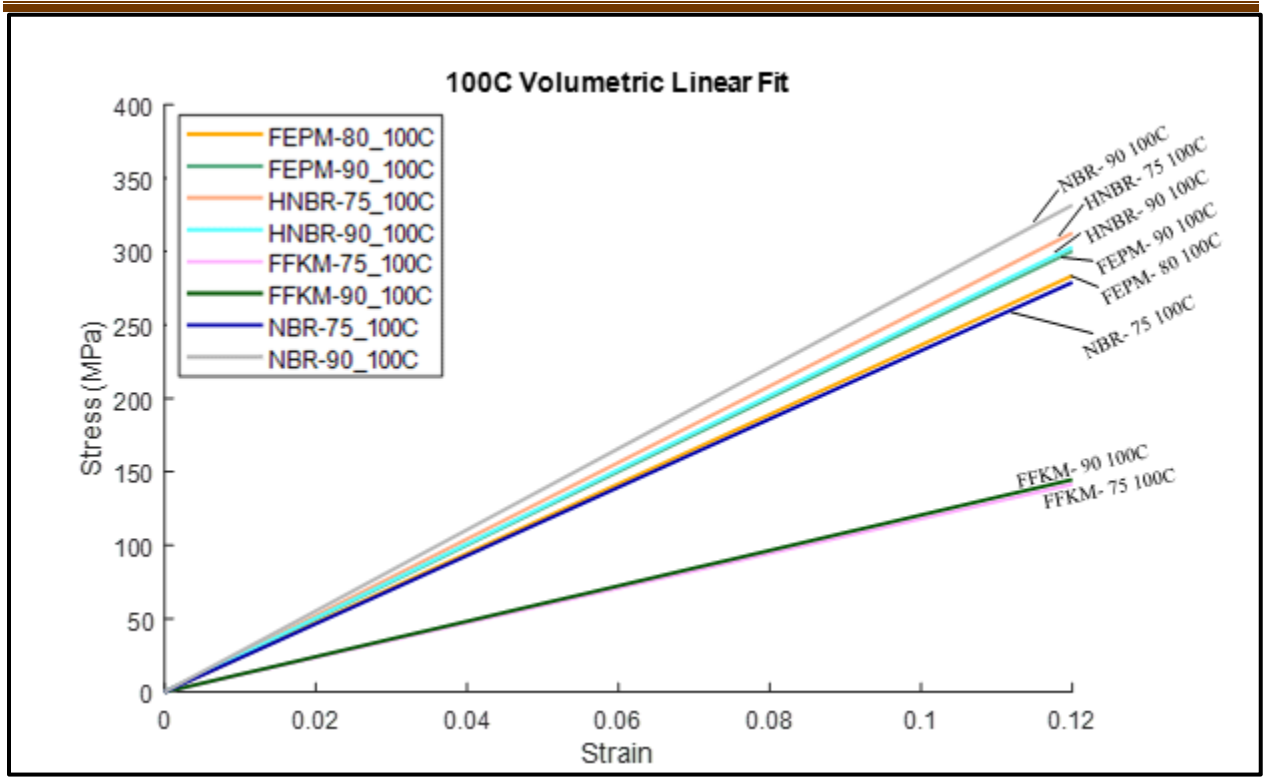


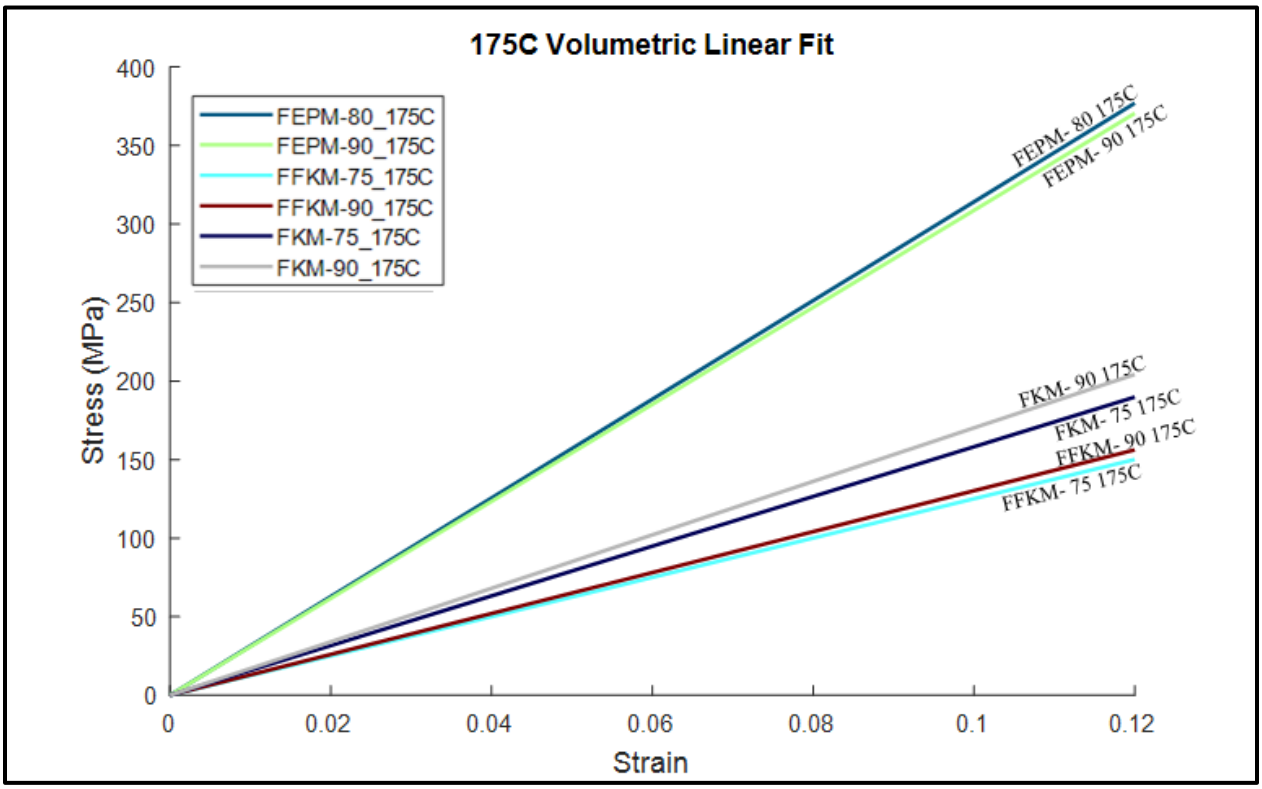


Figure A.4-9. Volumetric linear fit for all materials.

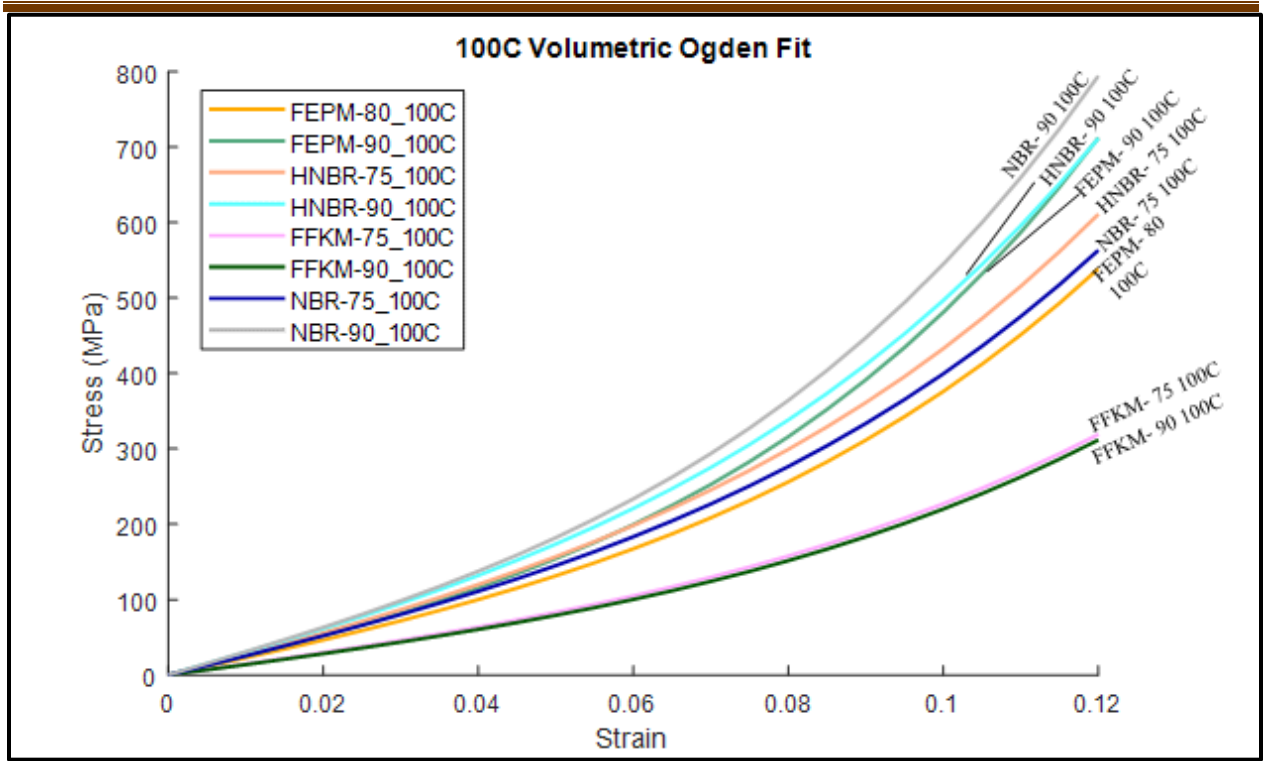


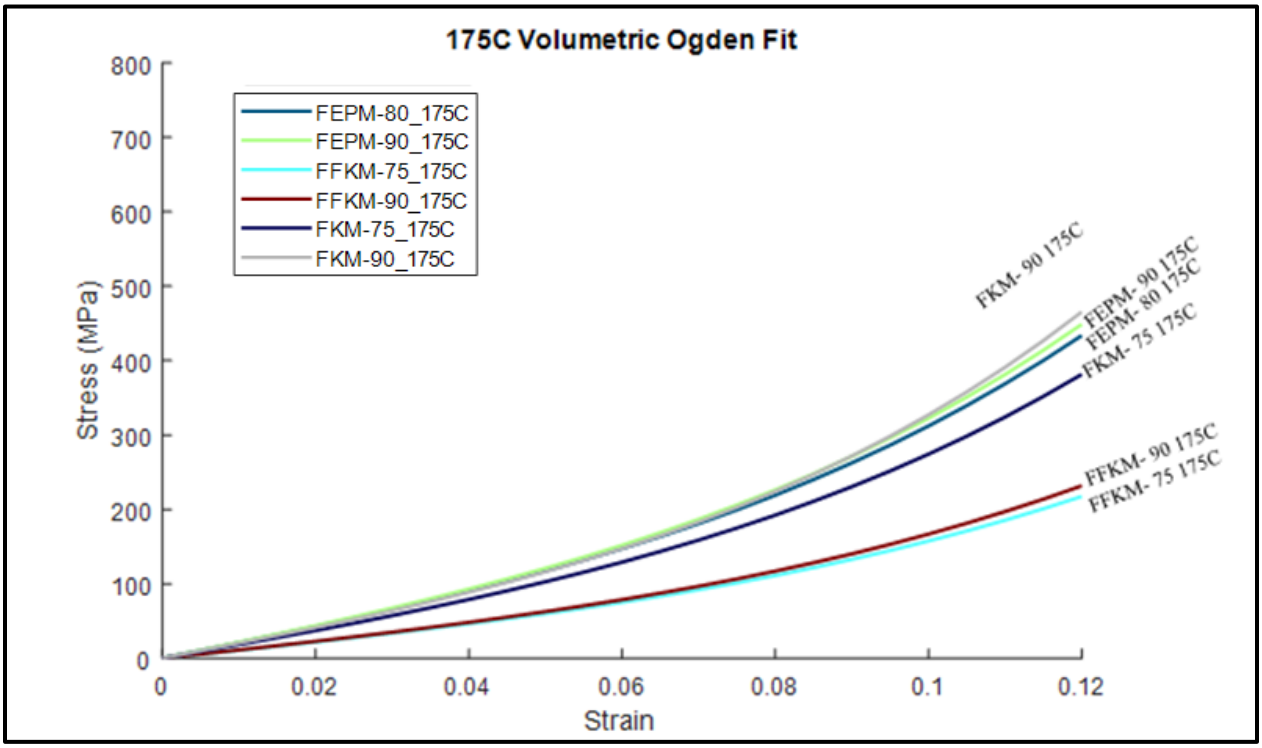


Figure A.4-10. Volumetric Ogden fit for all materials.

# Creep Crack Growth Module

## *Experiment 4: Creep Crack Growth*

Purpose: The rate of creep crack growth indicates how quickly damage will accumulate when an elastomer is held under load. Creep crack growth occurs in addition to cyclic crack growth when load is applied for an extended time. Measuring the creep crack growth rate gives a more complete picture of the total crack growth rate to more accurately estimate fatigue life.

Method: A planar tension specimen with initial cut is used. The specimen is loaded under an increasing strain during an extended time interval. The crack length is measured during the test to determine the crack growth rate at all strain levels during the test.

Specimen: Planar Tension with initial cut. Nominal dimensions 150 mm x 10 mm x 2 mm.
Initial Cut: 25 mm, inserted via razor blade.
Ambient temperature: 100 °C, 175 °C
Strain: small initial strain and slowly increasing until rapid crack growth.
Test Duration: Dependent on observing crack growth.

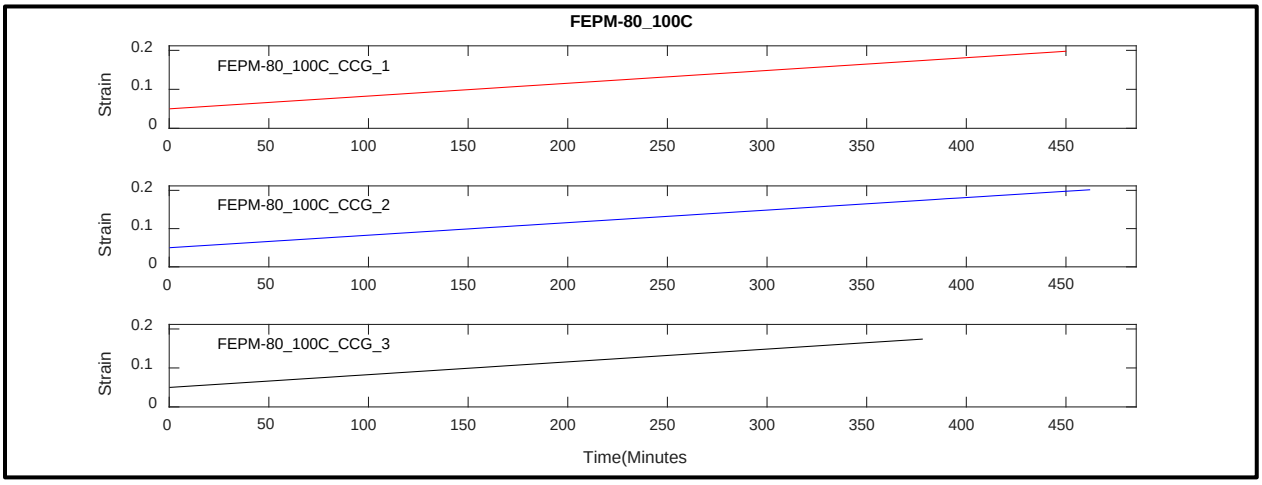

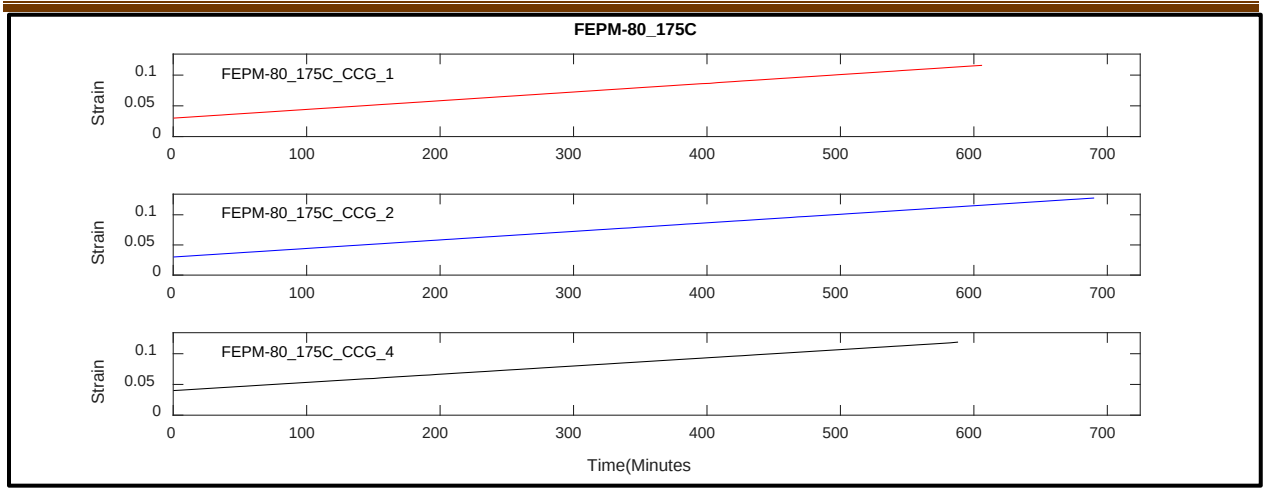
FEPM-80_175C
FEPM-80_175C_CCG_1
FEPM-80_175C_CCG_2
FEPM-80_175C_CCG_4
Strain
Time(Minutes

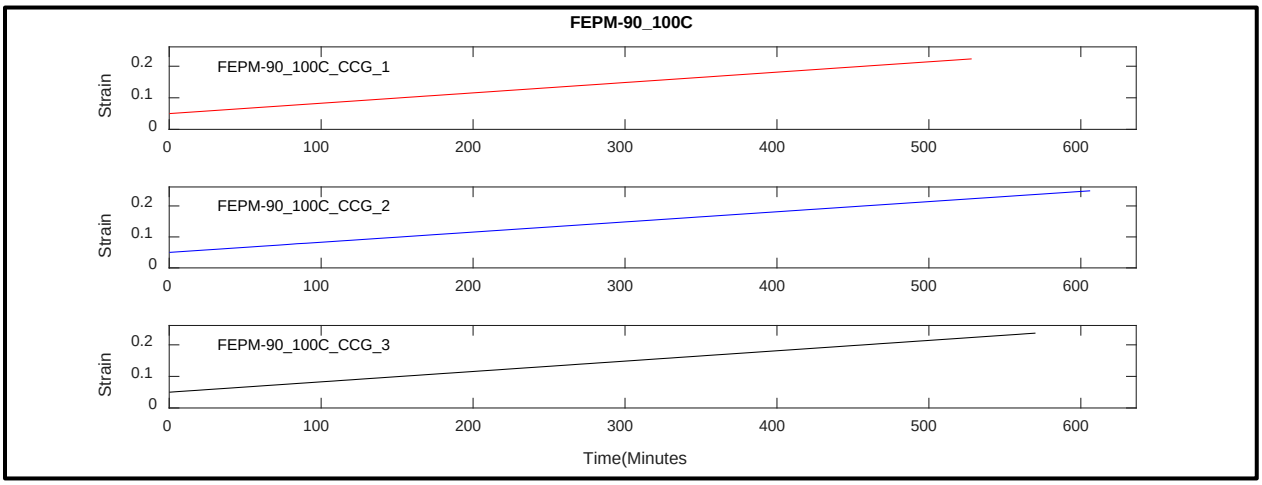
FEPM-90_100C
FEPM-90_100C_CCG_1
FEPM-90_100C_CCG_2
FEPM-90_100C_CCG_3
Strain
Time(Minutes

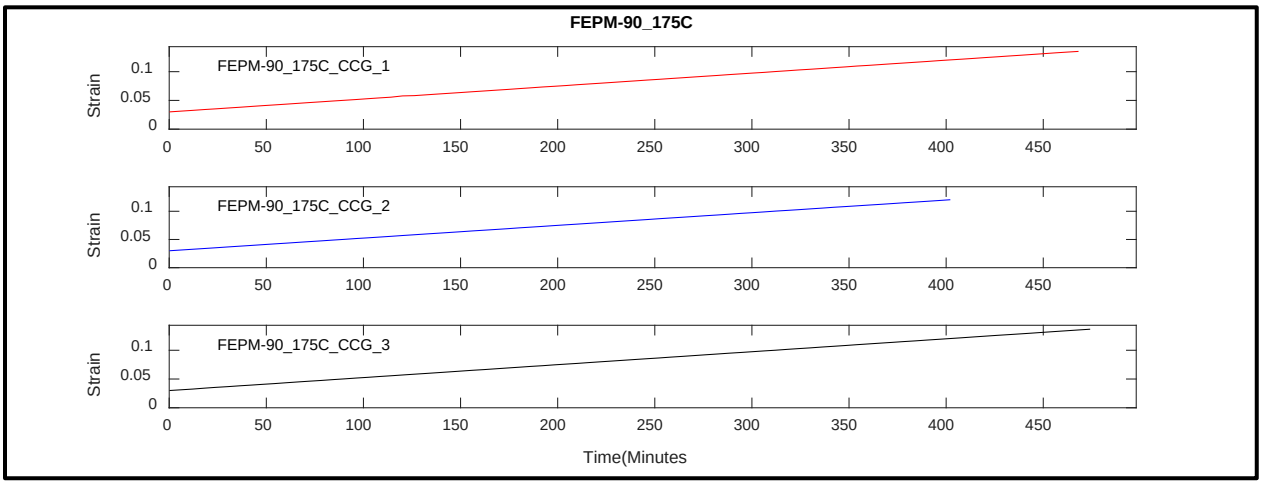
FEPM-90_175C
FEPM-90_175C_CCG_1
FEPM-90_175C_CCG_2
FEPM-90_175C_CCG_3
Strain
Time(Minutes

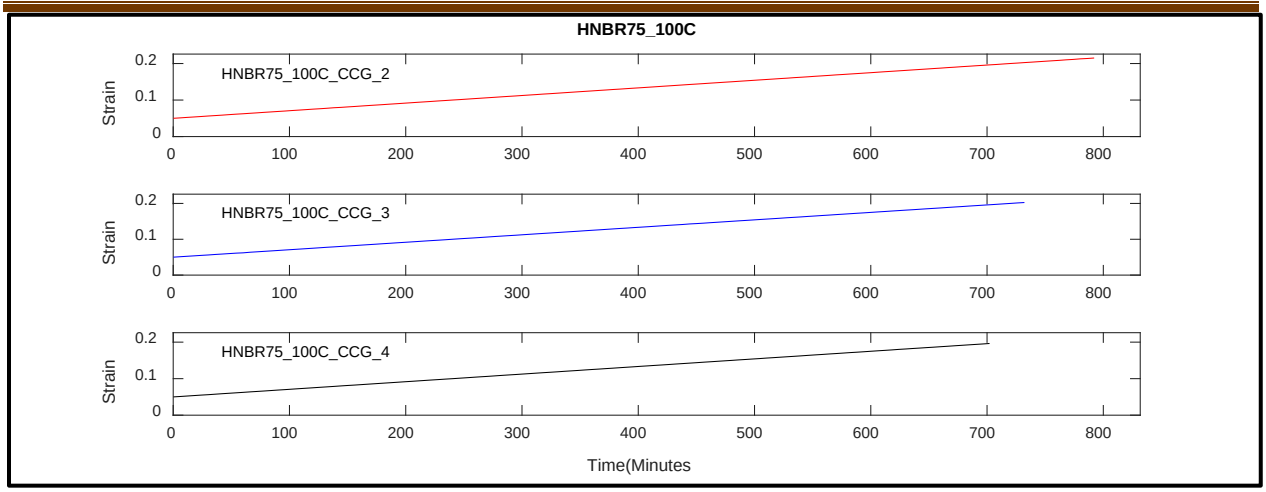
HNBR75_100C
HNBR75_100C_CCG_2
HNBR75_100C_CCG_3
HNBR75_100C_CCG_4
Strain
0.2
0.1
0
0
100
200
300
400
500
600
700
800
Time(Minutes

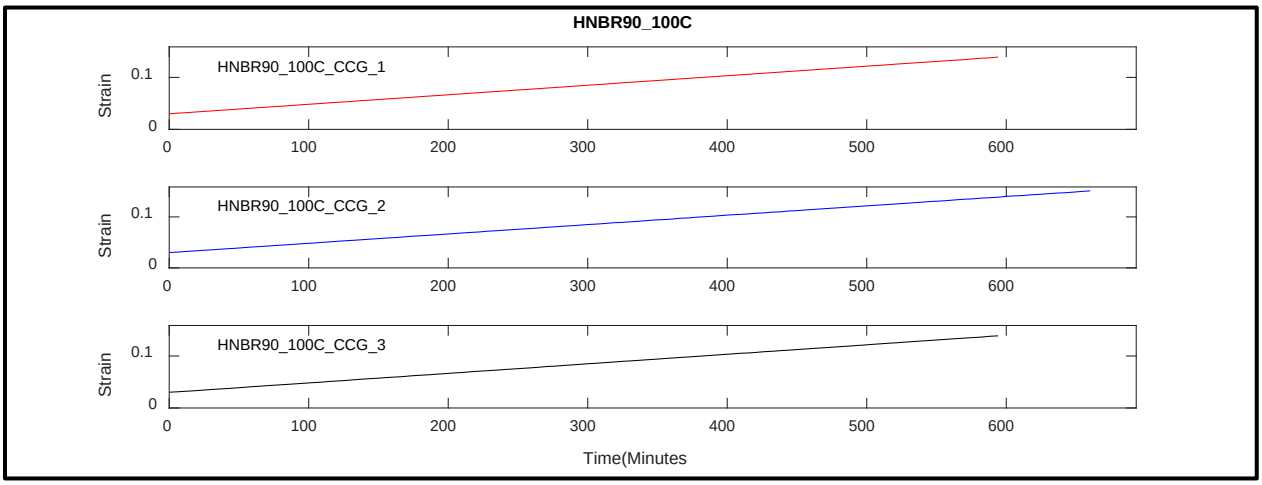
HNBR90_100C
HNBR90_100C_CCG_1
HNBR90_100C_CCG_2
HNBR90_100C_CCG_3
Strain
0.1
0
0
100
200
300
400
500
600
Time(Minutes

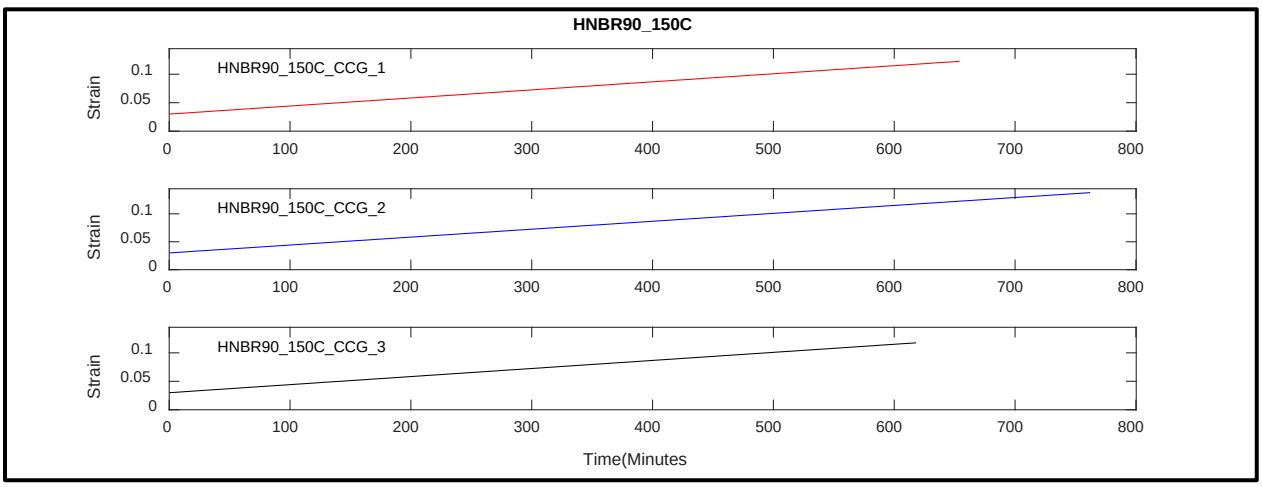
HNBR90_150C
HNBR90_150C_CCG_1
HNBR90_150C_CCG_2
HNBR90_150C_CCG_3
Strain
0.1
0.05
0
0
100
200
300
400
500
600
700
800
Time(Minutes

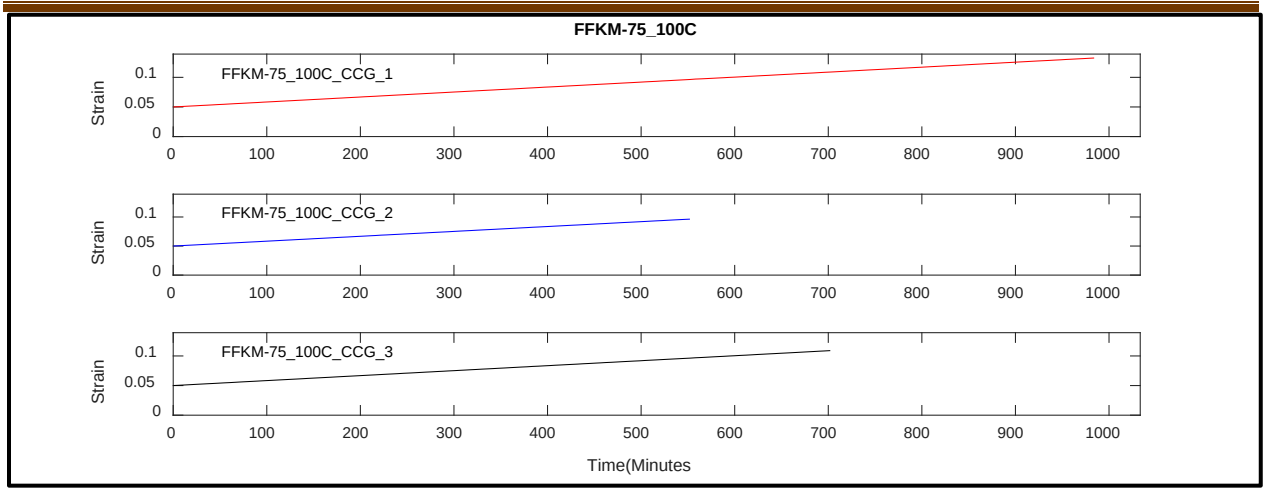
FFKM-75_100C
FFKM-75_100C_CCG_1
FFKM-75_100C_CCG_2
FFKM-75_100C_CCG_3
Strain
Time(Minutes

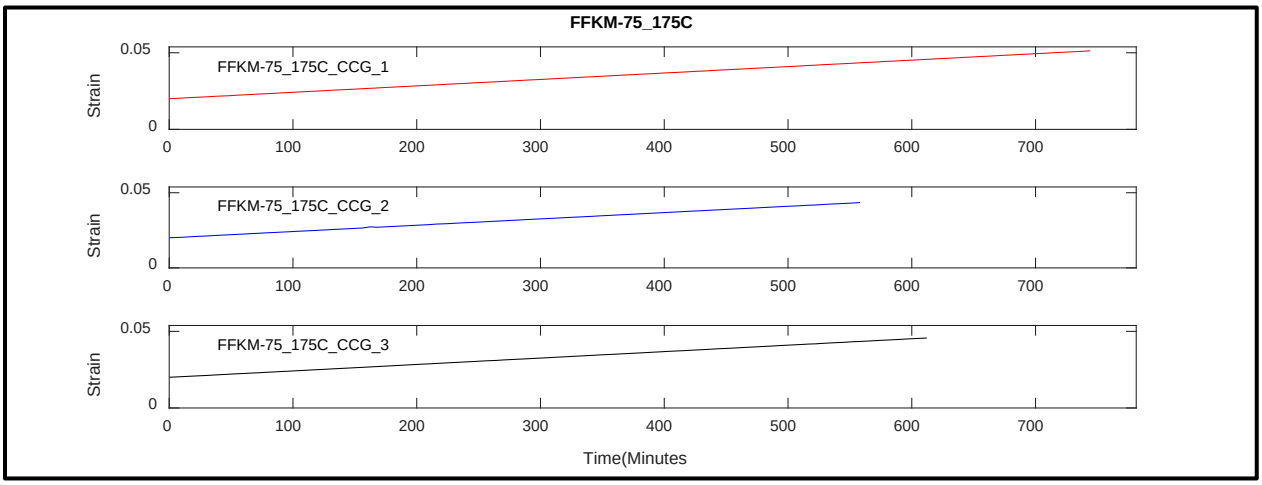
FFKM-75_175C
FFKM-75_175C_CCG_1
FFKM-75_175C_CCG_2
FFKM-75_175C_CCG_3
Strain
Time(Minutes

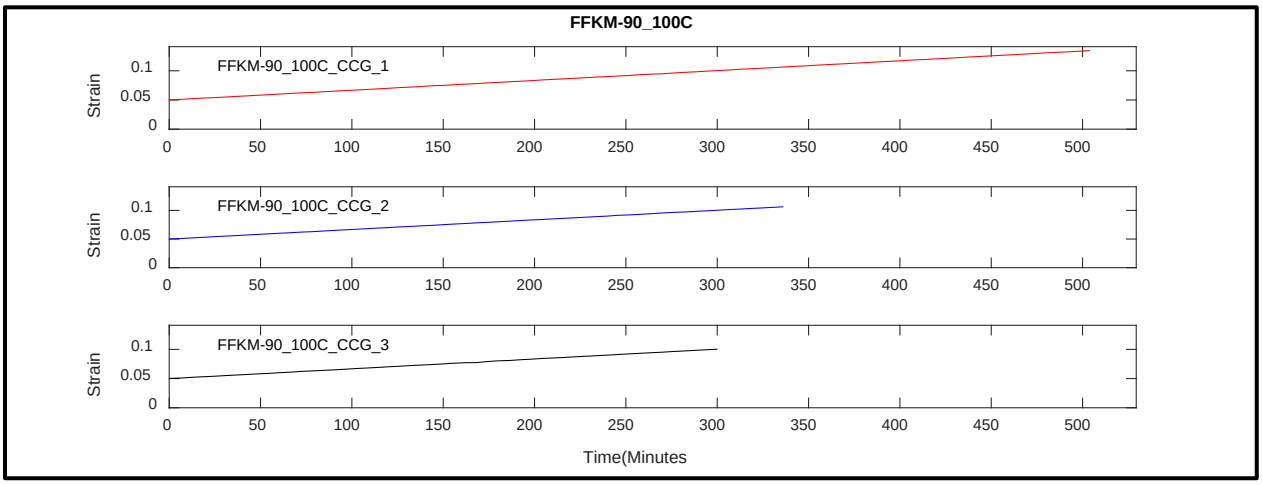
FFKM-90_100C
FFKM-90_100C_CCG_1
FFKM-90_100C_CCG_2
FFKM-90_100C_CCG_3
Strain
Time(Minutes

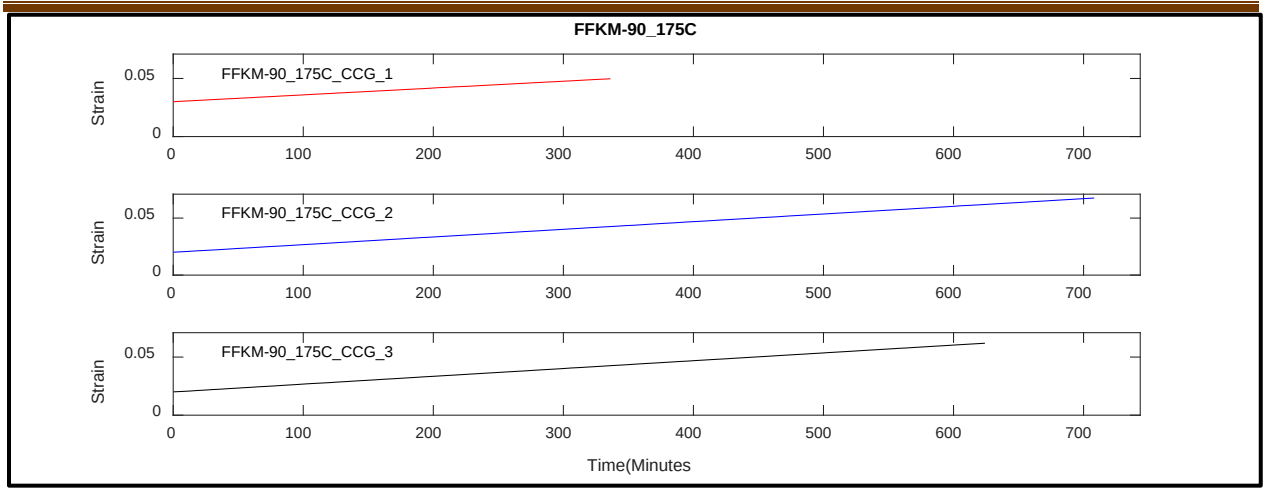
FFKM-90_175C
FFKM-90_175C_CCG_1
FFKM-90_175C_CCG_2
FFKM-90_175C_CCG_3
Strain
0.05
0
0
100
200
300
400
500
600
700
Time(Minutes

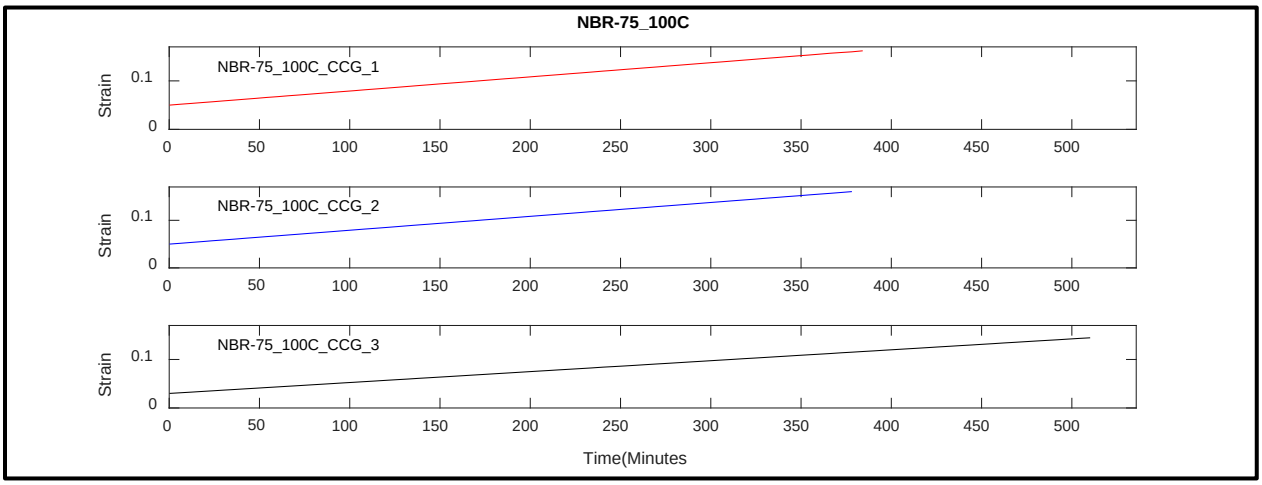
NBR-75_100C
NBR-75_100C_CCG_1
NBR-75_100C_CCG_2
NBR-75_100C_CCG_3
Strain
0.1
0
0
50
100
150
200
250
300
350
400
450
500
Time(Minutes

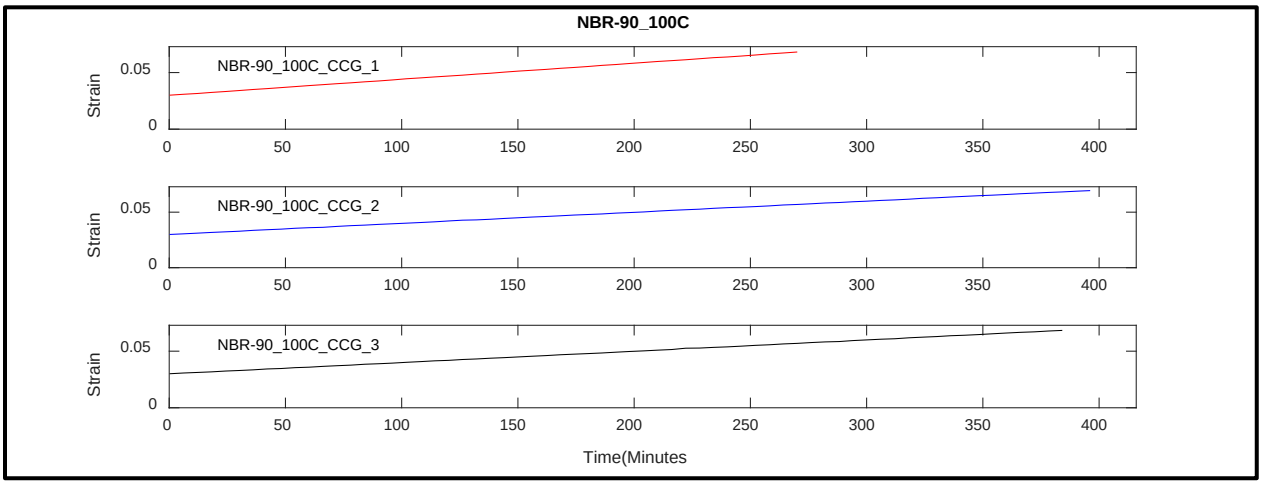
NBR-90_100C
NBR-90_100C_CCG_1
NBR-90_100C_CCG_2
NBR-90_100C_CCG_3
Strain
0.05
0
0
50
100
150
200
250
300
350
400
Time(Minutes

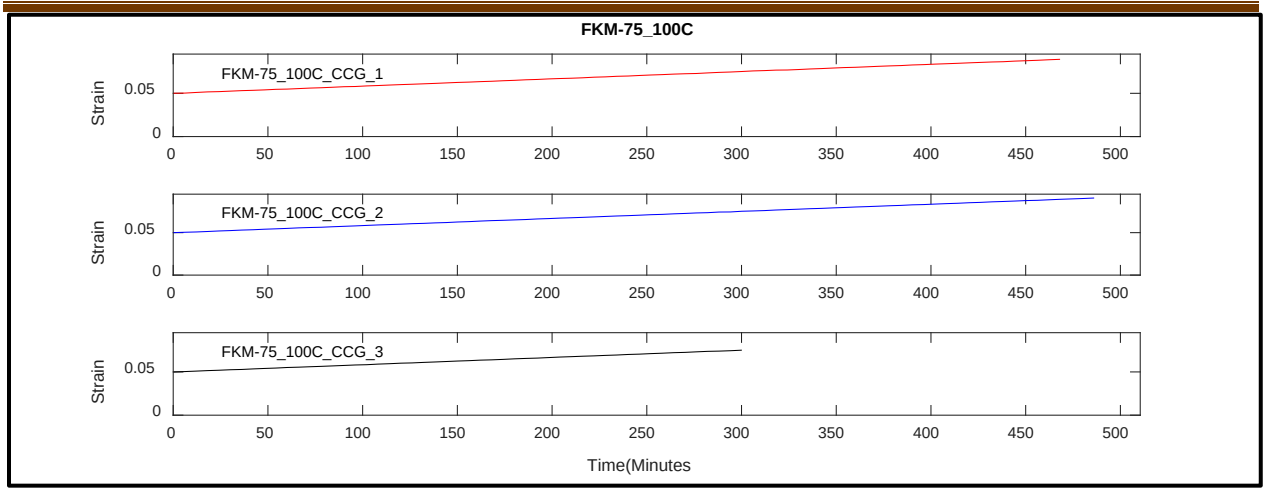
FKM-75_100C
FKM-75_100C_CCG_1
FKM-75_100C_CCG_2
FKM-75_100C_CCG_3
Strain
0.05
0
0
50
100
150
200
250
300
350
400
450
500
Time(Minutes

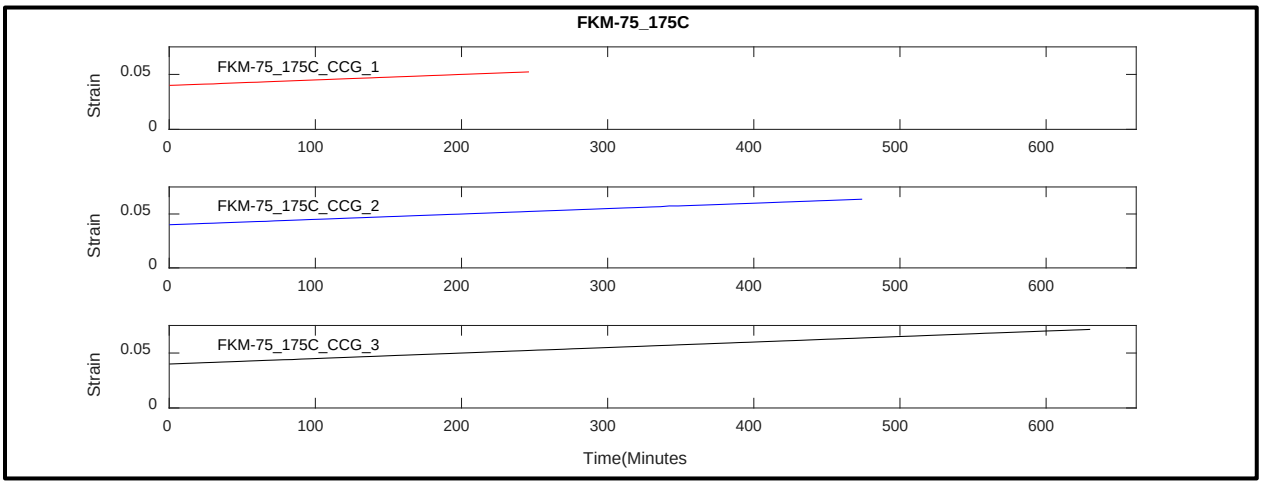
FKM-75_175C
FKM-75_175C_CCG_1
FKM-75_175C_CCG_2
FKM-75_175C_CCG_3
Strain
0.05
0
0
100
200
300
400
500
600
Time(Minutes

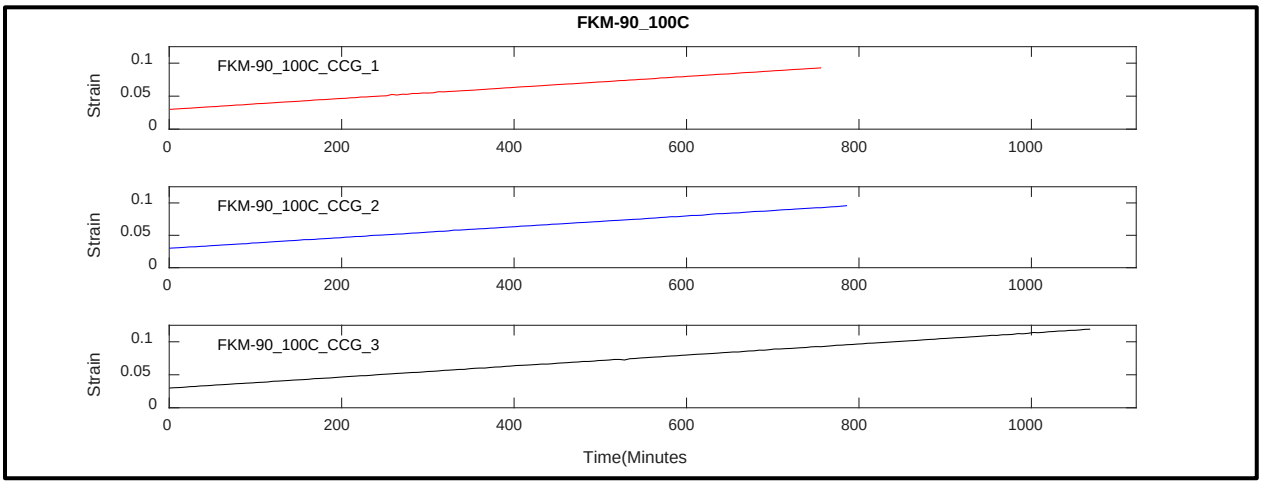
FKM-90_100C
FKM-90_100C_CCG_1
FKM-90_100C_CCG_2
FKM-90_100C_CCG_3
Strain
0.1
0.05
0
0
200
400
600
800
1000
Time(Minutes

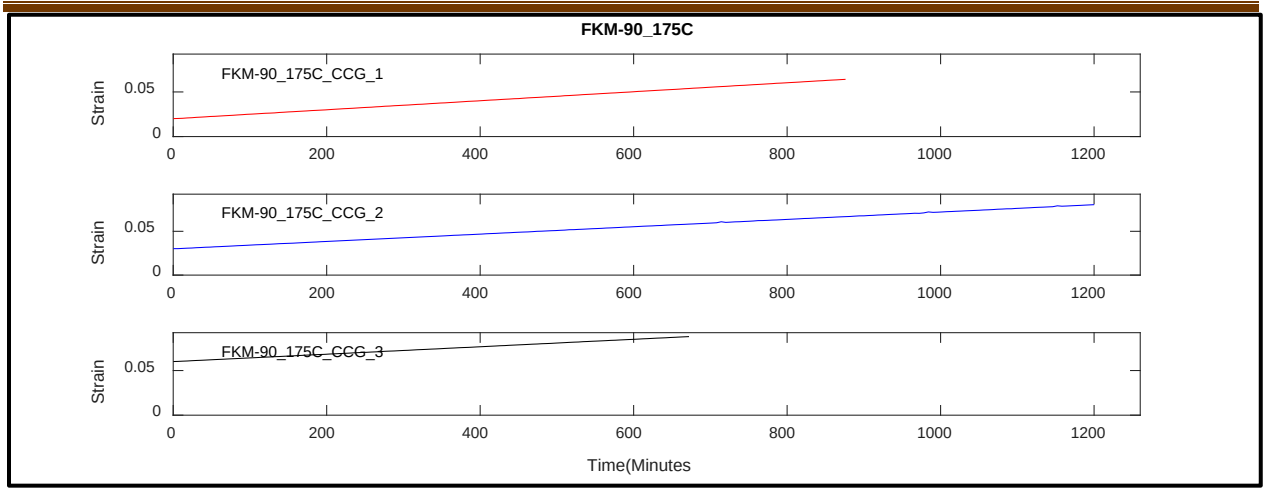


Figure A.4-11. Strain history during creep crack growth rate experiment.

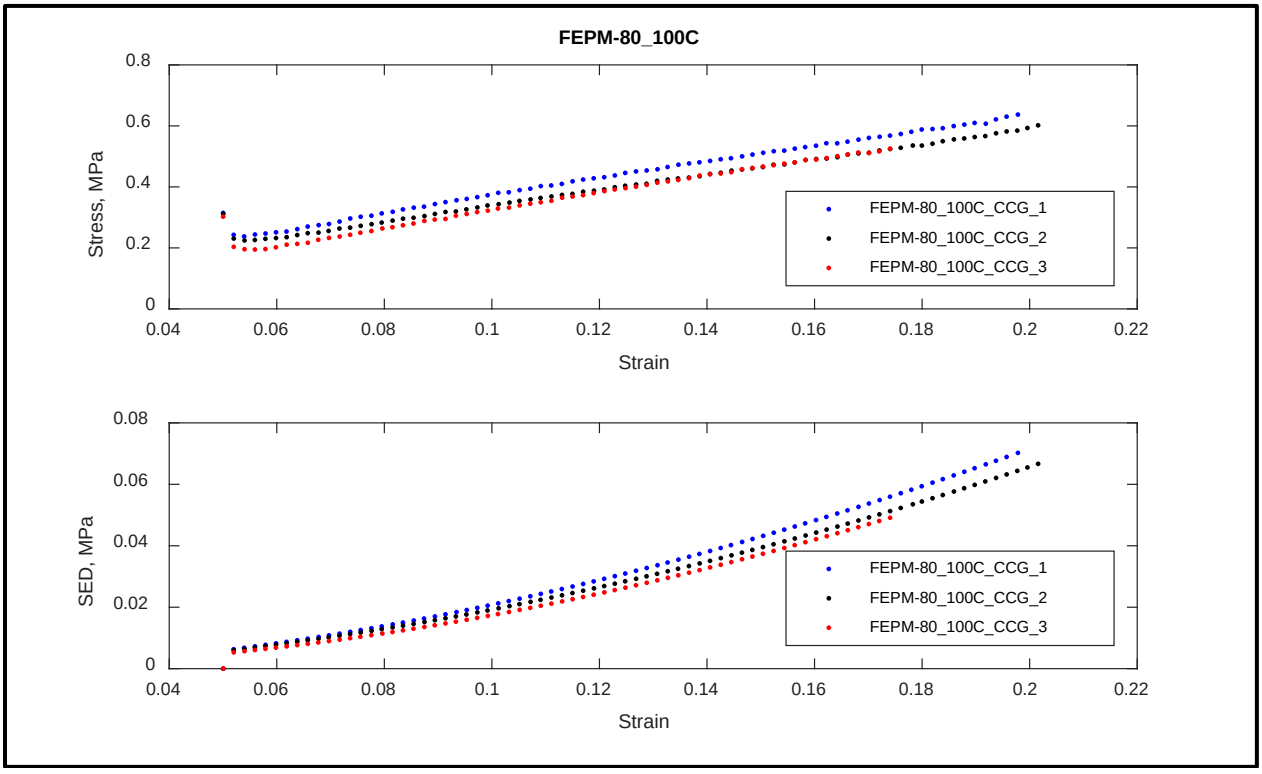

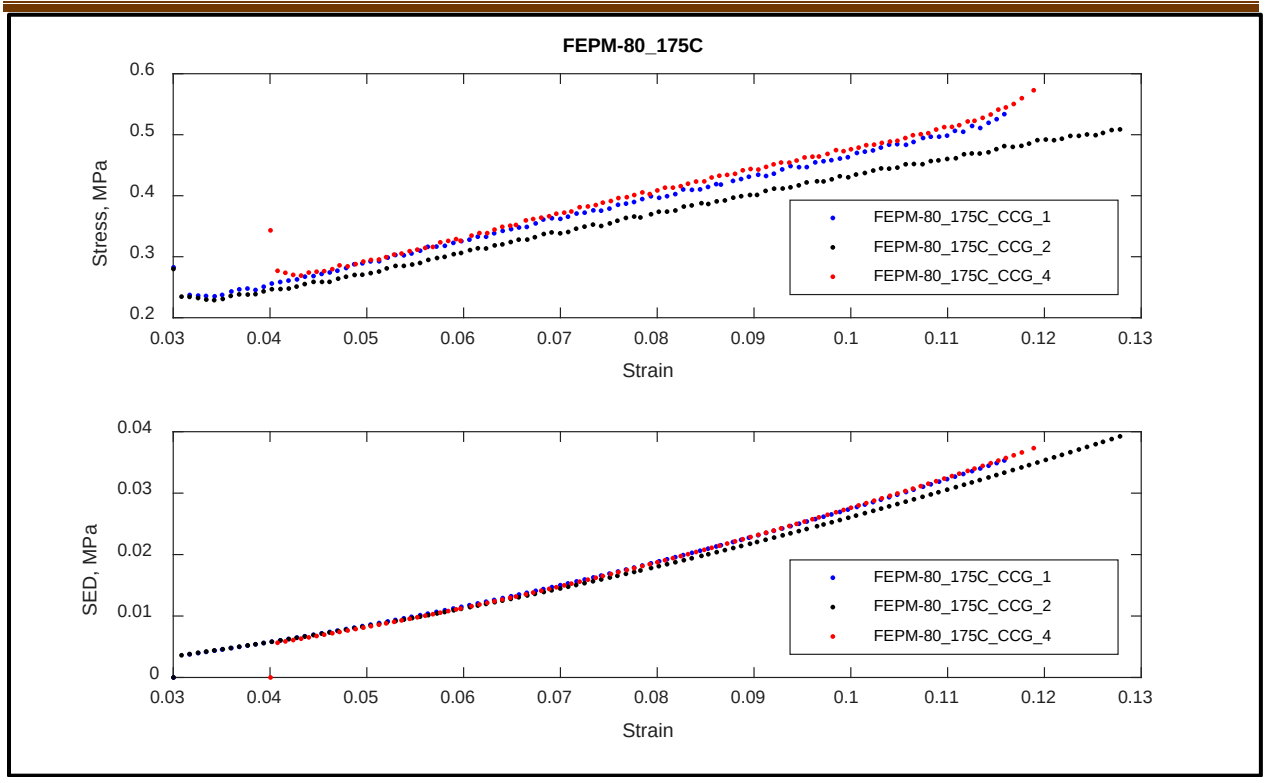
FEPM-80_175C
Stress, MPa
Strain
FEPM-80_175C_CCG_1
FEPM-80_175C_CCG_2
FEPM-80_175C_CCG_4
SED, MPa
Strain
FEPM-80_175C_CCG_1
FEPM-80_175C_CCG_2
FEPM-80_175C_CCG_4

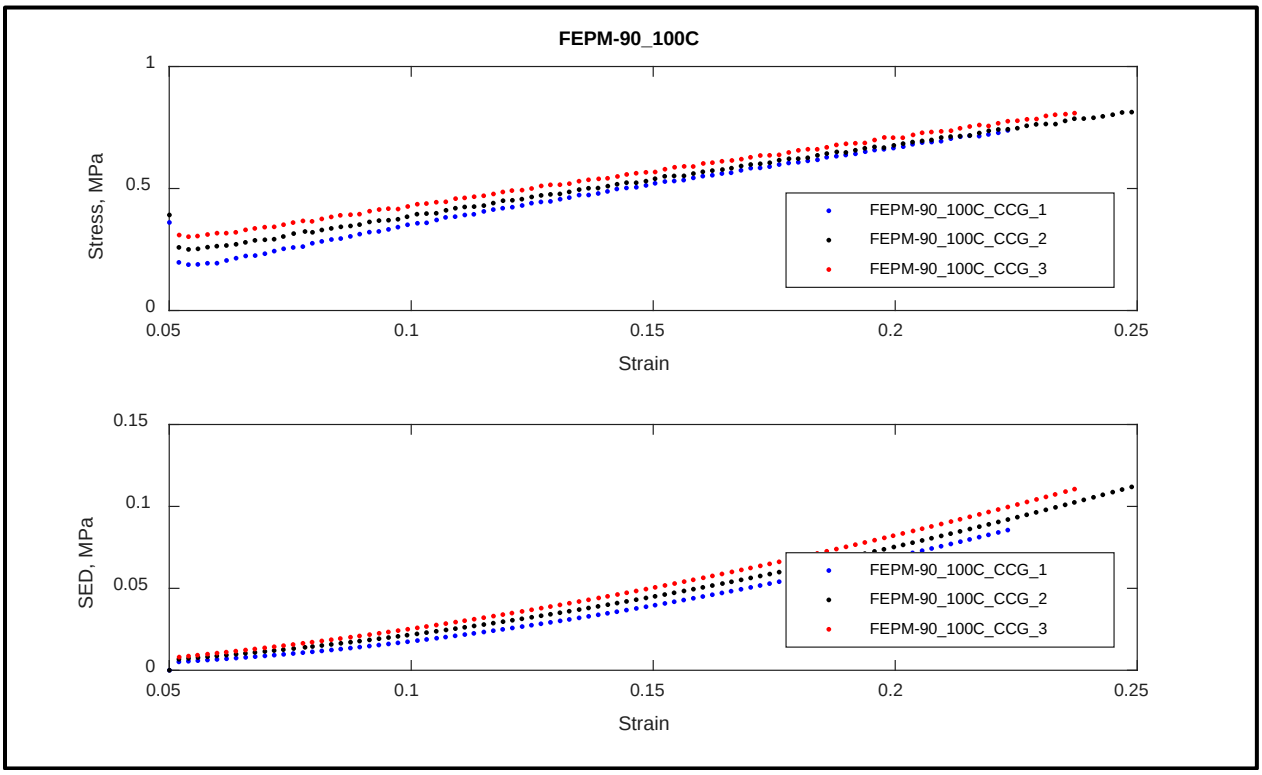
FEPM-90_100C
Stress, MPa
Strain
FEPM-90_100C_CCG_1
FEPM-90_100C_CCG_2
FEPM-90_100C_CCG_3
SED, MPa
Strain
FEPM-90_100C_CCG_1
FEPM-90_100C_CCG_2
FEPM-90_100C_CCG_3

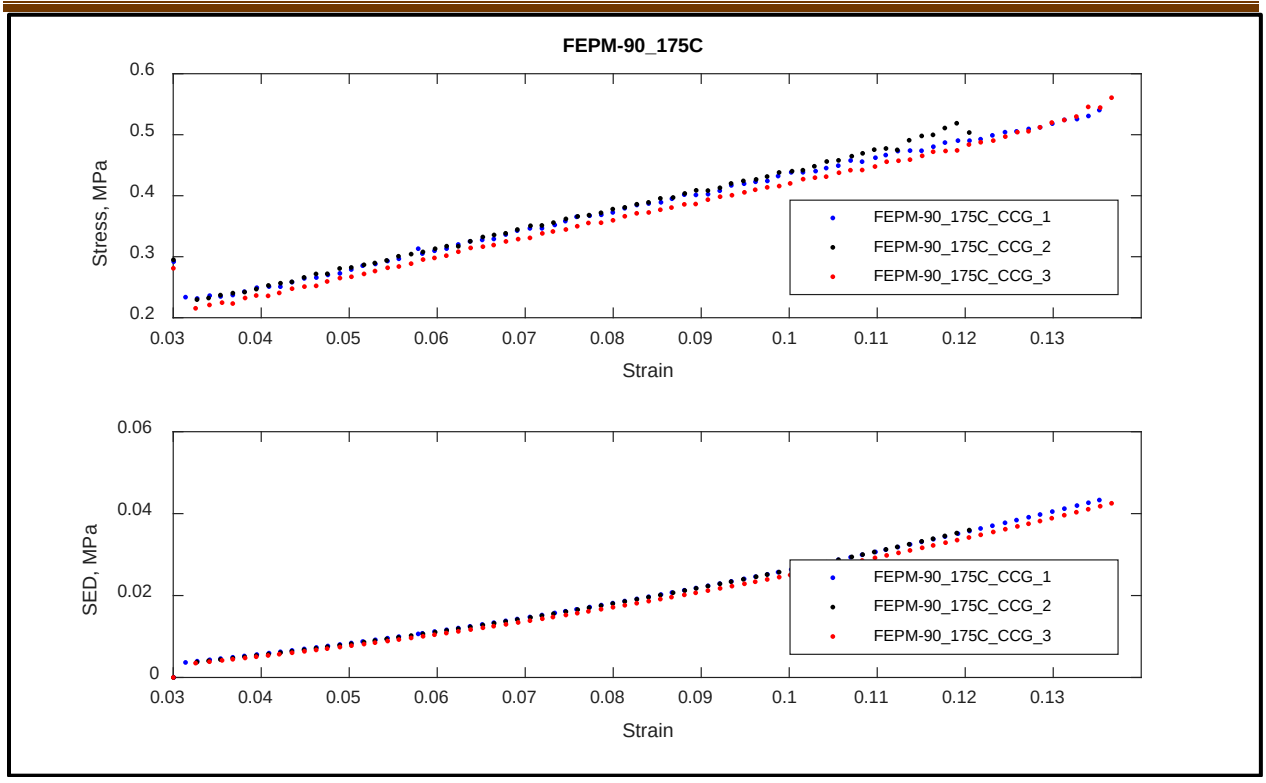
FEPM-90_175C
Stress, MPa
Strain
FEPM-90_175C_CCG_1
FEPM-90_175C_CCG_2
FEPM-90_175C_CCG_3
SED, MPa
Strain
FEPM-90_175C_CCG_1
FEPM-90_175C_CCG_2
FEPM-90_175C_CCG_3

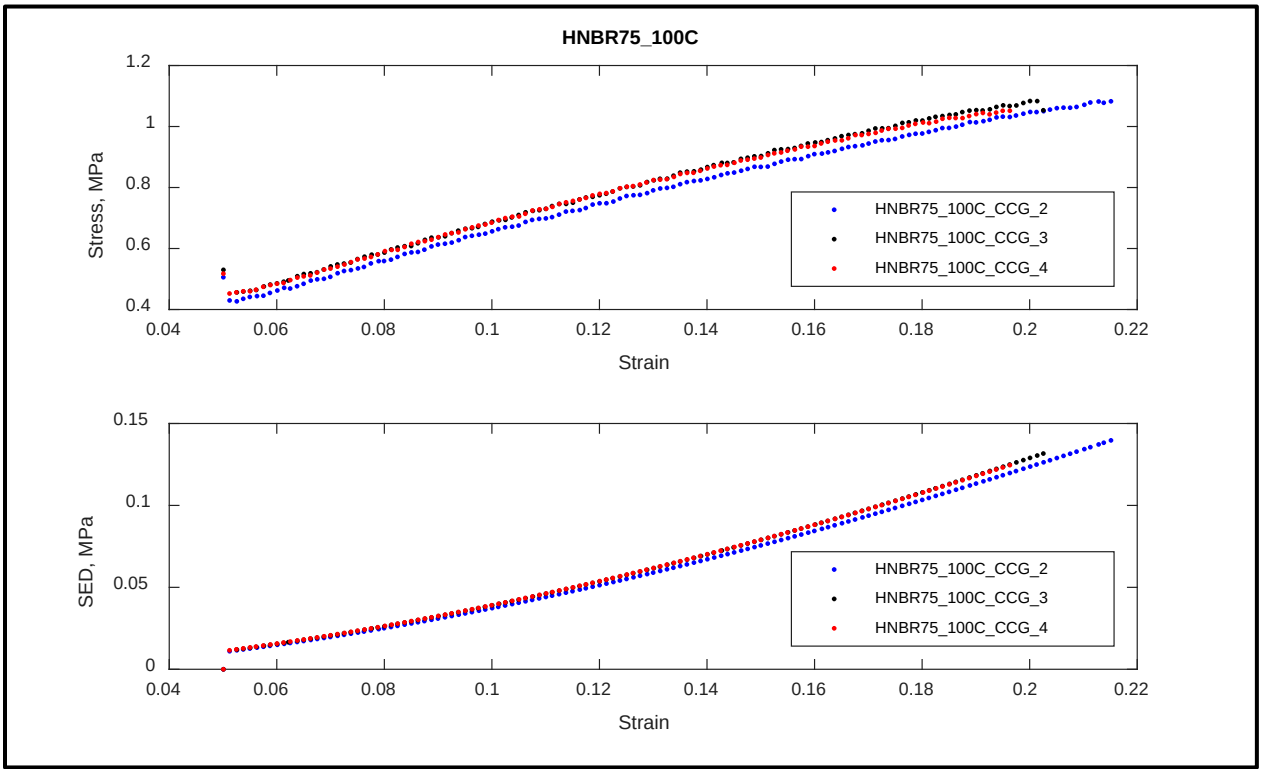
HNBR75_100C
Stress, MPa
Strain
HNBR75_100C_CCG_2
HNBR75_100C_CCG_3
HNBR75_100C_CCG_4
SED, MPa
Strain
HNBR75_100C_CCG_2
HNBR75_100C_CCG_3
HNBR75_100C_CCG_4

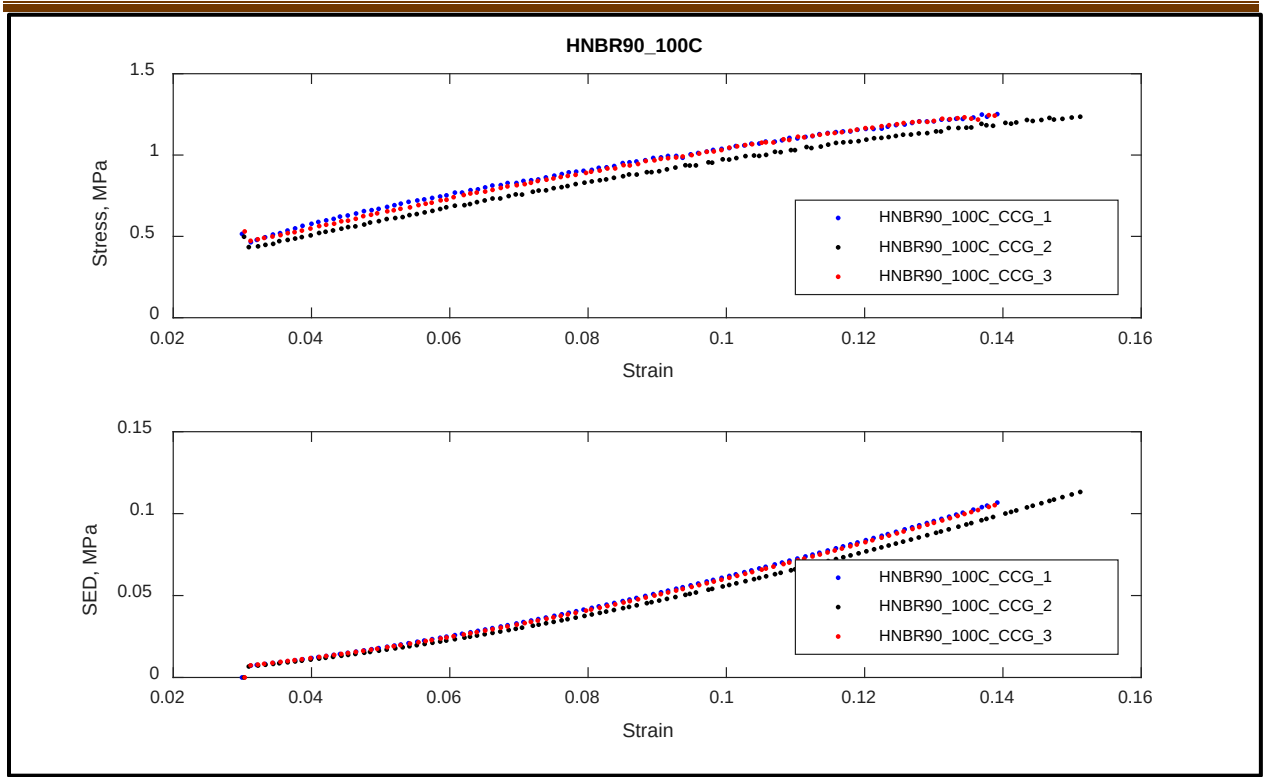
HNBR90_100C
Stress, MPa
Strain
HNBR90_100C_CCG_1
HNBR90_100C_CCG_2
HNBR90_100C_CCG_3
SED, MPa
Strain
HNBR90_100C_CCG_1
HNBR90_100C_CCG_2
HNBR90_100C_CCG_3

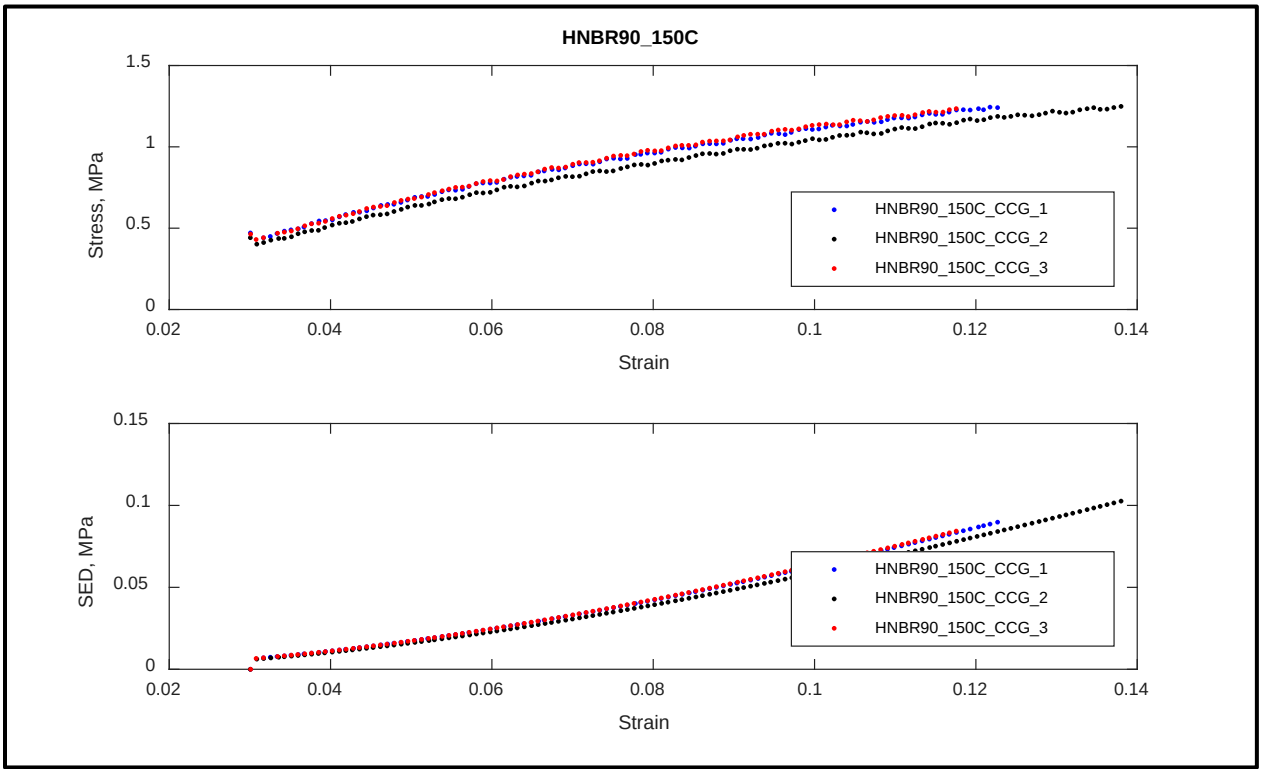
HNBR90_150C
Stress, MPa
Strain
HNBR90_150C_CCG_1
HNBR90_150C_CCG_2
HNBR90_150C_CCG_3
SED, MPa
Strain
HNBR90_150C_CCG_1
HNBR90_150C_CCG_2
HNBR90_150C_CCG_3

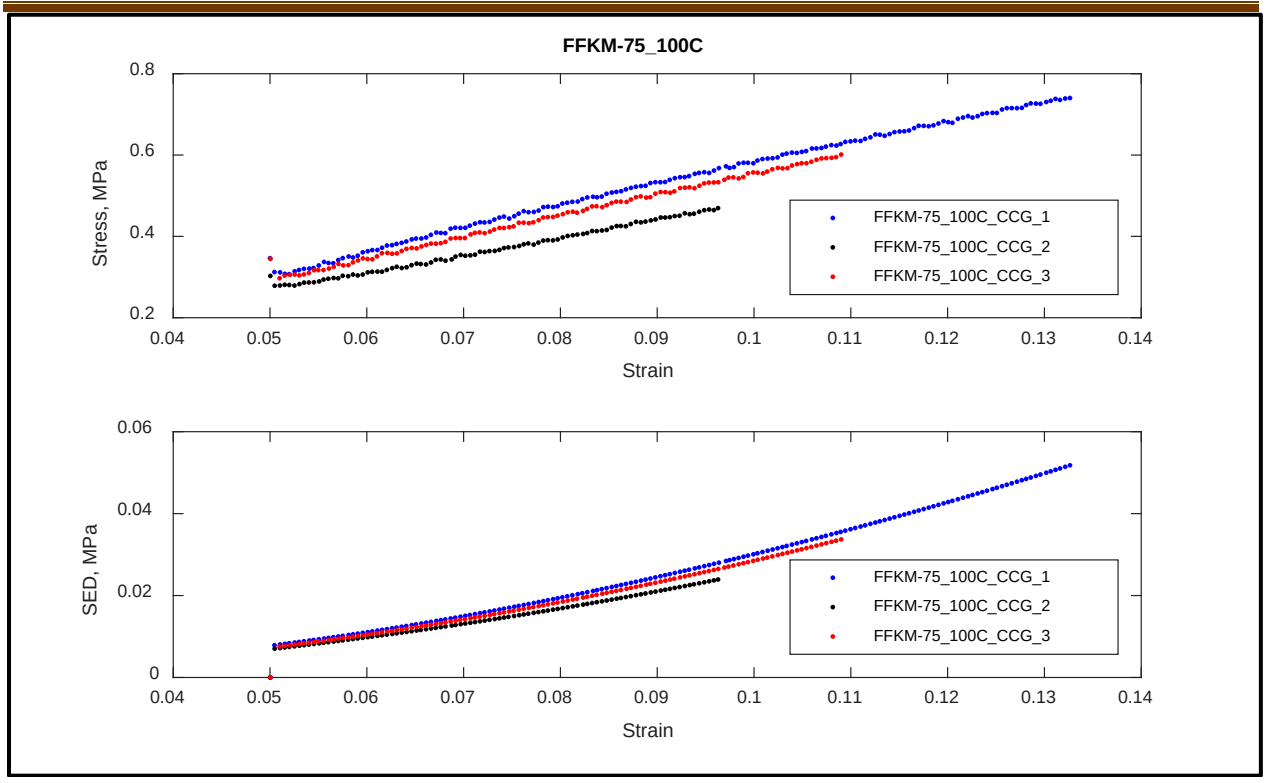
FFKM-75_100C
Stress, MPa
Strain
FFKM-75_100C_CCG_1
FFKM-75_100C_CCG_2
FFKM-75_100C_CCG_3
SED, MPa
Strain
FFKM-75_100C_CCG_1
FFKM-75_100C_CCG_2
FFKM-75_100C_CCG_3

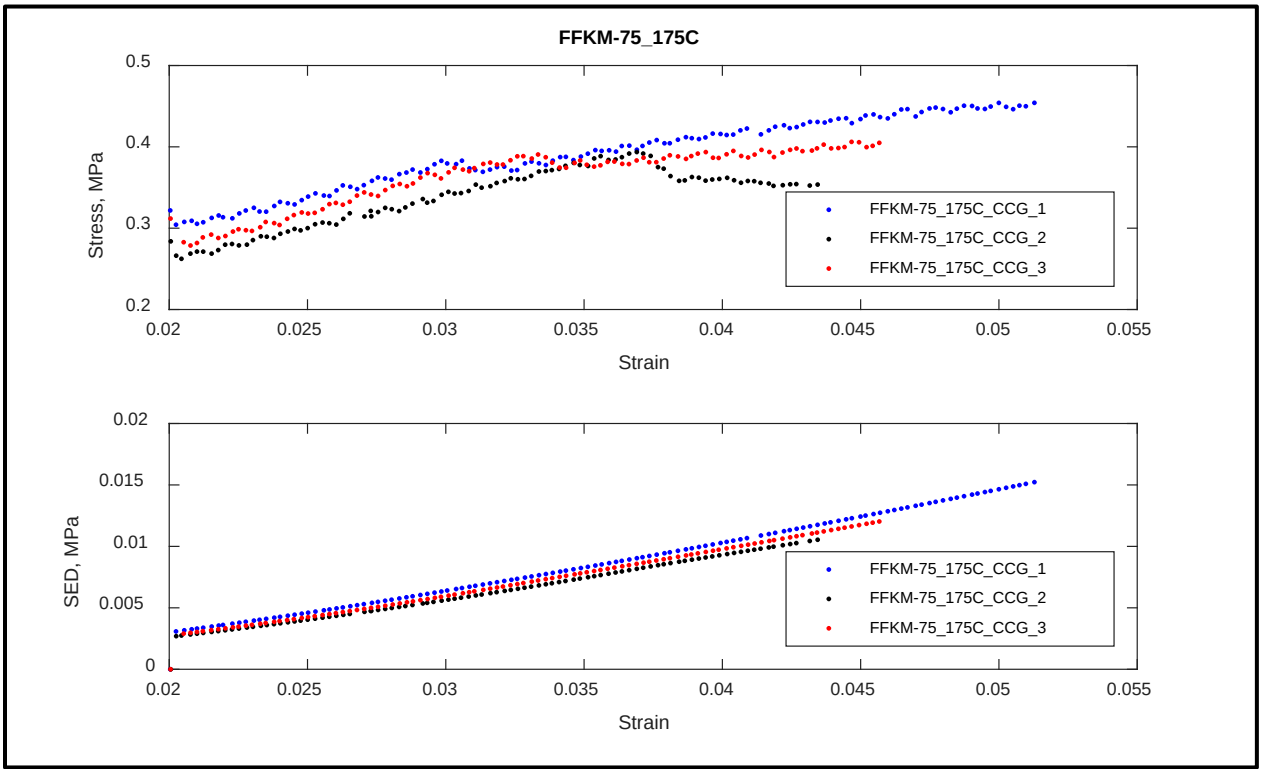
FFKM-75_175C
Stress, MPa
Strain
FFKM-75_175C_CCG_1
FFKM-75_175C_CCG_2
FFKM-75_175C_CCG_3
SED, MPa
Strain
FFKM-75_175C_CCG_1
FFKM-75_175C_CCG_2
FFKM-75_175C_CCG_3

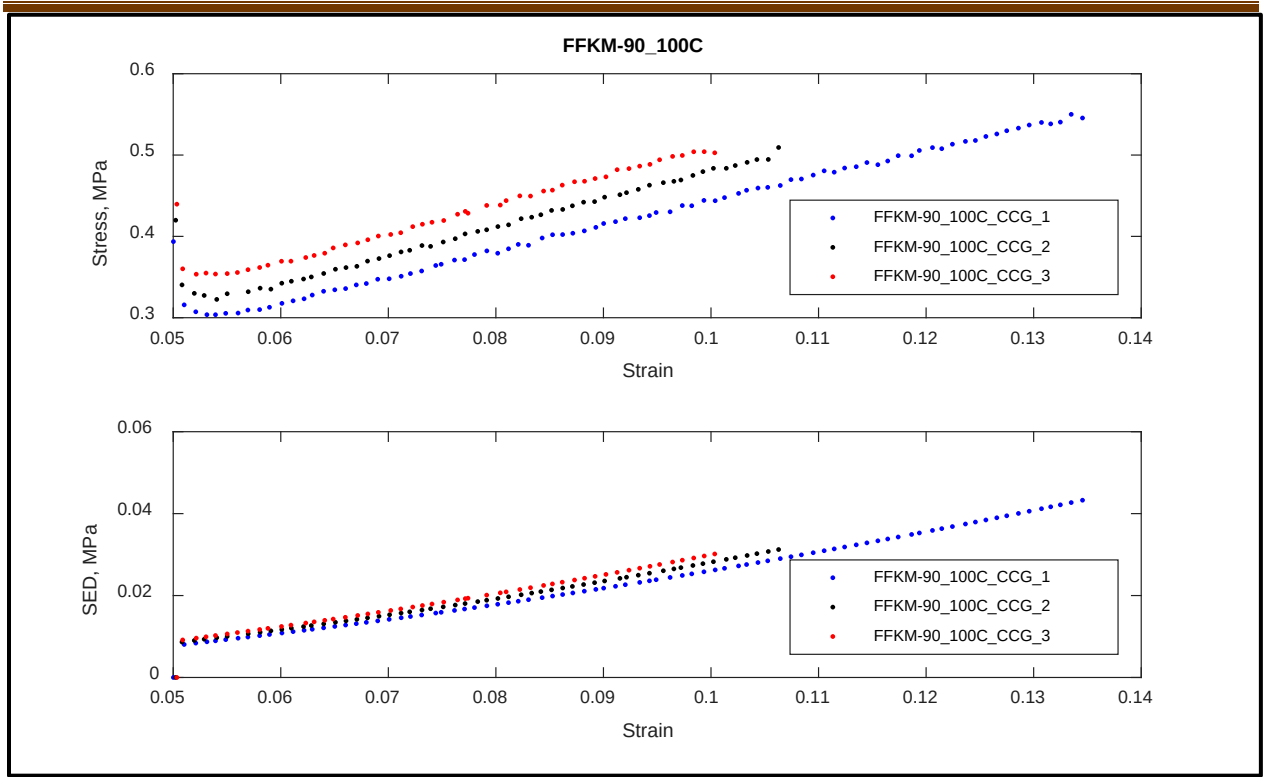
FFKM-90_100C
Stress, MPa
Strain
FFKM-90_100C_CCG_1
FFKM-90_100C_CCG_2
FFKM-90_100C_CCG_3
SED, MPa
Strain
FFKM-90_100C_CCG_1
FFKM-90_100C_CCG_2
FFKM-90_100C_CCG_3

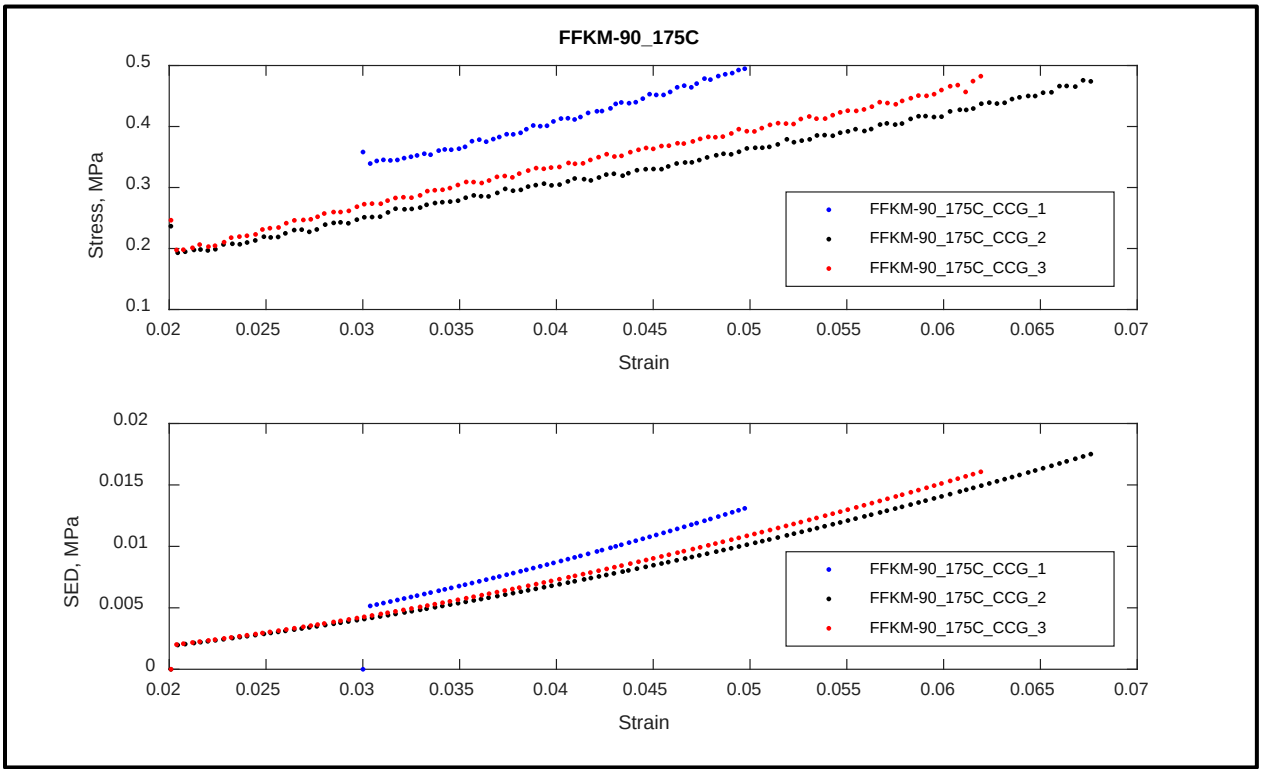
FFKM-90_175C
Stress, MPa
Strain
FFKM-90_175C_CCG_1
FFKM-90_175C_CCG_2
FFKM-90_175C_CCG_3
SED, MPa
Strain
FFKM-90_175C_CCG_1
FFKM-90_175C_CCG_2
FFKM-90_175C_CCG_3

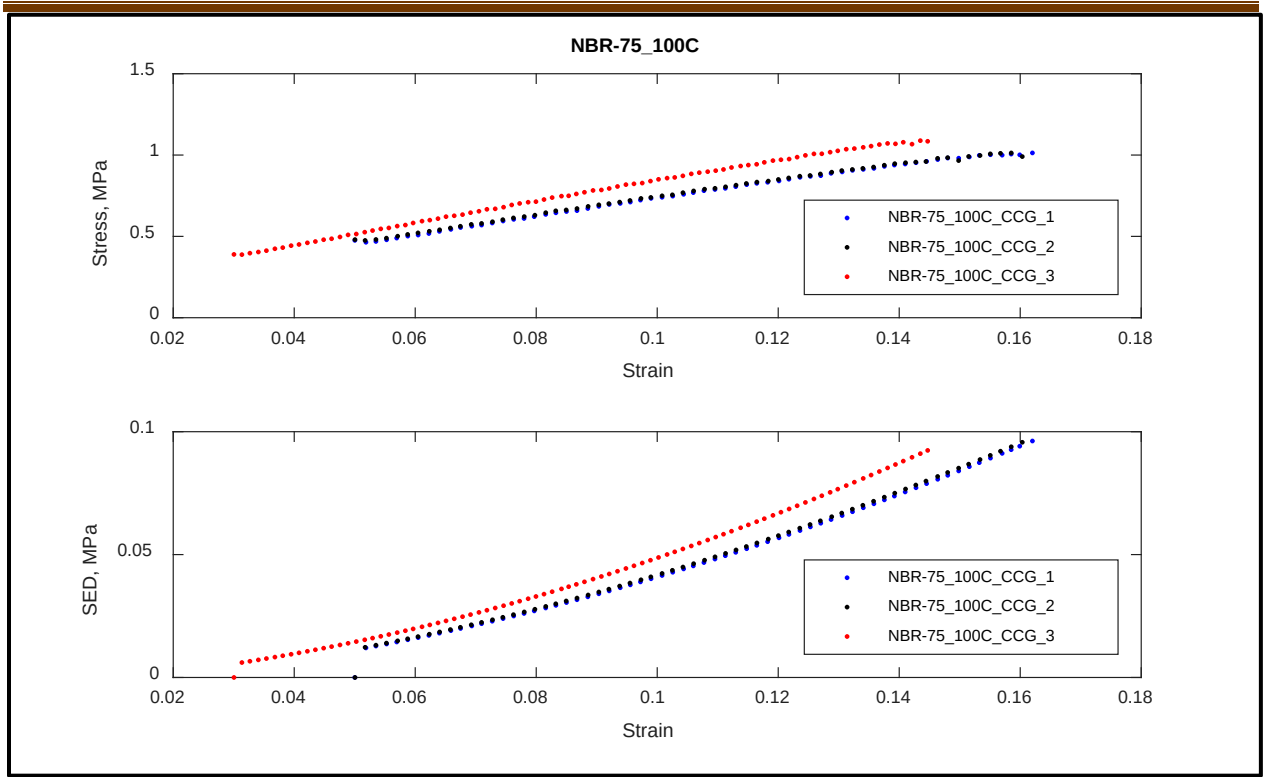
NBR-75_100C
Stress, MPa
Strain
NBR-75_100C_CCG_1
NBR-75_100C_CCG_2
NBR-75_100C_CCG_3
SED, MPa
Strain
NBR-75_100C_CCG_1
NBR-75_100C_CCG_2
NBR-75_100C_CCG_3

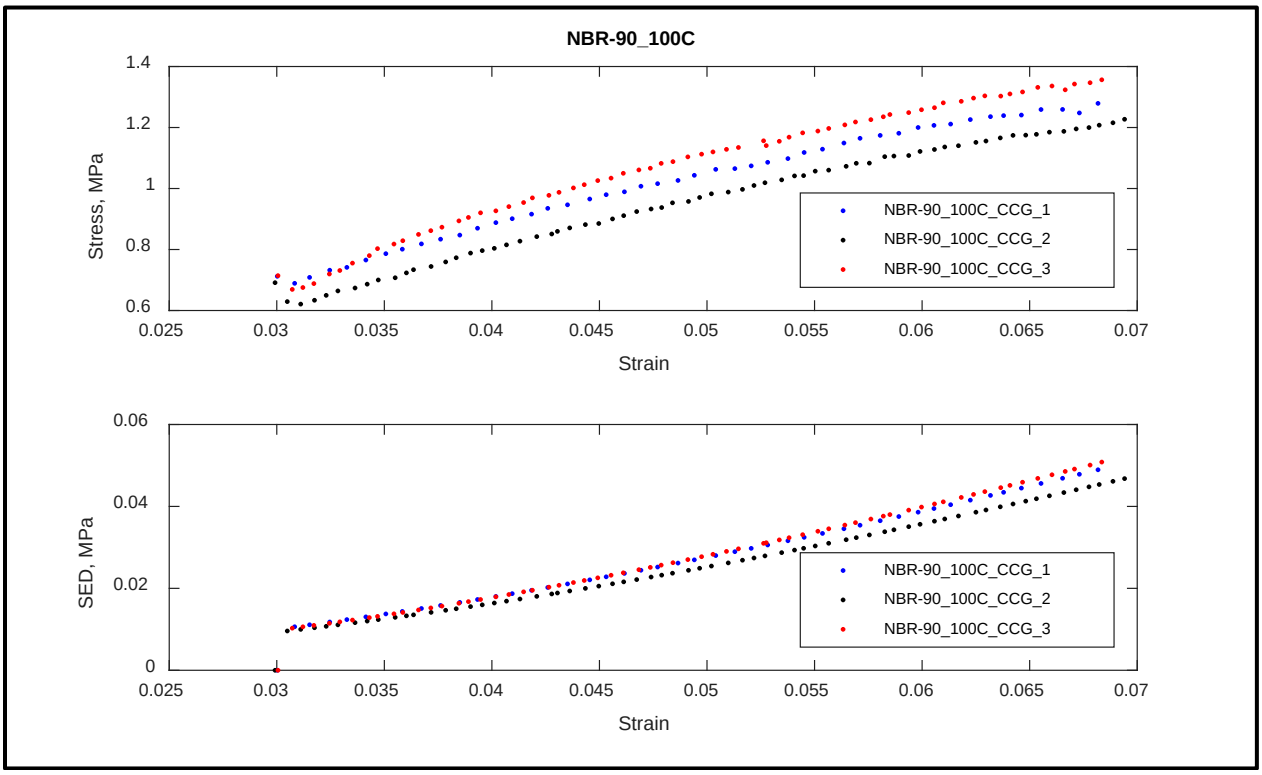
NBR-90_100C
Stress, MPa
Strain
NBR-90_100C_CCG_1
NBR-90_100C_CCG_2
NBR-90_100C_CCG_3
SED, MPa
Strain
NBR-90_100C_CCG_1
NBR-90_100C_CCG_2
NBR-90_100C_CCG_3

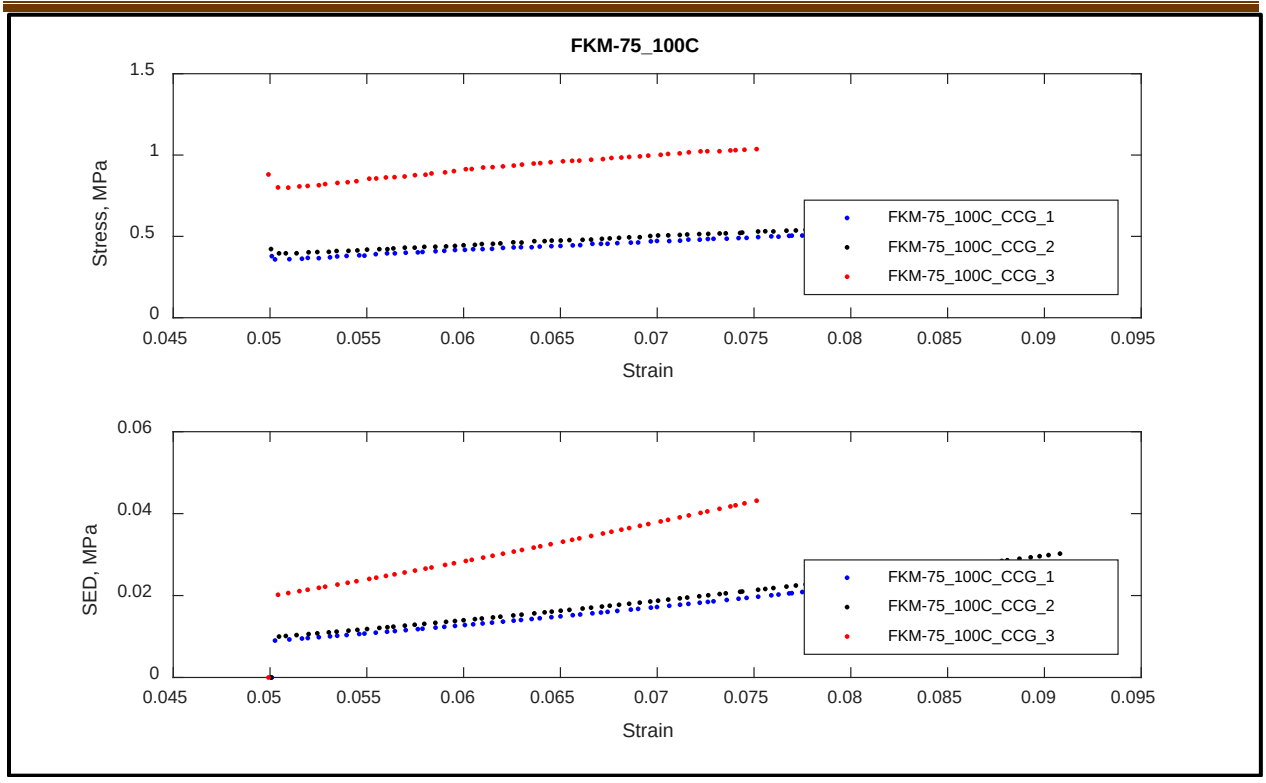
FKM-75_100C
Stress, MPa
Strain
FKM-75_100C_CCG_1
FKM-75_100C_CCG_2
FKM-75_100C_CCG_3
SED, MPa
Strain
FKM-75_100C_CCG_1
FKM-75_100C_CCG_2
FKM-75_100C_CCG_3

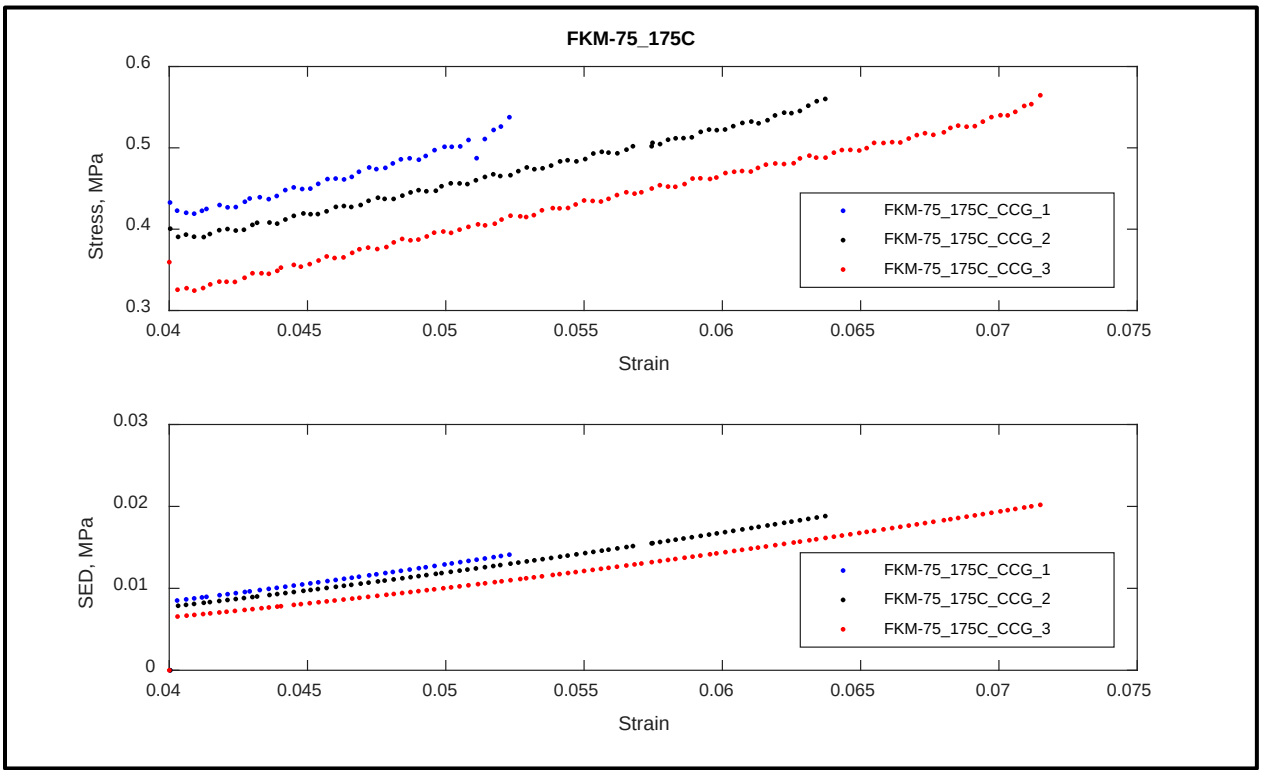
FKM-75_175C
Stress, MPa
Strain
FKM-75_175C_CCG_1
FKM-75_175C_CCG_2
FKM-75_175C_CCG_3
SED, MPa
Strain
FKM-75_175C_CCG_1
FKM-75_175C_CCG_2
FKM-75_175C_CCG_3

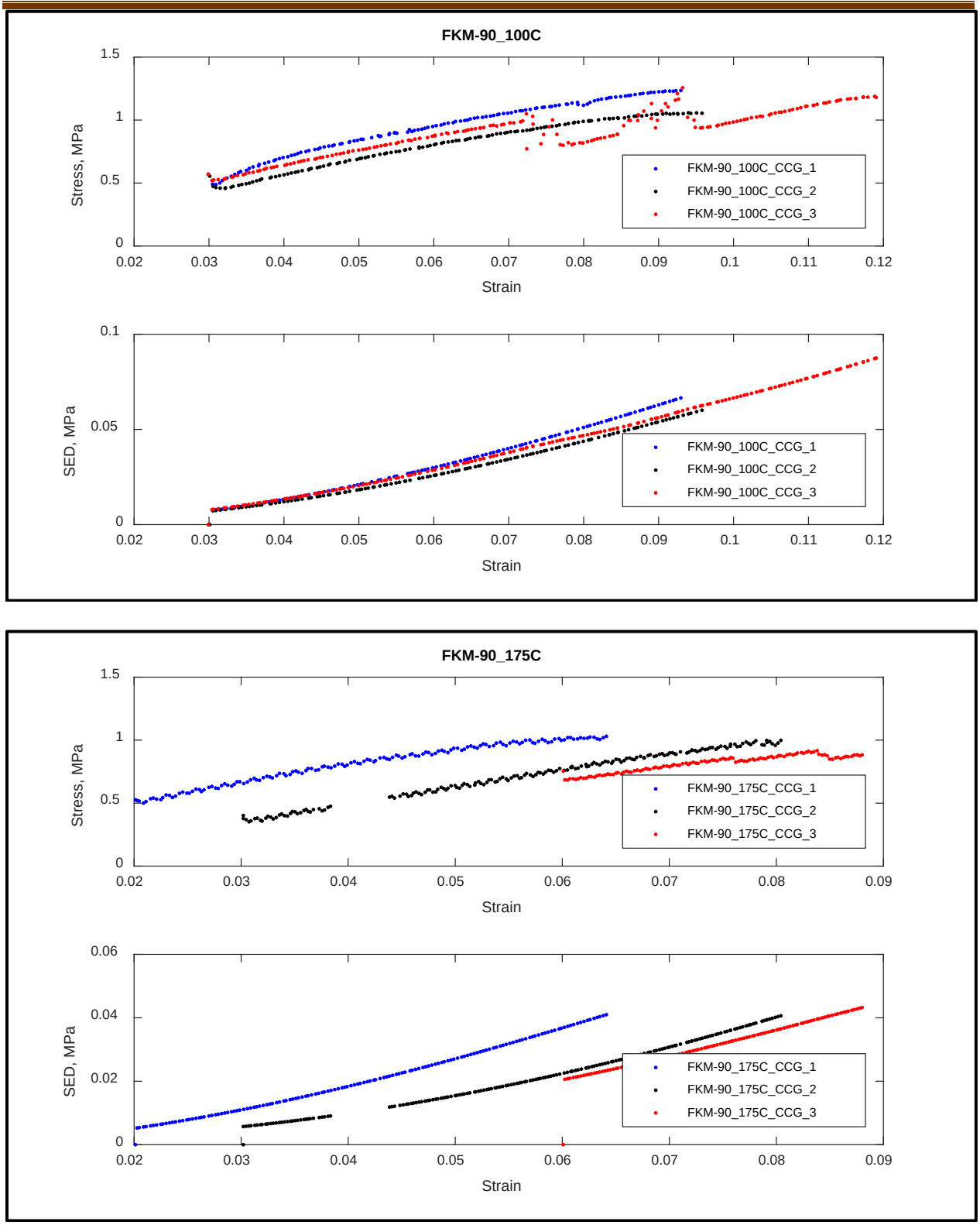


Figure A.4-12. Stress-Strain history and computed SED-Strain for creep crack growth replicates. SED was computed by numerically integrating the stress-strain curve.

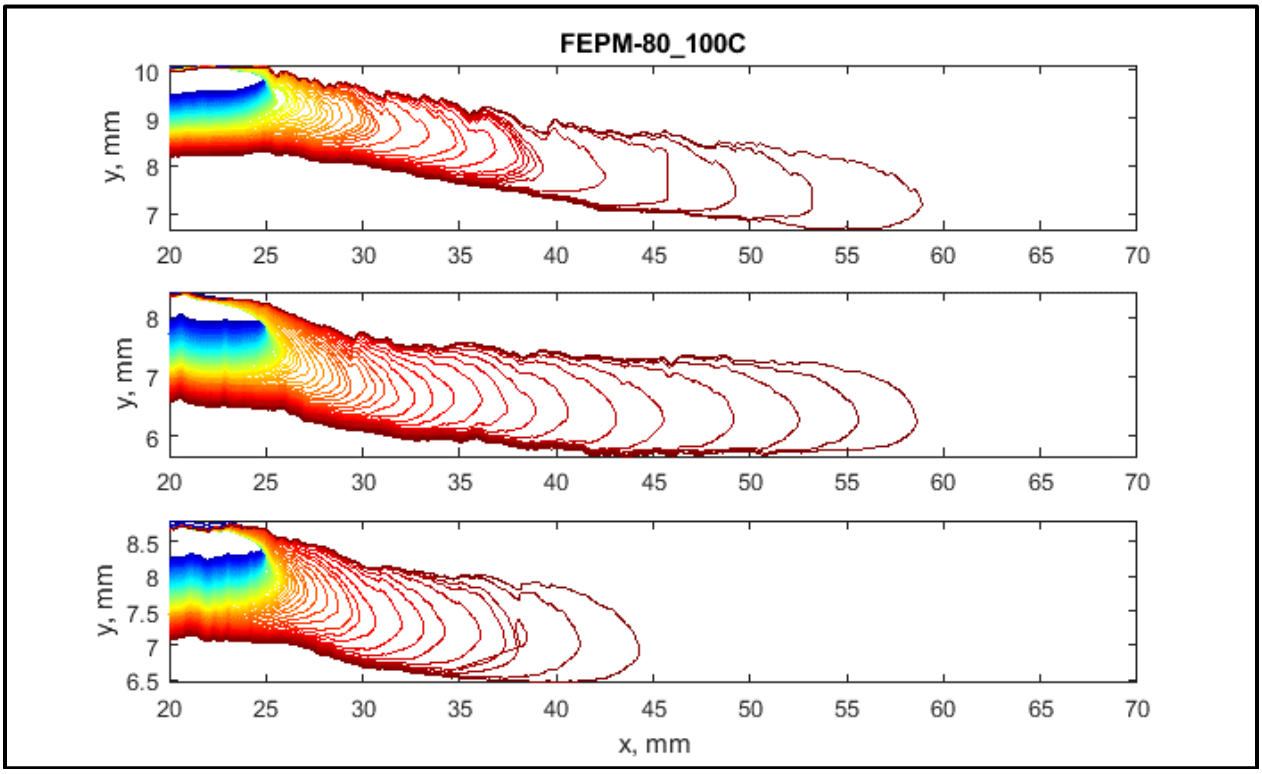
FEPM-80_100C
y, mm
x, mm

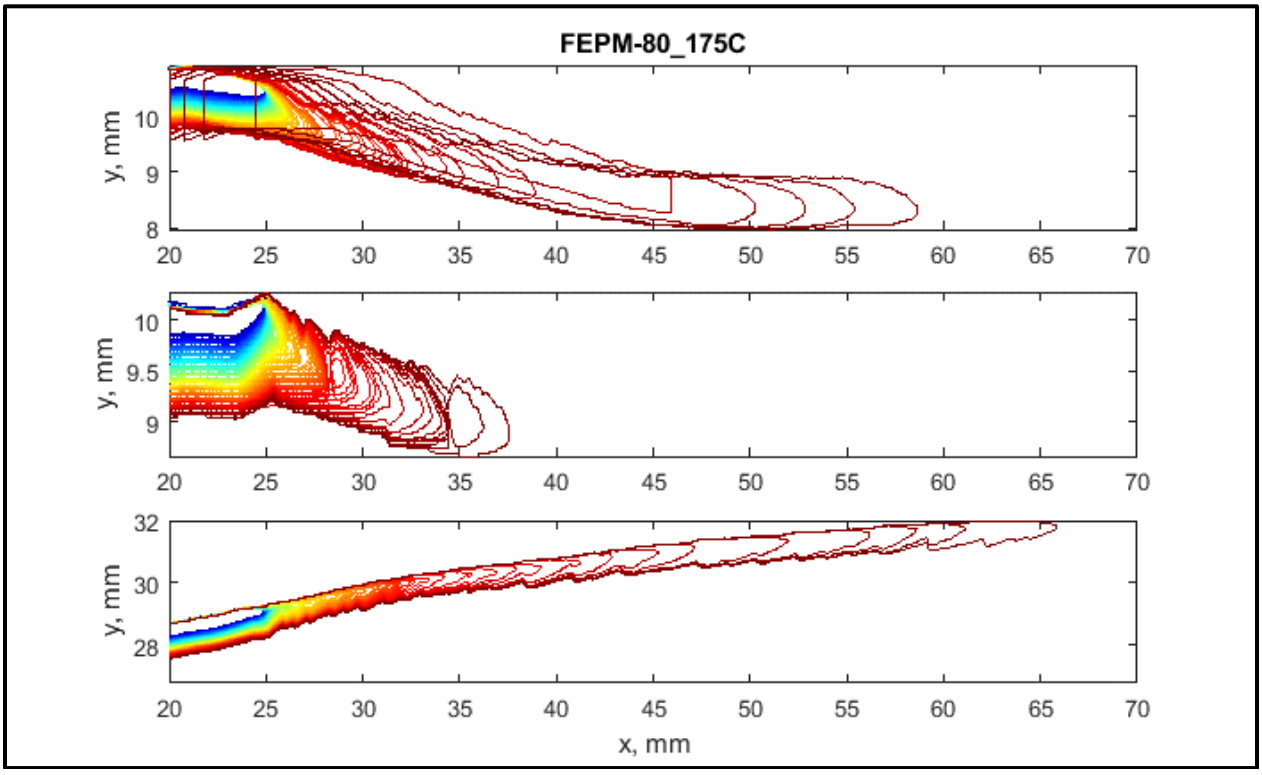
FEPM-80_175C
y, mm
x, mm

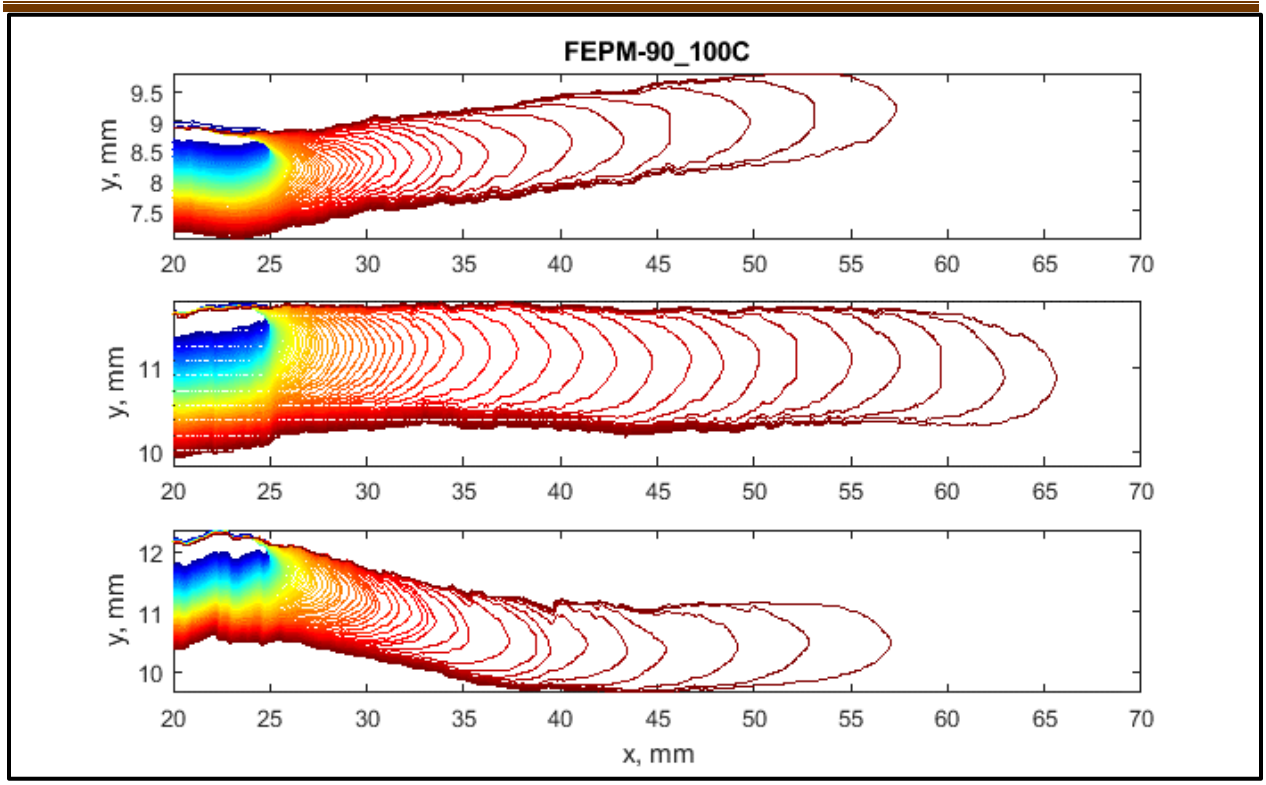
FEPM-90_100C
y, mm
9.5
9
8.5
8
7.5
11
10
12
11
10
20 25 30 35 40 45 50 55 60 65 70
x, mm

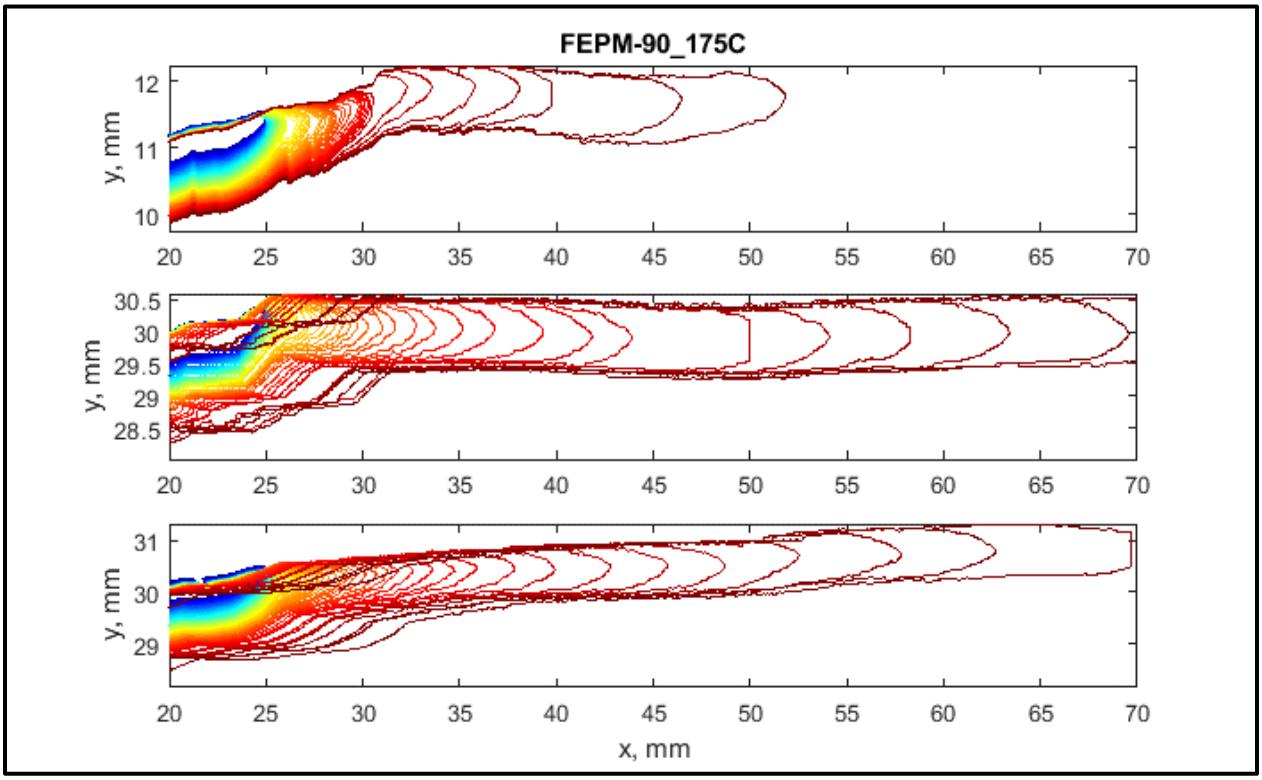
FEPM-90_175C
y, mm
12
11
10
30.5
30
29.5
29
28.5
31
30
29
20 25 30 35 40 45 50 55 60 65 70
x, mm

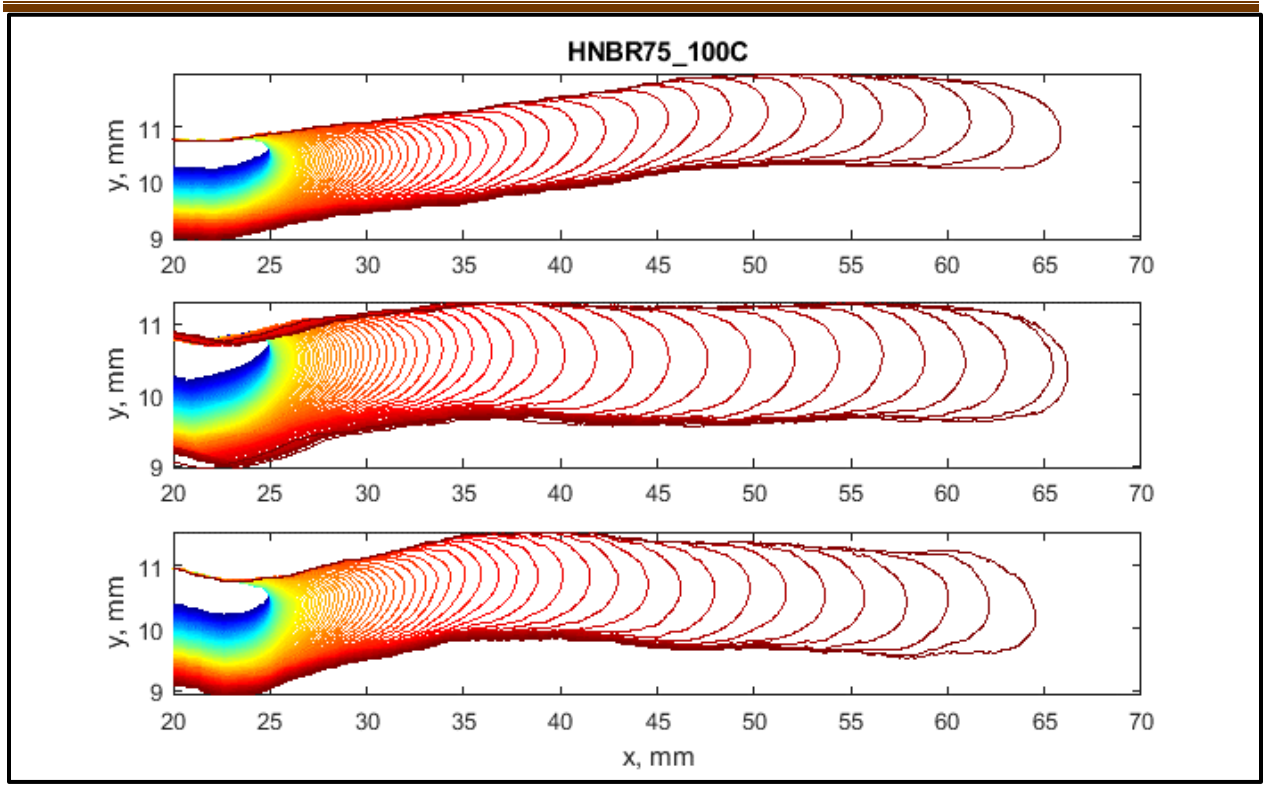
HNBR75_100C
y, mm
11
10
9
20
25
30
35
40
45
50
55
60
65
70
x, mm

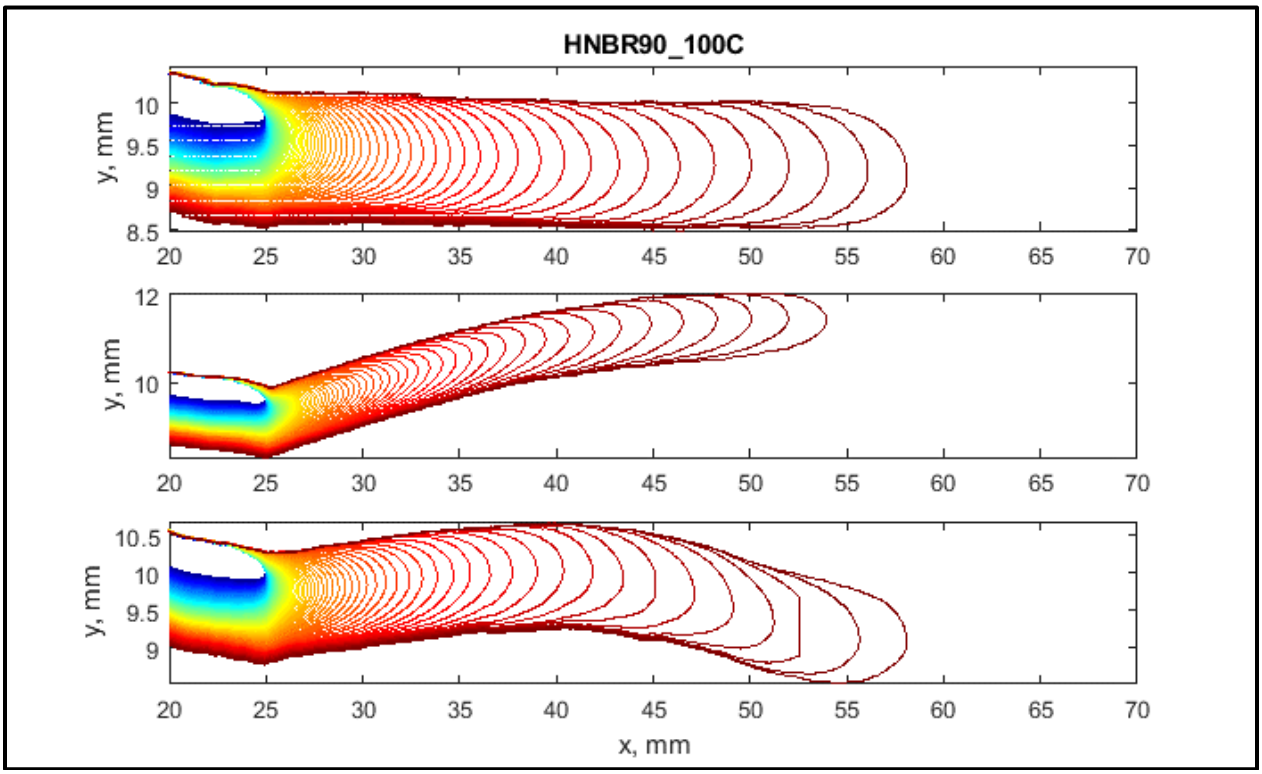
HNBR90_100C
y, mm
10
9.5
9
8.5
12
10.5
20
25
30
35
40
45
50
55
60
65
70
x, mm

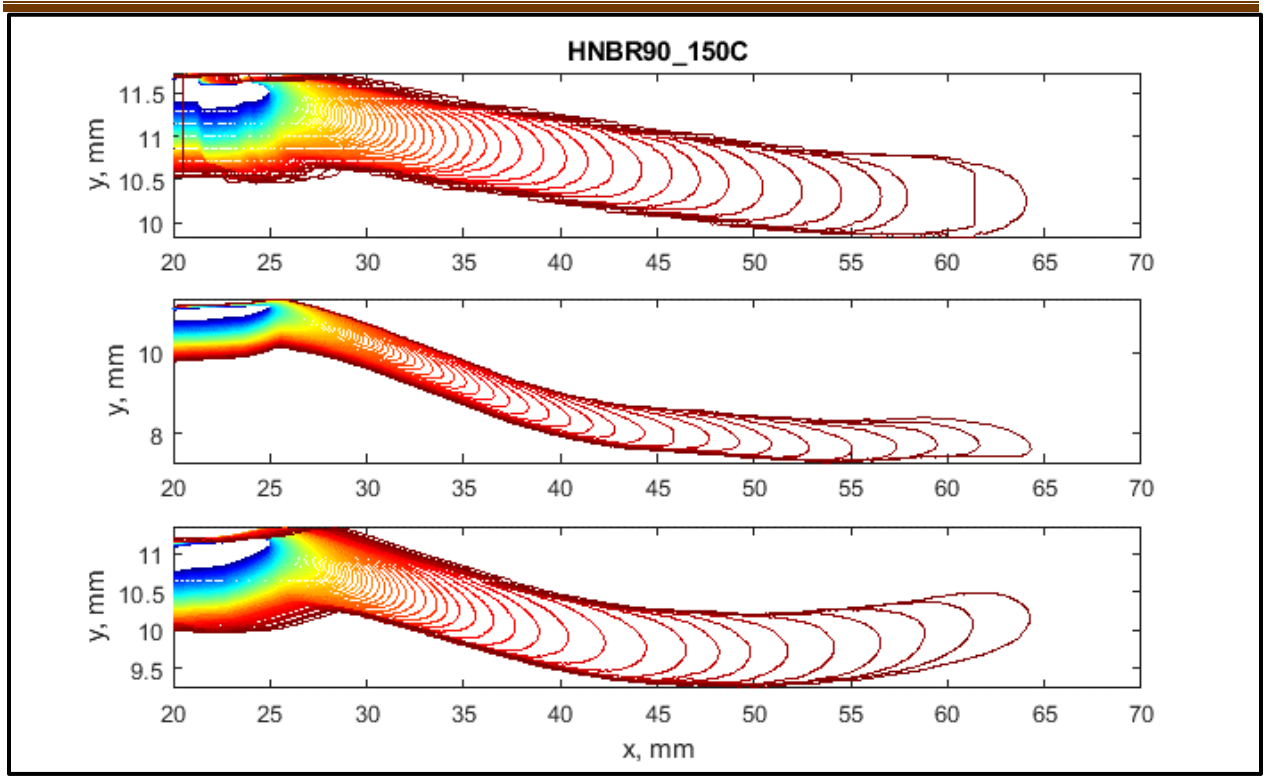
HNBR90_150C
y, mm
x, mm

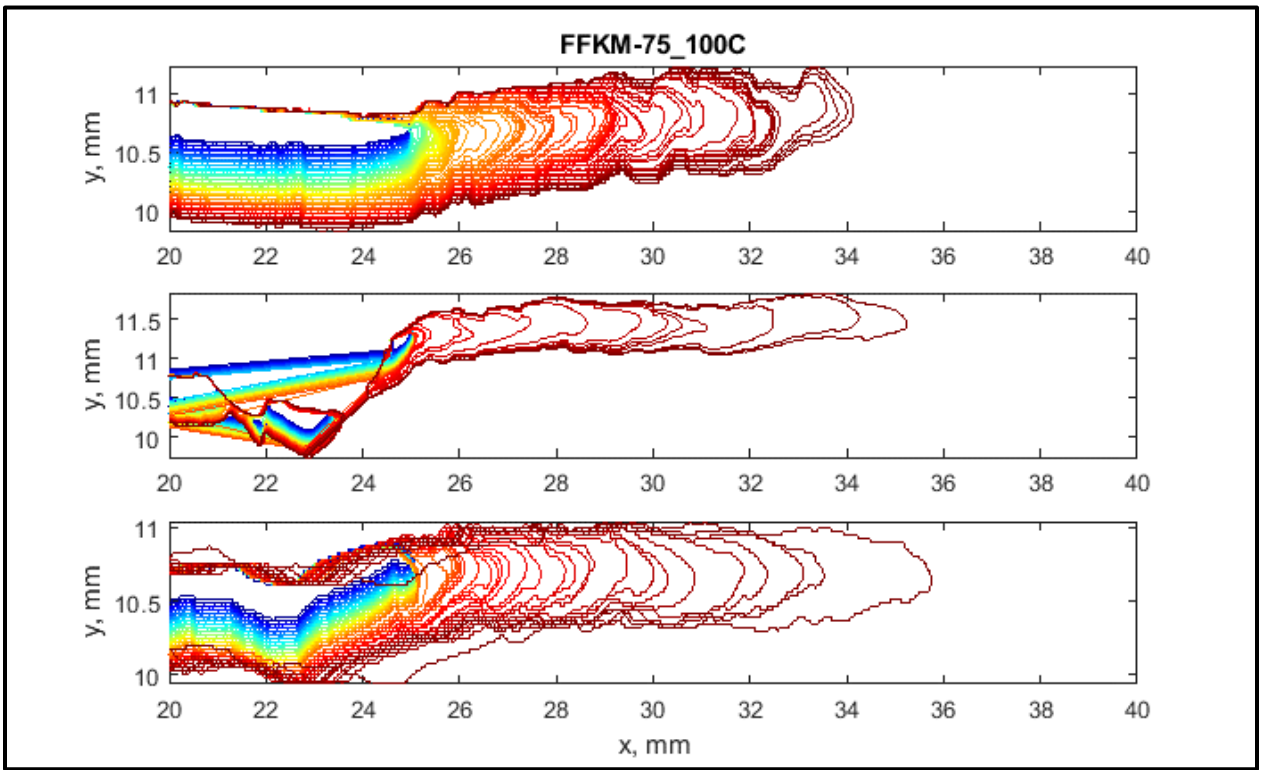
FFKM-75_100C
y, mm
x, mm

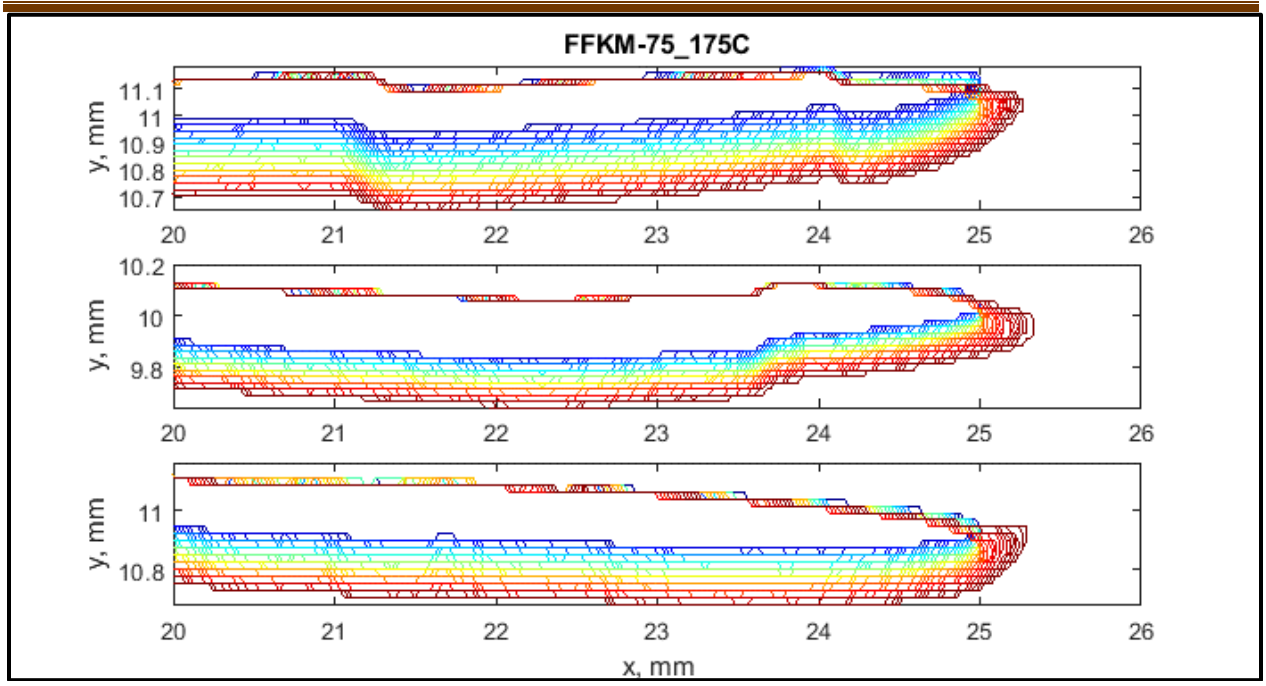
FFKM-75_175C
y, mm
11.1
11
10.9
10.8
10.7
20
21
22
23
24
25
26
y, mm
10.2
10
9.8
y, mm
11
10.8
x, mm

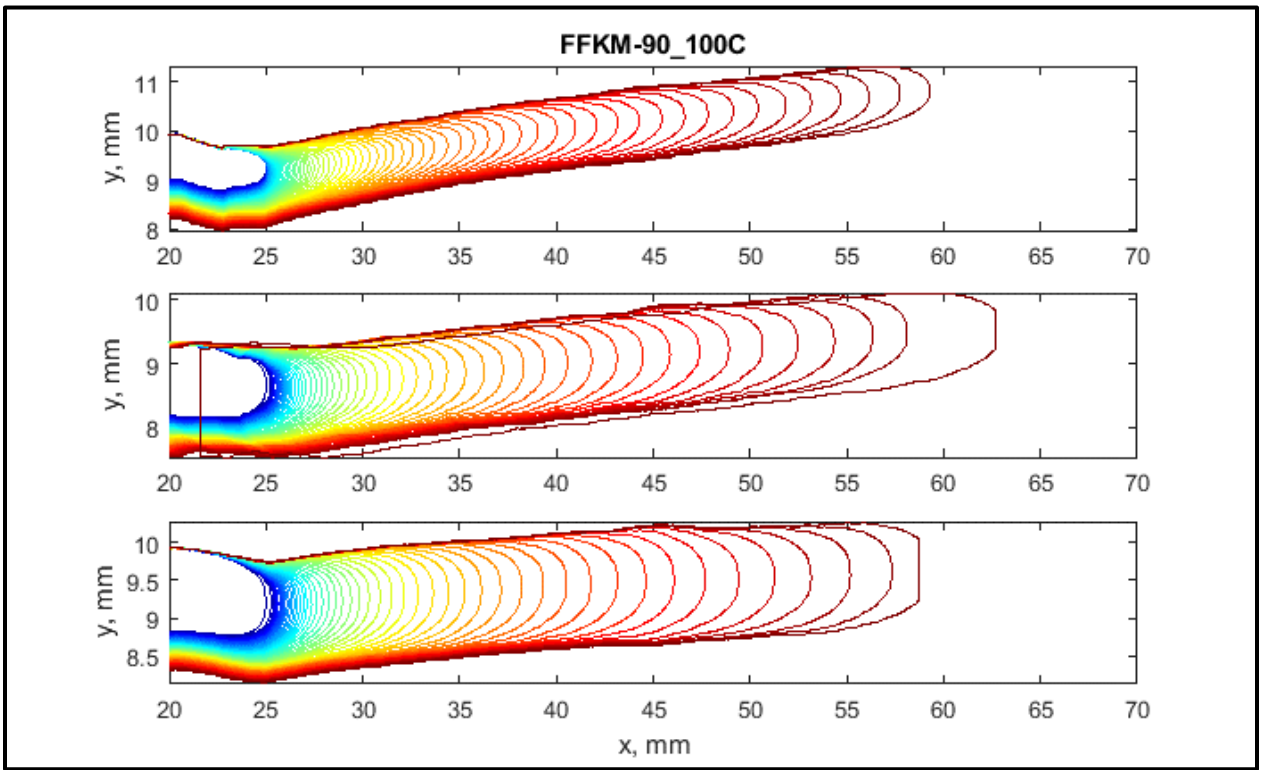
FFKM-90_100C
y, mm
11
10
9
8
20
25
30
35
40
45
50
55
60
65
70
y, mm
10
9
8
y, mm
10
9.5
9
8.5
x, mm

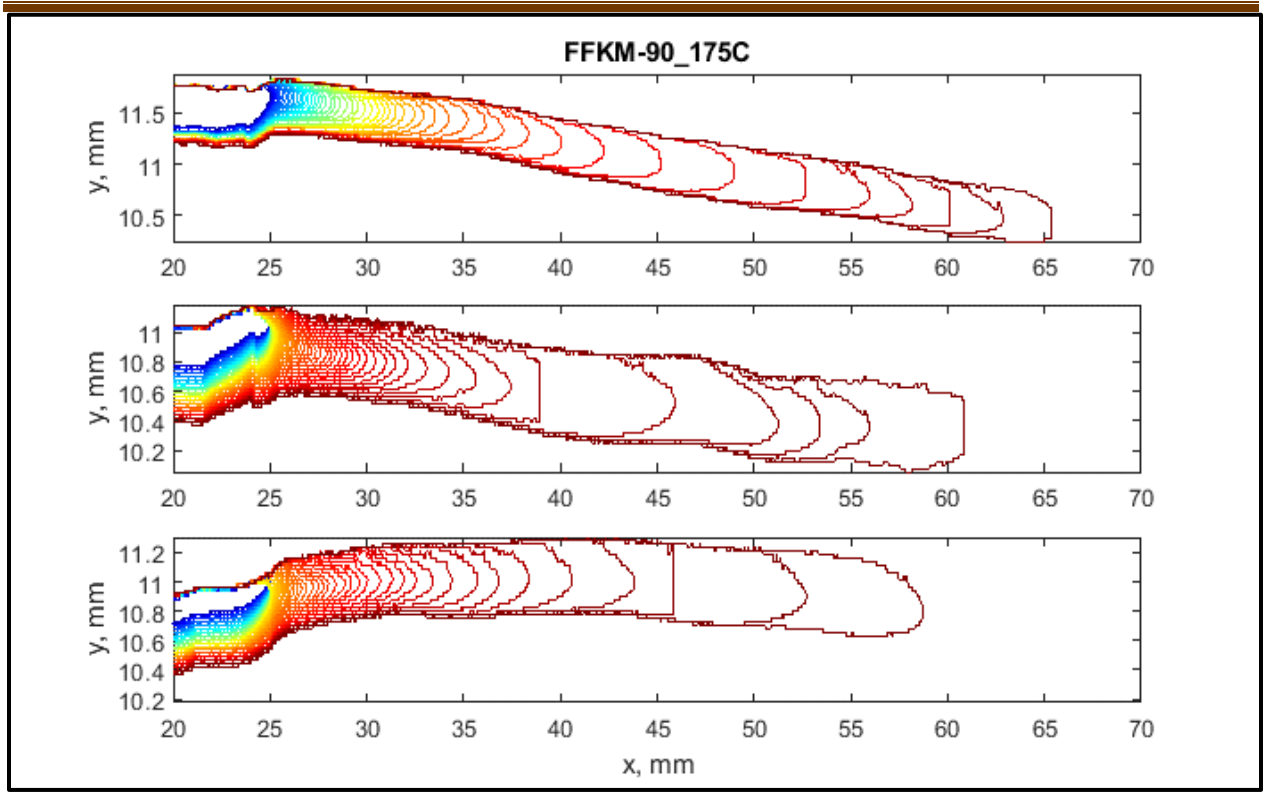
FFKM-90_175C
y, mm
x, mm

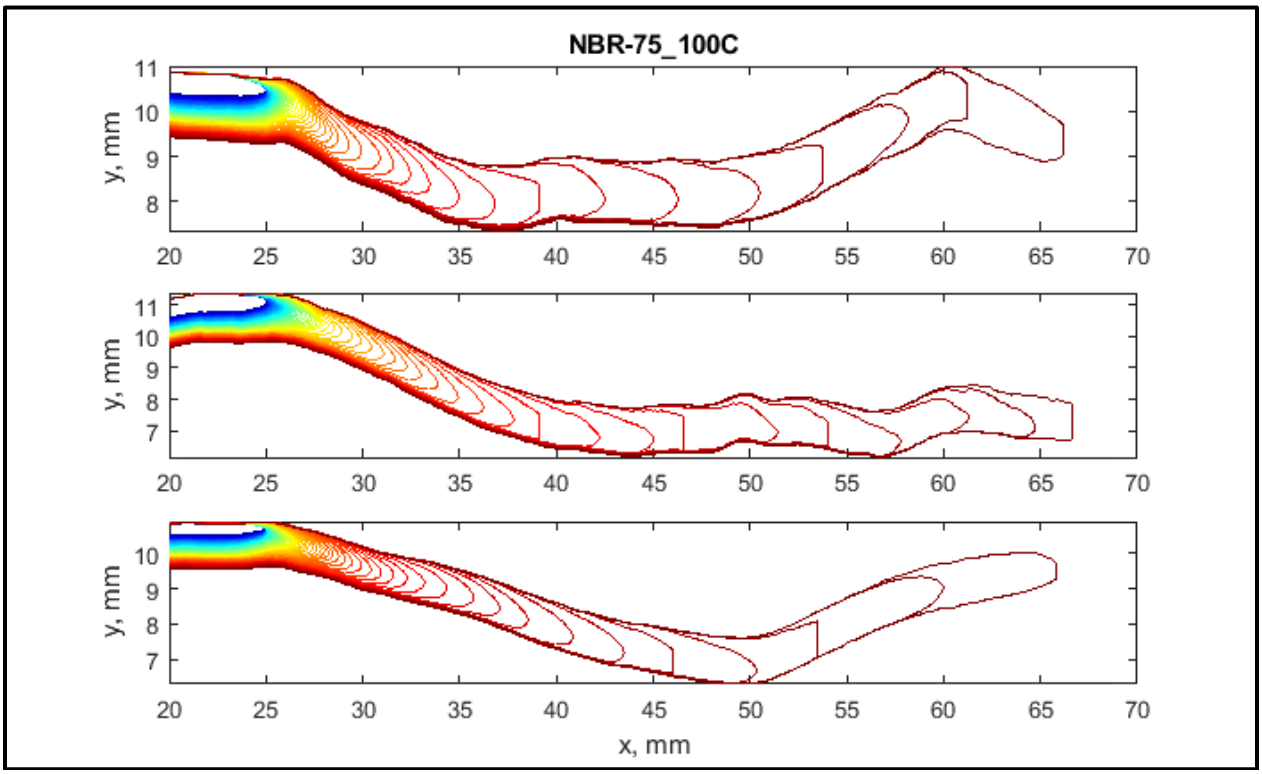
NBR-75_100C
y, mm
x, mm

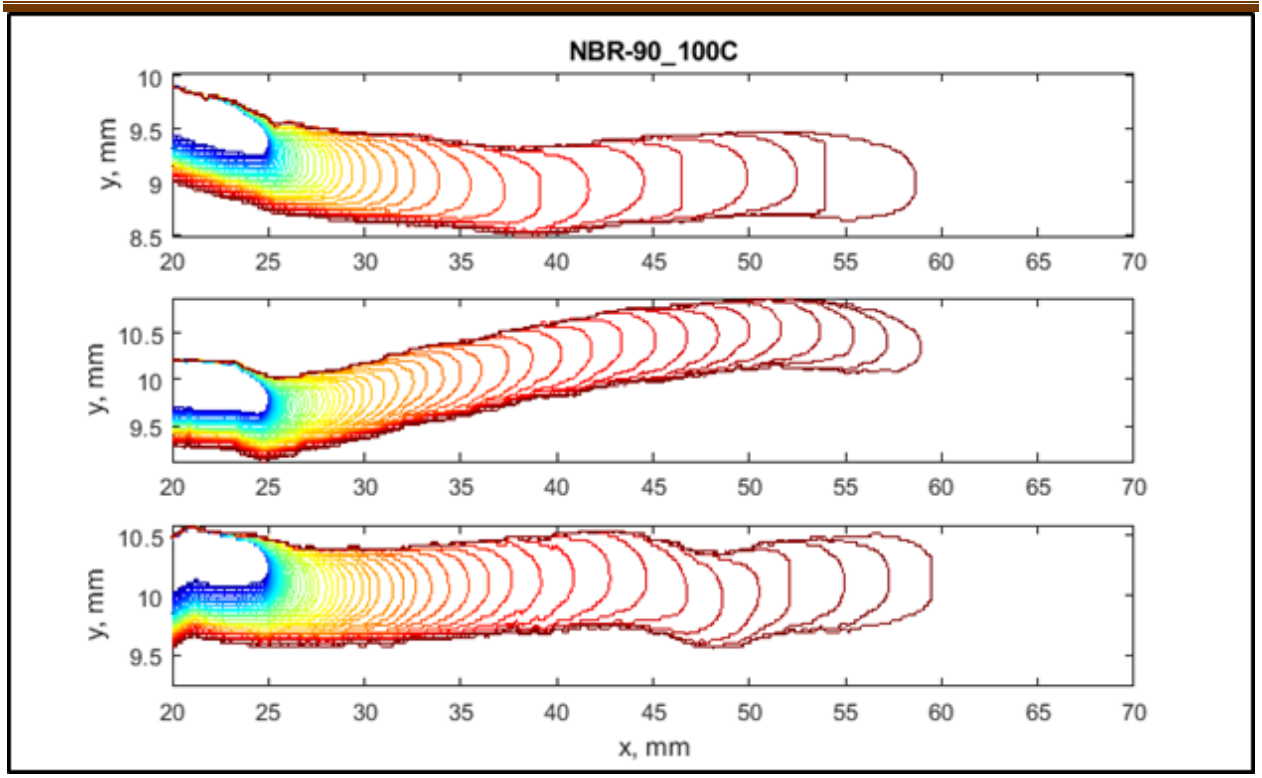
NBR-90_100C
y, mm
x, mm

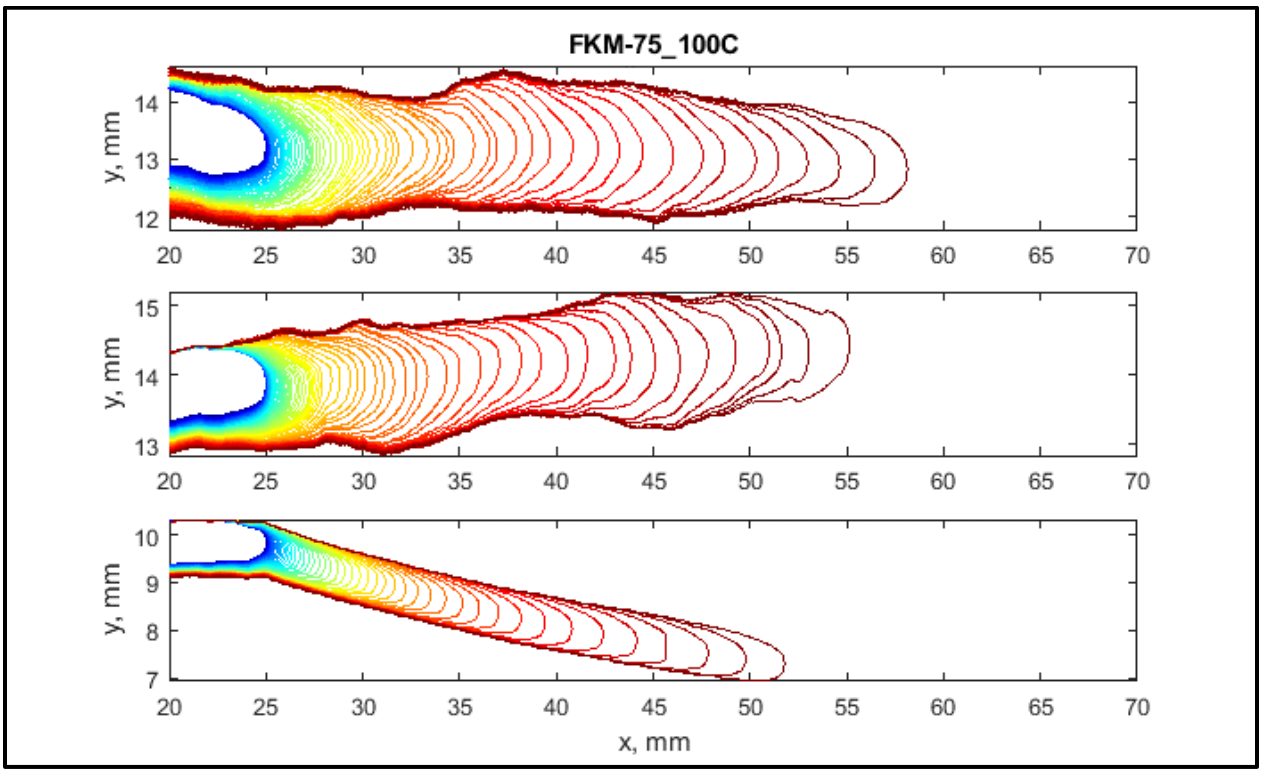
FKM-75_100C
y, mm
x, mm

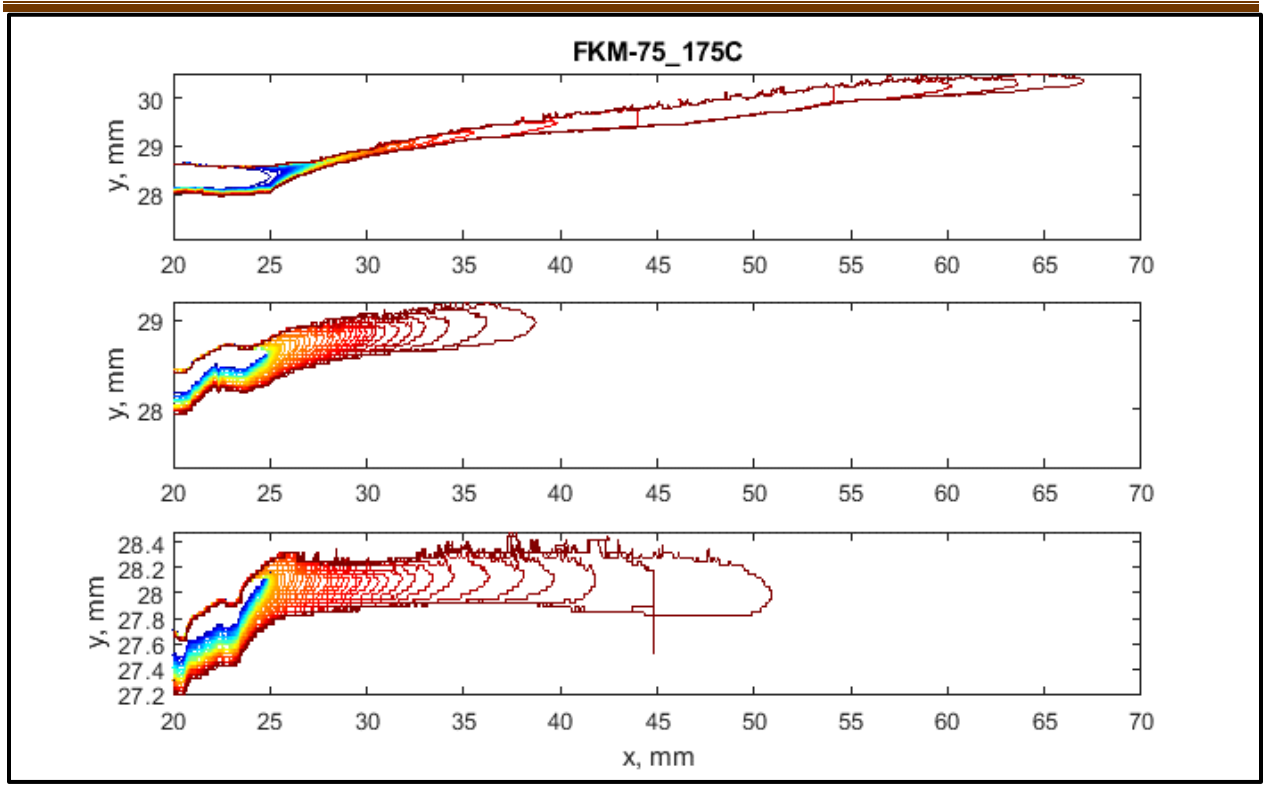
FKM-75_175C
y, mm
30
29
28
y, mm
29
28
y, mm
28.4
28.2
28
27.8
27.6
27.4
27.2
20 25 30 35 40 45 50 55 60 65 70
x, mm

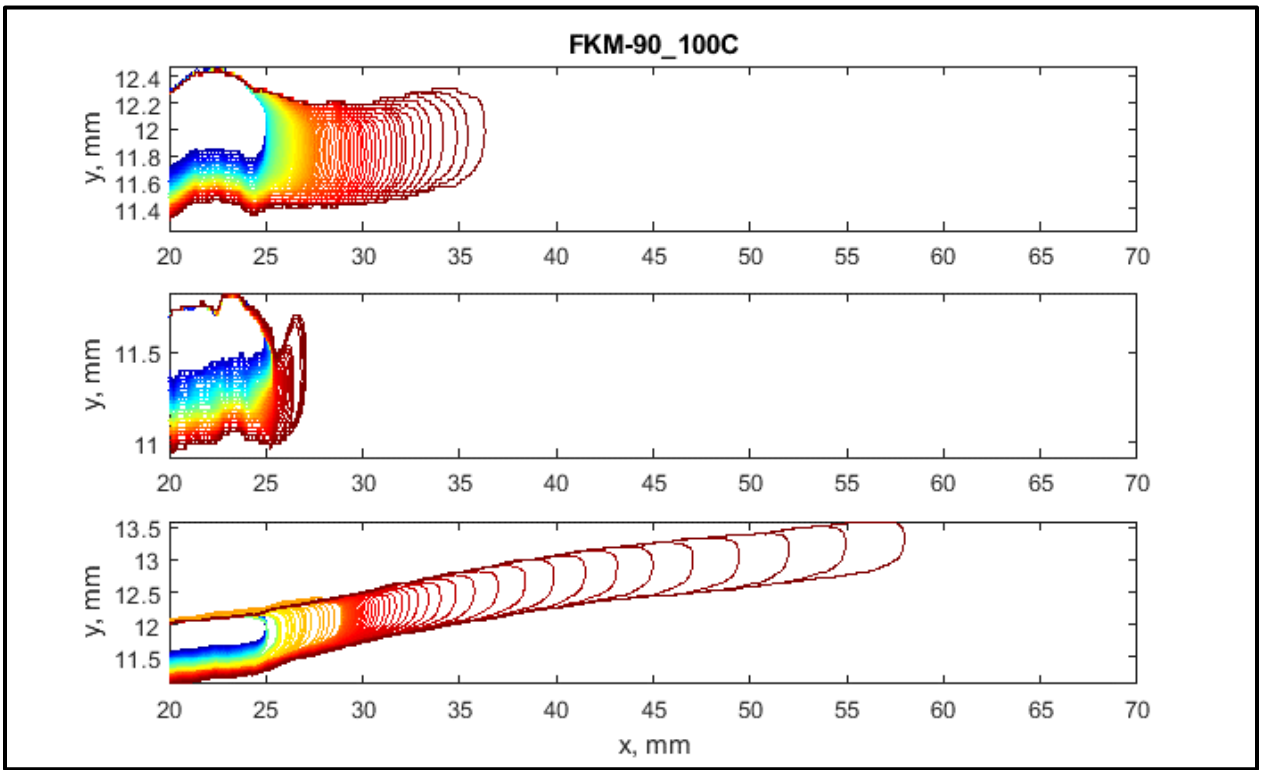
FKM-90_100C
y, mm
12.4
12.2
12
11.8
11.6
11.4
y, mm
11.5
11
y, mm
13.5
13
12.5
12
11.5
20 25 30 35 40 45 50 55 60 65 70
x, mm

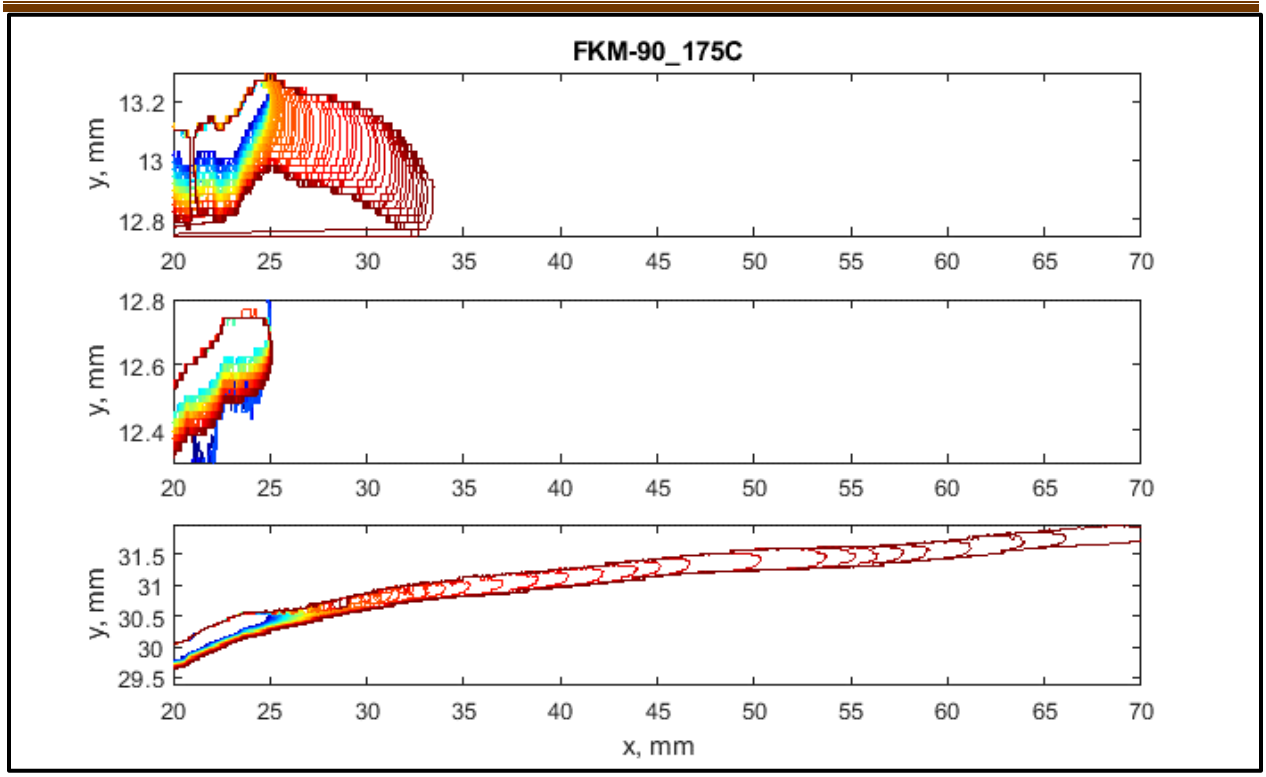


Figure A.4-13. Images of crack tip evolution during testing for compound H82, replicates 1-3. (top to bottom)

For each creep crack growth test, crack growth rates were estimated by fitting the following equation to the data shown Figure A.4-14, then differentiating with respect to time.

$$c = c_0 + r_q\left(\frac{h}{T_q}\right)^F \int_0^t W^{F_q} dt = c_0 + A\int_0^t W^{F_q} dt \qquad (4)$$

$c$ is the crack length
$c_0$ is the initial crack length, prior to application of any cycles
$t$ is time
$W$ is the strain energy density at time, t (based on loading curve)
$h$ is the specimen gauge height
$A$ is a parameter derived from the curve fitting process that reflects the combined influence of the material parameters $r_c$, $T_c$, and $F$.

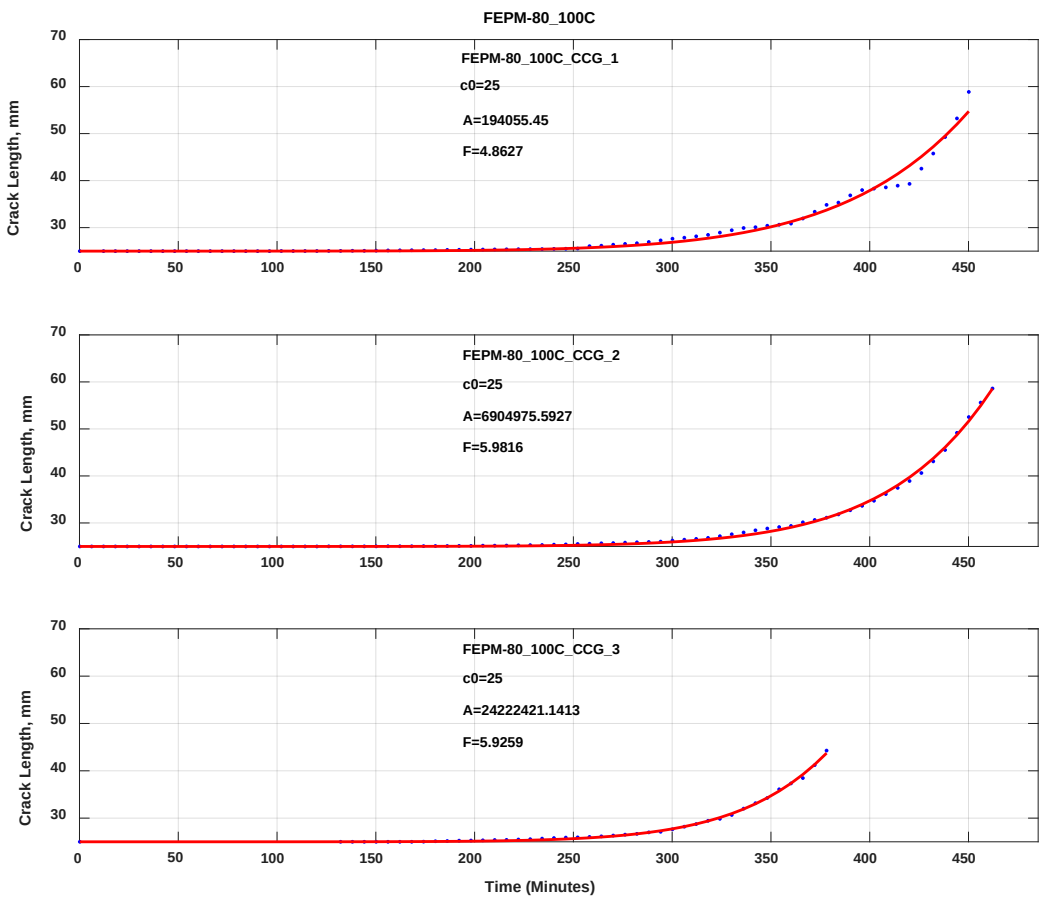
FEPM-80_100C
FEPM-80_100C_CCG_1
c0=25
A=194055.45
F=4.8627
FEPM-80_100C_CCG_2
c0=25
A=6904975.5927
F=5.9816
FEPM-80_100C_CCG_3
c0=25
A=24222421.1413
F=5.9259
Crack Length, mm
Time (Minutes)

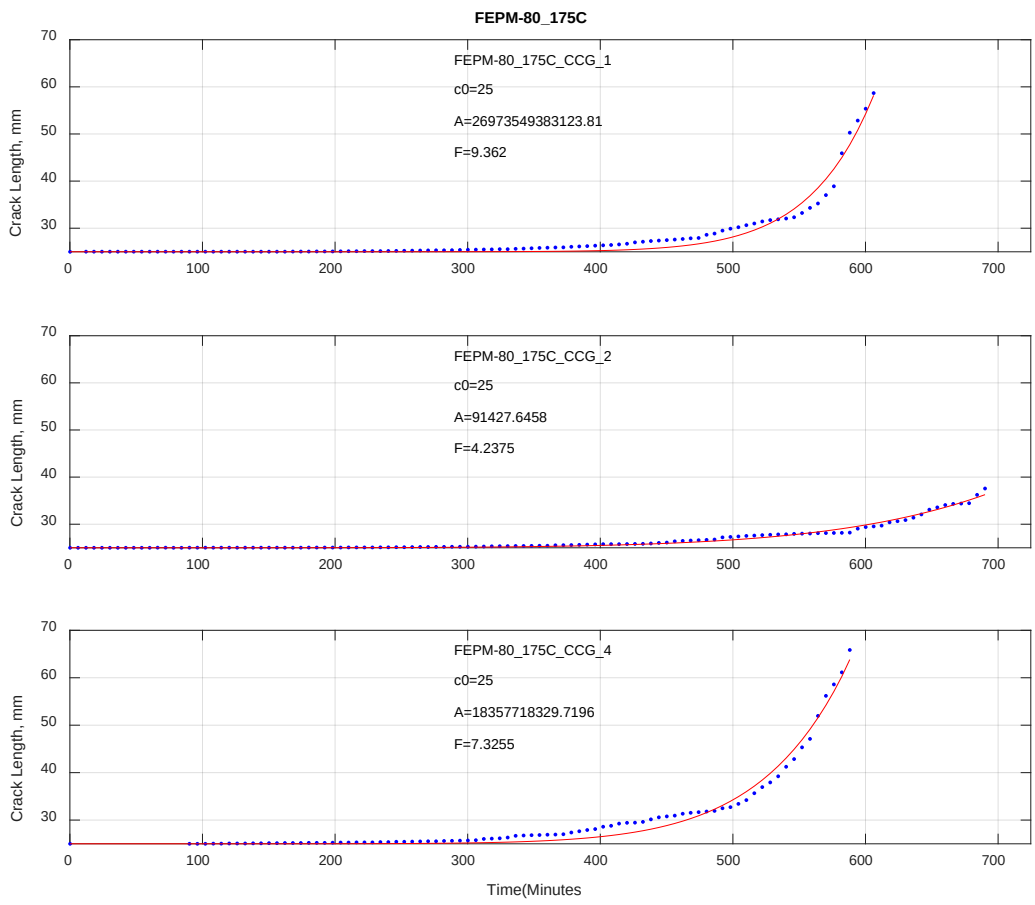
FEPM-80_175C
FEPM-80_175C_CCG_1
c0=25
A=26973549383123.81
F=9.362
FEPM-80_175C_CCG_2
c0=25
A=91427.6458
F=4.2375
FEPM-80_175C_CCG_4
c0=25
A=18357718329.7196
F=7.3255
Crack Length, mm
Time(Minutes

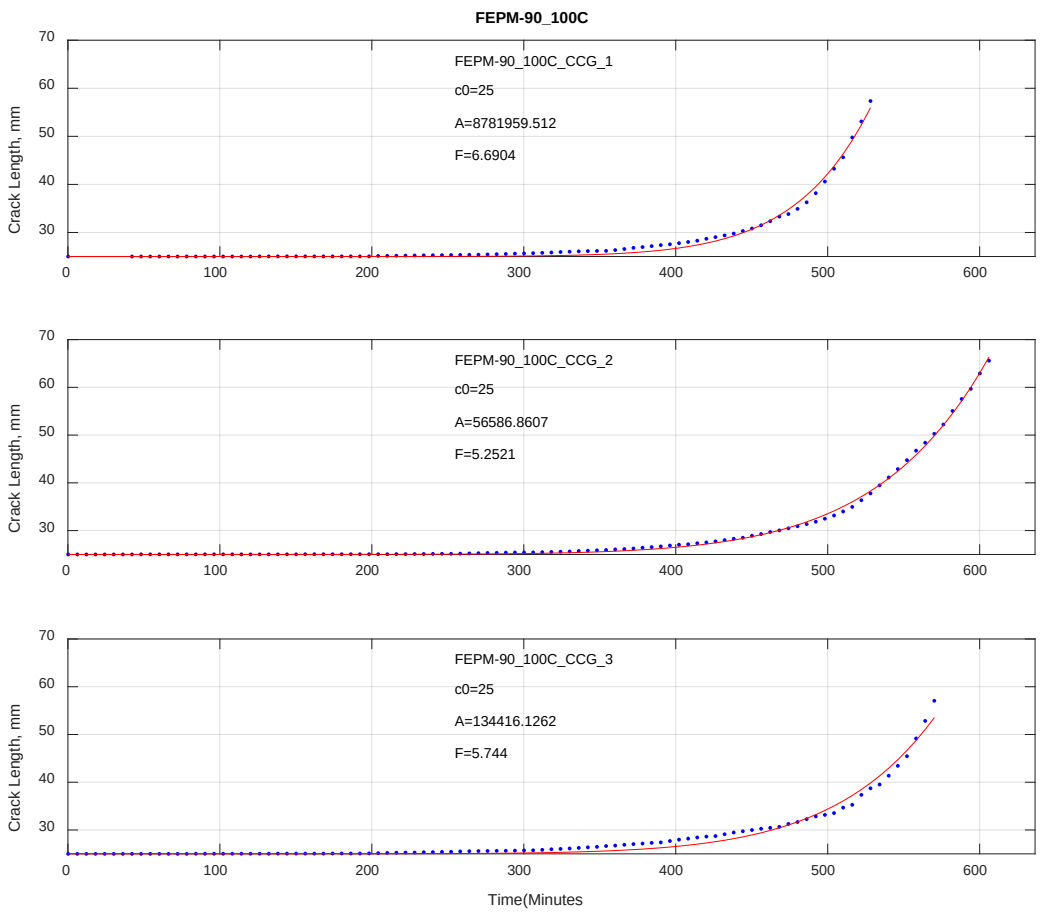
FEPM-90_100C
FEPM-90_100C_CCG_1
c0=25
A=8781959.512
F=6.6904
FEPM-90_100C_CCG_2
c0=25
A=56586.8607
F=5.2521
FEPM-90_100C_CCG_3
c0=25
A=134416.1262
F=5.744
Crack Length, mm
Time(Minutes
70
60
50
40
30
0
100
200
300
400
500
600

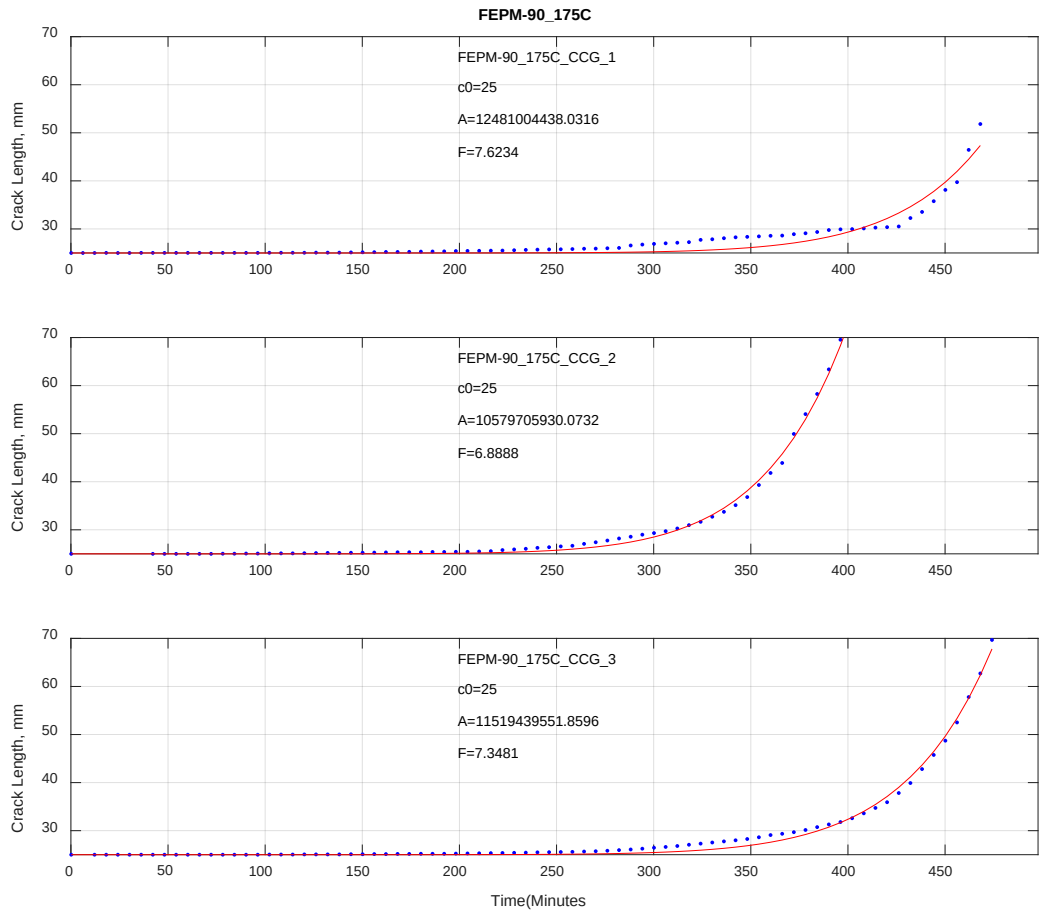
FEPM-90_175C
FEPM-90_175C_CCG_1
c0=25
A=12481004438.0316
F=7.6234
FEPM-90_175C_CCG_2
c0=25
A=10579705930.0732
F=6.8888
FEPM-90_175C_CCG_3
c0=25
A=11519439551.8596
F=7.3481
Crack Length, mm
Time(Minutes

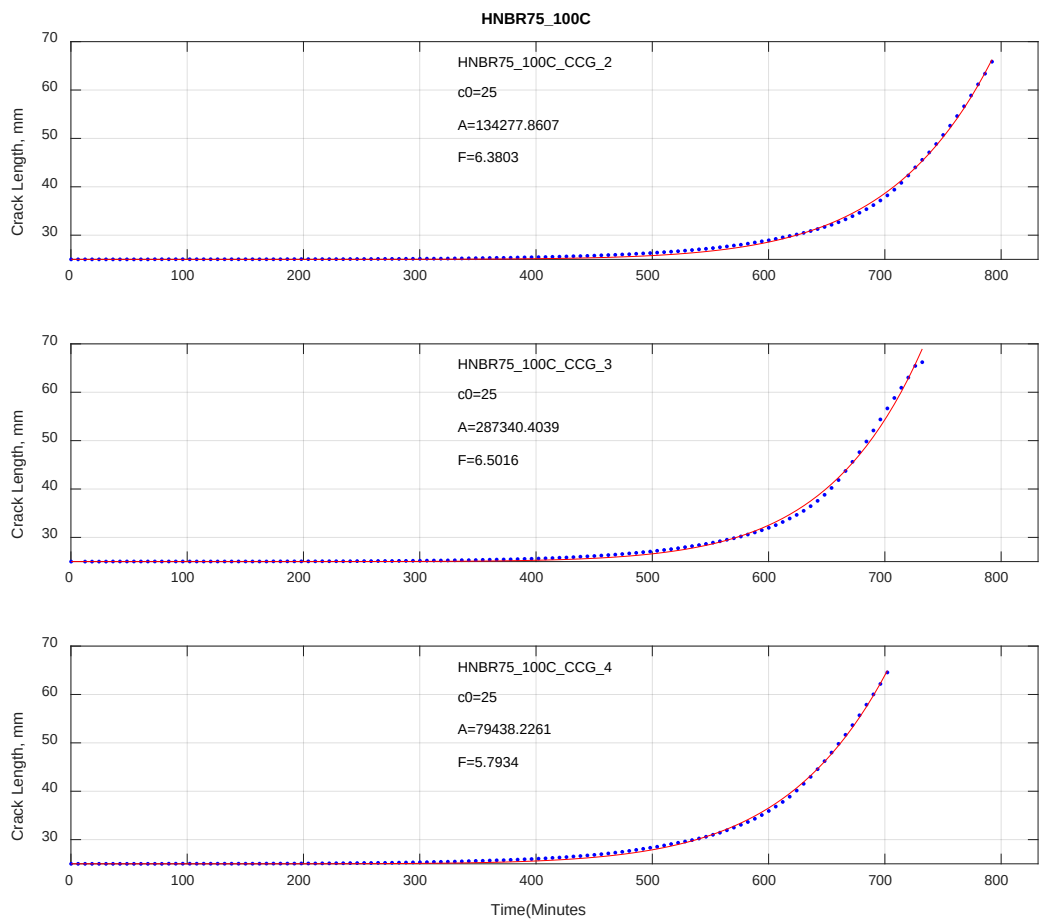
HNBR75_100C
HNBR75_100C_CCG_2
c0=25
A=134277.8607
F=6.3803
HNBR75_100C_CCG_3
c0=25
A=287340.4039
F=6.5016
HNBR75_100C_CCG_4
c0=25
A=79438.2261
F=5.7934
Crack Length, mm
Time(Minutes
0
100
200
300
400
500
600
700
800
30
40
50
60
70

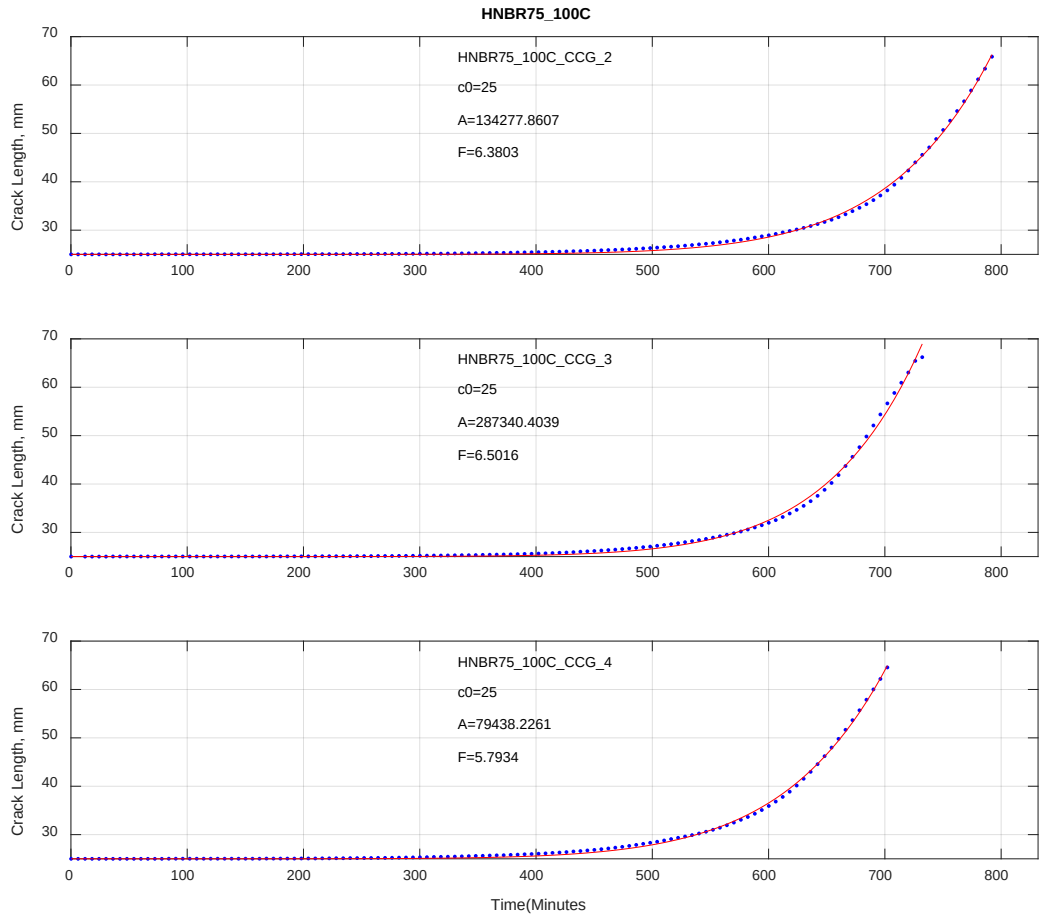
HNBR75_100C
HNBR75_100C_CCG_2
c0=25
A=134277.8607
F=6.3803
HNBR75_100C_CCG_3
c0=25
A=287340.4039
F=6.5016
HNBR75_100C_CCG_4
c0=25
A=79438.2261
F=5.7934
Crack Length, mm
Time(Minutes
0
100
200
300
400
500
600
700
800
30
40
50
60
70

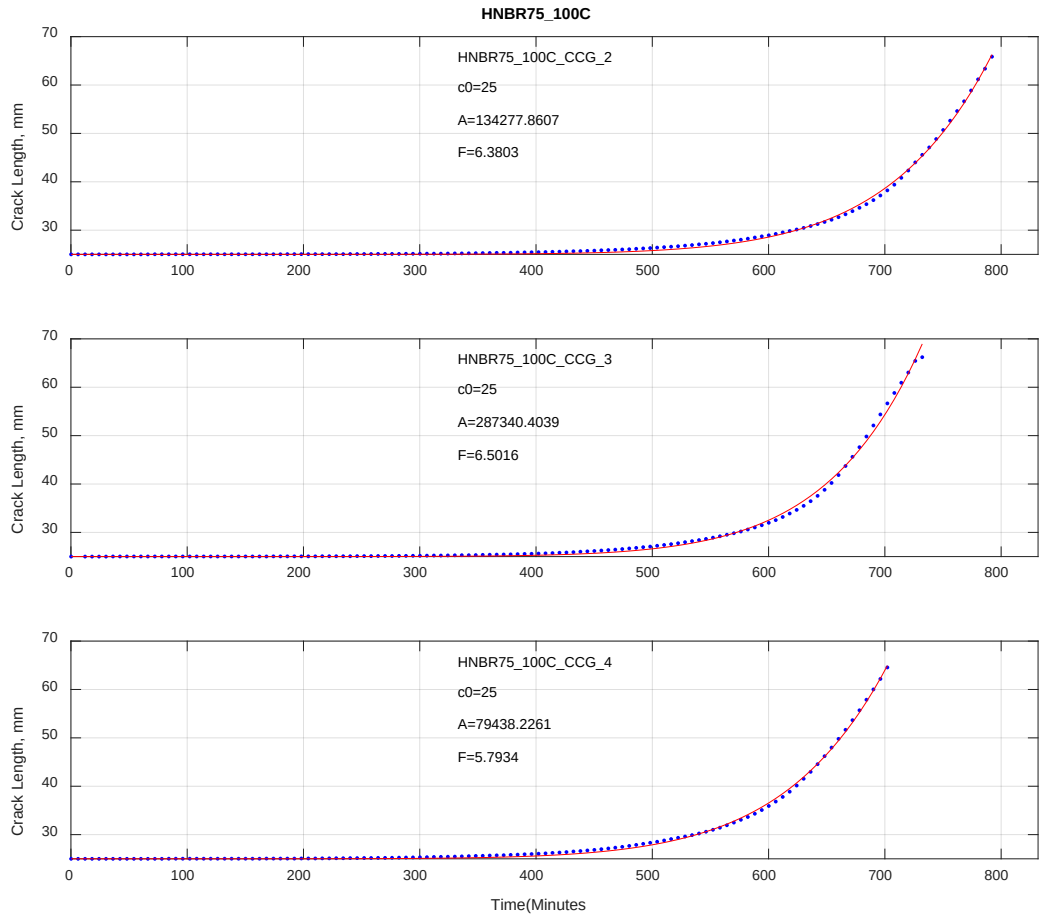
HNBR75_100C
HNBR75_100C_CCG_2
c0=25
A=134277.8607
F=6.3803
HNBR75_100C_CCG_3
c0=25
A=287340.4039
F=6.5016
HNBR75_100C_CCG_4
c0=25
A=79438.2261
F=5.7934
Crack Length, mm
Time(Minutes
0
100
200
300
400
500
600
700
800
30
40
50
60
70

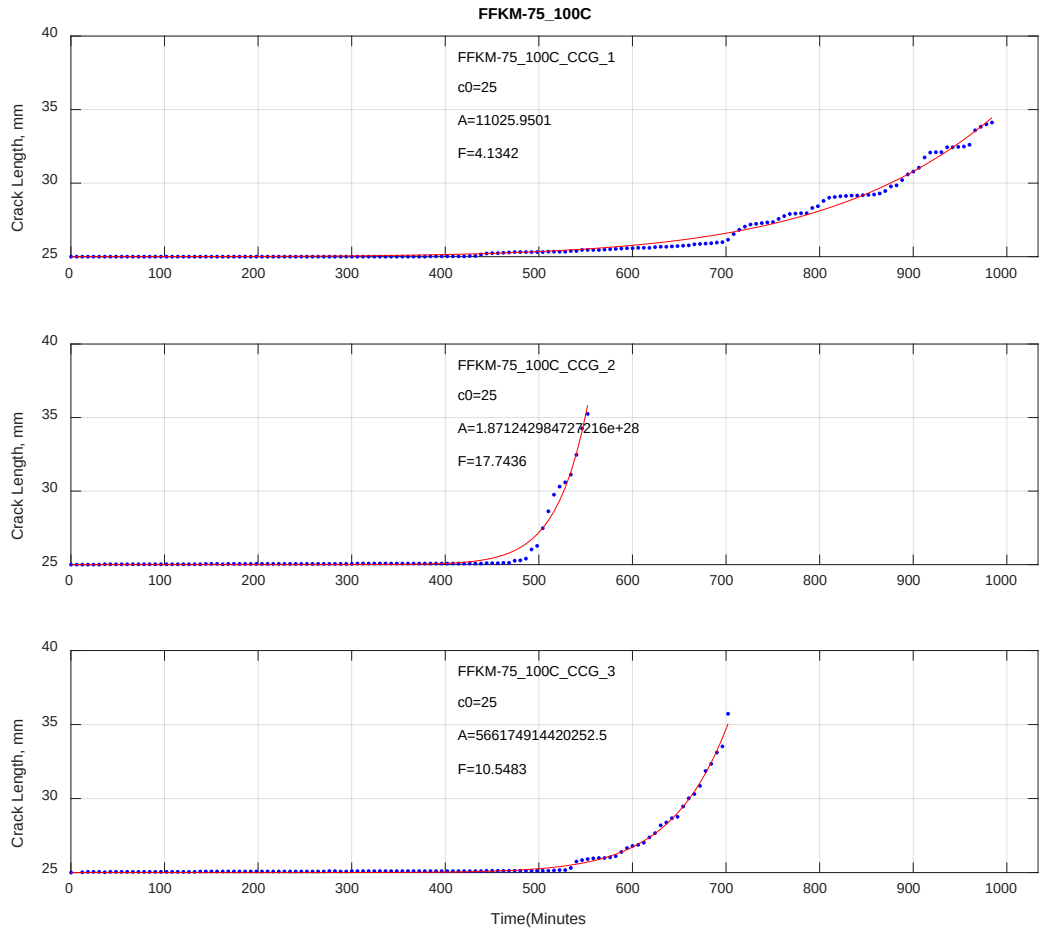
FFKM-75_100C
FFKM-75_100C_CCG_1
c0=25
A=11025.9501
F=4.1342
FFKM-75_100C_CCG_2
c0=25
A=1.87124298472721 6e+28
F=17.7436
FFKM-75_100C_CCG_3
c0=25
A=566174914420252.5
F=10.5483
Crack Length, mm
Time(Minutes

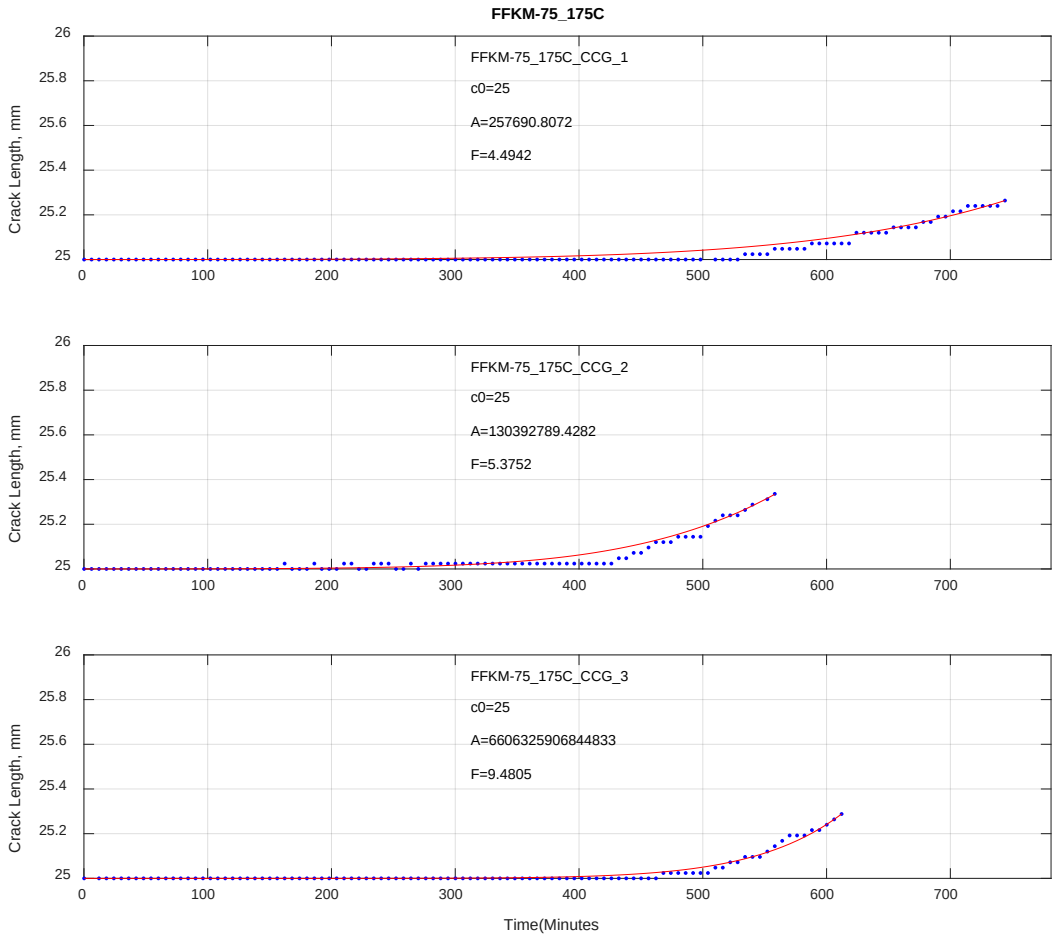
FFKM-75_175C
FFKM-75_175C_CCG_1
c0=25
A=257690.8072
F=4.4942
FFKM-75_175C_CCG_2
c0=25
A=130392789.4282
F=5.3752
FFKM-75_175C_CCG_3
c0=25
A=6606325906844833
F=9.4805
Crack Length, mm
Time(Minutes
26
25.8
25.6
25.4
25.2
25
0
100
200
300
400
500
600
700

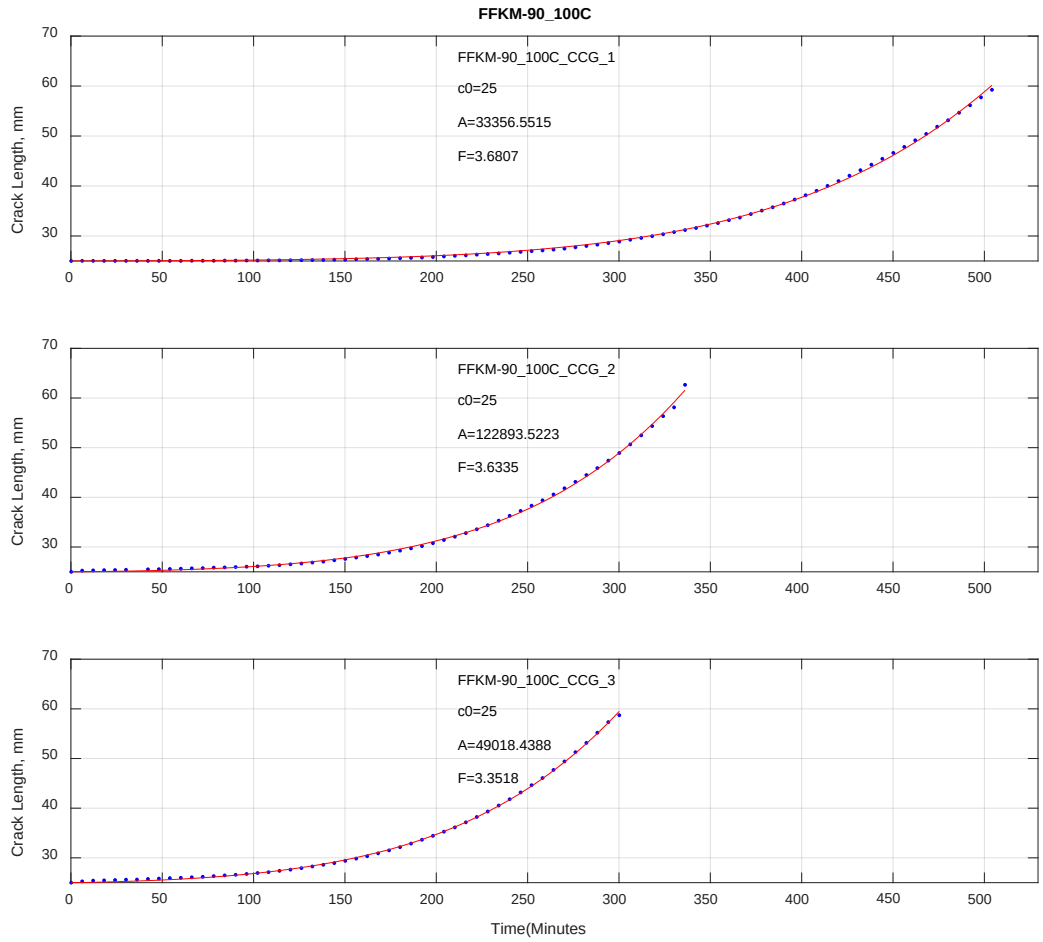
FFKM-90_100C
FFKM-90_100C_CCG_1
c0=25
A=33356.5515
F=3.6807
FFKM-90_100C_CCG_2
c0=25
A=122893.5223
F=3.6335
FFKM-90_100C_CCG_3
c0=25
A=49018.4388
F=3.3518
Crack Length, mm
Time(Minutes
70
60
50
40
30
0
50
100
150
200
250
300
350
400
450
500

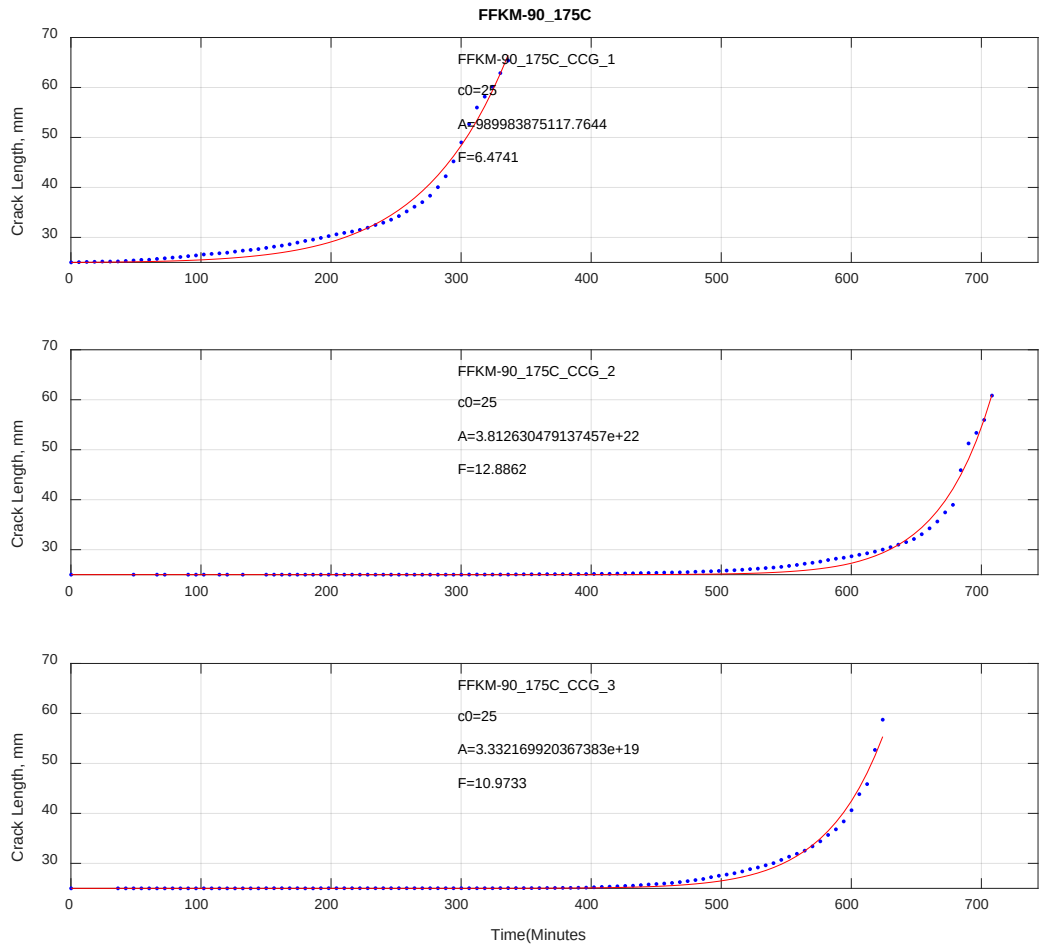
FFKM-90_175C
FFKM-90_175C_CCG_1
c0=25
A=989983875117.7644
F=6.4741
FFKM-90_175C_CCG_2
c0=25
A=3.812630479137457e+22
F=12.8862
FFKM-90_175C_CCG_3
c0=25
A=3.332169920367383e+19
F=10.9733
Crack Length, mm
Time(Minutes
70
60
50
40
30
0
100
200
300
400
500
600
700

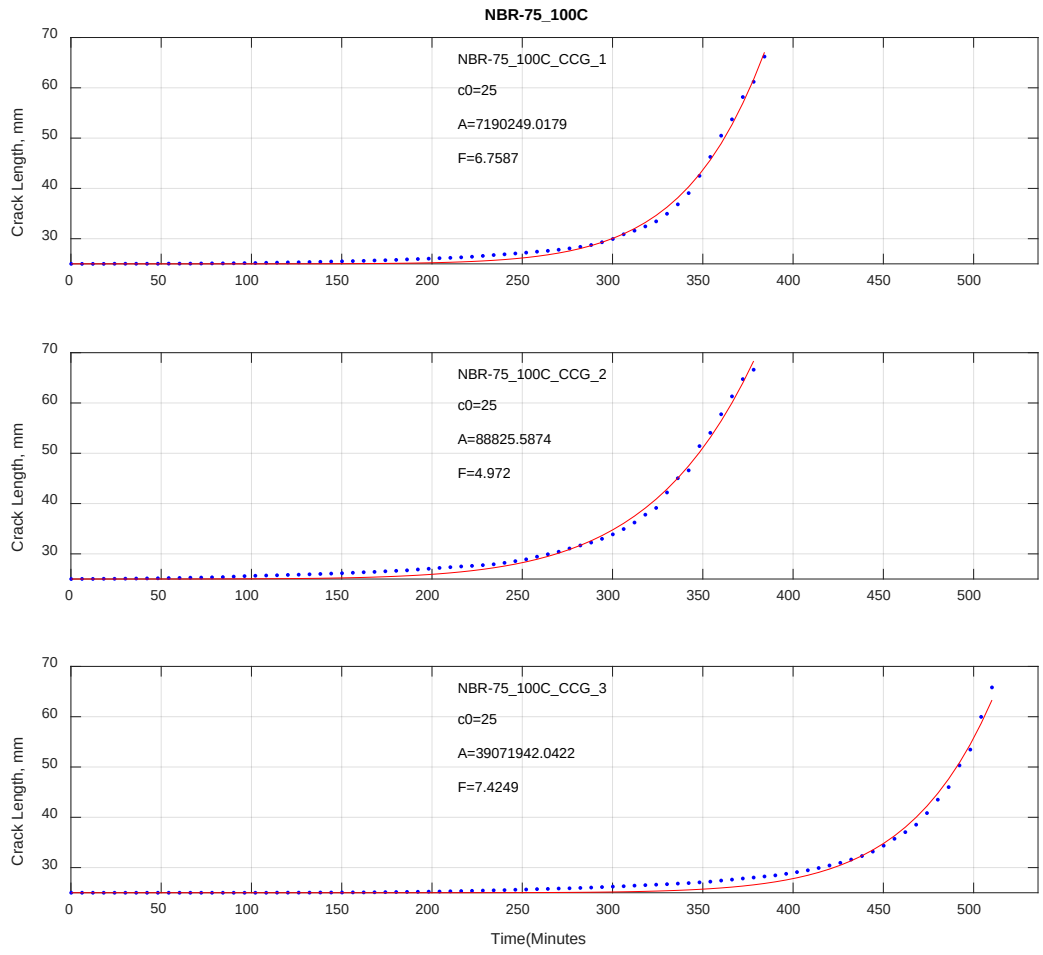
NBR-75_100C
NBR-75_100C_CCG_1
c0=25
A=7190249.0179
F=6.7587
NBR-75_100C_CCG_2
c0=25
A=88825.5874
F=4.972
NBR-75_100C_CCG_3
c0=25
A=39071942.0422
F=7.4249
Crack Length, mm
Time(Minutes

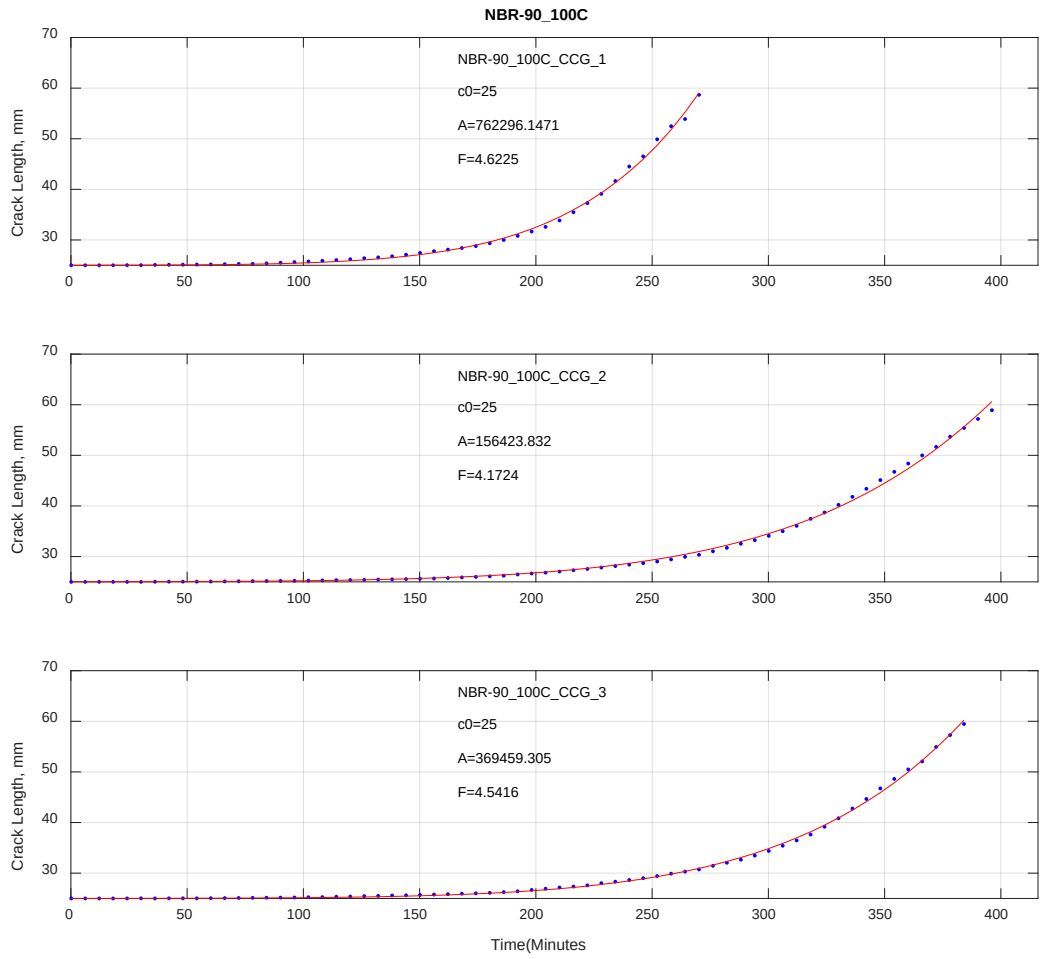
NBR-90_100C
NBR-90_100C_CCG_1
c0=25
A=762296.1471
F=4.6225
NBR-90_100C_CCG_2
c0=25
A=156423.832
F=4.1724
NBR-90_100C_CCG_3
c0=25
A=369459.305
F=4.5416
Crack Length, mm
Time(Minutes
70
60
50
40
30
0
50
100
150
200
250
300
350
400

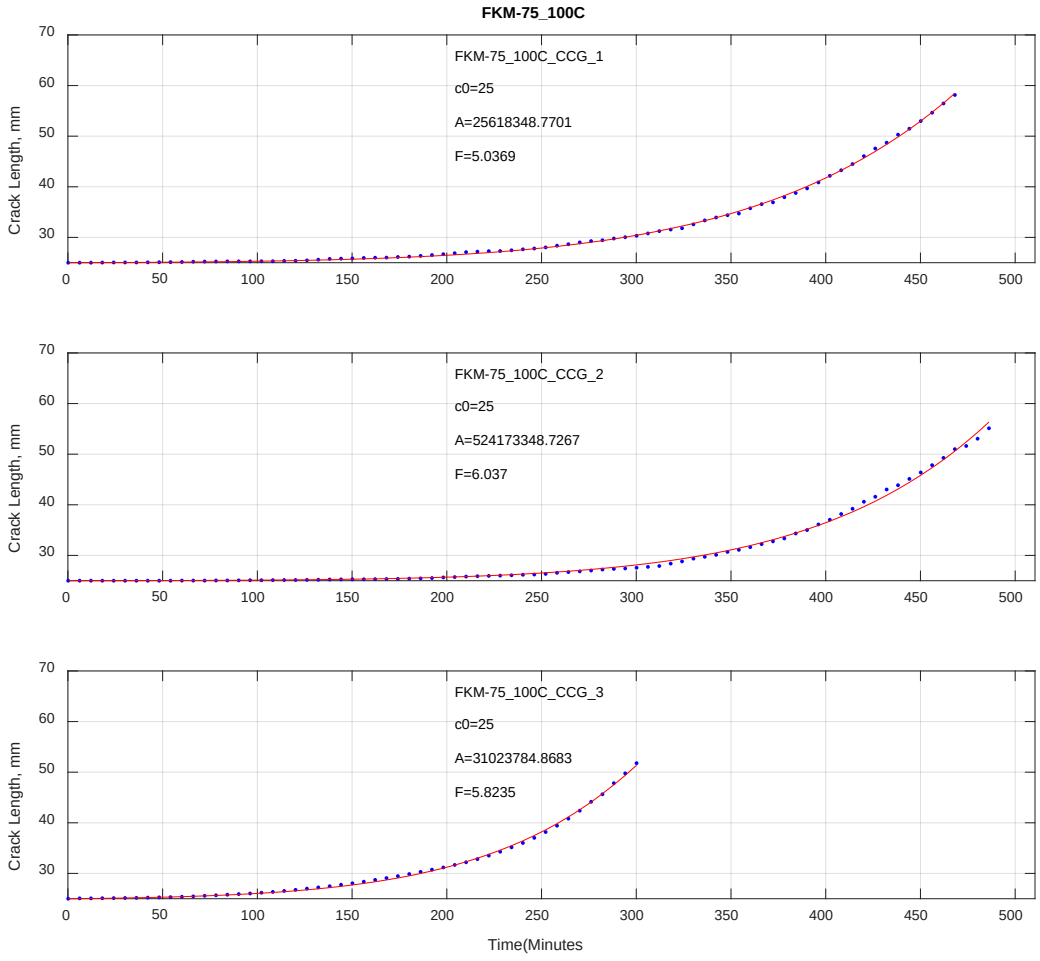
FKM-75_100C
FKM-75_100C_CCG_1
c0=25
A=25618348.7701
F=5.0369
FKM-75_100C_CCG_2
c0=25
A=524173348.7267
F=6.037
FKM-75_100C_CCG_3
c0=25
A=31023784.8683
F=5.8235
Crack Length, mm
Time(Minutes
70
60
50
40
30
0
50
100
150
200
250
300
350
400
450
500

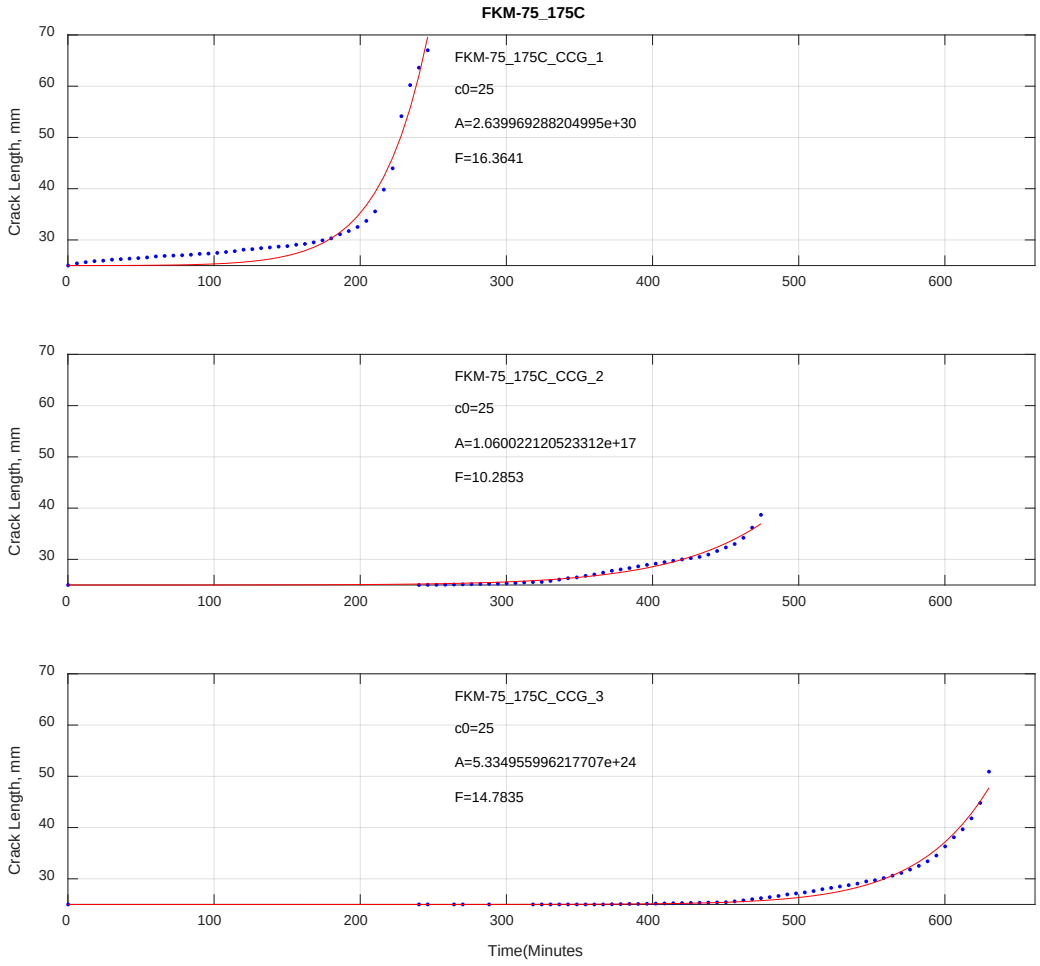
FKM-75_175C
FKM-75_175C_CCG_1
c0=25
A=2.6399692882049 95e+30
F=16.3641
FKM-75_175C_CCG_2
c0=25
A=1.060022120523312e+17
F=10.2853
FKM-75_175C_CCG_3
c0=25
A=5.334955996217707e+24
F=14.7835
Crack Length, mm
Time(Minutes
70
60
50
40
30
0
100
200
300
400
500
600

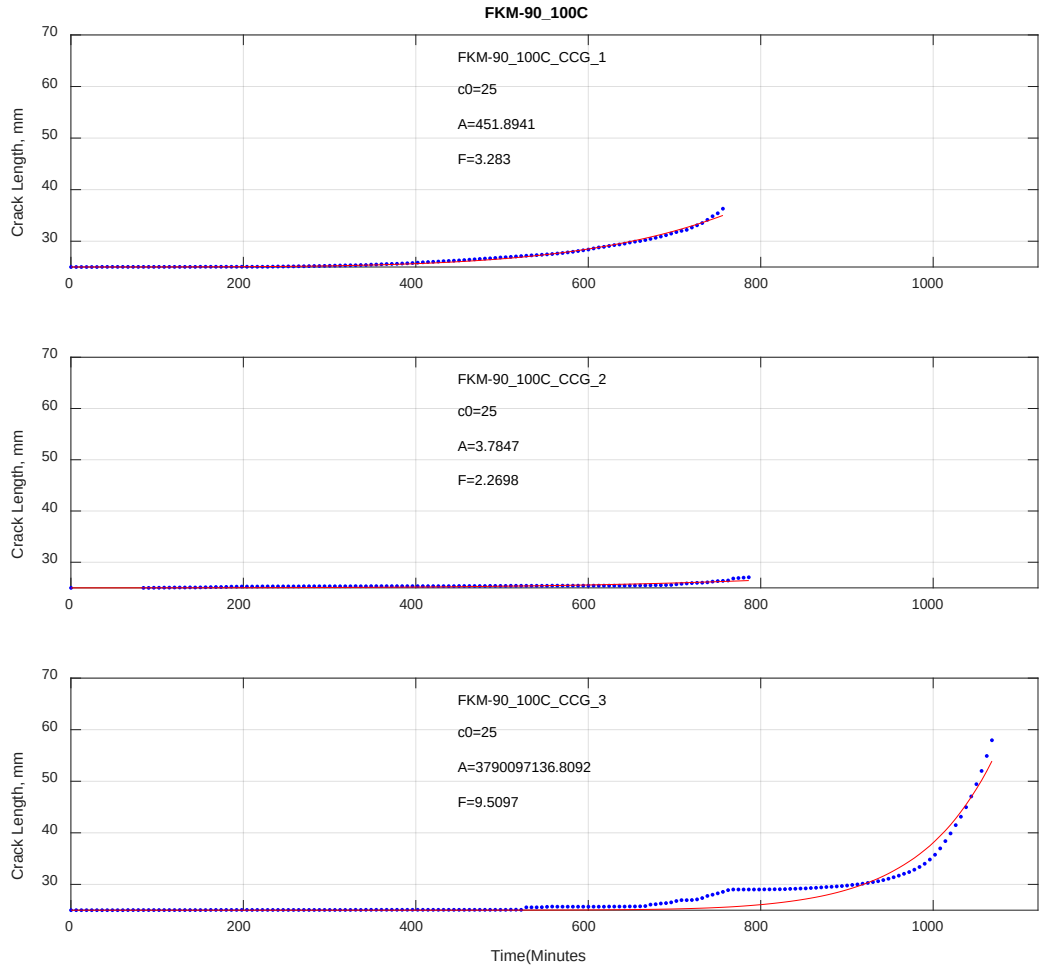
FKM-90_100C
FKM-90_100C_CCG_1
c0=25
A=451.8941
F=3.283
FKM-90_100C_CCG_2
c0=25
A=3.7847
F=2.2698
FKM-90_100C_CCG_3
c0=25
A=3790097136.8092
F=9.5097
Crack Length, mm
Time(Minutes
70
60
50
40
30
0
200
400
600
800
1000

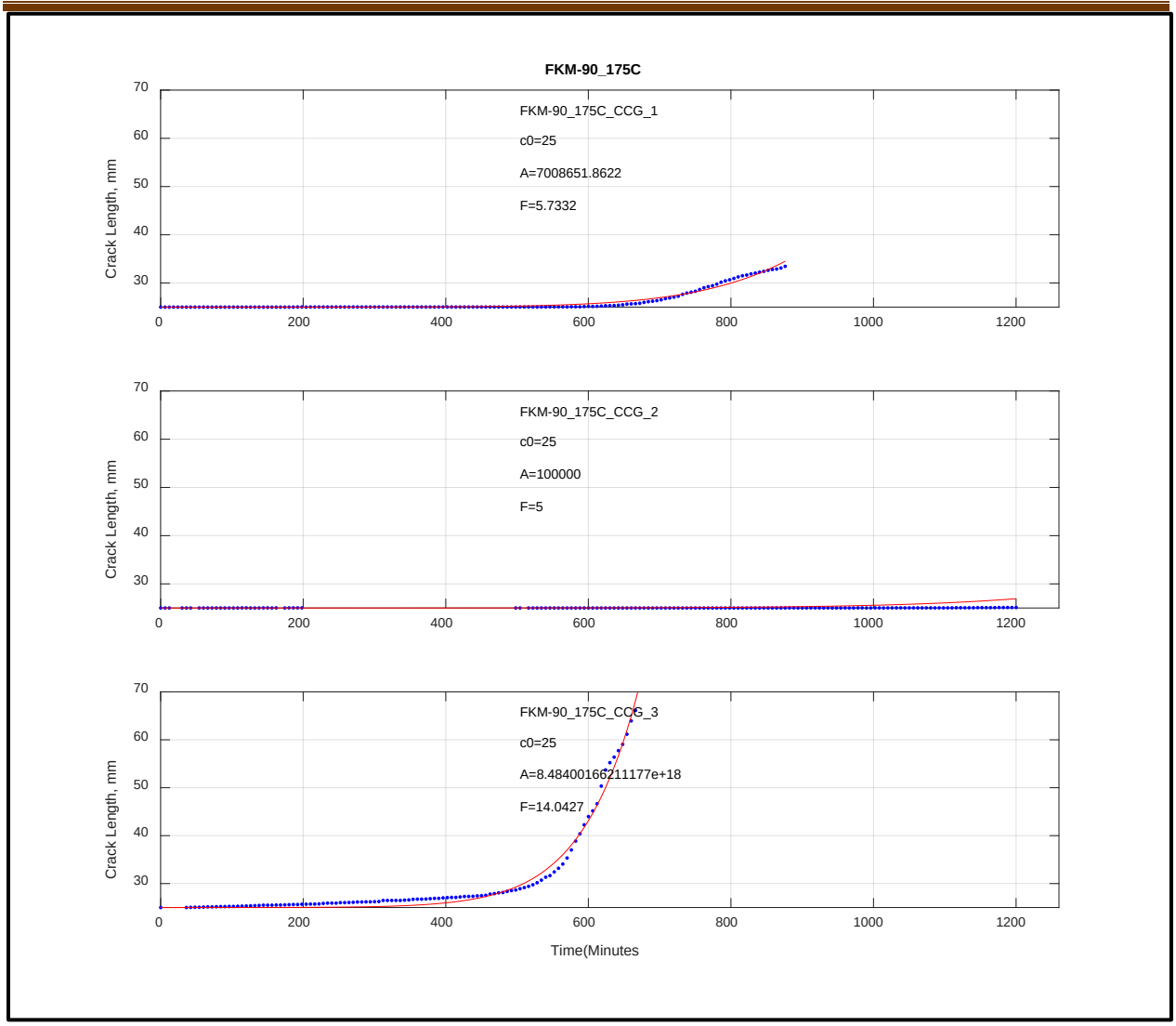


Figure A.4-14. Crack length evolution during tests for replicates 1-3.

The energy release rate, T, was computed using the following equation.

$$T = Wh \tag{5}$$

Crack growth rates *dc*/*dt* were then plotted as a function of the energy release rate *T*, as shown in Figure A.4-15. The following power law was then fit to the collection of measurements.

$$\frac{dc}{dt} = B(T)^F = r_q \left(\frac{T}{T_q}\right)^{F_q} \tag{6}$$

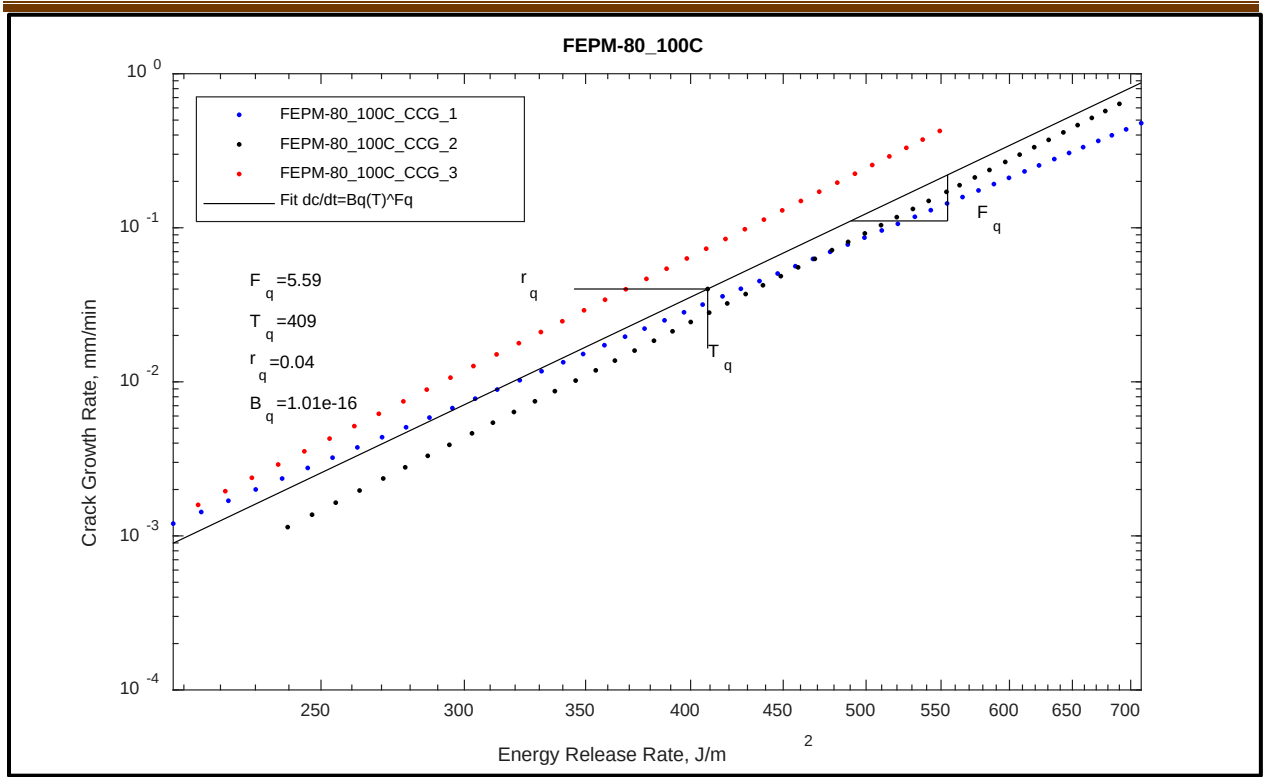
FEPM-80_100C
FEPM-80_100C_CCG_1
FEPM-80_100C_CCG_2
FEPM-80_100C_CCG_3
Fit dc/dt=Bq(T)^Fq
F q =5.59
T q =409
r q =0.04
B q =1.01e-16
r q
T q
F q
Crack Growth Rate, mm/min
Energy Release Rate, J/m 2
10 0
10 -1
10 -2
10 -3
10 -4
250
300
350
400
450
500
550
600
650
700

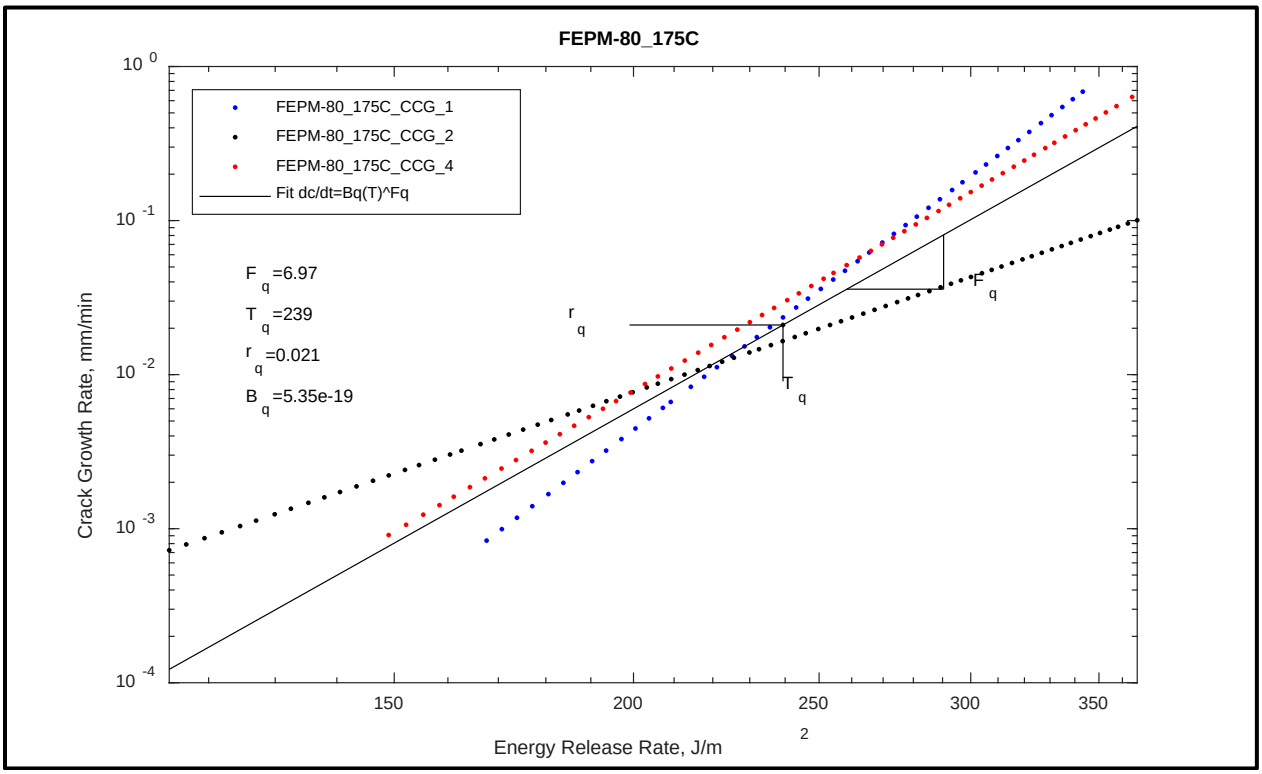
FEPM-80_175C
FEPM-80_175C_CCG_1
FEPM-80_175C_CCG_2
FEPM-80_175C_CCG_4
Fit dc/dt=Bq(T)^Fq
F q =6.97
T q =239
r q =0.021
B q =5.35e-19
r q
T q
F q
Crack Growth Rate, mm/min
Energy Release Rate, J/m 2
10 0
10 -1
10 -2
10 -3
10 -4
150
200
250
300
350

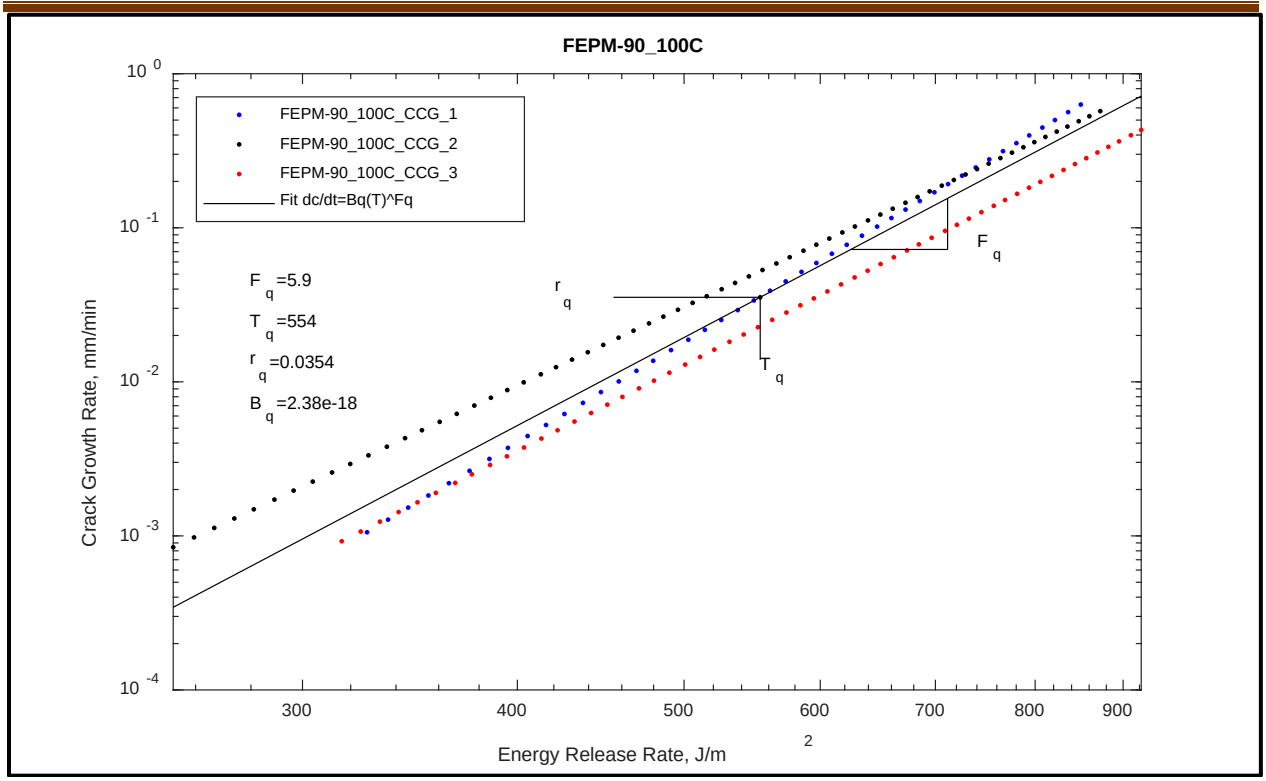
FEPM-90_100C
FEPM-90_100C_CCG_1
FEPM-90_100C_CCG_2
FEPM-90_100C_CCG_3
Fit dc/dt=Bq(T)^Fq
Fq=5.9
Tq=554
rq=0.0354
Bq=2.38e-18
rq
Tq
Fq
Crack Growth Rate, mm/min
Energy Release Rate, J/m2
10 0
10 -1
10 -2
10 -3
10 -4
300
400
500
600
700
800
900

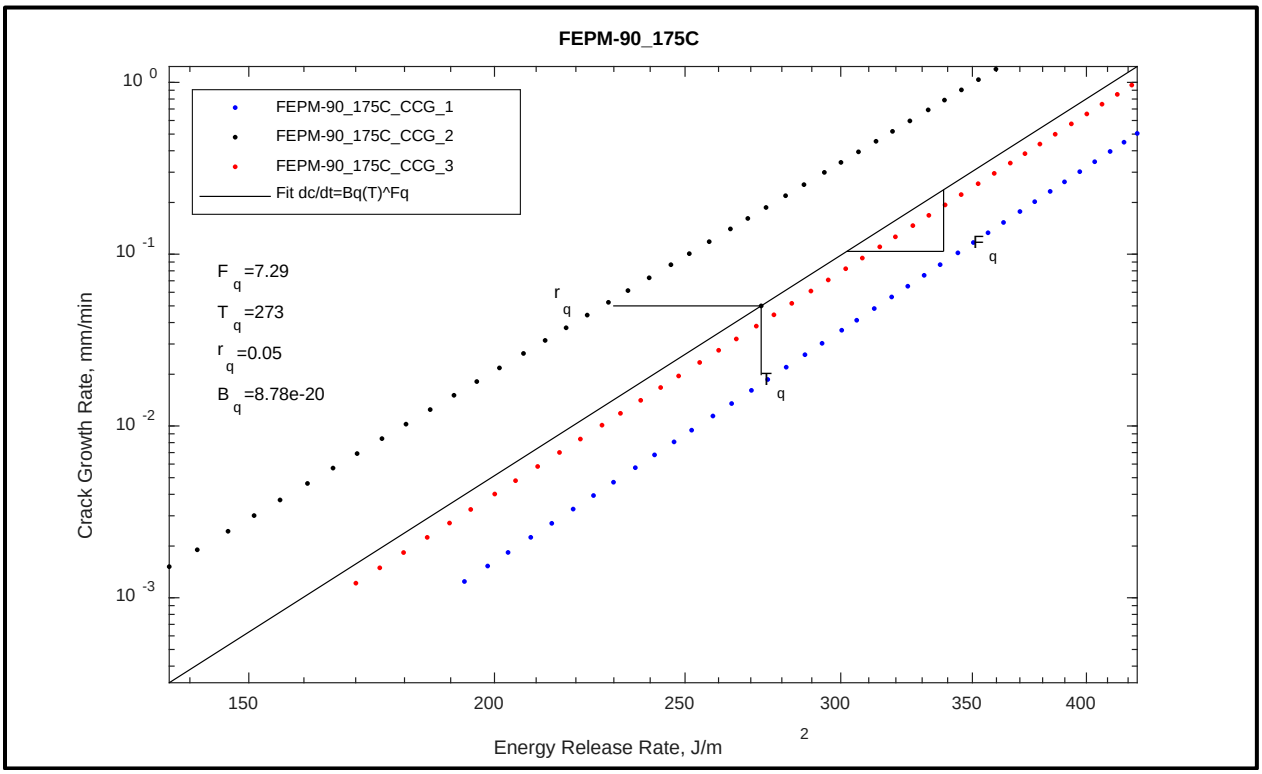
FEPM-90_175C
FEPM-90_175C_CCG_1
FEPM-90_175C_CCG_2
FEPM-90_175C_CCG_3
Fit dc/dt=Bq(T)^Fq
Fq=7.29
Tq=273
rq=0.05
Bq=8.78e-20
rq
Tq
Fq
Crack Growth Rate, mm/min
Energy Release Rate, J/m2
10 0
10 -1
10 -2
10 -3
150
200
250
300
350
400

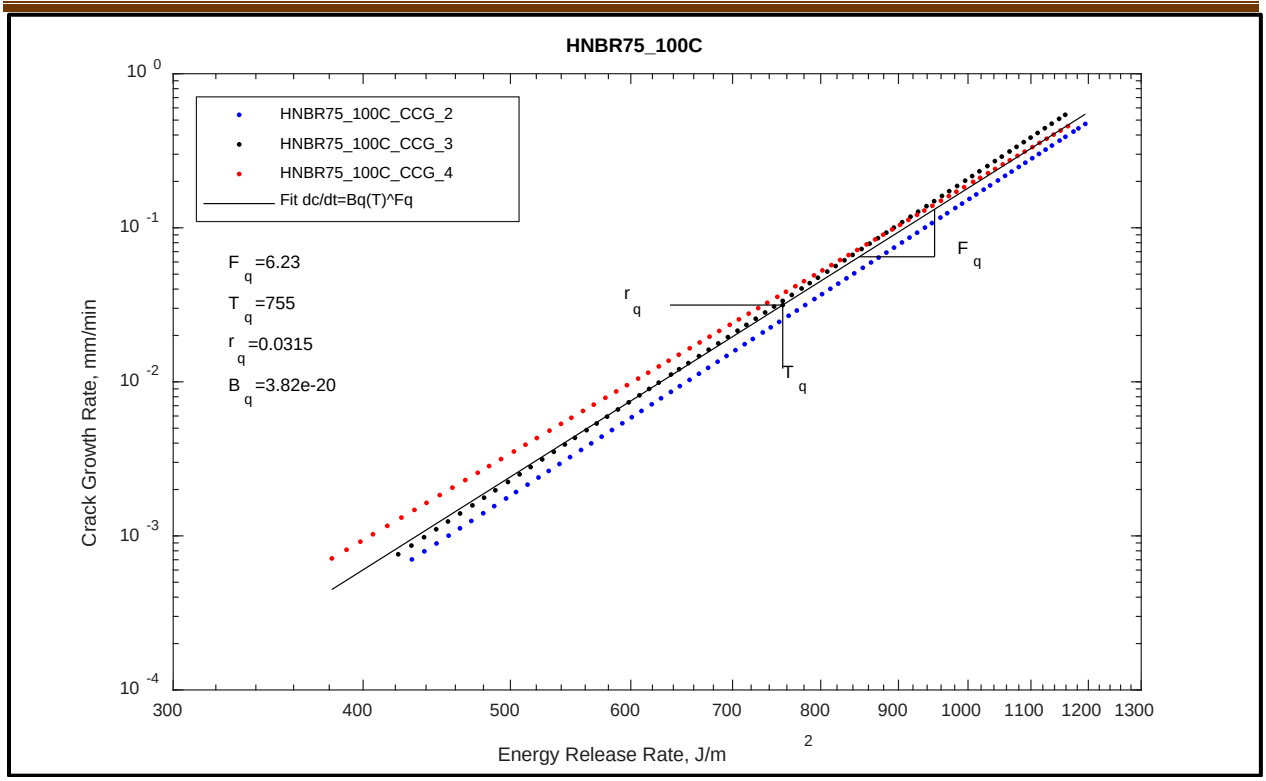
HNBR75_100C
HNBR75_100C_CCG_2
HNBR75_100C_CCG_3
HNBR75_100C_CCG_4
Fit dc/dt=Bq(T)^Fq
Fq=6.23
Tq=755
rq=0.0315
Bq=3.82e-20
Crack Growth Rate, mm/min
Energy Release Rate, J/m2

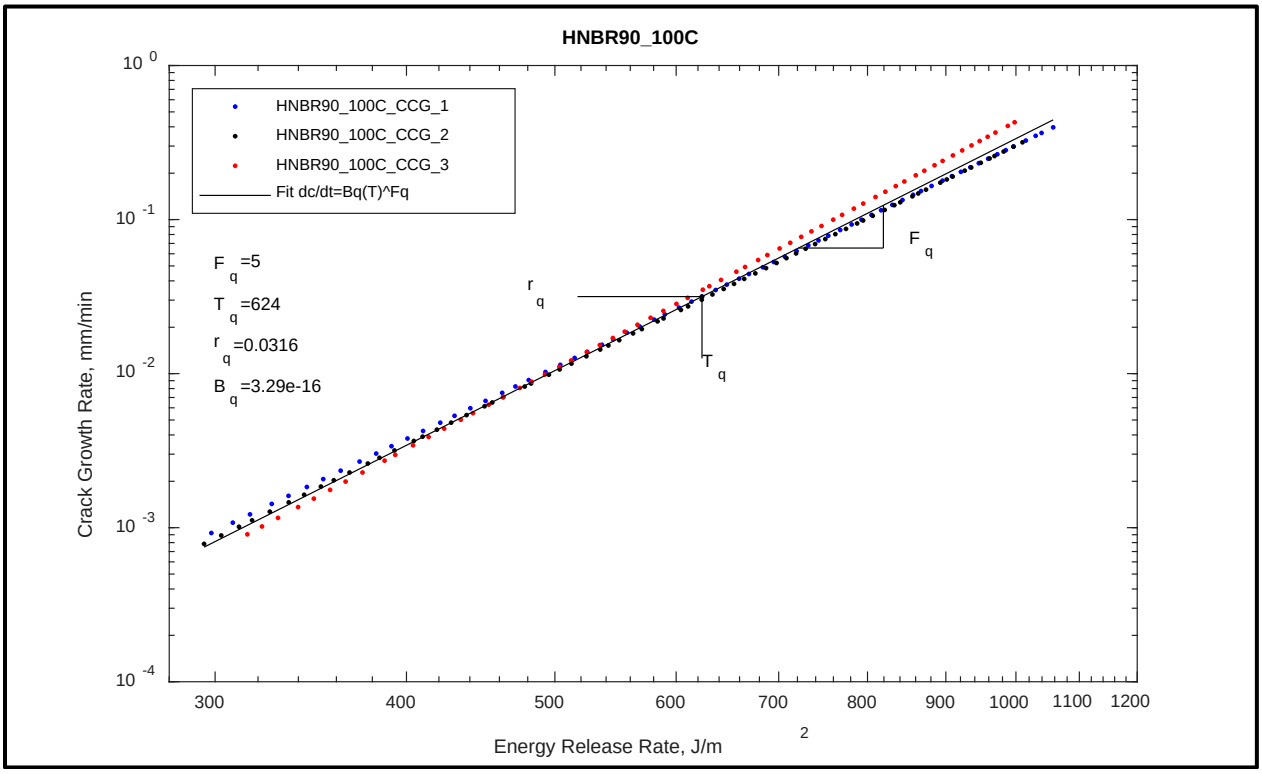
HNBR90_100C
HNBR90_100C_CCG_1
HNBR90_100C_CCG_2
HNBR90_100C_CCG_3
Fit dc/dt=Bq(T)^Fq
Fq=5
Tq=624
rq=0.0316
Bq=3.29e-16
Crack Growth Rate, mm/min
Energy Release Rate, J/m2

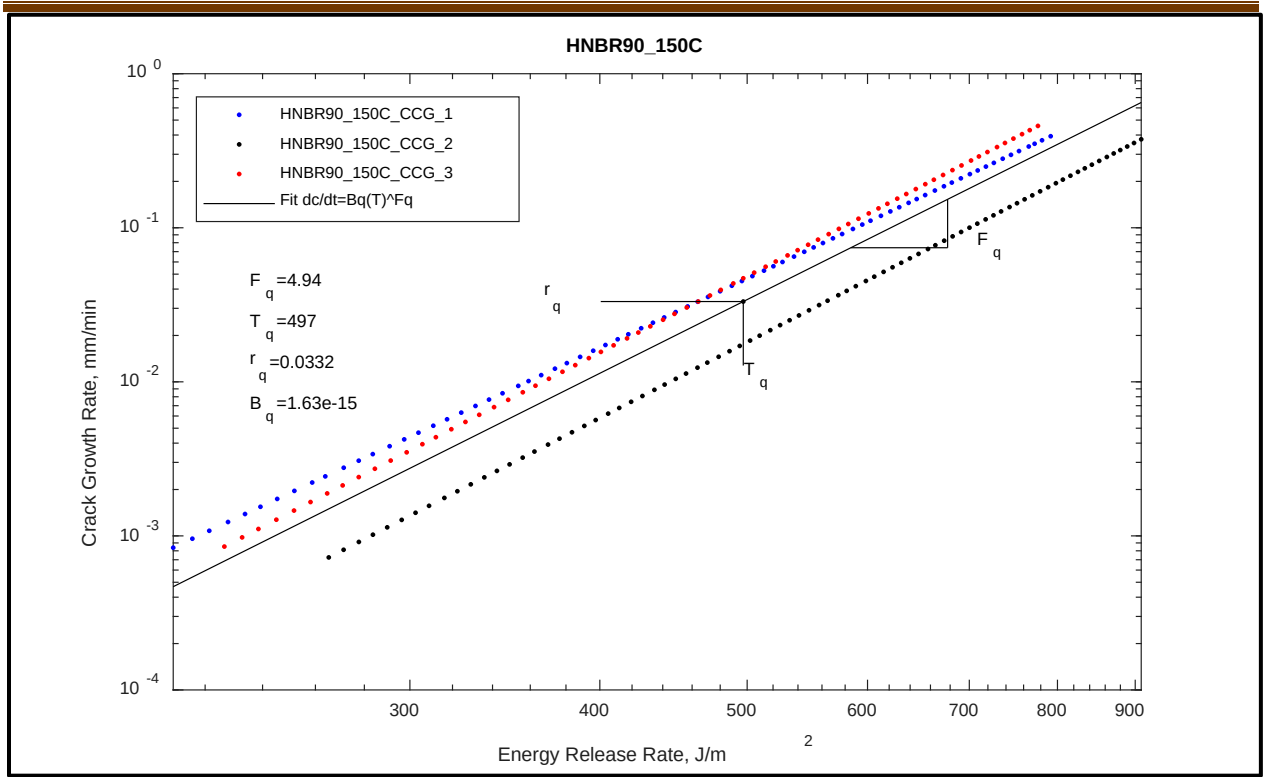
HNBR90_150C
HNBR90_150C_CCG_1
HNBR90_150C_CCG_2
HNBR90_150C_CCG_3
Fit dc/dt=Bq(T)^Fq
Fq=4.94
Tq=497
rq=0.0332
Bq=1.63e-15
rq
Tq
Fq
Crack Growth Rate, mm/min
Energy Release Rate, J/m2
10 0
10 -1
10 -2
10 -3
10 -4
300
400
500
600
700
800
900

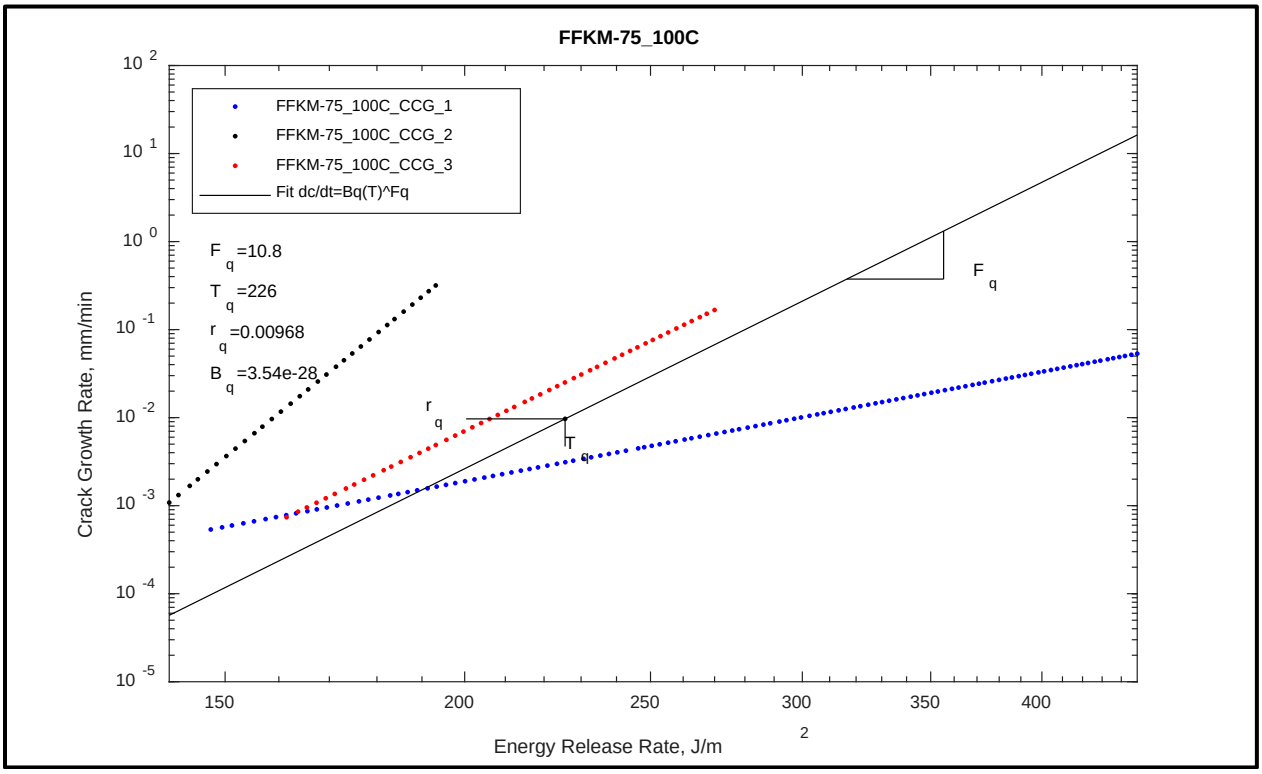
FFKM-75_100C
FFKM-75_100C_CCG_1
FFKM-75_100C_CCG_2
FFKM-75_100C_CCG_3
Fit dc/dt=Bq(T)^Fq
Fq=10.8
Tq=226
rq=0.00968
Bq=3.54e-28
rq
Tq
Fq
Crack Growth Rate, mm/min
Energy Release Rate, J/m2
10 2
10 1
10 0
10 -1
10 -2
10 -3
10 -4
10 -5
150
200
250
300
350
400

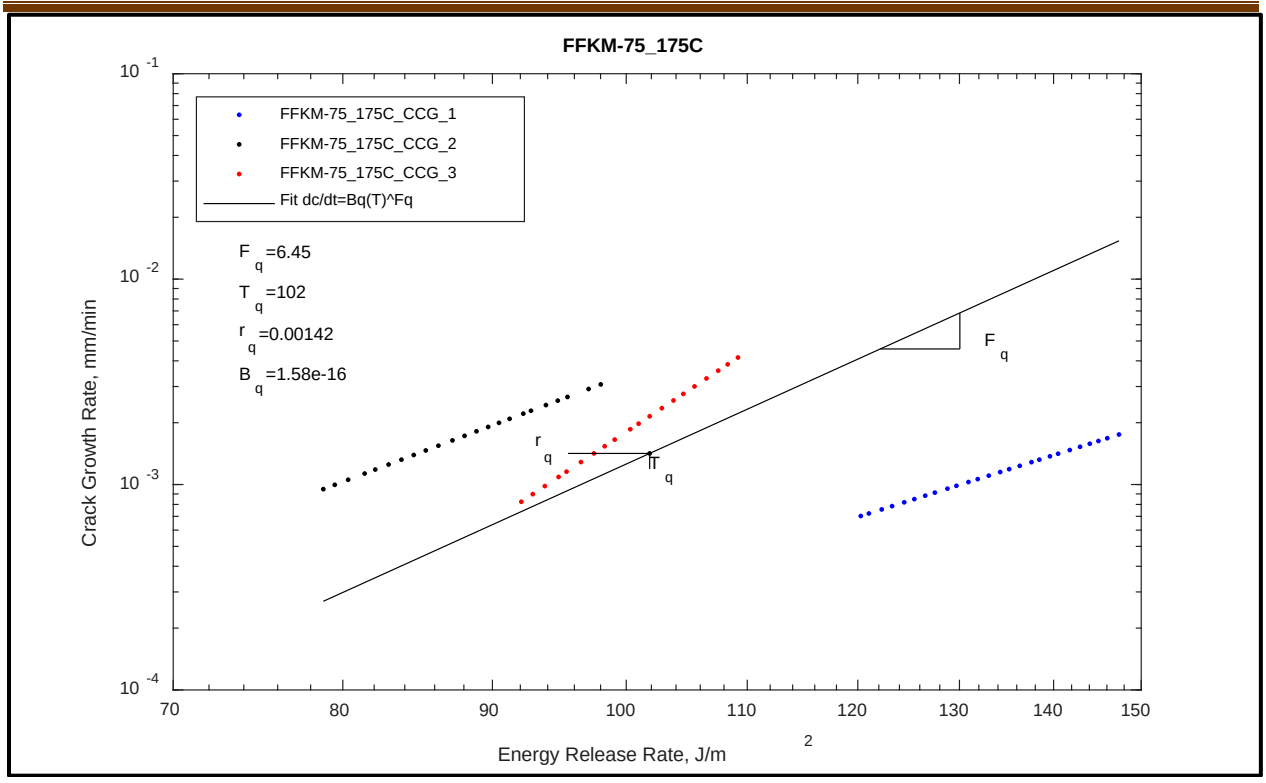
FFKM-75_175C
FFKM-75_175C_CCG_1
FFKM-75_175C_CCG_2
FFKM-75_175C_CCG_3
Fit dc/dt=Bq(T)^Fq
F q =6.45
T q =102
r q =0.00142
B q =1.58e-16
F q
r q
T q
Crack Growth Rate, mm/min
Energy Release Rate, J/m 2
10 -1
10 -2
10 -3
10 -4
70
80
90
100
110
120
130
140
150

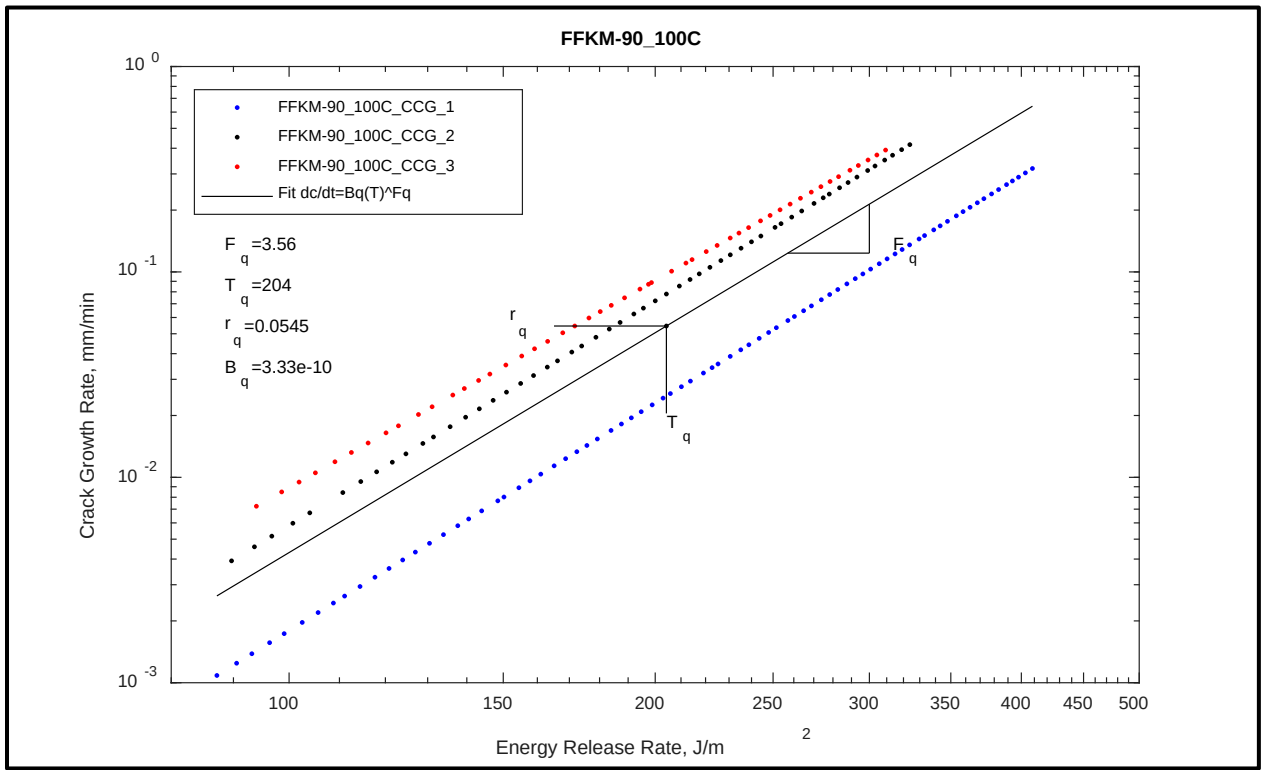
FFKM-90_100C
FFKM-90_100C_CCG_1
FFKM-90_100C_CCG_2
FFKM-90_100C_CCG_3
Fit dc/dt=Bq(T)^Fq
F q =3.56
T q =204
r q =0.0545
B q =3.33e-10
F q
r q
T q
Crack Growth Rate, mm/min
Energy Release Rate, J/m 2
10 0
10 -1
10 -2
10 -3
100
150
200
250
300
350
400
450
500

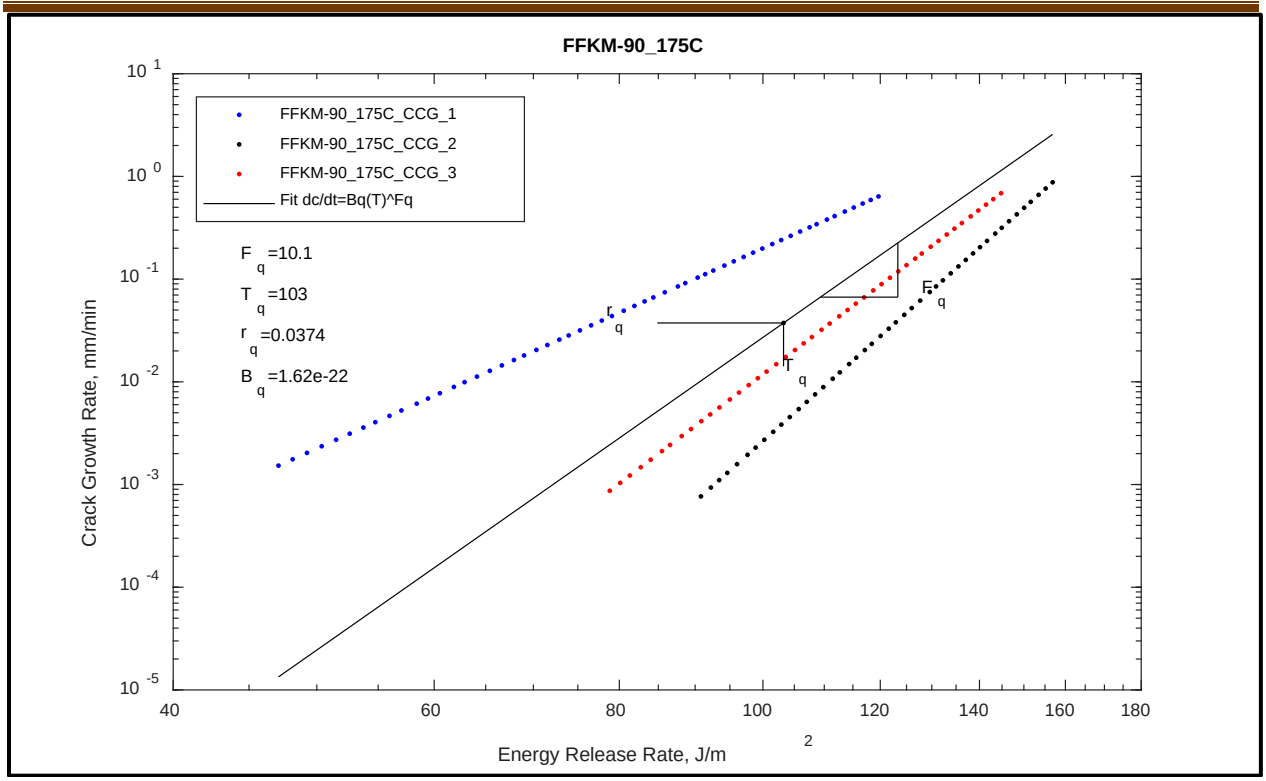
FFKM-90_175C
FFKM-90_175C_CCG_1
FFKM-90_175C_CCG_2
FFKM-90_175C_CCG_3
Fit dc/dt=Bq(T)^Fq
F q =10.1
T q =103
r q =0.0374
B q =1.62e-22
r q
T q
F q
Crack Growth Rate, mm/min
Energy Release Rate, J/m 2
10 1
10 0
10 -1
10 -2
10 -3
10 -4
10 -5
40
60
80
100
120
140
160
180

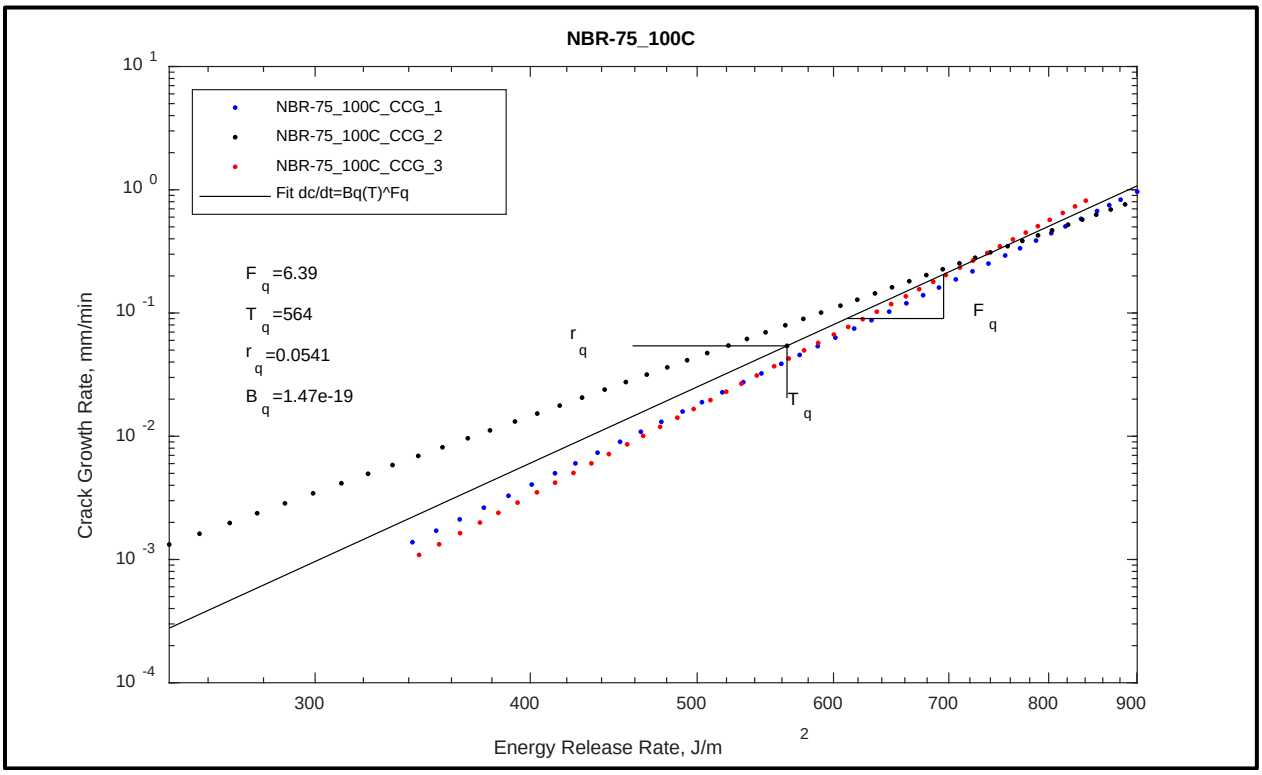
NBR-75_100C
NBR-75_100C_CCG_1
NBR-75_100C_CCG_2
NBR-75_100C_CCG_3
Fit dc/dt=Bq(T)^Fq
F q =6.39
T q =564
r q =0.0541
B q =1.47e-19
r q
T q
F q
Crack Growth Rate, mm/min
Energy Release Rate, J/m 2
10 1
10 0
10 -1
10 -2
10 -3
10 -4
300
400
500
600
700
800
900

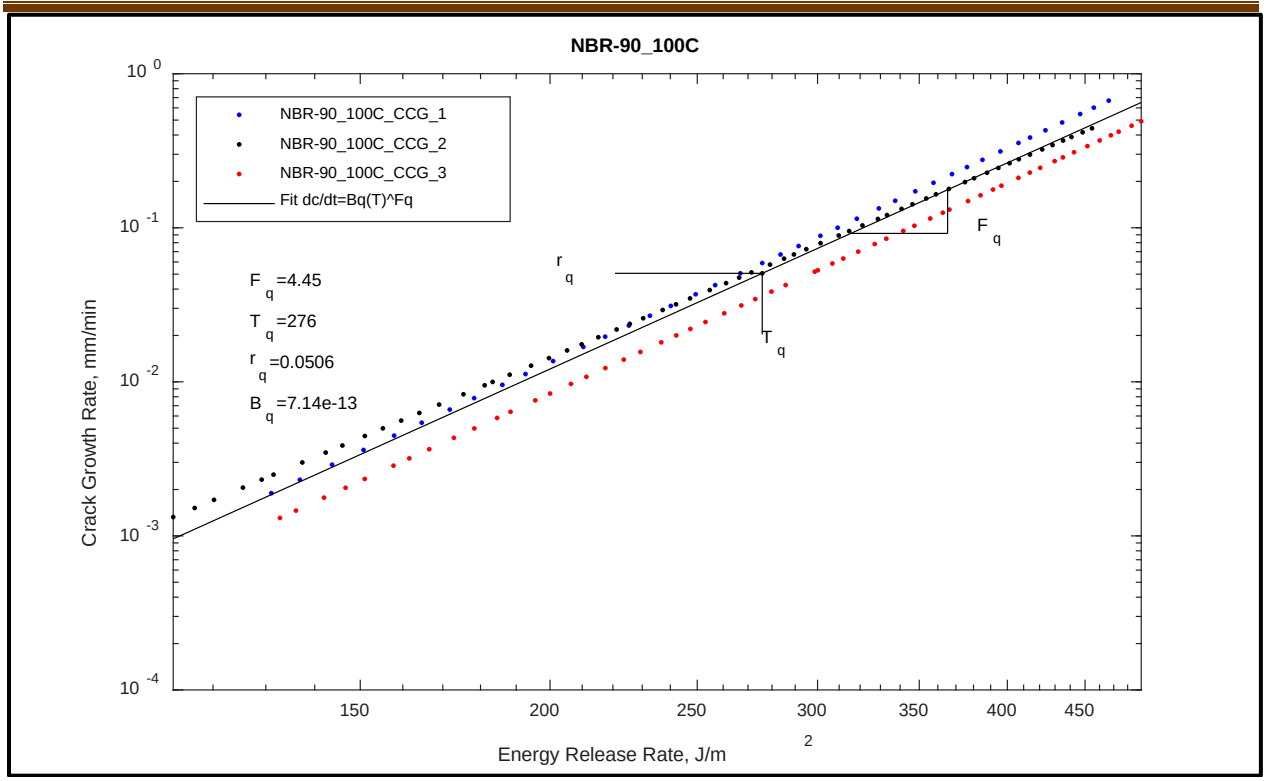
NBR-90_100C
NBR-90_100C_CCG_1
NBR-90_100C_CCG_2
NBR-90_100C_CCG_3
Fit dc/dt=Bq(T)^Fq
F q =4.45
T q =276
r q =0.0506
B q =7.14e-13
r q
T q
F q
Crack Growth Rate, mm/min
Energy Release Rate, J/m 2
10 0
10 -1
10 -2
10 -3
10 -4
150
200
250
300
350
400
450

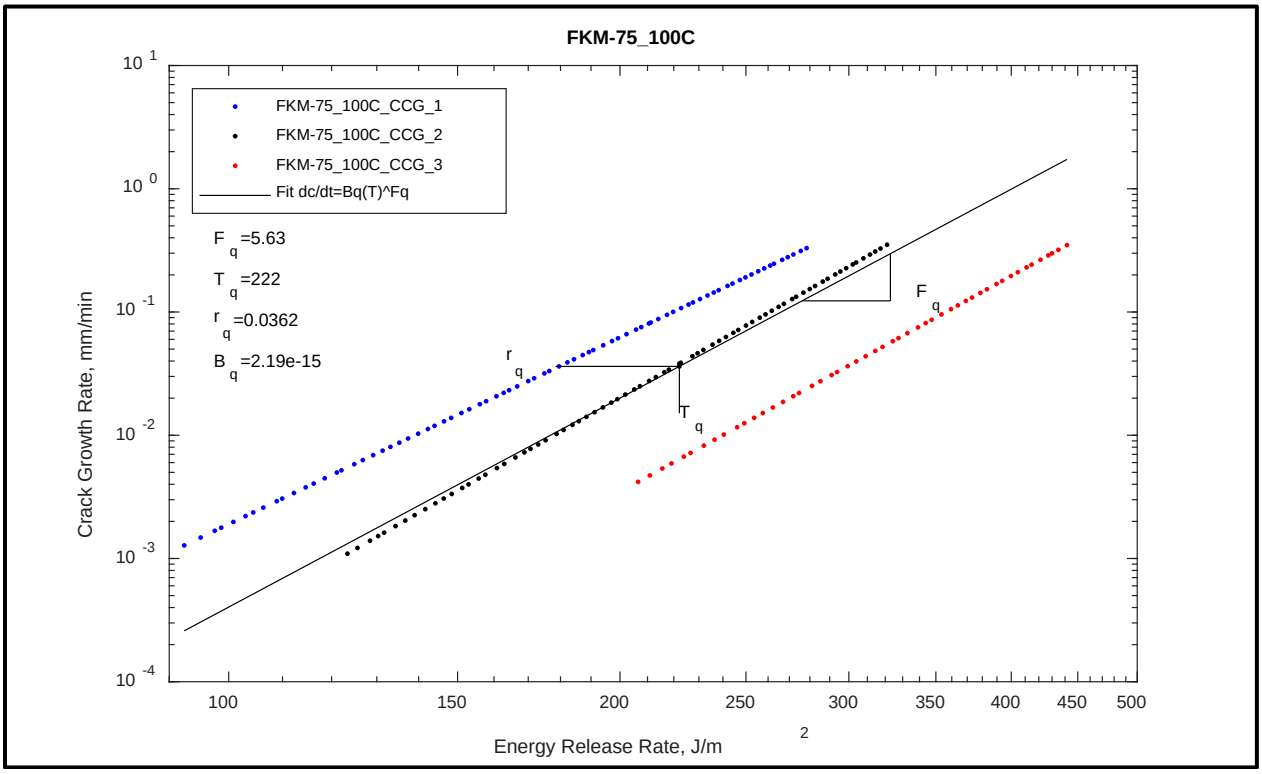
FKM-75_100C
FKM-75_100C_CCG_1
FKM-75_100C_CCG_2
FKM-75_100C_CCG_3
Fit dc/dt=Bq(T)^Fq
F q =5.63
T q =222
r q =0.0362
B q =2.19e-15
r q
T q
F q
Crack Growth Rate, mm/min
Energy Release Rate, J/m 2
10 1
10 0
10 -1
10 -2
10 -3
10 -4
100
150
200
250
300
350
400
450
500

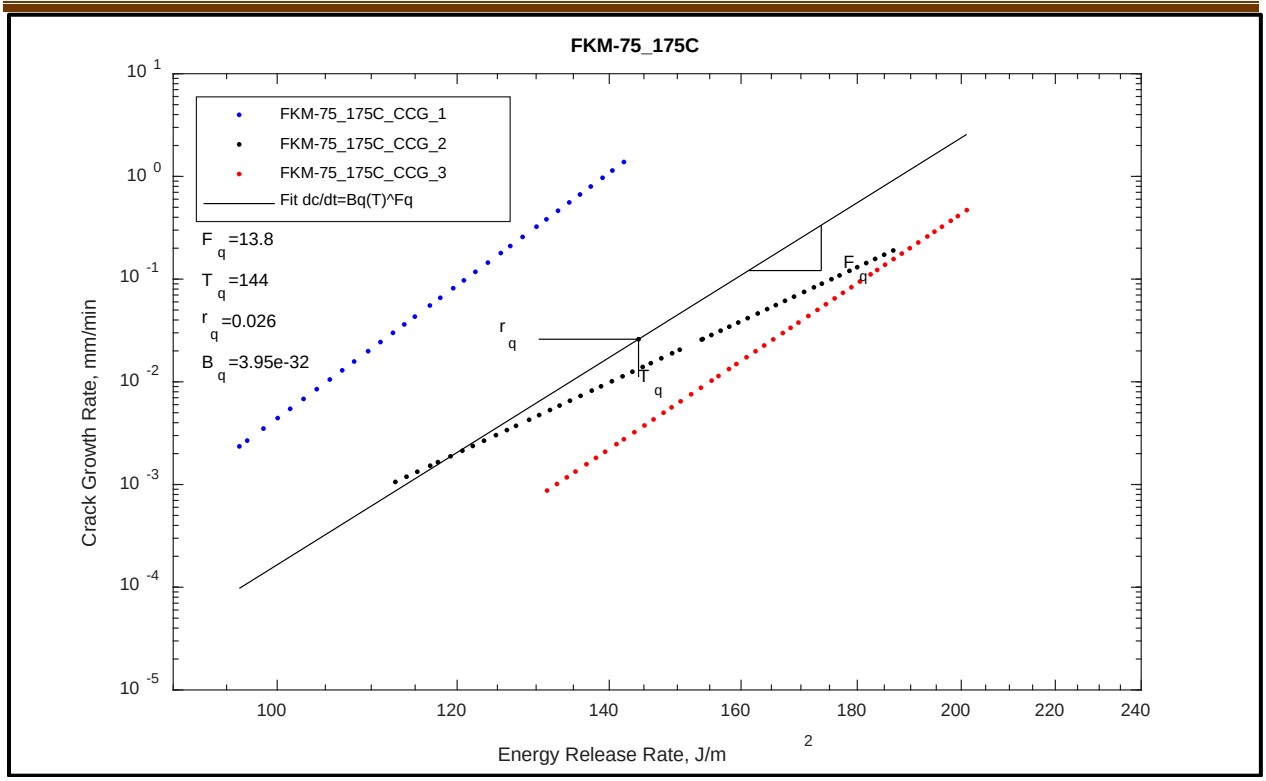
FKM-75_175C
FKM-75_175C_CCG_1
FKM-75_175C_CCG_2
FKM-75_175C_CCG_3
Fit dc/dt=Bq(T)^Fq
Fq=13.8
Tq=144
rq=0.026
Bq=3.95e-32
Crack Growth Rate, mm/min
Energy Release Rate, J/m2

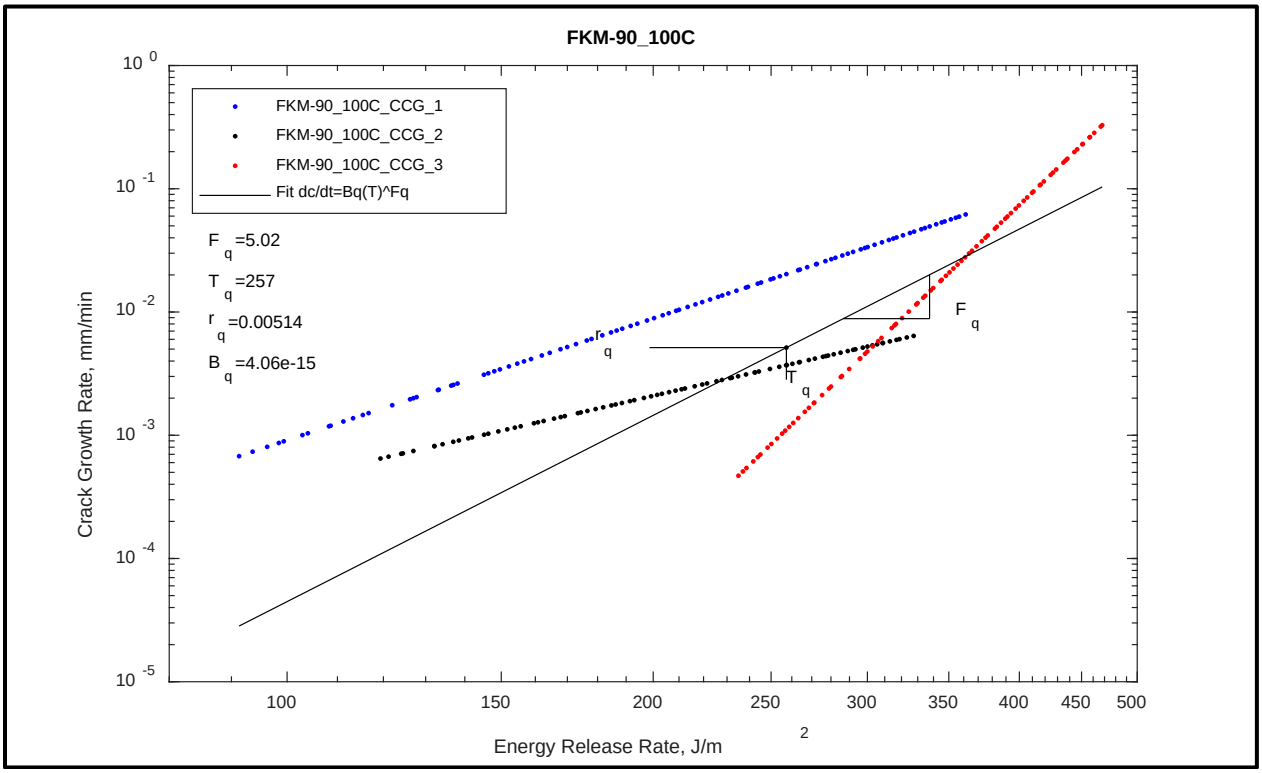
FKM-90_100C
FKM-90_100C_CCG_1
FKM-90_100C_CCG_2
FKM-90_100C_CCG_3
Fit dc/dt=Bq(T)^Fq
Fq=5.02
Tq=257
rq=0.00514
Bq=4.06e-15
Crack Growth Rate, mm/min
Energy Release Rate, J/m2

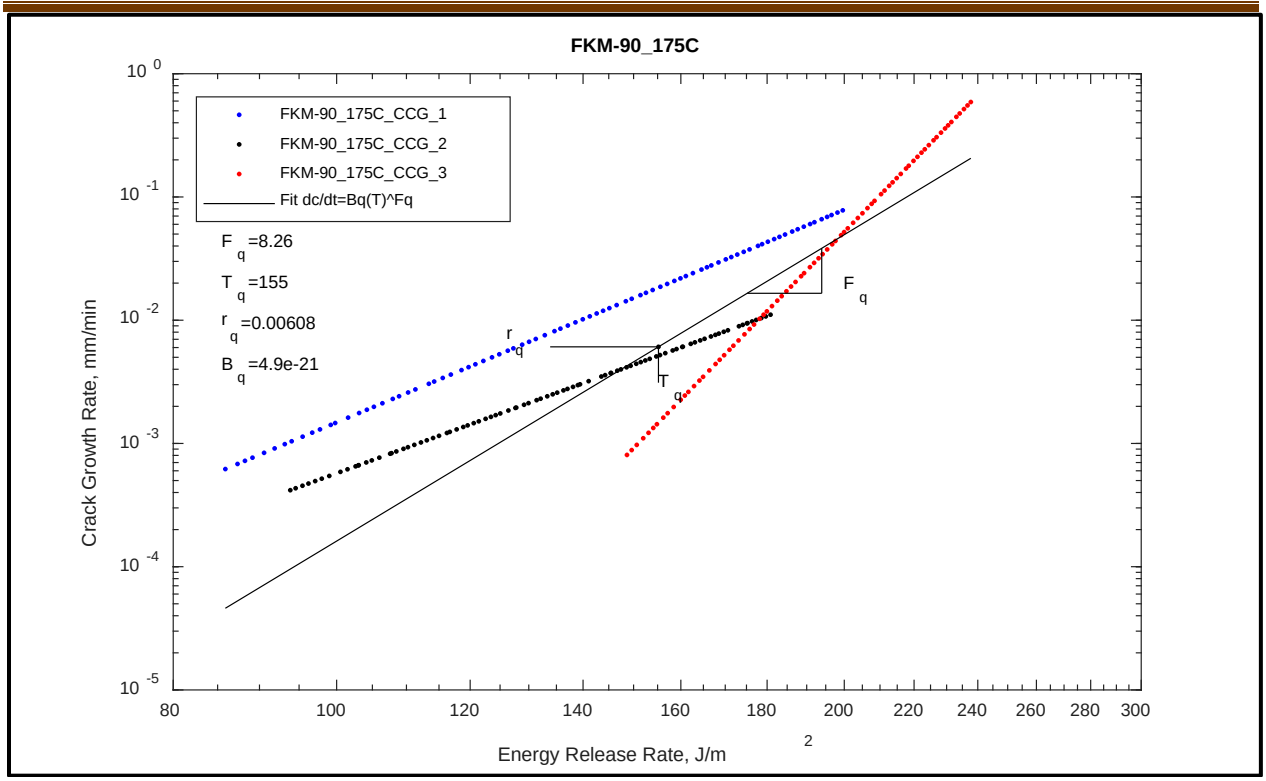


Figure A.4-15. Creep crack growth curves for replicates 1-3 and fitted creep crack growth law.

Table A.4-12. Fitted power law creep crack growth parameters. (mm/min vs. J/m$^2$)

| Material | Test Temperature, °C | $F_q$ | $T_q$ (J/m$^2$) | $r_q$ (mm/min) | $B_q$ |
|---|---|---|---|---|---|
| FEPM-80 | 100 | 5.59 | 409 | 0.04 | 1.01e-16 |
| FEPM-80 | 175 | 6.97 | 239 | 0.021 | 5.35e-19 |
| FEPM-90 | 100 | 5.9 | 554 | 0.0354 | 2.38e-18 |
| FEPM-90 | 175 | 7.29 | 273 | 0.05 | 8.78e-20 |
| HNBR-75 | 100 | 6.23 | 755 | 0.0315 | 3.82e-20 |
| HNBR-90 | 100 | 5.00 | 624 | 0.0316 | 3.29e-16 |
| HNBR-90 | 150 | 4.94 | 497 | 0.0332 | 1.63e-15 |
| FFKM-75 | 100 | 10.8 | 226 | 0.00968 | 3.54e-28 |
| FFKM-75 | 175 | 6.45 | 102 | 0.00142 | 1.58e-16 |
| FFKM 90 | 100 | 3.56 | 204 | 0.0545 | 3.33e-10 |
| FFKM-90 | 175 | 10.1 | 103 | 0.0374 | 1.66e-22 |
| NBR-75 | 100 | 6.39 | 564 | 0.0541 | 1.47e-19 |
| NBR-90 | 100 | 4.45 | 276 | 0.0506 | 7.14e-13 |
| FKM-75 | 100 | 5.63 | 222 | 0.0362 | 2.19e-15 |
| FKM-75 | 175 | 13.8 | 144 | 0.026 | 3.95e-32 |
| FKM-90 | 100 | 5.02 | 257 | 0.00514 | 4.06e-15 |
| FKM-90 | 175 | 8.26 | 155 | 0.00608 | 4.9e-21 |

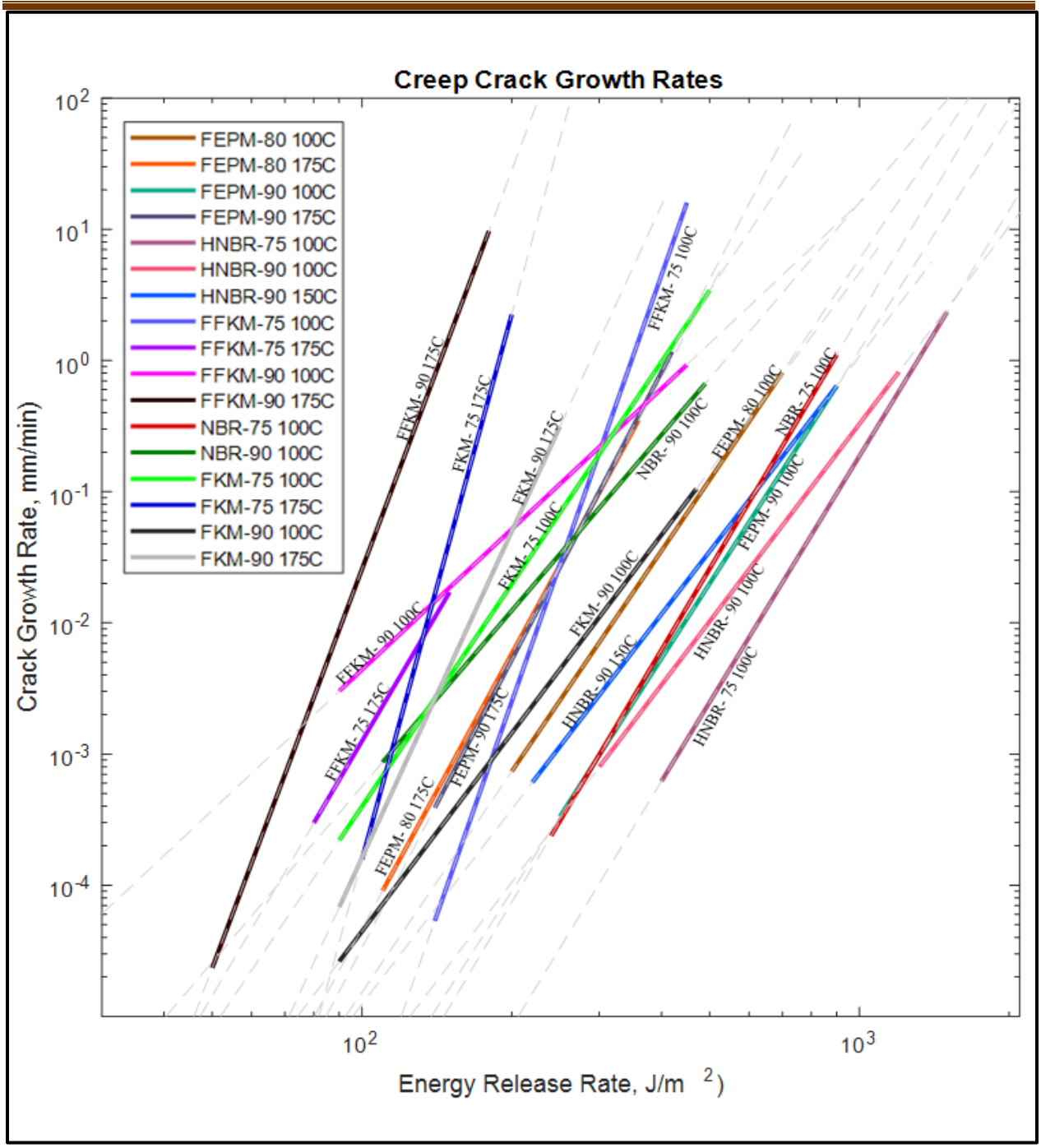


Figure A.4-16. Fitted creep crack growth rates are plotted for all materials and at each temperature measured. The bold colored line shows the part of the curve that was measured. Gray dashed lines extrapolate the measurements.

# Thermal Expansion

## *Experiment 5 – Thermal Expansion*

Purpose: Thermal expansion experiments are needed to define the thermal coefficient of expansion.

Specimen: Cylindrical specimen

Test Setup: A PerkinElmer Diamond Thermomechanical Analyzer is used to measure the expansion of materials under temperature changes.

Figure A.4-17. Thermomechanical Analyzer

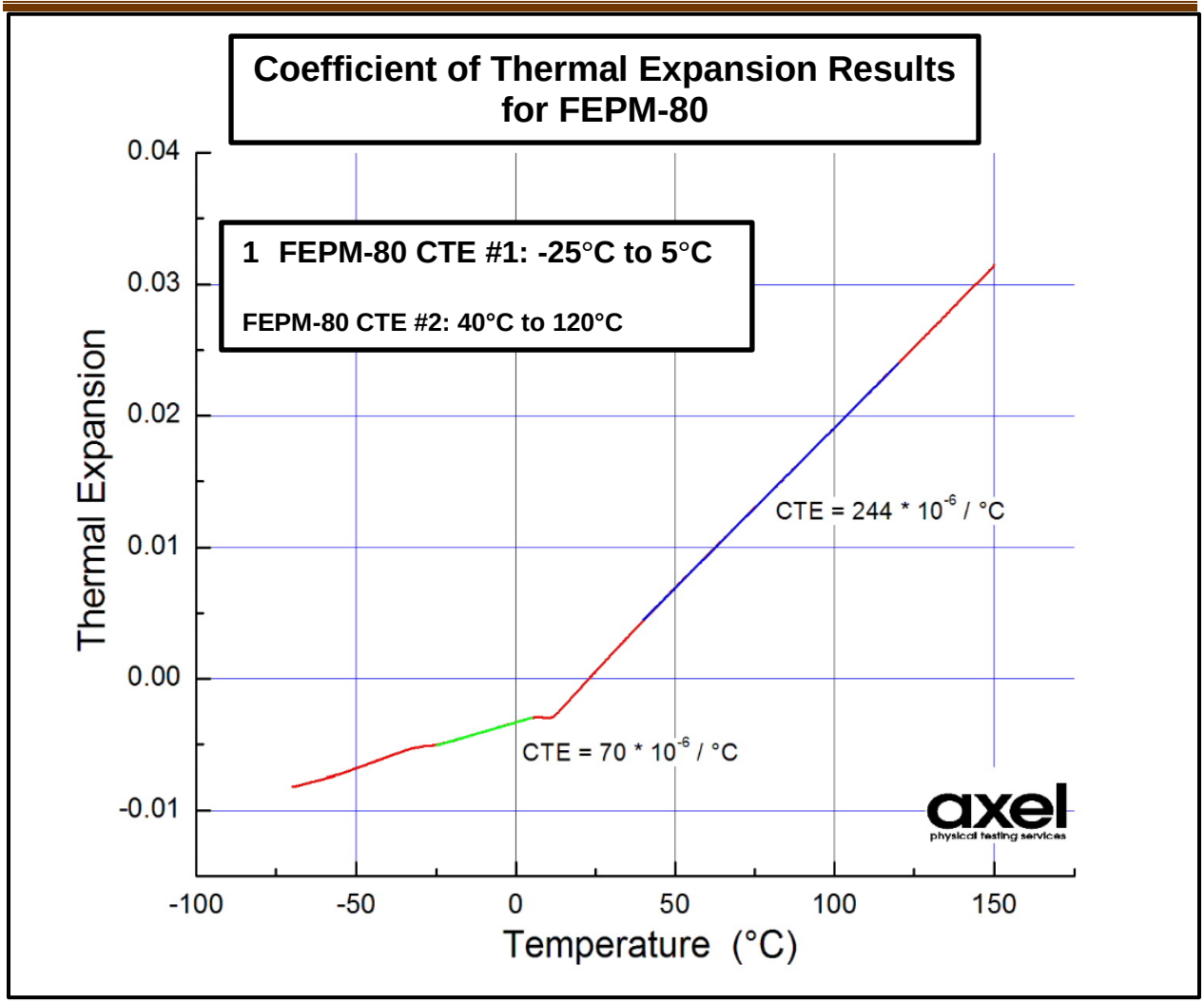
Coefficient of Thermal Expansion Results for FEPM-80
1 FEPM-80 CTE #1: -25°C to 5°C
FEPM-80 CTE #2: 40°C to 120°C
CTE = 244 * 10-6 / °C
CTE = 70 * 10-6 / °C
axel
physical testing services
Thermal Expansion
0.04
0.03
0.02
0.01
0.00
-0.01
-100
-50
0
50
100
150
Temperature (°C)

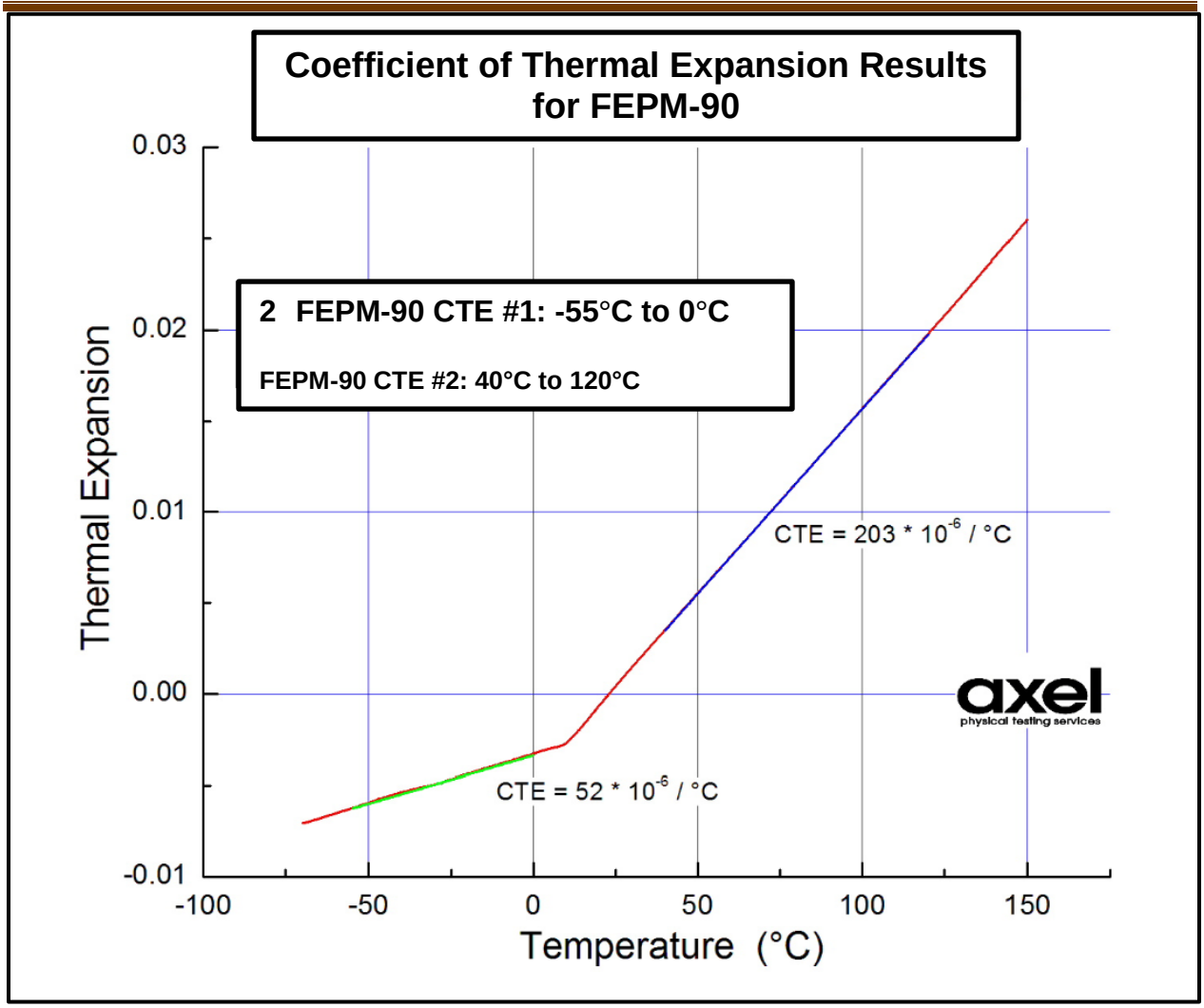
Coefficient of Thermal Expansion Results for FEPM-90
2 FEPM-90 CTE #1: -55°C to 0°C
FEPM-90 CTE #2: 40°C to 120°C
CTE = 203 * 10-6 / °C
CTE = 52 * 10-6 / °C
axel
physical testing services
Thermal Expansion
Temperature (°C)
0.03
0.02
0.01
0.00
-0.01
-100
-50
0
50
100
150

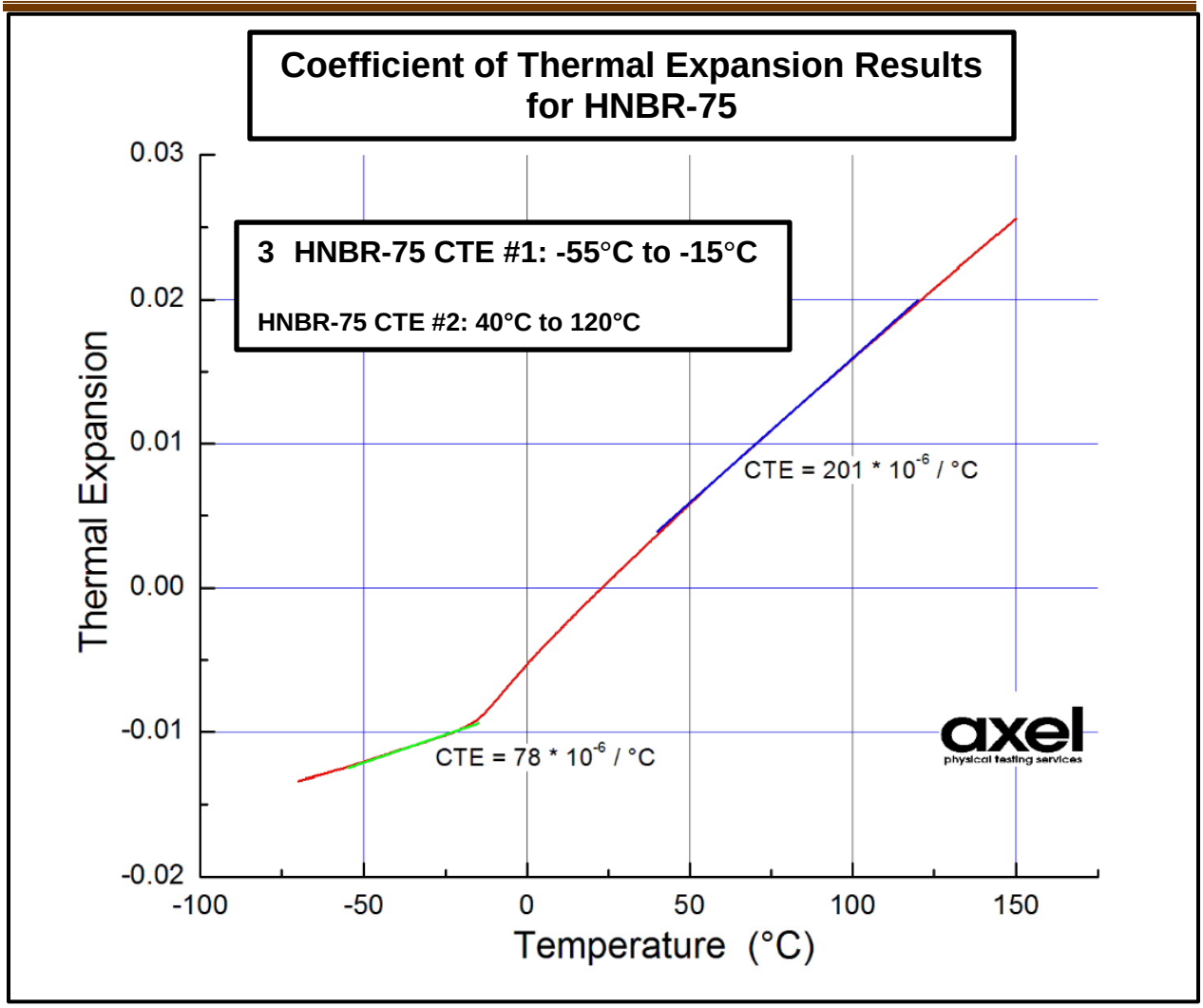
Coefficient of Thermal Expansion Results for HNBR-75
3 HNBR-75 CTE #1: -55°C to -15°C
HNBR-75 CTE #2: 40°C to 120°C
CTE = 201 * 10-6 / °C
CTE = 78 * 10-6 / °C
axel
physical testing services
Thermal Expansion
Temperature (°C)
0.03
0.02
0.01
0.00
-0.01
-0.02
-100
-50
0
50
100
150

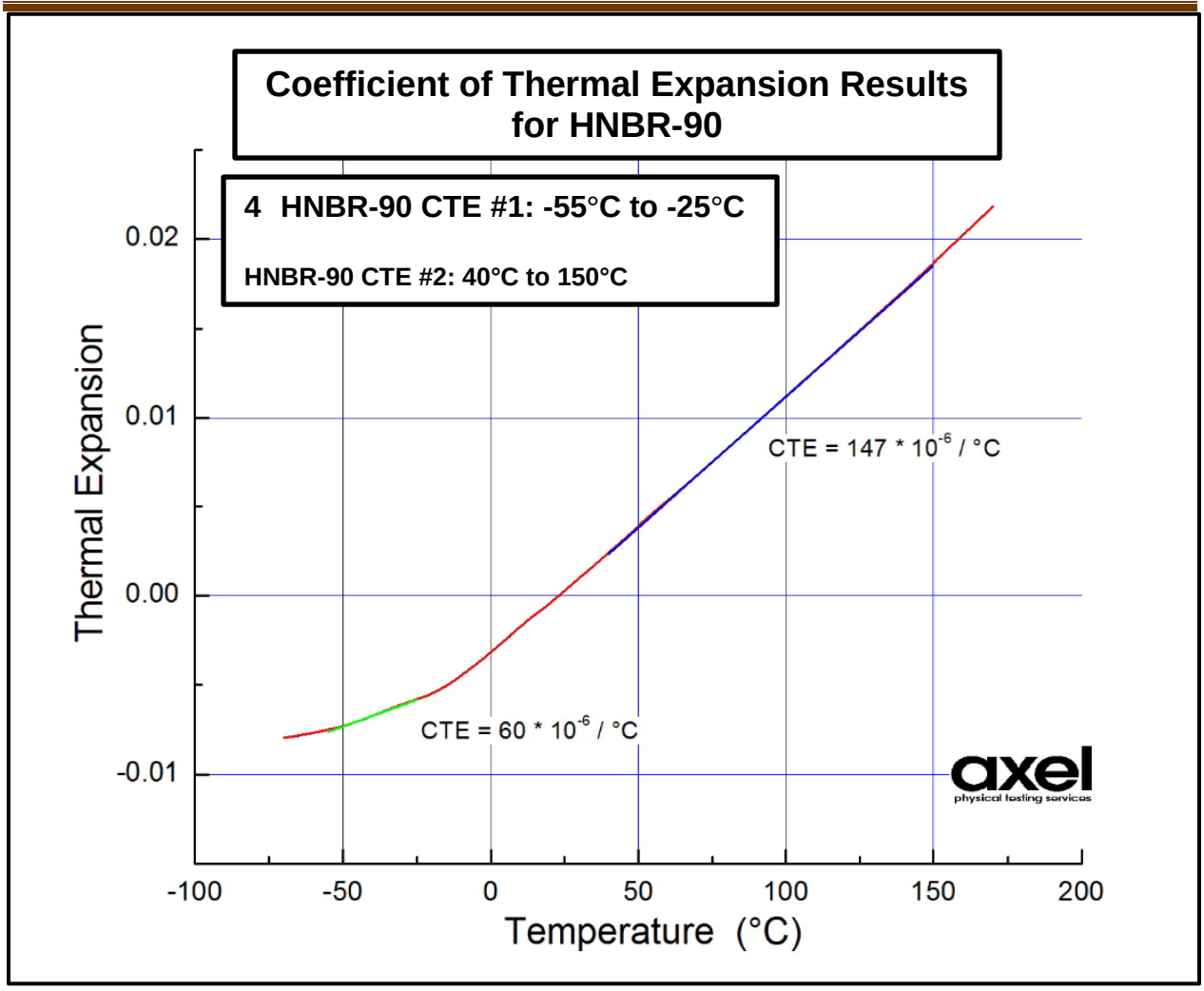
Coefficient of Thermal Expansion Results for HNBR-90
4 HNBR-90 CTE #1: -55°C to -25°C
HNBR-90 CTE #2: 40°C to 150°C
Thermal Expansion
0.02
0.01
0.00
-0.01
CTE = 147 * 10-6 / °C
CTE = 60 * 10-6 / °C
axel
physical testing services
-100
-50
0
50
100
150
200
Temperature (°C)

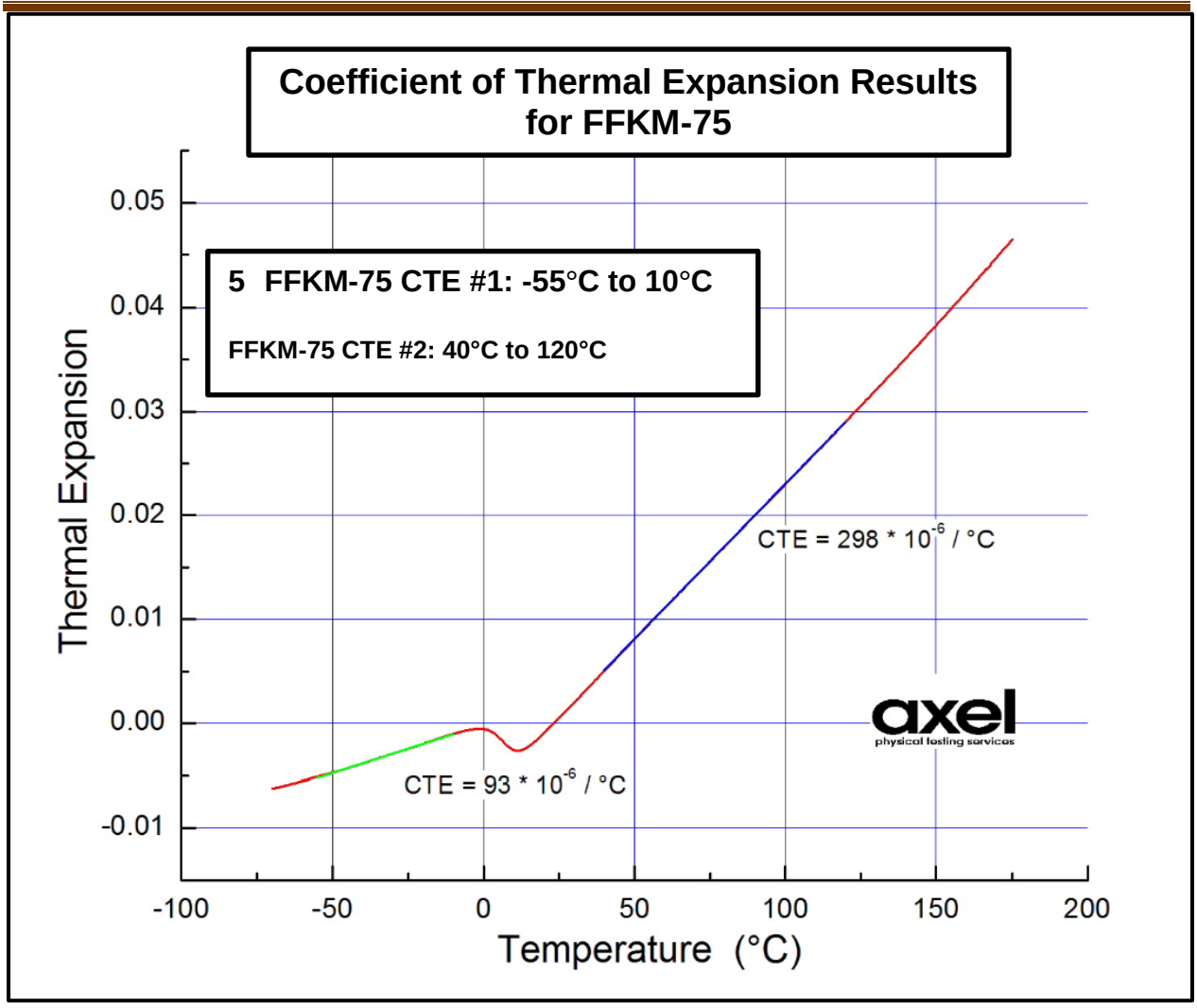
Coefficient of Thermal Expansion Results for FFKM-75
5 FFKM-75 CTE #1: -55°C to 10°C
FFKM-75 CTE #2: 40°C to 120°C
CTE = 298 * 10-6 / °C
CTE = 93 * 10-6 / °C
axel
physical testing services
Thermal Expansion
Temperature (°C)
0.05
0.04
0.03
0.02
0.01
0.00
-0.01
-100
-50
0
50
100
150
200

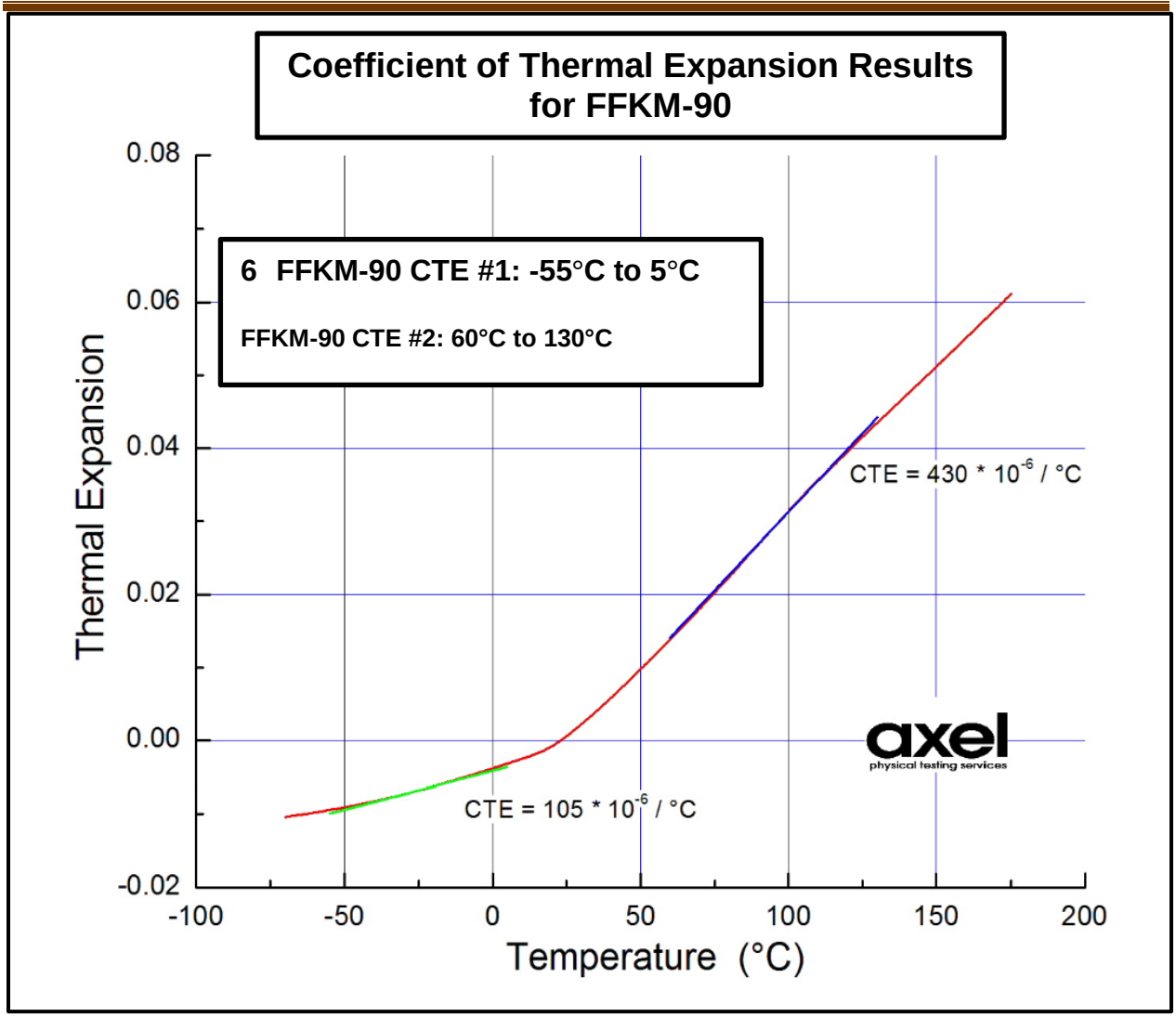
Coefficient of Thermal Expansion Results for FFKM-90
6 FFKM-90 CTE #1: -55°C to 5°C
FFKM-90 CTE #2: 60°C to 130°C
CTE = 430 * 10-6 / °C
CTE = 105 * 10-6 / °C
axel
physical testing services
Thermal Expansion
Temperature (°C)
0.08
0.06
0.04
0.02
0.00
-0.02
-100
-50
0
50
100
150
200

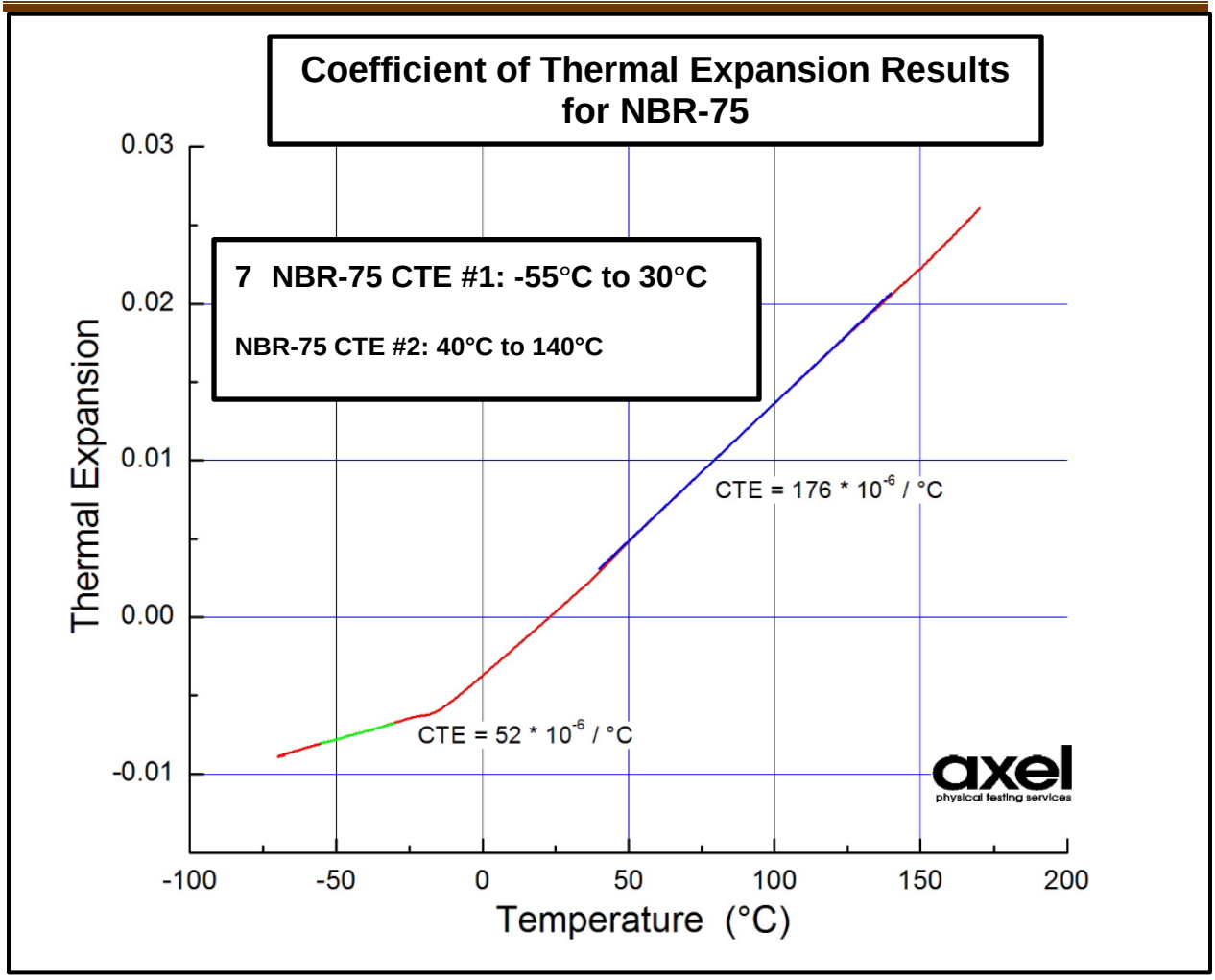
Coefficient of Thermal Expansion Results for NBR-75
7 NBR-75 CTE #1: -55°C to 30°C
NBR-75 CTE #2: 40°C to 140°C
CTE = 176 * 10-6 / °C
CTE = 52 * 10-6 / °C
axel
physical testing services
Thermal Expansion
0.03
0.02
0.01
0.00
-0.01
-100
-50
0
50
100
150
200
Temperature (°C)

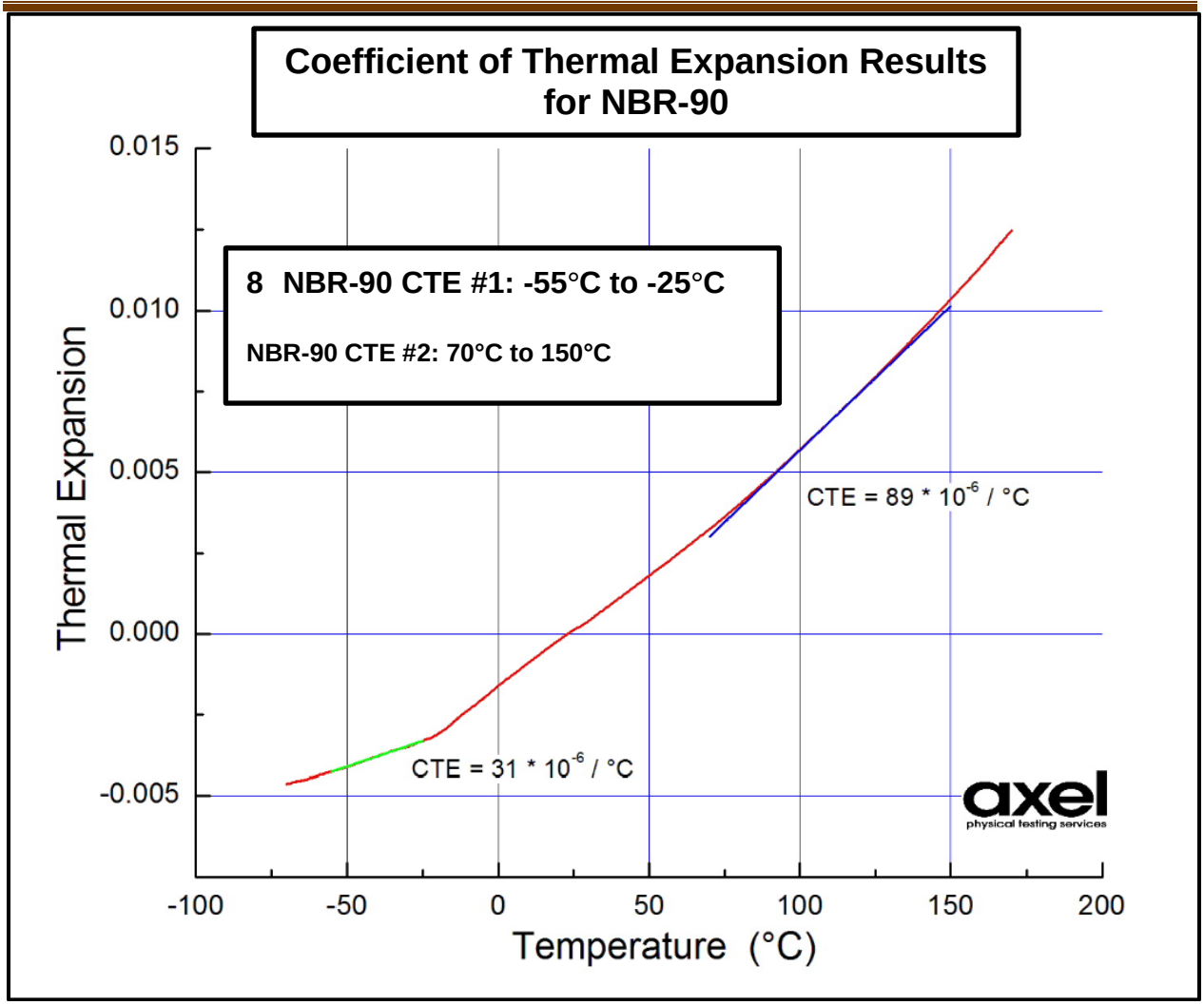
Coefficient of Thermal Expansion Results for NBR-90
8 NBR-90 CTE #1: -55°C to -25°C
NBR-90 CTE #2: 70°C to 150°C
CTE = 89 * 10-6 / °C
CTE = 31 * 10-6 / °C
axel
physical testing services
Thermal Expansion
0.015
0.010
0.005
0.000
-0.005
-100
-50
0
50
100
150
200
Temperature (°C)

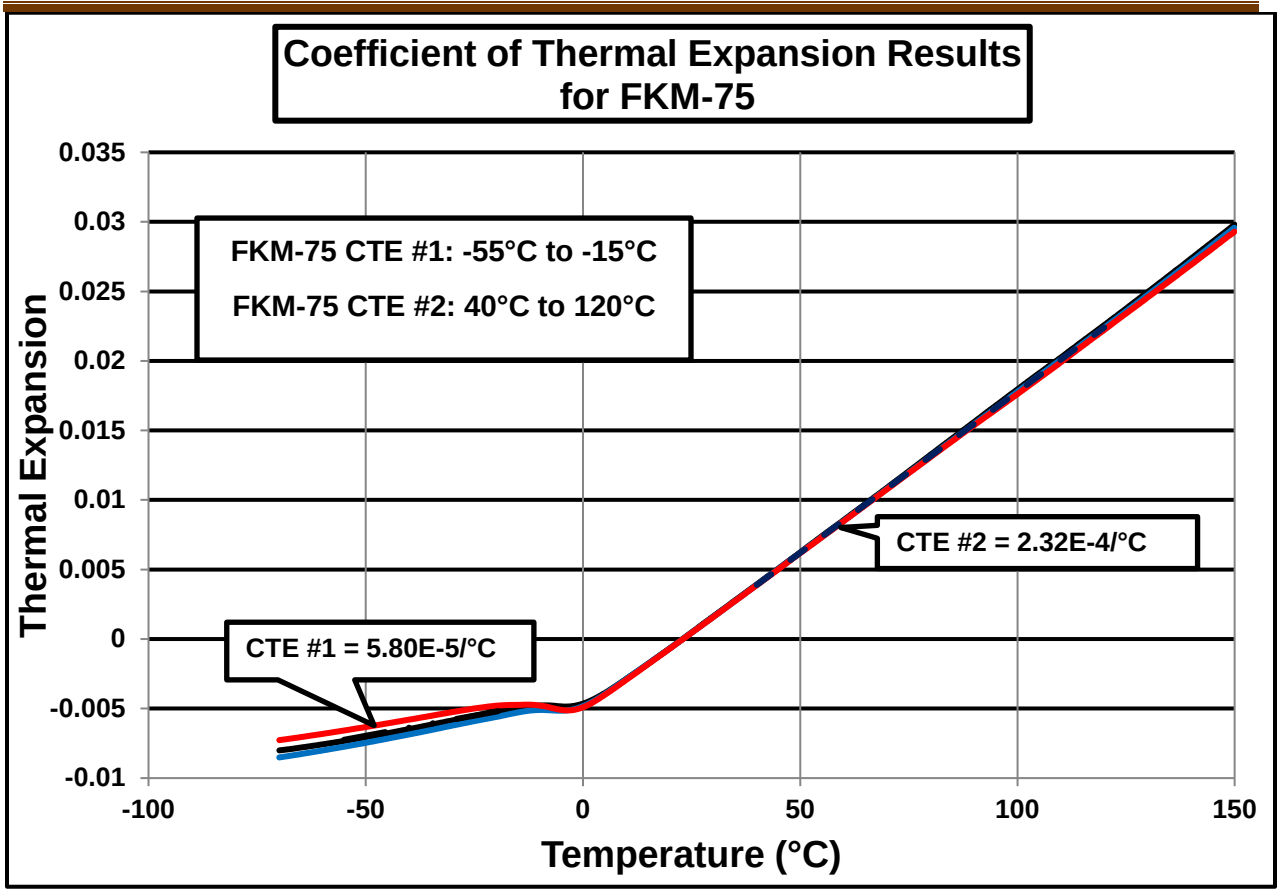


Figure A.4-18. Thermal expansion fit and observations of three replicates

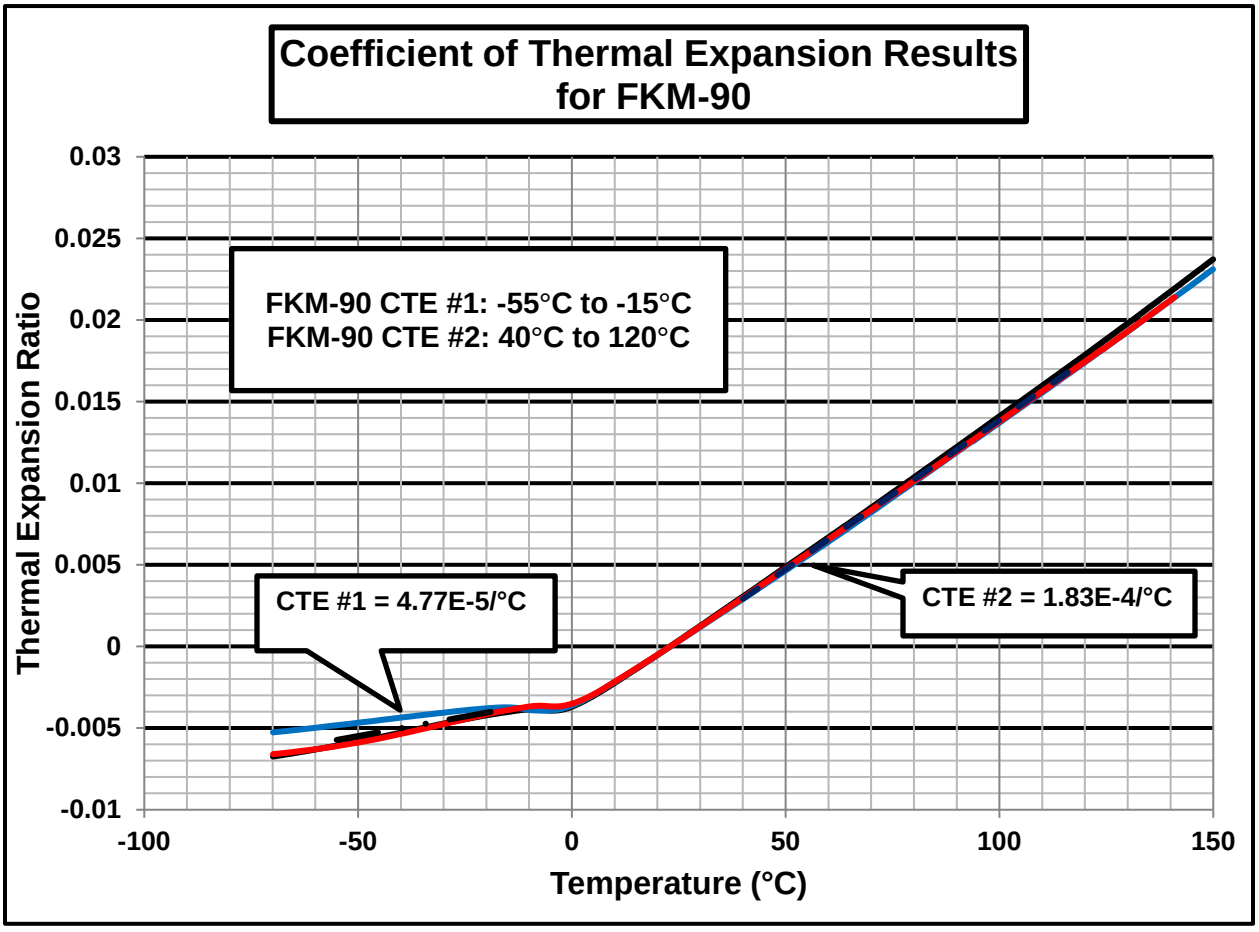
Coefficient of Thermal Expansion Results for FKM-90
FKM-90 CTE #1: -55°C to -15°C
FKM-90 CTE #2: 40°C to 120°C
CTE #1 = 4.77E-5/°C
CTE #2 = 1.83E-4/°C
Thermal Expansion Ratio
0.03
0.025
0.02
0.015
0.01
0.005
0
-0.005
-0.01
-100
-50
0
50
100
150
Temperature (°C)

Table A.4-13. Coefficient of Thermal Expansion.

| Material | Coefficient of Thermal Expansion -55°C to -15°C ($10^{-6}$ / °C) | Coefficient of Thermal Expansion 40°C to 120°C ($10^{-6}$ / °C) |
|---|---|---|
| FEPM-80 | 70 | 244 |
| FEPM-90 | 52 | 203 |
| HNBR-75 | 78 | 201 |
| HNBR-90 | 60 | 147 |
| FFKM-75 | 93 | 298 |
| FFKM-90 | 105 | 430 |
| NBR-75 | 52 | 176 |
| NBR-90 | 31 | 89 |
| FKM- 75 | 62 | 232 |
| FKM-90 | 54 | 185 |

# Appendix A.4-1. Raw Data File Contents.

*_PT_STE, *_ST_SL, *_SCL_*

Column: contents, units
A: Strain
B: Stress, MPa
C: Unused
D: time, sec
E: head displacement, mm

*_FCG

A: Cycles at the Current Strain Level. This is the number of cycles or pulses at the particular strain level.
B: Maximum Strain. This is the measured maximum engineering strain.
C: Minimum Strain. This is the measured minimum engineering strain.
D: Set at Zero Strain. This is the engineering strain occurring when the stress reaches zero on the unloading stroke.
E: Maximum Stress in MPa. This is the measured maximum engineering stress.
F: Minimum Stress in MPa. This is the measured minimum engineering stress.
G: Loading Tearing Energy in J/m2. This is the tearing energy calculated using the area under the loading stress strain curve.
H: Unloading Tearing Energy in J/m2. This is the tearing energy calculated using the area under the unloading stress strain curve.
I: Dissipative Tearing Energy in J/m2. This is the tearing energy calculated using the area inside the loading and unloading stress strain curve.
J: Air temperature in °C. Ambient temperature in the test chamber.
K: Specimen temperature in °C. Specimen surface temperature measured via infrared sensor.
L: Strain work density on loading stroke in mJ/mm3.
M: Strain work density on unloading stroke in mJ/mm3.
N: Hysteresis per cycle in mJ/mm3.
O: Recoverable strain work density (strain energy density) remaining in material at minimum strain in mJ/mm3.
P: Crack Width in mm. This is the total linear length of the crack only in the direction perpendicular to loading from the edge of the specimen.
Q: Specimen Height in mm. This is the height of the specimen.
R: Specimen Width in mm. This is the uncracked width of the specimen.
S: Specimen Thickness in mm. This is the thickness of the specimen.

*_CCG

A: Time in minutes. Total time since test started.
B: Strain. This is the measured engineering strain.
C: Stress in MPa. This is the measured engineering stress.

D: Crack Width in mm. This is the total linear length of the crack only in the direction perpendicular to loading from the edge of the specimen.
E: Specimen Width in mm. This is the uncracked width of the specimen.
F: Specimen Thickness in mm. This is the thickness of the specimen.
G: Specimen Height in mm. This is the height of the specimen.
H: Initial Crack in mm. This is the length of the initial crack precut in the specimen

*_R_Contours

i. Image 1
    1. Trigger line "-1,-1"
    2. Cycle Number, Fraction of peak strain used for imaging
    3. X, Y pairs…
ii. Image 2
    1. Trigger line "-1,-1"
    2. Cycle Number, Fraction of peak strain used for imaging
    3. X, Y pairs…
iii. …
iv. Image N

*_MechFatigue*

A: Engineering Strain
B: Cycles to failure

*_PT_CF_*

Column: contents, units
A: Time, sec
B: Stress, MPa
C: strain
D: head displacement, mm
E: cutting force, mN

# Appendix A.4-2. Useful Unit Conversions

The following table provides 3 typical consistent unit systems useful for analysis, along with conversion factors between SI and English units.

| Quantity | SI Units (m) | SI Units (mm) | English Units | Conversion Factor 1 SI (m) = X English |
|---|---|---|---|---|
| Temperature | ° C | ° C | ° F | 1.8 °F |
| Crack Driving Force (Tear Energy, Energy Release Rate) | $J/m^2$ | $kJ/m^2$ | $inlbf / in^2$ | $5.710 \times 10^{-3}$ $inlbf / in^2$ |
| R ratio | Unitless | Unitless | Unitless | |
| Flaw size, crack length, specimen dimensions | m | mm | in | 39.37 in |
| Modulus, Stress | Pa | MPa | $lbf / in^2$ | $1.450 \times 10^{-4}$ $lbf / in^2$ |
| Hysteresis, Strain energy density | $J/m^3$ | $mJ/mm^3$ | $inlbf / in^3$ | $1.450 \times 10^{-4}$ $inlbf / in^3$ |
| Mullins r, beta | Unitless | Unitless | Unitless | |
| Mullins m | Pa | MPa | $lbf / in^2$ | $1.450 \times 10^{-4}$ $lbf / in^2$ |
| Temperature Coefficient | 1 / °C | 1 / °C | 1 / °F | 0.5556 |
| Fatigue crack growth rate | m/cyc | mm/cyc | in/cyc | 39.37 in/cyc |
| Time | s | s | s | |
| Strain, Stretch Ratio | Unitless | Unitless | Unitless | |

## A.5 Appendix 5 – Additional Material Testing Results

Dynamic Mechanical Analysis (DMA)

Shown in Figure A-5-1 is a summary of the percent change in storage modulus (stiffness) of the elastomers in this study as the temperature is raised from 50°C, to 90°C, to 120°C, to 160°C and finally to 175°C.

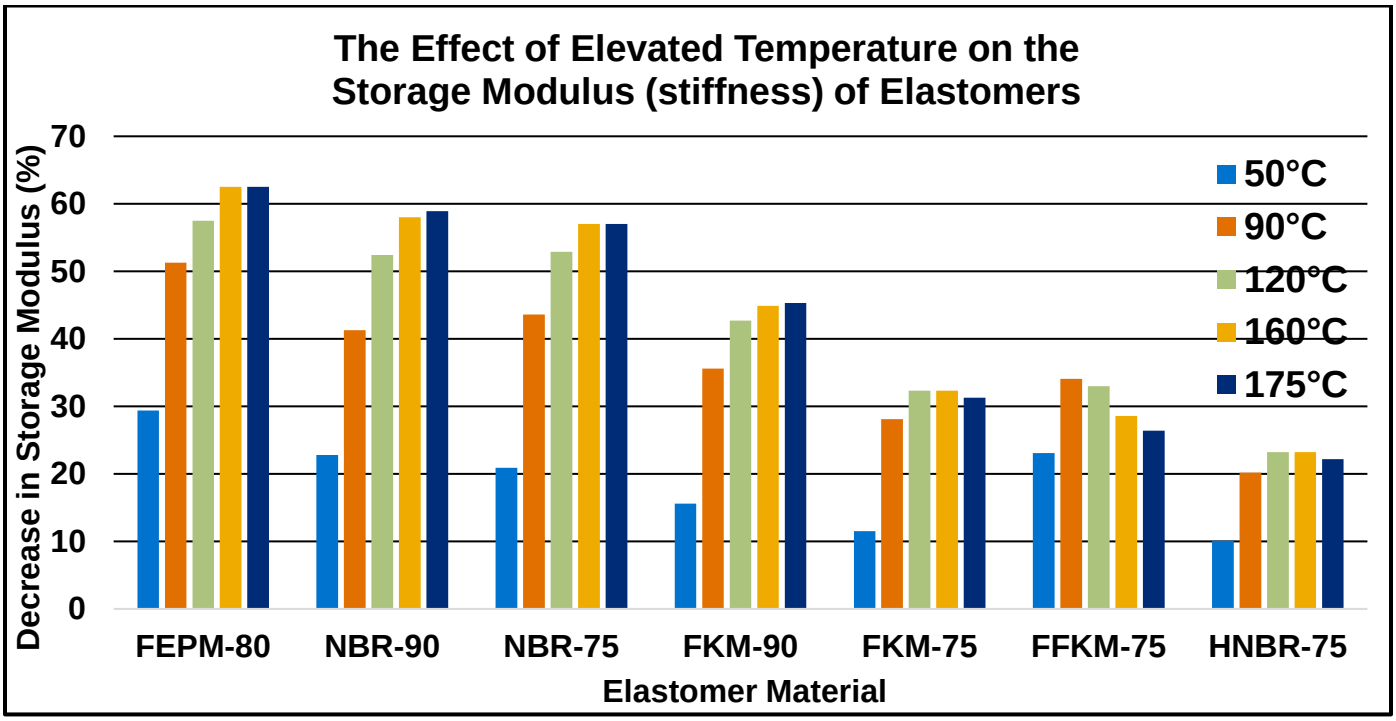


**Figure A.5-1. The Effect of Elevated Temperature on the Storage Modulus (stiffness) of Elastomers**

The results are ranked from left to right on the plot and show that FEPM had the greatest relative change and that HNBR had the lowest relative change. Plots of all the DMA test results are included in the following section of Appendix 5.

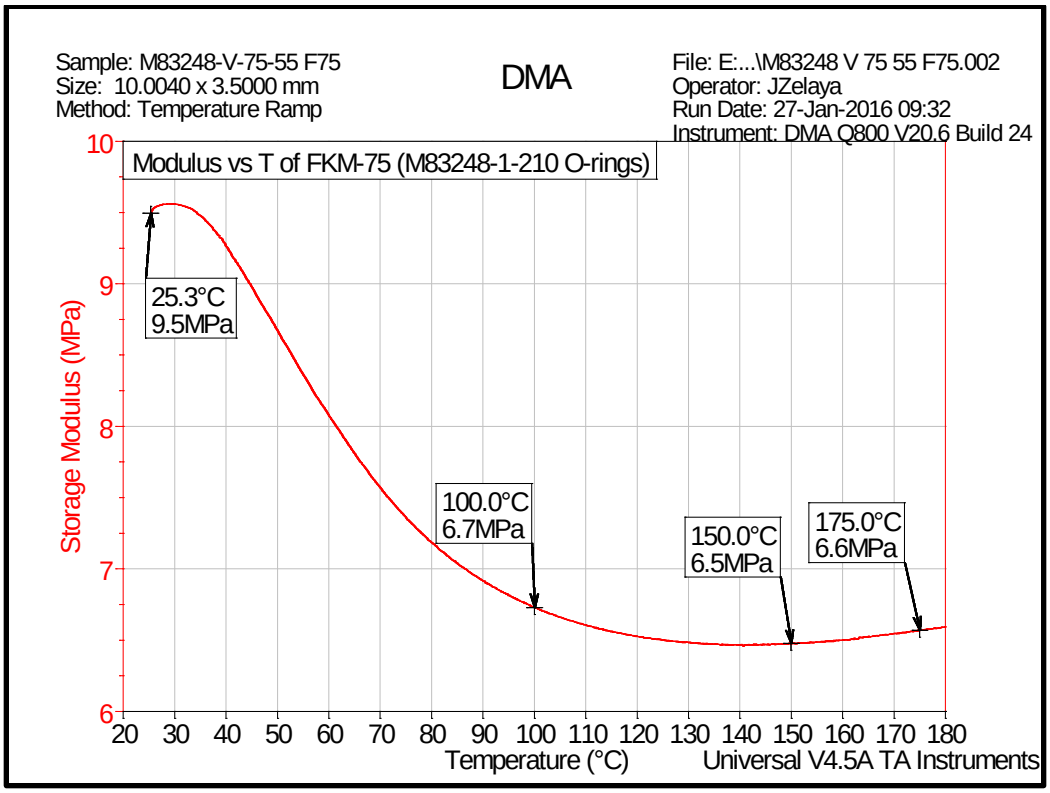


**Figure A.5-2. DMA of FKM-75 (M83248-1-210 O-ring).**

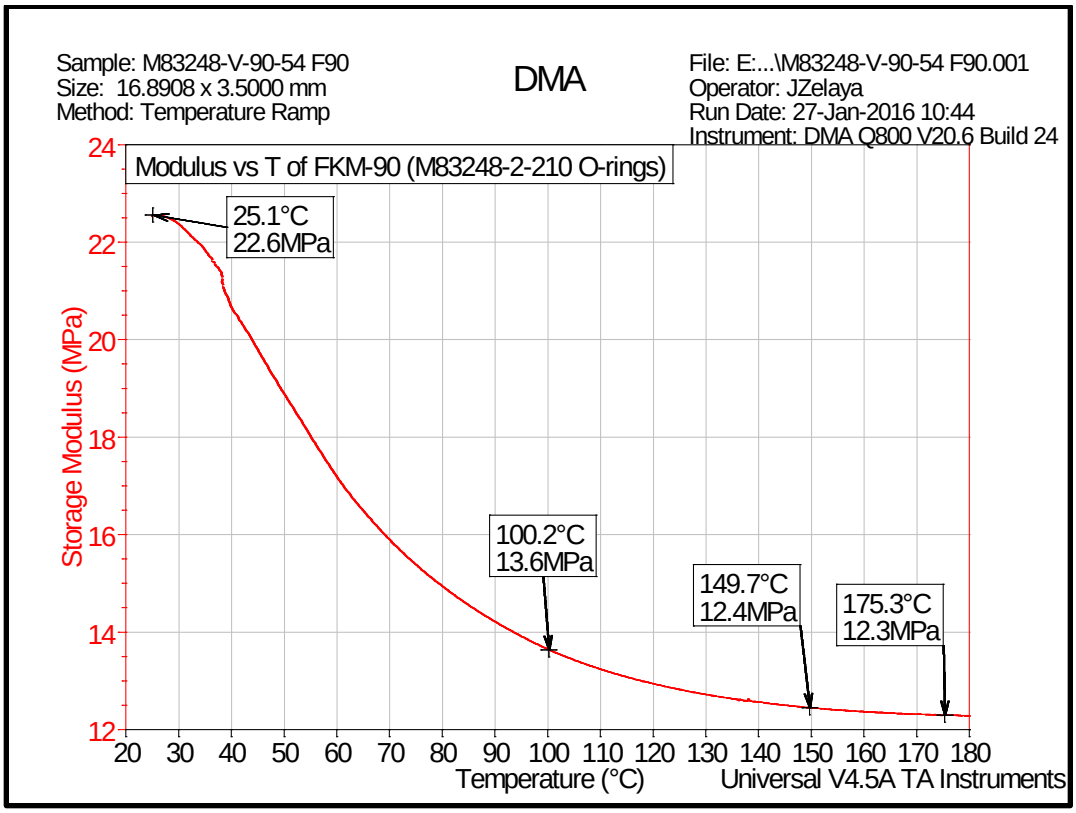


**Figure A.5-3. DMA of FKM-90 (M83248-2-210 O-ring).**

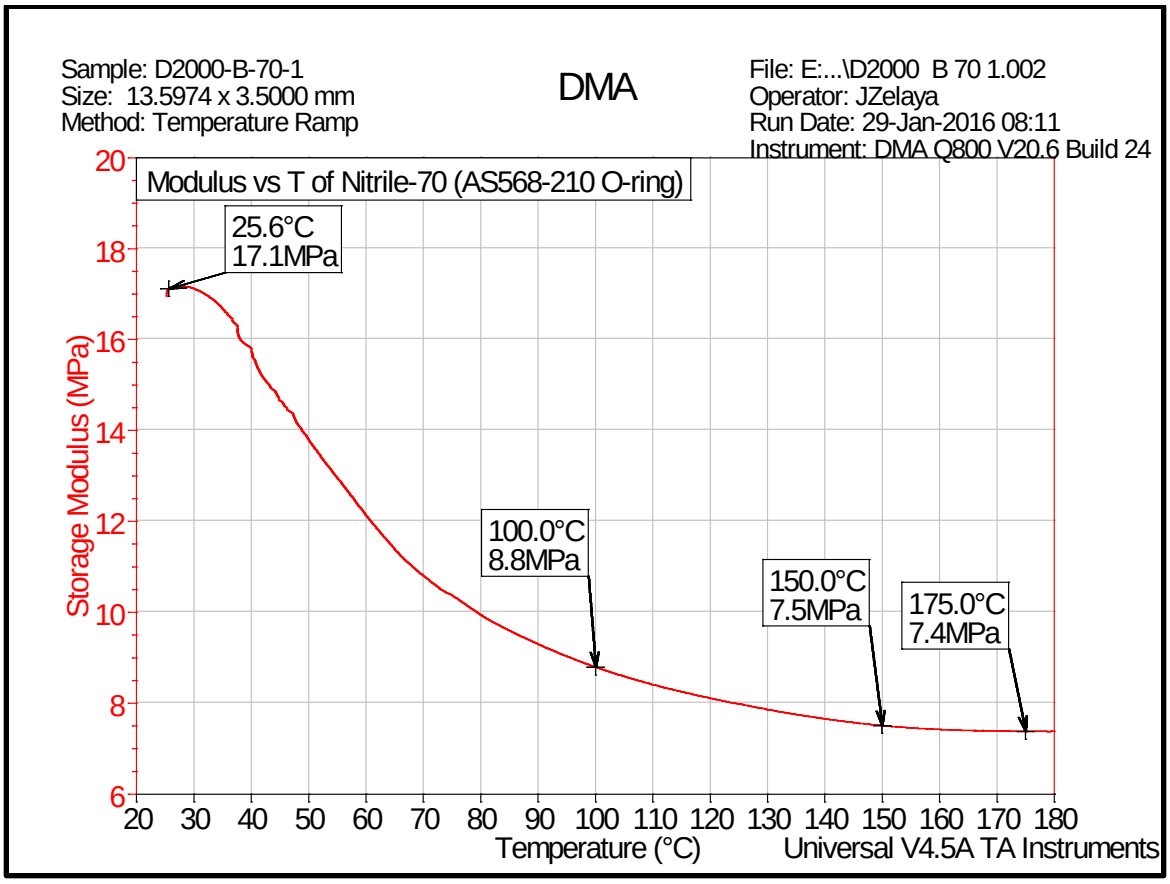


**Figure A.5-4. DMA of NBR-70 (AS568-210 O-ring).**

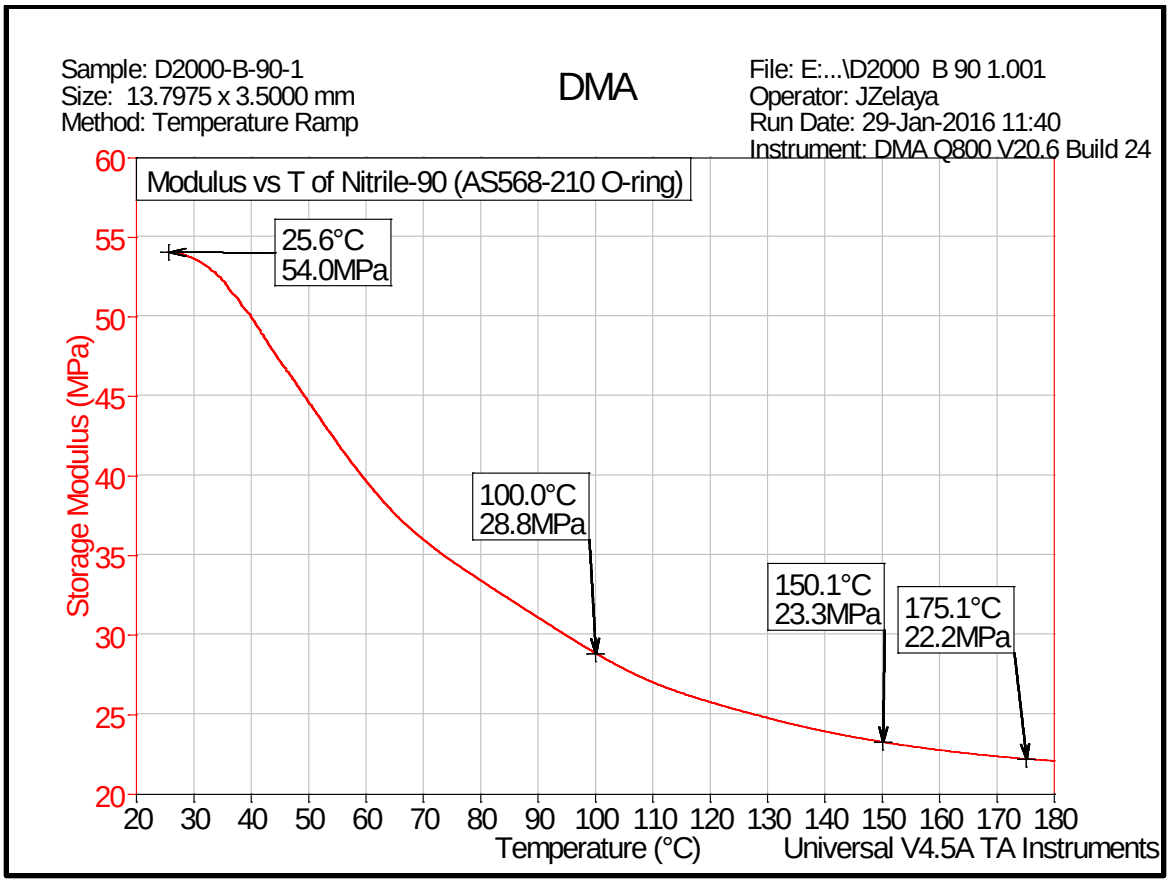


**Figure A.5-5. DMA of NBR-90 (AS568-210 O-ring).**

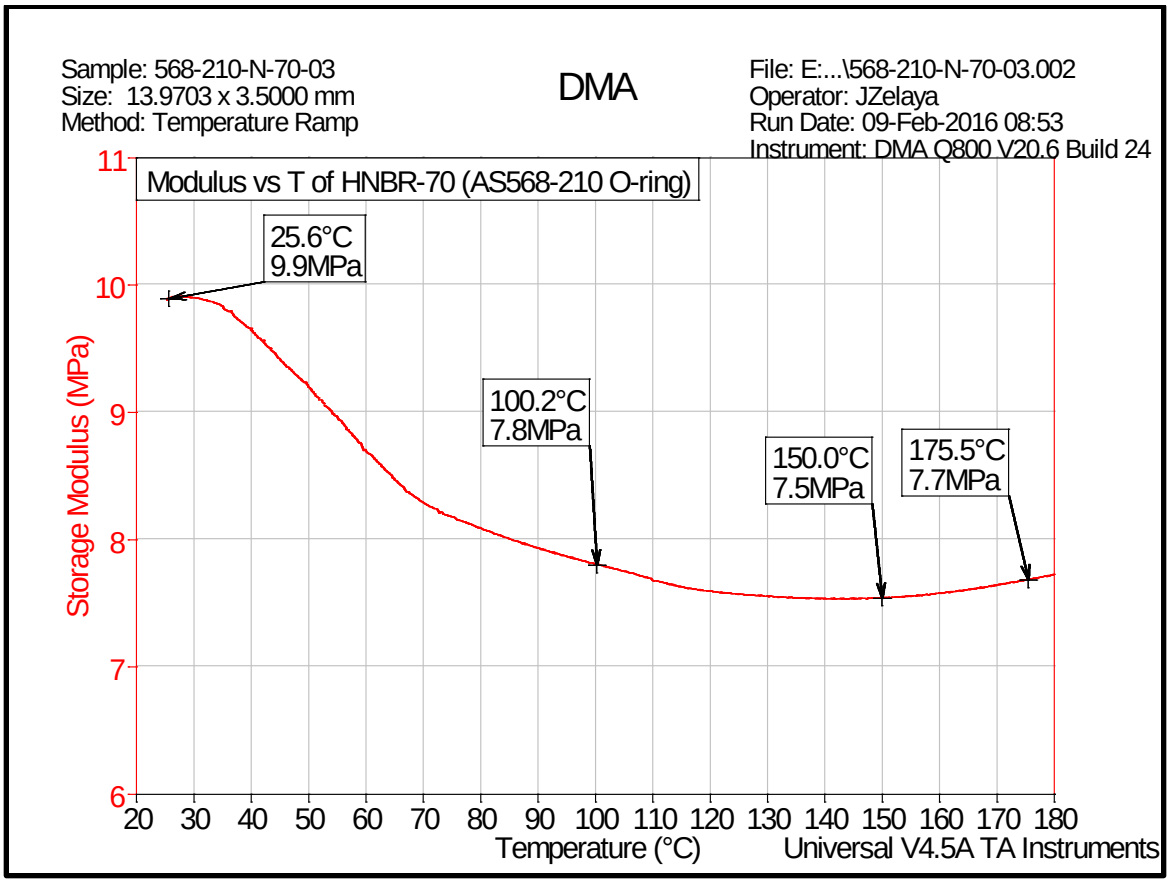


**Figure A.5-6. DMA of HNBR-70 (AS568-210 O-ring).**

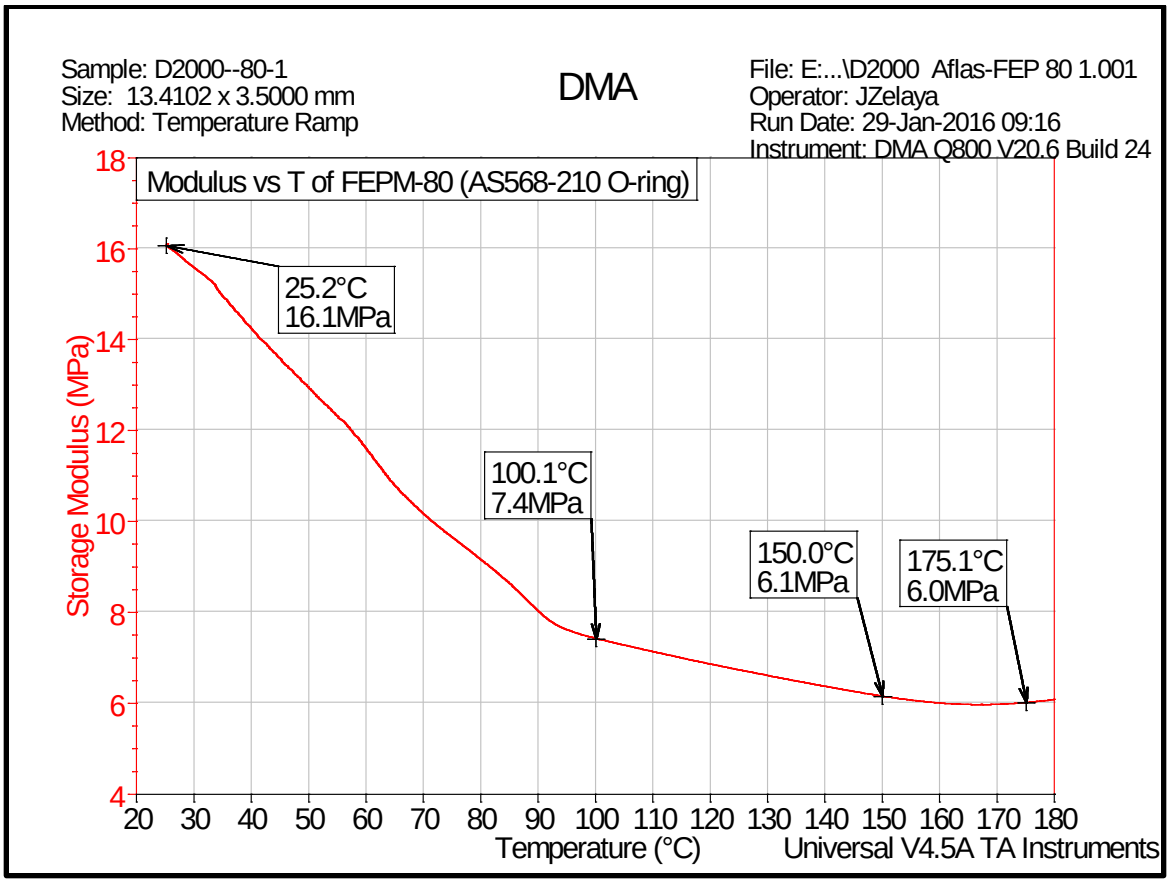


**Figure A.5-7. DMA of FEPM-80 (AS568-210 O-ring)**

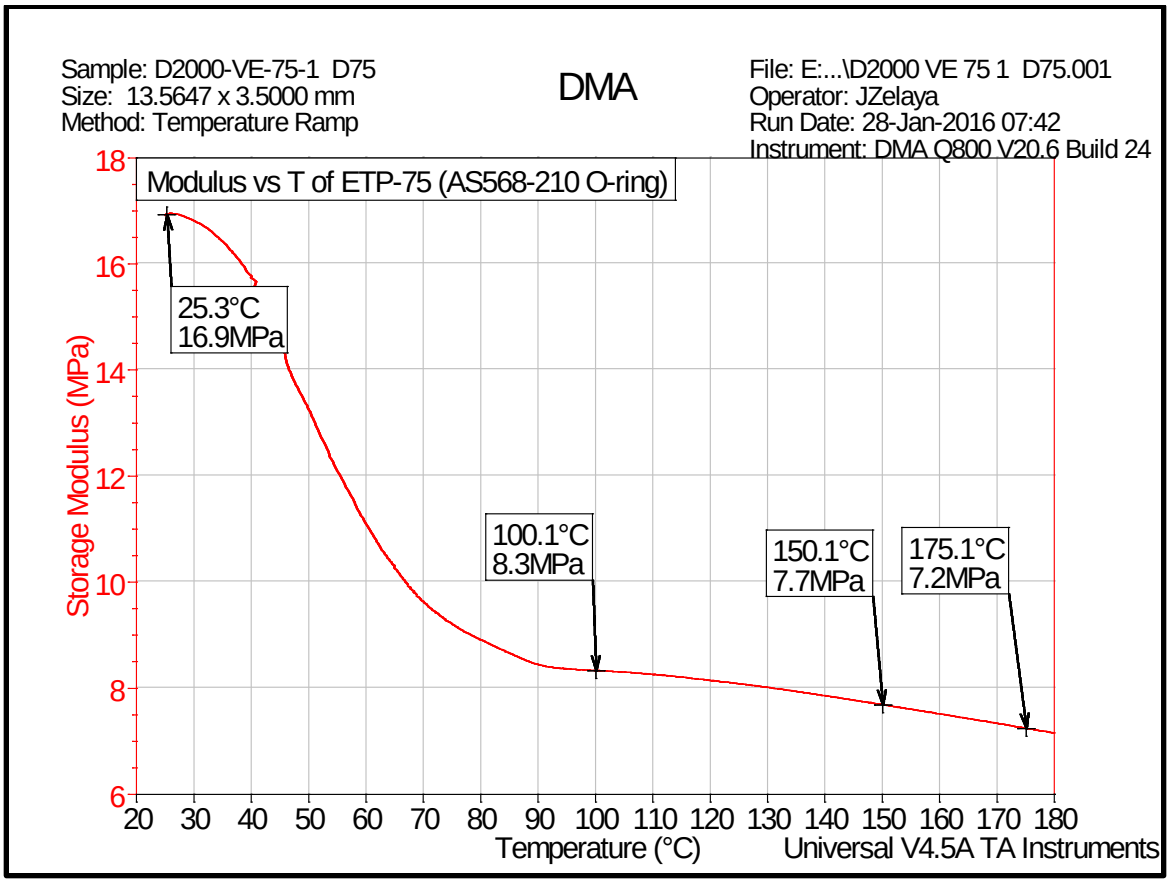


**Figure A.5-8. DMA of FEPM ETP-75 (AS568 -210 O-ring).**

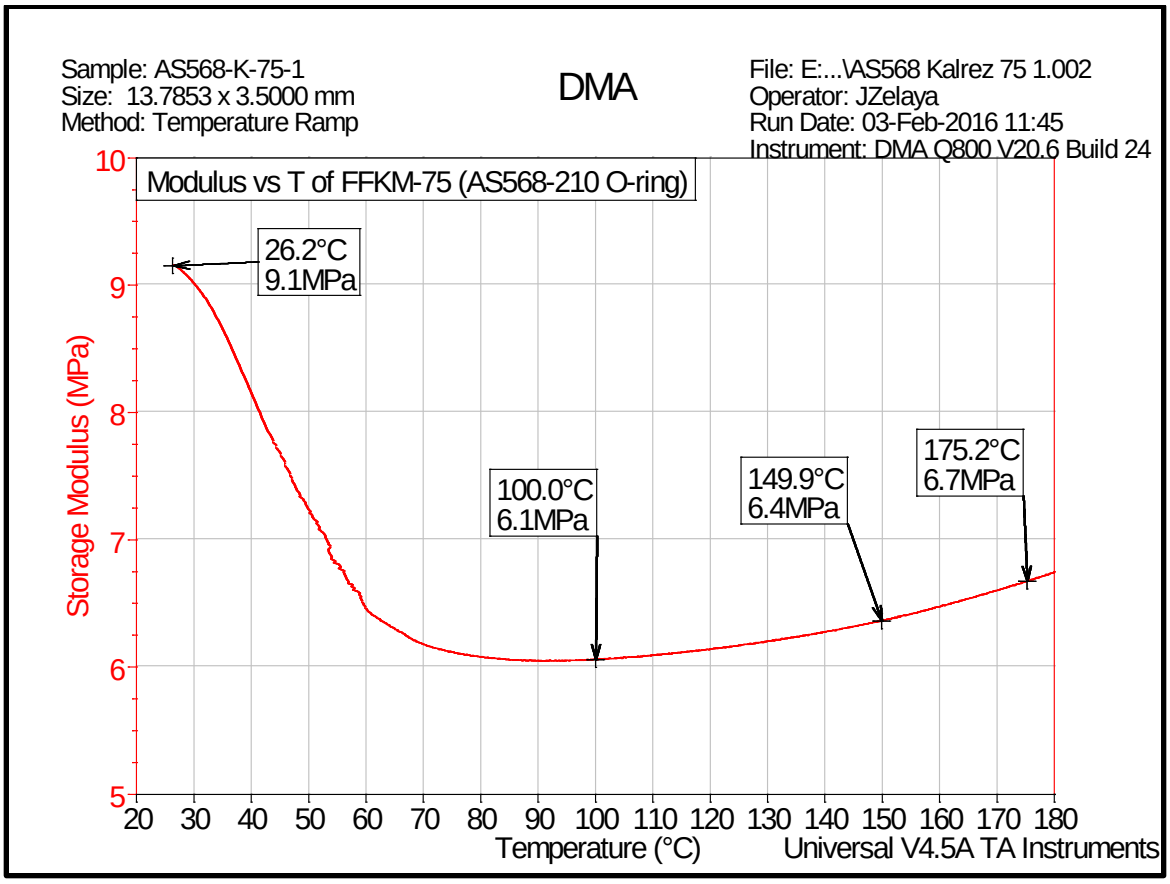


**Figure A.5-9. DMA of FFKM-75 AS568-210 O-ring.**

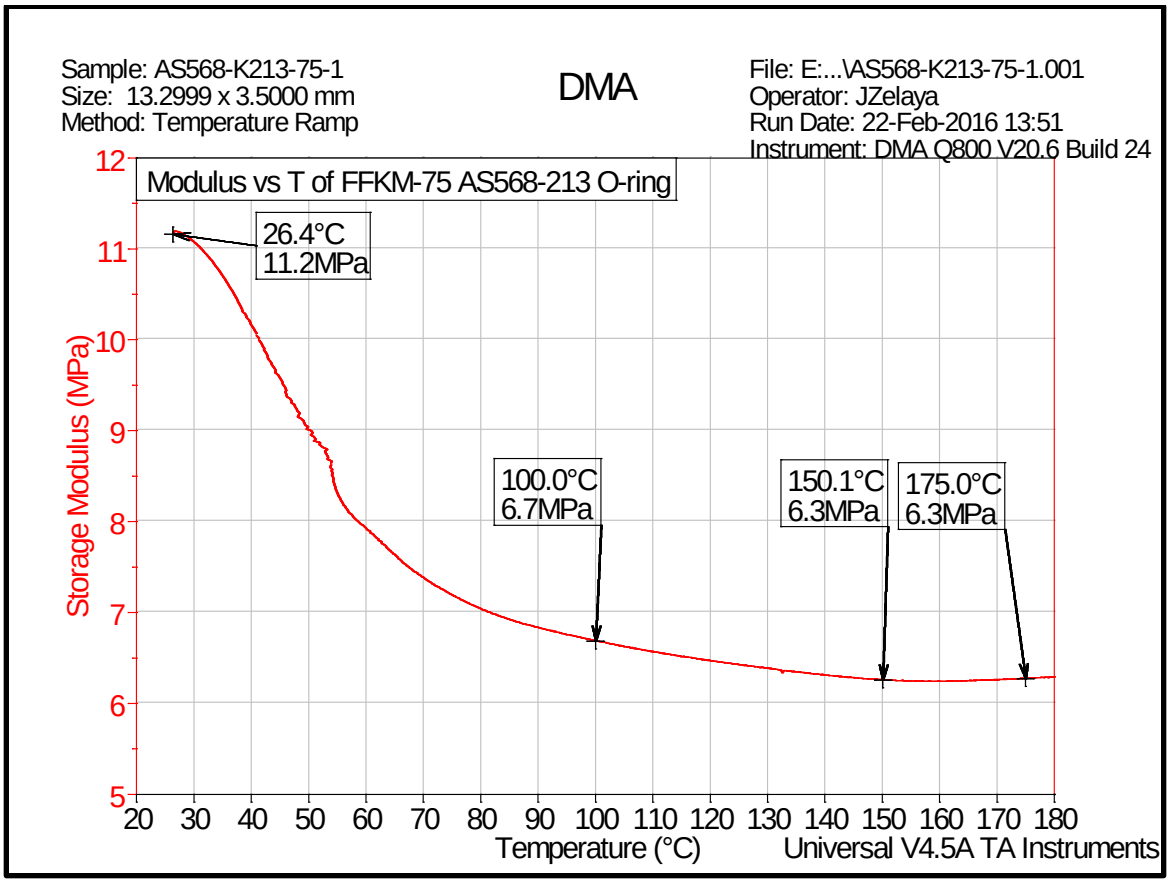


**Figure A.5-10. DMA of FFKM-75 (AS568-213 O-ring).**

Frequency Dependent DMA Plots

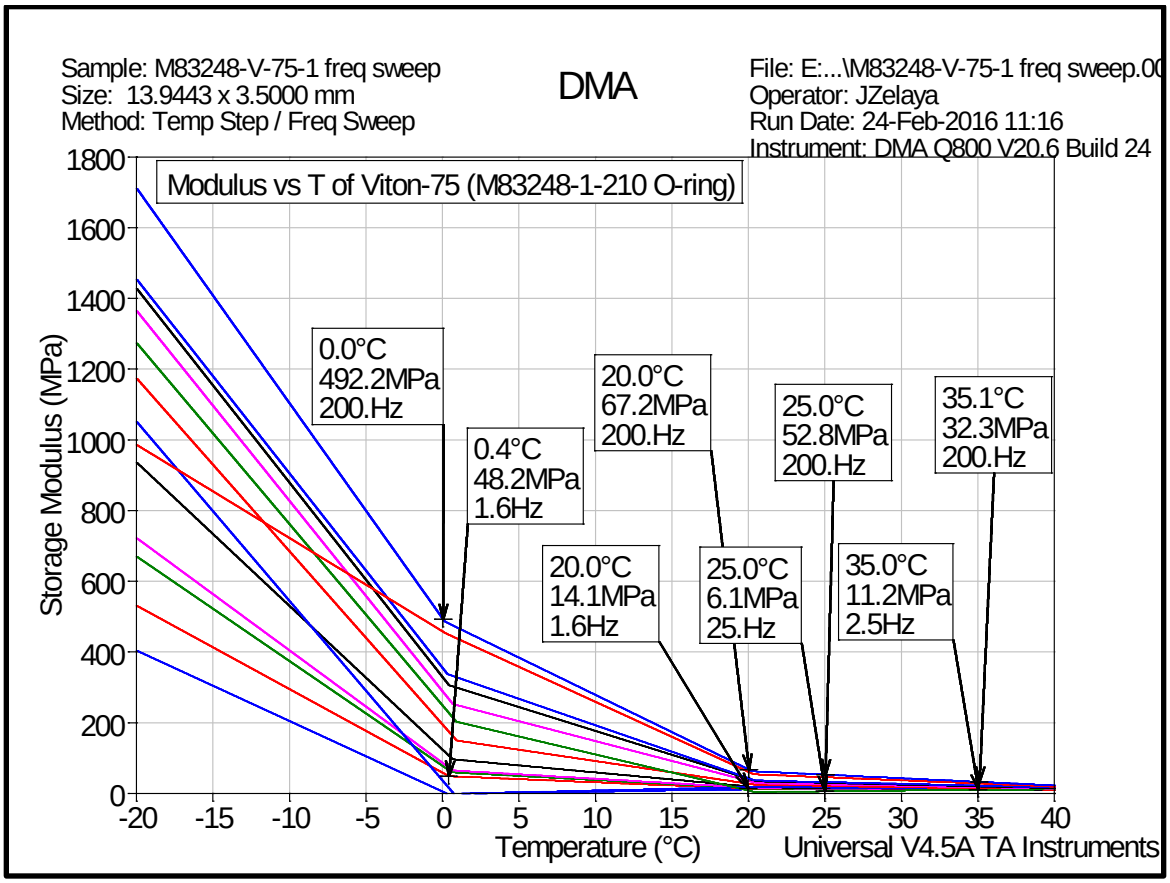


**Figure A.5-11. Frequency dependent DMA of FKM-75 (M83248-1-210) (-20ºC -40ºC).**

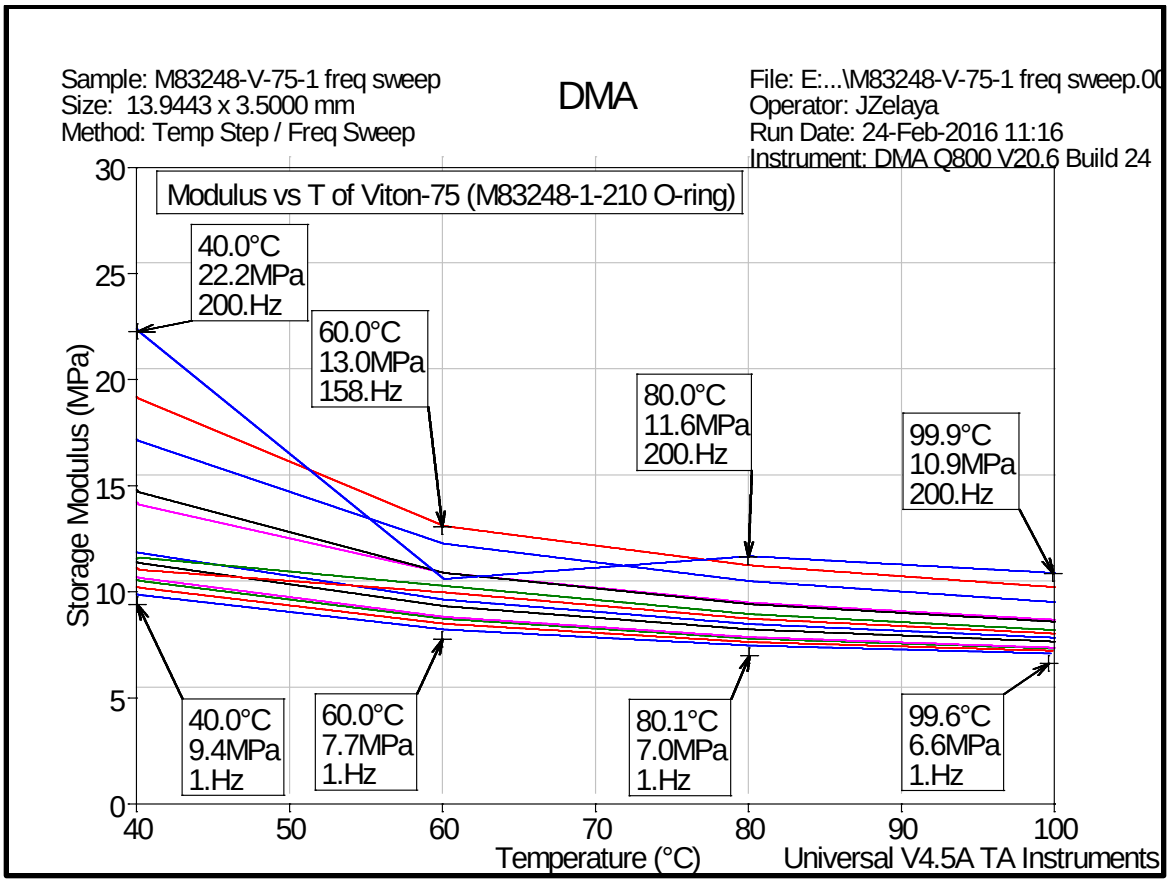


**Figure A.5-12. Frequency dependent (1 Hz-200 Hz) DMA for FKM-75 (M83248-1-210) 40 ºC- 100 ºC.**

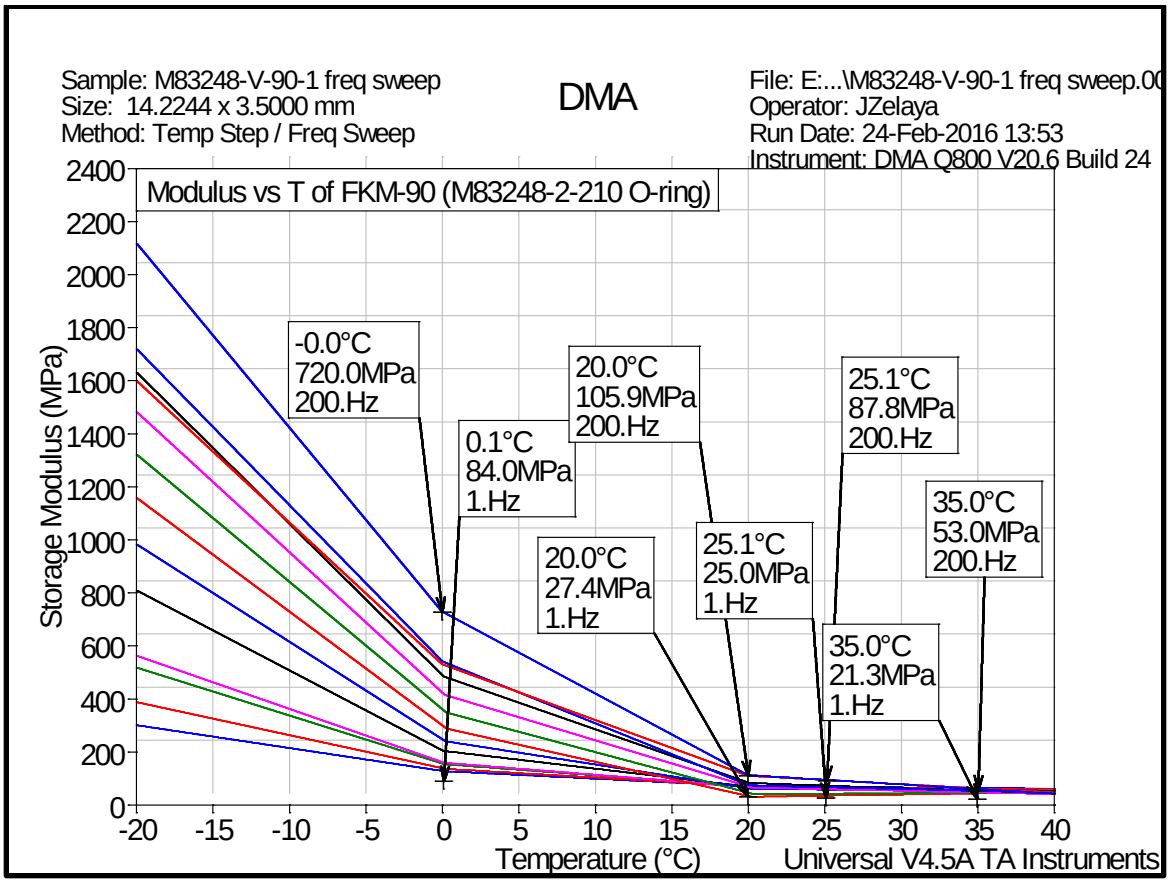


**Figure A.5-13. Frequency dependent DMA of FKM-90 (M83248-2-210) (-20ºC -40ºC).**

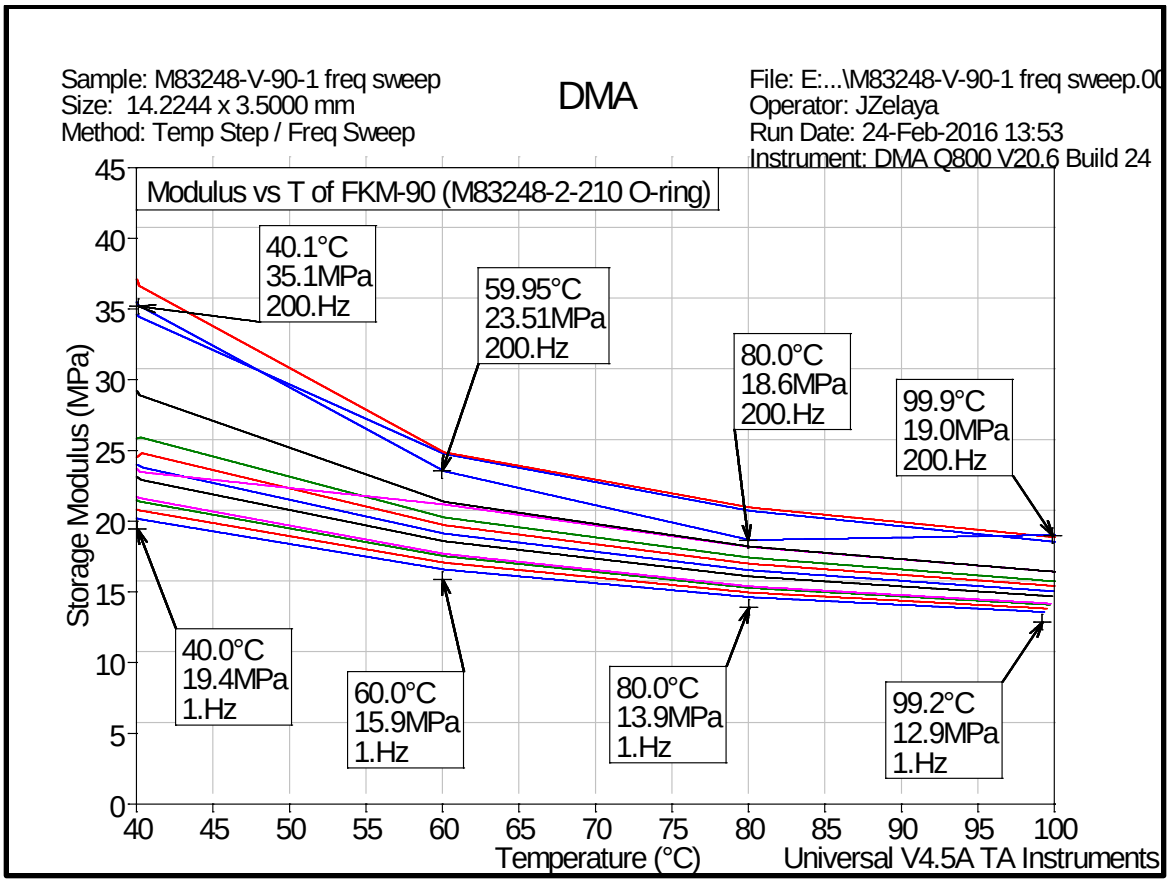


**Figure A.5-14. Frequency dependent DMA of FKM-90 (M83248-2-210) (40ºC -100ºC).**

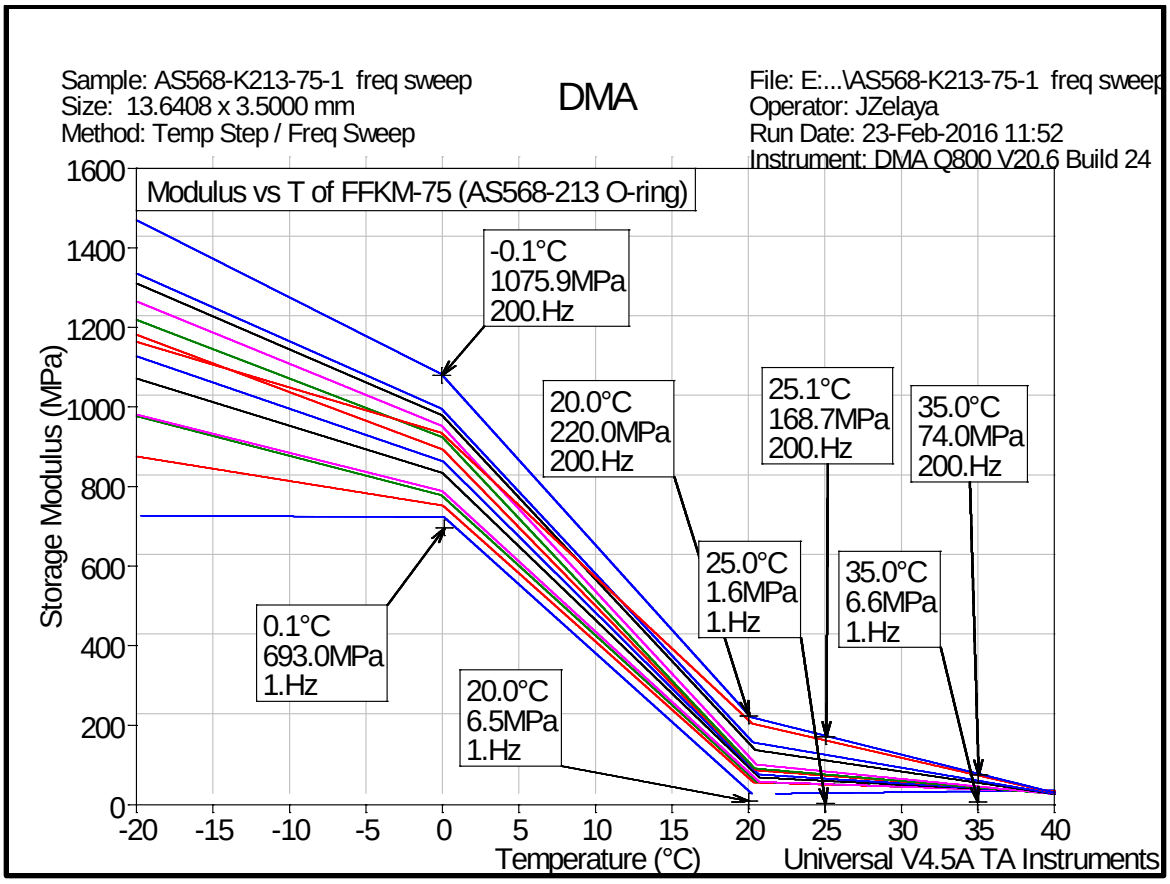


**Figure A.5-15. Frequency dependent (1 Hz - 200 Hz) DMA for FFKM-75 (AS568-213 O-ring) from -20 ºC to 40 ºC.**

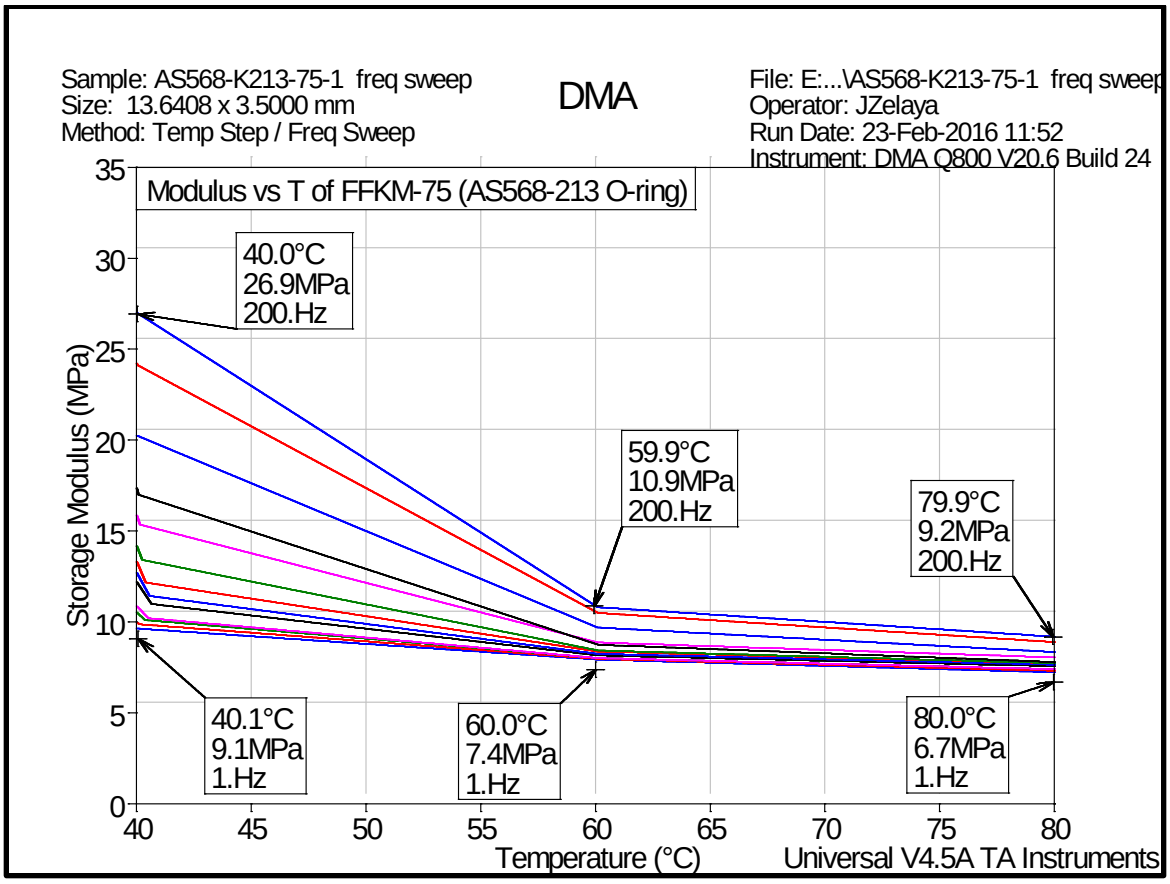


**Figure A.5-16. Frequency dependent (1 Hz - 200 Hz) DMA for FFKM-75 (AS568-213 O-ring) from 40 ºC to 80 ºC.**

Additional Membrane Inflation test results

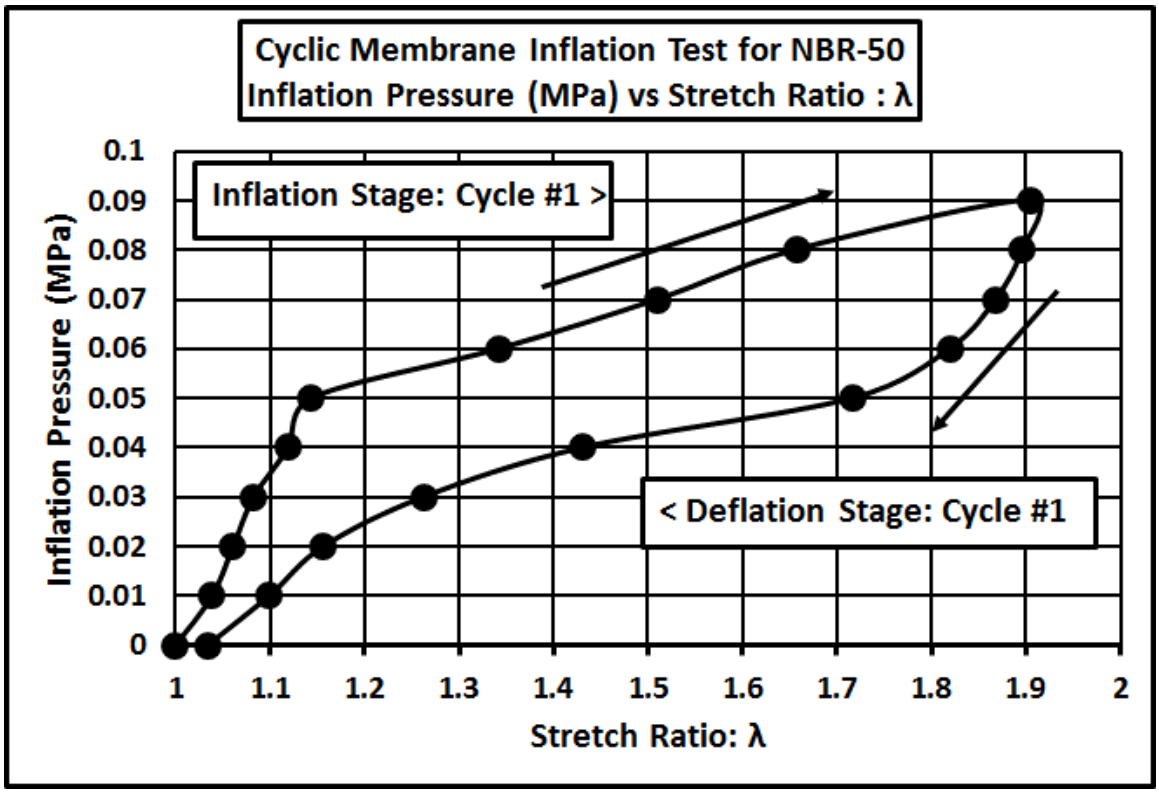


**Figure A.5-17. Cyclic membrane inflation test data for NBR-50 (hardness of 50).**

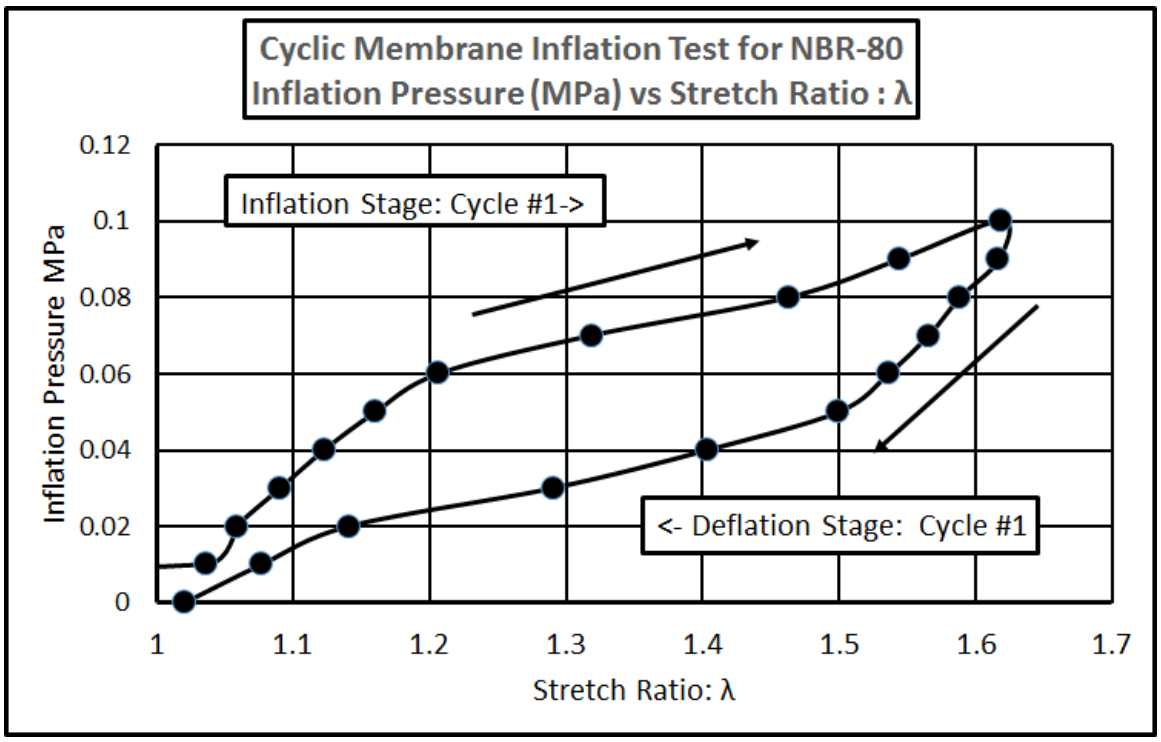


**Figure A.5-18. Cyclic membrane inflation test data for NRB-80 (80 Shore hardness).**

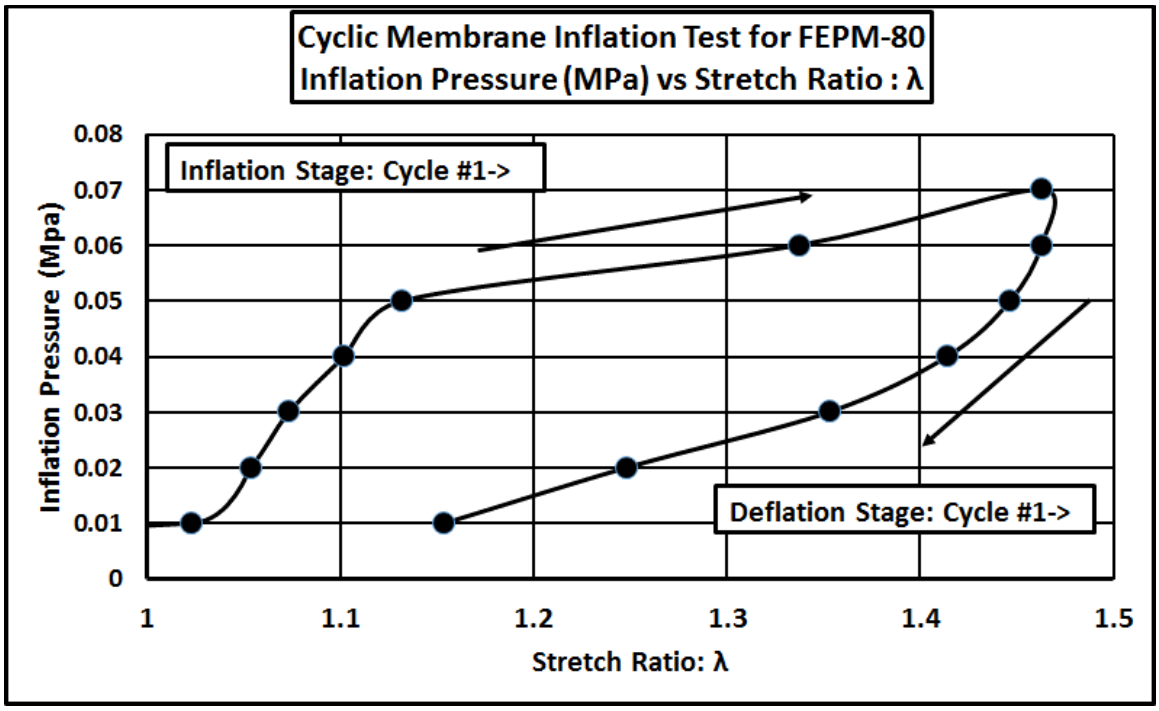


**Figure A.5-19. Cyclic membrane inflation test data for FEPM-80 (hardness of 80).**

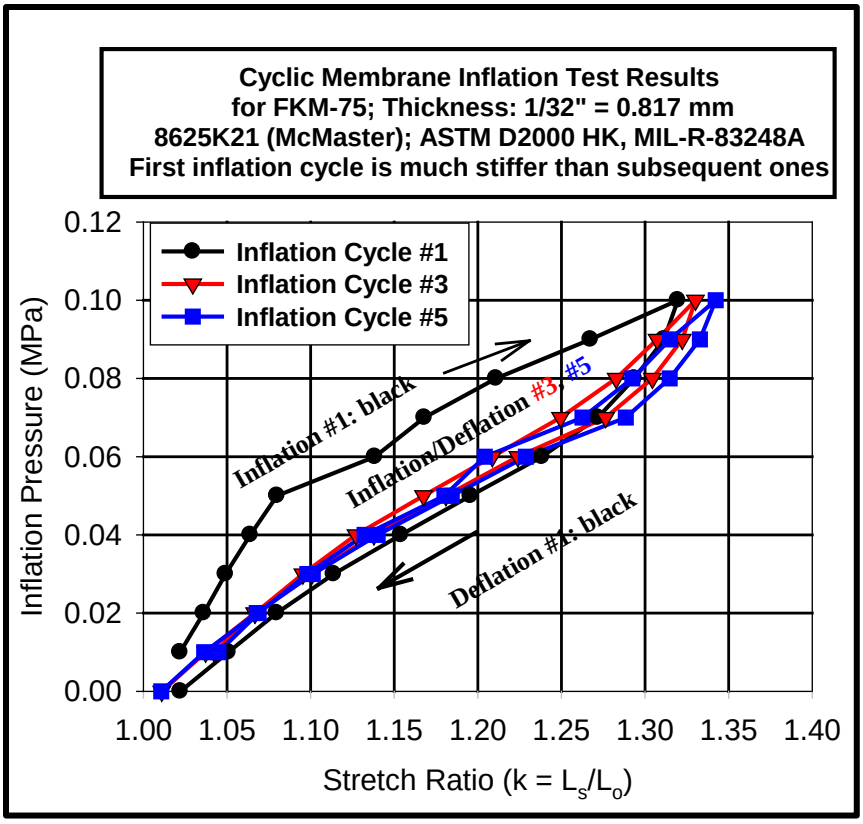


**Figure A.5-20a. Cyclic membrane inflation tests for FKM-75.**

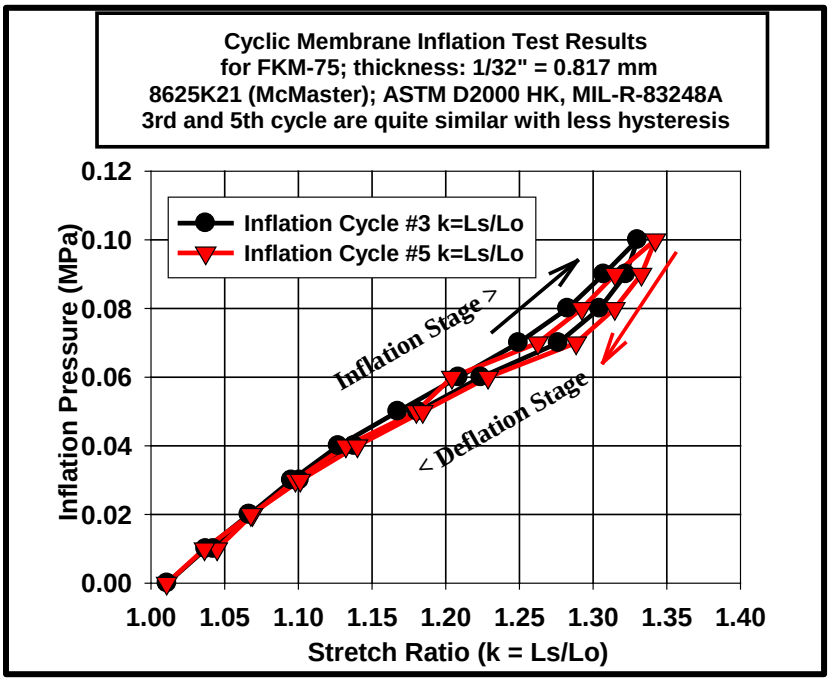


**Figure A.5-20b. Cyclic membrane inflation tests for FKM-75: third and fifth cycles.**

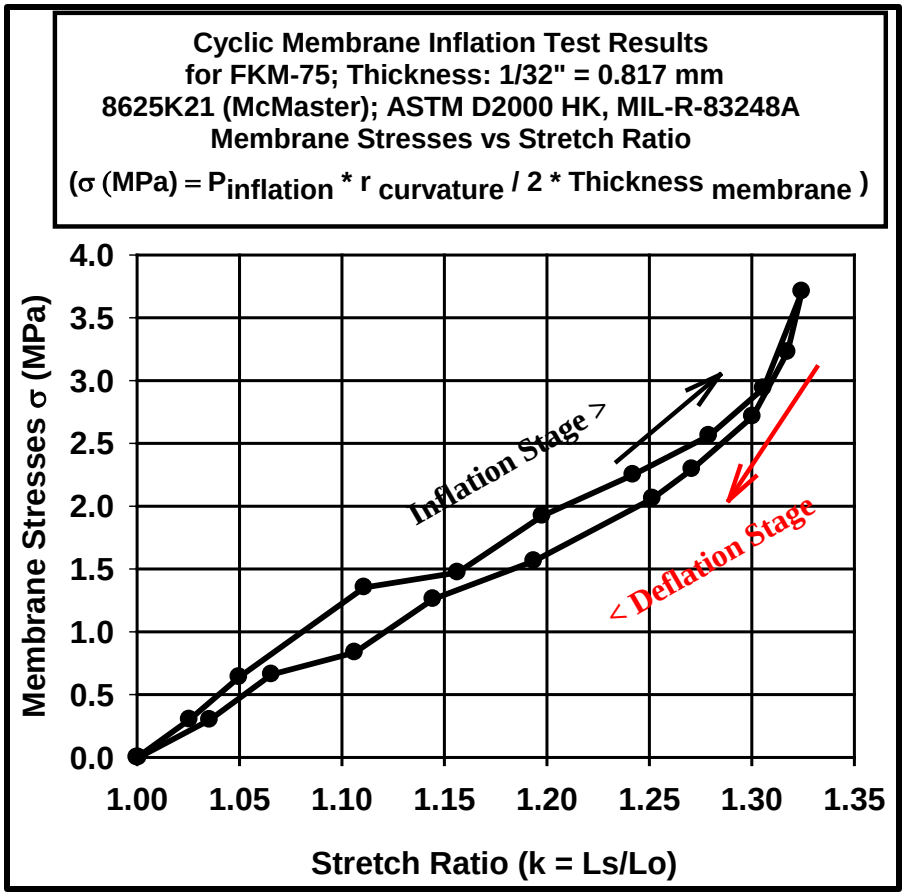


**Figure A.5-21. Membrane stresses calculated for FKM-75.**

| Mooney- Rivlin Constants (kPa) Complete Cycle #3 | |
|---|---|
| № | X |
| C1 | 231.348 |
| C2 | 503.945 |

**Figure A.5-22. Mooney-Rivlin constants calculated from membrane stress, radius of curvature, etc. (matrix solutions from http://matrix.reshish.com/matrixMethod.php).**

## A.6 Appendix 6 – HPHT Test Report (courtesy of PetroMar Technologies, Inc.)

Report

# HPHT O-ring Testing Results

**Purpose and Summary**: This report describes High-Pressure/High-Temperature (HPHT) testing performed with multiple arrays of AS568-210 O-rings extruded into clearance gaps ranging from 0.002” to 0.015”. The main purpose of the tests was to support Battelle’s HPHT elastomer research effort, in particular, the development of the Endurica’s Finite-Element model of elastomeric seals exposed to high pressure and temperature. Five different O-ring materials popular in the Oil & Gas industry have been tested per ASTM classification (ASTM D1418-17): NBR, HNBR, FEPM, FKM, and FFKM; two durometers (75 and 90 Shore A hardness) per material. The acquired data was used to determine values of the critical pressures (E-CTP) at which O-rings tearing is initiated under the specified range of test conditions. These critical pressures will be utilized for correlation with the critical tear pressures (M-CTP), critical tear energies and critical Tresca stresses derived from the FE model, as well as to calibrate and to validate the model’s results.



| REV. | Date | Drawn by | Revision Notes |
|---|---|---|---|
| **A** | July 2017 | SK | |

| Document Number: | Document Title: | |
|---|---|---|
| **D100562** | HPHT O-ring Testing Results, Final Report | PetroMar TECHNOLOGIES·INC<br>440 Creamery Way, Suite 100 |

# Table of Contents

## Table of Figures

## Table of Tables

# A.6-1 Test Objectives

## *A.6-1-1 Background*

FEA analysis success is limited by the accuracy of the underlying materials properties incorporated into the analysis. In addition, a given FEA material behavior model can converge on multiple solutions of varying degrees of reliability depending on the interplay between the design elements. For example, the FEA monitored sealing pressure of an O-ring depends on both the groove design and the clearance gap as depicted by a CAD drawing.

A main element of the proposed work is to suggest the laboratory testing procedures and analyses that should be performed to ensure the materials properties used in FEA design reflect the performance of the material in the service conditions. It is important that the results of a given FEA material model, however simple or sophisticated, be directly correlated to the results obtained by subjecting the candidate elastomers to a defined and reproducible set of conditions in an experimentally verifiable test rig.

The experimental results can be used to refine the FEA model through additional material properties or higher order interactions. Ultimately, the regulatory confidence in material suitability depends on demonstration of reasonable agreement between modeling and experiment on at least a laboratory scale. Extrapolation to more extreme down-hole conditions can be managed much more easily once the FEA material model's foundation has been established.[6]

## *A.6-1-2 Goal*

The main goal of the testing is, for the given range of test temperatures, determination of critical/minimal pressure levels at which O-ring tearing is initiated for the specified materials and durometers. These experimentally-observed pressure levels (E-CTP) where tearing begins may then be used for calibration and verification of the FEA model's predictions.

## *A.6-1-3 Test Matrix*

Table A.6-1 lists five O-ring materials/durometers specified for testing as well as the specified test temperatures:

[6] Safety Technology Verification for Materials and Corrosions in the U.S. Outer Continental Shelf, TECHNICAL PROPOSAL, BAA Solicitation E15PS00026, Battelle Memorial Institute

**Table A.6-1 Test Matrix**

| Material | Compound Reference | Nominal hardness | Actual hardness Mean | Service Temperature, [°C] | Test Temp#1, [°C] | Test Temp#2, [°C] |
|---|---|---|---|---|---|---|
| FKM (FKM--A) | F-13664 (F75) / Mil-83248 | 75 | 77 | -20 to +200 | 100 | 175 |
| FKM (FKM--A) | F-13681 (F90) / Mil-83248 | 90 | 91 | -20 to +200 | 100 | 175 |
| NBR (NBR-) | B1016 | 75 | 76 | -30 to +120 | 100 | n/a |
| NBR (NBR-) | B1001 | 90 | 94 | -30 to +120 | 100 | n/a |
| HNBR | R1006 | 75 | 76 | -35 to +160 | 100 | 150 |
| HNBR | R1003 | 90 | 92 | -35 to +160 | 100 | 150 |
| FEPM (FEPM-®) | L1000 | 80 | 89 | -20 to +230 | 100 | 175 |
| FEPM (FEPM-®) | 210-A-83 | 83 | 83 | -20 to +230 | 100 | 175 |
| FFKM (FFKM-) | K4079 | 75 | 76 | -2 to +316 | 100 | 175 |
| FFKM (FFKM-) | K3018 | 90 | 94 | -40 to +270 | 100 | 175 |

## A.6-2 Equipment

A specially designed hydraulic system was built to test O-rings under HPHT conditions.

**Figure** Figure A.6-1 illustrates the main components of the HPHT setup, which consists of:

- High-pressure hydraulic system rated to 30,000 psi that includes
  - manual fluid pump,
  - pressure vessel and a set of pistons accepting a AS568-210-size O-ring,
  - valves, tubes and fittings;
- Heater band;
- Oil-fill system capable of circulating oil under vacuum and filled with Rhodorsil 47V100;
- Pressure transducer and temperature sensors connected to the acquisition system;
- Laptop with a LabView-based application that controls the test regimes and records temperature and pressure amplitudes versus time.

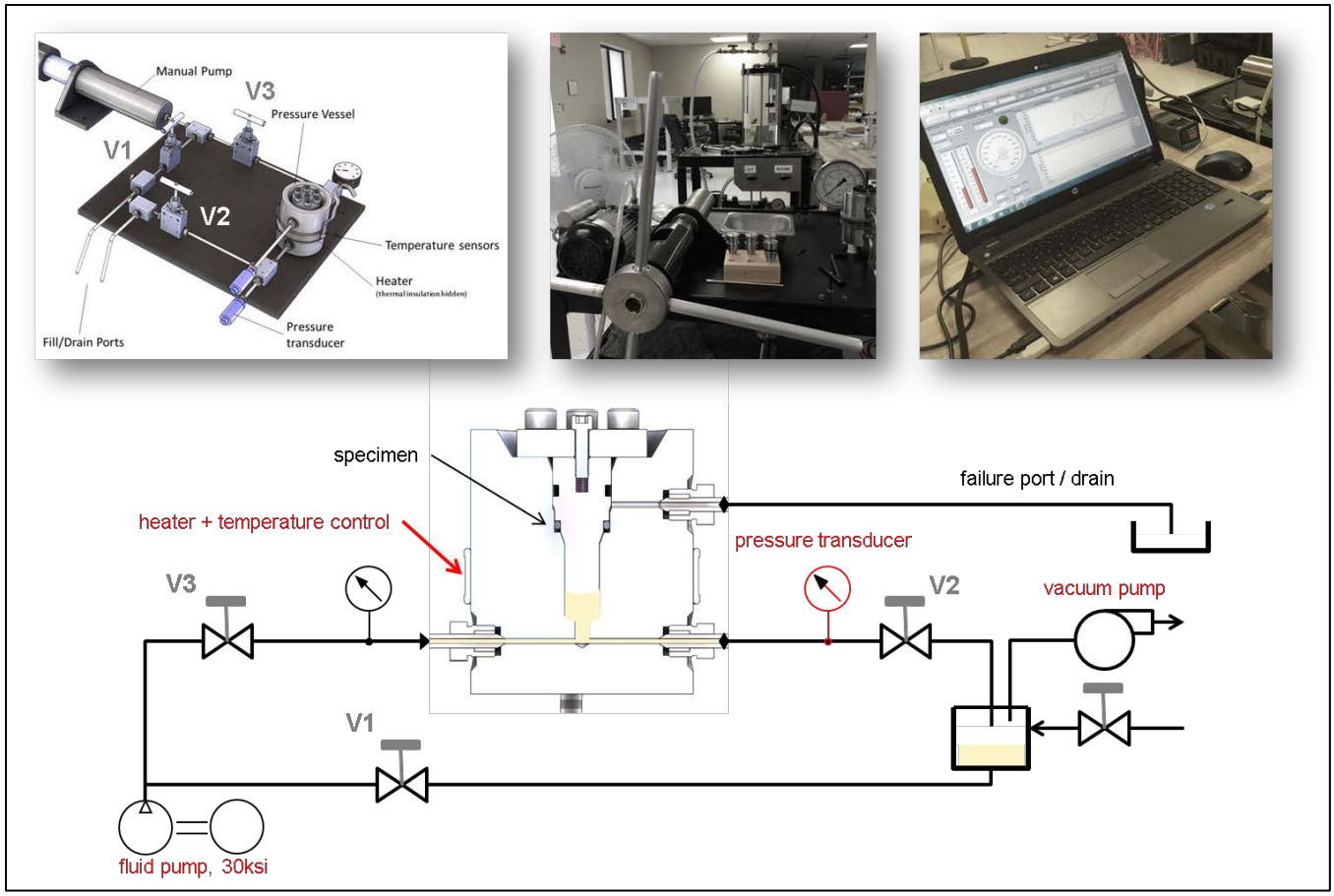


**Figure A.6-1** The HPHT O-ring test layout, the schematics for the hydraulic and the oil-fill systems.

Before pressure is applied, oil is de-aired and isolated by closing valves V1 and V2. While heating, the fluid pump is backed off to allow for oil to expand safely. When the target temperature is reached, the fluid pump is activated to set pressure up and to energize the specimen. For prolonged tests under fixed pressure, valve V3 could be closed to lock the pressure and to isolate the fluid pump. Petromar generated test procedure D100511 describes steps to operate the setup in more details.

By design, the extrusion gap between the vessel's bore and piston can be changed in five discrete steps by using pistons of slightly different diameters as outlined in Figure A.6-2.

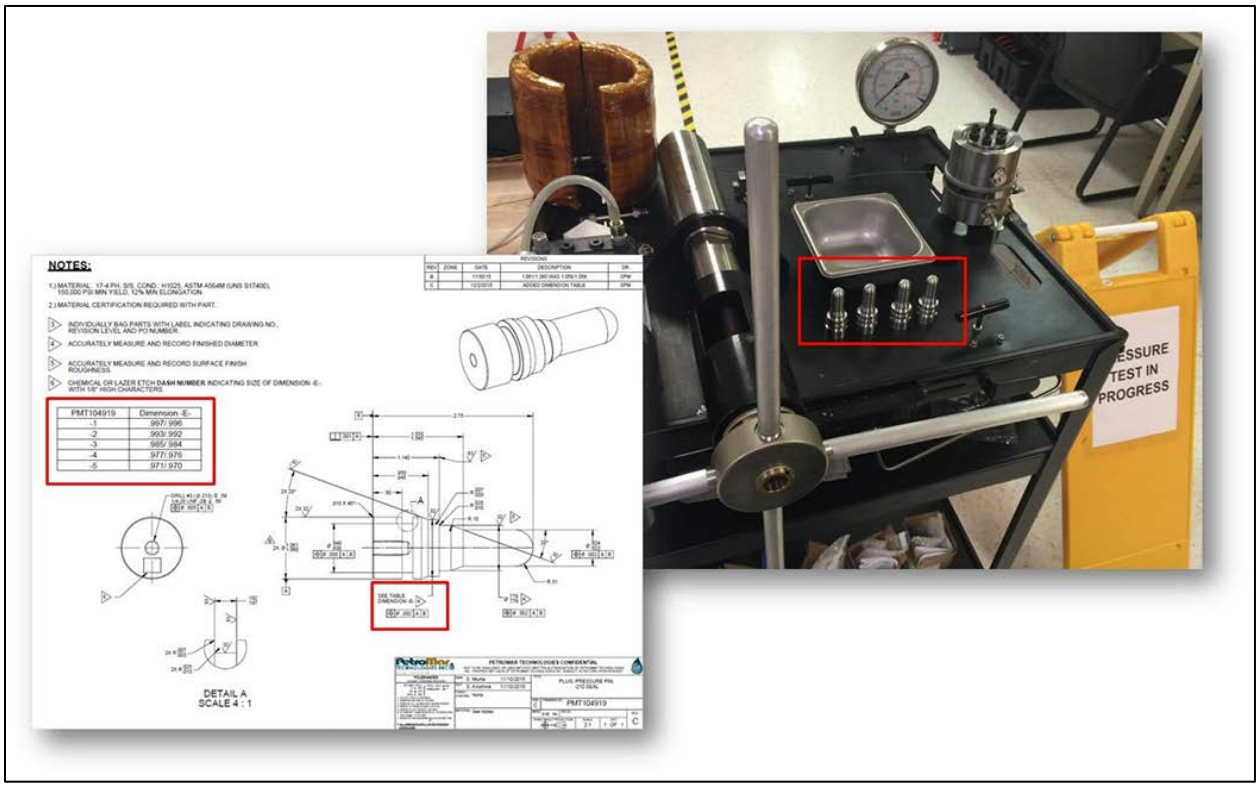


**Figure A.6-2** Five interchangeable pistons of slightly different diameters were utilized to control the clearance gap between the piston and vessel's bore.

After the pistons and the pressure vessel were fabricated, their actual dimensions and surface finishes were measured (see Figure A.6-3). These actual machined dimensions, as opposed to the nominal design dimensions, will be used for the FEA modeling to better match test conditions. In addition, during testing, the increase in pressure and temperature lead to a slight change in physical dimensions which have been calculated for each T,P case and used as correction factors. Under pressure, the vessel's bore diameter changes the most compared to the other vessel dimensions. The rate of this change is estimated to be 0.0004" per 25,000 psi (see Figure A.6-4):

$$\Delta Cp = 0.4/25000 = 1.6\ E\text{-}8 \quad [\text{inch/psi}] \qquad \text{Eq. 1}$$

Thermal changes of the largest clearance gap of 0.015" are negligible given the fact that both vessel and piston are made from the same material with CTE of 11 ppm/°C (for the alloy 17-4PH used).

Special attention has been given to minimize any unaccounted pre- and post-test disturbances of O-rings. To this end, the piston design allows for O-ring installation with the least stretch and the

most repeatability from one specimen to another. This design is to minimize the Mullins effect influence on the test outcome as well as to preserve the specimen's distortion after the test. Other important design/test considerations and parameters, chosen for enhanced accuracy/precision of results, were:

- Only new AS568-210-size O-rings utilized,
- Other than the clearance gap, the gland dimensions are based on the Parker O-ring Handbook recommendations for static seals,
- The initial squeeze is set to be 18%,
- All tests are single-cycle tests.

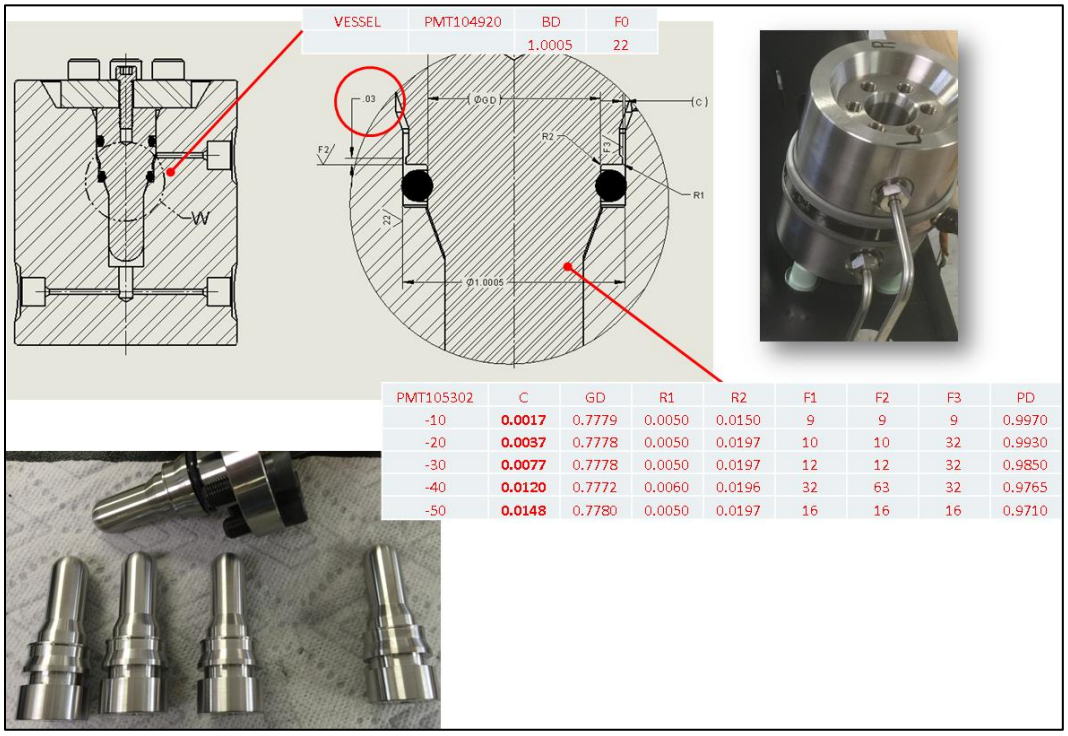


| PMT105302 | C | GD | R1 | R2 | F1 | F2 | F3 | PD |
|---|---|---|---|---|---|---|---|---|
| -10 | **0.0017** | 0.7779 | 0.0050 | 0.0150 | 9 | 9 | 9 | 0.9970 |
| -20 | **0.0037** | 0.7778 | 0.0050 | 0.0197 | 10 | 10 | 32 | 0.9930 |
| -30 | **0.0077** | 0.7778 | 0.0050 | 0.0197 | 12 | 12 | 32 | 0.9850 |
| -40 | **0.0120** | 0.7772 | 0.0060 | 0.0196 | 32 | 63 | 32 | 0.9765 |
| -50 | **0.0148** | 0.7780 | 0.0050 | 0.0197 | 16 | 16 | 16 | 0.9710 |

**Figure A.6-3** The actual dimensions of the pistons and the pressure vessel.

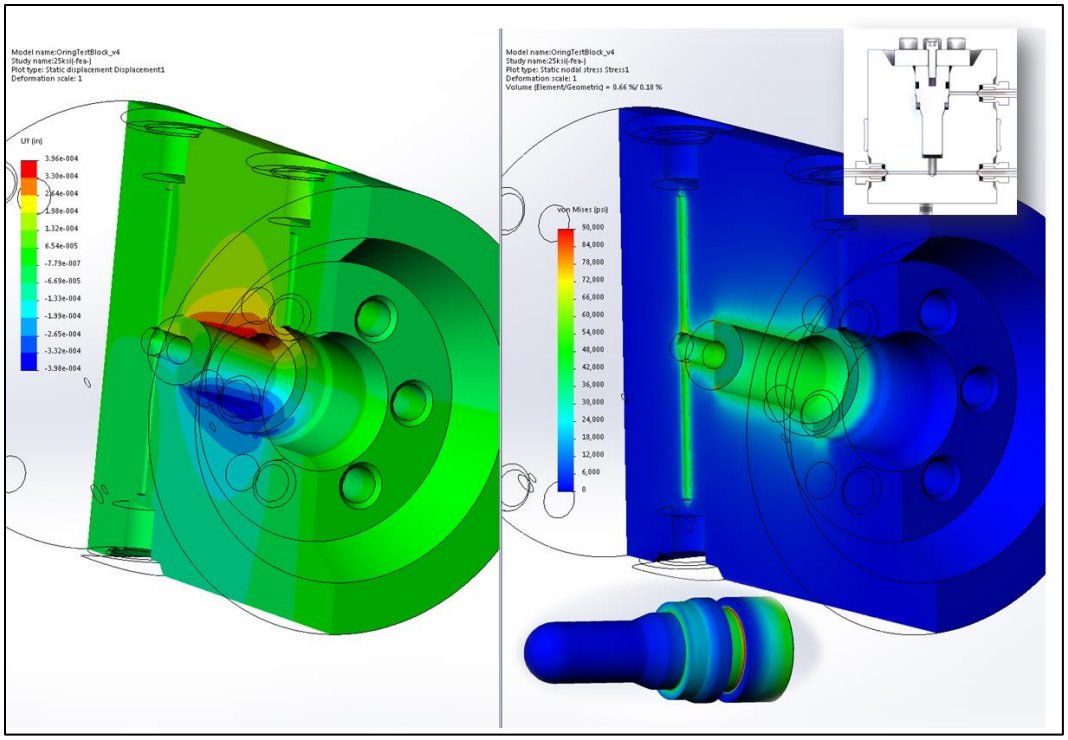


**Figure A.6-4** Deformation and stresses in vessel under 25,000 psi of pressure.

## A.6-3 Test Approach

The Endurica finite element model (FEM) analysis of the O-ring seal suggests that, when a certain pressure and temperature are applied, the O-ring deforms and may partially extrude into the clearance gap, C (Figure A.6-3). Physical testing of O-rings under matching HPHT loads qualitatively supports the FEM results. However, it is not practical to quantify the actual deformation of a specimen under the loads. The O-ring can only be examined after its post-test removal from the pressure cell, but the degree of the O-ring deformation changes significantly once the HPHT loads have been removed. Moreover, right after its extraction from the test apparatus, the deformation/extrusion continues to change for some time even when the specimen remains in unloaded (or resting) condition. This shape instability makes it difficult to correlate the physical deformations under loads with those predicted by the FEM.

One way to correlate the modeled and the physical deformations is to use some irreversible features that stay with a specimen after the HPHT loads have been removed and the specimen is extracted for its examination. Such irreversible yet measurable features include tiny tears or cuts indicative of the initiation of the tear process. Experience predicts that these tears/cuts will be found on a circular line the O-ring makes contact along with the fillet R1 (see Figure A.6-5, which shows the higest stress in the extruded O-ring where it is pressed against the fillet R1).

Furthermore, material tests conducted in another lab (as part of this overall project) provide the specific levels of the Critical Tearing Energy (E-CTP) for the same O-ring materials and durometers used in these tests.

In our test approach, these Critical Tearing Energy (E-CTP) levels will be used to link the FEM (M-CTP) results with the physical damage induced to the test specimens. The data of interest in this case are the presence of the tiny cuts/tears and the pressure/temperature combinations which caused these cuts/tears to occur. The tear/cut size of the interest is less than 0.010", only visible under a microscope. The main challenge here is to pre-determine the critical pressure that needs to be applied to just initiate an O-ring tear. The critical pressure level is very specific, which varies depending on the number of test conditions including temperature, exposure time to temperature, and pressure, clearance gap size, O-ring material/durometer, actual gland dimensions, and surface finish.

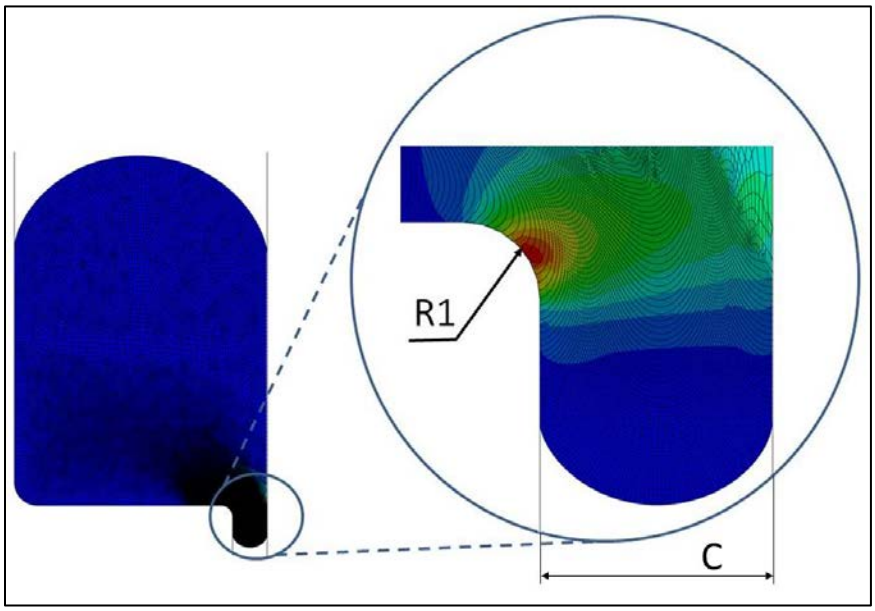


**Figure A.6-5** Finite element model of an O-ring deformed under pressure and extruded into gap, C.
The maximum stress in rubber is where O-ring contacts the fillet, R1.

### *A.6-3.1 Dwell Test*

A series of "exploratory" soak tests utilizing up to five nominally identical O-rings exposed to different HPHT levels was run to identify the minimal pressure at which an O-ring of particular material and durometer is expected to tear under the given conditions. The strategy is to test the first O-ring under a fixed pressure, examine the O-ring for damage and then determined how the fixed pressure should be adjusted for the next O-ring. If the next O-ring exhibits just a tiny cut (only visible under a microscope) then that pressure is defined to be the critical pressure for that

specific combination of material, durometer, clearance, and temperature. If the second O-ring suffers significantly larger damage than just a tiny cut, the third O-ring will be tested at a reduced fixed pressure. The iterations will continue until either a specimen with a tiny cut is obtained or the pressure difference between the damaged and undamaged O-rings is sufficiently small (less than about 15% of the mean) to allow for estimating the critical pressure to lie between the damage and no-damage values.

The HPHT profile used in the Dwell tests is shown in Figure A.6-6.

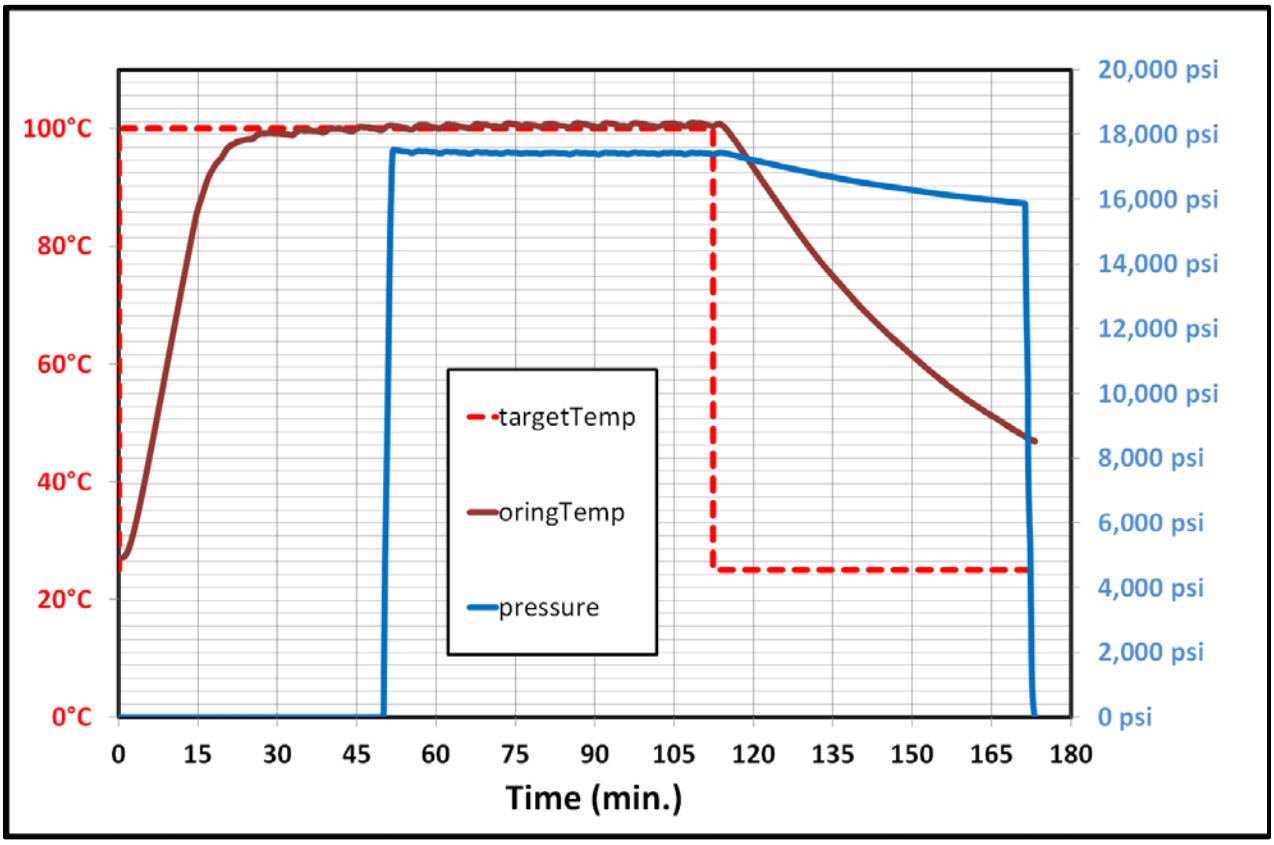


**Figure A.6-6** HPHT dwell test profile per the D100511 procedure.

The main steps are: (1) Heat to the target temperature, (2) when target Temperature is reached, wait for at least 10 minutes before starting application of pressure, (3) increase pressure slowly to the target pressure, (4) dwell for 1 hour and then turn the heater off, (5) wait until temperature decreases below 50°C before releasing pressure, (6) bleed pressure and stop logging.

### *A.6-3.2 Stepped Scans*

Another type of test, Stepped Scan, is designed to indicate (1) pressure levels at which a specimen starts to extrude and (2) the highest pressure an O-ring can take under given temperature and extrusion clearance before it either suffers the First Large Extrusion (SS-FLE) event or leaks.

The typical profile of Stepped Scan is shown in Figure A.6-7. Similar to the Dwell Test, the temperature is kept constant, but for the Stepped Scan, the specimen is soaked at a given pressure level for a short 5 minute duration, after which the pressure is stepped up in increments of 500 psi. Evaluation of pressure stability on each level reveals whether a specimen seals without extrusion (stable pressure levels) or it partially moves/extrudes into a clearance gap. When a specimen extrudes, it leaves an additional volume for oil to occupy, which results in a small but detectable pressure change (decrease) during that interval. For example, note the blue pressure curve at the nominal 9,000 psi interval in Figure A.6-7. During that interval, the pressure can be seen to drop slightly, as compared to the pressure during the nominal 8,000 psi interval during which the pressure remains steady, indicative of stable O-ring geometry and thus no significant extrusion.

Stepped Scans were run prior to each series of Dwell Tests. For the given combination of O-ring material/durometer, clearance, and temperature, the results of a Scan provided guidance in selecting the initial pressure level to use for the corresponding Dwell Testing of that material/durometer and clearance. In addition, O-ring response data from the Stepped Scan may prove useful for verification of the results of future advanced transient FE analysis of elastomers under HPHT.

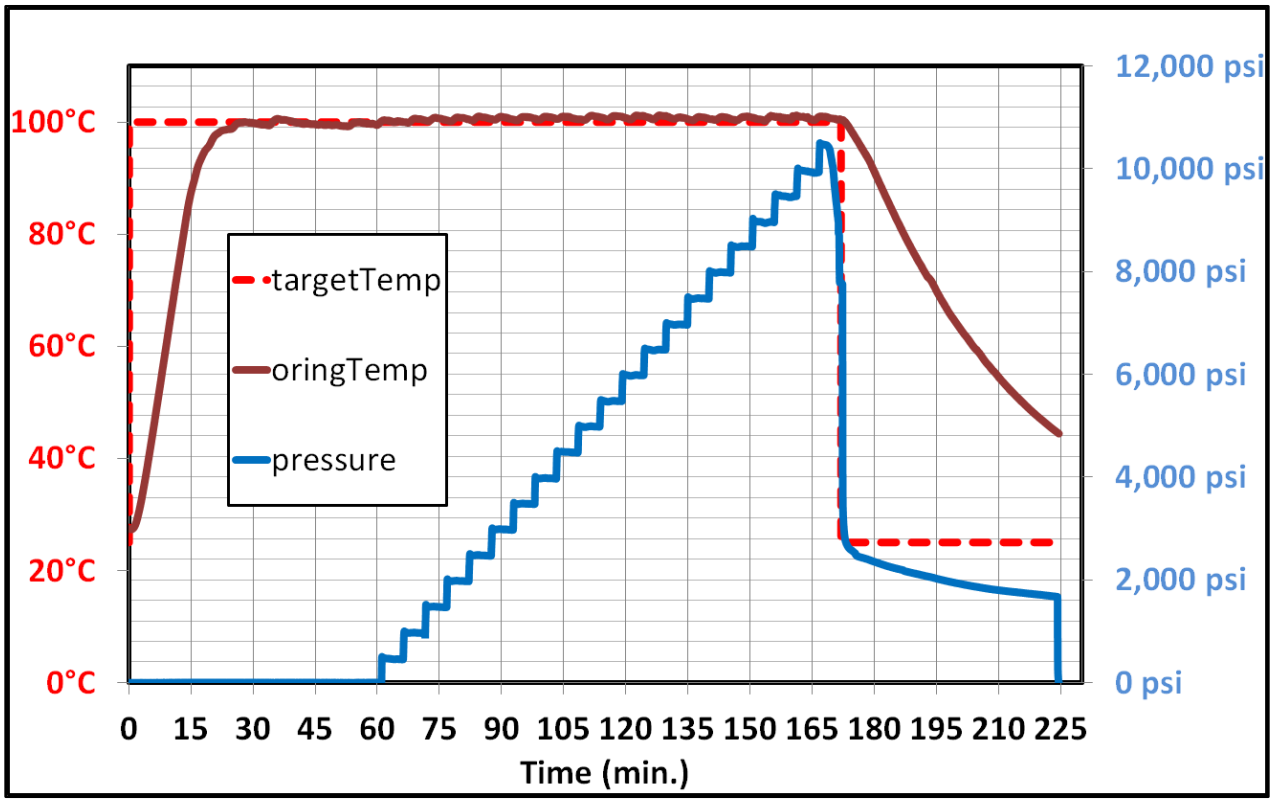


**Figure A.6-7** HPHT step test profile per the D100511 procedure.

The main steps are: (1) Heat to the target temperature, (2) when target Temp is reached, wait for at least 10 minutes before starting applying pressure, (3) increase pressure in increments of 500 psi, keeping it at each pressure setting for 5 minutes until reaching the level at which the specimen fails to hold pressure, (4) turn the heater off and wait until temperature decreases below 50°C, (5) bleed pressure and stop logging.

## A.6-4 Extrusion Grouping / Color Coding

As suggested above, the search for the critical pressure level that initiates tears/cuts on the O-ring surface was an iterative process and, for every combination of the test parameters, this search required a series of up to five specimens dwell-tested at different pressure levels. Although all tested specimens were documented and stored, only one specimen per series was used to define the experimentally-derived Critical Tear Pressure (E-CTP). Classification of the results for all tested specimens were sorted in three main groups: Green, Yellow, and Red. The sorting is based on the extent of the O-rings' damage:

**Green** group (Figure A.6-8):

- No visible damage
- Seating

**Yellow** group (Figure A.6-9):

- Thin-band cut-off
- Small-size extrusion with visible damage
- Visible localized cuts/tears
- Nibbled surface

**Red** group (Figure A.6-10):

- First Large Extrusion event (after Stepped Scans)
- Large extrusion / deep circumferential cuts

Each O-ring from the Green group was additionally examined under a microscope in an attempt to find small cuts/tears invisible by a naked eye. Should these tiny damages be found, the pressure to which this O-ring was subjected was then defined as the Critical Tear Pressure for that material/durometer and clearance. By definition, this pressure is on the borderline between the Green and Yellow groups, and such O-rings were then marked as green-yellow and kept in the Green group.


**Figure A.6-8** Examples of the Green group’s O-rings – some set/seating, but no cuts/tears. Samples of each elastomer are shown with the experimental conditions and results for each sample.

Figure A.6-11 illustrates an example of a color-coded test matrix and its graphical representation. The data in columns is grouped based on the piston’s size/clearance. The colored cells’ values indicate the pressure at which each specimen was tested in psi. The cells’ color (Green, Yellow, or Red) represents the extent of the induced damage at that pressure. Each piston’s series starts with a Stepped Scan test resulting in the SS-FLE event. The found SS-FLE pressure is then used as the initial pressure for the first Dwell test using the second O-ring and the same piston. Based on the result of the first Dwell test, a decision was made on the next pressure level and so on until either a ‘green-yellow’ O-ring is found or the pressure difference between ‘green’ and ‘yellow’ specimens is sufficiency small.


**Figure A.6-9** Examples of the Yellow group’s O-rings – cuts and tears are visible by a naked eye. Samples of each elastomer are shown with the experimental conditions and results for each sample.

**Figure A.6-10** Examples of the Red group's O-rings – large extrusion, deep cuts. Samples of each elastomer are shown with the experimental conditions and results for each sample.

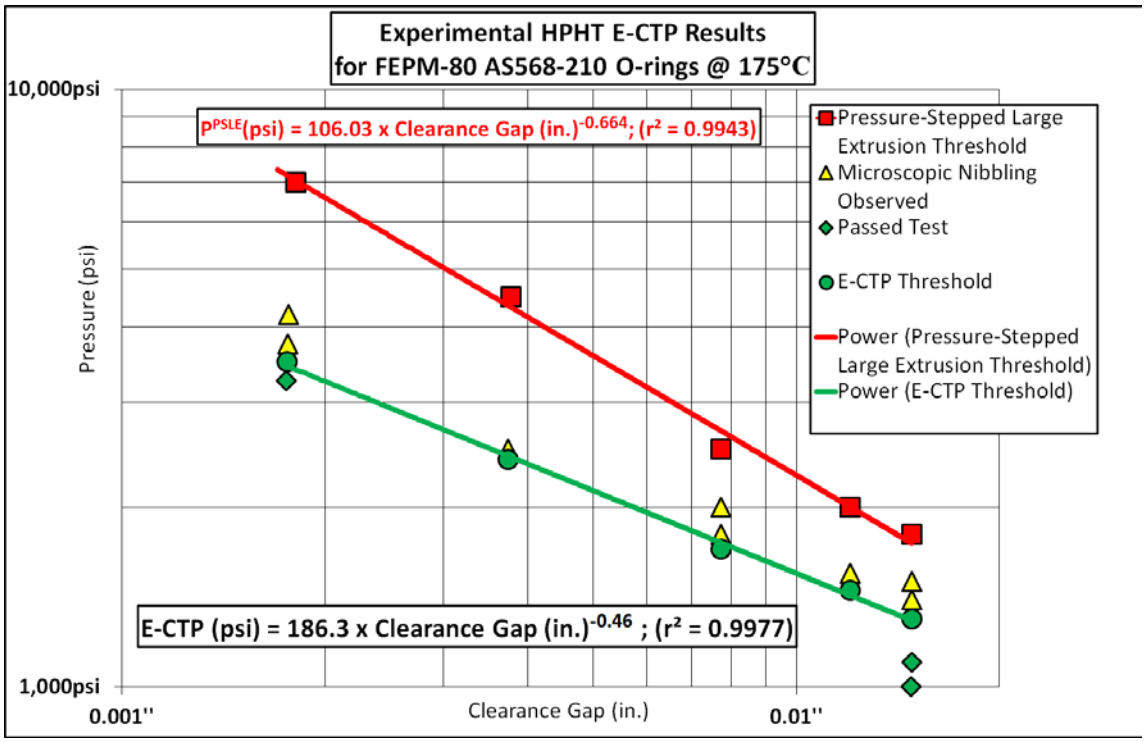


**Figure A.6-11** Example of the test matrix and its graphical representation using the color coding.

## A.6-5 Critical Tear Pressure

As stated above, for any given test condition, the minimum pressure level that initiates O-ring tearing is called the Critical Tear Pressure (E-CTP). In order to validate the final O-ring FE model, that model's results must reproduce the experimentallyderived E-CTPs as well as the experimentallyderived Critical Tear Energy obtained on the material sample slabs by another laboratory. Any differences must be understood and, if needed, further experimentation or model refinement will be needed until the satisfactory correlation is achieved.

### *A.6-5.1 Data Interpolation Using Power Regression*

To an acceptable degree of accuracy, the upper pressure level of the Green group will define the Critical Tear Pressure for each set of test parameters. It was found that the critical pressures for the five clearances tested could be interpolated using power regression

$$E\text{-}CTP = A * C^{B}, \qquad \text{Eq. 2}$$

where E-CTP is a critical tear pressure in [psi],
C is clearance gap in [inch],

A and B are coefficients.

Power regression is also well suited for interpolation of the SS-FLE data acquired in Stepped Scans.

Figure A.6-12 utilizes the data presented in Figure A.6-11 to illustrate how E-CTP is defined for each of the 5 clearance sizes (empty green circles), the power regression coefficients, and the corresponding fit curve. For this example, $R^2$, the goodness-of-fit coefficient, is almost 1 suggesting a very good fit of the curve to the data.

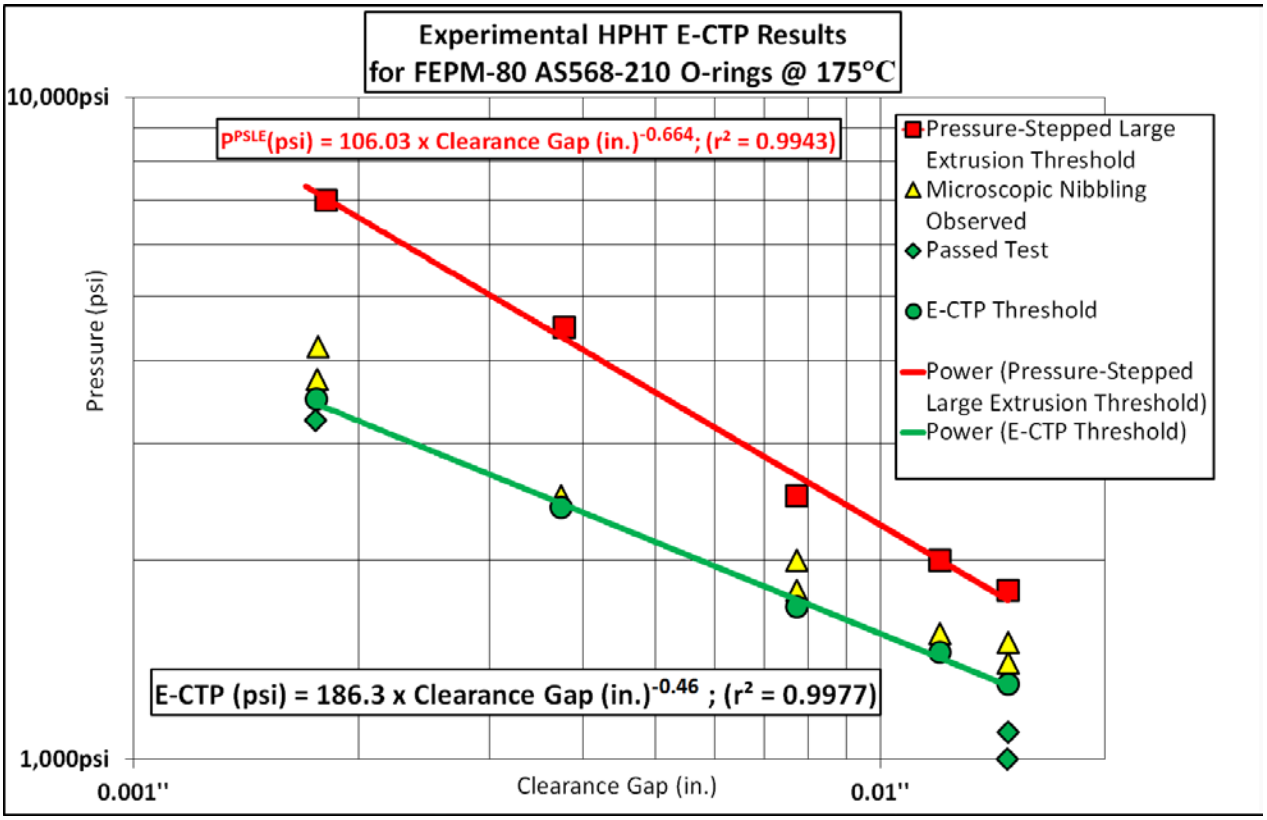


**Figure A.6-12** Example of the Critical Tear Pressure levels versus clearance and their interpolation using power regression with coefficients A=186.3 and B=-0.46 (green line). Red line represents interpolation of the SS-FLE results.

## *A.6-5.2 Interpolation Coefficients for E-CTP and SS-FLE*

Table A.6-2 and Table A.6-3 summarize coefficients of power regression for E-CTP (Dwell tests) and SS-FLE (Stepped Scans) based on the test results outlined in paragraph 0 and for the entire Test Matrix presented in Table A.6-4.

**Table A.6-2 Coefficients of power regression for extrusion tests conducted at 100°C**

| Power Regression Coefficients | | | | P=A*C^(B), where P [psi] & C [inch] | | | |
|---|---|---|---|---|---|---|---|
| | | | | E-CTP | | SS-FLE | |
| Material | Compound Reference | Durometer | Temp (°C) | A | B | A | B |
| FKM-75 | F-13664 (F75) | 75 | 100 | 184.572 | -0.584 | 73.010 | -0.904 |
| FKM-90 | F-13681 (F90) | 90 | 100 | 533.899 | -0.479 | 135.482 | -0.905 |
| NBR-75 | B1016 | 75 | 100 | 720.374 | -0.386 | 181.667 | -0.814 |
| NBR-90 | B1001 | 90 | 100 | 760.005 | -0.479 | 126.031 | -1.002 |
| HNBR-75 | R1006 | 75 | 100 | 133.608 | -0.608 | 127.474 | -0.701 |
| HNBR-90 | R1003 | 90 | 100 | 918.098 | -0.411 | 191.328 | -0.850 |
| FEPM-80 | L1000 | 89 | 100 | 217.904 | -0.490 | 120.629 | -0.715 |
| FEPM-83 | A-210 | 83 | 100 | 292.565 | -0.427 | 137.227 | -0.664 |
| FFKM-75 | K4079 | 75 | 100 | 304.152 | -0.481 | 5.802 | -1.445 |
| FFKM-90 | K3018 | 90 | 100 | 399.140 | -0.502 | 58.838 | -1.092 |

**Table A.6-3 Coefficients of power regression for extrusion tests conducted at 150°C and 175°C**

| Power Regression Coefficients | | | | P=A*C^(B), where P [psi] & C [inch] | | | |
|---|---|---|---|---|---|---|---|
| | | | | E-CTP | | SS-FLE | |
| Material | Compound Reference | Durometer | Temp (°C) | A | B | A | B |
| FKM-75 | F-13664 (F75) | 75 | 175 | 190.034 | -0.501 | 90.945 | -0.760 |
| FKM-90 | F-13681 (F90) | 90 | 175 | 500.792 | -0.416 | 148.567 | -0.779 |
| NBR-75 | B1016 | 75 | -- | | | | |
| NBR-90 | B1001 | 90 | -- | | | | |
| HNBR-75 | R1006 | 75 | 150 | 455.224 | -0.339 | 375.276 | -0.500 |
| HNBR-90 | R1003 | 90 | 150 | 737.688 | -0.426 | 268.642 | -0.759 |
| FEPM-80 | L1000 | 89 | 175 | 186.302 | -0.460 | 106.028 | -0.664 |
| FEPM-83 | A-210 | 83 | 175 | 373.009 | -0.343 | 129.339 | -0.647 |
| FFKM-75 | K4079 | 75 | 175 | 200.431 | -0.494 | 36.051 | -1.008 |
| FFKM-90 | K3018 | 90 | 175 | 254.974 | -0.423 | 110.993 | -0.758 |

### *A.6-5.3 Test Data for E-CTP and SS-FLE*

The actual test data used to derive the coefficients listed in Table A.6-4 and Table A.6-5 is presented in the following subsections.

### A.6-5.3.1 FKM- (FKM)

**Table A.6-4 E-CTP and SS-FLE pressures versus clearance gaps for FKM-75 and FKM-90 @ 100°C and 175°C**

| E-CTP FKM-75, FKM-90 | | | | | | | | |
|---|---|---|---|---|---|---|---|---|
| Nominal Clearance Gap (@ 25°C) | Clearance Gap (in.) @ 100°C | E-CTP, FKM-75 @ 100°C (psi) | Clearance Gap @ 100°C (in.) | E-CTP, FKM-90 (psi) | Clearance Gap (in.) @175°C | E-CTP, FKM-75@175°C (psi) | Clearance Gap @175°C (in.) | E-CTP, FKM-90 @ 175°C (psi) |
| 0.0148" | 0.0148336 | 2,100 | 0.0148672 | 4,200 | 0.014824 | 1,500 | 0.014848 | 3,000 |
| 0.012" | 0.0120392 | 2,450 | 0.0120672 | 4,200 | 0.012028 | 1,750 | 0.012048 | 3,000 |
| 0.0077" | 0.007752 | 3,250 | 0.007784 | 5,250 | 0.007736 | 2,250 | 0.0077612 | 3,825 |
| 0.0037" | 0.0037784 | 4,900 | 0.0038312 | 8,200 | 0.0037512 | 3,200 | 0.00378 | 5,000 |
| 0.0017" | 0.0018152 | 7,200 | 0.001868 | 10,500 | 0.0017704 | 4,400 | 0.001812 | 7,000 |
| SS-FLE FKM-75, FKM-90 | | | | | | | | |
| Nominal Clearance Gap (@ 25°C) | Clearance Gap (in.) @ 100°C | SS-FLE, FKM-75 @100°C (psi) | Clearance Gap @ 100°C (in.) | SS-FLE, FKM-90 @100°C (psi) | Clearance Gap (in.) @175°C | SS-FLE, FKM-75 @175°C (psi) | Clearance Gap @175°C (in.) | SS-FLE, FKM-90 @175°C (psi) |
| 0.0148" | 0.014856 | 3,500 | 0.014904 | 6,500 | 0.014832 | 2,000 | 0.014864 | 4,000 |
| 0.012" | 0.012064 | 4,000 | 0.012112 | 7,000 | 0.012048 | 3,000 | 0.01208 | 5,000 |
| 0.0077" | 0.007788 | 5,500 | 0.007868 | 10,500 | 0.007756 | 3500 | 0.007796 | 6,000 |
| 0.0037" | 0.00386 | 10,000 | 0.004028 | 20,500 | 0.003804 | 6,500 | 0.003868 | 10,500 |
| 0.0017" | 0.002044 | 21,500 | 0.0017 | Use power law | 0.001868 | 10,500 | 0.00202 | 20,000 |

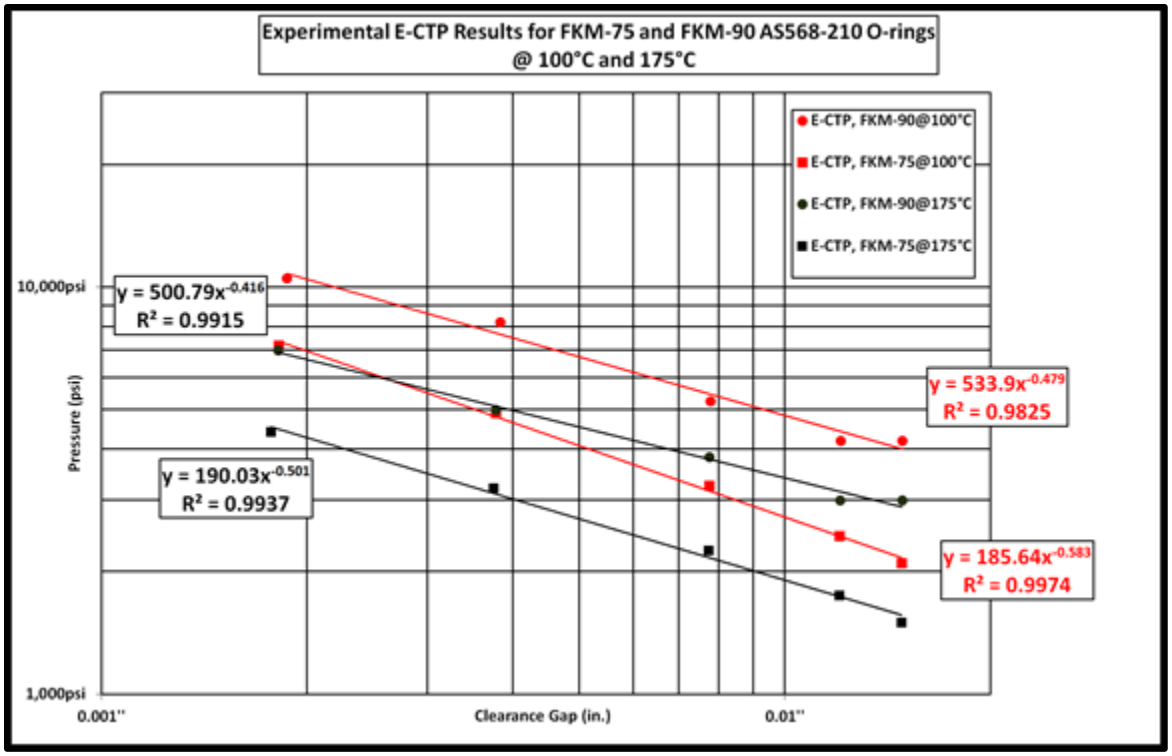


**Figure A.6-13** E-CTP versus clearance gaps for FKM-75 and FKM-90 @ 100°C and 175°C.

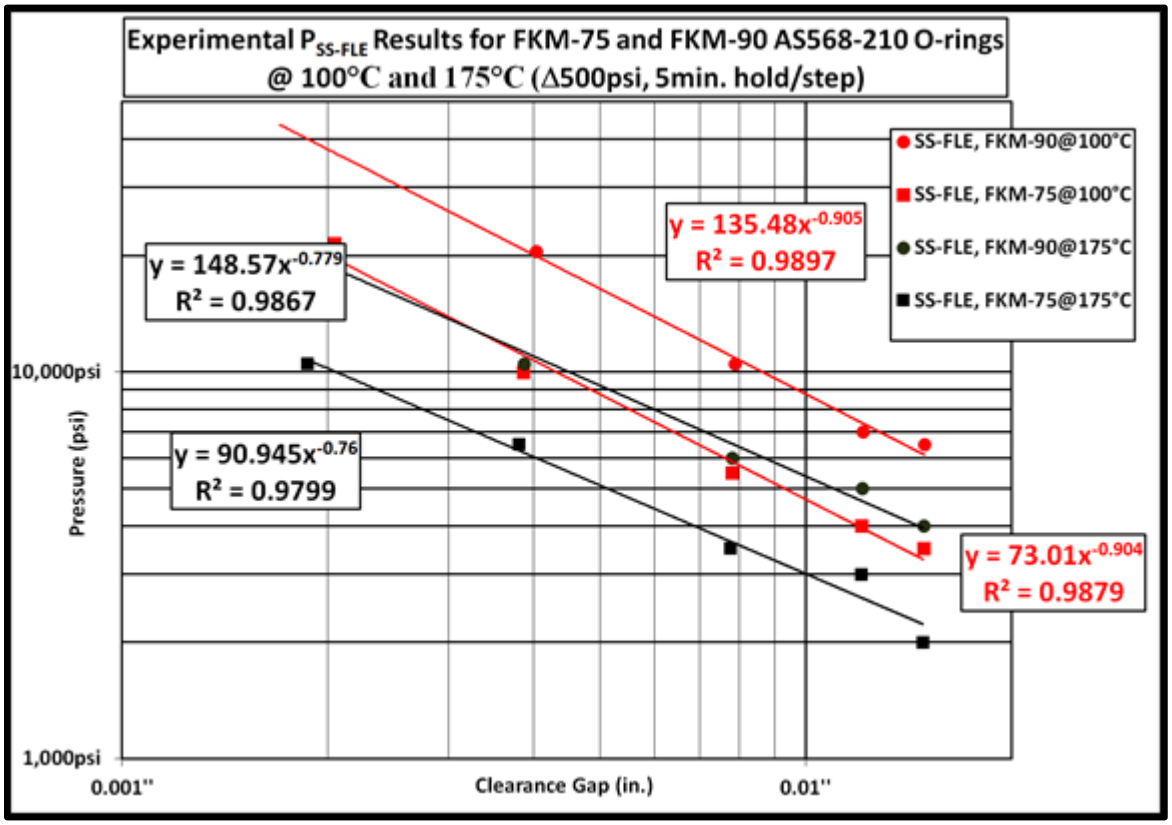


**Figure A.6-14** SS-FLE pressures versus clearance gaps for FKM-75 and FKM-90 @ 100°C and 175°C.

### A.6-5.3.2 NBR- (NBR)

**Table A.6-5 E-CTP and SS-FLE pressures versus clearance gaps for NBR-75 and NBR-90 @ 100°C**

| E-CTP NBR-75, NBR-90 | | | | |
|---|---|---|---|---|
| Nominal Clearance Gap (in.) @ 25°C | Clearance Gap (in.) @ 100°C | E-CTP (psi), NBR-75 @ 100°C | Clearance Gap (in.) @ 100°C | E-CTP (psi), NBR-90 @ 100°C |
| 0.0148 | 0.014856 | 3,500 | 0.0149 | 6,250 |
| 0.012 | 0.0120604 | 4,000 | 0.0121 | 6,250 |
| 0.0077 | 0.07776 | 4,750 | 0.07812 | 7,000 |
| 0.0037 | 0.03808 | 6,750 | 0.03868 | 10,500 |
| 0.0017 | 0.01824 | 7,750 | 0.01956 | 16,000 |
| **SS-FLE NBR-75, NBR-90** | | | | |
| Nominal Clearance Gap (in.) @ 25°C | Clearance Gap (in.) @ 100°C | SS-FLE (psi), NBR-75 @100°C | Clearance Gap (in.) @ 100°C | SS-FLE (psi), NBR-90 @100°C |
| 0.0148 | 0.014888 | 5,500 | 0.014.36 | 8,500 |
| 0.012 | 0.0120604 | 6,500 | 0.0121 | 10,500 |
| 0.0077 | 0.07844 | 9,000 | 0.07956 | 16,000 |
| 0.0037 | 0.04004 | 19,000 | 0.037 | Use Power Law |
| 0.0017 | 0.01876 | 25000 | 0.017 | Use Power Law |

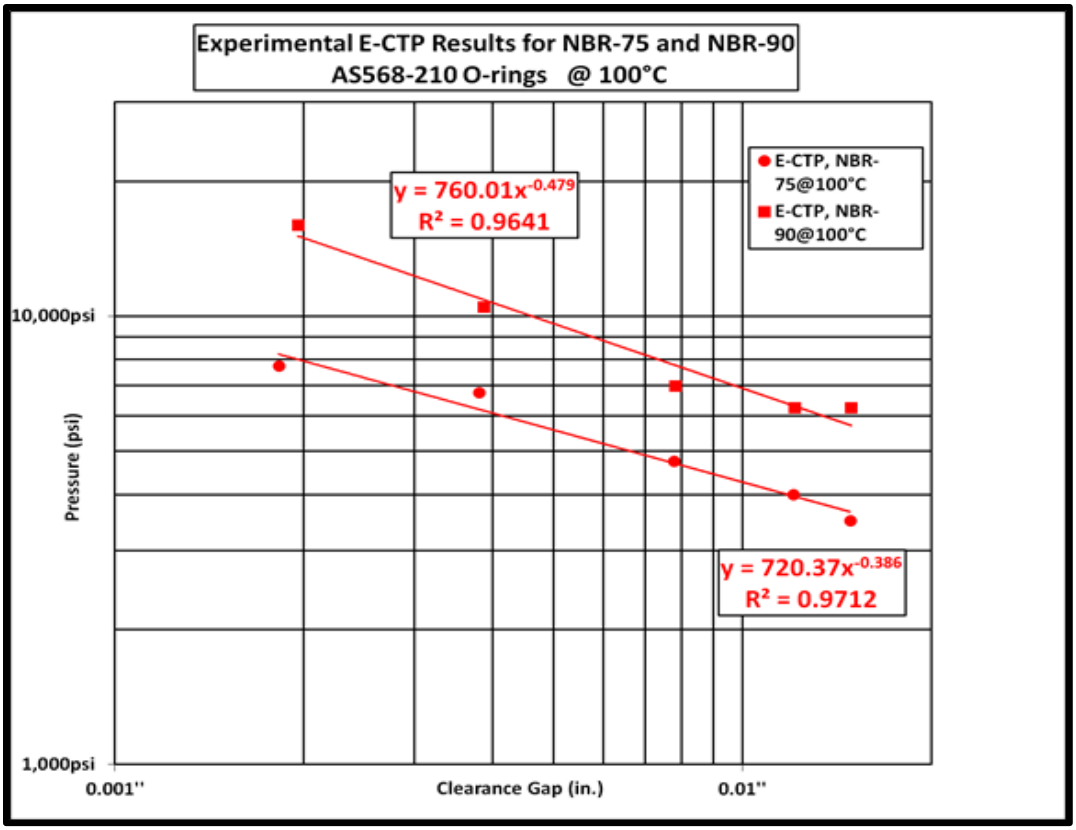


**Figure A.6-15** E-CTP versus clearance gaps for NBR-75 and NBR-90 @ 100°C.

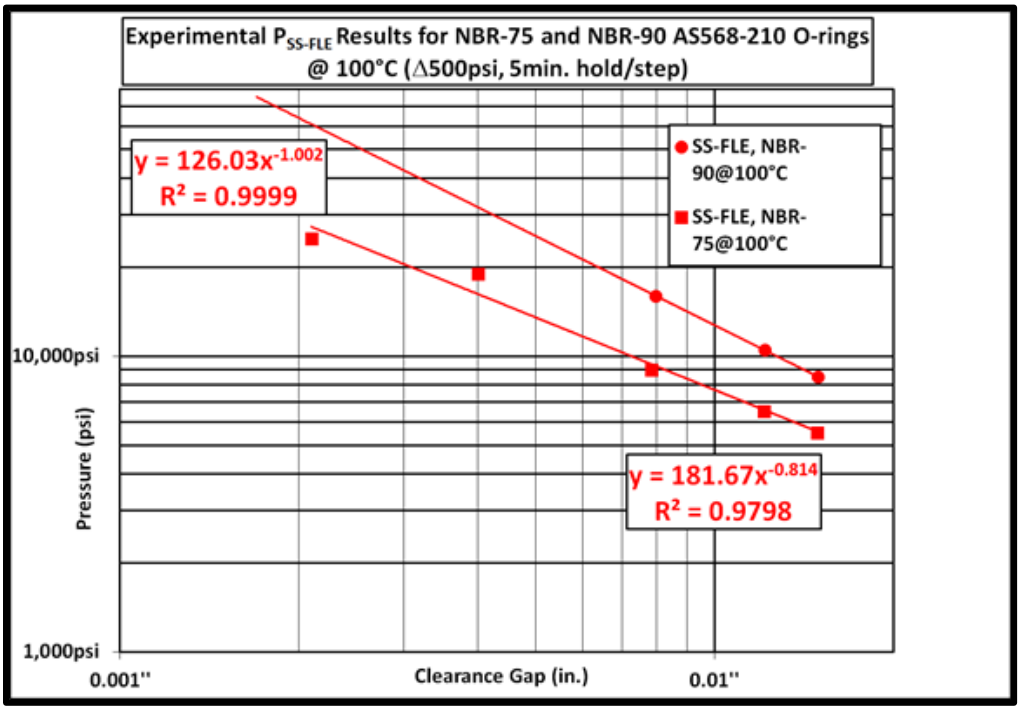


**Figure A.6-16** SS-FLE pressures versus clearance gaps for NBR-75 and NBR-90 @ 100°C.

### A.6-5.3.3 HNBR

**Table A.6-6 E-CTP and SS-FLE pressures versus clearance gaps for HNBR-75 and HNBR-90 @ 100°C and 150°C**

| E-CTP HNBR-75, HNBR-90 | | | | | | | | |
|---|---|---|---|---|---|---|---|---|
| Nominal Clearance Gap (in.) @ 25°C | Clearance Gap (in.) @ 100°C | E-CTP (psi), HNBR-75 @ 100°C | Clearance Gap (in.) @ 100°C | E-CTP (psi), HNBR-90 @ 100°C | Clearance Gap (in.) @175°C | E-CTP (psi), HNBR-75@175°C | Clearance Gap (in.) @175°C | E-CTP (psi), HNBR-90 @ 175°C |
| 0.0148 | 0.0148288 | 1,800 | 0.01488 | 5,000 | 0.014828 | 1,750 | 0.014872 | 4,500 |
| 0.012 | 0.0120304 | 1,900 | 0.012096 | 6,000 | 0.012036 | 2,250 | 0.012076 | 4,750 |
| 0.0077 | 0.0774 | 2,500 | 0.07804 | 6,500 | 0.07736 | 2,250 | 0.07796 | 6,000 |
| 0.0037 | 0.03764 | 4,000 | 0.03848 | 9,250 | 0.03752 | 3,250 | 0.0382 | 7,500 |
| 0.0017 | 0.018 | 6,250 | 0.01892 | 12,000 | 0.0176 | 3,750 | 0.01876 | 11,000 |
| **SS-FLE HNBR-75, HNBR-90** | | | | | | | | |
| Nominal Clearance Gap (in.) @ 25°C | Clearance Gap (in.) @ 100°C | SS-FLE (psi), HNBR-75 @100°C | Clearance Gap (in.) @ 100°C | SS-FLE (psi), HNBR-90 @100°C | Clearance Gap (in.) @175°C | SS-FLE (psi), HNBR-75 @175°C | Clearance Gap (in.) @175°C | SS-FLE (psi), HNBR-90 @175°C |
| 0.0148 | 0.01484 | 2,500 | 0.014912 | 7,000 | 0.01484 | 3,000 | 0.014848 | 6,500 |
| 0.012 | 0.012048 | 3,000 | 0.012128 | 8,000 | 0.012048 | 4,000 | 0.012048 | 7,500 |
| 0.0077 | 0.07756 | 3,500 | 0.07884 | 11,500 | 0.0778 | 4000 | 0.07764 | 11,000 |
| 0.0037 | 0.03796 | 6,000 | 0.04036 | 21,000 | 0.0386 | 5,000 | 0.038248 | 17,500 |
| 0.0017 | 0.01876 | 11000 | 0.017 | Use Power law | 0.01996 | 10,000 | 0.01908 | Use Power law |

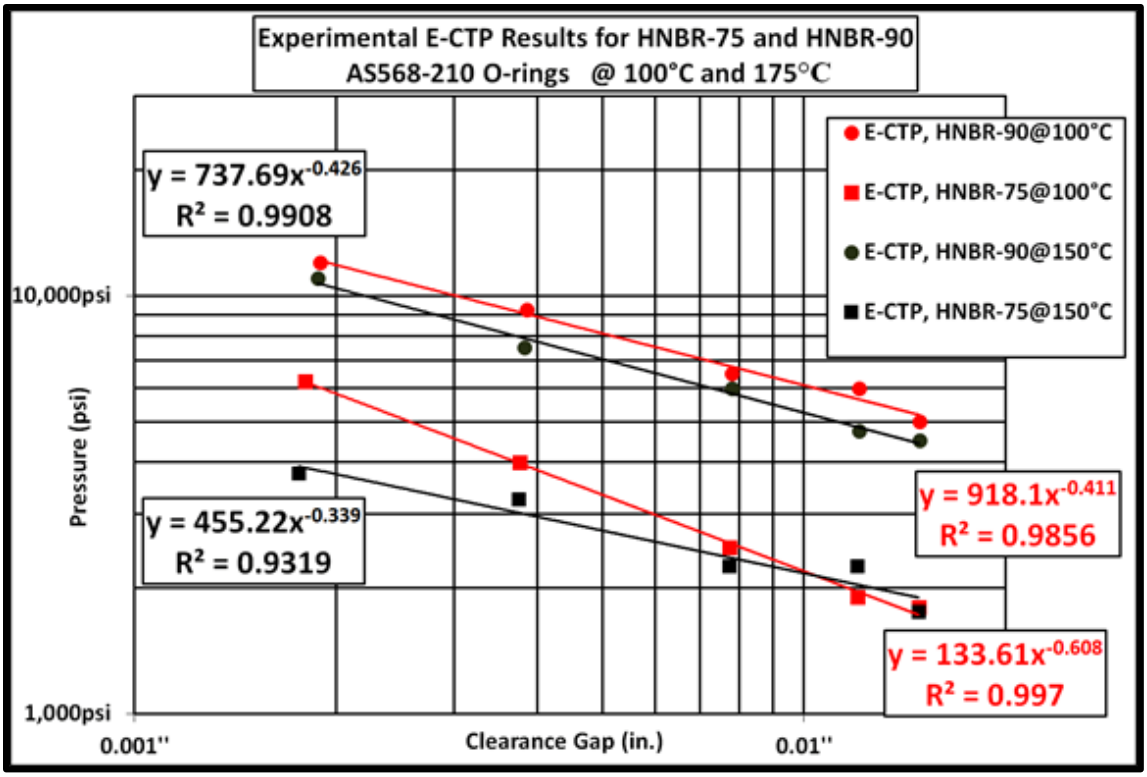


**Figure A.6-17** E-CTP versus clearance gaps for HNBR-75 and HNBR-90 @ 100°C and 150°C.

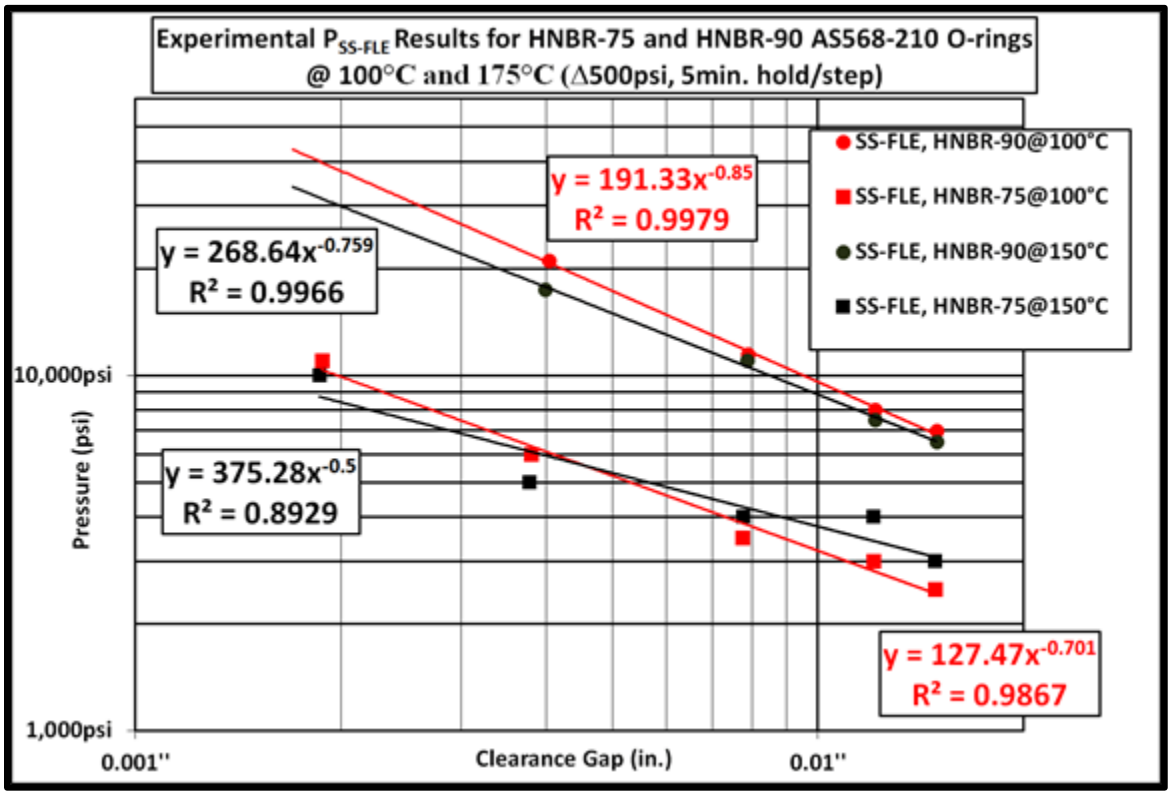


**Figure A.6-18** SS-FLE pressure versus clearance gaps for HNBR-75 and HNBR-90 @ 100°C and 150°C.

## A.6-5.3.4 FEPM- (FEPM)

**Table A.6-7 E-CTP and SS-FLE pressures versus clearance gaps for FEPM-80 and FEPM-83 @ 100°C and 175°C**

| E-CTP FEPM-80 (89), FEPM-83 | | | | | | | | |
|---|---|---|---|---|---|---|---|---|
| Nominal Clearance Gap (in.) @ 25°C | Clearance Gap (in.) @ 100°C | E-CTP (psi), FEPM-80 @ 100°C | Clearance Gap (in.) @ 100°C | E-CTP (psi), FEPM-83 @ 100°C | Clearance Gap (in.) @ 175°C | E-CTP (psi), FEPM-80 @ 175°C | Clearance Gap (in.) @ 175°C | E-CTP (psi), FEPM-83 @ 175°C |
| 0.0148 | 0.0148336 | 1,750 | 0.014856 | 1,750 | 0.0148256 | 1,300 | 0.014824 | 1,600 |
| 0.012 | 0.01204 | 1,900 | 0.0120576 | 1,900 | 0.012028 | 1,450 | 0.0120256 | 1,675 |
| 0.0077 | 0.07756 | 2,250 | 0.07772 | 2,350 | 0.07736 | 1,700 | 0.07732 | 1,950 |
| 0.0037 | 0.0378 | 3,500 | 0.03796 | 3,300 | 0.03752 | 2,400 | 0.03748 | 2,600 |
| 0.0017 | 0.01792 | 4,800 | 0.0186 | 4,250 | 0.01772 | 3,500 | 0.01756 | 3,250 |
| **SS-FLE FEPM-80 (89), FEPM-83** | | | | | | | | |
| Nominal Clearance Gap (in.) @ 25°C | Clearance Gap (in.) @ 100°C | SS-FLE (psi), FEPM-80 @ 100°C | Clearance Gap (in.) @ 100°C | SS-FLE (psi), FEPM-83 @ 100°C | Clearance Gap (in.) @175°C | SS-FLE (psi), FEPM-80 @175°C | Clearance Gap (in.) @175°C | SS-FLE (psi), FEPM-83 @175°C |
| 0.0148 | 0.01484 | 2,500 | 0.014896 | 2,500 | 0.01484 | 1,800 | 0.014848 | 2,000 |
| 0.012 | 0.012056 | 3,000 | 0.01212 | 2,500 | 0.012048 | 2,000 | 0.012048 | 2,200 |
| 0.0077 | 0.07804 | 3,500 | 0.07868 | 3,000 | 0.0778 | 2,500 | 0.07764 | 3,000 |
| 0.0037 | 0.03972 | 6,500 | 0.041 | 6,000 | 0.0386 | 4,500 | 0.038248 | 5,000 |
| 0.0017 | 0.017 | 11,000 | 0.017 | 9,000 | 0.01996 | 7,000 | 0.01908 | 7,500 |

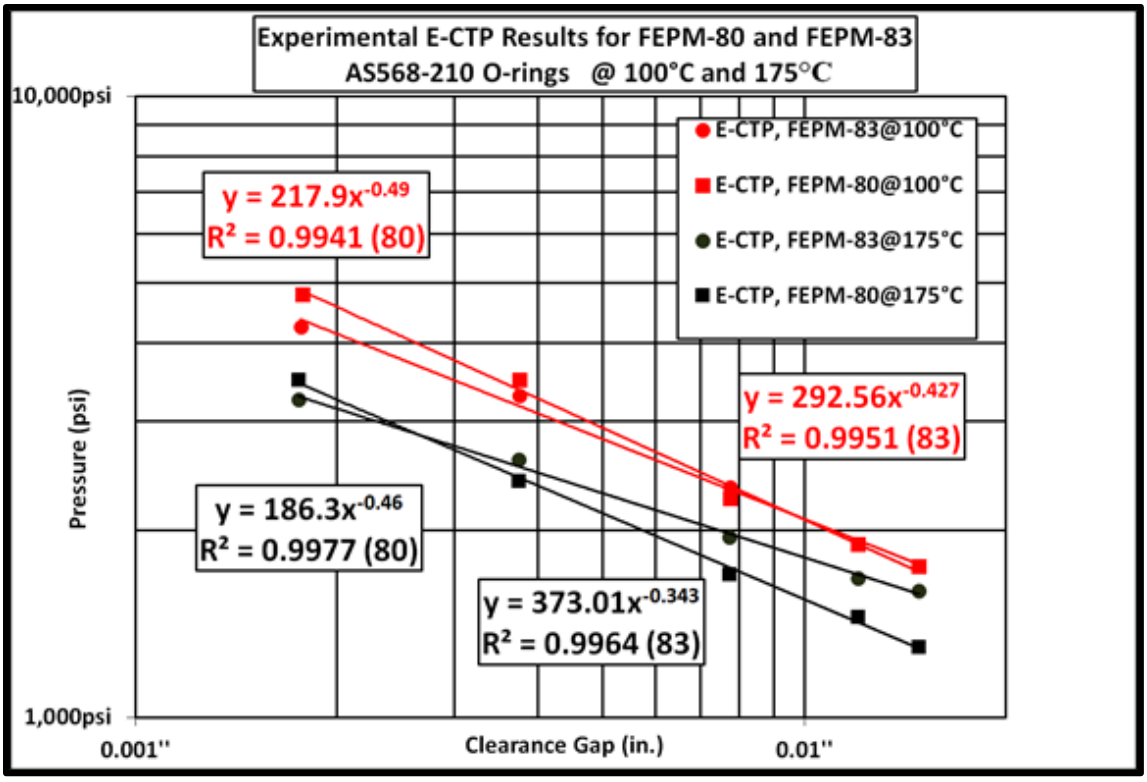


**Figure A.6-19** E-CTP versus clearance gaps for FEPM-80 and FEPM-83 @ 100°C and 175°C.

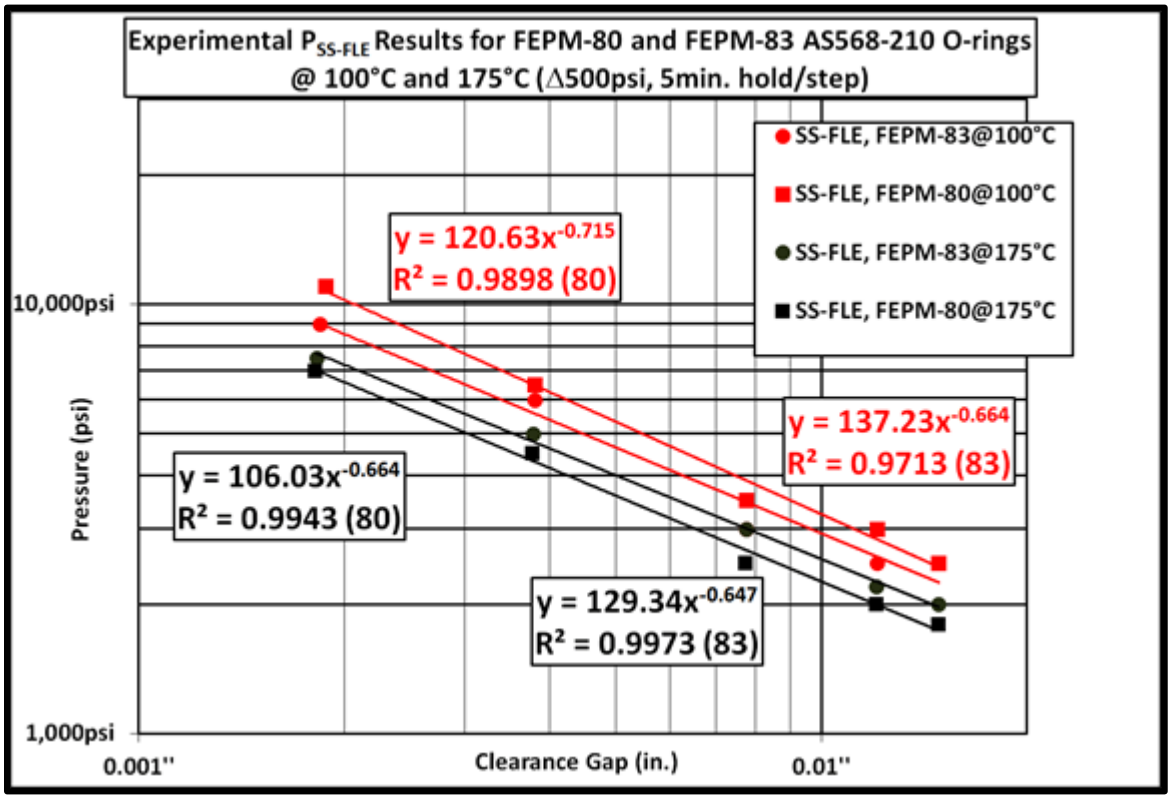


**Figure A.6-20** SS-FLE pressures versus clearance gaps for FEPM-80 and FEPM-83 @ 100°C and 175°C.

## A.6-5.3.5 FFKM- (FFKM)

**Table A.6-8 E-CTP and SS-FLE pressures versus clearance gaps for FFKM-75 and FFKM-90 @ 100°C and 175°C**

| E-CTP FFKM-75, FFKM-90 | | | | | | | | |
|---|---|---|---|---|---|---|---|---|
| Nominal Clearance Gap (in.) @ 25°C | Clearance Gap (in.) @ 100°C | E-CTP (psi), FFKM-75 @ 100°C | Clearance Gap (in.) @ 100°C | E-CTP (psi), FFKM-90 | Clearance Gap (in.) @175°C | E-CTP (psi), FFKM-75 @175°C | Clearance Gap (in.) @175°C | E-CTP (psi), FFKM-90 @ 175°C |
| 0.0148 | 0.0148336 | 2,100 | 0.014856 | 3,500 | 0.0148256 | 1,600 | 0.014824 | 1,500 |
| 0.012 | 0.01204 | 2,500 | 0.0120576 | 3,600 | 0.012028 | 1,750 | 0.0120256 | 1,600 |
| 0.0077 | 0.07756 | 3,500 | 0.07772 | 4,500 | 0.07736 | 2,250 | 0.07732 | 2,000 |
| 0.0037 | 0.0378 | 5,000 | 0.03796 | 6,000 | 0.03752 | 3,250 | 0.03748 | 3,000 |
| 0.0017 | 0.01792 | 5,750 | 0.0186 | 10,000 | 0.01772 | 4,500 | 0.01756 | 3,500 |
| **SS-FLE FFKM-75, FFKM-90** | | | | | | | | |
| Nominal Clearance Gap (in.) @ 25°C | Clearance Gap (in.) @ 100°C | SS-FLE (psi), FFKM-75 @ 100°C | Clearance Gap (in.) @ 100°C | SS-FLE (psi), FFKM-90 @ 100°C | Clearance Gap (in.) @175°C | SS-FLE (psi), FFKM-75 @175°C | Clearance Gap (in.) @ 175°C | SS-FLE (psi), FFKM-90 @ 175°C |
| 0.0148 | 0.01484 | 2,500 | 0.014896 | 6,000 | 0.01484 | 2,500 | 0.014848 | 3,000 |
| 0.012 | 0.012056 | 3,500 | 0.01212 | 7,500 | 0.012048 | 3,000 | 0.012048 | 3,000 |
| 0.0077 | 0.07804 | 6,500 | 0.07868 | 10,500 | 0.0778 | 5,000 | 0.07764 | 4,000 |
| 0.0037 | 0.03972 | 17,000 | 0.041 | 25,000 | 0.0386 | 10,000 | 0.038248 | 7,800 |
| 0.0017 | 0.017 | Use Power law | 0.017 | Use Power law | 0.01996 | 18,500 | 0.01908 | 13,000 |

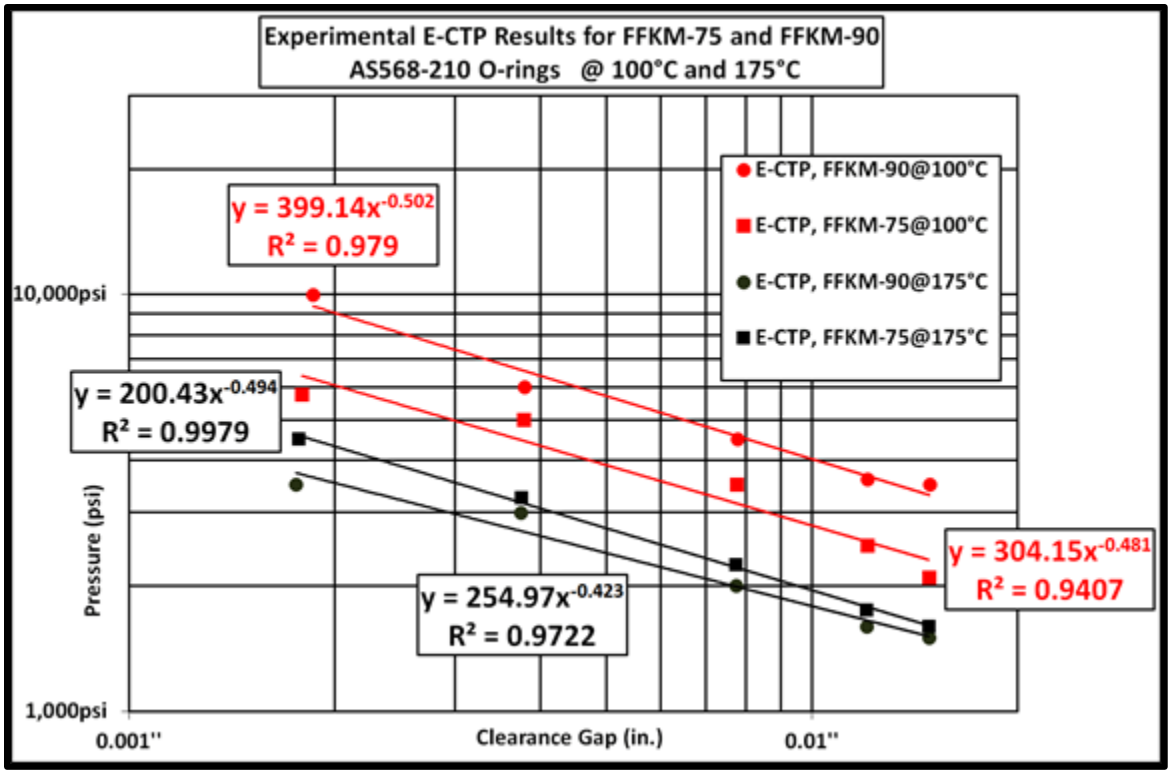


**Figure A.6-21** E-CTP versus clearance gaps for FFKM-75 and FFKM-90 @ 100°C and 175°C. Unlike all other materials tested, in terms of E-CTP, the low-durometer FFKM-75 slightly outperforms the high-durometer FFKM-90 at 175°C.

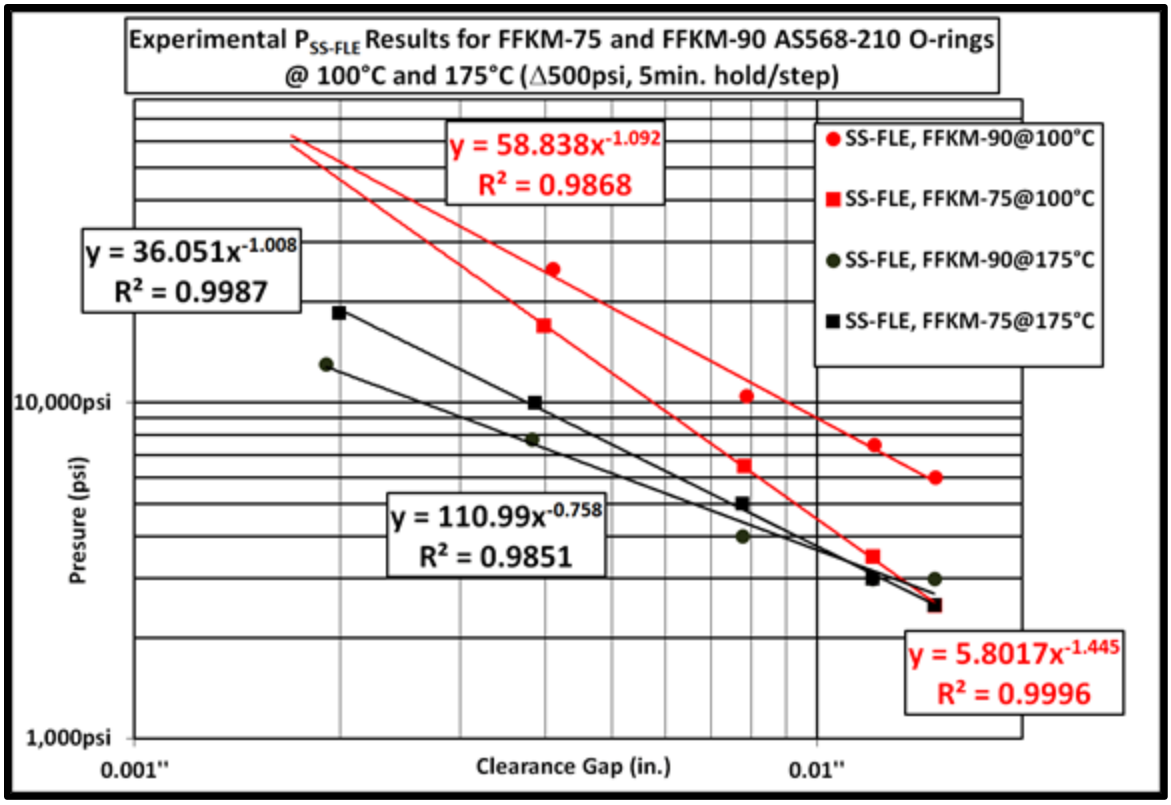


**Figure A.6-22** SS-FLE pressures versus clearance gaps for FFKM-75 and FFKM-90 @ 100°C & 175°C. Unlike all other materials tested, in terms of SS-FLE, the low-durometer FFKM-75 slightly outperforms the high-durometer FFKM-90 at 175°C.

## A.6-6 Cross-Material Plots of Critical Tear Pressures

The following charts summarize the different material O-rings based on their E-CTP levels for different temperatures and durometers. The testing was conducted according to the test conditions outlined in Figure A.6-6 (HPHT dwell test profile per the D100511 procedure) for a single-cycle Dwell test and new O-rings. The ability of the O-rings' material to resist tear may be affected by different factors that could alter their relative ranking, e.g. duration of exposure to temperature and pressure, aging and load prehistory, including Mullins effect, HPHT cycling, etc.

### *A.6-6.1 E-CTP Ranking @ 100°C, Durometer <83*

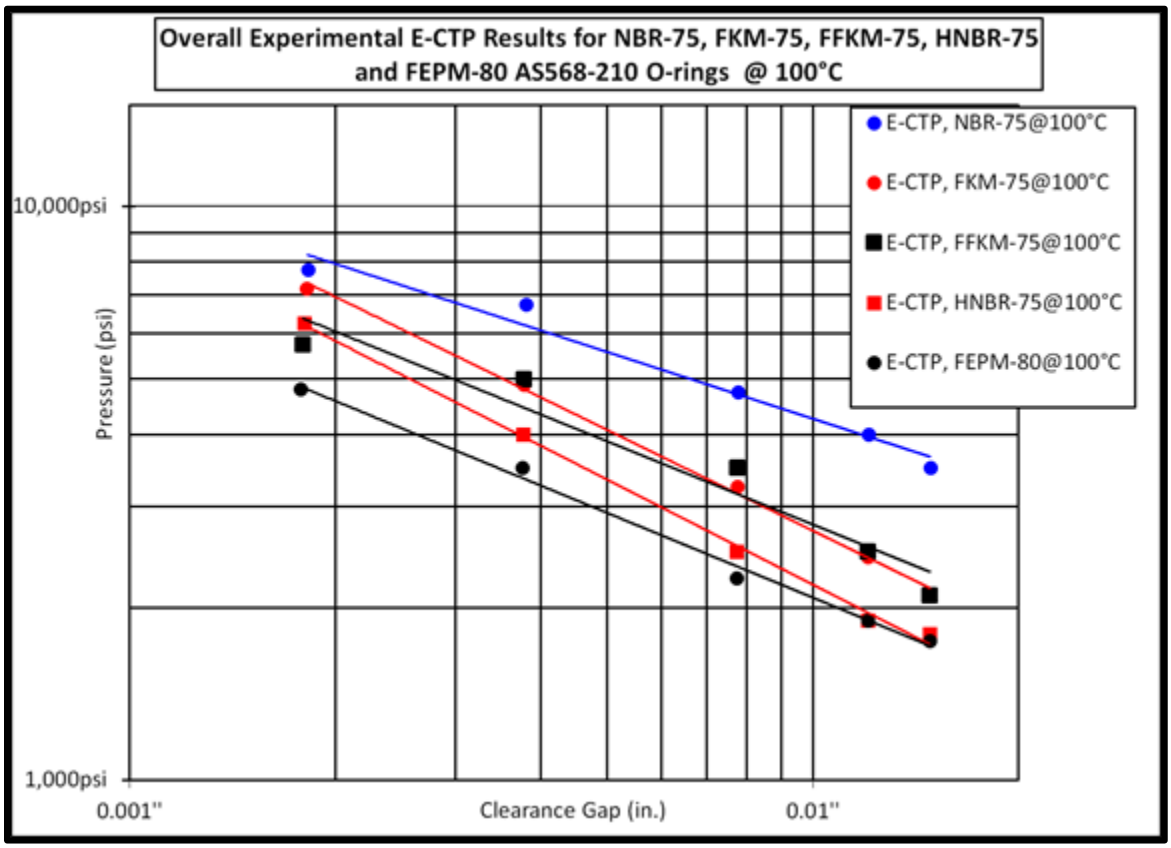


**Figure A.6-23** Critical Tear Pressure ranking for O-rings with Durometer <83 @ 100°C. The legend lists all materials in the descending E-CTP order.

### *A.6-6.2 E-CTP Ranking at 100°C, Durometer =90*

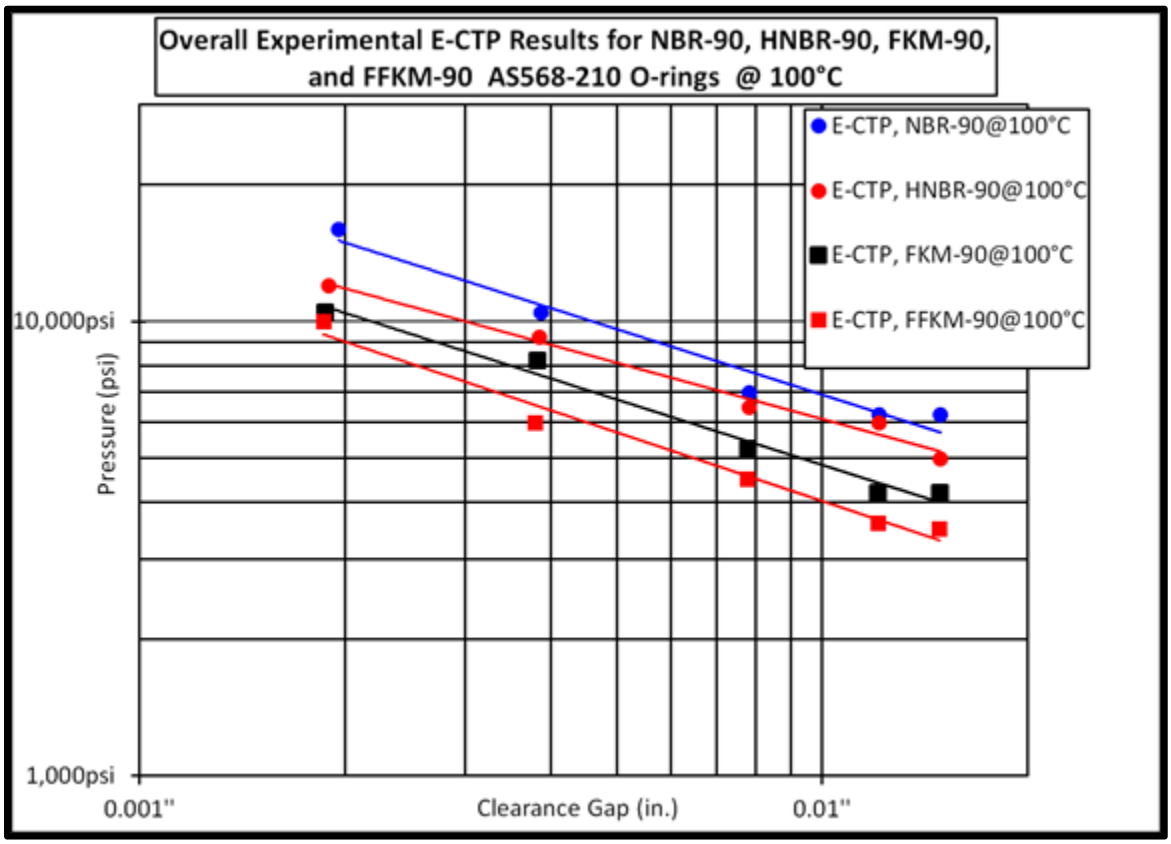


**Figure A.6-24** Critical Tear Pressure ranking for O-rings with Durometer =90 @ 100°C. The legend lists all materials in the descending E-CTP order.

### *A.6-6.3 E-CTP Ranking at 150°C & 175°C, Durometer <83*

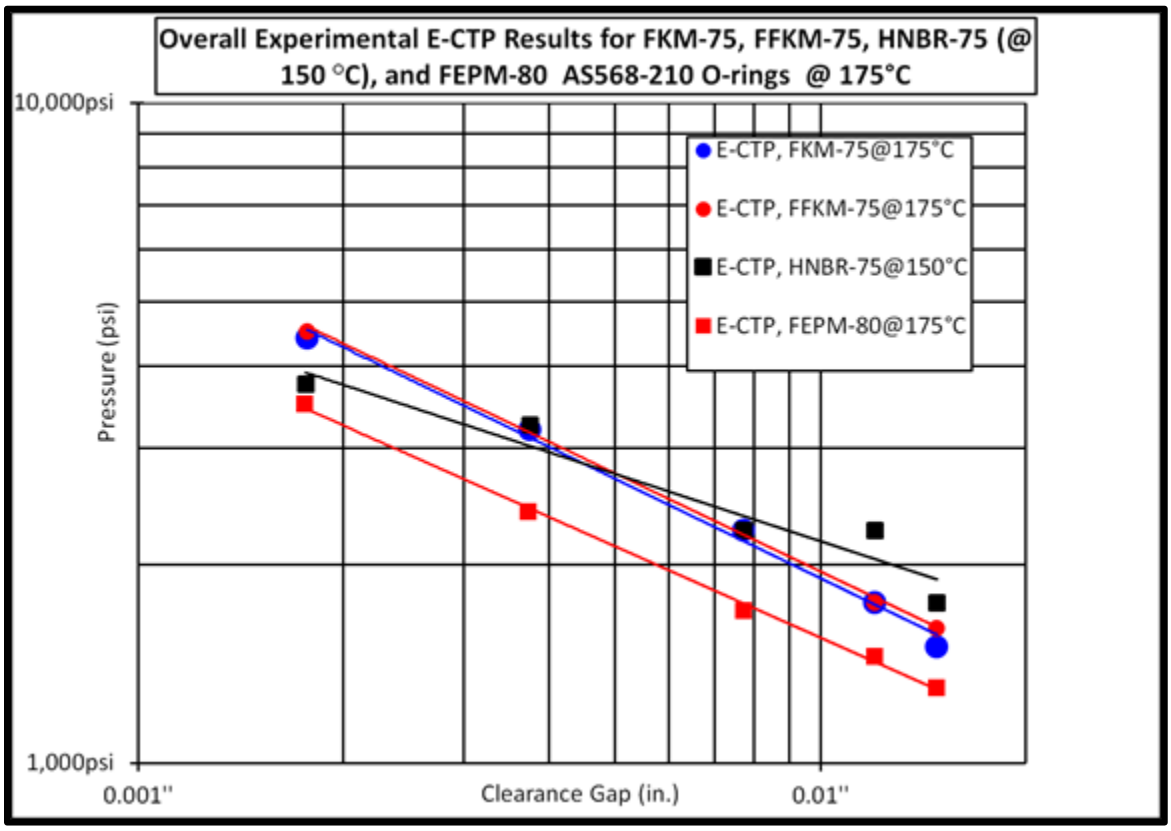


**Figure A.6-25** Critical Tear Pressure ranking for O-rings with Durometer <83 @ 150°C & 175°C.

The legend lists all materials in the descending E-CTP order.

### A.6-6.4 E-CTP Ranking at 150°C & 175°C, Durometer=90

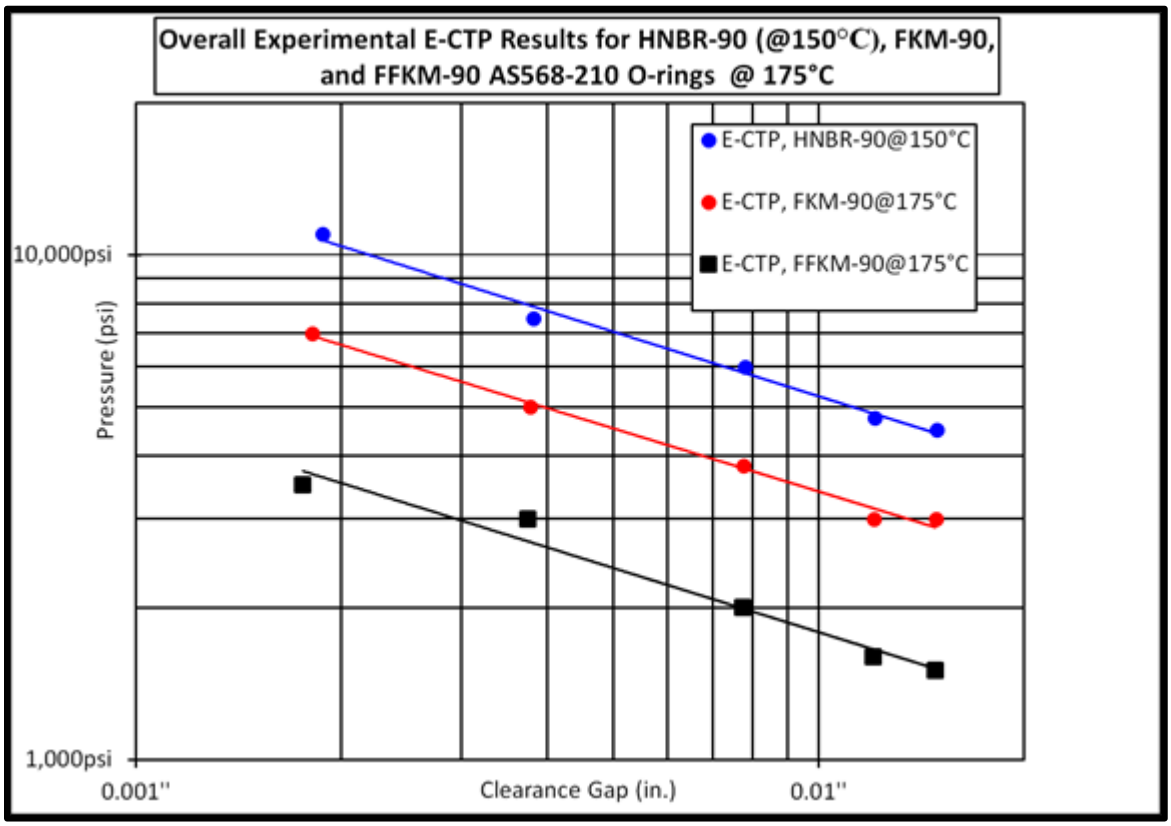


**Figure A.6-26** Critical Tear Pressure ranking for O-rings with Durometer =90 @ 150°C & 175°C.

The legend lists all materials in the descending E-CTP order.

### A.6-6.5 E-CTP-based Relative Material Ranking

Figure A.6-27 plots Critical Tear Pressure for all materials tested versus temperature. The E-CTP values are based on the power regression coefficients for clearance of 0.002". The plot's legend lists the materials in descending E-CTP@100°C order with NBR-90 on the top of the list with E-CTP=15,000 psi and FEPM-83 on the bottom with just 4,000 psi.

As expected, for all materials, their E-CTP levels decrease as temperature increases from 100°C to 175°C.

The most interesting temperature dependence is observed for FFKM-75 and FFKM-90 (black lines): The 90 durometer version has the highest rate of the E-CTP drop in the temperature range from 100°C to 175°C (~60%), while the 75 durometer version is in-line with other materials and its E-CTP decreases by only 29%. As a result, FFKM-75 slightly outperforms FFKM-90 at the highest temperature tested of 175°C.

For all other materials, their E-CTP ratings are always higher for the higher durometer versions. It is appropriate to mention here that the actual average durometer of FEPM-80 samples is 89,

while the FEPM-83 batch has average durometer of 83. This likely explains why FEPM-80 has a slightly higher E-CTP rating than FEPM-83.

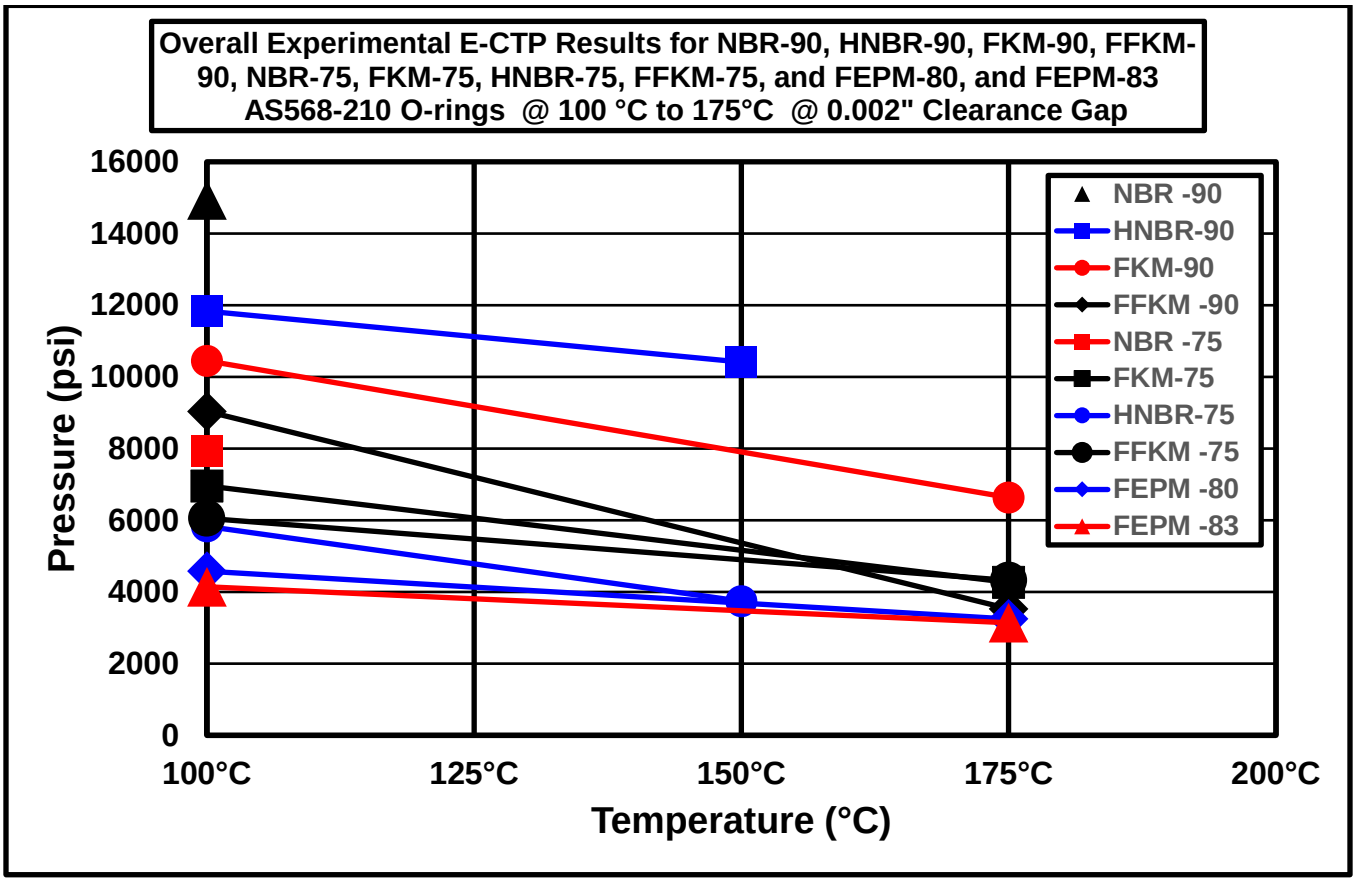


**Figure A.6-27** Critical Tear Pressures versus temperature for a 0.002” clearance gap. The legend lists all materials in the descending E-CTP order.

# A.6-7 Appendix A: Test Data Tables and Charts

The following subparagraphs summarize the results of all extrusion tests conducted with all O-ring materials and five pistons.

## *A.6-7.1 FKM*

### A.6-7.1.1 FKM-75 @ 100°C

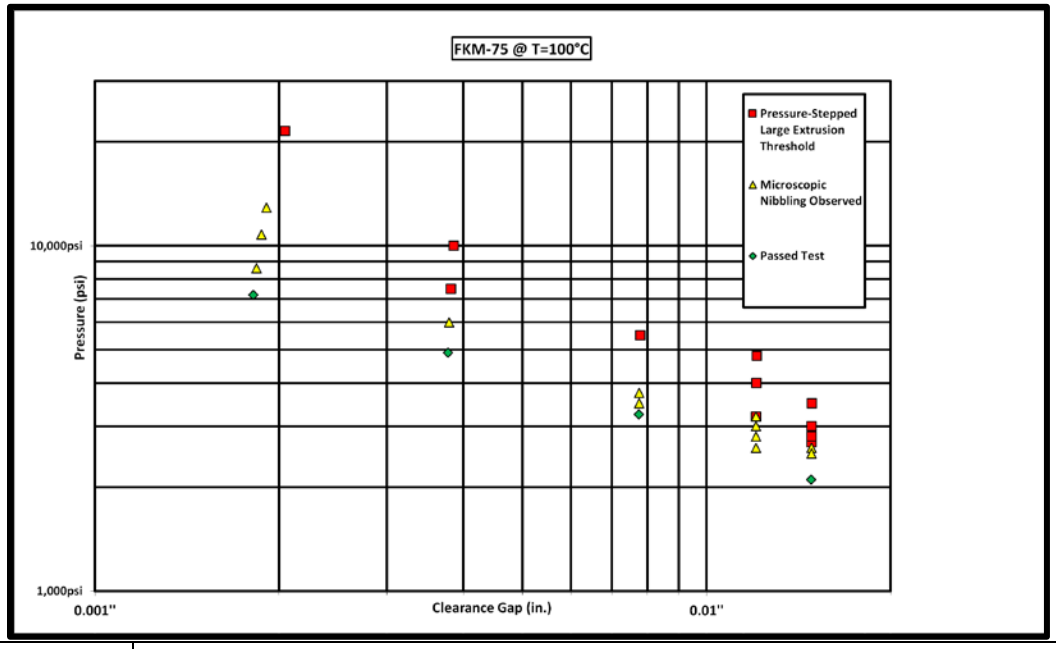


| | FKM-75, T= 100°C, (Piston Size / Clearance Gap) | | | | |
|---|---|---|---|---|---|
| | #50/0.015" | #40/0.012" | #30/0.008" | #20/0.004" | #10/0.002" |
| O-Ring # | 56 | 62 | 68 | 74 | 80 |
| Pressure (psi) | 3,500 | 4,000 | 5,500 | 10,000 | 21,500 |
| O-Ring # | 57 | 63 | 69 | 75 | 81 |
| Pressure (psi) | 2,700 | 4,800 | nt | nt | 10,750 |
| O-Ring # | 58 | 64 | 70 | 76 | 82 |
| Pressure (psi) | 2,100 | 3,000 | 3,750 | 7,500 | 12,900 |
| O-Ring # | 59 | 65 | 71 | 77 | 83 |
| Pressure (psi) | 2,600 | 3,200 | 3,500 | 6,000 | 10,750 |
| O-Ring # | 60 | 66 | 72 | 78 | 84 |
| Pressure (psi) | 3,000 | 3,200 | 3,250 | 6,000 | 8,600 |
| O-Ring # | 61 | 67 | 73 | 79 | 85 |
| Pressure (psi) | 2,800 | 2,800 | nt | 4,900 | 7,200 |

**Figure A.6-28** Test data plot (top) and table (bottom) for FKM-75 @ 100°C. Data points only.

### A.6-7.1.2 FKM-75 @ 175°C

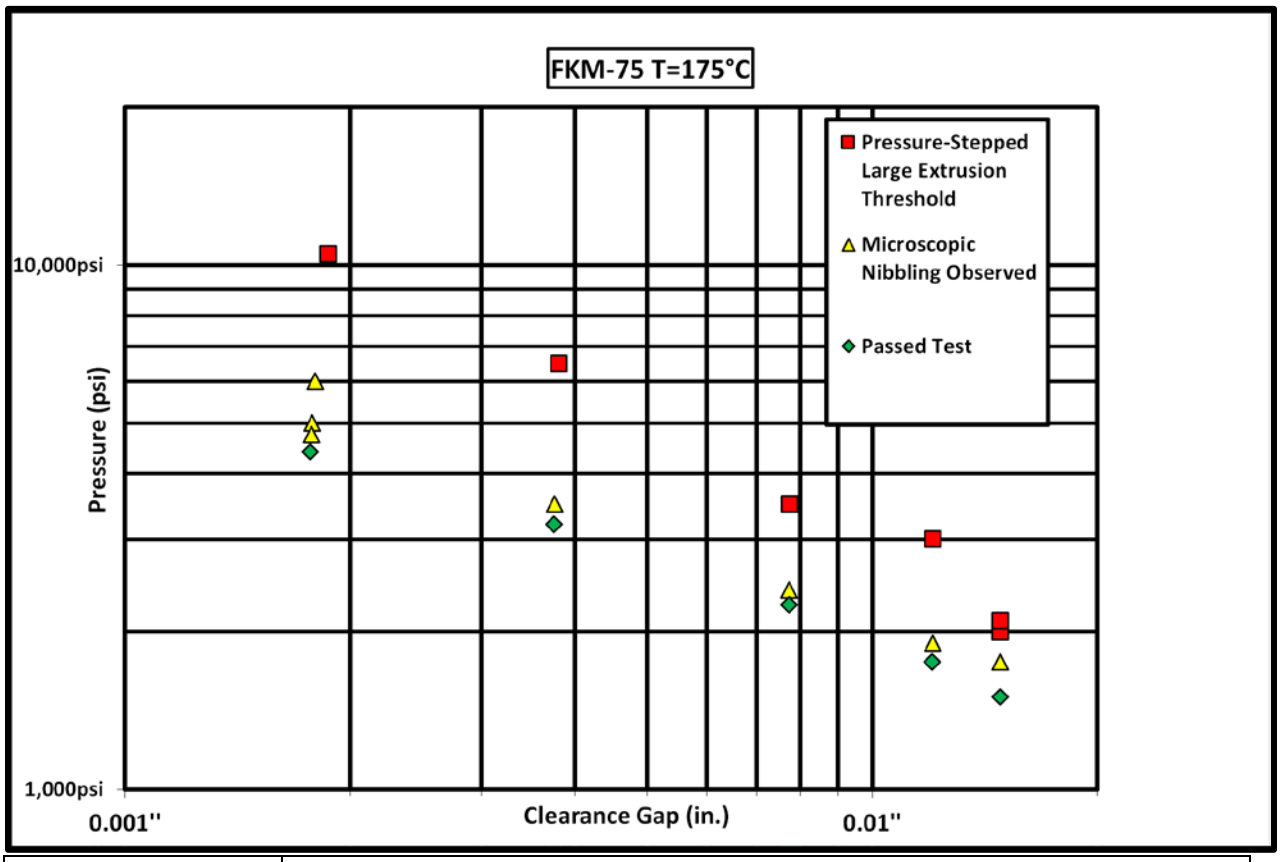


| | FKM-75, T= 175°C, (Piston Size / Clearance Gap) | | | | |
|---|---|---|---|---|---|
| | #50/0.015" | #40/0.012" | #30/0.008" | #20/0.004" | #10/0.002" |
| O-Ring # | 090 | 096 | 102 | 108 | 114 |
| Pressure (psi) | 2,000 | 3,000 | 3,500 | 6,500 | 10,500 |
| O-Ring # | 091 | 097 | 103 | 109 | 115 |
| Pressure (psi) | nt | nt | nt | nt | nt |
| O-Ring # | 092 | 098 | 104 | 110 | 116 |
| Pressure (psi) | 1500 | 1750 | 2400 | 3500 | 6000 |
| O-Ring # | 093 | 099 | 105 | 111 | 117 |
| Pressure (psi) | 2100 | 1900 | 2250 | 3200 | 5000 |
| O-Ring # | 094 | 100 | 106 | 112 | 118 |
| Pressure (psi) | 1750 | nt | nt | nt | 4750 |
| O-Ring # | 095 | 101 | 107 | 113 | 119 |
| Pressure (psi) | nt | nt | nt | nt | 4400 |

**Figure A.6-29** Test data plot (top) and table (bottom) for FKM-75 @ 175°C. Data points only. No regression lines are included.

### A.6-7.1.3 FKM-90 @ 100°C

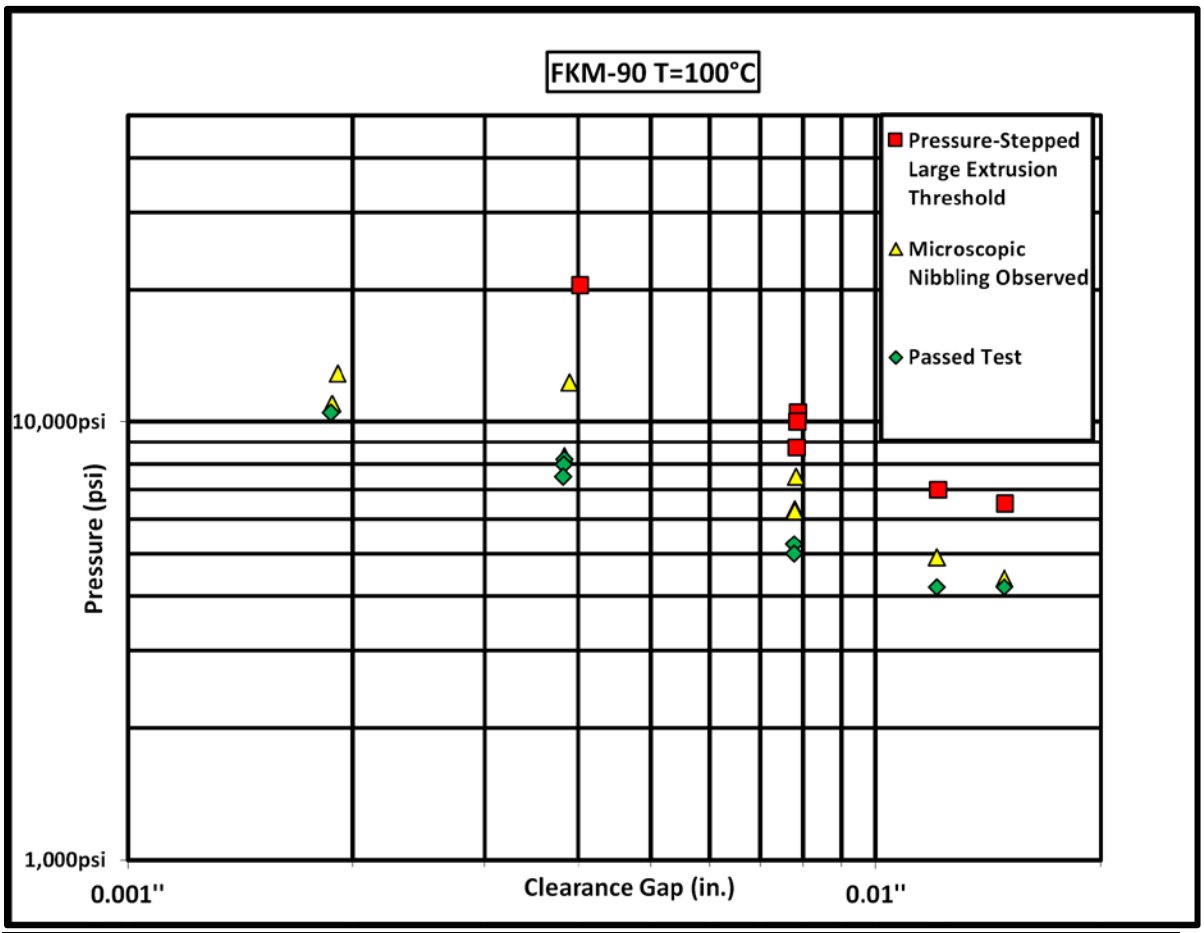


| | FKM-90, T= 100°C, (Piston Size / Clearance Gap) | | | | |
|---|---|---|---|---|---|
| | #50/0.015" | #40/0.012" | #30/0.008" | #20/0.004" | #10/0.002" |
| O-Ring # | 56 | 62 | 68 | 74 | 80 |
| Pressure (psi) | 8,500 | 7,000 | 10,500 | 20,500 | 25,000 |
| O-Ring # | 57 | 63 | 69 | 75 | 81 |
| Pressure (psi) | nt | nt | nt | 8,350 | nt |
| O-Ring # | 58 | 64 | 70 | 76 | 82 |
| Pressure (psi) | 4,400 | 4,200 | 6,300 | 12,300 | 12,900 |
| O-Ring # | 59 | 65 | 71 | 77 | 83 |
| Pressure (psi) | 4,200 | 4,900 | 5,250 | 7,500 | 11,000 |
| O-Ring # | 60 | 66 | 72 | 78 | 84 |
| Pressure (psi) | nt | nt | nt | 8,000 | 10,500 |
| O-Ring # | 61 | 67 | 73 | 79 | 85 |
| Pressure (psi) | nt | nt | nt | 8,200 | nt |

**Figure A.6-30** Test data plot (top) and table (bottom) for FKM-90 @ 100°C. Data points only.

### A.6-7.1.4 FKM-90 @ 175°C

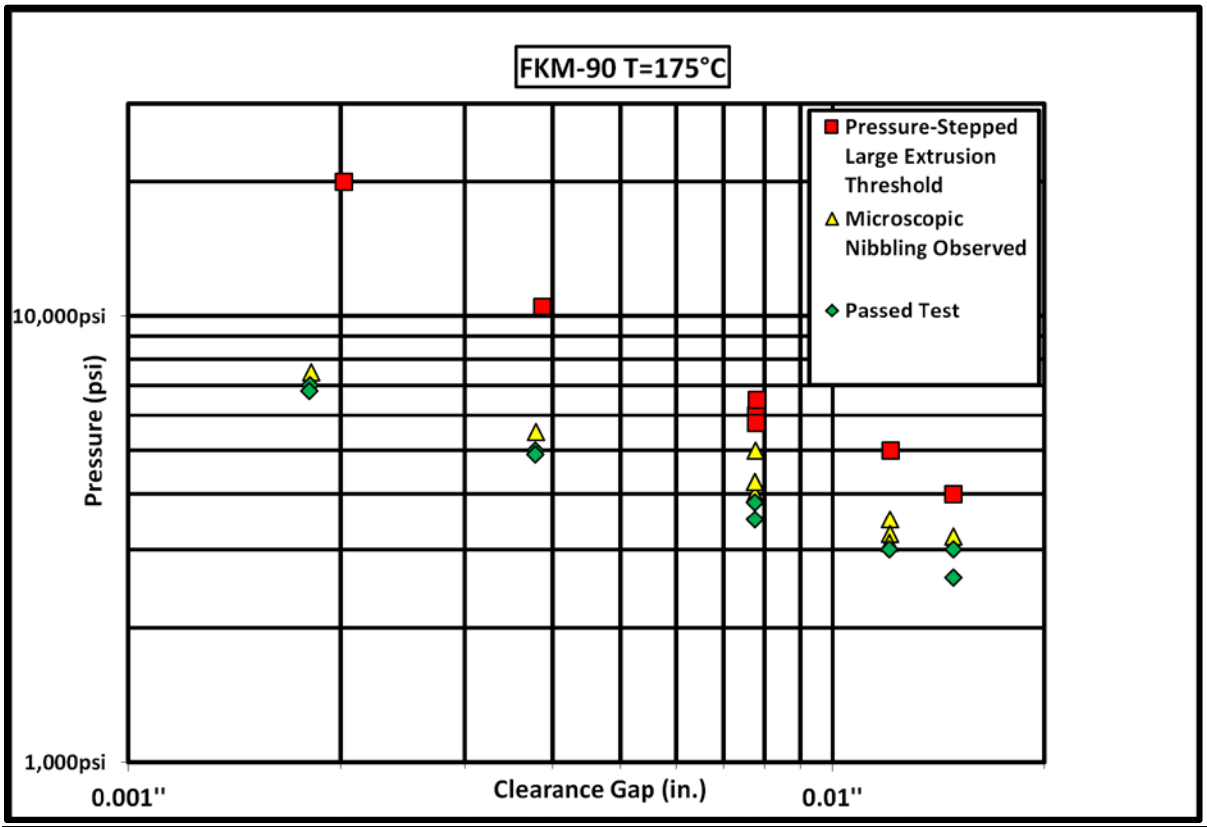


| | FKM-90, T= 175°C, (Piston Size / Clearance Gap) | | | | |
|---|---|---|---|---|---|
| | #50/0.015" | #40/0.012" | #30/0.008" | #20/0.004" | #10/0.002" |
| O-Ring # | 90 | 96 | 102 | 108 | 114 |
| Pressure (psi) | 4,000 | 5,000 | 5,000 | 10,500 | 20,000 |
| O-Ring # | 91 | 97 | 103 | 109 | 115 |
| Pressure (psi) | nt | nt | 3,825 | nt | nt |
| O-Ring # | 92 | 98 | 104 | 110 | 116 |
| Pressure (psi) | 2,600 | 3,500 | 4,250 | 5,000 | 7,480 |
| O-Ring # | 93 | 99 | 105 | 111 | 117 |
| Pressure (psi) | 3,000 | 3,250 | 4,000 | 5,500 | 7,000 |
| O-Ring # | 94 | 100 | 106 | 112 | 118 |
| Pressure (psi) | 3,200 | 3,100 | nt | 4,900 | 6,800 |
| O-Ring # | 95 | 101 | 107 | 113 | 119 |
| Pressure (psi) | nt | 3,000 | nt | nt | nt |

**Figure A.6-31** Test data plot (top) and table (bottom) for FKM-90 @ 175°C. Data points only.

## *A.6-7.2 NBR- (NBR)*

### A.6-7.2.1 NBR-75 @ 100°C

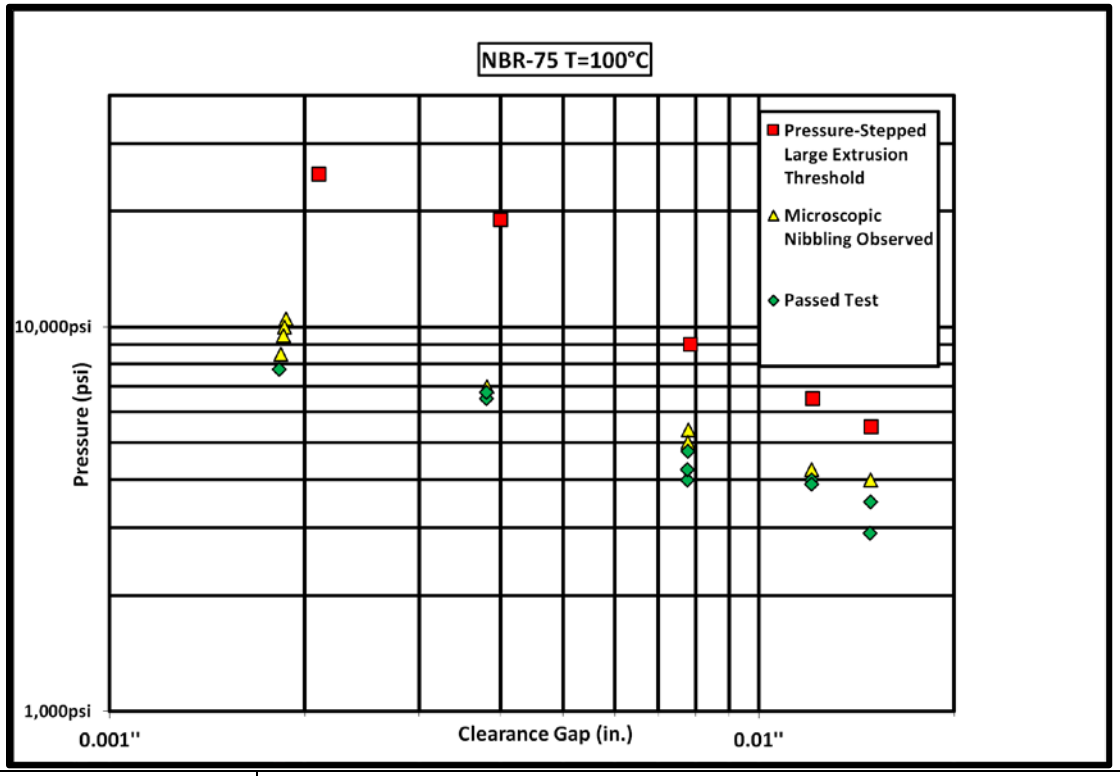


| | NBR-75, T= 100°C, (Piston Size / Clearance Gap) | | | | |
|---|---|---|---|---|---|
| | #50/0.015" | #40/0.012" | #30/0.008" | #20/0.004" | #10/0.002" |
| O-Ring # | 1 | 7 | 13 | 19 | 25 |
| Pressure (psi) | 5,500 | 6,500 | 9,000 | 19,000 | 25,000 |
| O-Ring # | 2 | 8 | 14 | 20 | 26 |
| Pressure (psi) | nt | nt | 5,000 | nt | 7,750 |
| O-Ring # | 3 | 9 | 15 | 21 | 27 |
| Pressure (psi) | 2,900 | 4,250 | 5,400 | 6,500 | 10,500 |
| O-Ring # | 4 | 10 | 16 | 22 | 28 |
| Pressure (psi) | 3,500 | 4,000 | 4,000 | 7,000 | 10,000 |
| O-Ring # | 5 | 11 | 17 | 23 | 29 |
| Pressure (psi) | 4,000 | 3,900 | 4,250 | 6,750 | 9,500 |
| O-Ring # | 6 | 12 | 18 | 24 | 30 |
| Pressure (psi) | nt | nt | 4,750 | nt | 8,500 |

**Figure A.6-32** Test data plot (top) and table (bottom) for NBR-75 @ 100°C. Data points only. No regression lines are included.

### A.6-7.2.2 NBR-90 @ 100°C

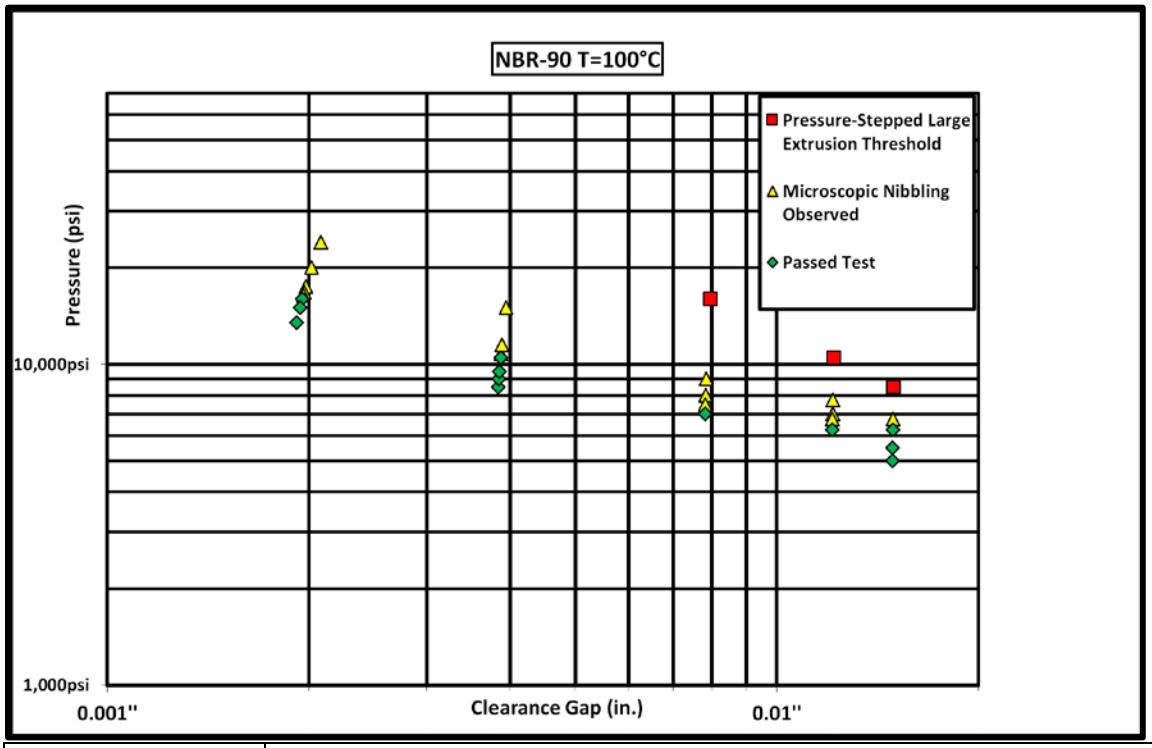


| | NBR-90, T= 100°C, (Piston Size / Clearance Gap) | | | | |
|---|---|---|---|---|---|
| | #50/0.015" | #40/0.012" | #30/0.008" | #20/0.004" | #10/0.002" |
| O-Ring # | 1 | 7 | 13 | 19 | 25 |
| Pressure (psi) | 8,500 | 10,500 | 16,000 | nt | nt |
| O-Ring # | 2 | 8 | 14 | 20 | 26 |
| Pressure (psi) | nt | nt | nt | 15,000 | 13,500 |
| O-Ring # | 3 | 9 | 15 | 21 | 27 |
| Pressure (psi) | 5,000 | 7,750 | 9,000 | 8,500 | 24,000 |
| O-Ring # | 4 | 10 | 16 | 22 | 28 |
| Pressure (psi) | 5,500 | 7,000 | 8,000 | 9,000 | 20,000 |
| O-Ring # | 5 | 11 | 17 | 23 | 29 |
| Pressure (psi) | 6,250 | 6,750 | 7,000 | 9,500 | 17,500 |
| O-Ring # | 6 | 12 | 18 | 24 | 30 |
| Pressure (psi) | 6,750 | 6,250 | 7,500 | 10500 | 15,000 |

**Figure A.6-33** Test data plot (top) and table (bottom) for NBR-90 @ 100°C. Data points only. No regression lines are included.

## *A.6-7.3 HNBR*

### A.6-7.3.1 HNBR-75 @ 100°C

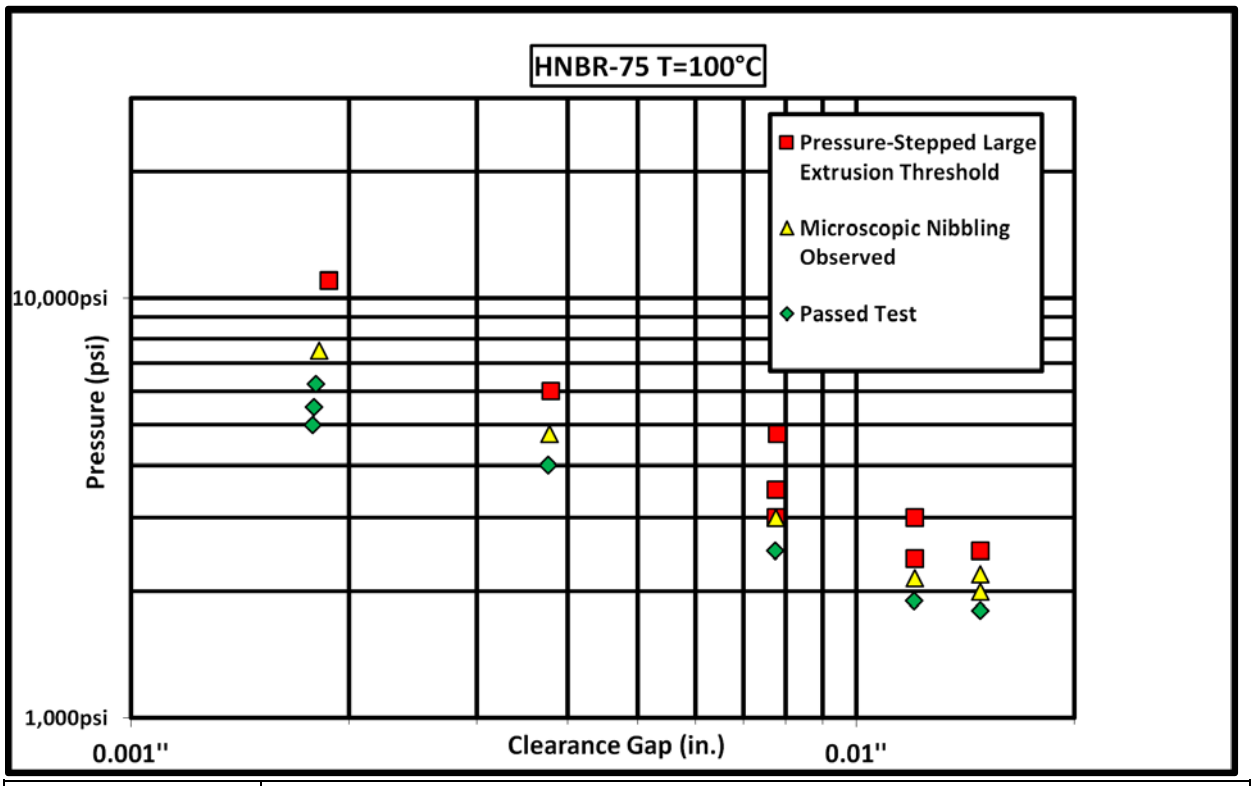


| | HNBR-75, T= 100°C, (Piston Size / Clearance Gap) | | | | |
|---|---|---|---|---|---|
| | #50/0.015" | #40/0.012" | #30/0.008" | #20/0.004" | #10/0.002" |
| O-Ring # | 1 | 7 | 13 | 19 | 25 |
| Pressure (psi) | 2,500 | 3,000 | 3,000 | 6,000 | 11,000 |
| O-Ring # | 2 | 8 | 14 | 20 | 26 |
| Pressure (psi) | nt | nt | 3,500 | nt | nt |
| O-Ring # | 3 | 9 | 15 | 21 | 27 |
| Pressure (psi) | 2,000 | 2,150 | 4,750 | 4,000 | 5,000 |
| O-Ring # | 4 | 10 | 16 | 22 | 28 |
| Pressure (psi) | 2,200 | 2,400 | 2,500 | 4,750 | 5,500 |
| O-Ring # | 5 | 11 | 17 | 23 | 29 |
| Pressure (psi) | 1,800 | 1,900 | 3,000 | nt | 6,250 |
| O-Ring # | 6 | 12 | 18 | 24 | 30 |
| Pressure (psi) | nt | nt | nt | nt | 7,500 |

**Figure A.6-34** Test data plot (top) and table (bottom) for HNBR-75 @ 100°C. Data points only. No regression lines are included.

### A.6-7.3.2 HNBR-75 @ 150°C

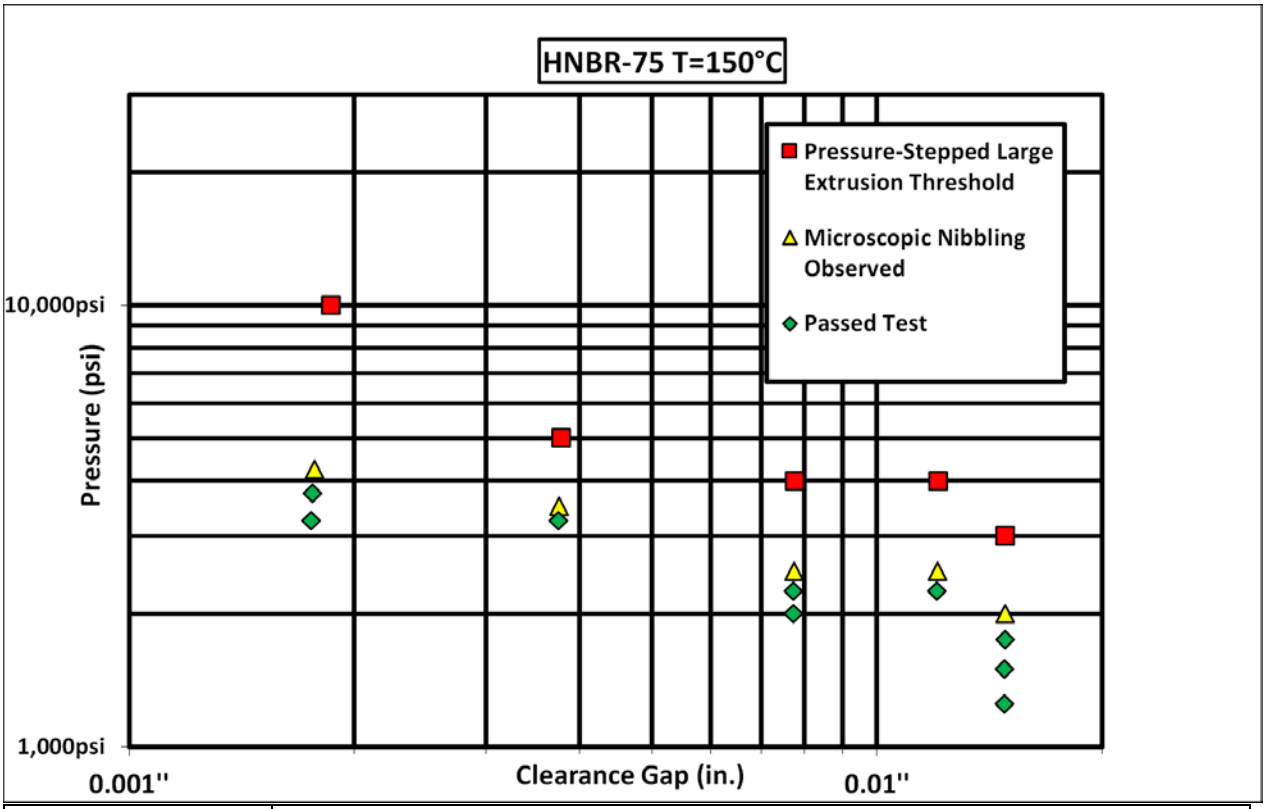


| | HNBR-75, T= 175°C, (Piston Size / Clearance Gap) | | | | |
|---|---|---|---|---|---|
| | #50/0.015" | #40/0.012" | #30/0.008" | #20/0.004" | #10/0.002" |
| O-Ring # | 50 | 56 | 62 | 68 | 74 |
| Pressure (psi) | 3,000 | 4,000 | 4,000 | 5,000 | 10,000 |
| O-Ring # | 51 | 57 | 63 | 69 | 75 |
| Pressure (psi) | nt | nt | nt | nt | nt |
| O-Ring # | 52 | 58 | 64 | 70 | 76 |
| Pressure (psi) | 1,250 | 2,250 | 2,000 | 3,250 | 3,250 |
| O-Ring # | 53 | 59 | 65 | 71 | 77 |
| Pressure (psi) | 1,500 | 2,500 | 2,250 | 3,500 | 3,750 |
| O-Ring # | 54 | 60 | 66 | 72 | 78 |
| Pressure (psi) | 1,750 | nt | 2,500 | 3,500 | 4,250 |
| O-Ring # | 55 | 61 | 67 | 73 | 79 |
| Pressure (psi) | 2,000 | nt | nt | nt | nt |

**Figure A.6-35** Test data plot (top) and table (bottom) for HNBR-75 @ 175°C. Data points only. No regression lines are included.

### A.6-7.3.3 HNBR-90 @ 100°C

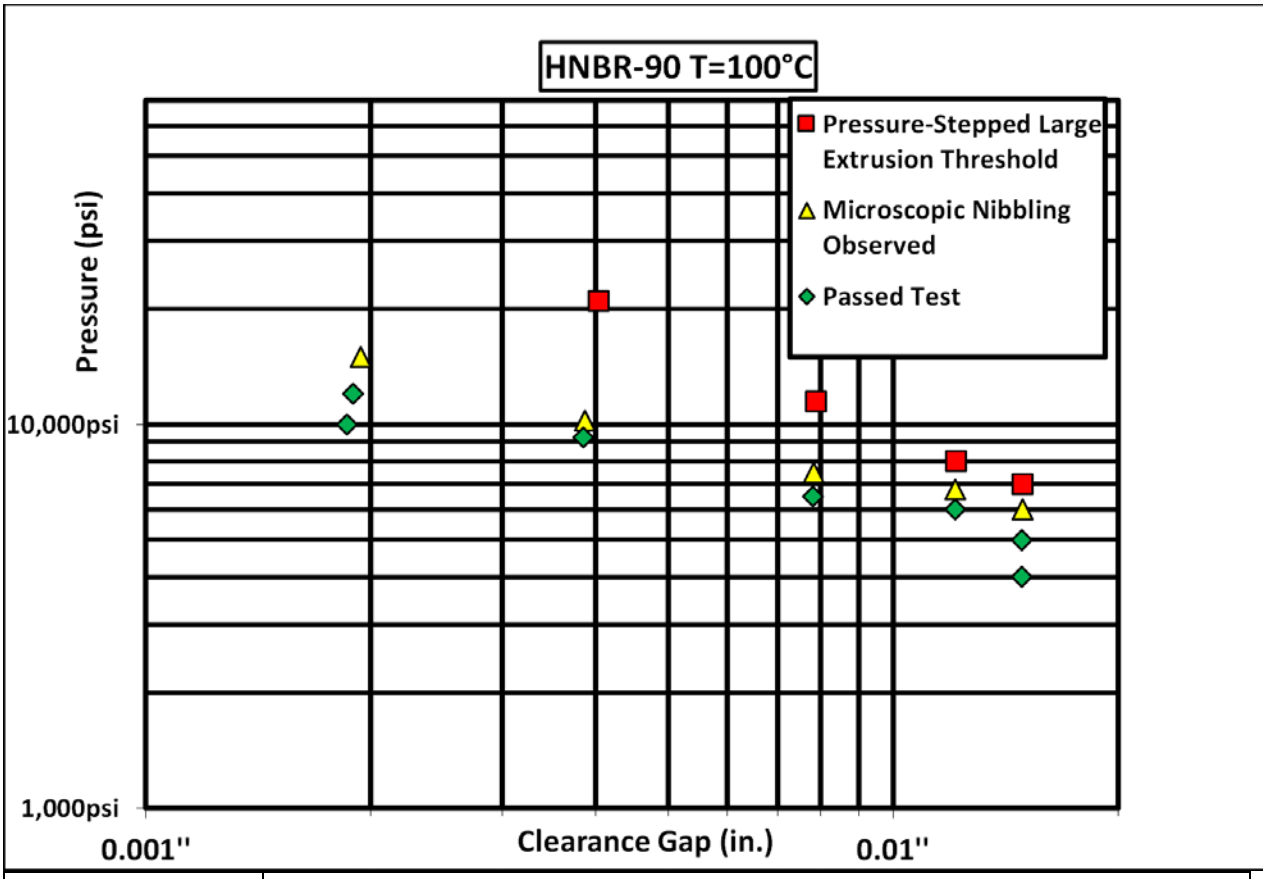


| | HNBR-90, T= 100°C, (Piston Size / Clearance Gap) | | | | |
|---|---|---|---|---|---|
| | #50/0.015" | #40/0.012" | #30/0.008" | #20/0.004" | #10/0.002" |
| O-Ring # | 1 | 7 | 13 | 19 | 25 |
| Pressure (psi) | 7,000 | 8,000 | 11,500 | 21,000 | nt |
| O-Ring # | 2 | 8 | 14 | 20 | 26 |
| Pressure (psi) | nt | nt | nt | nt | nt |
| O-Ring # | 3 | 9 | 15 | 21 | 27 |
| Pressure (psi) | 4,000 | 6,750 | 7,500 | 10,250 | 10,000 |
| O-Ring # | 4 | 10 | 16 | 22 | 28 |
| Pressure (psi) | 5,000 | 6,000 | 6,500 | 9,250 | 15,000 |
| O-Ring # | 5 | 11 | 17 | 23 | 29 |
| Pressure (psi) | 6,000 | nt | nt | nt | 12,000 |
| O-Ring # | 6 | 12 | 18 | 24 | 30 |
| Pressure (psi) | nt | nt | nt | nt | nt |

**Figure A.6-36** Test data plot (top) and table (bottom) for HNBR-90 @ 100°C. Data points only. No regression lines are included.

### A.6-7.3.4 HNBR-90 @ 150°C

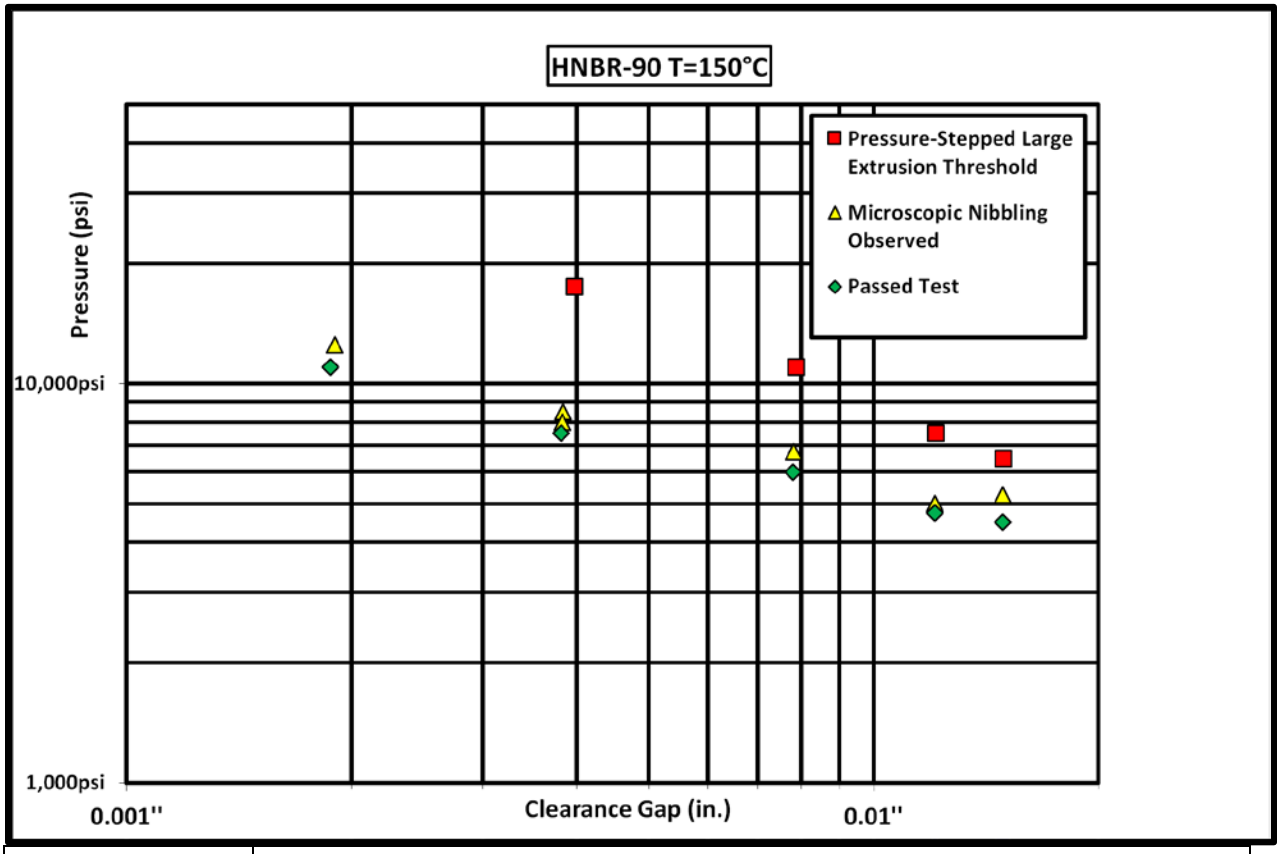


| | HNBR-90, T= 150°C, (Piston Size / Clearance Gap) | | | | |
|---|---|---|---|---|---|
| | #50/0.015" | #40/0.012" | #30/0.008" | #20/0.004" | #10/0.002" |
| O-Ring # | 50 | 56 | 62 | 68 | 74 |
| Pressure (psi) | 6,500 | 7,500 | 11,000 | 17,500 | nt |
| O-Ring # | 51 | 57 | 63 | 69 | 75 |
| Pressure (psi) | nt | nt | nt | nt | nt |
| O-Ring # | 52 | 58 | 64 | 70 | 76 |
| Pressure (psi) | 4,500 | 5,000 | 6,750 | 8,500 | 11,000 |
| O-Ring # | 53 | 59 | 65 | 71 | 77 |
| Pressure (psi) | 5,250 | 4,750 | 6,000 | 8,000 | 12,500 |
| O-Ring # | 54 | 60 | 66 | 72 | 78 |
| Pressure (psi) | nt | nt | nt | 7,500 | nt |
| O-Ring # | 55 | 61 | 67 | 73 | 79 |
| Pressure (psi) | nt | nt | nt | nt | nt |

**Figure A.6-37** Test data plot (top) and table (bottom) for HNBR-90 @ 175°C. Data points only.

## A.6-7.4 FEPM

### A.6-7.4.1 FEPM-80 @ 100°C

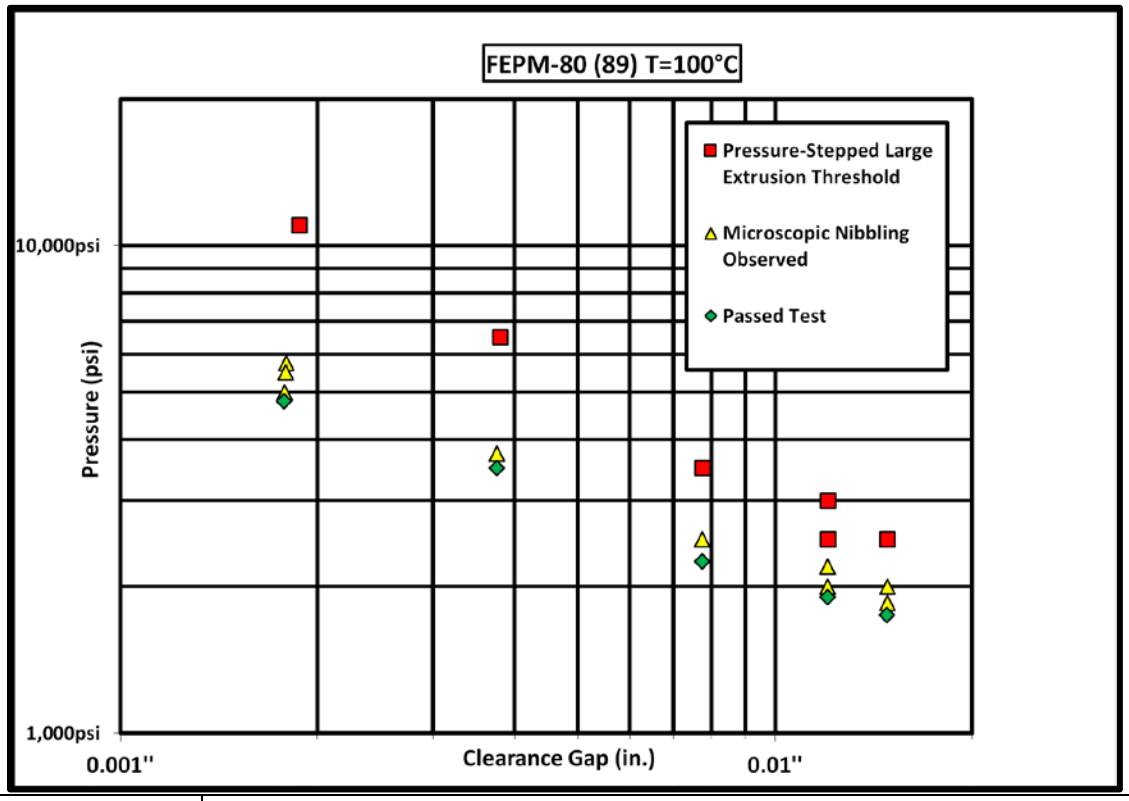


| | FEPM-80 (89), T= 100°C, (Piston Size / Clearance Gap) | | | | |
|---|---|---|---|---|---|
| | #50/0.015" | #40/.012" | #30/.008" | #20/0.004" | #10/0.002" |
| O-Ring # | 1 | 2 | 13 | 19 | 25 |
| Pressure (psi) | 2,500 | 2,500 | 3,500 | 6,500 | 11,000 |
| O-Ring # | 7 | 8 | 14 | 20 | 26 |
| Pressure (psi) | 2,500 | 3,000 | nt | nt | nt |
| O-Ring # | 3 | 9 | 15 | 21 | 27 |
| Pressure (psi) | 2,000 | 2,200 | 2,500 | 3,500 | 5,750 |
| O-Ring # | 4 | 10 | 16 | 22 | 28 |
| Pressure (psi) | 1,850 | 2,000 | 2,250 | 3,750 | 5,500 |
| O-Ring # | 5 | 11 | 17 | 23 | 29 |
| Pressure (psi) | 1,750 | 1,900 | nt | nt | 5,000 |
| O-Ring # | 6 | 12 | 18 | 24 | 30 |
| Pressure (psi) | nt | nt | nt | nt | 4,800 |

**Figure A.6-38** Test data plot (top) and table (bottom) for FEPM-80 (89) @ 100°C. Data points only. No regression lines are included.

## A.6-7.4.2 FEPM-80 @ 175°C

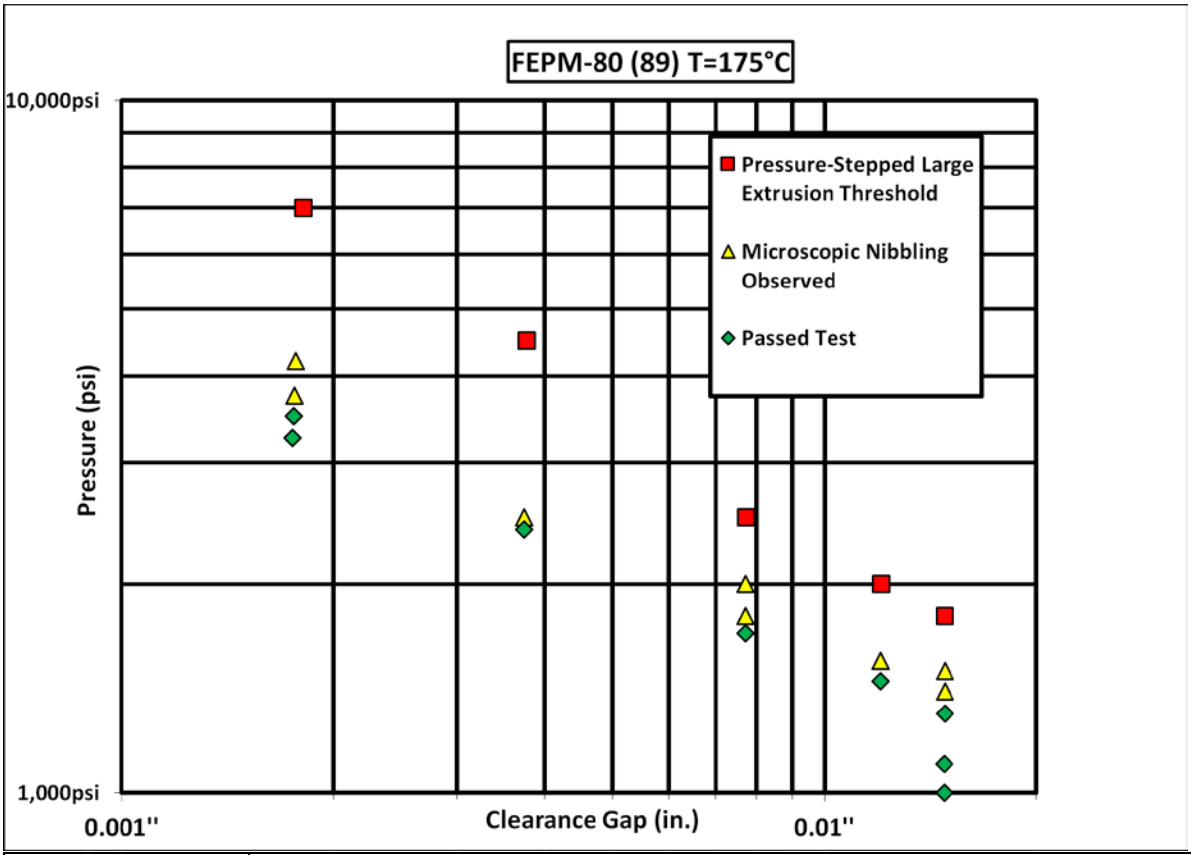


| | FEPM-80 (89), T= 175°C, (PistonSize / Clearance Gap) | | | | |
|---|---|---|---|---|---|
| | #50/0.015" | #40/0.012" | #30/0.008" | #20/0.004" | #10/0.002" |
| O-Ring # | 50 | 56 | 62 | 68 | 74 |
| Pressure (psi) | 1,800 | 2,000 | 2,500 | 4,500 | 7,000 |
| O-Ring # | 51 | 57 | 63 | 69 | 75 |
| Pressure (psi) | 1,400 | nt | nt | nt | nt |
| O-Ring # | 52 | 58 | 64 | 70 | 76 |
| Pressure (psi) | 1,000 | 1,450 | 2,000 | 2,400 | 4,200 |
| O-Ring # | 53 | 59 | 65 | 71 | 77 |
| Pressure (psi) | 1,100 | 1,550 | 1,800 | 2,500 | 3,250 |
| O-Ring # | 54 | 60 | 66 | 72 | 78 |
| Pressure (psi) | 1,300 | nt | 1,700 | nt | 3,500 |
| O-Ring # | 55 | 61 | 67 | 73 | 79 |
| Pressure (psi) | 1,500 | nt | nt | nt | 3,750 |

**Figure A.6-39** Test data plot (top) and table (bottom) for FEPM-80 (89) @ 175°C. Data points only. No regression lines are included.

### A.6-7.4.3 FEPM-83 @ 100°C

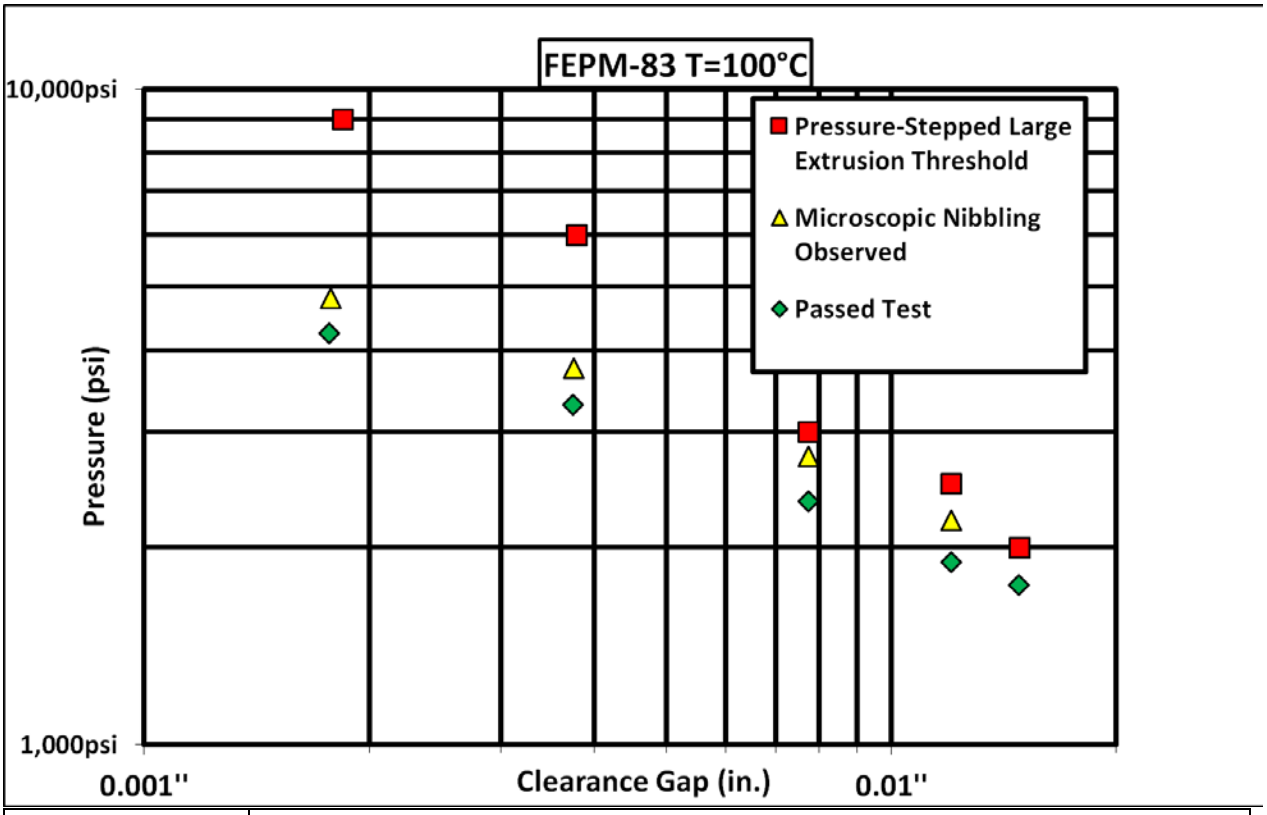


| | FEPM-83, T= 100°C, (Piston Size / Clearance Gap) | | | | |
|---|---|---|---|---|---|
| | #50/0.015" | #40/0.012" | #30/0.008" | #20/0.004" | #10/0.002" |
| O-Ring # | 1 | 7 | 13 | 19 | 25 |
| Pressure (psi) | 2,000 | 2,500 | 3,000 | 6000 | 9,000 |
| O-Ring # | 2 | 8 | 14 | 20 | 26 |
| Pressure (psi) | nt | nt | nt | nt | nt |
| O-Ring # | 3 | 9 | 15 | 21 | 27 |
| Pressure (psi) | 1,750 | 1,900 | 2,350 | 3,300 | 4,800 |
| O-Ring # | 4 | 10 | 16 | 22 | 28 |
| Pressure (psi) | 2,000 | 2,200 | 2,750 | 3,750 | 4,250 |
| O-Ring # | 5 | 11 | 17 | 23 | 29 |
| Pressure (psi) | nt | nt | nt | nt | nt |
| O-Ring # | 6 | 12 | 18 | 24 | 30 |
| Pressure (psi) | nt | nt | nt | nt | nt |

**Figure A.6-40** Test data plot (top) and table (bottom) for FEPM-83 @ 100°C. Data points only.

### A.6-7.4.4 FEPM-83 @ 175°C

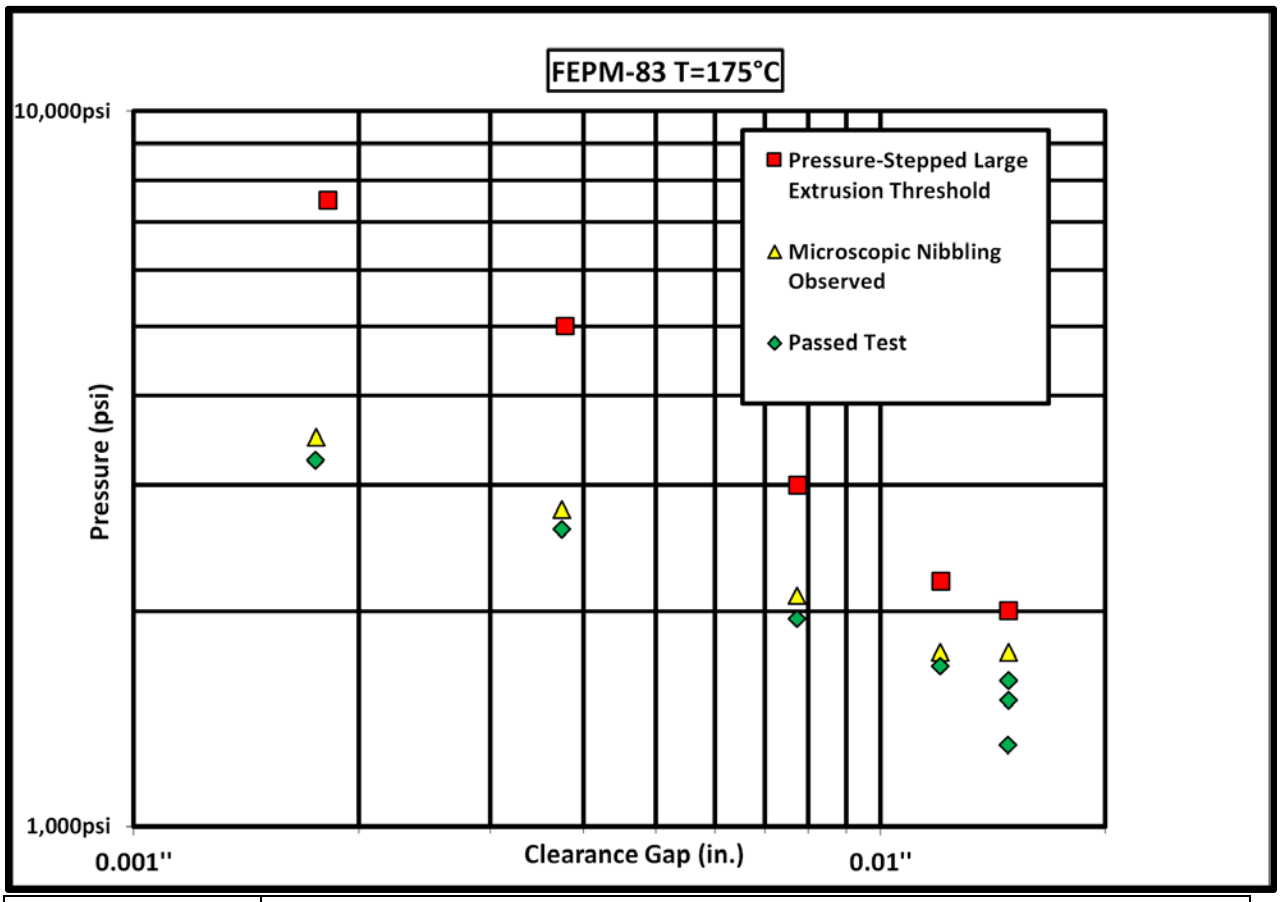


| | FEPM-83, T= 175°C, (Piston Size / Clearance Gap) | | | | |
|---|---|---|---|---|---|
| | #50/0.015" | #40/0.012" | #30/0.008" | #20/0.004" | #10/0.002" |
| O-Ring # | 50 | 56 | 62 | 68 | 74 |
| Pressure (psi) | 2,000 | 2,200 | 3,000 | 5,000 | 7,500 |
| O-Ring # | 51 | 57 | 63 | 69 | 75 |
| Pressure (psi) | nt | nt | nt | nt | nt |
| O-Ring # | 52 | 58 | 64 | 70 | 76 |
| Pressure (psi) | 1,300 | 1,750 | 2,100 | 2,600 | 3,500 |
| O-Ring # | 53 | 59 | 65 | 71 | 77 |
| Pressure (psi) | 1,500 | 1,675 | 1,950 | 2,775 | 3,250 |
| O-Ring # | 54 | 60 | 66 | 72 | 78 |
| Pressure (psi) | 1,750 | nt | nt | nt | nt |
| O-Ring # | 55 | 61 | 67 | 73 | 79 |
| Pressure (psi) | 1,600 | nt | nt | nt | nt |

**Figure A.6-41** Test data plot (top) and table (bottom) for FEPM-83 @175°C. Data points only.

## *A.6-7.5 FFKM*

### A.6-7.5.1 FFKM-75 @ 100°C

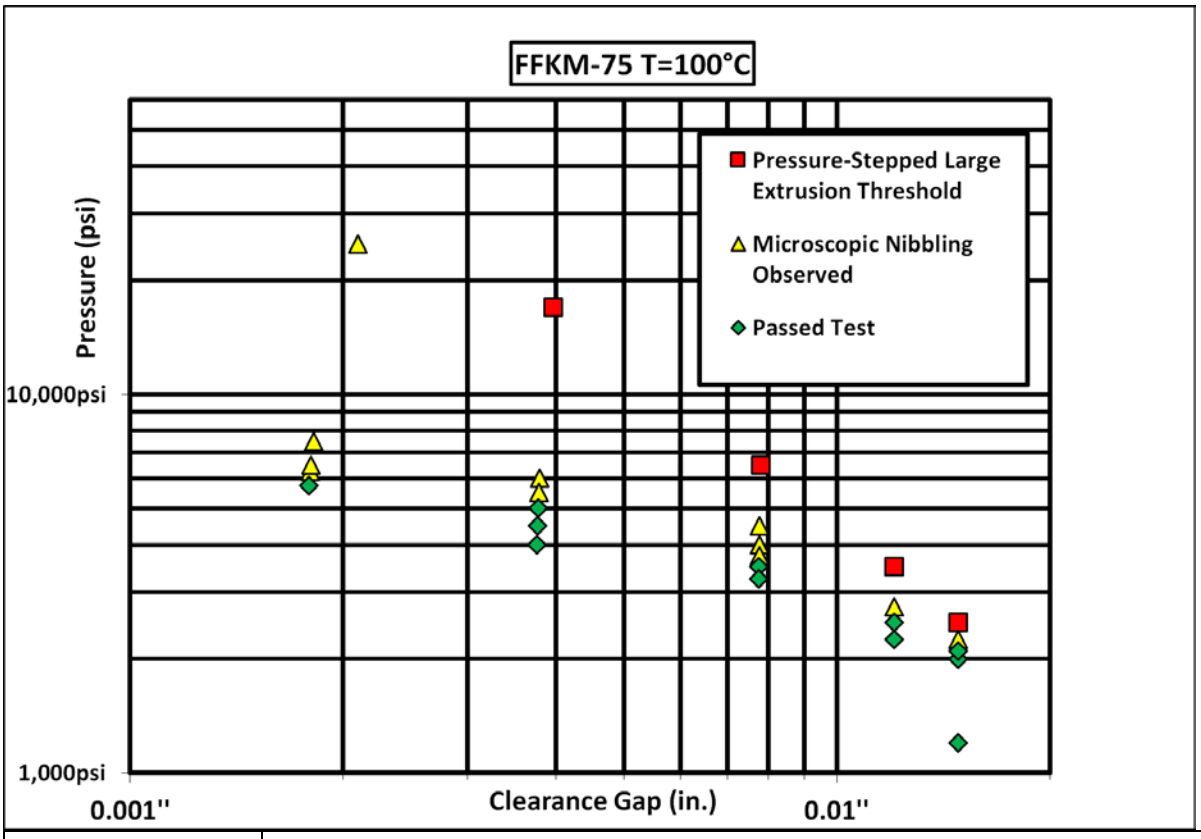


| | FFKM-75, T= 100°C, (Piston Size / Clearance Gap) | | | | |
|---|---|---|---|---|---|
| | #50/0.015" | #40/0.012" | #30/0.008" | #20/0.004" | #10/0.002" |
| O-Ring # | 1 | 7 | 13 | 19 | 25 |
| Pressure (psi) | 2,500 | 3,500 | 6,500 | 17,000 | 25,000 |
| O-Ring # | 2 | 8 | 14 | 20 | 26 |
| Pressure (psi) | nt | nt | 3,250 | 5,500 | nt |
| O-Ring # | 3 | 9 | 15 | 21 | 27 |
| Pressure (psi) | 1,200 | 2,250 | 4,500 | 4,000 | 7,500 |
| O-Ring # | 4 | 10 | 16 | 22 | 28 |
| Pressure (psi) | 2,000 | 2,500 | 4,000 | 4,500 | 6,500 |
| O-Ring # | 5 | 11 | 17 | 23 | 29 |
| Pressure (psi) | 2,250 | 2,750 | 3,750 | 5,000 | 6,250 |
| O-Ring # | 6 | 12 | 18 | 24 | 30 |
| Pressure (psi) | 2,100 | nt | 3,500 | 6,000 | 5,750 |

**Figure A.6-42** Test data plot (top) and table (bottom) for FFKM-75 @ 100°C. Data points only.

### A.6-7.5.2 FFKM-75 @ 175°C

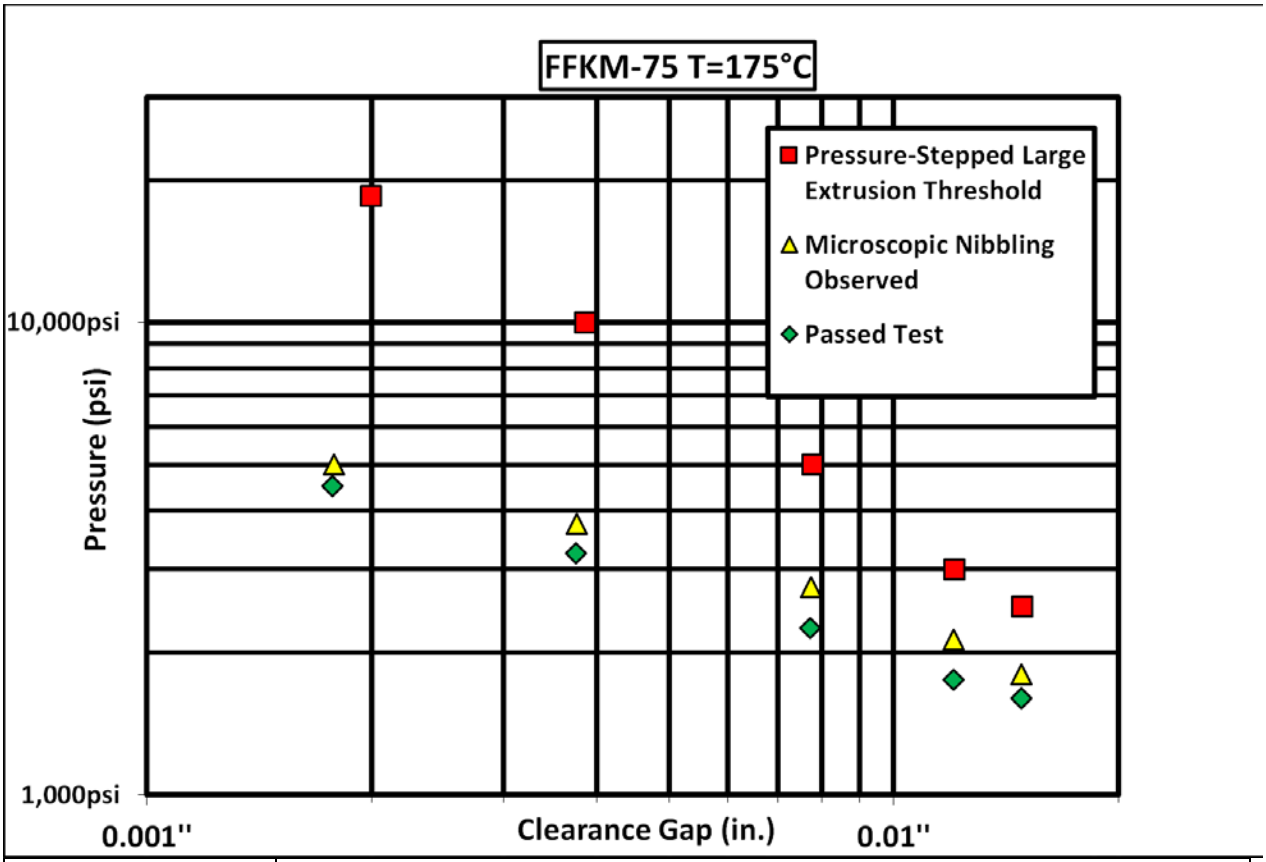


| | FFKM-75, T= 175°C, (Piston Size / Clearance Gap) | | | | |
|---|---|---|---|---|---|
| | #50/0.015" | #40/0.012" | #30/0.008" | #20/0.004" | #10/0.002" |
| O-Ring # | 50 | 56 | 62 | 68 | 74 |
| Pressure (psi) | 2,500 | 3,000 | 5,000 | 10,000 | 18,500 |
| O-Ring # | 51 | 57 | 63 | 69 | 75 |
| Pressure (psi) | nt | nt | nt | nt | nt |
| O-Ring # | 52 | 58 | 64 | 70 | 76 |
| Pressure (psi) | 1,600 | 1,750 | 2,250 | 3,250 | 4,500 |
| O-Ring # | 53 | 59 | 65 | 71 | 77 |
| Pressure (psi) | 1,800 | 2,125 | 2,750 | 3,750 | 5,000 |
| O-Ring # | 54 | 60 | 66 | 72 | 78 |
| Pressure (psi) | nt | nt | nt | nt | nt |
| O-Ring # | 55 | 61 | 67 | 73 | 79 |
| Pressure (psi) | nt | nt | nt | nt | nt |

**Figure A.6-43** Test data plot (top) and table (bottom) for FFKM-75 @ 175°C. Data points only.

### A.6-7.5.3 FFKM-90 @ 100°C

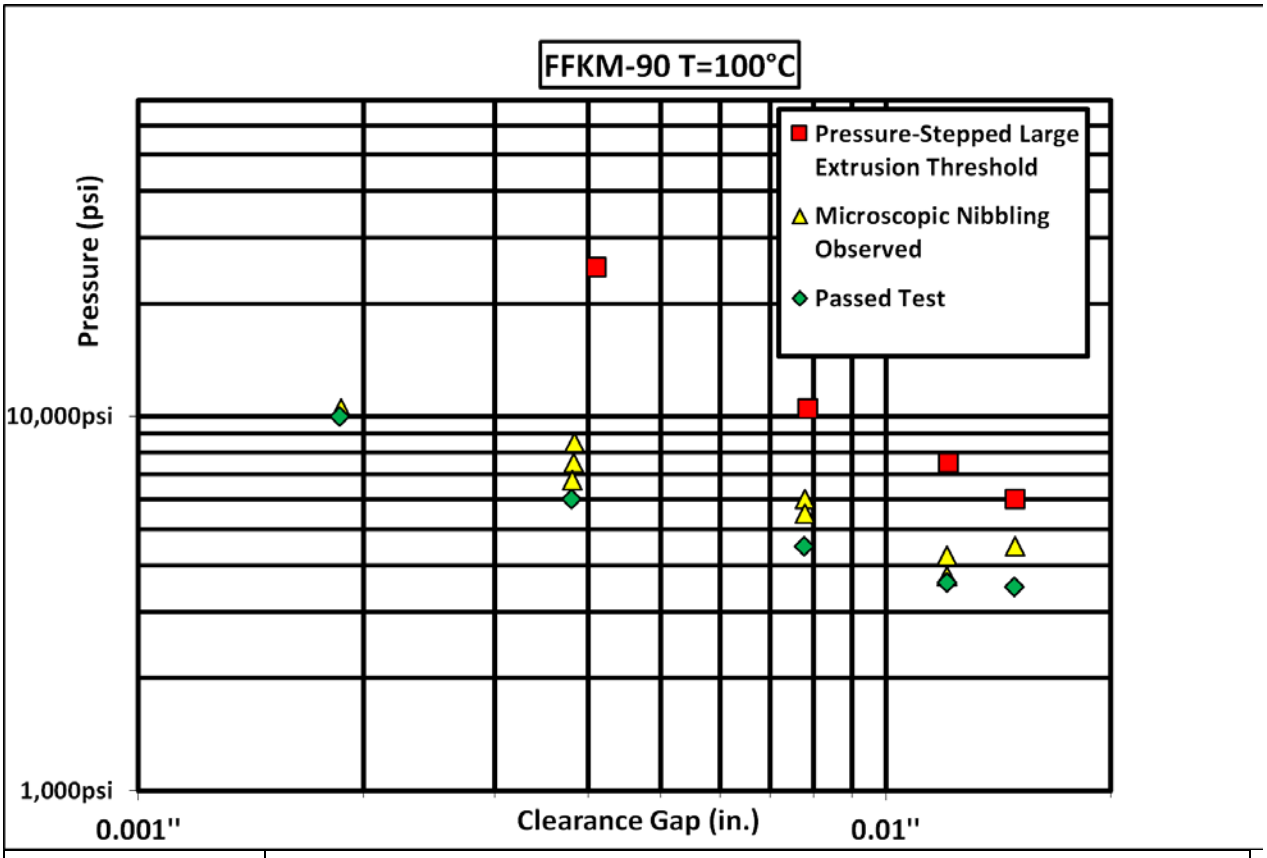


| | FFKM-90, T= 100°C, (Piston Size / Clearance Gap) | | | | |
|---|---|---|---|---|---|
| | #50/0.015" | #40/0.012" | #30/0.008" | #20/0.004" | #10/0.002" |
| O-Ring # | 1 | 7 | 13 | 19 | 25 |
| Pressure (psi) | 6,000 | 7,500 | 10,500 | 25,000 | nt |
| O-Ring # | 2 | 8 | 14 | 20 | 26 |
| Pressure (psi) | nt | nt | nt | nt | nt |
| O-Ring # | 3 | 9 | 15 | 21 | 27 |
| Pressure (psi) | 4,500 | 4,250 | 6,000 | 8,500 | 10,000 |
| O-Ring # | 4 | 10 | 16 | 22 | 28 |
| Pressure (psi) | 3,500 | 3,750 | 5,500 | 7,500 | 10,500 |
| O-Ring # | 5 | 11 | 17 | 23 | 29 |
| Pressure (psi) | nt | 3,600 | 4,500 | 6,750 | nt |
| O-Ring # | 6 | 12 | 18 | 24 | 30 |
| Pressure (psi) | nt | nt | nt | 6,000 | nt |

**Figure A.6-44** Test data plot (top) and table (bottom) for FFKM-90 @ 100°C. Data points only. No regression lines are included.

### A.6-7.5.4 FFKM-90 @ 175°C

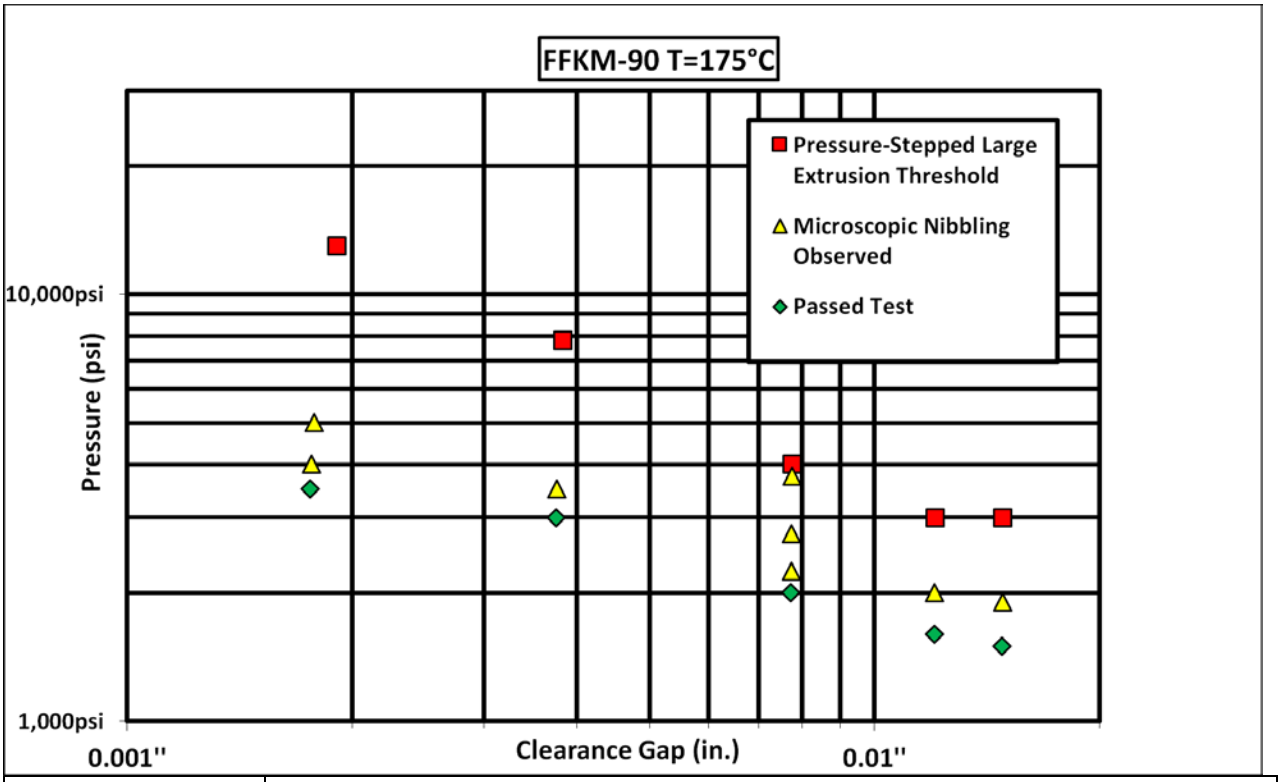


| | FFKM-90, T= 175°C, (Piston Size / Clearance Gap) | | | | |
|---|---|---|---|---|---|
| | #50/0.015" | #40/0.012" | #30/0.008" | #20/0.004" | #10/0.002" |
| O-Ring # | 50 | 56 | 62 | 68 | 74 |
| Pressure (psi) | 3,000 | 3,000 | 4,000 | 7,800 | 13,000 |
| O-Ring # | 51 | 57 | 63 | 69 | 75 |
| Pressure (psi) | nt | nt | nt | nt | nt |
| O-Ring # | 52 | 58 | 64 | 70 | 76 |
| Pressure (psi) | 1,500 | 1,600 | 3,750 | 3,000 | 5,000 |
| O-Ring # | 53 | 59 | 65 | 71 | 77 |
| Pressure (psi) | 1,900 | 2,000 | 2,750 | 3,500 | 4,000 |
| O-Ring # | 54 | 60 | 66 | 72 | 78 |
| Pressure (psi) | nt | nt | 2,250 | nt | 3,500 |
| O-Ring # | 55 | 61 | 67 | 73 | 79 |
| Pressure (psi) | nt | nt | 2,000 | nt | nt |

**Figure A.6-45** Test data plot (top) and table (bottom) for FFKM-90 @ 175°C. Data points only. No regression lines are included.

## A.7 Appendix 7 – FEA Modeling Report (courtesy of Endurica, LLC)

# Safety Technology Verification for Materials and Corrosions in the U.S. Outer Continental Shelf

## HPHT O-Ring Finite Element Analysis

Report Date: July 2017

| |
|---|
| Prepared For:<br><br>U.S. Department of the Interior<br>Bureau of Safety and Environmental Enforcement<br>45600 Woodland Road, VAE-ORP<br>Sterling, VA 20166<br>Attn: Bipin Patel, Contracting Officer's Representative |
| Analysis and Reporting<br>Prepared by:<br><br>William V. Mars, Ph.D. P.E., Mark A. Bauman<br>Endurica LLC<br>1219 W. Main Cross St., Ste 201<br>Findlay, Ohio 45840<br>www.endurica.com |

# HPHT O-Ring Finite Element Analysis

A series of Finite Element Analyses of the sealing integrity of O-rings operating in a High Pressure High Temperature test cell environment has been completed. Five different elastomer (rubber) materials (ASTM D1418-2017) types were evaluated as part of this project: NBR, HNBR, FKM, FEPM, and FFKM. Two hardness specifications (nominally, 75 and 90 Shore A), at two (2) operating temperatures (100 °C and 175°C) were included. The analyses consider the effects of the clearance gap (ranging from 0.002" to 0.015") on critical pressure at incipient tearing, and on various associated mechanical parameters. In the analysis, seal integrity is considered to be lost at the instant that incipient tearing begins, following a simple fracture-mechanical criterion. The finite element computed pressure-clearance relationship reconciles with experimental observations provided by Petromar, across the full range of materials and temperatures considered, to within a statistical uncertainty similar to experimental scatter. The results support that tearing of O-ring material is the primary mechanism governing loss of seal integrity, and provides a validated analysis procedure that may be applied generally in other sealing scenarios.

# Contents

# Table of Figures



# Table of Tables

# Legal Notices



# Background

O-ring seal integrity is essential to the safe operation of various systems in the Oil and Gas industry that operate under High Pressure / High Temperature conditions. In support of the Battelle project “Safety Technology Verification for Materials and Corrosions in the U.S. Outer Continental Shelf”, Endurica has developed a finite element model of the O-ring installation and operating process that occurs in a benchmark O-ring testing system developed by PetroMar. The finite element model uses previously measured material properties for the O-ring (Endurica LLC 13 July 2016).

# Objective

The purpose of the finite element analysis is to determine the relationships between the conditions occurring at incipient loss of seal integrity with the material properties of the O-ring, the geometric features of the gland, the thermal environment, and the loads carried through the seal. A successful model generation and validation will reproduce the experimental observations from Petromar and increase confidence in application of the developed simulation methods for other seal configurations and operating scenarios.

## Test Cell Gland / Seal Geometry

The test cell gland was designed and built to test size AS568-210 O-rings under HPHT conditions in a static radial seal. The test cell uses pistons of slightly different diameters to vary the extrusion gap between the test apparatus bore and the piston, as shown in Figure . Pressure is applied to the O-ring using a hydraulic system and manual pump. The test cell includes a heater with temperature control to test at high temperatures. A more detailed description of the test cell can be found in the Petromar report "HPHT O-ring Testing Results" (10 October 2016). The terms used to describe the testing are shown in Figure .

Figure A.7-1. Pistons and pressure vessel used for the HPHT O-ring testing.

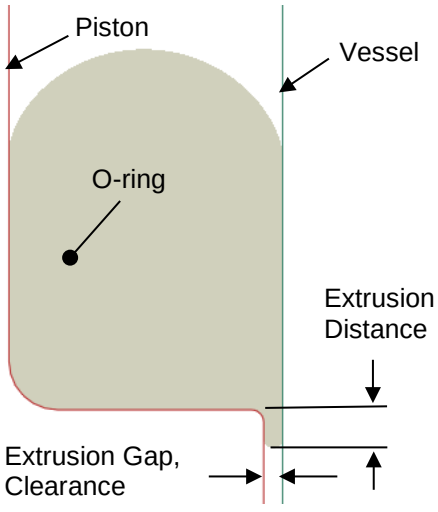


Figure A.7-2. Diagram of terms used to describe testing.

## Loads and Operating Scenarios

The finite element simulation was set up to mimic as closely as possible the experimental steps used in the HPHT O-ring Test Cell experiments executed by PetroMar. A video titled “Finite Element Modeling of O-ring Sealing Pressure Limits” (Endurica LLC, 14 September 2016) illustrating the simulation setup was previously delivered that presents the loading and operating steps in detail. The steps indicated in Figure A.7-3 were modeled, as follows:

1. Initial unstressed, room temperature geometry.
2. Installation of the O-Ring and interference fit on the inside gland diameter.
3. Closure of the test cell and contact with the outside cylinder wall.
4. Thermal equilibration at test temperature.
5. Establishment of initial, zero-pressure contact with the gland face.
6. Pressurization.

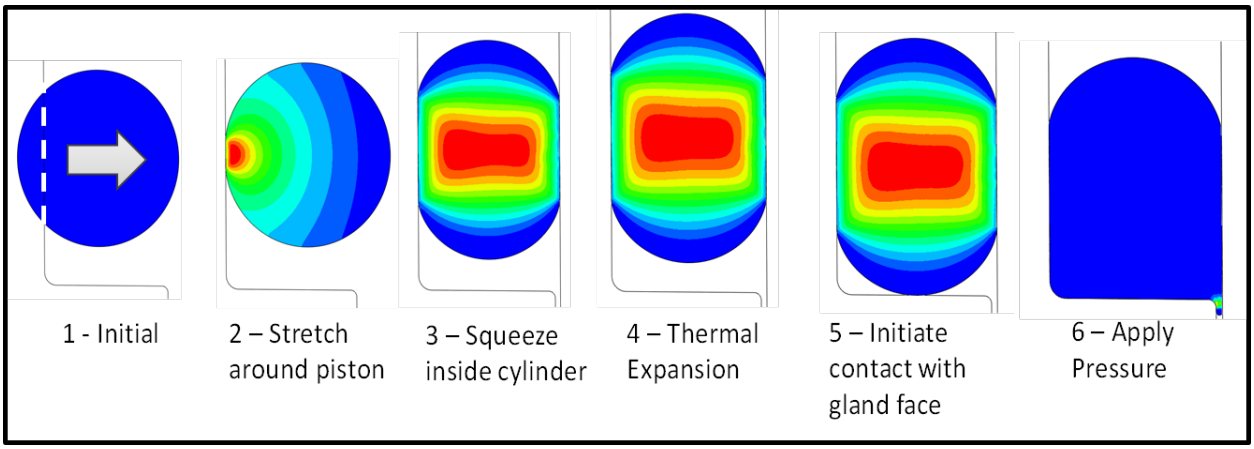


Figure A.7-3. Analysis steps for computing stress-distribution in O-ring as a function of pressure.

Note that in the simulation, the final pressurization step continues until convergence unless the model fails to converge (usually due to too large distortions of the mesh). The initiation of tearing is analyzed after the simulation has executed, using the theory detailed in the Tearing Criterion section.

In experiments, following tear initiation, further extrusion of the O-ring was observed to occur via the propagation of a crack along an inward-spiraling path. Tear propagation resulted in a flap of roughly constant thickness being separated from the O-ring, and fed through the gap clearance.

## Test Matrix

Table A.7-1 summarizes the materials and conditions for which material characterizations were completed. The characterization results have been used herein for defining material behavior in the O-ring simulation and failure analysis.

Table A.7-1. Material characterization test matrix.

| Material | Temp, °C | Critical Tearing Energy | Hyperelastic Properties | Mullins effect | Volumetric Compression | Creep Crack Growth | Thermal Expansion |
|---|---|---|---|---|---|---|---|
| **FEPM-80** | 100 | X | X | X | X | X | X |
| **FEPM-80** | 175 | X | X | X | X | X | |
| **FEPM-90** | 100 | X | X | X | X | X | X |
| **FEPM-90** | 175 | X | X | X | X | X | |
| **HNBR-75** | 100 | X | X | X | X | X | X |
| **HNBR-90** | 100 | X | X | X | X | X | X |
| **HNBR-90** | 150 | X | X | X | X | X | |
| **FFKM-75** | 100 | X | X | X | X | X | X |
| **FFKM- 75** | 175 | X | X | X | X | X | |
| **FFKM- 90** | 100 | X | X | X | X | X | X |
| **FFKM-90** | 175 | X | X | X | X | X | |
| **NBR-75** | 100 | X | X | X | X | X | X |
| **NBR-90** | 100 | X | X | X | X | X | X |
| **FKM-75** | 23 | | X | X | X | | X |
| **FKM-75** | 100 | X | | | | X | |
| **FKM-75** | 175 | X | X | X | X | X | |
| **FKM-90** | 23 | | X | X | X | | X |
| **FKM-90** | 100 | X | | | | X | |
| **FKM-90** | 175 | X | X | X | X | X | |

## Model Setup

The O-ring FE model consisted of three parts; O-ring, piston, and cylinder. The piston and cylinder were modeled as rigid. The deformation of the vessel bore under high pressure loading

was calculated by PetroMar. The minimal deformation calculated showed that treating them as rigid bodies was acceptable.

The FE model used the material properties measured by Endurica LLC for each material. The material properties used in the FEA are a three term Ogden Hyperelastic law including the volumetric compression response, a Mullins model, and the thermal expansion coefficient.

Surface-to-surface contact interactions were created between the O-ring and piston and between the O-ring and cylinder. The contact interactions allowed the friction to be modeled using the coefficient of friction that was calculated. Unless otherwise noted the coefficient of friction was 0.05.

A temperature field in the model allows the ambient temperature to be changed during the thermal expansion step. The thermal expansion coefficient for each material was measured and was input into the model to calculate the thermal expansion. A constant, steady-state temperature was modeled through the entire O-ring cross section since the experimental test allowed adequate time for the temperature to stabilize.

The fluid pressure was applied to the O-ring in the model using pressure penetration interactions. As pressure was applied to the O-ring, the area of the O-ring exposed to the fluid pressure changes as the O-ring deformed. The pressure penetration interactions apply fluid pressure only to the free surface area of the O-ring that was exposed to the fluid.

The O-ring mesh used an approximate element size of 0.0015” and was refined to smaller elements of approximate size 0.00018” near the portion that was extruded into the extrusion gap. The overall mesh is shown in Figure A.7-4, and a detail view of the clearance gap is shown in Figure A.7-5. The entire mesh on the O-ring includes 30,458 elements of type CAX4RH modeled using ABAQUS software. The CAX4RH element type is a linear axisymmetric stress element that uses a hybrid formulation and reduced integration. Hybrid formulation elements are recommended for materials such as rubber that have a high Poisson’s ratio value close to 0.5. In comparing the convergence of solutions for models under high deformation it was observed that using CAX4RH elements for the mesh allowed modeling of double the applied pressure versus using other alternative element types. CAX4RH elements were selected to best model the high deformation of the O-ring extruding into the clearance gap.

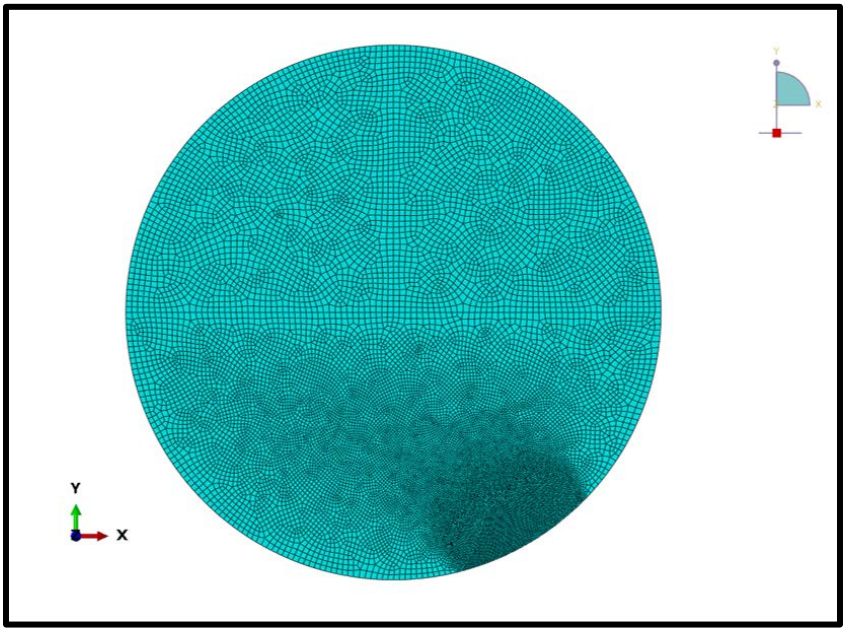


Figure A.7-4. Mesh on O-ring showing the refined mesh at area that will be extruded.

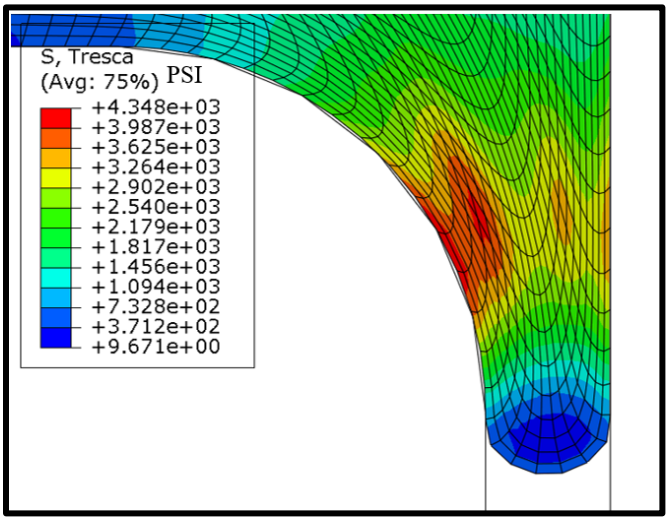


Figure A.7-5. Detail view of extrusion gap. The mesh shown is for an FEPM-80 O-ring at 100°C with a 0.002” nominal clearance gap at the critical tearing pressure. The mesh has enough elements across the smallest clearance gap to accurately capture the stress gradients.

## Model Outputs

The mechanical state of the O-ring was recorded as a function of time during the simulation. The following outputs were requested from the model:

1. Tresca Stress distribution
2. Total recoverable strain energy
3. Total deformed O-ring volume

4. Strain energy density distribution
5. Extrusion distance: The extrusion distance was measured as the axial distance from the lower gland face to the furthest extruded point of the O-ring in the extrusion gap. (see Figure A.7-2)
6. Applied pressure to O-ring

The raw results for each simulation are presented in Appendix A.7-1.

## Tearing Criterion

Tearing of an elastomer can occur whenever the incremental growth of some crack would cause a release of energy $U$ sufficient for creating new crack surface area $A$ (Rivlin and Thomas 1953). Formally, the general tearing criterion $T$ – the energy release rate - is defined as

$$T = -\frac{\partial U}{\partial A} \tag{7}$$

Tearing is predicted to occur whenever $T \geq T_c$, where $T_c$ is the critical fracture energy (Gent and Mars 2013) corresponding to unstable rupture propagation. In the typical case of a tear that initiates from a microscopic pre-existing feature of the elastomer microstructure, equation (7) can be specialized, considering that the energy release rate of a small crack is known to scale linearly with size $a_0$ (Ait Bachir et al 2012), and with the available part $W_a$ of the stored strain energy density $W$.

$$T = \alpha W_a a_0 \tag{8}$$

The constant of proportionality $\alpha = \pi / 4$ was set to give equivalence of equation (8) to the linear elastic solution for a crack under mode II loading with far-field shearing stress $\tau$, as given in Anderson (2005).

Because of crack closure that occurs under large hydrostatic compression, the energy release due to crack growth is maximized by the crack that experiences maximum shearing. The maximum shear stress is equal to the Tresca Stress $\tau$, defined as $\tau = (\sigma_1 - \sigma_3) / 2$, where $\sigma_1$ and $\sigma_3$ are the maximum and minimum principal stresses. The associated available strain energy density is therefore written in terms of the Tresca stress at break $\tau_b$ and shear modulus $G$, finally giving the criterion used with the finite element analyses presented herein.

$$T_c = \alpha \frac{\tau_b^2}{G} a_0 \tag{9}$$

In equation (9), the material parameters $T_c$ and $G$ have previously been measured (Endurica LLC 13 July 2016), and are known to depend on temperature. The crack precursor size $a_0$, on the

other hand, is a temperature-independent constant for a given material, depending only on compositional and manufacturing details of the elastomer.

In our analysis of finite element calculations, the parameter $a_0$ was calibrated for each material by evaluating equation (9) at the pressure associated with incipient tearing, as observed in the PetroMar experiments (see Figure A.7-6). The parameters $T_c$ and $G$ were obtained from the material characterization for the associated temperature. $\tau_b$ was obtained from the finite element model at the moment that the critical pressure for incipient tearing occurred, at the location on the gland lip where the Tresca stress was maximized.

Once the crack precursor size $a_0$ was calibrated for a given material, computations of the effects of gap clearance, gland fillet radius, etc. were executed following the procedure outlined in Figure A.7-7.

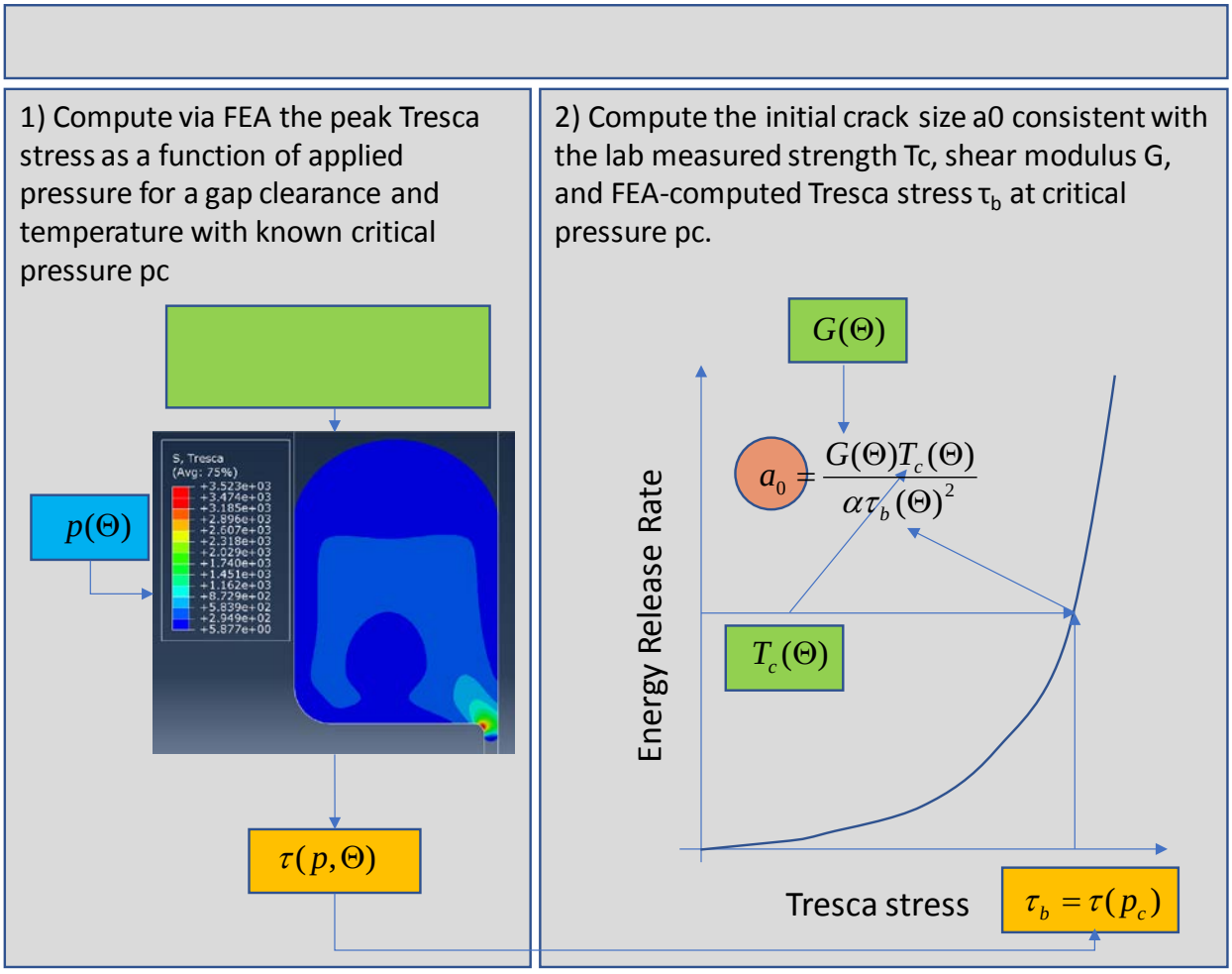


Figure A.7-6. Schematic process for calibrating the crack precursor size for a given material. Blue = known data from O-ring experiment testing, Green = known material characterization experiment data, Yellow = Output from FEA, Red = Final calibrated crack precursor size.

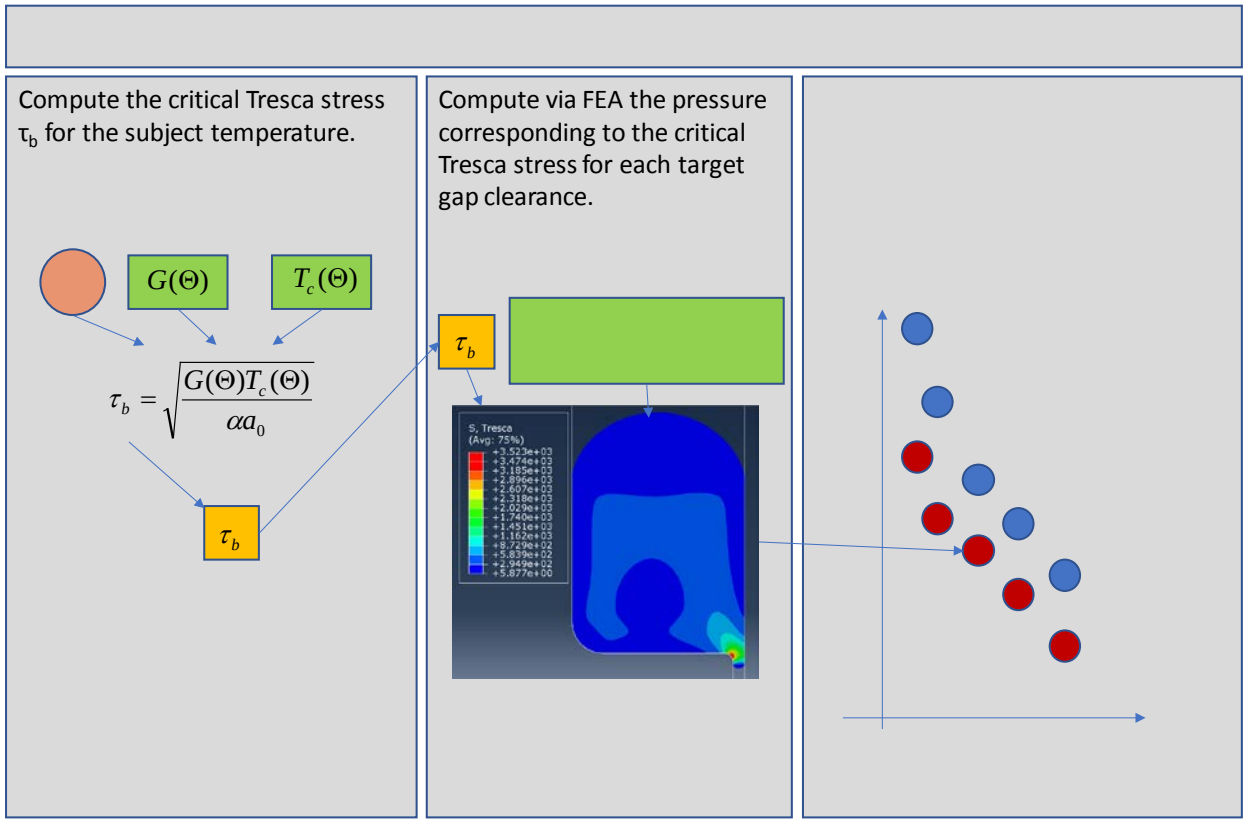


Figure A.7-7. Schematic process for computing pressure-clearance curves for a given material.

## Friction Coefficient Calculation

The coefficient of friction between the O-ring and the piston and the O-ring and the cylinder was calculated for the test setup. The friction coefficient was calculated by measuring the torque required to rotate the cylinder, calculating the normal forces in an FE model, and then solving the equation μ=F/r where F= Force and r = gland radius of curvature. Sliding occurs between either the O-ring and the piston or the O-ring and the cylinder.

The friction coefficient test was performed without pressure applied to the seal. Since no pressure was applied to the seal and the O-ring has space to move along the gland axially it is assumed that the frictional forces between the O-ring and the side of the gland wall are negligible.

Using the test cell gland for measuring the torque required to rotate the piston incorporates the surface finish of the piston and cylinder into the friction coefficient measurement as well as the effect of the hydraulic oil.

The assumption was made that the friction coefficient is the same for all O-ring materials, temperatures, and test pressures. The friction coefficient test was run for one FKM- 90 O-ring at 100C. The inputs to the friction coefficient calculation are shown in Table .

Table A.7-2. Friction coefficient calculation inputs.

| | |
|---|---|
| Measured torque to rotate cylinder by PetroMar | 2 in-lbs. |
| Normal force between O-ring and piston calculated using FEA | 95.2 lbs. |
| Normal force between O-ring and cylinder calculated using FEA | 108.5 lbs. |
| Cylinder inside diameter | 1.0005 in |
| Piston gland diameter | 0.772 in |

Sliding between piston gland outer diameter and O-ring: (The frictional forces between the end of the gland wall and the O-ring are assumed to be negligible)
F=2in-lbs/0.386
Mu=5.181 lbs./95.2 lbs.
Mu=0.054

Sliding between Cylinder and O-ring:
F=2in-lbs/0.500025
Mu=4 lbs. / 108.5 lbs.
Mu=0.037

Using Mu=0.054
Force to slide at piston = 5.181 lbs. (matches experimental results)
Force to slide at cylinder = 5.86 lbs. (above experimental force to slide. This shows that it is not sliding between O-ring and cylinder)

Using Mu=0.037
Force to slide at piston = 3.52 lbs. (below experimental value to slide, using this friction factor is not correct as it would result in a lower torque to spin than measured)
Force to slide at cylinder = 4 lbs. (matches experimental results)

The friction coefficient was calculated at 0.05. The friction coefficient was rounded to 1 significant figure to match the reported 2in-lbs torque value. The sliding that occurs in the friction test is between the piston and the O-ring.

## Result Summary

A detailed account of computed results for each material and temperature in the experimental matrix is provided in Appendix A.7-1.

## *FEA vs Experiment*

The FEA computed pressure at tear initiation is plotted below in Figure  vs experimentally observed tear initiation pressure (i.e., green) test results performed by PetroMar. The black 1:1 fit line indicates ideal agreement. The distance of a point from the line shows the difference between the two results. The average percent difference is 9.24%.  The correlation coefficient $R^2$ for the fit line is 0.96.  In the plot, data points are coded by polymer family (point style), shore hardness (open or closed points), and temperature (blue or red points).  Overall, scatter in the results increase as the pressure increases, and is similar in magnitude to experimental uncertainty occurring in the PetroMar results.

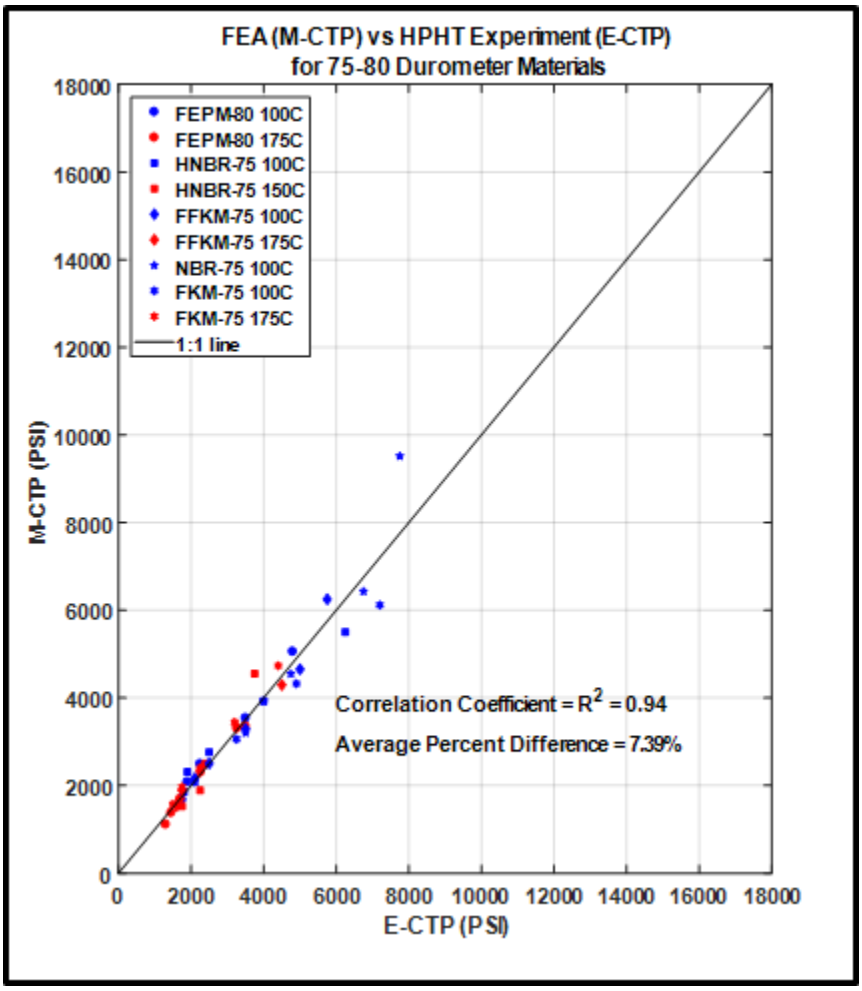

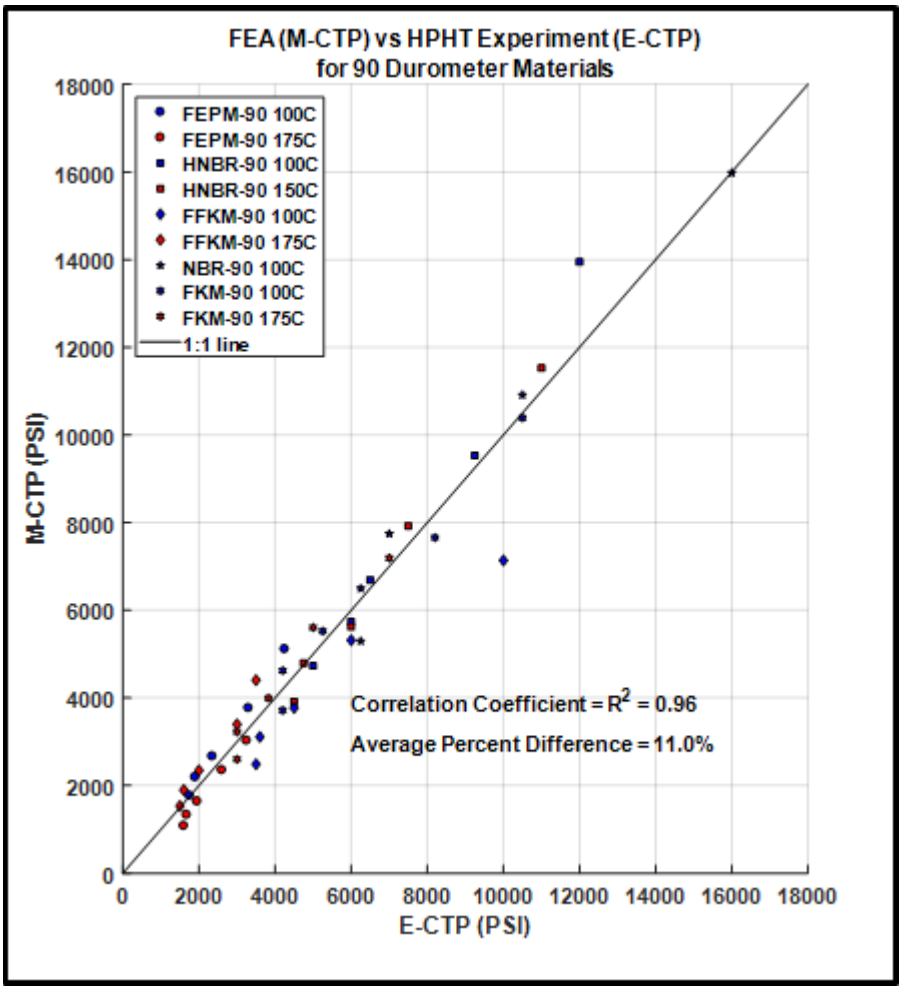
FEA (M-CTP) vs HPHT Experiment (E-CTP)
for 90 Durometer Materials
FEPM-90 100C
FEPM-90 175C
HNBR-90 100C
HNBR-90 150C
FFKM-90 100C
FFKM-90 175C
NBR-90 100C
FKM-90 100C
FKM-90 175C
1:1 line
Correlation Coefficient = R2 = 0.96
Average Percent Difference = 11.0%
M-CTP (PSI)
E-CTP (PSI)
0
2000
4000
6000
8000
10000
12000
14000
16000
18000

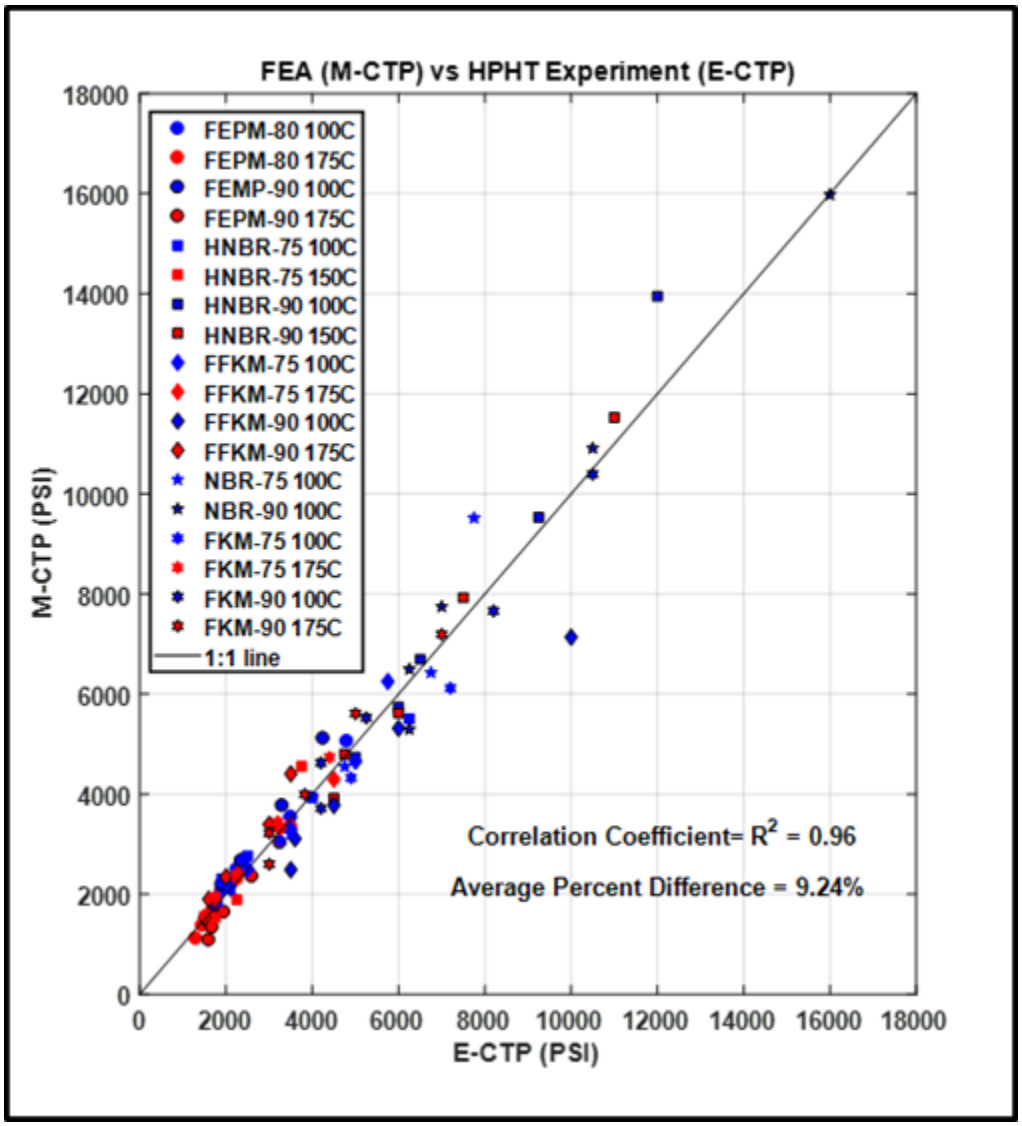


Figure A.7-8 a,b,c. Comparison of tear initiation pressure predictions by FEA vs experiment. Each polymer family uses a different point style. Red points are for elevated temperatures of 150°C to 175°C. Blue points are for low temperature of 100°C.

## *Effect of Gland Fillet Radius*

A fillet radius sensitivity study examined the effect of the fillet radius on the gland of the piston next to the clearance gap. The sensitivity study used one test setup, FKM-75 at 100°C with a 0.004” clearance gap and four different fillet radii. The Tresca stress at which tearing initiates was previously determined for the test setup. The pressure when the Tresca stress reaches the critical level when tearing initiates was determined for each fillet radius. The fillet radius vs. pressure results show that a larger fillet radius enables the O-ring to withstand greater pressure before tearing initiates. The fillet radius vs pressure relationship can be approximated by a log-linear relationship. The results of the sensitivity study are shown below in Figure A.7-9.

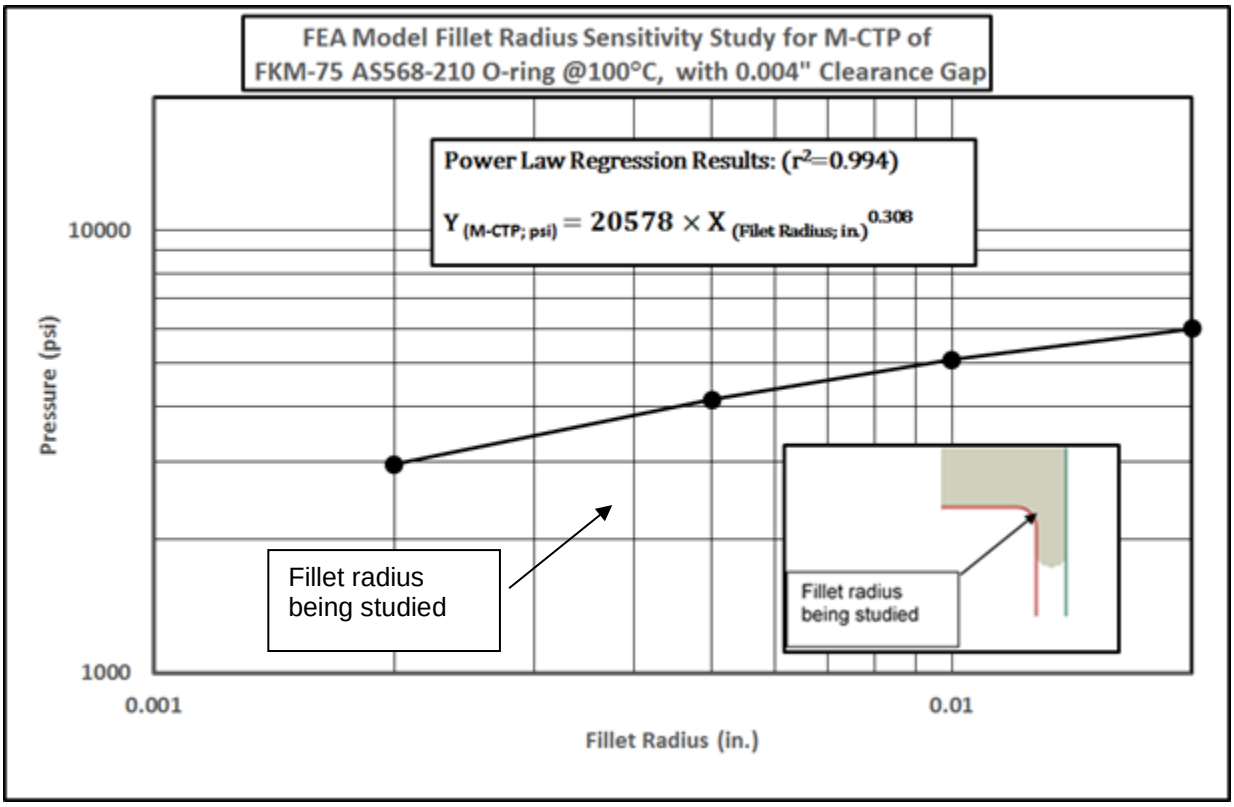


Figure A.7-9. Fillet Radius Sensitivity

## *Effect of Friction Coefficient*

A coefficient of friction sensitivity study was performed for FKM-90 at 100°C with a clearance gap of 0.008 inches. Five different outputs are graphed in Figure  versus the applied pressure; total recoverable strain energy, total O-ring volume, peak strain energy density, peak tresca stress, and extrusion distance. The critical tresca stress to initiate tearing was determined in the material experiments. An "X" shows the point at which the critical tresca stress is reached.

The last graph in Figure  shows the relationship between the critical tearing pressure and the friction factor. Smaller friction factors lead to more extrusion at the same pressure. The critical tearing pressure shows little dependence on friction factor due to the friction factor having little effect on the critical tresca stress.

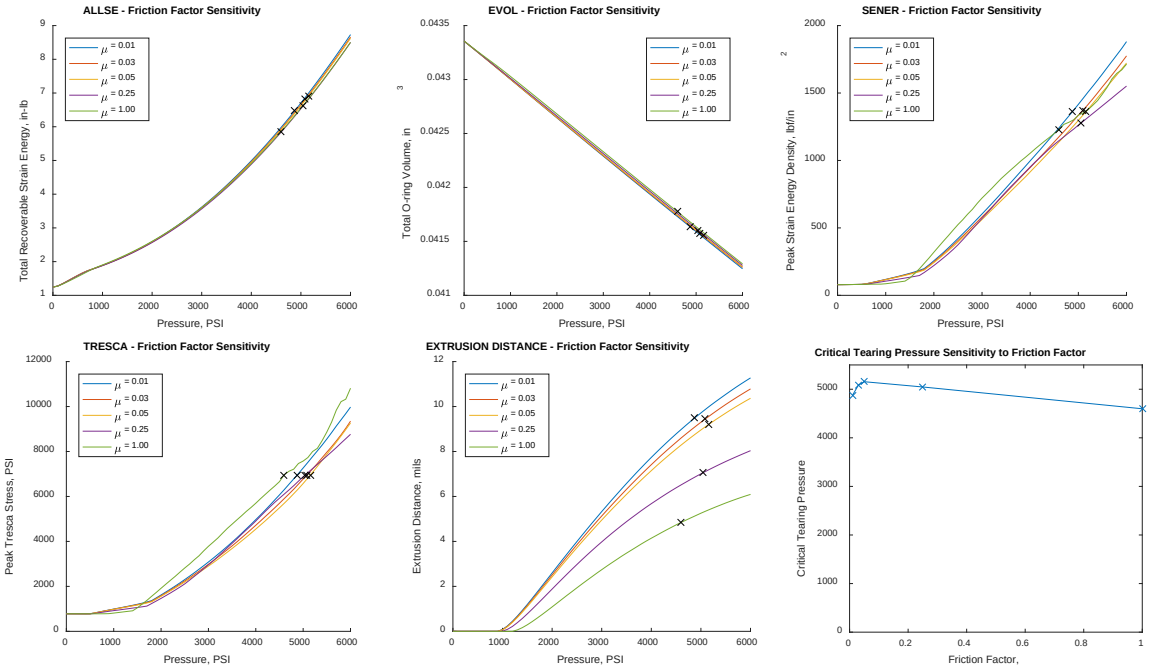


Figure A.7-10. Friction factor sensitivity graphs.

The sensitivity of the tear initiation angle to the friction factor was determined. The tear initiation angle varies 4° over the range of friction factors evaluated, 0.01 to 1. The tresca stress distribution, at the pressure of first tearing initiation, is shown in Figure A.7-11.

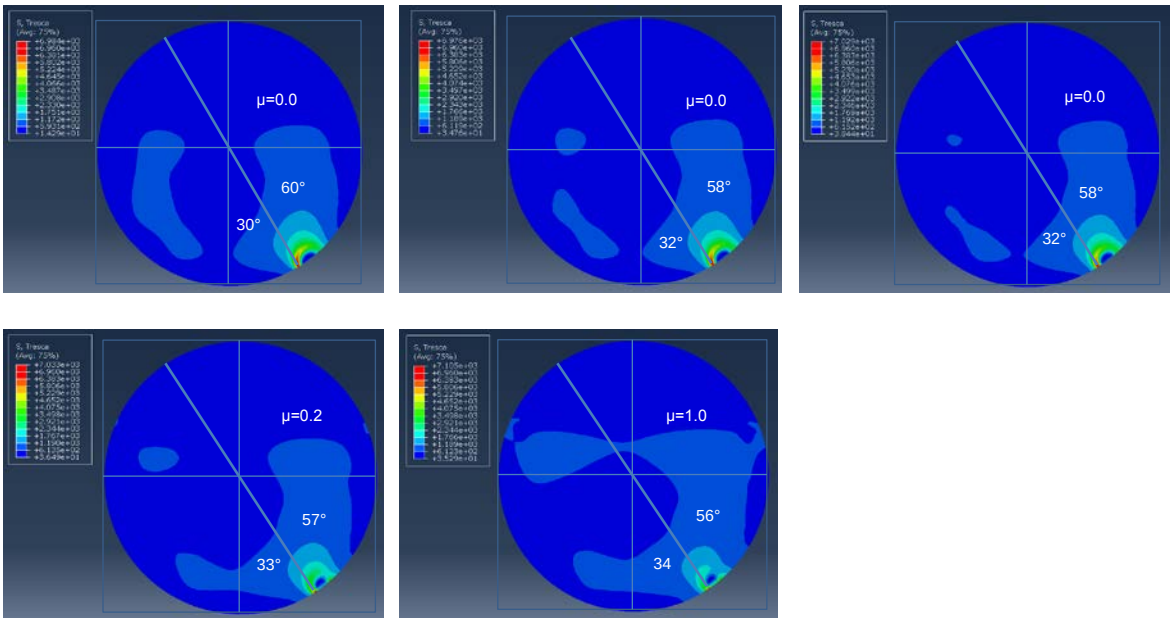


Figure A.7-11. Tear initiation angle sensitivity to friction factor.

### *Effect of Finite Element Mesh*

A mesh convergence study was performed on the O-ring to determine the incremental change in output results when refining the mesh to smaller elements. Four different mesh densities were analyzed in the mesh convergence study. The pressure vs. Tresca stress at the critical location was plotted for each of the mesh densities. Higher mesh densities resulted in a decrease of the Tresca stress at the critical location. The mesh element size was continually reduced until the change in Tresca stress was within 1% with a 50% increase in the number of elements. The results from meshes in the mesh convergence study are plotted below in Figure A7-12. Based on these results, the mesh with 30458 elements was used for all subsequent analyses.

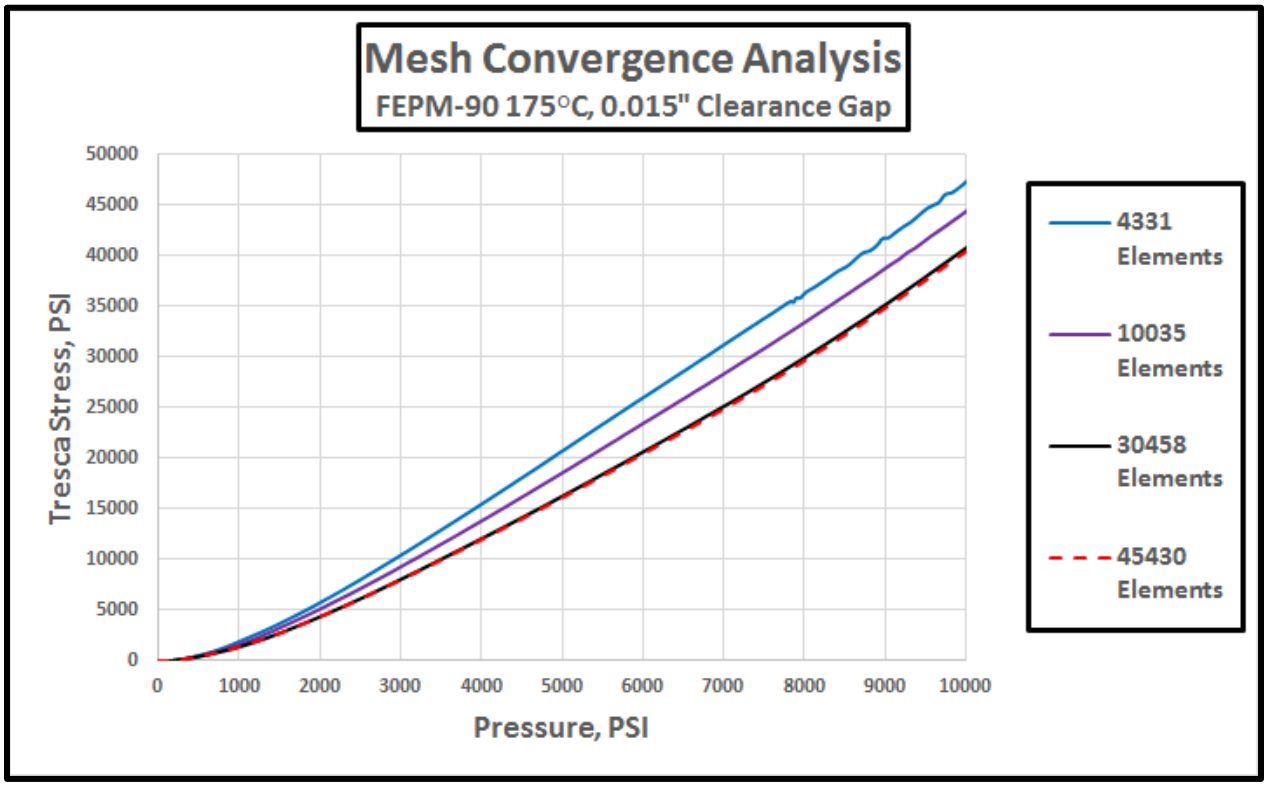


Figure A.7-12. Tresca Stress vs Pressure Results for the Mesh Convergence Study.

## Cross-Material Plots of Critical Tear Pressures

The following charts arrange FEA results of critical tearing pressure for O-rings of different materials for similar temperatures and durometers. It should be noted that the FE model is for a single-cycle dwell test of a new O-ring. The ability of the O-rings' material to resist tear may be affected by different factors that could alter the relative ranking, e.g. duration of exposure to temperature and pressure, ageing and load prehistory, including Mullins effect, HPHT cycling, etc.

## *M-CTP Ranking at 100°C, Durometer<83*

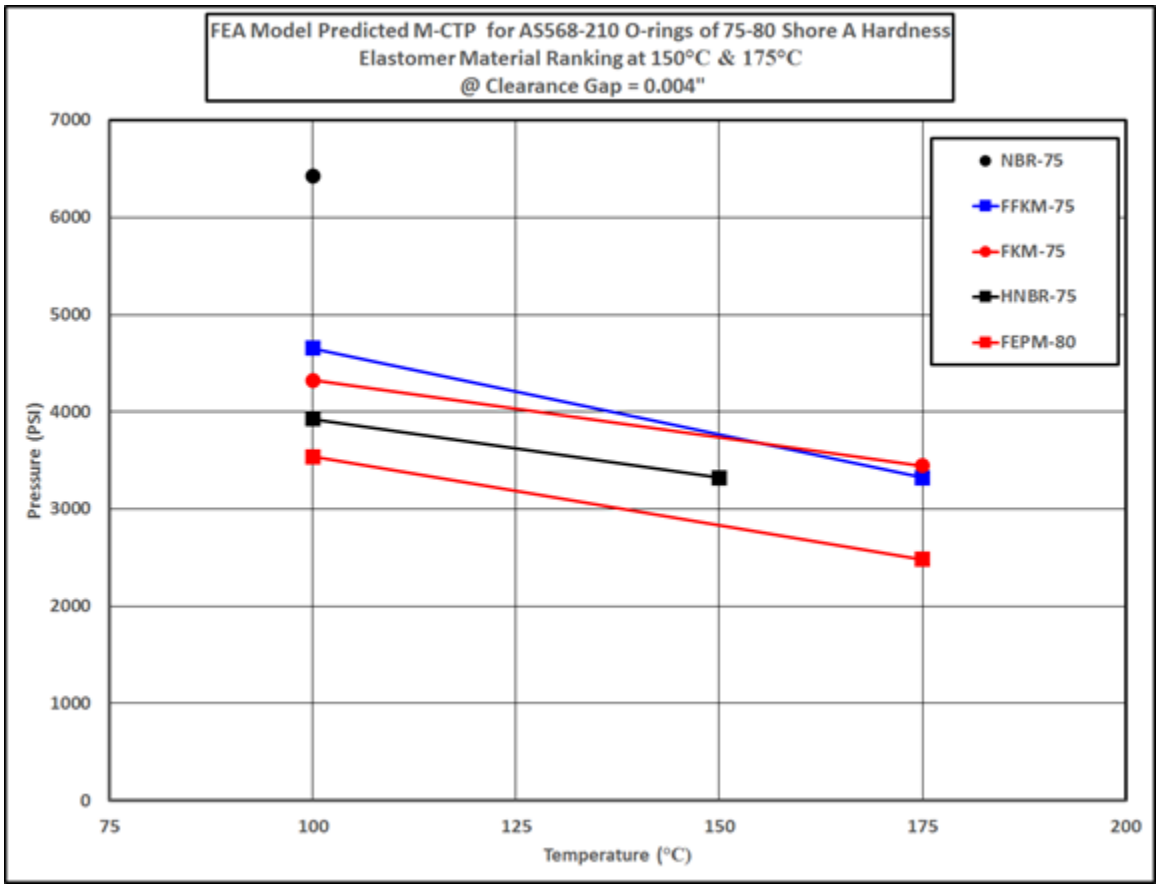


Figure A.7-13. Ranking of M-CTP for 75-80 shore A durometer materials at 100°C to 175°C for 0.004-inch clearance gap and AS568-210 size O-rings.

## *M-CTP Ranking at 100°C, Durometer=90*

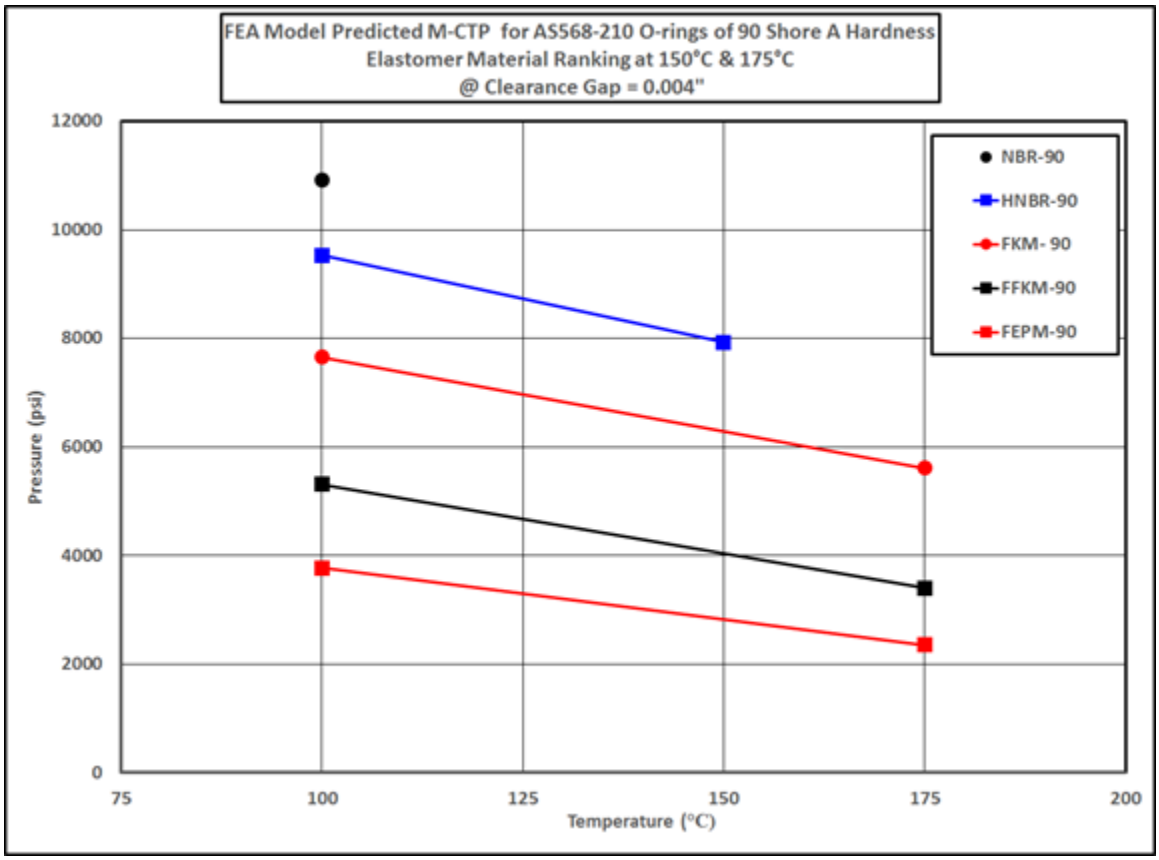


Figure A.7-14. Ranking of M-CTP for 90 shore A durometer materials at 100°C to 175°C for 0.004-inch clearance gap and AS568-210 size O-rings.

## *M-CTP Ranking at 150°C & 175°C, Hardness <83*

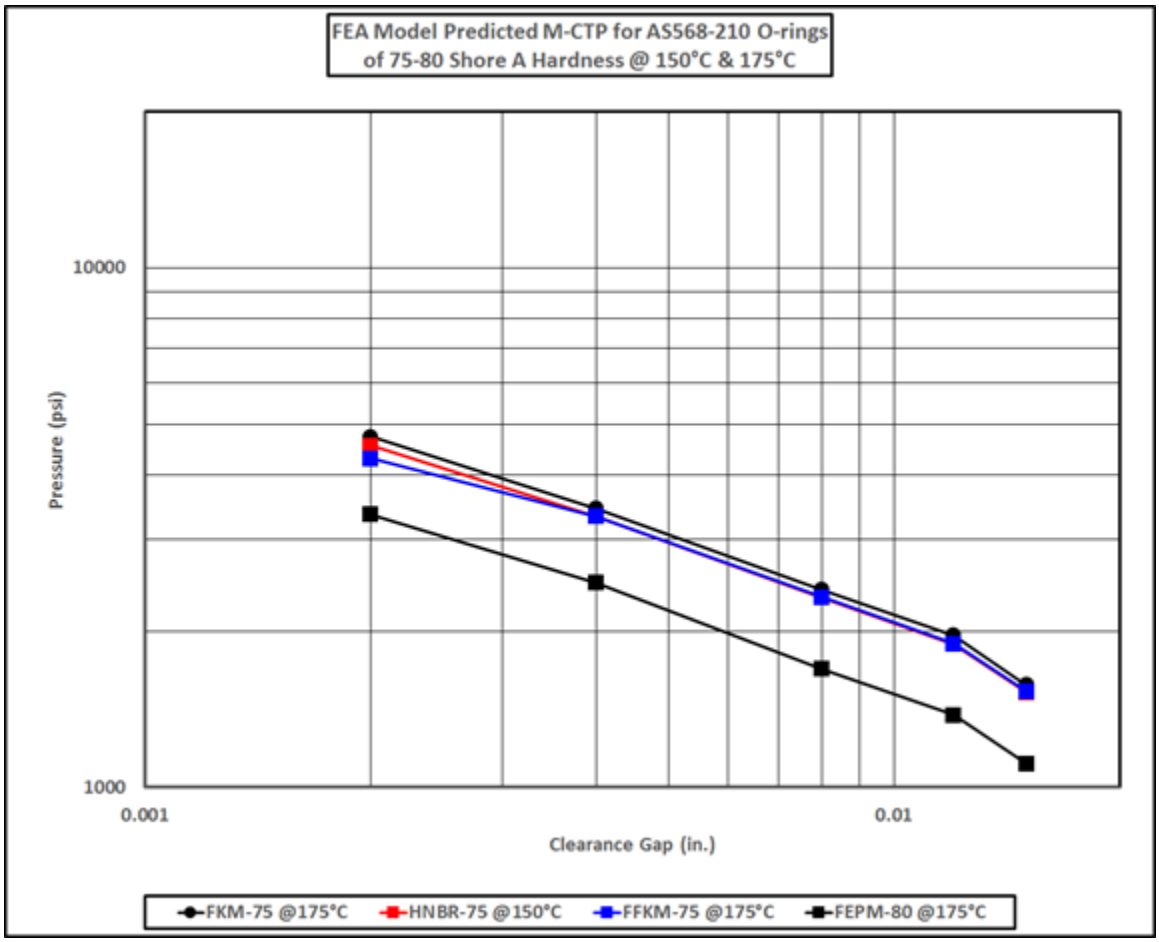


Figure A.7-15. M-CTP ranking for O-rings with 75 and 80 Shore A durometer at 150°C and 175°C (Endurica, LLC).

## *M-CTP Ranking at 150°C & 175°C, Durometer=90*

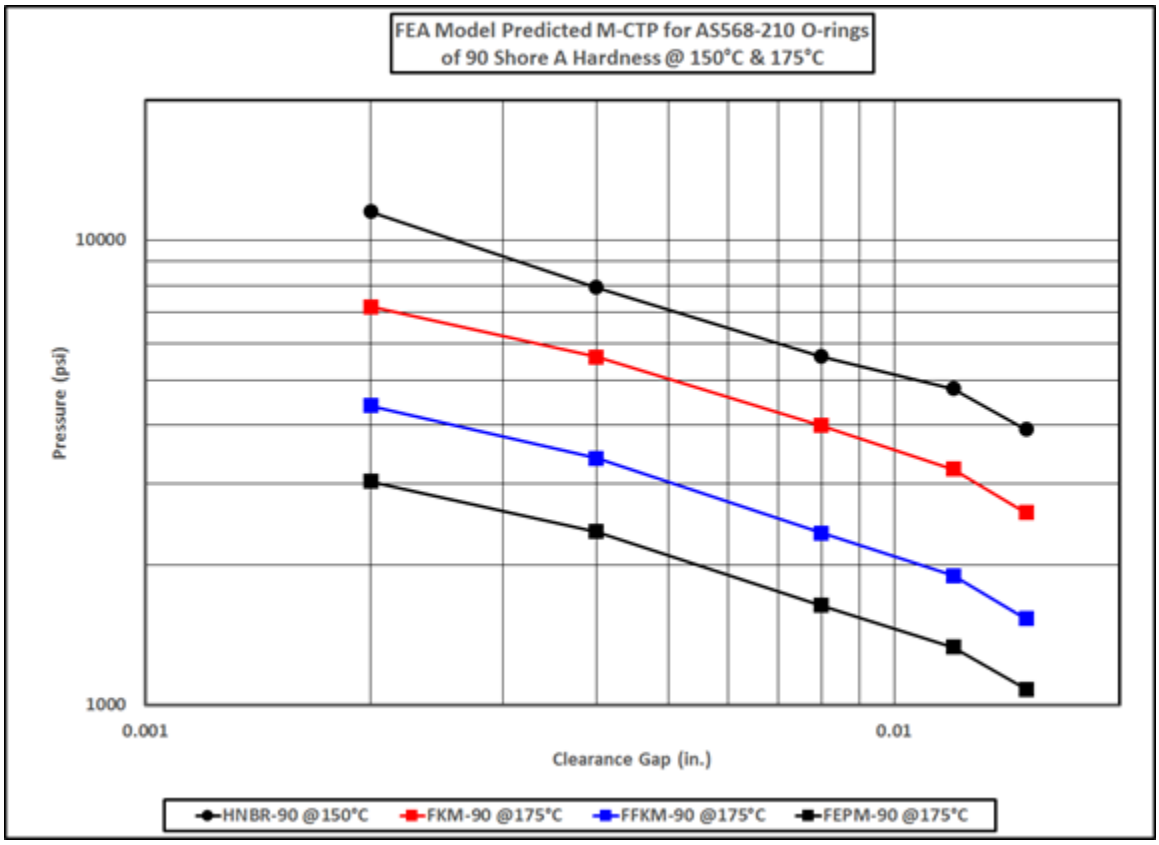


Figure A.7-16. M-CTP rankings for O-rings with a 90 Shore A Durometer at 150 and 175°C (Endurica, LLC).

## *M-CTP-based Relative Material Ranking*

The critical tearing pressure is plotted for all materials tested versus temperature in Figure A.7-17 for a 0.004” clearance gap and in Figure  for a 0.002” clearance gap. The materials are listed in the legend in descending critical tearing pressure at 100°C.

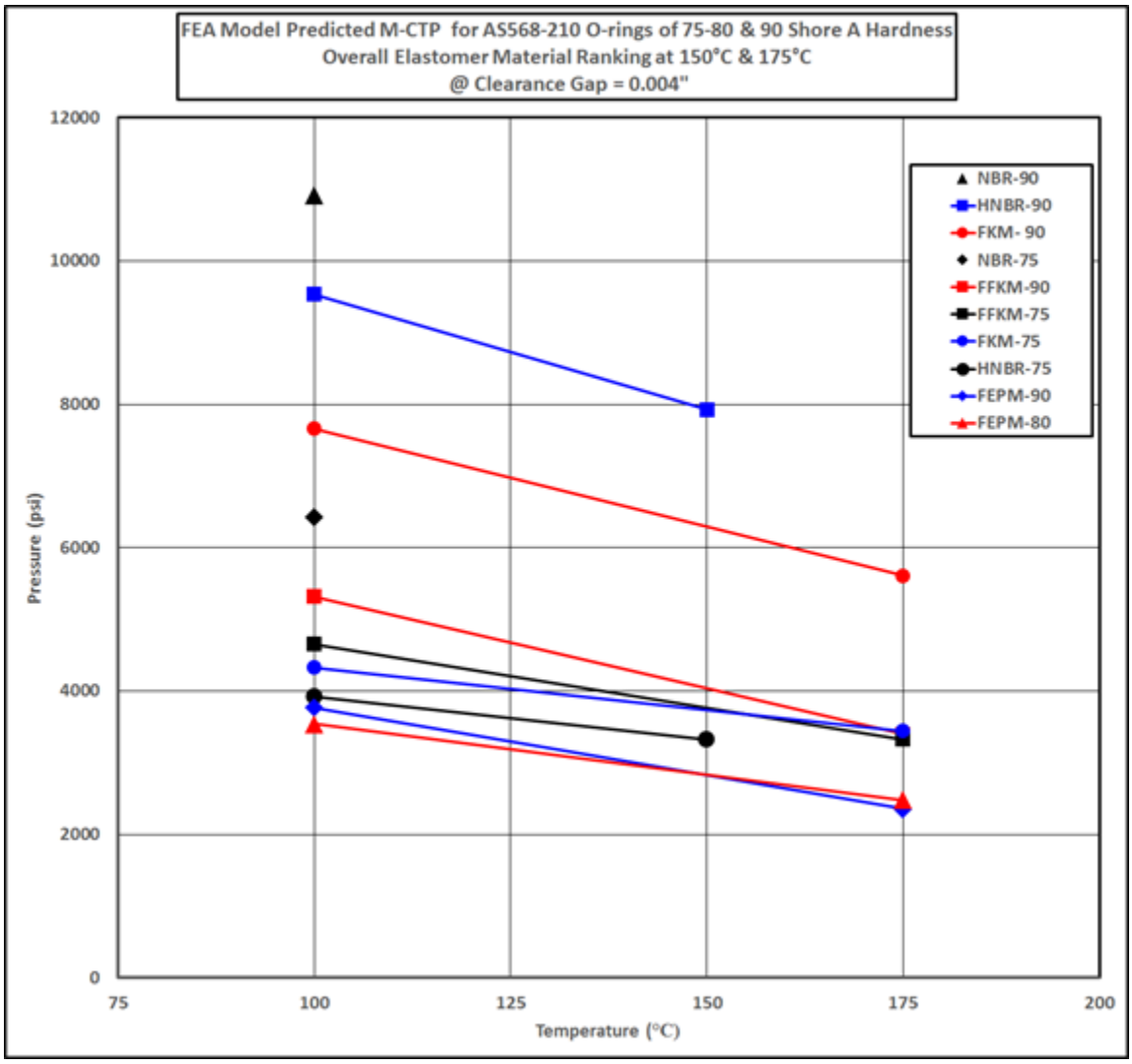


Figure A.7-17. Overall critical tear pressure ranking from FEA model (M-CTP) versus temperature for a 0.004” clearance gap and AS568-210 size O-rings. Note: NBR-75 and NBR-90 could only be tested at 100 °C (Endurica, LLC).

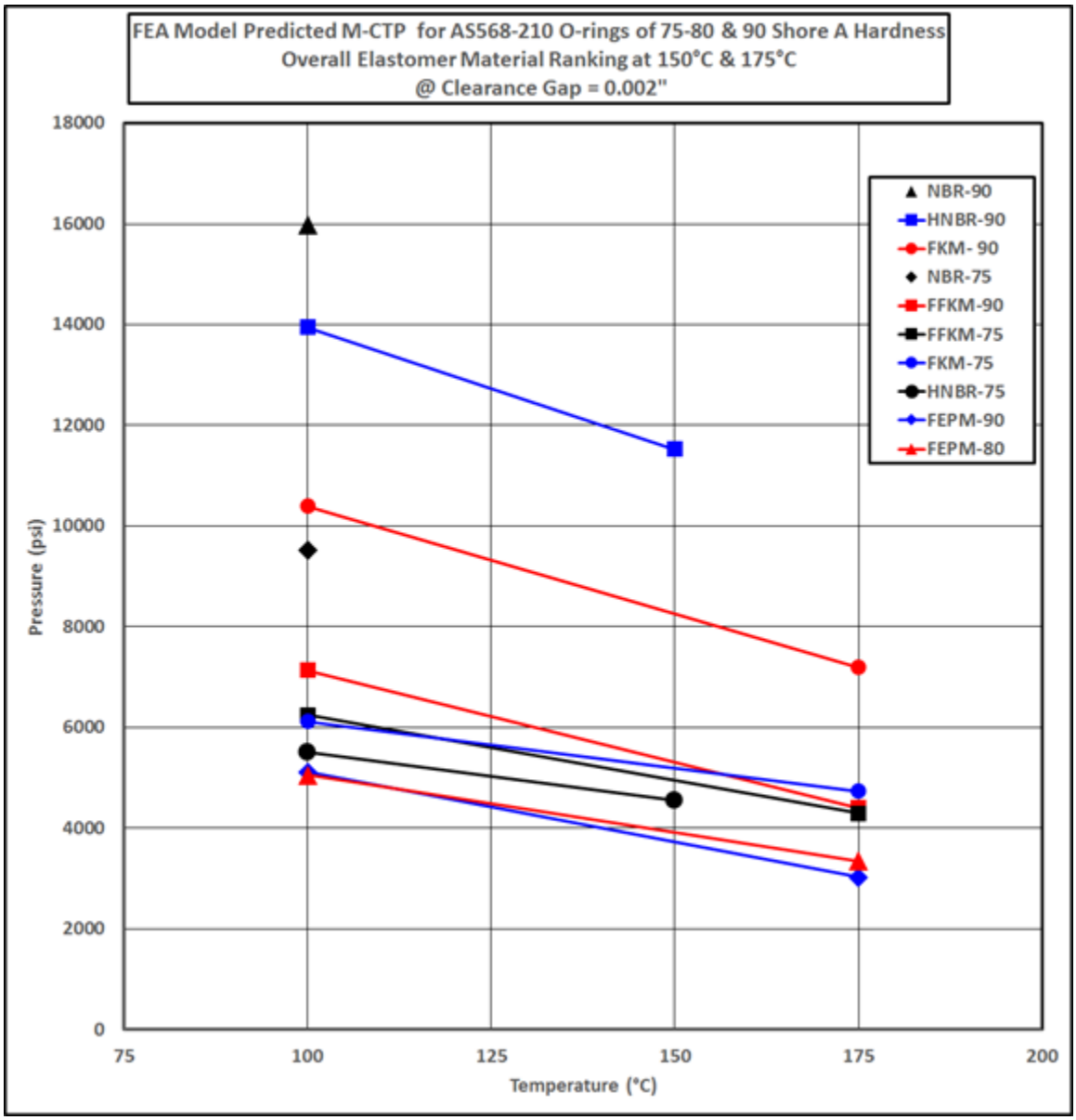


Figure A.7-18. Overall ranking of M-CTP materials at a clearance gap of 0.002 inch at 100°C to 175°C.

## Critical Tresca Stress

Based on the finite element simulation, the critical Tresca stress at which tearing initiates on the O-ring is listed in Table  and plotted in Figure .

Table A.7-3. Critical Tresca Stress for Elastomers

| Material | Critical Tresca Stress (PSI) |
|---|---|
| FEPM-80 100°C | 4,443 |
| FEPM-80 175°C | 2,351 |
| FEPM-90 100°C | 4,891 |
| FEPM-90 175°C | 2,384 |
| HNBR- 75 100°C | 4,408 |
| HNBR- 75 150°C | 3,194 |
| HNBR- 90 100°C | 16,064 |
| HNBR- 90 150°C | 11,678 |
| FFKM- 75 100°C | 6,755 |
| FFKM- 75 175°C | 3,404 |
| FFKM- 90 100°C | 6,773 |
| FFKM- 90 175°C | 3,175 |
| NBR- 75 100°C | 10,964 |
| NBR- 90 100°C | 14,044 |
| FKM- 75 100°C | 5,457 |
| FKM- 75 175°C | 3,582 |
| FKM- 90 100°C | 7,948 |
| FKM- 90 175°C | 4,680 |

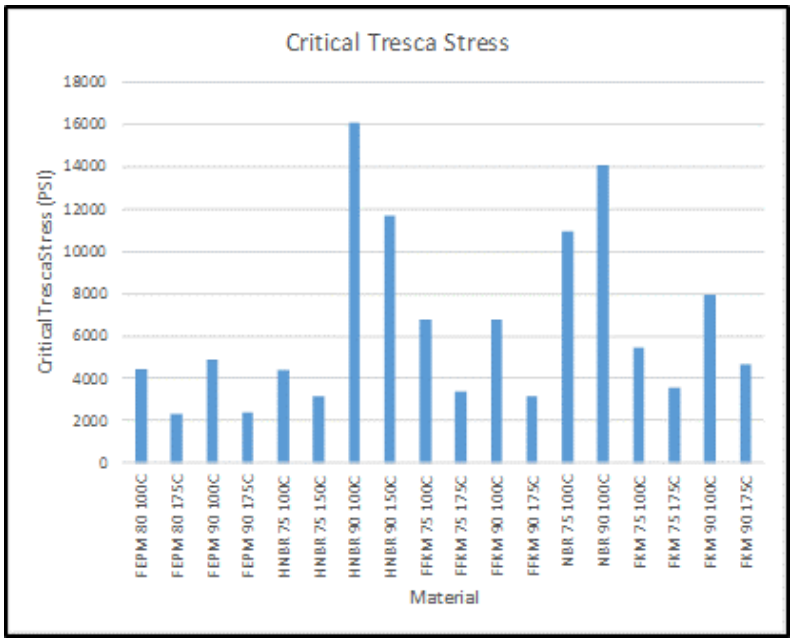


Figure A.7-19. Critical Tresca stress.

## Crack Precursor Size

All rubbers contain microscopic features from which cracks can develop. The initial size of such features is a key parameter that defines the strength and fatigue behavior of the rubber.

The crack precursor size is a temperature-independent constant that was inferred for each material by evaluating equation (9) at the pressure associated with incipient tearing, as observed in the PetroMar experiments, following the process in Figure A.7-6. The crack precursor size is listed in Table and plotted in Figure .

Table A.7-4. Crack precursor sizes.

| Material | Crack precursor size (μm) | Crack precursor size (x 0.001") |
|---|---|---|
| FEPM-80 | 1.202 | 0.04734 |
| FEPM-90 | 1.942 | 0.07646 |
| HNBR-75 | 2.323 | 0.09146 |
| HNBR-90 | 0.263 | 0.01036 |
| FFKM- 75 | 0.163 | 0.00642 |
| FFKM- 90 | 0.394 | 0.01551 |
| NBR- 75 | 0.296 | 0.01167 |
| NBR- 90 | 0.397 | 0.01562 |
| FKM- 75 | 0.469 | 0.01846 |
| FKM- 90 | 0.715 | 0.02814 |

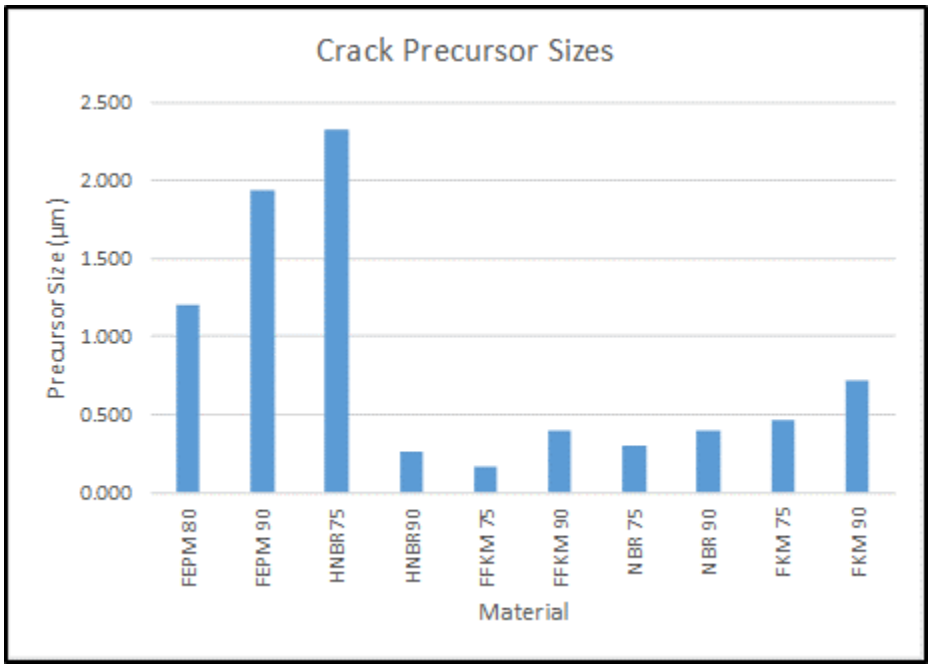


Figure A.7-20. Crack precursor sizes.

- NBR and HNBR-90 had highest Critical Tresca Stress Values and small Crack Precursor sizes
- FKM and FFKM had low Critical Tresca Stress and small Crack Precursor sizes
- FEPM had low Critical Tresca Stress and larger Crack Precursor sizes

# Conclusion

Statistical error is the degree to which a measurement agrees with the true value. Statistical uncertainty is an interval around the measurement in which repeated measurements will fall. Using the characterization, simulation and analysis methods presented herein, the critical pressure marking incipient tearing (M-CTP) and subsequent extrusion of the O-ring was calculated within an uncertainty that is similar to the variations observed in repeated experiments, across a wide range of materials, temperatures, and gap clearances. The success in validating the analysis with experiments strongly supports that the simulation and failure analysis procedures developed may be applied in other cases where seal safety depends on properly understanding the limits of the material, and the dependencies of the material on operating conditions. As the model exists today, it could reasonably be used to predict seal integrity for many other gland or lip geometries and loading / operating scenarios.

There are aspects of the O-ring sealing problem that have not been fully considered here, and which present opportunities for further study. We have suggested a model, based upon creep crack growth, for estimating the effects of long-duration pressurization periods (see Appendix A.7-2). The model has not been validated against long-term sealing experiments, but this could be done using the existing Petromar experimental hardware and longer exposure periods. The long-term effects of cyclic pressurization (and therefore fatigue crack growth effects) should also

be considered. Finally, the effects of thermochemical ageing on seal performance should be evaluated. Such evaluations would greatly benefit efforts to establish effective guidance on the conditions that ensure safe operating of O-rings in the long term.

## References

Anderson, Ted L., and T. L. Anderson. *Fracture mechanics: fundamentals and applications*. CRC press, 2005.

Aït-Bachir, Malik, W. V. Mars, and Erwan Verron. "Energy release rate of small cracks in hyperelastic materials." *International Journal of Non-Linear Mechanics* 47, no. 4 (2012): 22-29.

Gent, A. N., and W. V. Mars. "Strength of Elastomers, the Science and Technology of Rubber. Chapter 10." (2013).

Rivlin, R. S., and A. G. Thomas. "Rupture of rubber. I. Characteristic energy for tearing." Journal of Polymer Science 10, no. 3 (1953): 291-318.

Kadir, A., & Thomas, A. G. (1981). Tear behavior of rubbers over a wide range of rates. Rubber Chemistry and Technology, 54(1), 15-23.

HPHT O-ring Testing Results, Petromar Technologies Inc., Exton PA, 10 October 2016

Finite Element Modeling of O-ring Sealing Pressure Limits, FEA Video3.mp4, Endurica LLC, 14 September 2016.

Characterization of High Pressure / High Temperature (HPHT) Sealing Materials for Finite Element Analysis, Endurica LLC, 13 July 2016

# Appendix A.7-1. Computed Results for each Material

The computed results are given for each material from the FE model.

## *Model Results Summary Format*

The first result for each material is a graph of the applied pressure when tearing initiates versus the clearance gap. This graph includes results for the experimental test cell measured by PetroMar marked with an "X" symbol and FEA results calculated by Endurica marked with an "O" symbol. When two temperatures were tested for a material the higher temperature was plotted in red and the lower temperature in blue. The pressure calculated using FEA is at the critical peak Tresca stress that causes tearing of the O-ring as discussed previously in the tearing criterion section.

A table of results provides the value of each output for each clearance gap when O-ring tearing initiates due to the critical Tresca stress being reached. The outputs are applied pressure, strain energy, volume, strain energy density, and extrusion distance. Cases where the model fails to converge before reaching the critical Tresca stress are noted in the table with the abbreviation "NC" meaning the model did not converge. Model convergence failures were caused by excessively distorted finite elements that occurred in the stress concentration at the gland fillet radius.

Five different outputs are graphed versus the applied pressure; total recoverable strain energy, total O-ring volume, peak strain energy density, peak Tresca stress, and extrusion distance. An "X" shows the pressure at which the peak Tresca stress is reached in the model and the tearing initiates. The FE model does not include effects from the tear propagating through the O-ring. Results at pressures greater than the tearing initiation pressure include inaccuracies due to not modeling the tear propagation. The curve for each output continues until the model fails to converge or reaches the pressure input for the FE model step.

The first output graphed is the total recoverable strain energy which increases as pressure is increased. At a given pressure the total recoverable strain energy decreases at smaller clearance gaps.

The total O-ring volume is in the next graph. The total O-ring volume is nearly identical for all clearance gaps and decreases linearly with increasing pressure.

The strain energy density at the most critical location is in the next graph. The peak strain energy density increases at increasing pressures. At a given pressure the peak strain energy density decreases at smaller clearance gaps.

The Tresca stress at the most critical location is in the next graph. The peak Tresca stress increases as pressure increases. At a given pressure, the peak Tresca stress decreases at smaller clearance gaps. The same peak Tresca stress is used across all clearance gaps since it is a

material property. Tresca stress is temperature dependent since it is dependent upon the stress-strain law and critical tearing energy which are both temperature dependent.

The last output graph is of the extrusion distance. The extrusion distance approaches an upper limit as the pressure increases. At a given pressure the extrusion distance decreases at smaller clearance gaps. The extrusion distance is measured as the distance on the furthest point of the O-ring into the clearance gap to the lower gland face plane.

The last result for each material is a plot of the Tresca stress distribution at the pressure at which tearing initiates for the mid-size clearance gap of 0.008 inches. In the first plot on the left the O-ring is shown in the deformed position. The peak Tresca stress occurs along the fillet radius on the lip of the gland. The critical Tresca stress is set as the highest value in the legend and is colored red. The plot on the right shows the Tresca stress at the critical pressure plotted on the un-deformed O-ring. This purpose for this plot is to help visualize and compare the tearing location on the O-ring in the FE model to the tearing location observed on the physical test specimens from the PetroMar test. The angular location of tear initiation is noted for each material / temperature case for comparison against experiments.

## *FEPM-80*

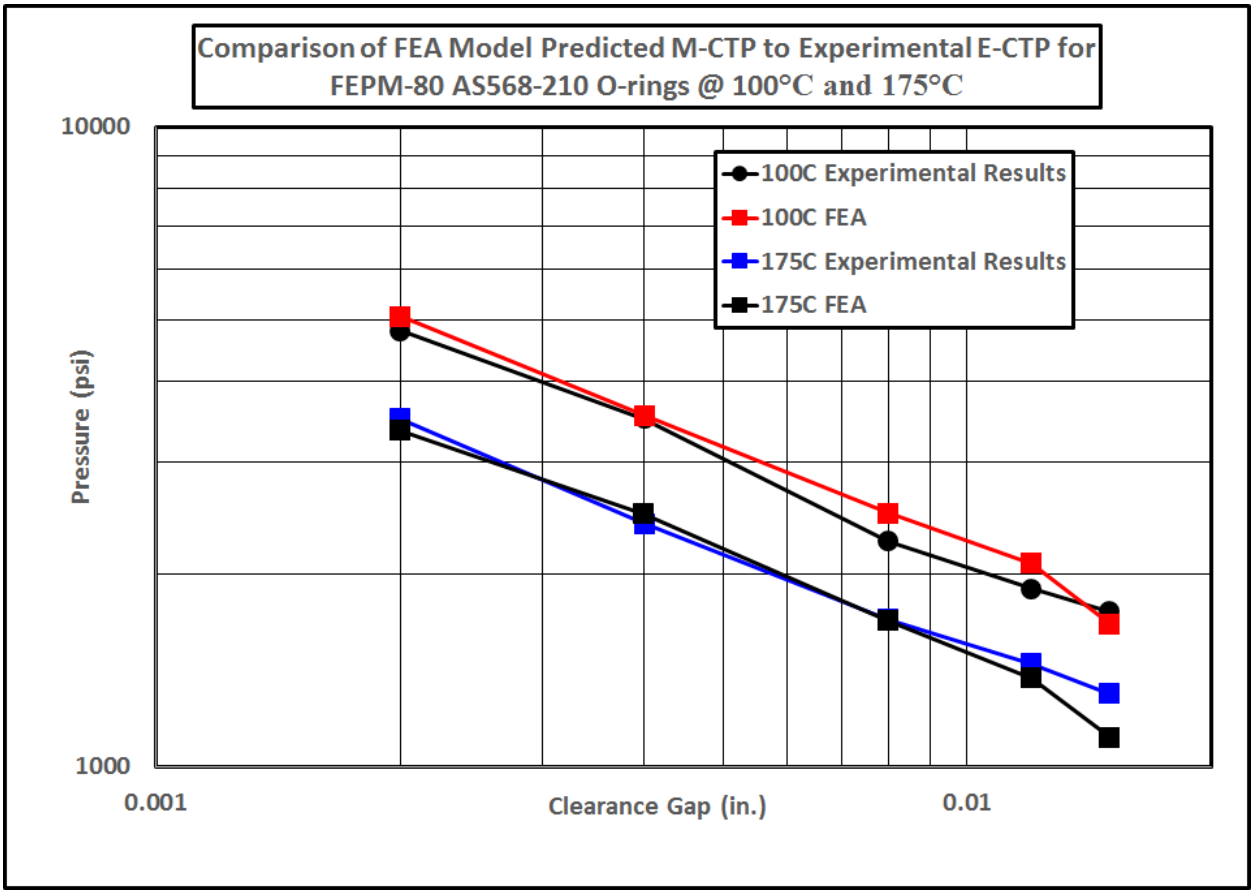


FEPM-80 100°C Simulation Output Parameters

| Clearance Gap | **0.015”** | **0.012”** | **0.008”** | **0.004”** | **0.002”** |
|---|---|---|---|---|---|
| **M-CTP Pressure (PSI)** | 1673 | 2080 | 2490 | 3540 | 5055 |
| **Strain Energy (in-lb.)** | 1.72 | 1.99 | 2.18 | 3.31 | 5.84 |
| **Volume ($in^3$)** | 0.04331 | 0.04315 | 0.04298 | 0.04256 | 0.04196 |
| **SED (PSI)** | 797 | 799 | 805 | 808 | 833 |
| **Extrusion Distance (mils)** | 18.17 | 17.30 | 12.07 | 8.02 | 5.79 |

FEPM-80 175°C Simulation Output Parameters

| Clearance Gap | **0.015”** | **0.012”** | **0.008”** | **0.004”** | **0.002”** |
|---|---|---|---|---|---|
| **M-CTP Pressure (PSI)** | 1113 | 1376 | 1692 | 2481 | 3350 |
| **Strain Energy (in-lb.)** | 1.36 | 1.50 | 1.63 | 2.32 | 3.46 |
| **Volume ($in^3$)** | 0.04587 | 0.04575 | 0.04560 | 0.04524 | 0.04484 |
| **SED (PSI)** | 463 | 464 | 466 | 473 | 477 |
| **Extrusion Distance (mils)** | 12.55 | 12.30 | 8.86 | 6.40 | 4.81 |

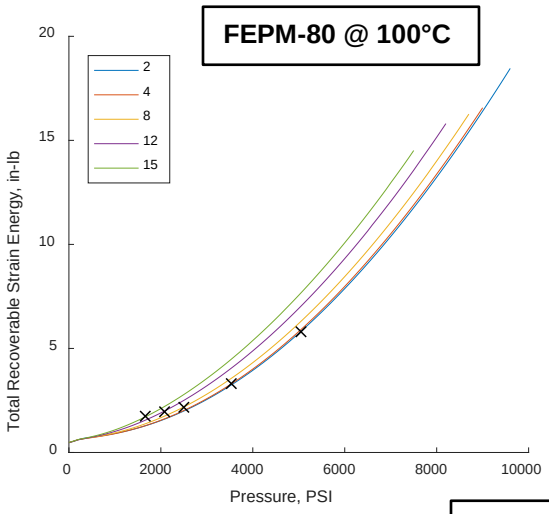
FEPM-80 @ 100°C
Total Recoverable Strain Energy, in-lb
Pressure, PSI
2
4
8
12
15

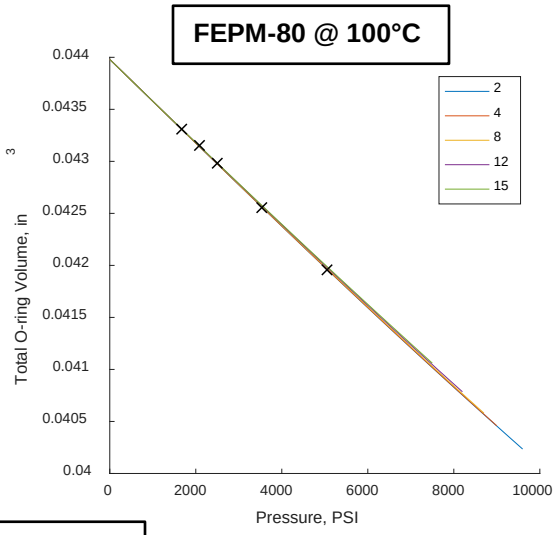
FEPM-80 @ 100°C
Total O-ring Volume, in3
Pressure, PSI
2
4
8
12
15

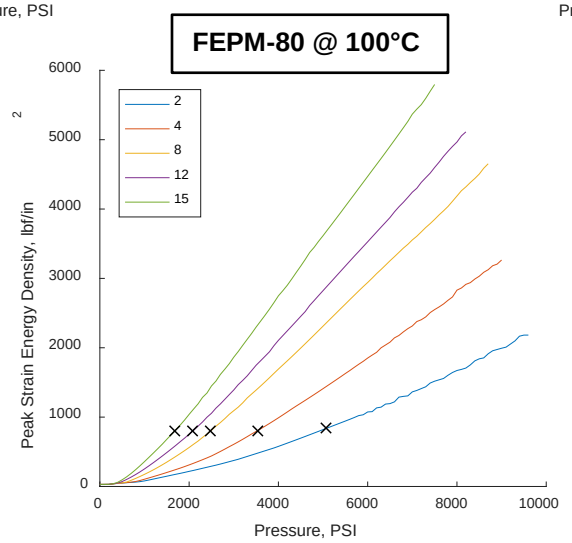
FEPM-80 @ 100°C
Peak Strain Energy Density, lbf/in2
Pressure, PSI
2
4
8
12
15

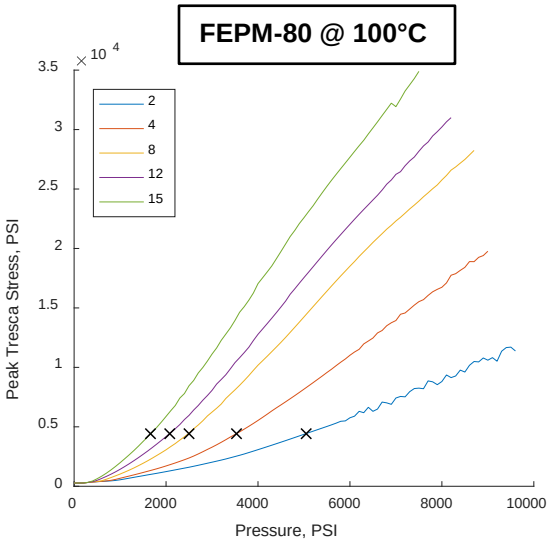
FEPM-80 @ 100°C
×10 4
Peak Tresca Stress, PSI
Pressure, PSI
2
4
8
12
15

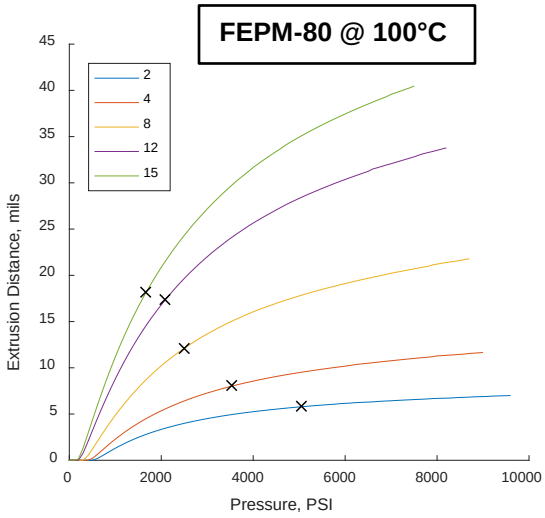
FEPM-80 @ 100°C
Extrusion Distance, mils
Pressure, PSI
2
4
8
12
15

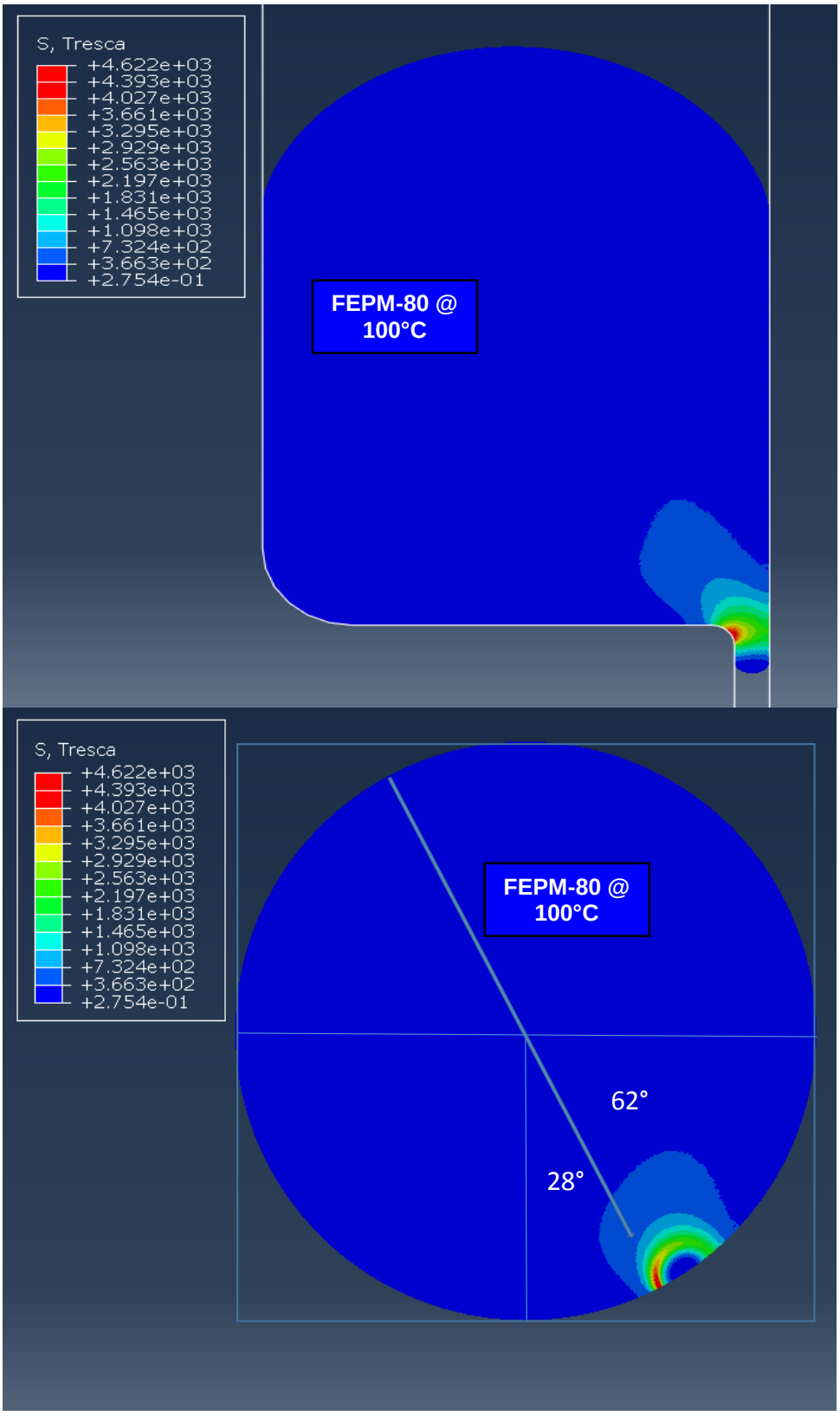
S, Tresca
+4.622e+03
+4.393e+03
+4.027e+03
+3.661e+03
+3.295e+03
+2.929e+03
+2.563e+03
+2.197e+03
+1.831e+03
+1.465e+03
+1.098e+03
+7.324e+02
+3.663e+02
+2.754e-01
FEPM-80 @ 100°C
S, Tresca
+4.622e+03
+4.393e+03
+4.027e+03
+3.661e+03
+3.295e+03
+2.929e+03
+2.563e+03
+2.197e+03
+1.831e+03
+1.465e+03
+1.098e+03
+7.324e+02
+3.663e+02
+2.754e-01
FEPM-80 @ 100°C
62°
28°

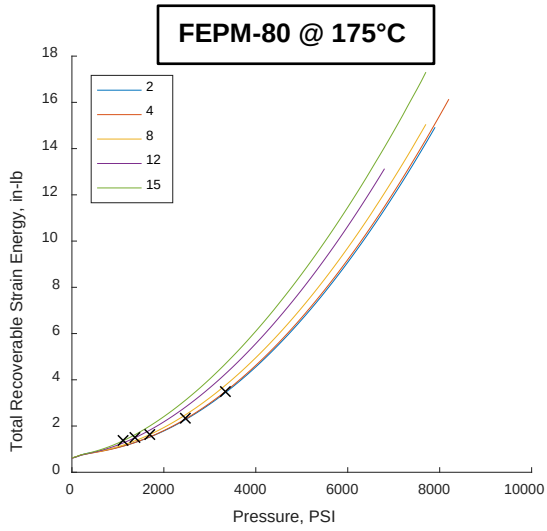
FEPM-80 @ 175°C
Total Recoverable Strain Energy, in-lb
Pressure, PSI
2
4
8
12
15

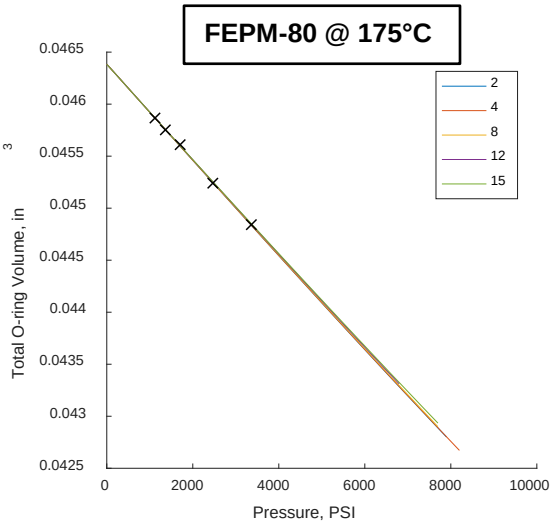
FEPM-80 @ 175°C
Total O-ring Volume, in 3
Pressure, PSI
2
4
8
12
15

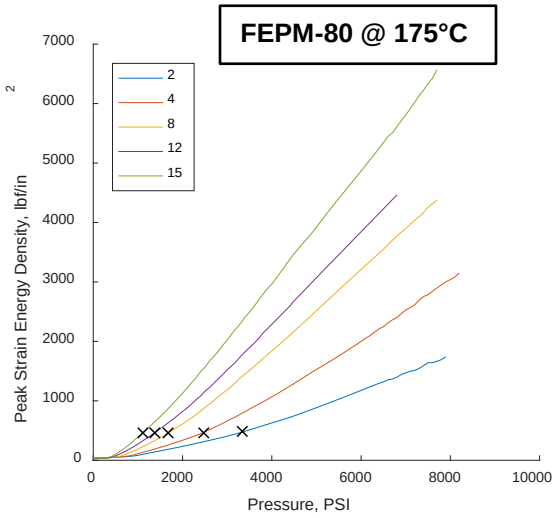
FEPM-80 @ 175°C
Peak Strain Energy Density, lbf/in 2
Pressure, PSI
2
4
8
12
15

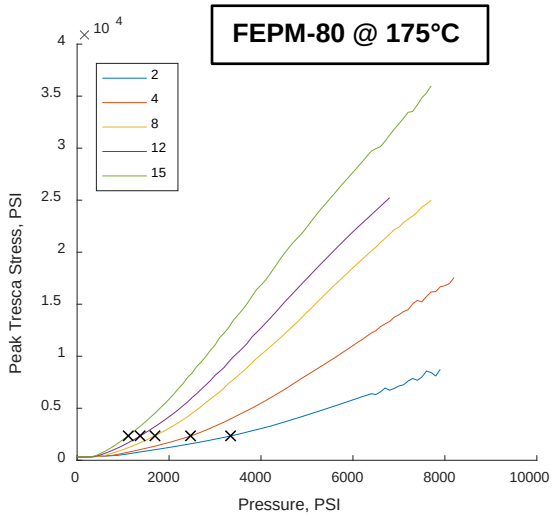
FEPM-80 @ 175°C
× 10 4
Peak Tresca Stress, PSI
Pressure, PSI
2
4
8
12
15

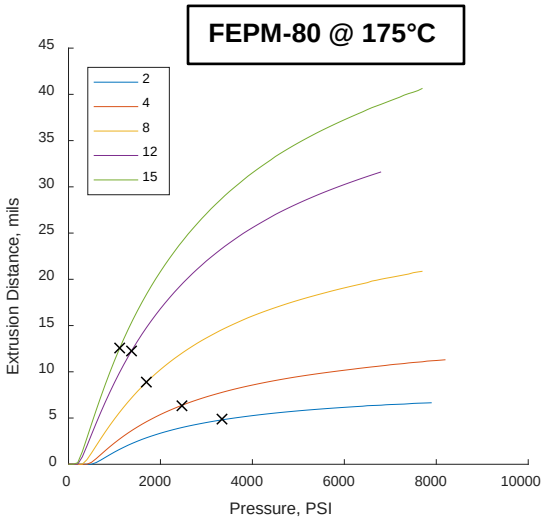
FEPM-80 @ 175°C
Extrusion Distance, mils
Pressure, PSI
2
4
8
12
15

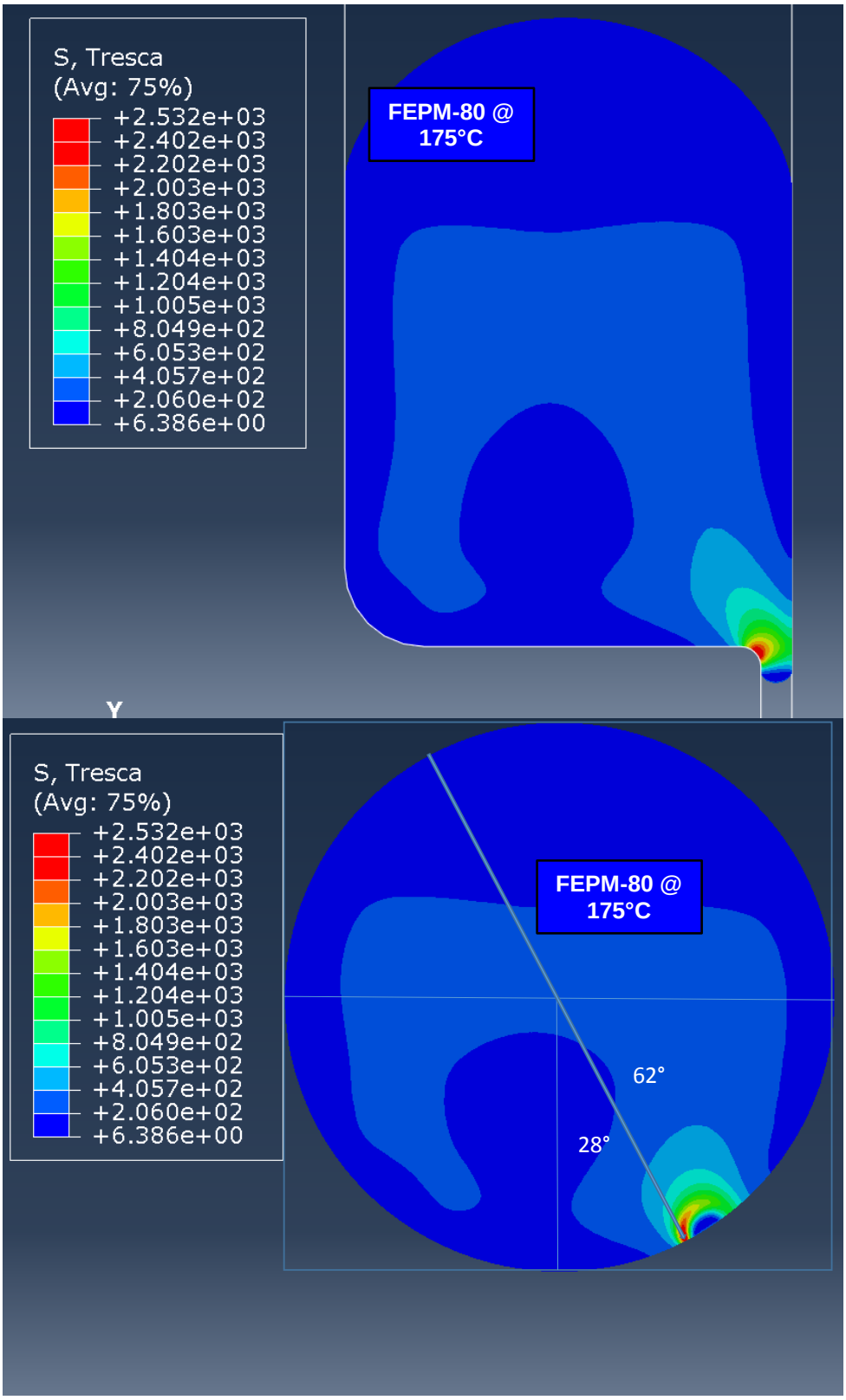
S, Tresca
(Avg: 75%)
+2.532e+03
+2.402e+03
+2.202e+03
+2.003e+03
+1.803e+03
+1.603e+03
+1.404e+03
+1.204e+03
+1.005e+03
+8.049e+02
+6.053e+02
+4.057e+02
+2.060e+02
+6.386e+00
FEPM-80 @
175°C
Y
S, Tresca
(Avg: 75%)
+2.532e+03
+2.402e+03
+2.202e+03
+2.003e+03
+1.803e+03
+1.603e+03
+1.404e+03
+1.204e+03
+1.005e+03
+8.049e+02
+6.053e+02
+4.057e+02
+2.060e+02
+6.386e+00
FEPM-80 @
175°C
62°
28°

## *FEPM-90*

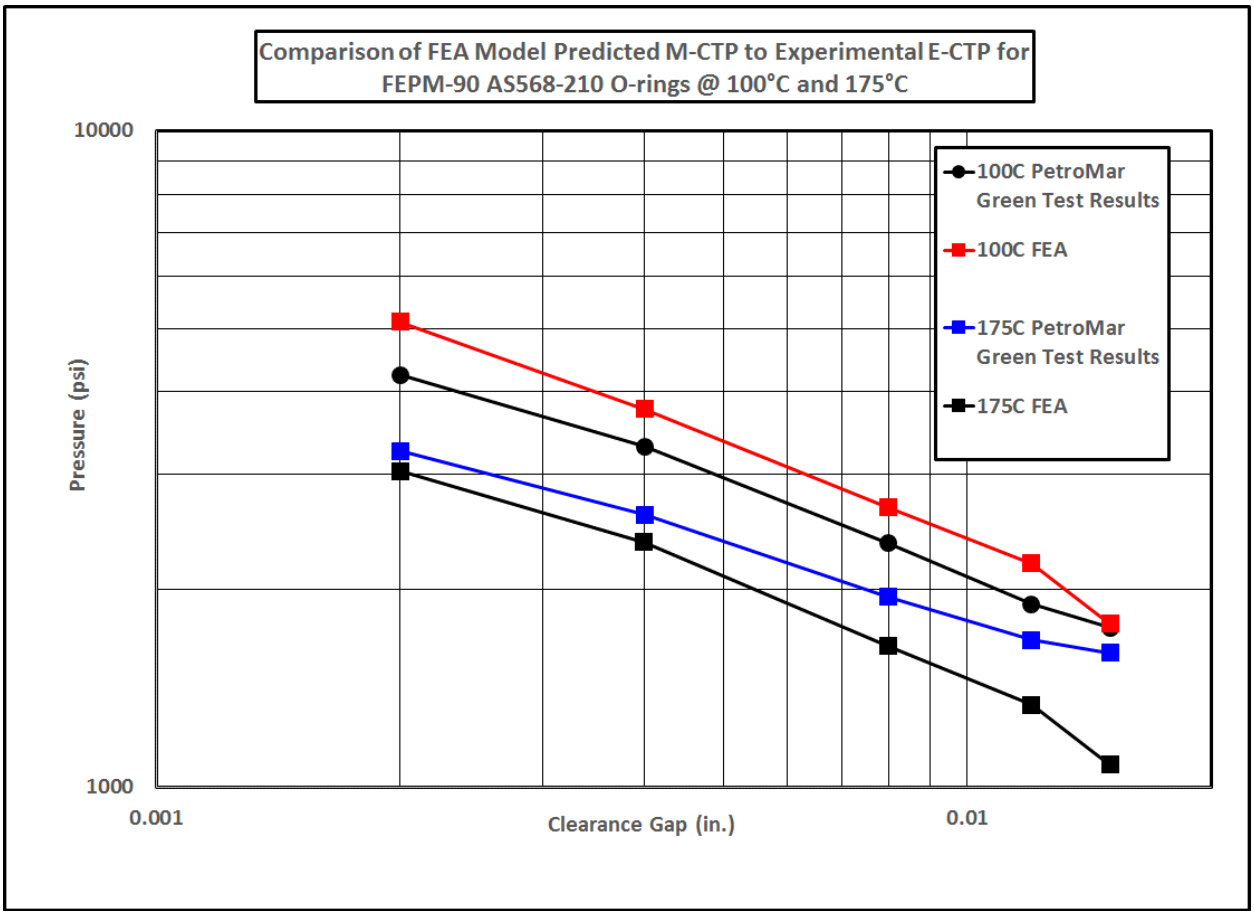


FEPM-90 100°C Simulation Output Parameters

| Clearance Gap | **0.015”** | **0.012”** | **0.008”** | **0.004”** | **0.002”** |
|---|---|---|---|---|---|
| **M-CTP Pressure (PSI)** | 1773 | 2193 | 2667 | 3769 | 5114 |
| **Strain Energy (in-lb.)** | 1.68 | 1.93 | 2.19 | 3.33 | 5.37 |
| **Volume ($in^3$)** | 0.04295 | 0.04280 | 0.04263 | 0.04224 | 0.04178 |
| **SED (PSI)** | 572 | 576 | 582 | 593 | 612 |
| **Extrusion Distance (mils)** | 14.96 | 13.94 | 9.75 | 6.52 | 4.77 |

FEPM-90 175°C Simulation Output Parameters

| Clearance Gap | **0.015”** | **0.012”** | **0.008”** | **0.004”** | **0.002”** |
|---|---|---|---|---|---|
| **M-CTP Pressure (PSI)** | 1083 | 1333 | 1640 | 2356 | 3028 |
| **Strain Energy (in-lb.)** | 1.24 | 1.36 | 1.48 | 2.05 | 2.82 |
| **Volume ($in^3$)** | 0.04508 | 0.04497 | 0.04484 | 0.04452 | 0.04423 |
| **SED (PSI)** | 339 | 340 | 342 | 346 | 347 |
| **Extrusion Distance (mils)** | 11.79 | 11.36 | 8.10 | 5.70 | 4.24 |

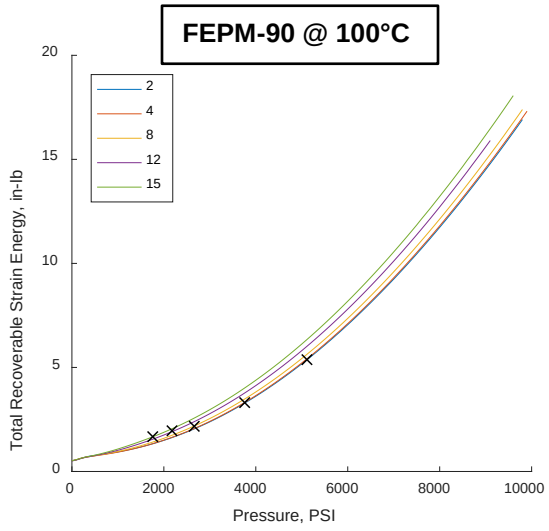
FEPM-90 @ 100°C
Total Recoverable Strain Energy, in-lb
Pressure, PSI
2
4
8
12
15

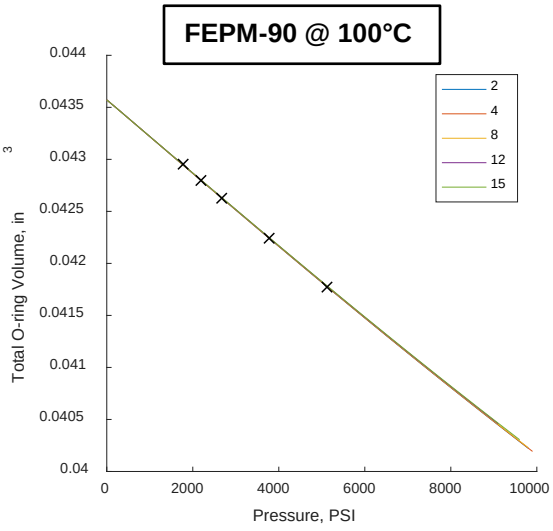
FEPM-90 @ 100°C
Total O-ring Volume, in 3
Pressure, PSI
2
4
8
12
15

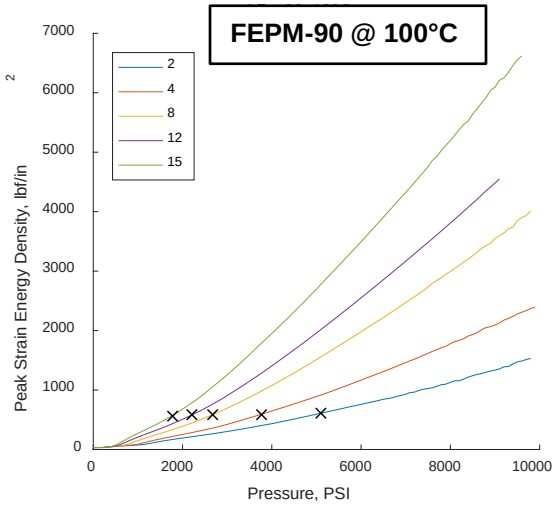
FEPM-90 @ 100°C
Peak Strain Energy Density, lbf/in 2
Pressure, PSI
2
4
8
12
15

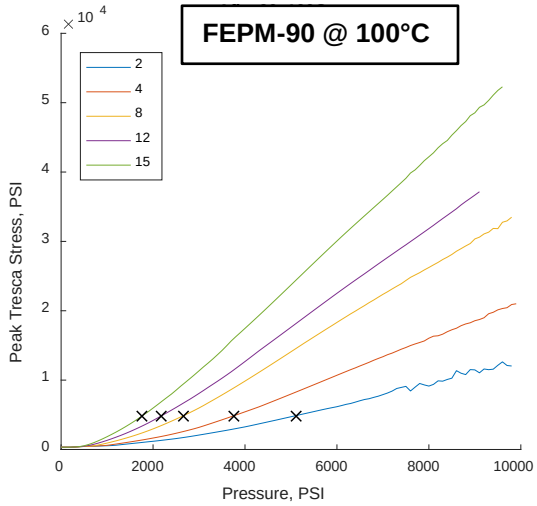
FEPM-90 @ 100°C
× 10 4
Peak Tresca Stress, PSI
Pressure, PSI
2
4
8
12
15

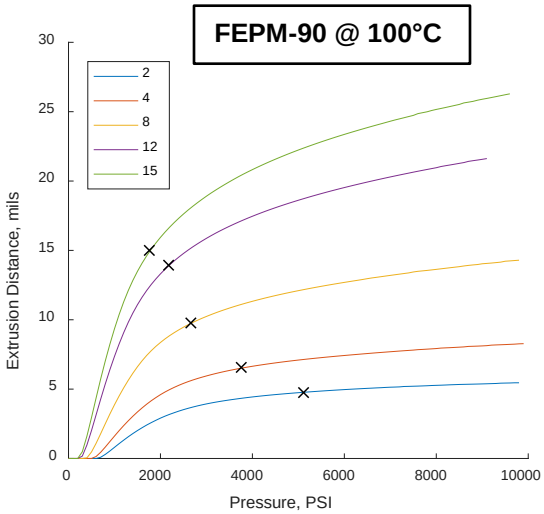
FEPM-90 @ 100°C
Extrusion Distance, mils
Pressure, PSI
2
4
8
12
15

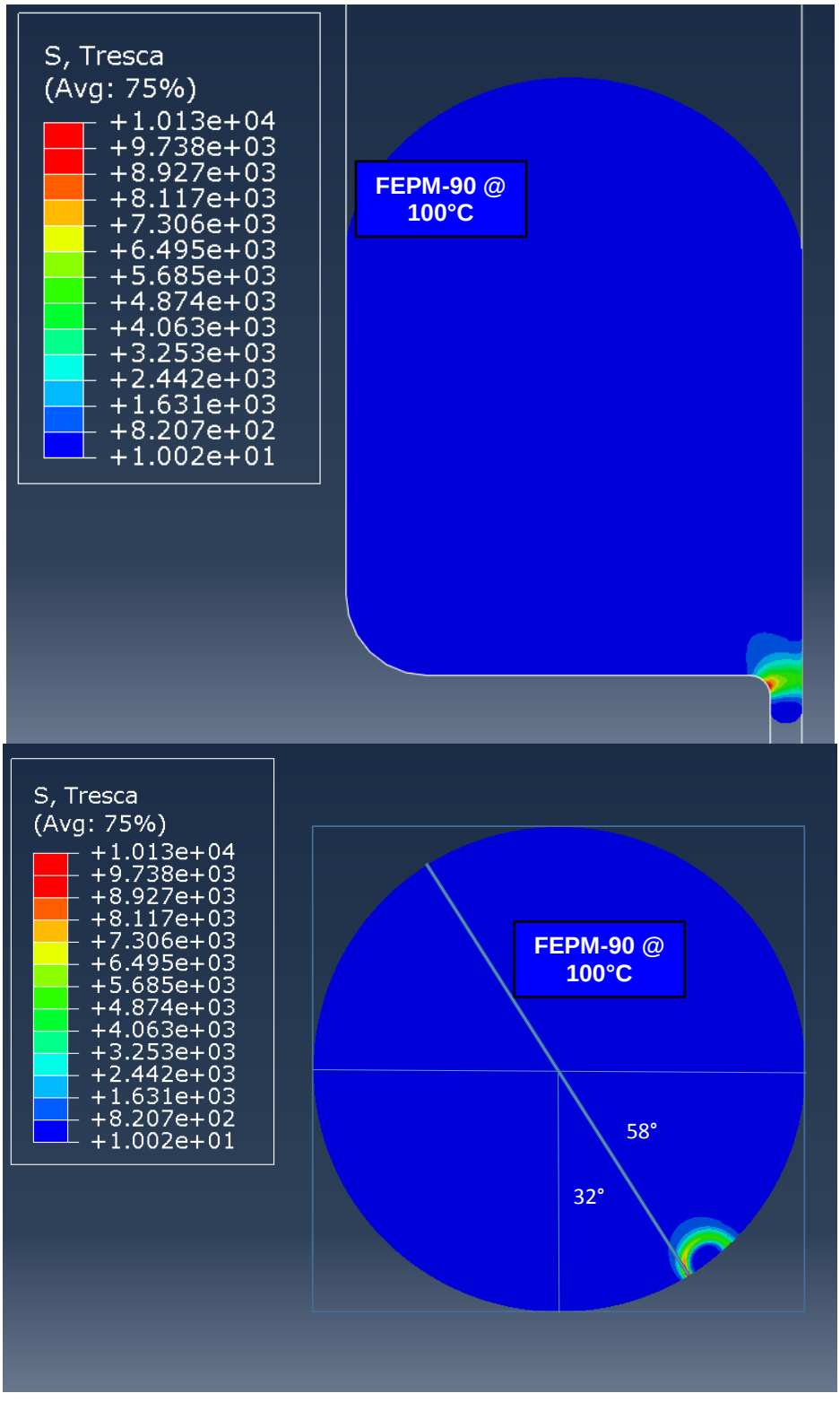
S, Tresca
(Avg: 75%)
+1.013e+04
+9.738e+03
+8.927e+03
+8.117e+03
+7.306e+03
+6.495e+03
+5.685e+03
+4.874e+03
+4.063e+03
+3.253e+03
+2.442e+03
+1.631e+03
+8.207e+02
+1.002e+01
FEPM-90 @
100°C
S, Tresca
(Avg: 75%)
+1.013e+04
+9.738e+03
+8.927e+03
+8.117e+03
+7.306e+03
+6.495e+03
+5.685e+03
+4.874e+03
+4.063e+03
+3.253e+03
+2.442e+03
+1.631e+03
+8.207e+02
+1.002e+01
FEPM-90 @
100°C
58°
32°

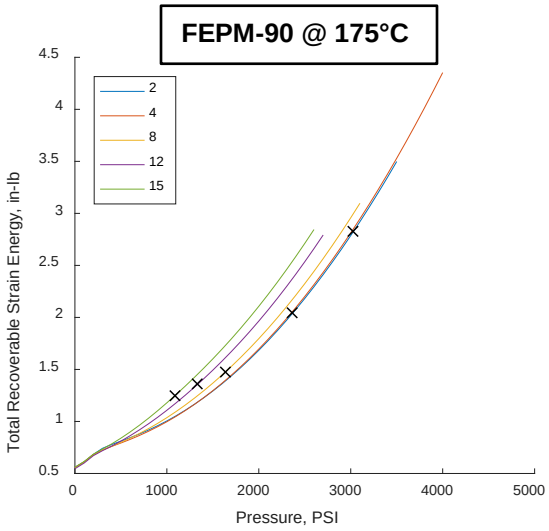
FEPM-90 @ 175°C
Total Recoverable Strain Energy, in-lb
Pressure, PSI
2
4
8
12
15

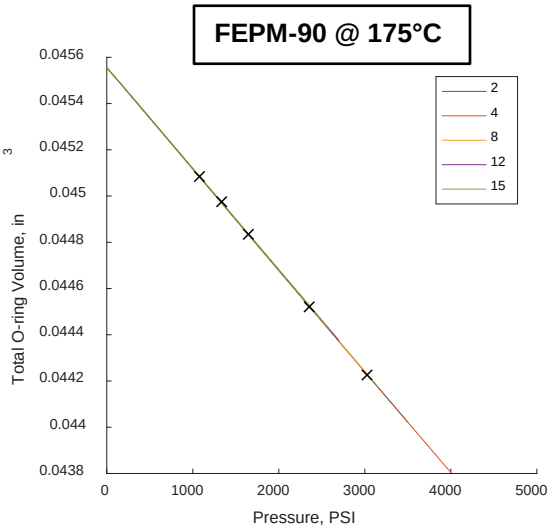
FEPM-90 @ 175°C
Total O-ring Volume, in3
Pressure, PSI
2
4
8
12
15

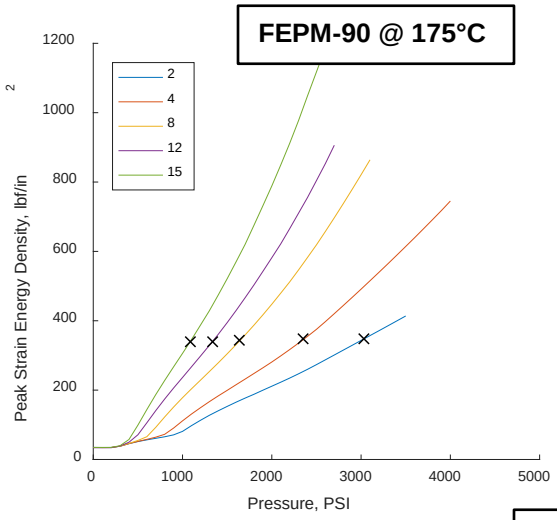
FEPM-90 @ 175°C
Peak Strain Energy Density, lbf/in2
Pressure, PSI
2
4
8
12
15

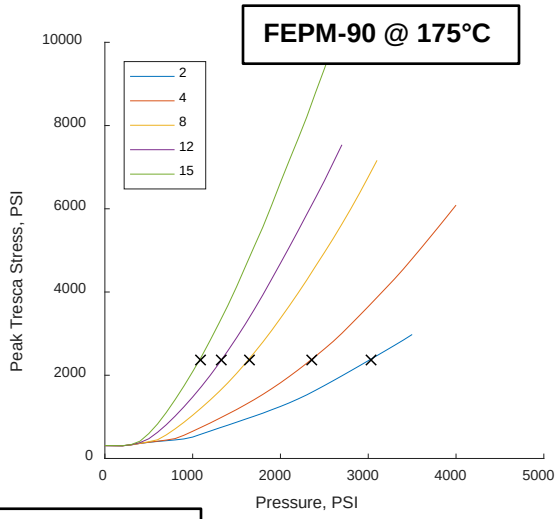
FEPM-90 @ 175°C
Peak Tresca Stress, PSI
Pressure, PSI
2
4
8
12
15

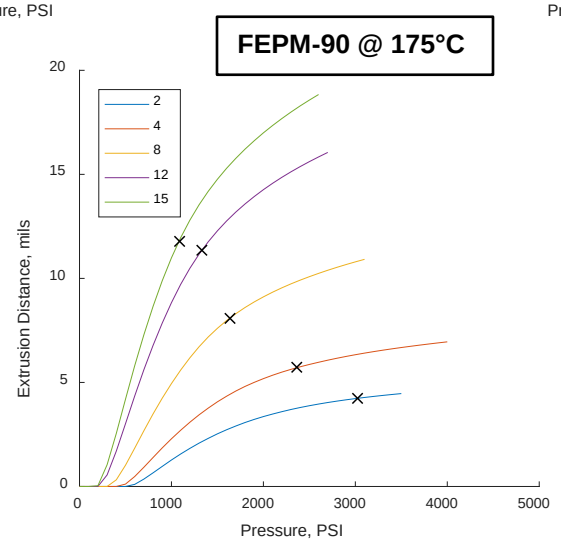
FEPM-90 @ 175°C
Extrusion Distance, mils
Pressure, PSI
2
4
8
12
15

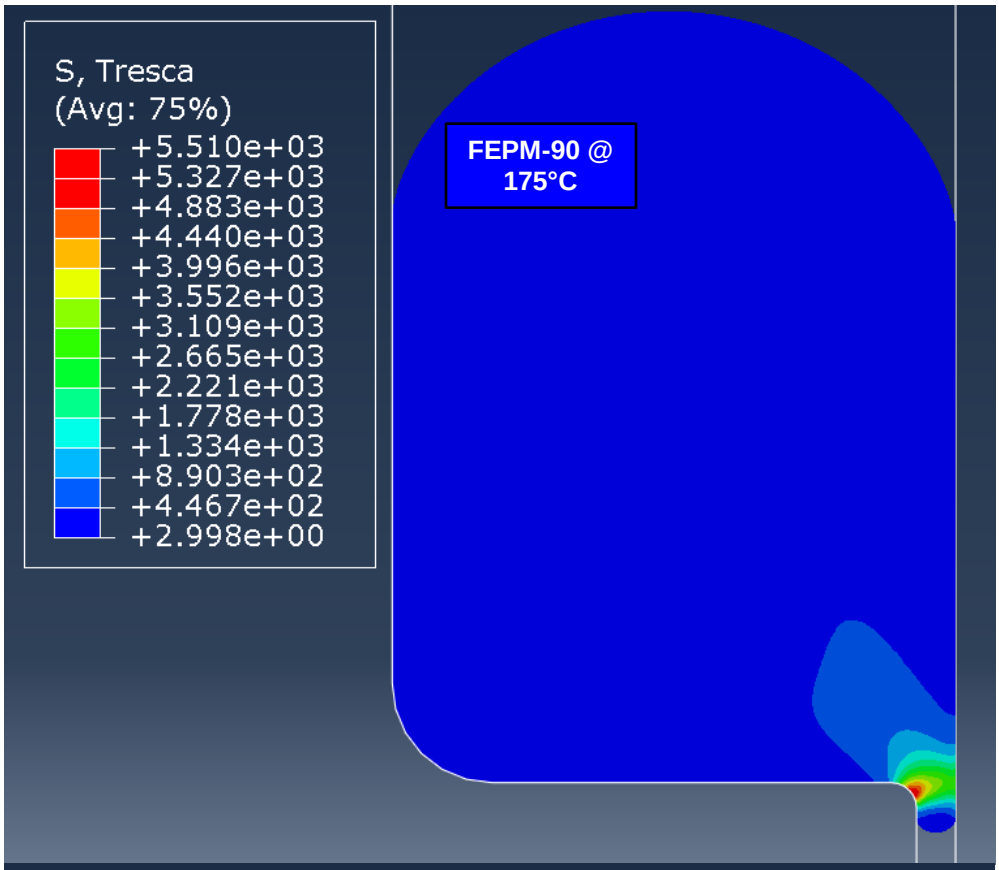
S, Tresca
(Avg: 75%)
+5.510e+03
+5.327e+03
+4.883e+03
+4.440e+03
+3.996e+03
+3.552e+03
+3.109e+03
+2.665e+03
+2.221e+03
+1.778e+03
+1.334e+03
+8.903e+02
+4.467e+02
+2.998e+00
FEPM-90 @
175°C

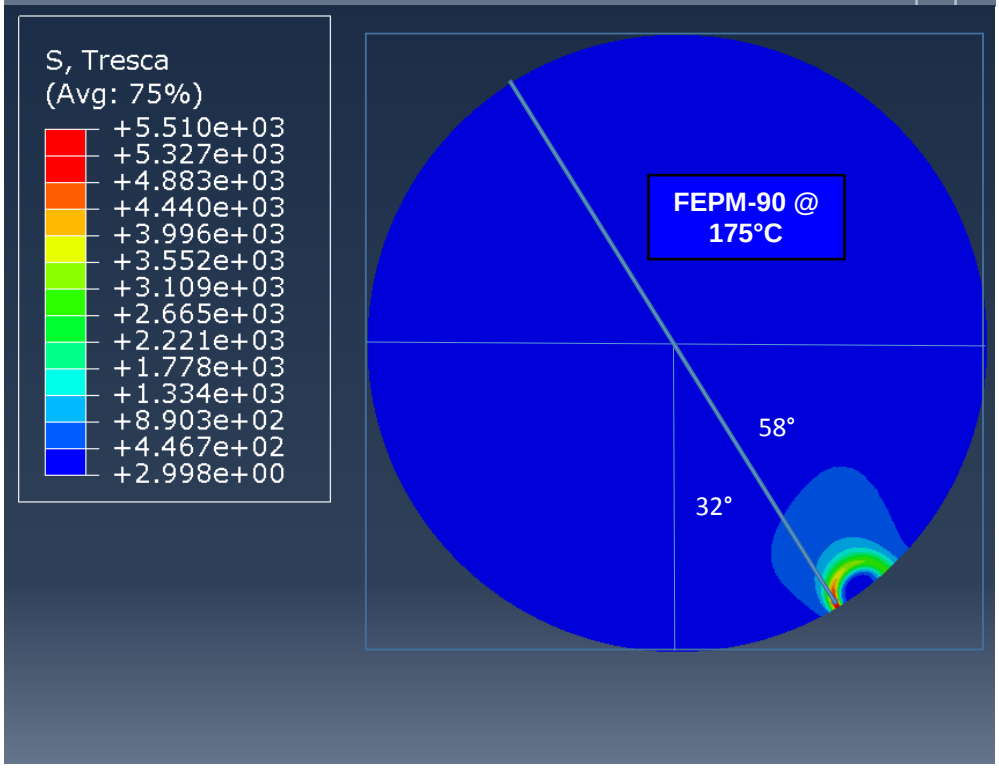
S, Tresca
(Avg: 75%)
+5.510e+03
+5.327e+03
+4.883e+03
+4.440e+03
+3.996e+03
+3.552e+03
+3.109e+03
+2.665e+03
+2.221e+03
+1.778e+03
+1.334e+03
+8.903e+02
+4.467e+02
+2.998e+00
FEPM-90 @
175°C
58°
32°

## *HNBR- 75*

Material properties for HNBR-75 were measured at 100°C. The material properties for HNBR-75 at 150°C were estimated based on the observed differences in properties of HNBR-90 between 100°C and 150°C. The same Hyperelastic properties were used for HNBR-75 at both 100°C and 150°C based on negligible differences in the observed in the Hyperelastic curve of HNBR-90 at 100°C and 150°C. The critical tearing energy for HNBR-75 at 150°C was calculated to be 1.215 kJ/m$^2$, following the same percent reduction of Tc observed in HNBR-90 from 100°C to 150°C.

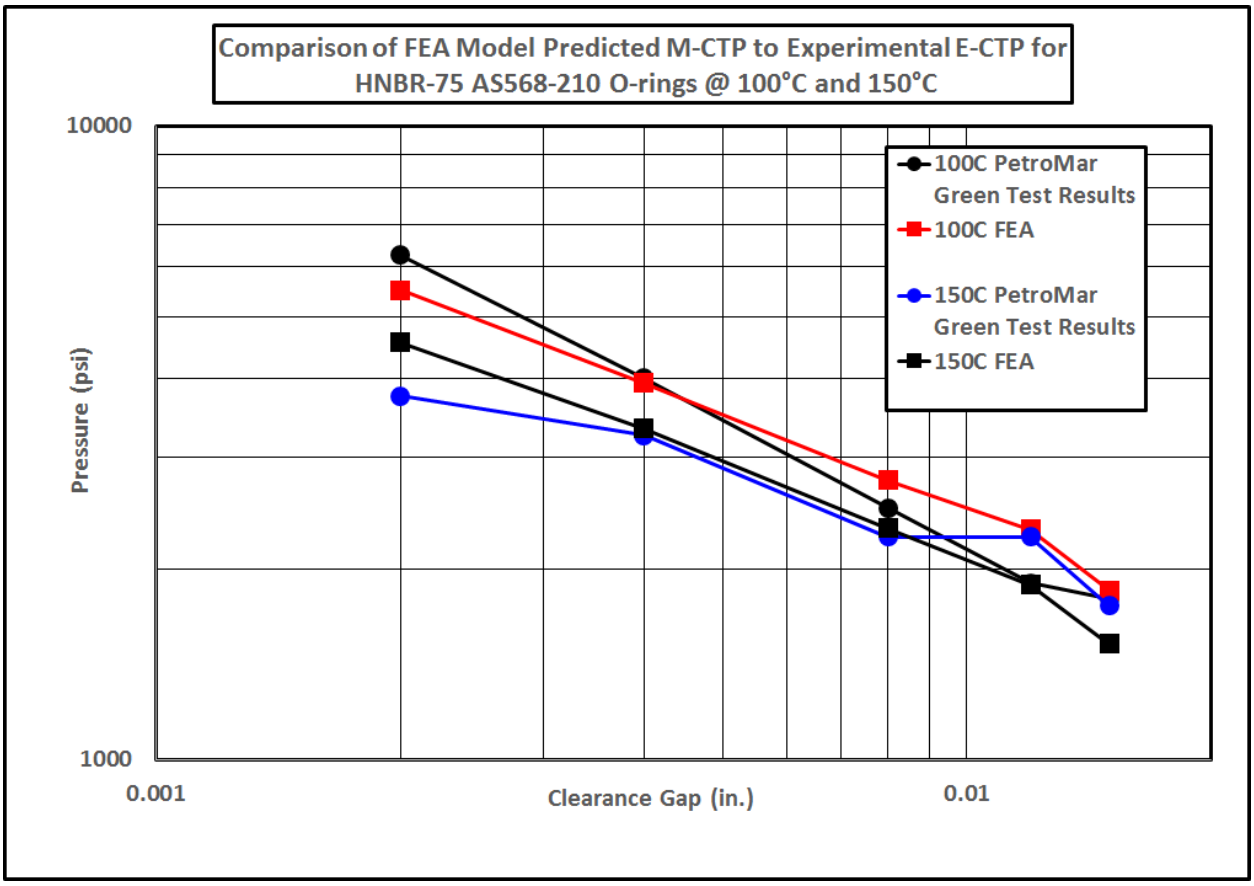


HNBR-75 100°C Simulation Output Parameters

| Clearance Gap | **0.015”** | **0.012”** | **0.008”** | **0.004”** | **0.002”** |
|---|---|---|---|---|---|
| **M-CTP Pressure (PSI)** | 1853 | 2309 | 2764 | 3927 | 5504 |
| **Strain Energy (in-lb.)** | 2.14 | 2.42 | 2.56 | 3.66 | 6.03 |
| **Volume (in$^3$)** | 0.04295 | 0.04280 | 0.04265 | 0.04226 | 0.04175 |
| **SED (PSI)** | 950 | 953 | 954 | 960 | 969 |
| **Extrusion Distance (mils)** | 17.67 | 17.24 | 12.04 | 8.12 | 5.85 |

HNBR-75 150°C Simulation Output Parameters

| Clearance Gap | **0.015”** | **0.012”** | **0.008”** | **0.004”** | **0.002”** |
|---|---|---|---|---|---|
| **M-CTP Pressure (PSI)** | 1525 | 1888 | 2321 | 3323 | 4552 |
| **Strain Energy (in-lb.)** | 1.91 | 2.09 | 2.26 | 3.10 | 4.69 |
| **Volume ($in^3$)** | 0.04434 | 0.04422 | 0.04407 | 0.04373 | 0.04332 |
| **SED (PSI)** | 704 | 706 | 708 | 713 | 719 |
| **Extrusion Distance (mils)** | 14.05 | 13.93 | 10.03 | 7.07 | 5.25 |

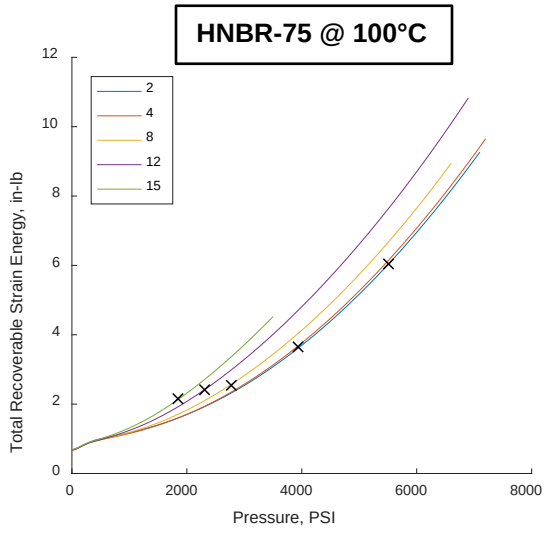
HNBR-75 @ 100°C
Total Recoverable Strain Energy, in-lb
Pressure, PSI
2
4
8
12
15

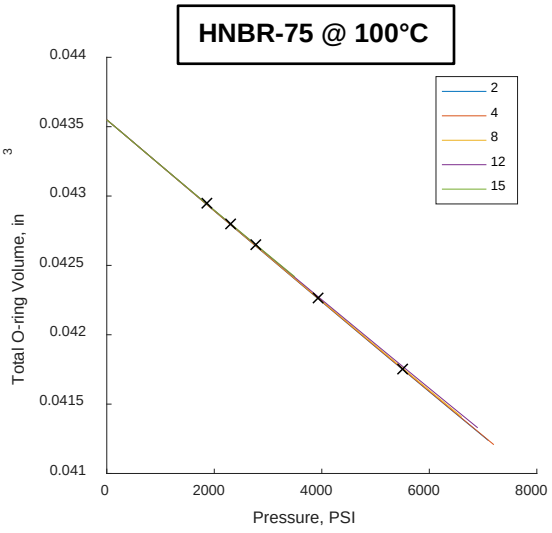
HNBR-75 @ 100°C
Total O-ring Volume, in3
Pressure, PSI
2
4
8
12
15

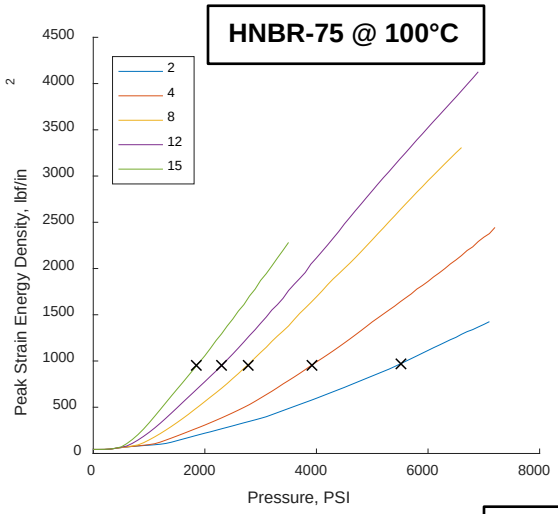
HNBR-75 @ 100°C
Peak Strain Energy Density, lbf/in2
Pressure, PSI
2
4
8
12
15

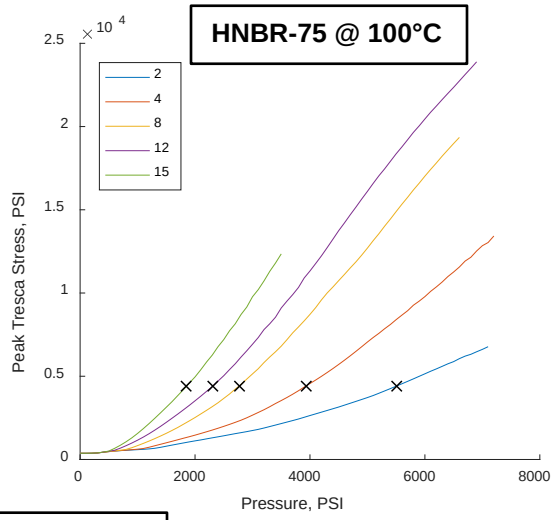
HNBR-75 @ 100°C
×10 4
Peak Tresca Stress, PSI
Pressure, PSI
2
4
8
12
15

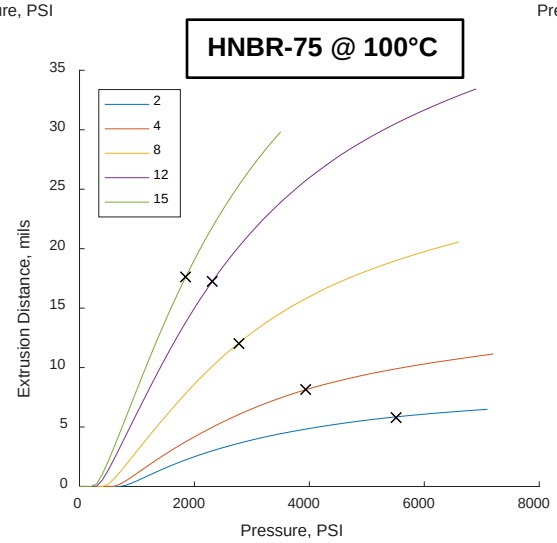
HNBR-75 @ 100°C
Extrusion Distance, mils
Pressure, PSI
2
4
8
12
15

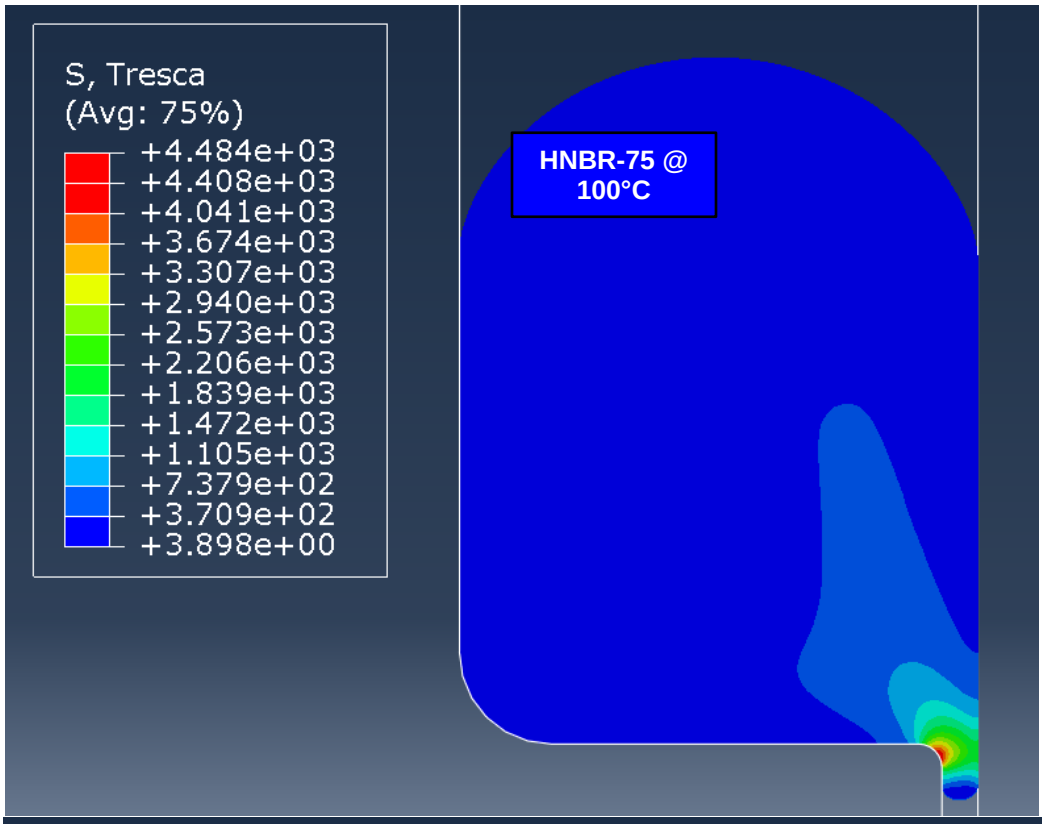
S, Tresca
(Avg: 75%)
+4.484e+03
+4.408e+03
+4.041e+03
+3.674e+03
+3.307e+03
+2.940e+03
+2.573e+03
+2.206e+03
+1.839e+03
+1.472e+03
+1.105e+03
+7.379e+02
+3.709e+02
+3.898e+00
HNBR-75 @
100°C

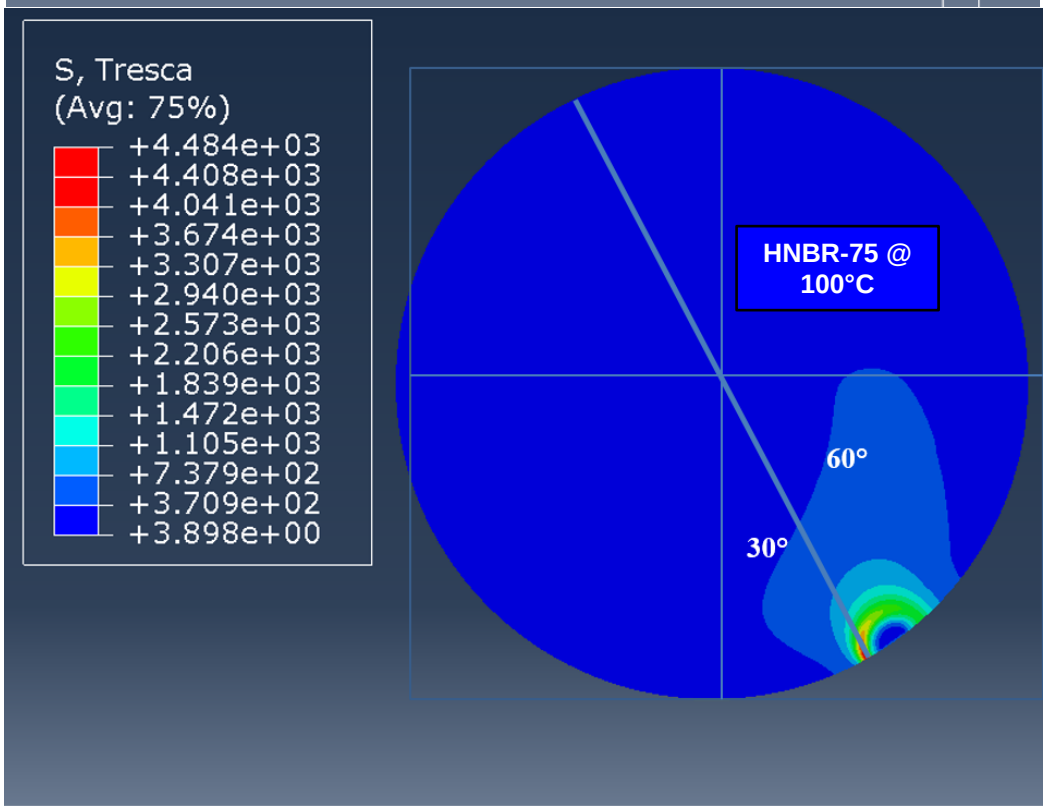
S, Tresca
(Avg: 75%)
+4.484e+03
+4.408e+03
+4.041e+03
+3.674e+03
+3.307e+03
+2.940e+03
+2.573e+03
+2.206e+03
+1.839e+03
+1.472e+03
+1.105e+03
+7.379e+02
+3.709e+02
+3.898e+00
HNBR-75 @
100°C
60°
30°

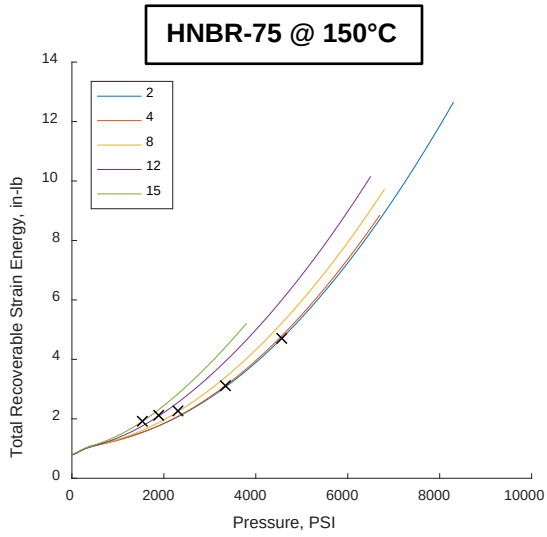
HNBR-75 @ 150°C
Total Recoverable Strain Energy, in-lb
Pressure, PSI
2
4
8
12
15

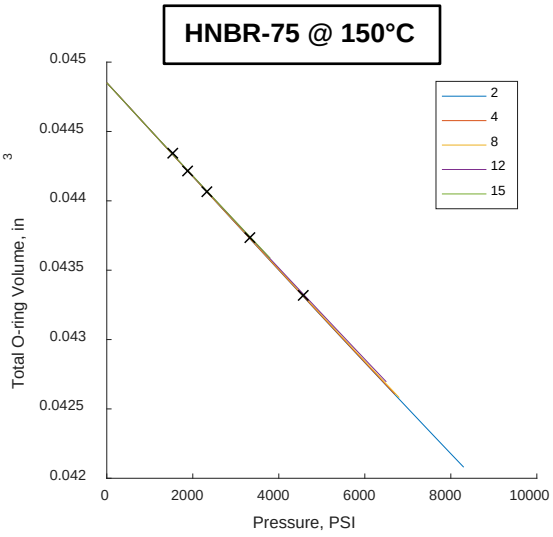
HNBR-75 @ 150°C
Total O-ring Volume, in 3
Pressure, PSI
2
4
8
12
15

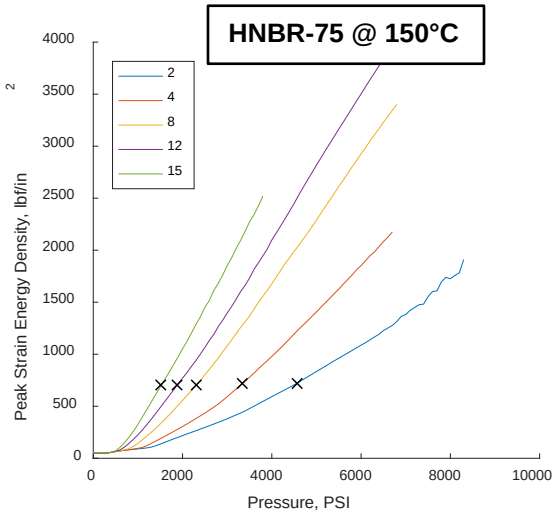
HNBR-75 @ 150°C
Peak Strain Energy Density, lbf/in 2
Pressure, PSI
2
4
8
12
15

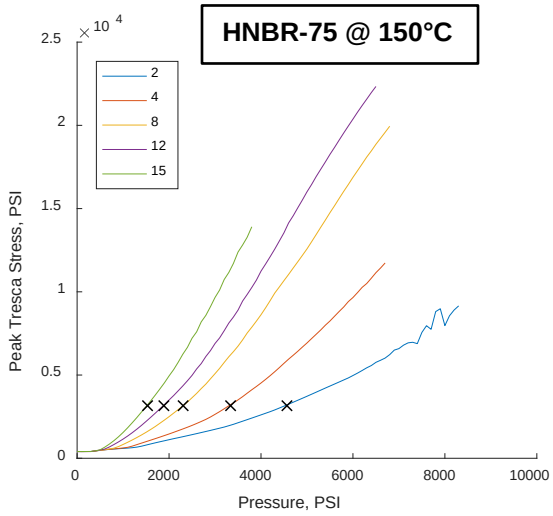
HNBR-75 @ 150°C
× 10 4
Peak Tresca Stress, PSI
Pressure, PSI
2
4
8
12
15

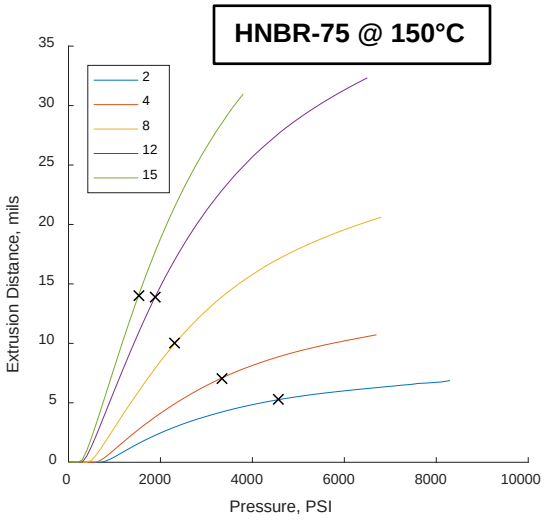
HNBR-75 @ 150°C
Extrusion Distance, mils
Pressure, PSI
2
4
8
12
15

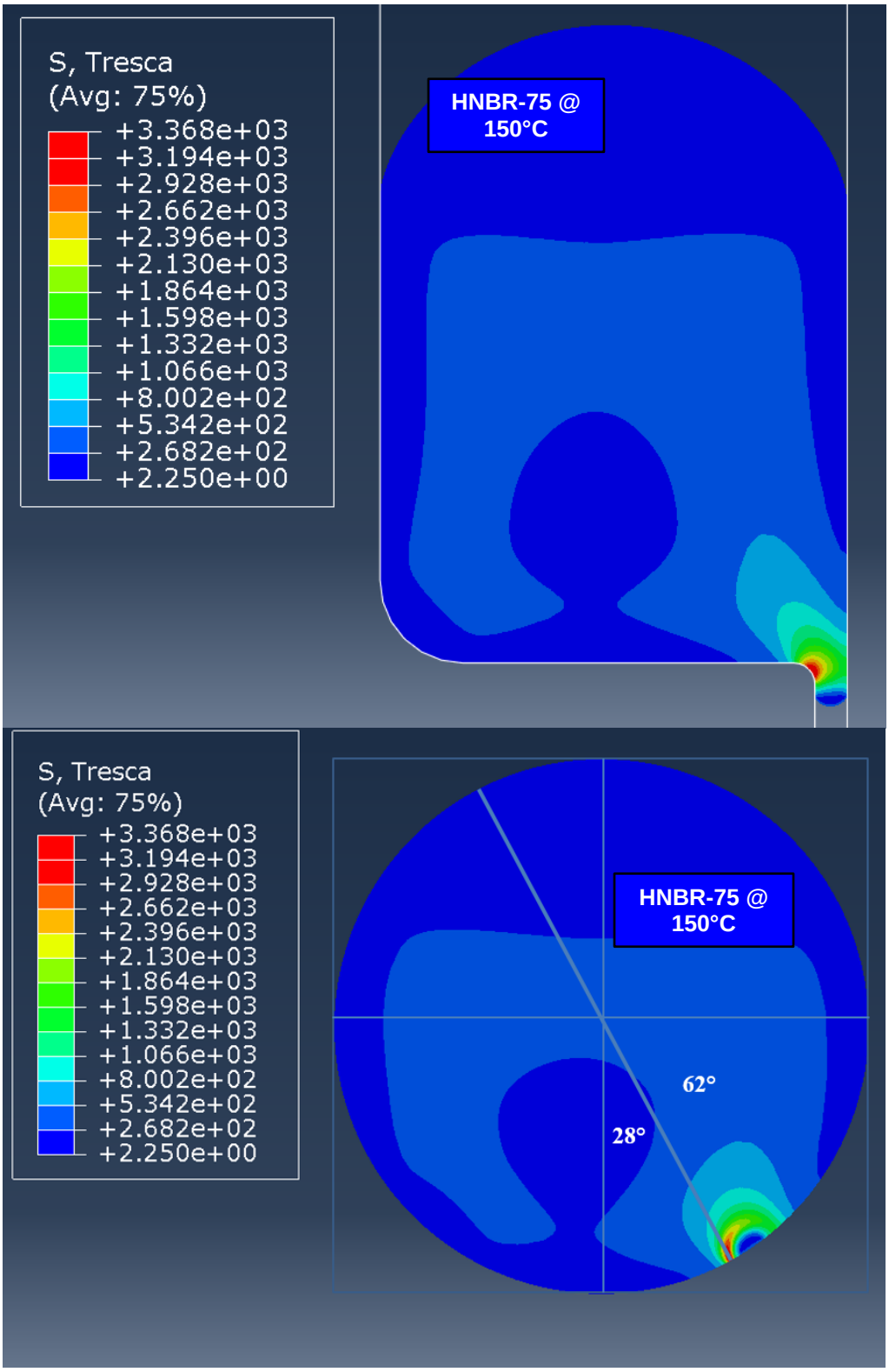
S, Tresca
(Avg: 75%)
+3.368e+03
+3.194e+03
+2.928e+03
+2.662e+03
+2.396e+03
+2.130e+03
+1.864e+03
+1.598e+03
+1.332e+03
+1.066e+03
+8.002e+02
+5.342e+02
+2.682e+02
+2.250e+00
HNBR-75 @
150°C
S, Tresca
(Avg: 75%)
+3.368e+03
+3.194e+03
+2.928e+03
+2.662e+03
+2.396e+03
+2.130e+03
+1.864e+03
+1.598e+03
+1.332e+03
+1.066e+03
+8.002e+02
+5.342e+02
+2.682e+02
+2.250e+00
HNBR-75 @
150°C
62°
28°

## *HNBR- 90*

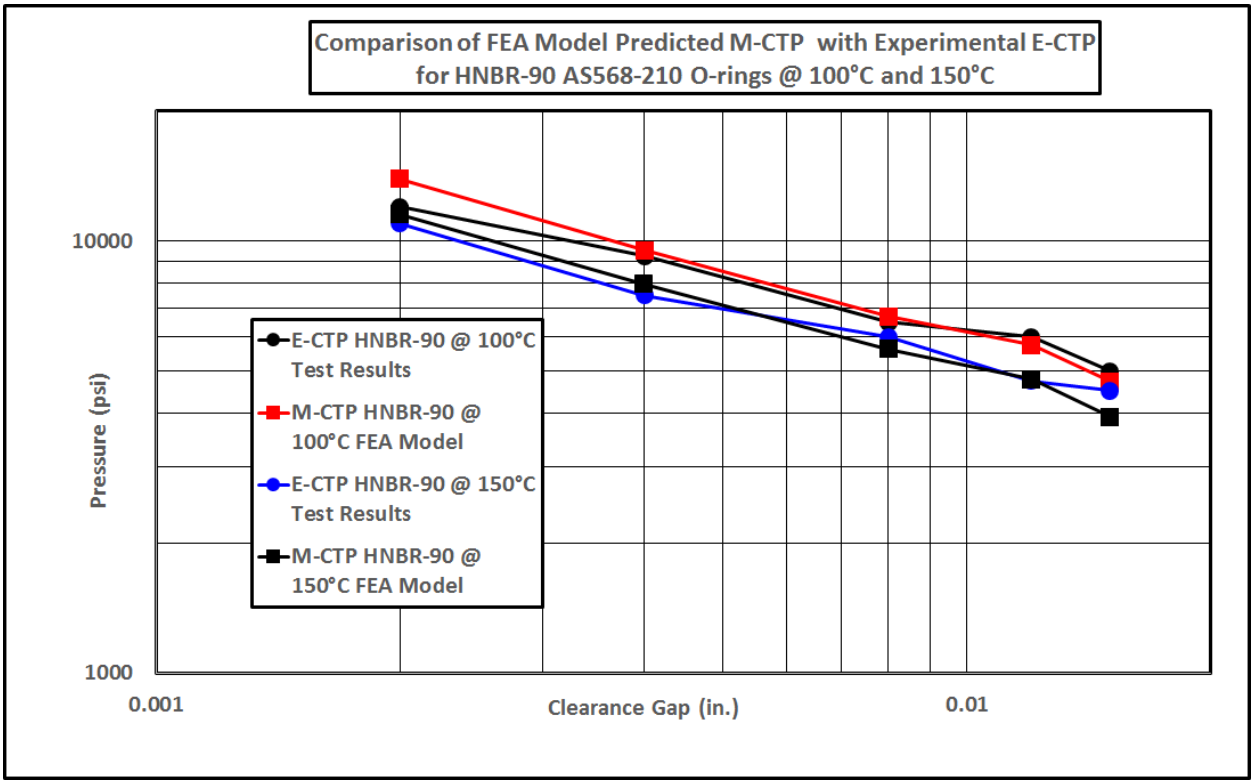


HNBR-90 100°C Simulation Output Parameters

| Clearance Gap | **0.015”** | **0.012”** | **0.008”** | **0.004”** | **0.002”** |
|---|---|---|---|---|---|
| **M-CTP Pressure (PSI)** | 4731 | 5739 | 6695 | 9521 | 13783 |
| **Strain Energy (in-lb.)** | 5.94 | 7.24 | 8.39 | 14.55 | 28.01 |
| **Volume ($in^3$)** | 0.04163 | 0.04133 | 0.04105 | 0.04023 | 0.03906 |
| **SED (PSI)** | 2527 | 2502 | 2468 | 2485 | 2758 |
| **Extrusion Distance (mils)** | 23.65 | 21.25 | 14.33 | 8.98 | 6.47 |

HNBR-90 150°C Simulation Output Parameters

| Clearance Gap | **0.015”** | **0.012”** | **0.008”** | **0.004”** | **0.002”** |
|---|---|---|---|---|---|
| **M-CTP Pressure (PSI)** | 3920 | 4792 | 5610 | 7926 | 11668 |
| **Strain Energy (in-lb.)** | 5.41 | 6.50 | 7.47 | 12.50 | 24.47 |
| **Volume ($in^3$)** | 0.04257 | 0.04226 | 0.04197 | 0.04117 | 0.03994 |
| **SED (PSI)** | 2154 | 2149 | 2125 | 2110 | 2358 |
| **Extrusion Distance (mils)** | 20.95 | 19.19 | 13.04 | 8.31 | 6.09 |

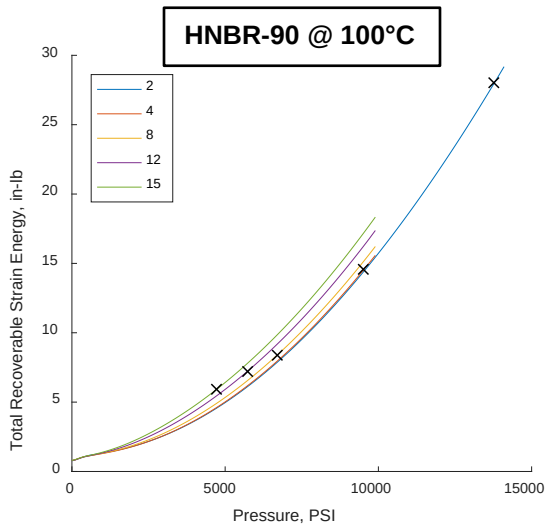
HNBR-90 @ 100°C
Total Recoverable Strain Energy, in-lb
Pressure, PSI
2
4
8
12
15

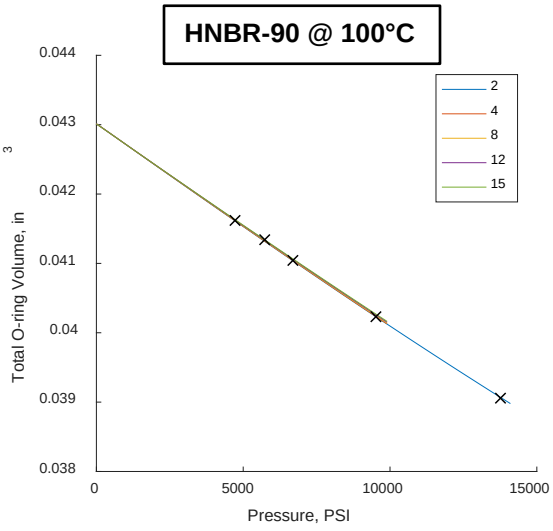
HNBR-90 @ 100°C
Total O-ring Volume, in 3
Pressure, PSI
2
4
8
12
15

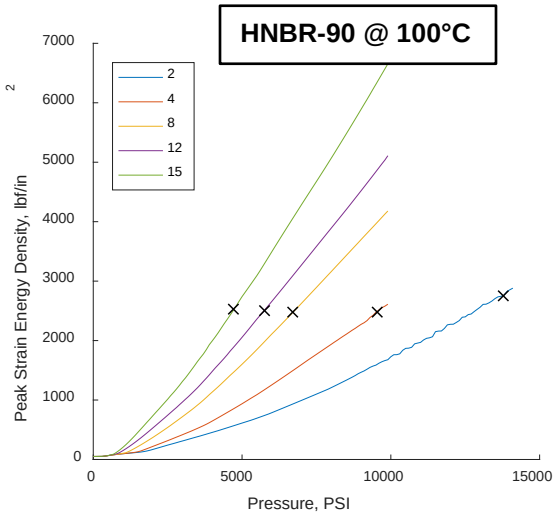
HNBR-90 @ 100°C
Peak Strain Energy Density, lbf/in 2
Pressure, PSI
2
4
8
12
15

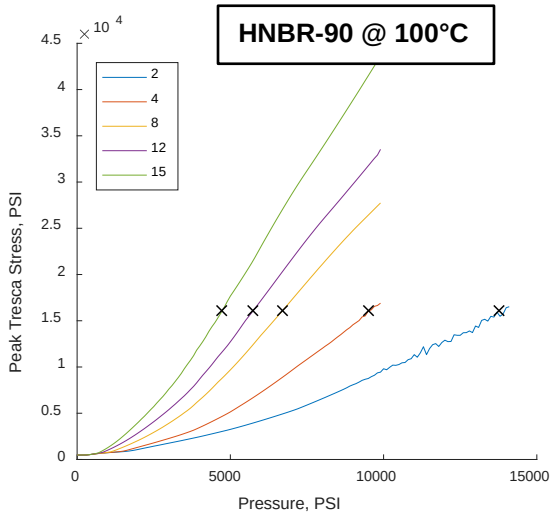
HNBR-90 @ 100°C
Peak Tresca Stress, PSI
Pressure, PSI
2
4
8
12
15

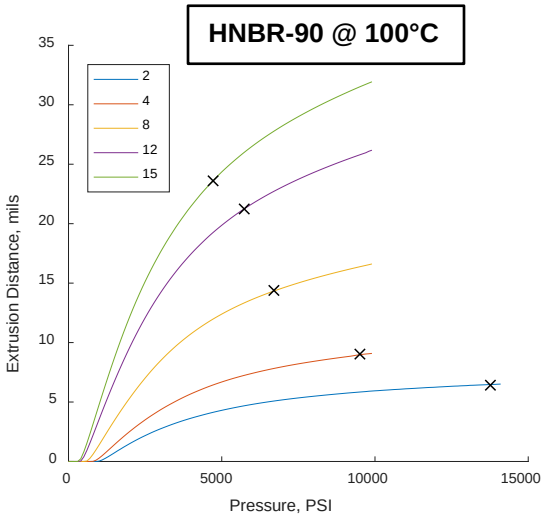
HNBR-90 @ 100°C
Extrusion Distance, mils
Pressure, PSI
2
4
8
12
15

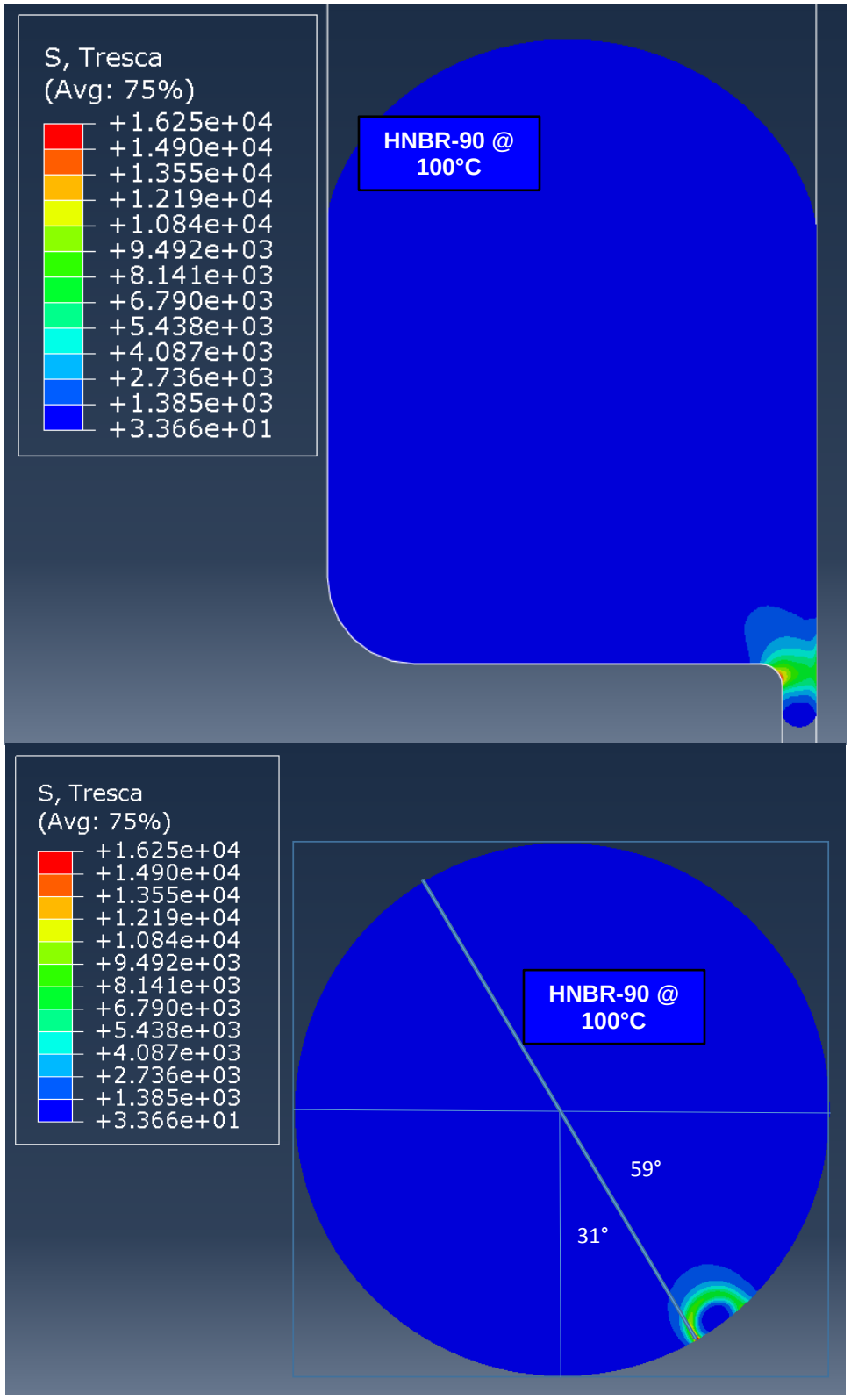
S, Tresca
(Avg: 75%)
+1.625e+04
+1.490e+04
+1.355e+04
+1.219e+04
+1.084e+04
+9.492e+03
+8.141e+03
+6.790e+03
+5.438e+03
+4.087e+03
+2.736e+03
+1.385e+03
+3.366e+01
HNBR-90 @ 100°C
S, Tresca
(Avg: 75%)
+1.625e+04
+1.490e+04
+1.355e+04
+1.219e+04
+1.084e+04
+9.492e+03
+8.141e+03
+6.790e+03
+5.438e+03
+4.087e+03
+2.736e+03
+1.385e+03
+3.366e+01
HNBR-90 @ 100°C
59°
31°

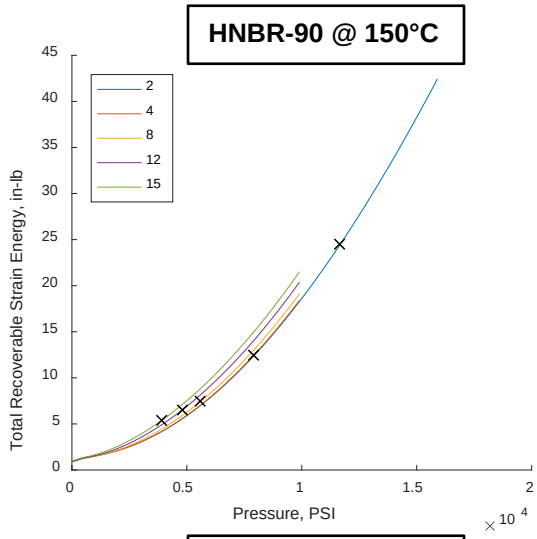
HNBR-90 @ 150°C
Total Recoverable Strain Energy, in-lb
Pressure, PSI
× 10 4
2
4
8
12
15

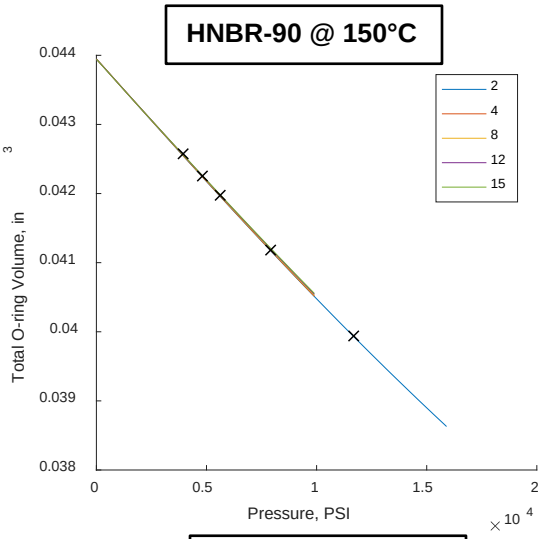
HNBR-90 @ 150°C
Total O-ring Volume, in 3
Pressure, PSI
× 10 4
2
4
8
12
15

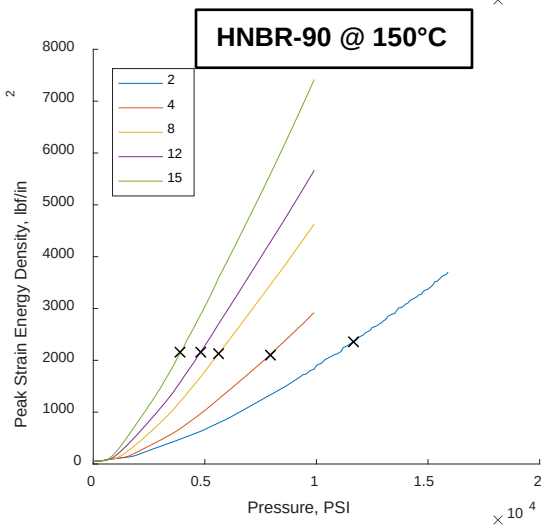
HNBR-90 @ 150°C
Peak Strain Energy Density, lbf/in 2
Pressure, PSI
× 10 4
2
4
8
12
15

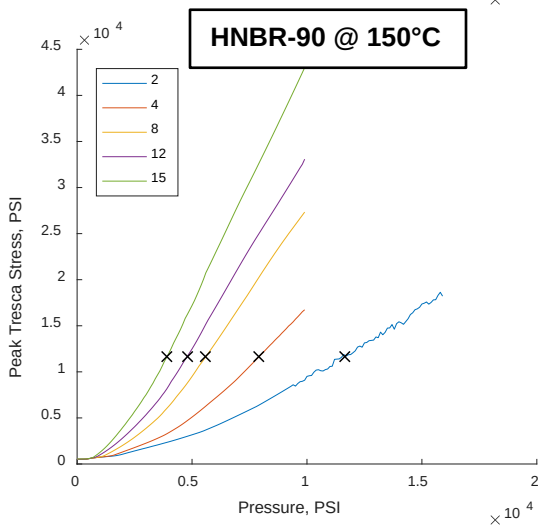
HNBR-90 @ 150°C
Peak Tresca Stress, PSI
× 10 4
Pressure, PSI
× 10 4
2
4
8
12
15

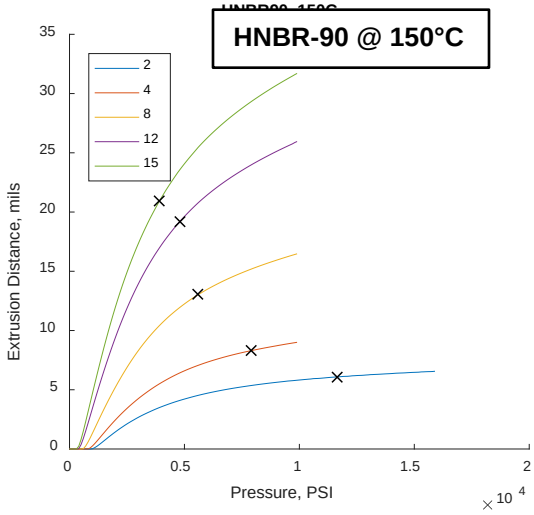
HNBR-90 @ 150°C
Extrusion Distance, mils
Pressure, PSI
× 10 4
2
4
8
12
15

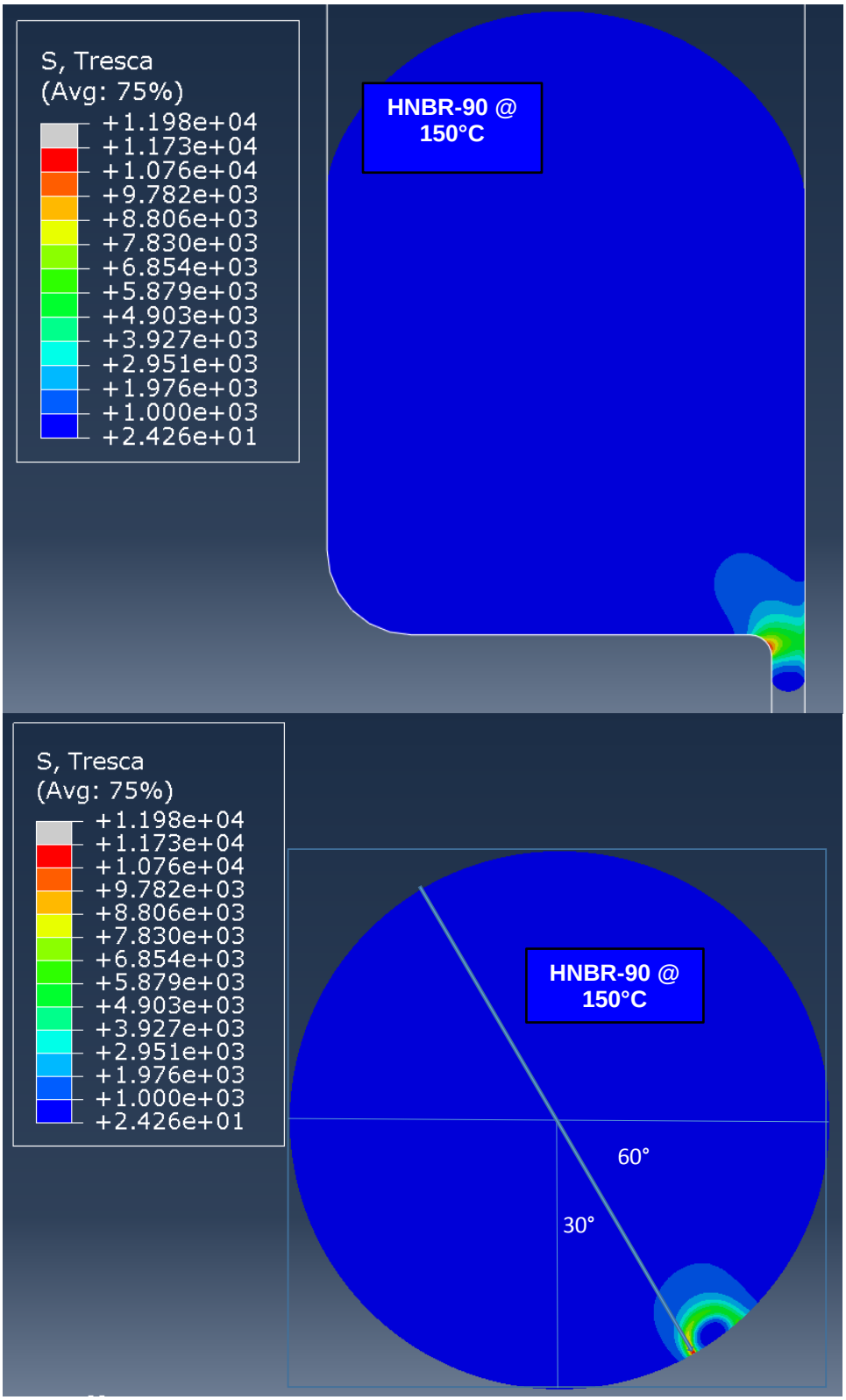
S, Tresca
(Avg: 75%)
+1.198e+04
+1.173e+04
+1.076e+04
+9.782e+03
+8.806e+03
+7.830e+03
+6.854e+03
+5.879e+03
+4.903e+03
+3.927e+03
+2.951e+03
+1.976e+03
+1.000e+03
+2.426e+01
HNBR-90 @
150°C
S, Tresca
(Avg: 75%)
+1.198e+04
+1.173e+04
+1.076e+04
+9.782e+03
+8.806e+03
+7.830e+03
+6.854e+03
+5.879e+03
+4.903e+03
+3.927e+03
+2.951e+03
+1.976e+03
+1.000e+03
+2.426e+01
HNBR-90 @
150°C
60°
30°

## *FFKM- 75*

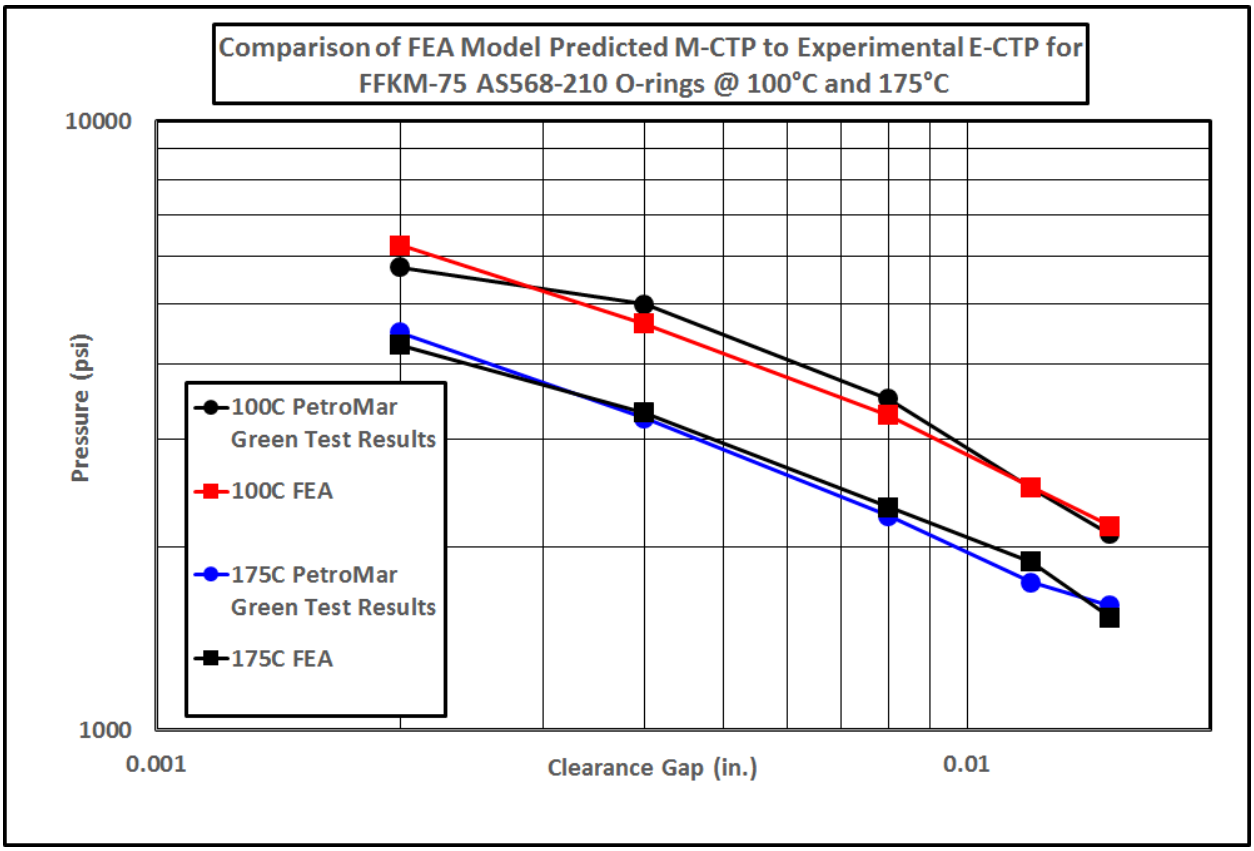


FFKM-75 100°C Simulation Output Parameters

| Clearance Gap | **0.015”** | **0.012”** | **0.008”** | **0.004”** | **0.002”** |
|---|---|---|---|---|---|
| **M-CTP Pressure (PSI)** | 2165 | 2504 | 3292 | 4653 | 6250 |
| **Strain Energy (in-lb.)** | 2.89 | 3.27 | 4.55 | 7.70 | 12.80 |
| **Volume ($in^3$)** | 0.04314 | 0.04293 | 0.04245 | 0.04162 | 0.04068 |
| **SED (PSI)** | 903 | 914 | 942 | 957 | 1005 |
| **Extrusion Distance (mils)** | 13.50 | 11.62 | 8.72 | 5.85 | 4.32 |

FFKM-75 175°C Simulation Output Parameters

| Clearance Gap | **0.015”** | **0.012”** | **0.008”** | **0.004”** | **0.002”** |
|---|---|---|---|---|---|
| **M-CTP Pressure (PSI)** | 1531 | 1892 | 2323 | 3325 | 4292 |
| **Strain Energy (in-lb.)** | 3.02 | 3.53 | 4.23 | 6.64 | 9.81 |
| **Volume ($in^3$)** | 0.04603 | 0.04571 | 0.04532 | 0.04443 | 0.04360 |
| **SED (PSI)** | 579 | 586 | 594 | 623 | 646 |
| **Extrusion Distance (mils)** | 9.95 | 9.53 | 6.76 | 4.76 | 3.60 |

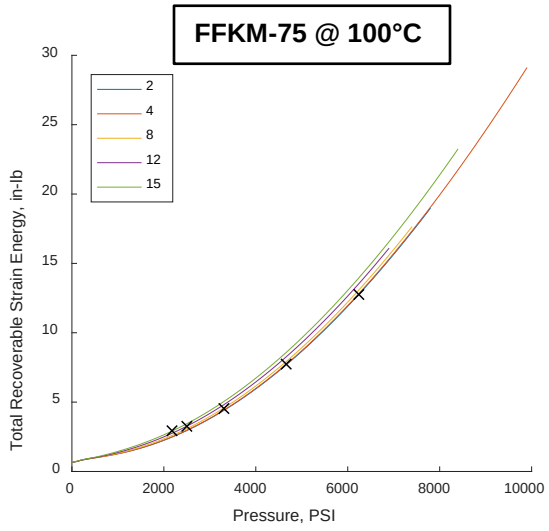
FFKM-75 @ 100°C
Total Recoverable Strain Energy, in-lb
Pressure, PSI
2
4
8
12
15

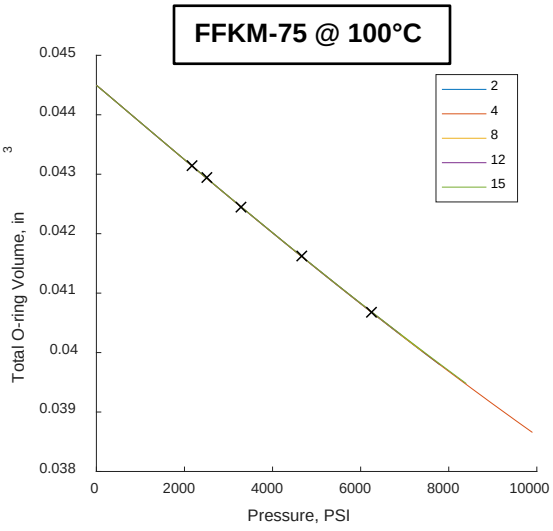
FFKM-75 @ 100°C
Total O-ring Volume, in 3
Pressure, PSI
2
4
8
12
15

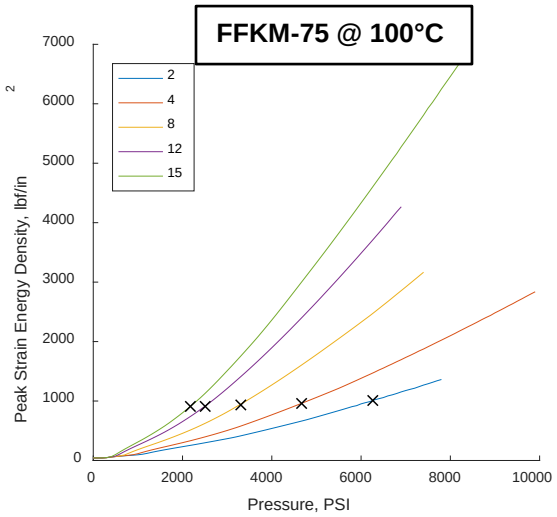
FFKM-75 @ 100°C
Peak Strain Energy Density, lbf/in 2
Pressure, PSI
2
4
8
12
15

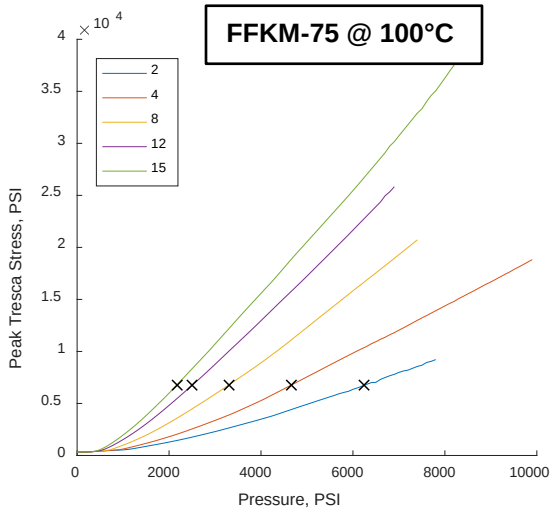
FFKM-75 @ 100°C
× 10 4
Peak Tresca Stress, PSI
Pressure, PSI
2
4
8
12
15

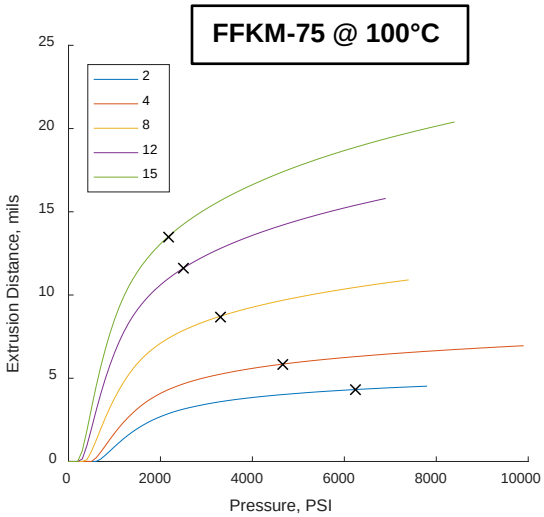
FFKM-75 @ 100°C
Extrusion Distance, mils
Pressure, PSI
2
4
8
12
15

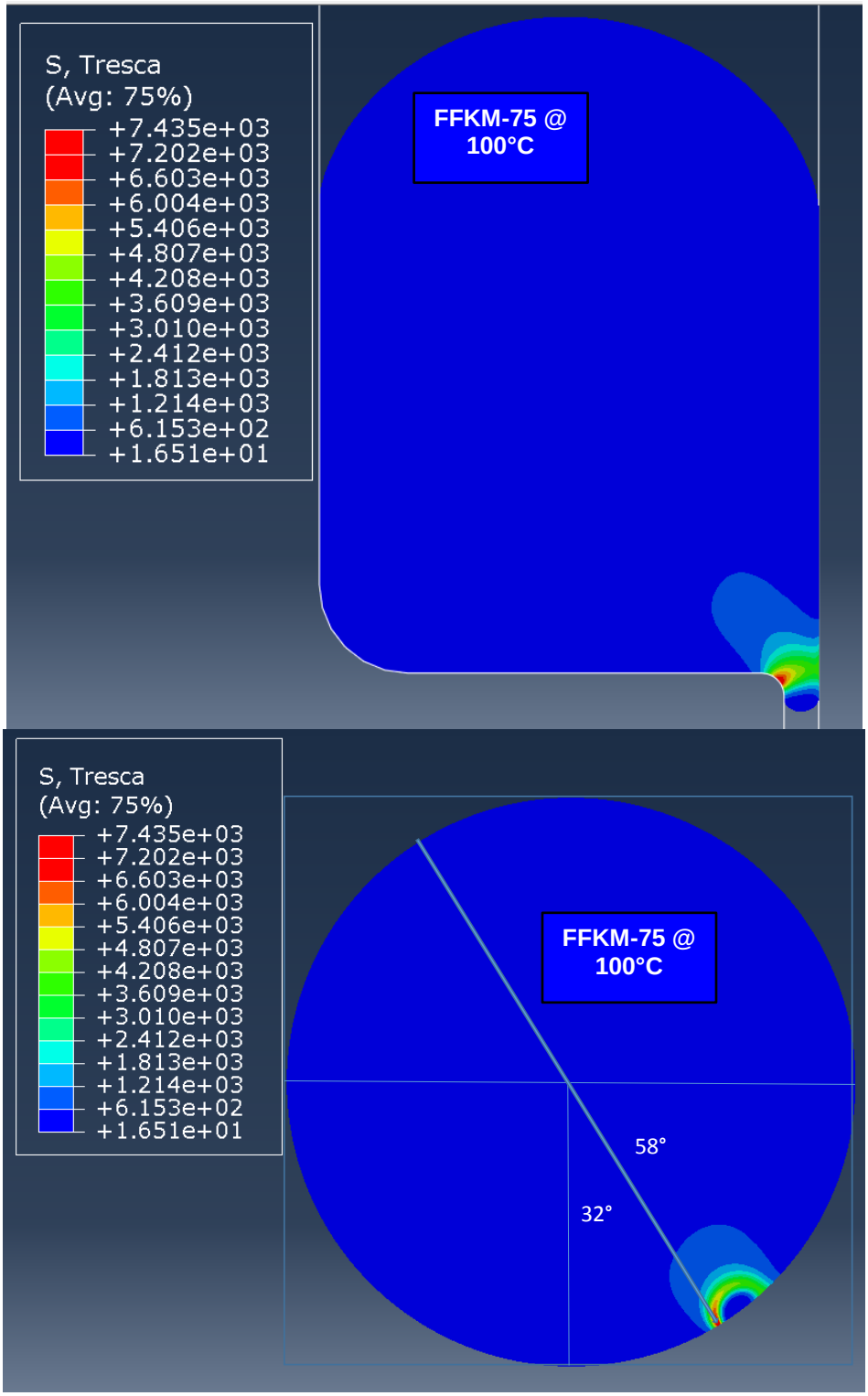
S, Tresca
(Avg: 75%)
+7.435e+03
+7.202e+03
+6.603e+03
+6.004e+03
+5.406e+03
+4.807e+03
+4.208e+03
+3.609e+03
+3.010e+03
+2.412e+03
+1.813e+03
+1.214e+03
+6.153e+02
+1.651e+01
FFKM-75 @
100°C
S, Tresca
(Avg: 75%)
+7.435e+03
+7.202e+03
+6.603e+03
+6.004e+03
+5.406e+03
+4.807e+03
+4.208e+03
+3.609e+03
+3.010e+03
+2.412e+03
+1.813e+03
+1.214e+03
+6.153e+02
+1.651e+01
FFKM-75 @
100°C
58°
32°

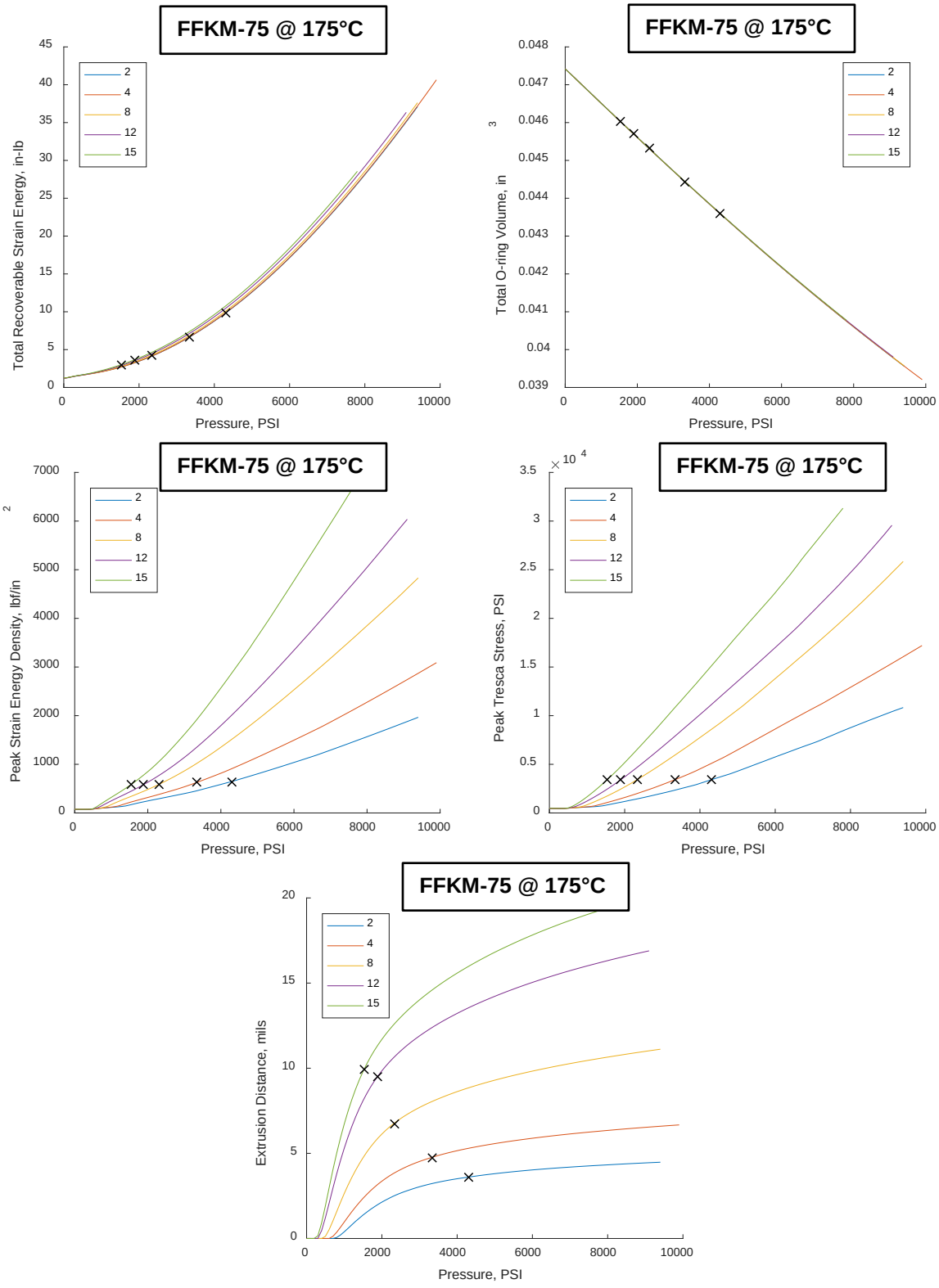
FFKM-75 @ 175°C
Total Recoverable Strain Energy, in-lb
Pressure, PSI
2
4
8
12
15
FFKM-75 @ 175°C
Total O-ring Volume, in3
Pressure, PSI
FFKM-75 @ 175°C
Peak Strain Energy Density, lbf/in2
Pressure, PSI
FFKM-75 @ 175°C
Peak Tresca Stress, PSI
×10 4
Pressure, PSI
FFKM-75 @ 175°C
Extrusion Distance, mils
Pressure, PSI

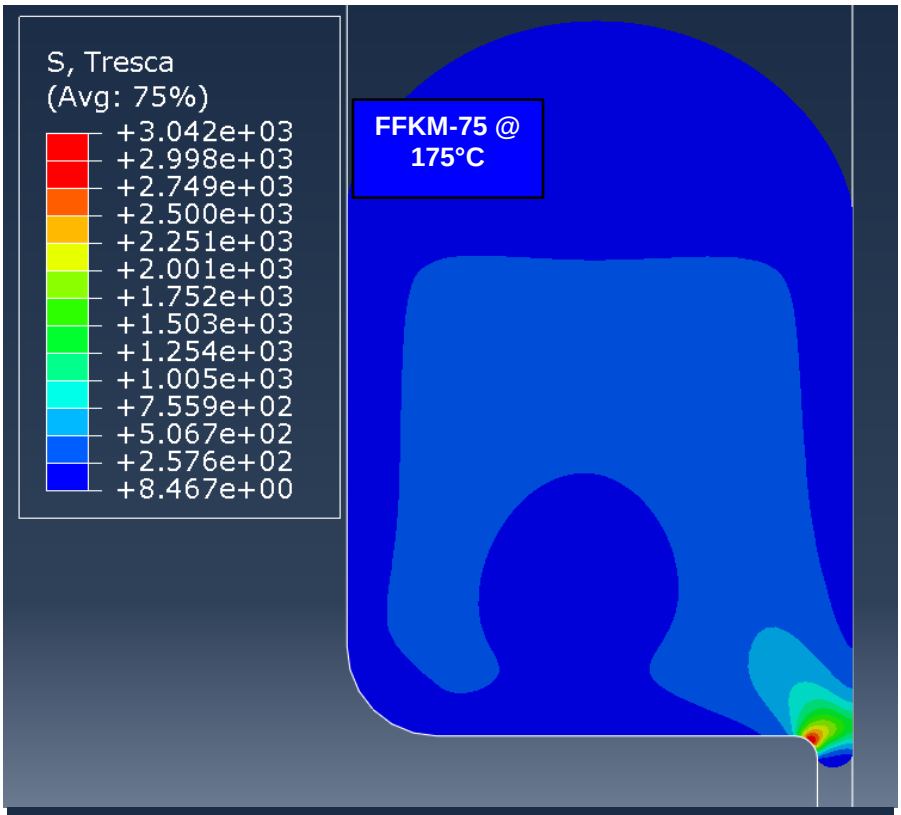
S, Tresca
(Avg: 75%)
+3.042e+03
+2.998e+03
+2.749e+03
+2.500e+03
+2.251e+03
+2.001e+03
+1.752e+03
+1.503e+03
+1.254e+03
+1.005e+03
+7.559e+02
+5.067e+02
+2.576e+02
+8.467e+00
FFKM-75 @
175°C

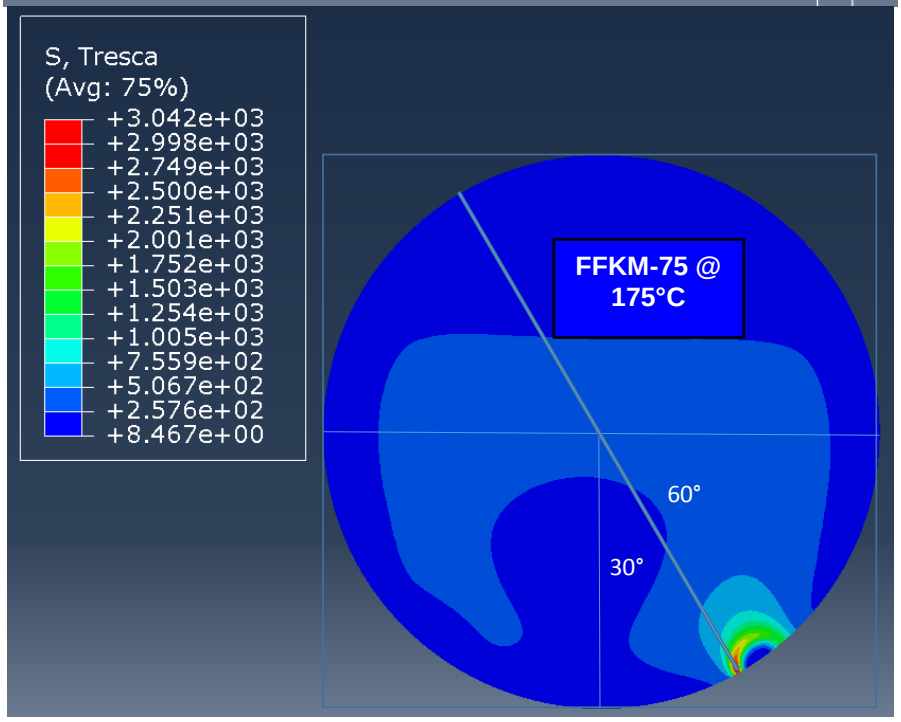
S, Tresca
(Avg: 75%)
+3.042e+03
+2.998e+03
+2.749e+03
+2.500e+03
+2.251e+03
+2.001e+03
+1.752e+03
+1.503e+03
+1.254e+03
+1.005e+03
+7.559e+02
+5.067e+02
+2.576e+02
+8.467e+00
FFKM-75 @
175°C
60°
30°

## *FFKM- 90*

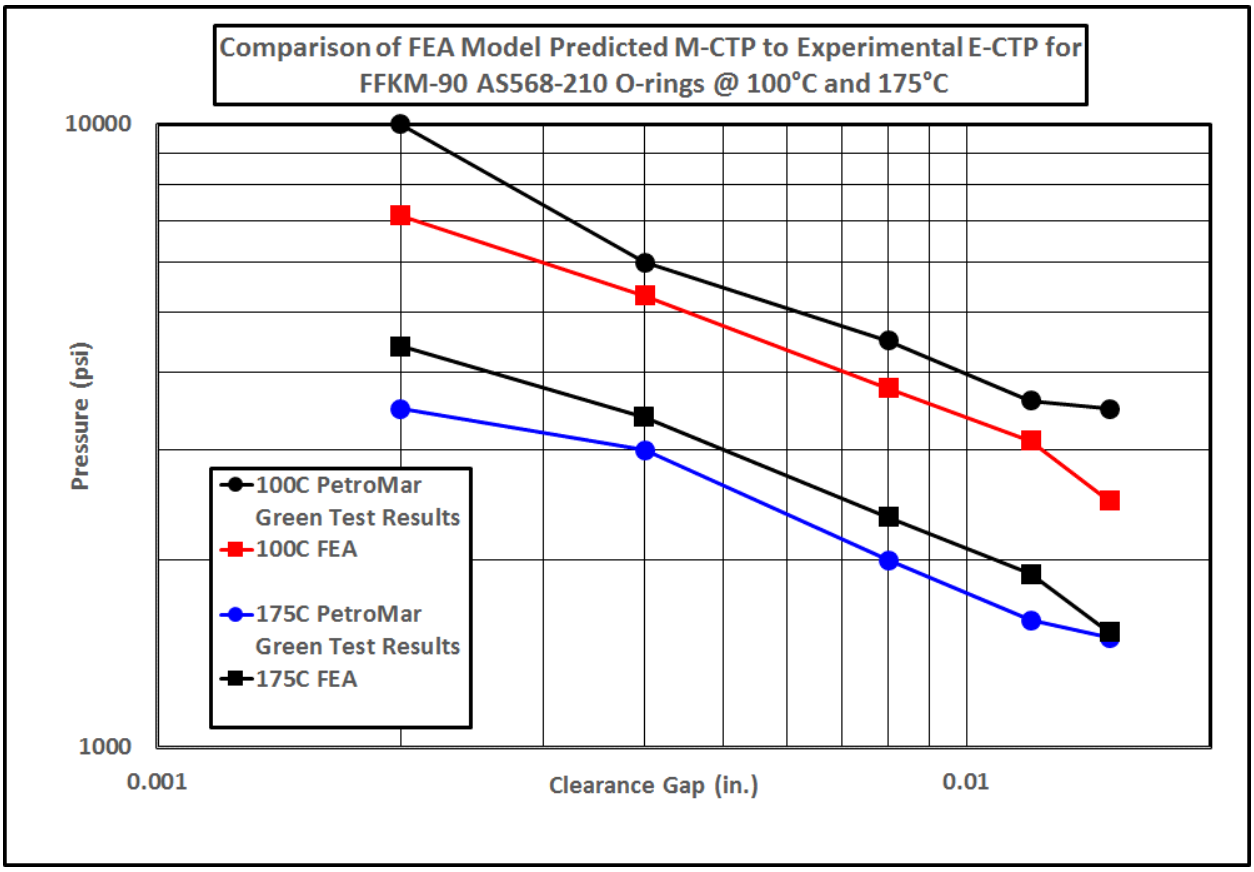


FFKM-90 100°C Simulation Output Parameters

| Clearance Gap | **0.015”** | **0.012”** | **0.008”** | **0.004”** | **0.002”** |
|---|---|---|---|---|---|
| **M-CTP Pressure (PSI)** | 2488 | 3109 | 3773 | 5315 | 7183 |
| **Strain Energy (in-lb.)** | 3.78 | 4.87 | 6.17 | 10.54 | 17.72 |
| **Volume ($in^3$)** | 0.04413 | 0.04372 | 0.04328 | 0.04228 | 0.04112 |
| **SED (PSI)** | 1012 | 1023 | 1047 | 1055 | 1106 |
| **Extrusion Distance (mils)** | 14.14 | 13.24 | 9.27 | 6.20 | 4.56 |

FFKM-90 175°C Simulation Output Parameters

| Clearance Gap | **0.015”** | **0.012”** | **0.008”** | **0.004”** | **0.002”** |
|---|---|---|---|---|---|
| **M-CTP Pressure (PSI)** | 1534 | 1899 | 2346 | 3394 | 4406 |
| **Strain Energy (in-lb.)** | 3.12 | 3.66 | 4.42 | 7.03 | 10.48 |
| **Volume ($in^3$)** | 0.04878 | 0.04845 | 0.04804 | 0.04709 | 0.04620 |
| **SED (PSI)** | 559 | 565 | 574 | 599 | 620 |
| **Extrusion Distance (mils)** | 9.97 | 9.69 | 6.94 | 4.99 | 3.78 |

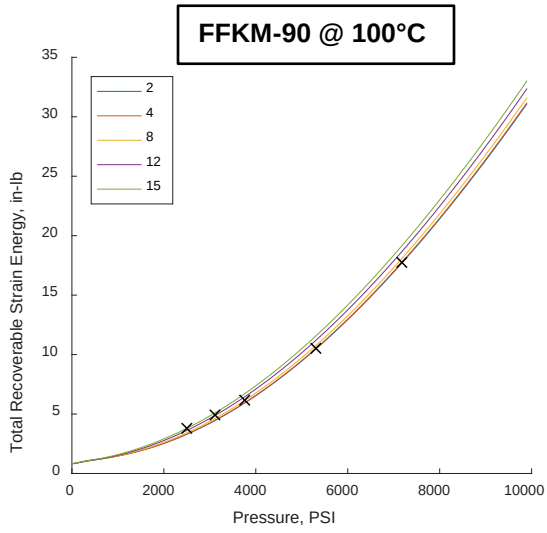
FFKM-90 @ 100°C
Total Recoverable Strain Energy, in-lb
Pressure, PSI
2
4
8
12
15

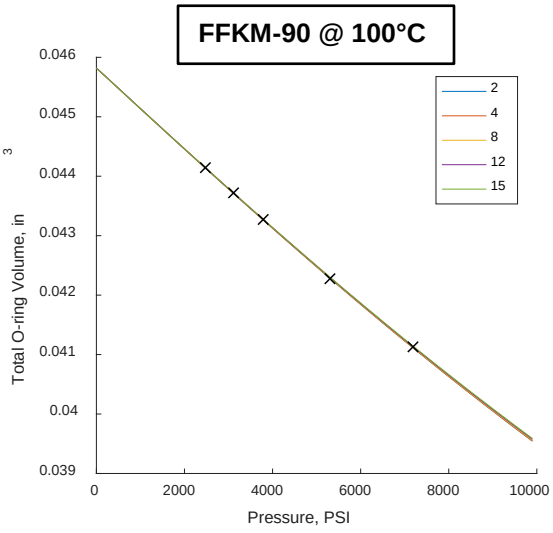
FFKM-90 @ 100°C
Total O-ring Volume, in 3
Pressure, PSI
2
4
8
12
15

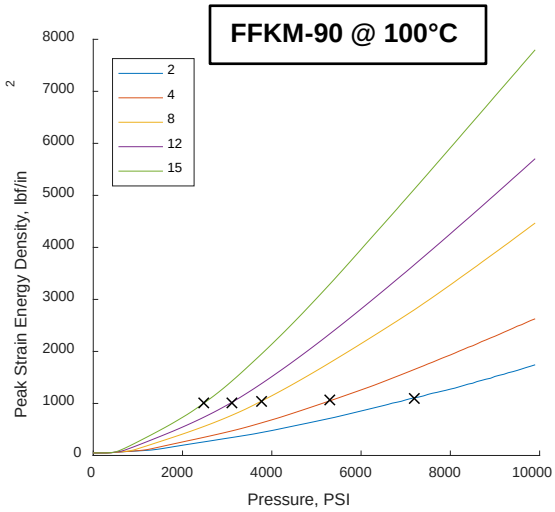
FFKM-90 @ 100°C
Peak Strain Energy Density, lbf/in 2
Pressure, PSI
2
4
8
12
15

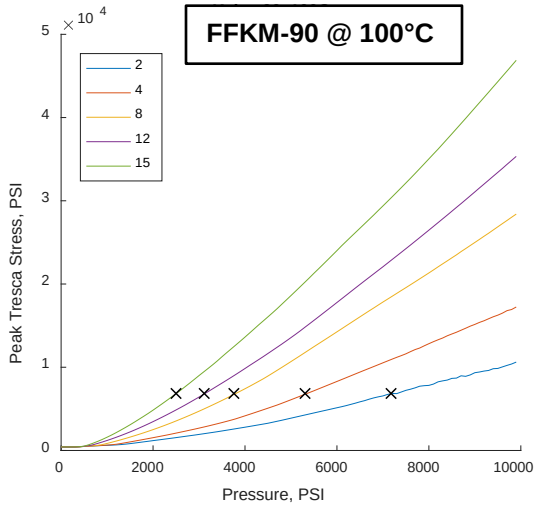
FFKM-90 @ 100°C
× 10 4
Peak Tresca Stress, PSI
Pressure, PSI
2
4
8
12
15

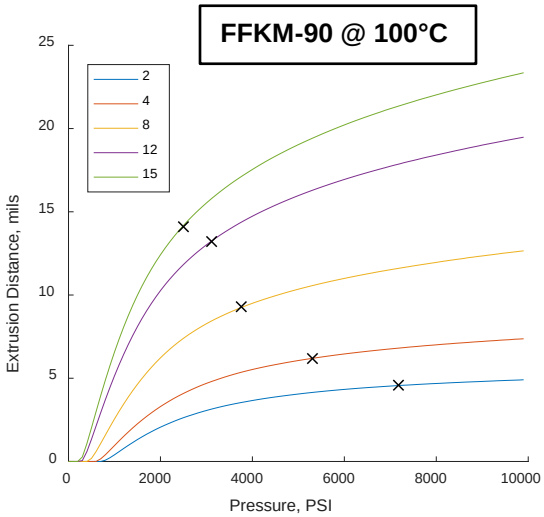
FFKM-90 @ 100°C
Extrusion Distance, mils
Pressure, PSI
2
4
8
12
15

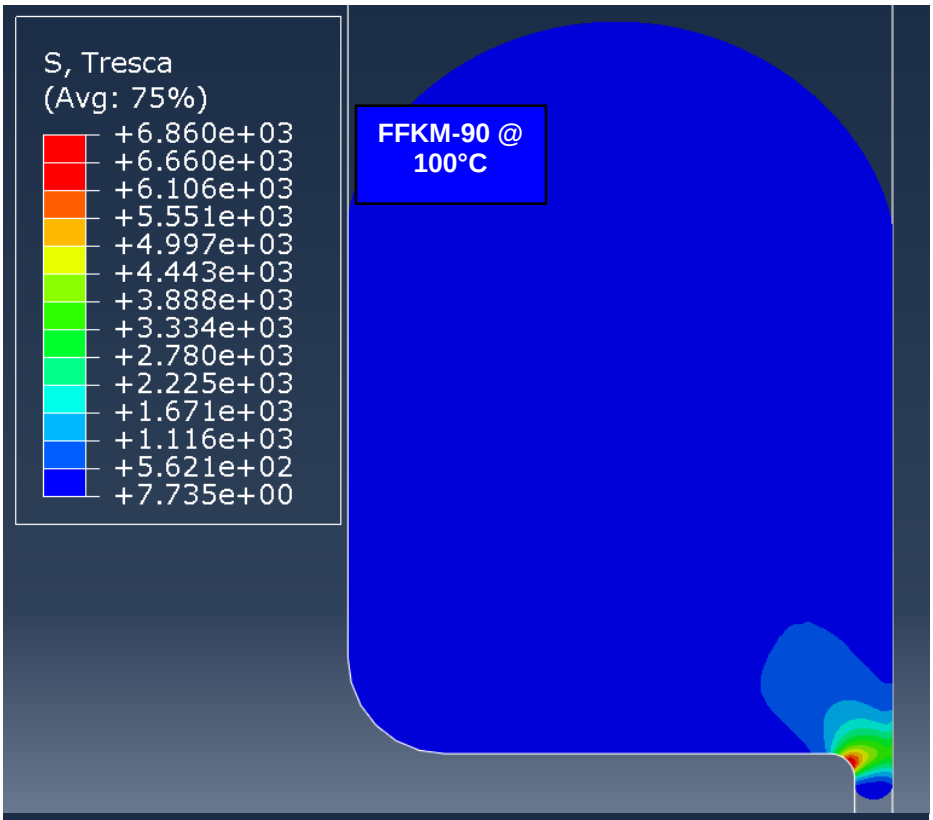
S, Tresca
(Avg: 75%)
+6.860e+03
+6.660e+03
+6.106e+03
+5.551e+03
+4.997e+03
+4.443e+03
+3.888e+03
+3.334e+03
+2.780e+03
+2.225e+03
+1.671e+03
+1.116e+03
+5.621e+02
+7.735e+00
FFKM-90 @
100°C

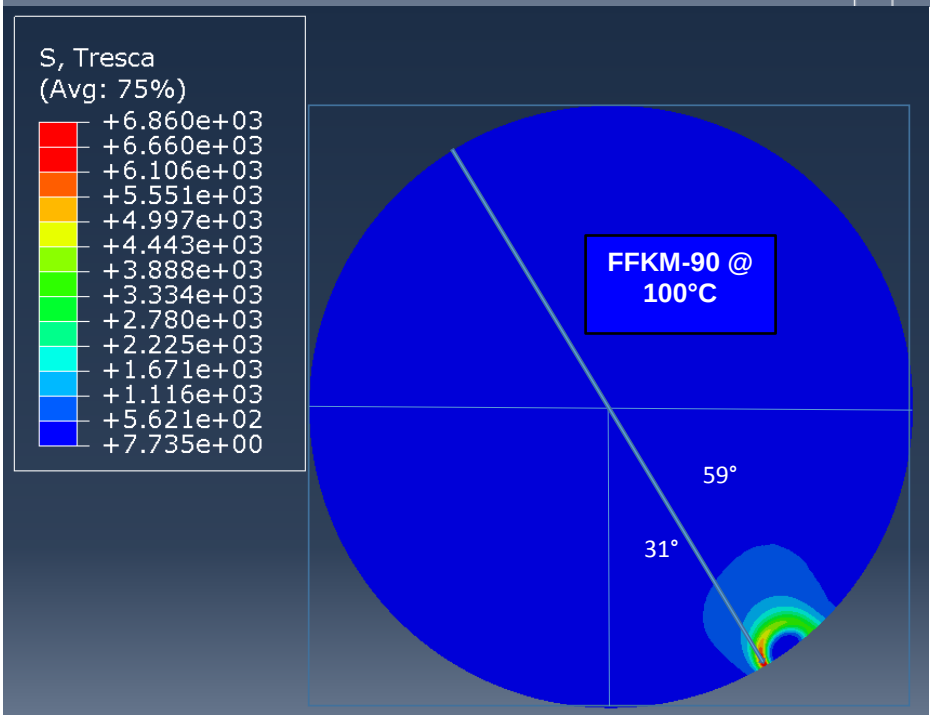
S, Tresca
(Avg: 75%)
+6.860e+03
+6.660e+03
+6.106e+03
+5.551e+03
+4.997e+03
+4.443e+03
+3.888e+03
+3.334e+03
+2.780e+03
+2.225e+03
+1.671e+03
+1.116e+03
+5.621e+02
+7.735e+00
FFKM-90 @
100°C
59°
31°

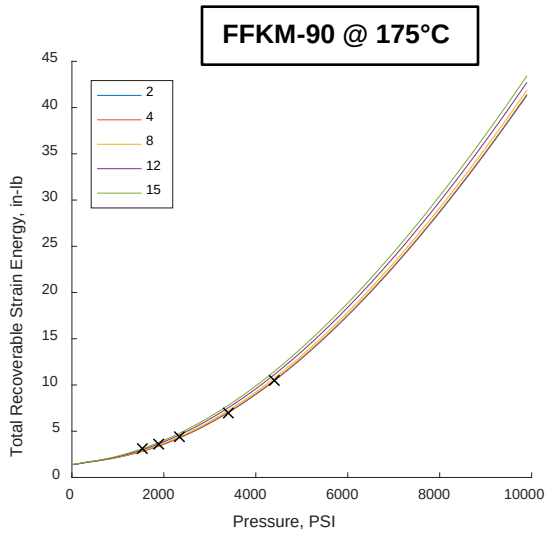
FFKM-90 @ 175°C
Total Recoverable Strain Energy, in-lb
Pressure, PSI
2
4
8
12
15

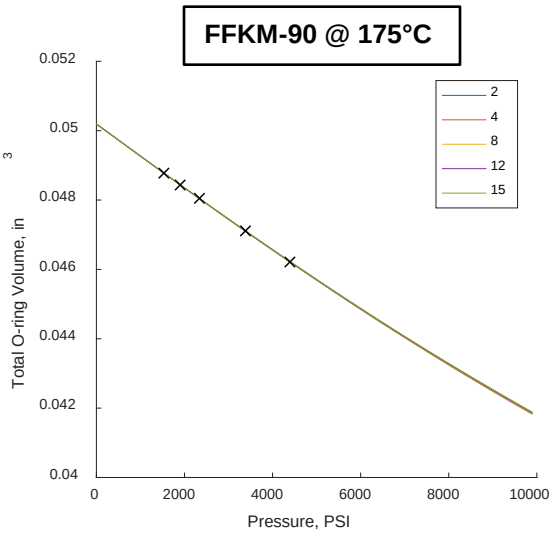
FFKM-90 @ 175°C
Total O-ring Volume, in 3
Pressure, PSI
2
4
8
12
15

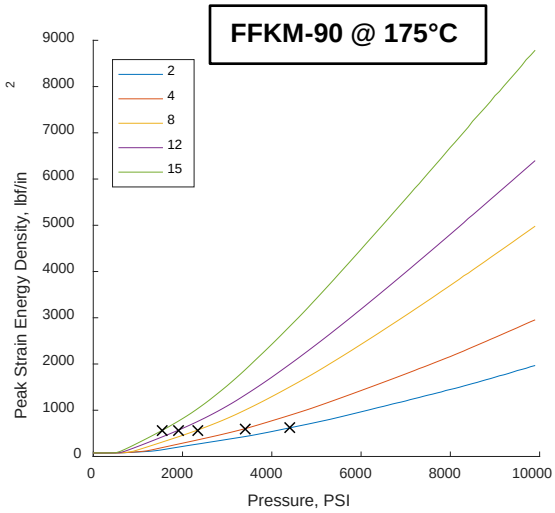
FFKM-90 @ 175°C
Peak Strain Energy Density, lbf/in 2
Pressure, PSI
2
4
8
12
15

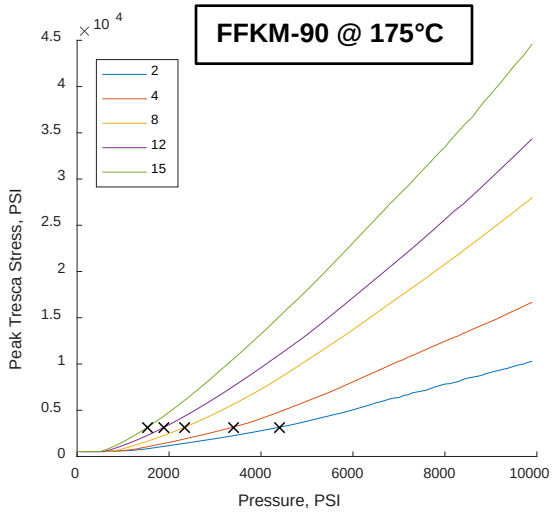
FFKM-90 @ 175°C
Peak Tresca Stress, PSI
Pressure, PSI
2
4
8
12
15

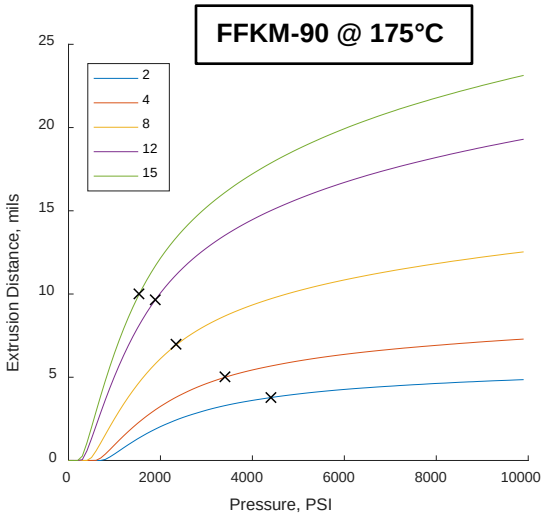
FFKM-90 @ 175°C
Extrusion Distance, mils
Pressure, PSI
2
4
8
12
15

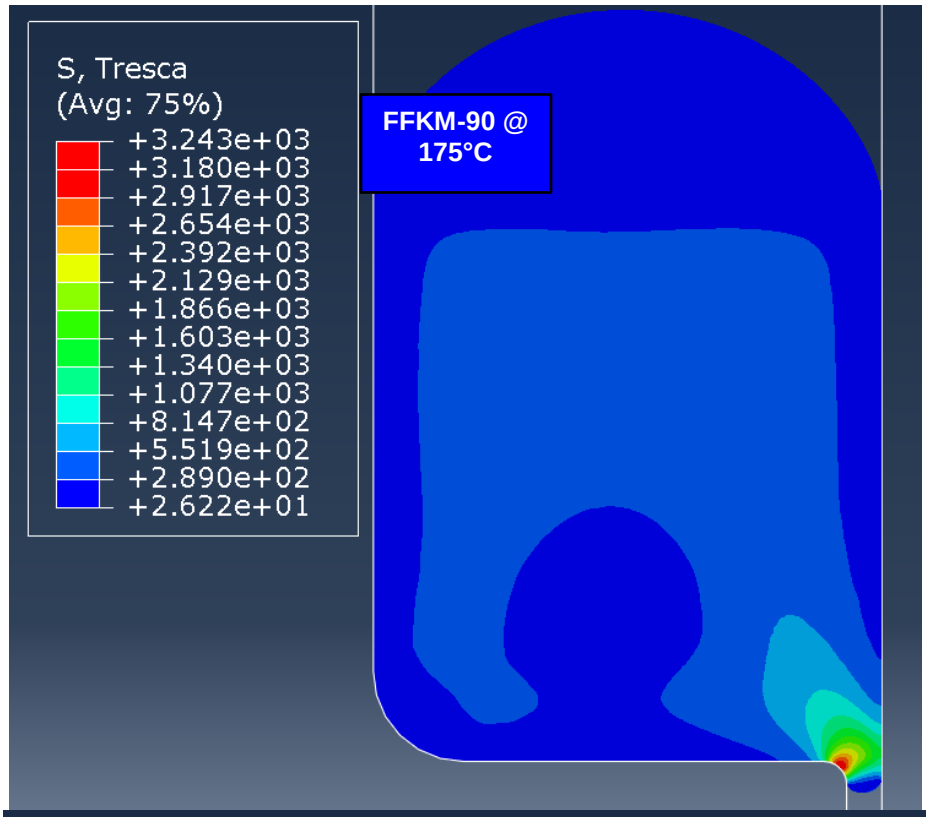
S, Tresca
(Avg: 75%)
+3.243e+03
+3.180e+03
+2.917e+03
+2.654e+03
+2.392e+03
+2.129e+03
+1.866e+03
+1.603e+03
+1.340e+03
+1.077e+03
+8.147e+02
+5.519e+02
+2.890e+02
+2.622e+01
FFKM-90 @
175°C

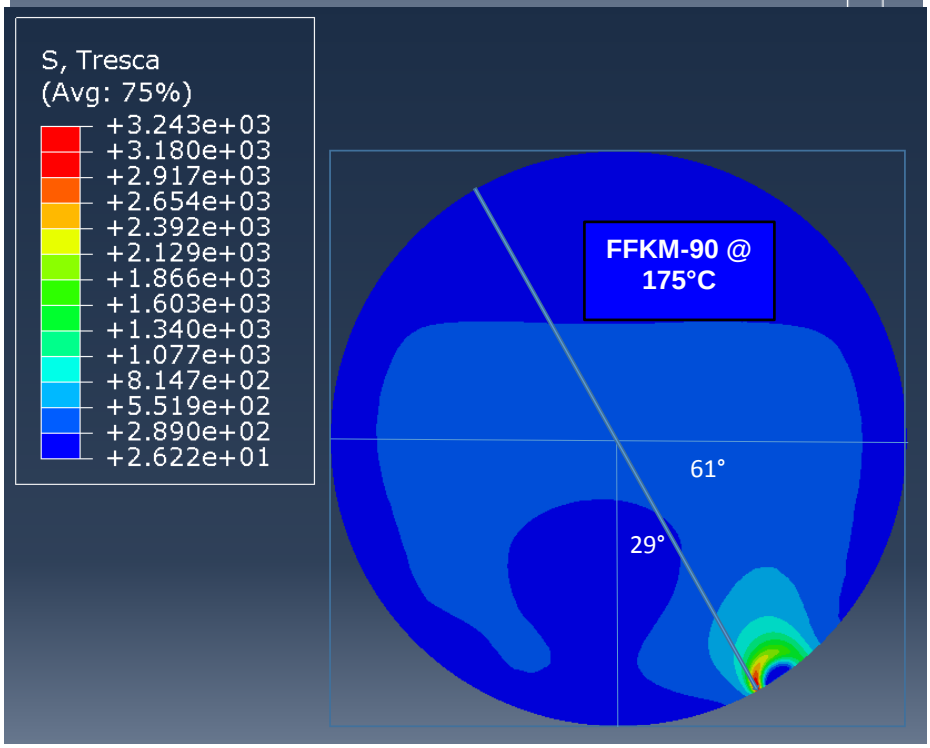
S, Tresca
(Avg: 75%)
+3.243e+03
+3.180e+03
+2.917e+03
+2.654e+03
+2.392e+03
+2.129e+03
+1.866e+03
+1.603e+03
+1.340e+03
+1.077e+03
+8.147e+02
+5.519e+02
+2.890e+02
+2.622e+01
FFKM-90 @
175°C
61°
29°

## *NBR- 75*

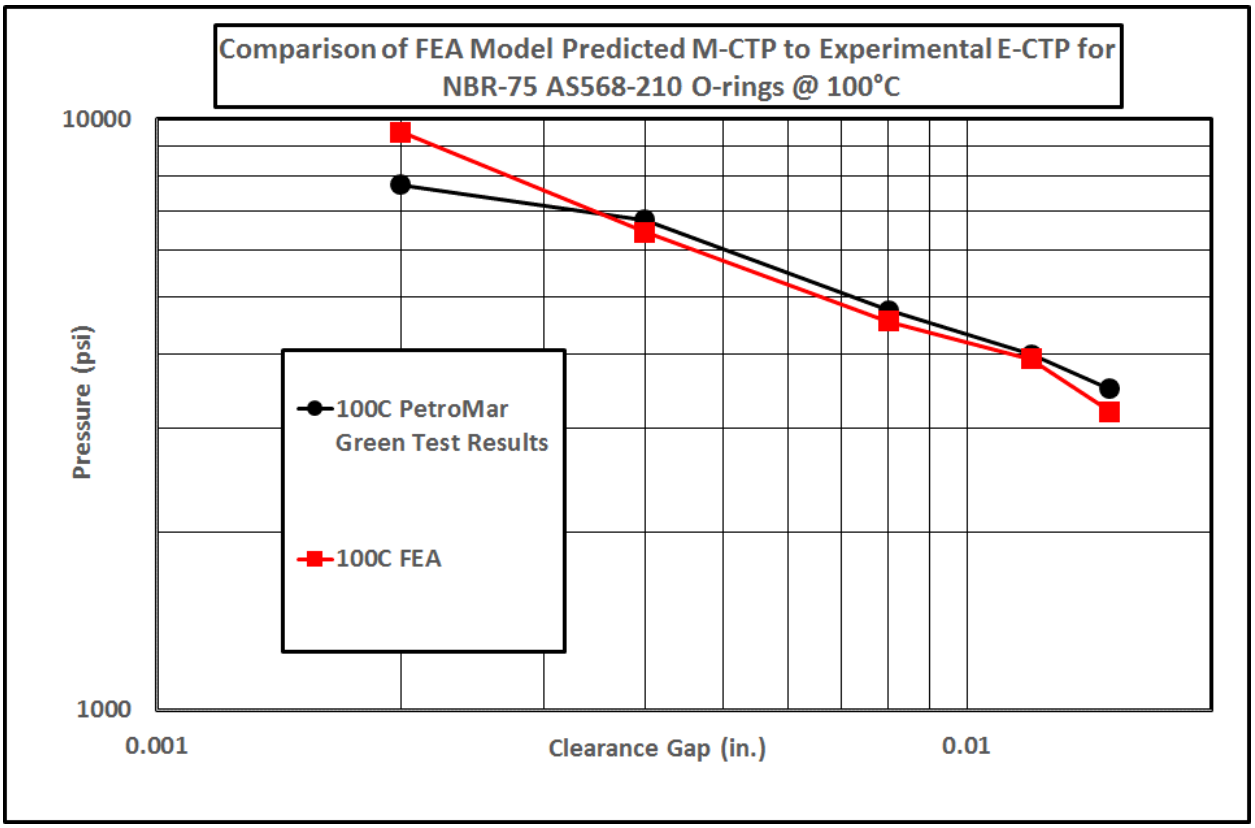


NBR-75 100C Simulation Output Parameters

| Clearance Gap | **0.015”** | **0.012”** | **0.008”** | **0.004”** | **0.002”** |
|---|---|---|---|---|---|
| **M-CTP Pressure (PSI)** | 3203 | 3931 | 4547 | 6428 | 9516 |
| **Strain Energy (in-lb.)** | 4.41 | 5.10 | 5.29 | 8.40 | 16.55 |
| **Volume ($in^3$)** | 0.04219 | 0.04194 | 0.04171 | 0.04106 | 0.04001 |
| **SED (PSI)** | 2626 | 2634 | 2617 | 2643 | 2815 |
| **Extrusion Distance (mils)** | 31.26 | 28.65 | 19.27 | 11.74 | 7.83 |

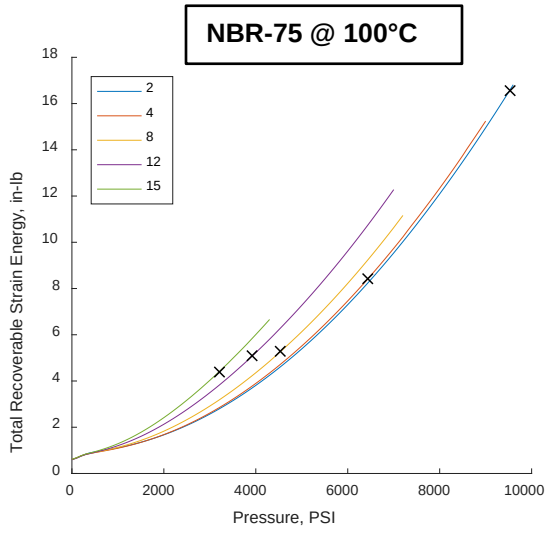
NBR-75 @ 100°C
Total Recoverable Strain Energy, in-lb
Pressure, PSI
2
4
8
12
15

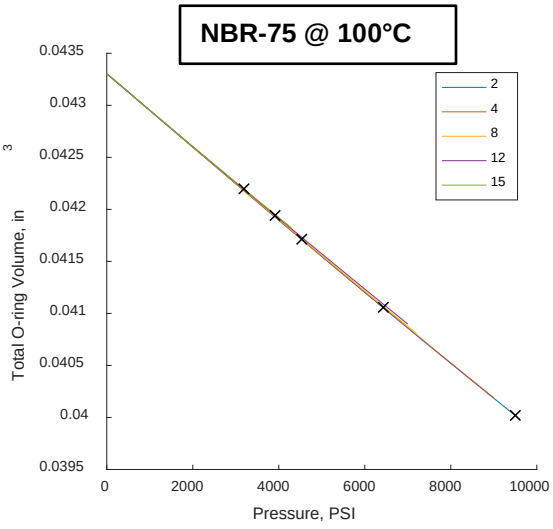
NBR-75 @ 100°C
Total O-ring Volume, in3
Pressure, PSI
2
4
8
12
15

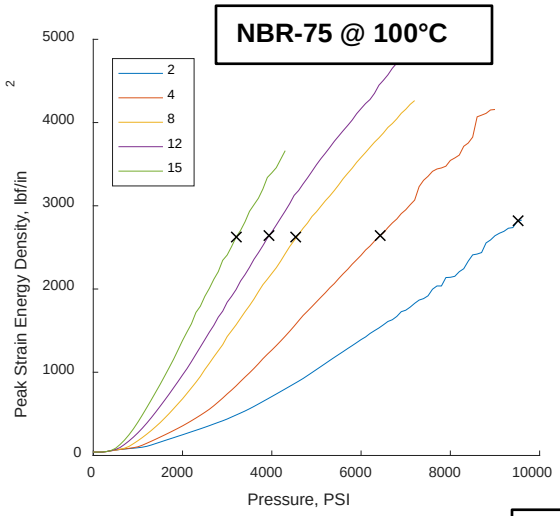
NBR-75 @ 100°C
Peak Strain Energy Density, lbf/in2
Pressure, PSI
2
4
8
12
15

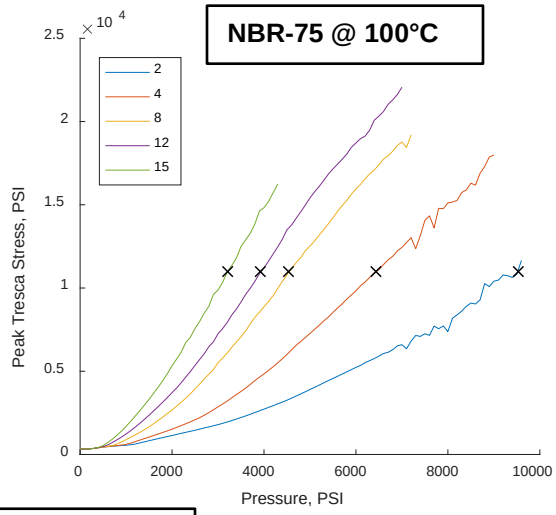
NBR-75 @ 100°C
×10 4
Peak Tresca Stress, PSI
Pressure, PSI
2
4
8
12
15

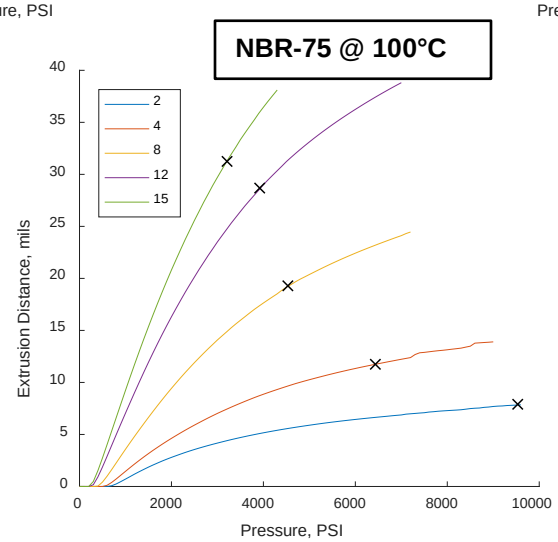
NBR-75 @ 100°C
Extrusion Distance, mils
Pressure, PSI
2
4
8
12
15

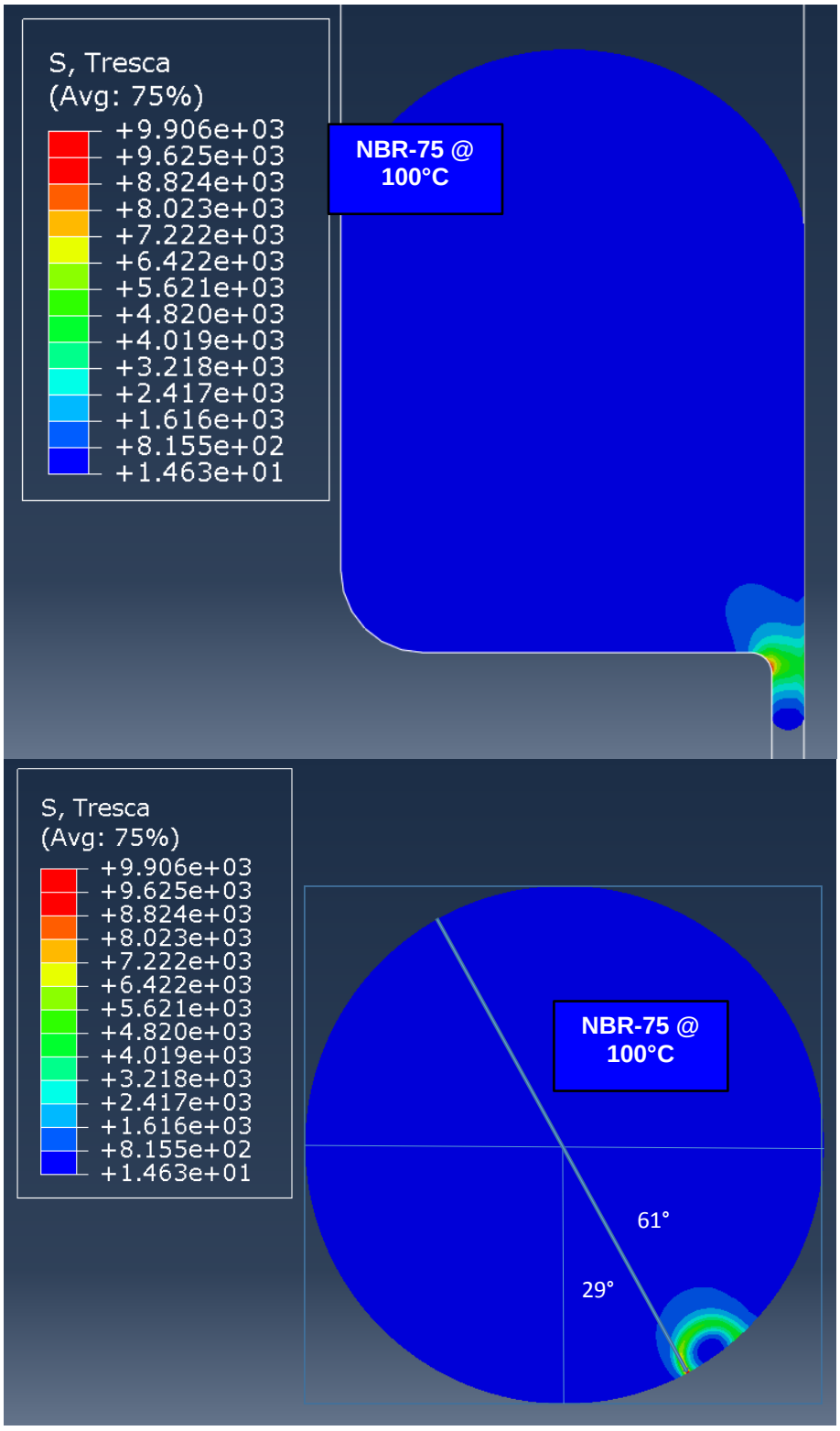
S, Tresca
(Avg: 75%)
+9.906e+03
+9.625e+03
+8.824e+03
+8.023e+03
+7.222e+03
+6.422e+03
+5.621e+03
+4.820e+03
+4.019e+03
+3.218e+03
+2.417e+03
+1.616e+03
+8.155e+02
+1.463e+01
NBR-75 @
100°C
S, Tresca
(Avg: 75%)
+9.906e+03
+9.625e+03
+8.824e+03
+8.023e+03
+7.222e+03
+6.422e+03
+5.621e+03
+4.820e+03
+4.019e+03
+3.218e+03
+2.417e+03
+1.616e+03
+8.155e+02
+1.463e+01
NBR-75 @
100°C
61°
29°

## *NBR- 90*

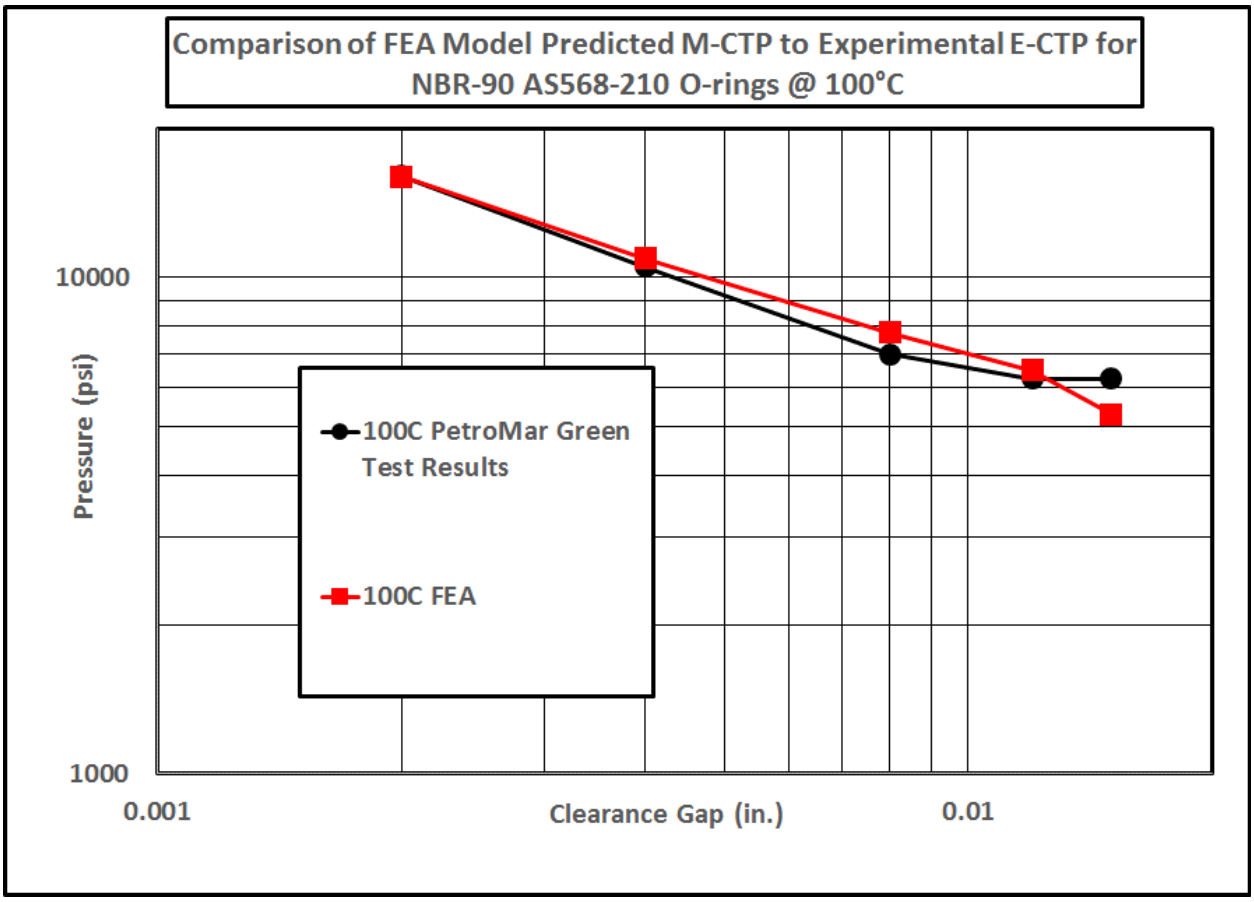


NBR-90 100°C Simulation Output Parameters

| Clearance Gap | **0.015”** | **0.012”** | **0.008”** | **0.004”** | **0.002”** |
|---|---|---|---|---|---|
| **M-CTP Pressure (PSI)** | 5294 | 6495 | 7746 | 10912 | 16123 |
| **Strain Energy (in-lb.)** | 7.99 | 9.73 | 11.31 | 18.67 | 36.16 |
| **Volume ($in^3$)** | 0.04095 | 0.04062 | 0.04027 | 0.03941 | 0.03810 |
| **SED (PSI)** | 4350 | 4337 | 4334 | 4397 | 4600 |
| **Extrusion Distance (mils)** | 20.58 | 19.26 | 13.25 | 9.38 | 6.60 |

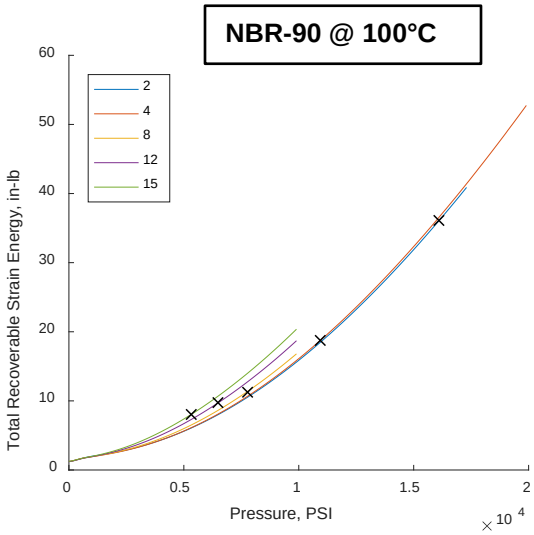
NBR-90 @ 100°C
Total Recoverable Strain Energy, in-lb
Pressure, PSI
2
4
8
12
15

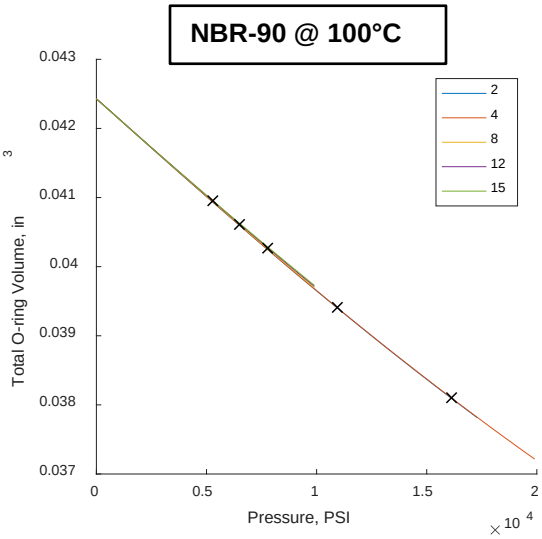
NBR-90 @ 100°C
Total O-ring Volume, in
Pressure, PSI
2
4
8
12
15

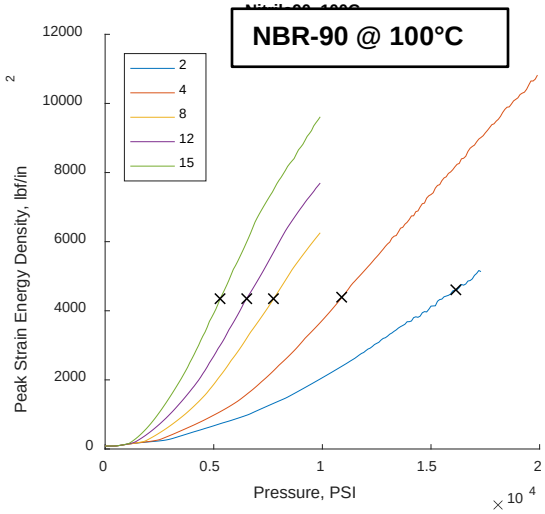
NBR-90 @ 100°C
Peak Strain Energy Density, lbf/in
Pressure, PSI
2
4
8
12
15

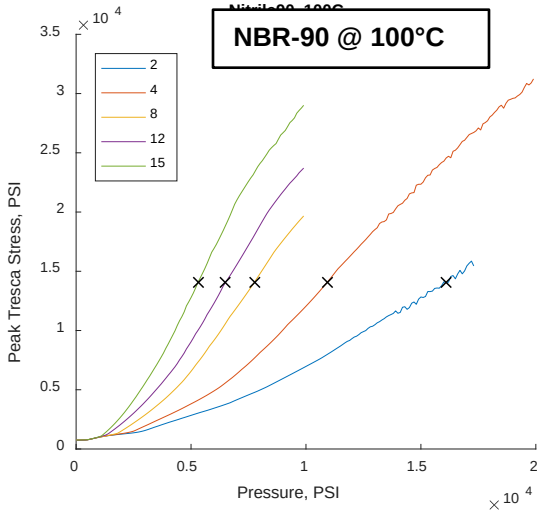
NBR-90 @ 100°C
Peak Tresca Stress, PSI
Pressure, PSI
2
4
8
12
15

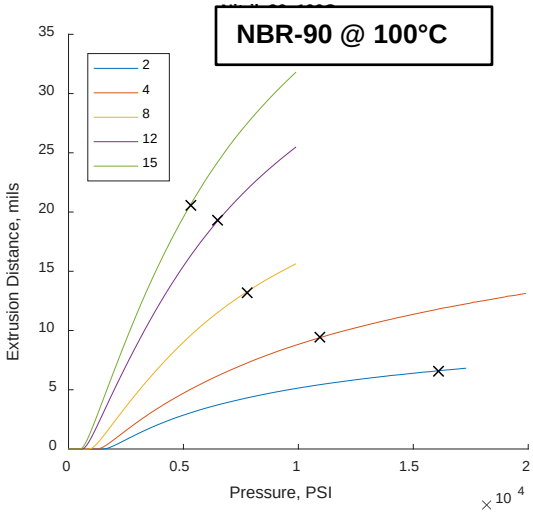
NBR-90 @ 100°C
Extrusion Distance, mils
Pressure, PSI
2
4
8
12
15

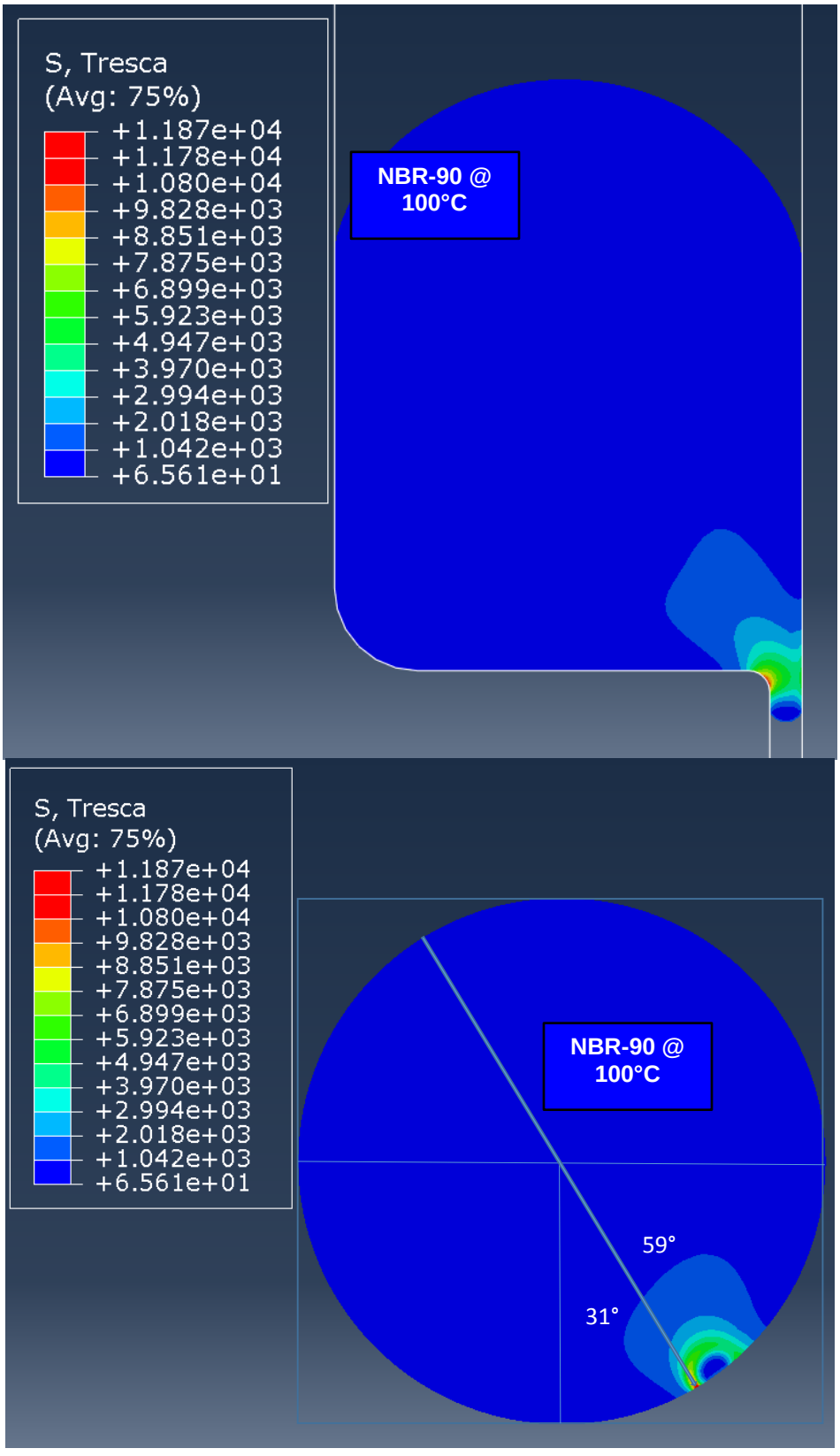
S, Tresca
(Avg: 75%)
+1.187e+04
+1.178e+04
+1.080e+04
+9.828e+03
+8.851e+03
+7.875e+03
+6.899e+03
+5.923e+03
+4.947e+03
+3.970e+03
+2.994e+03
+2.018e+03
+1.042e+03
+6.561e+01
NBR-90 @
100°C
S, Tresca
(Avg: 75%)
+1.187e+04
+1.178e+04
+1.080e+04
+9.828e+03
+8.851e+03
+7.875e+03
+6.899e+03
+5.923e+03
+4.947e+03
+3.970e+03
+2.994e+03
+2.018e+03
+1.042e+03
+6.561e+01
NBR-90 @
100°C
59°
31°

## *FKM- 75*

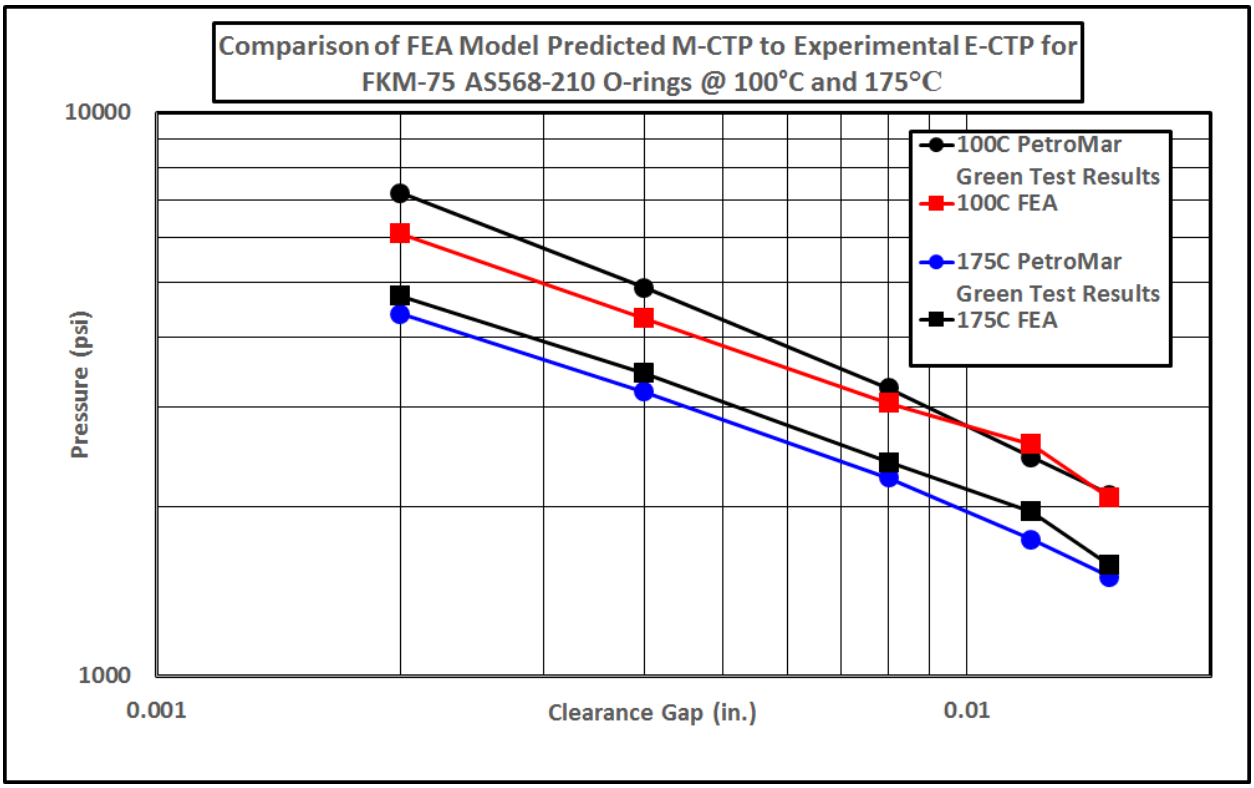


FKM-75 100°C Simulation Output Parameters

| Clearance Gap | **0.015”** | **0.012”** | **0.008”** | **0.004”** | **0.002”** |
|---|---|---|---|---|---|
| **M-CTP Pressure (PSI)** | 2077 | 2582 | 3058 | 4325 | 6119 |
| **Strain Energy (in-lb.)** | 2.67 | 3.07 | 3.27 | 4.90 | 8.49 |
| **Volume ($in^3$)** | 0.04302 | 0.04282 | 0.04263 | 0.04212 | 0.04142 |
| **SED (PSI)** | 1239 | 1247 | 1243 | 1245 | 1272 |
| **Extrusion Distance (mils)** | 18.88 | 17.95 | 12.38 | 8.14 | 5.81 |

FKM-75 175°C Simulation Output Parameters

| Clearance Gap | **0.015”** | **0.012”** | **0.008”** | **0.004”** | **0.002”** |
|---|---|---|---|---|---|
| **M-CTP Pressure (PSI)** | 1577 | 1963 | 2401 | 3447 | 4732 |
| **Strain Energy (in-lb.)** | 2.38 | 2.70 | 2.99 | 4.41 | 7.04 |
| **Volume ($in^3$)** | 0.04530 | 0.04510 | 0.04487 | 0.04433 | 0.04367 |
| **SED (PSI)** | 905 | 909 | 914 | 926 | 935 |
| **Extrusion Distance (mils)** | 15.07 | 14.74 | 10.51 | 7.25 | 5.31 |

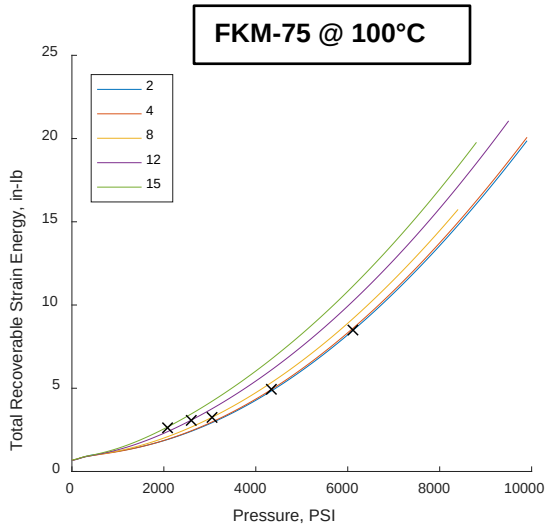
FKM-75 @ 100°C
Total Recoverable Strain Energy, in-lb
Pressure, PSI
2
4
8
12
15

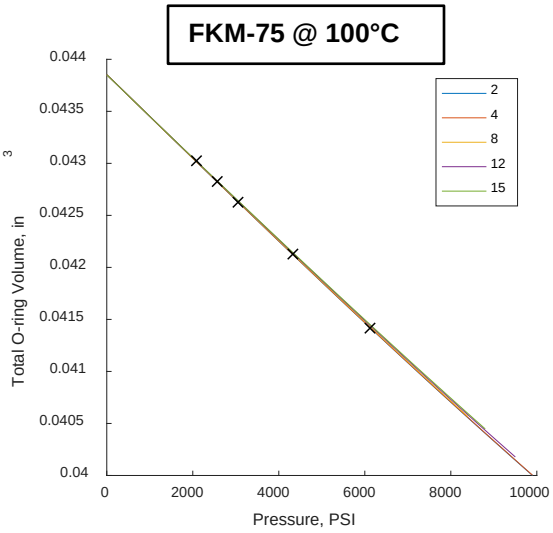
FKM-75 @ 100°C
Total O-ring Volume, in 3
Pressure, PSI
2
4
8
12
15

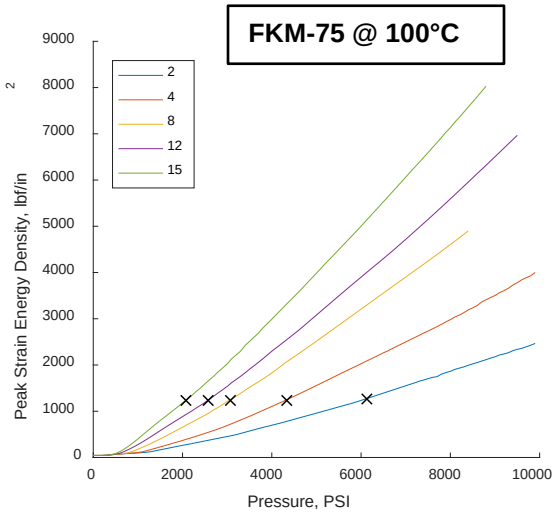
FKM-75 @ 100°C
Peak Strain Energy Density, lbf/in 2
Pressure, PSI
2
4
8
12
15

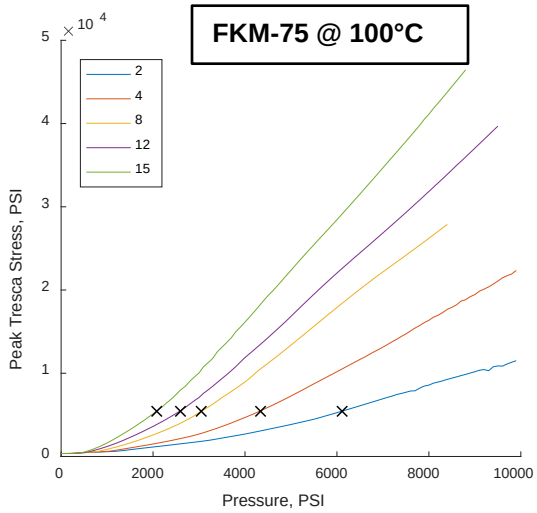
FKM-75 @ 100°C
× 10 4
Peak Tresca Stress, PSI
Pressure, PSI
2
4
8
12
15

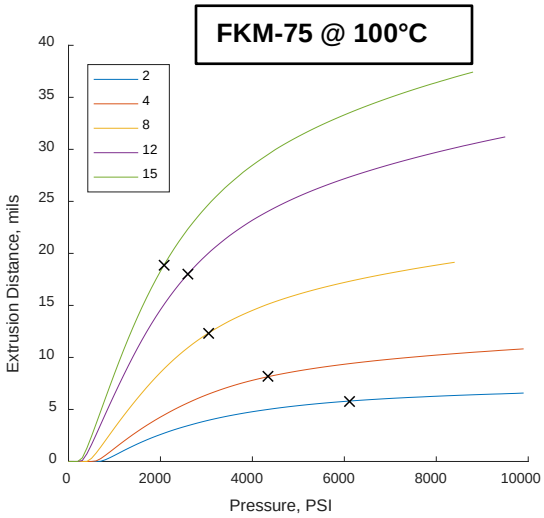
FKM-75 @ 100°C
Extrusion Distance, mils
Pressure, PSI
2
4
8
12
15

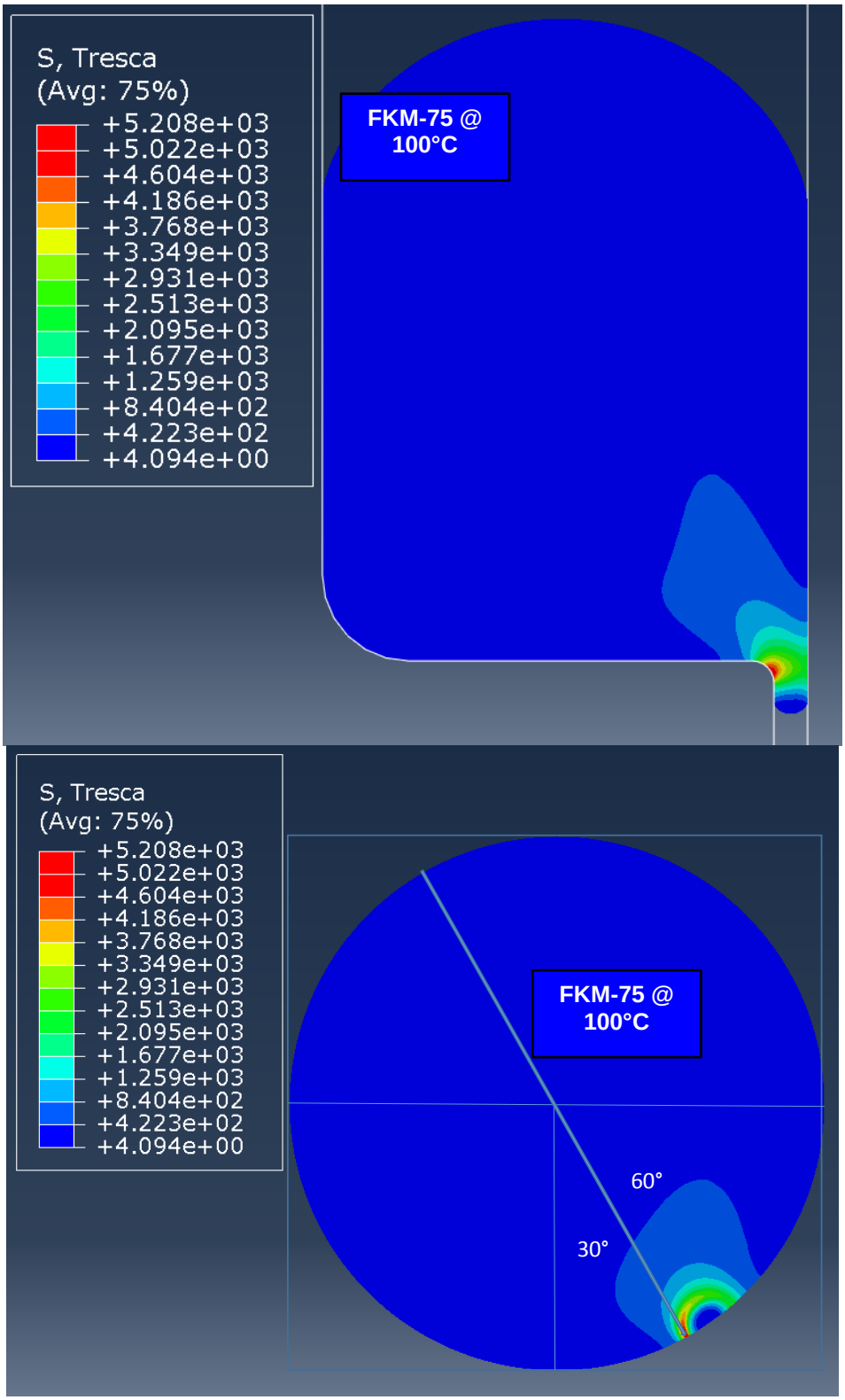
S, Tresca
(Avg: 75%)
+5.208e+03
+5.022e+03
+4.604e+03
+4.186e+03
+3.768e+03
+3.349e+03
+2.931e+03
+2.513e+03
+2.095e+03
+1.677e+03
+1.259e+03
+8.404e+02
+4.223e+02
+4.094e+00
FKM-75 @
100°C
S, Tresca
(Avg: 75%)
+5.208e+03
+5.022e+03
+4.604e+03
+4.186e+03
+3.768e+03
+3.349e+03
+2.931e+03
+2.513e+03
+2.095e+03
+1.677e+03
+1.259e+03
+8.404e+02
+4.223e+02
+4.094e+00
FKM-75 @
100°C
60°
30°

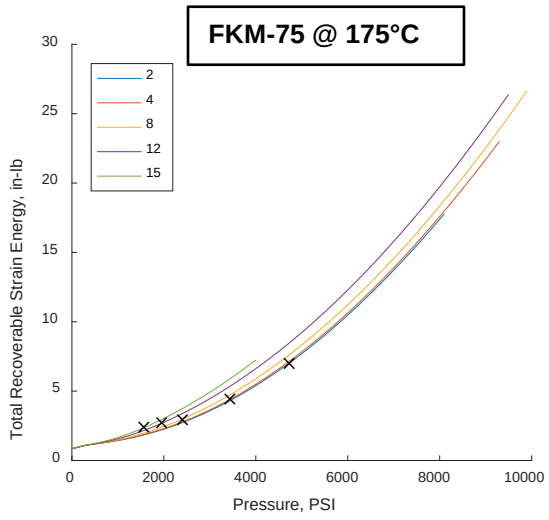
FKM-75 @ 175°C
Total Recoverable Strain Energy, in-lb
Pressure, PSI
2
4
8
12
15

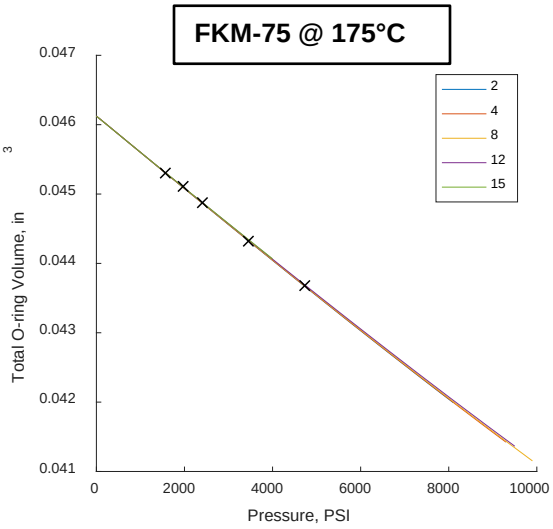
FKM-75 @ 175°C
Total O-ring Volume, in 3
Pressure, PSI
2
4
8
12
15

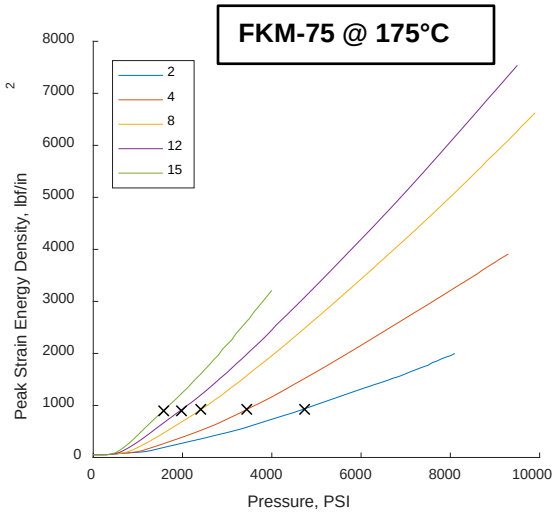
FKM-75 @ 175°C
Peak Strain Energy Density, lbf/in 2
Pressure, PSI
2
4
8
12
15

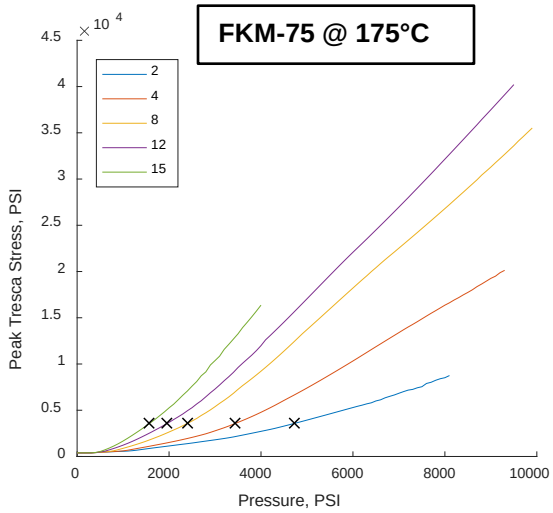
FKM-75 @ 175°C
Peak Tresca Stress, PSI
Pressure, PSI
2
4
8
12
15

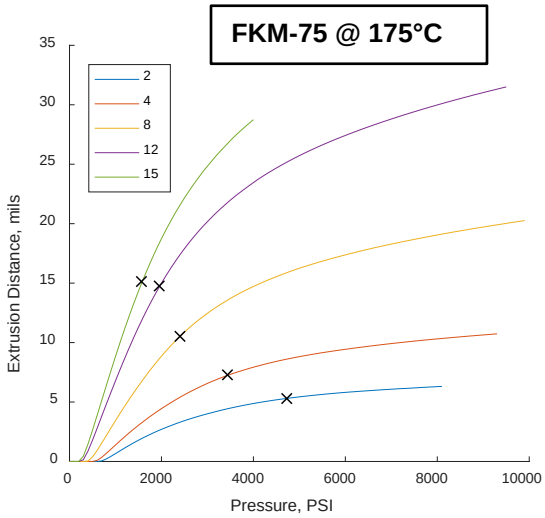
FKM-75 @ 175°C
Extrusion Distance, mils
Pressure, PSI
2
4
8
12
15

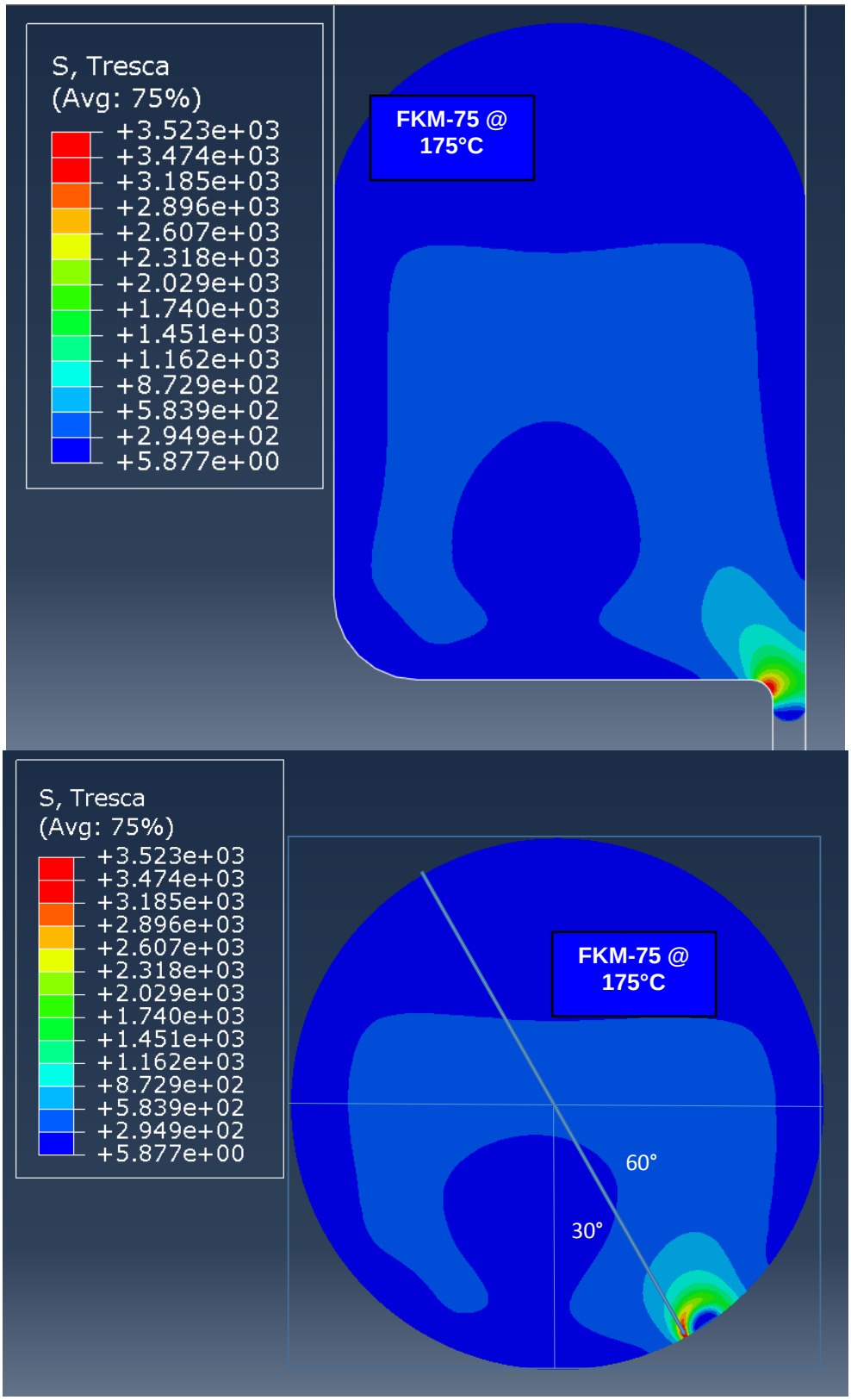
S, Tresca
(Avg: 75%)
+3.523e+03
+3.474e+03
+3.185e+03
+2.896e+03
+2.607e+03
+2.318e+03
+2.029e+03
+1.740e+03
+1.451e+03
+1.162e+03
+8.729e+02
+5.839e+02
+2.949e+02
+5.877e+00
FKM-75 @
175°C
S, Tresca
(Avg: 75%)
+3.523e+03
+3.474e+03
+3.185e+03
+2.896e+03
+2.607e+03
+2.318e+03
+2.029e+03
+1.740e+03
+1.451e+03
+1.162e+03
+8.729e+02
+5.839e+02
+2.949e+02
+5.877e+00
FKM-75 @
175°C
60°
30°

## *FKM-90*

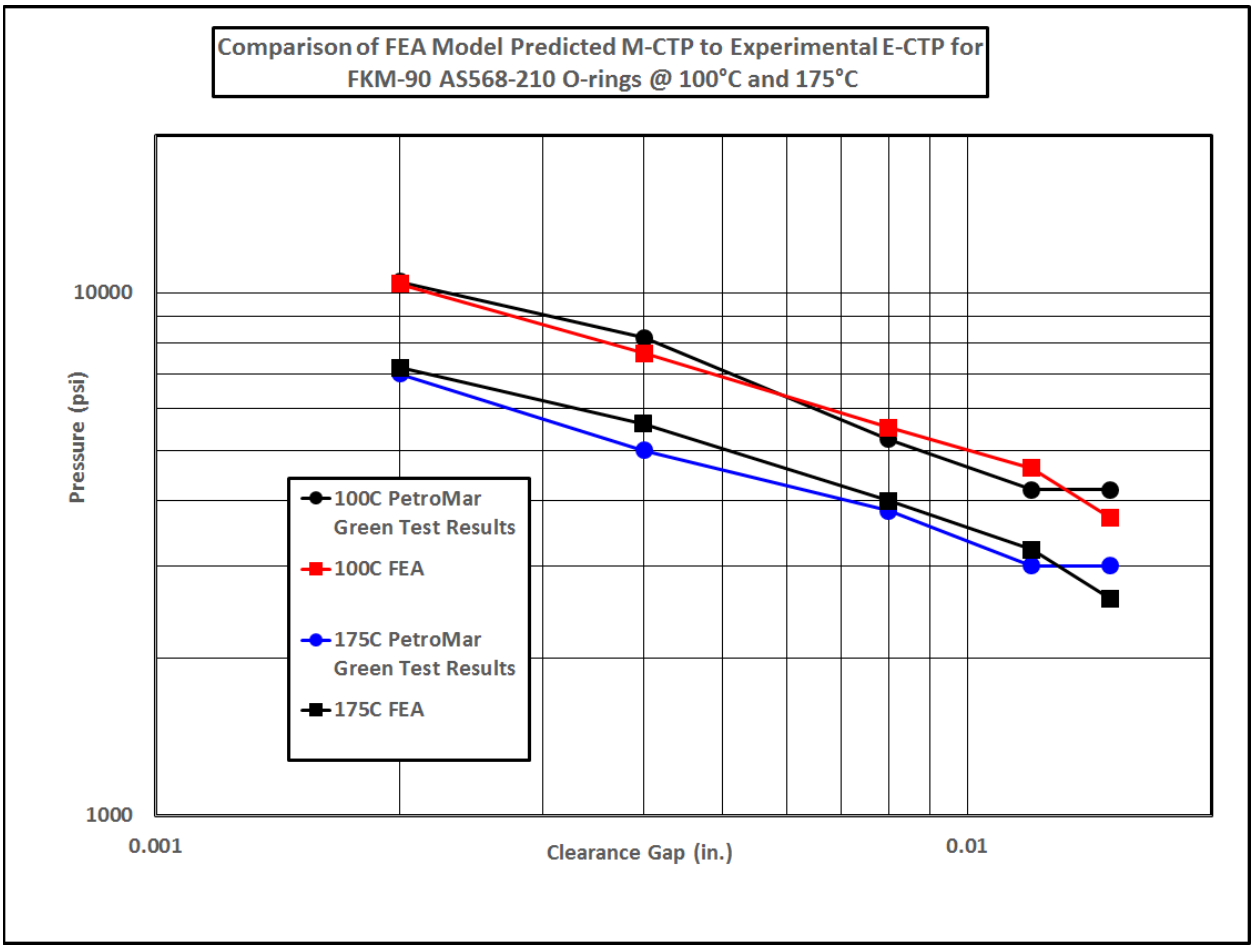


FKM-90 100°C Simulation Output Parameters

| Clearance Gap | **0.015”** | **0.012”** | **0.008”** | **0.004”** | **0.002”** |
|---|---|---|---|---|---|
| **M-CTP Pressure (PSI)** | 3714 | 4623 | 5521 | 7658 | 10392 |
| **Strain Energy (in-lb.)** | 5.16 | 6.41 | 7.62 | 12.12 | 20.07 |
| **Volume ($in^3$)** | 0.04206 | 0.04174 | 0.04143 | 0.04070 | 0.03981 |
| **SED (PSI)** | 1513 | 1526 | 1518 | 1508 | 1570 |
| **Extrusion Distance (mils)** | 14.56 | 14.07 | 9.75 | 6.52 | 4.98 |

FKM-90 175°C Simulation Output Parameters

| Clearance Gap | **0.015”** | **0.012”** | **0.008”** | **0.004”** | **0.002”** |
|---|---|---|---|---|---|
| **M-CTP Pressure (PSI)** | 2597 | 3221 | 3995 | 5610 | 7194 |
| **Strain Energy (in-lb.)** | 4.15 | 4.95 | 6.01 | 9.29 | 13.65 |
| **Volume ($in^3$)** | 0.04396 | 0.04368 | 0.04333 | 0.04261 | 0.04192 |
| **SED (PSI)** | 1028 | 1037 | 1046 | 1064 | 1070 |
| **Extrusion Distance (mils)** | 10.55 | 10.52 | 7.57 | 5.39 | 4.04 |

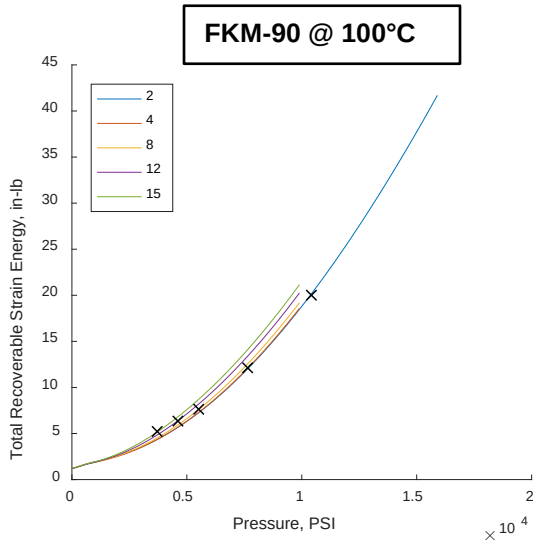
FKM-90 @ 100°C
Total Recoverable Strain Energy, in-lb
Pressure, PSI
× 10 4
2
4
8
12
15

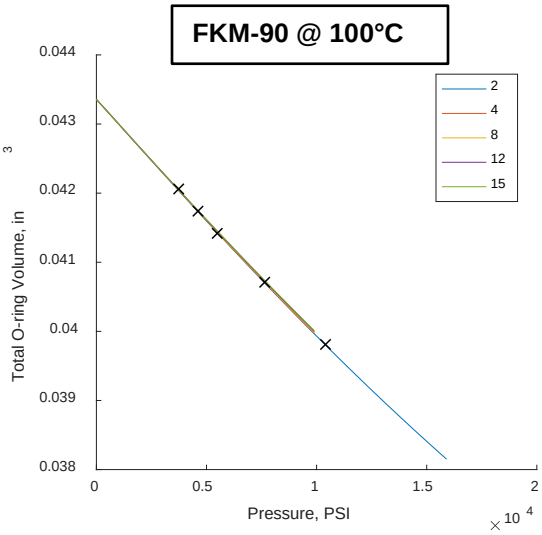
FKM-90 @ 100°C
Total O-ring Volume, in 3
Pressure, PSI
× 10 4
2
4
8
12
15

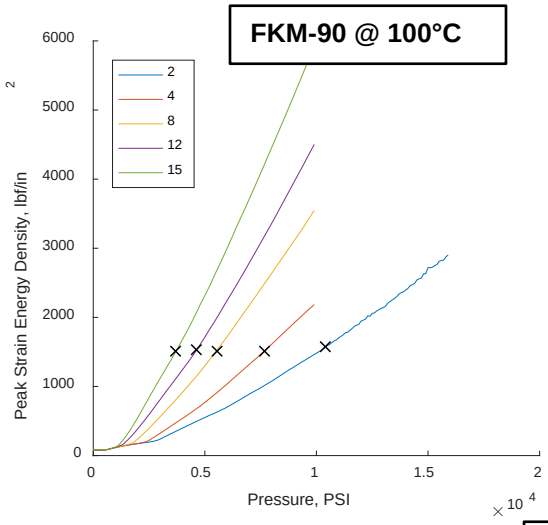
FKM-90 @ 100°C
Peak Strain Energy Density, lbf/in 2
Pressure, PSI
× 10 4
2
4
8
12
15

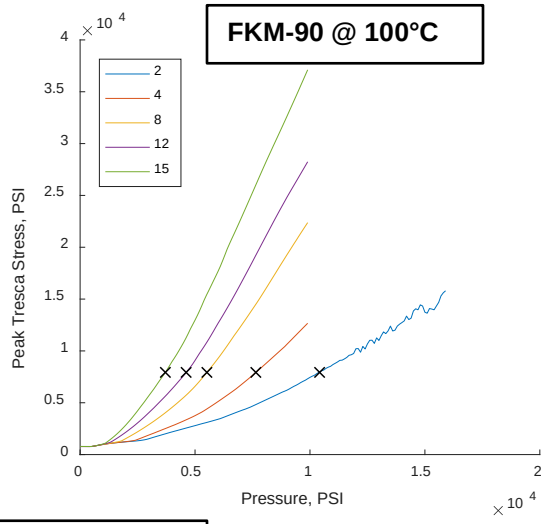
FKM-90 @ 100°C
× 10 4
Peak Tresca Stress, PSI
Pressure, PSI
× 10 4
2
4
8
12
15

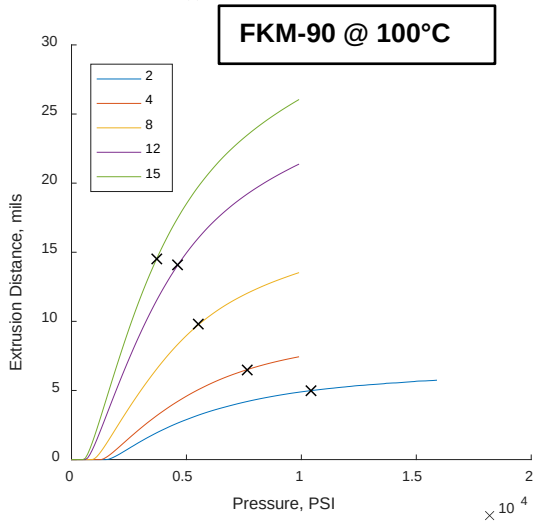
FKM-90 @ 100°C
Extrusion Distance, mils
Pressure, PSI
× 10 4
2
4
8
12
15

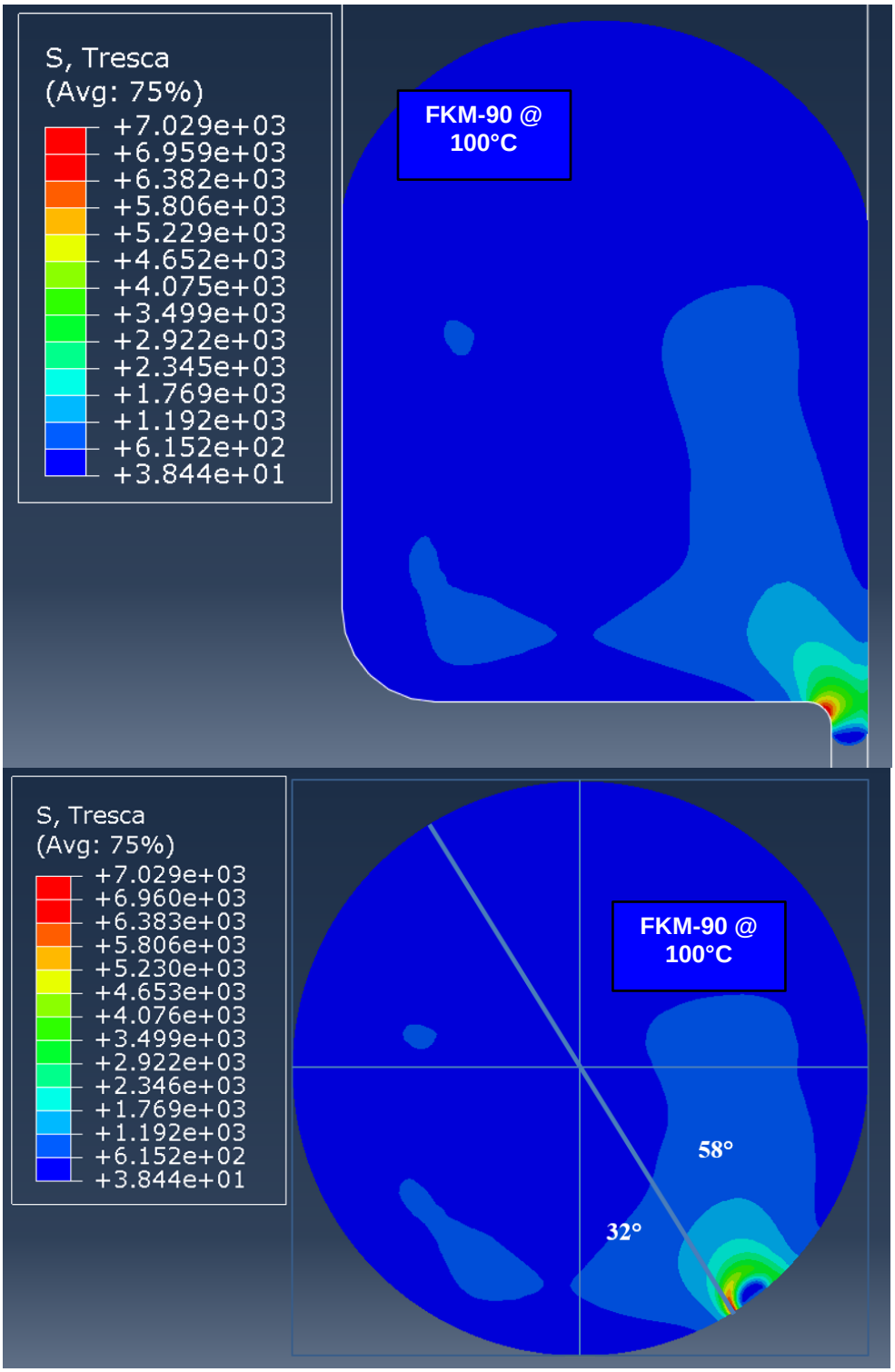
S, Tresca
(Avg: 75%)
+7.029e+03
+6.959e+03
+6.382e+03
+5.806e+03
+5.229e+03
+4.652e+03
+4.075e+03
+3.499e+03
+2.922e+03
+2.345e+03
+1.769e+03
+1.192e+03
+6.152e+02
+3.844e+01
FKM-90 @
100°C
S, Tresca
(Avg: 75%)
+7.029e+03
+6.960e+03
+6.383e+03
+5.806e+03
+5.230e+03
+4.653e+03
+4.076e+03
+3.499e+03
+2.922e+03
+2.346e+03
+1.769e+03
+1.192e+03
+6.152e+02
+3.844e+01
FKM-90 @
100°C
58°
32°

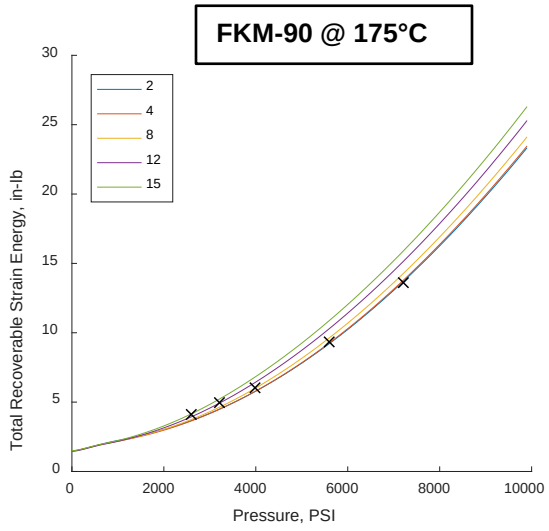
FKM-90 @ 175°C
Total Recoverable Strain Energy, in-lb
Pressure, PSI
2
4
8
12
15

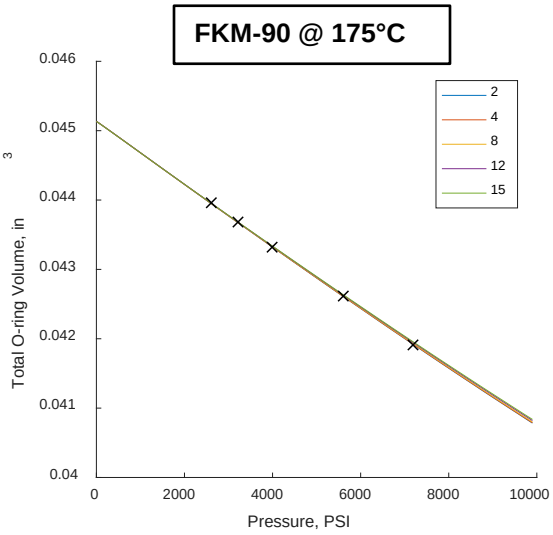
FKM-90 @ 175°C
Total O-ring Volume, in3
Pressure, PSI
2
4
8
12
15

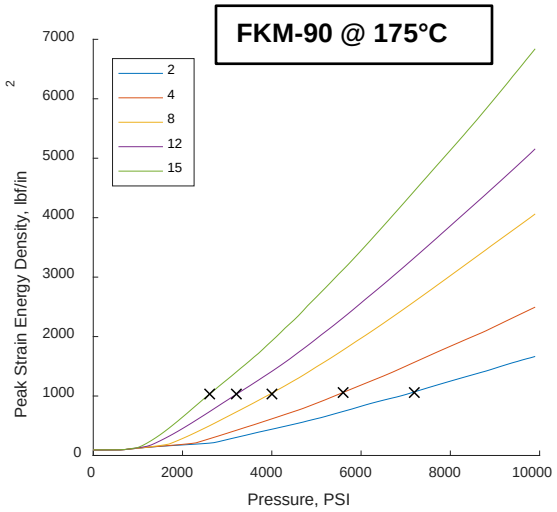
FKM-90 @ 175°C
Peak Strain Energy Density, lbf/in2
Pressure, PSI
2
4
8
12
15

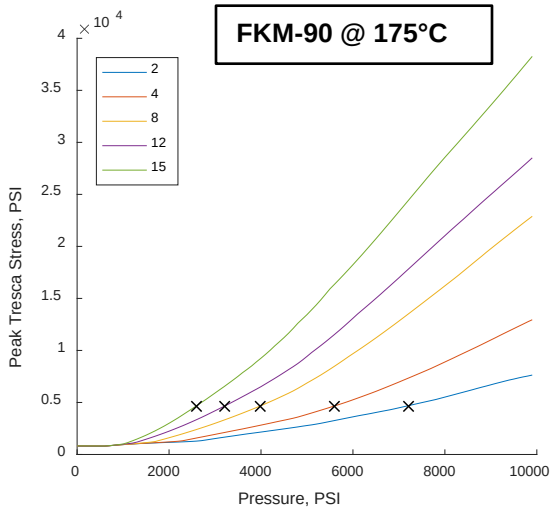
FKM-90 @ 175°C
Peak Tresca Stress, PSI
Pressure, PSI
2
4
8
12
15

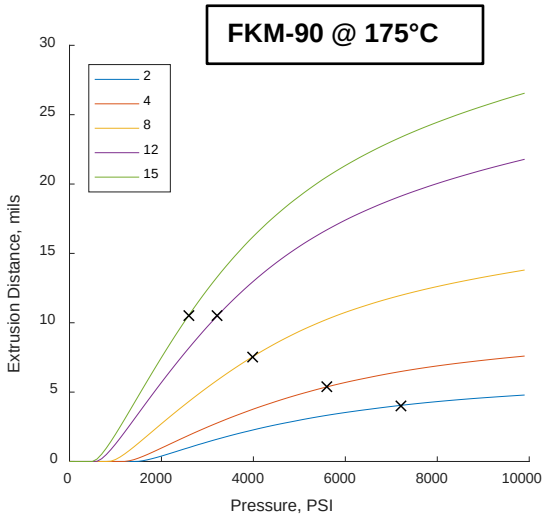
FKM-90 @ 175°C
Extrusion Distance, mils
Pressure, PSI
2
4
8
12
15

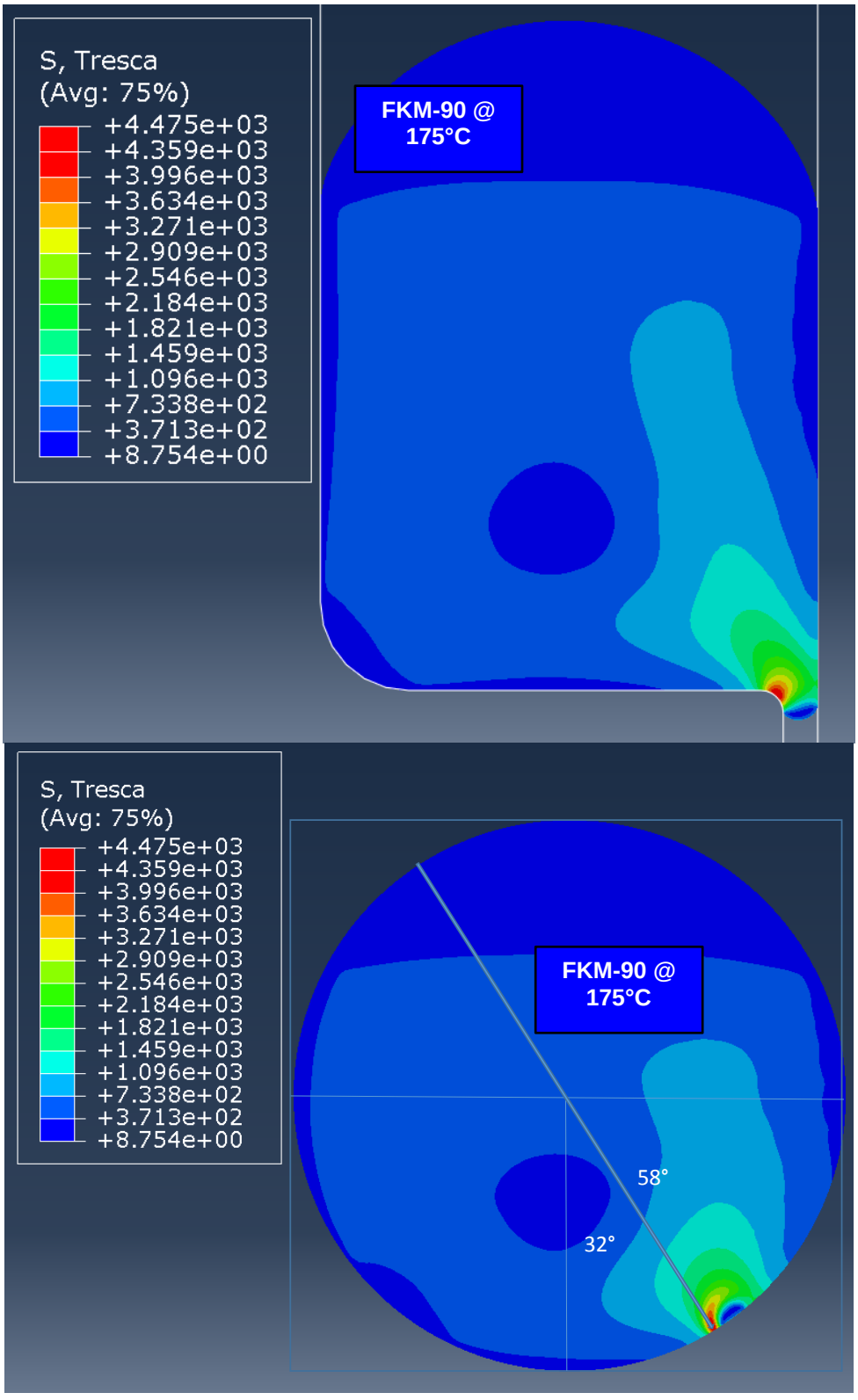
S, Tresca
(Avg: 75%)
+4.475e+03
+4.359e+03
+3.996e+03
+3.634e+03
+3.271e+03
+2.909e+03
+2.546e+03
+2.184e+03
+1.821e+03
+1.459e+03
+1.096e+03
+7.338e+02
+3.713e+02
+8.754e+00
FKM-90 @
175°C
S, Tresca
(Avg: 75%)
+4.475e+03
+4.359e+03
+3.996e+03
+3.634e+03
+3.271e+03
+2.909e+03
+2.546e+03
+2.184e+03
+1.821e+03
+1.459e+03
+1.096e+03
+7.338e+02
+3.713e+02
+8.754e+00
FKM-90 @
175°C
58°
32°

# Appendix A.7-2. Time-Dependent Effects on O-Ring Tearing

Petromar experiments on the O-ring used two procedures (Petromar Technologies Inc., 10 October 2016): 1) a Dwell test procedure, and 2) a Stepped Scan procedure. The Dwell procedure was aimed at identifying the smallest pressure at which any tearing could be observed. A pressurized dwell time of at least 60 minutes was used. The Stepped Scan procedure was aimed at finding the largest pressure that could be sustained for 5 minutes without leak or extrusion. In this Appendix, we consider to what extent time-dependent tearing effects, as characterized using creep crack growth rate measurements might influence observations of O-ring pressure retaining capability.

It is known in general that tearing in an elastomer occurs at a time rate $da/dt$ that is fixed by the instantaneous operating energy release rate $T$ (Kadir and Thomas, 1981), following a power-law of the form

$$\frac{da}{dt} = r_q \left( \frac{T}{T_q} \right)^{F_q} \tag{10}$$

$a$ is the crack length
$t$ is time
$T$ is the energy release rate (which in turn depends on pressure and on size of the crack)
$r_q$, $T_q$, and $F_q$ are the power law parameters describing the material response

The creep crack growth rate measurements can be used to estimate how different test time scales might impact the pressure required to produce tearing.

For a constant pressure test with duration $dt$, the tearing distance $da$ will be equal to the tearing distance in the reference test with $dt_{ref}$ whenever the following condition occurs

$$\frac{dt}{dt_{ref}} = \frac{da / dt_{ref}}{da / dt} = \frac{r_q \left( \frac{T_{ref}}{T_q} \right)^{F_q}}{r_q \left( \frac{T}{T_q} \right)^{F_q}} = \left( \frac{T_{ref}}{T} \right)^{F_q} \tag{11}$$

To illustrate, a 5 min hold time at pressure for NBR- 75 at 100 °C (which has $F_q$ = 6.39) would give a result of, relative to a 60 minute reference hold time

$$\frac{dt}{dt_{ref}} = \frac{5\,\text{min}}{60\,\text{min}} = \left( \frac{T_{ref}}{T} \right)^{6.39} \Rightarrow \frac{T}{T_{ref}} = \left( \frac{5\,\text{min}}{60\,\text{min}} \right)^{-\frac{1}{6.39}} = 1.475 \tag{12}$$

That is, tearing is predicted for a 5 min hold at an energy release rate of $T = 1.475\ T_{ref}$, where $T_{ref}$ is the energy release rate at tearing in the 60 minute observation. From equation (9), it follows that the Tresca stress at tearing for the 5 min test would be $\tau_b = (1.475)^{1/2}\,\tau_{b,ref}$ or simply $\tau_b = 1.215\,\tau_{b,ref}$. This information can be used with the finite element solution relating pressure and Tresca stress, as shown in Figure A.7-21. We see that, for the example considered for a 0.004 inch clearance, the pressure for the 5 min test is predicted to increase to 7800 psi, up from nearly 6000 psi for the 60 min test.

The corresponding Petromar-observed actual results were 6500 psi (green) for the 60 min Dwell test, 7000 psi (yellow), and 19000 psi (red) for the 5 minute Stepped Scan test. The difference between the predicted 5 min and 60 min results is roughly 1800 psi, which may be compared to the difference of 1500 psi observed between the Petromar 5 min (yellow) and 60 min (green) test. The red extrusion pressure occurs at significantly higher pressures, which may reflect not only the benefit gained from time-dependent crack growth but also from other interactions not included in the model as torn O-ring material partly "refills" the gap.

Given that each of the subject materials has a distinct power-law slope $F_q$, the specific ranking of materials for seal integrity at a given clearance may depend somewhat on test duration. Materials with larger values of $F_q$ are expected to show less dependence on test duration, while materials with smaller values of $F_q$ are expected to show strong dependence on test duration.

Although the characterization measurements and finite element solutions obtained under this program provide sufficient information to make this estimate of the time-dependence of seal integrity, it should be noted that this estimation method has not been validated against test-cell sealing experiments. Additional experiments over a series of test durations would be required, ideally for each material and temperature.

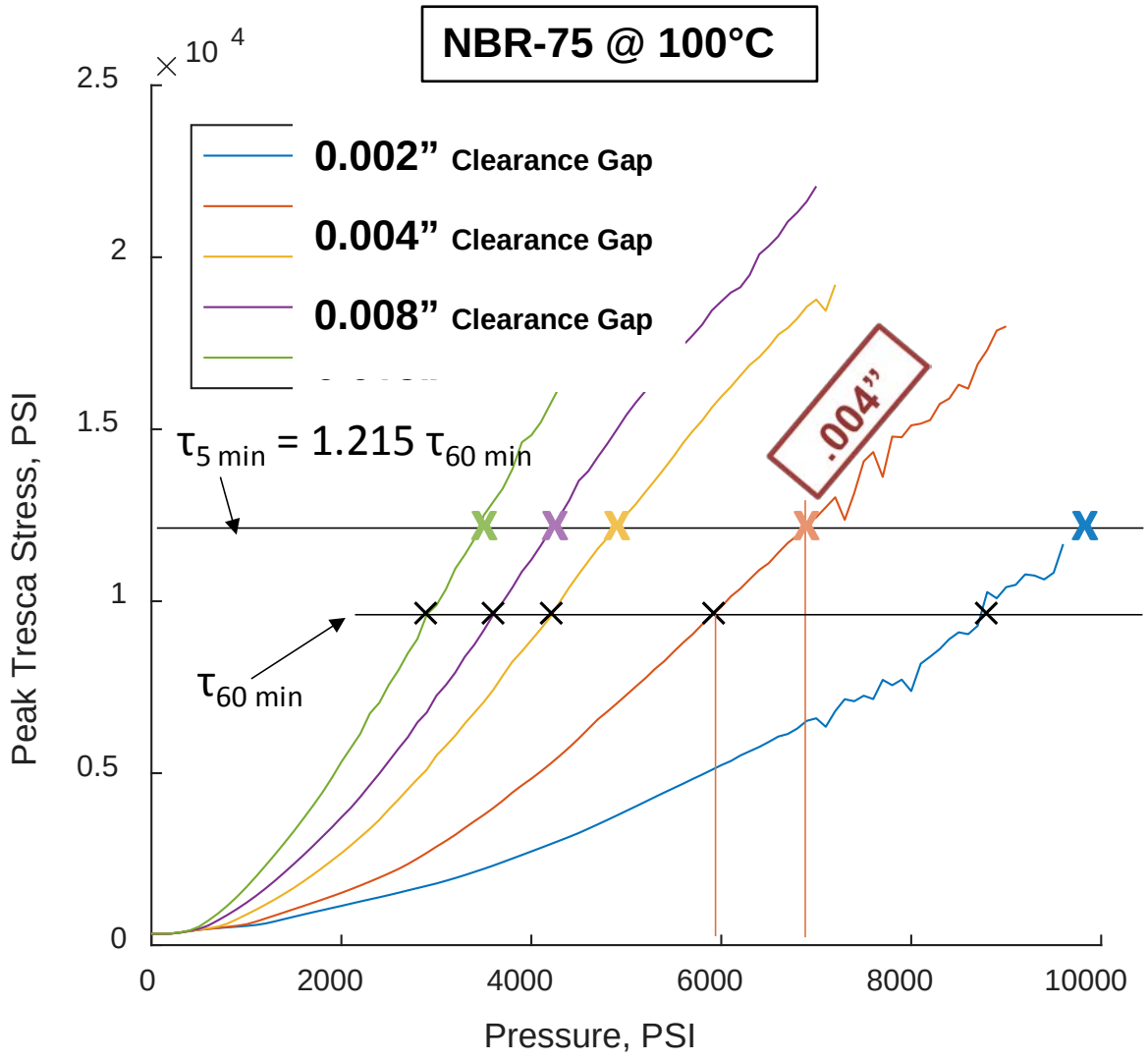


Figure A.7-21. Example calculation of increase in critical pressure for a test duration of 5 minutes, based on finite element computed solution for Tresca stress vs. pressure for NBR-75 @ 100°C.

## A.8 Appendix 8 – Finite Element Model Estimates of the Reduction in Critical Tear Pressure (M-CTP) for Elastomer O-rings @ 100°C and 175°C After 1 year Exposure at Maximum Pressure using 0.004-inch clearance gap.

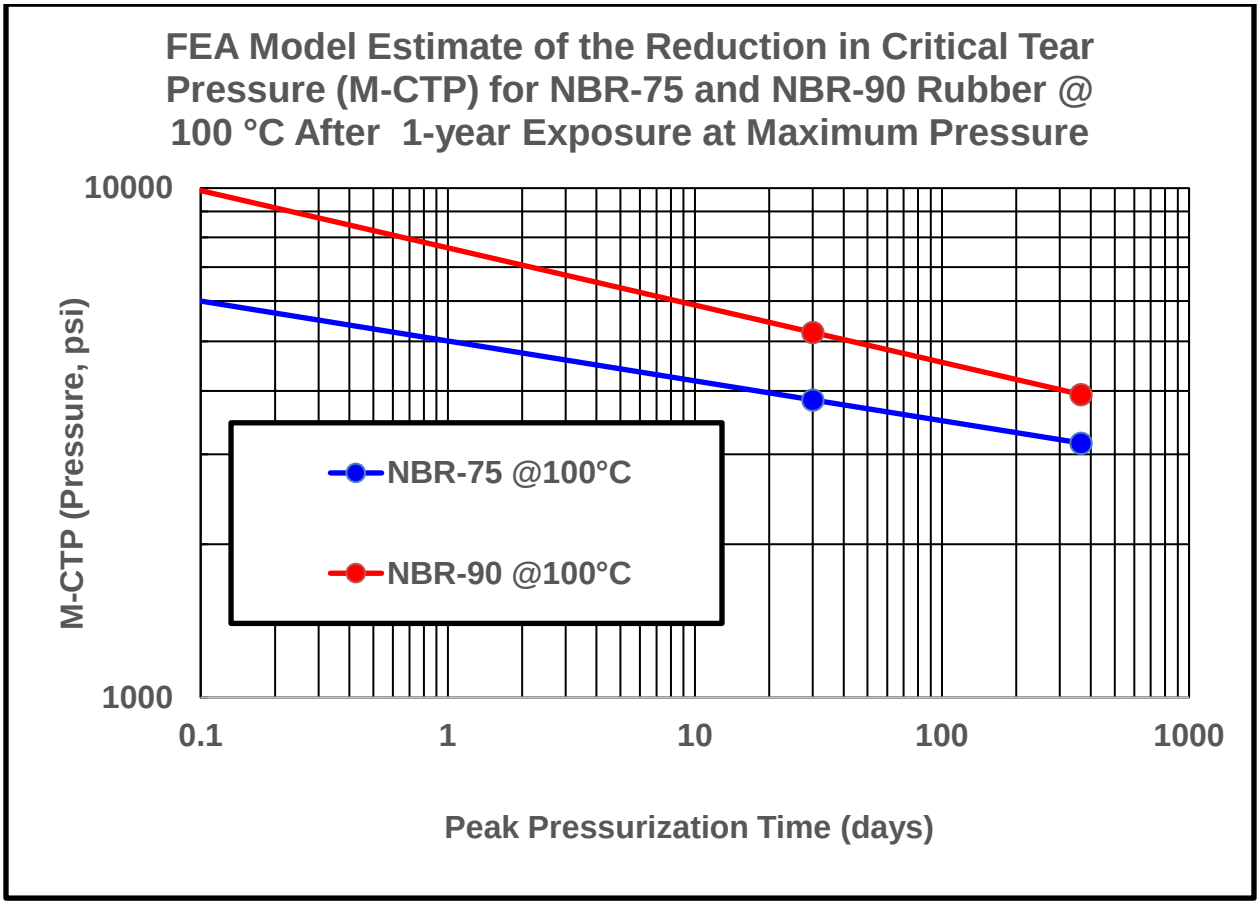


**Figure A.8-1. Predicted Reduction in M-CTP for NBR-75 and NBR-90 @ 100°C for 1 year exposure**

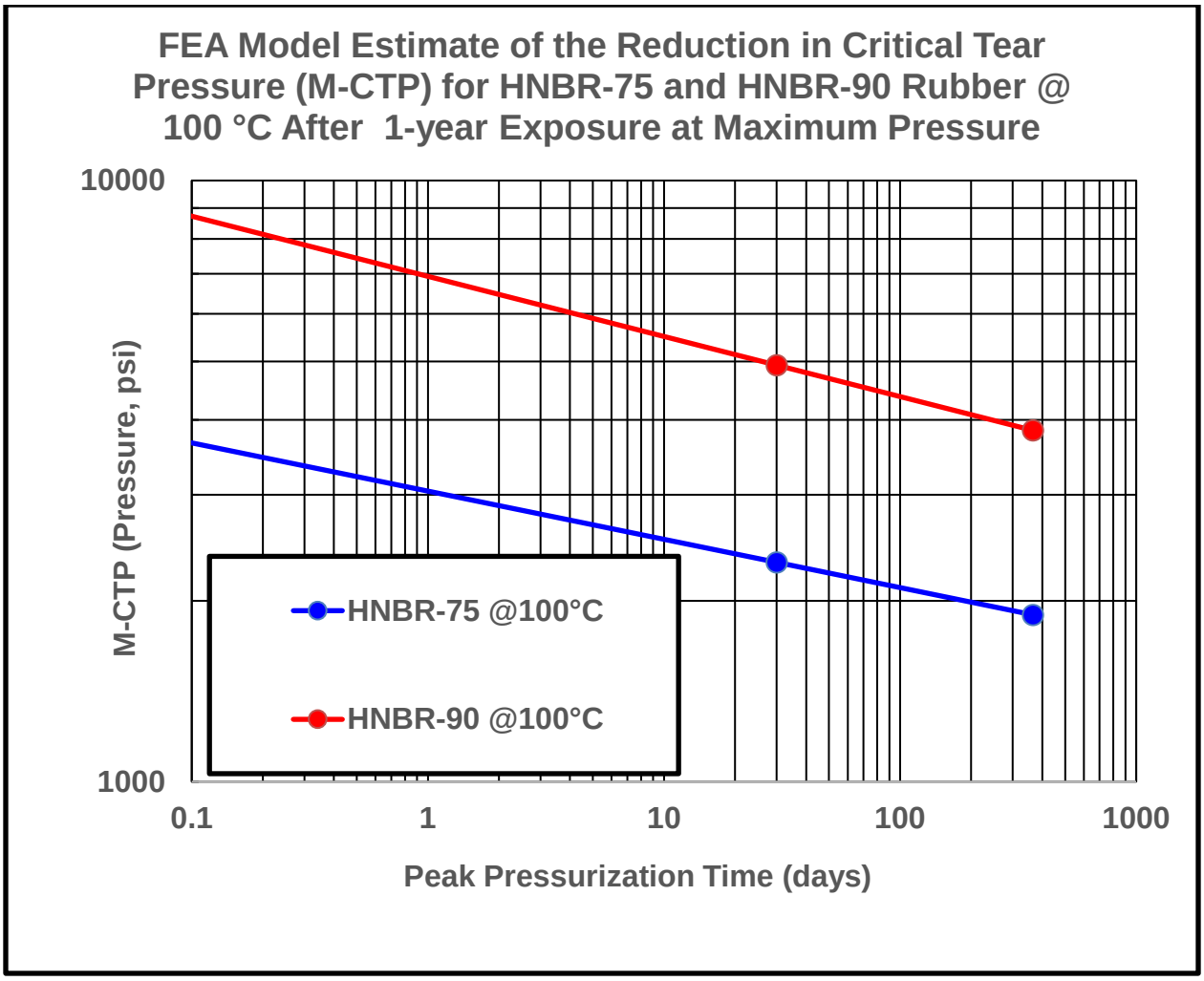


**Figure A.8-2. Predicted Reduction in M-CTP for HNBR-75 and HNBR-90 @ 100°C for 1 year exposure**

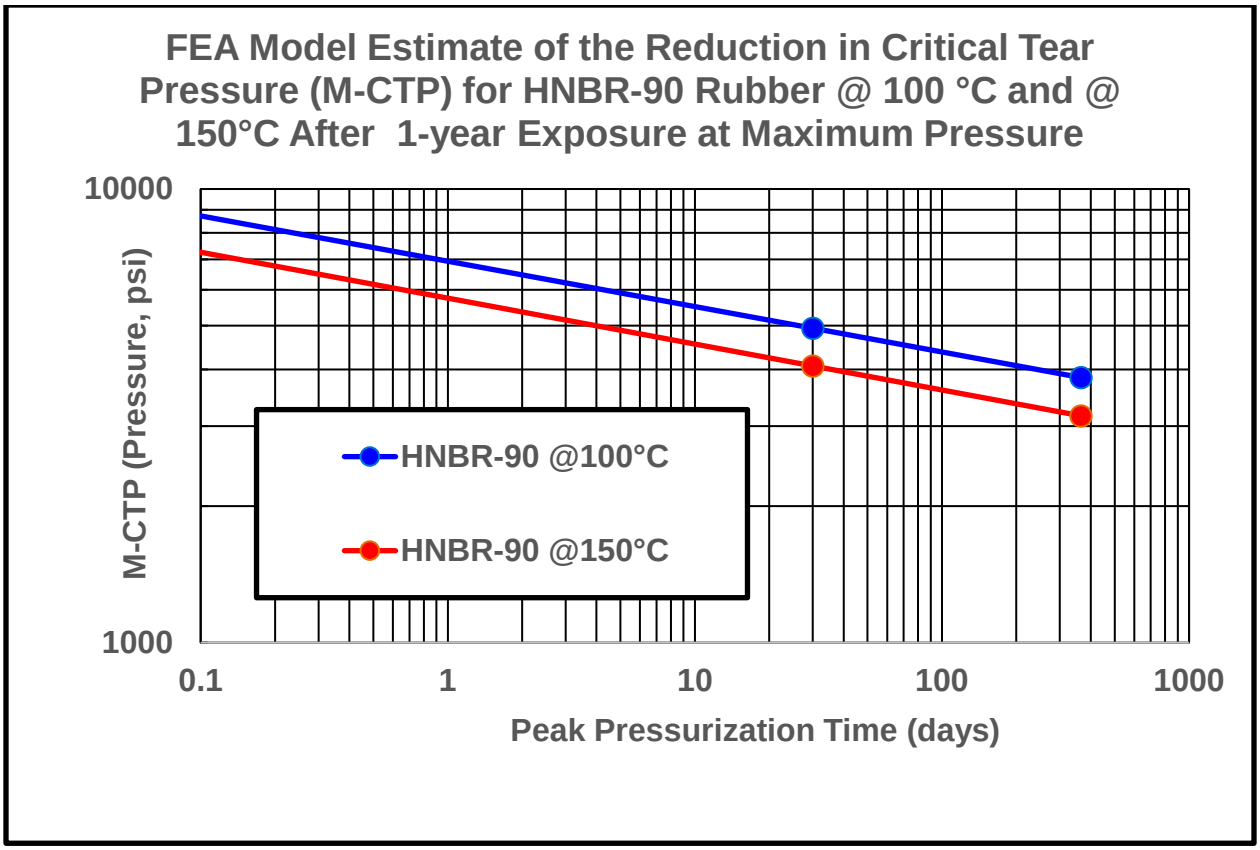


**Figure A.8-3. Predicted Reduction in M-CTP for HNBR-90 @ 100°C and @ 150°C for 1 year exposure**

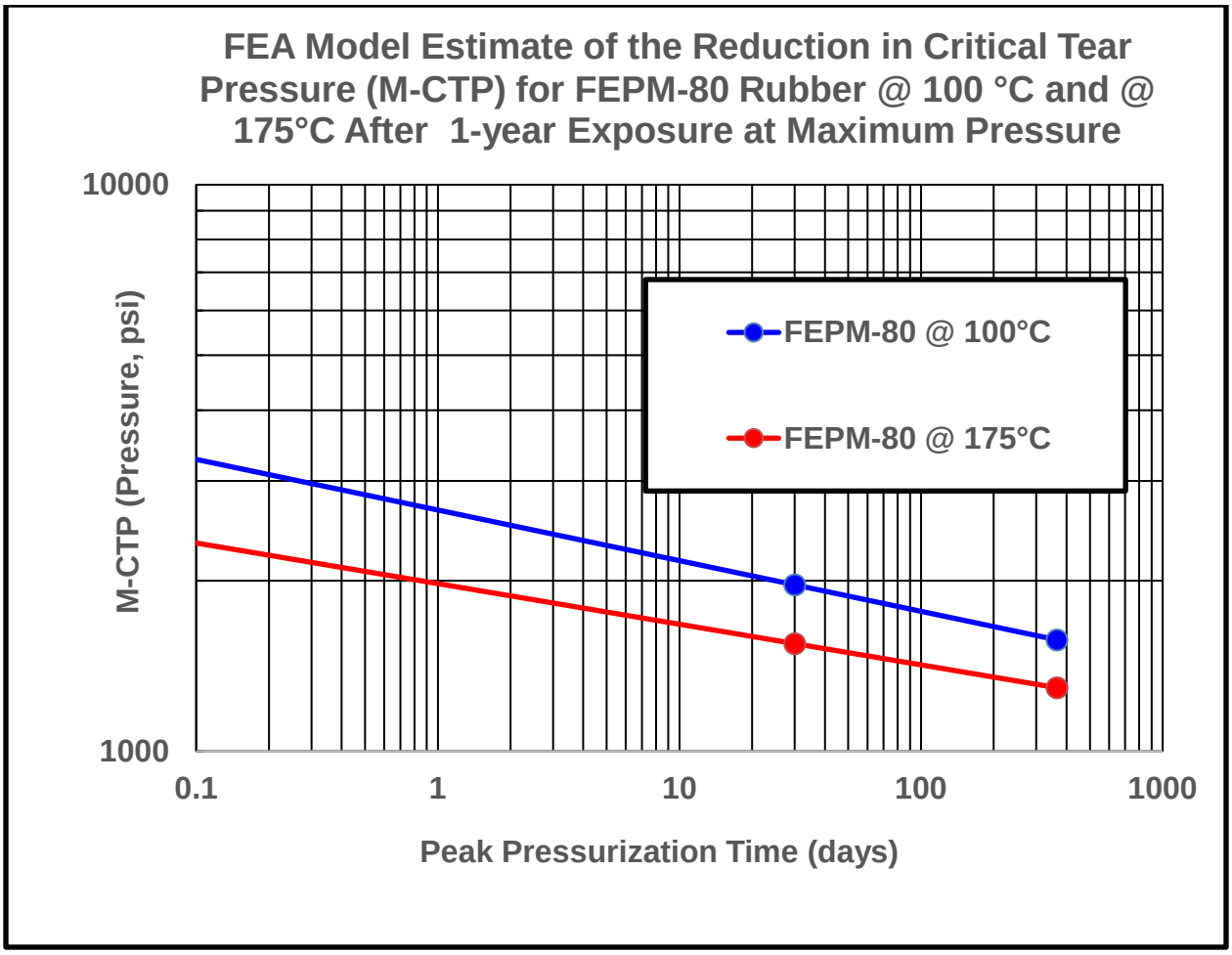


**Figure A.8-4. Predicted Reduction in M-CTP for FEPM-80 @ 100°C and @ 175°C for 1 year exposure**

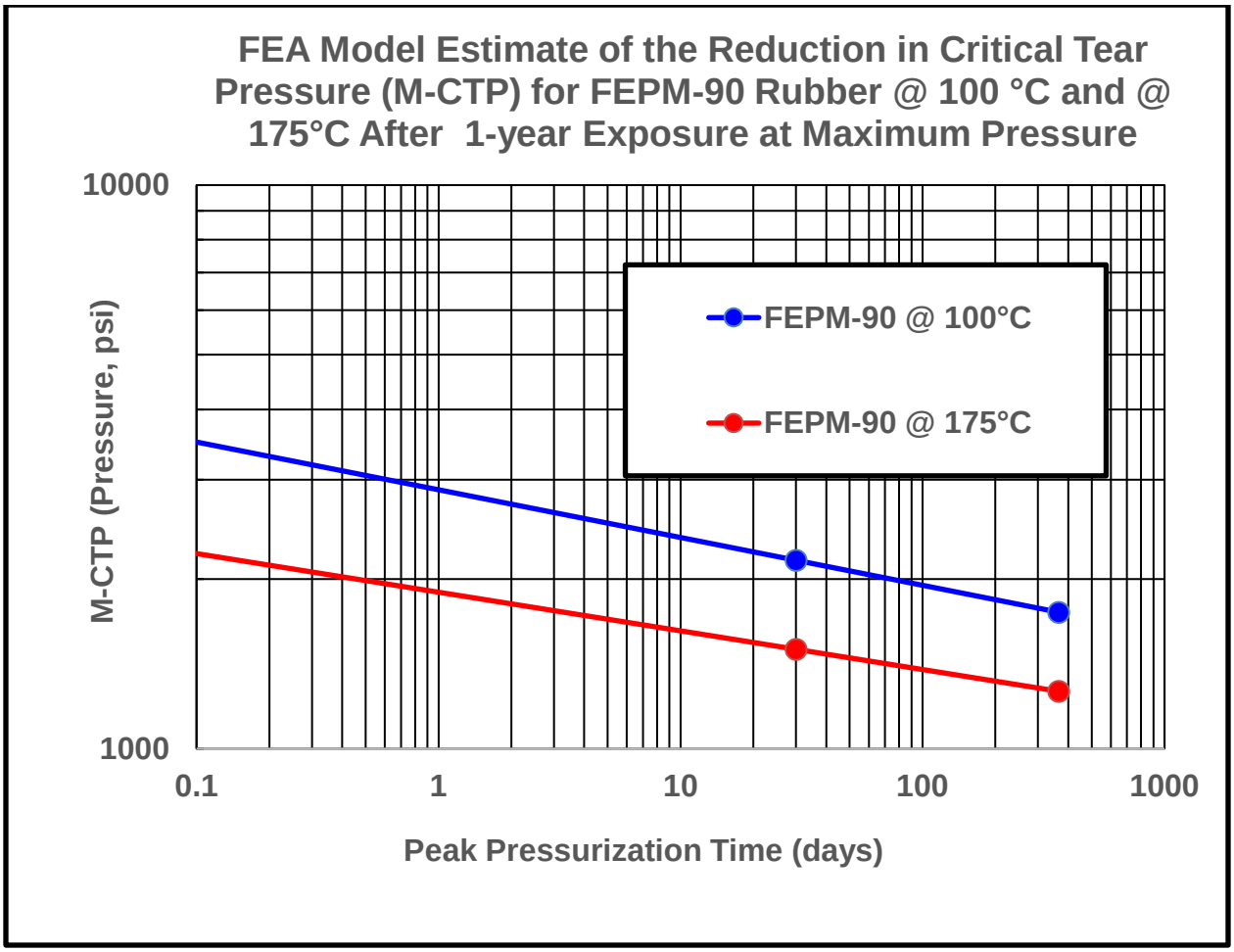


**Figure A.8-5. Predicted Reduction in M-CTP for FEPM-90 @ 100°C and @ 175°C for 1 year exposure**

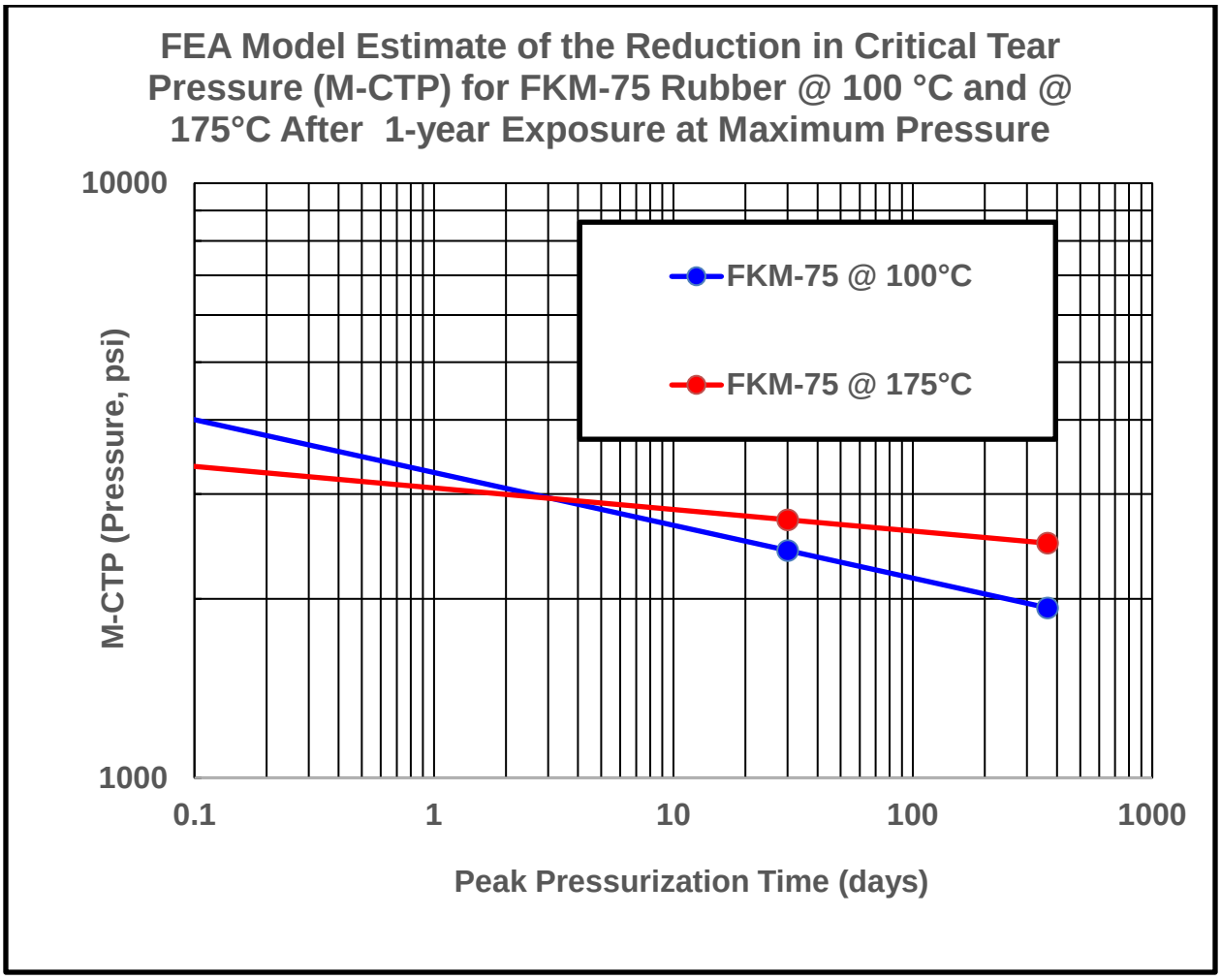


**Figure A.8-6. Predicted Reduction in M-CTP for FKM-75 @ 100°C and @ 175°C for 1 year exposure**

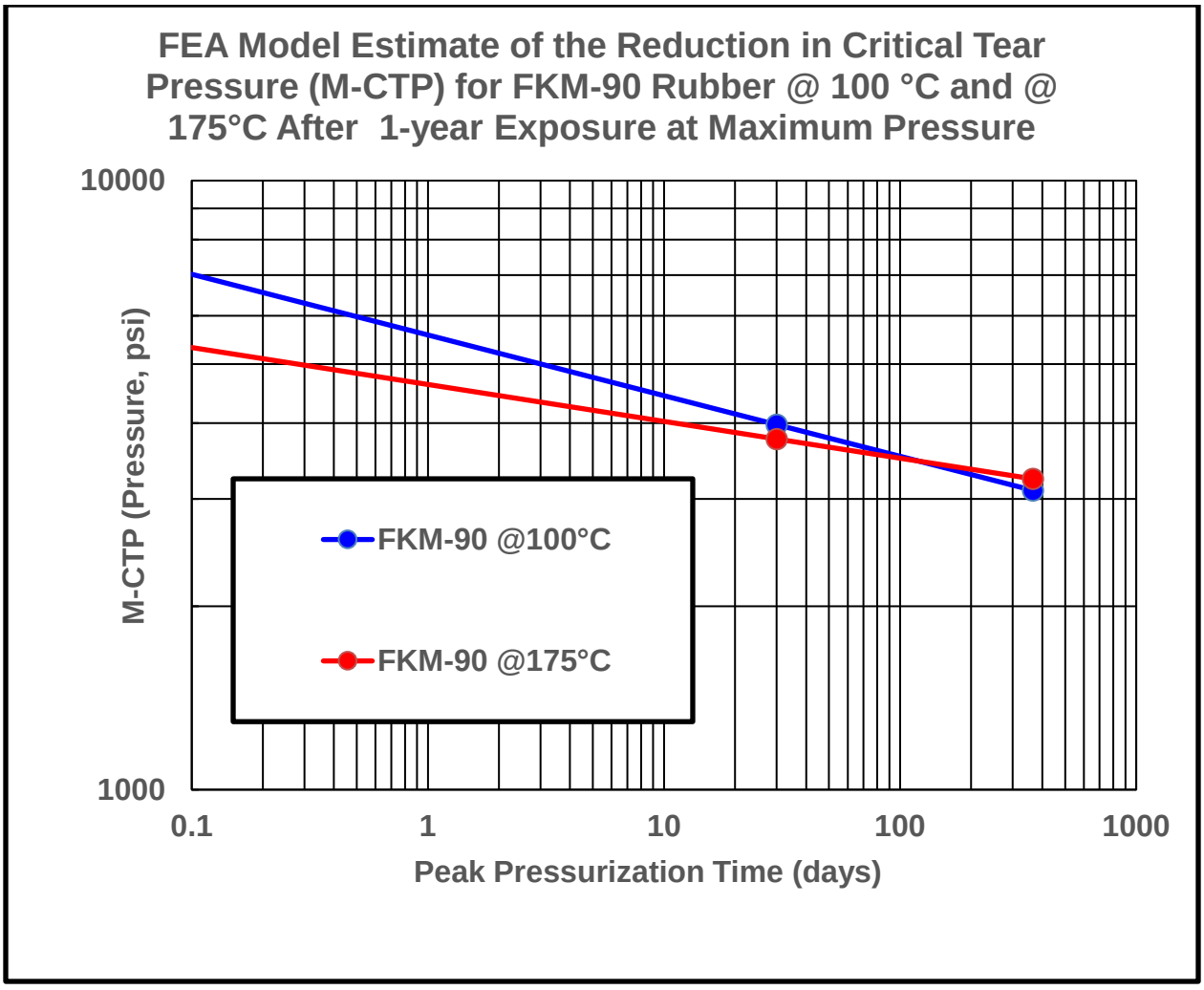


**Figure A.8-7. Predicted Reduction in M-CTP for FKM-90 @ 100°C and @ 175°C for 1 year exposure**

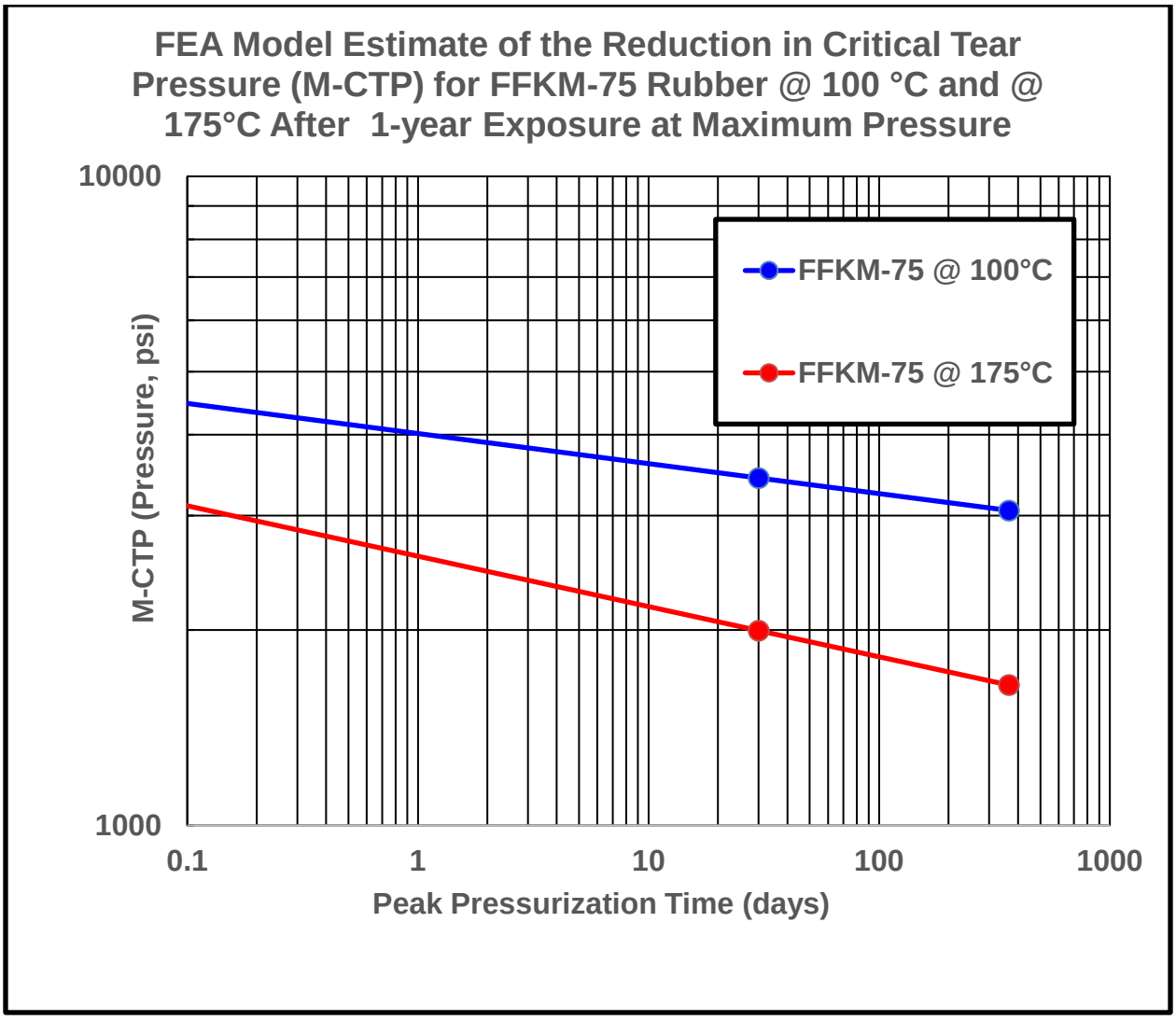


**Figure A.8-8. Predicted Reduction in M-CTP for FFKM-75 @ 100°C and @ 175°C for 1 year exposure**

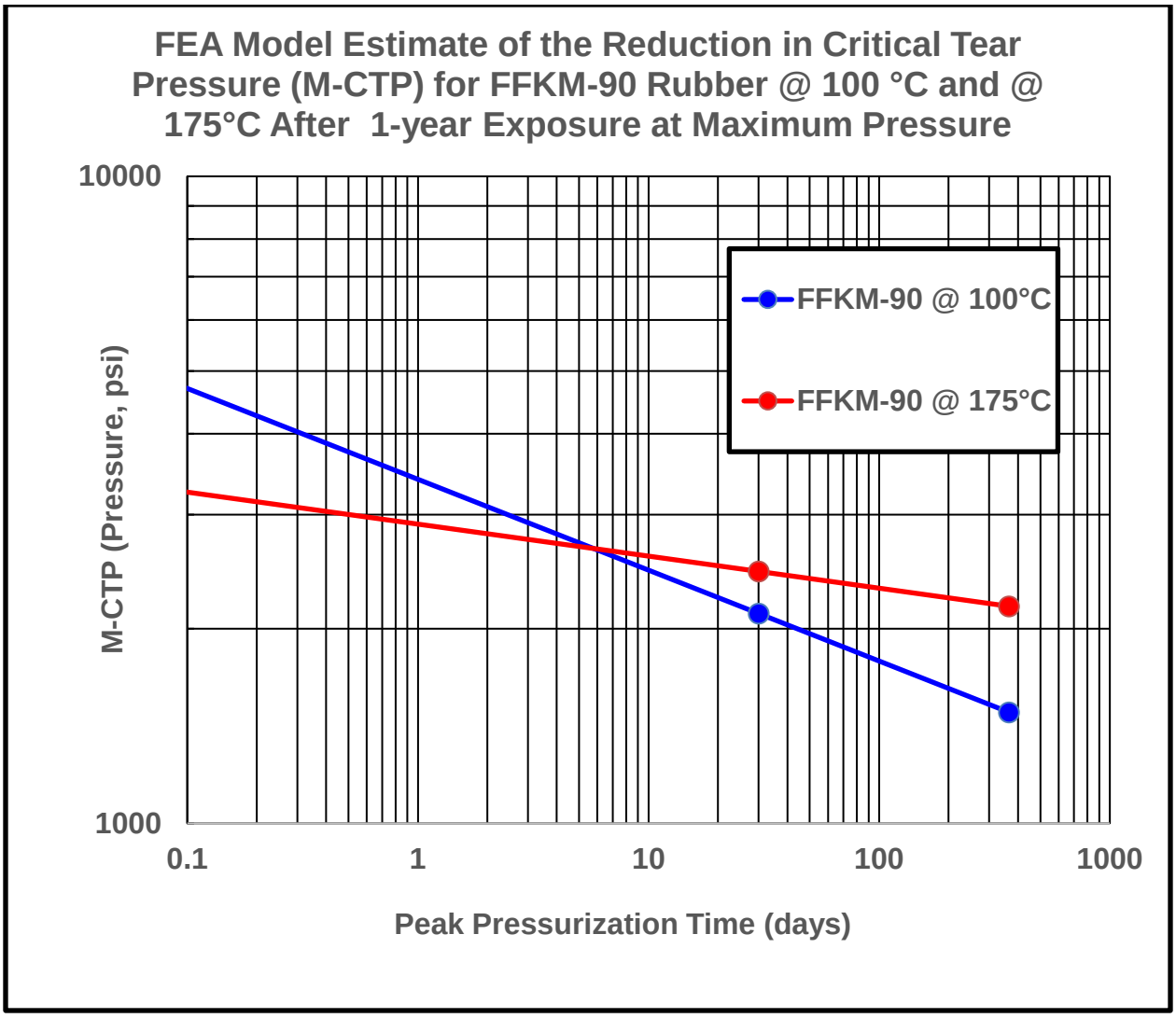


**Figure A.8-9. Predicted Reduction in M-CTP for FFKM-90 @ 100°C and @ 175°C for 1 year exposure**